

In this PhD research on axisymmetric groundwater flow in multilayered aquifer systems, existing analytical and numerical solutions are examined and compared, and new solutions are developed with the aim of modeling flow to pumping wells more realistically.

Solutions for layered aquifer systems also allow for the interpretation of multiple pumping tests, such as hydraulic tomography. Nevertheless, this study proves that the resolution of such tests is theoretically limited.

The superposition method is applicable when assuming a linear aquifer response. This approach is illustrated through a practical case involving the optimization of a drainage system using linear programming.

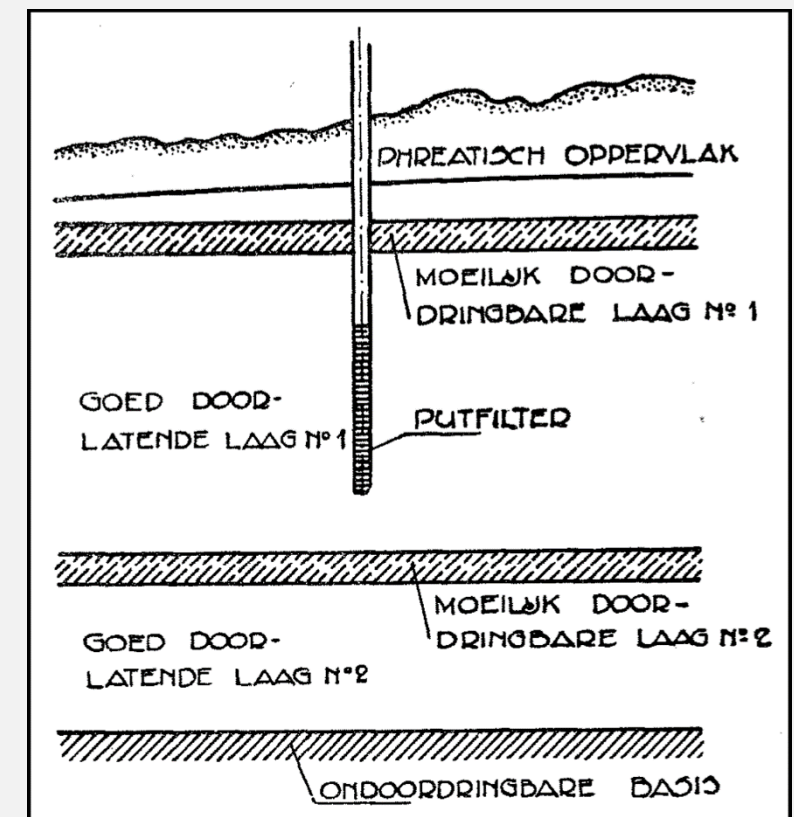
However, when assessing the environmental impact of groundwater extractions, it is essential to distinguish between linear and nonlinear models. Relying on empirical formulas to estimate the radius of influence is strongly discouraged due to their inconsistency with fundamental hydrogeological principles.

On the other hand, many groundwater studies face stringent time and budget constraints. In such cases, the use of axisymmetric models may serve as an acceptable and cost-effective alternative. Furthermore, these models offer valuable insights that can guide the decision-making process regarding the necessity of building a complex numerical model.

Axisymmetric Flow in Multilayer Aquifer Systems: Solutions and Theoretical Considerations

Andy Louwyck 2023

Axisymmetric Flow in Multilayer Aquifer Systems: Solutions and Theoretical Considerations



Andy Louwyck

September 2023

Axisymmetric Flow in Multilayer Aquifer Systems: Solutions and Theoretical Considerations

Andy Louwyck

**Dissertation submitted in fulfilment of the requirements for the award of the degree of
Doctor in Sciences: Geology**

**Publicly defended at the Auditorium Valère Billiet
Campus Sterre, Krijgslaan 281, Building S8, 9000 Gent**

On Friday 1 September 2023

Supervisor: Prof. Dr. Kristine Walraevens (Ghent University)

Co-supervisor: Dr. Alexander Vandenbohede (De Watergroep)

Members of the Jury:

Prof. Dr. Stephen Louwey, Ghent University, Belgium (**chairman**)

Prof. Dr. Thomas Hermans, Ghent University, Belgium (**secretary**)

Prof. Dr. Herman Peiffer, Ghent University, Belgium

Prof. Dr. Marijke Huysmans, Free University of Brussels, Belgium

Prof. Dr. Mark Bakker, Delft University of Technology, The Netherlands

Prof. Dr. Kristine Walraevens, Ghent University, Belgium

Dr. Alexander Vandenbohede, De Watergroep, Brussels, Belgium

Dean: Prof. Dr. Isabel Van Driessche

Rector: Prof. Dr. Rik Van de Walle

Please refer to this work as follows:

Louwyck, A., 2023. Axisymmetric Flow in Multilayer Aquifer Systems: Solutions and Theoretical Considerations. PhD thesis, Laboratory for Applied Geology and Hydrogeology, Department of Geology, Ghent University, Belgium.

An online version of this thesis is available at <https://github.com/alouwyck/PhD>

Printing: University Press

Copyright: © 2023

The author and the supervisors give the authorization to consult and to copy parts of this work for personal use only. Every other use is subject to the copyright laws and the source should be specified when using the results and the data from the thesis. Permission to reproduce any material contained in this work should be obtained from the author.

This PhD thesis is dedicated to my late father, Marc Alleman, who lives on in me.

Table of Contents

Executive Summary	xii
Nederlandse Samenvatting	xv
Preface.....	xix
About the Author	xx
About the Cover Illustration.....	xxi
Chapter 1. General Introduction	1
1.1. Research context	1
1.2. Research objective	3
1.3. Research overview	5
1.3.1. Hydraulic parameter identification in the Belgian coastal plain	5
1.3.2. Improving the finite-difference model for axisymmetric flow.....	8
1.3.3. Assessing the environmental impact of groundwater extractions	10
1.3.4. Developing semi-analytical solutions for multilayer well-flow	14
1.4. Dissertation outline	16
1.5. Publications	20
1.6. Developed software	22
1.7. References.....	23
Chapter 2. Semi-Analytical Solution Method for Simulating Multilayer Flow	32
2.1. Introduction.....	32
2.1.1 One-layer solutions	32
2.1.2 Two-layer solutions	33
2.1.3 Multilayer solutions.....	34
2.1.4 Generalized solution.....	35
2.2. Problem statement.....	36
2.2.1 The multilayered aquifer system.....	37
2.2.2 Groundwater flow equations	38
2.2.3 Initial and boundary conditions.....	39
2.3. Generalized semi-analytical solution	40
2.3.1 Laplace transform.....	40
2.3.2 Matrix formulation	41
2.3.3 General solution	43
2.3.4 Axisymmetric flow constants	45
2.3.5 Parallel flow constants	46
2.4. The superposition principle	47

2.4.1 Mathematical description	48
2.4.2 Superposition in time	50
2.4.3 Superposition in space	51
2.5. Well-known analytical solutions.....	52
2.5.1 Darcy's law.....	52
2.5.2 The Thiem-Dupuit equation	53
2.5.3 Areal recharge on a circular island	55
2.5.4 One-dimensional parallel flow with recharge	56
2.5.5 One-dimensional axisymmetric flow with recharge	57
2.5.6 The de Glee equation	58
2.5.7 The Theis equation	60
2.5.8 Effect of a well on the flow of a nearby stream	63
2.5.9 The Edelman equations	65
2.5.10 The model of Hantush-Jacob.....	67
2.5.11 Hemker's solution for steady flow in a leaky multi-aquifer system.....	68
2.5.12 Hemker's solution for unsteady flow in a multi-aquifer system	70
2.5.13 Steady flow in a confined multi-aquifer system.....	72
2.6. Summary.....	74
2.7. References.....	75
Chapter 3. Finite-Difference Approach for Simulating Multilayer Flow.....	82
3.1. Introduction.....	82
3.1.1. A brief history of numerical groundwater modeling.....	82
3.1.2. Axisymmetric numerical models	83
3.1.3. Simulating axisymmetric flow using MODFLOW.....	84
3.1.4. Software implementations.....	85
3.2. Problem statement.....	87
3.3. Finite-difference approach.....	88
3.3.1. Discretization.....	89
3.3.2. Flow equations	90
3.3.3. Initial and boundary conditions.....	90
3.3.4. Matrix system.....	92
3.3.5. Solvers	93
3.3.6. Interpolation.....	94
3.4. Axisymmetric MODFLOW procedure	95
3.4.1. General procedure	95
3.4.2. MODFLOW procedure	96

3.5. Summary.....	98
3.6. References.....	98
Chapter 4. A Critical Review of the Hybrid Finite-Difference Finite-Element Method	110
4.1. Introduction.....	110
4.1.1. HYPARIDEN	110
4.1.2. AS2D	111
4.1.3. Objective	112
4.2. Problem statement.....	114
4.3. Solution methods	115
4.3.1. Semi-analytical solution	115
4.3.2. Finite-difference approximation	116
4.3.3. Hybrid finite-difference finite-element method	119
4.4. Numerical experiments	123
4.4.1. Synthetic pumping test	123
4.4.2. The Theis model	125
4.4.3. Three-layer system	128
4.4.4. Random simulations.....	130
4.5. Discussion and conclusions	131
4.6. References.....	132
Chapter 5. Simulating Multilayer-Multizone Flow	141
5.1. Introduction.....	141
5.2. Problem statement.....	143
5.2.1. The multilayer-multizone aquifer system	143
5.2.2. Groundwater flow equations	144
5.2.3. Initial and boundary conditions.....	144
5.3. Semi-analytical solution	145
5.3.1. Matrix formulation	145
5.3.2. General solution	147
5.3.3. Particular solutions.....	149
5.3.4. Finding the integration constants	151
5.4. Finite-difference approach.....	153
5.5. Verification	155
5.5.1. Circular infiltration area	156
5.5.2. Formula of Blom	160
5.5.3. Steady state confined one-layer solutions	162
5.5.4. Steady state leaky one-layer solution	166

5.5.5. Transient state confined one-layer solution	170
5.5.6. Slug test in confined aquifer.....	173
5.5.7. Embanked river infiltrating a multilayer aquifer system.....	175
5.6. Skin effect.....	179
5.6.1. Linear and non-linear well losses	180
5.6.2. Dimensionless skin factor.....	182
5.6.3. Multi-zone skin factor	184
5.6.4. Skin effect in case of transient flow	185
5.6.5. Skin effect for a well in a multilayer system.....	186
5.7. Summary and conclusions.....	189
5.8. References.....	191
Chapter 6. Modeling Multilayer Wells	196
6.1. Introduction.....	196
6.1.1. Multi-aquifer wells	196
6.1.2. Partially penetrating wells.....	197
6.1.3. Numerical methods	201
6.1.4. Objectives	203
6.2. Problem statement.....	204
6.3. Semi-analytical solution	206
6.3.1. General solution	206
6.3.2. Particular solutions.....	209
6.3.3. Solution for homogeneous layers	212
6.3.4. Zero-thickness skin	215
6.4. Finite-difference solution	216
6.4.1. Wellbore storage	216
6.4.2. Connected cells	217
6.4.3. MODFLOW procedure	218
6.5. Verification	221
6.5.1. Steady flow to a multi-aquifer well	222
6.5.2. Transient flow to a multi-aquifer well.....	224
6.5.3. The UWD solution	227
6.5.4. Partially penetrating wells: UWD versus UWG	229
6.5.5. The KGS model	232
6.5.6. A multilayer well surrounded by multiple zones.....	235
6.6. Summary.....	238
6.7. References.....	239

Chapter 7. Radial Flow in Head-Dependent Two-Zone Multi-Aquifer Systems	249
7.1. Introduction.....	249
7.1.1. Confined-unconfined flow.....	249
7.1.2. Combined areal infiltration and drainage	250
7.1.3. Finite-difference method	251
7.1.4. Objective	252
7.2. Semi-analytical multilayer two-zone solution.....	254
7.2.1. Problem statement.....	254
7.2.2. Solution for one zone	255
7.2.3. Coupled solution for two zones	258
7.2.4. Verification	260
7.3. Multilayer head-dependent two-zone problems.....	260
7.3.1. Problem statement.....	261
7.3.2. Semi-analytical solution method.....	262
7.3.3. Finite-difference approach.....	268
7.4. Confined-unconfined flow.....	270
7.4.1. Problem statement.....	270
7.4.2. Semi-analytical solution method.....	271
7.4.3. Finite-difference approach.....	276
7.4.4. Verification	277
7.5. Combined areal infiltration and drainage	280
7.5.1. Solving the initial head problem	281
7.5.2. Problem statement.....	282
7.5.3. Semi-analytical solution method.....	283
7.5.4. Finite-difference approach.....	286
7.5.5. Verification	288
7.6. Summary and conclusions.....	295
7.7. References.....	297
Chapter 8. Modeling Unconfined Flow	302
8.1. Introduction.....	302
8.2. Nonlinear unconfined flow.....	303
8.2.1. Problem statement.....	305
8.2.2. Semi-analytical method.....	306
8.2.3. Finite-difference approach.....	307
8.2.4. Verification	308
8.3. Delayed yield	311

8.3.1. Problem statement.....	315
8.3.2. Semi-analytical solution	315
8.3.3. Finite-difference approach	318
8.3.4. Verification	318
8.4. Summary and conclusions.....	323
8.5. References.....	324
Chapter 9. Understanding Axisymmetric Multilayer Well-Flow	332
9.1. Introduction.....	332
9.1.1. Semi-analytical multi-aquifer solutions.....	332
9.1.2. Objective	333
9.2. Problem statement.....	334
9.3. Analytical solution	336
9.3.1. Exact solution in Laplace space	336
9.3.2. Steady state solution.....	338
9.3.3. Asymptotic solution for large values of time	342
9.4. Example	345
9.5. Verification	349
9.6. Hydraulic parameter identification	350
9.7. Summary and conclusions.....	353
9.8. References.....	354
Chapter 10. The Radius of Influence Myth.....	360
10.1. Introduction.....	360
10.1.1. The Sichardt formula	360
10.1.2. Objectives	362
10.2. One-dimensional axisymmetric flow: analytical solutions.....	364
10.2.1. Problem statement.....	364
10.2.2. Laplace transform.....	365
10.2.3. General solution	365
10.2.4. Particular solutions.....	366
10.2.5. Radial discharge and storage change	369
10.2.6. The Ernst model	370
10.3. Estimating the radius of influence.....	371
10.3.1. The Sichardt formula	372
10.3.2. The de Glee Equation	376
10.3.3. The Theis equation	378
10.3.4. The Hantush-Jacob model	380

10.3.5. The Ernst model	383
10.3.6. Validating the Ernst model	385
10.3.7. Transient state solution of the Ernst model.....	388
10.3.8. Finding the maximum radius of influence.....	391
10.4. Discussion	392
10.5. Summary and conclusions.....	395
10.6. References.....	396
Chapter 11. The Water Budget Myth and Its Recharge Controversy: Linear versus Nonlinear Systems	
.....	405
11.1. Introduction.....	405
11.1.1. The recharge controversy	406
11.1.2. Objective	409
11.2. The water budget equation revisited	410
11.3. Bredehoeft's island.....	414
11.4. Polder island.....	416
11.4.1. The linear case.....	416
11.4.2. The nonlinear case	418
11.5. Finite-difference approach.....	420
11.5.1. Finite-difference equations	421
11.5.2. Numerical example.....	424
11.6. Summary and conclusions.....	426
11.7. References.....	427
Chapter 12. Using Linear Programming to Revisit the Optimization of a Combined Pumping and Deep Infiltration System	
.....	432
12.1. Introduction.....	432
12.1.1. Inverse problems.....	432
12.1.2. Linear programming	433
12.1.3. Objective	433
12.2. The original study	434
12.2.1. Introduction.....	434
12.2.2. Methodology	436
12.2.3. Results	440
12.2.4. Conclusions.....	444
12.3. Revisiting the optimization.....	444
12.3.1. Methodology	445
12.3.2. Implementation.....	448

12.3.3. Conclusions.....	460
12.4. Summary	460
12.5. References.....	461
Chapter 13. Summary and Conclusions.....	465
13.1. Main objective.....	465
13.2. Existing solutions.....	465
13.3. New solutions	466
13.4. Theoretical considerations	469
13.5. A practical case study.....	471
13.6. Final conclusions and recommendations	471
13.7. References.....	472
Appendix: Analytical Solutions	476

Executive Summary

Axisymmetric flow in multilayer aquifer systems:

Solutions and theoretical considerations

Well hydraulics is the discipline that studies the aquifer response to hydraulic perturbations in a well. To simulate the flow toward or away from a well, mathematical models are applied, and a distinction is made between analytical and numerical models. Dupuit was the first who developed analytical solutions for steady radial flow to a well very shortly after Darcy published his fundamental law in 1856. Another milestone was the publication of the analytical solution for transient flow to a well by Theis in 1935. Many other analytical solutions have been developed after this publication, taking into account different hydraulic effects, such as leakage from an overlying aquitard, delayed water table response, partial penetration, and wellbore storage. For decades these solutions have been restricted to one or two layers.

Another breakthrough is the development of analytical solutions for multilayer flow in the 1980s. Hemker was the first to publish a solution method for steady and transient multilayer well-flow, respectively in 1984 and 1985. He expressed the governing system of differential equations in matrix form, and uncoupled these equations by applying eigendecomposition. Using matrix notation, it was possible to generalize the problem of flow to a well in a layered aquifer system, while stating the problem in a very concise manner. The introduction of numerical inversion techniques for the Laplace transform in the 1980s was another important step as it facilitated the development of semi-analytical multilayer solutions that include more realistic features such as partial penetration and wellbore storage.

Meanwhile numerical models were becoming increasingly popular, and starting from the 1960s, both the finite-difference and the finite-element method were applied to solve groundwater flow problems including axisymmetric flow to a pumping well. As these numerical solution methods discretize space and time, they are generally more efficient in solving more advanced problems that deal with aquifer heterogeneity and nonlinear flow behavior. At Ghent University, Lebbe developed a finite-difference model designed specifically for the simulation of axisymmetric flow to a well in a layered aquifer system. The model was called AS2D and its initial version was published in 1983. Later Lebbe modified the solution method by incorporating interpolations in space and time, which he called the hybrid finite-difference finite-element method. Lebbe also coupled AS2D to a nonlinear regression algorithm for deriving hydraulic parameters from pumping test data. The resulting inverse model was called HYPARIDEN, and Lebbe published a book in 1999 in which he presents this numerical model as a generalized interpretation method for single and multiple pumping tests.

This PhD research extends both the work of Hemker and Lebbe by investigating the semi-analytical approach as well as the finite-difference method to solve problems of axisymmetric flow in multilayered aquifer systems. The main objective is to get a better understanding of these problems by examining and comparing existing well-flow solutions, by developing new solutions, by implementing these solutions, and by applying some of these solutions to solve real-world problems. First, existing semi-analytical multilayer solutions are synthetized into a generalized solution that can handle both steady and transient flow in confined and leaky systems subject to areal recharge. The aquifer system may be laterally bounded or unbounded, and the inner model boundary condition can be a specified head or a constant discharge. In case of transient flow, the Laplace transform is applied and the inversion is performed numerically using the Stehfest algorithm. Because of the similarity

between two-dimensional axisymmetric and parallel flow, the developed solution also includes the latter.

The generalized semi-analytical approach is extended by defining multiple cylindrical zones around the pumping well. Wellbore storage can be taken into account, and a uniform head is defined at the face of well-screens extending over more than one layer, while the unscreened parts are impervious. Such a mixed-type boundary condition offers a more realistic way of conceptualizing partially penetrating wells and multi-aquifer wells. As the cylindrical zones are characterized by their own set of parameters and boundary conditions, this extension also allows for the incorporation of lateral heterogeneities. Possible applications are simulating the effect of gravel pack and skin or defining mixed boundary conditions at the top of the aquifer system. A two-zone model can be applied to solve the nonlinear problems of confined-unconfined flow and combined areal infiltration and drainage. The multilayer-multizone solution can also be used to simulate nonlinear unconfined flow by discretizing the radial distance in a similar way the finite-difference method does.

The hybrid numerical method by Lebbe is critically reviewed and it is concluded that the linear interpolations have no added value. The vertical interpolation is even problematic and could be omitted according to the Dupuit-Forchheimer approximation. The temporal interpolation is similar to the Crank-Nicholson method and may cause spurious oscillations at small values of time. Due to these issues, several new versions of the AS2D model were developed, finally resulting in the MAxSym tool written in Matlab. The code implements the backward Euler finite-difference method and it contains new features such as initial drawdowns, inactive and constant-head cells, recharge and drainage boundary conditions, and stress periods. It also allows for radial variation of input parameters. The presented finite-difference approach is basically the same as the formulation used by MODFLOW, and because of the similarity between axisymmetric and parallel flow, it is possible to trick the unmodified version of MODFLOW into simulating axisymmetric flow and to include all the features implemented in the MAxSym code.

The finite-difference approach is also written in Python and extended with the option to connect cells in the grid. A simple algorithm is developed to modify the matrix system of finite-difference equations, which can be solved easily by applying standard LU decomposition. The option to connect cells makes it possible to define multi-node wells, which are used to simulate more accurately the effect of partial penetration or flow to a multi-aquifer well. The newly-developed semi-analytical approach and the finite-difference method are compared and verified against several existing analytical solutions, and it is concluded that both methods are very accurate. The generalized semi-analytical solution simplifies to well-known analytical one- or two-layer solutions, although it is shown that neglecting effects due to well-skin, wellbore storage, delayed yield, and drainage may significantly over- or underestimate the drawdown. This underlines the importance of developing more advanced axisymmetric solutions that allow for defining more realistic boundary conditions.

Leakage from the layers adjacent to the extracted layer is an effect that cannot be ignored either, although it is proven here that this effect is limited in both space and time. The Laplace space solution for multilayer well-flow is expanded for large values of time and inverted analytically, which gives an approximate solution that is similar to the corresponding steady-state solution. This approximate solution shows that flow close to the well is redistributed according to the transmissive properties of the individual layers, while it is redistributed according to the storative properties further away from the well. Eventually, a pseudo-steady state is reached, resulting in time-drawdown curves that conform to the Theis solution of the equivalent comprehensive one-layer system. This confirms the spatial averaging in the measurements of pumping induced drawdown and the inherent limitations of multilevel pumping tests such as the hydraulic tomography.

Axisymmetric models are well-known to groundwater practitioners as they are frequently used to interpret aquifer tests. Additionally, these models are applied to simulate permanent wells, and in combination with the superposition method, they are powerful tools that can avoid building data-hungry and computationally expensive groundwater flow models. Under the assumption of axial symmetry, the governing differential equation is reduced by one dimension, making these superposition models relatively easy to set up and fast to run. As an illustration, a practical case study is presented in which a drainage system consisting of multiple pumping and injection wells is optimized. The drained aquifer comprises three permeable layers separated by semi-pervious layers. At the site, a double pumping test was conducted and interpreted to identify the hydraulic parameters. The effect of the drainage system is simulated by applying superposition to the analytical axisymmetric multilayer steady-state solution, and linear programming is applied to minimize the pumping and injection rates.

Similarly, axisymmetric models are also used to assess the environmental impact of permanent groundwater extractions. Empirical formulas to estimate the radius of influence, such as the Sichardt formula, are widely-used, although these formulas are not consistent with fundamental hydrogeological principles. As a consequence, their use should be discouraged in this context. On the other hand, when properly applied, axisymmetric models may offer valuable insights, and therefore, alternative formulas to calculate the radius of influence are given based on the de Glee and the Theis equations. It is even shown that the contested formula, which estimates the radius of influence by balancing pumping and infiltration rate, can be derived from an asymptotic solution of a model developed by Ernst in 1971 to simulate radial flow to a well in an aquifer subject to combined areal uniform infiltration and drainage.

If the superposition method is applied to evaluate sustainable pumping, one should keep in mind that this principle is valid only if the boundary value problem is expressed by linear equations. Since linear models tend to underestimate the cone of depression, applying them to assess sustainability should be subject to caution. Distinguishing between linear and nonlinear models is also the essence of the debate on the role of recharge in evaluating the sustainability of groundwater development. The controversy originates in the groundwater budget myth, which is the idea that safe pumping must not exceed the initial recharge. To refute this idea of safe yield, a simplified water budget equation is used, which equates the total pumping rate to the sum of capture and storage change. Since initial recharge and discharge are canceled out from this equation, one may conclude that sustainable pumping has nothing to do with recharge.

It is proven that this water budget equation expresses the superposition principle, in which case the calculated cone of depression indeed is independent of the initial conditions including initial recharge. However, like any other model assumption, this is a simplification of reality, as it implicitly assumes the groundwater reservoir can be depleted indefinitely and boundary conditions are an infinite source of water. In reality, capture and storage are limited, and this requires modeling nonlinear responses, in which case the superposition principle is not applicable, and simulating the initial conditions is inevitable. Moreover, the initial conditions determine the limits of the system, and as a consequence, they paradoxically indicate whether the assumption of linearity is valid or not. In some cases, using superposition models is justified indeed, but in other cases, defining nonlinear and time-dependent stresses on the groundwater system is inevitable, making recharge a relevant parameter. And this is why hydrogeologists model.

Nederlandse Samenvatting

Axiaal-symmetrische stroming in gelaagde aquifersystemen: oplossingen en theoretische beschouwingen

Well hydraulics – wat kan vertaald worden als de hydraulica van putten – is de discipline die de grondwaterstroming in een aquifer naar een pompput bestudeert. Men maakt hiervoor gebruik van wiskundige modellen, waarbij men een onderscheid maakt tussen analytische en numerieke modellen. Dupuit was de eerste die enkele analytische oplossingen voor permanente radiale stroming naar een pompput uitwerkte, zeer kort nadat Darcy zijn fundamentele wet publiceerde in 1856. Een andere mijlpaal was de publicatie van Theis in 1935 met de analytische oplossing voor tijdsafhankelijke stroming naar een pompput. Sinds die publicatie werden vele andere analytische oplossingen afgeleid om allerhande hydraulische effecten in rekening te brengen zoals lek vanuit een bovenliggende aquitard, invloed van de watertafel, onvolkomen filters en putberging. Decennialang bleven deze oplossingen echter beperkt tot één of twee lagen.

Een andere doorbraak vond plaats in de jaren 1980 toen analytische oplossingen werden ontwikkeld voor het simuleren van stroming in gelaagde systemen. Hemker was de eerste die een oplossing publiceerde voor permanente en tijdsafhankelijke grondwaterstroming naar een pompput in een aquifersysteem dat uit meerdere lagen bestaat. Hij deed dat respectievelijk in 1984 en 1985. Het probleem wordt wiskundig beschreven door een stelsel differentiaalvergelijkingen dat hij als een matrixstelsel formuleerde, waardoor hij de vergelijkingen kon ontkoppelen door het toepassen van eigenwaardenontbinding. Door matrices te gebruiken kon hij het probleem van grondwaterstroming naar een put eenvoudig veralgemenen naar een in theorie onbeperkt aantal lagen. Een andere belangrijke stap vond ook plaats in de jaren 1980 toen numerieke algoritmes voor het inverteren van de Laplacetransformatie hun intrede deden. Hierdoor werd het mogelijk om semi-analytische oplossingen te ontwikkelen die meer realistische kenmerken in rekening brengen zoals onvolkomen filters en putberging.

Ondertussen werden numerieke modellen alsmaar populairder, en vanaf de jaren 1960 al werden zowel de eindige-differentie- als de eindige-elementenmethode toegepast om grondwaterstromingsproblemen op te lossen, waaronder ook axiaal-symmetrische stroming naar een pompput. In deze methoden worden afstanden en tijd gediscretiseerd, waardoor ze over het algemeen efficiënter zijn in het oplossen van meer complexe problemen die rekening houden met de aquiferheterogeniteit en niet-lineair stromingsgedrag. Aan de Universiteit Gent ontwikkelde Lebbe een eindigverschilmmodel dat speciaal ontworpen was om axiaal-symmetrische stroming naar een pompput in een gelaagd aquifersysteem te simuleren. Het model werd AS2D genoemd, en een eerste versie werd in 1983 gepubliceerd. Later paste Lebbe de oplossingsmethode aan en voegde hij lineaire interpolaties in functie van afstanden en tijd toe, wat hij de hybride eindige-differentie en eindige-elementenmethode noemde. Lebbe koppelde ook het AS2D model aan een algoritme voor niet-lineaire regressie voor het afleiden van hydraulische parameters van pompproefdata. Het resulterende invers model noemde hij HYPARIDEN, en in het boek dat hij in 1999 publiceerde, stelde hij dit numerieke model voor als een veralgemeende interpretatiemethode voor enkel- en meervoudige pompproeven.

Dit doctoraatsonderzoek bouwt verder op het werk van Hemker en Lebbe, met als hoofddoel meer inzicht te krijgen in het probleem van axiaal-symmetrische stroming in gelaagde aquifersystemen. Hierbij worden zowel de semi-analytische oplossingsmethode als de eindigverschilmethode

toegepast. Niet alleen bestaande oplossingen worden bestudeerd, maar ook nieuwe oplossingen worden ontwikkeld en geïmplementeerd, en sommige van die oplossingen worden in de praktijk toegepast. Eerst en vooral wordt een veralgemeende semi-analytische oplossing uitgewerkt die een synthese is van bestaande oplossingen. Deze oplossing kan permanente en tijdsafhankelijke stroming simuleren in afgesloten en half-afgesloten gelaagde aquifersystemen waarbij ook infiltratie in rekening kan worden gebracht. Die aquifersystemen kunnen lateraal begrensd of onbegrensd zijn, en aan de binnenste modelgrens kan een vaste stijghoogte of een constant debiet als randvoorwaarde gedefinieerd worden. Bij tijdsafhankelijke stroming wordt de Laplacetransformatie toegepast die met behulp van het numerieke Stehfest algoritme wordt geïnverteerd. Omwille van de overeenkomst tussen beide is het eenvoudig om de veralgemeende oplossing voor radiale stroming uit te breiden naar parallelle stroming.

De veralgemeende oplossing wordt ook verder uitgebred. Zo wordt de mogelijkheid voorzien om meerdere cilindrische zones rond de pompput te definiëren en ook het effect van de verandering in putberging kan in rekening worden gebracht. Wanneer een putfilter zich over meerdere lagen uitstrekkt, dan wordt een uniforme stijghoogte opgelegd aan de binnenste modelrand die overeenkomt met de putfilterrand. Omdat de modelranden die niet overeenkomen met een putfilter ondoorlatend zijn, spreekt men van een gemengde randvoorwaarde. Hiermee kunnen onvolkomen putten of putten waarvan de filter zich in meerdere aquifers bevindt, op een realistischer manier gemodelleerd worden. Doordat de cilindrische zones hun eigen parameters en randvoorwaarden krijgen toegekend, is het mogelijk om laterale heterogeniteit toe te laten. Op die manier kan het effect van de putomstorting of van verstopping van de put gesimuleerd worden. Een andere toepassing is het definiëren van gemengde randvoorwaarden aan de bovengrens van het aquifersysteem. Het is zelfs mogelijk om niet-lineaire stroming in een freatische toplaat te simuleren door het discretiseren van de radiale afstand zoals dat ook wordt gedaan in eindigverschilmodellen.

De hybride numerieke oplossingsmethode van Lebbe wordt kritisch onder de loep genomen, met als conclusie dat de lineaire interpolaties geen meerwaarde hebben. Het verticaal interpoleren van verlagingen is zelfs problematisch en kan beter weggeleggen worden, wat volledig in overeenstemming is met de Dupuit-Forchheimer benadering. De interpolatie in de tijd is gelijkaardig aan de Crank-Nicholson methode en kan bij kleine simulatietijden leiden tot numerieke instabiliteit in de vorm van oscillaties. Omwille van die problemen werden verschillende nieuwe versies van het AS2D model geïmplementeerd, wat uiteindelijk leidde tot de ontwikkeling van de Matlab tool MAxSym, die een achterwaartse eindige-differentiebenadering met betrekking tot de tijd toepast. De tool bevat ook nieuwe features zoals de mogelijkheid om initiële verlagingen te definiëren, inactieve cellen en cellen met een vaste verlaging, infiltratie en drainage, en stressperiodes. Het is ook mogelijk om parameters te laten variëren in de radiale richting. De toegepaste eindigverschilmethode is in feite dezelfde als de benadering die MODFLOW toepast, en door de overeenkomst tussen axiaal-symmetrische en parallelle stroming, is het zelfs mogelijk om MODFLOW radiale stroming te laten simuleren zonder de code aan te passen. Hierbij kunnen alle features gebruikt worden die ook beschikbaar zijn in de MAxSym tool.

Het eindigverschilmodel werd ook in Python gecodeerd en uitgebred met de optie om cellen te connecteren. Een eenvoudig algoritme werd ontwikkeld om in dat geval het matrixstelsel met eindige-differentievergelijkingen aan te passen, wat makkelijk met standaard LU-decompositie kan worden opgelost. Die extra optie maakt het mogelijk om zogenaamde multi-node wells te definiëren, putten die meerdere knooppunten bevatten. Die kunnen gebruikt worden om het effect van een onvolkomen filter nauwkeuriger te simuleren of stroming naar een putfilter die zich over meerdere aquifers uitstrekkt. De nieuw ontwikkelde semi-analytische oplossingsmethode en het

eindigverschilmmodel worden met elkaar vergeleken en geverifieerd aan de hand van bestaande analytische oplossingen, waaruit men kan besluiten dat beide methodes zeer nauwkeurig zijn. De veralgemeende semi-analytische oplossing kan vereenvoudigd worden tot welgekende analytische oplossingen van modellen die uit slechts één of twee lagen bestaan. Er wordt echter aangetoond dat het verwaarlozen van bepaalde effecten zoals putverstopping, putberging, watertafel en drainage kan leiden tot significante over- of onderschatting van de verlaging. Dit onderstreept het belang van het ontwikkelen van geavanceerde axiaal-symmetrische modellen die toelaten om meer realistische randvoorwaarden te definiëren.

Lek vanuit de lagen die grenzen aan de aangepompte laag is een effect dat evenmin kan verwaarloosd worden, hoewel het hier wordt bewezen dat dit effect beperkt is in tijd en afstand. De exacte oplossing voor axiaal-symmetrische stroming naar een pompput in een gelaagd aquifersysteem wordt opgesteld in de Laplaceruimte, en een benadering voor grote waarden van de tijd kan analytisch worden geïnverteerd tot een oplossing die gelijkaardig is aan de overeenkomstige tijdsafhankelijke oplossing. Deze benaderende oplossing voor late tijden toont aan dat de stroming nabij de put wordt herverdeeld op basis van de doorlaatvermogens van de afzonderlijke lagen, terwijl de stroming verder van de put wordt herverdeeld op basis van de bergingscoëfficiënten. Uiteindelijk komt het systeem in een pseudo-permanente toestand, die zich vertaalt in tijdsverlagingscurven die overeenkomen met de Theis-oplossing voor de equivalente samengestelde aquifer. Dit bevestigt dat verlagingen geobserveerd tijdens pompproeven onderhevig zijn aan een ruimtelijke uitmiddeling, en dat bewijst dat meervoudige pompproeven, zoals de hydraulische tomografie, inherente beperkingen hebben.

Axiaal-symmetrische modellen worden heel vaak toegepast bij het interpreteren van aquifertesten. Daarnaast kunnen deze modellen ook gebruikt worden om permanente winningen te simuleren. In combinatie met de superpositiemethode zijn het zeer efficiënte instrumenten die zelfs het bouwen van complexe grondwatermodellen kunnen voorkomen. De veronderstelling van axiale symmetrie zorgt er immers voor dat de stromingsvergelijking met één dimensie wordt verminderd, waardoor deze superpositiemodellen eenvoudig op te zetten zijn en zeer snel rekenen. Dat wordt geïllustreerd aan de hand van een praktijkvoorbeeld waarin een drainagesysteem wordt geoptimaliseerd dat uit meerdere pomp- en injectieputten bestaat. De aquifer die wordt gedraineerd is opgebouwd uit drie goed doorlatende lagen die door slecht doorlatende lagen van elkaar worden gescheiden. Ter plaatse werd een dubbele pompproef uitgevoerd, en die werd geïnterpreteerd om de relevante hydraulische parameters te identificeren. Het effect van het drainagesysteem wordt gesimuleerd door toepassing van de superpositiemethode, waarbij gebruik wordt gemaakt van de analytische axiaal-symmetrische oplossing voor permanente stroming in een gelaagde aquifer. Voor het optimaliseren van de pomp- en injectiedebieten wordt lineaire programmering toegepast.

Axiaal-symmetrische modellen worden ook toegepast om de impact van permanente grondwaterwinningen op het milieu na te gaan. Vaak gebruikt men empirische formules om de invloedstraal te schatten, zoals de formule van Sichardt, ook al zijn die formules niet in overeenstemming met fundamentele hydrogeologische principes. Om die reden kunnen empirische formules best worden vermeden in de context van milieueffectrapportage. Anderzijds kunnen axiaal-symmetrische modellen wel waardevolle inzichten opleveren, op voorwaarde dat ze correct worden toegepast. Als alternatief worden daarom formules om de invloedstraal te berekenen afgeleid van de vergelijkingen van de Glee en Theis. Er wordt zelfs aangetoond dat de betwiste formule die de invloedstraal berekent door pompdebit en infiltratie in evenwicht te brengen, kan afgeleid worden uit een asymptotische oplossing van een model dat Ernst ontwikkelde in 1971. Dat model simuleert stroming naar een pompput in een aquifer met gebiedsdekkende uniforme infiltratie en drainage.

Wanneer de superpositiemethode wordt toegepast om de duurzaamheid van een grondwaterwinning te evalueren, dan moet men er rekening mee houden dat deze methode enkel geldig is als het probleem wiskundig wordt uitgedrukt aan de hand van lineaire vergelijkingen. Lineaire modellen hebben echter de neiging om de depressietrechter te onderschatten, en dus is er voorzichtigheid geboden. Het onderscheid tussen lineaire en niet-lineaire modellen is ook de essentie van het debat over de rol van voeding bij het evalueren van de duurzaamheid van grondwaterwinningen. Het is een controversie die zijn oorsprong vindt in de grondwaterbalansmythe, het idee dat het onttrekken van grondwater veilig is zolang de initiële voeding niet wordt overschreden. Om dit idee te weerleggen, gebruikt men een vereenvoudigde waterbalansvergelijking die het totale pompdebiet gelijkstelt aan de som van de verandering in voeding, de verandering in afvoer, en de verandering in berging. Omdat de initiële voeding ontbreekt in deze vergelijking, kan men inderdaad tot de conclusie komen dat duurzame grondwaterwinning niets te maken heeft met de voeding.

Er wordt echter aangetoond dat deze vereenvoudigde waterbalansvergelijking het principe van superpositie toepast. In dit geval is de depressietrechter inderdaad onafhankelijk van de initiële condities, en dus ook van de initiële voeding. Maar net als elke andere modelaanname is dit een vereenvoudigde weergave van de werkelijkheid, die hier impliciet veronderstelt dat het grondwaterreservoir onuitputtelijk is, net zoals de randvoorwaarden. In werkelijkheid zijn voeding, afvoer en berging uiteraard beperkt, en dat vereist het modelleren van niet-lineaire verbanden. In dat geval is superpositie niet toegestaan, waardoor het simuleren van de initiële condities onvermijdelijk is. Het is zelfs zo dat die initiële condities de limieten van het systeem bepalen, waardoor ze paradoxaal genoeg bepalen of het systeem al dan niet als lineair kan beschouwd worden. In sommige gevallen is het gebruik van superpositiemodellen zeker en vast verantwoord, maar in andere gevallen is het noodzakelijk om tijdsafhankelijke en niet-lineaire randvoorwaarden te definiëren, waarbij de voeding een relevante parameter is. En dat is nu eenmaal waarom hydrogeologen modelleren.

Preface

In “An interview with C.V. Theis”, Dr. John D. Bredehoeft (2008) mentions how Dr. Charles V. Theis “commented on the difficulty of having your ideas accepted by your colleagues”, which “reminds us of how he struggled to have his transient ideas accepted”. In the interview, Dr. Bredehoeft could “sense Theis’ efforts, and frustration in getting his transient idea accepted by the community”. Undoubtedly, the Theis (1935) solution was a major breakthrough in the field of well hydraulics, yet in my opinion, his contribution is still being undervalued, definitely in Flanders, due to the prevailing conviction that the theoretical model of unsteady-state flow to a pumping well in a confined aquifer is only applicable in a few cases.

Leakage from the layers adjacent to the extracted layer is an effect that cannot be ignored indeed, but as I prove in chapter 9 of this dissertation, the effect is limited in both space and time. It is well-known that leakage is negligibly small at early times, in which case the Theis solution is applicable. Additionally, time-drawdown curves conform to the Theis solution again after a certain time of pumping. As I explain in chapter 9, this is true when the leakage close to the pumping well is maximal and the aquifer system has reached a pseudo-steady state.

Certainly, this insight is not a major breakthrough, and I am not a brilliant scientist like Dr. Charles Theis was. I do, however, feel sympathy with the man, as I know what it is having your ideas not being taken seriously, and for sure, this dissertation stems from my efforts and frustrations in getting some of my work accepted by my colleagues. Therefore, I am very grateful to Prof. Dr. Kristine Walraevens for appreciating those efforts and taking my ideas seriously. This dissertation would never have been written without her continuous support and encouragement. The same holds for Dr. Alexander Vandenbohede, whose help was indispensable in continuing my research. He is a coauthor on all of the papers I have published within the context of this research, for which I am very grateful.

I acknowledge Prof. Dr. Luc Lebbe for giving me the opportunity to start a PhD and for supervising my earliest research activities. He introduced me to the fascinating world of groundwater modeling. I would like to thank Prof. Dr. Mark Bakker, who is a coauthor on two of my publications. Despite the short period of cooperation, he taught me a lot about analytical modeling. I am also grateful to my other coauthors, Dr. Griet Heuvelmans, MSc. Marc Van Camp, and MSc. Dirk Libbrecht. I thank the chairman of the jury, Prof. Dr. Stephen Louwey, and the other members of the jury, Prof. Dr. Thomas Hermans, Prof. Dr. Herman Peiffer, Prof. Dr. Marijke Huysmans, and Prof. Dr. Mark Bakker for taking the time to carefully review this dissertation.

I appreciate Dr. Peter Tanghe’s help in the final stage of completing this work. Last but not least, I am very grateful to my grandparents, Gilberte Lecluse and Cyrille Allemeersch, for having supported me my entire life.

Gent, August 2023



Andy Louwyck

About the Author



Andy Louwyck earned a Bachelor of Science degree in Geology from the Catholic University of Leuven (KU Leuven) in 1999, and a Master of Science degree in Geology with a major in Hydrogeology from Ghent University (UGent) in 2001. In 2002, he started his PhD research at the Laboratory for Applied Geology and Hydrogeology (LTGH) of Ghent University. The project was financed by the Special Research Fund of Ghent University, and the objective was to conduct research on hydraulic parameter identification in the Belgian coastal plain. Andy participated in the studies on the realization of a new drainage system at an archeological site situated in one of the dune areas of the western North Sea coast of Belgium. A summary of these studies was presented at a conference organized by the Flanders Marine Institute (VLIZ) and published in the proceedings. The numerical analysis of a step-drawdown test conducted at the site was published in *Journal of Hydrology*.

The main focus of the PhD research was on the hydraulic tomography. Unfortunately, the interpretation of the field tests did not give satisfying results. After his scholarship ended in 2006, Andy continued his research, primarily focusing on improving the finite-difference model for radial well-flow, which finally resulted in the development of the MAxSym tool and a procedure to trick MODFLOW into simulating axisymmetric flow. Two papers on this subject were published, one in *Computers & Geosciences*, and one in *Hydrogeology Journal*. The finite-difference model and the MODFLOW procedure were also used to study axisymmetric reactive solute transport and heat transport, and Andy coauthored one proceedings paper and three papers in peer-reviewed journals discussing the results of this research.

For two years, Andy was a project engineer in integral water management for the International Marine and Dredging Consultants (IMDC). He did the groundwater modeling for several water management studies, and worked on a data project for the sedimentological laboratory of Flanders Hydraulics (WL). In 2008, Andy started working as a groundwater modeler at the Flemish Environment Agency (VMM), where he participated in several projects on groundwater management. The insights he gained during this work led to the publication of a paper in *Water* about assessing the environmental impact of a groundwater extraction by estimating the radius of influence, and a paper in *Groundwater* on the water budget myth and the role of recharge in evaluating sustainable pumping. He also coauthored one paper published in *Journal of Hydrology* about distinguishing between management-induced and climatic trends in phreatic groundwater levels. From 2012 to 2020, Andy was responsible for the interpretation of slug tests conducted in observation wells belonging to the groundwater monitoring network exploited by the Flemish Environment Agency.

In 2015, Andy earned an associate degree in Software Development, and in 2019, he obtained a micro-degree in Artificial Intelligence and Data Science. In 2020, he took a new challenge and started doing research in artificial intelligence at the Vives University of Applied Sciences. As a lecturer, Andy taught several courses on programming and on artificial intelligence. Nowadays, he still teaches courses on machine learning and deep learning. During his PhD research, he used his programming skills to develop new analytical and numerical solutions for axisymmetric flow in multilayer aquifer systems. The MAxSym tool can be downloaded from <https://github.com/alouwyck/MAxSym>; the Jupyter notebooks accompanying this thesis are available at <https://github.com/alouwyck/PhD>.

About the Cover Illustration

The cover was designed with the help of Alexander Vandenbohede. The figures are taken from the PhD dissertation of Dutch engineer Gerrit Jan de Glee, who defended his thesis at the Technical University of Delft in the Netherlands on Wednesday, April 2, 1930. The title of the dissertation is "*Over grondwaterstroomingen bij wateronttrekkingen door middel van putten*", which translates as "About groundwater flow due to water extractions through wells". It can be downloaded from <http://resolver.tudelft.nl/uuid:c3e13209-4626-41b9-9038-c223d61e35c4>.

In the Netherlands and in Flanders, the de Glee formula refers to the steady-state solution for axisymmetric flow to a pumping well with infinitesimal radius fully penetrating a leaky aquifer. However, this solution had already been developed in 1914 by another Dutch engineer, Johan Kooper, to whom de Glee refers in his dissertation. Kooper (1914) even considered the more general case of a well with finite radius, while de Glee (1930) generalized the solution to a partially penetrating well. De Glee (1930) also defined different boundary conditions at the top of the aquifer: a constant-head boundary, a no-flux boundary, and leakage from an overlying aquitard. In the English literature, American hydrologist Charles E. Jacob was the first to publish the steady-state solution for a well in a leaky aquifer in 1946. The equation also appears in the PhD thesis of Iraqi-born American hydrologist Mahdi S. Hantush (1949).

The figure on the front cover is Fig. 45 on page 134 of de Glee's dissertation, and it is captioned "*Putfilter tusschen twee moeilijk doordringbare lagen*", which translates as "Well-screen between two semi-pervious layers". The text on page 135 explains the figure as follows:

"Een andere complicatie ontstaat, wanneer het putfilter geplaatst is tusschen twee moeilijk doordringbare lagen No. 1 en 2 (fig. 45), waaronder zich nog een goed doorlatend pakket bevindt. De moeilijk doordringbare laag No. 2 zal dan niet als waterkeerende basis kunnen worden opgevat. De spanningsverhanglijn kan in dit geval worden ingesloten tusschen de verhanglijnen van twee eenvoudiger gevallen; bij de eerste situatie wordt de moeilijk doordringbare laag No. 2 als waterkeerende basis opgevat, bij de tweede situatie wordt aan deze laag dezelfde doorlatendheid toegekend als aan de goed watervoerende lagen. In het eerste geval vindt men te grote, in het laatste te kleine waarden voor de potentiaalverlaging. Door vergelijking van de aldus berekende waarden met de spanningsverhanglijn, die uit de waarnemingen wordt gevonden, kan men in verschillende gevallen een inzicht verkrijgen in de meer of mindere waterkeerendheid van de afdekkende laag."

Het verdient aanbeveling, in dat geval tevens een waarnemingsfilter te plaatsen onder de moeilijk doordringbare laag no. 2 op korte afstand van den pompput. Blijkt, dat hierin geen peilverlaging wordt waargenomen, dan kan men voor het primaire veld de moeilijk doordringbare laag no. 2 als ondoordringbare basis opvatten."

This translates into English as: "Another complication arises when the well-screen is placed between two semi-pervious layers, No. 1 and 2 (fig. 45), beneath which lies a permeable layer. The semi-pervious layer No. 2 cannot be considered as an impermeable base in this case. The distance-drawdown curve in this scenario can be enclosed between the curves of two simpler cases: in the first situation, the semi-pervious layer No. 2 is considered an impermeable base, while in the second situation, the same conductivity is assigned to this layer as to the permeable layers. In the first case, overly large values for the drawdown are obtained; in the latter case, the values are too small. By comparing the values calculated in this manner with the observed drawdowns, insights into the permeability of the covering layer can be obtained for different cases.

It is also recommended to place an observation well below the semi-pervious layer No. 2 at a short distance from the pumping well. If no drawdown is observed, then the semi-pervious layer No. 2 may be considered an impermeable base.”

At that time, solutions that consider more than one layer did not exist yet. Only in 1951 did Dutch engineers Huisman and Kemperman develop the steady-state solution for a pumping well in a leaky two-aquifer system bounded by an impervious base. It took more than 50 years until Dutch hydrogeologist Kick Hemker published the solution that generalizes the de Glee formula to multiple layers, in 1984. It is interesting to read how de Glee, who did not yet have access to the two-layer solution, creatively applied the single-layer solutions he had developed to approximate the solution of the two-layer problem.

The illustration on the back cover is part of Fig. 40 on page 117 of de Glee’s dissertation. It demonstrates the principle of superposition and the method of images to simulate steady flow to a well near an infiltrating stream. A similar solution was published by American hydrogeologist Charles V. Theis in 1941, who applied his famous equation developed in 1935 to simulate transient flow to a well near a stream by superimposing the head rise due to an imaginary injection well on the drawdown caused by the actual pumping well.

The de Glee formula and the multilayer solutions developed by Hemker are frequently discussed and applied in this PhD thesis, as is the equation of Theis. The superposition method is a powerful technique that is also exhaustively addressed. Its applicability in the context of sustainable pumping is critically reviewed, and a practical case study is discussed in which this method is applied to the Hemker (1984) solution in order to simulate the effect of a drainage system consisting of multiple pumping and injection wells in a multilayer aquifer system.

Chapter 1. General Introduction

1.1. Research context

Groundwater is an important alternative resource to surface water for agriculture, industry, and domestic use (Yeh & Chang, 2013). In fact, it provides most of the drinking water for billions of people and nearly half of the water used for agricultural irrigation (Jasechko & Perrone, 2021). The development of groundwater is carried out mainly through wells, which permit the withdrawal of water from aquifers. Wells are excavations into the earth not only for developing groundwater, but also for oil, brine, and gas. They are being used in many engineering geology operations (Barrocu et al., 2018). Wells are also indispensable instruments to groundwater practitioners for exploring the subsurface, monitoring groundwater flow and chemistry, collecting groundwater samples, remediating polluted groundwater, and testing the hydraulic properties of aquifers (Sterrett, 2007). There are different types of wells, such as dug wells and driven wells, although most modern wells are drilled. Drilled wells that penetrate unconsolidated material require installation of a well-casing and a well-screen to prevent inflow of sediment and collapse (Barrocu et al., 2018; Waller, 1982).

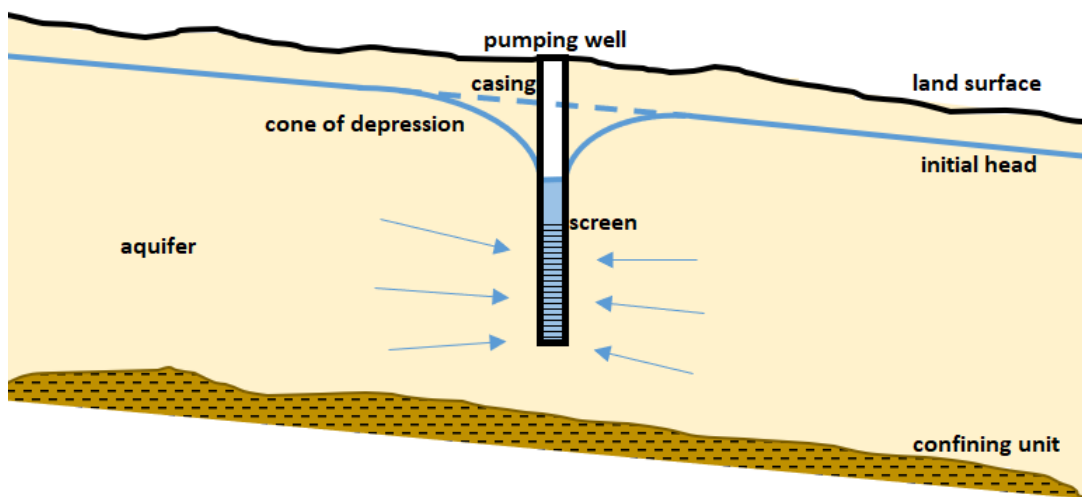


Figure 1. Sketch of a pumping well extracting groundwater from a phreatic aquifer bounded by a confining unit. The well has a casing and a screen through which water flows from the aquifer to the well due to the lowering of the water level in the well. As a consequence, the hydraulic head in the aquifer also lowers, which results in a cone of depression.

When the water level in a well is lowered, for instance by pumping the well, a cone of depression occurs in the aquifer, and groundwater flows from the aquifer into the well (Figure 1). The discipline that specifically studies the aquifer response to hydraulic perturbations in a well is called well hydraulics (Renard, 2005a). Mathematical models are used to simulate flow to a well, and traditionally, a distinction is made between analytical and numerical models (Yeh & Chang, 2013). As groundwater wells have always been extremely important to all societies, it is no surprise that the first analytical solutions were developed very shortly after Darcy (1856) published his fundamental law (Renard, 2005b). In fact, it was Dupuit (1857, 1863) who derived the well-known formulas to calculate the steady drawdown caused by a pumping well, already distinguishing between shallow and deep wells by respectively treating unconfined and confined flow. More than 150 years later, well hydraulics is still a highly relevant field of study, considering that present-day groundwater levels are declining in many aquifers around the globe putting millions of wells at risk of running dry (Jasechko & Perrone, 2021).

Another milestone in well hydraulics is the publication of the well-known equation by Theis (1935) for simulating transient flow to a well fully penetrating a confined aquifer. Many other analytical solutions have been developed rapidly and steadily after this publication, accounting for different hydraulic effects, such as leakage from a bounding semi-pervious aquitard, delayed water table response, partial penetration, wellbore storage, and well-skin. Some of these analytical solutions were used to develop type curves for the interpretation of pumping tests (Yeh & Chang, 2013). Well testing is used to analyze the aquifer response and to quantify the hydraulic properties of the aquifer. Well hydraulics and well testing are intimately related since they respectively solve the direct and the inverse problem (Renard, 2005a). Still it took almost half a century before Thiem (1906) applied for the first time the Dupuit (1857, 1863) equations for well-test interpretation (Renard, 2005b). At present day, pumping tests are the standard method to estimate the transmissivity and storativity of aquifers (Dashti et al., 2022).

Analytical well-flow models are restricted to idealized homogeneous aquifers in which flow occurs under simplifying conditions, whereas real-world well-flow problems often involve heterogeneous aquifers and complicated boundary conditions. Numerical models can deal more effectively with this kind of circumstances, and as a consequence, numerical approaches such as the finite-difference method and the finite-element method, have been used extensively since the mid 1960s (Yeh & Chang, 2013). The introduction of the numerical Laplace inversion in the field of well hydraulics in the 1980s gave rise to the development of a broad range of semi-analytical models that would be tedious to program otherwise using traditional analytical solution methods (Renard, 2005a, 2005b). Also starting from the 1980s, numerical regression algorithms joined the graphical type curve fitting procedures used to analyze pumping tests. These inverse models couple an analytical or numerical model that simulates pumping induced drawdown to an automatic curve fitting method that optimizes the hydraulic parameters and calculates the confidence intervals for the derived parameter values (Renard, 2005b). Nowadays, machine learning methods may be applied to interpret aquifer tests, and although further research in the field is required, these methods are very promising (Dashti et al., 2022).

A major breakthrough in well hydraulics also took place in the 1980s when several researchers developed analytical solutions to simulate flow to a well in an aquifer system consisting of multiple layers. Previously, analytical solutions for well-flow were restricted to one or two layers, despite the fact that an extracted aquifer is often part of a system consisting of multiple aquifers that are also affected by the pumping (Hemker, 2000). The use of the Laplace transform in combination with a numerical inversion algorithm made it even possible to include more realistic well conditions in these multilayer models, such as wellbore storage, the presence of a well-skin, and well-screens that are open to more than one layer (Hemker, 2000). In this way, the semi-analytical multilayer solution method performs equally well as numerical models developed specifically to simulate flow to a well in vertically heterogeneous aquifers. In this work, this is illustrated for several multilayer well-flow problems.

In fact, this study extends both the work of Lebbe (1999), who proposed a generalized interpretation method for single and multiple pumping tests, and the PhD research by Hemker (2000), who developed a semi-analytical solution method for groundwater flow in layered aquifer systems. The generalized interpretation method by Lebbe (1999) is an example of an inverse model that couples a numerical model to simulate axisymmetric flow to a pumping well in a multilayer aquifer system to the Gauss-Newton algorithm for nonlinear regression. An earlier version of this inverse model was developed by Lebbe (1988), and the axisymmetric multilayer model is a modified version of the

finite-difference model developed by Lebbe (1983). The inverse model has been applied in many hydrogeological studies conducted in Flanders during the last 30 years.

The dissertation by Hemker (2000) bundles the different papers he published in developing a semi-analytical model to simulate axisymmetric flow to a multilayer well of finite diameter with zero-thickness skin (Hemker, 1984, 1985a, 1999a, 1999b; Hemker & Maas, 1987). Actually, Hemker (1984, 1985a) was the first in the English literature to present the analytical solution for respectively steady and transient flow to a well in an aquifer system consisting of multiple layers. Hemker and Maas (1987) and Hemker (1999a, 1999b) numerically inverted the Laplace transform using the algorithm of Stehfest (1970), and extended the transient state solution by Hemker (1985a). In particular, Hemker (1999b) included the effect of partial penetration and wellbore storage, and Hemker (1999a) also considered a zero-thickness skin and uniform well-face drawdown if the well-screen is open to more than one layer. The popular MLU code (Hemker & Post, 2019) developed for the interpretation of pumping tests, combines the final semi-analytical solution by Hemker (1999a) with the Levenberg-Marquardt regression algorithm (Hemker, 1985b).

1.2. Research objective

The research presented in this PhD dissertation is within the field of well hydraulics. The main objective is to get a better understanding of axisymmetric groundwater flow to a well in a multilayered aquifer system. This goal is pursued in four ways: (1) studying and comparing existing well-flow solutions, (2) developing new solutions, (3) implementing these solutions, and (4) applying some of these solutions to solve real-world problems of groundwater flow to a well.

First, existing solutions are studied thoroughly and compared to each other. Not only different solution methods are verified against each other, in particular analytical and finite-difference models, also relations between different models are investigated. Most of these solutions are mathematically related as they are the result of solving the same partial differential equation that describes radial flow. The difference only lies in the discretization and the boundary conditions. For instance, the solution by Hantush and Jacob (1955) simulating transient flow to a well in a leaky aquifer approximates the Theis (1935) equation at early times when leakage is negligibly small, and it is asymptotic to the steady state formula of de Glee (1930) at late times when storage change is negligibly small. Many other examples are given in this dissertation, and one of the key findings is that the transient multilayer well-flow solution is asymptotic to the single-layer Theis (1935) solution.

Second, several new multilayer solutions are developed in this study, with the focus on semi-analytical methods, as they provide more insight than numerical approaches do (Haitjema, 2006). Undeniably, the theory of multilayer well-flow is well-established within the field of hydrogeology, and applying integral transforms, it is even possible to solve the problem of transient radial flow to a partially penetrating well in a multi-aquifer system, taking the vertical direction fully into account (Veling & Maas, 2009). Nevertheless, many problems remain unsolved, especially problems that are dealing with heterogeneity or nonlinearity. Concerning the first, the Hemker (1984, 1985a, 1999a, 1999b) solution is extended in this work to include lateral heterogeneity, and a MODFLOW procedure is presented with the same purpose. Unconfined flow and drainage boundary conditions are examples of nonlinearities, which occur, for instance, in water table aquifers. Both are examined here, and applied to multilayer aquifer systems. As axisymmetric models usually apply the superposition method, which is valid only for linear systems, it is investigated if this assumption of linearity is still justified in the context of sustainable pumping.

Third, these studied and newly-developed solutions are implemented in different programming languages, where the primary aim is to verify these solutions, not to optimize the implemented

algorithms. Although it seems obvious to code a solution once the mathematical derivation is found, it is actually not. Numerical approaches, such as the finite-difference method, require implementing the right solvers, which are iterative in most cases. Coding these iterative solvers gives a better insight in the convergence process and the related accuracy of the simulated solutions. For instance, by rewriting the axisymmetric model by Lebbe (1988, 1999), its numerical issues could be explained and solved, and a new procedure to trick MODFLOW (Harbaugh, 2005) into simulating axisymmetric flow was developed. Semi-analytical solutions also rely on numerical methods. Additionally, special mathematical functions need to be evaluated, such as the exponential integral. Implementing these functions usually requires applying some series expansions, which may be truncated for small or large values of distance or time. The best-known example within the field of well hydraulics is the Cooper and Jacob (1946) approximation of the Theis (1935) solution. The modified Bessel functions constituting the multilayer solution may be approximated in a similar way, also revealing interesting relations between different well-flow solutions.

Fourth, well hydraulics needs to be studied in the field. This implies the validation of multilayer well-flow solutions by means of real data obtained through practical applications. Aquifer tests are the most frequently applied field experiments that are usually analyzed by fitting an axisymmetric model to observations. In order to fit field data more accurately, well-test interpretations have stimulated the development of more realistic models. As discussed in previous section 1.1, two major breakthroughs were the transition from steady-state to transient-state models, and the extension from one-layer to two-layer solutions, and eventually, to multilayer solutions. Boundary conditions defining the well also became more realistic, evolving from fully penetrating wells with infinitesimal radius to partially penetrating finite-diameter wells with finite-thickness skin. Similarly, a more realistic conceptualization of the aquifer system required more complicated boundary conditions, such as defining a moving water table or including the effect of drainage.

Following these four approaches in pursuing a better understanding of multilayer flow, the dissertation can be divided into four major parts:

1. Chapters 2 to 4 synthesize and compare the semi-analytical and finite-difference methods originating from the work of Hemker (1984, 1985a, 1999b) and Lebbe (1983, 1988, 1999). It is also shown how the multilayer solution under certain conditions simplifies to well-known solutions for one or two layers.
2. Chapters 5 to 8 extend these solution methods to solve more complicated problems such as multilayer-multizone flow, multilayer wells, conversion from confined to unconfined conditions, flow in multilayer systems with draining upper boundary, and nonlinear unconfined flow.
3. Chapters 9 to 11 discuss some theoretical considerations. It is clarified how transient multilayer well-flow must be understood, some reflections are given on using the radius of influence to assess the environmental impact of an extraction, and it is explained why distinguishing between linear and nonlinear models in simulating the cone of depression of a groundwater development is important;
4. Finally, chapter 12 presents the practical case of optimizing a drainage system consisting of pumping and deep-infiltration wells that operates in a multilayer aquifer system.

In reality, these four points were not performed sequentially as presented here. Research usually is an iterative process, and several topics can be studied easily in parallel. Therefore, the next section discusses the different steps that were conducted in this PhD research, and more importantly, why these steps were taken. In fact, it is a chronological overview of the research on axisymmetric multilayer flow I carried out or participated in during the last 2 decades. The subsequent section

gives a detailed outline of this dissertation, and briefly discusses how the different chapters are interrelated. In other words, it explains the logical coherence of the research. Finally, there is a section summarizing the relevant publications and a section briefly discussing the developed software.

1.3. Research overview

The research spans a period of two decades, and it can be divided into four phases, each characterized by a main topic of research. From 2002 to 2006, I officially worked as a PhD student at Ghent University. Focus of the research was on hydraulic parameter identification in the Belgian coastal plain, and in particular, on the interpretation of hydraulic tomography (Yeh & Liu, 2000) to characterize the vertical heterogeneity of an aquifer. I also participated in the studies that were carried out to realize a new drainage system at the archeological site ‘Duinenabdij’ (Lebbe et al., 2002; Louwyck et al., 2005). After my scholarship ended, I continued my research, and primarily focused on improving Lebbe’s (1988, 1999) finite-difference model for axisymmetric flow, which finally resulted in the development of the MAxSym code (Louwyck, 2011).

In 2008, I started working as a groundwater modeler at the Flemish Environment Agency, where I participated in several projects on groundwater management. I also developed a tool that applied the MAxSym model (Louwyck, 2011) to assess the environmental impact of groundwater extractions. In 2020, I took a new challenge and started doing research in artificial intelligence at the Vives University of Applied Sciences. In this period, I switched from Matlab to Python, which made it possible to develop new semi-analytical solutions for multilayer well-flow more rapidly.

Although this dissertation synthesizes all of my research on multilayer flow from the last 2 decades, most topics were implemented during these last 3 years. Next sections discuss each phase in more detail.

1.3.1. Hydraulic parameter identification in the Belgian coastal plain

After graduating as Master in Geology, I started my PhD research at the Laboratory for Applied Geology and Hydrogeology (abbreviated as LTGH) of Ghent university in 2002. The project was financed by the Special Research Fund of Ghent University, and the objective was to conduct research on hydraulic parameter identification in the Belgian coastal plain. Inspired by a paper published by Yeh and Liu (2000), it was decided to study the hydraulic tomography, a sequential aquifer test used to characterize aquifer heterogeneity, that was proposed independently by several researchers (Bohling, 1993; Gottlieb & Dietrich, 1995; Neuman, 1987; Tosaka et al., 1993). The Quaternary deposits in the Belgian coastal plain, which are very heterogeneous by nature (Baeteman, 1999), are excellent sediments to examine the feasibility of this new aquifer test. Instead of applying an iterative geostatistical inverse method as proposed by Yeh and Liu (2000), the inverse model HYPARIDEN developed by Lebbe (1999) was used.

The model by Lebbe (1999) is deterministic and can only deal with layered heterogeneity. Therefore, the idea was to divide the tested aquifer into sublayers and to conduct a short-term pumping test in each sublayer while observing the drawdown at different levels in the aquifer (Figure 2). The simultaneous interpretation of these pumping tests would give an idea of the aquifer’s vertical heterogeneity. The first theoretical experiments were promising, so it was decided to test the procedure in the field. Two probes were constructed, one for pumping and one for measuring. In these probes, pump and pressure sensors were isolated by means of inflatable packers. Two hydraulic tomography tests were conducted in a sandy aquifer in the western coastal plain of Belgium. The tests were successful and the observed drawdowns looked fine. However, the

observations did not reflect the expected vertical heterogeneity, as the time-drawdown curves for each test coincided, although they represented different levels. Bohling et al. (2007) encountered the same problem: “One major challenge to effective implementation of hydraulic tomography is our limited ability to induce measurable vertical differences in pressure over significant distances, especially in high-permeability media.”

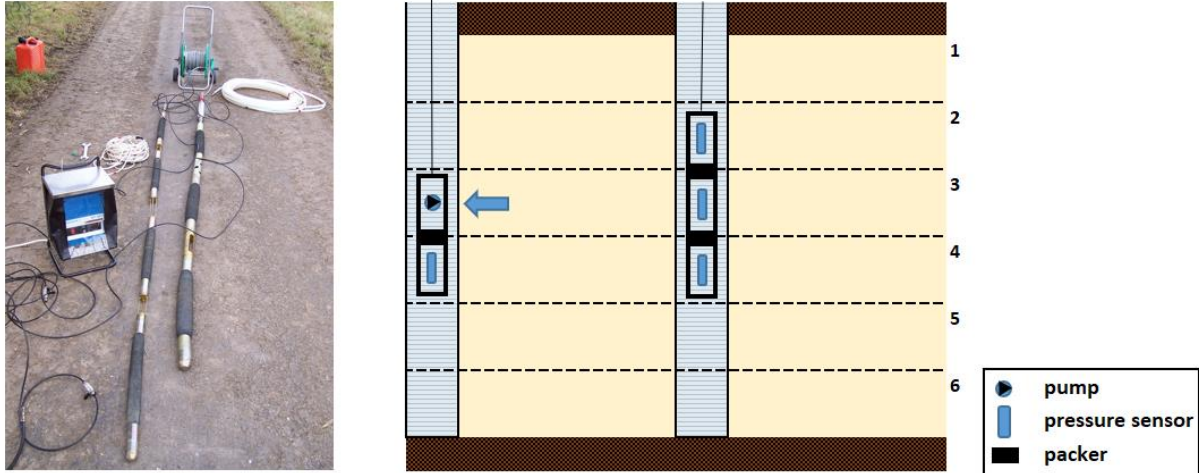


Figure 2. Left: Picture of the probes used for the two hydraulic tomography tests that were performed in sandy sediments in the western coastal plain of Belgium. The probe on the right is used for pumping, the probe on the left for measuring. In these probes, pump and pressure sensors are isolated by means of black inflatable packers. Right: Setup of the hydraulic tomography. The aquifer is divided into a number of sublayers; in this example, there are 6 sublayers. A small-scale pumping test is conducted on each sublayer. The plot shows the pumping test that extracts from layer 3. In the pumping well, the pumping probe extracts water from the aquifer and a pressure sensor measures drawdown in the layer underneath. An observation well is used to measure drawdown in the pumped layer and the adjacent layers using the measuring probe.

A possible explanation was the occurrence of a hydraulic short circuit (Chapuis & Chenaf, 1998) along the unsealed gravel pack surrounding the monitoring well. Therefore, a new test was conducted, and this time, drawdown was measured in a monitoring well without gravel pack in order to prevent hydraulic short circuiting. Unfortunately, the time-drawdown curves still coincided, and it was decided to stop the experiments in the field, and to further investigate the problem of interpreting the hydraulic tomography theoretically. To facilitate the simulation of these sequential pumping tests, I wrote a Matlab wrapper for the HYPARIDEN executables, which are basically compiled FORTRAN code. Matlab offers a more interactive environment for simulation and data visualization, and a large number of synthetic tests could be simulated and analyzed in this way.

Two important conclusions could be drawn from these numerical tests: (1) the axisymmetric model AS2D (Lebbe, 1988, 1999) implemented in HYPARIDEN was not accurate in some cases, and (2) vertical flow between layers becomes negligibly small at a certain distance from the pumping well, which could explain why the observed time-drawdown curves coincided, even in the absence of a hydraulic short circuit. Chapter 4 elaborates on the first conclusion, which also resulted into the development of OGMA-RF (Louwyck et al., 2007) and MAXSYM (Louwyck, 2011). The development of software to simulate multilayer well-flow is discussed in the next section 1.3.2. Concerning the second conclusion, it was already proven analytically for steady-state flow that there is virtually no vertical flow far from a pumping well extracting a multi-aquifer system (Bakker & Strack, 2003). Proving that this is also true for transient flow is, however, mathematically more challenging.

Hunt and Scott (2007) showed that the approximate solution for large values of time for transient axisymmetric well-flow in a two-layer system is asymptotic to the Theis (1935) solution for the comprehensive system. Eventually, I succeeded in generalizing this approximate solution to multiple

layers applying Hemker's (1985a, 1999b) solution method. The mathematical proof is given in Chapter 9. The approximate solution for large values of time can be summarized as follows:

$$s(r, t) \sim s_{\text{steady}}(r) - s_{\text{thiem}}(r) + s_{\text{theis}}(r, t) \quad (t \rightarrow \infty) \quad (1)$$

where $s(r, t)$ is the transient drawdown [L] for large values of time t [T] at distance r [L] from the well, $s_{\text{steady}}(r)$ is the drawdown [L] according to the corresponding steady-state multilayer model, and $s_{\text{thiem}}(r)$ and $s_{\text{theis}}(r, t)$ are the drawdown [L] in the equivalent one-layer system according to the Thiem (1870; 1906) and Theis (1935) equations, respectively. The equivalent one-layer system is determined by simply taking the sum of all pumping rates and all layer transmissivities, and in case of the Theis (1935) model, the sum of all layer storativities.

Interesting is that the term $s_{\text{steady}}(r) - s_{\text{thiem}}(r)$ in (1) is negligibly small if distance r is larger than a finite distance R_m [L] determined by the largest leakage factor of the aquifer system (Bakker & Strack, 2003). In other words, the multilayer aquifer system behaves as a homogeneous layer beyond distance R_m at large values of time. Expression (1) indicates these large values of time by $t \rightarrow \infty$, but actually, the approximate solution is valid for finite values of time. Consequently, the theory summarized by expression (1) supports the steady-shape analysis of tomographic pumping tests proposed by Bohling et al. (2002, 2007), and it also confirms the inherent limitations of the hydraulic tomography, as discussed by Bohling (2009) and Bohling and Butler (2010). In Chapter 9, it is shown that there is only a small window of opportunity indeed in both space and time to observe the vertical heterogeneity in measured drawdowns. This slightly contradicts other researchers who are very enthusiastic about this kind of sequential pumping tests, substantiating their optimism by probabilistic reasoning (Yeh et al., 2014).

During this 4 year period of research at Ghent university, I also participated in the hydrogeological studies that were carried out to realize a more effective drainage system at the archeological site 'Duinenabdij' situated in the dunes of Koksijde on the western North Sea coast of Belgium. The aquifer system consists of three permeable layers separated by two semi-pervious layers, where the upper semi-pervious layer caused problems of flooding at the site. The new drainage system is a combination of pumping wells enclosing the site and extracting groundwater from the middle permeable layer, and injection wells deep-infiltrating the extracted water back into the aquifer system to protect the surrounding dunes. In my MSc thesis (Louwyck, 2001), the effectiveness of this system of combined pumping and injection was investigated first through mathematical modeling. A double pumping test was executed at the site and interpreted to identify the hydraulic properties of the different layers in the aquifer system (Lebbe et al., 2002; Lust, 2002). An overview of these hydrogeological studies was presented at the international conference on nature restoration practices in European coastal habitats organized by the Flanders Marine Institute (abbreviated as VLIZ). Chapter 12 presents the proceedings paper by Louwyck et al. (2005) and revisits the optimization of the drainage system using linear programming.

A step-drawdown test was also conducted at the 'Duinenabdij' site, and just like the double pumping test, this test was interpreted using HYPARIDEN (Lebbe, 1999). The paper by Louwyck et al. (2010) discusses the interpretation of this and two other step-drawdown tests. In general, step-drawdown tests are used to evaluate well-performance (Kruseman & de Ridder, 1990). This is accomplished by extracting groundwater from a single well in a number of consecutive time-intervals during which the pumping rate is constant but increases steadily with the number of time-intervals (Driscoll, 1986). Analyzing the drawdown measured in the pumping well during a step-drawdown test enables to distinguish between aquifer losses and well-losses, the latter consisting of linear and nonlinear head losses (Kruseman & de Ridder, 1990). Linear well-loss is usually attributed to the presence of a gravel

pack and/or a well-skin around the pumping well (Houben, 2015). Traditionally, the skin effect is simulated using a dimensionless skin factor which assumes the skin has an infinitesimal thickness (Kruseman & de Ridder, 1990). However, Louwyck et al. (2010) only consider nonlinear well-loss and even derive negative values for the well-loss coefficient, while Louwyck et al. (2014) discuss the simulation of the effect of a finite-thickness skin for a well in a multi-layer system. In Chapter 5, the analyses by Louwyck et al. (2010, 2014) are revisited, and it is theoretically explained why a negative well-loss coefficient is obtained if the pumping well is effectively developed.

1.3.2. Improving the finite-difference model for axisymmetric flow

HYPARIDEN (Lebbe, 1999) is written in the FORTRAN programming language and compiled to Windows executables that run from the MS-DOS command prompt. These executables read input from text files, and write output to text files. So, it is similar in use as MODFLOW (Harbaugh, 2005; Harbaugh et al., 2000; Harbaugh & McDonald, 1996a; McDonald & Harbaugh, 1984, 1988). Just like FloPy enables development of MODFLOW models using Python scripting (Bakker et al., 2016), I wrote a Matlab wrapper that automated the reading and writing of HYPARIDEN text files and that invoked the Windows executables from the Matlab prompt. In this way, a large number of models could be simulated and batch-processed. As already mentioned in previous section 1.3.1, it turned out the AS2D model (Lebbe, 1988, 1999) used for the simulation of axisymmetric multilayer flow was not accurate in some cases.

It was discovered the exchange of water between layers is not simulated correctly, which could be checked easily by verifying the volumetric balances for the different layers in the AS2D model.

Initially, the model applied the finite-difference method to solve the governing differential equation (Lebbe, 1983). Later, Lebbe (1988) tried to enhance the convergence rate by interpolating the simulated drawdowns in both time and space. As inspiration for these interpolations was found in the finite-element method, this new approach was called the hybrid finite-difference finite-element method (Lebbe & de Breuck, 1995). Lebbe (1988) himself already encountered a problem caused by the vertical interpolation as he observed head rises in layers adjacent to the extracted layer. He called this issue “a numerical Noordbergum effect”, and to attenuate it, Lebbe (1988, 1999) introduced empirically derived correction factors.

As will be explained in Chapter 4, the temporal interpolation applied by Lebbe (1988) is similar to the Crank-Nicholson finite-difference scheme, which may cause spurious oscillations (LeVeque, 2007). Lebbe (1988, 1999) does not mention these oscillations explicitly, but reports inaccurate results at small values of time. Lebbe (1988, 1999) further ‘tweaked’ the AS2D model and abandoned the usual criteria of convergence as he discovered “after a certain experience with the iteration process” that the required number of iterations for simulation time t in minutes is equal to $(t + 5)/5$. The number of iterations indeed increases with the time step (Wang & Anderson, 1982), but it also rises nonlinearly with the size of the domain (Mehl & Hill, 2001). This implies the linear relation between convergence rate and simulation time proposed by Lebbe (1988) is not valid if the model comprises a large number of layers, which again results in inaccurate calculations as the iterative process is aborted too soon. These and other issues are discussed exhaustively in Chapter 4, which presents a critical review of the hybrid finite-difference finite-element method and verifies it against the finite-difference approach (Lebbe, 1983; Louwyck et al., 2012) and the semi-analytical solution (Hemker, 1985a, 1999b).

Although the AS2D model was verified and validated for simulating large-scale pumping tests (Lebbe, 1988, 1999; Lebbe & de Breuck, 1995), it clearly was less suited for modeling small-scale pumping tests such as the hydraulic tomography, since the calculated drawdowns close to the well at small

values of time are unreliable. Therefore, I rewrote the axisymmetric model from scratch applying the finite-difference method as it is implemented in MODFLOW (Harbaugh et al., 2000; Harbaugh & McDonald, 1996b; McDonald & Harbaugh, 1984, 1988). Actually, the new model had the option to choose between a ‘pure’ finite-difference approach and the hybrid method by Lebbe (1988, 1999). To prevent quitting the iterative process too early, it used a maximum relative head difference and a maximum number of iterations specified by the user as stop criteria. The code was still written in FORTRAN, but it was compiled to a mex-file, which is a Matlab executable that can be run from the Matlab prompt just like standard m-files. This avoided the use of text files for model input and output.

A conceptual improvement to the model was the possibility to define hydraulic parameters for each grid node. Unlike the AS2D model that assumes homogeneous layers (Lebbe, 1988, 1999), this new feature allowed for lateral variations in hydraulic parameters, which makes it possible to include wellbore storage and a finite-thickness skin (Louwyck et al., 2012, 2014). The new model was combined with the Levenberg-Marquardt regression algorithm for the purpose of parameter identification. The collinear diagnostic tools proposed by Lebbe (1999) to determine whether the inverse model is well-posed or not, were adopted and rewritten in Matlab. The model was also coupled to a particle tracking algorithm for the simulation of flow paths, capture zones, and advective transport. A user-friendly graphical interface was developed, and the resulting Matlab tool was called OGMA-RF, which stands for Optimized and Generalized Model for Analyzing Radial Flow (Louwyck et al., 2007). It was used to interpret the step-drawdown tests discussed by Louwyck et al. (2010). The tool also contained a module ReacTrans developed by Dr. Alexander Vandenbohede to simulate axisymmetric reactive solute transport, for instance during push-pull tests (Vandenbohede et al., 2008a). ReacTrans can also be used to simulate axisymmetric heat transport, as the governing partial differential equation is similar to the one describing solute transport (Vandenbohede et al., 2008b, 2009).

The core of the OGMA-RF tool was the new version of the axisymmetric model, which certainly was an improvement over the AS2D model, but still inherited some of its flaws. For instance, it was only capable of simulating transient flow to a constant-discharge well, and it did not support constant heads or inactive cells. Another weakness was the iterative ADI solver, which was found to be inefficient in case of more complex models. At that time, Matlab no longer supported the Lahey compiler we used to compile the Fortran code. So I decided again to start from scratch, and developed MAxSym, a Matlab tool for simulating two-dimensional axisymmetric groundwater flow (Louwyck, 2011). Because Matlab provided a standard C compiler, the ADI solver was rewritten in C, and additionally, the more efficient SIP method (Stone, 1968) was implemented, which is also a standard solver for MODFLOW (Harbaugh, 2005; Harbaugh et al., 2000; Harbaugh & McDonald, 1996a, 1996b; McDonald & Harbaugh, 1984, 1988).

The MAxSym tool has an object oriented design and it contains features such as initial drawdowns, inactive and constant-head cells, recharge, and stress periods. Steady as well as transient flow can be simulated, and its use is therefore not limited to the simulation of constant-discharge pumping tests. The MAxSym code can be downloaded online¹, along with an exhaustive documentation (Louwyck, 2011). The applied finite-difference approach is published by Louwyck et al. (2012). The code was extensively tested and verified against numerous analytical solutions (Louwyck, 2011), and compared to the semi-analytical TTIm solver (Louwyck et al., 2012, 2014). TTIm (Bakker, 2013a, 2013b) is available as Python package² and solves the problem of multilayer flow to a well in the same way as

¹ <https://github.com/alouwyck/MAxSym>

² <https://pypi.org/project/ttim>

Hemker (1999a, 1999b) does, except for the numerical inversion of the Laplace transform, which is performed using the algorithm of de Hoog et al. (1982) instead of the Stehfest (1970) algorithm.

Both axisymmetric and parallel flow are simulated using two-dimensional vertical profile models. Because of this similarity, it is possible to simulate axisymmetric flow using a finite-difference model with rectilinear grid geometry (Anderson & Woessner, 1992). In particular, the unmodified versions of MODFLOW (Harbaugh, 2005), MT3DMS (Zheng & Wang, 1999), and SEAWAT (Langevin et al., 2007) can be used to model accurately both axisymmetric flow and solute transport by means of a simple correction of the input parameters (Langevin, 2008). Based on the finite-difference approach implemented in the MAxSym code, a MODFLOW procedure was developed as straightforward as the method of Langevin (2008), yet more flexible in defining radial variations in input parameters, making it possible, for instance, to include the effect of a finite-thickness skin (Louwyck et al., 2012, 2014). Chapter 3 discusses both the finite-difference method and the corresponding MODFLOW procedure that are published by Louwyck et al. (2012, 2014). Vandenbohede et al. (2014) apply the method by Langevin (2008) to simulate axisymmetric heat transport using SEAWAT and compare the traditional WEL package (Harbaugh, 2005) with the MNW package (Konikow et al., 2009). MNW stands for multi-node well, which is a multilayer well that is open to more than one layer. Simulating flow to multilayer wells is the subject of Chapter 6.

1.3.3. Assessing the environmental impact of groundwater extractions

In 2008, I started as a groundwater modeler at the Flemish Environment Agency (abbreviated as VMM), where I was part of the team developing the Flemish Groundwater Model (abbreviated as VGM). As opposed to what its name suggests, VGM is not a single model, rather a collection of datasets, groundwater models, and tools used to support groundwater related decision making (Lermytte & Thomas, 2008). VMM officially coordinates the integrated water policy in Flanders, and in that capacity, it is legally responsible for managing Flanders' groundwater reserves. One of the legal tasks assigned to VMM is to advise local authorities on the approval of environmental permits and environmental impact assessments. For almost one decade, VMM used – as part of VGM – the AS2D model developed by Lebbe (1988, 1999) to estimate the radius of influence of permanent groundwater extractions (Lebbe & Vandenbohede, 2004). In 2012, the AS2D model was replaced by MAxSym (Louwyck, 2011), and I developed a nice graphical user interface so that colleagues without modeling and programming background could easily setup an axisymmetric multilayer model to simulate the cone of depression for a groundwater extraction that required an environmental permit (Figure 3).

The MAxSym tool was used internally at VMM, although the aim was to release it to the public. In particular, the tool would have been very useful to environmental impact assessment experts within the groundwater discipline, considering the guidelines at that time recommended the use of the Sichardt formula to estimate the radius of influence of an extraction (Willems et al., 2009). The Sichardt formula (Kyrieleis & Sichardt, 1930) is an empirical formula derived by German engineers in the early 20th century to estimate the radius of influence, which is needed to apply the steady-state equations by Dupuit (1857, 1863) and by Thiem (1870; 1906). At that time, the Theis (1935) solution was not known yet, and the concept of aquifer storage was not fully understood. Nowadays, the Sichardt formula is still being used by geotechnical engineers to estimate the initial pumping rate of a dewatering well, as it yields a safe and conservative estimate of the required pumping rate in most cases (Peiffer, personal communication, March 7, 2023). Chapter 10, which is an extended version of the paper by Louwyck et al. (2022), elaborates on this issue, and proposes alternative formulas derived from well-known analytical solutions, such as the Theis (1935) and the de Glee (1930) equations.

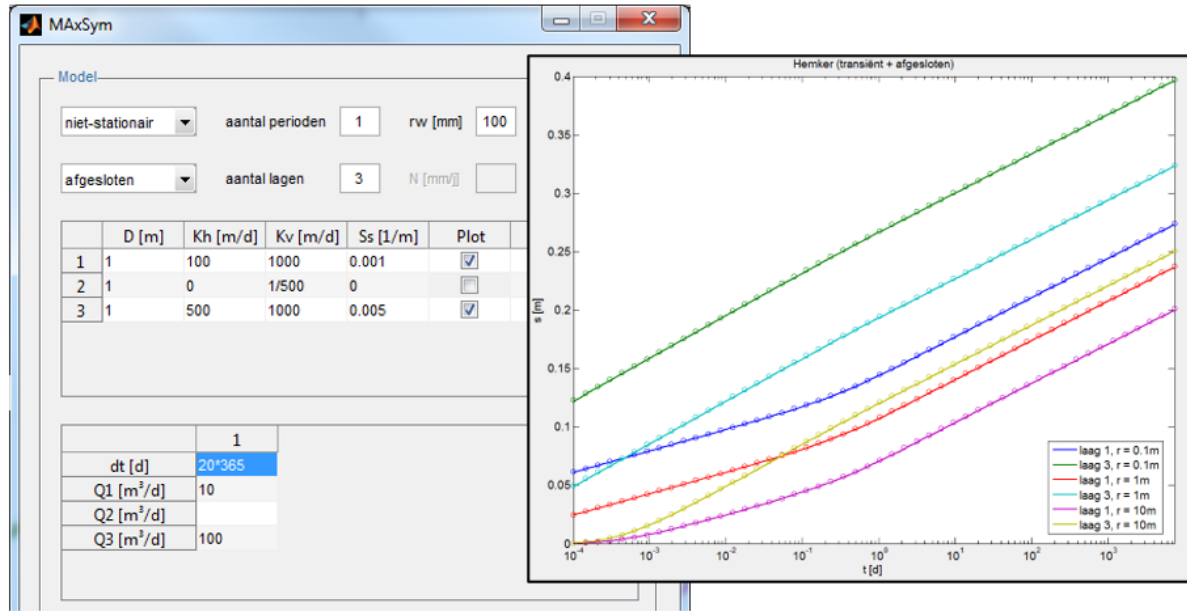


Figure 3. Screenshot of the MAxSym tool used at the Flemish Environment Agency. The tool simulates transient flow to a well in a three-layer system. The plot shows the time-drawdown curves for different layers at different distances from the well. Drawdown is simulated by the tool (solid lines) and verified against the corresponding Hemker (1985a) solution (circles).

Compared to these alternative equations, it is seen that the Sichardt formula tends to underestimate the radius of influence. This conclusion confirms it may be justified indeed to apply the Sichardt formula in case of a dewatering well, while it is problematic in the context of an environmental impact assessment. This can be explained easily considering the Thiem (1870; 1906) equation:

$$s(r) = \frac{Q}{2\pi T} \ln\left(\frac{R}{r}\right) \quad (2)$$

with s the drawdown [L] at distance r [L] from a well pumping a homogeneous aquifer with transmissivity T [L^2/T] at constant rate Q [L^3/T]. Distance R [L] is the distance of the outer model boundary at which drawdown is zero; hence, R is the radius of influence by definition. If R is estimated too small, then it is clear from expression (2) that the cone of depression described by function $s(r)$ is underestimated. In the context of assessing the environmental impact of the extraction, it would be safer to overestimate R , and therefore, the use of the Sichardt formula should be discouraged (Louwyck et al., 2022). To get an overestimation of pumping rate Q , equation (2) shows that this is achieved by underestimating distance R , which may explain its effectiveness in dimensioning dewatering wells. In both cases, it is assumed aquifer transmissivity T is known. In analyzing pumping tests, pumping rate Q is known, and transmissivity T is derived from observed drawdowns s .

When discussing the use of the Sichardt formula, it is important to keep in mind that groundwater models serve different purposes throughout different fields of study (Peiffer, personal communication, March 7, 2023). According to Sun (1999), deriving discharges for dimensioning a dewatering well is a type 2 inverse problem, whereas simulating the cone of depression, which is required to assess the environmental impact of an extraction, is a forward problem. Type 1 inverse problems are solved to derive hydraulic aquifer parameters, for instance, by fitting drawdown observations from a pumping test. Solving these different kinds of groundwater problems is illustrated in Chapter 12 revisiting the realization of the drainage system at the archeological site 'Duinenabdij' (Louwyck et al., 2005). In this study, the inverse problems are the interpretation of a

double pumping test and the optimization of the pumping and injection rates for the drainage system, which both require a forward model coupled to an optimization algorithm. In general, solving these inverse problems is mathematically more challenging than calculating the cone of depression for a given set of parameters and boundary conditions.

As argued by Louwyck et al. (2022), assessing the sustainability of a groundwater development by merely estimating the radius of influence is insufficient as sustainability includes other factors such as water quality, ecology, and socioeconomic considerations (Devlin & Sophocleous, 2005). On the other hand, most groundwater studies are subject to very strict time and budget constraints, in which case the use of axisymmetric models could be an acceptable and inexpensive alternative. Moreover, these models offer valuable insights and may help to decide whether to build a complex numerical model or not (Louwyck et al., 2022). In that sense, the MAxSym tool would have been an improvement to the environmental impact assessment guidelines recommending the use of the Sichardt formula (Willems et al., 2009), as it simulates the hydraulic effect of an extraction in all layers of the aquifer system. Similar to the Theis (1935) and de Glee (1930) solutions, the radius of influence is determined, respectively, by the diffusivities or the leakage factors of the layers, which is in agreement with the multilayer well-flow theory (Bakker & Strack, 2003; Hemker, 1985a). Alternatively, recharge could be included in the MAxSym model, in which case the radius of influence is derived by balancing the pumping and infiltration rate. There was, however, no consensus about this option among the groundwater modeling experts at VMM, and as a consequence, the MAxSym tool has never been released to the public.

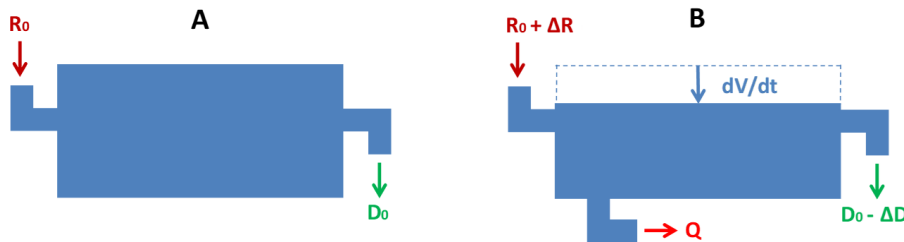


Figure 4. Visualization of the total water budget equation for an aquifer system that initially is in a state of dynamic equilibrium if the total recharge R_0 equals the total discharge D_0 (left plot A). If the system is extracted, then the total pumping rate Q is equal to the sum of total storage change dV/dt , total increase in recharge ΔR , and total decrease in discharge ΔD . The sum of ΔR and ΔD is called the capture (right plot B).

But why is considering recharge an issue when evaluating sustainable pumping? The discussion goes back to an editorial written by Bredehoeft (1997) for the Ground Water journal in which he claimed that sustainable groundwater development has almost nothing to do with recharge. Bredehoeft (1997) referred to the water budget myth, a term introduced by Bredehoeft et al. (1982) to reject the concept of safe yield, which limits groundwater pumping to the natural recharge. The invalidity of the safe yield approach can be proven using the famous water budget equation (Lohman, 1972) that is part of almost every paper discussing the water budget myth (Figure 4):

$$Q = \Delta R + \Delta D + \frac{dV}{dt} \quad (3)$$

where Q is the constant total pumping rate [L^3/T] of the extractions; ΔR and ΔD are the total change in recharge [L^3/T] and discharge [L^3/T], respectively; V is the total volume [L^3] of water in the groundwater reservoir; t is the time [T]; dV/dt is the total storage change. Equation (3) does not contain the initial recharge R_0 and the initial discharge D_0 at time $t = 0$. As it is assumed the aquifer system initially is in a steady state, which implies $R_0 = D_0$, these quantities are canceled out. Equation (3) indeed proves the concept of safe yield, which states that $Q < R_0$, is fallacious.

Additionally, Bredehoeft (1997) concludes initial recharge such as infiltration due to rainfall, is not relevant in estimating the cone of depression, as R_0 is missing from (3).

Equation (3) only accounts for the changes the aquifer system undergoes due to the extraction. Actually, it expresses the total volumetric balance for models that simulate drawdown due to pumping, such as the model of Theis (1935). These models do not consider recharge as they apply the principle of superposition. Bredehoeft (2002, 2007) clarifies that this traditional method of analysis applies to many aquifers since they can be analyzed mathematically as if they are linear systems. In Chapter 11, which is an extended version of the paper by Louwyck et al. (2023), it is proven that equation (3) is valid only if the model is linear. However, if the model is nonlinear, then the initial conditions cannot be ignored, and the initial recharge R_0 is relevant. This is illustrated by analyzing the model of Ernst (1971), which simulates radial flow to a pumping well extracting from a homogeneous aquifer that is recharged and drained.

In essence, the Ernst (1971) model is the same as the de Glee (1930) model, except that the leaky boundary condition is restricted to remove water from the aquifer. As this boundary condition is not allowed to recharge, it becomes inactive at distances where the head drops below the drainage level. This is a nonlinear boundary condition similar to a MODFLOW drain (Harbaugh, 2005). Because of this nonlinearity, the initial conditions cannot be ignored, and neither can the infiltration flux. Louwyck et al. (2022, 2023) even show that the asymptotic solution for zero drainage resistance yields the contested formula that determines the radius of influence R [L] by balancing pumping rate Q [L^3/T] and infiltration rate N [L/T]:

$$R = \sqrt{\frac{Q}{\pi N}} \quad (4)$$

Equation (4) is the well-known formula to calculate the radius of the capture zone of a single well in a homogeneous aquifer that is being recharged (Haitjema, 1995). In general, capture zone and cone of depression do not coincide, as illustrated by Brown (1963). However, they do coincide in this exceptional case of a well pumping a heavily drained aquifer, which implies equation (4) is also valid to estimate the radius of influence. Chapter 10 and Chapter 11 go into detail about the applicability of formula (4), and in Chapter 10, the formula is validated by a MODFLOW model simulating flow to a pumping well subject to nonuniform drainage.

Ernst (1971) also elaborates on the applicability of his solution, and presents a thorough analysis of annual hydraulic head fluctuations observed in different parts of the Netherlands. In the low-lying polder areas characterized by a dense network of ditches, the average drainage resistance is very small, whereas it is much larger in the higher areas, where only few and widely spaced watercourses give discharge. Therefore, I extended the MAxSym code (Louwyck, 2011) with the option to include drainage boundary conditions, so it became possible to simulate transient flow to a well in a phreatic multilayer system with areal recharge and drainage. Unfortunately, I could not convince my colleagues at VMM of the relevance of the Ernst solution, although the hydrological and geological conditions in many parts of Flanders are very similar to those in the Netherlands. This is why the final version of the MAxSym tool, which I developed to fulfill my associate degree in programming (Louwyck, 2015), has never been used in practice. However, the extended MAxSym code has been applied to test some of the semi-analytical solutions developed during this research.

As a hydrogeologist at the Flemish Environment Agency, I participated in several projects and studies about groundwater management (e.g. Heuvelmans et al., 2011). One interesting study in particular was conducted to answer the question how much groundwater may be extracted from Flemish

aquifers in a sustainable way. A methodology was developed based on a simulation-optimization approach using a multi-criteria analysis tool (Van Camp et al., 2010). The simulations were performed using MODFLOW, the optimization was employed by applying either nonlinear regression or linear programming. The latter inspired me to revisit the optimization of the drainage system at the archeological site ‘Duinenabdij’ discussed in Chapter 12. During this study, the literature on safe yield and the water budget myth was investigated, which is discussed exhaustively in Chapter 11.

From 2012 to 2020, I was responsible for the interpretation of slug tests conducted in observation wells belonging to the groundwater monitoring network exploited by the Flemish Environment Agency. Dozens of wells located in different aquifers were tested all over Flanders, and the data were analyzed using the KGS model (Hyder et al., 1994). Several students from Ghent University (UGent) and the Catholic University of Leuven (KU Leuven) participated in this project under supervision of Dr. Alexander Vandenbohede (UGent), Prof. Dr. Kristine Walraevens (UGent), Dr. Pieter Jan Haest (KU Leuven), and Prof. Dr. Marijke Huysmans (KU Leuven). Unfortunately, the Flemish Environment Agency has not published the identified parameters. The interpretation of these slug tests is also not part of this PhD research. However, the KGS model, originally coded with FORTRAN by Hyder et al. (1994), is rewritten in Python, and used to test the semi-analytical and finite-difference methods developed in Chapter 6 to simulate axisymmetric flow to a partially penetrating well with finite-thickness skin. In Chapter 5, the semi-analytical multilayer-multizone solution is verified against the solution by Cooper et al. (1967) for simulating slug tests conducted in a well fully penetrating a confined aquifer.

1.3.4. Developing semi-analytical solutions for multilayer well-flow

In 2019, I attained a micro degree in Artificial Intelligence, and in 2020, I started doing research in artificial intelligence at the Vives University of Applied Sciences. That is how I became acquainted with the Python ecosystem. Previously, I almost exclusively coded with Matlab, which offers great toolboxes to do scientific computing. However, Python has very similar packages which are open-source and free to use. This probably explains why Python has become increasingly popular among groundwater practitioners (Bakker, 2014). Besides basic libraries for scientific computing, such as NumPy, SciPy, and Matplotlib, there are many other packages available for specific tasks. One of them is PuLP³, a linear programming modeler which is used to optimize the pumping and injection rates for the drainage system discussed in Chapter 12.

Another great feature is the Jupyter notebook⁴, which is a web-based interactive file for Python scripting. These notebooks combine live code, markdown text, equations, plots, and widgets, making the development of graphical user interfaces to run model simulations obsolete. That is why I did not put any effort anymore in maintaining the MAxSym tool (Louwyck, 2011, 2015). Instead, I implemented the finite-difference approach (Louwyck et al., 2012) with Python, and applied standard LU-decomposition available with SciPy to solve the system of finite-difference equations. As explained in Chapter 3, a direct solver may even be more efficient in solving small two-dimensional problems than an iterative solver (Harbaugh, 1995). In Chapter 6, the finite-difference approach is extended to simulate flow to multilayer wells, which are wells open to more than one layer (Neville & Tonkin, 2004). In this case, the matrix system is no longer pentadiagonal, which is a problem for standard iterative solvers such as SIP (Stone, 1968), but not for LU decomposition.

Using the finite-difference method in combination with Picard iterations (Mehl, 2006), it is very straightforward to simulate flow to a well in a multilayer system subject to areal recharge and

³ <https://pypi.org/project/PuLP>

⁴ <https://jupyter.org>

drainage. Solving this problem analytically is more challenging. Ernst (1971) already suggested to assume “that the aquifer is consisting of a succession of horizontal, homogeneous layers with alternatively large and small permeabilities. The direction of flow is horizontal in the layers of large permeability and vertical in the layers of small permeability”. This is exactly the approach followed by Hemker (1984), although in his model, the top of the multilayer aquifer system is leaky, which corresponds to a linear constant-head boundary condition. Because of this linearity, the superposition principle is valid, and recharge is canceled out if drawdown is simulated. The superposition method is explained in Chapter 2, which synthesizes the semi-analytical multilayer solutions by Hemker (1984, 1985a, 1999b) and Bakker and Strack (2003).

Instead of a leaky top, Ernst (1971) defined a nonlinear draining boundary condition, in which case recharge cannot be ignored. At that time, the multilayer solution was not known yet, and Ernst (1971) stated the problem for one layer only. His analytical solution is found by considering two cylindrical zones around the pumping well: in the proximal zone, drainage is inactive due to the lowering of the water table; in the distal zone, drainage is still active. The Ernst (1971) solution is discussed in Chapter 7, Chapter 10, and Chapter 11. The distance of the boundary between the two zones depends on the head in the aquifer, as drainage becomes inactive when the head is lower than the drainage level. This explains why the problem is nonlinear. According to Sun (1999), finding this distance is a type 4 inverse problem, as it involves deriving a boundary condition. Indeed, the two zones can be seen as two models sharing a common boundary at which there is continuity of flow.

This inverse problem is easy to solve using a standard nonlinear solver available with Matlab or Python. Applying the steady-state solution method by Hemker (1984), it is also straightforward to extend the Ernst solution to an arbitrary number of layers. The transient-state problem, however, is much more involved, as the proximal zone expands with time, which implies the distance between the two zones is time-dependent. Chapter 7 presents a solution method based on the Laplace transform, which assumes the initial conditions in the proximal zone are irrelevant. Solving the inverse problem to find the distance of the boundary between the non-draining and the draining zone is also more challenging in case of transient flow. The unbounded nonlinear solver available with Matlab even fails for small values of time. Fortunately, the SciPy library provides a bounded nonlinear solver, which makes it possible to find this distance for small values of time by using the distance at a later time as upper bound.

Summarizing, a two-zone multilayer model is developed, and the distance defining the boundary between the two zones is derived from a specified head or drawdown at that distance. A similar problem that can be solved in this way is the conversion from confined to unconfined flow. This conversion occurs when the head drops below the top of a confined aquifer system due to pumping. The one-layer solution for confined-unconfined flow to a well was developed by Moench and Prickett (1972). In Chapter 7, this solution is generalized to the multilayer case. A two-zone model is also used to include the effect of a finite-thickness skin. In this case, the proximal zone represents the skin or the gravel pack around the well, whereas the distal zone is the actual aquifer system. As the distance between the two zones is fixed and known, the problem is linear and no inverse problem needs to be solved here.

In reality, however, it is possible that there is a gravel pack as well as a skin around the pumping well (Houben et al., 2016). Therefore, the general problem of having multiple zones around the well is solved in Chapter 5. In Chapter 6, the semi-analytical solution for multilayer wells (Hemker, 1999a) is extended to multilayer-multizone flow. Mathematically, a multilayer well is conceptualized as a mixed-type boundary, defining a Dirichlet boundary condition at the well-face which equates the head at that boundary to the water level in the well, and a Neumann boundary condition for the

impervious non-screened parts of the aquifer system (Cassiani & Kabala, 1998). This type of well can be applied to simulate both multi-aquifer wells and partially penetrating wells. In the context of the finite-difference model MODFLOW, the term multi-node well is used (Konikow et al., 2009). As already mentioned, a new finite-difference formulation for multi-node wells is also presented in Chapter 6, and it is verified against the developed semi-analytical solution.

The conversion from confined to unconfined flow discussed in Chapter 7 is expressed mathematically by merely replacing the elastic storage coefficient by the specific yield. For the sake of simplicity, the change in transmissivity is not taken into account. In Chapter 8, unconfined flow with head-dependent transmissivity is discussed. Using Picard iterations, the MAxSym code is capable of simulating unconfined flow in the top layer of the multilayer aquifer system (Louwyck, 2011). The nonlinear problem of unconfined flow is linearized by discretizing the radial distance into cylindrical zones around the well. The semi-analytical multilayer-multizone solution method presented in Chapter 5 can be used in a similar way to approximate the unconfined flow in the top layer of a multilayer system.

Chapter 8 also discusses the effect of delayed yield, a term introduced by Boulton (1954) to explain the typically S-shaped time-drawdown curves obtained from constant-rate pumping tests conducted in water table aquifers (Kruseman & de Ridder, 1990). The Boulton (1954, 1963) solution, however, is semi-empirical, and it was shown by Cooley and Case (1973) that it can be reproduced by a two-layer system, where the lower layer represents the actual layer that is pumped, and the upper layer simulates the effect of the dewatering that accompanies the falling water table. Based on this equivalence, Hemker (1999b) uses his multilayer solution to reproduce not only the Boulton solution but also the Moench (1995, 1996) solution that combines the models of Boulton (1954, 1963) and Neuman (1972, 1974). Hemker (1999b) simulates the effect of delayed yield by defining a dummy layer on top of the model. However, in Chapter 8, the semi-analytical multilayer problem by Hemker (1999b) is restated to define the effect of delayed yield explicitly as a draining boundary condition. A solution for head-dependent unconfined flow that also takes into account the effect of delay yield has not been developed.

1.4. Dissertation outline

The PhD dissertation is structured into 13 chapters. As already discussed in section 1.2, chapters 2 to 4 present and compare existing solution methods for axisymmetric multilayer flow, chapters 5 to 8 extend these solutions to solve more advanced multilayer problems, chapters 9 to 11 provide some theoretical considerations, and chapter 12 discusses a practical case. This section briefly explains the contents of each chapter.

Chapter 1 is a general introduction discussing background, main objective, and chronological overview of the research. The outline of the dissertation is presented, it is indicated which parts of it have already been published in peer-reviewed journals, and an overview of the developed software is given.

Chapter 2 presents the generalized semi-analytical solution for axisymmetric flow to a well in a multilayer aquifer system. It is based on solutions presented by Hemker (1984, 1985a, 1999b) and Bakker and Strack (2003). Both steady and transient flow are considered in confined and leaky systems which may include areal recharge. In case of transient flow, the Laplace transform is applied. The aquifer system can be laterally bounded or unbounded, and the source or sink at the inner boundary is characterized by a specified head or constant discharge. Similarity between axisymmetric flow and parallel flow has already been mentioned in section 1.3.2 discussing the finite-difference method. Since this is also true for the semi-analytical multilayer solution, the corresponding parallel

flow solution is also presented. The superposition method is explained in detail, as it enables defining a time-varying inner boundary condition and simulating flow due to multiple wells. Finally, it is shown how the general solution simplifies to well-known analytical solutions, such as Thiem (1870; 1906), de Glee (1930), Theis (1935), Edelman (1947), and Hantush and Jacob (1955).

Chapter 3 summarizes the papers by Louwyck et al. (2012, 2014) about the finite-difference method and the corresponding MODFLOW procedure. The presented finite-difference approach is implemented in the Matlab code MAxSym (Louwyck, 2011), and recently, it is rewritten in Python. Because memory is not an issue anymore in simulating this kind of small problems, the Python code applies standard LU decomposition available with SciPy instead of the iterative solvers implemented in MAxSym. The presented MODFLOW procedure is very similar to the method proposed by Langevin (2008), yet it is more flexible when dealing with radially varying aquifer parameters.

Chapter 4 is a critical review of the hybrid finite-difference finite-element method developed by Lebbe (1988, 1999) to simulate axisymmetric flow to a well in a multilayer aquifer system. Basically, this method is a finite-difference approximation that applies linear interpolations in space and time. It is compared with the finite-difference approach by Louwyck et al. (2012) presented in Chapter 3. It is also verified against the semi-analytical solution by Hemker (1985a, 1999b). The multilayer example by Lebbe (1988, 1999) and Lebbe and De Breuck (1995) to validate the inverse model HYPARIDEN, is simulated by applying these three solution methods. The Theis (1935) solution is used to investigate the individual effect of the radial and temporal interpolations, and the individual effect of the vertical interpolation is analyzed by comparing a homogeneous and a heterogeneous three-layer system. Finally, a thousand random multilayer models are simulated to check the accuracy of the different solution methods. The vertical interpolation of drawdowns at nodes in adjacent layers is problematic and results in inaccurate results. It is shown the temporal interpolation is similar to the Crank-Nicolson (1947) scheme which may cause spurious oscillations.

Chapter 5 generalizes the semi-analytical solution method presented in Chapter 2 to include lateral heterogeneity by defining multiple cylindrical zones around the well. It discusses how this multilayer-multizone solution can be applied to include areal recharge and to simulate the effect of a gravel pack and finite-thickness skin. It also revisits the analyses of the skin effect by Louwyck et al. (2010, 2014). The solution method is developed for both axisymmetric and parallel flow, and it is carefully verified against existing analytical solutions (Bakker & Strack, 2003; Blom, 1973; Butler, 1988; Haitjema, 1995; Strack, 1989) and compared with the finite-difference method presented in Chapter 3. It is shown how defining a high-transmissivity zone can include the effect of wellbore storage, although next Chapter 6 presents a mathematically more rigorous way. The multilayer-multizone solution is also applied in Chapter 7 to solve the problem of confined-unconfined flow and to include areal drainage. In Chapter 8, it is used to simulate nonlinear unconfined flow.

Chapter 6 extends the multilayer-multizone solution to include multilayer wells, also called multi-node wells. These are used to model partially penetrating wells and multi-aquifer wells, which are wells open to more than one aquifer. At the face of the well, a uniform flux can be defined, which is very straightforward, although a more realistic approach requires a mixed-type boundary condition (Hemker, 1999a). Such a mixed-type boundary condition is mathematically more involved as the head at the well-face in the screened layers must equal the water level in the well, while there is a no-flow boundary in the non-screened layers. Applying the finite-difference method, multilayer wells are implemented by connecting the grid cells that represent the well, and a new algorithm is presented to modify the system of finite-difference equations accordingly. In the semi-analytical method, the layers at the well-face must also be connected, which is done by applying the uniform well-face drawdown solution by Hemker (1999a). Wellbore storage is taken into account, and using

the solution method developed in Chapter 5, it is possible to include multiple zones characterized by different hydraulic properties. This extends the Hemker (1999a) solution which is only capable of simulating the effect of a zero-thickness skin. The modified finite-difference method and the extended semi-analytical approach are compared and verified against some analytical and semi-analytical solutions presented in the literature (Hemker, 1999a; Hyder et al., 1994; Neville & Tonkin, 2004; Papadopoulos, 1966; Sokol, 1963; Wikramaratna, 1984). Both steady and transient flow are considered, and although all test cases deal with axisymmetric flow, the developed solutions may also be applied to solve parallel flow problems involving multilayer streams.

Chapter 7 articulates the semi-analytical multilayer-multizone solution developed in Chapter 5 for the special case of two zones, and uses it to solve the problems of confined-unconfined flow and areal drainage. The one-dimensional transient-state problem for confined-unconfined flow was solved initially by Moench and Prickett (1972), the one-dimensional steady-state problem for a well in an aquifer subject to areal infiltration and drainage by Ernst (1971). Due to the pumping induced lowering of the head, the proximal zone around the well in the first model is characterized by water table conditions, while the areal drainage becomes inactive in the latter. The distal zone in the first model remains confined, while there is still drainage in the latter. To find the boundary between the two zones, an inverse problem must be solved, as it corresponds to the distance where the head equals the top of the aquifer in the Moench and Prickett (1972) model, and the drainage level in the Ernst (1971) model. Using the multilayer solution for two zones, both models are generalized for a multilayer aquifer system where the top layer is subject to confined-unconfined conditions or areal drainage, respectively. The finite-difference method is used to test the semi-analytical solutions. Confined-unconfined flow is simulated using the MODFLOW procedure by Louwyck et al. (2012, 2014), where the limited convertible layer option implemented in the BCF6 package is used (Harbaugh, 2005). Areal infiltration and drainage are options available with the extended version of MAXSYM (Louwyck, 2015).

Chapter 8 discusses two important aspects of radial flow to a well in a phreatic aquifer: the nonlinearity associated with the head-dependent transmissivity and the effect of delayed yield. Combining the finite-difference method with Picard iterations, it is straightforward to take into account the head-dependent transmissivity in the top layer of a phreatic multilayer aquifer system (Louwyck, 2011; Louwyck et al., 2012). Alternatively, the MODFLOW procedure by Louwyck et al. (2012, 2014) can be applied. The multilayer-multizone solution developed in Chapter 5 can also be applied if the radial distance is discretized in the same way in order to linearize the nonlinear differential equation describing unconfined flow. Both solution methods are compared and verified against the analytical Dupuit (1857, 1863) solution. The effect of delayed yield can be simulated by defining on top of the model a highly transmissive dummy layer to which the specific yield is assigned (Hemker, 1999b). This ‘modeling trick’ is based on the equivalence between the semi-empirical solution by Boulton (1954, 1963) and the solution for well-flow in an aquifer-aquitard system (Cooley & Case, 1973). However, instead of defining a dummy layer, Chapter 8 extends the solution presented in Chapter 2 and defines the delayed water table drainage as an upper boundary condition.

Chapter 9 is about understanding transient flow to a pumping well extracting from a confined multilayer system. For that purpose, the semi-analytical solution method presented by Hemker (1984, 1985a, 1999b) is examined carefully. This method is also discussed in Chapter 2 and Chapter 4. The exact solution in the Laplace domain is compared with the corresponding steady-state solution. By expanding this Laplace space solution for large values of time, an asymptotic solution is found that is equal to the steady state solution (Bakker & Strack, 2003), in which the comprehensive potential

term expressed by the Thiem (1870; 1906) formula is replaced by the Theis (1935) equation. Using this approximate solution for large values of time, the water budget for the individual layers is examined. It is shown that close to the well at distances smaller than about 8 times the largest leakage factor, flow is redistributed according to the transmissive properties of the individual layers and the hydraulic gradient does not change anymore, resulting in a pseudo-steady state. At distances larger than the distance determined by the largest leakage factor, flow continues to be redistributed according to the storative properties of the layers if there are no external sources or sinks. The associated vertical flow is, however, negligibly small because of the large volumes involved. Hence, drawdown in the individual layers is virtually the same at distances larger than about 8 times the largest leakage factor, a conclusion that also holds for steady multilayer flow (Bakker & Strack, 2003). The developed theory thus proves the spatial averaging in the measurements of pumping induced drawdown, and confirms the inherent limitations of hydraulic tomography, as discussed by Bohling and Butler (2010).

Chapter 10 critically reviews the use of the radius of influence to assess the environmental impact of a groundwater extraction. Especially the use of empirical formulas such as the Sichardt formula (Kyrieleis & Sichardt, 1930) is questioned as they are not consistent with fundamental hydrogeological principles. Alternative formulations based on the well-known de Glee (1930) and Theis (1935) equations are presented. Comparing these formulas with the Sichardt formula reveals the latter indeed tends to underestimate the extent of the cone of depression. The contested formula that estimates the radius of influence by balancing pumping and infiltration rate, is derived from the asymptotic solution of the Ernst (1971) model for zero drainage resistance. This formula is validated by means of a MODFLOW (Harbaugh, 2005) model that simulates flow to a well in a recharged aquifer with non-uniform drainage. The transient state solution of the Ernst (1971) model is developed applying the Laplace transform, and it is compared with the finite-difference solution implemented in the MAxSym tool (Louwyck, 2011, 2015). A slightly different approach is taken here compared to the semi-analytical method proposed in Chapter 7. Examining drawdown and total storage change reveals the relations between the presented one-dimensional radial flow solutions. The assumptions underlying these solutions are discussed in detail to show their limitations and to refute misunderstandings about their applicability. They offer valuable insights on relevant parameter combinations, but cannot be regarded as substitutes for advanced modeling. Chapter 10 is a revised and extended version of the paper by Louwyck et al. (2022): the sections are reordered conform the structure of the other chapters, the literature is updated, plots are added to visualize the assumptions that hold for the presented equations, and the validation of the Ernst (1971) model is supplementary.

Chapter 11 discusses the controversy in the hydrogeological literature about the role of recharge in evaluating sustainable pumping, which originates in the water budget myth (Bredehoeft, 2002; Bredehoeft et al., 1982). To refute the concept of safe yield, a simplified water budget equation is used, which equals the total pumping rate to the sum of capture and storage change. Since initial recharge and discharge are canceled out from this equation, it is concluded that sustainable pumping has nothing to do with recharge (Bredehoeft, 1997, 2002, 2007). The literature about the recharge controversy is summarized, and the assumptions underlying the water budget equation are investigated. It is seen that it indeed expresses the superposition principle, which assumes the aquifer system can be analyzed as if it is a linear system. The solution for unconfined flow to a well pumping a circular island subject to areal recharge (Verruijt, 1970) and the solution by Ernst (1971) are presented to demonstrate that recharge cannot be ignored if the model is not linear. The finite-difference approximation of the simplified water budget equation is given, which shows the superposition principle not only applies to analytical models. This is illustrated by revisiting a

numerical example discussed by Zhou (2009). Chapter 11 is a revised and extended version of the paper by Louwyck et al. (2023): the literature is updated and a section is added that discusses the finite-difference approximation of the water budget equation.

Chapter 12 revisits the optimization of the drainage system realized at the archeological site ‘Duinenabdij’. The aquifer system at the site comprises three permeable layers separated by two semi-pervious layers. The shallow semi-pervious layer caused problems of flooding at the site. The new drainage system extracts water from the middle permeable layer and injects the pumped water into the middle and lower permeable layers to protect the dunes surrounding the site. A double pumping test was conducted at the site to identify the hydraulic parameters of the aquifer system (Lebbe et al., 2002; Lust, 2002), and the effectiveness of the drainage system was evaluated through mathematical modeling (Louwyck, 2001; Lust, 2002). Originally, the optimal pumping and injection rates were determined via trial-and-error (Louwyck et al., 2005; Lust, 2002). In Chapter 12, linear programming is applied to find the minimum pumping rate that is required to achieve the desired lowering of the water table. Drawdown in the three permeable layers due to the combined pumping and deep-infiltration is simulated by applying the superposition method to the multilayer steady-state well-flow solution by Hemker (1984), as discussed in Chapter 2. The simulation-optimization method is coded with Python. Package PuLP is used for implementing the linear programming model. Chapter 12 is a revised version of the paper by Louwyck et al. (2005), which is extended here with a section discussing the optimization through linear programming.

Chapter 13 terminates the dissertation with a summary and some important conclusions that can be drawn from this work. The **Appendix** gives an overview of the analytical and semi-analytical solutions discussed in this thesis.

Although there is a logical structure in the sequence of the chapters, it is possible to read each chapter without having gone through the previous ones. Each chapter is structured in the same way as scientific papers are, starting with an introduction summarizing the relevant literature and stating the objectives, followed by a methodology section, a section discussing the results, and finishing with a summary highlighting the most important conclusions. The methodology section for the chapters discussing existing or newly developed solutions always provides a clear and unambiguous mathematical statement of the problem, after which it is explained how the semi-analytical and the finite-difference method are applied to solve the stated problem. The results are the different test cases used to verify and compare both methods.

The decision to write each chapter in isolation from the others results in the repetition of certain parts throughout the dissertation. Another consequence is the varying use of symbols for some parameters and variables, as well as a possible difference in sign convention. For example, in some chapters, pumping rates and associated drawdowns are defined as negative, while in others, they are represented as positive. To prevent any confusion, each chapter unambiguously defines its parameters and variables, usually within the section that states the solved problem. Additionally, each chapter makes clear references to the content from previous chapters it develops further or is related to.

1.5. Publications

Parts of this PhD dissertation have already been published in peer-reviewed journals or were included in conference proceedings. This section gives an overview of these papers.

Chapter 12 is an extended version of the following proceedings paper summarizing the hydrogeological studies that were conducted to realize a new drainage system at the archeological site ‘Duinenabdij’:

Louwyck, A., Vandenbohede, A., and Lebbe, L. (2005). The role of hydrogeological research in the realization of a combined pumping and deep infiltration system at the excavation Duinenabdij. In: *Herrier, J.-L., Mees, J., Salman, A., Seys, J., Van Nieuwenhuyse, H., and Dobbelaere, I. (Eds.) Proceedings of ‘Dunes and Estuaries 2005’ – International Conference on Nature Restoration Practices in European Coastal Habitats, Koksijde, Belgium. VLIZ Special Publication 19*, 317- 326.

Author contributions: Conceptualization: L.L.; Methodology: L.L.; Software: A.L. and L.L.; Validation: A.L., A.V., and L.L.; Formal Analysis: L.L.; Investigation: A.L., A.V., and L.L.; Resources: L.L.; Data Curation: A.L., A.V., and L.L.; Writing – Original Draft Preparation: A.L.; Writing – Review and Editing: A.V. and L.L.; Visualization: A.L., A.V., and L.L.; Supervision: L.L.; Project Administration: L.L.; Funding Acquisition: L.L.

One of the topics discussed in Chapter 5 is the concept of well-loss. It is an indication of the well-performance and it can be identified through interpretation of step-drawdown tests. The following paper presents the interpretation of three step-drawdown tests. One of the tests, the Dune test, is conducted at the archeological site ‘Duinenabij’. Chapter 5 theoretically explains why the authors derive a negative well-loss coefficient from the data collected during this test.

Louwyck, A., Vandenbohede, A., and Lebbe, L. (2010). Numerical analysis of step-drawdown tests: parameter identification and uncertainty. *Journal of Hydrology*, 380 (1-2), 165-179.
doi: 10.1016/j.jhydrol.2009.10.034

Author contributions: Conceptualization: L.L.; Methodology: L.L.; Software: A.L. and L.L.; Validation: A.L., A.V., and L.L.; Formal Analysis: A.L., A.V., and L.L.; Investigation: A.L., A.V., and L.L.; Resources: A.L., A.V., and L.L.; Data Curation: A.L., A.V., and L.L.; Writing – Original Draft Preparation: A.L., A.V., and L.L.; Writing – Review and Editing: A.L., A.V., and L.L.; Visualization: A.L., A.V., and L.L.; Supervision: L.L.; Project Administration: L.L.; Funding Acquisition: L.L.

The finite-difference approach and the associated MODFLOW procedure summarized in Chapter 3 are published in the following paper:

Louwyck, A., Vandenbohede, A., Bakker, M., Lebbe, L. (2012). Simulation of axi-symmetric flow towards wells: A finite-difference approach. *Computers & Geosciences* 44, 136-145.
doi: 10.1016/j.cageo.2011.09.004

Author contributions: Conceptualization: A.L., A.V., M.B., and L.L.; Methodology: A.L.; Software: A.L.; Validation: A.L. and M.B.; Formal Analysis: A.L., A.V., and M.B.; Investigation: A.L., A.V., and M.B.; Resources: A.L., A.V., and M.B.; Data Curation: A.L. and M.B.; Writing – Original Draft Preparation: A.L.; Writing – Review and Editing: A.V., M.B., and L.L.; Visualization: A.L. and A.V.; Supervision: L.L.; Project Administration: A.L.

The MODFLOW procedure presented in Chapter 3 is also published in the following paper, which focuses on the effect of a finite-thickness skin around a well extracting from a multilayer aquifer system. The authors’ analysis of the dimensionless skin factor is revisited and extended for multiple zones in Chapter 5.

Louwyck, A., Vandenbohede, A., Bakker, M., Lebbe, L. (2014). MODFLOW procedure to simulate axisymmetric flow in heterogeneous multi-aquifer systems. *Hydrogeology Journal*, 22 (5), 1217-1226.
doi: 10.1007/s10040-014-1150-0.

Author contributions: Conceptualization: A.L., A.V., M.B.; Methodology: A.L.; Software: A.L.; Validation: A.L. and M.B.; Formal Analysis: A.L., A.V., and M.B.; Investigation: A.L., A.V., and M.B.; Resources: A.L., A.V., and

M.B.; Data Curation: A.L. and M.B.; Writing – Original Draft Preparation: A.L.; Writing – Review and Editing: A.V., M.B., and L.L.; Visualization: A.L. and A.V.; Supervision: L.L.; Project Administration: A.L.

In Chapter 6, it is explained how the MODFLOW procedure can be applied to simulate radial flow to a multilayer well using the multi-node well (MNW) package. The following paper employs this procedure to simulate axisymmetric heat transport:

Vandenbohede, A., Louwyck, A., and Vlamynck, N. (2014). SEAWAT-based simulation of axisymmetric heat transport. *Groundwater*, 52 (6), 908–915 . doi: 10.1111/gwat.12137.

Author contributions: Conceptualization: A.V.; Methodology: A.V. and A.L.; Software: A.V; Validation: A.V. and N.V.; Formal Analysis: A.V. and A.L.; Investigation: A.V. and N.V.; Resources: A.V. and N.V.; Data Curation: A.V. and N.V.; Writing – Original Draft Preparation: A.V. and N.V.; Writing – Review and Editing: A.L.; Visualization: A.V. and N.V.; Supervision: A.V.; Project Administration: A.V. ; Funding Acquisition: A.V.

Chapter 10 discussing the radius of influence is an extended version of the following paper:

Louwyck, A., Vandenbohede, A., Libbrecht, D., Van Camp, M., Walraevens, K. (2022). The radius of influence myth. *Water*, 14 (2), 149. doi: 10.3390/w14020149.

Author contributions: Conceptualization: A.L, A.V., D.L., M.V.C., and K.W.; Methodology: A.L.; Software: A.L.; Validation: A.L. and A.V.; Formal Analysis: A.L.; Investigation: A.L.; Resources: A.L, A.V., D.L., M.V.C., and K.W.; Data Curation: A.L.; Writing – Original Draft Preparation: A.L.; Writing – Review and Editing: A.V., D.L., M.V.C., and K.W.; Visualization: A.L.; Supervision: K.W.; Project Administration: K.W.

Chapter 11 concerning the water budget myth and its recharge controversy and explaining why it is important to distinguish between linear and nonlinear models is an extended version of the following paper:

Louwyck, A., Vandenbohede, A., Heuvelmans, G., Van Camp, M., Walraevens, K. (2023). The water budget myth and its recharge controversy: linear vs. nonlinear models. *Groundwater*, 61 (1), 100-110. doi: 10.1111/gwat.13245.

Author contributions: Conceptualization: A.L, A.V., G.H., M.V.C., and K.W.; Methodology: A.L.; Software: A.L.; Validation: A.L.; Formal Analysis: A.L.; Investigation: A.L.; Resources: A.L, A.V., G.H., M.V.C., and K.W.; Data Curation: A.L.; Writing – Original Draft Preparation: A.L. and A.V.; Writing – Review and Editing: G.H., M.V.C., and K.W.; Visualization: A.L. and A.V.; Supervision: K.W.; Project Administration: K.W.

1.6. Developed software

A lot of software has been developed during the two decades of this research. Programming languages that have been used are Python, Matlab, R, C, and FORTRAN.

The first Matlab tool I developed to simulate and analyze radial flow was OGMA-RF, which was presented at the ModelCARE 2007 conference:

Louwyck, A., Vandenbohede, A., and Lebbe, L. (2007). OGMA-RF: a user-friendly, modular program package to simulate and analyse radial flow. *Poster session presented at ModelCARE 2007, Sixth International Conference on Calibration and Reliability in Groundwater Modelling: Credibility in Modelling, Copenhagen, Denmark, 9-13 September 2007*, 88–93.

OGMA-RF has been applied in the following studies:

Vandenbohede, A., Louwyck, A., and Lebbe, L. (2008). Heat transport in a push-pull test: parameter identification and sensitivity analyses. In: Refsgaard, J.C., Kovar, K., Haarder, E., and Nygaard, E. (Eds.), *Proceedings of an International Conference on Calibration and Reliability in Groundwater Modelling: Credibility in Modelling, Copenhagen, Denmark, 9-13 September 2007*, 257–261.

Vandenbohede, A., Louwyck, A., and Lebbe, L. (2008). Identification and reliability of microbial aerobic respiration and denitrification kinetics using a single-well push-pull field test. *Journal of Contaminant Hydrology*, 95 (1-2), 42–56 . doi: 10.1016/j.jconhyd.2007.07.003.

Vandenbohede, A., Louwyck, A., and Lebbe, L. (2009). Conservative Solute Versus Heat Transport in Porous Media During Push-pull Tests. *Transport in Porous Media*, 76 (2), 265–287. doi: 10.1007/s11242-008-9246-4.

OGMA-RF is not available anymore since it was replaced by the MAxSym tool, which is also written in Matlab:

Louwyck, A. (2011). MAxSym - A MATLAB Tool to Simulate Two-Dimensional Axi-Symmetric Groundwater Flow. <https://github.com/alouwyck/MAxSym>.

Code and documentation can still be downloaded from the GitHub repository mentioned in the reference. MAxSym has been used in chapters 7, 8, and 10 to test the semi-analytical solutions.

All recent software is written in Python, except for the simulations in chapters 9 and 10, which are executed in Matlab. The Python software includes:

- all semi-analytical solutions developed in chapters 2, 4, 5, 6, 7, and 8;
- the finite-difference method presented in chapter 3 and 4;
- the hybrid numerical method (Lebbe, 1988, 1999) reviewed in chapter 4;
- the finite-difference formulation for connected cells presented in chapter 6;
- all analytical solutions from the literature discussed in chapters 5, 6, 7, 8, and 11;
- the linear programming example presented in chapter 12.

The Appendix gives an overview of the analytical and semi-analytical solutions that are discussed in this study. All of these solutions are coded with Python.

It is not the objective of this PhD research to develop professional software that can be released to the public. The code is written with the only objective to verify the newly developed solutions. It is not always well-documented, and in many cases, it is badly structured. For sure, computational performance of some algorithms can also be enhanced. However, I would like to contribute to the Python groundwater community, and therefore, notebooks for the different chapters are available on GitHub⁵, which implement the developed solutions and most of the examples discussed in this dissertation. It is also my objective to make a refactored version of the software available in the near future. I have also put a lot of effort to write all equations down and to extensively discuss the solution methods. This should make it possible for readers to implement the solutions by themselves in the programming language of their choice.

1.7. References

Anderson, M. P., & Woessner, W. W. (1992). *Applied Groundwater Modeling—Simulation of Flow and Advection Transport*. San Diego: Academic Press.

Baeteman, C. (1999). The Holocene depositional history of the IJzer paleovalley (western Belgian coastal plain) with reference to the factors controlling the formation of intercalated peat beds. *Geologica Belgica* , 2(3–4), 39–72.

⁵ <https://github.com/alouwyck/PhD>

- Bakker, M. (2013a). Analytic Modeling of Transient Multilayer Flow. In P. K. Mishra & K. Kuhlman (Eds.), *Advances in Hydrogeology* (pp. 95–114). Springer, Heidelberg.
https://doi.org/10.1007/978-1-4614-6479-2_5
- Bakker, M. (2013b). Semi-analytic modeling of transient multi-layer flow with TTim. *Hydrogeology Journal*, 21(4), 935–943. <https://doi.org/10.1007/s10040-013-0975-2>
- Bakker, M. (2014). Python Scripting: The Return to Programming. *Groundwater*, 52(6), 821–822.
<https://doi.org/10.1111/gwat.12269>
- Bakker, M., Post, V., Langevin, C. D., Hughes, J. D., White, J. T., Starn, J. J., & Fienen, M. N. (2016). Scripting MODFLOW Model Development Using Python and FloPy. *Groundwater*, 54(5), 733–739. <https://doi.org/10.1111/gwat.12413>
- Bakker, M., & Strack, O. D. L. (2003). Analytic elements for multiaquifer flow. *Journal of Hydrology*, 271(1–4). [https://doi.org/10.1016/S0022-1694\(02\)00319-0](https://doi.org/10.1016/S0022-1694(02)00319-0)
- Barrocu, G., Eslamian, S., Ostad-Ali-Askari, K., & Singh, V. P. (2018). Wells. In P. T. Bobrowsky & B. Marker (Eds.), *Encyclopedia of Engineering Geology* (pp. 1–2). Springer International Publishing AG. https://doi.org/10.1007/978-3-319-12127-7_297-1
- Blom, J. (1973). *Verlagingen van het freatisch vlak bij grondwateronttrekking in een gebied met vrije afwatering (Drenthe) (in Dutch)*. RID Mededeling 74-7, Rijksinstituut voor Drinkwatervoorziening (RID), The Netherlands.
- Bohling, G. C. (1993). Hydraulic tomography in two-dimensional, steady state groundwaterflow (abstract). *Eos Trans. AGU*, 74(16), Spring Meet. Suppl., 141.
- Bohling, G. C. (2009). Sensitivity and resolution of tomographic pumping tests in an alluvial aquifer. *Water Resources Research*, 45(2), 1–21. <https://doi.org/10.1029/2008WR007249>
- Bohling, G. C., & Butler, J. J. (2010). Inherent Limitations of Hydraulic Tomography. *Ground Water*, 48(6), 809–824. <https://doi.org/10.1111/j.1745-6584.2010.00757.x>
- Bohling, G. C., Butler, J. J., Zhan, X., & Knoll, M. D. (2007). A field assessment of the value of steady shape hydraulic tomography for characterization of aquifer heterogeneities. *Water Resources Research*, 43(5), W05430 1–23. <https://doi.org/10.1029/2006WR004932>
- Bohling, G. C., Zhan, X., Butler, J. J., & Zheng, L. (2002). Steady shape analysis of tomographic pumping tests for characterization of aquifer heterogeneities. *Water Resources Research*, 38(12), 60 1–15. <https://doi.org/10.1029/2001WR001176>
- Boulton, N. S. (1954). Unsteady radial flow to a pumped well allowing for delayed yield from storage. *General Assembly of Rome, Tome II, Groundwater, IAHS publ.* 37, 472–477.
- Boulton, N. S. (1963). Analysis of data from non-equilibrium pumping tests allowing for delayed yield from storage. *Proceedings of the Institution of Civil Engineers*, 26(3), 469–482.
<https://doi.org/10.1680/iicep.1963.10409>
- Bredehoeft, J. D. (1997). Safe Yield and the Water Budget Myth. *Ground Water*, 35(6), 929–929.
<https://doi.org/10.1111/j.1745-6584.1997.tb00162.x>
- Bredehoeft, J. D. (2002). The Water Budget Myth Revisited: Why Hydrogeologists Model. *Ground Water*, 40(4). <https://doi.org/10.1111/j.1745-6584.2002.tb02511.x>

- Bredehoeft, J. D. (2007). It Is the Discharge. *Ground Water*, 45(5), 523–523.
<https://doi.org/10.1111/j.1745-6584.2007.00305.x>
- Bredehoeft, J. D., Papadopoulos, S. S., & Cooper, H. H. (1982). The water budget myth. In *Scientific Basis of Water Resources management Studies in Geophysics* (pp. 51–57). National Academy Press.
- Brown, R. H. (1963). *The cone of depression and the area of diversion around a discharging well in an infinite strip aquifer subject to uniform recharge*. U.S. Geological Survey Water-Supply Paper 1545C; U.S. Government Printing Office, Washington, D.C.
- Butler, J. J. (1988). Pumping tests in nonuniform aquifers — The radially symmetric case. *Journal of Hydrology*, 101(1–4), 15–30. [https://doi.org/10.1016/0022-1694\(88\)90025-X](https://doi.org/10.1016/0022-1694(88)90025-X)
- Cassiani, G., & Kabala, Z. J. (1998). Hydraulics of a partially penetrating well: solution to a mixed-type boundary value problem via dual integral equations. *Journal of Hydrology*, 211(1–4), 100–111. [https://doi.org/10.1016/S0022-1694\(98\)00223-6](https://doi.org/10.1016/S0022-1694(98)00223-6)
- Chapuis, R. P., & Chenaf, D. (1998). Detecting a hydraulic short circuit along a monitoring well with the recovery curve of a pumping test in a confined aquifer: method and example. *Canadian Geotechnical Journal*, 35(5), 790–800. <https://doi.org/10.1139/t98-046>
- Cooley, R. L., & Case, C. M. (1973). Effect of a water table aquitard on drawdown in an underlying pumped aquifer. *Water Resources Research*, 9(2), 434–447.
<https://doi.org/10.1029/WR009i002p00434>
- Cooper, H. H., Bredehoeft, J. D., & Papadopoulos, I. S. (1967). Response of a finite-diameter well to an instantaneous charge of water. *Water Resources Research*, 3(1), 263–269.
<https://doi.org/10.1029/WR003i001p00263>
- Cooper, H. H., & Jacob, C. E. (1946). A generalized graphical method for evaluating formation constants and summarizing well-field history. *Transactions, American Geophysical Union*, 27(4), 526–534. <https://doi.org/10.1029/TR027i004p00526>
- Crank, J., & Nicolson, P. (1947). A practical method for numerical evaluation of solutions of partial differential equations of the heat-conduction type. *Mathematical Proceedings of the Cambridge Philosophical Society*, 43(1), 50–67. <https://doi.org/10.1017/S0305004100023197>
- Darcy, H. (1856). *Les fontaines publiques de la ville de Dijon (In French)*. Paris: Dalmont.
- Dashti, Z., Nakhaei, M., Vadiati, M., Karami, G. H., & Kisi, O. (2022). A literature review on pumping test analysis (2000–2022). *Environmental Science and Pollution Research*, 30(4), 9184–9206. <https://doi.org/10.1007/s11356-022-24440-4>
- de Glee, G. J. (1930). *Over grondwaterstroomingen bij wateronttrekking door middel van putten (in Dutch)* [PhD thesis]. Technische Hoogeschool Delft, Drukkerij J. Waltman. Jr.
- de Hoog, F. R., Knight, J. H., & Stokes, A. N. (1982). An Improved Method for Numerical Inversion of Laplace Transforms. *SIAM Journal on Scientific and Statistical Computing*, 3(3), 357–366. <https://doi.org/10.1137/0903022>
- Devlin, J. F., & Sophocleous, M. (2005). The persistence of the water budget myth and its relationship to sustainability. *Hydrogeology Journal*, 13(4). <https://doi.org/10.1007/s10040-004-0354-0>
- Driscoll, F. G. (1986). *Groundwater and Wells* (2nd ed.). St. Paul: Johnson Division.

- Dupuit, J. (1857). Mouvement de l'eau à travers les terrains perméables (in French). *Comptes Rendus de l'Académie Des Sciences*, 45, 92–96.
- Dupuit, J. (1863). *Etude Théoriques et Pratiques Sur le Mouvement Des Eaux Dans Les Canaux Découverts et à Travers Les Terrains Perméables* (in French). Paris: Dunot.
- Edelman, J. H. (1947). *Over de berekening van grondwaterstroomingen* (in Dutch). TU Delft.
- Ernst, L. F. (1971). Analysis of groundwater flow to deep wells in areas with a non-linear function for the subsurface drainage. *Journal of Hydrology*, 14(2). [https://doi.org/10.1016/0022-1694\(71\)90004-7](https://doi.org/10.1016/0022-1694(71)90004-7)
- Gottlieb, J., & Dietrich, P. (1995). Identification of the permeability distribution in soil by hydraulic tomography. *Inverse Problems*, 11(2), 353–360. <https://doi.org/10.1088/0266-5611/11/2/005>
- Haitjema, H. (1995). *Analytic Element Modeling of Groundwater Flow*. San Diego: Academic Press. <https://doi.org/10.1016/B978-0-12-316550-3.X5000-4>
- Haitjema, H. (2006). The Role of Hand Calculations in Ground Water Flow Modeling. *Ground Water*, 44(6). <https://doi.org/10.1111/j.1745-6584.2006.00189.x>
- Hantush, M. S., & Jacob, C. E. (1955). Non-steady radial flow in an infinite leaky aquifer. *Transactions, American Geophysical Union*, 36(1), 95–100. <https://doi.org/10.1029/TR036i001p00095>
- Harbaugh, A. W. (1995). *Direct solution package based on alternating diagonal ordering for the U.S. Geological Survey modular finite-difference ground-water flow model*. U.S. Geological Survey Open-File Report 95-288. <https://doi.org/https://doi.org/10.3133/ofr95288>
- Harbaugh, A. W. (2005). *MODFLOW-2005, the U.S. Geological Survey modular ground-water model - the Ground-Water Flow Process*. U.S. Geological Survey Techniques and Methods 6-A16. <https://doi.org/https://doi.org/10.3133/tm6A16>
- Harbaugh, A. W., Banta, E. R., Hill, M. C., & McDonald, M. G. (2000). *MODFLOW-2000, The U.S. Geological Survey Modular Ground-Water Model: User Guide to Modularization Concepts and the Ground-Water Flow Process*. U.S. Geological Survey Open-File Report 00-92. <https://doi.org/https://doi.org/10.3133/ofr200092>
- Harbaugh, A. W., & McDonald, M. G. (1996a). *User's documentation for MODFLOW-96, an update to the U.S. Geological Survey modular finite-difference ground-water flow model*. U.S. Geological Survey Open-File Report 96-485. <https://doi.org/https://doi.org/10.3133/ofr96485>
- Harbaugh, A. W., & McDonald, M. G. (1996b). *Programmer's documentation for MODFLOW-96, an update to the U.S. Geological Survey modular finite-difference ground-water flow model*. U.S. Geological Survey Open-File Report 96-486. <https://doi.org/https://doi.org/10.3133/ofr96486>
- Hemker, C. J. (1984). Steady groundwater flow in leaky multiple-aquifer systems. *Journal of Hydrology*, 72(3–4), 355–374. [https://doi.org/10.1016/0022-1694\(84\)90089-1](https://doi.org/10.1016/0022-1694(84)90089-1)
- Hemker, C. J. (1985a). Transient well flow in leaky multiple-aquifer systems. *Journal of Hydrology*, 81(1–2), 111–126. [https://doi.org/10.1016/0022-1694\(85\)90170-2](https://doi.org/10.1016/0022-1694(85)90170-2)
- Hemker, C. J. (1985b). A General Purpose Microcomputer Aquifer Test Evaluation Technique. *Ground Water*, 23(2), 247–253. <https://doi.org/10.1111/j.1745-6584.1985.tb02799.x>

- Hemker, C. J. (1999a). Transient well flow in layered aquifer systems: the uniform well-face drawdown solution. *Journal of Hydrology*, 225(1–2), 19–44. [https://doi.org/10.1016/S0022-1694\(99\)00093-1](https://doi.org/10.1016/S0022-1694(99)00093-1)
- Hemker, C. J. (1999b). Transient well flow in vertically heterogeneous aquifers. *Journal of Hydrology*, 225(1–2), 1–18. [https://doi.org/10.1016/S0022-1694\(99\)00137-7](https://doi.org/10.1016/S0022-1694(99)00137-7)
- Hemker, C. J. (2000). *Groundwater flow in layered aquifer systems* [PhD thesis]. VU, Amsterdam.
- Hemker, C. J., & Maas, C. (1987). Unsteady flow to wells in layered and fissured aquifer systems. *Journal of Hydrology*, 90(3–4), 231–249. [https://doi.org/10.1016/0022-1694\(87\)90069-2](https://doi.org/10.1016/0022-1694(87)90069-2)
- Hemker, C. J., & Post, V. E. A. (2019). *MLU for Windows*. Retrieved from <https://www.microfem.com/products/mlu.html>
- Heuvelmans, G., Louwyck, A., & Lermytte, J. (2011). Distinguishing between management-induced and climatic trends in phreatic groundwater levels. *Journal of Hydrology*, 411(1–2). <https://doi.org/10.1016/j.jhydrol.2011.09.039>
- Houben, G. J. (2015). Review: Hydraulics of water wells—head losses of individual components. *Hydrogeology Journal*, 23(8), 1659–1675. <https://doi.org/10.1007/s10040-015-1313-7>
- Houben, G. J., Halisch, M., Kaufhold, S., Weidner, C., Sander, J., & Reich, M. (2016). Analysis of Wellbore Skin Samples-Typology, Composition, and Hydraulic Properties. *Groundwater*, 54(5), 634–645. <https://doi.org/10.1111/gwat.12403>
- Hunt, B., & Scott, D. (2007). Flow to a Well in a Two-Aquifer System. *Journal of Hydrologic Engineering*, 12(2), 146–155. [https://doi.org/10.1061/\(ASCE\)1084-0699\(2007\)12:2\(146\)](https://doi.org/10.1061/(ASCE)1084-0699(2007)12:2(146))
- Hyder, Z., Butler, J. J., McElwee, C. D., & Liu, W. (1994). Slug tests in partially penetrating wells. *Water Resources Research*, 30(11), 2945–2957. <https://doi.org/10.1029/94WR01670>
- Jasechko, S., & Perrone, D. (2021). Global groundwater wells at risk of running dry. *Science*, 372(6540), 418–421. <https://doi.org/10.1126/science.abc2755>
- Konikow, L. F., Hornberger, G. Z., Halford, K. J., Hanson, R. T., & Harbaugh, A. W. (2009). *Revised multi-node well (MNW2) package for MODFLOW ground-water flow model*. U.S. Geological Survey Techniques and Methods 6-A30.
- Kruseman, G. P., & de Ridder, N. A. (1990). *Analysis and Evaluation of Pumping Test Data* (2nd ed.). ILRI Publication 47, Wageningen.
- Kyrieleis, W., & Sichardt, W. (1930). *Grundwasserabsenkung bei Fundierungsarbeiten (in German)*. Berlin: Springer.
- Langevin, C. D. (2008). Modeling Axisymmetric Flow and Transport. *Ground Water*, 46(4), 579–590. <https://doi.org/10.1111/j.1745-6584.2008.00445.x>
- Langevin, C. D., Thorne, D. T., Dausman, A. M., Sukop, M. C., & Guo, W. (2007). *SEAWAT Version 4: A Computer Program for Simulation of Multi-Species Solute and Heat Transport*. U.S. Geological Survey Techniques and Methods 6-A22. <https://doi.org/https://doi.org/10.3133/tm6A22>
- Lebbe, L. C. (1983). Een matematisch model van de niet-permanente grondwaterstroming naar een pompput in een veellagig grondwaterreservoir en enkele beschouwingen over de stroomtijd (in Dutch). *Tijdschrift BECEWA*, 70, 35–48.

- Lebbe, L. C. (1988). *Uitvoering van pompproeven en interpretatie door middel van een invers model* (in Dutch). Ghent University.
- Lebbe, L. C. (1999). *Hydraulic Parameter Identification. Generalized Interpretation Method for Single and Multiple Pumping Tests*. Berlin Heidelberg: Springer-Verlag.
- Lebbe, L. C., & de Breuck, W. (1995). Validation of an inverse numerical model for interpretation of pumping tests and a study of factors influencing accuracy of results. *Journal of Hydrology*, 172(1–4), 61–85. [https://doi.org/10.1016/0022-1694\(95\)02747-D](https://doi.org/10.1016/0022-1694(95)02747-D)
- Lebbe, L. C., & Vandenbohede, A. (2004). *Ontwikkeling van een lokaal axi-symmetrisch model op basis van de HCOV kartering ter ondersteuning van de adviesverlening voor grondwaterwinningen* (in Dutch). Onderzoeksopdracht voor het Ministerie van de Vlaamse Gemeenschap, AMINAL, afdeling Water, Brussels.
- Lebbe, L. C., Vandenbohede, A., & Louwyck, A. (2002). *Uitvoering en interpretatie van dubbele pompproef nabij de abdijsite te Koksijde* (in Dutch). Report GROMO2002/01, Ghent University.
- Lermytte, J., & Thomas, P. (2008). Het Vlaams Grondwatermodel: een gebiedsdekkend modelinstrumentarium voor Vlaanderen, toepasbaar van regionale tot lokale schaal (in Dutch). *Stromingen*, 14(4), 63–71.
- LeVeque, R. J. (2007). *Finite Difference Methods for Ordinary and Partial Differential Equations: Steady-State and Time-Dependent Problems*. Society for Industrial and Applied Mathematics.
- Lohman, S. W. (1972). *Ground-water Hydraulics*. U.S. Geological Survey.
- Louwyck, A. (2001). *Hydrogeologische studie van de archeologische site ‘Duinenabdij’, Koksijde* (in Dutch) [MSc. Thesis]. Ghent University.
- Louwyck, A. (2011). *MAXSym - A MATLAB Tool to Simulate Two-Dimensional Axi-Symmetric Groundwater Flow*. Research Unit Groundwater Modeling, Ghent University. Retrieved from <https://github.com/alouwyck/MAXSym>
- Louwyck, A. (2015). *Module Projectwerk programmeren B5 - Ontwikkeling MAXSymMer* (in Dutch) [Associate Degree Programming]. CVO Lethas, Brussels.
- Louwyck, A., Vandenbohede, A., Bakker, M., & Lebbe, L. C. (2012). Simulation of axi-symmetric flow towards wells: A finite-difference approach. *Computers & Geosciences*, 44, 136–145. <https://doi.org/10.1016/j.cageo.2011.09.004>
- Louwyck, A., Vandenbohede, A., Bakker, M., & Lebbe, L. C. (2014). MODFLOW procedure to simulate axisymmetric flow in radially heterogeneous and layered aquifer systems. *Hydrogeology Journal*, 22(5), 1217–1226. <https://doi.org/10.1007/s10040-014-1150-0>
- Louwyck, A., Vandenbohede, A., Heuvelmans, G., Van Camp, M., & Walraevens, K. (2023). The Water Budget Myth and Its Recharge Controversy: Linear vs. Nonlinear Models. *Groundwater*, 61(1), 100–110. <https://doi.org/10.1111/gwat.13245>
- Louwyck, A., Vandenbohede, A., & Lebbe, L. C. (2005). The role of hydrogeological research in the realization of a combined pumping and deep infiltration system at the excavation “Duinenabdij.” In J.-L. Herrier, J. Mees, A. Salman, J. Seys, H. Van Nieuwenhuyse, & I. Dobbelaere (Eds.), *Proceedings “Dunes and Estuaries 2005”: International Conference on nature*

restoration practices in European coastal habitats, Koksijde, Belgium 19-23 September 2005.
(pp. 317–326). VLIZ Special Publication 19.

Louwyck, A., Vandenbohede, A., & Lebbe, L. C. (2007). OGMA-RF: a user-friendly, modular program package to simulate and analyse radial flow. *ModelCARE 2007, Sixth International Conference on Calibration and Reliability in Groundwater Modelling: Credibility in Modelling, Copenhagen, Denmark, 9-13 September 2007*, 88–93.

Louwyck, A., Vandenbohede, A., & Lebbe, L. C. (2010). Numerical analysis of step-drawdown tests: Parameter identification and uncertainty. *Journal of Hydrology*, 380(1–2), 165–179.
<https://doi.org/10.1016/j.jhydrol.2009.10.034>

Louwyck, A., Vandenbohede, A., Libbrecht, D., Van Camp, M., & Walraevens, K. (2022). The Radius of Influence Myth. *Water*, 14(2), 149. <https://doi.org/10.3390/w14020149>

Lust, H. (2002). *Bijdrage tot de optimalisatie van de diepe drainage op de Duinenabdijsite te Koksijde (in Dutch)* [MSc. Thesis]. Ghent University.

McDonald, M. G., & Harbaugh, A. W. (1984). *A modular three-dimensional finite-difference ground-water flow model*. U.S. Geological Survey Open-File Report 83-875.
<https://doi.org/https://doi.org/10.3133/ofr83875>

McDonald, M. G., & Harbaugh, A. W. (1988). *A modular three-dimensional finite-difference ground-water flow model*. U.S. Geological Survey Techniques of Water-Resources Investigations 06-A1.
<https://doi.org/10.3133/twri06A1>

Mehl, S. W. (2006). Use of Picard and Newton Iteration for Solving Nonlinear Ground Water Flow Equations. *Ground Water*, 44(4), 583–594. <https://doi.org/10.1111/j.1745-6584.2006.00207.x>

Mehl, S. W., & Hill, M. C. (2001). *MODFLOW-2000, the U. S. Geological Survey modular ground-water model; user guide to the Link-AMG (LMG) package for solving matrix equations using an algebraic multigrid solver*. U.S. Geological Survey Open-File Report 2001-177.
<https://doi.org/https://doi.org/10.3133/ofr01177>

Moench, A. F. (1995). Combining the Neuman and Boulton Models for Flow to a Well in an Unconfined Aquifer. *Ground Water*, 33(3), 378–384. <https://doi.org/10.1111/j.1745-6584.1995.tb00293.x>

Moench, A. F. (1996). Flow to a Well in a Water-Table Aquifer: An Improved Laplace Transform Solution. *Ground Water*, 34(4), 593–596. <https://doi.org/10.1111/j.1745-6584.1996.tb02045.x>

Moench, A. F., & Prickett, T. A. (1972). Radial flow in an infinite aquifer undergoing conversion from artesian to water table conditions. *Water Resources Research*, 8(2), 494–499.
<https://doi.org/10.1029/WR008i002p00494>

Neuman, S. P. (1972). Theory of flow in unconfined aquifers considering delayed response of the water table. *Water Resources Research*, 8(4), 1031–1045.
<https://doi.org/10.1029/WR008i004p01031>

Neuman, S. P. (1974). Effect of partial penetration on flow in unconfined aquifers considering delayed gravity response. *Water Resources Research*, 10(2), 303–312.
<https://doi.org/10.1029/WR010i002p00303>

- Neuman, S. P. (1987). Stochastic continuum representation of fractured rock permeability as an alternative to the REV and fracture network concepts. *Proc. U.S. Rock Mech. Symp.*, 28, 533–561.
- Neville, C. J., & Tonkin, M. J. (2004). Modeling Multiaquifer Wells with MODFLOW. *Ground Water*, 42(6), 910–919. <https://doi.org/10.1111/j.1745-6584.2004.t01-9-x>
- Papadopoulos, I. S. (1966). Nonsteady flow to multiaquifer wells. *Journal of Geophysical Research*, 71(20), 4791–4797. <https://doi.org/10.1029/JZ071i020p04791>
- Renard, P. (2005a). Hydraulics of Wells and Well Testing. In M. G. Anderson (Ed.), *Encyclopedia of Hydrological Sciences* (Vol. 4). John Wiley & Sons, Ltd. <https://doi.org/10.1002/0470848944.hsa154a>
- Renard, P. (2005b). The future of hydraulic tests. *Hydrogeology Journal*, 13(1), 259–262. <https://doi.org/10.1007/s10040-004-0406-5>
- Sokol, D. (1963). Position and fluctuations of water level in wells perforated in more than one aquifer. *Journal of Geophysical Research*, 68(4), 1079–1080. <https://doi.org/10.1029/JZ068i004p01079>
- Stehfest, H. (1970). Algorithm 368: Numerical inversion of Laplace transforms [D5]. *Communications of the ACM*, 13(1), 47–49. <https://doi.org/10.1145/361953.361969>
- Sterrett, R. J. (Ed.). (2007). *Groundwater and wells* (3rd ed.). New Brighton: Johnson Screens.
- Stone, H. L. (1968). Iterative Solution of Implicit Approximations of Multidimensional Partial Differential Equations. *SIAM Journal on Numerical Analysis*, 5(3), 530–558. <https://doi.org/10.1137/0705044>
- Strack, O. D. L. (1989). *Groundwater Mechanics*. Old Tappan, N. J.: Prentice-Hall.
- Sun, N.-Z. (1999). *Inverse Problems in Groundwater Modeling* (Vol. 6). Springer Netherlands. <https://doi.org/10.1007/978-94-017-1970-4>
- Theis, C. V. (1935). The relation between the lowering of the Piezometric surface and the rate and duration of discharge of a well using ground-water storage. *Transactions, American Geophysical Union*, 16(2), 519–524. <https://doi.org/10.1029/TR016i002p00519>
- Thiem, A. (1870). Die Ergiebigkeit artesischer Bohrlöcher, Schachtbrunnen und Filtergalerien (in German). *Journal Für Gasbeleuchtung Und Wasserversorgung*, 13, 450–467.
- Thiem, G. (1906). *Hydrologische Methoden* (in German). Leipzig: Gebhardt.
- Tosaka, H., Masumoto, K., & Kojima, K. (1993). Hydropulse tomography for identifying 3-d permeability distribution, in High Level Radioactive Waste Management. *Proceedings of the Fourth Annual International Conference of the ASCE, Am. Soc. of Civ. Eng.*, Reston VA, 955–959.
- Van Camp, M., Martens, K., D'hont, D., Lermytte, J., Louwyck, A., & Walraevens, K. (2010). A methodology for determining sustainable groundwater exploitation in aquifer systems based on a simulation-optimisation approach using a multi-criteria analysis tool. In A. Zuber, J. Kania, & E. Kmiecik (Eds.), *Extended Abstracts, XXXVIII IAH Congress, Groundwater Quality Sustainability, Krakow, 12–17 September 2010* (pp. 1319–1321). University of Silesia Press .

- Vandenbohede, A., Louwyck, A., & Lebbe, L. C. (2008a). Identification and reliability of microbial aerobic respiration and denitrification kinetics using a single-well push–pull field test. *Journal of Contaminant Hydrology*, 95(1–2), 42–56. <https://doi.org/10.1016/j.jconhyd.2007.07.003>
- Vandenbohede, A., Louwyck, A., & Lebbe, L. C. (2008b). Heat transport in a push-pull test: parameter identification and sensitivity analyses. In J. C. Refsgaard, K. Kovar, E. Haarder, & E. Nygaard (Eds.), *Proceedings of an International Conference on Calibration and Reliability in Groundwater Modelling: Credibility of Modelling, Copenhagen, Denmark, 9-13 September 2007* (pp. 257–261).
- Vandenbohede, A., Louwyck, A., & Lebbe, L. C. (2009). Conservative Solute Versus Heat Transport in Porous Media During Push-pull Tests. *Transport in Porous Media*, 76(2), 265–287. <https://doi.org/10.1007/s11242-008-9246-4>
- Vandenbohede, A., Louwyck, A., & Vlamynck, N. (2014). SEAWAT-Based Simulation of Axisymmetric Heat Transport. *Groundwater*, 52(6), 908–915. <https://doi.org/10.1111/gwat.12137>
- Veling, E. J. M., & Maas, C. (2009). Strategy for solving semi-analytically three-dimensional transient flow in a coupled N-layer aquifer system. *Journal of Engineering Mathematics*, 64(2), 145–161. <https://doi.org/10.1007/s10665-008-9256-9>
- Verruijt, A. (1970). *Theory of Groundwater Flow*. London: Macmillan Press.
- Waller, R. M. (1982). *Ground Water and the Rural Homeowner*. US Geological Survey Pamphlet.
- Wang, H. F., & Anderson, M. P. (1982). *Introduction to Groundwater Modeling: Finite Difference and Finite Element Methods*. San Francisco: WH Freeman and Company.
- Wikramaratna, R. S. (1984). An Analytical Solution for the Effects of Abstraction From a Multiple-Layered Confined Aquifer With No Cross Flow. *Water Resources Research*, 20(8), 1067–1074. <https://doi.org/10.1029/WR020i008p01067>
- Willems, E., Monseré, T., & Dierckx, J. (2009). *Geactualiseerd richtlijnenboek milieueffectrapportage - Basisrichtlijnen per activiteitengroep – Landbouwdieren (in Dutch)*. Dienst MER, Afdeling Milieu-, Natuur- en Energiebeleid, Departement Leefmilieu, Natuur en Energie, Brussels.
- Yeh, H.-D., & Chang, Y.-C. (2013). Recent advances in modeling of well hydraulics. *Advances in Water Resources*, 51, 27–51. <https://doi.org/10.1016/j.advwatres.2012.03.006>
- Yeh, T.-C. J., & Liu, S. (2000). Hydraulic tomography: Development of a new aquifer test method. *Water Resources Research*, 36(8), 2095–2105. <https://doi.org/10.1029/2000WR900114>
- Yeh, T.-C. J., Mao, D., Zha, Y., Hsu, K.-C., Lee, C.-H., Wen, J.-C., Lu, W., & Yang, J. (2014). Why Hydraulic Tomography Works? *Groundwater*, 52(2), 168–172. <https://doi.org/10.1111/gwat.12129>
- Zheng, C., & Wang, P. P. (1999). *MT3DMS : a modular three-dimensional multispecies transport model for simulation of advection, dispersion, and chemical reactions of contaminants in groundwater systems; documentation and user's guide*. Contract Report SERDP-99-1, U.S. Army Engineer Research and Development Center, Vicksburg, MI.
- Zhou, Y. (2009). A critical review of groundwater budget myth, safe yield and sustainability. *Journal of Hydrology*, 370(1–4). <https://doi.org/10.1016/j.jhydrol.2009.03.009>

Chapter 2. Semi-Analytical Solution Method for Simulating Multilayer Flow

2.1. Introduction

Radial groundwater flow can be thought of as groundwater that flows along the radii of an imaginary circle towards or away from the center of this circle. Mathematically, it is described using a three-dimensional cylindrical coordinate system (r, θ, z) , with r the radial distance, θ the angular position, and z the vertical distance. If the flow is also axially symmetric around the vertical axis containing the center of the circle, then it is called axisymmetric. In this case, the flow does not change in the angular direction θ , and the mathematical problem is reduced by one dimension, as it can be described using a two-dimensional coordinate system (r, z) . If the axisymmetric flow is also strictly horizontal, then it is one-dimensional, as it only varies in the radial dimension r .

The canonical example of radial groundwater flow is a well that extracts water from an aquifer. In this case, the vertical axis of the well acts as the axis of symmetry. In the study of groundwater flow systems, knowledge of flow to pumping wells is essential, as they are used to extract groundwater for human use, which represents a substantial part of the discharge of those systems. Wells are also applied for observation and testing of the groundwater regime. As a consequence, the theory of axisymmetric groundwater flow towards a well is an important specialized topic of groundwater hydraulics (Bennett et al., 1990), which has been studied for more than one and a half century.

2.1.1 One-layer solutions

The first known publications on well hydraulics are written by Dupuit (1857, 1863), who proposed the first series of analytical solutions for steady-state flow to a well in an idealized confined or unconfined aquifer (Mishra & Kuhlman, 2013; Renard, 2005; Ritzi & Bobeck, 2008). More than 40 years later, Günther Thiem (1906) used his well-known formula to simulate steady radial flow to a fully penetrating well in a homogeneous confined aquifer. His PhD-thesis is often cited as the source of the Thiem equation, although his father, Adolf Thiem, should get credit for it as his first paper on groundwater (Thiem, 1870) already applied this equation (Houben & Batelaan, 2021). As already mentioned, Dupuit (1857, 1863) derived the equations for both unconfined and confined well-flow, to which he referred as ordinary and artesian wells, respectively. In the Netherlands, Kooper (1914) found the analytical solution for steady radial flow to a fully penetrating well in a homogeneous leaky aquifer (Hemker, 2000). About 15 years later, de Glee (1930) applied Kooper's formula to evaluate field data, and extended it to partially penetrating wells. This probably explains why Kooper's solution is generally referred to as the de Glee formula in the Netherlands and in Flanders. More than 30 years later, the same solution was published in the English literature by Jacob (1946) and by Hantush (1949).

The next milestone in well hydraulics is the publication of Theis (1935), who presented the solution for transient radial flow to a well in a homogeneous confined aquifer. Until then, the design of well fields was mainly based on empirically found relations between pumping rate and drawdown measured during pumping tests (Hemker, 2000). A well-known example is the Sichardt formula (Kyrieleis & Sichardt, 1930) that will be discussed in Chapter 10. By recognizing the physical analogy between heat flow and groundwater flow, Theis (1935) introduced the concept of aquifer storage, and with the help of the mathematician Lubin (Bredehoeft, 2008), he was able to fully describe transient flow to a well, although it should be noted that Boussinesq (1904) was the first to give the

transient version of the differential equation governing confined groundwater flow (Mishra & Kuhlman, 2013). The Theis (1935) solution made the use of empirically derived formulas unnecessary and obsolete, as from then on, pumping test data could be compared graphically with the theoretical Theis type curve to determine aquifer transmissivity and storage (e.g. Jacob, 1940). The well-known late-time approximation of the Theis (1935) solution was used by Cooper and Jacob (1946) in their simplified graphical interpretation method, which only involves matching a straight line to the pumping test data. More than three decades after Kooper (1914) found the steady state solution for radial flow in a leaky aquifer, Jacob (1946) developed the transient state solution for a pumping well in a leaky aquifer that is laterally bounded, and almost a decade later, Hantush and Jacob (1955) published the transient state solution for a leaky aquifer of infinite extent. About fifteen years later, Ernst (1971) presented the steady state solution for a well in an aquifer subject to areal uniform drainage and recharge.

All of these models assume a single homogeneous aquifer from which groundwater is extracted by a fully penetrating well. Under this assumption, flow to the well is strictly horizontal and axially symmetric, which reduces the mathematical problem to one spatial dimension only. The time-dependent solutions are mostly simplified by assuming the well has an infinitesimal radius and the aquifer has an infinite extent. In case of a leaky aquifer, the leakage from the adjoining aquitard is simplified by defining an upper boundary condition which assumes a constant head in the unpumped aquifer and reduces the aquitard to its vertical resistance. These assumptions greatly facilitated the mathematical treatment of the problem. However, in reality, such idealized conditions are rare (Lebbe, 1999; Yeh & Chang, 2013): pumping wells have a finite diameter and penetrate the aquifer only partially in many cases, and the pumped aquifer mostly is part of a multi-aquifer system, i.e. a succession of aquifers separated by relatively less permeable yet compressible aquitards.

2.1.2 Two-layer solutions

Therefore it is no surprise researchers in the 1960s started to investigate the feasibility of the simplified solutions that have been applied before, and this gave rise to a variety of new solutions. An exhaustive discussion is not within the scope of this study, but it is worth mentioning some well-known solutions that were published in these years to illustrate how axisymmetric well-flow models became more complex in the pursuit of defining more realistic boundary conditions and considering flow in the adjacent unpumped layers. Hantush (1960) extended the solution for transient flow to a fully penetrating well in a leaky aquifer by including the storage of the overlying aquitard, and more than 25 years after Theis (1935) published his model of transient flow to a fully penetrating well, Hantush (1961a) presented the same model for a partially penetrating well, while Hantush (1961b) applied it to pumping test data. Remarkable is the work of Hantush (1964) in which several transient state solutions are presented that were derived by applying integral transforms such as the Laplace transform. One of these solutions concerns radial flow to a partially penetrating well in a homogeneous leaky aquifer. Papadopoulos and Cooper (1967) extended the Theis (1935) solution to include wellbore storage in case the well has a large diameter. Wellbore storage is also important when simulating slug tests, and Cooper et al. (1967) presented a solution where radial flow to a fully-penetrating finite-diameter well in a homogeneous confined aquifer is induced by an instantaneous head change in the well instead of steady pumping.

Although researchers at that time were aware of the impossibility to develop a complete understanding of flow in the pumped aquifer without analyzing the multi-aquifer system as a whole (Neuman & Witherspoon, 1969a), all analytical multilayer solutions that were published then considered two aquifers only. Hemker (1985, 2000) presumed the complexity of notation was the main reason for the lack of analytical models in which more than two layers were involved. This

statement should be nuanced, however, since Neuman (1968) developed an analytical solution for drawdown in a confined system consisting of three aquifers separated by two aquitards, which was evaluated only 40 years later by Li and Neuman (2007). According to Strack (1989), the first to consider flow in a leaky system of an arbitrary number of aquifers separated by leaky layers was Mjatliev (1947), who published his work in Russian. Huisman and Kemperman (1951) independently developed a solution for steady flow to a well in a leaky two-aquifer system bounded by an impervious base. The solution for a two-layer system with leaky base was given by Polubarinova-Kochina (1962), who applied the technique introduced by Mjatliev (1947).

It was Hantush (1967) again who published a transient state solution for a confined two-aquifer system, and his work was extended by Neuman and Witherspoon (1969b) who included elastic storage within the aquitard that separates the pumped and unpumped aquifer. Neuman and Witherspoon (1972) applied this theory to develop a new interpretation method in which drawdown is not only measured in the pumped aquifer, but also in the adjacent layers. These transient state solutions were obtained by applying the Laplace and Hankel transforms. Using the same integral transforms, Bruggeman (1972) developed solutions for steady and transient flow in two-aquifer systems that are recharged through top and bottom aquitards. More than 10 years later, a solution for transient flow to a partially penetrating well in a two-layer system was published by Javandel and Witherspoon (1983), and a solution for transient flow to a large-diameter well in an aquifer with elastic semi-confining layers was presented by Moench (1985).

Not only solutions for leaky and confined systems were developed in those days, the problem of unconfined flow was also studied extensively. Boulton (1954, 1963) presented a solution to simulate radial flow in a homogeneous unconfined aquifer. His delayed-yield solution, however, is semi-empirical, and only later, it was shown by Cooley (1972) and Cooley and Case (1973) that the Boulton model corresponds to a two-layer model in which the lower layer is extracted by a fully penetrating well, and where the delayed-yield effect results from vertical drainage through the semi-pervious upper layer. In the pumped layer only horizontal flow is considered, whereas the flow in the top layer is assumed to be strictly vertical. Neuman (1972) developed a full theoretical solution for flow to a well fully penetrating a homogeneous unconfined aquifer, and Neuman (1974) extended the solution to account for the effect of partial penetration. However, the Neuman (1972, 1974) solutions are complex, and it is no surprise that even in recent studies the delayed-yield approach is still being applied, especially in multi-aquifer systems (e.g. Hunt & Scott, 2007). On the other hand, Moench (1993) presented a more efficient solution method for the Neuman (1972, 1974) model by numerically inverting the Laplace transform using the Stehfest (1970) algorithm, and a similar method was applied by Moench (1995, 1996) to combine the Neuman (1972, 1974) and the Boulton (1954, 1963) models. In Chapter 8 discussing unconfined flow, a more exhaustive overview is given of the literature on delayed yield.

2.1.3 Multilayer solutions

In the 1980s, several researchers developed steady as well as transient state solutions to simulate flow in a multi-aquifer system consisting of as many layers as required. In the English literature, Hemker (1984) was the first to publish the generalized solution for steady flow in a leaky multi-aquifer system in which the aquitards are incompressible. However, according to Hemker (1984), earlier work on multilayer well flow problems was published in Russian and Hungarian by Hungarian hydrologists (Halász, 1975; Halász & Székely, 1979; Székely, 1978). They applied integral transforms and polynomial techniques, whereas Hemker (1984) made use of matrix analysis techniques to solve the system of ordinary differential equations. Since his method requires a numerical solution for an eigenvalue problem, the obtained solution is semi-analytical. Hunt (1985, 1986) modified the method

applied by Hemker (1984) by using the solution of a generalized eigenvalue problem. Maas (1986, 1987a) applied matrix differential calculus to solve the same problem, and Yu (1987) published a method similar to the one developed by Hemker (1984). Steady flow in systems of aquifers separated by leaky layers was also treated by Strack (1989).

Hemker (1985), Hunt (1985), and Maas (1987b) extended their steady state solution method to obtain a solution for transient flow to a well in a confined or leaky multi-aquifer system. Hemker (1985) applied the Laplace and Hankel transforms, Maas (1987b) the Hankel and generalized Fourier transforms. Maas (1987b) also considered the compressibility of the separating aquitards. Both Hemker (1985) and Maas (1987b) applied analytical inversion techniques, whereas Hemker and Maas (1987) used the Stehfest (1970) algorithm to invert the obtained solution in Laplace space. According to Hemker (2000), inspiration was found in the work of Moench and Ogata (1981, 1984), who clearly demonstrated the simplicity of this numerical inversion technique. The solution by Hemker and Maas (1987) completely accounted for the effect of elastic storage in separating and bounding aquitards. Unaware of these results, Cheng and Morohunfola (1993) published a similar but less concise solution several years later (Hemker, 2000). Bruggeman (1999) presented an alternative expression to the one found by Hemker (1985).

By resolving the limitation on the number of aquifers, the generalized multi-aquifer solutions were a major breakthrough in well hydraulics. On the other hand, these models still adopted some of the simplifying assumptions made by their predecessors. Since each aquifer in multi-aquifer models is represented by a single layer in which vertical resistance to flow is neglected according to the Dupuit-Forchheimer approximation, Bakker (1999) called them multilayer Dupuit models, and he suggested to divide the aquifer layer in a number of sublayers separated by resistance layers of thickness zero when vertical flow is important. This suggestion was not new as Hemker (1984, 1985) already discussed the possibility to subdivide the aquifer layers. Hemker (1999a) called it a finite-difference technique, since finite-difference models apply the same approximation to simulate vertical flow (e.g. Reilly & Harbaugh, 1993).

Hemker (1999a) also considered a finite-diameter well by including the effect of wellbore storage, and Hemker (1999b) defined an additional boundary condition for the inner model boundary to account for uniform drawdown along the well screen. Bakker (2001) applied the finite-difference technique to the steady multi-aquifer solution in order to study the effect of partial penetration. Solutions for steady state groundwater flow in layered anisotropic aquifers were developed by Bakker and Hemker (2002) and Meesters et al. (2004). These solutions showed the possibility of whirling groundwater flow (Bakker & Hemker, 2004; Hemker & Bakker, 2006). Finally, Veling and Maas (2009) presented efficient strategies using integral transforms for solving the problem of transient radial flow to a partially penetrating well in a multi-aquifer system, where the vertical direction is fully taken into account, and where aquitards are treated in the same way as aquifers.

2.1.4 Generalized solution

In this chapter, the solution technique presented by Hemker (1984, 1985) is applied to derive a generalized semi-analytical solution for axisymmetric and parallel flow in multilayer systems. As illustrated by Hemker (1984), parallel flow towards a stream interacting with a multi-aquifer system can be treated in the same way as axisymmetric flow towards a well. The solution presented here is not restricted to leaky aquifer systems, but also includes confined systems, and even recharge may be taken into account. This allows for the simulation of flow in a multilayered aquifer system with a phreatic top layer. Hemker (1984, 1985) considered a well with infinitesimal radius in an unbounded aquifer system. Using the generalized solution, it is also possible to define an inner and outer

boundary at finite distance. Wellbore storage is not taken into account yet; this effect is considered and discussed in Chapter 6.

By conducting the Laplace transform as recommended by Hemker (1999a, 2000), both steady and transient flow solutions can be derived simultaneously, as the transient state solution in the Laplace domain is very similar to the steady state solution. Moreover, the use of the Laplace transform has proven to be very efficient (Hemker, 2000). It is implemented in the frequently used software program MLU (Hemker & Post, 2019), which has been reviewed very positively (Carlson & Randall, 2012). The multilayer transient analytic element model TTIm (Bakker, 2022) applies the same solution technique. The main difference between MLU and TTIm is that the first uses the Stehfest (1970) algorithm to perform the numerical inversion, whereas the latter uses the algorithm of de Hoog et al. (1982) (Bakker, 2013a, 2013b). Recall that the simulation of vertical flow in these models is treated similarly as in finite-difference models (Bakker, 1999; Hemker, 1984, 1985, 1999a, 2000).

After stating and solving the generalized problem of axisymmetric and parallel flow in a multilayer system, the principle of superposition is explained and applied to extend the solution to define time-dependent boundary conditions, and to simulate drawdown due to multiple wells. Superposition is a powerful mathematical technique that is discussed in many textbooks on hydrogeology (e.g. Bear, 1979; Bruggeman, 1999; Kruseman & de Ridder, 1990; Verruijt, 1970), and it also plays a key role in the analytic element method (Haitjema, 1995; Strack, 1989). Chapter 11 discusses the use of superposition models in the context of sustainable pumping. Finally, the generalized solution is used to derive some of the well-known analytical solutions discussed above. The solutions by de Glee (1930), Theis (1935), and Hantush and Jacob (1955) are also addressed in Chapter 10, where they are used to derive equations for estimating the radius of influence.

Historically, there was an evolution from simple one-dimensional steady-state solutions to the generalized transient-state multi-layer solutions, because the latter are mathematically much more involved. In this chapter, the generalized solution is presented first, from which the simpler well-known solutions are derived. In this way, it is clearly illustrated that these simple equations are special cases of the generalized solution, a fact that some groundwater practitioners do not realize. For instance, Lebbe (1999) presents these analytical models as less applicable compared to his generalized numerical multilayer approach, unaware of the fact that the same multilayer problem was solved semi-analytically almost fifteen years earlier by Hemker (1985). Moreover, using an axisymmetric model that is vertically discretized into many sublayers is not always required and even not recommended. This will be proven and demonstrated in Chapter 9.

2.2. Problem statement

In this section, the problem of axisymmetric and parallel flow in a multilayered aquifer system is stated mathematically. Both steady and transient flow are considered. The aquifer system may be bounded or unbounded, and the lower and upper boundary is leaky or confined. Each layer can be recharged by constant infiltration. The inner model boundary can be infinitesimal or finite, and it defines a constant head or a constant discharge.

Figure 1 visualizes the problem stated in this section. It shows how both axisymmetric flow to a well (A) and parallel flow to a stream (B) in a multilayered aquifer system can be represented by a vertical profile model (C). The aquifer is schematized into a number of horizontal homogeneous layers (colored in yellow) with constant transmissivity and storage coefficient. The layers are separated by zero-thickness resistance layers (colored in brown). Four layers are plotted in Figure 1 and the top layer is recharged by a constant infiltration flux. In practice, as many layers as necessary can be defined. The well or stream occurs at the left of the profile model, and it extracts water at constant

rate from each layer of the aquifer system. It is also possible to define a constant level in the well or the stream. The next paragraphs state this problem mathematically and define the parameters indicated on Figure 1.

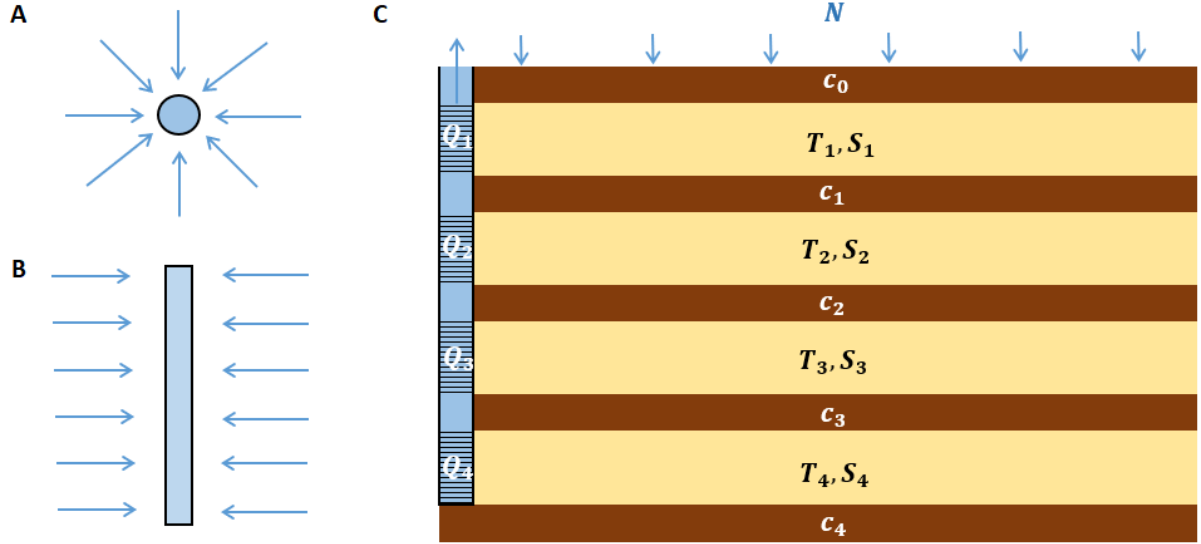


Figure 1. Visualization of the problem stated and solved analytically in this chapter. (A) Plan view of axisymmetric flow to a well. (B) Plan view of parallel flow to a stream. (C) Both are treated mathematically by defining a vertical profile model consisting of horizontal layers characterized by constant transmissivity T and constant storativity S , and separated by zero-thickness layers of constant resistance c . A system of 4 layers is shown; in practice, any number of layers can be defined. The top of the aquifer system is recharged by constant infiltration flux N , although it is possible to recharge each layer. Top and bottom resistances may be finite to implement a leaky boundary, or infinitely large to define an impervious boundary. The well or stream at the left of the profile model interacts with the aquifer system. Here, it discharges each layer at constant rate Q ; alternatively, a constant water level can be defined. See text for a more detailed explanation and definitions.

2.2.1 The multilayered aquifer system

As shown in Figure 1, the groundwater reservoir is assumed to consist of n_l horizontal layers, in which flow is strictly horizontal. Layers are numbered from the top down. Hydraulic head in layer i is denoted by h_i [L]. Each layer i is characterized by constant transmissivity T_i [L^2/T], which is the product of the layer thickness D_i [L] and the horizontal conductivity K_i^h [L/T]:

$$T_i = K_i^h D_i \quad (1 \leq i \leq n_l) \quad (1)$$

Each layer i is also characterized by a constant storativity S_i [-], which is the product of the layer thickness D_i and the specific elastic storage S_i^S [L^{-1}]:

$$S_i = S_i^S D_i \quad (1 \leq i \leq n_l) \quad (2)$$

Adjacent layers i and $i + 1$ are separated by an incompressible resistance layer with zero thickness characterized by hydraulic resistance c_i [T]. Flow between two layers is assumed to be strictly vertical. Resistances c_0 and c_{n_l} are assigned to the upper and lower boundary of the aquifer system, respectively. If the boundary is impervious, then the resistance is infinitely large.

If the i -th resistance layer between layers i and $i + 1$ corresponds to an aquitard, then its hydraulic resistance c_i is defined as the thickness of the aquitard D'_i [L] divided by its vertical conductivity $K_i^{v'}$ [L/T]:

$$c_i = \frac{D'_i}{K_i^{v'}} \quad (0 \leq i \leq n_l + 1) \quad (3)$$

Aquitards are not incompressible, however, and therefore, it is more appropriate to use the resistance layers to discretize the vertical flow in the aquifer system. In this case, resistance c_i between layers i and $i + 1$ is defined as:

$$c_i = \frac{D_i}{2K_i^v} + \frac{D_{i+1}}{2K_{i+1}^v} \quad (1 \leq i < n_l) \quad (4)$$

Calculating vertical resistance according to (4) comes down to the finite-difference approach (Hemker, 1999a). Figure 2 visualizes the two possible interpretations: the left plot corresponds to expression (3), the right plot to equation (4).

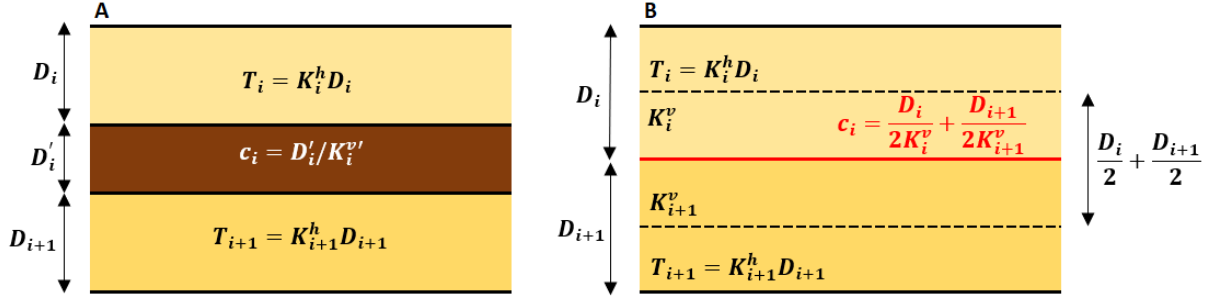


Figure 2. The left plot (A) visualizes the interpretation in which aquifers i and $i+1$ (yellow) are separated by an incompressible aquitard (brown). In this case, the flow in the aquifers is strictly horizontal and determined by transmissivities T_i and T_{i+1} , whereas the flow in the aquitard is strictly vertical and determined by resistance c_i . The right plot (B) shows the finite-difference approach where layers i and $i+1$ (yellow) are separated by a zero-thickness resistance layer (red line), to which the average vertical resistance c_i of both layers is assigned. This resistance determines the vertical flow between the two layers. Horizontal flow in the layers is still determined by transmissivities T_i and T_{i+1} . Parameter D is the thickness, parameters K^h and K^v are the horizontal and vertical conductivity, respectively. See text for the definition and the units of the parameters.

Each layer i may also be recharged at a constant flux N_i [L/T], which is positive in case of infiltration. In practice, only the top layer ($i = 1$) is recharged by infiltration when it is phreatic. In this case, recharge flux N_1 is not zero, storativity S_1 is set to specific yield S^y [-], resistance c_0 is infinitely large, and layer thickness D_1 is equal to the initial hydraulic head in this layer. As a constant layer thickness is assumed, the change in head in a phreatic top layer should be relatively small at all times. Chapter 8 discusses the problem of unconfined flow in the top layer considering a head-dependent thickness.

2.2.2 Groundwater flow equations

If axisymmetric radial flow towards a point sink or source is considered (Figure 1A), then groundwater flow in layer i is governed by the following partial differential equation:

$$\frac{\partial^2 h_i}{\partial r^2} + \frac{1}{r} \frac{\partial h_i}{\partial r} = \frac{S_i}{T_i} \frac{\partial h_i}{\partial t} + \frac{-N_i}{T_i} + \frac{h_i - h_{i-1}}{c_{i-1} T_i} + \frac{h_i - h_{i+1}}{c_i T_i} \quad (1 \leq i \leq n_l) \quad (5)$$

If parallel flow towards a horizontal line sink or source is considered (Figure 1B), then groundwater flow in layer i is governed by the following partial differential equation:

$$\frac{\partial^2 h_i}{\partial r^2} = \frac{S_i}{T_i} \frac{\partial h_i}{\partial t} + \frac{-N_i}{T_i} + \frac{h_i - h_{i-1}}{c_{i-1} T_i} + \frac{h_i - h_{i+1}}{c_i T_i} \quad (1 \leq i \leq n_l) \quad (6)$$

In equation (5), hydraulic head h_i is considered at radial distance r [L] from the point sink or source, whereas it is at horizontal distance r [L] from the line sink or source in equation (6). In both equation (5) and equation (6), hydraulic head h_i is also a function of time t [T]. The head within a layer is assumed not to vary in the vertical direction according to the Dupuit-Forchheimer approximation.

If flow is in a steady state, then $\frac{\partial h_i}{\partial t} = 0$, by definition, and equation (5) and equation (6) reduce to, respectively:

$$\frac{d^2 h_i}{dr^2} + \frac{1}{r} \frac{dh_i}{dr} = \frac{-N_i}{T_i} + \frac{h_i - h_{i-1}}{c_{i-1} T_i} + \frac{h_i - h_{i+1}}{c_i T_i} \quad (1 \leq i \leq n_l) \quad (7)$$

$$\frac{d^2 h_i}{dr^2} = \frac{-N_i}{T_i} + \frac{h_i - h_{i-1}}{c_{i-1} T_i} + \frac{h_i - h_{i+1}}{c_i T_i} \quad (1 \leq i \leq n_l) \quad (8)$$

In both equation (7) and equation (8), hydraulic head h_i is dependent on distance r only.

Hydraulic head h_i can be used to calculate the horizontal discharge applying Darcy's law. In case of axisymmetric flow, horizontal discharge $Q^h(r, t)$ [L^3/T] is defined as the amount of water per unit of time that flows radially at time t through the cylindrical surface with radius r :

$$Q_i^h(r, t) = -2\pi T_i r \frac{\partial h_i}{\partial r} \quad (9)$$

If radial flow is steady, then horizontal discharge is not a function of time:

$$Q_i^h(r) = -2\pi T_i r \frac{dh_i}{dr} \quad (10)$$

In case of parallel flow, horizontal discharge $Q^h(r, t)$ [L^2/T] is defined as the amount of water per unit of time that flows horizontally at time t through a vertical surface with unit width at distance r :

$$Q_i^h(r, t) = -T_i \frac{\partial h_i}{\partial r} \quad (11)$$

In case of steady parallel flow, then (11) must be written as:

$$Q_i^h(r) = -T_i \frac{dh_i}{dr} \quad (12)$$

To know the hydraulic head in a given layer and at a given distance and given time, system of differential equations (5), (6), (7), or (8) need to be solved for h , depending on the characteristics of the flow: radial or parallel, and transient or steady. To find a unique solution to these systems of equations, boundary conditions are required, and initial conditions in case of transient flow.

2.2.3 Initial and boundary conditions

The upper and the lower boundary of the layered aquifer system are characterized by resistances c_0 and c_{n_l} , and constant heads φ_0 [L] and φ_{n_l+1} [L], respectively:

$$h_0(r, t) = \varphi_0 \quad (13)$$

$$h_{n_l+1}(r, t) = \varphi_{n_l+1} \quad (14)$$

The outer boundary of the aquifer system is at distance r_{out} [L], at which a constant head φ_i [L] is defined in each layer i :

$$h_i(r_{out}, t) = \varphi_i \quad (1 \leq i \leq n_l) \quad (15)$$

The inner boundary of the aquifer system is at distance r_{in} [L], at which either a constant head H_i [L] is defined in each layer i or a constant flux q_i [L/T]. In case of a constant head, the inner boundary conditions are:

$$h_i(r_{in}, t) = H_i \quad (1 \leq i \leq n_l) \quad (16)$$

In case of a constant flux, the inner boundary conditions are given by Darcy's law:

$$K_i^h \frac{\partial h_i}{\partial r} = -q_i \quad (r = r_{in}; 1 \leq i \leq n_l) \quad (17)$$

Note that q_i is positive if water is added to the aquifer system. It is more convenient, however, to define a constant discharge Q_i [L^3/T] at the inner boundary of each layer i , and to reformulate equation (17) in terms of Q_i and transmissivity $T_i = K_i^h D_i$. In case of axisymmetric flow, this gives:

$$r \frac{\partial h_i}{\partial r} = \frac{-Q_i}{2\pi T_i} \quad (r = r_{in}; 1 \leq i \leq n_l) \quad (18)$$

In case of parallel flow, discharge Q_i [L^2/T] is defined per unit length of the line source or sink:

$$\frac{\partial h_i}{\partial r} = \frac{-Q_i}{T_i} \quad (r = r_{in}; 1 \leq i \leq n_l) \quad (19)$$

As constant heads and fluxes are considered which are time-independent, the boundary conditions are the same in the steady-state case. The only difference is that hydraulic head h_i is also time-independent, and therefore the partial derivative in (17), (18) and (19) must be replaced by $\frac{dh_i}{dr}$.

Finally, initial conditions at $t = 0$ are required in case of transient flow. These conditions are defined by setting the initial head in layer i to the constant head φ_i at the outer model boundary:

$$h_i(r, 0) = \varphi_i \quad (1 \leq i \leq n_l) \quad (20)$$

2.3. Generalized semi-analytical solution

To solve the problem stated in previous section 2.2, the method proposed by Hemker (1984, 1985) is used, which applies eigendecomposition to uncouple the system of differential equations defined in section 2.2.2. The transient state equations and corresponding initial and boundary conditions discussed in section 2.2.3, are Laplace transformed as suggested by Hemker (1999a, 2000). This transformation makes the transient state problem very similar to the steady state problem.

2.3.1 Laplace transform

In case of transient flow, the governing equations (5) and (6) are second-order partial differential equations, whereas steady-state equations (7) and (8) are second-order ordinary differential equations. Solving the latter is more straightforward, although it is possible to convert the former into ordinary differential equations by applying the Laplace transform in time variable t :

$$\mathcal{L}\{h_i(r, t)\}(p) = \bar{h}_i(r, p) \quad (21)$$

where the Laplace transform of head h is denoted by \bar{h} , and p is the frequency variable [T^{-1}].

Applying the Laplace transform (21) to partial differential equations (5) and (6) using initial condition (20), gives:

$$\nabla^2 \bar{h}_i = \frac{S_i}{T_i} p \bar{h}_i - \frac{S_i}{T_i} \varphi_i + \frac{-N_i}{p T_i} + \frac{\bar{h}_i - \bar{h}_{i-1}}{c_{i-1} T_i} + \frac{\bar{h}_i - \bar{h}_{i+1}}{c_i T_i} \quad (1 \leq i \leq n_l) \quad (22)$$

with $\nabla^2 \bar{h}_i = \frac{\partial^2 \bar{h}_i}{\partial r^2} + \frac{1}{r} \frac{\partial \bar{h}_i}{\partial r}$ in case of transient flow, and $\nabla^2 \bar{h}_i = \frac{\partial^2 \bar{h}_i}{\partial r^2}$ in case of steady flow.

The Laplace transform of horizontal discharge Q^h is:

$$\mathcal{L}\{Q_i^h(r, t)\}(p) = \bar{Q}_i^h(r, p) \quad (23)$$

In case of axisymmetric flow, the Laplace transform of horizontal discharge (23) can be calculated using the definition of horizontal discharge (9) and the Laplace transform of hydraulic head (21):

$$\bar{Q}_i^h(r, p) = -2\pi T_i r \frac{\partial \bar{h}_i}{\partial r} \quad (24)$$

In case of parallel flow, (21) and (23) are applied to definition (11):

$$\bar{Q}_i^h(r, p) = -T_i \frac{\partial \bar{h}_i}{\partial r} \quad (25)$$

Boundary conditions (13), (14), (15), and (16) are Laplace transformed into, respectively:

$$\bar{h}_0(r, p) = \frac{\varphi_0}{p} \quad (26)$$

$$\bar{h}_{n_l+1}(r, p) = \frac{\varphi_{n_l+1}}{p} \quad (27)$$

$$\bar{h}_i(r_{out}, p) = \frac{\varphi_i}{p} \quad (1 \leq i \leq n_l) \quad (28)$$

$$\bar{h}_i(r_{in}, p) = \frac{H_i}{p} \quad (1 \leq i \leq n_l) \quad (29)$$

Equation (29) is the Laplace transform of the inner constant-head boundary. In case of a constant discharge and axisymmetric flow, equation (18) is Laplace transformed:

$$r \frac{\partial \bar{h}_i}{\partial r} = \frac{-Q_i}{2\pi p T_i} \quad (r = r_{in}; 1 \leq i \leq n_l) \quad (30)$$

In case of parallel flow, equation (19) is Laplace transformed:

$$\frac{\partial \bar{h}_i}{\partial r} = \frac{-Q_i}{p T_i} \quad (r = r_{in}; 1 \leq i \leq n_l) \quad (31)$$

2.3.2 Matrix formulation

Steady-state equations (7) and (8) and the Laplace transformed transient state equation (22) define a system of n_l equations, which can be written more conveniently in matrix form:

$$\nabla^2 \mathbf{h} = \mathbf{A} \mathbf{h} - \mathbf{b} \quad (32)$$

where \mathbf{h} and \mathbf{b} are $n_l \times 1$ vectors, and \mathbf{A} is an $n_l \times n_l$ tridiagonal matrix. Recall that $\nabla^2 \mathbf{h} = \frac{\partial^2 \mathbf{h}}{\partial r^2} + \frac{1}{r} \frac{\partial \mathbf{h}}{\partial r}$ in case of radial flow, and $\nabla^2 \mathbf{h} = \frac{\partial^2 \mathbf{h}}{\partial r^2}$ in case of parallel flow.

If (32) expresses steady flow, then:

$$\mathbf{h}_i = h_i(r) \quad (33)$$

$$\mathbf{b}_i = \begin{cases} \frac{N_1}{T_1} + \frac{\varphi_0}{c_0 T_1} & (i = 1) \\ \frac{N_{n_l}}{T_{n_l}} + \frac{\varphi_{n_l+1}}{c_{n_l} T_{n_l}} & (i = n_l) \\ \frac{N_i}{T_i} & (1 < i < n_l) \end{cases} \quad (34)$$

$$A_{ij} = \begin{cases} \frac{1}{c_{i-1} T_i} + \frac{1}{c_i T_i} & (1 \leq i \leq n_l; j = i) \\ \frac{-1}{c_{i-1} T_i} & (1 < i \leq n_l; j = i - 1) \\ \frac{-1}{c_i T_i} & (1 \leq i < n_l; j = i + 1) \end{cases} \quad (35)$$

In the Laplace transformed transient-state case, \mathbf{h} , \mathbf{b} , and \mathbf{A} are defined as:

$$\mathbf{h}_i = \bar{h}_i(r, p) \quad (36)$$

$$\mathbf{b}_i = \begin{cases} \frac{N_1}{p T_1} + \frac{\varphi_0}{p c_0 T_1} + \frac{S_1}{T_1} \varphi_1 & (i = 1) \\ \frac{N_{n_l}}{p T_{n_l}} + \frac{\varphi_{n_l+1}}{p c_{n_l} T_{n_l}} + \frac{S_{n_l}}{T_{n_l}} \varphi_{n_l} & (i = n_l) \\ \frac{N_i}{p T_i} + \frac{S_i}{T_i} \varphi_i & (1 < i < n_l) \end{cases} \quad (37)$$

$$A_{ij} = \begin{cases} \frac{1}{c_{i-1} T_i} + \frac{1}{c_i T_i} + \frac{S_i}{T_i} p & (1 \leq i \leq n_l; j = i) \\ \frac{-1}{c_{i-1} T_i} & (1 < i \leq n_l; j = i - 1) \\ \frac{-1}{c_i T_i} & (1 \leq i < n_l; j = i + 1) \end{cases} \quad (38)$$

The i -th entry in \mathbf{h} and \mathbf{b} is denoted by \mathbf{h}_i and \mathbf{b}_i , respectively, and the entry on the i -th row and the j -th column of matrix \mathbf{A} is denoted by A_{ij} . If $j = i$, then the entry is on the main diagonal of \mathbf{A} ; if $j = i - 1$, then the entry is on the lower diagonal; and if $j = i + 1$, then the entry is on the upper diagonal; all other elements in \mathbf{A} are zero.

Definitions (10) and (12) of steady horizontal discharge and the Laplace-transformed expressions (24) and (25) of transient horizontal discharge can also be written in matrix form:

$$\mathbf{Q}^h = -\mathbf{T} \nabla \mathbf{h}(r) \quad (39)$$

In case of steady flow, then the i -th entry of \mathbf{Q}^h is:

$$\mathbf{Q}_i^h = Q_i^h(r) \quad (40)$$

In the transient case, the Laplace transform is considered:

$$\mathbf{Q}_i^h = \bar{Q}_i^h(r, p) \quad (41)$$

In case of axisymmetric flow, $\nabla \mathbf{h} = r \frac{\partial \bar{h}}{\partial r}$; in case of parallel flow, $\nabla \mathbf{h} = \frac{\partial \bar{h}}{\partial r}$; if flow is steady, then $\frac{\partial \bar{h}}{\partial r}$ must be replaced by $\frac{dh}{dr}$. In (39), \mathbf{T} is an $n_l \times n_l$ diagonal matrix. In case of axisymmetric flow, the nonzero entries are equal to:

$$\mathbf{T}_{ii} = 2\pi T_i \quad (42)$$

In case of parallel flow, the nonzero entries are:

$$\mathbf{T}_{ii} = T_i \quad (43)$$

The upper and the lower boundary condition are taken into account in elements \mathbf{b}_1 and \mathbf{b}_{n_l} , respectively. Using vector \mathbf{h} , the conditions at inner and outer boundary may also be written in matrix form. The outer boundary conditions are reformulated as:

$$\mathbf{h}(r_{out}) = \boldsymbol{\varphi} \quad (44)$$

with $\boldsymbol{\varphi}$ an $n_l \times 1$ vector. If flow is steady, the i -th entry of $\boldsymbol{\varphi}$ is defined as:

$$\boldsymbol{\varphi}_i = \varphi_i \quad (45)$$

In the Laplace transformed transient-state case, the i -th entry is:

$$\boldsymbol{\varphi}_i = \frac{\varphi_i}{p} \quad (46)$$

The constant-head inner boundary conditions are in matrix form expressed as:

$$\mathbf{h}(r_{in}) = \mathbf{H} \quad (47)$$

with \mathbf{H} an $n_l \times 1$ vector. In the steady-state case, the i -th element of \mathbf{H} is:

$$\mathbf{H}_i = H_i \quad (48)$$

In the Laplace transformed transient-state case, the i -th element is:

$$\mathbf{H}_i = \frac{H_i}{p} \quad (49)$$

The constant-flux inner boundary conditions are reformulated as follows:

$$\nabla \mathbf{h}(r_{in}) = -\mathbf{T}^{-1} \mathbf{Q} \quad (50)$$

with \mathbf{Q} an $n_l \times 1$ vector. In case of steady state, it is defined as:

$$\mathbf{Q}_i = Q_i \quad (51)$$

In the Laplace transformed transient-state case, the i -th entry is:

$$\mathbf{Q}_i = \frac{Q_i}{p} \quad (52)$$

2.3.3 General solution

System of equations (32) is solved by decomposing matrix \mathbf{A} using its eigenvalues and corresponding eigenvectors:

$$\nabla^2 \mathbf{h} = \mathbf{V} \mathbf{D} \mathbf{V}^{-1} \mathbf{h} - \mathbf{b} \quad (53)$$

where \mathbf{D} is an $n_l \times n_l$ diagonal matrix containing the n_l eigenvalues d_i , and \mathbf{V} is an $n_l \times n_l$ matrix containing the corresponding eigenvectors in its columns. Multiplying both sides of (53) by \mathbf{V}^{-1} , and substituting $\mathbf{V}^{-1} \mathbf{h}$ by \mathbf{g} and $\mathbf{V}^{-1} \mathbf{b}$ by \mathbf{v} gives:

$$\nabla^2 \mathbf{g} = \mathbf{D} \mathbf{g} - \mathbf{v} \quad (54)$$

Because \mathbf{D} is a diagonal matrix, equation (54) expresses a system of uncoupled ordinary differential equations. In case of axisymmetric flow, the general solution of this system is:

$$\mathbf{g}_i(r) = \begin{cases} \boldsymbol{\alpha}_i \ln(r) + \boldsymbol{\beta}_i - \frac{\mathbf{v}_i r^2}{4} & (d_i = 0) \\ \boldsymbol{\alpha}_i I_0(r\sqrt{d_i}) + \boldsymbol{\beta}_i K_0(r\sqrt{d_i}) + \frac{\mathbf{v}_i}{d_i} & (d_i \neq 0) \end{cases} \quad (55)$$

Functions I_0 and K_0 are the zero order modified Bessel functions of the first and second kind, respectively. In case of parallel flow, the general solution is:

$$\mathbf{g}_i(r) = \begin{cases} \boldsymbol{\alpha}_i r + \boldsymbol{\beta}_i - \frac{\mathbf{v}_i r^2}{2} & (d_i = 0) \\ \boldsymbol{\alpha}_i e^{(r\sqrt{d_i})} + \boldsymbol{\beta}_i e^{-(r\sqrt{d_i})} + \frac{\mathbf{v}_i}{d_i} & (d_i \neq 0) \end{cases} \quad (56)$$

The only case in which one of the eigenvalues d_i is zero, is when flow is steady and the aquifer system is confined, i.e. $c_0 = c_{nl} = \infty$.

In (55) and (56), $\boldsymbol{\alpha}$ and $\boldsymbol{\beta}$ are $n_l \times 1$ vectors with constants that are determined by applying the boundary conditions. Multiplying both sides of equations (44), (47), and (50) by \mathbf{V}^{-1} , and substituting $\mathbf{V}^{-1}\mathbf{h}$ by \mathbf{g} , $\mathbf{V}^{-1}\boldsymbol{\varphi}$ by \mathbf{w} , $\mathbf{V}^{-1}\mathbf{H}$ by \mathbf{u} , and $\mathbf{V}^{-1}\mathbf{T}^{-1}\mathbf{Q}$ by \mathbf{q} , gives:

$$\mathbf{g}(r_{out}) = \mathbf{w} \quad (57)$$

$$\mathbf{g}(r_{in}) = \mathbf{u} \quad (58)$$

$$\nabla \mathbf{g}(r_{in}) = -\mathbf{q} \quad (59)$$

Recall that $\nabla \mathbf{g} = r \frac{\partial \mathbf{g}}{\partial r}$ in case of axisymmetric flow, which is found using (55):

$$\nabla \mathbf{g}_i(r) = \begin{cases} \boldsymbol{\alpha}_i - \frac{\mathbf{v}_i r^2}{2} & (d_i = 0) \\ (r\sqrt{d_i})[\boldsymbol{\alpha}_i I_1(r\sqrt{d_i}) - \boldsymbol{\beta}_i K_1(r\sqrt{d_i})] & (d_i \neq 0) \end{cases} \quad (60)$$

In case of parallel flow, $\nabla \mathbf{g} = \frac{\partial \mathbf{g}}{\partial r}$, which is found using (56):

$$\nabla \mathbf{g}_i(r) = \begin{cases} \boldsymbol{\alpha}_i - \mathbf{v}_i r & (d_i = 0) \\ \sqrt{d_i} [\boldsymbol{\alpha}_i e^{(r\sqrt{d_i})} - \boldsymbol{\beta}_i e^{-(r\sqrt{d_i})}] & (d_i \neq 0) \end{cases} \quad (61)$$

Recall that $\frac{\partial \mathbf{g}}{\partial r}$ must be replaced by $\frac{d \mathbf{g}}{dr}$ if flow is steady.

In the next two sections, the expressions to calculate $\boldsymbol{\alpha}_i$ and $\boldsymbol{\beta}_i$ are derived for all possible cases. Once $\boldsymbol{\alpha}$ and $\boldsymbol{\beta}$ are determined, hydraulic heads in all layers and at any given distance r are found by evaluating:

$$\mathbf{h}(r) = \mathbf{V} \mathbf{g}(r) \quad (62)$$

since $\mathbf{V}^{-1}\mathbf{h} = \mathbf{g}$, where \mathbf{g} is calculated using (55) or (56), depending on whether flow is axisymmetric or parallel, respectively. In the transient case, $\mathbf{h}_i = \bar{h}_i(r, p)$ according to (36), and therefore, \mathbf{h} calculated using (62) needs to be inverted to the real time domain. This can be done numerically, for instance, by applying the Stehfest (1970) algorithm:

$$h_i(r, t) = \frac{\ln 2}{t} \sum_{k=1}^N \omega_k \bar{h}_i(r, k \ln 2/t) \quad (63)$$

where N is an even integer, and ω_k is calculated as:

$$\omega_k = (-1)^{N/2+k} \sum_{j=\frac{k+1}{2}}^{\min(k,N/2)} \frac{j^{N/2}(2j)!}{(N/2-j)!(j)!(j-1)!(k-j)!(2j-k)!} \quad (64)$$

The optimal value for Stehfest number N is problem-specific. Theoretically, greater values improve the result; in practice, rounding errors limit this value. Hemker and Maas (1987) recommend $N = 10$.

Horizontal discharges in all layers and at any given distance r are found by multiplying both sides of equation (39) by $\mathbf{V}^{-1}\mathbf{T}^{-1}$, substituting $\mathbf{V}^{-1}\nabla\mathbf{h}$ by $\nabla\mathbf{g}$, and finally, multiplying both sides by \mathbf{TV} :

$$\mathbf{Q}^h(r) = -\mathbf{TV}\nabla\mathbf{g}(r) \quad (65)$$

Recall that $\nabla\mathbf{g}$ is evaluated using (60) or (61), depending on whether flow is axisymmetric or parallel, respectively. In the transient case, $\mathbf{Q}_i^h = \bar{Q}_i^h(r, p)$ according to (41), and the inversion to the real time domain can also be done numerically applying the Stehfest (1970) algorithm:

$$Q_i^h(r, t) = \frac{\ln 2}{t} \sum_{k=1}^N \omega_k \bar{Q}_i^h(r, k \ln 2/t) \quad (66)$$

2.3.4 Axisymmetric flow constants

In case of axisymmetric flow and constant head at the inner boundary, α_i and β_i are found by introducing (55) into (57) and (58). If $d_i \neq 0$, this gives:

$$\alpha_i = \frac{K_0(r_{in}\sqrt{d_i}) \left[\frac{\mathbf{v}_i}{d_i} - \mathbf{w}_i \right] + K_0(r_{out}\sqrt{d_i}) \left[\mathbf{u}_i - \frac{\mathbf{v}_i}{d_i} \right]}{K_0(r_{out}\sqrt{d_i}) I_0(r_{in}\sqrt{d_i}) - K_0(r_{in}\sqrt{d_i}) I_0(r_{out}\sqrt{d_i})} \quad (67)$$

$$\beta_i = \frac{I_0(r_{out}\sqrt{d_i}) \left[\frac{\mathbf{v}_i}{d_i} - \mathbf{u}_i \right] + I_0(r_{in}\sqrt{d_i}) \left[\mathbf{w}_i - \frac{\mathbf{v}_i}{d_i} \right]}{K_0(r_{out}\sqrt{d_i}) I_0(r_{in}\sqrt{d_i}) - K_0(r_{in}\sqrt{d_i}) I_0(r_{out}\sqrt{d_i})} \quad (68)$$

If $d_i = 0$, then:

$$\alpha_i = \frac{\frac{\mathbf{v}_i}{4} [r_{in}^2 - r_{out}^2] + \mathbf{u}_i - \mathbf{w}_i}{\ln\left(\frac{r_{in}}{r_{out}}\right)} \quad (69)$$

$$\beta_i = \frac{\ln(r_{in}) \left[\frac{\mathbf{v}_i r_{out}^2}{4} + \mathbf{w}_i \right] - \ln(r_{out}) \left[\frac{\mathbf{v}_i r_{in}^2}{4} + \mathbf{u}_i \right]}{\ln\left(\frac{r_{in}}{r_{out}}\right)} \quad (70)$$

To obtain a real and finite solution in this case, r_{in} may not be equal to zero, and if one of the eigenvalues equals zero, r_{out} may not be infinitely large. If all eigenvalues are nonzero, then $\alpha_i \rightarrow 0$ if $r_{out} \rightarrow \infty$, and:

$$\beta_i \rightarrow \frac{\mathbf{u}_i - \frac{\mathbf{v}_i}{d_i}}{K_0(r_{in}\sqrt{d_i})} \quad (r_{out} \rightarrow \infty) \quad (71)$$

In case of axisymmetric flow and constant discharge at the inner boundary, α_i and β_i are found by introducing (55) into (57) and introducing (60) into (59). If $d_i \neq 0$, this gives:

$$\alpha_i = \frac{(r_{in}\sqrt{d_i})K_1(r_{in}\sqrt{d_i})\left[\mathbf{w}_i - \frac{\mathbf{v}_i}{d_i}\right] - K_0(r_{out}\sqrt{d_i})\mathbf{q}_i}{(r_{in}\sqrt{d_i})[K_0(r_{out}\sqrt{d_i})I_1(r_{in}\sqrt{d_i}) + K_1(r_{in}\sqrt{d_i})I_0(r_{out}\sqrt{d_i})]} \quad (72)$$

$$\beta_i = \frac{(r_{in}\sqrt{d_i})I_1(r_{in}\sqrt{d_i})\left[\mathbf{w}_i - \frac{\mathbf{v}_i}{d_i}\right] + I_0(r_{out}\sqrt{d_i})\mathbf{q}_i}{(r_{in}\sqrt{d_i})[K_0(r_{out}\sqrt{d_i})I_1(r_{in}\sqrt{d_i}) + K_1(r_{in}\sqrt{d_i})I_0(r_{out}\sqrt{d_i})]} \quad (73)$$

If $d_i = 0$, then:

$$\alpha_i = \frac{\mathbf{v}_i r_{in}^2}{2} - \mathbf{q}_i \quad (74)$$

$$\beta_i = \frac{\mathbf{v}_i r_{out}^2}{4} + \mathbf{w}_i - \alpha_i \ln(r_{out}) \quad (75)$$

If $d_i = 0$, then r_{in} may be equal to zero. However, from (75), it follows that heads become infinitely large if $r_{out} \rightarrow \infty$.

If $d_i \neq 0$, then $\alpha_i \rightarrow 0$ if $r_{out} \rightarrow \infty$, and:

$$\beta_i = \frac{\mathbf{q}_i}{r_{in}\sqrt{d_i}K_1(r_{in}\sqrt{d_i})} \quad (r_{out} \rightarrow \infty) \quad (76)$$

If $d_i \neq 0$, then $\beta_i \rightarrow \mathbf{q}_i$ if $r_{in} \rightarrow 0$, and:

$$\alpha_i = \frac{\mathbf{w}_i - \frac{\mathbf{v}_i}{d_i} - \mathbf{q}_i K_0(r_{out}\sqrt{d_i})}{I_0(r_{out}\sqrt{d_i})} \quad (r_{in} \rightarrow 0) \quad (77)$$

If $d_i \neq 0$, then $\alpha_i \rightarrow 0$ and $\beta_i \rightarrow \mathbf{q}_i$ if $r_{in} \rightarrow 0$ and $r_{out} \rightarrow \infty$.

2.3.5 Parallel flow constants

In case of parallel flow and constant head at the inner boundary, α_i and β_i are found by introducing (56) into (57) and (58). If $d_i \neq 0$, this gives:

$$\alpha_i = \frac{e^{-(r_{in}\sqrt{d_i})}\left[\frac{\mathbf{v}_i}{d_i} - \mathbf{w}_i\right] + e^{-(r_{out}\sqrt{d_i})}\left[\mathbf{u}_i - \frac{\mathbf{v}_i}{d_i}\right]}{e^{(r_{in}-r_{out})\sqrt{d_i}} - e^{(r_{out}-r_{in})\sqrt{d_i}}} \quad (78)$$

$$\beta_i = \frac{e^{(r_{out}\sqrt{d_i})}\left[\frac{\mathbf{v}_i}{d_i} - \mathbf{u}_i\right] + e^{(r_{in}\sqrt{d_i})}\left[\mathbf{w}_i - \frac{\mathbf{v}_i}{d_i}\right]}{e^{(r_{in}-r_{out})\sqrt{d_i}} - e^{(r_{out}-r_{in})\sqrt{d_i}}} \quad (79)$$

If $d_i = 0$, then:

$$\alpha_i = \frac{\frac{\mathbf{v}_i}{2}[r_{in}^2 - r_{out}^2] + \mathbf{u}_i - \mathbf{w}_i}{r_{in} - r_{out}} \quad (80)$$

$$\beta_i = \frac{\left[\frac{\mathbf{v}_i r_{out}^2}{2} + \mathbf{w}_i\right]r_{in} - \left[\frac{\mathbf{v}_i r_{in}^2}{2} + \mathbf{u}_i\right]r_{out}}{r_{in} - r_{out}} \quad (81)$$

If $d_i = 0$, then r_{out} must be finite. If $d_i \neq 0$, then $\alpha_i \rightarrow 0$ if $r_{out} \rightarrow \infty$, and:

$$\beta_i \rightarrow \frac{\mathbf{u}_i - \frac{\mathbf{v}_i}{d_i}}{e^{-(r_{in}\sqrt{d_i})}} \quad (r_{out} \rightarrow \infty) \quad (82)$$

In case of parallel flow and constant discharge at the inner boundary, α_i and β_i are found by introducing (56) into (57) and introducing (61) into (59). If $d_i \neq 0$, this gives:

$$\alpha_i = \frac{\sqrt{d_i} e^{-(r_{in}\sqrt{d_i})} \left[\mathbf{w}_i - \frac{\mathbf{v}_i}{d_i} \right] - e^{-(r_{out}\sqrt{d_i})} \mathbf{q}_i}{\sqrt{d_i} \left[e^{(r_{in}-r_{out})\sqrt{d_i}} + e^{(r_{out}-r_{in})\sqrt{d_i}} \right]} \quad (83)$$

$$\beta_i = \frac{e^{(r_{out}\sqrt{d_i})} \mathbf{q}_i + \sqrt{d_i} e^{(r_{in}\sqrt{d_i})} \left[\mathbf{w}_i - \frac{\mathbf{v}_i}{d_i} \right]}{\sqrt{d_i} \left[e^{(r_{in}-r_{out})\sqrt{d_i}} + e^{(r_{out}-r_{in})\sqrt{d_i}} \right]} \quad (84)$$

If $d_i = 0$, then:

$$\alpha_i = \mathbf{v}_i r_{in} - \mathbf{q}_i \quad (85)$$

$$\beta_i = \frac{\mathbf{v}_i r_{out}^2}{2} + \mathbf{w}_i - \alpha_i r_{out} \quad (86)$$

If $d_i = 0$, then r_{out} must be finite. If $d_i \neq 0$, then $\alpha_i \rightarrow 0$ if $r_{out} \rightarrow \infty$, and:

$$\beta_i \rightarrow \frac{\mathbf{q}_i}{e^{-(r_{in}\sqrt{d_i})}\sqrt{d_i}} \quad (r_{out} \rightarrow \infty) \quad (87)$$

If flow is parallel, r_{in} may be set to zero in all cases.

2.4. The superposition principle

The generalized solution derived in previous section 2.3 defines constant boundary conditions, i.e. conditions that are not varying with time. In many cases, this is acceptable, like for the impervious or leaky boundary on top and at the bottom of the system. But sometimes boundary conditions are time dependent, like a well extracting groundwater at time-varying pumping rates, or a stream in which the water level fluctuates over time. Also groundwater problems often involve multiple wells whose effect cannot be simulated applying the axisymmetric solution presented in this chapter.

Fortunately, the principle of superposition provides a straightforward way to overcome these shortcomings. Superposition solves a complex problem by adding solutions of individual parts of that problem, or in other words, it calculates the total effect of multiple stresses by summing the individual effects of these stresses (Reilly et al., 1987). The classical example is the simulation of the total drawdown due to several pumping wells by summing the drawdown caused by the individual wells.

The theory of superposition only applies to linear systems in which groundwater flow is governed by linear differential equations (Reilly et al., 1987). Bruggeman (1999) even states that the superposition or linearity principle only applies to homogeneous linear differential equations, although it is justified in some cases to superimpose solutions of the homogeneous Laplace equation on a solution of the nonhomogeneous Poisson equation (e.g. Haitjema, 1995). Bruggeman (1999) also explains that in case of boundary value problems both the individual solutions and the resulting composite solution must satisfy all boundary and initial conditions. According to Reilly et al. (1987), one should keep in mind that the individual solutions describe changes in head rather than actual heads in the system.

This implies that a boundary condition in a model that simulates an individual solution represents the change in head or flux at that boundary.

2.4.1 Mathematical description

Mathematically, the superposition principle is valid if a linear combination of individual solutions is a solution to the boundary value problem that must be solved. Here, a linear combination of the hydraulic head $h_i(r, t)$ in a multi-layer system is considered:

$$h_i(r, t) = \sum_k a_k s_{i,k}(r, t) \quad (88)$$

with a_k an arbitrary constant and $s_{i,k}(r, t)$ the head change [L] in layer i at distance r and time t . If the head change expresses a lowering of the head, then s is also called drawdown. Subscript k refers to the k -th solution. As $s_{i,k}(r, t)$ is a solution to the boundary value problem stated in section 2.2, it is a solution to the following set of partial differential equations:

$$\nabla^2 s_i = \frac{S_i}{T_i} \frac{\partial s_i}{\partial t} + \frac{-\Delta N_i}{T_i} + \frac{s_i - s_{i-1}}{c_{i-1} T_i} + \frac{s_i - s_{i+1}}{c_i T_i} \quad (1 \leq i \leq n_l) \quad (89)$$

where $\nabla^2 s = \frac{\partial^2 s}{\partial r^2} + \frac{1}{r} \frac{\partial s}{\partial r}$ in case of axisymmetric flow, and $\nabla^2 s = \frac{\partial^2 s}{\partial r^2}$ in case of parallel flow. Subscript k is omitted for notational convenience. Note that (89) takes into account a change in recharge ΔN . Head change $s_{i,k}(r, t)$ must also satisfy the initial and the boundary conditions:

$$s_i(r, 0) = \Delta \varphi_i \quad (1 \leq i \leq n_l) \quad (90)$$

$$s_0(r, t) = \Delta \varphi_0 \quad (91)$$

$$s_{n_l+1}(r, t) = \Delta \varphi_{n_l+1} \quad (92)$$

$$s_i(r_{out}, t) = \Delta \varphi_i \quad (1 \leq i \leq n_l) \quad (93)$$

$$s_i(r_{in}, t) = \Delta H_i \quad (1 \leq i \leq n_l) \quad (94)$$

$$\nabla s_i(r_{in}, t) = \frac{-\Delta Q_i}{T_i} \quad (1 \leq i \leq n_l) \quad (95)$$

where $\nabla s = 2\pi r \frac{\partial s}{\partial r}$ in case of radial flow, and $\nabla s = \frac{\partial s}{\partial r}$ in case of parallel flow. In each of these equations, a change in constant head or discharge is considered, which is denoted by the Δ symbol. Recall that the inner boundary condition is defined by either a constant change in head or discharge, defined by (94) or (95), respectively.

The governing differential equations are linear, since head h or head change s and the derivatives of h or s with respect to distance r or time t that appear in these equations, are of the first degree (Bruggeman, 1999). Here, the linearity property also holds for the first and second derivatives of h with respect to r and t :

$$\nabla h_i(r, t) = \sum_k a_k \nabla s_{i,k}(r, t) \quad (96)$$

$$\nabla^2 h_i(r, t) = \sum_k a_k \nabla^2 s_{i,k}(r, t) \quad (97)$$

$$\frac{\partial h_i(r, t)}{\partial t} = \sum_k a_k \frac{\partial s_{i,k}(r, t)}{\partial t} \quad (98)$$

Finally, the linear combination should also be applied to recharge and discharge, and to initial and constant heads:

$$N_i = \sum_k a_k \Delta N_{i,k} \quad (99)$$

$$Q_i = \sum_k a_k \Delta Q_{i,k} \quad (100)$$

$$\varphi_i = \sum_k a_k \Delta \varphi_{i,k} \quad (101)$$

$$H_i = \sum_k a_k \Delta H_{i,k} \quad (102)$$

These equations clearly show why it is common practice to assume that the conditions at the lower, upper and outer model boundaries do not vary with time (Reilly et al., 1987). Indeed, if there is no change in recharge, or $\Delta N_{i,k} = 0$, and the specified heads at those boundaries are constant, or $\Delta \varphi_{i,k} = 0$, then applying the superposition method is very straightforward, since all individual solutions $s_{i,k}$ as well as the composite solution h_i automatically satisfy the zero-potential and zero-flux initial and boundary conditions. That is also why Bruggeman (1999) restricts the superposition principle to homogeneous differential equations that describe groundwater flow without recharge, or $N_i = 0$. The role of recharge in simulating the cone of depression of an extraction applying the superposition method is elaborated on in Chapter 11.

The specified heads or discharges at the inner model boundary representing the well in case of radial flow or the stream in case of parallel flow are nonzero, and the calculated head change s_i is due to this well or stream only, in case the other boundary conditions do not change. It is possible, however, to superimpose these head changes on the heads that are simulated using the same model but defining zero-head or zero-discharge at the inner model boundary and nonzero constant heads and/or nonzero recharge at the other model boundaries. These heads could be interpreted as the initial heads $h_i(r, 0)$ that reflect the pre-development conditions in the aquifer system:

$$h_i(r, t) = h_i(r, 0) + s_i(r, t) \quad (1 \leq i \leq n_l) \quad (103)$$

The well-known island example discussed in section 2.5.3 clearly demonstrates this. From (103), it follows that in most cases, the initial no-flow condition commonly assumed in pumping test interpretation (e.g. Kruseman & de Ridder, 1990) is too strict.

Equations (100) and (102) also show that the extraction of water from the individual layers may be simulated separately, after which the resulting changes in head $s_{i,k}$ can be summed to obtain the total head change s_i^{tot} in each layer i :

$$s_i^{tot}(r, t) = \sum_{k=1}^{n_l} s_{i,k}(r, t) \quad (1 \leq i \leq n_l) \quad (104)$$

In equation (104), $s_{i,k}$ is the head change due to pumping in layer k only, or $Q_k \neq 0$ and $Q_{i \neq k} = 0$.

If pumping rates or water levels at the inner model boundary are multiplied by a factor, then the resulting head change is multiplied by the same factor. This means the following relation is true:

$$\mathbf{s}(r, t) = \mathbf{H}\boldsymbol{\sigma}(r, t) \quad (105)$$

or:

$$\mathbf{s}(r, t) = \mathbf{Q}\boldsymbol{\sigma}(r, t) \quad (106)$$

where vector \mathbf{s} contains the head change for each layer i :

$$s_i = s_i(r, t) \quad (1 \leq i \leq n_l) \quad (107)$$

and vector $\boldsymbol{\sigma}$ contains the head change for each layer i corresponding to unit discharge or unit head change at the inner boundary:

$$\sigma_i(r_{in}, t) = 1 \quad (1 \leq i \leq n_l) \quad (108)$$

$$\nabla\sigma_i(r_{in}, t) = \frac{-1}{T_i} \quad (1 \leq i \leq n_l) \quad (109)$$

Making use of property (105) or (106) can save a lot of computation time, for instance when solving problems of maximizing pumping rates that are subject to drawdown constraints. This is illustrated in Chapter 12 for the optimization of a drainage system consisting of multiple pumping and injection wells.

In the examples discussed in this paragraph, the individual solutions and the composite solution are all solutions to the boundary value problem that is stated in section 2.2. In the next two paragraphs, individual solutions to this boundary value problem are superimposed to solve more complex boundary value problems, illustrating the real added value of the superposition technique.

2.4.2 Superposition in time

Suppose the inner model boundary condition is varying with time. In this case, it is common to discretize the total simulation period into stress periods in which the stresses are constant:

$$h_i(r_{in}, t) = H_{i,k} \quad (1 \leq i \leq n_l, \tau_{k-1} \leq t < \tau_k) \quad (110)$$

$$\nabla h_i(r_{in}, t) = \frac{-Q_{i,k}}{T_i} \quad (1 \leq i \leq n_l, \tau_{k-1} \leq t < \tau_k) \quad (111)$$

Equation (110) defines a time-varying specified head at the inner model boundary, whereas condition (111) defines a time-varying and specified discharge. In the k -th stress period between times τ_{k-1} and τ_k , head $H_{i,k}$ or discharge $Q_{i,k}$ is constant. The starting time of the first stress period is τ_0 and it corresponds to the start of the simulation, i.e. $\tau_0 = 0$. As the inner boundary value is constant within a stress period, the solution derived in section 2.3 may be used to simulate the head change during each stress period. Applying the superposition principle in this way could be thought of as if a new well is added to the first well at the beginning of each stress period to simulate the change in head due to the change in discharge or head at the inner boundary. Mathematically, this is expressed as follows (e.g. Lebbe, 1999):

$$\mathbf{s}(r, t) = \sum_k (\mathbf{W}_k - \mathbf{W}_{k-1})\boldsymbol{\sigma}(r, \Delta t_k) \quad \text{with } \Delta t_k = t - \tau_{k-1} \quad (112)$$

where vector \mathbf{W}_k holds the constant heads $H_{i,k}$ or constant pumping rates $Q_{i,k}$ for stress period k . Recall that vector $\boldsymbol{\sigma}$ contains the head changes in each layer i corresponding to unit discharge or unit head change at the inner boundary. Note that these head changes are calculated at time Δt_k

relatively to the beginning of stress period k . In this case, the initial heads are zero, as are the constant heads at the other model boundaries, i.e. $\Delta\varphi_{i,k} = 0$. Infiltration is also canceled out, i.e. $\Delta N_{i,k} = 0$, although vector s may be superimposed on initial heads that do take into account recharge N and nonzero constant heads φ , according to equation (103).

2.4.3 Superposition in space

The superposition principle is also applied to simulate the total head change due to multiple wells. In this case, groundwater flow is described using a Cartesian coordinate system, and the governing system of partial differential equations (89) is reformulated as:

$$\frac{\partial^2 s_i}{\partial x^2} + \frac{\partial^2 s_i}{\partial y^2} = \frac{S_i}{T_i} \frac{\partial s_i}{\partial t} + \frac{s_i - s_{i-1}}{c_{i-1} T_i} + \frac{s_i - s_{i+1}}{c_i T_i} \quad (1 \leq i \leq n_l) \quad (113)$$

In (113), head change $s_i(x, y, t)$ in layer i at time t does not depend on distance r from the well, but on the coordinate (x, y) of the point in which the head change is defined. As the change in head is simulated, infiltration is omitted in (113), and initial heads and constant heads at the boundaries are also set to zero. It is justified, however, to superimpose the head changes $s_i(x, y, t)$ to the initial heads $h_i(x, y, 0)$ that describe the flow in the multi-layered aquifer system before pumping started. As explained in 2.4.1, this initial flow may take into account infiltration and linearly responding sources and sinks.

As expression (113) defines a system of homogeneous linear differential equations, the superposition property is valid, and the total head change caused by multiple wells can be calculated as the sum of the head changes due to the individual wells (e.g. Lebbe, 1999):

$$s(x, y, t) = \sum_w Q_w \sigma(\rho_w, t) \quad \text{with } \rho_w = \sqrt{(x - x_w)^2 + (y - y_w)^2} \quad (114)$$

where (x_w, y_w) is the coordinate of well w which extracts from or injects into layer i at rate $Q_{i,w}$. These pumping rates are the entries of vector \mathbf{Q}_w . Recall that vector σ contains the head changes in each layer i due to pumping at unit rate. These are calculated using the axisymmetric solution derived in section 2.3, where the radial distance ρ_w equals the distance between point (x, y) and well w . Note that this distance reflects the conversion from Cartesian to polar coordinates.

In the strict mathematical sense, solution (114) only holds for radial flow to wells with infinitesimal radius. Finite-diameter wells indeed disturb the groundwater flow, although this effect may be neglected if the well diameter is relatively small. Specified-head wells are not allowed as the change in head caused by the other wells must be added to the head in the well, which violates the constant-head condition. Therefore, only wells with specified discharges are allowed, although these rates may vary with time applying expression (112).

A final condition concerns the outer boundary. In the axisymmetric solution, this boundary is a circle, and therefore, it should be at an infinitely large distance when applying superposition according to (114). If the aquifer system has a leaky upper or lower boundary, or if the flow regime is transient, then this condition is feasible. In case of steady confined flow, however, an outer boundary at infinity leads to infinite changes in head. In this case, one should define a zero-drawdown boundary condition in one point (x_0, y_0) that lies at a finite distance from each well. Distance $r_{out,w}$ of the outer boundary in the model simulating the steady change in head due to well w is equal to $\sqrt{(x_0 - x_w)^2 + (y_0 - y_w)^2}$. Bakker & Strack (2003) show that superposition applied in this way may be used to simulate steady confined multi-aquifer flow that also considers the effect of areal recharge and line sinks.

The assumption of an aquifer system of infinite extent may be circumvented by applying the method of images. As suggested by its name, this method uses superimposed image wells to bound the aquifer system laterally. It is a well-known technique discussed in many hydrogeology textbooks (e.g. Bruggeman, 1999; Haitjema, 1995; Lebbe, 1999; Strack, 1989; Verruijt, 1970). An example of a well extracting a homogeneous aquifer and depleting a nearby stream is given in section 2.5.8.

2.5. Well-known analytical solutions

In this section, the general solution derived in section 2.3 is simplified to well-known solutions for groundwater flow in one- and two-layer systems. Most of these solutions were discussed in the introduction 2.1. and are well-known and frequently used in daily hydrogeological practice. Here, they are used to verify the generalized semi-analytical multilayer solution.

2.5.1 Darcy's law

Consider a homogeneous aquifer with constant transmissivity T from which groundwater is drained at constant rate Q by a fully penetrating stream with a half-width equal to r_{in} . As there is one layer only, $n_l = 1$, and subscript $i = 1$ is omitted. At distance r_{out} , a constant head φ is considered. The aquifer may be interpreted as confined, i.e. $c_0 = c_1 = \infty$ and $N = 0$; hence, the right-hand side of the governing differential equation (32) is zero, and consequently, $v = 0$.

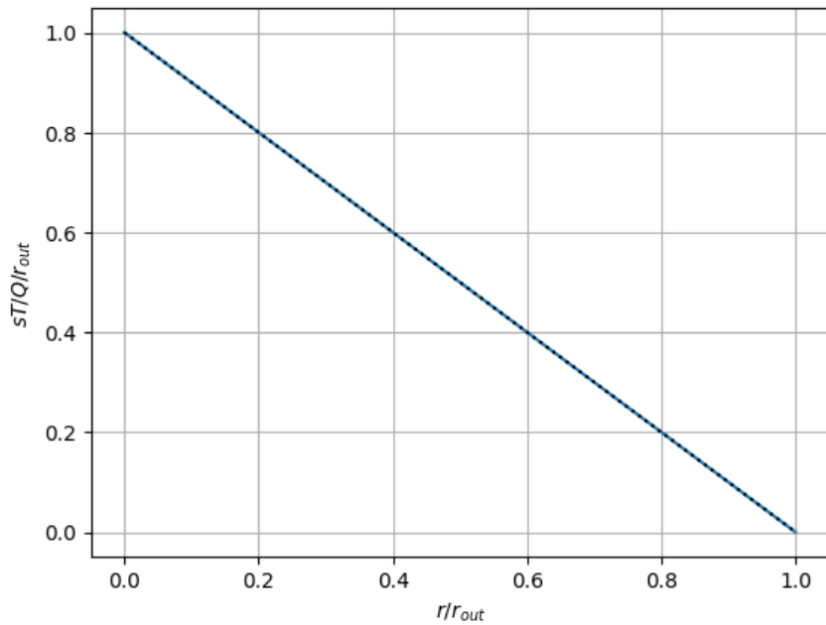


Figure 3. Plot of dimensionless head change versus relative distance due to parallel flow between a constant-discharge and a constant-head boundary. The solid blue line is calculated using Darcy's (1856) law, the black dotted line is simulated using the generalized semi-analytical solution developed in this chapter. See text for definition of variables and details about the applied solutions.

In this case, there is only one eigenvalue $d = 0$, and the corresponding eigenvector equals 1. This means the right-hand side of boundary conditions (57) and (59) simplifies to $w = \varphi$ and $q = \frac{Q}{T}$, respectively. If steady flow is considered, then $g = h$, and the general solution is given by (56), in which constants α and β are substituted by (85) and (86), respectively, to obtain:

$$h(r) = \varphi + \frac{Q}{T}(r_{out} - r) \quad (115)$$

Equation (115) can be rearranged to obtain the fundamental law of hydrogeology that was formulated first by Darcy (1856):

$$Q = -T \frac{\varphi - h}{r_{out} - r} \quad (116)$$

Figure 3 shows dimensionless head change $(sT)/(Qr_{out})$ as a function of relative distance r/r_{out} , with head change $s = h - \varphi$. Results are calculated according to (115) and simulated using the generalized solution developed in section 2.3.

If the stream is characterized by a constant head H instead of a constant discharge Q , then $u = H$ according to (58), and constants α and β are given by (80) and (81), respectively, which yields:

$$h(r) = \frac{H(r - r_{out}) + \varphi(r_{in} - r)}{r_{in} - r_{out}} \quad (117)$$

This equation corresponds to equation 2.2 in Haitjema (1995). Note that (117) simplifies to $h(r) = H$ if $\varphi = H$. Figure 4 shows relative head h/H as a function of relative distance r/r_{out} for different values of relative constant head φ/H according to (117) and simulated using the generalized solution developed in section 2.3.

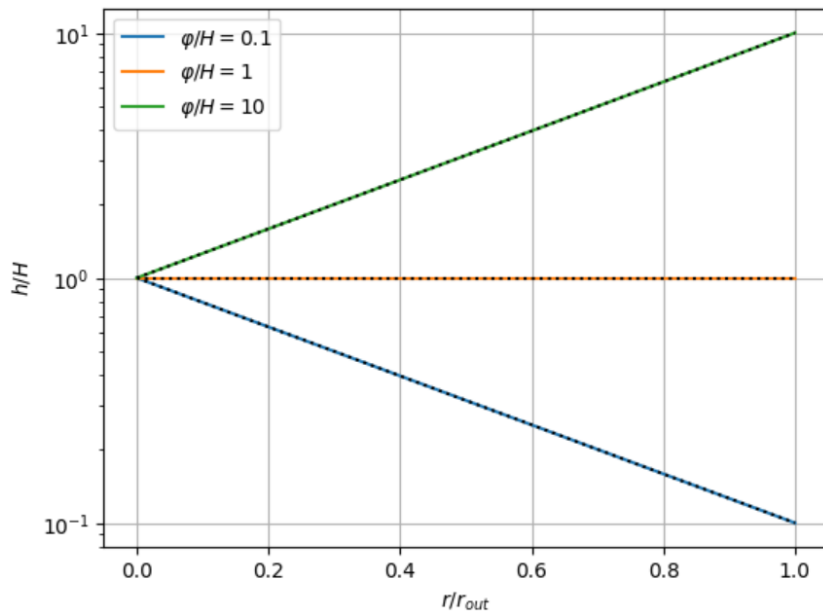


Figure 4. Plot of relative head versus relative distance due to parallel flow between two constant heads H and φ . The colored solid lines are calculated using the analytical expression (Haitjema, 1995), the black dotted lines using the generalized semi-analytical solution developed in this chapter. See text for definition of variables and details about the applied solutions.

2.5.2 The Thiem-Dupuit equation

Consider steady axisymmetric flow towards a fully penetrating well in a homogeneous aquifer with constant transmissivity T . The well has radius r_{in} and extracts groundwater at constant pumping rate Q . At distance r_{out} from the center of the well, a constant head φ is considered. Subscript i is omitted as there is one layer only. The aquifer boundaries are impervious, or $c_0 = c_1 = \infty$, and there is no recharge, or $N = 0$. Consequently, $v = 0$, and the only eigenvalue, $d = 0$, has eigenvector 1.

Concerning outer boundary condition (57) and inner boundary condition (59), it is found that $q = \frac{Q}{2\pi T}$ and $w = \varphi$. The general solution is given by (55), and constants α and β are substituted by (74) and (75), respectively, which gives the following solution for $g = h$:

$$h(r) = \varphi + \frac{Q}{2\pi T} \ln \left(\frac{r_{out}}{r} \right) \quad (118)$$

Equation (118) is the well-known Thiem-Dupuit equation (Dupuit, 1857, 1863; A. Thiem, 1870; G. Thiem, 1906) for confined flow to a fully penetrating well in a homogeneous aquifer. In the hydrogeological literature, it is usually simply referred to as the Thiem equation.

Figure 5 shows dimensionless drawdown $2\pi Ts/Q$ as a function of relative distance r/r_{out} , with drawdown $s = h - \varphi$. Results are calculated according to (118) and simulated using the generalized solution developed in section 2.3.

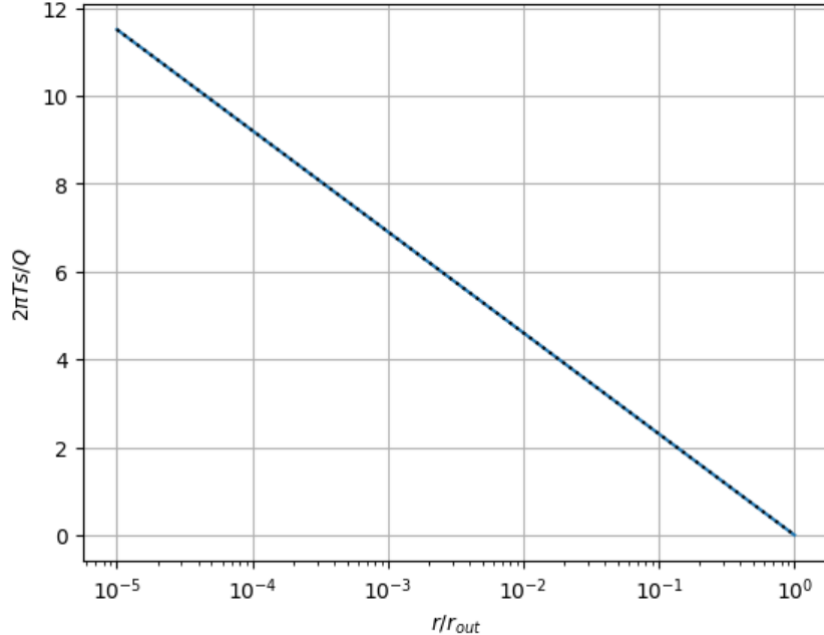


Figure 5. Plot of dimensionless drawdown as a function of relative distance according to the Thiem (1870, 1906) equation (blue solid line) and the generalized semi-analytical solution developed in this chapter (black dotted line). See text for definition of variables and details about the applied solutions.

If the pumping well has a constant head H , then $u = H$ according to (58), and constants α and β are given by (69) and (70), respectively, which gives the following equation:

$$h(r) = \frac{H \ln\left(\frac{r}{r_{out}}\right) + \varphi \ln\left(\frac{r_{in}}{r}\right)}{\ln\left(\frac{r_{in}}{r_{out}}\right)} \quad (119)$$

Figure 6 shows relative head h/H as a function of relative distance r/r_{out} for different values of relative constant head φ/H . Results are calculated according to (119) and simulated using the generalized solution developed in section 2.3.

Note that equation (119) simplifies to $h(r) = H$ if $\varphi = H$. Comparing equations (118) and (119) to the corresponding solutions (115) and (117) for parallel flow derived in previous section 2.5.1, it is seen that pumping rate Q must be replaced by $\frac{Q}{2\pi}$ and the logarithm of the distances must be considered to go from parallel flow to axisymmetric flow.

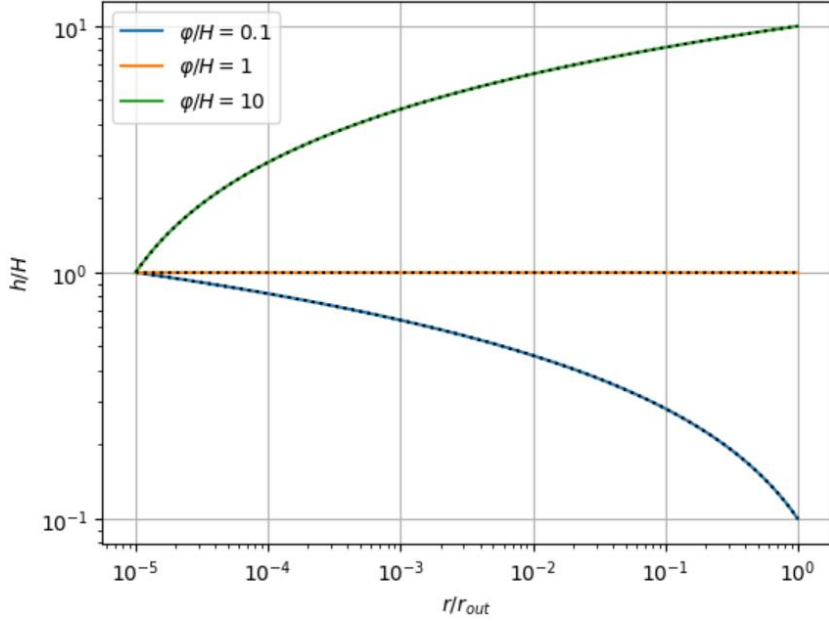


Figure 6. Plot of relative head versus relative distance due to radial flow between two constant heads H and φ . The colored solid lines are calculated using the analytical expression, the black dotted lines using the generalized semi-analytical solution developed in this chapter. See text for definition of variables and details about the applied solutions.

2.5.3 Areal recharge on a circular island

Consider a circular island with radius r_{out} surrounded by a lake with constant water level φ . Areal infiltration N recharges the island's aquifer with constant transmissivity T . The inner model boundary r_{in} is zero, as it is at the center of the island; it is a no-flow boundary, thus $q = 0$ in (59). As one-dimensional steady state confined flow is considered, there is one eigenvalue equal to 0 with eigenvector equal to 1; hence, $v = \frac{N}{T}$, and $w = \varphi$.

Substituting the values for these variables into the general solution (55) for radial flow using expressions (74) and (75), respectively, for α and β , gives:

$$h(r) = \varphi + \frac{N}{4T} (r_{out}^2 - r^2) \quad (120)$$

This equation corresponds to equation 3.174 in Haitjema (1995).

Suppose a fully penetrating well with nonzero radius r_{in} at the center of the island extracts groundwater at constant pumping rate Q . In this case, $q = \frac{Q}{2\pi T}$, which gives the following solution:

$$h(r) = \varphi + \left(\frac{Nr_{in}^2}{2T} - \frac{Q}{2\pi T} \right) \ln \left(\frac{r}{r_{out}} \right) + \frac{N}{4T} (r_{out}^2 - r^2) \quad (121)$$

Figure 7 shows dimensionless head change $2\pi Ts/Q$ as a function of relative distance r/r_{out} for different values of dimensionless recharge $N\pi r_{out}^2/Q$, with head change $s = h - \varphi$, and $r_{in}/r_{out} = 10^{-5}$. Results are calculated according to (121) and simulated using the generalized solution developed in section 2.3. Because both Q and s are negative in case of pumping, the dimensionless head change is positive. However, in order to actually observe whether the head is decreasing or increasing, the dimensionless head change is multiplied by -1 in Figure 7.

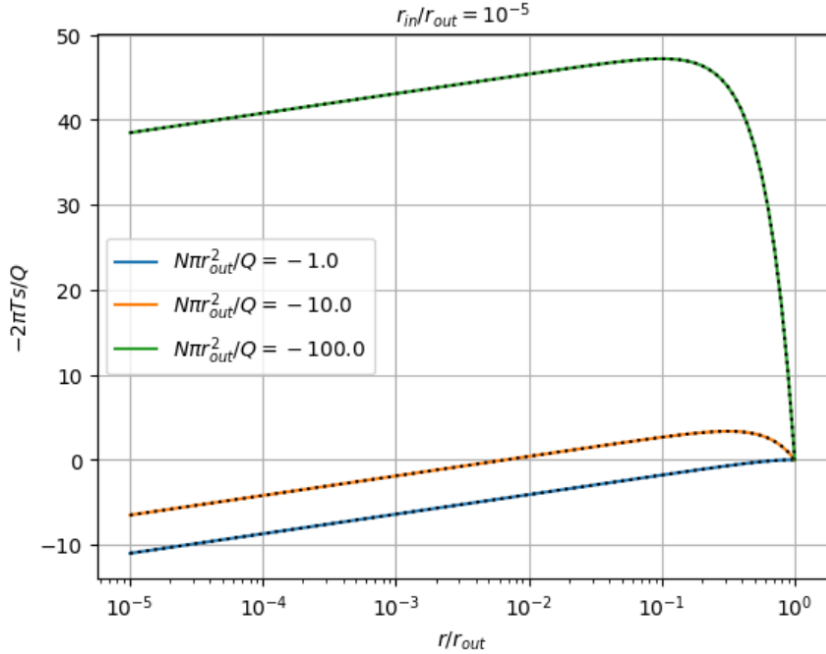


Figure 7. Plot of dimensionless head change versus relative distance for different values of dimensionless recharge according to the solution of a circular island with uniform recharge and a pumping well at the center of the island. The colored solid lines are calculated using the analytical expression, the black dotted lines using the generalized semi-analytical solution developed in this chapter. See text for definition of variables and details about the applied solutions.

Equation (121) corresponds to equation 3.175 in Haitjema (1995) if the well radius is neglected, i.e. $r_{in} = 0$, and it reduces to (120) if there is no well, i.e. $r_{in} = 0$ and $Q = 0$. In fact, if $r_{in} = 0$, then the solution is found by superimposing the drawdown caused by the well according to the Thiem-Dupuit formula (118) on the initial head that is given by equation (120). Note that this example of a circular island with recharge and pumping is used by Bredehoeft et al. (1982) and Bredehoeft (2002) to discuss the water budget myth. Chapter 11 elaborates on this example and also discusses the nonlinear solution for unconfined flow.

2.5.4 One-dimensional parallel flow with recharge

Consider two parallel streams fully penetrating an aquifer with constant transmissivity T , recharged by constant areal infiltration N . The first stream is at distance r_{in} and has a constant water level H , whereas the second stream with constant level φ is at distance r_{out} .

As a single layer is considered, there is only one eigenvalue, which is zero in case of steady flow and if $c_0 = c_1 = \infty$. The corresponding eigenvector equals 1, which reduces v to $\frac{N}{T}$, u to H , and w to φ . The general solution is given by (56), and constants α and β are given by (80) and (81), respectively. The particular solution is:

$$h(r) = \frac{H(r - r_{out}) + \varphi(r_{in} - r)}{r_{in} - r_{out}} + \frac{N}{2T} \frac{(r_{in}^2 - r_{out}^2)r + (r_{out}^2 - r^2)r_{in} + (r^2 - r_{in}^2)r_{out}}{r_{in} - r_{out}} \quad (122)$$

Note that the first term in the right-hand side of (122) is the same as equation (117) which describes uniform flow. The last term describes the groundwater mounding due to areal recharge. This means equation (122) can be found by superimposing the solution for areal recharge on the uniform flow equation.

Figure 8 shows dimensionless head $2Th/(Nr_{out}^2)$ as a function of relative distance r/r_{out} for different values of dimensionless constant head $2TH/(Nr_{out}^2)$ at the inner model boundary and with

dimensionless constant head $2T\varphi/(Nr_{out}^2)$ at the outer model boundary equal to 1. Results are calculated according to (122) and simulated using the generalized solution developed in section 2.3.

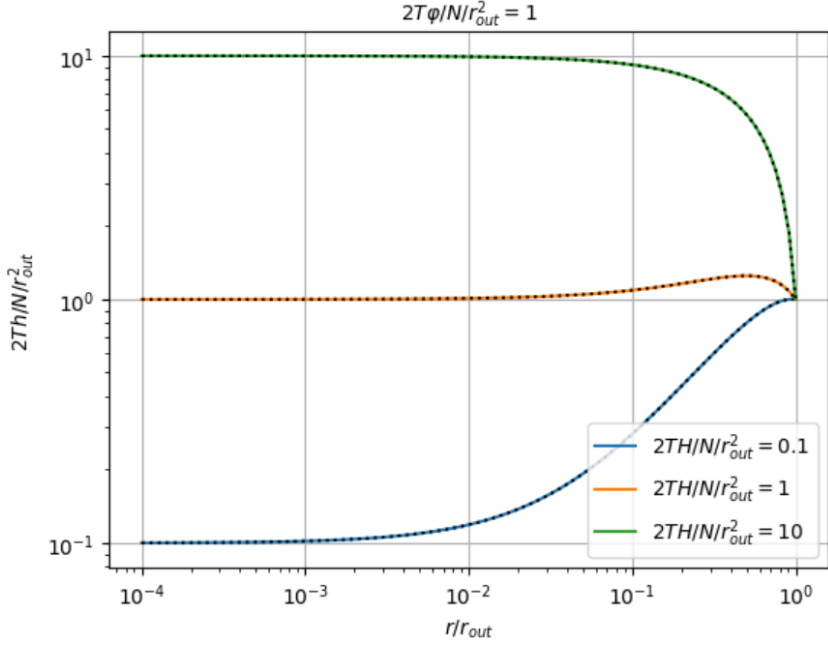


Figure 8. Plot of dimensionless head versus relative distance due to parallel flow between two constant heads and uniform recharge. Different values for the dimensionless constant head at the inner boundary are considered, whereas the dimensionless constant head at the outer boundary equals 1. The colored solid lines are calculated using the analytical expression, the black dotted lines using the generalized semi-analytical solution developed in this chapter. See text for definition of variables and details about the applied solutions.

If $r_{in} = 0$, then (122) simplifies to:

$$h(r) = H + \frac{Nr}{2T}(r_{out} - r) + \frac{\varphi - H}{r_{out}}r \quad (123)$$

This equation corresponds to equation 3.157 in Haitjema (1995). If the levels in both streams are the same, or $\varphi = H$, then equation (123) reduces to:

$$h(r) = H + \frac{Nr}{2T}(r_{out} - r) \quad (124)$$

This equation corresponds to equation 3.165 in Haitjema (1995).

2.5.5 One-dimensional axisymmetric flow with recharge

Consider a fully penetrating well with radius r_{in} and constant head H in an aquifer with constant transmissivity T , recharged by constant areal infiltration N . There is no leakage; hence $c_0 = c_1 = \infty$. At radial distance r_{out} from the well, the head is constant and equal to φ .

In case of confined, one-dimensional flow, there is only one eigenvalue equal to zero with eigenvector equal to 1, which reduces v to $\frac{N}{T}$, u to H , and w to φ . Substituting these values into general solution (55), with constants α and β respectively given by (69) and (70), gives:

$$h(r) = \frac{H \ln\left(\frac{r}{r_{out}}\right) + \varphi \ln\left(\frac{r_{in}}{r}\right)}{\ln\left(\frac{r_{in}}{r_{out}}\right)} + \frac{N}{4T} \frac{(r_{in}^2 - r_{out}^2) \ln(r) + (r_{out}^2 - r^2) \ln(r_{in}) + (r^2 - r_{in}^2) \ln(r_{out})}{\ln\left(\frac{r_{in}}{r_{out}}\right)} \quad (125)$$

Equation (125) can also be interpreted as the superposition of uniform flow equation (119), which is the first term in the right-hand side, and the solution for groundwater mounding due to areal recharge, which is the second term. If $\varphi = H$, then the first term in equation (125) simplifies to H .

Figure 9 shows dimensionless head $4Th/(Nr_{out}^2)$ as a function of relative distance r/r_{out} for different values of dimensionless constant head $4T\varphi/(Nr_{out}^2)$ at the outer model boundary and with dimensionless constant head $4TH/(Nr_{out}^2)$ at the inner model boundary equal to 1. Results are calculated according to (125) and simulated using the generalized solution developed in section 2.3.

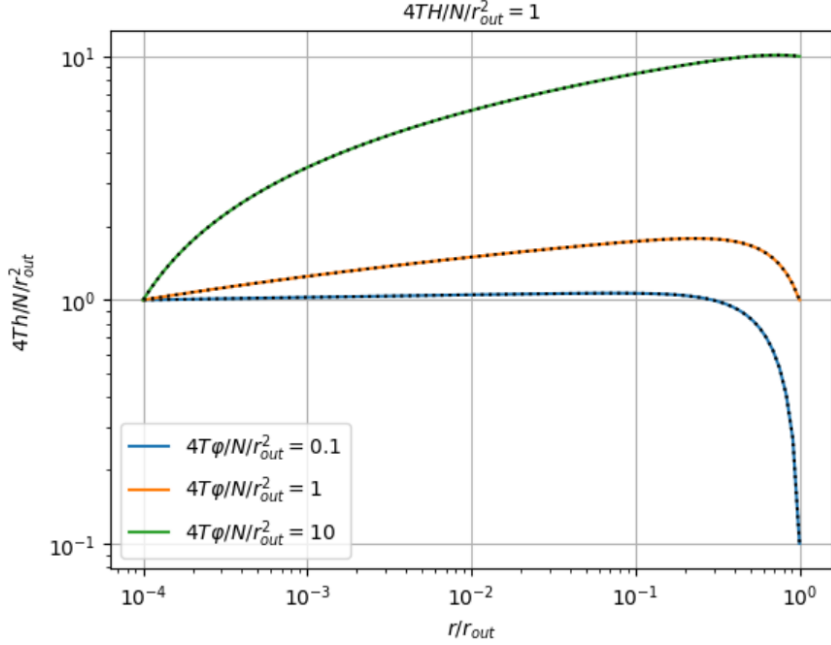


Figure 9. Plot of dimensionless head versus relative distance due to radial flow between two constant heads and uniform recharge. Different values for the dimensionless constant head at the outer boundary are considered, whereas the dimensionless constant head at the inner boundary equals 1. The colored solid lines are calculated using the analytical expression, the black dotted lines using the generalized semi-analytical solution developed in this chapter. See text for definition of variables and details about the applied solutions.

2.5.6 The de Glee equation

Consider a leaky aquifer of infinite extent with constant transmissivity T , bounded on top by an aquitard with vertical resistance $c_0 = c_{top}$ and constant head $\varphi_0 = \varphi_{top}$. Suppose a fully penetrating well extracts water from the aquifer at constant pumping rate Q . If the well radius is infinitesimal small, i.e. $r_{in} \rightarrow 0$, and the lower aquifer boundary is impervious, i.e. $c_1 = c_{bot} = \infty$, then the steady head in the aquifer during pumping is calculated using the following formula:

$$h(r) = \varphi_{top} + \frac{Q}{2\pi T} K_0 \left(r \sqrt{\frac{1}{c_{top} T}} \right) \quad (126)$$

In this case, matrix A defined by (35) has one entry only, which equals the eigenvalue $d = \frac{1}{c_{top} T}$. The corresponding eigenvector is 1. Vector b defined by (34) also has one element, i.e. $b = v = \frac{\varphi_{top}}{c_{top} T}$.

The inner boundary is zero and the outer boundary is at an infinitely large distance; hence $\alpha = 0$ and $\beta = q = \frac{Q}{2\pi T}$. Substituting these values into general solution (55) gives equation (126).

If the initial head φ_1 before pumping is equal to the constant head φ_{top} in the aquitard, then subtracting this initial head from both sides of equation (126) gives the well-known de Glee formula to calculate steady drawdown due to pumping in a leaky aquifer (de Glee, 1930; Hantush, 1949; Jacob, 1946; Kooper, 1914).

Note that the leakage factor λ [L] of a leaky aquifer is defined as:

$$\lambda = \sqrt{c_{top}T} \quad (127)$$

From (127) it follows that $d = \frac{1}{\lambda^2}$.

If the well-radius cannot be neglected, then β is defined by (76), which results in the following equation (de Glee, 1930; Kooper, 1914):

$$h(r) = \varphi_{top} + \frac{Q}{2\pi T} \frac{K_0(r\sqrt{d})}{r_{in}\sqrt{d}K_1(r_{in}\sqrt{d})} \quad \text{with } d = \frac{1}{c_{top}T} \quad (128)$$

If equation (128) is expressed in terms of drawdown, then it corresponds to equation 227.14 in Bruggeman (1999). Equation (128) approximates equation (126) if $r_{in} \rightarrow 0$, as $xK_1(x) \rightarrow 1$ if $x \rightarrow 0$.

Figure 10 shows dimensionless drawdown $2\pi Ts/Q$ as a function of relative distance $r/\sqrt{Tc_{top}}$ for different values of dimensionless well-radius $r_{in}/\sqrt{Tc_{top}}$, with drawdown $s = h - \varphi_{top}$. Results are calculated according to (128) and simulated using the generalized solution developed in section 2.3.

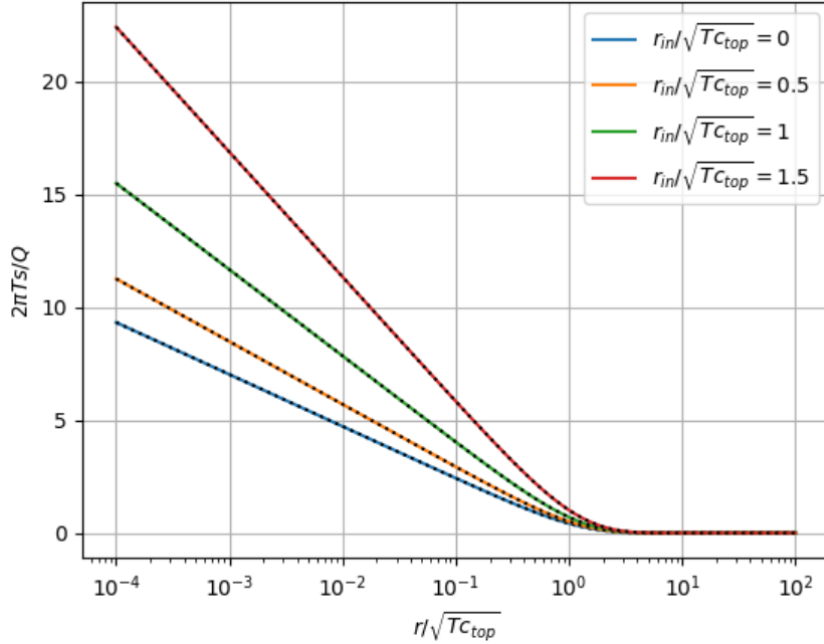


Figure 10. Plot of dimensionless drawdown versus dimensionless distance for a pumping well in a leaky aquifer. Different values for the dimensionless radius of the pumping well are considered. The colored solid lines are calculated using the analytical expression (de Glee, 1930), the black dotted lines using the generalized semi-analytical solution developed in this chapter. See text for definition of variables and details about the applied solutions.

If the aquifer is also bounded below by a leaky aquitard in which the constant head is $\varphi_2 = \varphi_{bot}$, then the following generalized equation is obtained:

$$h(r) = \frac{\varphi_{top}c_{bot} + \varphi_{bot}c_{top}}{c_{top} + c_{bot}} + \frac{Q}{2\pi T} \frac{K_0(r\sqrt{d})}{r_{in}\sqrt{d}K_1(r_{in}\sqrt{d})} \quad \text{with } d = \frac{1}{c_{top}T} + \frac{1}{c_{bot}T} \quad (129)$$

In this case, $b = v = \frac{\varphi_{top}}{c_{top}T} + \frac{\varphi_{bot}}{c_{bot}T}$. As the eigenvalue is $d = \frac{1}{c_{top}T} + \frac{1}{c_{bot}T}$, the leakage factor for an aquifer bounded by two leaky aquitards is:

$$\lambda = \sqrt{\frac{c_{top}c_{bot}T}{c_{top} + c_{bot}}} \quad (130)$$

Figure 11 plots several curves of head versus distance according to (129) using the following dimensionless parameters: $h^* = 2\pi Th/Q$; $\varphi_{top}^* = 2\pi T\varphi_{top}/Q$; $\varphi_{bot}^* = 2\pi T\varphi_{bot}/Q$; $r^* = r/\sqrt{Tc_{tot}}$; $r_{in}^* = r_{in}/\sqrt{Tc_{tot}}$; $c_{top}^* = c_{tot}/c_{top}$; $c_{bot}^* = c_{bot}/c_{tot}$; with $c_{tot} = c_{top} + c_{bot}$. The curves in Figure 11 are also simulated using the generalized solution developed in section 2.3.

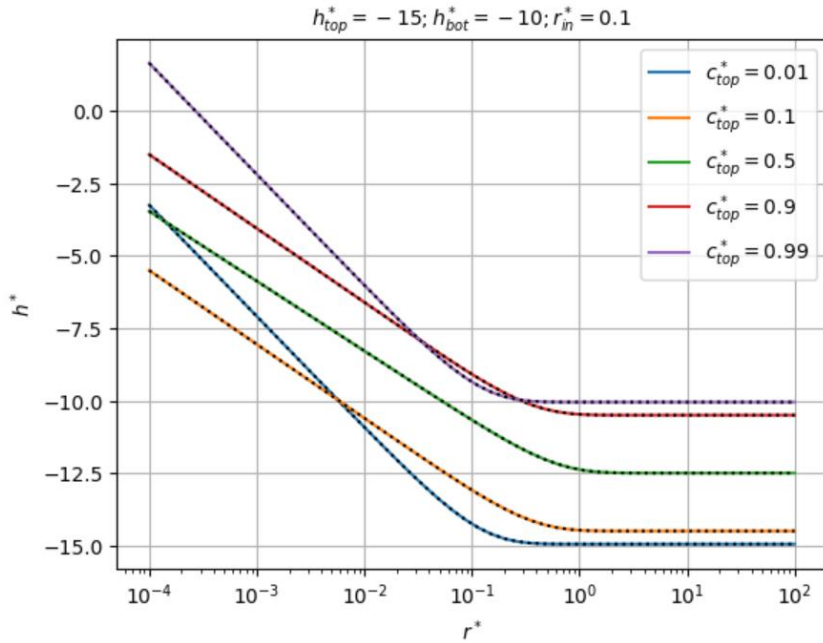


Figure 11. Plot of dimensionless head versus dimensionless distance for a pumping well in an aquifer bounded by two leaky aquitards. The well has a dimensionless radius of 0.1. The dimensionless constant head in top and bottom aquitard are -15 and -10, respectively. Different values for the dimensionless resistance of the top aquitard are considered. The dimensionless resistance of the bottom aquitard is one minus the dimensionless resistance of the top aquitard. The colored solid lines are calculated using the analytical expression, the black dotted lines using the generalized semi-analytical solution developed in this chapter. See text for definition of variables and details about the applied solutions.

Chapter 10 also discusses the de Glee equation and derives formulas to estimate the radius of influence from this equation.

2.5.7 The Theis equation

Consider transient flow towards a fully penetrating well in an aquifer with constant transmissivity T and constant storativity S . The aquifer is not recharged by infiltration or leakage; hence, $c_0 = c_1 = \infty$ and $N = 0$. The well extracts groundwater at a constant pumping rate Q .

Simulating one-dimensional axisymmetric flow toward the well only requires one model layer in this case; hence, there is one eigenvalue which equals the single entry in system matrix \mathbf{A} . From definition (38), it follows that eigenvalue $d = \frac{S}{T}p$; the corresponding eigenvector equals 1. The only element in vector \mathbf{b} defined by (37) equals $\frac{S}{T}\varphi$, with φ the initial head, from which it follows that $v = \frac{S}{T}\varphi$. The well has an infinitesimal radius, i.e. $r_{in} \rightarrow 0$, and the aquifer has an infinite extent, which

means the outer model boundary is at an infinitely large distance, i.e. $r_{out} \rightarrow \infty$. As a consequence, $\alpha = 0$ and $\beta = q = \frac{Q}{2\pi T p}$. The latter is derived from the inner boundary condition (59).

The general solution for axisymmetric transient flow is given by (55), with $g = \bar{h}$ in this case.

Introducing all values discussed above into the general solution gives:

$$\bar{h}(r, p) = \frac{\varphi}{p} + \frac{Q}{2\pi T p} K_0 \left(r \sqrt{\frac{S}{T}} p \right) \quad (131)$$

Expression (131) gives the solution in Laplace space, which can be inverted analytically to the real time domain using known Laplace transforms (e.g. page 303 of Hantush, 1964):

$$h(r, t) = \varphi + \frac{Q}{4\pi T} W \left(\frac{r^2 S}{4tT} \right) \quad (132)$$

Subtracting initial head φ from both sides of equation (132) gives the well-known Theis equation to calculate transient drawdown due to pumping in a confined aquifer (Theis, 1935). Function W , which is called the Theis well function or the exponential integral, is defined as:

$$W(u) = \int_u^\infty \frac{e^{-x}}{x} dx = -\gamma - \ln(u) - \sum_{n=1}^{\infty} \frac{(-u)^n}{n \cdot n!} \quad (133)$$

with γ the Euler-Mascheroni constant equal to 0.57721.... The Cooper-Jacob approximation is justified if u is smaller than 0.02, in which case only the first two terms, i.e. $-\gamma - \ln(u)$, are considered to calculate the well function (Cooper & Jacob, 1946). Chapter 10 also discusses the Theis equation and derives formulas to estimate the radius of influence from the Cooper-Jacob approximation of this equation.

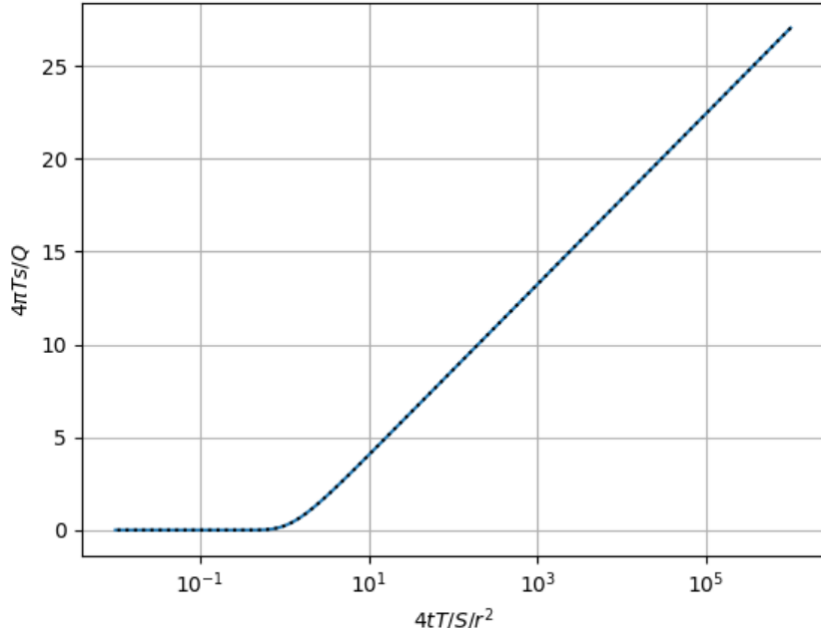


Figure 12. Plot of dimensionless drawdown versus dimensionless time for a pumping well fully penetrating a confined aquifer. The blue solid line is calculated using the Theis (1935) equation, the black dotted line using the generalized semi-analytical solution developed in this chapter. See text for definition of variables and details about the applied solutions.

Figure 12 shows dimensionless drawdown $4\pi Ts/Q$ as a function of dimensionless time $4tT/(Sr^2)$, with drawdown $s = h - \varphi$. The result is calculated according to (132) and simulated using the generalized solution developed in section 2.3.

Applying superposition equation (112) to equation (132) for $\varphi = 0$, it is possible to determine the residual drawdown s' [L] after pumping (Theis, 1935):

$$s'(r, t) = \frac{Q}{4\pi T} \left[W\left(\frac{r^2 S}{4tT}\right) - W\left(\frac{r^2 S'}{4\Delta t T}\right) \right] \quad \text{with } \Delta t = t - \tau \quad (134)$$

where τ is the time [T] when the pump is shut down and the recovery starts, and S' is the aquifer storativity [-] during recovery. It is possible indeed that the interpretation of a recovery test results in different values for the storage coefficient during pumping and recovery (Ashjari, 2013; Jacob, 1963; Kruseman & de Ridder, 1990). This difference can be caused by several phenomena such as the consolidation of deposits during pumping, especially in newly developed aquifers (Jacob, 1963), a hysteresis effect due to the lag time in response between aquifer and confining unit, material displacement inside the aquifer, or air entrapment when hydraulic head drops below the confining layer (Ashjari, 2013).

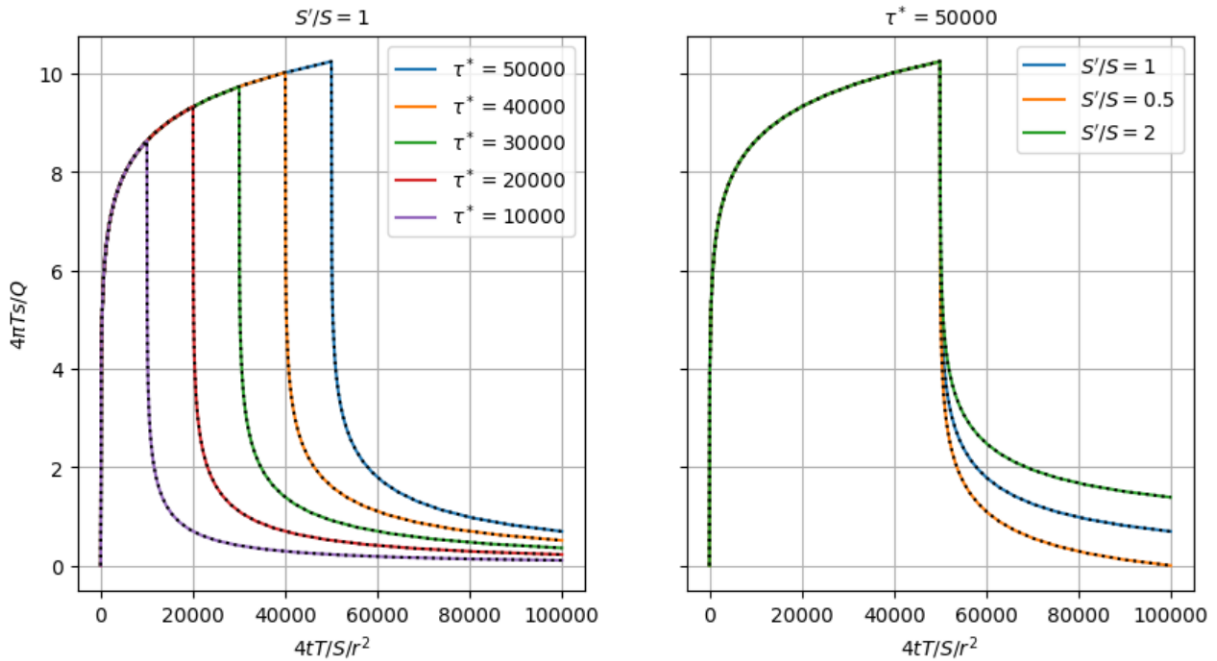


Figure 13. Simulation of recovery tests conducted in a pumping well fully penetrating a confined aquifer. Both plots show dimensionless drawdown as a function of dimensionless time. The colored solid lines are calculated using the analytical expression (Theis, 1935), the black dotted lines are simulated using the generalized semi-analytical solution developed in this chapter. Left: Aquifer storativity during pumping and recovery, respectively S and S' , are the same. The pump is shut down at different dimensionless times τ^* . Right: The pump shuts down at dimensionless time $\tau^* = 50\,000$. Different values for S'/S are considered. See text for definition of variables and details about the applied solutions.

Figure 13 shows two plots of dimensionless drawdown $4\pi Ts/Q$ as a function of dimensionless time $4tT/(Sr^2)$. The results are calculated applying superposition to equation (132) and to the generalized solution developed in section 2.3. The time-drawdown curves in left graph are calculated for different dimensionless times $\tau^* = 4tT/(Sr^2)$ at which the recovery starts. The same storage coefficient is defined for pumping and recovery, that is $S = S'$. The right graph compares the equal storativity curve for $\tau^* = 50000$ with the curves calculated using a storativity S' during recovery which is two times greater and smaller, respectively, than the storativity S during pumping. The difference between S and S' is exaggerated to the extent that the corresponding curves visibly deviate from the

equal storativity curve. In practice, the storage coefficient during recovery usually is smaller (Jacob, 1963), although it is possible a greater value is derived from recovery test data (Ashjari, 2013).

2.5.8 Effect of a well on the flow of a nearby stream

Applying the method of images, Theis (1941) derived a solution to calculate the drawdown caused by a fully penetrating pumping well close to a fully penetrating stream. Defining the distance between the well and the stream as L , an image well injecting water at rate $-Q$ is defined at distance $2L$ from the real well with pumping rate Q . If the coordinate of the pumping well is $(0,0)$, then the coordinate of the imaginary injection well is $(-2L, 0)$, and the stream coincides with line $x = -L$ parallel to the y -axis.

Applying superposition equation (114) to equation (132) for $\varphi = 0$, the total drawdown due to both the pumping and the injection well is obtained:

$$s(x, y, t) = \frac{Q}{4\pi T} \left[W\left(\frac{[x^2 + y^2]S}{4tT}\right) - W\left(\frac{[(x + 2L)^2 + y^2]S}{4tT}\right) \right] \quad (135)$$

The line representing the stream of infinite length actually is a constant-head boundary where drawdown is zero. A no-flow boundary is achieved by using an image well that extracts water at the same rate Q .

After a certain time of pumping, the well-discharge will be balanced by the recharge from the stream. In this new state of steady flow, the Cooper and Jacob (1946) approximation is valid, and equation (135) simplifies to:

$$s(x, y) = \frac{Q}{4\pi T} \ln\left(\frac{(x + 2L)^2 + y^2}{x^2 + y^2}\right) \quad (136)$$

A new state of equilibrium is reached when the total storage change in the semi-infinite aquifer is negligibly small. The total storage change is defined as:

$$\frac{dV}{dt} = \int_{-\infty}^{\infty} \int_{-L}^{\infty} S \frac{\partial s}{\partial t} dx dy \quad (137)$$

with V the volume [L^3] of groundwater in the semi-infinite aquifer. To find a solution for (137), the partial derivative of well function W with respect to time t is needed:

$$\frac{\partial W}{\partial t} = \frac{dW}{du} \frac{\partial u}{\partial t} = \frac{e^{-u}}{u} \frac{\partial u}{\partial t} = \frac{e^{-u}}{u} \frac{-u}{t} = \frac{-e^{-u}}{t} \quad (138)$$

Introducing solution (135) into (137) and using (138) to calculate $\frac{\partial s}{\partial t}$ gives:

$$\frac{dV}{dt} = \frac{Qv}{\pi} \int_{-\infty}^{\infty} \int_{-L}^{\infty} [e^{-(x+2L)^2+y^2}v - e^{-x^2+y^2}v] dx dy \quad (139)$$

where $\frac{S}{4tT}$ is substituted for v . Substituting $(x + 2L)$ for w and rearranging (139) gives:

$$\frac{dV}{dt} = \frac{Qv}{\pi} \int_{-\infty}^{\infty} e^{-vy^2} \int_L^{\infty} e^{-vw^2} dw dy - \frac{Qc}{\pi} \int_{-\infty}^{\infty} e^{-vy^2} \int_{-L}^{\infty} e^{-vx^2} dx dy \quad (140)$$

Considering the following known solution (Gradshteyn & Ryzhik, 2007), with erf the error function:

$$\int_a^b e^{-vy^2} dy = \sqrt{\frac{\pi}{4v}} [\operatorname{erf}(b\sqrt{v}) - \operatorname{erf}(a\sqrt{v})] \quad (141)$$

and applying $\lim_{u \rightarrow \infty} \operatorname{erf}(u) = 1$ and $\lim_{u \rightarrow -\infty} \operatorname{erf}(u) = -1$:

$$\int_{-\infty}^{\infty} e^{-vy^2} dy = \sqrt{\frac{\pi}{v}} \quad (142)$$

Using (141) and (142) to simplify (140) finally gives:

$$\frac{dV}{dt} = \frac{Q}{2} \left[\operatorname{erf}\left(-\sqrt{\frac{SL^2}{4tT}}\right) - \operatorname{erf}\left(\sqrt{\frac{SL^2}{4tT}}\right) \right] \quad (143)$$

Figure 14 shows these solutions for drawdown and total storage change expressed in terms of dimensionless drawdown $4\pi Ts/Q$, relative coordinates x/L and y/L , and dimensionless time $4tT/(SL^2)$. The left plot draws the contour lines of dimensionless drawdown calculated using (135) for dimensionless time equal to 10. The well is located in the center of the map, while the stream is parallel to the y-axis and coincides with the left boundary of the map. The upper graph on the right plots dimensionless total storage change $\frac{dV/Q}{dt}$ versus dimensionless time calculated using (143), while the lower graph is the dimensionless drawdown as a function of dimensionless time at four points located on the x-axis. It is seen that steady state is reached approximately at dimensionless time equal to 100. The time-drawdown curves are calculated using (135) and by applying superposition to the generalized solution developed in section 2.3.

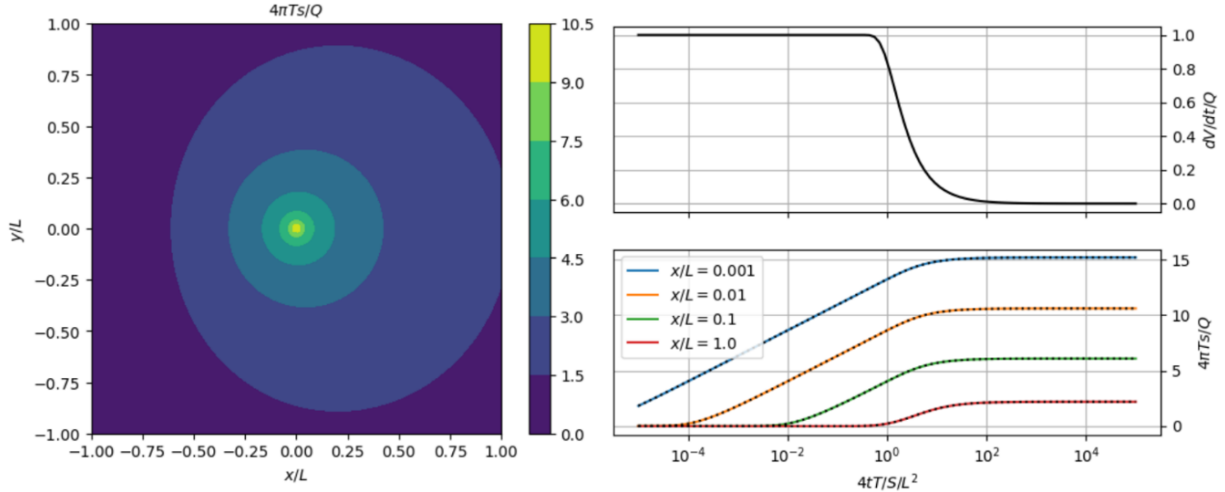


Figure 14. Simulation of dimensionless drawdown due to a pumping well fully penetrating a confined aquifer and located at distance L from a stream with constant head. Left: Contour plot of dimensionless drawdown as a function of relative coordinates x/L and y/L at dimensionless time $4tT/SL^2 = 10$. The well is located at point $(0, 0)$; the stream is north-south oriented and coincides with the straight line $x/L = -1$. Upper left: Relative total storage change in the aquifer as a function of dimensionless time. Lower left: Dimensionless drawdown as a function of dimensionless time at different points $(x/L, 0)$ lying on the x-axis ($y=0$). The colored solid lines and the black dotted lines are calculated by applying superposition respectively to the Theis (1935) equation and to the generalized semi-analytical solution developed in this chapter. See text for definition of variables and details about the applied solutions.

2.5.9 The Edelman equations

Consider transient flow toward a fully penetrating stream in an aquifer with constant transmissivity T and constant storativity S . The aquifer is not recharged by infiltration or leakage; hence $c_0 = c_1 = \infty$ and $N = 0$.

According to (38), matrix \mathbf{A} contains one element which equals the only eigenvalue $d = \frac{S}{T}p$ with corresponding eigenvector 1. According to (37), vector \mathbf{b} also contains one element only, which is equal to $v = \frac{S}{T}\varphi$, with φ the initial head. The aquifer is semi-infinite, i.e. $r_{out} \rightarrow \infty$, from which it follows that $\alpha \rightarrow 0$. The stream has an infinitesimal width; hence, $r_{in} \rightarrow 0$.

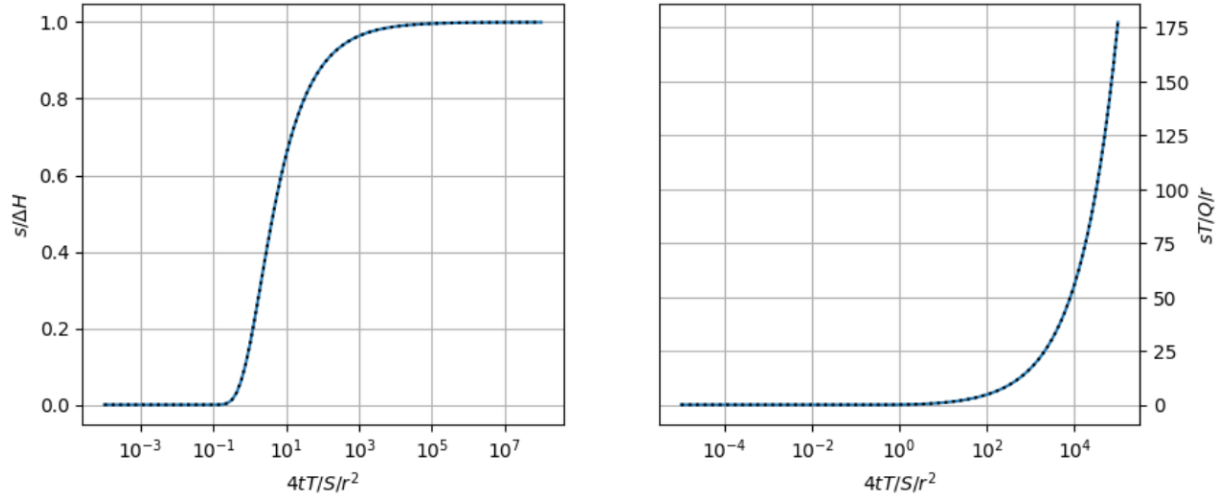


Figure 15. Plot of the Edelman (1947) equations for simulating parallel flow to a stream with constant water level (case 0) or constant discharge (case 1). Left: relative head change versus dimensionless time for the constant water level case. Right: dimensionless head change versus dimensionless time for the constant discharge case. The blue solid lines are calculated using the respective Edelman (1947) equations, the black dotted lines using the generalized semi-analytical solution developed in this chapter. See text for definition of variables and details about the applied solutions.

If the stream has a constant water level H , then inner boundary condition (58) is applied with $u = \frac{H}{p}$. In this case, $\beta \rightarrow \frac{H-\varphi}{p}$ according to (82). Substituting these values into general solution (56) and taking into account that $g = \bar{h}$, the solution in the Laplace domain is obtained:

$$\bar{h}(r, p) = \frac{\varphi}{p} + \left(\frac{H - \varphi}{p} \right) e^{-\left(r \sqrt{\frac{S}{T}p} \right)} \quad (144)$$

Expression (144) can be inverted analytically using known Laplace transforms (e.g. page 303 in Hantush, 1964):

$$h(r, t) = \varphi + (H - \varphi) \operatorname{erfc} \left(r \sqrt{\frac{S}{4tT}} \right) \quad (145)$$

with erfc the complementary error function. If initial head φ is set to zero, equation (145) corresponds to solution “case 0” derived by Edelman (1947).

If the stream drains groundwater at constant rate Q , then inner boundary condition (59) is applied with $q = \frac{Q}{Tp}$. In this case, $\beta \rightarrow \frac{q}{\sqrt{d}}$ according to (87). Introducing these values into general solution (56) gives:

$$\bar{h}(r, p) = \frac{\varphi}{p} + \frac{Q}{\sqrt{ST}} \frac{e^{-\left(r\sqrt{\frac{S}{T}}p\right)}}{p\sqrt{p}} \quad (146)$$

Inverting expression (146) analytically to the real time domain is a bit more involved, but it can be proven that it is equal to solution “case 1” derived by Edelman (1947):

$$h(r, t) = \varphi + 2Q \sqrt{\frac{t}{\pi ST}} e^{-\frac{r^2 S}{4tT}} - \frac{Qr}{T} \operatorname{erfc}\left(\sqrt{\frac{r^2 S}{4tT}}\right) \quad (147)$$

Edelman (1947) also derives a solution for the cases where the water level and the drainage rate are a linear function of time. According to Olsthoorn (2006), solution 123.05 in Bruggeman (1999) is a generalized solution for this kind of problems, and it also includes the cases presented by Edelman (1947).

Figure 15 visualizes both Edelman (1947) equations using dimensionless parameters. The left graph plots relative head change $s/\Delta H$ versus dimensionless time $4tT/(Sr^2)$ for the constant-head case, while the right graph plots dimensionless head change $sT/(Qr)$ versus dimensionless time $4tT/(Sr^2)$ for the constant-discharge case. In both cases, head change s is defined as $h - \varphi$, and accordingly, $\Delta H = H - \varphi$ in the first case. The blue lines in the left and right plot are calculated using equations (145) and (147), respectively. In both plots, the black dotted lines are simulated using the generalized solution developed in section 2.3.

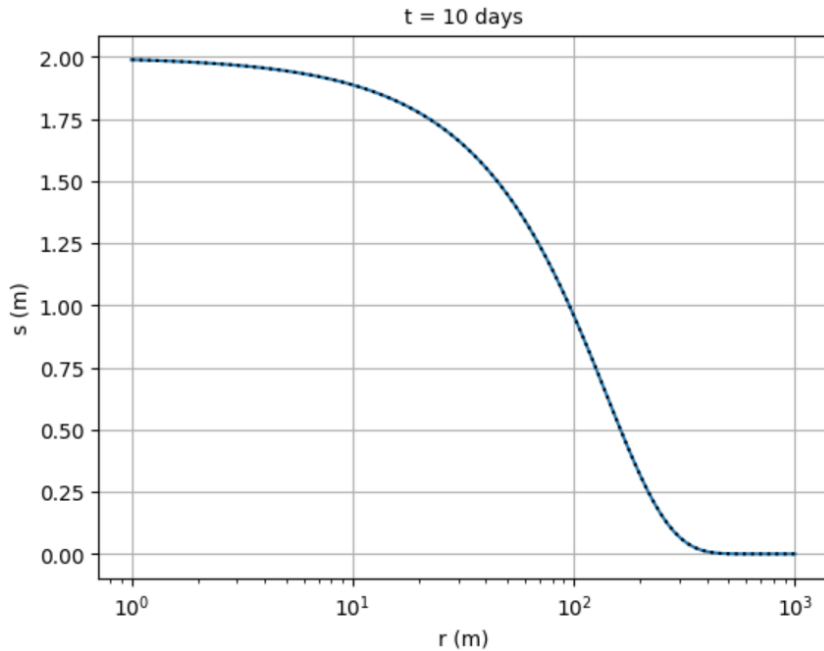


Figure 16. Plot of head rise versus horizontal distance in an aquifer with transmissivity of $100 \text{ m}^2/\text{d}$ and storage coefficient of 0.1. The plotted head change is due to a water level rise of 2 m that happened 10 days ago in a river open to the aquifer. The blue solid line is calculated using the Edelman (1947) equation (case 0), the black dotted line using the generalized semi-analytical solution developed in this chapter. See text for definition of variables and details about the applied solutions.

The dimensionless parameter curves in Figure 15 are not intuitively and easy to interpret, and therefore, Figure 16 shows the result of a specific example involving a river in which the water level is increased by 2 m. The river is connected to an aquifer characterized by a transmissivity of $100 \text{ m}^2/\text{d}$ and a storage coefficient of 0.1. The plot shows the head rise in the aquifer as a function of the

horizontal distance after 10 days. The blue line is calculated according to equation (145), the black dotted line is simulated using the generalized solution developed in section 2.3.

2.5.10 The model of Hantush-Jacob

Consider transient flow toward a fully penetrating well in an aquifer with constant transmissivity T and constant storativity S . The aquifer is recharged by leakage through an overlying aquitard with resistance $c_0 = c_{top}$ and constant head $\varphi_0 = \varphi_{top}$. The lower boundary of the aquifer is impervious, i.e. $c_1 = \infty$, and there is no infiltration, i.e. $N = 0$. The well extracts groundwater at a constant pumping rate Q .

Definition (38) determines the single entry in \mathbf{A} which is also the only eigenvalue, $d = \frac{1}{c_{top}T} + \frac{S}{T}p$; the corresponding eigenvector equals 1. Vector \mathbf{b} defined by (37) also contains one element equal to $v = \frac{\varphi_{top}}{pc_{top}T} + \frac{S}{T}\varphi$, with φ the initial head, which is assumed equal to the constant head in the aquitard, i.e. $\varphi = \varphi_{top}$. If the well has an infinitesimal radius, i.e. $r_{in} \rightarrow 0$, and the aquifer has an infinite extent, i.e. $r_{out} \rightarrow \infty$, then $\alpha \rightarrow 0$ and $\beta \rightarrow q = \frac{Q}{2\pi T p}$. Introducing these values into general solution (55) with $g = \bar{h}$ gives:

$$\bar{h}(r, p) = \frac{\varphi}{p} + \frac{Q}{2\pi T p} K_0(r\sqrt{d}) \quad \text{with } d = \frac{1}{c_{top}T} + \frac{S}{T}p \quad (148)$$

It is possible to invert equation (148) analytically (e.g. page 303 in Hantush, 1964):

$$h(r, t) = \varphi + \frac{Q}{4\pi T} W\left(\frac{r^2 S}{4tT}, \frac{r}{\sqrt{c_{top}T}}\right) \quad (149)$$

Subtracting initial head φ from both sides of equation (149) gives the well-known solution of Hantush and Jacob (1955) to calculate transient drawdown due to pumping in a leaky aquifer. Function W in (149) is the Hantush well function, which is defined as:

$$W(u, v) = \int_u^\infty \frac{e^{-x-v^2/4x}}{x} dx \quad (150)$$

Veling and Maas (2010) give an overview of existing analytical and numerical methods to calculate or approximate the Hantush well function. If the aquifer is confined, i.e. $c_{top} = \infty$, then $v = 0$, and the Hantush well function equals the Theis well function. If $t \rightarrow \infty$, then $u \rightarrow 0$, and $W(u, v) \rightarrow 2K_0(v)$. In practice, however, the aquifer already reaches a new state of equilibrium after a finite period of pumping, in which case equation (149) may be approximated using the formula of de Glee (126). Chapter 10 elaborates on the Hantush and Jacob (1955) solution and shows the relation with the de Glee (1930) and Theis (1935) equations.

Veling and Maas (2010) also present the following fast approximation of equation (149):

$$h(r, t) \cong \varphi + \frac{Q}{4\pi T} F(\rho, \tau)$$

with:

$$F(\rho, \tau) = \begin{cases} \omega W\left(\frac{e^{-\tau}\rho}{2}\right) - (\omega - 1)W(\rho \cosh(\tau)) & (\tau \leq 0) \\ 2K_0(\rho) - \omega W\left(\frac{e^\tau\rho}{2}\right) + (\omega - 1)W(\rho \cosh(\tau)) & (\tau > 0) \end{cases}$$

$$\rho = \frac{r}{\sqrt{c_{top}T}}$$

$$\tau = \ln\left(\frac{2t}{\rho c_{top}S}\right)$$

$$\omega = \frac{W(\rho) - K_0(\rho)}{W(\rho) - W\left(\frac{\rho}{2}\right)}$$
(151)

Note that function W in (151) is the Theis well function, also known as the exponential integral.

Figure 17 shows dimensionless drawdown $4\pi Ts/Q$ as a function of dimensionless time $4tT/(Sr^2)$, with drawdown $s = h - \varphi$. The curves correspond to different values for the dimensionless resistance $c_{top}T/r^2$ of the bounding aquitard. Results are calculated according to (149) and simulated using the generalized solution developed in section 2.3. Numerically inverting Laplace domain solution (148) using the Stehfest (1970) algorithm and applying the fast approximation (151) by Veling and Maas (2010) virtually give the same result (not shown in Figure 17).

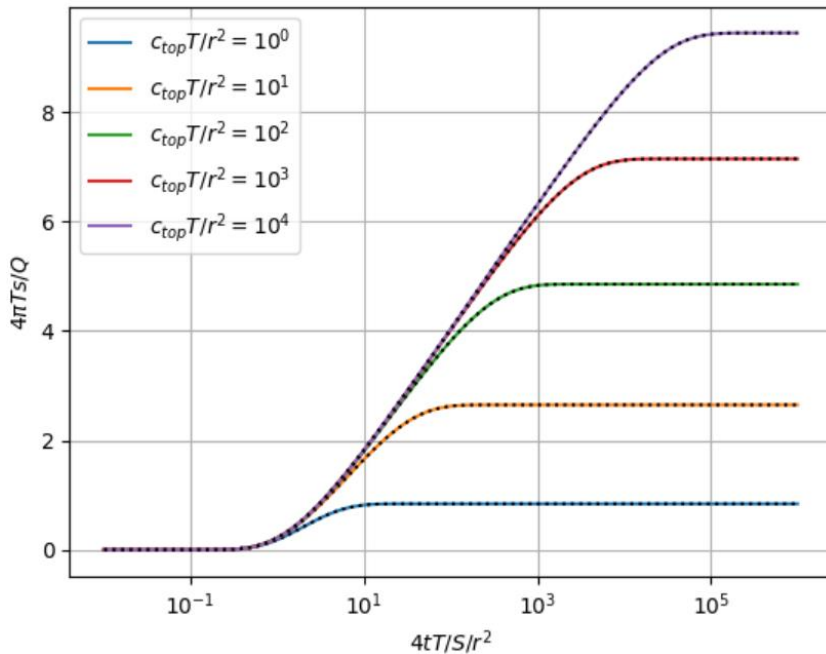


Figure 17. Plot of dimensionless drawdown versus dimensionless time for a pumping well fully penetrating a leaky aquifer. The plotted curves correspond to different values for the dimensionless resistance of the overlying aquitard. The colored solid lines are calculated using the analytical expression (Hantush & Jacob, 1955), the black dotted lines using the generalized semi-analytical solution developed in this chapter. See text for definition of variables and details about the applied solutions.

2.5.11 Hemker's solution for steady flow in a leaky multi-aquifer system

Consider a leaky multi-aquifer system in which aquifer i has a constant transmissivity T_i . Aquifers i and $i + 1$ are separated by an aquitard with constant resistance c_i . Each aquifer has a fully penetrating well-screen through which groundwater flows at constant pumping rate Q_i .

If there is no infiltration, and if the constant heads at the model boundaries are zero, then $\mathbf{b} = \mathbf{v} = \mathbf{0}$. The well has an infinitesimal radius, i.e. $r_{in} \rightarrow 0$; the aquifer system has an infinite extent, i.e. $r_{out} \rightarrow \infty$. Under these assumptions, $\alpha \rightarrow \mathbf{0}$ and $\beta \rightarrow \mathbf{q}$. If the system is leaky, all eigenvalues are

nonzero, and general solution (55) can be written easily in matrix form, recalling that $\mathbf{q} = \mathbf{V}^{-1}\mathbf{T}^{-1}\mathbf{Q}$ and $\mathbf{g} = \mathbf{V}^{-1}\mathbf{h}$:

$$\mathbf{h} = \mathbf{VKV}^{-1}\mathbf{T}^{-1}\mathbf{Q} \quad (152)$$

where matrix \mathbf{K} is a diagonal matrix with nonzero entries $K_{ii} = K_0(r\sqrt{d_i})$. As all constant heads are zero, \mathbf{h} may be interpreted as drawdown due to pumping.

Solution (152) was presented by Hemker (1984), who also discussed parallel flow in a leaky multi-aquifer system. In this case, solution (56) is valid, and $\beta_i \rightarrow q_i/\sqrt{d_i}$, from which it follows that the diagonal terms in \mathbf{K} are $K_{ii} = e^{-(r\sqrt{d_i})}/\sqrt{d_i}$. Recall that diagonal matrix \mathbf{T} is also dependent on the type of flow: $T_{ii} = 2\pi T_i$ in case of axisymmetric flow and $T_{ii} = T_i$ in case of parallel flow.

In general, the eigendecomposition $\mathbf{A} = \mathbf{VDV}^{-1}$ is performed numerically, although it can be done analytically if the number of layers is limited. For instance, the analytical solution for a leaky two-layer system with impervious lower boundary is:

$$\begin{cases} h_1(r) = \frac{y_2 x_1 x_2 (k_1 - k_2) - y_1 (x_1 k_1 - x_2 k_2)}{x_2 - x_1} \\ h_2(r) = \frac{y_2 (x_2 k_1 - x_1 k_2) - y_1 (k_1 - k_2)}{x_2 - x_1} \end{cases}$$

with:

$$\begin{aligned} k_i &= K_0(r\sqrt{d_i}) \\ y_i &= \frac{Q_i}{2\pi T_i} \\ x_i &= 1 - d_i L_2 \\ L_i &= T_i c_{i-1} \\ d_1 &= \frac{L_1 + L_2 + T_2 c_0 - \sqrt{(L_1 + L_2 + T_2 c_0)^2 - 4L_1 L_2}}{2L_1 L_2} \\ d_2 &= \frac{L_1 + L_2 + T_2 c_0 + \sqrt{(L_1 + L_2 + T_2 c_0)^2 - 4L_1 L_2}}{2L_1 L_2} \end{aligned} \quad (153)$$

Solution (153) also holds for parallel flow, except for $k_i = e^{-(r\sqrt{d_i})}/\sqrt{d_i}$ and $y_i = Q_i/T_i$. Alternative solution methods for steady multi-aquifer flow are presented by Hunt (1985, 1986) and by Maas (1986, 1987a). In Chapter 12, solution (152) is applied in combination with the superposition method explained in section 2.4.3 to simulate the effect of a drainage system consisting of pumping and injection wells in a three-layer system.

As an example, consider a leaky aquifer system with impervious lower boundary consisting of two permeable layers with transmissivities $T_1 = 10 \text{ m}^2/\text{d}$ and $T_2 = 100 \text{ m}^2/\text{d}$, respectively. The layers are separated by a semi-pervious layer with resistance $c_1 = 200 \text{ d}$, and the upper layer is covered by a semi-pervious layer with resistance $c_0 = 25 \text{ d}$. Figure 18 shows drawdown s (m) versus distance r (m) due to a well extracting water from both layers respectively at constant pumping rate $Q_1 = -50 \text{ m}^3/\text{d}$ and $Q_2 = -500 \text{ m}^3/\text{d}$ (left graph), and caused by a stream draining water from both layers respectively at constant rate $Q_1 = -0.5 \text{ m}^2/\text{d}$ and $Q_2 = -5 \text{ m}^2/\text{d}$ (right graph). Recall that drawdown s is defined as

the head h minus the initial head in the system. Results are calculated according to (153) and simulated using the generalized solution developed in section 2.3.

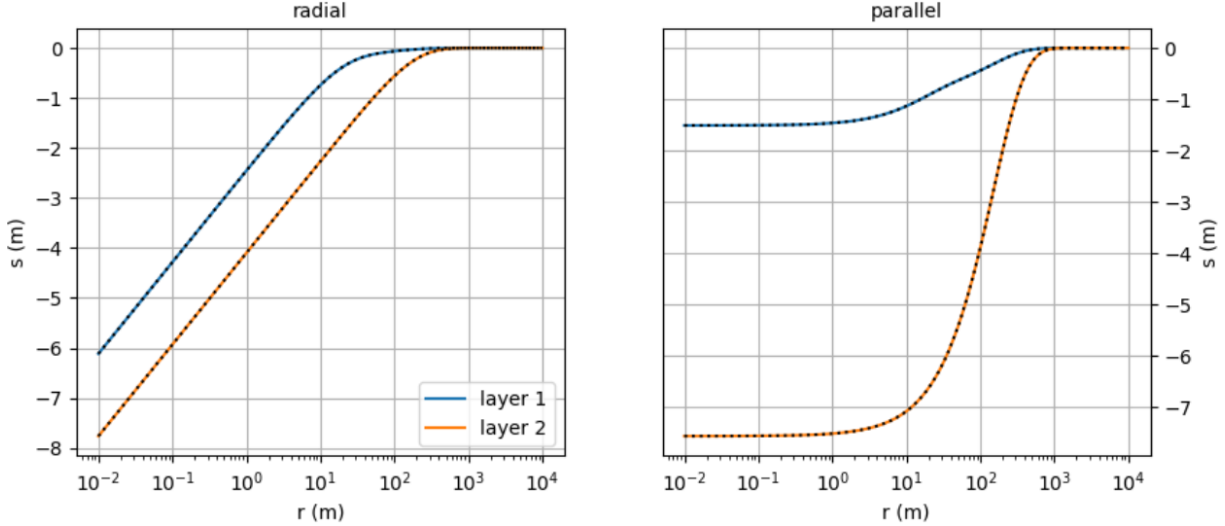


Figure 18. Example of a steady-state leaky two-layer model. Left: Drawdown versus distance plot in case of radial flow to a well extracting from both layers. Right: Drawdown versus distance plot in case of parallel flow to a stream draining both layers. The colored solid lines are calculated using the analytical expression (Hemker, 1984), the black dotted lines using the generalized semi-analytical solution developed in this chapter. See text for definition of variables and details about the model and the applied solutions.

2.5.12 Hemker's solution for unsteady flow in a multi-aquifer system

Consider a multi-aquifer system in which aquifer i has constant transmissivity T_i and constant storativity S_i . Aquifers i and $i + 1$ are separated by an incompressible aquitard with constant resistance c_i . Each aquifer has a fully penetrating well-screen through which groundwater is pumped at constant rate Q_i .

If there is no infiltration, and if the initial heads and constant heads at the model boundaries are zero, then $\mathbf{b} = \mathbf{v} = \mathbf{0}$. If the well has an infinitesimal radius, then $r_{in} \rightarrow 0$. If the aquifer system has an infinite extent, then $r_{out} \rightarrow \infty$. In this case, $\boldsymbol{\alpha} \rightarrow \mathbf{0}$ and $\boldsymbol{\beta} \rightarrow \mathbf{q}$. In case of transient flow, all eigenvalues are nonzero, and Laplace-transformed solution (55) can be written easily in matrix form, recalling that $\mathbf{q} = \mathbf{V}^{-1}\mathbf{T}^{-1}\mathbf{Q}$ and $\mathbf{g} = \mathbf{V}^{-1}\bar{\mathbf{h}}$:

$$\bar{\mathbf{h}} = \mathbf{V}\mathbf{K}\mathbf{V}^{-1}\mathbf{T}^{-1}\mathbf{Q} \quad (154)$$

where matrix \mathbf{K} is a diagonal matrix with nonzero elements $K_{ii} = K_0(r\sqrt{d_i})$. As initial and constant heads are zero, $\bar{\mathbf{h}}$ may be interpreted as the Laplace transform of drawdown due to pumping. Recall that vector \mathbf{Q} contains the Laplace transform of the pumping rates Q_i/p .

Solution (154) is also valid for transient parallel flow in a semi-infinite multi-aquifer system. In this case, general solution (56) must be applied, and $\boldsymbol{\beta}_i \rightarrow \mathbf{q}_i/\sqrt{d_i}$; hence, the diagonal terms in \mathbf{K} are $K_{ii} = e^{-(r\sqrt{d_i})}/\sqrt{d_i}$. Recall that $\mathbf{T}_{ii} = 2\pi T_i$ in case of axisymmetric flow and $\mathbf{T}_{ii} = T_i$ in case of parallel flow.

Hemker (1985) gives the solution for transient axisymmetric multi-aquifer flow in the real time domain, which he obtained by also applying the Hankel transform and inverting the obtained solution analytically. However, as this inverted solution contains an improper integral which must be approximated numerically, Hemker (2000) states it is computationally more efficient to invert solution (154) numerically, for instance, by applying the Stehfest (1970) algorithm.

The eigendecomposition of system matrix A is also performed numerically, although finding an analytical expression for the eigenvalues and eigenvectors is also possible if the number of layers is small. For instance, the exact solution in Laplace space for a confined two-aquifer system with a well in the lower aquifer only, is:

$$\begin{cases} \bar{h}_1(r, p) = \frac{yx_1x_2(k_2 - k_1)}{aL_2} \\ \bar{h}_2(r, p) = \frac{y(x_2k_1 - x_1k_2)}{a} \end{cases}$$

with:

$$k_i = K_0(r\sqrt{d_i})$$

$$y = \frac{Q}{2\pi T_2 p}$$

$$a = \sqrt{(z_1 - z_2)^2 + 4L_1 L_2}$$

$$x_i = d_i - z_2$$

$$L_i = T_i c$$

$$z_i = (1 + S_i cp)L_i$$

$$d_1 = \frac{z_1 + z_2 - a}{2}$$

$$d_2 = \frac{z_1 + z_2 + a}{2} \quad (155)$$

Solution (155) is valid for axisymmetric flow. If it is applied to simulate transient parallel flow in a confined two-aquifer system, then $y = Q/(T_2 p)$ and $k_i = e^{-(r\sqrt{d_i})}/\sqrt{d_i}$. Because $c_0 = c_2 = \infty$ and $Q_1 = 0$, some subscripts were omitted in (155) for notational convenience: the resistance of the aquitard separating the two aquifers is denoted by c , and the pumping rate of the well in the lower aquifer by Q .

Another exact Laplace-transformed solution for the same two-aquifer problem is given by Hunt & Scott (2007), who use the solution of a generalized eigenvalue problem as suggested by Hunt (1985, 1986). They also perform the Stehfest (1970) algorithm to transform the solution in the Laplace domain back to the real time domain. An alternative solution method was presented by Maas (1987b). In Chapter 4, solution (154) is used to verify the hybrid finite-difference finite-element method developed by Lebbe (1988, 1999). The numerical inversion is performed by applying the Stehfest (1970) algorithm. In Chapter 9, the same solution is further investigated to get a better understanding of radial flow to a well in a confined multilayered aquifer system.

As an example, consider a confined aquifer system consisting of two permeable layers with transmissivities $T_1 = 10 \text{ m}^2/\text{d}$ and $T_2 = 100 \text{ m}^2/\text{d}$, and storativities $S_1 = 0.2$ and $S_2 = 0.001$, respectively. The layers are separated by a semi-pervious layer with resistance $c = 200 \text{ d}$. Figure 19 shows drawdown s (m) versus time t (d) at distance $r = 1 \text{ m}$ due to a well extracting water from the lower layer at constant pumping rate $Q = -500 \text{ m}^3/\text{d}$ (left graph), and caused by a stream draining water from the lower layer at constant rate $Q = -0.5 \text{ m}^2/\text{d}$ (right graph). Recall that drawdown s is defined as the head h minus the initial head in the system. Results are calculated according to (155)

and simulated using the generalized solution developed in section 2.3. In both cases, the Laplace domain solution is numerically inverted using the Stehfest (1970) algorithm.

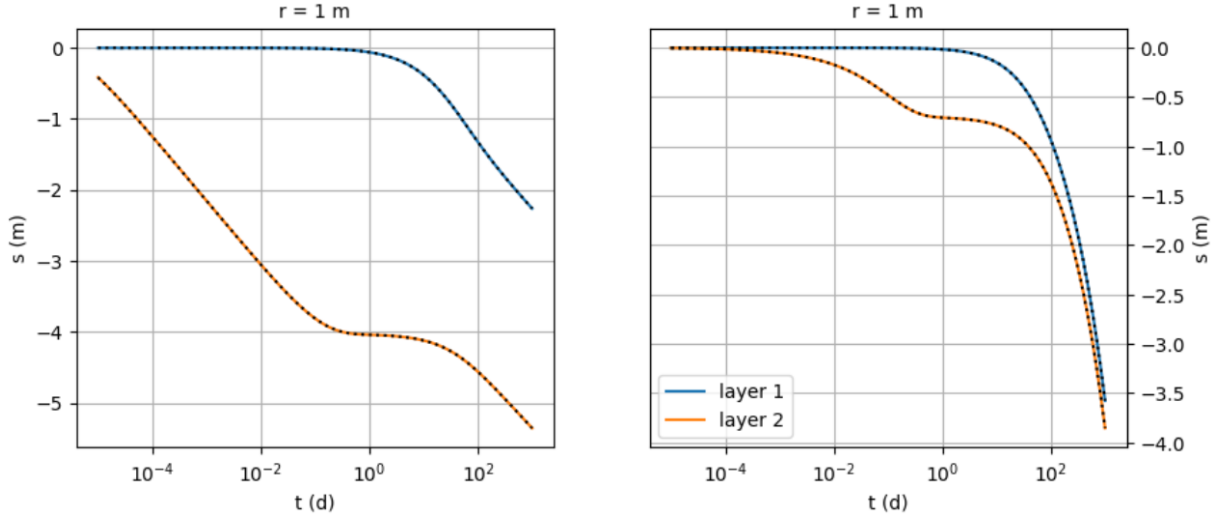


Figure 19. Example of a transient-state confined two-layer model. Left: Drawdown versus time plot in case of radial flow to a well extracting from the lower layer. Right: Drawdown versus time plot in case of parallel flow to a stream draining the lower layer. In both plots, drawdown is shown at a distance of 1 m from the well or stream, respectively. The colored solid lines are calculated using the analytical expression (Hemker, 1985), the black dotted lines using the generalized semi-analytical solution developed in this chapter. See text for definition of variables and details about the model and the applied solutions.

2.5.13 Steady flow in a confined multi-aquifer system

Consider a confined multi-aquifer system in which aquifer i has a constant transmissivity T_i . Aquifers i and $i + 1$ are separated by an aquitard with constant resistance c_i . As the system is confined, $c_0 = c_{n_l} = \infty$. Each aquifer has a fully penetrating well screen through which groundwater flows at constant pumping rate Q_i .

In this case, the solution method of Hemker (1984) is still applicable, although some modifications are required. First, a constant head φ is required at a finite distance r_{out} ; otherwise, the head in the multi-aquifer system would be infinitely large if $r_{out} \rightarrow \infty$. Second, there is always one eigenvalue that equals zero in this case. Bakker (2001) shows that this eigenvalue yields a term in the solution that calculates the head in the equivalent single-aquifer system characterized by total transmissivity $T = \sum_i T_i$ and total discharge $Q = \sum_i Q_i$.

As an example, consider a two-aquifer system where the two aquifers with transmissivities T_1 and T_2 , respectively, are separated by an aquitard with resistance $c_1 = c$. In this case, the first eigenvalue is $d_1 = d = T/(T_1 T_2 c)$ and the second eigenvalue is zero (Haitjema, 2006). Matrix \mathbf{V} holding the corresponding eigenvectors must be inverted:

$$\mathbf{V} = \begin{bmatrix} -T_2/T_1 & 1 \\ 1 & 1 \end{bmatrix} \quad \text{and} \quad \mathbf{V}^{-1} = \frac{T_1}{T} \begin{bmatrix} -1 & 1 \\ 1 & T_2/T_1 \end{bmatrix} \quad (156)$$

If there is no infiltration, i.e. $N = 0$, then $\mathbf{b} = \mathbf{v} = \mathbf{0}$. Evaluating the right-hand side of the outer boundary condition (57) and the inner boundary condition (59), respectively, gives $\mathbf{w}_1 = \mathbf{0}$, $\mathbf{w}_2 = \varphi$, and $\mathbf{q}_1 = (T_1 Q_2 / T_2 - Q_1) / (2\pi T)$, $\mathbf{q}_2 = Q / (2\pi T)$.

According to (55), entry \mathbf{g}_1 corresponding to the nonzero eigenvalue is $\alpha_1 I_0(r\sqrt{d}) + \beta_1 K_0(r\sqrt{d})$. If the well has an infinitesimal radius, i.e. $r_{in} \rightarrow 0$, then $\alpha_1 = -\mathbf{q}_1 K_0(r_{out}\sqrt{d}) / I_0(r_{out}\sqrt{d})$ according to

(77), and $\beta_1 = \mathbf{q}_1$. Entry \mathbf{g}_2 corresponding to the zero eigenvalue is $\alpha_2 \ln(r) + \beta_2$, with $\alpha_2 = -\mathbf{q}_2$ and $\beta_2 = \mathbf{w}_2 + \mathbf{q}_2 \ln(r_{out})$, according to (74) and (75), respectively. Evaluating $\mathbf{h} = \mathbf{V}\mathbf{g}$ finally gives the solution for steady well-flow in a confined two-layer system without areal recharge:

$$\begin{cases} h_1(r) = \varphi + \frac{Q}{2\pi T} \ln\left(\frac{r_{out}}{r}\right) + \frac{xy}{2\pi T T_1} \\ h_2(r) = \varphi + \frac{Q}{2\pi T} \ln\left(\frac{r_{out}}{r}\right) - \frac{xy}{2\pi T T_2} \end{cases}$$

with:

$$x = \frac{I_0(r_{out}\sqrt{d})K_0(r\sqrt{d}) - I_0(r\sqrt{d})K_0(r_{out}\sqrt{d})}{I_0(r_{out}\sqrt{d})}$$

$$y = Q_1 T_2 - Q_2 T_1 \quad (157)$$

Note that the first two terms in both equations of (157) indeed correspond to the Thiem-Dupuit equation (118) to calculate the head in the equivalent single-layer system with total transmissivity T and total pumping rate Q .

The solution for areal recharge on a circular island with a two-aquifer system is derived in the same way. Eigenvalues and eigenvectors are the same; only some of the boundary conditions are different. Suppose there is constant infiltration in the upper aquifer or $N_1 = N$ and $N_2 = 0$; then $\mathbf{b}_1 = N/T_1$ and $\mathbf{b}_2 = 0$ according to (34). From $\mathbf{v} = \mathbf{V}^{-1}\mathbf{b}$, it follows that $\mathbf{v}_1 = -N/T$ and $\mathbf{v}_2 = N/T$. There is no pumping; hence $\mathbf{Q} = \mathbf{q} = \mathbf{0}$. The outer boundary condition is the same; hence $\mathbf{w}_1 = 0$ and $\mathbf{w}_2 = \varphi$.

As the inner model boundary is zero, $\alpha_1 = -\mathbf{v}_1/(dI_0(r_{out}\sqrt{d}))$ according to (77), $\beta_1 = \mathbf{q}_1 = 0$, $\alpha_2 = 0$ according to (74), and $\beta_2 = \mathbf{w}_2 + \mathbf{v}_2 r_{out}^2/4$ according to (75). Element \mathbf{g}_1 corresponding to the nonzero eigenvalue is $\alpha_1 I_0(r\sqrt{d}) + \mathbf{v}_1/d$; element \mathbf{g}_2 corresponding to the zero eigenvalue is $\beta_2 - \mathbf{v}_2 r^2/4$. Evaluating $\mathbf{h} = \mathbf{V}\mathbf{g}$ gives:

$$\begin{cases} h_1(r) = \varphi + \frac{N}{4T}(r_{out}^2 - r^2) + \frac{T_2}{T_1} \frac{N}{Td} \left[1 - \frac{I_0(r\sqrt{d})}{I_0(r_{out}\sqrt{d})} \right] \\ h_2(r) = \varphi + \frac{N}{4T}(r_{out}^2 - r^2) - \frac{N}{Td} \left[1 - \frac{I_0(r\sqrt{d})}{I_0(r_{out}\sqrt{d})} \right] \end{cases} \quad (158)$$

The first two terms in the equations of (158) also correspond to the equivalent single-layer solution (120). As explained by Bakker and Strack (2003), the drawdown caused by the well, which is given by solution (157) for $\varphi = 0$, can be superimposed on the solution for areal recharge (158) to obtain the steady head during pumping. Chapter 5 discusses in more detail the solution for a well and a circular infiltration pond in a multilayer aquifer system and also presents the solution method by Bakker and Strack (2003).

As an example, consider a phreatic aquifer system with impervious lower boundary consisting of two permeable layers with transmissivities $T_1 = 10 \text{ m}^2/\text{d}$ and $T_2 = 100 \text{ m}^2/\text{d}$, respectively. The layers are separated by a semi-pervious layer with resistance $c = 200 \text{ d}$. There is recharge at the top of the system characterized by a constant flux $N = 0.0005 \text{ m}/\text{d}$. A pumping well extracts water from both layers respectively at constant pumping rate $Q_1 = -50 \text{ m}^3/\text{d}$ and $Q_2 = -100 \text{ m}^3/\text{d}$. The aquifer system is laterally bounded, with $r_{out} = 1000 \text{ m}$. At the outer model boundary, a constant head φ is defined in

both layers, which is equal to 10 m. Figure 20 shows head h (m) versus distance r (m) for the case without recharge (left graph) and with recharge (right graph). The results that neglect recharge are calculated using (157), while the results that consider recharge are obtained by superposition of (157) and (158). Results are also simulated using the generalized solution developed in section 2.3.

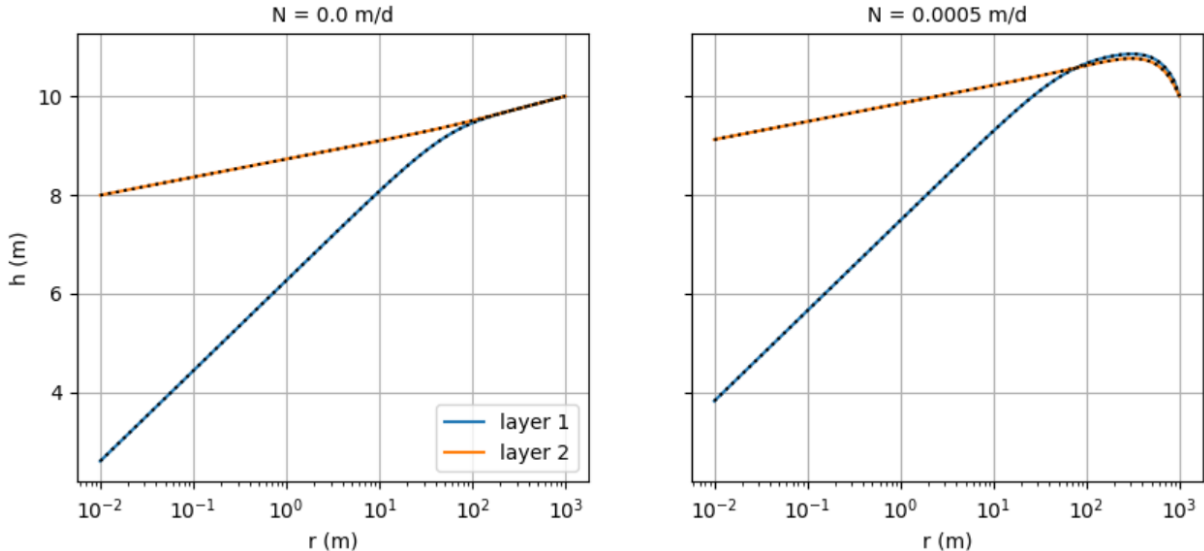


Figure 20. Example of a steady-state two-layer model simulating flow to a well extracting from both layers. Left: Drawdown versus distance plot for the case without recharge. Right: Drawdown versus distance plot for the case with recharge. The colored solid lines are calculated using the analytical expression (Bakker & Strack, 2003), the black dotted lines using the generalized semi-analytical solution developed in this chapter. See text for definition of variables and details about the model and the applied solutions.

2.6. Summary

This chapter presents a generalized solution for the simulation of axisymmetric or parallel flow in a multilayered aquifer system. It can handle both steady and transient flow in confined and leaky systems subject to areal recharge. The aquifer system is laterally bounded or unbounded, and the source or sink at the inner boundary is characterized by a constant head or constant discharge.

Applying the superposition method, a time-varying inner boundary value can be defined. Using the same technique, it is also possible to simulate flow in a multilayer system in which multiple wells are located. This is demonstrated in Chapter 12 presenting the optimization of a combined pumping and deep-infiltration system, while Chapter 11 discusses the limitations of these superposition models in the context of sustainable pumping. Finally, this chapter illustrates how the generalized solution can be simplified to well-known one- and two-layer solutions described in the hydrogeological literature. The generalized semi-analytical solution method is verified against these simpler solutions. Some of the one-dimensional solutions presented in this chapter are discussed in more detail in Chapter 10, where they are used to derive formulas to estimate the radius of influence.

The presented semi-analytical solution is not new, but synthesizes several multilayer solutions described in the hydrogeological literature (Bakker & Strack, 2003; Hemker, 1984, 1985, 1999a). In Chapter 5 and Chapter 6, the solution is extended, respectively to include radial variations in hydraulic parameters and to define more realistic conditions at the well face. The resulting multilayer-multizone solution can be applied to solve nonlinear problems involving drainage and unconfined flow, as is illustrated in Chapter 7 and Chapter 8. In chapters 5 to 8, the extended semi-analytical solution methods are carefully verified against existing analytical models and compared with the finite-difference method discussed in next Chapter 3. This is required as the semi-analytical solution method actually is an approximation because of the numerical inversion in case of transient

flow. In Chapter 4, both the semi-analytical and the finite-difference method are used to verify the hybrid finite-difference finite-element method developed by Lebbe (1988, 1999) to simulate axisymmetric flow to a pumping well in a confined multilayer aquifer system. In Chapter 9, an approximate semi-analytical solution for large values of time is developed which offers some new insights in the hydraulics of confined multilayer well-flow.

2.7. References

- Ashjari, J. (2013). Determination of Storage Coefficients During Pumping and Recovery. *Ground Water*, 51(1), 122–127. <https://doi.org/10.1111/j.1745-6584.2012.00917.x>
- Bakker, M. (1999). Simulating groundwater flow in multi-aquifer systems with analytical and numerical Dupuit-models. *Journal of Hydrology*, 222(1–4), 55–64. [https://doi.org/10.1016/S0022-1694\(99\)00089-X](https://doi.org/10.1016/S0022-1694(99)00089-X)
- Bakker, M. (2001). An analytic, approximate method for modeling steady, three-dimensional flow to partially penetrating wells. *Water Resources Research*, 37(5). <https://doi.org/10.1029/2000WR900400>
- Bakker, M. (2013a). Analytic Modeling of Transient Multilayer Flow. In P. K. Mishra & K. Kuhlman (Eds.), *Advances in Hydrogeology* (pp. 95–114). New York, NY: Springer, Heidelberg. https://doi.org/10.1007/978-1-4614-6479-2_5
- Bakker, M. (2013b). Semi-analytic modeling of transient multi-layer flow with TTIm. *Hydrogeology Journal*, 21(4), 935–943. <https://doi.org/10.1007/s10040-013-0975-2>
- Bakker, M. (2022). TTIm, A Multi-Layer, Transient, Analytic Element Model. Retrieved from <https://github.com/mbakker7/ttim>
- Bakker, M., & Hemker, C. J. (2002). A Dupuit formulation for flow in layered, anisotropic aquifers. *Advances in Water Resources*, 25(7), 747–754. [https://doi.org/10.1016/S0309-1708\(02\)00074-X](https://doi.org/10.1016/S0309-1708(02)00074-X)
- Bakker, M., & Hemker, C. J. (2004). Analytic solutions for groundwater whirls in box-shaped, layered anisotropic aquifers. *Advances in Water Resources*, 27(11), 1075–1086. <https://doi.org/10.1016/j.advwatres.2004.08.009>
- Bakker, M., & Strack, O. D. L. (2003). Analytic elements for multiaquifer flow. *Journal of Hydrology*, 271(1–4). [https://doi.org/10.1016/S0022-1694\(02\)00319-0](https://doi.org/10.1016/S0022-1694(02)00319-0)
- Bear, J. (1979). *Hydraulics of Groundwater. McGraw-Hill series in water resources and environmental engineering*. New York: McGraw-Hill.
- Bennett, G. D., Reilly, T. E., & Hill, M. C. (1990). *Technical training notes in ground-water hydrology: radial flow to a well*. U.S. Geological Survey. <https://doi.org/10.3133/wri894134>
- Boulton, N. S. (1954). Unsteady radial flow to a pumped well allowing for delayed yield from storage. *General Assembly of Rome, Tome II, Groundwater, IAHS publ. 37*, 472–477.
- Boulton, N. S. (1963). Analysis of data from non-equilibrium pumping tests allowing for delayed yield from storage. *Proceedings of the Institution of Civil Engineers*, 26(3), 469–482. <https://doi.org/10.1680/iicep.1963.10409>
- Boussinesq, J. (1904). Recherches théoriques sur l’écoulement des nappes d’eau infiltrées dans le sol et sur le débit des sources (in French). *Journal De Mathématiques Pures Et Appliquées*, 10, 5–78.

- Bredehoeft, J. D. (2002). The Water Budget Myth Revisited: Why Hydrogeologists Model. *Ground Water*, 40(4). <https://doi.org/10.1111/j.1745-6584.2002.tb02511.x>
- Bredehoeft, J. D. (2008). An interview with C.V. Theis. *Hydrogeology Journal*, 16(1). <https://doi.org/10.1007/s10040-007-0248-z>
- Bredehoeft, J. D., Papadopoulos, S. S., & Cooper, H. H. (1982). The water budget myth. In *Scientific Basis of Water Resources management Studies in Geophysics* (pp. 51–57). National Academy Press.
- Bruggeman, G. A. (1972). The Reciprocity Principle in Flow Through Heterogeneous Porous Media. In *Developments in Soil Science* (Vol. 2, pp. 136–149). Amsterdam: Elsevier. [https://doi.org/10.1016/S0166-2481\(08\)70535-X](https://doi.org/10.1016/S0166-2481(08)70535-X)
- Bruggeman, G. A. (1999). *Analytical solutions of geohydrological problems. Developments in Water Science* 46. Amsterdam: Elsevier.
- Carlson, F., & Randall, J. (2012). MLU: A Windows Application for the Analysis of Aquifer Tests and the Design of Well Fields in Layered Systems. *Groundwater*, 50(4), 504–510. <https://doi.org/10.1111/j.1745-6584.2012.00945.x>
- Cheng, A. H.-D., & Morohunfola, O. K. (1993). Multilayered leaky aquifer systems: 1. Pumping well solutions. *Water Resources Research*, 29(8), 2787–2800. <https://doi.org/10.1029/93WR00768>
- Cooley, R. L. (1972). Numerical simulation of flow in an aquifer overlain by a water table aquitard. *Water Resources Research*, 8(4), 1046–1050. <https://doi.org/10.1029/WR008i004p01046>
- Cooley, R. L., & Case, C. M. (1973). Effect of a water table aquitard on drawdown in an underlying pumped aquifer. *Water Resources Research*, 9(2), 434–447. <https://doi.org/10.1029/WR009i002p00434>
- Cooper, H. H., & Jacob, C. E. (1946). A generalized graphical method for evaluating formation constants and summarizing well-field history. *Transactions, American Geophysical Union*, 27(4), 526–534. <https://doi.org/10.1029/TR027i004p00526>
- Cooper, H. H., Bredehoeft, J. D., & Papadopoulos, I. S. (1967). Response of a finite-diameter well to an instantaneous charge of water. *Water Resources Research*, 3(1), 263–269. <https://doi.org/10.1029/WR003i001p00263>
- Darcy, H. (1856). *Les fontaines publiques de la ville de Dijon (In French)*. Paris: Dalmont.
- de Glee, G. J. (1930). *Over grondwaterstroomingen bij wateronttrekking door middel van putten (in Dutch)* (PhD thesis). Technische Hoogeschool Delft, Drukkerij J. Waltman. Jr., Delft.
- de Hoog, F. R., Knight, J. H., & Stokes, A. N. (1982). An Improved Method for Numerical Inversion of Laplace Transforms. *SIAM Journal on Scientific and Statistical Computing*, 3(3), 357–366. <https://doi.org/10.1137/0903022>
- Dupuit, J. (1857). Mouvement de l'eau à travers les terrains perméables (in French). *Comptes Rendus de l'Académie Des Sciences*, 45, 92–96.
- Dupuit, J. (1863). *Etude Théoriques et Pratiques Sur le Mouvement Des Eaux Dans Les Canaux Découverts et à Travers Les Terrains Perméables (in French)*. Paris: Dunot.
- Edelman, J. H. (1947). *Over de berekening van grondwaterstroomingen (in Dutch)*. TU Delft, Delft.

- Ernst, L. F. (1971). Analysis of groundwater flow to deep wells in areas with a non-linear function for the subsurface drainage. *Journal of Hydrology*, 14(2). [https://doi.org/10.1016/0022-1694\(71\)90004-7](https://doi.org/10.1016/0022-1694(71)90004-7)
- Gradshteyn, I., & Ryzhik, I. (2007). *Table of integrals, series, and products (Translated from the Russian)* (Seventh edition). Amsterdam: Elsevier/Academic Press.
- Haitjema, H. (1995). *Analytic Element Modeling of Groundwater Flow*. San Diego: Academic Press. <https://doi.org/10.1016/B978-0-12-316550-3.X5000-4>
- Haitjema, H. (2006). The Role of Hand Calculations in Ground Water Flow Modeling. *Ground Water*, 44(6). <https://doi.org/10.1111/j.1745-6584.2006.00189.x>
- Halász, B. (1975). Eigenheiten von geschichteten hydrogeologischen Systemen (in Hungarian). *Hidrol. Közl.*, 11, 505–507.
- Halász, B., & Székely, F. (1979). Computation of drawdown in wells in stratified aquifer systems (In Russian). In *I.A.H. Methods for Evaluation of Groundwater Resources. XV-1. Congr. Vilnius* (pp. 50–53). Moscow.
- Hantush, M. S. (1949). *Plain potential flow of ground water with linear leakage*. (PhD Thesis). University of Utah, Salt Lake City.
- Hantush, M. S. (1960). Modification of the theory of leaky aquifers. *Journal of Geophysical Research*, 65(11), 3713–3725. <https://doi.org/10.1029/JZ065i011p03713>
- Hantush, M. S. (1961a). Drawdown around a partially penetrating well. *Journal of the Hydraulics Division, Proceedings of the American Society of Civil Engineers*, 87(HY4), 83–98.
- Hantush, M. S. (1961b). Aquifer tests on partially penetrating wells. *Journal of the Hydraulics Division, Proceedings of the American Society of Civil Engineers*, 87(HY5), 171–194.
- Hantush, M. S. (1964). Hydraulics of wells. In V. T. Chow (Ed.), *Advances in Hydroscience* (Vol. I, pp. 281–432). New York and London: Academic Press.
- Hantush, M. S. (1967). Flow to wells in aquifers separated by a semipervious layer. *Journal of Geophysical Research*, 72(6), 1709–1720. <https://doi.org/10.1029/JZ072i006p01709>
- Hantush, M. S., & Jacob, C. E. (1955). Non-steady radial flow in an infinite leaky aquifer. *Transactions, American Geophysical Union*, 36(1), 95–100. <https://doi.org/10.1029/TR036i001p00095>
- Hemker, C. J. (1984). Steady groundwater flow in leaky multiple-aquifer systems. *Journal of Hydrology*, 72(3–4), 355–374. [https://doi.org/10.1016/0022-1694\(84\)90089-1](https://doi.org/10.1016/0022-1694(84)90089-1)
- Hemker, C. J. (1985). Transient well flow in leaky multiple-aquifer systems. *Journal of Hydrology*, 81(1–2), 111–126. [https://doi.org/10.1016/0022-1694\(85\)90170-2](https://doi.org/10.1016/0022-1694(85)90170-2)
- Hemker, C. J. (1999a). Transient well flow in vertically heterogeneous aquifers. *Journal of Hydrology*, 225(1–2), 1–18. [https://doi.org/10.1016/S0022-1694\(99\)00137-7](https://doi.org/10.1016/S0022-1694(99)00137-7)
- Hemker, C. J. (1999b). Transient well flow in layered aquifer systems: the uniform well-face drawdown solution. *Journal of Hydrology*, 225(1–2), 19–44. [https://doi.org/10.1016/S0022-1694\(99\)00093-1](https://doi.org/10.1016/S0022-1694(99)00093-1)
- Hemker, C. J. (2000). *Groundwater flow in layered aquifer systems* (PhD thesis). VU, Amsterdam.

- Hemker, C. J., & Bakker, M. (2006). Analytical solutions for whirling groundwater flow in two-dimensional heterogeneous anisotropic aquifers. *Water Resources Research*, 42(12). <https://doi.org/10.1029/2006WR004901>
- Hemker, C. J., & Maas, C. (1987). Unsteady flow to wells in layered and fissured aquifer systems. *Journal of Hydrology*, 90(3–4), 231–249. [https://doi.org/10.1016/0022-1694\(87\)90069-2](https://doi.org/10.1016/0022-1694(87)90069-2)
- Hemker, C. J., & Post, V. E. A. (2019). MLU for Windows. Amsterdam. Retrieved from <https://www.microfem.com/products/mlu.html>
- Houben, G. J., & Batelaan, O. (2021). The Thiem team – Adolf and Günther Thiem, two forefathers of hydrogeology. *Hydrology and Earth System Sciences Discussions*.
- Huisman, L., & Kemperman, J. (1951). Bemaling van spanningsgrondwater (in Dutch). *Ingenieur*, 62, B.29-B.35.
- Hunt, B. (1985). Flow to a Well in a Multiaquifer System. *Water Resources Research*, 21(11), 1637–1641. <https://doi.org/10.1029/WR021i011p01637>
- Hunt, B. (1986). Solutions for steady groundwater flow in multi-layer aquifer systems. *Transport in Porous Media*, 1(4), 419–429. <https://doi.org/10.1007/BF00208046>
- Hunt, B., & Scott, D. (2007). Flow to a Well in a Two-Aquifer System. *Journal of Hydrologic Engineering*, 12(2), 146–155. [https://doi.org/10.1061/\(ASCE\)1084-0699\(2007\)12:2\(146\)](https://doi.org/10.1061/(ASCE)1084-0699(2007)12:2(146))
- Jacob, C. E. (1940). On the flow of water in an elastic artesian aquifer. *Transactions, American Geophysical Union*, 21(2), 574. <https://doi.org/10.1029/TR021i002p00574>
- Jacob, C. E. (1946). Radial flow in a leaky artesian aquifer. *Transactions, American Geophysical Union*, 27(2). <https://doi.org/10.1029/TR027i002p00198>
- Jacob, C. E. (1963). The recovery method for determining the coefficient of transmissibility. In *Methods of Determining Permeability, Transmissibility and Drawdown*. USGS Water Supply Paper 1536-I.
- Javandel, I., & Witherspoon, P. A. (1983). Analytical solution of a partially penetrating well in a two-layer aquifer. *Water Resources Research*, 19(2), 567–578. <https://doi.org/10.1029/WR019i002p00567>
- Kooper, J. (1914). Beweging van het water in den bodem bij onttrekking door bronnen (in Dutch). *Ingenieur*, 29, 697–716.
- Kruseman, G. P., & de Ridder, N. A. (1990). *Analysis and Evaluation of Pumping Test Data* (2nd ed.). Wageningen: ILRI Publication 47.
- Kyrieleis, W., & Sichardt, W. (1930). *Grundwasserabsenkung bei Fundierungsarbeiten (in German)*. Berlin: Springer.
- Lebbe, L. C. (1988). *Uitvoering van pomproeven en interpretatie door middel van een invers model (in Dutch)*. Ghent University, Ghent, Belgium.
- Lebbe, L. C. (1999). *Hydraulic Parameter Identification. Generalized Interpretation Method for Single and Multiple Pumping Tests*. Berlin Heidelberg: Springer-Verlag.
- Li, Y., & Neuman, S. P. (2007). Flow to a Well in a Five-Layer System with Application to the Oxnard Basin. *Ground Water*, 45(6), 672–682. <https://doi.org/10.1111/j.1745-6584.2007.00357.x>

- Maas, C. (1986). The use of matrix differential calculus in problems of multiple-aquifer flow. *Journal of Hydrology*, 88(1–2). [https://doi.org/10.1016/0022-1694\(86\)90196-4](https://doi.org/10.1016/0022-1694(86)90196-4)
- Maas, C. (1987a). Groundwater flow to a well in a layered porous medium: 1. Steady flow. *Water Resources Research*, 23(8), 1675–1681. <https://doi.org/10.1029/WR023i008p01675>
- Maas, C. (1987b). Groundwater flow to a well in a layered porous medium: 2. Nonsteady multiple-aquifer flow. *Water Resources Research*, 23(8), 1683–1688. <https://doi.org/10.1029/WR023i008p01683>
- Meesters, A. G. C. A., Hemker, C. J., & van den Berg, E. H. (2004). An approximate analytical solution for well flow in anisotropic layered aquifer systems. *Journal of Hydrology*, 296(1–4), 241–253. <https://doi.org/10.1016/j.jhydrol.2004.03.021>
- Mishra, P. K., & Kuhlman, K. L. (2013). Unconfined Aquifer Flow Theory: From Dupuit to Present. In P. K. Mishra & K. L. Kuhlman (Eds.), *Advances in Hydrogeology* (pp. 185–202). New York, NY: Springer New York. https://doi.org/10.1007/978-1-4614-6479-2_9
- Mjatlev, A. N. (1947). Pressure complex of underground water and wells (in Russian). *Izv. Akad. Nauk SSSR Otd. Tekh. Nauk.*, 9.
- Moench, A. F. (1985). Transient Flow to a Large-Diameter Well in an Aquifer With Storative Semiconfining Layers. *Water Resources Research*, 21(8), 1121–1131. <https://doi.org/10.1029/WR021i008p01121>
- Moench, A. F. (1993). Computation of Type Curves for Flow to Partially Penetrating Wells in Water-Table Aquifers. *Ground Water*, 31(6), 966–971. <https://doi.org/10.1111/j.1745-6584.1993.tb00870.x>
- Moench, A. F. (1995). Combining the Neuman and Boulton Models for Flow to a Well in an Unconfined Aquifer. *Ground Water*, 33(3), 378–384. <https://doi.org/10.1111/j.1745-6584.1995.tb00293.x>
- Moench, A. F. (1996). Flow to a Well in a Water-Table Aquifer: An Improved Laplace Transform Solution. *Ground Water*, 34(4), 593–596. <https://doi.org/10.1111/j.1745-6584.1996.tb02045.x>
- Moench, A. F., & Ogata, A. (1981). A numerical inversion of the laplace transform solution to radial dispersion in a porous medium. *Water Resources Research*, 17(1), 250–252. <https://doi.org/10.1029/WR017i001p00250>
- Moench, A. F., & Ogata, A. (1984). Analysis of constant discharge wells by numerical inversion of Laplace transform solutions. In J. Rosensheim & G. D. Bennett (Eds.), *Groundwater Hydraulics. Water Resour. Monogr. Ser. 9.* (pp. 146–170). Washington D.C.: Am. Geophys. Union.
- Neuman, S. P. (1968). *Transient Flow of Ground Water to Wells in Multiple-Aquifer Systems*. (PhD). University of California, Berkley, California.
- Neuman, S. P. (1972). Theory of flow in unconfined aquifers considering delayed response of the water table. *Water Resources Research*, 8(4), 1031–1045. <https://doi.org/10.1029/WR008i004p01031>
- Neuman, S. P. (1974). Effect of partial penetration on flow in unconfined aquifers considering delayed gravity response. *Water Resources Research*, 10(2), 303–312. <https://doi.org/10.1029/WR010i002p00303>

- Neuman, S. P., & Witherspoon, P. A. (1969a). Applicability of Current Theories of Flow in Leaky Aquifers. *Water Resources Research*, 5(4). <https://doi.org/10.1029/WR005i004p00817>
- Neuman, S. P., & Witherspoon, P. A. (1969b). Theory of Flow in a Confined Two Aquifer System. *Water Resources Research*, 5(4), 803–816. <https://doi.org/10.1029/WR005i004p00803>
- Neuman, S. P., & Witherspoon, P. A. (1972). Field determination of the hydraulic properties of leaky multiple aquifer systems. *Water Resources Research*, 8(5), 1284–1298. <https://doi.org/10.1029/WR008i005p01284>
- Olsthoorn, T. N. (2006). Van Edelman naar Bruggeman (in Dutch). *Stromingen*, 12(1), 5–12.
- Papadopoulos, I. S., & Cooper, H. H. (1967). Drawdown in a well of large diameter. *Water Resources Research*, 3(1), 241–244. <https://doi.org/10.1029/WR003i001p00241>
- Polubarnova-Kochina, P. Y. (1962). *Theory of Groundwater Movement*. Princeton, N.J.: Princeton University Press.
- Reilly, T. E., & Harbaugh, A. W. (1993). Simulation of cylindrical flow to a well using the U.S. Geological Survey Modular Finite-Difference Ground-Water Flow Model. *Ground Water*, 31(3), 489–494. <https://doi.org/10.1111/j.1745-6584.1993.tb01851.x>
- Reilly, T. E., Franke, O. L., & Bennett, G. D. (1987). *The principle of superposition and its application in ground-water hydraulics*. U.S. Geological Survey.
- Renard, P. (2005). Hydraulics of Wells and Well Testing. In M. G. Anderson (Ed.), *Encyclopedia of Hydrological Sciences* (Vol. 4). Chichester, UK: John Wiley & Sons, Ltd. <https://doi.org/10.1002/0470848944.hsa154a>
- Ritzi, R. W., & Bobeck, P. (2008). Comprehensive principles of quantitative hydrogeology established by Darcy (1856) and Dupuit (1857). *Water Resources Research*, 44(10). <https://doi.org/10.1029/2008WR007002>
- Stehfest, H. (1970). Algorithm 368: Numerical inversion of Laplace transforms [D5]. *Communications of the ACM*, 13(1), 47–49. <https://doi.org/10.1145/361953.361969>
- Strack, O. D. L. (1989). *Groundwater Mechanics*. Old Tappan, N. J.: Prentice-Hall.
- Székely, F. (1978). *Computing problems in well hydraulics (in Hungarian)*, Res. Cent. Water Resour. Res. Dev. (VITUKI), Budapest. Budapest.
- Theis, C. V. (1935). The relation between the lowering of the Piezometric surface and the rate and duration of discharge of a well using ground-water storage. *Transactions, American Geophysical Union*, 16(2), 519–524. <https://doi.org/10.1029/TR016i002p00519>
- Theis, C. V. (1941). The effect of a well on the flow of a nearby stream. *Transactions, American Geophysical Union*, 22(3), 734. <https://doi.org/10.1029/TR022i003p00734>
- Thiem, A. (1870). Die Ergiebigkeit artesischer Bohrlöcher, Schachtbrunnen und Filtergalerien (in German). *Journal Für Gasbeleuchtung Und Wasserversorgung*, 13, 450–467.
- Thiem, G. (1906). *Hydrologische Methoden (in German)*. Leipzig: Gebhardt.
- Veling, E. J. M., & Maas, C. (2009). Strategy for solving semi-analytically three-dimensional transient flow in a coupled N-layer aquifer system. *Journal of Engineering Mathematics*, 64(2), 145–161. <https://doi.org/10.1007/s10665-008-9256-9>

Veling, E. J. M., & Maas, C. (2010). Hantush Well Function revisited. *Journal of Hydrology*, 393(3–4).
<https://doi.org/10.1016/j.jhydrol.2010.08.033>

Verruijt, A. (1970). *Theory of Groundwater Flow*. London: Macmillan Press.

Yeh, H.-D., & Chang, Y.-C. (2013). Recent advances in modeling of well hydraulics. *Advances in Water Resources*, 51, 27–51. <https://doi.org/10.1016/j.advwatres.2012.03.006>

Yu, W. S. (1987). Steady ground-water flow through layered media. *Transport in Porous Media*, 2(2), 103–127. <https://doi.org/10.1007/BF00142654>

Chapter 3. Finite-Difference Approach for Simulating Multilayer Flow

3.1. Introduction

The finite-difference method is well-known and frequently used by groundwater practitioners, as it is implemented in the MODFLOW family of codes, which may be considered the de facto standard code for groundwater modeling. In this chapter, the finite-difference approach developed by Louwyck (2011) and verified by Louwyck (2011) and Louwyck et al. (2012, 2014) is presented and applied to solve the problem stated in previous Chapter 2 numerically instead of semi-analytically. The approach is very similar to the finite-difference formulation implemented in MODFLOW versions that use a structured grid (Harbaugh, 2005; Harbaugh et al., 2000; Harbaugh & McDonald, 1996a, 1996b; McDonald & Harbaugh, 1984, 1988). Using this approach, it is even possible to trick MODFLOW into simulating axisymmetric multilayer flow by merely modifying some of the input parameters (Louwyck et al., 2012, 2014). Another option is to use the software code MAxSym written in Matlab (Louwyck, 2011). Before introducing this finite-difference approach and its implementations, the history of numerical groundwater modeling is summarized. Unlike the other chapters presenting solutions for simulating multilayer flow, this chapter does not contain specific examples. Interested readers are referred to Louwyck (2011) and Louwyck et al. (2012, 2014).

3.1.1. A brief history of numerical groundwater modeling

In the previous chapter, the history of analytical well-flow models was discussed briefly starting with the work of Dupuit (1857, 1863). The dawn of numerical groundwater modeling is situated about one century later. Different numerical approaches were applied; the most common are the finite-difference and the finite-element methods (Saatsaz & Eslamian, 2020; Yeh, 1999). Saatsaz and Eslamian (2020) refer to Raats and Knight (2018) to state the finite-difference method was introduced by Richardson (1910, 1925), whereas they mention Turner et al. (1956) as the first to theorize the finite-element method, as known in its present form. Both methods are discussed in detail in several textbooks on groundwater modeling (Anderson et al., 2015; Anderson & Woessner, 1992; Wang & Anderson, 1982). The control volume finite-difference method implemented in MODFLOW 6 (Langevin et al., 2017) is the third important numerical approach that was applied in one of the first numerical groundwater models by Tyson and Weber (1964), and that was explored in more detail by Narasimhan and Witherspoon (1976). In those early applications, the method was called integrated finite differences (Anderson et al., 2015).

According to Pinder and Bredehoeft (1968), numerical methods were introduced into hydrogeology by Stallman (1956), and the next important application of the numerical approach was published by Fayers and Sheldon (1962). Pinder and Bredehoeft (1968) also refer to Freeze (1966), Bittenger et al. (1967), and Rubin (1968). According to Pinder (1988), saturated flow problems were among the earliest to be considered numerically, and he refers to Remson et al. (1965), Freeze and Witherspoon (1966), Bittenger et al. (1967), Pinder and Bredehoeft (1968), Javandel and Witherspoon (1968), and Freeze (1971). Zhou and Li (2011) give a brief history in regional groundwater flow modeling and they name Freeze and Witherspoon (1966, 1967, 1968) as the first to use numerical models for the simulation of steady state regional flow patterns. Narasimhan and Witherspoon (1982) give an overview of the finite-element method and refer to Zienkiewicz et al. (1966), Taylor and Brown (1967), Javandel and Witherspoon (1968, 1969), and Neuman and Witherspoon (1970, 1971). Digital computer modeling was also part of some groundwater studies carried out by the British Institute of

Geological Sciences between 1965 and 1977 (Gray, 2004). For instance, Lloyd (1969) constructed the first numerical groundwater model in the Middle East (Lloyd, 2004).

At about the same time as numerical techniques were developed to solve more complicated groundwater problems, soil physicists were independently pursuing the simulation of flow in the unsaturated zone using numerical methods, which is mathematically even more complex due to the coexistence of water and air in this zone. Pinder (1988) refers to Klute (1952), Day and Luthin (1956), Youngs (1957), Whisler and Klute (1965), Rubin (1968), and Green et al. (1970). Of particular interest is the work of Drake et al. (1969) and Drake and Ellingson (1970a, 1970b) since they solve the problem of radial flow of soil moisture using numerical techniques.

At the U.S. Geological Survey, the two- and three-dimensional finite-difference models described by Trescott (1975), Trescott and Larson (1976), and Trescott et al. (1976) were used extensively before the first version of MODFLOW (McDonald & Harbaugh, 1984) entered the picture. The purpose of this first MODFLOW version was to integrate all the commonly used simulation capabilities into a single code (Langevin et al., 2017; McDonald & Harbaugh, 2003). The finite-difference model of Trescott et al. (1976) superseded the “digital model for aquifer elevation” developed by Pinder (1970), whereas Trescott (1975) was inspired by Remson et al. (1971). MODFLOW-88 (McDonald & Harbaugh, 1988) was largely the same as the first MODFLOW version developed by McDonald and Harbaugh (1984), and by the early 1990s, it had become the most widely used groundwater flow model (Langevin et al., 2017; McDonald & Harbaugh, 2003).

MODFLOW-96 (Harbaugh & McDonald, 1996a, 1996b) was an overall update primarily to improve ease of use, whereas the modular design was expanded in the MODFLOW-2000 version (Harbaugh et al., 2000) to facilitate the incorporation of related equations (Langevin et al., 2017; McDonald & Harbaugh, 2003). The parts of the code that solve a major equation or set of related equations are called processes, and this concept was further expanded in MODFLOW-2005 (Harbaugh, 2005), which was followed by the development of numerous MODFLOW variants (Langevin et al., 2017). One of these variants particularly interesting for the design of axisymmetric models, is MODFLOW-USG (Panday et al., 2013) as it can handle other than rectilinear grids. The latest version, MODFLOW 6 (Langevin et al., 2017), is designed to support many of the capabilities that have been implemented in those variants. For instance, it also applies the control volume finite-difference formulation implemented in MODFLOW-USG (Panday et al., 2013) that allows the use of flexible unstructured grid geometries.

3.1.2. Axisymmetric numerical models

The assumption of axial symmetry reduces the governing flow equation by one dimension, which simplifies the mathematical description and makes it easier to find closed-form analytical solutions. If the governing equation is solved numerically, then the benefit of assuming axial symmetry is a substantial reduction of computer runtime (Langevin, 2008). This is advantageous in applications that require a large number of computer runs, such as interpretation methods for aquifer tests that use a groundwater flow model coupled to a numerical optimization algorithm (e.g. Hemker, 1985; Lebbe, 1999; Louwyck et al., 2010). The use of an axisymmetric model in such applications is justified, as the groundwater flow close to the pumping well exhibits radial symmetry in most cases. Using an analytical forward model has the advantage that it does not require discretization of space and time, whereas a numerical model may facilitate defining nonlinear boundary conditions and including aquifer heterogeneities.

Pinder and Bredehoeft (1968) give credit to Fiering (1964) for making the first attempt to evaluate numerically the response of a groundwater reservoir to extraction. They also mention Eshett and

Longenbaugh (1965) who describe a more general technique for long-term aquifer evaluation. Highly relevant is the publication of Bredehoeft and Pinder (1970) who simulate transient flow towards a well in a two-aquifer system applying the finite-difference method. The pumping well is located in the lower aquifer, the upper aquifer is phreatic, and both aquifers are separated by an incompressible aquitard. The head-dependent saturated thickness of the top aquifer is taken into account, and the numerical results are compared with the corresponding analytical solution developed by Hantush (1967).

Although Bredehoeft and Pinder (1970) simulate radial flow towards a well, they do not formulate the problem using a cylindrical coordinate system. An axisymmetric finite-difference formulation is, however, applied by Cooley (1971) to simulate flow towards a single well that penetrates one or more layers in an unconfined aquifer system. Cooley (1971) was inspired by the work of Spanier (1967) who solved axisymmetric heat conduction problems. Approximately the same numerical approach as the one described by Cooley (1971), was applied by Cooley (1972) and Cooley and Case (1973) to evaluate the concept of delayed yield introduced by Boulton (1954). In the last fifty years, many others also used the finite-difference method to solve a radial form of the governing flow equation (e.g. Bohling & Butler, 2001; Johnson et al., 2001; Lakshminarayana & Rajagopalan, 1977, 1978; Lebbe, 1983; Louwyck et al., 2012; Mansour et al., 2011; Rathod & Rushton, 1984, 1991; Rushton, 1974; Rushton & Booth, 1976; Rushton & Redshaw, 1979; Rushton & Turner, 1974; Rutledge, 1991; Salama et al., 2013; Streltsova & Rushton, 1973; Upton et al., 2019).

The axisymmetric finite-difference model created by Lebbe (1983) to simulate flow towards a well in a multi-aquifer system, was superseded by the axisymmetric numerical model developed by Lebbe (1988), who implemented a linear change of drawdown between the nodal circles. Because this property is characteristic to the finite-element method, Lebbe (1999) and Lebbe & de Breuck (1995) termed it a hybrid finite-difference finite-element method. Langevin (2008) points to the flexibility of finite-element meshes as the main advantage of the finite-element method. This flexibility enables a straightforward representation of the radially convergent flow patterns that result from extraction wells. In fact, there are no special considerations to simulate axisymmetric flow using a finite-element model (Langevin, 2008). Nevertheless, some finite-element models were designed specifically to simulate radially symmetric flow (e.g. Cooley, 1992; Cooley & Cunningham, 1979; Pandit & Abi Aoun, 1994; Reilly, 1984), while other models, such as FEFLOW (Diersch, 2002), have an option to perform simulations in “axisymmetric mode” (Bedekar et al., 2019).

3.1.3. Simulating axisymmetric flow using MODFLOW

Finite-difference models used to simulate axisymmetric flow require a two-dimensional axisymmetric grid consisting of coaxial rings around the axis of symmetry. MODFLOW versions up to MODFLOW-2005 (Harbaugh, 2005) use a three-dimensional rectilinear grid making the simulation of axisymmetric flow impossible without modifications. Fortunately, it is not necessary to adapt the software code, as MODFLOW can be tricked into simulating axisymmetric flow by merely modifying the input parameters (Langevin, 2008; Louwyck et al., 2012, 2014). This converts the horizontal flow between adjacent cells in the MODFLOW grid into radial flow between the corresponding rings of the axisymmetric grid. The basic idea behind this approach was briefly discussed by Anderson and Woessner (1992), and applied by, amongst others, Barrash and Dougherty (1997) and Halford and Yobbi (2006).

Reilly and Harbaugh (1993) developed the RADMOD pre-processor (which is no longer supported by recent MODFLOW versions) to modify interblock conductances between MODFLOW cells. A limitation of RADMOD is that it can only be applied to confined systems consisting of homogeneous

layers with constant thickness. RADMOD also requires a uniform logarithmic spacing of nodes in the radial direction based on a user defined expansion factor. The use of the latter is criticized by Samani et al. (2004), who present a log scaling method in which mesh spacing is based on flow geometry and parameters. As a result, the method can handle unconfined flow, axisymmetric nonhomogeneous aquifers, and effects of well skin and wellbore storage. Although Samani et al. (2004) conclude the log scaling method is general, efficient, and accurate, it is not as straightforward as the method described by Langevin (2008), since it requires modification of the MODFLOW code.

Langevin (2008) shows that the unmodified version of MODFLOW can accurately simulate axisymmetric flow by means of a simple correction. The aquifer parameters of each cell are multiplied by the radial distance of its node and the angular extent of the axisymmetric grid; interblock transmissivities are calculated using the logarithmic mean, a standard option in MODFLOW. The radial discretization is defined by the user, but not restricted to a uniform logarithmic scheme. Confined as well as unconfined flow may be simulated, and wellbore storage can be taken into account. If the flow is confined, it is possible to define a wellbore skin or other axisymmetric aquifer inhomogeneities, although radial variations of both layer thickness and horizontal conductivity are not handled accurately with the method of Langevin (2008).

Louwyck et al. (2012, 2014) describe an approach as straightforward as the method of Langevin (2008), and capable of dealing with radially varying layer thickness and horizontal conductivity. In this approach, the width and length of all cells are set to unity, and the aquifer parameters are modified to simulate radial flow. In this fashion, the default harmonic mean is used to compute intercell conductivities, and a more flexible approach is obtained without any restrictions on the parameter values, the type of flow, or the radial discretization. The method of Langevin (2008) and the method of Louwyck et al. (2012, 2014) are used not only to simulate radial flow (e.g. Bianchi et al., 2020), they are also applied to simulate solute and reactive transport under radial flow conditions (e.g. Vandenbohede et al., 2019; Wallis et al., 2012), axisymmetric variable-density groundwater flow (e.g. Khadra et al., 2017), and axisymmetric heat transport (e.g. Vandenbohede et al., 2014), using unmodified versions of MT3DMS (Zheng & Wang, 1999), PHT3D (Prommer & Post, 2010), and/or SEAWAT (Langevin et al., 2007).

As already mentioned, MODFLOW-USG (Panday et al., 2013) and MODFLOW 6 (Langevin et al., 2017) support the definition of unstructured finite-difference grids, which makes it possible to directly build an axisymmetric grid consisting of coaxial rings. This is illustrated by Bedekar et al. (2019), who propose a method to simulate axisymmetric flow using MODFLOW-USG by calculating the intercell interface area arrays to accurately represent the coaxial cylindrical model cells. They demonstrate the method by three examples: well-flow with delayed yield effects, a vadose zone flow model simulating an infiltration basin, and a density-dependent saltwater intrusion problem for a circular island.

3.1.4. Software implementations

The finite-difference approach published by Louwyck et al. (2012) and presented in this chapter is also implemented in software tools that are designed specifically for the simulation of axisymmetric multilayer flow. These tools could be regarded as further developments of the axisymmetric finite-difference model AS2D developed by Lebbe (1988, 1999). The AS2D code is written in FORTRAN-77, runs under MS-DOS or UNIX, uses fixed format ASCII files for data exchange, and creates HP-GL/2 files as graphical output. The system of finite-difference equations is solved by applying the Alternating Direction Implicit (ADI) method (Douglas & Rachford, 1956; Peaceman & Rachford, 1955), which is also described in textbooks on numerical modeling (e.g. Ferziger & Peric, 2002; Wang &

Anderson, 1982). The AS2D code was used in many hydrogeological studies involving simulation and interpretation of aquifer tests (e.g. Lebbe et al., 1992, 1995; Lebbe & Bougriba, 1995; Lebbe & de Breuck, 1994, 1995, 1997; Lebbe & van Meir, 2000; Louwyck et al., 2005; van Meir & Lebbe, 2005; Vandenbohede & Lebbe, 2003).

In the early 2000s, the need to integrate AS2D into a more interactive and user-friendly environment initiated the development of a Matlab wrapper, simply using functions to write and read the AS2D input and output files, and to invoke the compiled AS2D Windows executables. Later, the AS2D code was rewritten entirely, mainly because it does not support radial variation of hydraulic parameters. The ADI solver was coded in FORTRAN-95 and compiled to a Matlab MEX function, and additional code was written in Matlab. This new code was the core of the OGMA-RF program (Louwyck et al., 2007), that stands for “Optimised and Generalised Model for Analysing Radial Flow”. It was a numerical model to simulate and analyze axisymmetric groundwater flow, solute transport, and heat transport, provided with a user-friendly Matlab GUI. Although OGMA-RF was successfully applied in several studies (Louwyck et al., 2010; Vandenbohede et al., 2008a, 2008b, 2009), it is no longer available.

OGMA-RF adopted AS2D’s hybrid numerical method, in which drawdowns are averaged over grid cells and time steps (Lebbe, 1988, 1999). Because this averaging was optional in OGMA-RF, the hybrid method could be compared easily with the pure finite-difference formulation, and it was seen that the latter gave more accurate results when simulating drawdown within and near the well at very small values of time. The reason why is discussed in more detail in next Chapter 4. It was also found that the iterative ADI solver used by AS2D and OGMA-RF was inefficient in case of more complex models. These conclusions led to the development of MAxSym (Louwyck, 2011), an axisymmetric groundwater flow model coded in Matlab, that applies a pure finite-difference approach, which has been carefully verified (Louwyck, 2011; Louwyck et al., 2012, 2014).

Besides the ADI solver used by AS2D and OGMA-RF, the more efficient Strongly Implicit Procedure (SIP) developed by Stone (1968) is implemented in MAxSym. The SIP solver is one of the original MODFLOW solvers (McDonald & Harbaugh, 1984), and it is also described in Ferziger and Peric (2002). Both the ADI and SIP solver are written in ANSI C instead of FORTRAN, and compiled into MEX functions. MAxSym has an object-oriented design, and it is extended with model features such as initial drawdowns, discharges, inactive and constant-head cells, and stress periods, to cover a much broader range of axisymmetric models than AS2D does. As a consequence, its use is not limited to the simulation of pumping tests, but also includes simulation of slug tests, steady-state models, and models considering areal infiltration. MAxSym was used at the Flemish Environment Agency, and it is still available on GitHub⁶ and the MathWorks File Exchange⁷, where it can be downloaded by groundwater students, practitioners, and researchers (e.g. Hoving, 2015; Oliveti & Cardarelli, 2017).

Although Matlab is a powerful scientific computing language, it is proprietary commercial software that is relatively expensive, and thus not accessible to many groundwater practitioners. A free and open-source alternative for Matlab is the Python programming language, which is becoming increasingly popular among hydrogeologists (e. g. Bakker, 2014; Bakker et al., 2016; Bakker & Kelson, 2009; Bakker & Post, 2022). Therefore, the presented finite-difference approach has been implemented in Python recently. Because of the similarity between two-dimensional axisymmetric and parallel flow, the Python version is extended with the option to construct vertical profile models. This idea of implementing a linear and radial flow model in one code is not new (e.g. Bohling &

⁶ <https://github.com/alouwyck/MAxSym>

⁷ <https://nl.mathworks.com/matlabcentral/fileexchange/34361-maxsym>

Butler, 2001). The option of simulating nonlinear flow in the top layer of the model provided with MAxSym is omitted; hence, the matrix system is always linear, and a standard linear algebra solver is used to solve the system. As the Python version of MAxSym is not restricted to the simulation of pumping tests, it solves the mathematical problem in terms of heads instead of drawdowns. The Python version is used in Chapter 5 to test the newly-developed semi-analytical multilayer-multizone solution. The code is also available on GitHub⁸.

3.2. Problem statement

The problem of two-dimensional axisymmetric and parallel flow has been stated mathematically in previous Chapter 2. In this chapter, the same problem is solved numerically applying the finite-difference method (Louwyck, 2011; Louwyck et al., 2012). Using this method, it is very straightforward to define parameters that are function of radial or horizontal distance, and that are time dependent. Therefore, the problem is restated to account for lateral heterogeneities and time-varying boundary conditions, which requires reformulating the governing differential equations and associated boundary conditions.

In case of axisymmetric flow, the new system of partial differential equations is:

$$\frac{\partial}{\partial r} \left(T_i \frac{\partial h_i}{\partial r} \right) + \frac{T_i}{r} \frac{\partial h_i}{\partial r} = S_i \frac{\partial h_i}{\partial t} - N_i + \frac{h_i - h_{i-1}}{c_{i-1}} + \frac{h_i - h_{i+1}}{c_i} \quad (1 \leq i \leq n_l) \quad (1)$$

In case of parallel flow, the new system of equations is:

$$\frac{\partial}{\partial r} \left(T_i \frac{\partial h_i}{\partial r} \right) = S_i \frac{\partial h_i}{\partial t} - N_i + \frac{h_i - h_{i-1}}{c_{i-1}} + \frac{h_i - h_{i+1}}{c_i} \quad (1 \leq i \leq n_l) \quad (2)$$

Recall that hydraulic head $h_i(r, t)$ [L] in layer i is a function of distance r [L] and time t [T]. Transmissivity $T_i(r)$ [L^2/T] and storativity $S_i(r)$ [-] of layer i are not constant in this case, but function of distance r , as is vertical resistance $c_i(r)$ [T] between layers i and $i + 1$. Infiltration flux $N_i(r, t)$ [L/T] is dependent on both r and t . Partial differential equations (1) and (2) define transient flow as head h is time-dependent. In case of steady state, however, these equations simplify to ordinary differential equations, as $\partial h_i / \partial t = 0$ by definition, and h is dependent on distance r only.

Recall that transmissivity T_i [L^2/T] is the product of the layer thickness D_i [L] and the horizontal conductivity K_i^h [L/T]:

$$T_i(r) = K_i^h(r) \cdot D_i \quad (1 \leq i \leq n_l) \quad (3)$$

Storativity S_i [-] is the product of the layer thickness D_i and the specific elastic storage S_i^S [L^{-1}]:

$$S_i(r) = S_i^S(r) \cdot D_i \quad (1 \leq i \leq n_l) \quad (4)$$

If the conditions in layer i are phreatic, then $S_i(r)$ is set to the specific yield $S_i^Y(r)$ [-]. The resistance between two layers is calculated using the vertical conductivity K^v [L/T] of those layers:

$$c_i(r) = \frac{D_i}{2K_i^v(r)} + \frac{D_{i+1}}{2K_{i+1}^v(r)} \quad (1 \leq i < n_l) \quad (5)$$

Note that conductivities K^h and K^v and specific storage and yield S^S and S^Y are functions of radial distance r .

⁸ <https://github.com/alouwyck/PhD>

Although the flexibility of the finite-difference method allows to easily define all kinds of conditions at any distance r , the focus remains on the initial and boundary conditions defined in previous Chapter 2. In case of transient state, initial heads φ [L] are required, which may vary with distance r :

$$h_i(r, 0) = \varphi_i(r) \quad (1 \leq i \leq n_l) \quad (6)$$

Heads are also specified at the upper, the lower, and the outer model boundary, respectively:

$$h_0(r, t) = \varphi_0(r, t) \quad (7)$$

$$h_{n_l+1}(r, t) = \varphi_{n_l+1}(r, t) \quad (8)$$

$$h_i(r_{out}, t) = \varphi_i(t) \quad (1 \leq i \leq n_l) \quad (9)$$

Recall that the upper and lower boundary conditions combine specified heads φ_0 and φ_{n_l+1} with resistances c_0 and c_{n_l+1} , respectively, to define the leaky boundaries of the aquifer system. The specified heads may vary with distance r and time t . The specified head at the outer model boundary at distance r_{out} [L] may also be time-dependent.

At the inner model boundary at distance r_{in} [L], head H [L] or discharge Q [L^3/T] is specified:

$$h_i(r_{in}, t) = H_i(t) \quad (1 \leq i \leq n_l) \quad (10)$$

$$r_{in} \frac{\partial h_i(r_{in}, t)}{\partial r} = \frac{-Q_i(t)}{2\pi T_i} \quad (1 \leq i \leq n_l) \quad (11)$$

$$\frac{\partial h_i(r_{in}, t)}{\partial r} = \frac{-Q_i(t)}{T_i} \quad (1 \leq i \leq n_l) \quad (12)$$

Equation (11) holds for axisymmetric flow, equation (12) for parallel flow. Note that the specified head H and specified discharge Q are time-dependent.

The superposition technique is also applicable to heads that are simulated using a numerical model (e.g. Lebbe, 1999). However, it is more straightforward to incorporate time-dependent boundary conditions in the finite-difference method. For instance, in MODFLOW (Harbaugh, 2005; Harbaugh et al., 2000; Harbaugh & McDonald, 1996a, 1996b; McDonald & Harbaugh, 1984, 1988), stress periods are used to easily account for time-varying sources and sinks.

3.3. Finite-difference approach

To solve the problem stated in previous section 3.2, an implicit finite-difference method is applied (Louwyck, 2011; Louwyck et al., 2012). Finite-difference methods solve differential equations by approximating the derivatives with finite differences. These are obtained by discretizing the spatial domain and the time interval: the first is done by defining a regular model grid, the latter by defining time steps. In this way, a finite number of points in space and time are considered resulting in a set of algebraic finite-difference equations.

In case of groundwater flow problems, these equations correspond to the water budget for each cell in the grid and for each time step. Hydraulic parameters determining the groundwater flow can be assigned to each cell separately, which explains why it is straightforward to account for aquifer heterogeneities. In the same way, different initial and boundary values can be defined easily in each cell and for each time step.

The governing differential equations (1) and (2) are linear; hence, the finite-difference equations are also linear. Solving the stated problem thus comes down to solving a system of linear equations by

applying matrix algebra techniques. As the matrix system is sparse, specialized solvers may be used, although in this case, a standard direct solver is still efficient, as the number of equations is relatively small for most problems of two-dimensional axisymmetric or parallel flow.

3.3.1. Discretization

Since the stated problem concerns two-dimensional flow, the model grid consists of n_l rows and n_r columns. The rows correspond to the model layers; hence, the height of row i equals layer thickness D_i . The columns represent the discretization of the horizontal or radial distance r . Column j is defined between distances $r_{b,j}$ and $r_{b,j+1}$. The distance r_j at which the hydraulic head $h_{i,j}$ in cell j is calculated, depends on whether axisymmetric or parallel flow is simulated. In case of parallel flow, a rectilinear grid of unit width is used, and the nodes are defined at the center of the cells:

$$r_j = \frac{r_{b,j} + r_{b,j+1}}{2} \quad (1 \leq j \leq n_r) \quad (13)$$

In case of an axisymmetric grid, the cells are coaxial rings and the nodes are nodal circles. Radius r_j of the nodal circle of ring j is defined as the harmonic mean of the distances of the cell boundaries:

$$r_j = \sqrt{r_{b,j} \cdot r_{b,j+1}} \quad (1 \leq j \leq n_r) \quad (14)$$

Expression (14) is equivalent to the arithmetic mean of the log-transformed distances of the cell boundaries:

$$\ln(r_j) = \frac{\ln(r_{b,j}) + \ln(r_{b,j+1})}{2} \quad (1 \leq j \leq n_r) \quad (15)$$

This is consistent with the Thiem (1870; 1906) equation expressing a logarithmic relation between head and radial distance. It is common practice, indeed, to discretize the radial dimension into logarithmically spaced distances:

$$r_{j+1} = a_r r_j \quad (1 \leq j \leq n_r - 1) \quad (16)$$

which is equivalent to:

$$\ln(r_{j+1}) = \ln(r_j) + \ln(a_r) \quad (1 \leq j \leq n_r - 1) \quad (17)$$

with a_r a constant greater than 1. Reilly and Harbaugh (1993) use an expansion factor between 1.1 and 2 to define consecutively increasing cell widths, Anderson and Woessner (1992) advise to apply an expansion factor smaller than 1.5 to avoid large truncation errors related to the finite-difference expression for the second derivative, Barrash and Dougherty (1997) apply an expansion factor between 1.2 and 1.5, and Lebbe (1999) mostly chooses $a_r = 10^{0.1} = 1.259$.

As the cells in the rectilinear grid used to simulate parallel flow have unit width, the horizontal surface area A^h [L^2] of cell j is in this case:

$$A_j^h = r_{b,j+1} - r_{b,j} \quad (1 \leq j \leq n_r) \quad (18)$$

In the axisymmetric grid, it is:

$$A_j^h = \pi(r_{b,j+1}^2 - r_{b,j}^2) \quad (1 \leq j \leq n_r) \quad (19)$$

In case of transient state simulations, the time dimension is discretized into n_t simulation times t_k . The first simulation time $t_{k=1}$ is set to zero as it is the time $t = 0$ for which the initial conditions hold. For $t > 0$, it is also efficient in many cases to define logarithmically spaced simulation times:

$$t_{k+1} = a_t t_k \quad (1 \leq k \leq n_t - 1) \quad (20)$$

with a_t a constant greater than 1. In the AS2D code (Lebbe, 1988, 1999), a_t is always equal to a_r .

3.3.2. Flow equations

Using the discretization of space and time discussed in previous section 3.3.1, and the hydraulic parameters K_{ij}^h , K_{ij}^v , and S_{ij}^s assigned to each cell ij , it is straightforward to determine the in- and outflow for each grid cell by applying Darcy's law.

In case of parallel flow, the horizontal flow Q^h [L³/T] between two adjacent cells in column j and column $j + 1$ at time t_k is:

$$Q_{ijk}^h = \frac{2(h_{ijk} - h_{i,j-1,k})}{\frac{r_{b,j+1} - r_{b,j}}{T_{ij}} + \frac{r_{b,j} - r_{b,j-1}}{T_{i,j-1}}} = Q_{ij}^{hc}(h_{ijk} - h_{i,j-1,k}) \quad (1 \leq i \leq n_l; 2 \leq j \leq n_r; 1 \leq k \leq n_t) \quad (21)$$

In case of axisymmetric flow, it is (Louwyck, 2011; Louwyck et al., 2012):

$$Q_{ijk}^h = \frac{4\pi(h_{ijk} - h_{i,j-1,k})}{\frac{\ln(r_{b,j+1}/r_{b,j})}{T_{ij}} + \frac{\ln(r_{b,j}/r_{b,j-1})}{T_{i,j-1}}} = Q_{ij}^{hc}(h_{ijk} - h_{i,j-1,k}) \quad (1 \leq i \leq n_l; 2 \leq j \leq n_r; 1 \leq k \leq n_t) \quad (22)$$

Constant Q_{ij}^{hc} is the horizontal or radial conductance [L²/T] between cells $j - 1$ and j . Matrix Q^{hc} has n_l rows and $n_r + 1$ columns. As the model grid has impervious boundaries, $Q_{i,1}^{hc} = Q_{i,n_r+1}^{hc} = 0$. Recall that transmissivity T_{ij} in cell ij is calculated according to (3).

In both flow cases, the vertical flow Q^v [L³/T] between two adjacent cells in layer i and layer $i + 1$ at time t_k is defined as:

$$Q_{ijk}^v = A_j^h \frac{h_{ijk} - h_{i-1,j,k}}{c_{i-1,j}} = Q_{ij}^{vc}(h_{ijk} - h_{i-1,j,k}) \quad (2 \leq i \leq n_l; 1 \leq j \leq n_r; 1 \leq k \leq n_t) \quad (23)$$

Constant Q_{ij}^{vc} is the vertical conductance [L²/T] between cells $i - 1$ and i , and Q^{vc} is an $(n_l + 1) \times n_r$ matrix. The impervious grid boundaries require that $Q_{1,j}^{vc} = Q_{n_l+1,j}^{vc} = 0$. Recall that the vertical resistance c_{ij} is calculated according to (5).

If the simulation is time dependent, the storage change Q^s [L³/T] is also required for each cell ij and for each time step between simulation times t_{k-1} and t_k :

$$Q_{ij,k-1}^s = A_j^h S_{ij} \frac{h_{ijk} - h_{i,j,k-1}}{t_k - t_{k-1}} = Q_{ij,k-1}^{sc}(h_{ijk} - h_{i,j,k-1}) \quad (1 \leq i \leq n_l; 1 \leq j \leq n_r; 2 \leq k \leq n_t) \quad (24)$$

If storage change Q^s is positive, then water is added to the groundwater reservoir. Recall that storativity S_{ij} in cell ij is calculated according to (4). Expression (24) expresses a backward finite-difference approximation with respect to time t , as the initial heads at time $t_{k=1}$ are known, and the heads at the end of time step $k - 1$ are used to calculate the heads at the end of time step k .

3.3.3. Initial and boundary conditions

Initial and boundary conditions may be defined in each cell of the finite-difference grid. A distinction is made between inactive, constant-head, and variable-head cells. Inactive cells are excluded from the model grid as they do not contain groundwater. The head in constant-head cells is specified and thus known, whereas it is not in variable-head cells. In a variable-head cell, it is possible, however, to define flux boundary conditions.

Inactive and constant-head cells are used to define model boundaries. If cell ij is inactive, then $Q_{ij}^{hc} = Q_{i,j+1}^{hc} = Q_{ij}^{vc} = Q_{i+1,j}^{vc} = Q_{ijk}^{sc} = 0$ for all k . If cell ij is a constant-head cell, then $h_{ijk} = \varphi_{ijk}$ for all k , with φ_{ijk} the specified head [L]. In case of transient flow, the heads $h_{i,j,1}$ at time $t_{k=1}$ are required model input for the variable-head cells, as they define the initial conditions at time $t = 0$.

Variable-head cells may have an extra flow term Q_{ijk} [L^3/T], which is used, for instance, to simulate pumping or areal infiltration. Note that Q_{ijk} is positive in case of recharge, and negative in case of discharge. It is also possible to define a head-dependent flux boundary condition in each variable-head cell ij . In this case, not only a constant head φ_{ijk} is defined, but also a corresponding resistance γ_{ij} [T]. Together, they induce additional recharge or discharge Q^c [L^3/T] in cells where such a boundary condition is defined. Q^c is calculated as follows:

$$Q_{ijk}^c = A_j^h \frac{\varphi_{ijk} - h_{ijk}}{\gamma_{ij}} = Q_{ij}^{cc}(h_{ijk} - \varphi_{ijk}) \quad (1 \leq i \leq n_l; 1 \leq j \leq n_r; 1 \leq k \leq n_t) \quad (25)$$

Note that cell ij is recharged if Q_{ijk}^c is positive; otherwise it is drained.

The outer model boundary condition defined by equation (9) is implemented by defining constant heads $\varphi_{i,n_r,k}$ in the cells of the last column $j = n_r$ of the model grid. If distance r_{out} of the outer model boundary is infinitely large, then the last cell must be at a very large distance. This can be accomplished by discretizing r into logarithmically spaced distances according to (16). If the outer boundary is at a finite distance, then it is advised to assign a very small width δ to the last column in the model grid: $r_{b,n_r-1} = r_{out}$ and $r_{b,n_r} = r_{out} + \delta$.

When specified heads $H_i(t)$ according to (10) are defined at the inner model boundary, then the first column of the model grid consists of constant-head cells with $\varphi_{i,1,k} = H_i(t_k)$. When the inner boundary conditions are specified discharges according to (11) or (12), depending on the type of flow, then the cells in the first column are variable-head cells with extra flow term $Q_{i,1,k} = Q_i(t_k)$. In order to simulate the effect of the inner boundary condition accurately, it is also recommended to assign a very small width δ to the first column of the model grid (Louwyck et al., 2012), or $r_{b,2} = r_{in}$ and $r_{b,1} = r_{in} - \delta$. Barrash and Dougherty (1997) recommend to additionally assign a very small value to the width of the cell adjacent to the first cell. When axisymmetric flow is simulated and r_{in} is infinitesimal, then a very small value should be assigned to $r_{b,1}$ as it is not possible to set $r_{b,1}$ to zero because of the logarithmic singularity at the origin. Therefore, defining logarithmically spaced distances is also useful in this case.

Concerning the upper and lower boundary conditions, there are three possibilities: a no-flow boundary, a leaky boundary, or a water table. In case of a zero-flux boundary, no additional input is required, as the boundaries of the model grid are impervious. A leaky boundary may be defined using the head-dependent flux boundary condition. If the upper boundary is leaky, then (25) is applied with $\varphi_{1,j,k} = \varphi_0(r_j, t_k)$ and $\gamma_{1,j} = c_0(r_j)$. If the lower boundary is leaky, then $\varphi_{n_l,j,k} = \varphi_{n_l+1}(r_j, t_k)$ and $\gamma_{n_l,j} = c_{n_l}(r_j)$. Alternatively, an extra dummy layer of low transmissivity with constant-head cells could be defined on top or at the bottom of the model grid. If the top layer is phreatic, then storativity S_1 should be equal to the specific yield. Therefore, $S^y(r_j)/D_1$ must be assigned to $S_{1,j}^s$. If there is infiltration $N(r, t)$ [L/T] in the top layer, then:

$$Q_{1,j,k} = A_j^h N(r_j, t_k) \quad (26)$$

Recall that A_j^h is the horizontal surface area of the cells in column j of the model grid. Note that the layer thickness D_1 remains constant here. In Chapter 8, nonlinear unconfined flow is discussed.

3.3.4. Matrix system

Having defined in- and outflow and all boundary conditions for each variable-head cell ij and for each time step k , the following set of water budget equations can be set up:

$$Q_{ij+1,k}^h - Q_{ijk}^h + Q_{i+1,j,k}^v - Q_{ijk}^v + Q_{ij,k-1}^s + Q_{ijk} + Q_{ijk}^c = 0 \quad (1 \leq i \leq n_l; 1 \leq j \leq n_r; 2 \leq k \leq n_t) \quad (27)$$

For each time step k , expression (27) is a system of $n_l \times n_r$ equations, which can be rearranged and written in matrix form:

$$\mathbf{A}_k \mathbf{h}_k = \mathbf{b}_k \quad (2 \leq k \leq n_t) \quad (28)$$

Matrix \mathbf{A}_k is an $n \times n$ matrix, and both \mathbf{h}_k and \mathbf{b}_k are $n \times 1$ vectors, with $n = n_l \cdot n_r$. If linear index l is defined as $(i-1)n_r + j$, then vector \mathbf{h}_k contains the unknown hydraulic heads h_{ijk} which are ‘flattened’ row-wise:

$$\mathbf{h}_{lk} = h_{ijk} \quad (1 \leq i \leq n_l; 1 \leq j \leq n_r) \quad (29)$$

Two-dimensional matrix \mathbf{A}_k holds the known conductance terms. It is symmetric, positive definite, and sparse, and its nonzero elements are located on just five diagonals:

$$\begin{aligned} \mathbf{A}_{llk} &= Q_{i,j+1}^{hc} + Q_{ij}^{hc} + Q_{i+1,j}^{vc} + Q_{ij}^{vc} + Q_{i,j,k+1}^{sc} - Q_{ij}^{cc} & (1 \leq i \leq n_l; 1 \leq j \leq n_r) \\ \mathbf{A}_{l,l+1,k} &= \mathbf{A}_{l+1,l,k} = -Q_{i,j+1}^{hc} & (1 \leq i \leq n_l; 1 \leq j \leq n_r) \\ \mathbf{A}_{l,l+n_r,k} &= \mathbf{A}_{l+n_r,l,k} = -Q_{i+1,j}^{vc} & (1 \leq i \leq n_l; 1 \leq j \leq n_r) \end{aligned} \quad (30)$$

Vector \mathbf{b}_k contains the known terms of water budget equation (27):

$$\mathbf{b}_{lk} = Q_{i,j,k+1}^{sc} h_{i,j,k-1} + Q_{ijk} - Q_{ij}^{cc} \varphi_{ijk} \quad (1 \leq i \leq n_l; 1 \leq j \leq n_r) \quad (31)$$

Expressions (30) and (31) hold for variable-head cells only. Rows in \mathbf{A}_k and elements in \mathbf{b}_k that correspond to inactive cells are removed. If cell ij is a constant-head cell, then element $\mathbf{b}_{lk} = \varphi_{ijk}$, and the entries of the corresponding l -th row in \mathbf{A}_k are all set to zero, or $\mathbf{A}_{l,l+1,k} = \mathbf{A}_{l,l+n_r,k} = 0$, with the exception of the entry on the main diagonal, which is set to one, or $\mathbf{A}_{llk} = 1$.

Another way to deal with constant-head cells is to add the terms that contain a constant head to vector \mathbf{b}_k , after which the constant heads are removed from the matrix system. Suppose there are n_c constant-head cells. Let \mathbf{A}'_k be the $n \times n_c$ matrix that contains the columns in \mathbf{A}_k that correspond to those constant-head cells, and let $\boldsymbol{\varphi}_k$ be the vector that contains the n_c constant heads for time step k ; then vector \mathbf{b}_k is modified as follows:

$$\mathbf{b}_k \leftarrow \mathbf{b}_k - \mathbf{A}'_k \boldsymbol{\varphi}_k \quad (32)$$

After updating \mathbf{b}_k according to (32), the rows and columns in \mathbf{A}_k and the elements in \mathbf{b}_k corresponding to the constant heads are removed. As it is no use to consider storage change for constant-head cell ij , Q_{ijk}^{sc} is set to zero for all time steps k .

When constructing \mathbf{A}_k , it is also possible to order the heads column-wise by defining the linear index l as $(j-1)n_l + i$. In this case, only the nonzero entries in matrix \mathbf{A}_k that are not on the main diagonal must be modified:

$$\begin{aligned} \mathbf{A}_{l,l+1,k} &= \mathbf{A}_{l+1,l,k} = -Q_{i,j+1}^{vc} & (1 \leq i \leq n_l; 1 \leq j \leq n_r) \\ \mathbf{A}_{l,l+n_l,k} &= \mathbf{A}_{l+n_l,l,k} = -Q_{i+1,j}^{hc} & (1 \leq i \leq n_l; 1 \leq j \leq n_r) \end{aligned} \quad (33)$$

As matrix \mathbf{A}_k and vector \mathbf{b}_k are known, the unknown heads \mathbf{h}_k at time t_k are found by solving matrix system (28) recursively starting with $k = 2$, and so on:

$$\mathbf{h}_k = \mathbf{A}_k^{-1} \mathbf{b}_k \quad (2 \leq k \leq n_t) \quad (34)$$

Next section discusses different methods to obtain solution (34).

3.3.5. Solvers

In general, a direct or an iterative solver can be applied to solve a system of linear equations such as (28) (Harbaugh, 1995; Yeh, 1999). Direct solvers use one large computational step to solve the matrix system, whereas iterative solvers approach the solution gradually. In the absence of rounding errors due to a computer's finite precision, an exact solver would give an exact solution, while an iterative solver converges to the exact solution, if the problem is well-conditioned. In case of convergence, the residual error, i.e. the difference in heads between two successive iterations, decreases with the number of iteration steps. Theoretically, the exact solution is reached only after an infinite number of iterations. As a consequence, a stopping criterion, also called convergence or error tolerance criterion, is required to finish the iterative procedure as soon as the approximation error has become acceptable (Anderson et al., 2015).

Concerning the iterative methods, Anderson et al. (2015) distinguish between point iteration methods that were used in the early years of groundwater modeling, and methods that combine iteration with a direct solution. The first methods use at every iteration the heads from the previous iteration, whereas the latter simplify the matrix system so that a more efficient direct solver can be used. As this simplified matrix is not accurate, iterations are required to improve the solution. Barrett et al. (1994) make a similar distinction between stationary and non-stationary iterative solvers, where the latter differ from the first in that the computations involve information that changes at each iteration. Examples of stationary iterative solvers are the Jacobi method, the Gauss-Seidel method and its derived methods Successive Overrelaxation (SOR) and Symmetric Successive Overrelaxation (SSOR). Conjugate gradient methods are examples of non-stationary iterative solvers. Gaussian elimination and LU decomposition are widely known methods of direct solution, where the latter may be viewed as the matrix form of the first.

In the early years of groundwater modeling, ADI (Peaceman & Rachford, 1955) and SOR (Young, 1950) were prevalent (e.g. Bredehoeft & Pinder, 1970; Cooley, 1971; Pinder & Bredehoeft, 1968; Trescott et al., 1976), and in the first MODFLOW versions (Harbaugh & McDonald, 1996b; McDonald & Harbaugh, 1984, 1988), the user could choose between SSOR (Young, 1950) and SIP (Stone, 1968). The latter method was also implemented in MODFLOW's predecessors (Trescott, 1975; Trescott et al., 1976). The Preconjugated Conjugate Gradient (PCG) method was made available as a solver by Hill (1990), and Harbaugh (1995) developed the DE4 package which implements a direct solver. The MODFLOW-2000 release (Harbaugh et al., 2000) came with an algebraic multigrid method LMG (Mehl & Hill, 2001), and later, the geometric multigrid (GMG) solver package was released (Wilson & Naff, 2004). Both solvers were developed to enhance the performance of complex simulations involving large grids. In general, no single solver is well suited for solving the matrix system for all problems, and even if multiple solvers can correctly solve the same problem, the execution speed and the amount of memory used will be different. Therefore, it is indispensable to modelers to have several solvers at their disposal (Harbaugh, 1995).

As already mentioned, the AS2D code developed by Lebbe (1988, 1999) solves the system of equations applying the ADI method (Peaceman & Rachford, 1955), which does not give satisfactory results in all cases. Indeed, Wang and Anderson (1982) report the possibility of obtaining large errors using ADI, referring to Bennett (1976), and they propose an iterative ADI method to avoid these errors as applied by Prickett and Lonnquist (1971) and Trescott et al. (1976). They also mention SOR (Young, 1950) as an efficient iterative solver for groundwater problems. However, because SIP

(Stone, 1968) is used in MODFLOW and its predecessors, and as it is explained extensively in McDonald & Harbaugh (1988), it was implemented in MAxSym (Louwyck, 2011) as an alternative solver to ADI. Nonlinear problems that involve a phreatic top layer with head-dependent thickness are solved iteratively, which is sometimes referred to as Picard iterations (Harbaugh, 1995; Hill, 1990). The ADI and the SIP algorithm implemented in MAxSym both are discussed in detail in the documentation (Louwyck, 2011).

Daily practice has proven that SIP is more efficient indeed than ADI for relatively small two-dimensional axisymmetric flow problems. However, a number of reasons has led to the decision to use a standard solver implemented in SciPy (Peterson et al., 2022) for the Python version of MAxSym. The first reason is practical. Using existing code not only saves a lot of time, it is also more reliable as the code has been tested thoroughly. Moreover, SciPy uses LAPACK routines written in FORTRAN which are very fast. Second, as pointed out by Anderson et al. (2015), direct method solutions are desirable as they are theoretically exact. Unfortunately, they often require large amounts of computer memory, but in case of relatively small linear two-dimensional problems, this is not an issue, and according to Harbaugh (1995), they may execute faster than an iterative method when solving such problems.

Finally, the SciPy solver applies LU decomposition which imposes less restrictions on the matrix system. As already mentioned, matrix \mathbf{A} in equation (28) is symmetric, positive definite, and sparse with nonzero elements located on five diagonals. Some methods exploit these properties to solve the system more efficiently (Yeh, 1999). PCG, for instance, is valid only for symmetric and positive definite matrices, while ADI and SIP require sparse matrices with nonzero entries occurring exclusively on some of the diagonals. In Chapter 6, the finite-difference approach is extended so it can handle connected cells, for instance, to simulate flow to multi-aquifer wells. In this case, matrix \mathbf{A} must be modified and will have nonzero entries that are not located on the five diagonals. As a consequence, this modified matrix system cannot be solved using ADI or SIP, but LU decomposition can do the job without problem.

Assessing the accuracy of the numerical solution is typically done by checking the total water budget (Anderson et al., 2015; Wang & Anderson, 1982). The continuity principle states that inflow equals outflow for each cell in the model grid, and for the model grid as a whole. Therefore, summing water budget equation (27) for all cells should give a value that is very close to zero. Mathematically, the solution of the system of finite-difference equations may be considered accurate, if the following condition is satisfied for each time step k :

$$|\mathbf{1}^T(\mathbf{A}_k \mathbf{h}_k - \mathbf{b}_k)| < \epsilon \quad (2 \leq k \leq n_t) \quad (35)$$

The left-hand side of (35) is the absolute value of the total water balance, and ϵ is a small positive value. Checking the balance for each time step is also good practice when a direct solver is used. Recall that even direct solution methods do not give an exact solution, because they suffer from rounding errors.

3.3.6. Interpolation

Once all heads h_{ijk} are calculated accurately, head $h_i(r, t)$ in layer i at any distance r and at any time t is computed using bilinear interpolation. Hydraulic head is assumed to vary linearly as a function of r or $\ln(r)$ between nodal distances r_j and r_{j+1} , and as a function of t or $\ln(t)$ between two simulation times t_k and t_{k+1} . These assumptions are justified if distance r and time t are sufficiently discretized. Within layer i the head is assumed not to vary in the vertical direction

according to the Dupuit-Forchheimer approximation, and a more accurate simulation of the vertical variation in hydraulic head is obtained by dividing layers into sublayers.

At time t_k , hydraulic head $h_i(r, t_k)$ in layer i and at any distance r between r_j and r_{j+1} is calculated as follows:

$$h_i(r, t_k) = h_{ijk} + \frac{h_{i,j+1,k} - h_{ijk}}{r_{j+1} - r_j} (r - r_j) \quad (r_j \leq r \leq r_{j+1}) \quad (36)$$

In (36), it assumed there is a linear relation between h and r . If $\ln(r)$ is used instead of r , then the spatial interpolation is:

$$h_i(r, t_k) = h_{ijk} + \frac{h_{i,j+1,k} - h_{ijk}}{\ln(r_{j+1}/r_j)} \ln(r/r_j) \quad (r_j \leq r \leq r_{j+1}) \quad (37)$$

If it is assumed the head varies linearly between two simulation times, then $h_i(r_j, t)$ in layer i at distance r_j and at any time t between t_k and t_{k+1} is:

$$h_i(r_j, t) = h_{ijk} + \frac{h_{i,j,k+1} - h_{ijk}}{t_{k+1} - t_k} (t - t_k) \quad (t_k \leq t \leq t_{k+1}) \quad (38)$$

If a linear relation between h and $\ln(t)$ is assumed, then the temporal interpolation is:

$$h_i(r_j, t) = h_{ijk} + \frac{h_{i,j,k+1} - h_{ijk}}{\ln(t_{k+1}/t_k)} \ln(t/t_k) \quad (t_k \leq t \leq t_{k+1}) \quad (39)$$

Hydraulic head $h_i(r, t)$ in layer i at any distance r and at any time t is obtained by first calculating $h_i(r, t_k)$ and $h_i(r, t_{k+1})$ using (36) or (37), after which $h_i(r, t)$ is computed using (38) or (39).

3.4. Axisymmetric MODFLOW procedure

Parallel flow is simulated using a profile model that represents a vertical slice or cross section of the groundwater flow system. The longitudinal axis of such a model is oriented parallel to the groundwater flow, because no water flows perpendicular to the profile. The thickness of the profile is set to one unit of the aquifer (Anderson et al., 2015).

Finite-difference models such as MODFLOW (Harbaugh, 2005; Harbaugh et al., 2000; Harbaugh & McDonald, 1996b, 1996a; McDonald & Harbaugh, 1984, 1988) that use a three-dimensional rectilinear grid are well-suited for the simulation of parallel flow, as profile models simply require a grid consisting of n_l layers, n_r columns, and 1 row of unit width. Layer thicknesses and column widths can be set without modification, as are all input parameters and initial and boundary values defined in previous section 3.3.

As already mentioned in section 3.1.3, simulating axisymmetric flow using a Cartesian grid geometry is also possible (Anderson & Woessner, 1992; Halford & Yobbi, 2006; Reilly & Harbaugh, 1993), but in this case, the model input requires some modifications to account for the required cylindrical grid geometry (Langevin, 2008; Louwyck et al., 2012, 2014). In other words, the parallel flow equations must be transformed to the corresponding axisymmetric flow equations by modifying the input parameters.

3.4.1. General procedure

Similar to parallel flow simulations, a model grid consisting of n_l layers, n_r columns, and 1 row of unit width is defined when simulating axisymmetric flow. Layer thicknesses are also adopted, but

unit width is assigned to the columns. As a consequence, $r_{b,j+1} - r_{b,j} = A_j^h = 1$, which makes it straightforward to convert the parallel flow equations into axisymmetric flow equations.

Comparing equation (21) to equation (22) and taking into account column j has unit width gives:

$$T_{ij}^* = \frac{2\pi T_{ij}}{\ln(r_{b,j+1}/r_{b,j})} \quad (40)$$

Recall that the horizontal surface area of the cells in the rectilinear MODFLOW grid is 1; hence from (19) and (23), it follows that:

$$c_{ij}^* = \frac{c_{ij}}{\pi(r_{b,j+1}^2 - r_{b,j}^2)} \quad (41)$$

and from (19) and (24), it follows that:

$$S_{ij}^* = \pi(r_{b,j+1}^2 - r_{b,j}^2) S_{ij} \quad (42)$$

In (40), (41), and (42), the transformed input parameters are denoted by an asterisk superscript. These parameter values are input for the profile model that is used to simulate axisymmetric flow.

The resistance required for head-dependent flux boundary condition (25) is modified in the same way as the vertical resistance between layers:

$$\gamma_{ij}^* = \frac{\gamma_{ij}}{\pi(r_{b,j+1}^2 - r_{b,j}^2)} \quad (43)$$

Specified discharges are not transformed, but infiltration fluxes require a similar modification:

$$N_{ijk}^* = \pi(r_{b,j+1}^2 - r_{b,j}^2) N_{ijk} \quad (44)$$

with N_{ijk} the vertical infiltration flux in cell ij at time t_k .

3.4.2. MODFLOW procedure

All standard MODFLOW versions up to MODFLOW-2005 (Harbaugh, 2005) use a rectilinear model grid composed of rows, columns, and layers of rectangular-prismatic cells. The latest version, MODFLOW 6 (Langevin et al., 2017), also allows for the use of unstructured grids, which were only supported before in MODFLOW-USG (Panday et al., 2013).

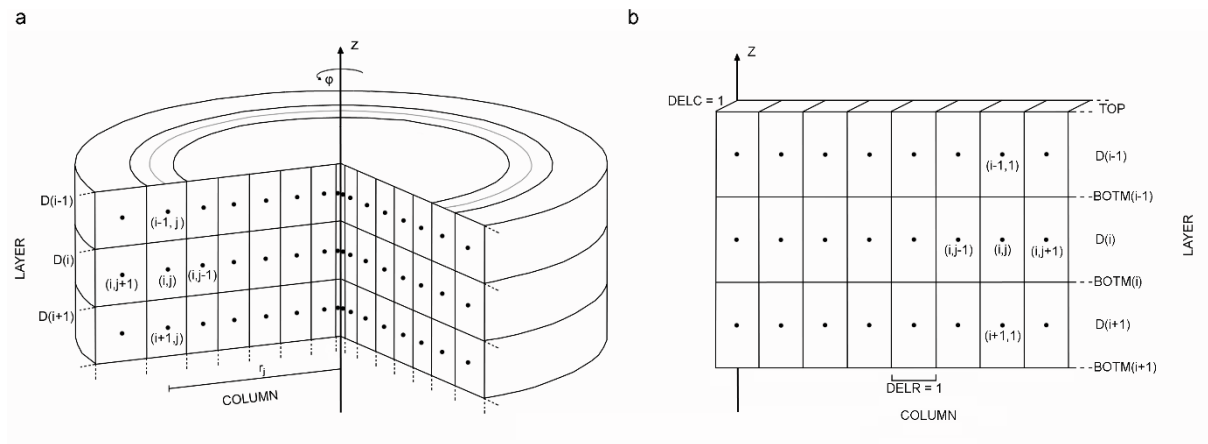


Figure 1. (a) Axisymmetric, finite-difference grid and (b) corresponding MODFLOW grid. See text for explanation and definitions. The figure is adopted from Louwyck et al. (2014).

Louwyck et al. (2014) describe in detail the MODFLOW procedure to simulate axisymmetric flow using the modifications to the input parameters discussed in previous section 3.4.1. The procedure is developed for MODFLOW-2005 (Harbaugh, 2005), but it may also be performed using MODFLOW 6, as the latter contains most of the functionality of the first (Langevin et al., 2017).

The simulations discussed by Louwyck et al. (2014) are executed with the double-precision version of MODFLOW-2005 using the following packages: BA6, DIS, LPF, WEL, SIP, and OC. MODFLOW variables relevant to the simulation of axisymmetric flow are discussed, where variable names are adopted from the MODFLOW-2005 manual (Harbaugh, 2005).

1. The finite-difference grid (Figure 1a) is defined in the DIS file. It consists of 1 row (NROW = 1) of unit width (DELC = 1), n_l layers (NLAY = n_l), and n_r columns (NCOL = n_r). Layer i is characterized by its thickness D_i ; variables BOTM and TOP, defining top and bottom of each layer, are set accordingly (Figure 1b). Cell width DELR is set to 1, since the width of each ring is included by modifying the aquifer parameters. Variable LAYCBD is set to 0 for each layer as no confining beds are considered.
2. Stress periods and time steps are also defined in the DIS file by assigning variables NPER, PERLEN, NSTP, TSMULT, and SS/TR. No corrections are required for axisymmetric flow, although a time step multiplier TSMULT > 1 may reduce computational time.
3. Aquifer parameters are defined in the LPF file. They are modified to include discretization of radial distance r . Horizontal conductivity HK for cell ij in the LPF file is corrected as follows:

$$HK_{ij} = \frac{2\pi K_{ij}^h}{\ln(r_{b,j+1}/r_{b,j})} \quad (45)$$

In addition, variable LAYAVG is set to 0 to use the harmonic mean for calculation of effective conductivities, and variable LAYTYP is set to 0 for each layer to keep its thickness constant.

Since the horizontal surface area of the cells in the MODFLOW grid is equal to 1 (DELC = DELR = 1), all other aquifer parameters must be multiplied by the horizontal surface area of the corresponding rings:

$$VKA_{ij} = \pi(r_{b,j+1}^2 - r_{b,j}^2)K_{ij}^v \quad (46)$$

$$SS_{ij} = \pi(r_{b,j+1}^2 - r_{b,j}^2)S_{ij}^s \quad (47)$$

with VKA the vertical conductivity, and SS the specific storage in the LPF file. Variable LAYVKA is set to 0 to indicate VKA is the vertical conductivity. There is no horizontal anisotropy, hence, variable CHANI is set to -1 and HANI is set to 1 for each layer. Assigning 0 to LAYWET disables the wetting option.

4. Constant heads are defined in the BA6 file by setting the IBOUND variable to -1, as are inactive cells by setting IBOUND to 0. The starting or initial heads are also defined in the BA6 file by setting variable STRT.
5. Flux dependent boundary conditions are defined in the WEL file. Pumping or injection rates for the well at the inner model boundary are assigned to variable Q without modification. Vertical infiltration is defined by setting Q as follows:

$$Q_{ij} = \pi(r_{b,j+1}^2 - r_{b,j}^2)N_{ij} \quad (48)$$

Alternatively, the RCH package may be used, in which case the infiltration flux is also modified according to (48).

6. A solver package is chosen and the OC file is prepared to define output control. Louwyck et al. (2014) use the SIP solver with variables NPARM = 5, ACCL = 1, and IPCALC = 1. Criterion for convergence HCLOSE is set to 10^{-7} . No corrections are required for the calculated heads and volumetric budget terms.

Louwyck et al. (2012, 2014) show that the MODFLOW procedure discussed in this section is very accurate. They verify it against existing analytical solutions, and compare it with the analytic element solver TTIm (Bakker, 2013b, 2013a, 2022). In all test cases, the MODFLOW results are virtually the same as the analytical calculations. It should be kept in mind, however, that accuracy also depends on the applied discretization scheme and the defined solver criteria.

As already mentioned, checking the total volumetric budget of the axisymmetric MODFLOW model is a good practice, although small rounding errors might result into large budget discrepancies if the outer model boundary is defined at large distance to approximate the no-drawdown condition at infinity. The PCG package seems less susceptible to rounding errors than the SIP package, but accuracy of simulated head is not enhanced significantly using PCG as those errors merely affect the storage change of individual cells with large volumes (Louwyck et al., 2014).

3.5. Summary

This chapter explains the finite-difference approach developed by Louwyck (2011) and presented by Louwyck et al. (2012) to simulate axisymmetric flow in multilayered aquifer systems. The approach is inspired by earlier work of Lebbe (1988, 1999), although a pure finite-difference technique is opted for, similar to the MODFLOW formulation (Harbaugh, 2005; Harbaugh et al., 2000; Harbaugh & McDonald, 1996b, 1996a; McDonald & Harbaugh, 1984, 1988). In the latter, the variation in head between nodes is discontinuous instead of linear. The difference between both methods is investigated in next Chapter 4.

The finite-difference approach is implemented in the Matlab tool MAxSym (Louwyck, 2011), which has been verified thoroughly against several analytical solutions (Louwyck, 2011; Louwyck et al., 2012). A Python version is also developed, which is used in Chapter 5 to test the semi-analytical multilayer-multizone solution. This version is extended with the option to simulate parallel flow. Because memory is not an issue anymore when simulating two-dimensional models, it uses the standard solver available with SciPy instead of the iterative solvers implemented in MAxSym. The first is a direct method that applies LU decomposition, which may be faster and more accurate for small linear problems (Harbaugh, 1995). In Chapter 6, the presented finite-difference formulation is extended to define connected cells, which can be used to simulate flow to multi-aquifer wells.

As explained by Louwyck et al. (2012, 2014), it is also possible to use MODFLOW to solve the system of finite-difference equations, without having to modify the software. It suffices to adapt the input parameters to account for the axisymmetric grid geometry. In this way, the parallel flow simulated by MODFLOW is transformed into radial flow. The procedure presented by Louwyck et al. (2012, 2014) is similar to the approach proposed by Langevin (2008), although it is more flexible, as it can deal more accurately with radially varying aquifer parameters.

3.6. References

Anderson, M. P., & Woessner, W. W. (1992). *Applied Groundwater Modeling—Simulation of Flow and Advective Transport*. San Diego, California: Academic Press.

Anderson, M. P., Woessner, W. W., & Hunt, R. J. (2015). *Applied Groundwater Modeling - Simulation of Flow and Advective Transport (Second Edition)* (2nd ed.). Academic Press.

- Bakker, M. (2013a). Analytic Modeling of Transient Multilayer Flow. In P. K. Mishra & K. Kuhlman (Eds.), *Advances in Hydrogeology* (pp. 95–114). New York, NY: Springer, Heidelberg. https://doi.org/10.1007/978-1-4614-6479-2_5
- Bakker, M. (2013b). Semi-analytic modeling of transient multi-layer flow with TTIm. *Hydrogeology Journal*, 21(4), 935–943. <https://doi.org/10.1007/s10040-013-0975-2>
- Bakker, M. (2014). Python Scripting: The Return to Programming. *Groundwater*, 52(6), 821–822. <https://doi.org/10.1111/gwat.12269>
- Bakker, M. (2022). TTIm, A Multi-Layer, Transient, Analytic Element Model. Retrieved from <https://github.com/mbakker7/ttim>
- Bakker, M., & Kelson, V. A. (2009). Writing Analytic Element Programs in Python. *Ground Water*, 47(6), 828–834. <https://doi.org/10.1111/j.1745-6584.2009.00583.x>
- Bakker, M., & Post, V. E. A. (2022). *Analytical Groundwater Modeling: Theory and Applications using Python* (1st ed.). London: CRC Press.
- Bakker, M., Post, V., Langevin, C. D., Hughes, J. D., White, J. T., Starn, J. J., & Fienen, M. N. (2016). Scripting MODFLOW Model Development Using Python and FloPy. *Groundwater*, 54(5), 733–739. <https://doi.org/10.1111/gwat.12413>
- Barrash, W., & Dougherty, M. E. (1997). Modeling Axially Symmetric and Nonsymmetric Flow to a Well with MODFLOW, and Application to Goddard2 Well Test, Boise, Idaho. *Ground Water*, 35(4), 602–611. <https://doi.org/10.1111/j.1745-6584.1997.tb00125.x>
- Barrett, R., Berry, M., Chan, T. F., Demmel, J., Donato, J., Dongarra, J., et al. (1994). *Templates for the Solution of Linear Systems: Building Blocks for Iterative Methods*. Philadelphia: Society for Industrial and Applied Mathematics. <https://doi.org/10.1137/1.9781611971538>
- Bedekar, V., Scantlebury, L., & Panday, S. (2019). Axisymmetric Modeling Using MODFLOW-USG. *Groundwater*, 57(5), 772–777. <https://doi.org/10.1111/gwat.12861>
- Bennett, G. D. (1976). *Introduction to ground-water hydraulics, a programmed text for self-instruction*. U.S. Geological Survey Techniques of Water-Resources Investigations 03-B2. <https://doi.org/10.3133/twri03B2>
- Bianchi, M., MacDonald, A. M., Macdonald, D. M. J., & Asare, E. B. (2020). Investigating the Productivity and Sustainability of Weathered Basement Aquifers in Tropical Africa Using Numerical Simulation and Global Sensitivity Analysis. *Water Resources Research*, 56(9). <https://doi.org/10.1029/2020WR027746>
- Bittenger, M. W., Duke, H. R., & Longenbaugh, R. A. (1967). Mathematical Simulations for Better Aquifer Management. *IASH, Pub. No. 72*, 509–519.
- Bohling, G. C., & Butler, J. J. (2001). Ir2dinv: A finite-difference model for inverse analysis of two-dimensional linear or radial groundwater flow. *Computers & Geosciences*, 27(10), 1147–1156. [https://doi.org/10.1016/S0098-3004\(01\)00036-X](https://doi.org/10.1016/S0098-3004(01)00036-X)
- Boulton, N. S. (1954). The drawdown of the watertable under non-steady conditions near a pumped well in an unconfined formation. *Proceedings of the Institution of Civil Engineers*, 3(4), 564–579. <https://doi.org/10.1680/ipeds.1954.12586>

- Bredehoeft, J. D., & Pinder, G. F. (1970). Digital Analysis of Areal Flow in Multiaquifer Groundwater Systems: A Quasi Three-Dimensional Model. *Water Resources Research*, 6(3), 883–888. <https://doi.org/10.1029/WR006i003p00883>
- Cooley, R. L. (1971). A Finite Difference Method for Unsteady Flow in Variably Saturated Porous Media: Application to a Single Pumping Well. *Water Resources Research*, 7(6), 1607–1625. <https://doi.org/10.1029/WR007i006p01607>
- Cooley, R. L. (1972). Numerical simulation of flow in an aquifer overlain by a water table aquitard. *Water Resources Research*, 8(4), 1046–1050. <https://doi.org/10.1029/WR008i004p01046>
- Cooley, R. L. (1992). *A modular finite-element model (MODFE) for areal and axisymmetric ground-water-flow problems, Part 2: Derivation of finite-element equations and comparisons with analytical solutions*. U.S. Geological Survey Techniques of Water-Resources Investigations 06-A4. <https://doi.org/10.3133/twri06A4>
- Cooley, R. L., & Case, C. M. (1973). Effect of a water table aquitard on drawdown in an underlying pumped aquifer. *Water Resources Research*, 9(2), 434–447. <https://doi.org/10.1029/WR009i002p00434>
- Cooley, R. L., & Cunningham, A. B. (1979). Consideration of total energy loss in theory of flow to wells. *Journal of Hydrology*, 43(1–4), 161–184. [https://doi.org/10.1016/0022-1694\(79\)90171-9](https://doi.org/10.1016/0022-1694(79)90171-9)
- Day, P. R., & Luthin, J. N. (1956). A Numerical Solution of the Differential Equation of Flow for a Vertical Drainage Problem1. *Soil Science Society of America Journal*, 20(4), 443. <https://doi.org/10.2136/sssaj1956.03615995002000040001x>
- Diersch, H. J. G. (2002). FEFLOW Finite Element Subsurface Flow and Transport Simulation System - User's Manual/Reference Manual/White Papers. Release 5.0., WASY Ltd., Berlin. Berlin, Germany: WASY Ltd.
- Douglas, J., & Rachford, H. H. (1956). On the Numerical Solution of Heat Conduction Problems in Two and Three Space Variables. *Transactions of the American Mathematical Society*, 82(2), 421. <https://doi.org/10.2307/1993056>
- Drake, R. L., & Ellingson, M. B. (1970a). Numerical Solutions for the Radial Subsurface Flow Problem. *Ground Water*, 8(6), 39–47. <https://doi.org/10.1111/j.1745-6584.1970.tb03680.x>
- Drake, R. L., & Ellingson, M. B. (1970b). The application of a local similarity concept in solving the radial flow problem. *Journal of Computational Physics*, 6(2), 200–218. [https://doi.org/10.1016/0021-9991\(70\)90021-5](https://doi.org/10.1016/0021-9991(70)90021-5)
- Drake, R. L., Molz, F. J., Remson, I., & Fungaroli, A. A. (1969). Similarity Approximation for the Radial Subsurface Flow Problem. *Water Resources Research*, 5(3), 673–684. <https://doi.org/10.1029/WR005i003p00673>
- Dupuit, J. (1857). Mouvement de l'eau à travers les terrains perméables (in French). *Comptes Rendus de l'Académie Des Sciences*, 45, 92–96.
- Dupuit, J. (1863). *Etude Théoriques et Pratiques Sur le Mouvement Des Eaux Dans Les Canaux Découverts et à Travers Les Terrains Perméables* (in French). Paris: Dunot.
- Eshett, A., & Longenbaugh, R. A. (1965). *Mathematical model for transient flow in porous media*. Progress Report, Civil Engineering Section, Colorado State University. Fort Collins, Colorado.

- Fayers, F. J., & Sheldon, J. W. (1962). The use of a high-speed digital computer in the study of the hydrodynamics of geologic basins. *Journal of Geophysical Research*, 67(6), 2421–2431. <https://doi.org/10.1029/JZ067i006p02421>
- Ferziger, J. H., & Peric, M. (2002). *Computational Method for Fluid Dynamics, 3th edition*. New York: Springer-Verlag Berlin Heidelberg.
- Fiering, M. B. (1964). A Digital Computer Solution For Well Field Draw-down. *International Association of Scientific Hydrology. Bulletin*, 9(4), 16–23. <https://doi.org/10.1080/02626666409493683>
- Freeze, R. A. (1966). *Theoretical analysis of regional ground water flow*. (PhD). University of California, Berkely.
- Freeze, R. A. (1971). Three-Dimensional, Transient, Saturated-Unsaturated Flow in a Groundwater Basin. *Water Resources Research*, 7(2), 347–366. <https://doi.org/10.1029/WR007i002p00347>
- Freeze, R. A., & Witherspoon, P. A. (1966). Theoretical analysis of regional groundwater flow: 1. Analytical and numerical solutions to the mathematical model. *Water Resources Research*, 2(4), 641–656. <https://doi.org/10.1029/WR002i004p00641>
- Freeze, R. A., & Witherspoon, P. A. (1967). Theoretical analysis of regional groundwater flow: 2. Effect of water-table configuration and subsurface permeability variation. *Water Resources Research*, 3(2), 623–634. <https://doi.org/10.1029/WR003i002p00623>
- Freeze, R. A., & Witherspoon, P. A. (1968). Theoretical Analysis of Regional Ground Water Flow: 3. Quantitative Interpretations. *Water Resources Research*, 4(3), 581–590. <https://doi.org/10.1029/WR004i003p00581>
- Gray, D. A. (2004). Groundwater studies in the Institute of Geological Sciences between 1965 and 1977. *Geological Society, London, Special Publications*, 225(1), 295–318. <https://doi.org/10.1144/GSL.SP.2004.225.01.22>
- Green, D. W., Dabiri, H., Weinaug, C. F., & Prill, R. (1970). Numerical Modeling of Unsaturated Groundwater Flow and Comparison of the Model to a Field Experiment. *Water Resources Research*, 6(3), 862–874. <https://doi.org/10.1029/WR006i003p00862>
- Halford, K. J., & Yobbi, D. (2006). Estimating Hydraulic Properties Using a Moving-Model Approach and Multiple Aquifer Tests. *Ground Water*, 44(2), 284–291. <https://doi.org/10.1111/j.1745-6584.2005.00109.x>
- Hantush, M. S. (1967). Flow to wells in aquifers separated by a semipervious layer. *Journal of Geophysical Research*, 72(6), 1709–1720. <https://doi.org/10.1029/JZ072i006p01709>
- Harbaugh, A. W. (1995). *Direct solution package based on alternating diagonal ordering for the U.S. Geological Survey modular finite-difference ground-water flow model*. U.S. Geological Survey Open-File Report 95-288. <https://doi.org/https://doi.org/10.3133/ofr95288>
- Harbaugh, A. W. (2005). *MODFLOW-2005, the U.S. Geological Survey modular ground-water model - the Ground-Water Flow Process*. U.S. Geological Survey Techniques and Methods 6-A16. <https://doi.org/https://doi.org/10.3133/tm6A16>

- Harbaugh, A. W., & McDonald, M. G. (1996a). *Programmer's documentation for MODFLOW-96, an update to the U.S. Geological Survey modular finite-difference ground-water flow model*. U.S. Geological Survey Open-File Report 96-486. [https://doi.org/https://doi.org/10.3133/ofr96486](https://doi.org/10.3133/ofr96486)
- Harbaugh, A. W., & McDonald, M. G. (1996b). *User's documentation for MODFLOW-96, an update to the U.S. Geological Survey modular finite-difference ground-water flow model*. U.S. Geological Survey Open-File Report 96-485. [https://doi.org/https://doi.org/10.3133/ofr96485](https://doi.org/10.3133/ofr96485)
- Harbaugh, A. W., Banta, E. R., Hill, M. C., & McDonald, M. G. (2000). *MODFLOW-2000, The U.S. Geological Survey Modular Ground-Water Model: User Guide to Modularization Concepts and the Ground-Water Flow Process*. U.S. Geological Survey Open-File Report 00-92. [https://doi.org/https://doi.org/10.3133/ofr200092](https://doi.org/10.3133/ofr200092)
- Hemker, C. J. (1985). A General Purpose Microcomputer Aquifer Test Evaluation Technique. *Ground Water*, 23(2), 247–253. <https://doi.org/10.1111/j.1745-6584.1985.tb02799.x>
- Hill, M. C. (1990). *PRECONDITIONED CONJUGATE-GRADIENT 2 (PCG2), a computer program for solving ground-water flow equations*. U.S. Geological Survey Water-Resources Investigations Report 90-4048. <https://doi.org/10.3133/wri904048>
- Hoving, J. H. K. (2015). *Maintaining ATES Balance Using Continuous Commissioning and Model Predictive Control - Development of a reference model and analysis of method potential based on a case study at the Kropman Utrecht office*. (Master Thesis). Eindhoven University of Technology, Eindhoven, The Netherlands.
- Javandel, I., & Witherspoon, P. A. (1968). Application of the Finite Element Method to Transient Flow in Porous Media. *Society of Petroleum Engineers Journal*, 8(03), 241–252. <https://doi.org/10.2118/2052-PA>
- Javandel, I., & Witherspoon, P. A. (1969). A Method of Analyzing Transient Fluid Flow in Multilayered Aquifers. *Water Resources Research*, 5(4), 856–869. <https://doi.org/10.1029/WR005i004p00856>
- Johnson, G. S., Cosgrove, D. M., & Frederick, D. B. (2001). A Numerical Model and Spreadsheet Interface for Pumping Test Analysis. *Ground Water*, 39(4), 582–592. <https://doi.org/10.1111/j.1745-6584.2001.tb02346.x>
- Khadra, W. M., Stuyfzand, P. J., & Khadra, I. M. (2017). Mitigation of saltwater intrusion by 'integrated fresh-keeper' wells combined with high recovery reverse osmosis. *Science of The Total Environment*, 574, 796–805. <https://doi.org/10.1016/j.scitotenv.2016.09.156>
- Klute, A. (1952). A Numerical Method for Solving the Flow Equation for Water in Unsaturated Materials. *Soil Science*, 73(2), 105–116. <https://doi.org/10.1097/00010694-195202000-00003>
- Lakshminarayana, V., & Rajagopalan, S. P. (1977). Digital Model Studies of Steady-State Radial Flow to Partially Penetrating Wells in Alluvial Plains. *Ground Water*, 15(3), 223–230. <https://doi.org/10.1111/j.1745-6584.1977.tb03167.x>
- Lakshminarayana, V., & Rajagopalan, S. P. (1978). Digital model studies of unsteady-state radial flow to partially penetrating wells in unconfined anisotropic aquifers. *Journal of Hydrology*, 38(3–4), 249–262. [https://doi.org/10.1016/0022-1694\(78\)90072-0](https://doi.org/10.1016/0022-1694(78)90072-0)
- Langevin, C. D. (2008). Modeling Axisymmetric Flow and Transport. *Ground Water*, 46(4), 579–590. <https://doi.org/10.1111/j.1745-6584.2008.00445.x>

- Langevin, C. D., Thorne, D. T., Dausman, A. M., Sukop, M. C., & Guo, W. (2007). *SEAWAT Version 4: A Computer Program for Simulation of Multi-Species Solute and Heat Transport*. U.S. Geological Survey Techniques and Methods 6-A22. Reston, Virginia.
<https://doi.org/https://doi.org/10.3133/tm6A22>
- Langevin, C. D., Hughes, J. D., Banta, E. R., Niswonger, R. G., Panday, S., & Provost, A. M. (2017). *Documentation for the MODFLOW 6 Groundwater Flow Model*. U.S. Geological Survey Techniques and Methods 6-A55. <https://doi.org/10.3133/tm6A55>
- Lebbe, L. C. (1983). Een matematisch model van de niet-permanente grondwaterstroming naar een pompput in een veellagig grondwaterreservoir en enkele beschouwingen over de stroomtijd (in Dutch). *Tijdschrift BECEWA*, 70, 35–48.
- Lebbe, L. C. (1988). *Uitvoering van pomproeven en interpretatie door middel van een invers model (in Dutch)*. Ghent University, Ghent, Belgium.
- Lebbe, L. C. (1999). *Hydraulic Parameter Identification. Generalized Interpretation Method for Single and Multiple Pumping Tests*. Berlin Heidelberg: Springer-Verlag.
- Lebbe, L. C., & Bougriba, M. (1995). Interpretation of a double pumping test at Assenede (N.W. Belgium) by means of an inverse numerical model and the comparison of the ordinary and biweighted least square solution. *BULLETIN DE LA SOCIETE BELGE DE GEOLOGIE = BULLETIN VAN DE BELGISCHE VERENIGING VOOR GEOLOGIE*, 104(1–2), 163–172.
- Lebbe, L. C., & de Breuck, W. (1994). The Application of an Inverse Numerical Model for the Interpretation of Single or Multiple Pumping Tests. In A. Peters, G. Wittum, B. Herrling, U. Messner, C. A. Brebbia, W. G. Gray, & G. F. Pinder (Eds.), *Water Science and Technology Library* (Vol. 12, pp. 769–767). Dordrecht, The Netherlands: Kluwers Academic.
- Lebbe, L. C., & de Breuck, W. (1995). Validation of an inverse numerical model for interpretation of pumping tests and a study of factors influencing accuracy of results. *Journal of Hydrology*, 172(1–4), 61–85. [https://doi.org/10.1016/0022-1694\(95\)02747-D](https://doi.org/10.1016/0022-1694(95)02747-D)
- Lebbe, L. C., & de Breuck, W. (1997). Analysis of a Pumping Test in an Anisotropic Aquifer by Use of an Inverse Numerical Model. *Hydrogeology Journal*, 5(3), 44–59.
<https://doi.org/10.1007/s100400050112>
- Lebbe, L. C., & van Meir, N. (2000). Hydraulic Conductivities of Low Permeability Sediments Inferred from a Triple Pumping Test and Observed Vertical Gradients. *Ground Water*, 38(1), 76–88.
<https://doi.org/10.1111/j.1745-6584.2000.tb00204.x>
- Lebbe, L. C., Mahauden, M., & de Breuck, W. (1992). Execution of a triple pumping test and interpretation by an inverse numerical model. *Applied Hydrogeology*, 1(4), 20–34.
- Lebbe, L. C., Tarhouni, J., van Houtte, E., & de Breuck, W. (1995). Results Of An Artificial Recharge Test And A Double Pumping Test As Preliminary Studies For Optimizing Water Supply In The Western Belgian Coastal Plain. *Hydrogeology Journal*, 3(3), 53–63.
<https://doi.org/10.1007/s100400050067>
- Lloyd, J. W. (1969). *The hydrogeology of the southern desert of Jordan*. UNDP/FAO Publications, Technical Report, 1, Special Fund 212.

- Lloyd, J. W. (2004). British hydrogeologists in North Africa and the Middle East: an historical perspective. *Geological Society, London, Special Publications*, 225(1), 219–227.
<https://doi.org/10.1144/GSL.SP.2004.225.01.15>
- Louwyck, A. (2011). *MAxSym - A MATLAB Tool to Simulate Two-Dimensional Axi-Symmetric Groundwater Flow*, Research Unit Groundwater Modeling, Ghent University. Ghent, Belgium.
Retrieved from <https://github.com/alouwyck/MAxSym>
- Louwyck, A., Vandenbohede, A., & Lebbe, L. C. (2005). The role of hydrogeological research in the realization of a combined pumping and deep infiltration system at the excavation “Duinenabdij.” In J.-L. Herrier, J. Mees, A. Salman, J. Seys, H. Van Nieuwenhuyse, & I. Dobbelaere (Eds.), *Proceedings “Dunes and Estuaries 2005”: International Conference on nature restoration practices in European coastal habitats, Koksijde, Belgium 19-23 September 2005.* (pp. 317–326). Oostende, Belgium: VLIZ Special Publication 19.
- Louwyck, A., Vandenbohede, A., & Lebbe, L. C. (2007). OGMA-RF: a user-friendly, modular program package to simulate and analyse radial flow. In *ModelCARE 2007, Sixth International Conference on Calibration and Reliability in Groundwater Modelling: Credibility in Modelling, Copenhagen, Denmark, 9-13 September 2007* (pp. 88–93).
- Louwyck, A., Vandenbohede, A., & Lebbe, L. C. (2010). Numerical analysis of step-drawdown tests: Parameter identification and uncertainty. *Journal of Hydrology*, 380(1–2), 165–179.
<https://doi.org/10.1016/j.jhydrol.2009.10.034>
- Louwyck, A., Vandenbohede, A., Bakker, M., & Lebbe, L. C. (2012). Simulation of axi-symmetric flow towards wells: A finite-difference approach. *Computers & Geosciences*, 44, 136–145.
<https://doi.org/10.1016/j.cageo.2011.09.004>
- Louwyck, A., Vandenbohede, A., Bakker, M., & Lebbe, L. C. (2014). MODFLOW procedure to simulate axisymmetric flow in radially heterogeneous and layered aquifer systems. *Hydrogeology Journal*, 22(5), 1217–1226. <https://doi.org/10.1007/s10040-014-1150-0>
- Mansour, M. M., Hughes, A. G., Spink, A. E. F., & Riches, J. (2011). Pumping test analysis using a layered cylindrical grid numerical model in a complex, heterogeneous chalk aquifer. *Journal of Hydrology*, 401(1–2), 14–21. <https://doi.org/10.1016/j.jhydrol.2011.02.005>
- McDonald, M. G., & Harbaugh, A. W. (1984). *A modular three-dimensional finite-difference ground-water flow model*. U.S. Geological Survey Open-File Report 83-875.
<https://doi.org/https://doi.org/10.3133/ofr83875>
- McDonald, M. G., & Harbaugh, A. W. (1988). *A modular three-dimensional finite-difference ground-water flow model*. U.S. Geological Survey Techniques of Water-Resources Investigations 06-A1.
<https://doi.org/10.3133/twri06A1>
- McDonald, M. G., & Harbaugh, A. W. (2003). The History of MODFLOW. *Ground Water*, 41(2), 280–283. <https://doi.org/10.1111/j.1745-6584.2003.tb02591.x>
- Mehl, S. W., & Hill, M. C. (2001). *MODFLOW-2000, the U. S. Geological Survey modular ground-water model; user guide to the Link-AMG (LMG) package for solving matrix equations using an algebraic multigrid solver*. U.S. Geological Survey Open-File Report 2001-177.
<https://doi.org/https://doi.org/10.3133/ofr01177>

- Narasimhan, T. N., & Witherspoon, P. A. (1976). An integrated finite difference method for analyzing fluid flow in porous media. *Water Resources Research*, 12(1), 57–64.
<https://doi.org/10.1029/WR012i001p00057>
- Narasimhan, T. N., & Witherspoon, P. A. (1982). Overview of the Finite Element Method in Groundwater Hydrology. In K. P. Holz, U. Meissner, W. Zielke, C. A. Brebbia, G. Pinder, & W. Gray (Eds.), *Finite Elements in Water Resources* (pp. 29–44). Berlin, Heidelberg: Springer-Verlag.
https://doi.org/10.1007/978-3-662-02348-8_2
- Neuman, S. P., & Witherspoon, P. A. (1970). Finite Element Method of Analyzing Steady Seepage with a Free Surface. *Water Resources Research*, 6(3), 889–897.
<https://doi.org/10.1029/WR006i003p00889>
- Neuman, S. P., & Witherspoon, P. A. (1971). Analysis of Nonsteady Flow with a Free Surface Using the Finite Element Method. *Water Resources Research*, 7(3), 611–623.
<https://doi.org/10.1029/WR007i003p00611>
- Oliveti, I., & Cardarelli, E. (2017). 2D approach for modelling self-potential anomalies: application to synthetic and real data. *Bollettino Di Geofisica Teorica Ed Applicata*, 58(4), 415–430.
- Panday, S., Langevin, C. D., Niswonger, R. G., Ibaraki, M., & Hughes, J. D. (2013). *MODFLOW-USG version 1: An unstructured grid version of MODFLOW for simulating groundwater flow and tightly coupled processes using a control volume finite-difference formulation*. U.S. Geological Survey Techniques and Methods 6-A45. <https://doi.org/10.3133/tm6A45>
- Pandit, A., & Abi Aoun, J. M. (1994). Numerical Modeling of Axisymmetric Flow. *Ground Water*, 32(3), 458–464. <https://doi.org/10.1111/j.1745-6584.1994.tb00663.x>
- Peaceman, D. W., & Rachford, Jr. , H. H. (1955). The Numerical Solution of Parabolic and Elliptic Differential Equations. *Journal of the Society for Industrial and Applied Mathematics*, 3(1), 28–41. <https://doi.org/10.1137/0103003>
- Peterson, P., Oliphant, T., & Vanderplas, J. (2022). SciPy (version 1.8.1) documentation for function linalg.solve. Retrieved July 18, 2022, from <https://docs.scipy.org/doc/scipy/reference/generated/scipy.linalg.solve.html>
- Pinder, G. F. (1970). *A digital model for aquifer evaluation*. U.S. Geological Survey Techniques of Water-Resources Investigations 07-C1. https://doi.org/10.3133/twri07C1_1970
- Pinder, G. F. (1988). An Overview of Groundwater Modelling. In E. Custodio, A. Gurgui, & J. P. L. Ferreira (Eds.), *Groundwater Flow and Quality Modelling. NATO ASI Series*. (Vol. vol 224, pp. 119–134). Dordrecht: Springer Netherlands. https://doi.org/10.1007/978-94-009-2889-3_7
- Pinder, G. F., & Bredehoeft, J. D. (1968). Application of the Digital Computer for Aquifer Evaluation. *Water Resources Research*, 4(5), 1069–1093. <https://doi.org/10.1029/WR004i005p01069>
- Prickett, T. A., & Lonnquist, C. G. (1971). *Selected digital computer techniques for groundwater resource evaluation* (Bulletin 55). State of Illinois, Department of Registration and Education.
- Prommer, H., & Post, V. E. A. (2010). *PHT3D, a reactive multicomponent transport model for saturated media, User's Manual Vol 2.10*. Retrieved from <http://www.pht3d.org>

- Raats, P. A. C., & Knight, J. H. (2018). The Contributions of Lewis Fry Richardson to Drainage Theory, Soil Physics, and the Soil-Plant-Atmosphere Continuum. *Frontiers in Environmental Science*, 6. <https://doi.org/10.3389/fenvs.2018.00013>
- Rathod, K. S., & Rushton, K. R. (1984). Numerical Method of Pumping Test Analysis Using Microcomputers. *Ground Water*, 22(5), 602–608. <https://doi.org/10.1111/j.1745-6584.1984.tb01431.x>
- Rathod, K. S., & Rushton, K. R. (1991). Interpretation of Pumping from Two-Zone Layered Aquifers Using a Numerical Model. *Ground Water*, 29(4), 499–509. <https://doi.org/10.1111/j.1745-6584.1991.tb00541.x>
- Reilly, T. E. (1984). *A Galerkin finite-element flow model to predict the transient response of a radially symmetric aquifer*. U.S. Geological Survey Water Supply Paper 2198. <https://doi.org/10.3133/wsp2198>
- Reilly, T. E., & Harbaugh, A. W. (1993). Simulation of Cylindrical Flow to a Well Using the U.S. Geological Survey Modular Finite-Difference Ground-Water Flow Model. *Ground Water*, 31(3), 489–494. <https://doi.org/10.1111/j.1745-6584.1993.tb01851.x>
- Remson, I., Appel, C. A., & Webster, R. A. (1965). Ground-Water Models Solved by Digital Computer. *Journal of the Hydraulics Division*, 91(3), 133–147. <https://doi.org/10.1061/JYCEAJ.0001234>
- Remson, I., Hornberger, G. M., & Molz, F. J. (1971). *Numerical methods in subsurface hydrology*. New York: Wiley-Interscience. [https://doi.org/10.1016/0148-9062\(74\)92313-4](https://doi.org/10.1016/0148-9062(74)92313-4)
- Richardson, L. F. (1910). The approximate arithmetical solution by finite differences of physical problems involving differential equations, with an application to the stresses in a masonry dam. *Philosophical Transactions of the Royal Society London Series , A* 210, 307–357.
- Richardson, L. F. (1925). How to solve differential equations approximately by arithmetic. *The Mathematical Gazette*, 12, 415–421.
- Rubin, J. (1968). Theoretical Analysis of Two-Dimensional, Transient Flow of Water in Unsaturated and Partly Unsaturated Soils. *Soil Science Society of America Journal*, 32(5), 607–615. <https://doi.org/10.2136/sssaj1968.03615995003200050013x>
- Rushton, K. R. (1974). Extensive Pumping From Unconfined Aquifers. *Journal of the American Water Resources Association*, 10(1), 32–41. <https://doi.org/10.1111/j.1752-1688.1974.tb00538.x>
- Rushton, K. R., & Booth, S. J. (1976). Pumping-test analysis using a discrete time-discrete space numerical method. *Journal of Hydrology*, 28(1), 13–27. [https://doi.org/10.1016/0022-1694\(76\)90049-4](https://doi.org/10.1016/0022-1694(76)90049-4)
- Rushton, K. R., & Redshaw, S. C. (1979). *Seepage and Groundwater Flow: Numerical Analysis by Digital Methods*. New York: Wiley.
- Rushton, K. R., & Turner, A. (1974). Numerical Analysis of Pumping from Confined-Unconfined Aquifers. *Journal of the American Water Resources Association*, 10(6), 1255–1269. <https://doi.org/10.1111/j.1752-1688.1974.tb00642.x>
- Rutledge, A. T. (1991). *An Axisymmetric finite-difference flow model to simulate drawdown in and around a pumped well*. U.S. Geological Survey Water-Resources Investigations Report 90-4098. <https://doi.org/10.3133/wri904098>

- Saatsaz, M., & Eslamian, S. (2020). Groundwater Modeling and Its Concepts, Classifications, and Applications for Solute Transport Simulation in Saturated Porous Media. In S. Eslamian & F. Eslamian (Eds.), *Advances in Hydrogeochemistry Research* (pp. 91–126). New York, USA: Nova Science Publishers, Inc.
- Salama, A., Li, W., & Sun, S. (2013). Finite volume approximation of the three-dimensional flow equation in axisymmetric, heterogeneous porous media based on local analytical solution. *Journal of Hydrology*, 501, 45–55. <https://doi.org/10.1016/j.jhydrol.2013.07.036>
- Samani, N., Kompani-Zare, M., & Barry, D. A. (2004). MODFLOW equipped with a new method for the accurate simulation of axisymmetric flow. *Advances in Water Resources*, 27(1), 31–45. <https://doi.org/10.1016/j.advwatres.2003.09.005>
- Spanier, J. (1967). Alternating direction methods applied to heat conduction problems. In A. Ralston & H. S. Wilf (Eds.), *Mathematical Methods for Digital Computers* (Vol. 2, pp. 215–245). New York: John Wiley.
- Stallman, R. W. (1956). Numerical analysis of regional water levels to define aquifer hydrology. *Transactions, American Geophysical Union*, 37(4), 451. <https://doi.org/10.1029/TR037i004p00451>
- Stone, H. L. (1968). Iterative Solution of Implicit Approximations of Multidimensional Partial Differential Equations. *SIAM Journal on Numerical Analysis*, 5(3), 530–558. <https://doi.org/10.1137/0705044>
- Streltsova, T. D., & Rushton, K. R. (1973). Water table drawdown due to a pumped well in an unconfined aquifer. *Water Resources Research*, 9(1), 236–242. <https://doi.org/10.1029/WR009i001p00236>
- Taylor, R. L., & Brown, C. B. (1967). Darcy Flow Solutions with a Free Surface. *Journal of the Hydraulics Division*, 93(2), 25–33. <https://doi.org/10.1061/JYCEAJ.0001590>
- Thiem, A. (1870). Die Ergiebigkeit artesischer Bohrlöcher, Schachtbrunnen und Filtergalerien (in German). *Journal Für Gasbeleuchtung Und Wasserversorgung*, 13, 450–467.
- Thiem, G. (1906). *Hydrologische Methoden* (in German). Leipzig: Gebhardt.
- Trescott, P. C. (1975). *Documentation of finite-difference model for simulation of three-dimensional groundwater flow*. U.S. Geological Survey Open-File Report 75-438. <https://doi.org/https://doi.org/10.3133/ofr75438>
- Trescott, P. C., & Larson, S. P. (1976). *Supplement to Open-File Report 75-438: Documentation of finite-difference model for simulation of three-dimensional ground-water flow*. U.S. Geological Survey Open-File Report 76-591. <https://doi.org/https://doi.org/10.3133/ofr76591>
- Trescott, P. C., Pinder, G. F., & Larson, S. P. (1976). *Finite-difference Model for Aquifer Simulation in Two Dimensions With Results of Numerical Experiments*. U.S. Geological Survey Techniques of Water-Resources Investigations 07-C1. <https://doi.org/https://doi.org/10.3133/twri07C1>
- Turner, M. J., Clough, R. W., Martin, H. C., & Topp, L. J. (1956). Stiffness and Deflection Analysis of Complex Structures. *Journal of the Aeronautical Sciences*, 23(9), 805–823. <https://doi.org/10.2514/8.3664>

- Tyson, H. N., & Weber, E. M. (1964). Ground-Water Management for the Nation's Future—Computer Simulation of Ground-Water Basins. *Journal of the Hydraulics Division*, 90(4), 59–77.
<https://doi.org/10.1061/JYCEAJ.0001093>
- Upton, K. A., Butler, A. P., Jackson, C. R., & Mansour, M. (2019). Modelling boreholes in complex heterogeneous aquifers. *Environmental Modelling & Software*, 118, 48–60.
<https://doi.org/10.1016/j.envsoft.2019.03.018>
- Vandenbohede, A., & Lebbe, L. C. (2003). Combined interpretation of pumping and tracer tests: theoretical considerations and illustration with a field test. *Journal of Hydrology*, 277(1–2), 134–149. [https://doi.org/10.1016/S0022-1694\(03\)00090-8](https://doi.org/10.1016/S0022-1694(03)00090-8)
- Vandenbohede, A., Louwyck, A., & Lebbe, L. C. (2008a). Heat transport in a push-pull test: parameter identification and sensitivity analyses. In J. C. Refsgaard, K. Kovar, E. Haarder, & E. Nygaard (Eds.), *Proceedings of an International Conference on Calibration and Reliability in Groundwater Modelling: Credibility of Modelling, Copenhagen, Denmark, 9-13 September 2007* (pp. 257–261). Copenhagen, Denmark.
- Vandenbohede, A., Louwyck, A., & Lebbe, L. C. (2008b). Identification and reliability of microbial aerobic respiration and denitrification kinetics using a single-well push–pull field test. *Journal of Contaminant Hydrology*, 95(1–2), 42–56. <https://doi.org/10.1016/j.jconhyd.2007.07.003>
- Vandenbohede, A., Louwyck, A., & Lebbe, L. C. (2009). Conservative Solute Versus Heat Transport in Porous Media During Push-pull Tests. *Transport in Porous Media*, 76(2), 265–287.
<https://doi.org/10.1007/s11242-008-9246-4>
- Vandenbohede, A., Louwyck, A., & Vlaminck, N. (2014). SEAWAT-Based Simulation of Axisymmetric Heat Transport. *Groundwater*, 52(6), 908–915. <https://doi.org/10.1111/gwat.12137>
- Vandenbohede, A., Wallis, I., & Alleman, T. (2019). Trace metal behavior during in-situ iron removal tests in Leuven, Belgium. *Science of The Total Environment*, 648, 367–376.
<https://doi.org/10.1016/j.scitotenv.2018.08.126>
- Van Meir, N., & Lebbe, L. C. (2005). Parameter identification for axi-symmetric density-dependent groundwater flow based on drawdown and concentration data. *Journal of Hydrology*, 309(1–4), 167–177. <https://doi.org/10.1016/j.jhydrol.2004.11.019>
- Wallis, I., Prommer, H., Post, V. E. A., Vandenbohede, A., & Simmons, C. T. (2012). Simulating MODFLOW-Based Reactive Transport Under Radially Symmetric Flow Conditions. *Ground Water*, 51(3), 398–413. <https://doi.org/10.1111/j.1745-6584.2012.00978.x>
- Wang, H. F., & Anderson, M. P. (1982). *Introduction to Groundwater Modeling: Finite Difference and Finite Element Methods*. San Francisco: WH Freeman and Company.
- Whisler, F. D., & Klute, A. (1965). The Numerical Analysis of Infiltration, Considering Hysteresis, Into a Vertical Soil Column at Equilibrium Under Gravity. *Soil Science Society of America Journal*, 29(5), 489. <https://doi.org/10.2136/sssaj1965.03615995002900050008x>
- Wilson, J. D., & Naff, R. L. (2004). *MODFLOW-2000, The U.S. Geological Survey Modular Ground-Water Model -- GMG Linear Equation Solver Package Documentation*. U.S. Geological Survey Open-File Report 2004-1261. <https://doi.org/10.3133/ofr20041261>

Yeh, G.-T. (1999). Numerical Methods Applied to Subsurface Hydrology. In *Computational Subsurface Hydrology* (pp. 27–176). Boston, MA: Springer US. https://doi.org/10.1007/978-1-4757-3038-8_2

Young, D. M. (1950). *Iterative methods for solving partial difference equations of elliptical type* (PhD Thesis). Harvard University, Cambridge.

Youngs, E. G. (1957). Moisture Profiles During Vertical Infiltration. *Soil Science*, 84(4), 283–290. <https://doi.org/10.1097/00010694-195710000-00003>

Zheng, C., & Wang, P. P. (1999). *MT3DMS : a modular three-dimensional multispecies transport model for simulation of advection, dispersion, and chemical reactions of contaminants in groundwater systems; documentation and user's guide*. Contract Report SERDP-99-1, U.S. Army Engineer Research and Development Center, Vicksburg, MI. Vicksburg, MI.

Zhou, Y., & Li, W. (2011). A review of regional groundwater flow modeling. *Geoscience Frontiers*, 2(2), 205–214. <https://doi.org/10.1016/j.gsf.2011.03.003>

Zienkiewicz, O., Mayer, P., & Cheung, Y. K. (1966). Solution of Anisotropic Seepage by Finite Elements. *Journal of the Engineering Mechanics Division*, 92(1), 111–120. <https://doi.org/10.1061/JMCEA3.0000706>

Chapter 4. A Critical Review of the Hybrid Finite-Difference Finite-Element Method

4.1. Introduction

A hybrid finite-difference finite-element method was developed by Lebbe (1988) to simulate axisymmetric flow towards a pumping well in a confined multilayered aquifer system. The method was implemented in the AS2D code, which is part of the HYPARIDEN software package (Lebbe, 1999), a set of FORTRAN routines to simulate and analyze single and multiple pumping tests by means of an inverse numerical model. Both the axisymmetric flow model and the inverse model were verified by Lebbe (1988, 1999) and Lebbe and De Breuck (1995), and were used frequently during the past thirty-five years at the Department of Geology of Ghent University.

Hydraulic parameters for a wide range of lithological layers in Flanders were identified through application of HYPARIDEN (e.g. Lebbe et al., 1992, 1995; Lebbe and Bougriba, 1995; Lebbe and De Breuck, 1994, 1997; Lebbe and Van Meir, 2000; Louwyck et al., 2005; Van Meir and Lebbe, 2005; Vandenbohede and Lebbe, 2003), and the AS2D model was combined with algorithms to simulate solute transport (e.g. Van Meir and Lebbe, 2005). HYPARIDEN was employed extensively in an educational context, foremost in the ‘hydraulic parameter identification’ course taught by Prof. Dr. Luc Lebbe from 1993 until 2017. Several students interpreted aquifer tests using HYPARIDEN in the context of their Master thesis, while Mertooetomo (1995), Van Meir (2001), and Vandenbohede (2004) utilized the software in their PhD research. Numerous hydrogeological studies carried out at Ghent University as an academic service to society made use of the HYPARIDEN software. These include environmental impact assessments, groundwater remediation studies, design of groundwater extractions, and hydro-ecological studies. The Flemish Environment Agency used the AS2D model for almost one decade to estimate the radius of influence of permanent groundwater extractions that require an environmental permit (Lebbe & Vandenbohede, 2004).

4.1.1. HYPARIDEN

The functionalities of HYPARIDEN are very similar to those of the more popular MLU program (Hemker & Post, 2019). Basically, both programs combine an axisymmetric groundwater flow model with a regression algorithm to automatically estimate hydraulic parameters from pumping test data. In this fashion, they provide a more reliable alternative to the curve fitting methods developed during the early years of pumping test interpretation (e.g. Kruseman & de Ridder, 1970, 1990; Reed, 1980; Walton, 1962). Another functionality they have in common is the option to simulate groundwater flow due to multiple pumped wells by applying the superposition method. The most notable difference between both programs is the user interface: MLU is equipped with a graphical user interface, whereas HYPARIDEN has a command-line interface which makes use of text-files for input and output similar to the native versions of MODFLOW.

There are also methodological dissimilarities between HYPARIDEN and MLU. For instance, the nonlinear regression method is different: the former applies the Gauss-Newton algorithm, which was validated by Lebbe and De Breuck (1995), whereas the latter applies the Levenberg-Marquardt algorithm, as proposed by Hemker (1985a). The most important difference within the scope of this study is the solution method applied to simulate the transient axisymmetric well-flow: HYPARIDEN

uses the numerical model AS2D, while MLU applies a semi-analytical approach. The solution method implemented in AS2D is described first by Lebbe (1988), and later by Lebbe and De Breuck (1995) and Lebbe (1999), who call it a hybrid finite-difference finite-element method. The hybrid analytical-numerical method implemented in MLU is described by Hemker (1999a, 1999b). The latter applies an eigenvalue analysis technique which was developed previously by Hemker (1984, 1985b) for steady and transient axisymmetric multi-aquifer flow, respectively. Hemker and Maas (1987) applied the same technique for transient flow, but instead of inverting the solution in the Laplace domain analytically, they performed a numerical inversion using the Stehfest (1970) algorithm. According to Hemker (2000), this was inspired by the work of Moench and Ogata (1981, 1984), and since the numerical inversion is more efficient, it is also adopted by MLU.

4.1.2. AS2D

Analytical solutions for transient axisymmetric well-flow published in the English literature before Hemker (1985b) presented the multilayer solution, were restricted to one-aquifer systems (e.g. Hantush and Jacob, 1955; Theis, 1935), two-aquifer systems (e.g. Hantush, 1967; Neuman and Witherspoon, 1969), or three-aquifer systems (e.g. Neuman, 1968). On the other hand, numerical solutions were not new at the time Lebbe (1988) introduced the AS2D model. Pinder and Bredehoeft (1968), for instance, used a “digital computer” for aquifer evaluation, and gave credit to Fiering (1964) for making the first numerical evaluation of the response of a groundwater reservoir to pumping. Bredehoeft and Pinder (1970) used the finite-difference method to simulate flow to a well in a two-aquifer system, and they compared the result with the analytical solution developed by Hantush (1967). Although Bredehoeft and Pinder (1970) simulate radial flow, they do not use an axisymmetric formulation like Cooley (1971, 1972) and Cooley and Case (1973) do to validate the concept of delayed yield introduced by Boulton (1954, 1963). Other researchers who applied the finite-difference method to solve a radial form of the governing flow equation in the early days of digital computing are, amongst others, Lakshminarayana and Rajagopalan (1977, 1978), Rathod and Rushton (1984), Rushton (1974), Rushton and Booth (1976), Rushton and Redshaw (1979), Rushton and Turner (1974), and Streltsova and Rushton (1973). Finite-element models were also used at that time, and some of them were designed specifically for simulating radial flow (e.g. Cooley and Cunningham, 1979; Reilly, 1984).

Lebbe (1983) developed a finite-difference model to simulate transient flow toward a pumping well in a multilayered groundwater reservoir. This model may be regarded as the predecessor of the AS2D model (Lebbe, 1988, 1999), and it was used in a few hydrogeological studies (e.g. Lebbe et al., 1984). It applied a central finite-difference approximation with respect to the radial and the vertical distance, and a backward finite-difference approximation with respect to the time (Lebbe, 1983). A similar implicit finite-difference formulation for three-dimensional flow is implemented in all MODFLOW versions up to 2005 (Harbaugh, 2005; Harbaugh et al., 2000; Harbaugh & McDonald, 1996; McDonald & Harbaugh, 1984, 1988) and in the MODFLOW predecessors (Pinder, 1969, 1970; Trescott, 1975; Trescott et al., 1976; Trescott & Larson, 1976). Despite the effectiveness of this finite-difference formulation, Lebbe (1988, 1999) modified it to attenuate the abrupt changes in drawdown between adjacent nodes and subsequent time steps by applying linear interpolations in space and time. In this way, a continuous variation of drawdown between nodes and successive points of time is assumed, similar to the finite-element method.

In essence, Lebbe (1988, 1999) solves the same problem numerically as Hemker (1985b) does semi-analytically, i.e. the problem of axisymmetric flow towards a well with infinitesimal radius in a multilayered aquifer system of infinite extent. Remarkably, Lebbe (1988, 1999) does not refer to the work of Hemker (1984, 1985b) or Hunt (1985, 1986) who independently developed a similar solution

technique to solve the same problem semi-analytically. Conversely, Hemker (1999b) refers to Lebbe and de Breuck (1995) whose results were used to test MLU (Hemker & Post, 2019). Hemker (1999b) also extended the transient state solution presented by Hemker (1985b) to include wellbore storage in case of a finite-diameter well, and Hemker (1999a) developed the solution for a multilayer well with screen extending over more than one layer. The latter is also capable of taking into account the effects of wellbore storage and a zero thickness skin.

Although it is straightforward to define laterally varying hydraulic parameters in numerical models, the AS2D model does not account for the effects of wellbore storage, well skin, or gravel pack. It can, however, correct drawdown in the pumping well to account for nonlinear well losses. These may be estimated, for instance, from step-drawdown test data (Louwyck et al., 2010). The inability of the AS2D model to define lateral heterogeneities led to the development of the MAxSym code (Louwyck, 2011). Besides lateral variation of input parameters, this model also allows to define nonuniform initial heads, constant heads, and recharge, by extending the finite-difference formulation implemented in the original model developed by Lebbe (1983). The applied finite-difference approach is discussed by Louwyck et al. (2012), who also present a MODFLOW procedure to solve the same system of finite-difference equations. This procedure is similar to the method proposed by Langevin (2008). Louwyck et al. (2012, 2014) show that both the finite-difference approach and the MODFLOW procedure are very accurate through verification against several analytical solutions (e.g. Butler, 1988; Cooper et al., 1967; Hantush, 1961, 1964; Hyder et al., 1994; Kitterød, 2004; Şen, 2014; Theis, 1935), and against the analytical element solver TTim (Bakker, 2013a, 2013b), which applies the same semi-analytical approach as Hemker (1999a, 1999b) to simulate axisymmetric flow in a multilayered aquifer system.

Lebbe (1988, 1999) also carefully verifies the AS2D model against well-known analytical one- and two-aquifer solutions (e.g. Boulton, 1954, 1963; Hantush, 1960, 1961, 1964; Hantush & Jacob, 1955; Neuman & Witherspoon, 1969; Theis, 1935) and concludes these solutions can be simulated exactly using AS2D if an appropriate discretization of time and space is defined. Apparently unaware of its existence, Lebbe (1988, 1999) does not compare his numerical approach with the semi-analytical multi-aquifer solution developed by Hemker (1985b). A comprehensive comparison between AS2D and the previous version that applied a pure finite-difference approximation (Lebbe, 1983) is also missing. Lebbe (1988) only briefly discusses the influence of the linear interpolations, and he concludes the radial and temporal interpolations do not affect the accuracy of calculated drawdown, but result into more accurate water balances and faster convergence compared to the pure finite-difference approach. The vertical interpolation, however, is problematic, as it causes a head rise close to the pumping well in layers adjacent to the pumped layer. Lebbe (1988) calls this a “numerical Noordbergum effect”, and to attenuate it, Lebbe (1988, 1999) introduces empirically derived correction factors. Unfortunately, the numerical experiments which substantiate all of these findings are not documented.

4.1.3. Objective

As a consequence, it is still an open question whether the applied interpolations in the hybrid finite-difference finite-element method developed by Lebbe (1988, 1999) effectively lead to an improved accuracy or not. Because the AS2D model has been used frequently in the past thirty-five years, the objective of this study is to answer this highly relevant question. Moreover, the “numerical Noordbergum effect” is not the only issue encountered in practice, as numerical instabilities may also occur at small values of time. This is seen, for instance, on the time-drawdown graph in fig 4.7 of Lebbe (1999), and the upper left graph of Figure 6 in Chapter 12.

As will be explained further, the temporal interpolation proposed by Lebbe (1988, 1999) results into a finite-difference approximation which is very similar to the Crank-Nicolson method (Crank & Nicolson, 1947, 1996). This method applies central differences to approximate the time derivative, and it is still being used by several groundwater researchers (e.g. Aime Feulefack et al., 2019; Atangana and Botha, 2013; Samarinis et al., 2022; Wang et al., 2022; Yadav and Agarwal, 2019). It is, however, not as popular as the backward finite-difference approach that is implemented, for instance, in MODFLOW (Harbaugh, 2005; Harbaugh et al., 2000; Harbaugh & McDonald, 1996; McDonald & Harbaugh, 1984, 1988). Although it has been proven that the Crank-Nicolson method is also unconditionally stable and theoretically even more accurate, in practice, it may suffer from spurious oscillations (e.g. Britz et al., 2003; Hellevik, 2020; LeVeque, 2007; Suárez-Carreño and Rosales-Romero, 2021). Spurious oscillations are relatively common issues for numerical analysis, for instance, if the standard Galerkin method or the central finite-difference method is used to solve the one-dimensional convection-diffusion equation in salt water intrusion problems (Wikramaratna & Wood, 1983). Lebbe (1988, 1999) does not mention these oscillations explicitly, but reports larger deviations between numerically and analytically calculated drawdowns at small values of time. Lebbe (1988, 1999) also recognizes the large influence of the initial time on the accuracy, and recommends a value that is ten times smaller than the smallest time at which accurate drawdown simulations are needed.

A theoretical analysis could be conducted to mathematically investigate both the stability and the accuracy of the hybrid finite-difference finite-element method developed by Lebbe (1988, 1999). Similar analyses are presented in textbooks discussing the mathematics behind the finite-difference method (e.g. LeVeque, 2007; Li et al., 2017), and therefore, it is opted for some well thought-out numerical experiments that clearly illustrate the issues of the hybrid finite-difference finite-element method. Three interpolations are applied in this approach: a radial and vertical interpolation, and an interpolation in time. Each of these interpolations can be switched on and off independently, and if they are all inactive, the pure finite-difference approach is obtained (Lebbe, 1988, 1999). As a consequence, it is straightforward to simulate the individual effect of each of these interpolations.

The synthetic pumping test conducted by Lebbe (1988, 1999) and Lebbe and De Breuck (1995) to verify HYPERIDEN is presented as the first test case. Oscillating drawdowns in the pumping well at small values of time are encountered, which disappear if the initial time is set to a much smaller value than recommended by Lebbe (1988, 1999). The Theis (1935) solution is used to investigate the individual effect of the radial and temporal interpolations. The individual effect of the vertical interpolation is analyzed by comparing a homogeneous and a heterogeneous three-layer system. Finally, thousand random multilayer models are simulated to check the accuracy of the different solution methods.

The semi-analytical approach developed by Hemker (1985b, 1999b) is used as a reference. Although this method does not give an exact solution either, it is reasonable to assume it is more accurate than the numerical methods as it does not require a discretization of radial distance and time. Because Lebbe (1988, 1999) did not compare the hybrid finite-difference finite-element method with the finite-difference approach previously presented by Lebbe (1983), the latter is also included in the numerical experiments to investigate if the linear interpolations improve the accuracy of the calculated drawdowns. As the three solution methods were coded again from scratch in Python, they are recapitulated before discussing the results from the numerical experiments. The methods solve the same groundwater flow problem, which is stated mathematically in the next section.

4.2. Problem statement

The problem of axisymmetric flow in a multilayered aquifer system has been stated mathematically in Chapter 2. In this chapter, the stated problem is reduced to the problem solved by AS2D and discussed by Lebbe (1988, 1999). The AS2D model is designed specifically to simulate axisymmetric flow towards a pumping well in an aquifer system consisting of multiple horizontal homogeneous layers of infinite extent (Lebbe, 1988, 1999). Each layer i in the aquifer system has constant transmissivity T_i [L²/T] and constant storativity S_i [-]. Between layers i and $i + 1$, an incompressible resistance layer occurs with zero thickness and vertical resistance c_i [T]. Transmissivity T_i is the product of layer thickness D_i [L] and horizontal conductivity K_i^h [L/T]:

$$T_i = K_i^h D_i \quad (1 \leq i \leq n_l) \quad (1)$$

Storativity S_i is the product of layer thickness D_i and specific elastic storage S_i^s [1/L]:

$$S_i = S_i^s D_i \quad (1 \leq i \leq n_l) \quad (2)$$

If the top layer is phreatic, then S_1 is set to the specific yield S^y [-]. The resistance between two layers is calculated using the vertical conductivity K^v [L/T] of those layers:

$$c_i = \frac{D_i}{2K_i^v} + \frac{D_{i+1}}{2K_{i+1}^v} \quad (1 \leq i < n_l) \quad (3)$$

The upper and lower boundaries of the aquifer system are impervious, i.e. $c_0 = c_{n_l} = \infty$.

Axisymmetric flow in layer i is described by the following partial differential equation:

$$\frac{\partial^2 s_i}{\partial r^2} + \frac{1}{r} \frac{\partial s_i}{\partial r} = \frac{S_i}{T_i} \frac{\partial s_i}{\partial t} + \frac{s_i - s_{i-1}}{c_{i-1} T_i} + \frac{s_i - s_{i+1}}{c_i T_i} \quad (1 \leq i \leq n_l) \quad (4)$$

where n_l is the number of layers. In (4), drawdown s_i [L] is defined as:

$$s_i(r, t) = h_i(r, 0) - h_i(r, t) \quad (5)$$

with $h_i(r, t)$ the hydraulic head [L] in layer i at distance r and time t , and $h_i(r, 0)$ the initial head in layer i at distance r and time $t = 0$. From (5), it follows that the initial drawdown at $t = 0$ is zero:

$$s_i(r, 0) = 0 \quad (1 \leq i \leq n_l) \quad (6)$$

At the outer model boundary, a constant head is defined. This boundary is at an infinitely large distance from the well:

$$s_i(\infty, t) = 0 \quad (1 \leq i \leq n_l) \quad (7)$$

At the inner model boundary of each layer i , a constant pumping rate Q_i [L³/T] is defined, which is positive in case of extraction. This boundary coincides with the well-face as it conceptualizes the well having a separate screen in each layer of the aquifer system. Because AS2D does not consider wellbore storage, an infinitesimal well radius is assumed:

$$\lim_{r \rightarrow 0} \left(r \frac{\partial s_i(r, t)}{\partial r} \right) = \frac{Q_i}{2\pi T_i} \quad (1 \leq i \leq n_l) \quad (8)$$

A constant pumping rate is defined, although it is straightforward to simulate variable-rate pumping tests applying the superposition method as explained in Lebbe (1999) and in section 2.4 of Chapter 2. The superposition principle is valid in this case since the governing partial differential equations (4) are linear.

4.3. Solution methods

As already mentioned in the introduction 4.1, three solution methods are discussed: (1) the semi-analytical approach developed by Hemker (1985b, 1999b), in which the exact solution in the Laplace domain is inverted numerically, (2) the finite-difference approach presented by Lebbe (1983) and Louwyck et al. (2012), and (3) the hybrid finite-difference finite-element method proposed by Lebbe (1988, 1999).

4.3.1. Semi-analytical solution

Hemker (1985b) is the first in the English literature who solved the problem stated in previous section analytically by successive application of the Laplace transform with respect to time t and the infinite zero-order Hankel transform with respect to radial distance r . By performing an eigendecomposition, the system of transformed equations are uncoupled in a similar way as Hemker (1984) solved the corresponding steady state problem. These uncoupled equations are inverted analytically to obtain a closed-form solution containing an improper integral. As both the eigendecomposition and the evaluation of this integral are performed numerically, the solution method is called semi-analytical.

The numerical integration requires extensive computer calculations, and therefore, it is more efficient to only apply the Laplace transform, perform the eigendecomposition, and finally invert the obtained solution in the Laplace domain numerically, e.g. by using the Stehfest (1970) algorithm (Hemker, 2000). This solution method is used here, and it is also applied by Hemker and Maas (1987) and Hemker (1999a, 1999b) to solve similar yet more complex problems of transient axisymmetric flow in multilayered aquifer systems. The same approach is also implemented in the TTim code (Bakker, 2022) that uses the algorithm of de Hoog et al. (1982) for the numerical inversion (Bakker, 2013a, 2013b). The method has already been discussed briefly in section 2.5.12 of Chapter 2.

First, the Laplace transform of drawdown s is defined:

$$\mathcal{L}\{s_i(r, t)\}(p) = \bar{s}_i(r, p) \quad (9)$$

Rewriting system of equations (4) in matrix form and applying the Laplace transform gives:

$$\nabla^2 \bar{\mathbf{s}} = \mathbf{A} \bar{\mathbf{s}} \quad (10)$$

The i -th entry of vector $\bar{\mathbf{s}}$ is:

$$\bar{s}_i = \bar{s}_i(r, p) \quad (1 \leq i \leq n_l) \quad (11)$$

Matrix \mathbf{A} is an $n_l \times n_l$ tridiagonal matrix with nonzero entries calculated as:

$$\mathbf{A}_{ij} = \begin{cases} \frac{1}{c_{i-1}T_i} + \frac{1}{c_iT_i} + \frac{S_i}{T_i}p & (i = j) \\ -\frac{1}{c_{i-1}T_i} & (i = j + 1) \\ -\frac{1}{c_iT_i} & (i = j - 1) \end{cases} \quad (12)$$

The associated boundary conditions at outer and inner model boundary, respectively (7) and (8), are also transformed and written in matrix form:

$$\bar{\mathbf{s}}(\infty, p) = \mathbf{0} \quad (13)$$

$$\lim_{r \rightarrow 0} \left(r \frac{\partial \bar{s}}{\partial r} \right) = \mathbf{q} \quad (14)$$

where the elements of vector \mathbf{q} in (14) are defined as:

$$\mathbf{q}_i = \frac{Q_i}{2\pi T_i p} \quad (1 \leq i \leq n_l) \quad (15)$$

By decomposing system matrix \mathbf{A} into its eigenvalues and corresponding eigenvectors, equation (10) can be written as:

$$\nabla^2 \bar{s} = \mathbf{V} \mathbf{D} \mathbf{V}^{-1} \bar{s} \quad (16)$$

where \mathbf{D} is an $n_l \times n_l$ diagonal matrix containing the n_l eigenvalues d_i , and \mathbf{V} is an $n_l \times n_l$ matrix containing the corresponding eigenvectors in its columns. Multiplying both sides of (16), (13), and (14) by \mathbf{V}^{-1} , and substituting $\mathbf{V}^{-1} \bar{s}$ by \mathbf{g} , gives an uncoupled system of modified Bessel equations and associated boundary conditions:

$$\nabla^2 \mathbf{g} = \mathbf{D} \mathbf{g} \quad (17)$$

$$\mathbf{g}(\infty, p) = 0 \quad (18)$$

$$\lim_{r \rightarrow 0} \left(r \frac{\partial \mathbf{g}}{\partial r} \right) = \mathbf{V}^{-1} \mathbf{q} \quad (19)$$

The general solution of (17) is:

$$\mathbf{g}_i(r, p) = \boldsymbol{\alpha}_i I_0(r\sqrt{d_i}) + \boldsymbol{\beta}_i K_0(r\sqrt{d_i}) \quad (20)$$

with $\boldsymbol{\alpha}$ and $\boldsymbol{\beta}$ vectors containing n_l constants that are derived from introducing the general solution into the boundary conditions. If solution (17) is introduced in inner boundary condition (19), then it is seen that $\boldsymbol{\alpha} = \mathbf{0}$ as $I_0(x) \rightarrow \infty$ if $x \rightarrow \infty$. Introducing (17) in outer boundary condition (18) gives $\boldsymbol{\beta} = -\mathbf{V}^{-1} \mathbf{q}$ as $x K_0(x) \rightarrow 1$ if $x \rightarrow 0$. Substituting $\boldsymbol{\alpha}$ and $\boldsymbol{\beta}$ into equation (20) written in matrix form, and multiplying both sides by matrix \mathbf{V} , finally gives the solution in the Laplace domain:

$$\bar{s} = -\mathbf{V} \mathbf{K} \mathbf{V}^{-1} \mathbf{q} \quad (21)$$

with \mathbf{K} an $n_l \times n_l$ diagonal matrix with nonzero entries $\mathbf{K}_{ii} = K_0(r\sqrt{d_i})$. Note that expression (21) is similar to the corresponding steady state solution (Hemker, 1984). The numerical inversion of (21) is performed by applying the Stehfest (1970) algorithm, sometimes referred to as the Gaver-Stehfest algorithm, as the calculation method originates from Gaver (1966). In this study, the number of terms used to approximate the inverted Laplace transform is 12.

4.3.2. Finite-difference approximation

The finite-difference approach presented by Lebbe (1983) and Louwyck et al. (2012) and discussed in Chapter 3, is the second method that is applied to solve the stated problem. Considering the objective of the study, the finite-difference formulation is restricted to homogeneous layers, and both radial distance r and time t are discretized using a uniformly spaced logarithmic series (Lebbe, 1983, 1988, 1999):

$$r_j = a_r r_{j-1} = a_r^{j-1} r_1 \quad (2 \leq j \leq n_r) \quad (22)$$

$$t_k = a_t t_{k-1} = a_t^{k-1} t_1 \quad (2 \leq k \leq n_t) \quad (23)$$

Expression (22) shows that the n_r distances r_j are calculated recursively using expansion factor $a_r > 1$ and starting with $r_1 > 0$. Both a_r and r_1 are defined by the user. In the same way, expression (23) generates n_t simulation times t_k using factor $a_t > 1$ and starting with $t_1 > 0$. If r and t are logarithmically transformed, then it is seen that the difference between two adjacent nodes is constant and equal to $\ln(a_r)$, and that the fixed period between two successive times is $\ln(a_t)$.

Vertical distance z [L] is discretized by means of the layer thicknesses. Let B be the cumulative thickness [L]:

$$B_i = \sum_{m=1}^i D_m \quad (1 \leq i \leq n_l) \quad (24)$$

then drawdown in layer i is simulated at the middle of the layer at distance z_i :

$$z_i = B_{i-1} + \frac{D_i}{2} \quad (1 \leq i \leq n_l) \quad (25)$$

with $B_0 = 0$. In the same way, distance r_j is at the center of coaxial ring j between $r_{j-0.5}$ and $r_{j+0.5}$, although in this case, the center is defined by the harmonic mean (Louwyck et al., 2012).

The radial flow Q_{ijk}^h [L^3/T] in layer i between the nodes at distances r_j and r_{j+1} at time t_k is given by the well-known Thiem (1870, 1906) equation:

$$Q_{ijk}^h = 2\pi T_i \frac{s_{i,j+1,k} - s_{ijk}}{\ln(r_{j+1}/r_j)} \quad (1 \leq i \leq n_l; 1 \leq j \leq n_r - 1; 1 \leq k \leq n_t) \quad (26)$$

with s_{ijk} the drawdown in layer i at distance r_j and at time t_k . From (26) and (22), it follows that the conductance Q_{ij}^{hc} [L^2/T] in layer i between the nodes at distances r_j and r_{j+1} is:

$$Q_{ij}^{hc} = \begin{cases} 0 & (j = 0 \text{ or } j = n_r) \\ 2\pi T_i / \ln(a_r) & (0 < j < n_r) \end{cases} \quad (1 \leq i \leq n_l) \quad (27)$$

Note that the conductance $Q_{i,0}^{hc}$ at the inner model boundary of layer i is set to zero, although the radial flow through this boundary is not zero but equal to the constant pumping rate Q_i according to condition (8):

$$Q_{i,0,k}^h = Q_i \quad (1 \leq i \leq n_l; 1 \leq k \leq n_t) \quad (28)$$

Since the pumping rates are known, however, they will be added as an extra sink term to the water budget equation, which will be set up below. The inner model boundary coincides with the well face and its radius is infinitesimal. Because of the singularity at $r = 0$, setting r_1 to zero is numerically not possible, and therefore, a very small value is assigned to r_1 .

At the outer model boundary, condition (7) states that drawdown is zero in all layers. Analytically, this model boundary is at an infinitely large distance; numerically, a very large value is assigned to r_{n_l} so that drawdown $s_{i,n_l,k}$ at this distance remains negligibly small in all layers i and at all times t_k . In this way, defining a constant head is not required, and it suffices to set Q_{i,n_r}^{hc} to zero for all layers i , which is easier to implement.

The vertical flow Q_{ijk}^v [L^3/T] between layers i and $i + 1$ at distance r_j and at time t_k is determined by Darcy's law:

$$Q_{ijk}^v = \pi(r_{j+0.5}^2 - r_{j-0.5}^2) \frac{s_{i+1,j,k} - s_{ijk}}{c_i} \quad (1 \leq i \leq n_l - 1; 1 \leq j \leq n_r; 1 \leq k \leq n_t) \quad (29)$$

From (29) and (22), it follows that the vertical conductance Q_{ij}^{vc} [L²/T] between layers i and $i + 1$ at distance r_j is:

$$Q_{ij}^{vc} = \begin{cases} 0 & (i = 0 \text{ or } i = n_l) \\ \pi r_1^2 a_r^{2j-3} (a_r^2 - 1)/c_i & (0 < i < n_l) \end{cases} \quad (1 \leq j \leq n_r) \quad (30)$$

Recall that $c_0 = c_{n_l} = \infty$ as the aquifer system is confined; hence, $Q_{0,j}^{vc} = Q_{n_l,j}^{vc} = 0$ for all distances r_j .

The storage change Q_{ijk}^s [L³/T] in layer i at distance r_j during time step k is:

$$Q_{ijk}^s = \pi(r_{j+0.5}^2 - r_{j-0.5}^2) S_i \frac{s_{ijk} - s_{i,j,k-1}}{t_k - t_{k-1}} \quad (1 \leq i \leq n_l; 1 \leq j \leq n_r; 1 \leq k \leq n_t) \quad (31)$$

Equation (31) expresses a backward finite-difference approximation with respect to time t . The initial condition (6) states that $s_{i,j,0} = 0$ at time $t_0 = 0$ for all layers i and all distances r_j . However, Lebbe (1983, 1988, 1999) assigns a very small value to t_0 , mostly 0.1 minute, so that $t_1 = t_0 a_t$. Similar to the known conductance terms defined for the radial and vertical flow, a constant storage change term Q_{ijk}^{sc} [L²/T] is derived from (31):

$$Q_{ijk}^{sc} = \frac{\pi r_1^2 a_r^{2j-3} (a_r^2 - 1)}{t_1 a_t^{k-2} (a_t - 1)} S_i \quad (1 \leq i \leq n_l; 1 \leq j \leq n_r; 1 \leq k \leq n_t) \quad (32)$$

Continuity of flow in layer i at distance r_j during time step k states that:

$$Q_{ijk}^h - Q_{i,j-1,k}^h + Q_{ijk}^v - Q_{i-1,j,k}^v + Q_{ijk}^s = \begin{cases} Q_i & (j = 1) \\ 0 & (2 \leq j \leq n_r) \end{cases} \quad (1 \leq i \leq n_l; 1 \leq k \leq n_t) \quad (33)$$

The first four terms in (33) express a central finite-difference approximation with respect to the radial and vertical distance. Note that a distinction is made between the first node at distance r_1 , where the specified discharge Q_i must be taken into account, and the other nodes, for which no extra sources or sinks are defined.

For each time step k , water budget equation (33) is a system of $n_l \times n_r$ equations, which can be rearranged as a matrix equation:

$$[\mathbf{F} + \mathbf{G}_k] \mathbf{s}_k = \mathbf{G}_k \mathbf{s}_{k-1} + \mathbf{q} \quad (1 \leq k \leq n_t) \quad (34)$$

where \mathbf{F} and \mathbf{G}_k are $n \times n$ matrices, and \mathbf{s}_k and \mathbf{q} are $n \times 1$ vectors, with $n = n_l \cdot n_r$. Vector \mathbf{s}_k contains the unknown drawdowns s_{ijk} which are ‘flattened’ row-wise:

$$s_{lk} = s_{ijk} \quad (1 \leq i \leq n_l; 1 \leq j \leq n_r) \quad (35)$$

with linear index $l = (i - 1)n_r + j$. Vector \mathbf{s}_{k-1} contains the known drawdowns from previous time step $k - 1$. Matrix \mathbf{F} contains the known conductance terms (27) and (30). It is symmetric, positive definite, and sparse, and its nonzero elements are located on just five diagonals:

$$\begin{cases} \mathbf{F}_{ll} = Q_{ij}^{hc} + Q_{i,j-1}^{hc} + Q_{ijk}^{vc} + Q_{i-1,j}^{vc} \\ \mathbf{F}_{l,l+1} = \mathbf{F}_{l+1,l} = -Q_{ij}^{hc} \\ \mathbf{F}_{l,l+n_r} = \mathbf{F}_{l+n_r,l} = -Q_{ijk}^{vc} \end{cases} \quad (1 \leq i \leq n_l; 1 \leq j \leq n_r) \quad (36)$$

Matrix \mathbf{G}_k is a diagonal matrix with nonzero entries equal to the known storage change terms (32):

$$\mathbf{G}_{lk} = Q_{ijk}^{sc} \quad (1 \leq i \leq n_l; 1 \leq j \leq n_r) \quad (37)$$

Vector \mathbf{q} holds the known pumping rates:

$$\mathbf{q}_{lk} = \begin{cases} Q_i & (j = 1) \\ 0 & (2 \leq j \leq n_r) \end{cases} \quad (1 \leq i \leq n_l) \quad (38)$$

The unknown drawdowns s_k at time t_k are found by solving matrix system (34) recursively starting with $k = 1$:

$$\mathbf{s}_k = [\mathbf{F} + \mathbf{G}_k]^{-1}[\mathbf{G}_k \mathbf{s}_{k-1} + \mathbf{q}] \quad (1 \leq k \leq n_t) \quad (39)$$

Recall that the initial heads are zero, i.e. $\mathbf{s}_0 = \mathbf{0}$. Calculating (39) is done using the standard solver implemented in SciPy (Peterson et al., 2022) that applies LU decomposition. As pointed out by Anderson et al. (2015), direct method solutions are desirable as they are theoretically exact. The disadvantage of requiring large amounts of computer memory is not an issue here, as the stated problem is two-dimensional. According to Harbaugh (1995), a direct solver may even execute faster than an iterative method when solving relatively small and linear problems such as (34).

Alternatively, MODFLOW may be used to solve the system of finite-difference equations by converting some of the input parameters to account for the cylindrical grid geometry (Louwyck et al., 2012, 2014). This MODFLOW procedure is explained in section 3.4 of previous Chapter 3.

4.3.3. Hybrid finite-difference finite-element method

The method proposed by Lebbe (1988, 1999) applies an identical discretization of radial distance r and time t , respectively defined by (22) and (23). However, it uses the same expansion factor a for both schemes, i.e. $a = a_r = a_t$. The main difference with the pure finite-difference formulation discussed in previous section 4.3.2 is it assumes a linear variation instead of an abrupt change of drawdown between layers, nodes, and times:

$$s(z_i, r, t_k) = s_{ijk} + \frac{s_{i,j+1,k} - s_{ijk}}{\ln(r_{j+1}/r_j)} \ln(r/r_j) \quad (1 \leq i \leq n_l; r_j \leq r \leq r_{j+1}; 1 \leq k \leq n_t) \quad (40)$$

$$s(z, r_j, t_k) = s_{ijk} + 2 \frac{s_{i+1,j,k} - s_{ijk}}{D_{i+1} + D_i} (z - z_i) \quad (z_i \leq z \leq z_{i+1}; 1 \leq j \leq n_r; 1 \leq k \leq n_t) \quad (41)$$

$$s(z_i, r_j, t) = s_{ijk} + \frac{s_{i,j,k+1} - s_{ijk}}{\ln(t_{k+1}/t_k)} \ln(t/t_k) \quad (1 \leq i \leq n_l; 1 \leq j \leq n_r; t_{k-1} \leq t \leq t_k) \quad (42)$$

Drawdown s between two nodes at distances r_j and r_{j+1} varies linearly as a function of $\ln(r)$ according to (40), between two nodes at distances z_i and z_{i+1} , it is a linear function of z expressed by (41), and between two simulation times t_k and t_{k+1} , it changes linearly as a function of $\ln(t)$ according to (42). Lebbe (1988, 1999) justifies the assumption of a semi-logarithmic change by referring to the well-known Cooper and Jacob (1946) approximation of the Theis (1935) solution. Curiously, he does not mention the Thiem (1870, 1906) equation, which expresses an exact semi-logarithmic relation between drawdown and radial distance.

Based on the assumptions expressed by (40), (41), and (42), Lebbe (1988, 1999) calculates the mean drawdown s_{ijk}^r in layer i at time t_k over the horizontal surface of ring j as:

$$s_{ijk}^r = \frac{2\pi \int_{r_{j-0.5}}^{r_j} s(z_i, r, t_k) rdr + 2\pi \int_{r_j}^{r_{j+0.5}} s(z_i, r, t_k) rdr}{\pi(r_{j+0.5}^2 - r_{j-0.5}^2)} \quad (43)$$

Solving the definite integrals in (43) using (22), and simplifying the result, Lebbe (1988, 1999) obtains the following expression:

$$s_{ijk}^r = c_1^r s_{i,j-1,k} + c_2^r s_{ijk} + c_3^r s_{i,j+1,k} \quad (44)$$

with radial interpolation constants:

$$\begin{cases} c_1^r = \frac{a - \ln(a) - 1}{2\ln(a)(a^2 - 1)} \\ c_3^r = \frac{a + a^2\ln(a) - a^2}{2\ln(a)(a^2 - 1)} \\ c_2^r = 1 - c_1^r - c_3^r \end{cases} \quad (45)$$

In the same way, Lebbe (1988, 1999) calculates the mean drawdown s_{ijk}^z in layer i at time t_k over the cylindrical surface with radius r_j as:

$$s_{ijk}^z = \frac{2\pi r_j \int_{B_{i-1}}^{Z_i} s(z, r_j, t_k) dz + 2\pi r_j \int_{Z_i}^{B_i} s(z, r_j, t_k) dz}{2\pi r_j D_i} \quad (46)$$

Solving (46) using (22), Lebbe (1988, 1999) finds:

$$s_{ijk}^z = c_1^z s_{i-1,j,k} + c_2^z s_{ijk} + c_3^z s_{i+1,j,k} \quad (47)$$

with vertical interpolation constants:

$$\begin{cases} c_{i,1}^z = \frac{D_i f_{i-1}}{4(D_{i-1} + D_i)} \\ c_{i,3}^z = \frac{D_i f_i}{4(D_i + D_{i+1})} \\ c_{i,2}^z = 1 - c_{i,1}^z - c_{i,3}^z \end{cases} \quad (48)$$

Additionally, Lebbe (1988, 1999) defines correction factor f_i to prevent “the numerical Noordbergum effect”:

$$f_i = \frac{1}{10} \left[\left(1 - \left| \frac{K_i^h - K_{i+1}^h}{K_i^h + K_{i+1}^h} \right| \right) \left(1 - \left| \frac{K_i^h - K_i^v}{K_i^h + K_i^v} \right| \right) \left(1 - \left| \frac{K_{i+1}^h - K_i^v}{K_{i+1}^h + K_i^v} \right| \right) \left(1 - \left| \frac{S_i^s - S_{i+1}^s}{S_i^s + S_{i+1}^s} \right| \right) \right]^{1/4} \quad (49)$$

By introducing correction factors defined by (49), the influence of the drawdown in the adjacent layers $i - 1$ and $i + 1$ is attenuated as constants $c_{i,1}^z$ and $c_{i,3}^z$ approximate zero when there is a high contrast in hydraulic parameters between layer i and its neighboring layers. Unfortunately, the derivation of (49) is not further substantiated by Lebbe (1988, 1999).

The mean drawdown over the entire volume of ring j in layer i at time t_k is found by combining (44) and (47):

$$s_{ijk}^{rz} = c_1^r s_{i,j-1,k}^z + c_2^r s_{ijk}^z + c_3^r s_{i,j+1,k}^z \quad (50)$$

Finally, Lebbe (1988, 1999) also defines the mean drawdown for time step k :

$$s_{ijk}^t = \frac{\int_{t_{k-1}}^{t_k} s(z_i, r_j, t) dt}{t_k - t_{k-1}} \quad (51)$$

Solving (51) using (23) gives:

$$s_{ijk}^t = c_1^t s_{i,j,k-1} + c_2^t s_{ijk} \quad (52)$$

with temporal interpolation constants:

$$\begin{cases} c_2^t = \frac{a \ln(a) - a + 1}{\ln(a)(a - 1)} \\ c_1^t = 1 - c_2^t \end{cases} \quad (53)$$

Lebbe (1988, 1999) uses the mean drawdowns s^z over the cylindrical surface to calculate the radial flow, and the mean drawdowns s^r over the horizontal surface to calculate the vertical flow, respectively:

$$\bar{Q}_{ijk}^h = 2\pi T_i r_{j+0.5} \frac{s_{i,j+1,k}^z - s_{ijk}^z}{r_{j+1} - r_j} \quad (1 \leq i \leq n_l; 1 \leq j \leq n_r - 1; 1 \leq k \leq n_t) \quad (54)$$

$$\bar{Q}_{ijk}^v = Q_{ij}^{vc} (s_{i+1,j,k}^r - s_{ijk}^r) \quad (1 \leq i \leq n_l - 1; 1 \leq j \leq n_r; 1 \leq k \leq n_t) \quad (55)$$

Remarkably, Lebbe (1988, 1999) does not apply the Thiem formula to calculate the radial flow between two nodes. However, equation (54) approximates the Thiem formula if expansion factor a is close to 1. Indeed, $r_{j+0.5}/(r_{j+1} - r_j) = \sqrt{a} - 1/\sqrt{a}$, and using the Taylor series expansion for a^x , it can be shown easily that $\sqrt{a} - 1/\sqrt{a} \rightarrow \ln(a)$ if $a \rightarrow 1$. Therefore, to be consistent with the finite-difference approach discussed in previous section 4.3.2, equation (54) may be replaced by the exact expression based on the Thiem equation:

$$\bar{Q}_{ijk}^h = Q_{ij}^{hc} (s_{i,j+1,k}^z - s_{ijk}^z) \quad (1 \leq i \leq n_l; 1 \leq j \leq n_r - 1; 1 \leq k \leq n_t) \quad (56)$$

To calculate the storage change in ring j during time step k , Lebbe (1988, 1999) uses the mean drawdown s^{rz} over the entire ring volume:

$$\bar{Q}_{ijk}^s = Q_{ijk}^{sc} (s_{ijk}^{rz} - s_{i,j,k-1}^{rz}) \quad (1 \leq i \leq n_l; 1 \leq j \leq n_r; 1 \leq k \leq n_t) \quad (57)$$

The net in- and outflow ΔQ_{ijk} [L^3/T] for ring j in layer i during time step k is:

$$\Delta Q_{ijk} = \bar{Q}_{ijk}^h - \bar{Q}_{i,j-1,k}^h + \bar{Q}_{ijk}^v - \bar{Q}_{i-1,j,k}^v \quad (1 \leq i \leq n_l; 1 \leq j \leq n_r; 1 \leq k \leq n_t) \quad (58)$$

To set up the water budget equation, the temporal interpolation is applied (Lebbe, 1988, 1999):

$$c_1^t \Delta Q_{i,j,k-1} + c_2^t \Delta Q_{ijk} + \bar{Q}_{ijk}^s = \begin{cases} -Q_i & (j = 1) \\ 0 & (2 \leq j \leq n_r) \end{cases} \quad (1 \leq i \leq n_l; 1 \leq k \leq n_t) \quad (59)$$

Equation (59) expresses a system of n equations for each time step k , which can be rearranged into the following matrix equation:

$$[\bar{\mathbf{G}}_k + c_2^t \bar{\mathbf{F}}] \mathbf{s}_k = [\bar{\mathbf{G}}_k - c_1^t \bar{\mathbf{F}}] \mathbf{s}_{k-1} + \mathbf{q} \quad (1 \leq k \leq n_t) \quad (60)$$

Matrix equation (60) is similar to the finite-difference equation (34). In the same manner, $\bar{\mathbf{F}}$ contains the known conductances, and $\bar{\mathbf{G}}_k$ the known storage change terms. However, because of the radial and vertical interpolations, both matrices have nine nonzero diagonals in this approach. Using linear index $l = (i - 1)n_r + j$, the nonzero entries in $\bar{\mathbf{F}}$ are:

$$\begin{cases} \bar{\mathbf{F}}_{ll} = [c_{i,2}^z(Q_{ij}^{hc} + Q_{i,j-1}^{hc}) + c_2^r(Q_{ij}^{vc} + Q_{i-1,j}^{vc})] \\ \bar{\mathbf{F}}_{l,l-1} = [c_1^r(Q_{ij}^{vc} + Q_{i-1,j}^{vc}) - c_{i,2}^zQ_{i,j-1}^{hc}] \\ \bar{\mathbf{F}}_{l,l+1} = [c_3^r(Q_{ij}^{vc} + Q_{i-1,j}^{vc}) - c_{i,2}^zQ_{ij}^{hc}] \\ \bar{\mathbf{F}}_{l,l-n_r} = [c_{i,1}^z(Q_{ij}^{hc} + Q_{i-1,j}^{hc}) - c_2^rQ_{i-1,j}^{vc}] \\ \bar{\mathbf{F}}_{l,l+n_r} = [c_{i,3}^z(Q_{ij}^{hc} + Q_{i-1,j}^{hc}) - c_2^rQ_{ij}^{vc}] \\ \bar{\mathbf{F}}_{l,l-n_r-1} = -[c_{i,1}^zQ_{i-1,j}^{hc} + c_1^rQ_{i-1,j}^{vc}] \\ \bar{\mathbf{F}}_{l,l-n_r+1} = -[c_{i,1}^zQ_{ij}^{hc} + c_3^rQ_{i-1,j}^{vc}] \\ \bar{\mathbf{F}}_{l,l+n_r-1} = -[c_{i,3}^zQ_{i-1,j}^{hc} + c_1^rQ_{ij}^{vc}] \\ \bar{\mathbf{F}}_{l,l+n_r+1} = -[c_{i,3}^zQ_{ij}^{hc} + c_3^rQ_{ij}^{vc}] \end{cases} \quad (1 \leq i \leq n_l; 1 \leq j \leq n_r) \quad (61)$$

The nonzero entries in $\bar{\mathbf{G}}_k$ are:

$$\begin{cases} \bar{\mathbf{G}}_{llk} = c_{i,2}^z c_2^r Q_{ijk}^{sc} \\ \bar{\mathbf{G}}_{l,l-1,k} = c_{i,2}^z c_1^r Q_{ijk}^{sc} \\ \bar{\mathbf{G}}_{l,l+1,k} = c_{i,2}^z c_3^r Q_{ijk}^{sc} \\ \bar{\mathbf{G}}_{l,l-n_r,k} = c_{i,1}^z c_2^r Q_{ijk}^{sc} \\ \bar{\mathbf{G}}_{l,l+n_r,k} = c_{i,3}^z c_2^r Q_{ijk}^{sc} \\ \bar{\mathbf{G}}_{l,l-n_r-1,k} = c_{i,1}^z c_1^r Q_{ijk}^{sc} \\ \bar{\mathbf{G}}_{l,l-n_r+1,k} = c_{i,1}^z c_3^r Q_{ijk}^{sc} \\ \bar{\mathbf{G}}_{l,l+n_r-1,k} = c_{i,3}^z c_1^r Q_{ijk}^{sc} \\ \bar{\mathbf{G}}_{l,l+n_r+1,k} = c_{i,3}^z c_3^r Q_{ijk}^{sc} \end{cases} \quad (1 \leq i \leq n_l; 1 \leq j \leq n_r) \quad (62)$$

Note that matrix system (60) simplifies to system (34) if no interpolation is performed, or if $c_1^r = c_3^r = 0$, $c_{i,1}^z = c_{i,3}^z = 0$ for all i , and $c_1^t = 0$. This relation between the two solutions is used to compare both methods and their respective implementations. The interpolations may also be switched on and off separately to investigate their individual effect.

Once the matrices are constructed, matrix system (60) can be solved recursively starting with $k = 1$:

$$\mathbf{s}_k = [\bar{\mathbf{G}}_k + c_2^t \bar{\mathbf{F}}]^{-1} \{[\bar{\mathbf{G}}_k - c_1^t \bar{\mathbf{F}}] \mathbf{s}_{k-1} + \mathbf{q}\} \quad (1 \leq k \leq n_t) \quad (63)$$

Lebbe (1988, 1999) applies the Alternating Direction Implicit (ADI) method (Douglas & Rachford, 1956; Peaceman & Rachford, 1955). In initial versions of AS2D, the iterative process was terminated when the total water balance was smaller than a certain percentage of the total pumping rate, while later implementations use an empirical formula based on “a certain experience” to determine the number of ADI iteration for each time step k : $[(1440t_k + 5)/5]$ (Lebbe, 1983, 1988, 1999).

In our experience, the required number of iterations to reach convergence indeed increases with the time step, which is also confirmed by Wang and Anderson (1982). However, the rate of convergence also depends on other factors, such as the initial conditions and the number of grid cells, and according to Mehl and Hill (2001), the rate of convergence for traditional iterative solvers increases nonlinearly with the size of the domain. Stability and rate of convergence for ADI and other iterative solvers is analyzed mathematically by Varga (2000), whereas Anderson et al. (2015) discuss convergence issues from a practical point of view. To avoid all kind of convergence problems, however, the direct solver implemented in SciPy (Peterson et al., 2022) is used here, in the same way as it is used to solve finite-difference matrix system (34).

4.4. Numerical experiments

In this section, four numerical experiments are carried out. Before conducting a more systematic analysis of the effect of the interpolations applied by the hybrid solution method developed by Lebbe (1988, 1999), the synthetic problem discussed by Lebbe (1988, 1999) and Lebbe and De Breuck (1995) is simulated first. This is an interesting example as it was used to demonstrate and verify the inverse model. Numerical instabilities occur at small values of time, and in the next case, the Theis (1935) model, it will be shown that these are caused by the temporal interpolation, which results into a finite-difference approximation that is similar to the Crank-Nicolson method (Crank & Nicolson, 1947, 1996). In the third example, the influence of the vertical interpolation will be further investigated by comparing results of a homogeneous and a heterogeneous three-layer model. In the last case, thousand random multilayer models are simulated to get a more global view on the accuracy of the finite-difference and the hybrid numerical method.

4.4.1. Synthetic pumping test

Consider a groundwater reservoir consisting of three layers that is bounded below by an aquiclude and on top by the water table. Each layer is homogeneous and has a thickness of 10 m. The lower and upper layers are isotropic aquifers with conductivity equal to 10 m/d and specific elastic storage equal to $8 \times 10^{-5} \text{ m}^{-1}$ and $4 \times 10^{-4} \text{ m}^{-1}$, respectively. The specific yield is 0.2. The separating aquitard is anisotropic and has a horizontal conductivity of 0.5 m/d and a vertical conductivity of 0.1 m/d; its specific elastic storage is $4 \times 10^{-5} \text{ m}^{-1}$. A pumping well with a fully penetrating screen in the lower aquifer extracts water from the system at a constant rate of $180 \text{ m}^3/\text{d}$. Drawdown is observed in the pumping well and in three observation wells at a distance of 5.01 m, 15.85 m, and 50.12 m from the pumping well, respectively. Each observation well has a separate screen in the middle of the pumped aquifer and in the middle of the aquitard. Drawdown is measured during a period ranging between 1 minute and 1585 minutes after the start of the test. Observation times are spaced evenly on a logarithmic scale.

The observations are simulated using the semi-analytical solution method discussed in section 4.3.1, where drawdowns smaller than 0.5 cm are omitted. These simulated drawdowns are the reference data. The pumping test data are also simulated using the finite-difference approach discussed in section 4.3.2 and the hybrid finite-difference finite-element method discussed in section 4.3.3. In both numerical models, the vertical discretization defined by Lebbe (1988, 1999) and Lebbe and De Breuck (1995) is adopted: the aquitard is divided up in three sublayers of equal thickness, and the upper aquifer in two model layers of 9 m and 1 m thickness, respectively. The top layer of 1 m represents the water table, and therefore, its storage coefficient equals the specific yield. Neither Lebbe (1988, 1999) nor Lebbe and De Breuck (1995) discuss the radial and temporal discretization. However, Lebbe (1988, 1999) sets r_1 to 0.1 in most examples, suggests an expansion factor α equal to $10^{0.1}$, and recommends an initial time that is 10 times smaller than the first observation time, which means t_0 equals 0.1 minute in this example. The number of rings n_r is 70; the number of time steps n_t is 45.

Figure 1 shows the result of the simulations. Observations calculated using the three methods are virtually the same, except for the drawdowns in the pumping well simulated using the hybrid numerical method developed by Lebbe (1988, 1999). The red dashed curve indeed shows oscillations that are large for small values of time and dampen with time. Therefore, the initial time is set 100 times smaller, i.e. $t_0 = 10^{-3}$ minutes, and 65 time steps are simulated. The black dashed curve on the plot in Figure 1 shows that the oscillations disappear by defining a much smaller initial time than

recommended by Lebbe (1988, 1999). It is noticeable that neither Lebbe (1988, 1999) nor Lebbe and De Breuck (1995) include the drawdowns simulated in the pumping well to interpret the test.

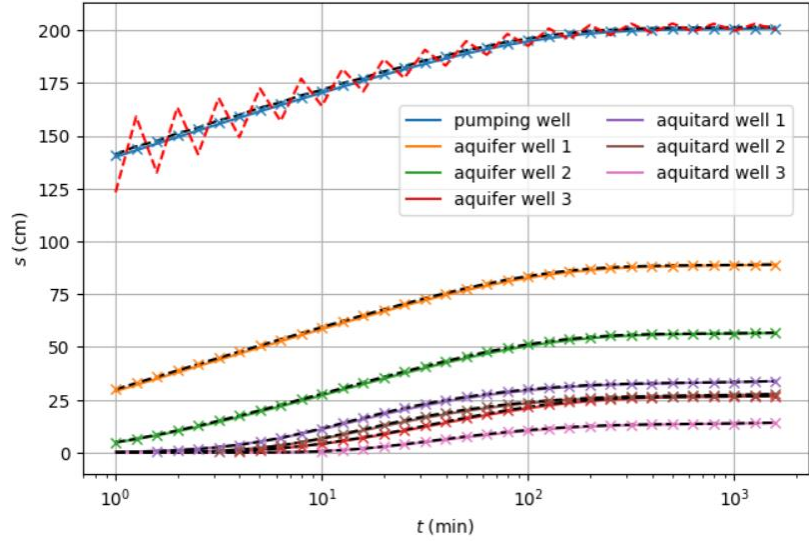


Figure 1. Drawdown versus time for the synthetic pumping test conducted in a two-aquifer system with observation wells in the pumped aquifer and in the separating aquitard. Crosses are calculated using the semi-analytical approach (Hemker, 1985b, 1999b), colored lines are simulated using the finite-difference method (Lebbe, 1983; Louwyck et al., 2012), and black dashed lines are simulated using the hybrid finite-difference finite-element method (Lebbe, 1998, 1999). The red dashed line is also simulated using the latter method, but in this simulation, the initial time is 0.1 instead of 0.001 minute. See text for a detailed description of the test and the models.

Although the simulated data virtually coincide on the time-drawdown graph, they are not exactly the same. The difference between the drawdowns s_{ref} calculated using the semi-analytical approach and the drawdowns s_{num} simulated using the numerical methods can be summarized using the root-mean-square error (RMSE):

$$\text{RMSE} = \sqrt{\frac{1}{N} \sum_{i=1}^N (s_{i,ref} - s_{i,num})^2} \quad (64)$$

with N the total number of data observed in all wells. The RMSE for the finite-difference method is 0.52 cm, and for the hybrid finite-difference finite-element method, it is 0.28 cm. The simulation that suffers from oscillations has a RMSE of 3.07 cm. In this example, it seems the hybrid method is more accurate, if there are no numerical instabilities. However, if the expansion factor α is set to $10^{0.01}$ and the number of rings and the number of time steps are multiplied by 10 accordingly, then the RMSE for the finite-difference simulation is 0.049 cm, whereas the hybrid method does not result in a significantly improved accuracy, as it has a RMSE of 0.27 cm. The model applying the hybrid method and defining $t_0 = 0.1$ minute is numerically more stable if $\alpha = 10^{0.01}$, and it has a RMSE of 0.46 cm.

As expected, the discretization error for the finite-difference approximation is smaller if the grid has a higher resolution. Remarkably, this is not the case for the hybrid finite-difference finite-element method. Unfortunately, using an expansion factor α equal to $10^{0.01}$ is computationally expensive, and therefore, $\alpha = 10^{0.1}$ will be used in the next cases, as suggested by Lebbe (1988, 1999). Moreover, analyzing the influence of the grid resolution is out of scope. The objective is to study the effect of the linear interpolations applied by the hybrid finite-difference finite-element method. In that sense, it is worth mentioning the values of the different interpolation constants. If $\alpha = 10^{0.1}$,

then the radial interpolation constants are $c_1^r = 0.11$, $c_2^r = 0.75$, and $c_3^r = 0.14$, and the temporal interpolation constants are $c_1^t = 0.48$ and $c_2^t = 0.52$. Because of the correction factors defined by (49), c_2^z is always higher than 0.98, which means the vertical interpolation is almost completely undone by this correction. In the next example, it will be shown that the time interpolation is similar to the Crank-Nicolson formulation.

4.4.2. The Theis model

The well-known one-aquifer solution developed by Theis (1935) is an interesting test case, as it is restricted to transient radial flow without vertical component. The aquifer is homogeneous and has constant transmissivity T and storativity S . There is no leakage; hence, partial differential equation (4) simplifies to:

$$\frac{\partial^2 s}{\partial r^2} + \frac{1}{r} \frac{\partial s}{\partial r} = \frac{S}{T} \frac{\partial s}{\partial t} \quad (65)$$

As there is one layer only, subscript $i = 1$ is omitted. Initial condition (6) and boundary conditions (7) and (8) are adopted with $n_l = 1$. Recall that the aquifer has an infinite extent, and drawdown is zero at the outer boundary at all times t :

$$s(\infty, t) = 0 \quad (66)$$

The well has an infinitesimal radius and a fully penetrating screen, and it extracts water from the aquifer at constant rate Q :

$$\lim_{r \rightarrow 0} \left(r \frac{\partial s(r, t)}{\partial r} \right) = \frac{Q}{2\pi T} \quad (67)$$

Drawdown before the pumping starts is zero at all distances r :

$$s(r, 0) = 0 \quad (68)$$

Applying the semi-analytical solution method discussed in section 4.3.1, it is seen the only eigenvalue equals the single entry in \mathbf{A} , i.e. $d = \frac{S}{T} p$, and the corresponding eigenvector equals 1; hence, solution (21) simplifies to:

$$\bar{s}(r, p) = \frac{-Q}{2\pi T p} K_0 \left(r \sqrt{\frac{S}{T} p} \right) \quad (69)$$

Equation (69) gives the solution in the Laplace domain, which can be inverted analytically to the real time domain (Hantush, 1964; Loaiciga, 2010):

$$s(r, t) = \frac{-Q}{4\pi T} W \left(\frac{r^2 S}{4tT} \right) = \frac{Q}{4\pi T} \left[\gamma + \ln \left(\frac{r^2 S}{4tT} \right) + \sum_{n=1}^{\infty} \frac{1}{n \cdot n!} \left(-\frac{r^2 S}{4tT} \right)^n \right] \quad (70)$$

with γ the Euler-Mascheroni constant equal to 0.57721..., and W the exponential integral, which is called the Theis well function in the hydrogeological literature. If the semi-analytical approach is used, then (69) is inverted numerically using the Stehfest (1970) algorithm. This solution has already been discussed in more detail in section 2.5.7 of Chapter 2.

The finite-difference approximation of (65) applying the approach explained in section 4.3.2 is:

$$2\pi T \frac{s_{j+1,k} - s_{jk}}{\ln(r_{j+1}/r_j)} - 2\pi T \frac{2s_{jk} - s_{j-1,k}}{\ln(r_j/r_{j-1})} = \pi (r_{j+0.5}^2 - r_{j-0.5}^2) S \frac{s_{jk} - s_{j,k-1}}{t_k - t_{k-1}} \quad (71)$$

Using (22) and (23), expression (71) may be rewritten as a function of expansion factor a :

$$\frac{s_{j+1,k} - 2s_{jk} + s_{j-1,k}}{(\ln a)^2} = \frac{S}{T} \frac{r_j^2}{t_{k-0.5}} \frac{s_{jk} - s_{j,k-1}}{\ln a} \quad (72)$$

where use is made of:

$$\lim_{a \rightarrow 1^+} \frac{(r_{j+0.5}^2 - r_{j-0.5}^2)}{2} = \lim_{a \rightarrow 1^+} r_j^2 \frac{(a-1)(a+1)}{2\sqrt{a}} \cong \lim_{a \rightarrow 1^+} r_j^2 \ln a \quad (73)$$

Finite-difference formulation (72) indeed corresponds to partial differential equation (65), which can be rearranged to:

$$\frac{\partial^2 s}{\partial (\ln r)^2} = \frac{S}{T} \frac{r^2}{t} \frac{\partial s}{\partial \ln t} \quad (74)$$

The left-hand side of (72) clearly shows this is a second-order central difference for the space derivative at position r_j . Concerning the time, finite-difference approximation (72) can be generalized using the θ -method (Hellevik, 2020; Li et al., 2017):

$$\theta \frac{s_{j+1,k-1} - 2s_{jk} + s_{j-1,k-1}}{(\ln a)^2} + (1-\theta) \frac{s_{j+1,k} - 2s_{jk} + s_{j-1,k}}{(\ln a)^2} = \frac{S}{T} \frac{r_j^2}{t_{k-0.5}} \frac{s_{jk} - s_{j,k-1}}{\ln a} \quad (75)$$

If $\theta = 0$, equation (75) simplifies to (72), which is a backward finite-difference approximation with respect to time t , also called the backward Euler method; if $\theta = 1$, a forward difference is used, also called the explicit Euler method (Li et al., 2017). If $\theta = 0.5$, then it is a central difference at time $t_{k-0.5}$, also known as the Crank-Nicolson method (Crank & Nicolson, 1947, 1996). If $0 \leq \theta \leq 0.5$, then the method is unconditionally stable; if $\theta > 0.5$, then it is conditionally stable (Hellevik, 2020; Li et al., 2017). The forward difference approximation leads to an explicit scheme, the backward Euler and the Crank-Nicolson methods are implicit methods. The local truncation error is always quadratic over the space step, i.e. $O(\Delta^2)$ with $\Delta = \ln a$. In case of the backward and explicit Euler method, the error is linear over the time step, i.e. $O(\Delta)$, whereas it is quadratic or $O(\Delta^2)$ if the Crank-Nicolson method is used (Hellevik, 2020; Li et al., 2017). Backward, central, and forward finite-difference approximations with respect to the time, applied to solve differential equations that describe groundwater flow, are also discussed by Wang and Anderson (1982), who show that the Crank-Nicolson method may have a faster convergence rate.

If the hybrid numerical approach developed by Lebbe (1988, 1999) is applied to solve the problem of one-dimensional transient radial flow numerically, the following approximation of differential equation (65) is obtained:

$$c_1^t \frac{s_{j+1,k-1} - 2s_{jk} + s_{j-1,k-1}}{(\ln a)^2} + c_2^t \frac{s_{j+1,k} - 2s_{jk} + s_{j-1,k}}{(\ln a)^2} = \frac{S}{T} \frac{r_j^2}{t_{k-0.5}} \frac{s_{jk}^r - s_{j,k-1}^r}{\ln a} \quad (76)$$

with $s_{jk}^r = c_1^r s_{j-1,k} + c_2^r s_{jk} + c_3^r s_{j+1,k}$ according to (44). Comparing the left-hand side of expressions (75) and (76), it is clear that $\theta = c_1^t$. Recall that $c_1^t = 0.48$ and $c_2^t = 0.52$ if $a = 10^{0.1}$, which means the temporal interpolation applied by Lebbe (1988, 1999) approximately leads to a central finite-difference approximation with respect to time t . This contradicts Lebbe (1988, 1999), who states his hybrid method applies a backward finite-difference approximation with respect to the time. Since $\theta < 0.5$, the method is unconditionally stable. However, it is very close to the Crank-Nicolson approximation, and it has already been mentioned in the introduction 4.1 that this method may suffer from spurious oscillations due to sharp initial transitions. Previous example clearly illustrated

that the temporal interpolation indeed may cause oscillations at small values of time if the initial time is too large.

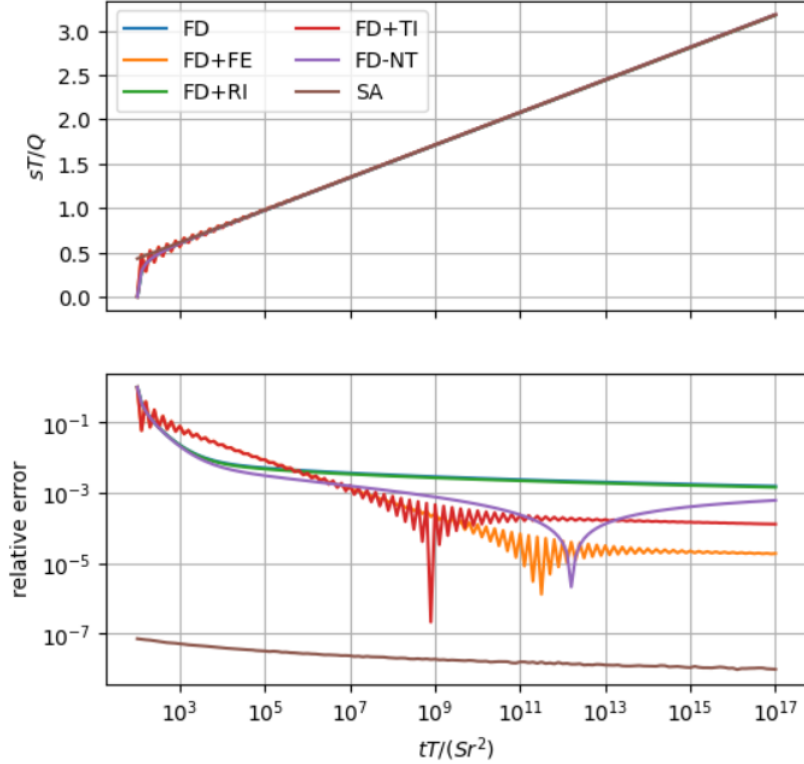


Figure 2. Upper: Dimensionless drawdown versus dimensionless time for the Theis (1935) model calculated using different methods: FD = finite-difference, FD+FE = hybrid finite-difference finite-element, FD+RI = finite-difference with radial interpolation, FD+TI = finite-difference with temporal interpolation, FD-NT = finite-difference in which radial flow is not calculated using the Thiem formula, SA = semi-analytical. Lower: corresponding relative error versus dimensionless time for the different solution methods compared with the analytical solution. See text for a more detailed explanation.

The upper plot in Figure 2 shows the dimensionless drawdown sT/Q as a function of the dimensionless time $tT/(r^2S)$ calculated using the semi-analytical approach (SA), the finite-difference method (FD), and the hybrid finite-difference finite-element method (FD+FE). To illustrate the individual effect of the interpolations in the latter method, simulations are carried out applying radial interpolation (FD+RI) and temporal interpolation (FD+TI) only. The FD-NT simulation applies the finite-difference method and uses equation (54) to calculate the radial flow between adjacent nodes instead of the Thiem formula (56). It is seen that all drawdown curves are virtually the same. For small values of time, the numerical solutions deviate from the semi-analytical solution because the initial time is not zero. The numerical solutions that apply the time interpolation (FD+FE and FD+TI) also suffer from numerical instabilities. As is the case in previous example, the oscillations vanish if a smaller value is assigned to t_0 . From this example, it is clear that these are caused by the temporal interpolation.

All solutions are compared with the analytical solution by means of the relative error (RE):

$$RE = \left| \frac{s_{ref}^* - s_{num}^*}{s_{ref}^*} \right| \quad (77)$$

where s_{ref}^* is the dimensionless drawdown sT/Q calculated using the analytical solution given by (70), and s_{num}^* is the dimensionless drawdown sT/Q simulated using one of the numerical methods or the semi-analytical approach. The lower plot in Figure 2 shows the result. As expected the semi-

analytical solution is very close to the analytical solution. For small values of time, the numerical solutions are not accurate due to the initial condition which is not defined at $t = 0$. The radial interpolation has no effect on the accuracy as the FD and the FD+RI curves coincide. Using the Thiem equation gives less accurate results, although the relative error slowly decreases for the FD method, while the error for the FD-NT method increases at large values of time. The time interpolation has a positive effect on the accuracy as both FD+FE and FD+TI have smaller errors. This is in accordance with the theoretical statement the Crank-Nicolson method is more accurate than the backward Euler method.

4.4.3. Three-layer system

In this experiment, an aquifer system consisting of three layers is analyzed to check the effect of the vertical interpolation proposed by Lebbe (1988, 1999).

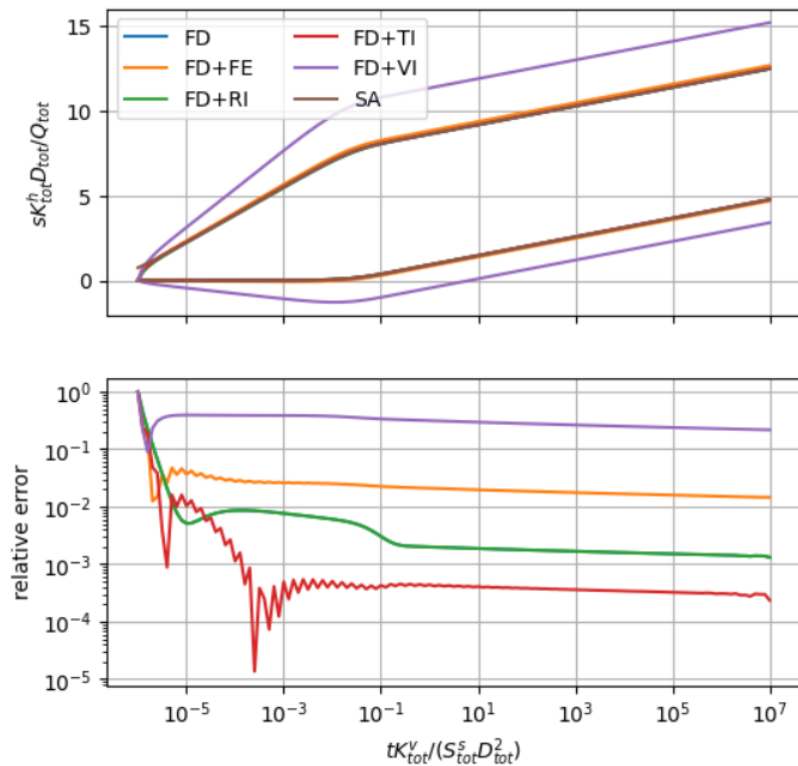


Figure 3. Upper: dimensionless drawdown versus dimensionless time at dimensionless distance 0.001 for the homogeneous three-layer system calculated using different methods: FD = finite-difference, FD+FE = hybrid finite-difference finite-element, FD+RI = finite-difference with radial interpolation, FD+TI = finite-difference with temporal interpolation, FD+VI = finite-difference with vertical interpolation, SA = semi-analytical. Lower: corresponding relative error of the dimensionless drawdowns in the pumped layer compared with the semi-analytical solution. See text for a more detailed explanation. Note that all curves virtually coincide in the upper plot, except the purple curve, which corresponds to the FD+VI simulation. In the lower plot, the green and blue curve coincide, which implies the relative error for the FD and the FD+RI simulations are virtually the same.

The layers have the same thickness, and water is extracted from the middle layer only. The following set of dimensionless parameters are defined:

$$\begin{cases} s_i^* = s_i K_{tot}^h D_{tot} / Q_{tot} \\ r^* = r / (K_{tot}^h D_{tot}^2 / K_{tot}^v)^{1/2} \\ t^* = t K_{tot}^v / (S_{tot}^s D_{tot}^2) \\ D_i^* = D_i / D_{tot} \\ K_i^{h*} = K_i^h / K_{tot}^h \\ K_i^{v*} = K_i^v / K_{tot}^v \\ S_i^{s*} = S_i^s / S_{tot}^s \\ Q_i^* = Q_i / Q_{tot} \end{cases} \quad (78)$$

The dimensionless parameters have an asterisk as superscript; subscript ‘tot’ refers to the sum of all parameters defined for each layer i .

Two scenarios are simulated: in the first, all layers have the same parameter values; in the second, the pumped layer has larger parameter values than those of the surrounding layers: the horizontal conductivity is 100 times larger, the vertical conductivity is 1000 times larger, and the specific elastic storage is 10 times larger. Because the upper and lower layers have the same parameter values in both scenarios, drawdown at a given distance and time is always the same in both layers.

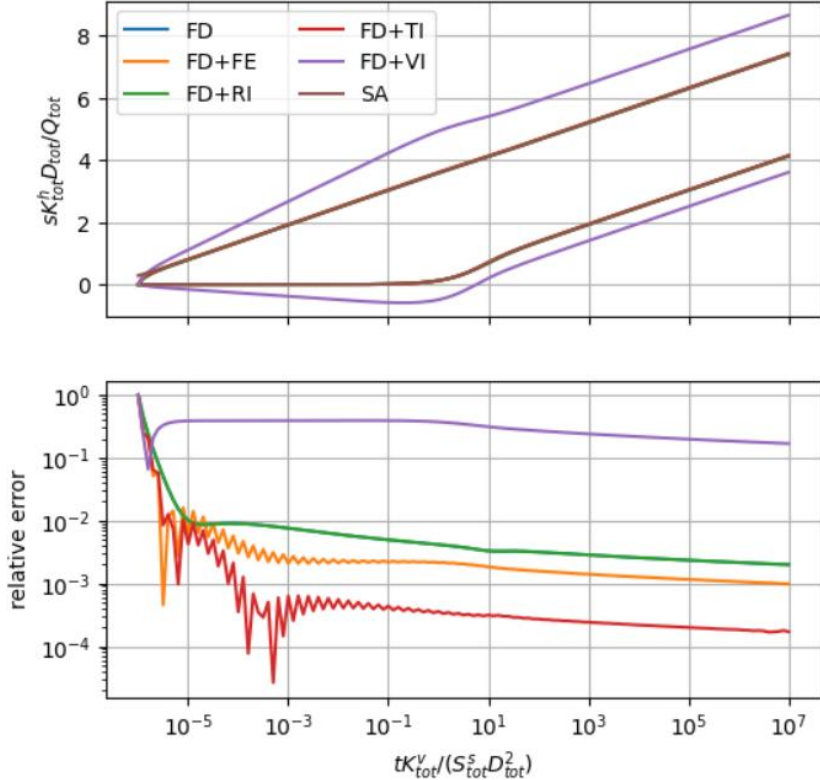


Figure 4. Upper: dimensionless drawdown versus dimensionless time at dimensionless distance 0.001 for the heterogeneous three-layer system calculated using different methods: FD = finite-difference, FD+FE = hybrid finite-difference finite-element, FD+RI = finite-difference with radial interpolation, FD+TI = finite-difference with temporal interpolation, FD+VI = finite-difference with vertical interpolation, SA = semi-analytical. Lower: corresponding relative error of the dimensionless drawdowns in the pumped layer compared with the semi-analytical solution. See text for a more detailed explanation. Note that all curves virtually coincide in the upper plot, except the purple curve, which corresponds to the FD+VI simulation. In the lower plot, the green and blue curve coincide, which implies the relative error for the FD and the FD+RI simulations are virtually the same.

The upper plot in Figure 3 shows the dimensionless drawdown s^* as a function of the dimensionless time t^* at dimensionless distance $r^* = 0.001$ for the homogeneous system, calculated using the semi-analytical approach (SA), the finite-difference method (FD), and the hybrid finite-difference

finite-element method (FD+FE). The individual effect of the interpolations in the latter method is demonstrated by simulations that apply radial interpolation only (FD+RI), temporal interpolation only (FD+TI), and vertical interpolation only without correction (FD+VI). The lower plot in Figure 3 visualizes the corresponding relative error defined by (77), where the semi-analytical solution (SA) is used as reference s_{ref}^* .

It is clear the vertical interpolation without correction does not give accurate results at all. In the layers that are not extracted, there is even a head rise, which Lebbe (1988) calls a “numerical Noordbergum effect”. The hybrid numerical method FD+FE is not very accurate either as relative errors are not below 1%. The radial interpolation has no significant effect as the FD+RI solution coincides with the FD solution. On the other hand, the time interpolation has a significant positive effect as the FD+TI result is the most accurate simulation.

Figure 4 shows the results for the heterogeneous aquifer system, from which the same conclusions are drawn. The vertical interpolation without correction gives inaccurate results, the radial interpolation has no significant effect as FD and FD+RI results are virtually the same, and the time interpolation has a significant positive effect on the accuracy. The only difference is that the hybrid method FD+FE is more accurate in this scenario, which is probably because the vertical interpolation is attenuated more than in the homogeneous case. The correction factor defined by (49) is smaller indeed if the parameter values are more dissimilar. In this example, c_2^t for the middle layer is in both scenarios equal to 0.75 without correction. If the correction is applied, then it is 0.975 for the homogeneous system, and 0.998 for the heterogeneous system. This means the vertical interpolation is almost completely removed from the FD+FE simulation in the second scenario, which clearly leads to more accurate calculations.

4.4.4. Random simulations

In the final test case, random simulations are carried out, and both the finite-difference (FD) and the hybrid finite-difference finite-element method (FD+FE) are compared with the semi-analytical approach. Because previous examples showed that applying a linear interpolation in time could also be beneficial, the finite-difference method only applying a temporal interpolation (FD+TI) is also included in the analysis.

Thousands of models in total are automatically constructed by means of randomly sampled input parameters. The number of layers is randomly chosen between 2 and 10, i.e. $2 \leq n_l \leq 10$, and the thickness of each layer is a random number between 0 and 50, i.e. $0 < D_i < 50$. The hydraulic parameters are sampled from a lognormal distribution:

$$\begin{cases} K_i^h = 10^{1.5Z} + 10^{-5} \\ K_i^v = K_i^h \cdot 10^{-|Z|} \\ S_i^s = 10^{-|3Z|} \end{cases} \quad (79)$$

with Z a standard normal variable. To avoid numerical problems, a minimum value of 10^{-5} is assigned to the horizontal conductivity. The vertical conductivity is always smaller than or equal to the horizontal conductivity; the specific elastic storage is always smaller than or equal to 1. After sampling parameter values according to (79), the corresponding dimensionless parameters are calculated according to (78). Concerning the pumping rates, only the most transmissive layer is extracted:

$$Q_i^* = \begin{cases} 1 & \text{if } i = \arg \max_i (K_i^h D_i) \\ 0 & \text{else} \end{cases} \quad (80)$$

Figure 5 shows the minimum and maximum relative error defined by (77) as a function of dimensionless time t^* at dimensionless distance $r^* = 0.001$ for all simulations. This means that for a given dimensionless time, the minimum and maximum relative error of the thousand simulations is determined. The reference drawdowns s_{ref}^* are calculated using the semi-analytical approach. The inaccurate simulations at small values of time could be reduced by defining a smaller initial time. The large errors at large values of time will also diminish if a more appropriate discretization is used. If these errors at small and large values of time are ignored, then it is seen the FD method is accurate with maximum relative errors smaller than 1%. Looking at the minimum relative errors, then it is concluded that the FD+FE method is sometimes more accurate than the FD method, but in some cases it may also be less accurate, with maximum relative errors even larger than 1%. The same is true for the FD+TI method that only applies a temporal interpolation, although this method has smaller maximum relative errors than the FD method if $t^* > 0.5$.

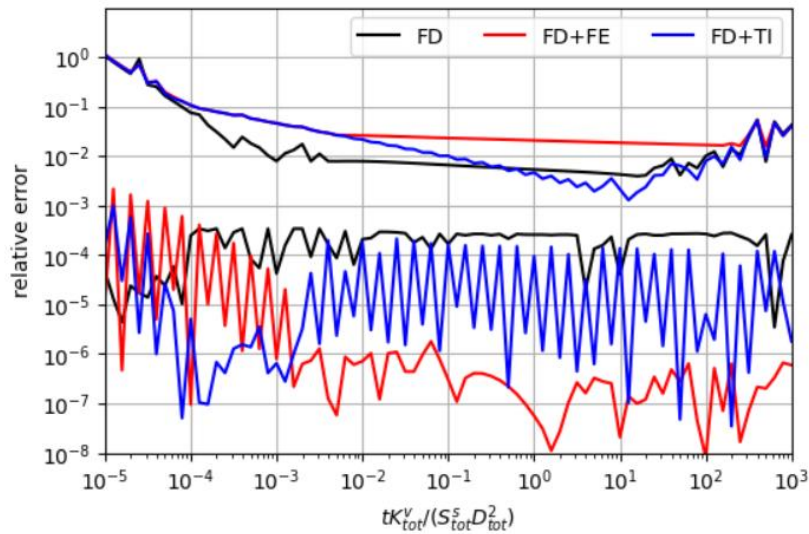


Figure 5. Minimum and maximum relative error as a function of dimensionless time at a dimensionless radial distance of 0.001 for 1000 random axisymmetric multilayer models simulated using the finite-difference method (FD), the hybrid finite-difference finite-element method (FD+FE), and the finite-difference method that applies a linear interpolation in time (FD+TI). The semi-analytical solution is used as reference to calculate the relative error. See text for a detailed explanation.

4.5. Discussion and conclusions

Lebbe (1988, 1999) proposed a finite-difference method to simulate transient axisymmetric groundwater flow in a multilayered aquifer system in which drawdowns at the grid nodes are replaced by drawdowns that are linearly interpolated and integrated over the cylindrical grid cells and over the time steps. The numerical experiments conducted in this study clearly show that these interpolations may cause numerical problems. Moreover, performing these interpolations is computationally more expensive, and there is no guarantee the calculated results are more accurate.

The vertical interpolation is even problematic as it results in unrealistic head rises instead of drawdowns. This issue has already been addressed by Lebbe (1988, 1999), who introduced empirical correction factors to bypass this unwanted effect of the vertical interpolation. In practice, this correction comes down to inactivating the vertical interpolation almost completely. Therefore, it is more convenient to remove the vertical interpolation, which is also theoretically justified by the Dupuit-Forchheimer approximation. As illustrated by Bakker (1999), multilayer Dupuit models are capable of simulating vertical flow accurately if aquifers and aquitards are divided in a sufficient number of sublayers.

The experiments carried out in this study could not indicate a significant positive effect on the accuracy due to the radial interpolation. Therefore, it is also computationally more efficient to remove this interpolation. It is shown that the temporal interpolation is similar to the Crank-Nicolson method (Crank & Nicolson, 1947, 1996), which is theoretically more accurate than the backward Euler method. However, the Crank-Nicolson method could suffer from spurious oscillations, which was confirmed by some of the numerical experiments. As these oscillations occur only at small values of time, they can be avoided by defining an appropriate time discretization. On the other hand, the backward Euler method, which is also implemented in MODFLOW, does not have these numerical instabilities, and is computationally more efficient.

A pertinent question is about the impact of the computational errors on the derived hydraulic parameters applying the inverse model by Lebbe (1988, 1999). Optimal parameter values are obtained through minimization of the sum of squared residuals, which are the differences between observed and calculated drawdowns. These residuals are a combination of measurement errors and errors arising from the mathematical model, where the latter can be subdivided in conceptual and computational errors (Carrera & Neuman, 1986). Conceptual errors are due to simplified or wrong model assumptions, whereas computational errors are caused, for instance, by the numerical discretization or the use of iterative solvers that approximate the exact solution. The reliability of the derived parameters is determined by the residuals; hence, it is influenced by these sources of error. Unfortunately, these are often difficult to isolate (Carrera & Neuman, 1986).

In this study, focus is solely on the computational errors, which are the differences between simulated and true drawdowns. In the absence of other sources of error, it is reasonable to state the magnitude of the error on the derived parameters is similar to the magnitude of the computational error, since the results of the experiments are expressed using dimensionless parameters. The maximum relative error of dimensionless drawdown for the thousand random finite-difference finite-element simulations is not larger than 5%. Assuming the measurement error on observed drawdowns and pumping rates and the conceptual errors are usually higher in the analysis of long-term pumping test data, it is concluded that the computational errors due to the interpolations in the hybrid numerical method by Lebbe (1988, 1999) did not have a significant effect on the reliability of the identified parameters.

The semi-analytical approach developed by Hemker (1985b, 1999b) does not require discretization of radial distance and time, which may be considered a great advantage over numerical solution methods. However, as it applies a numerical inversion technique (Stehfest, 1970), it is not free of computational error either. Still, it is the recommended solution method to simulate axisymmetric multilayer flow. On the other hand, numerical models offer more flexibility in defining aquifer heterogeneities and nonlinear behavior such as unconfined flow or the effect of subsurface drainage, which is discussed in subsequent chapters 5 to 8. In case of such nonlinear models, applying the Crank-Nicolson method instead of the more popular backward Euler method is worth considering, as the former is proven to be more accurate.

4.6. References

- Aime Feulefack, P., Daniel Djida, J., & Abdon, A. (2019). A new model of groundwater flow within an unconfined aquifer: Application of Caputo-Fabrizio fractional derivative. *Discrete & Continuous Dynamical Systems - B*, 24(7), 3227–3247. <https://doi.org/10.3934/dcdsb.2018317>
- Anderson, M. P., Woessner, W. W., & Hunt, R. J. (2015). *Applied Groundwater Modeling - Simulation of Flow and Advection Transport (Second Edition)* (2nd ed.). Academic Press.

- Atangana, A., & Botha, J. F. (2013). A generalized groundwater flow equation using the concept of variable-order derivative. *Boundary Value Problems*, 2013(1), 53. <https://doi.org/10.1186/1687-2770-2013-53>
- Bakker, M. (1999). Simulating groundwater flow in multi-aquifer systems with analytical and numerical Dupuit-models. *Journal of Hydrology*, 222(1–4), 55–64. [https://doi.org/10.1016/S0022-1694\(99\)00089-X](https://doi.org/10.1016/S0022-1694(99)00089-X)
- Bakker, M. (2013a). Analytic Modeling of Transient Multilayer Flow. In P. K. Mishra & K. Kuhlman (Eds.), *Advances in Hydrogeology* (pp. 95–114). Springer, Heidelberg. https://doi.org/10.1007/978-1-4614-6479-2_5
- Bakker, M. (2013b). Semi-analytic modeling of transient multi-layer flow with TTIm. *Hydrogeology Journal*, 21(4), 935–943. <https://doi.org/10.1007/s10040-013-0975-2>
- Bakker, M. (2022). *TTIm, A Multi-Layer, Transient, Analytic Element Model*. (0.6.3.). Retrieved from <https://github.com/mbakker7/ttim>
- Boulton, N. S. (1954). Unsteady radial flow to a pumped well allowing for delayed yield from storage. *General Assembly of Rome, Tome II, Groundwater, IAHS publ.* 37, 472–477.
- Boulton, N. S. (1963). Analysis of data from non-equilibrium pumping tests allowing for delayed yield from storage. *Proceedings of the Institution of Civil Engineers*, 26(3), 469–482. <https://doi.org/10.1680/iicep.1963.10409>
- Bredehoeft, J. D., & Pinder, G. F. (1970). Digital Analysis of Areal Flow in Multiaquifer Groundwater Systems: A Quasi Three-Dimensional Model. *Water Resources Research*, 6(3), 883–888. <https://doi.org/10.1029/WR006i003p00883>
- Britz, D., Østerby, O., & Strutwolf, J. (2003). Damping of Crank–Nicolson error oscillations. *Computational Biology and Chemistry*, 27(3), 253–263. [https://doi.org/10.1016/S0097-8485\(02\)00075-X](https://doi.org/10.1016/S0097-8485(02)00075-X)
- Butler, J. J. (1988). Pumping tests in nonuniform aquifers — The radially symmetric case. *Journal of Hydrology*, 101(1–4), 15–30. [https://doi.org/10.1016/0022-1694\(88\)90025-X](https://doi.org/10.1016/0022-1694(88)90025-X)
- Carrera, J., & Neuman, S. P. (1986). Estimation of Aquifer Parameters Under Transient and Steady State Conditions: 1. Maximum Likelihood Method Incorporating Prior Information. *Water Resources Research*, 22(2), 199–210. <https://doi.org/10.1029/WR022i002p00199>
- Cooley, R. L. (1971). A Finite Difference Method for Unsteady Flow in Variably Saturated Porous Media: Application to a Single Pumping Well. *Water Resources Research*, 7(6), 1607–1625. <https://doi.org/10.1029/WR007i006p01607>
- Cooley, R. L. (1972). Numerical simulation of flow in an aquifer overlain by a water table aquitard. *Water Resources Research*, 8(4), 1046–1050. <https://doi.org/10.1029/WR008i004p01046>
- Cooley, R. L., & Case, C. M. (1973). Effect of a water table aquitard on drawdown in an underlying pumped aquifer. *Water Resources Research*, 9(2), 434–447. <https://doi.org/10.1029/WR009i002p00434>
- Cooley, R. L., & Cunningham, A. B. (1979). Consideration of total energy loss in theory of flow to wells. *Journal of Hydrology*, 43(1–4), 161–184. [https://doi.org/10.1016/0022-1694\(79\)90171-9](https://doi.org/10.1016/0022-1694(79)90171-9)

- Cooper, H. H., Bredehoeft, J. D., & Papadopoulos, I. S. (1967). Response of a finite-diameter well to an instantaneous charge of water. *Water Resources Research*, 3(1), 263–269.
<https://doi.org/10.1029/WR003i001p00263>
- Cooper, H. H., & Jacob, C. E. (1946). A generalized graphical method for evaluating formation constants and summarizing well-field history. *Transactions, American Geophysical Union*, 27(4), 526–534. <https://doi.org/10.1029/TR027i004p00526>
- Crank, J., & Nicolson, P. (1947). A practical method for numerical evaluation of solutions of partial differential equations of the heat-conduction type. *Mathematical Proceedings of the Cambridge Philosophical Society*, 43(1), 50–67. <https://doi.org/10.1017/S0305004100023197>
- Crank, J., & Nicolson, P. (1996). A practical method for numerical evaluation of solutions of partial differential equations of the heat-conduction type. *Advances in Computational Mathematics*, 6(1), 207–226. <https://doi.org/10.1007/BF02127704>
- de Hoog, F. R., Knight, J. H., & Stokes, A. N. (1982). An Improved Method for Numerical Inversion of Laplace Transforms. *SIAM Journal on Scientific and Statistical Computing*, 3(3), 357–366.
<https://doi.org/10.1137/0903022>
- Douglas, J., & Rachford, H. H. (1956). On the Numerical Solution of Heat Conduction Problems in Two and Three Space Variables. *Transactions of the American Mathematical Society*, 82(2), 421.
<https://doi.org/10.2307/1993056>
- Fiering, M. B. (1964). A Digital Computer Solution For Well Field Draw-down. *International Association of Scientific Hydrology. Bulletin*, 9(4), 16–23.
<https://doi.org/10.1080/02626666409493683>
- Gaver, D. P. (1966). Observing Stochastic Processes, and Approximate Transform Inversion. *Operations Research*, 14(3), 444–459. <https://doi.org/10.1287/opre.14.3.444>
- Hantush, M. S. (1960). Modification of the theory of leaky aquifers. *Journal of Geophysical Research*, 65(11), 3713–3725. <https://doi.org/10.1029/JZ065i011p03713>
- Hantush, M. S. (1961). Drawdown around a partially penetrating well. *Journal of the Hydraulics Division, Proceedings of the American Society of Civil Engineers*, 87(HY4), 83–98.
- Hantush, M. S. (1964). Hydraulics of wells. In V. T. Chow (Ed.), *Advances in Hydroscience: Vol. I* (pp. 281–432). New York and London: Academic Press.
- Hantush, M. S. (1967). Flow to wells in aquifers separated by a semipervious layer. *Journal of Geophysical Research*, 72(6), 1709–1720. <https://doi.org/10.1029/JZ072i006p01709>
- Hantush, M. S., & Jacob, C. E. (1955). Non-steady radial flow in an infinite leaky aquifer. *Transactions, American Geophysical Union*, 36(1), 95–100. <https://doi.org/10.1029/TR036i001p00095>
- Harbaugh, A. W. (1995). *Direct solution package based on alternating diagonal ordering for the U.S. Geological Survey modular finite-difference ground-water flow model*. U.S. Geological Survey Open-File Report 95-288. <https://doi.org/https://doi.org/10.3133/ofr95288>
- Harbaugh, A. W. (2005). *MODFLOW-2005, the U.S. Geological Survey modular ground-water model - the Ground-Water Flow Process*. U.S. Geological Survey Techniques and Methods 6-A16.
<https://doi.org/https://doi.org/10.3133/tm6A16>

- Harbaugh, A. W., Banta, E. R., Hill, M. C., & McDonald, M. G. (2000). *MODFLOW-2000, The U.S. Geological Survey Modular Ground-Water Model: User Guide to Modularization Concepts and the Ground-Water Flow Process*. U.S. Geological Survey Open-File Report 00-92. <https://doi.org/https://doi.org/10.3133/ofr200092>
- Harbaugh, A. W., & McDonald, M. G. (1996). *User's documentation for MODFLOW-96, an update to the U.S. Geological Survey modular finite-difference ground-water flow model*. U.S. Geological Survey Open-File Report 96-485. <https://doi.org/https://doi.org/10.3133/ofr96485>
- Hellevik, L. R. (2020, January 13). *Numerical Methods for Engineers*. <https://folk.ntnu.no/leifh/teaching/tkt4140/>
- Hemker, C. J. (1984). Steady groundwater flow in leaky multiple-aquifer systems. *Journal of Hydrology*, 72(3–4), 355–374. [https://doi.org/10.1016/0022-1694\(84\)90089-1](https://doi.org/10.1016/0022-1694(84)90089-1)
- Hemker, C. J. (1985a). A General Purpose Microcomputer Aquifer Test Evaluation Technique. *Ground Water*, 23(2), 247–253. <https://doi.org/10.1111/j.1745-6584.1985.tb02799.x>
- Hemker, C. J. (1985b). Transient well flow in leaky multiple-aquifer systems. *Journal of Hydrology*, 81(1–2), 111–126. [https://doi.org/10.1016/0022-1694\(85\)90170-2](https://doi.org/10.1016/0022-1694(85)90170-2)
- Hemker, C. J. (1999a). Transient well flow in layered aquifer systems: the uniform well-face drawdown solution. *Journal of Hydrology*, 225(1–2), 19–44. [https://doi.org/10.1016/S0022-1694\(99\)00093-1](https://doi.org/10.1016/S0022-1694(99)00093-1)
- Hemker, C. J. (1999b). Transient well flow in vertically heterogeneous aquifers. *Journal of Hydrology*, 225(1–2), 1–18. [https://doi.org/10.1016/S0022-1694\(99\)00137-7](https://doi.org/10.1016/S0022-1694(99)00137-7)
- Hemker, C. J. (2000). *Groundwater flow in layered aquifer systems* [PhD thesis]. VU, Amsterdam.
- Hemker, C. J., & Maas, C. (1987). Unsteady flow to wells in layered and fissured aquifer systems. *Journal of Hydrology*, 90(3–4), 231–249. [https://doi.org/10.1016/0022-1694\(87\)90069-2](https://doi.org/10.1016/0022-1694(87)90069-2)
- Hemker, C. J., & Post, V. E. A. (2019). *MLU for Windows*. Retrieved from <https://www.microfem.com/products/mlu.html>
- Hunt, B. (1985). Flow to a Well in a Multiaquifer System. *Water Resources Research*, 21(11), 1637–1641. <https://doi.org/10.1029/WR021i011p01637>
- Hunt, B. (1986). Solutions for steady groundwater flow in multi-layer aquifer systems. *Transport in Porous Media*, 1(4), 419–429. <https://doi.org/10.1007/BF00208046>
- Hyder, Z., Butler, J. J., McElwee, C. D., & Liu, W. (1994). Slug tests in partially penetrating wells. *Water Resources Research*, 30(11), 2945–2957. <https://doi.org/10.1029/94WR01670>
- Kitterød, N.-O. (2004). Dupuit-Forchheimer solutions for radial flow with linearly varying hydraulic conductivity or thickness of aquifer. *Water Resources Research*, 40(11). <https://doi.org/10.1029/2004WR003115>
- Kruseman, G. P., & de Ridder, N. A. (1970). *Analysis and Evaluation of Pumping Test Data: Vol. Bulletin 11*. International Institute for Land Reclamation and Improvement, Wageningen.
- Kruseman, G. P., & de Ridder, N. A. (1990). *Analysis and Evaluation of Pumping Test Data* (2nd ed.). ILRI Publication 47, Wageningen.

- Lakshminarayana, V., & Rajagopalan, S. P. (1977). Digital Model Studies of Steady-State Radial Flow to Partially Penetrating Wells in Alluvial Plains. *Ground Water*, 15(3), 223–230. <https://doi.org/10.1111/j.1745-6584.1977.tb03167.x>
- Lakshminarayana, V., & Rajagopalan, S. P. (1978). Digital model studies of unsteady-state radial flow to partially penetrating wells in unconfined anisotropic aquifers. *Journal of Hydrology*, 38(3–4), 249–262. [https://doi.org/10.1016/0022-1694\(78\)90072-0](https://doi.org/10.1016/0022-1694(78)90072-0)
- Langevin, C. D. (2008). Modeling Axisymmetric Flow and Transport. *Ground Water*, 46(4), 579–590. <https://doi.org/10.1111/j.1745-6584.2008.00445.x>
- Lebbe, L. C. (1983). Een matematisch model van de niet-permanente grondwaterstroming naar een pompput in een veellagig grondwaterreservoir en enkele beschouwingen over de stroomtijd (in Dutch). *Tijdschrift BECEWA*, 70, 35–48.
- Lebbe, L. C. (1988). *Uitvoering van pompproeven en interpretatie door middel van een invers model (in Dutch)*. Ghent University.
- Lebbe, L. C. (1999). *Hydraulic Parameter Identification. Generalized Interpretation Method for Single and Multiple Pumping Tests*. Berlin Heidelberg: Springer-Verlag.
- Lebbe, L. C., & Bougriba, M. (1995). Interpretation of a double pumping test at Assenede (N.W. Belgium) by means of an inverse numerical model and the comparison of the ordinary and biweighted least square solution. *BULLETIN DE LA SOCIETE BELGE DE GEOLOGIE = BULLETIN VAN DE BELGISCHE VERENIGING VOOR GEOLOGIE*, 104(1–2), 163–172.
- Lebbe, L. C., & de Breuck, W. (1994). The Application of an Inverse Numerical Model for the Interpretation of Single or Multiple Pumping Tests. In A. Peters, G. Wittum, B. Herrling, U. Messner, C. A. Brebbia, W. G. Gray, & G. F. Pinder (Eds.), *Water Science and Technology Library* (Vol. 12, pp. 769–767). Kluwers Academic.
- Lebbe, L. C., & de Breuck, W. (1995). Validation of an inverse numerical model for interpretation of pumping tests and a study of factors influencing accuracy of results. *Journal of Hydrology*, 172(1–4), 61–85. [https://doi.org/10.1016/0022-1694\(95\)02747-D](https://doi.org/10.1016/0022-1694(95)02747-D)
- Lebbe, L. C., & de Breuck, W. (1997). Analysis of a Pumping Test in an Anisotropic Aquifer by Use of an Inverse Numerical Model. *Hydrogeology Journal*, 5(3), 44–59. <https://doi.org/10.1007/s100400050112>
- Lebbe, L. C., Mahauden, M., & de Breuck, W. (1992). Execution of a triple pumping test and interpretation by an inverse numerical model. *Applied Hydrogeology*, 1(4), 20–34.
- Lebbe, L. C., Pede, K., & Van Houtte, E. (1984). Analyse van pompproeven in een veellagig grondwaterreservoir met behulp van een matematisch model (in Dutch). *Tijdschrift Becewa*, 78, 132–146.
- Lebbe, L. C., Tarhouni, J., van Houtte, E., & de Breuck, W. (1995). Results Of An Artificial Recharge Test And A Double Pumping Test As Preliminary Studies For Optimizing Water Supply In The Western Belgian Coastal Plain. *Hydrogeology Journal*, 3(3), 53–63. <https://doi.org/10.1007/s100400050067>
- Lebbe, L. C., & van Meir, N. (2000). Hydraulic Conductivities of Low Permeability Sediments Inferred from a Triple Pumping Test and Observed Vertical Gradients. *Ground Water*, 38(1), 76–88. <https://doi.org/10.1111/j.1745-6584.2000.tb00204.x>

- Lebbe, L. C., & Vandenbohede, A. (2004). *Ontwikkeling van een lokaal axi-symmetrisch model op basis van de HCOV kartering ter ondersteuning van de adviesverlening voor grondwaterwinningen (in Dutch)*. Onderzoeksopdracht voor het Ministerie van de Vlaamse Gemeenschap, AMINAL, afdeling Water, Brussels.
- LeVeque, R. J. (2007). *Finite Difference Methods for Ordinary and Partial Differential Equations: Steady-State and Time-Dependent Problems*. Society for Industrial and Applied Mathematics, Philadelphia.
- Li, Z., Qiao, Z., & Tang, T. (2017). *Numerical Solution of Differential Equations - Introduction to Finite Difference and Finite Element Methods*. Cambridge University Press.
<https://doi.org/10.1017/9781316678725>
- Loáiciga, H. A. (2010). Derivation Approaches for the Theis (1935) Equation. *Ground Water*, 48(1), 2–5. <https://doi.org/10.1111/j.1745-6584.2009.00568.x>
- Louwyck, A. (2011). *MAxSym - A MATLAB Tool to Simulate Two-Dimensional Axi-Symmetric Groundwater Flow*. Research Unit Groundwater Modeling, Ghent University. Retrieved from <https://github.com/alouwyck/MAxSym>
- Louwyck, A., Vandenbohede, A., Bakker, M., & Lebbe, L. C. (2012). Simulation of axi-symmetric flow towards wells: A finite-difference approach. *Computers & Geosciences*, 44, 136–145. <https://doi.org/10.1016/j.cageo.2011.09.004>
- Louwyck, A., Vandenbohede, A., Bakker, M., & Lebbe, L. C. (2014). MODFLOW procedure to simulate axisymmetric flow in radially heterogeneous and layered aquifer systems. *Hydrogeology Journal*, 22(5), 1217–1226. <https://doi.org/10.1007/s10040-014-1150-0>
- Louwyck, A., Vandenbohede, A., & Lebbe, L. C. (2005). The role of hydrogeological research in the realization of a combined pumping and deep infiltration system at the excavation “Duinenabdij.” In J.-L. Herrier, J. Mees, A. Salman, J. Seys, H. Van Nieuwenhuyse, & I. Dobbelaere (Eds.), *Proceedings “Dunes and Estuaries 2005”: International Conference on nature restoration practices in European coastal habitats, Koksijde, Belgium 19-23 September 2005*. (pp. 317–326). VLIZ Special Publication 19.
- Louwyck, A., Vandenbohede, A., & Lebbe, L. C. (2010). Numerical analysis of step-drawdown tests: Parameter identification and uncertainty. *Journal of Hydrology*, 380(1–2), 165–179. <https://doi.org/10.1016/j.jhydrol.2009.10.034>
- McDonald, M. G., & Harbaugh, A. W. (1984). *A modular three-dimensional finite-difference ground-water flow model*. U.S. Geological Survey Open-File Report 83-875. <https://doi.org/https://doi.org/10.3133/ofr83875>
- McDonald, M. G., & Harbaugh, A. W. (1988). *A modular three-dimensional finite-difference ground-water flow model*. U.S. Geological Survey Techniques of Water-Resources Investigations 06-A1. <https://doi.org/10.3133/twri06A1>
- Mehl, S. W., & Hill, M. C. (2001). *MODFLOW-2000, the U. S. Geological Survey modular ground-water model; user guide to the Link-AMG (LMG) package for solving matrix equations using an algebraic multigrid solver*. U.S. Geological Survey Open-File Report 2001-177. <https://doi.org/https://doi.org/10.3133/ofr01177>

- Mertooetomo, M. (1995). *Modellering van een grondwaterwinning op basis van de hydrogeologische kenmerken van het veellagig grondwaterreservoir te Koksijde-Oostduinkerke (België)* (in Dutch) [PhD thesis]. Ghent University.
- Moench, A. F., & Ogata, A. (1981). A numerical inversion of the laplace transform solution to radial dispersion in a porous medium. *Water Resources Research*, 17(1), 250–252. <https://doi.org/10.1029/WR017i001p00250>
- Moench, A. F., & Ogata, A. (1984). Analysis of constant discharge wells by numerical inversion of Laplace transform solutions. In J. Rosensheim & G. D. Bennett (Eds.), *Groundwater Hydraulics. Water Resour. Monogr. Ser. 9.* (pp. 146–170). Am. Geophys. Union.
- Neuman, S. P. (1968). *Transient Flow of Ground Water to Wells in Multiple-Aquifer Systems*. [PhD Thesis]. University of California.
- Neuman, S. P., & Witherspoon, P. A. (1969). Theory of Flow in a Confined Two Aquifer System. *Water Resources Research*, 5(4), 803–816. <https://doi.org/10.1029/WR005i004p00803>
- Peaceman, D. W., & Rachford, Jr. , H. H. (1955). The Numerical Solution of Parabolic and Elliptic Differential Equations. *Journal of the Society for Industrial and Applied Mathematics*, 3(1), 28–41. <https://doi.org/10.1137/0103003>
- Peterson, P., Oliphant, T., & Vanderplas, J. (2022). *SciPy (version 1.8.1) documentation for function linalg.solve*. Retrieved from <https://docs.scipy.org/doc/scipy/reference/generated/scipy.linalg.solve.html>
- Pinder, G. F. (1969). *An iterative digital model for aquifer evaluation*. U.S. Geological Survey Open-File Report 69-207. <https://doi.org/https://doi.org/10.3133/ofr69207>
- Pinder, G. F. (1970). *A digital model for aquifer evaluation*. U.S. Geological Survey Techniques of Water-Resources Investigations 07-C1. https://doi.org/10.3133/twri07C1_1970
- Pinder, G. F., & Bredehoeft, J. D. (1968). Application of the Digital Computer for Aquifer Evaluation. *Water Resources Research*, 4(5), 1069–1093. <https://doi.org/10.1029/WR004i005p01069>
- Rathod, K. S., & Rushton, K. R. (1984). Numerical Method of Pumping Test Analysis Using Microcomputers. *Ground Water*, 22(5), 602–608. <https://doi.org/10.1111/j.1745-6584.1984.tb01431.x>
- Reed, J. E. (1980). *Type curves for selected problems of flow to wells in confined aquifers*. U.S. Geological Survey Techniques of Water-Resources Investigations 03-B3. <https://doi.org/10.3133/twri03B3>
- Reilly, T. E. (1984). *A Galerkin finite-element flow model to predict the transient response of a radially symmetric aquifer*. U.S. Geological Survey Water Supply Paper 2198. <https://doi.org/10.3133/wsp2198>
- Rushton, K. R. (1974). Extensive Pumping From Unconfined Aquifers. *Journal of the American Water Resources Association*, 10(1), 32–41. <https://doi.org/10.1111/j.1752-1688.1974.tb00538.x>
- Rushton, K. R., & Booth, S. J. (1976). Pumping-test analysis using a discrete time-discrete space numerical method. *Journal of Hydrology*, 28(1), 13–27. [https://doi.org/10.1016/0022-1694\(76\)90049-4](https://doi.org/10.1016/0022-1694(76)90049-4)

- Rushton, K. R., & Redshaw, S. C. (1979). *Seepage and Groundwater Flow: Numerical Analysis by Digital Methods*. New York: Wiley.
- Rushton, K. R., & Turner, A. (1974). Numerical Analysis of Pumping from Confined-Unconfined Aquifers. *Journal of the American Water Resources Association*, 10(6), 1255–1269. <https://doi.org/10.1111/j.1752-1688.1974.tb00642.x>
- Samarinas, N., Tzimopoulos, C., & Evangelides, C. (2022). An efficient method to solve the fuzzy Crank–Nicolson scheme with application to the groundwater flow problem. *Journal of Hydroinformatics*, 24(3), 590–609. <https://doi.org/10.2166/hydro.2022.150>
- Şen, Z. (2014). Hydraulic Conductivity Variation in a Confined Aquifer. *Journal of Hydrologic Engineering*, 19(3), 654–658. [https://doi.org/10.1061/\(ASCE\)HE.1943-5584.0000832](https://doi.org/10.1061/(ASCE)HE.1943-5584.0000832)
- Stehfest, H. (1970). Algorithm 368: Numerical inversion of Laplace transforms [D5]. *Communications of the ACM*, 13(1), 47–49. <https://doi.org/10.1145/361953.361969>
- Streltsova, T. D., & Rushton, K. R. (1973). Water table drawdown due to a pumped well in an unconfined aquifer. *Water Resources Research*, 9(1), 236–242. <https://doi.org/10.1029/WR009i001p00236>
- Suárez-Carreño, F., & Rosales-Romero, L. (2021). Convergency and Stability of Explicit and Implicit Schemes in the Simulation of the Heat Equation. *Applied Sciences*, 11(10), 4468. <https://doi.org/10.3390/app11104468>
- Theis, C. V. (1935). The relation between the lowering of the Piezometric surface and the rate and duration of discharge of a well using ground-water storage. *Transactions, American Geophysical Union*, 16(2), 519–524. <https://doi.org/10.1029/TR016i002p00519>
- Thiem, A. (1870). Die Ergiebigkeit artesischer Bohrlöcher, Schachtbrunnen und Filtergalerien (in German). *Journal Für Gasbeleuchtung Und Wasserversorgung*, 13, 450–467.
- Thiem, G. (1906). *Hydrologische Methoden (in German)*. Leipzig: Gebhardt.
- Trescott, P. C. (1975). *Documentation of finite-difference model for simulation of three-dimensional groundwater flow*. U.S. Geological Survey Open-File Report 75-438. <https://doi.org/https://doi.org/10.3133/ofr75438>
- Trescott, P. C., & Larson, S. P. (1976). *Supplement to Open-File Report 75-438: Documentation of finite-difference model for simulation of three-dimensional ground-water flow*. U.S. Geological Survey Open-File Report 76-591. <https://doi.org/https://doi.org/10.3133/ofr76591>
- Trescott, P. C., Pinder, G. F., & Larson, S. P. (1976). *Finite-difference Model for Aquifer Simulation in Two Dimensions With Results of Numerical Experiments*. U.S. Geological Survey Techniques of Water-Resources Investigations 07-C1. <https://doi.org/https://doi.org/10.3133/twri07C1>
- Van Meir, N. (2001). *Density-dependent groundwater flow: design of a parameter identification test and 3D-simulation of sea-level rise* [PhD. Thesis]. Ghent University.
- Van Meir, N., & Lebbe, L. C. (2005). Parameter identification for axi-symmetric density-dependent groundwater flow based on drawdown and concentration data. *Journal of Hydrology*, 309(1–4), 167–177. <https://doi.org/10.1016/j.jhydrol.2004.11.019>

- Vandenbohede, A. (2004). *Solute transport in heterogeneous aquifers - parameter identification and its use in groundwater pollution and salt water intrusion problems* [PhD. Thesis]. Ghent University.
- Vandenbohede, A., & Lebbe, L. C. (2003). Combined interpretation of pumping and tracer tests: theoretical considerations and illustration with a field test. *Journal of Hydrology*, 277(1–2), 134–149. [https://doi.org/10.1016/S0022-1694\(03\)00090-8](https://doi.org/10.1016/S0022-1694(03)00090-8)
- Varga, R. S. (2000). *Matrix Iterative Analysis* (2nd ed., Vol. 27). Berlin Heidelberg: Springer. <https://doi.org/10.1007/978-3-642-05156-2>
- Walton, W. C. (1962). *Selected analytical methods for well and aquifer evaluation*. Illinois State Water Survey Bulletin 49, Department of Registration and Education, State of Illinois.
- Wang, H. F., & Anderson, M. P. (1982). *Introduction to Groundwater Modeling: Finite Difference and Finite Element Methods*. San Francisco: WH Freeman and Company.
- Wang, Q., Kim, P., & Qu, W. (2022). A Hybrid Localized Meshless Method for the Solution of Transient Groundwater Flow in Two Dimensions. *Mathematics*, 10(3), 515. <https://doi.org/10.3390/math10030515>
- Wikramaratna, R. S., & Wood, W. L. (1983). Control of spurious oscillations in the salt water intrusion problem. *International Journal for Numerical Methods in Engineering*, 19(8), 1243–1251. <https://doi.org/10.1002/nme.1620190811>
- Yadav, M. P., & Agarwal, R. (2019). Numerical investigation of fractional-fractal Boussinesq equation. *Chaos: An Interdisciplinary Journal of Nonlinear Science*, 29(1), 013109. <https://doi.org/10.1063/1.5080139>

Chapter 5. Simulating Multilayer-Multizone Flow

5.1. Introduction

In this chapter, the semi-analytical axisymmetric multilayer solution discussed in Chapter 2 is extended to take into account lateral variations in hydraulic parameters. Examples of cylindrical aquifer inhomogeneities include a variety of geologic structures, such as patchy aquifers (Barker & Herbert, 1982), a cutoff meander channel in a flood-plain matrix (Butler, 1988), or axisymmetric delta structures (Kitterød, 2004). Another well-known use is the case of a finite-thickness skin around a pumping well (e.g. Barua & Bora, 2010; Butler, 1988; Chang & Chen, 2002; Chang et al., 2010; Chiu et al., 2007a, 2007b; Feng & Wen, 2016; Feng & Zhan, 2016, 2019; Huang et al., 2015; Hyder et al., 1994; Louwyck et al., 2014; Novakowski, 1993; Perina & Lee, 2006; Yang et al., 2014; Yang & Yeh, 2005, 2009; Yeh & Yang, 2006). The simulation of a circular infiltration pond recharging a multi-aquifer system is another application (e.g. Bakker & Strack, 2003; Hunt, 1986). Solutions in the hydrogeological literature are mostly restricted to two zones. In case of a finite-thickness skin, for instance, the inner zone conceptualizes this wellbore skin, whereas the outer zone represents the aquifer. If a circular infiltration area is simulated, then there are also two zones: an inner one with recharge and an outer one without.

The solution presented in this chapter generalizes the concept of cylindrical inhomogeneities to multiple zones, meaning that as many cylindrical zones as necessary may be defined. For instance, there could be a zone that coincides with the well-skin, and one with the gravel pack, which are both part of a zone with areal recharge, surrounded by a zone without recharge. In essence, each of these zones should be regarded as a separate model in which axisymmetric multilayer flow is simulated as discussed in Chapter 2. The models representing these zones are coupled by preserving continuity of flow at their shared boundaries. This implies that heads and fluxes in adjacent zones must be the same at the common boundary.

The first section of this chapter states the problem mathematically. Flow in each zone is governed by a system of differential equations. Both axisymmetric and parallel flow are considered. Preserving continuity of flow between adjacent zones is mathematically translated into the definition of head and flux conditions at the boundaries between these zones. The general solution for the system of differential equations for each zone is found by performing an eigendecomposition of the system matrix (Hemker, 1984, 1985, 1999a). In case of transient flow, the Laplace transform is applied first, which transforms the partial differential equations into ordinary differential equations. The resulting solution in Laplace space is inverted back numerically applying the Stehfest (1970) algorithm. This solution method was presented in detail in Chapter 2 and is recapitulated in this chapter.

Particular solutions are found by applying the boundary conditions. This is the step where the solution method discussed in this chapter generalizes the method presented in Chapter 2. Indeed, the problem solved in Chapter 2 considers a single zone, for which only two sets of boundary conditions are defined, at the inner and outer model boundary, respectively. Therefore, determining the integration constants to find the particular solution can be done analytically. In the general case of multiple zones, the number of boundary conditions is two times the number of zones. As a consequence, the integration constants can only be determined numerically in this general case. A new algorithm inspired by the Thomas (1949) algorithm is developed to solve the system of boundary conditions. It is a simplified form of Gaussian elimination that takes advantage of the

diagonal structure of the matrix system. LU decomposition is an alternative to this new algorithm, which is implemented in standard linear algebra solvers available with Matlab and SciPy.

After discussing the solution method, it is verified against several analytical solutions presented in the literature, and compared with the finite-difference solution presented in Chapter 3. In particular, solutions for a circular infiltration area in single and multiple aquifer systems are presented, and the effect of well-skin and gravel pack is discussed in more detail. The multilayer-multizone solution may also be used to include the effect of wellbore storage in case of a finite-diameter well, or to model the draining or irrigating effect of a wide stream interacting with a multi-aquifer system. In these applications, the well or stream is conceptualized as a separate zone of high transmissivity. This ‘high-transmissivity’ approach is a well-known modeling trick (Neville & Tonkin, 2004) which is also applied successfully here. In the next Chapter 6, the multilayer-multizone solution presented in this chapter is extended to model multilayer wells with a finite diameter by defining more realistic inner model boundary conditions, which is a mathematically more rigorous way to take into account the effect of wellbore storage.

The first test case presents different analytical solutions to simulate steady radial flow due to a circular infiltration area. The solution for a single homogeneous aquifer is given, for instance, by Strack (1989) and Haitjema (1995). Hunt (1986) and Bakker and Strack (2003) generalize this solution to the multi-aquifer case by applying an eigendecomposition of the system matrix. The solution of a circular infiltration pond can also be combined with the formula of de Glee (1930) to calculate the steady drawdown caused by a fully penetrating well in a phreatic aquifer system drained by a dense network of ditches. The nonlinear one-layer solution developed by Ernst (1971) is discussed exhaustively in Chapter 7, Chapter 10, and Chapter 11. In this chapter, a similar formula by Blom (1973) is used as a second test case, which is easier to implement as it assumes the distance of the boundary between the infiltrated and the drained zone is known.

The analytical steady state solutions for axisymmetric and parallel flow in a single confined aquifer consisting of multiple zones of differing transmissivities is derived in the third test case, whereas the steady state solution for axisymmetric flow in a leaky two-zone aquifer is presented in the fourth case. The fifth test case discusses the model of Butler (1988) to simulate transient flow to a pumping well in a radially symmetric nonuniform confined aquifer, that is a single confined aquifer consisting of two zones characterized by different transmissivities and storativities. Butler (1988) presents the exact solution in the Laplace domain, which is inverted numerically by applying the Stehfest (1970) algorithm. The solution for large values of time was presented earlier by Barker and Herbert (1982).

In the last two test cases, it is demonstrated how to use the ‘high-transmissivity’ approach to model axisymmetric flow toward or away from a finite-diameter well, and parallel flow caused by a river of finite width. First, the approach is applied to approximate the Cooper et al. (1967) solution for a slug test conducted in a well fully penetrating a confined aquifer. In the last test case, the effect of a permanent water level rise in a wide embanked river infiltrating a multi-aquifer system is simulated. This example is similar to an example presented by Hemker (1984), who solves the problem by coupling two multi-layer models, which is essentially the same approach as the semi-analytical solution method developed in this chapter.

Although the primary objective of this chapter is to present and verify a generalized semi-analytical solution for two-dimensional multilayer-multizone flow, the last section goes into more detail on the skin effect as this is an important topic within the discipline of well hydraulics. The traditional approach involving a dimensionless skin factor (Kruseman & de Ridder, 1990) is discussed and generalized to include multiple cylindrical zones of different hydraulic conductivities around the

pumping well. It is also investigated whether or not it is justified to use the dimensionless skin factor for estimating the linear well-loss in a pumping well extracting groundwater from a multilayered aquifer system. Recent insights on the individual components of the total well-loss (Houben, 2015; Houben et al., 2016; Houben & Kenrick, 2022) are addressed briefly, and the analysis presented by Louwyck et al. (2010, 2014) is revisited. In particular, it is theoretically explained why the inverse numerical model developed by Lebbe (1999) and applied by Louwyck et al. (2010) to interpret step-drawdown tests results in a negative well-loss coefficient if the pumping well is effectively developed.

5.2. Problem statement

In this section, the problem of axisymmetric and parallel flow in a multilayered aquifer system consisting of multiple zones is stated mathematically. Each zone and each layer is characterized by constant hydraulic parameters. Both steady and transient flow are considered. The upper and lower boundary of the multilayer system is confined or leaky, and the system may be laterally bounded or unbounded. Specified-discharge as well as specified-head conditions can be defined at the inner model boundary, and a constant infiltration flux may be included in each layer and each zone of the system. Figure 1 shows an example of an aquifer system consisting of 4 layers and 4 zones. The parameters are defined in the next sections.

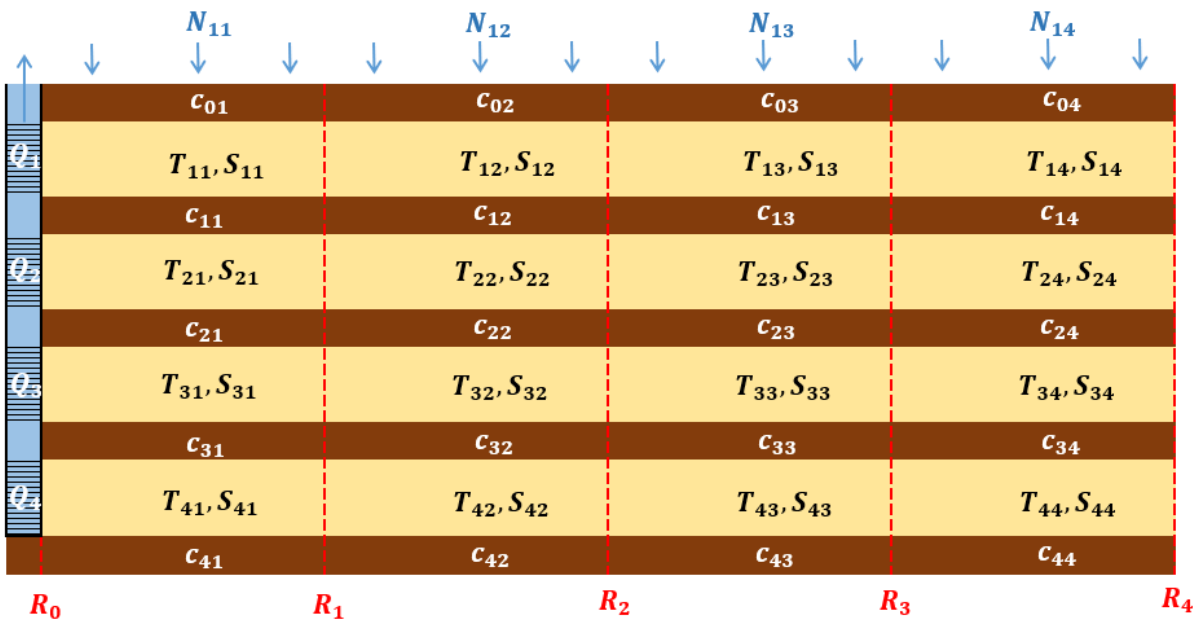


Figure 1. Visualization of an aquifer system consisting of 4 layers and 4 zones. In practice, any number of layers, and independently, any number of zones can be defined. Each zone is characterized by its own set of hydraulic parameters. Here, only the top layer is recharged, although the zones in the other layers can also be recharged. The inner model boundary at distance R_0 can have specified discharge defined, as shown here, or constant heads. See text for the mathematical statement of the problem and the definition of the parameters.

5.2.1. The multilayer-multizone aquifer system

The groundwater reservoir consists of n_l horizontal layers and n_z zones, in which flow is strictly horizontal. Layers are numbered from the top down; zones are numbered from inner to outer boundary. Each layer i has constant thickness D_i [L]; the boundary between zones j and $j + 1$ is at distance R_j [L]. The inner and outer boundary of the aquifer system is at distances R_0 and R_{n_z} , respectively. Hydraulic head in layer i and zone j is denoted by h_{ij} [L].

Each zone j in layer i is characterized by constant transmissivity T_{ij} [L^2/T] and constant storativity S_{ij} [-], which are respectively defined as:

$$T_{ij} = K_{ij}^h D_i \quad (1 \leq i \leq n_l; 1 \leq j \leq n_z) \quad (1)$$

$$S_{ij} = S_{ij}^s D_i \quad (1 \leq i \leq n_l; 1 \leq j \leq n_z) \quad (2)$$

with K_{ij}^h the constant horizontal conductivity [L/T] and S_{ij}^s the constant specific elastic storage [L^{-1}] defined for zone j in layer i .

Zones j in adjacent layers i and $i + 1$ are separated by an incompressible resistance layer with zero thickness characterized by hydraulic resistance c_{ij} [T]:

$$c_{ij} = \frac{D_i}{2K_{ij}^v} + \frac{D_{i+1}}{2K_{i+1,j}^v} \quad (1 \leq i < n_l; 1 \leq j \leq n_z) \quad (3)$$

with K_{ij}^v the constant vertical conductivity [L/T] defined for zone j in layer i . Flow between two layers is assumed to be strictly vertical. Resistance c_{ij} may also represent an incompressible aquitard. The upper and lower boundary of the aquifer system is characterized by resistances $c_{0,j}$ and $c_{n_l,j}$, respectively. If a boundary is impervious, then its resistance is infinitely large.

Each zone j in layer i may also be recharged by a constant flux N_{ij} [L/T], which is positive in case of infiltration.

5.2.2. Groundwater flow equations

The groundwater flow in zone j and layer i is governed by the following partial differential equation:

$$\nabla^2 h_{ij} = \frac{S_{ij}}{T_{ij}} \frac{\partial h_{ij}}{\partial t} + \frac{-N_{ij}}{T_{ij}} + \frac{h_{ij} - h_{i-1,j}}{c_{i-1,j} T_{ij}} + \frac{h_{ij} - h_{i+1,j}}{c_{ij} T_{ij}} \quad (1 \leq i \leq n_l; 1 \leq j \leq n_z) \quad (4)$$

with $\nabla^2 h = \frac{\partial^2 h}{\partial r^2} + \frac{1}{r} \frac{\partial h}{\partial r}$ in case of radial flow, and $\nabla^2 h = \frac{\partial^2 h}{\partial x^2}$ in case of parallel flow. Hydraulic head h_{ij} is a function of time t [T] and of radial or horizontal distance r [L], depending on the type of flow. If flow is in a steady state, $\partial h_{ij}/\partial t = 0$, by definition, and equation (4) simplifies to an ordinary differential equation as head h_{ij} is dependent on distance r only.

In case of axisymmetric flow, radial discharge $Q^h(r, t)$ [L^3/T] is defined as the amount of water per unit of time that flows radially through the cylindrical surface with radius r at time t :

$$Q_{ij}^h(r, t) = -2\pi T_{ij} r \frac{\partial h_{ij}}{\partial r} \quad (1 \leq i \leq n_l; 1 \leq j \leq n_z) \quad (5)$$

In case of parallel flow, horizontal discharge $Q^h(r, t)$ [L^2/T] is defined as the amount of water per unit of time that flows horizontally through a vertical surface with unit width at distance r and time t :

$$Q_{ij}^h(r, t) = -T_{ij} \frac{\partial h_{ij}}{\partial r} \quad (1 \leq i \leq n_l; 1 \leq j \leq n_z) \quad (6)$$

In case of steady state flow, Q^h in (5) and (6) is dependent on radial distance r only, and the partial derivative is replaced by dh_{ij}/dr .

5.2.3. Initial and boundary conditions

The upper and the lower boundary of the aquifer system are characterized by resistances $c_{0,j}$ and $c_{n_l,j}$, and constant heads $\varphi_{0,j}$ [L] and $\varphi_{n_l+1,j}$ [L], respectively:

$$h_{0,j}(r, t) = \varphi_{0,j} \quad (1 \leq j \leq n_z) \quad (7)$$

$$h_{n_l+1,j}(r, t) = \varphi_{n_l+1,j} \quad (1 \leq j \leq n_z) \quad (8)$$

The outer boundary of the aquifer system is at distance R_{n_z} [L], at which a constant head φ_{i,n_z} [L] is defined in each layer i :

$$h_{i,n_z}(R_{n_z}, t) = \varphi_{i,n_z} \quad (1 \leq i \leq n_l) \quad (9)$$

The inner boundary of the aquifer system is at distance R_0 [L], at which either a constant head H_i [L] is defined in each layer i , or a constant discharge Q_i [L^3/T]. In case of constant heads, the inner boundary conditions are:

$$h_{i,1}(R_0, t) = H_i \quad (1 \leq i \leq n_l) \quad (10)$$

In case of specified discharges, the inner boundary conditions are given by:

$$Q_{i,1}^h(R_0, t) = Q_i \quad (1 \leq i \leq n_l) \quad (11)$$

where Q_i is positive if water is added to the aquifer system. If axisymmetric flow is simulated, then discharge $Q_{i,1}^h(R_0, t)$ is defined by (5), in case of parallel flow, it is defined by (6).

At the boundary between zones j and $j + 1$, the hydraulic head cannot be discontinuous:

$$h_{ij}(R_j, t) = h_{i,j+1}(R_j, t) \quad (1 \leq i \leq n_l; 1 \leq j < n_z) \quad (12)$$

This is true for all layers i . There is also continuity of flow between zones j and $j + 1$:

$$Q_{ij}^h(R_j, t) = Q_{i,j+1}^h(R_j, t) \quad (1 \leq i \leq n_l; 1 \leq j < n_z) \quad (13)$$

Finally, initial conditions at $t = 0$ are required in case of transient flow. These conditions are defined by setting the initial head in each zone j and each layer i to the initial head φ_{ij} :

$$h_{ij}(r, 0) = \varphi_{ij} \quad (1 \leq i \leq n_l; 1 \leq j \leq n_z) \quad (14)$$

Note that the initial heads φ_{i,n_z} in the outer zones equal the constant heads at the outer model boundary defined by (9).

5.3. Semi-analytical solution

The method proposed by Hemker (1984, 1985) is applied to uncouple the system of differential equations for each zone. As this method performs eigendecomposition, the stated problem is rewritten in matrix form, and the transient state problem is Laplace transformed, as suggested by Hemker (1999a, 2000). The general solution for each zone is the same as the general solution for multilayer flow without zones presented in Chapter 2. To obtain particular solutions, the integration constants are determined by solving the system of boundary conditions numerically. In the transient case, particular solutions in the Laplace domain must be inverted numerically, e.g. by applying the Stehfest (1970) algorithm.

5.3.1. Matrix formulation

Expression (4) defines a system of n equations, with $n = n_l \cdot n_z$. The differential equations for zone j are coupled, and may be written more conveniently in matrix form:

$$\nabla^2 \mathbf{h}_j = \mathbf{A}_j \mathbf{h}_j - \mathbf{b}_j \quad (1 \leq j \leq n_z) \quad (15)$$

where \mathbf{h}_j and \mathbf{b}_j are $n_l \times 1$ vectors, and \mathbf{A}_j is an $n_l \times n_l$ tridiagonal matrix. If (15) expresses steady flow, then:

$$\mathbf{h}_{ji} = h_{ij}(r) \quad (16)$$

$$\mathbf{b}_{ji} = \begin{cases} \frac{N_{1,j}}{T_{1,j}} + \frac{\varphi_{0,j}}{c_{0,j} T_{1,j}} & (i = 1) \\ \frac{N_{n_l,j}}{T_{n_l,j}} + \frac{\varphi_{n_l+1,j}}{c_{n_l,j} T_{n_l,j}} & (i = n_l) \\ \frac{N_{ij}}{T_{ij}} & (1 < i < n_l) \end{cases} \quad (17)$$

$$\mathbf{A}_{jik} = \begin{cases} \frac{1}{c_{i-1,j} T_{ij}} + \frac{1}{c_{ij} T_{ij}} & (i = k) \\ \frac{-1}{c_{i-1,j} T_{ij}} & (i = k + 1) \\ \frac{-1}{c_{ij} T_{ij}} & (i = k - 1) \end{cases} \quad (18)$$

In the transient-state case, \mathbf{h}_j , \mathbf{b}_j , and \mathbf{A}_j are defined as:

$$\mathbf{h}_{ji} = \mathcal{L}\{h_{ij}(r, t)\}(p) = \bar{h}_{ij}(r, p) \quad (19)$$

$$\mathbf{b}_{ji} = \begin{cases} \frac{N_{1,j}}{p T_{1,j}} + \frac{\varphi_{0,j}}{p c_{0,j} T_{1,j}} + \frac{S_{1,j}}{T_{1,j}} \varphi_{1,j} & (i = 1) \\ \frac{N_{n_l,j}}{p T_{n_l,j}} + \frac{\varphi_{n_l+1,j}}{p c_{n_l,j} T_{n_l,j}} + \frac{S_{n_l,j}}{T_{n_l,j}} \varphi_{n_l,j} & (i = n_l) \\ \frac{N_{ij}}{p T_{ij}} + \frac{S_{ij}}{T_{ij}} \varphi_{ij} & (1 < i < n_l) \end{cases} \quad (20)$$

$$\mathbf{A}_{jik} = \begin{cases} \frac{1}{c_{i-1,j} T_{ij}} + \frac{1}{c_{ij} T_{ij}} + \frac{S_{ij}}{T_{ij}} p & (i = k) \\ \frac{-1}{c_{i-1,j} T_{ij}} & (i = k + 1) \\ \frac{-1}{c_{ij} T_{ij}} & (i = k - 1) \end{cases} \quad (21)$$

where \bar{h} is the Laplace transform \mathcal{L} of head h , and p is the frequency variable [T^{-1}]. The i -th entry in \mathbf{h}_j and \mathbf{b}_j is denoted by \mathbf{h}_{ji} and \mathbf{b}_{ji} , respectively. The entry on the i -th row and the k -th column of matrix \mathbf{A}_j is denoted by \mathbf{A}_{jik} . If $i = k$, then the entry is on the main diagonal of \mathbf{A}_j ; if $i = k + 1$, then the entry is on the lower diagonal; and if $i = k - 1$, then the entry is on the upper diagonal. All other elements in \mathbf{A}_j are zero.

The horizontal discharge Q^h is also written in matrix form:

$$\mathbf{Q}_j^h = -\mathbf{T}_j \nabla \mathbf{h}_j \quad (1 \leq j \leq n_z) \quad (22)$$

In case of steady axisymmetric flow, $\nabla \mathbf{h}_j = r \frac{d \mathbf{h}_j}{dr}$; in case of steady parallel flow, $\nabla \mathbf{h}_j = \frac{d \mathbf{h}_j}{dr}$; in case of transient flow, the Laplace transform is considered, i.e. $\frac{d \mathbf{h}}{dr}$ must be replaced by $\frac{\partial \bar{\mathbf{h}}}{\partial r}$. In (22), \mathbf{T}_j is an $n_l \times n_l$ diagonal matrix. In case of axi-symmetric flow, the nonzero entries are equal to:

$$\mathbf{T}_{jii} = 2\pi T_{ij} \quad (23)$$

In case of parallel flow, the nonzero entries are:

$$\mathbf{T}_{jii} = T_{ij} \quad (24)$$

Using vector \mathbf{h}_j , the boundary conditions are also written in matrix form. The outer boundary conditions are reformulated as:

$$\mathbf{h}_{n_z}(R_{n_z}) = \boldsymbol{\varphi}_{n_z} \quad (25)$$

with $\boldsymbol{\varphi}_{n_z}$ an $n_l \times 1$ vector. If flow is steady, the i -th entry in $\boldsymbol{\varphi}_{n_z}$ is:

$$\boldsymbol{\varphi}_{n_z,i} = \varphi_{i,n_z} \quad (26)$$

In the transient-state case, the i -th entry is:

$$\boldsymbol{\varphi}_{n_z,i} = \frac{\varphi_{i,n_z}}{p} \quad (27)$$

The constant-head inner boundary conditions are in matrix form expressed as:

$$\mathbf{h}_1(R_0) = \mathbf{H} \quad (28)$$

with \mathbf{H} an $n_l \times 1$ vector. In the steady-state case, the i -th entry in \mathbf{H} is:

$$\mathbf{H}_i = H_i \quad (29)$$

In the transient-state case, the i -th entry is:

$$\mathbf{H}_i = \frac{H_i}{p} \quad (30)$$

The constant-discharge inner boundary conditions are reformulated as follows:

$$\mathbf{Q}_1^h(R_0) = \mathbf{Q} \quad (31)$$

with \mathbf{Q} an $n_l \times 1$ vector. In case of steady state, it is defined as:

$$\mathbf{Q}_i = Q_i \quad (32)$$

In the transient-state case, the i -th entry is:

$$\mathbf{Q}_i = \frac{Q_i}{p} \quad (33)$$

Finally, the boundary conditions between zones j and $j + 1$ are in matrix form expressed as:

$$\mathbf{h}_j(R_j) = \mathbf{h}_{j+1}(R_j) \quad (1 \leq j < n_z) \quad (34)$$

$$\mathbf{Q}_j^h(R_j) = \mathbf{Q}_{j+1}^h(R_j) \quad (1 \leq j < n_z) \quad (35)$$

5.3.2. General solution

System of equations (15) is solved by decomposing matrix \mathbf{A}_j using its eigenvalues and corresponding eigenvectors as suggested by Hemker (1984, 1985, 1999a):

$$\nabla^2 \mathbf{h}_j = \mathbf{V}_j \mathbf{D}_j \mathbf{V}_j^{-1} \mathbf{h}_j - \mathbf{b}_j \quad (36)$$

where \mathbf{D}_j is an $n_l \times n_l$ diagonal matrix containing the n_l eigenvalues d_{ij} , and \mathbf{V}_j is an $n_l \times n_l$ matrix holding the corresponding eigenvectors in its columns. The eigenvalues are always positive. The only case in which one of the eigenvalues d_{ij} is zero, is when flow is steady and $c_{0,j} = c_{n_l,j} = \infty$.

Multiplying both sides of (36) by \mathbf{V}_j^{-1} , and substituting $\mathbf{V}_j^{-1}\mathbf{h}_j$ by \mathbf{g}_j and $\mathbf{V}_j^{-1}\mathbf{b}_j$ by \mathbf{v}_j gives:

$$\nabla^2 \mathbf{g}_j = \mathbf{D}_j \mathbf{g}_j - \mathbf{v}_j \quad (37)$$

Because \mathbf{D}_j is a diagonal matrix, equation (37) expresses a system of uncoupled ordinary differential equations. The general solution of this system of equations is:

$$\mathbf{g}_j(r) = \mathbf{I}_j(r)\boldsymbol{\alpha}_j + \mathbf{K}_j(r)\boldsymbol{\beta}_j + \mathbf{m}_j(r) \quad (38)$$

where \mathbf{I}_j and \mathbf{K}_j are $n_l \times n_l$ diagonal matrices, and $\boldsymbol{\alpha}_j$, $\boldsymbol{\beta}_j$, and \mathbf{m}_j are $n_l \times 1$ vectors. Vectors $\boldsymbol{\alpha}_j$ and $\boldsymbol{\beta}_j$ contain the unknown integration constants. In case of axisymmetric flow, the nonzero entries of \mathbf{I}_j , \mathbf{K}_j , and \mathbf{m}_j are defined as, respectively:

$$\mathbf{I}_{jii}(r) = \begin{cases} \ln(r) & (d_{ij} = 0) \\ I_0\left(r\sqrt{d_{ij}}\right) & (d_{ij} \neq 0) \end{cases} \quad (39)$$

$$\mathbf{K}_{jii}(r) = \begin{cases} 1 & (d_{ij} = 0) \\ K_0\left(r\sqrt{d_{ij}}\right) & (d_{ij} \neq 0) \end{cases} \quad (40)$$

$$\mathbf{m}_{ji}(r) = \begin{cases} -\frac{\mathbf{v}_{ji}r^2}{4} & (d_{ij} = 0) \\ \frac{\mathbf{v}_{ji}}{d_{ij}} & (d_{ij} \neq 0) \end{cases} \quad (41)$$

Functions I_0 and K_0 are the zero order modified Bessel functions of the first and second kind, respectively. In case of parallel flow, these entries are:

$$\mathbf{I}_{jii}(r) = \begin{cases} r & (d_{ij} = 0) \\ e^{(r\sqrt{d_{ij}})} & (d_{ij} \neq 0) \end{cases} \quad (42)$$

$$\mathbf{K}_{jii}(r) = \begin{cases} 1 & (d_{ij} = 0) \\ e^{-(r\sqrt{d_{ij}})} & (d_{ij} \neq 0) \end{cases} \quad (43)$$

$$\mathbf{m}_{ji}(r) = \begin{cases} -\frac{\mathbf{v}_{ji}r^2}{2} & (d_{ij} = 0) \\ \frac{\mathbf{v}_{ji}}{d_{ij}} & (d_{ij} \neq 0) \end{cases} \quad (44)$$

To calculate the radial or horizontal discharge, the first derivative of \mathbf{g} with respect to r is needed:

$$\nabla \mathbf{g}_j(r) = \mathbf{I}'_j(r)\boldsymbol{\alpha}_j + \mathbf{K}'_j(r)\boldsymbol{\beta}_j + \mathbf{m}'_j(r) \quad (45)$$

with \mathbf{I}'_j and \mathbf{K}'_j $n_l \times n_l$ diagonal matrices, and \mathbf{m}'_j an $n_l \times 1$ vector. In case of axisymmetric flow, $\nabla \mathbf{g}_j = r \frac{\partial \mathbf{g}_j}{\partial r}$, and the nonzero entries of \mathbf{I}'_j , \mathbf{K}'_j , and \mathbf{m}'_j are defined as, respectively:

$$\mathbf{I}'_{jii}(r) = \begin{cases} 1 & (d_{ij} = 0) \\ \left(r\sqrt{d_{ij}}\right)\text{I}_1\left(r\sqrt{d_{ij}}\right) & (d_{ij} \neq 0) \end{cases} \quad (46)$$

$$\mathbf{K}'_{jii}(r) = \begin{cases} 0 & (d_{ij} = 0) \\ -\left(r\sqrt{d_{ij}}\right)\text{K}_1\left(r\sqrt{d_{ij}}\right) & (d_{ij} \neq 0) \end{cases} \quad (47)$$

$$\mathbf{m}'_{ji}(r) = \begin{cases} -\frac{\nu_{ji}r^2}{2} & (d_{ij} = 0) \\ 0 & (d_{ij} \neq 0) \end{cases} \quad (48)$$

Functions I_1 and K_1 are the first order modified Bessel functions of the first and second kind, respectively. In case of parallel flow, $\nabla \mathbf{g}_j = \frac{\partial \mathbf{g}_j}{\partial r}$, and these nonzero entries are:

$$\mathbf{I}'_{jii}(r) = \begin{cases} 1 & (d_{ij} = 0) \\ \left(\sqrt{d_{ij}}\right)e^{(r\sqrt{d_{ij}})} & (d_{ij} \neq 0) \end{cases} \quad (49)$$

$$\mathbf{K}'_{jii}(r) = \begin{cases} 0 & (d_{ij} = 0) \\ -\left(\sqrt{d_{ij}}\right)e^{-(r\sqrt{d_{ij}})} & (d_{ij} \neq 0) \end{cases} \quad (50)$$

$$\mathbf{m}'_{ji}(r) = \begin{cases} -\nu_{ji}r & (d_{ij} = 0) \\ 0 & (d_{ij} \neq 0) \end{cases} \quad (51)$$

5.3.3. Particular solutions

In (38) and (45), vectors $\boldsymbol{\alpha}_j$ and $\boldsymbol{\beta}_j$ contain unknown constants that are determined by applying the boundary conditions. Therefore, these conditions need to be rewritten as a function of \mathbf{g} . The constant-head boundary conditions at outer and inner model boundary (25) and (28) are reformulated as, respectively:

$$\mathbf{V}_{n_z}\mathbf{g}_{n_z}(R_{n_z}) = \boldsymbol{\varphi}_{n_z} \quad (52)$$

$$\mathbf{V}_1\mathbf{g}_1(R_0) = \mathbf{H} \quad (53)$$

If the inner boundary conditions define constant discharges, then condition (31) is replaced by:

$$\mathbf{T}_1\mathbf{V}_1\nabla\mathbf{g}_1(R_0) = -\mathbf{Q} \quad (54)$$

Boundary conditions (34) and (35) between zones j and $j + 1$ are also written as a function of \mathbf{g} :

$$\mathbf{V}_j\mathbf{g}_j(R_j) = \mathbf{V}_{j+1}\mathbf{g}_{j+1}(R_j) \quad (1 \leq j < n_z) \quad (55)$$

$$\mathbf{T}_j\mathbf{V}_j\nabla\mathbf{g}_j(R_j) = \mathbf{T}_{j+1}\mathbf{V}_{j+1}\nabla\mathbf{g}_{j+1}(R_j) \quad (1 \leq j < n_z) \quad (56)$$

Using (38) and (45), vectors $\mathbf{V}_j\mathbf{g}_j$ and $\mathbf{T}_j\mathbf{V}_j\nabla\mathbf{g}_j$ are written as a function of vectors $\boldsymbol{\alpha}_j$ and $\boldsymbol{\beta}_j$:

$$\mathbf{V}_j\mathbf{g}_j(r) = \mathbf{X}_j(r)\boldsymbol{\alpha}_j + \mathbf{Y}_j(r)\boldsymbol{\beta}_j + \mathbf{z}_j(r) \quad (57)$$

$$\mathbf{T}_j\mathbf{V}_j\nabla\mathbf{g}_j(r) = \mathbf{X}'_j(r)\boldsymbol{\alpha}_j + \mathbf{Y}'_j(r)\boldsymbol{\beta}_j + \mathbf{z}'_j(r) \quad (58)$$

with $\mathbf{X}_j = \mathbf{V}_j\mathbf{I}_j$; $\mathbf{Y}_j = \mathbf{V}_j\mathbf{K}_j$; $\mathbf{z}_j = \mathbf{V}_j\mathbf{m}_j$; $\mathbf{X}'_j = \mathbf{T}_j\mathbf{V}_j\mathbf{I}'_j$; $\mathbf{Y}'_j = \mathbf{T}_j\mathbf{V}_j\mathbf{K}'_j$; $\mathbf{z}'_j = \mathbf{T}_j\mathbf{V}_j\mathbf{m}'_j$.

All boundary conditions taken together yields a system of $2n$ equations. If constant heads are defined at the inner model boundary, this system of equations is:

$$\begin{cases} -X_1\alpha_1 - Y_1\beta_1 = z_1 - H & (r = R_0) \\ X_j\alpha_j + Y_j\beta_j - X_{j+1}\alpha_{j+1} - Y_{j+1}\beta_{j+1} = z_{j+1} - z_j & (r = R_j; 1 \leq j < n_z) \\ X'_j\alpha_j + Y'_j\beta_j - X'_{j+1}\alpha_{j+1} - Y'_{j+1}\beta_{j+1} = z'_{j+1} - z'_j & (r = R_j; 1 \leq j < n_z) \\ X_{n_z}\alpha_{n_z} + Y_{n_z}\beta_{n_z} = \varphi_{n_z} - z_{n_z} & (r = R_{n_z}) \end{cases} \quad (59)$$

In case of specified discharges at the inner boundary, the system of equations is:

$$\begin{cases} -X'_1\alpha_1 - Y'_1\beta_1 = z'_1 + Q & (r = R_0) \\ X_j\alpha_j + Y_j\beta_j - X_{j+1}\alpha_{j+1} - Y_{j+1}\beta_{j+1} = z_{j+1} - z_j & (r = R_j; 1 \leq j < n_z) \\ X'_j\alpha_j + Y'_j\beta_j - X'_{j+1}\alpha_{j+1} - Y'_{j+1}\beta_{j+1} = z'_{j+1} - z'_j & (r = R_j; 1 \leq j < n_z) \\ X_{n_z}\alpha_{n_z} + Y_{n_z}\beta_{n_z} = \varphi_{n_z} - z_{n_z} & (r = R_{n_z}) \end{cases} \quad (60)$$

Solving (59) or (60) gives the integration constants which are the entries of vectors α_j and β_j :

$$\gamma = M^{-1}\omega \quad (61)$$

where vector γ in (61) contains the $2n$ unknown integration constants:

$$\gamma = \begin{bmatrix} \beta_1 \\ \alpha_1 \\ \vdots \\ \beta_{n_z} \\ \alpha_{n_z} \end{bmatrix} \quad (62)$$

The $2n \times 2n$ entries in matrix M are the known coefficients:

$$M = \begin{bmatrix} -M_{10} & \mathbf{0} & \cdots & \cdots & \mathbf{0} \\ M_{11} & -M_{21} & \mathbf{0} & & \vdots \\ \mathbf{0} & M_{22} & -M_{32} & \mathbf{0} & \\ \vdots & \mathbf{0} & & & \vdots \\ \vdots & & \mathbf{0} & M_{n_z-1,n_z-1} & -M_{n_z,n_z-1} \\ \mathbf{0} & \cdots & \cdots & \mathbf{0} & M_{n_z,n_z} \end{bmatrix} \quad (63)$$

with:

$$M_{10} = [Y_1(R_0) \quad X_1(R_0)] \quad \text{or} \quad M_{10} = [Y'_1(R_0) \quad X'_1(R_0)] \quad (64)$$

$$M_{jk} = \begin{bmatrix} Y_j(R_k) & X_j(R_k) \\ Y'_j(R_k) & X'_j(R_k) \end{bmatrix} \quad (0 < k < n_z; j \in \{k, k+1\}) \quad (65)$$

$$M_{n_z,n_z} = [Y_{n_z}(R_{n_z}) \quad X_{n_z}(R_{n_z})] \quad (66)$$

In (64), the expression on the left is used when constant heads are defined at the inner model boundary, whereas the expression on the right is used in the case of specified discharges. The entries of vector ω in (61) are the $2n$ known terms in the right-hand side of the equations in (59) or (60), respectively:

$$\boldsymbol{\omega} = \begin{bmatrix} \mathbf{z}_1(R_0) - \mathbf{H} \\ \mathbf{z}_2(R_1) - \mathbf{z}_1(R_1) \\ \mathbf{z}'_2(R_1) - \mathbf{z}'_1(R_1) \\ \vdots \\ \mathbf{z}_{n_z}(R_{n_z-1}) - \mathbf{z}_{n_z-1}(R_{n_z-1}) \\ \mathbf{z}'_{n_z}(R_{n_z-1}) - \mathbf{z}'_{n_z-1}(R_{n_z-1}) \\ \boldsymbol{\varphi}_{n_z} - \mathbf{z}_{n_z}(R_{n_z}) \end{bmatrix} \text{ or } \boldsymbol{\omega} = \begin{bmatrix} \mathbf{z}'_1(R_0) + \mathbf{Q} \\ \mathbf{z}_2(R_1) - \mathbf{z}_1(R_1) \\ \mathbf{z}'_2(R_1) - \mathbf{z}'_1(R_1) \\ \vdots \\ \mathbf{z}_{n_z}(R_{n_z-1}) - \mathbf{z}_{n_z-1}(R_{n_z-1}) \\ \mathbf{z}'_{n_z}(R_{n_z-1}) - \mathbf{z}'_{n_z-1}(R_{n_z-1}) \\ \boldsymbol{\varphi}_{n_z} - \mathbf{z}_{n_z}(R_{n_z}) \end{bmatrix} \quad (67)$$

The expression on the left in (67) holds for the case in which constant heads are defined at the inner model boundary, whereas the expression on the right is used in case of the specified discharges.

The next section discusses how to solve system (61). Once the integration constants α_j and β_j are determined for all j , hydraulic heads for all zones j , for all layers i , and at any given distance r , are found by evaluating:

$$\mathbf{h}_j(r) = \mathbf{V}_j \mathbf{g}_j(r) \quad (68)$$

Horizontal discharges for all zones j , for all layers i , and at any given distance r , are found by evaluating:

$$\mathbf{q}_j^h(r) = -\mathbf{T}_j \mathbf{V}_j \nabla \mathbf{g}_j(r) \quad (69)$$

In the transient-state case, the Laplace transformed heads \mathbf{h}_j and Laplace transformed discharges \mathbf{q}_j^h need to be inverted to the real time domain. This is done numerically by applying the Stehfest (1970) algorithm.

The principle of superposition may be applied to simulate time-dependent stresses at the inner model boundary as explained in section 2.4 of Chapter 2. Because of the radial variations in hydraulic parameters, superposition in space is generally not possible.

5.3.4. Finding the integration constants

In this section, two methods are discussed to solve system of equations (61) in order to find the integration constants α_j and β_j for all zones j . The first method is similar to the Thomas (1949) algorithm for solving tridiagonal matrix systems. Just like the Thomas (1949) algorithm, a simplified form of Gaussian elimination is applied, consisting of a forward and a backward sweep to obtain a diagonal matrix. There are, however, two differences compared with the Thomas (1949) algorithm. First, matrix \mathbf{M} is pentadiagonal instead of tridiagonal, as some of the entries on the second upper and lower diagonal are nonzero. Second, the entries of \mathbf{M} are $n_l \times n_l$ submatrices, as are all intermediate variables declared in the algorithm.

Before starting the algorithm, the number of zones N is determined in which integration constants α_j and β_j are nonzero. These are the zones in which a change of head occurs. If there is no head change in zone j , then $r\sqrt{d_{ij}} \rightarrow \infty$ in all layers i , and at all distances r for which $R_{j-1} \leq r \leq R_j$. This may be the case for large distances and/or for small values of time since $p \rightarrow \infty$ if $t \rightarrow 0$. As in this case, $I_{jii}(r) \rightarrow \infty$ and $I'_{jii}(r) \rightarrow \infty$ for all i , integration constants α_{ji} must be zero. As $K_{jii}(r) \rightarrow 0$ and $K'_{jii}(r) \rightarrow 0$ for all i , integration constants β_{ji} cannot be determined and are also set to zero. This is true for both axisymmetric and parallel flow. If there is no head change in zone j , there is no head change in all subsequent zones k either, where $j < k \leq n_z$. This means that only the first N zones should be involved in the algorithm, where N is also the index of the last zone for which both α_j and β_j are nonzero. In practice, N is determined by searching the first zone for which matrix

$\mathbf{X}_{N+1}(R_N)$ or $\mathbf{X}'_{N+1}(R_N)$ contains at least one infinitely large value, and for which matrix $\mathbf{X}_{N+1}(R_{N+1})$ or $\mathbf{X}'_{N+1}(R_{N+1})$ contains at least one infinitely large value.

Once the number of relevant zones N is found, the algorithm is started by initializing matrices \mathbf{G}'_0 and \mathbf{H}'_0 . In case of specified discharges at the inner model boundary, they are calculated as follows:

$$\mathbf{G}'_0 = \mathbf{Y}'_{10}^{-1} \mathbf{X}'_{10} \quad (70)$$

$$\mathbf{H}'_0 = -\mathbf{Y}'_{10}^{-1} (\mathbf{z}'_{10} + \mathbf{Q}) \quad (71)$$

In case of specified heads:

$$\mathbf{G}'_0 = \mathbf{Y}_{10}^{-1} \mathbf{X}_{10} \quad (72)$$

$$\mathbf{H}'_0 = -\mathbf{Y}_{10}^{-1} (\mathbf{z}_{10} - \mathbf{H}) \quad (73)$$

Note that \mathbf{X}_{ij} , \mathbf{Y}_{ij} , \mathbf{z}_{ij} , \mathbf{X}'_{ij} , \mathbf{Y}'_{ij} , and \mathbf{z}'_{ij} are short notations for $\mathbf{X}_i(R_j)$, $\mathbf{Y}_i(R_j)$, $\mathbf{z}_i(R_j)$, $\mathbf{X}'_i(R_j)$, $\mathbf{Y}'_i(R_j)$, and $\mathbf{z}'_i(R_j)$, respectively.

Once \mathbf{G}'_0 and \mathbf{H}'_0 are initialized, the forward sweep can be executed, starting with $k = 1$:

$$\begin{cases} \mathbf{L}_k = [\mathbf{Y}_{kk}^{-1} \mathbf{X}_{kk} - \mathbf{G}'_{k-1}]^{-1} \\ \mathbf{F}_k = -\mathbf{L}_k \mathbf{Y}_{kk}^{-1} \mathbf{Y}_{k+1,k} \\ \mathbf{G}_k = -\mathbf{L}_k \mathbf{Y}_{kk}^{-1} \mathbf{X}_{k+1,k} \\ \mathbf{H}_k = \mathbf{L}_k [\mathbf{Y}_{kk}^{-1} (\mathbf{z}_{k+1,k} - \mathbf{z}_{kk}) - \mathbf{H}'_{k-1}] \\ \mathbf{L}'_k = [\mathbf{Y}'_{kk}^{-1} \mathbf{X}'_{kk} - \mathbf{G}'_{k-1}]^{-1} \\ \mathbf{F}'_k = -\mathbf{L}'_k \mathbf{Y}'_{kk}^{-1} \mathbf{Y}'_{k+1,k} - \mathbf{F}_k \\ \mathbf{G}'_k = -\mathbf{F}'_k^{-1} [\mathbf{L}'_k \mathbf{Y}'_{kk}^{-1} \mathbf{X}'_{k+1,k} + \mathbf{G}_k] \\ \mathbf{H}'_k = \mathbf{F}'_k^{-1} \{ \mathbf{L}'_k [\mathbf{Y}'_{kk}^{-1} (\mathbf{z}'_{k+1,k} - \mathbf{z}'_{kk}) - \mathbf{H}'_{k-1}] - \mathbf{H}_k \} \end{cases} \quad k = 1, \dots, N-1 \quad (74)$$

The forward sweep ends with $k = N$:

$$\begin{cases} \mathbf{L}_N = [\mathbf{Y}_{NN}^{-1} \mathbf{X}_{NN} - \mathbf{G}'_{N-1}]^{-1} \\ \mathbf{H}_N = \mathbf{L}_N [\mathbf{Y}_{NN}^{-1} (\boldsymbol{\omega}_N - \mathbf{z}_{NN}) - \mathbf{H}'_{N-1}] \end{cases} \quad (75)$$

The back substitution starts with $k = N$:

$$\begin{cases} \boldsymbol{\alpha}_N = \mathbf{H}_N \\ \boldsymbol{\beta}_N = \mathbf{H}'_{N-1} - \mathbf{G}'_{N-1} \boldsymbol{\alpha}_N \end{cases} \quad (76)$$

It continues until $k = 1$:

$$\begin{cases} \boldsymbol{\alpha}_k = \mathbf{H}_k - \mathbf{F}_k \boldsymbol{\beta}_{k+1} - \mathbf{G}_k \boldsymbol{\alpha}_{k+1} \\ \boldsymbol{\beta}_k = \mathbf{H}'_{k-1} - \mathbf{G}'_{k-1} \boldsymbol{\alpha}_k \end{cases} \quad k = N-1, \dots, 1 \quad (77)$$

It is possible the outer boundary of last zone N gives infinitely large values. Indeed, if $R_N \sqrt{d_{i,N}} \rightarrow \infty$, then $I_0(R_N \sqrt{d_{i,N}}) \rightarrow \infty$; hence $\boldsymbol{\alpha}_N = \mathbf{0}$. In this case, the final step (75) of the forward sweep is skipped, and \mathbf{G}'_{N-1} is not calculated.

The algorithm works fine as long as the system matrices \mathbf{A}_j are not singular. This is not the case, for instance, if steady flow is considered in a confined aquifer system. Alternatively, solving (61) can be done by applying a standard linear equation solver, for instance, SciPy function ‘solve’ (Peterson et al., 2022). In this case, matrix \mathbf{M} and vector $\boldsymbol{\omega}$ are also restricted to the first N zones. If $R_N \sqrt{d_{i,N}} \rightarrow \infty$,

∞ , then the last n_l rows and n_l columns are removed from the restricted matrix \mathbf{M} , as are the last n_l elements from restricted vector $\boldsymbol{\omega}$. A more convenient way to ignore the zero integration constants, is to look for the first occurrence of an infinitely large value in matrix \mathbf{M} , after which all subsequent rows and columns are removed from the matrix system. After these operations, \mathbf{M} is an $N \times N$ matrix where $N = \min_{i,j}(\mathbf{M}_{ij} = \infty)$.

A final note on implementing these algorithms involves the limits of expressions containing modified Bessel or exponential functions. Although program languages for scientific computing such as Matlab or Python can deal with infinitely large values, it is still possible some calculations result into NaN-values, where NaN stands for ‘Not-a-Number’. For instance, calculating $I_0(\infty)$ or $(-\infty)e^{-\infty}$ using NumPy and SciPy returns NaN in both cases. Therefore, it is important to check matrices \mathbf{I}_j , \mathbf{K}_j , \mathbf{I}'_j , and \mathbf{K}'_j for NaN-values, and replace them appropriately according to the limits given in Table 1. The correctness of these limits can be verified easily.

Table 1. Limits of expressions involving modified Bessel functions and exponential functions. The first are relevant for solving problems of axisymmetric flow, the latter for solving parallel flow problems.

	$I_0(x)$	$K_0(x)$	$xI_1(x)$	$xK_1(x)$	e^x	e^{-x}	xe^x	$-xe^{-x}$
$x \rightarrow 0$	1	∞	0	1	1	1	0	0
$x \rightarrow \infty$	∞	0	∞	0	∞	0	∞	0

5.4. Finite-difference approach

The finite-difference approach presented in Chapter 3 can also be applied without any modification to solve the problem stated in section 5.2. In fact, the finite-difference method is very well-suited for taking into account aquifer heterogeneities, as it is straightforward to assign hydraulic parameter values to each individual cell in the finite-difference grid. As a consequence, it is easy to include lateral variations of those parameters. As explained in section 3.4 of Chapter 3, it is also possible to trick MODFLOW into simulating axisymmetric flow. However, the method presented by Langevin (2008) is not recommended for radially nonuniform systems, whereas the method by Louwyck et al. (2012) is easily applicable.

This is clearly demonstrated by Louwyck et al. (2014) who verify the MODFLOW procedure developed by Louwyck et al. (2012) against several analytical models with radially varying aquifer parameters (Butler, 1988; Kitterød, 2004; Şen, 2014). Louwyck et al. (2014) also simulate a synthetic pumping test conducted in a well with finite-thickness skin and clay seal that partially penetrates an aquifer that is part of a larger multi-aquifer system. The MODFLOW results are compared with those simulated using the analytic element solver TTIm (Bakker, 2013), and it is concluded that the MODFLOW procedure is accurate.

However, to obtain accurate results applying the finite-difference method, it is necessary to discretize each zone into a number of grid cells. As already discussed in Chapter 3, it is common practice to discretize the radial dimension into logarithmically spaced distances if axisymmetric flow is simulated. In case of multiple zones characterized by different hydraulic parameters, the radial discretization should be performed for each individual zone. If zone j between R_{j-1} and R_j must be discretized into $n_{r,j}$ cells, then a very small width δ [L] is assigned to the first and last cell in order to accurately simulate flow between zone j and its neighboring zones. The distances $r_{b,j,k}$ [L] of the boundaries of the remaining $n_{r,j} - 2$ cells between $R_{j-1} + \delta$ and $R_j - \delta$ may be calculated as follows:

$$r_{b,j,k+1} = R_{j-1} + 10^{(\log_{10}(\delta) + k\Delta)} \quad (0 \leq k \leq n_{r,j} - 2) \quad (78)$$

with:

$$\Delta = \frac{\log_{10}(R_j - R_{j-1} - \delta) + \log_{10}(\delta)}{n_{r,j} - 2} \quad (79)$$

Note that $R_{j-1} = r_{b,j,0}$ and $R_j = r_{b,j,n_{r,j}+1}$. Alternatively, an expansion factor $a_{r,j}$ greater than 1 may be defined, in which case expressions (78) and (79) are replaced by:

$$r_{b,j,k+1} = R_{j-1} + \delta + \sum_{i=1}^k a_{r,j}^{i-1} \Delta \quad (0 \leq k \leq n_{r,j} - 2) \quad (80)$$

with:

$$\Delta = (R_j - R_{j-1} - 2\delta) \left(\frac{a_{r,j} - 1}{a_{r,j}^{n_{r,j}-2} - 1} \right) \quad (81)$$

This discretization scheme is applied by MODFLOW to determine the time steps within a stress period (Harbaugh, 2005; Harbaugh et al., 2000).

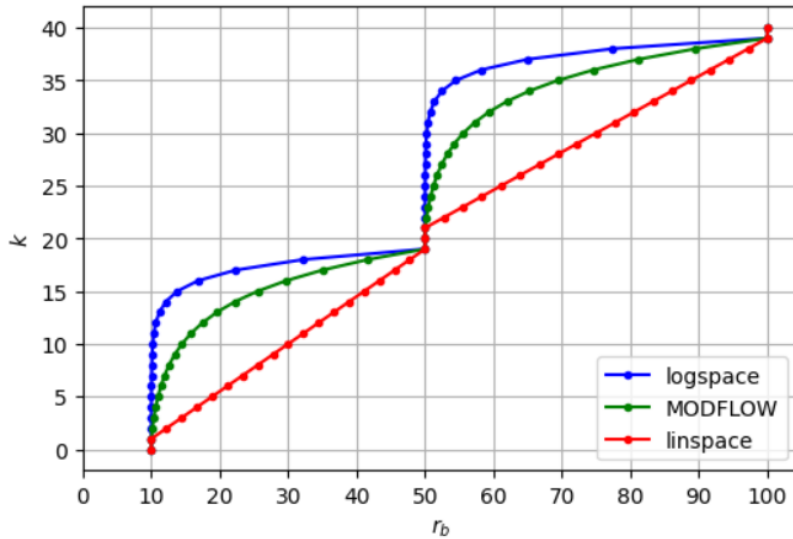


Figure 2. Comparing the three discretization schemes for the horizontal or radial distance discussed in the text: *logspace*, *MODFLOW*, and *linspace*. The three schemes are applied to two zones with boundaries at 10 m, 50 m, and 100 m. Each zone is discretized into 20 cells with boundaries r_b and indices k . The width of the first and last cell in each zone is 0.001 m. The *MODFLOW* scheme applies an expansion factor of $10^{0.1}$. See text for definition of the discretization schemes.

Both schemes may also be used in case of parallel flow. In this case, it is also possible to define linearly spaced distances:

$$r_{b,j,k+1} = R_{j-1} + \delta + k\Delta \quad (0 \leq k \leq n_{r,j} - 2) \quad (82)$$

with:

$$\Delta = \frac{R_j - R_{j-1} - 2\delta}{n_{r,j} - 2} \quad (83)$$

Expressions (82) and (83) replace expressions (78) and (79), respectively. Using NumPy or Matlab, function ‘*linspace*’ may be used to calculate the first, and function ‘*logspace*’ to calculate the latter.

In both cases, the start and stop value are $R_{j-1} + \delta$ and $R_j - \delta$, respectively, and the number of points is $n_{r,j} - 1$.

To have an idea of how the distances r_b are spaced according to the three proposed schemes, Figure 2 shows an example of two zones, where each zone is discretized into $n_r = 20$ cells. The first zone is between 10 m and 50 m; the second zone between 50 m and 100 m. In both zones, the width of the first and last cell is $\delta = 10^{-3}$. The ‘logspace’ scheme corresponds to expressions (78) and (79), the ‘MODFLOW’ scheme to expressions (80) and (81), and the ‘linspace’ scheme to expressions (82) and (83). In case of the ‘MODFLOW’ scheme, an expansion factor $a_r = 10^{0.1}$ is used for both zones.

In next section 5.5, the finite-difference method is used to test the semi-analytical solution developed in section 5.3. In all test cases, the ‘logspace’ scheme is applied. The width δ is mostly set to 10^{-4} , and the number of cells $n_{r,j}$ within each zone j is mostly equal to 50.

5.5. Verification

This section discusses some analytical solutions for groundwater flow models that consider two or more cylindrical zones. These solutions may be regarded as special cases of the generalized multilayer-multizone solution presented in section 5.3, and therefore, they are excellent test cases, especially if they apply a different approach to solve the boundary-value problem. Besides these analytical solutions, the finite-difference solution is also used to test the generalized solution, as explained in previous section 5.4.

In the first test cases, steady flow to a well in the middle of a circular infiltration area is simulated. The one-layer solution is well-known and discussed, for instance, by Strack (1989) and Haitjema (1995). Although the semi-analytical multilayer solution was presented first by Hunt (1986), the solution developed by Bakker and Strack (2003) is used here to verify the generalized multilayer-multizone solution. The second test case solves a similar problem using the formula of Blom (1973) which combines the solution for a circular infiltration pond in a single aquifer with the solution for a large-diameter well in a leaky aquifer.

The third test case involves steady flow to a fully penetrating pumping well or stream in a confined aquifer consisting of multiple zones. Both axisymmetric and parallel flow are considered, and the solutions for specified-discharge as well as specified-head conditions at the inner model boundary are developed. Deriving these solutions is straightforward and can be done simply by hand. The analytical steady state solution for a fully penetrating pumping well in a leaky aquifer is more involved, and therefore, this model is restricted to two zones. This solution presented in the fourth test case extends the well-known de Glee (1930) formula to the more general case of a well with finite-thickness skin extracting a leaky aquifer.

The next test case discusses the semi-analytical solution developed by Butler (1988) that considers transient flow toward a pumping well in a confined aquifer consisting of two zones. The solution method also applies the Laplace transform, and performs the inversion numerically using the Stehfest (1970) algorithm. In fact, the generalized multilayer-multizone solution would simplify to Butler’s (1988) solution if only one confined layer and two zones is considered. The approximate solution for large values of time was presented earlier by Barker and Herbert (1982).

In all of these examples, the well-face coincides with the inner model boundary and the pumping well itself is not part of the model domain but simplified to a constant-discharge boundary condition. In the next test case, the well is conceptualized as a separate zone in the model to which a high transmissivity value is assigned. In this way, it is possible to consider the wellbore storage, which is

illustrated by the Cooper et al. model (1967) for simulating a slug test conducted in a finite-diameter well fully penetrating a confined aquifer. The ‘high-transmissivity’ approach can also be applied to simulate more accurately the draining or irrigating effect of a wide embanked river interacting with a multi-aquifer system, which is demonstrated in the final test case.

5.5.1. Circular infiltration area

As already mentioned, the solution for a circular infiltration pond situated in the top aquifer of a multilayered aquifer system is presented first by Hunt (1986), who solves a generalized eigenvalue problem numerically to obtain closed-form solutions for steady flow in leaky multilayer aquifer systems. The method described by Hunt (1986) is similar to the method presented by Hemker (1984) to simulate steady well-flow in a leaky multi-aquifer system without recharge. Inspired by previous work of Hemker (1984), Hunt (1986), and Strack (1989), analytic element equations for wells, line sinks, and circular infiltration areas to simulate groundwater flow in multi-aquifer systems were developed by Bakker and Strack (2003). Applying the principle of superposition, these elements are combined to simulate regional multi-aquifer flow.

In this section, the analytic element solutions for a well and a circular infiltration pond presented by Bakker and Strack (2003) are used to solve the problem of steady axisymmetric flow towards a well located in the center of a circular infiltration pond that recharges a bounded multilayer aquifer system. The obtained solution is compared with the generalized multilayer-multizone solution method presented in section 5.3.

5.5.1.1. Problem statement

Consider an arbitrary number of n_l layers, and two cylindrical zones, i.e. $n_z = 2$. The proximal zone conceptualizes an infiltration pond, which is recharged at constant flux N , while there is no infiltration in the distal zone. As steady flow is simulated and only two zones are considered, system of partial differential equations (4) simplifies to the following two sets of ordinary differential equations:

$$\begin{cases} \frac{d^2 h_{i,1}}{dr^2} + \frac{1}{r} \frac{dh_{i,1}}{dr} = \frac{-N}{T_i} + \frac{h_{i,1} - h_{i-1,1}}{c_{i-1} T_i} + \frac{h_{i,1} - h_{i+1,1}}{c_i T_i} & (1 \leq i \leq n_l; R_0 \leq r \leq R_1) \\ \frac{d^2 h_{i,2}}{dr^2} + \frac{1}{r} \frac{dh_{i,2}}{dr} = \frac{h_{i,2} - h_{i-1,2}}{c_{i-1} T_i} + \frac{h_{i,2} - h_{i+1,2}}{c_i T_i} & (1 \leq i \leq n_l; R_1 \leq r \leq R_2) \end{cases} \quad (84)$$

Recall that subscript i is the layer number, whereas subscript 1 refers to the zone with recharge, and subscript 2 to the zone without recharge. The aquifer system has an impermeable bottom and a phreatic top layer; hence, $c_0 = c_{n_l} = \infty$.

The circular infiltration pond has a radius equal to R_1 , which is also the distance of the boundary between the two zones. At the boundary between zones 1 and 2 in layer i , hydraulic head and radial flow cannot be discontinuous. Internal boundary conditions (12) and (13) reduce to, respectively:

$$h_{i,1}(R_1) = h_{i,2}(R_1) \quad (1 \leq i \leq n_l) \quad (85)$$

$$Q_{i,1}^h(R_1) = Q_{i,2}^h(R_1) \quad (1 \leq i \leq n_l) \quad (86)$$

A constant head φ [L] is defined at the outer model boundary at distance R_2 ; hence, outer boundary conditions (9) reduces to:

$$h_{i,2}(R_2) = \varphi \quad (1 \leq i \leq n_l) \quad (87)$$

The inner boundary of the aquifer system is at distance R_0 [L], the radius of the well, at which a specified discharge Q_i is defined for each layer i . As it is assumed the well has an infinitesimal radius, inner boundary conditions (11) are reformulated as:

$$\lim_{R_0 \rightarrow 0} Q_{i,1}^h(R_0) = Q_i \quad (1 \leq i \leq n_l) \quad (88)$$

Recall that Q_i is positive if water is added to the aquifer system.

5.5.1.2. Solution

Because transmissivities T_i and resistances c_i are the same for both zones 1 and 2, the respective system matrices are also the same. Bakker and Strack (2003) formulate the problem in terms of discharge potentials $\phi_i = T_i h_i$ [L^3/T]. As a consequence, the resulting system matrix \mathbf{A} is the transpose of the matrix defined by (15):

$$A_{ik} = \begin{cases} \frac{1}{c_{i-1}T_i} + \frac{1}{c_iT_i} & (i = k) \\ \frac{-1}{c_iT_i} & (i = k+1) \\ \frac{-1}{c_{i-1}T_i} & (i = k-1) \end{cases} \quad (89)$$

Recall that $c_0 = c_{n_l} = \infty$. As steady flow is considered, there is one eigenvalue equal to zero that corresponds to the comprehensive potential, which is defined as the sum of the potentials of all aquifers (Bakker, 2001; Bakker & Strack, 2003). Chapter 9 elaborates on the concept of the comprehensive potential. The eigenvectors of the $n_l - 1$ nonzero eigenvalues d_i are put in the columns of matrix \mathbf{V} , which means it has n_l rows and $n_l - 1$ columns. Bakker and Strack (2003) also define vector $\boldsymbol{\tau}$:

$$\boldsymbol{\tau}_i = T_i / \sum_{k=1}^{n_l} T_k \quad (1 \leq i \leq n_l) \quad (90)$$

Expression (90) defines the i -th entry in vector $\boldsymbol{\tau}$ as the relative transmissivity of layer i .

The superposition principle is applied to calculate the total head change due to infiltration and pumping in each layer. Vector \mathbf{s}_p containing the drawdowns s_i [L] due to the extraction of groundwater at constant rate Q_p in layer p is determined as follows:

$$\mathbf{s}_p(r) = \left\{ Q_p \ln\left(\frac{R_2}{r}\right) \boldsymbol{\tau} + \mathbf{V}[\mathbf{K}(R_2) - \mathbf{K}(r)] \mathbf{a}_p \right\} \mathbf{T}^{-1} \quad (1 \leq p \leq n_l) \quad (91)$$

with \mathbf{K} a diagonal matrix with $n_l - 1$ rows and columns, and with nonzero diagonal entries $K_{ii}(r) = K_0(r\sqrt{d_i})$. Recall that \mathbf{T} is an $n_l \times n_l$ diagonal matrix with $T_{ii} = 2\pi T_i$. Vector \mathbf{a}_p contains $n_l - 1$ constants that are determined by solving the following system of equations:

$$\mathbf{a}_p = Q_p \mathbf{V}_{\neq p}^{-1} \boldsymbol{\tau}_{\neq p} \quad (1 \leq p \leq n_l) \quad (92)$$

with Q_p the pumping rate assigned to the well screen in layer p , whereas subscript $\neq p$ means that the p -th row is omitted in \mathbf{V} and the p -th element is removed from $\boldsymbol{\tau}$. Note that the first term in (91) is the Thiem (1870, 1906) formula that computes the drawdown in the corresponding aquifer system with comprehensive transmissivity $\sum_{k=1}^{n_l} T_k$.

The head change s_N [L] caused by the infiltration pond is:

$$\mathbf{s}_N(r) = \begin{cases} 2\pi \left\{ N \left[\frac{(R_1^2 - r^2)}{4} + \frac{R_1^2}{2} \ln \left(\frac{R_2}{R_1} \right) \right] \boldsymbol{\tau} + \mathbf{V}[\mathbf{Z}(R_2) - \mathbf{U}(r)] \mathbf{a}_N \right\} \mathbf{T}^{-1} & (0 < r \leq R_1) \\ 2\pi \left\{ N \frac{R_1^2}{2} \left[\ln \left(\frac{R_1}{r} \right) + \ln \left(\frac{R_2}{R_1} \right) \right] \boldsymbol{\tau} + \mathbf{V}[\mathbf{Z}(R_2) - \mathbf{Z}(r)] \mathbf{a}_N \right\} \mathbf{T}^{-1} & (R_1 < r \leq R_2) \end{cases} \quad (93)$$

with \mathbf{U} and \mathbf{Z} diagonal matrices with $n_l - 1$ rows and columns, and with nonzero diagonal entries $\mathbf{U}_{ii}(r) = [1/(R_1\sqrt{d_i}) - K_1(R_1\sqrt{d_i})I_0(r\sqrt{d_i})]$ and $\mathbf{Z}_{ii}(r) = I_1(R_1\sqrt{d_i})K_0(r\sqrt{d_i})$, respectively. Vector \mathbf{a}_N is found by solving the following matrix system:

$$\mathbf{a}_N = NR_1 \mathbf{L} \mathbf{V}_{\neq 1}^{-1} \boldsymbol{\tau}_{\neq 1} \quad (94)$$

where subscript $\neq 1$ means that the first row is removed from \mathbf{V} and the first element from $\boldsymbol{\tau}$. Matrix \mathbf{L} is a diagonal matrix with $n_l - 1$ rows and columns, and with nonzero diagonal entries $L_{ii} = 1/\sqrt{d_i}$. Again, the first term in the equations of (93) corresponds to the comprehensive one-layer solution.

The head \mathbf{h} is finally obtained through superposition of the solutions for wells (91) and infiltration pond (93):

$$\mathbf{h}(r) = \varphi + \mathbf{s}_N(r) + \sum_{p=1}^{n_l} \mathbf{s}_p(r) \quad (95)$$

If there is no well in layer p , then \mathbf{s}_p is set to zero. If only one layer is considered, then solution (95) reduces to:

$$h(r) = \begin{cases} \varphi + \frac{N}{T} \left[\frac{(R_1^2 - r^2)}{4} + \frac{R_1^2}{2} \ln \left(\frac{R_2}{R_1} \right) \right] + \frac{Q}{2\pi T} \ln \left(\frac{R_2}{r} \right) & (0 < r \leq R_1) \\ \varphi + \frac{NR_1^2}{T} \left[\ln \left(\frac{R_1}{r} \right) + \ln \left(\frac{R_2}{R_1} \right) \right] + \frac{Q}{2\pi T} \ln \left(\frac{R_2}{r} \right) & (R_1 < r \leq R_2) \end{cases} \quad (96)$$

Solution (96) is also found in Strack (1989) and in Haitjema (1995).

In case of two layers, the comprehensive head h_{tot} is calculated first using the corresponding one-layer solution (96) in which $T = T_1 + T_2$ and $Q = Q_1 + Q_2$. Using the multilayer solutions (91) and (93), the additional terms are found that determine the head difference between the two layers due to pumping and infiltration. The resulting head h_1 in the upper layer is:

$$h_1(r) = \begin{cases} h_{tot}(r) + \frac{NT_2R_1}{T_1T\sqrt{d}} \left[\frac{1}{R_1\sqrt{d}} - K_1(R_1\sqrt{d})I_0(r\sqrt{d}) - I_1(R_1\sqrt{d})K_0(R_2\sqrt{d}) \right] \\ \quad + \left[\frac{Q_1T_2}{T_1} - Q_2 \right] \frac{[K_0(r\sqrt{d}) - K_0(R_2\sqrt{d})]}{2\pi T} & (0 < r \leq R_1) \\ h_{tot}(r) + \frac{NT_2R_1}{T_1T\sqrt{d}} [I_1(R_1\sqrt{d})K_0(r\sqrt{d}) - I_1(R_1\sqrt{d})K_0(R_2\sqrt{d})] \\ \quad + \left[\frac{Q_1T_2}{T_1} - Q_2 \right] \frac{[K_0(r\sqrt{d}) - K_0(R_2\sqrt{d})]}{2\pi T} & (R_1 < r \leq R_2) \end{cases} \quad (97)$$

The head h_2 in the lower layer is:

$$h_2(r) = \begin{cases} h_{tot}(r) - \frac{NR_1}{T\sqrt{d}} \left[\frac{1}{R_1\sqrt{d}} - K_1(R_1\sqrt{d})I_0(r\sqrt{d}) - I_1(R_1\sqrt{d})K_0(R_2\sqrt{d}) \right] \\ \quad + \left[\frac{Q_2 T_1}{T_2} - Q_1 \right] \frac{[K_0(R_2\sqrt{d}) - K_0(r\sqrt{d})]}{2\pi T} & (0 < r \leq R_1) \\ h_{tot}(r) - \frac{NR_1}{T\sqrt{d}} [I_1(R_1\sqrt{d})K_0(r\sqrt{d}) - I_1(R_1\sqrt{d})K_0(R_2\sqrt{d})] \\ \quad + \left[\frac{Q_2 T_1}{T_2} - Q_1 \right] \frac{[K_0(R_2\sqrt{d}) - K_0(r\sqrt{d})]}{2\pi T} & (R_1 < r \leq R_2) \end{cases} \quad (98)$$

5.5.1.3. Example

Consider a phreatic three-layer system with impervious lower boundary, i.e. $c_3 = \infty$. The dimensionless parameters assigned to each layer are summarized in the left part of Table 2 referring to the three-layer model. These parameters are:

- the dimensionless transmissivities defined as T_i/T with $T = T_1 + T_2 + T_3$;
- the dimensionless resistances defined as c_i/c with $c = c_1 + c_2$;
- the dimensionless pumping rates defined as Q_i/Q with $Q = Q_1 + Q_2 + Q_3$.

The circular infiltration area around the pumping well has a dimensionless radius $R_1/\sqrt{Tc} = 1$. The dimensionless infiltration flux NTc/Q is -0.1 . The dimensionless distance R_2/\sqrt{Tc} of the outer model boundary is 100, and its constant head is zero.

Next, consider a two-layer model in which the upper layer is adopted from the three-layer model and the lower layer comprises the two lower layers of the three-layer model. Finally, consider a one-layer model which comprises the three layers. The dimensionless parameters of these equivalent two-layer and one-layer models are also given in Table 2. Dimensionless infiltration flux and dimensionless boundaries are the same in all three models.

Table 2. Dimensionless parameters for the different layers in the three-layer model and the equivalent two-layer and one-layer model. The lower layer in the two-layer model comprises the two lower layers of the three-layer model; the one-layer model comprises the three layers. Note that c_i is the vertical resistance between layers i and $i+1$. In each model, the lower model boundary is impervious which explains the infinitely large lower resistance.

Three-layer model				Two-layer model				One-layer model			
Layer	T_i/T	c_i/c	Q_i/Q	Layer	T_i/T	c_i/c	Q_i/Q	Layer	T_i/T	c_i/c	Q_i/Q
$i = 1$	0.5	0.2	0.0	$i = 1$	0.5	0.2	0.0	$i = 1$	1.0	∞	1.0
$i = 2$	0.2	0.8	0.1	$i = 2$	0.5	∞	1.0				
$i = 3$	0.3	∞	0.9								

Figure 3 is a plot of dimensionless drawdown $-sT/Q$ as a function of dimensionless radial distance r/\sqrt{Tc} for the three-layer model and its equivalent two-layer and one-layer model. The solid lines are calculated applying the method developed by Bakker and Strack (2003). For the two-layer model, equations (97) and (98) are used, and the solution for the one-layer model is given by equation (96). The dotted black lines are simulated using the generalized semi-analytical solution method derived in section 5.3 of this chapter, and the black dots are the corresponding finite-difference solution. It is seen that all methods result in virtually the same solutions.

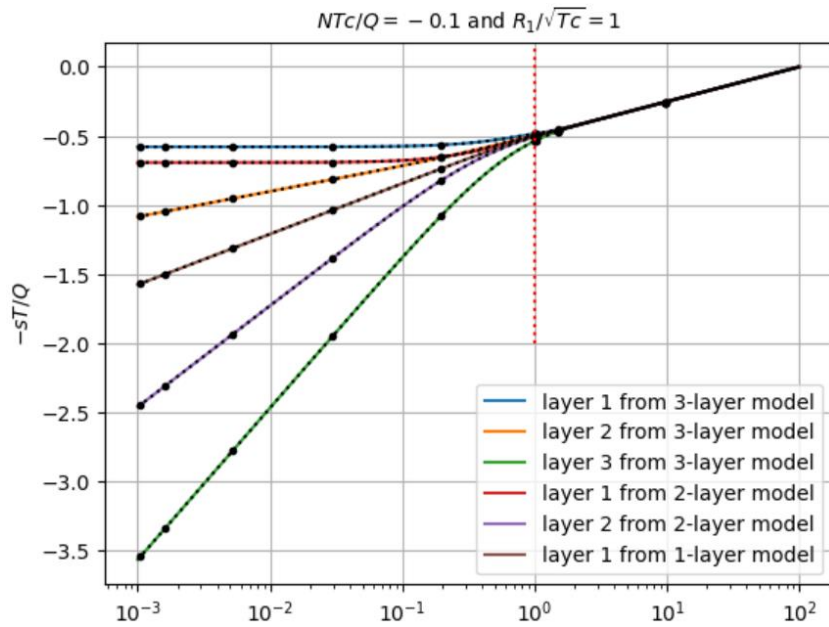


Figure 3. Dimensionless drawdown as a function of dimensionless radial distance for the three-layer model and the equivalent two-layer and one-layer model discussed in the text. The models simulate flow to a pumping well extracting groundwater at total pumping rate Q from a phreatic aquifer system with total transmissivity T and total resistance c . The system is recharged by a circular infiltration area around the well with constant flux N and radius R_1 . Distance R_1 is indicated by the vertical red dotted line. The solid lines are calculated by applying the method of Bakker and Strack (2003), the black dotted lines are simulated using the semi-analytical solution presented in this chapter, and the black dots are the finite-difference solution. See text for definition of parameters and derivation of solutions.

5.5.2. Formula of Blom

Blom (1973) combines the solution for a circular infiltration pond with the formula of de Glee (1930) to calculate the steady drawdown caused by a fully penetrating well in a phreatic aquifer drained by a dense network of ditches. The lowering of the water table causes the ditches to go dry in the proximal zone around the well, while there is still drainage in the distal zone. According to Blom (1973), this situation is characteristic for middle-high areas in the Netherlands. In the low-lying polder areas, where drainage levels are constant, the formula of de Glee (1930) is applicable, or the corresponding transient solution of Hantush and Jacob (1955), whereas the Thiem (1870, 1906) equation is valid in the areas of highest altitude, or the corresponding transient solution of Theis (1935). In Chapter 10, the applicability of these solutions are discussed in much more detail, and in Chapter 11, it is investigated whether recharge is relevant or not when simulating the cone of depression of a groundwater extraction.

5.5.2.1. Problem statement

The model discussed by Blom (1973) considers steady flow in two zones: a proximal zone with infiltration and a distal zone with drainage. In this case, system of partial differential equations (4) simplifies to the following set of two ordinary differential equations:

$$\begin{cases} \frac{d^2 s_1}{dr^2} + \frac{1}{r} \frac{ds_1}{dr} = \frac{-N}{T} & (0 < r \leq R_1) \\ \frac{d^2 s_2}{dr^2} + \frac{1}{r} \frac{ds_2}{dr} = \frac{s_2}{cT} & (R_1 \leq r < \infty) \end{cases} \quad (99)$$

where s_1 and s_2 is the head change [L] in the proximal and the distal zone, respectively. As there is one layer only, subscript $i = 1$ is omitted. The boundary between the two zones is R_1 . Distance R_0 of the inner model boundary is zero, and distance R_2 of the outer model boundary is infinitely large.

The aquifer has constant transmissivity $T_1 = T_2 = T$, and it is bounded below by an impervious layer, i.e. $c_{11} = c_{12} = \infty$.

In the proximal zone, there is no drainage; hence $c_{01} = \infty$. The precipitation excess in this zone is not drained anymore, but infiltrated with constant flux $N_1 = N$. In the distal zone, the precipitation excess is drained; hence $N_2 = 0$. The dense network of ditches in this zone is conceptualized by a head-dependent flux boundary condition with drainage resistance $c_{02} = c$. The pumping well extracts groundwater from the aquifer at constant rate Q , which reduces inner model boundary condition (11) to:

$$\lim_{R_0 \rightarrow 0} Q_1^h(R_0) = Q \quad (100)$$

The head at the outer model boundary is constant, which reduces outer model boundary condition (9) to:

$$s_2(\infty) = 0 \quad (101)$$

The head change at distance R_1 is equal to s_{R_1} ; hence, internal boundary condition (12) becomes:

$$s_1(R_1) = s_2(R_1) = s_{R_1} \quad (102)$$

There is also continuity of flow at the boundary between the two zones, generally expressed by (13). As steady flow is considered, the radial flow at distance R_1 is the difference between the pumping rate Q and the infiltration rate $N\pi R_1^2$ in the proximal zone:

$$Q_1^h(R_1) = Q_2^h(R_1) = Q + N\pi R_1^2 \quad (103)$$

Recall that Q is negative in case of discharge, and N is positive in case of recharge.

5.5.2.2. Solution

The solution for the first differential equation in (99) subject to boundary conditions (100) and (102) is the solution for a well on a circular island with areal infiltration given in section 2.5.3 (equation 121):

$$s_1(r) = s_{R_1} + \frac{N}{4T}(R_1^2 - r^2) + \frac{Q}{2\pi T} \ln\left(\frac{R_1}{r}\right) \quad (0 < r \leq R_1) \quad (104)$$

The solution for the second differential equation in (99) subject to boundary conditions (101) and (103) is the solution for a well with finite radius R_1 and pumping rate $Q + N\pi R_1^2$ in a leaky aquifer derived in section 2.5.6 (equation 128):

$$s_2(r) = \frac{Q + N\pi R_1^2}{2\pi T} \frac{K_0(r\sqrt{d})}{R_1\sqrt{d}K_1(R_1\sqrt{d})} \quad (r \geq R_1) \quad (105)$$

with $d = 1/(cT)$.

Blom (1973) assumes that both distance R_1 and head change s_{R_1} at this distance are known, although only one of these two parameters is required as the other can be found by solving $s_{R_1} = s_2(R_1)$ according to boundary condition (102). If R_1 is given, then it is straightforward to determine s_{R_1} , whereas a nonlinear solver is required to find R_1 if s_{R_1} is known. The nonlinear model in which R_1 is unknown, is developed by Ernst (1971), who also shows that $s_{R_1} = -Nc$, as the initial head before pumping is Nc above the drainage level. The nonlinear Ernst (1971) solution is discussed in more detail in Chapter 7, Chapter 10, and Chapter 11. Here, the linear model is used in which R_1 is given and s_{R_1} is derived from boundary condition (102).

5.5.2.3. Example

Figure 4 shows dimensionless head change $-sT/Q$ as a function of dimensionless distance r/\sqrt{Tc} , for different values of dimensionless recharge $-NTc/Q$, and with dimensionless distance $R_1/\sqrt{Tc} = 1.25$. Recall that \sqrt{Tc} is the leakage factor [L]. By expressing the problem using these dimensionless parameters, it is not required to explicitly specify parameters T , Q , and c ; hence, their input values are set to 1. The solid lines correspond to the analytical solution according to Blom (1973) given by equations (104) and (105), the black dotted lines are obtained by applying the generalized semi-analytical multi-zone solution derived in section 5.3, and the black dots represent the finite-difference solution. It is seen that all solutions are virtually the same. In case of the largest recharge, an unrealistic head rise occurs due to the fact that distance R_1 of the boundary between infiltrated and drained area is set by the user. The model of Ernst (1971) does not have this shortcoming as it derives distance R_1 from the condition that the head change at this boundary must be equal to $-Nc$.

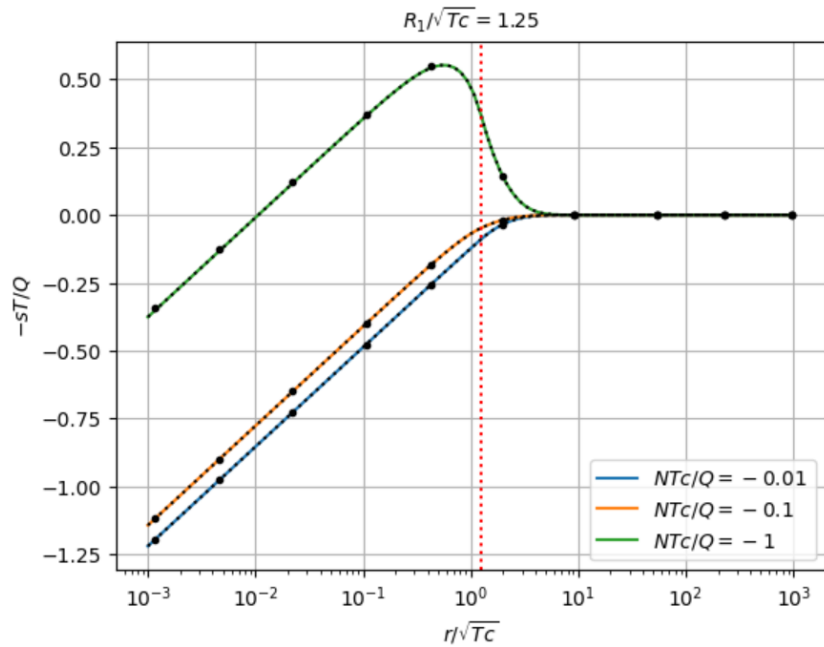


Figure 4. Dimensionless head change as a function of dimensionless radial distance for different values of dimensionless recharge according to the model that simulates steady flow to a fully penetrating pumping well extracting water at constant rate Q from a drained phreatic aquifer with constant transmissivity T and constant infiltration flux N . At distances $r < R_1$, there is no more drainage due to the pumping; at distances $r > R_1$, the aquifer is still drained with constant drainage resistance c . Distance R_1 is indicated by the vertical red dotted line. The solid lines are calculated using the formula of Blom (1973), the black dotted lines are simulated using the semi-analytical solution presented in this chapter, and the black dots are the finite-difference solution. See text for definition of parameters and derivation of solutions.

5.5.3. Steady state confined one-layer solutions

It is straightforward to find solutions for steady flow in a confined layer consisting of multiple zones. In this section, the solution for the following cases is presented:

1. steady parallel flow to a fully penetrating stream draining at constant rate;
2. steady axisymmetric flow to a fully penetrating well pumping at constant rate;
3. steady parallel flow to a fully penetrating stream with constant water level;
4. steady axisymmetric flow to a fully penetrating constant-head well.

5.5.3.1. Problem statement

In case of steady flow in a single confined aquifer, the system of equations (4) reduces to:

$$\nabla^2 h_j = 0 \quad (1 \leq j \leq n_z) \quad (106)$$

where subscript $i = 1$ is omitted for notational convenience. In case of parallel flow, the general solution to (106) is:

$$h_j(r) = \alpha_j r + \beta_j \quad (1 \leq j \leq n_z) \quad (107)$$

In case of axisymmetric flow, the general solution is:

$$h_j(r) = \alpha_j \ln(r) + \beta_j \quad (1 \leq j \leq n_z) \quad (108)$$

To find the integration constants α_j and β_j for each zone j , the boundary conditions need to be taken into account. Constant-head condition (10) at the inner model boundary simplifies to:

$$h_1(R_0) = H \quad (109)$$

In case of parallel flow, constant-discharge condition (11) at the inner model boundary reduces to:

$$T_1 \frac{dh_1(R_0)}{dr} = -Q \quad (110)$$

If axisymmetric flow is simulated, the constant-discharge boundary condition is:

$$2\pi T_1 R_0 \frac{dh_1(R_0)}{dr} = -Q \quad (111)$$

The outer model boundary condition (9) reduces to:

$$h_{n_z}(R_{n_z}) = \varphi \quad (112)$$

Finally, head and flux conditions (12) and (13) at the zone boundaries also need to be taken into account:

$$h_j(R_j) = h_{j+1}(R_j) \quad (0 < j < n_z) \quad (113)$$

$$T_j \frac{dh_j(R_j)}{dr} = T_{j+1} \frac{dh_{j+1}(R_j)}{dr} \quad (0 < j < n_z) \quad (114)$$

5.5.3.2. Solutions

The solutions for parallel or axisymmetric flow toward the inner model boundary with constant-head or constant-discharge are found by recursively applying the boundary conditions, in a similar way the algorithm described in section 5.3.4 works. However, in this case, the equations are much simpler, and therefore, deriving the constants can be done easily by hand.

The resulting solution for parallel flow with specified discharge Q at R_0 is:

$$h_j(r) = \varphi + Q \left(\frac{R_j - r}{T_j} + \sum_{k=j}^{n_z-1} \frac{R_{k+1} - R_k}{T_{k+1}} \right) \quad (R_{j-1} \leq r \leq R_j; 1 \leq j \leq n_z) \quad (115)$$

The equivalent solution for axisymmetric flow is:

$$h_j(r) = \varphi + \frac{Q}{2\pi} \left(\frac{\ln(R_j/r)}{T_j} + \sum_{k=j}^{n_z-1} \frac{\ln(R_{k+1}/R_k)}{T_{k+1}} \right) \quad (R_{j-1} \leq r \leq R_j; 1 \leq j \leq n_z) \quad (116)$$

The solution for parallel flow with specified head H at R_0 :

$$h_j(r) = H + \frac{\varphi - H}{w_{n_z}} \left(\frac{r}{T_j} + w_{j-1} \right) \quad (R_{j-1} \leq r \leq R_j; 1 \leq j \leq n_z) \quad (117)$$

with:

$$w_j = \sum_{k=0}^j \left(\frac{1}{T_k} - \frac{1}{T_{k+1}} \right) R_k$$

and $T_0 = T_{n_z+1} = \infty$.

The equivalent solution for axisymmetric flow is:

$$h_j(r) = H + \frac{\varphi - H}{w_{n_z}} \left(\frac{\ln(r)}{T_j} + w_{j-1} \right) \quad (R_{j-1} \leq r \leq R_j; 1 \leq j \leq n_z) \quad (118)$$

with:

$$w_j = \sum_{k=0}^j \left(\frac{1}{T_k} - \frac{1}{T_{k+1}} \right) \ln(R_k)$$

and $T_0 = T_{n_z+1} = \infty$.

It is seen that the axisymmetric solutions are found by replacing the distances in the corresponding parallel flow solutions by the logarithm of these distances. In case of specified discharge at the inner boundary, Q must also be replaced by $Q/2\pi$.

It is interesting to take a closer look at the axisymmetric two-zone solution for a well with constant pumping rate:

$$\begin{cases} s_1(r) = \frac{Q}{2\pi T_1} \ln(R_1/r) + \frac{Q}{2\pi T_2} \ln(R_2/R_1) & (R_0 \leq r \leq R_1) \\ s_2(r) = \frac{Q}{2\pi T_2} \ln(R_2/r) & (R_1 \leq r \leq R_2) \end{cases} \quad (119)$$

where the constant head φ at the outer boundary is set to zero to obtain drawdown s [L]. Drawdown s_2 in the distal zone is given by the well-known Thiem (1870, 1906) equation, as is drawdown s_1 in the proximal zone, but in this case, it is augmented by the drawdown $s_2(R_1)$ at the outer boundary of the zone at distance R_1 , which is given by the second term of the first equation in (119). Equation (116) shows that this may be generalized to multiple zones: the head in each zone is governed by the Thiem equation, and the head at the outer boundary of the zone is calculated by recursively applying the Thiem equation for all subsequent zones. This observation will be used in section 5.6 to generalize the concept of the dimensionless well-skin parameter.

5.5.3.3. Effective transmissivity

Using the solution for steady multizone flow, it is straightforward to derive expressions for the effective transmissivity, that is the equivalent transmissivity of the corresponding homogeneous aquifer. The difference between the heads at the inner and outer model boundaries is given by expression (116) for $r = R_0$:

$$h_1(R_0) - \varphi = \frac{Q}{2\pi} \sum_{k=0}^{n_z-1} \frac{\ln(R_{k+1}/R_k)}{T_{k+1}} \quad (120)$$

Using the effective transmissivity T_e [L^2/T], the head difference may also be expressed applying the Thiem (1870, 1906) formula:

$$h_1(R_0) - \varphi = \frac{Q}{2\pi} \frac{\ln(R_{n_z}/R_0)}{T_e} \quad (121)$$

The left-hand side of equations (120) and (121) is the same, from which it follows that:

$$T_e = \frac{\ln(R_{n_z}/R_0)}{\sum_{k=0}^{n_z-1} \frac{\ln(R_{k+1}/R_k)}{T_{k+1}}} \quad (122)$$

Expression (122) shows that the effective transmissivity is the weighted harmonic mean of the transmissivities of the zones, where the weights are determined by the logarithmically transformed widths of the zones. In case of parallel flow, the same expression is derived, except that the widths are not logarithmically transformed in this case:

$$T_e = \frac{R_{n_z} - R_0}{\sum_{k=0}^{n_z-1} \frac{R_{k+1} - R_k}{T_{k+1}}} \quad (123)$$

Expressions (122) and (123) are applied in the finite-difference formulation presented in Chapter 3 to calculate the effective transmissivity of two grid cells having different hydraulic conductivities. In this case, the number of zones n_z equals 2, and the distances are determined by the nodes of the two cells. Expressions (122) and (123) are also consistent to the way the total vertical resistance is calculated for an accumulation of heterogeneous layers in which vertical flow occurs. The vertical resistance of each layer is defined as the layer thickness divided by its vertical conductivity, and the total resistance is the sum of the individual layer resistances, which indeed comes down to calculating the harmonic mean of the vertical conductivities weighted by the layer thicknesses. The mathematical derivation is similar to the one presented here, and can be found, for instance, in Lebbe (1999).

5.5.3.4. Example

Consider a confined aquifer consisting of four zones with relative transmissivities $T_1/T = 0.1$, $T_2/T = 0.4$, $T_3/T = 0.2$, and $T_4/T = 0.3$, respectively, with $T = \sum_{j=1}^4 T_j$. The relative distances of the outer boundaries of the zones are $R_1/R_0 = 10$, $R_2/R_0 = 10^2$, $R_3/R_0 = 10^3$, and $R_4/R_0 = 10^4$, respectively. A fully penetrating well with radius R_0 extracts water from the aquifer at constant rate Q . The dimensionless constant head $\varphi T/Q$ at the outer model boundary at distance R_4 is 1.

The left plot in Figure 5 shows the dimensionless head hT/Q as a function of relative distance r/R_0 for this model. The head is also simulated for the case where the transmissivities of the zones are reversed: $T_1/T = 0.3$, $T_2/T = 0.2$, $T_3/T = 0.4$, and $T_4/T = 0.1$. The result of this second scenario is also plotted on the left graph of Figure 5.

To test solution (118) for a specified-head well, the same scenarios are simulated again using this solution, where $H = h(R_0)$ is adopted from the previous simulations using solution (116) for a specified-discharge well. The results for both scenarios with known head H are visualized in the right graph of Figure 5. This plot is exactly the same as the left plot in Figure 5, as it should.

The colored solid lines correspond to the analytical solutions (116) and (118) derived in this section, the black dotted lines are obtained by applying the generalized semi-analytical multi-zone solution derived in section 5.3, and the black dots represent the finite-difference solution. All solutions are virtually the same.

The gray solid line in each plot of Figure 5 is the equivalent one-zone solution. In case of a specified-discharge well, this solution is obtained by applying the Thiem equation (121) with the effective transmissivity given by expression (122). In case of a specified-head well, the corresponding one-zone solution is given in section 2.5.2 of Chapter 2 (equation 119).

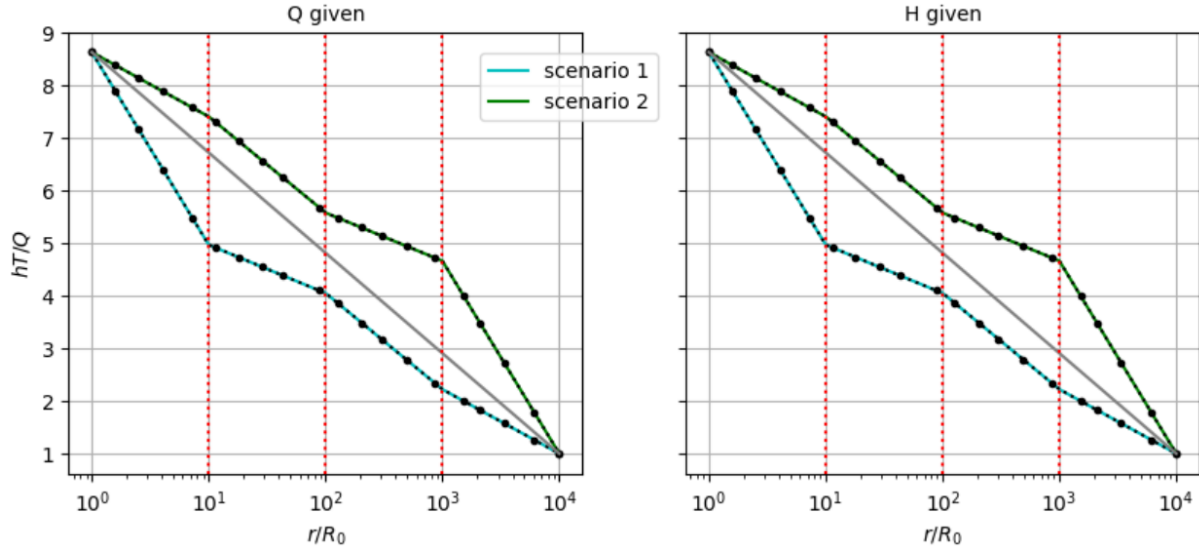


Figure 5. Left plot: Dimensionless head as a function of dimensionless radial distance for the model that simulates steady flow to a fully penetrating pumping well extracting water at constant rate Q from a confined aquifer consisting of 4 zones characterized by different transmissivities. The boundaries between the zones are indicated by the vertical red dotted lines. Two scenarios are simulated where the transmissivities of the zones are reversed in the second scenario. The sum of the transmissivities of the zones equals T . Right plot: Dimensionless head as a function of dimensionless radial distance for the same model with specified-head well. Head H in the well is adopted from the model with specified-discharge well. In both plots, the solid lines are calculated using the analytical solutions derived in this section, the black dotted lines are simulated using the generalized semi-analytical solution presented in this chapter, and the black dots are the finite-difference solution. The gray solid line in each plot is the solution for the equivalent one-zone model with effective transmissivity. See text for definition of parameters and derivation of solutions.

5.5.4. Steady state leaky one-layer solution

In this section, the steady state solution is given for a fully penetrating well in a leaky aquifer consisting of two cylindrical zones around the well. The proximal zone may be interpreted as a finite-thickness skin or gravel pack, whereas the distal zone is the actual aquifer. The well extracts groundwater from the aquifer at constant pumping rate. The solution may be regarded as an extension of the formula for steady flow toward a fully penetrating well of infinitesimal diameter without skin in a leaky aquifer (de Glee, 1930; Hantush, 1949; Jacob, 1946; Kooper, 1914).

5.5.4.1. Problem statement

System of equations (4) is simplified to a set of two modified Bessel equations that describe radial flow in the proximal and the distal zone, denoted by subscript 1 and 2, respectively:

$$\begin{cases} \frac{d^2 s_1}{dr^2} + \frac{1}{r} \frac{ds_1}{dr} = \left(\frac{1}{c_0 T_1} + \frac{1}{c_1 T_1} \right) s_1 & (r \leq R_1) \\ \frac{d^2 s_2}{dr^2} + \frac{1}{r} \frac{ds_2}{dr} = \left(\frac{1}{c_0 T_2} + \frac{1}{c_1 T_2} \right) s_2 & (r \geq R_1) \end{cases} \quad (124)$$

The subscript referring to the layer is omitted as there is one layer only. Parameters c_0 and c_1 are the resistances of the upper and lower bounding aquitard, respectively. The distance of the boundary between the two zones is R_1 . The principle of superposition is applied, and therefore, the problem is formulated in terms of drawdown s [L] instead of head h . This implies the drawdown in the bounding

aquitards is zero, as a constant-head boundary condition is defined for these boundaries. The drawdown at the outer boundary at infinity is constant and also equal to zero, which simplifies outer model boundary condition (9) to:

$$s_2(\infty) = 0 \quad (125)$$

The pumping well has a radius equal to R_0 , and it extracts water at constant rate Q , which reduces inner model boundary condition (11) to:

$$Q_1^h(R_0) = Q \quad (126)$$

where Q is positive if water is added to the aquifer system. At the boundary between the two zones, there is continuity of flow, and internal boundary conditions (12) and (13) are reformulated as, respectively:

$$s_1(R_1) = s_2(R_1) \quad (127)$$

$$Q_1^h(R_1) = Q_2^h(R_1) \quad (128)$$

5.5.4.2. Solution

The generalized solution presented in section 5.3 can be used to solve the stated problem, although in this case, there is no need to use matrices. Indeed, the two system matrices \mathbf{A}_1 and \mathbf{A}_2 have one entry only, which is equal to the eigenvalues d_1 and d_2 , respectively. The corresponding eigenvectors \mathbf{V}_1 and \mathbf{V}_2 are equal to 1. All constant and initial heads are set to 0, and there is no recharge; hence $\mathbf{b}_1 = \mathbf{b}_2 = 0$. In this way, the general solution for both differential equations in (124) reduces to:

$$\begin{cases} s_1(r) = \alpha_1 I_0(r\sqrt{d_1}) + \beta_1 K_0(r\sqrt{d_1}) & (r \leq R_1) \\ s_2(r) = \alpha_2 I_0(r\sqrt{d_2}) + \beta_2 K_0(r\sqrt{d_2}) & (r \geq R_1) \end{cases} \quad (129)$$

The eigenvalues d_1 and d_2 are:

$$d_j = \frac{1}{c_0 T_j} + \frac{1}{c_1 T_j} = \frac{c_0 + c_1}{c_0 c_1 T_j} \quad (j = 1,2) \quad (130)$$

Because $s_2(\infty)$ is zero according to boundary condition (125), α_2 must be zero as $I_0(x) \rightarrow \infty$ if $x \rightarrow \infty$. The other integration constants are found by applying the remaining boundary conditions (126), (127), and (128), which gives the following particular solution:

$$\begin{cases} s_1 = \frac{-Q}{2\pi T_1 R_0 \sqrt{d_1}} \left[\frac{a I_0(r\sqrt{d_1}) + K_0(r\sqrt{d_1})}{a I_1(R_0\sqrt{d_1}) - K_1(R_0\sqrt{d_1})} \right] & (r \leq R_1) \\ s_2 = \frac{-Q}{2\pi T_1 R_0 \sqrt{d_1}} \left[\frac{a I_0(R_1\sqrt{d_1}) + K_0(R_1\sqrt{d_1})}{a I_1(R_0\sqrt{d_1}) - K_1(R_0\sqrt{d_1})} \right] \left[\frac{K_0(r\sqrt{d_2})}{K_0(R_1\sqrt{d_2})} \right] & (r \geq R_1) \end{cases} \quad (131)$$

with:

$$a = \frac{T_1 R_1 \sqrt{d_1} K_1(R_1\sqrt{d_1}) K_0(R_1\sqrt{d_2}) - T_2 R_1 \sqrt{d_2} K_1(R_1\sqrt{d_2}) K_0(R_1\sqrt{d_1})}{T_1 R_1 \sqrt{d_1} I_1(R_1\sqrt{d_1}) K_0(R_1\sqrt{d_2}) + T_2 R_1 \sqrt{d_2} K_1(R_1\sqrt{d_2}) I_0(R_1\sqrt{d_1})}$$

If there is one zone only, then $T_1 = T_2 = T$ and $d_1 = d_2 = d$. In this case $a = 0$, and solution (131) simplifies to:

$$s = \frac{Q}{2\pi T R_0 \sqrt{d}} \left[\frac{K_0(r\sqrt{d})}{K_1(R_0\sqrt{d})} \right] \quad (132)$$

Equation (132) is found in Bruggeman (1999). If $R_0 \rightarrow 0$, then $[R_0\sqrt{d}K_1(R_0\sqrt{d})] \rightarrow 1$, in which case expression (132) reduces to the well-known de Glee (1930) formula, which is discussed more extensively in section 2.5.6 from Chapter 2.

A very interesting approximation relates solution (131) to the steady-state confined two-zone solution (119) presented in section 5.5.3. If $x < 0.1$, then the following approximations involving the modified Bessel functions are justified (Butler, 1988): $I_0(x) \approx 1$, $xI_1(x) \approx x^2/2$, $K_0(x) \approx \ln(2/(\eta x))$, and $xK_1(x) \approx 1$, with $\eta = e^\gamma$, and γ the Euler-Mascheroni constant equal to 0.57721.... If also an infinitesimal well-radius is assumed, i.e. $R_0 \rightarrow 0$, then the equations in (131) can be approximated as:

$$\begin{cases} s_1 = \frac{Q}{2\pi T_1} \ln\left(\frac{R_1}{r}\right) + \frac{Q}{2\pi T_2} \ln\left(\frac{2}{\eta\sqrt{d_2}R_1}\right) & (r \leq R_1) \\ s_2 = \frac{Q}{2\pi T_2} \ln\left(\frac{2}{\eta\sqrt{d_2}r}\right) & (r \geq R_1) \end{cases} \quad (133)$$

In practice, solution (133) is valid if the radii R_0 and R_1 are much smaller than the leakage factors $1/\sqrt{d_1}$ and $1/\sqrt{d_2}$. If the equations in (133) are compared to the steady-state solution (119) for a well in a confined two-zone aquifer, then it is seen that they are the same if distance R_2 of the outer model boundary in the steady-state solution is substituted by:

$$R_2 = \frac{2}{\eta\sqrt{d_2}} \approx 1.123 \sqrt{\frac{c_0 c_1 T_2}{c_0 + c_1}} \quad (134)$$

Equation (134) is the formula to estimate the radius of influence of a pumping well extracting water from a leaky homogeneous aquifer (Louwyck et al., 2022). This formula is discussed in Chapter 10.

As the steady-state solutions for confined and leaky aquifers are related, solution (133) may be generalized to n_z zones applying steady-state solution (116) for flow towards a well in a confined aquifer with multiple zones:

$$s_j(r, t) = \frac{Q}{2\pi} \left(\frac{\ln(R_j/r)}{T_j} + \sum_{k=j}^{n_z-1} \frac{\ln(R_{k+1}/R_k)}{T_{k+1}} \right) \quad (R_{j-1} \leq r \leq R_j; 1 \leq j \leq n_z) \quad (135)$$

where the initial head φ in (116) is set to zero to obtain drawdowns instead of heads. In equation (135), R_{n_z} is the radius of influence derived from the leakage factor of the most distal zone in which drawdown is not negligibly small:

$$R_{n_z} = \frac{2}{\eta\sqrt{d_{n_z}}} \approx 1.123 \sqrt{\frac{c_0 c_1 T_{n_z}}{c_0 + c_1}} \quad (136)$$

5.5.4.3. Example

Consider a pumping well with radius R_0 extracting water at constant rate Q from a leaky aquifer with constant transmissivity T_2 . The resistances of upper and lower aquifer boundary are the same, i.e. $c_0 = c_1$. The well is surrounded by a finite-thickness skin with radius R_1 and transmissivity T_1 . Three scenarios are simulated: in the first scenario, skin transmissivity is 10 times smaller than the aquifer transmissivity; in the second scenario, there is no skin or $T_1 = T_2$; in the last scenario, the skin transmissivity is 10 times larger than the aquifer transmissivity.

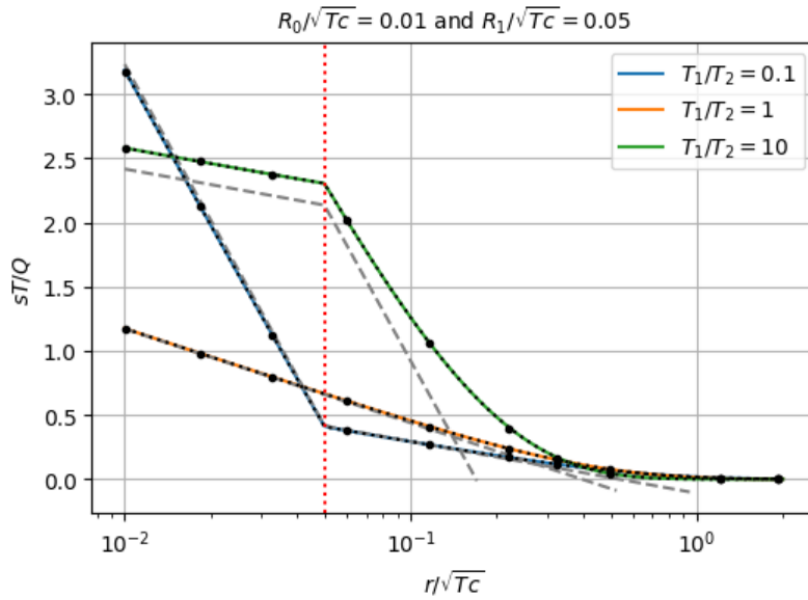


Figure 6. Dimensionless drawdown as a function of dimensionless radial distance for the model that simulates steady flow to a fully penetrating pumping well with radius R_0 , surrounded by a finite-thickness skin with radius R_1 and constant transmissivity T_1 . Distance R_1 is indicated by the vertical red dotted line. The well extracts water at constant rate Q from a leaky aquifer with constant transmissivity T_2 and resistances $c_0 = c_1$. Parameters T and c are the total transmissivity and resistance, respectively. The solid lines are calculated using the analytically derived formula, the black dotted lines are simulated using the generalized semi-analytical solution presented in this chapter, and the black dots are the finite-difference solution. The gray dashed lines represent the approximate analytical solution derived from the confined aquifer solution. See text for definition of parameters and derivation of solutions.

Figure 6 is a plot of dimensionless drawdown sT/Q as a function of dimensionless distance r/\sqrt{Tc} for the three scenarios, with $T = T_1 + T_2$ and $c = c_0 + c_1$. Dimensionless well radius R_0/\sqrt{Tc} is 0.01; dimensionless skin radius R_1/\sqrt{Tc} is 0.05. The solid lines correspond to the analytical solution (131) derived in this section, the black dotted lines are obtained by applying the generalized semi-analytical multi-zone solution derived in section 5.3, and the black dots represent the finite-difference solution. It is seen that all solutions are virtually the same.

In the first scenario, the lower conductivity of the skin causes drawdown in the well to be larger than in the case when there is no skin, whereas a higher skin conductivity gives a lower drawdown in the well, as is seen in the last scenario. The higher drawdown in the first scenario is called positive skin effect, the lower drawdown in the last scenario negative skin effect (Kruseman & de Ridder, 1990). In this example, dimensionless radius of the well-skin is the same in the three scenarios, which explains why drawdown in the well is lowest in the no-skin case. However, it is clearly seen that the drawdown curve becomes steeper at distances smaller than R_1 in the first scenario, while it becomes less steep in the last scenario. The skin effect will be discussed in more detail in section 5.6.

The approximate analytical solution (133) that is equivalent to the confined aquifer solution is plotted as gray dashed lines. It is seen that in this example the approximation is not valid for the case with the lowest aquifer leakage factor. In the two other cases, the approximate solution is acceptable for distances close to the well. The approximate radius of influence given by equation (134) corresponds to the point where the gray dashed lines cross the x-axis, which is clearly an underestimation of the actual radius of influence in all cases. Chapter 10 elaborates on the concept of the radius of influence.

5.5.5. Transient state confined one-layer solution

Barker and Herbert (1982) and Butler (1988) treat the case of transient axisymmetric flow toward a pumping well in a confined aquifer consisting of two cylindrical zones around the well. Barker and Herbert (1982) call it a patchy aquifer, while Butler (1988) uses the term radially symmetric non-uniform aquifer. Both apply the Laplace transform to solve the problem. However, Barker and Herbert (1982) only consider large values of times, which simplifies the solution in the Laplace domain to an expression that can be inverted analytically, whereas Butler (1988) applies the Stehfest (1970) algorithm to invert the exact solution in the Laplace domain numerically.

5.5.5.1. Problem statement

System of equations (4) is simplified to a set of two diffusion equations that govern radial flow in the proximal and the distal zone, denoted by subscript 1 and 2, respectively:

$$\begin{cases} \frac{\partial^2 s_1}{\partial r^2} + \frac{1}{r} \frac{\partial s_1}{\partial r} = \frac{S_1}{T_1} \frac{\partial s_1}{\partial t} & (r \leq R) \\ \frac{\partial^2 s_2}{\partial r^2} + \frac{1}{r} \frac{\partial s_2}{\partial r} = \frac{S_2}{T_2} \frac{\partial s_2}{\partial t} & (r \geq R) \end{cases} \quad (137)$$

As there is one layer only, the subscript referring to this layer is omitted. The distance of the boundary between the two zones is R_1 . Subscript 1 is also missing because the inner model boundary R_0 is infinitesimal, and the outer boundary is at the infinitely large distance R_2 . Applying the principle of superposition, the problem is formulated in terms of drawdown s [L] instead of head h . Hence, initial condition (14) is simplified by setting the initial drawdown at $t = 0$ to zero in both zones:

$$s_1(r, 0) = s_2(r, 0) = 0 \quad (138)$$

Similarly, outer boundary condition (9) is simplified as the drawdown at the outer boundary at infinity is constant and also equal to zero:

$$s_2(\infty, t) = 0 \quad (139)$$

The pumping well has an infinitesimal radius and extracts water at constant rate Q , which reduces inner model boundary condition (11) to:

$$\lim_{r \rightarrow 0} Q_1^h(r, t) = Q \quad (140)$$

where Q is positive if water is added to the aquifer system. At the boundary between the two zones, there is continuity of flow, which is expressed by internal boundary conditions (12) and (13), which simplify to, respectively:

$$s_1(R, t) = s_2(R, t) \quad (141)$$

$$Q_1^h(R, t) = Q_2^h(R, t) \quad (142)$$

5.5.5.2. Solution

The generalized solution presented in section 5.3 is used to solve the stated problem, where in this case the two system matrices A_1 and A_2 reduce to the eigenvalues d_1 and d_2 , respectively, and the corresponding eigenvectors are equal to 1. All constant and initial heads are zero, as are the infiltration fluxes N_1 and N_2 , from which it follows that $b_1 = b_2 = 0$. The general solution to both Laplace transformed differential equations in (137) thus reduces to:

$$\begin{cases} \bar{s}_1(r, p) = \alpha_1 I_0(r\sqrt{d_1}) + \beta_1 K_0(r\sqrt{d_1}) & (r \leq R) \\ \bar{s}_2(r, p) = \alpha_2 I_0(r\sqrt{d_2}) + \beta_2 K_0(r\sqrt{d_2}) & (r \geq R) \end{cases} \quad (143)$$

with \bar{s} the Laplace transform of drawdown s . The eigenvalues are $d_1 = pS_1/T_1$ and $d_2 = pS_2/T_2$. As $I_0(x) \rightarrow \infty$ if $x \rightarrow \infty$, α_2 must be zero to fulfill boundary condition (139). By applying the remaining boundary conditions (140), (141), and (142), the integration constants can be derived analytically, which gives the particular solution in the Laplace domain (Butler, 1988):

$$\begin{cases} \bar{s}_1 = \frac{Q}{2\pi T_1 p} \left[K_0(r\sqrt{d_1}) + \frac{K_1(R\sqrt{d_1})K_0(R\sqrt{d_2}) - \frac{T_2}{T_1}\sqrt{\frac{d_2}{d_1}}K_0(R\sqrt{d_1})K_1(R\sqrt{d_2})}{I_1(R\sqrt{d_1})K_0(R\sqrt{d_2}) + \frac{T_2}{T_1}\sqrt{\frac{d_2}{d_1}}I_0(R\sqrt{d_1})K_1(R\sqrt{d_2})} I_0(r\sqrt{d_1}) \right] \\ \bar{s}_2 = \frac{Q}{2\pi T_1 p} \left[\frac{K_1(R\sqrt{d_1})I_0(R\sqrt{d_1}) + K_0(R\sqrt{d_1})I_1(R\sqrt{d_1})}{I_1(R\sqrt{d_1})K_0(R\sqrt{d_2}) + \frac{T_2}{T_1}\sqrt{\frac{d_2}{d_1}}I_0(R\sqrt{d_1})K_1(R\sqrt{d_2})} K_0(r\sqrt{d_2}) \right] \end{cases} \quad (144)$$

The following approximations are valid if $x < 0.1$ (Butler, 1988): $I_0(x) \approx 1$, $I_1(x) \approx x/2$, $K_0(x) \approx \ln(2/(\eta x))$, and $K_1(x) \approx 1/x$, with $\eta = e^\gamma$, and γ the Euler-Mascheroni constant equal to 0.57721.... These approximations simplify expression (144) to:

$$\begin{cases} \bar{s}_1 = \frac{Q}{2\pi T_1 p} \left[\ln\left(\frac{2}{\eta r\sqrt{d_1}}\right) + \frac{1}{R\sqrt{d_1}} \frac{\ln(2/(\eta R\sqrt{d_2})) + \frac{T_2}{T_1}\ln(\eta R\sqrt{d_1}/2)}{\frac{R\sqrt{d_1}}{2}\ln(2/(\eta R\sqrt{d_2})) + \frac{T_2}{T_1}\frac{1}{R\sqrt{d_1}}} \right] \\ \bar{s}_2 = \frac{Q}{2\pi T_1 p} \left[\frac{\frac{R\sqrt{d_1}}{2}\ln(2/(\eta R\sqrt{d_1})) + \frac{1}{R\sqrt{d_1}}}{\frac{R\sqrt{d_1}}{2}\ln(2/(\eta R\sqrt{d_2})) + \frac{T_2}{T_1}\frac{1}{R\sqrt{d_1}}} \ln\left(\frac{2}{\eta r\sqrt{d_2}}\right) \right] \end{cases} \quad (145)$$

According to Butler (1988), the term $\left[\frac{R\sqrt{d_1}}{2}\ln(2/(\eta R\sqrt{d_j}))\right]$ can be ignored in most cases, which further simplifies (145) to expressions that can be inverted analytically to:

$$\begin{cases} s_1 = \frac{Q}{4\pi T_2} \ln\left(\frac{4T_2 t}{\eta S_2 R^2}\right) + \frac{Q}{2\pi T_1} \ln\left(\frac{R}{r}\right) & (r \leq R) \\ s_2 = \frac{Q}{4\pi T_2} \ln\left(\frac{4T_2 t}{\eta S_2 r^2}\right) & (r \geq R) \end{cases} \quad (146)$$

where use is made of the following Laplace transform inversion: $\mathcal{L}^{-1}[(a/p)\ln(bp)] = a\ln(\eta b/t)$ (Bateman, 1954). Due to these approximations, solution (146) is valid only for large values of time. This approximate solution is also given by Barker and Herbert (1982). The first term in both equations of solution (146) is the well-known series truncation of the Theis (1935) formula for large times (Cooper & Jacob, 1946).

Comparing solution (146) to the steady-state solution (119) for a well in a confined two-zone aquifer, it is seen that both are the same if distance R_2 of the outer model boundary in the steady-state solution is substituted by:

$$R_2 = \sqrt{\frac{4T_2 t}{\eta S_2}} \approx 1.5 \sqrt{\frac{T_2 t}{S_2}} \quad (147)$$

Equation (147) is the well-known formula to estimate the time-dependent radius of influence of a well extracting water from a confined homogeneous aquifer. This formula is derived from the Cooper and Jacob (1946) approximation of the Theis (1935) solution (Bear, 1972; Louwyck et al., 2022). It is also discussed in Chapter 10.

Using steady-state solution (116) for flow towards a well in a confined aquifer with multiple zones, transient state solution (146) for large values of time can be generalized to n_z zones:

$$s_j(r, t) = \frac{Q}{2\pi} \left(\frac{\ln(R_j/r)}{T_j} + \sum_{k=j}^{n_z-1} \frac{\ln(R_{k+1}/R_k)}{T_{k+1}} \right) \quad (R_{j-1} \leq r \leq R_j; 1 \leq j \leq n_z) \quad (148)$$

where the initial head φ in (116) is set to zero to obtain drawdowns instead of heads. In equation (148), R_{n_z} is the time-dependent radius of influence in the most distal zone of the aquifer system in which drawdown is not negligibly small:

$$R_{n_z}(t) = \sqrt{\frac{4T_{n_z} t}{\eta S_{n_z}}} \approx 1.5 \sqrt{\frac{T_{n_z} t}{S_{n_z}}} \quad (149)$$

5.5.5.3. Example

Consider a fully penetrating well extracting water at constant rate Q from a confined aquifer with transmissivity T_2 and storativity S_2 . The well has an infinitesimal radius and is surrounded by a gravel pack with radius R . Transmissivity T_1 of the gravel pack is 10 times larger than the aquifer transmissivity and its storativity S_1 is 10 times smaller than the aquifer storativity.

Figure 7 shows the dimensionless drawdown sT/Q as a function of dimensionless distance r/R at different dimensionless times $\frac{tT}{SR^2}$, with $T = T_1 + T_2$ and $S = S_1 + S_2$. The solid lines correspond to the semi-analytical solution developed by Butler (1988), which is equation (144) inverted numerically using the Stehfest (1970) algorithm. The black dotted lines are obtained by applying the generalized semi-analytical multizone solution derived in section 5.3, whereas the black dots represent the finite-difference solution. All methods simulate virtually the same results.

The approximate analytical solution (146) given by Barker and Herbert (1982) is also plotted as a gray dashed line for the two largest dimensionless times. It is seen that in this example the approximation is valid only if dimensionless time is larger than 1000 and dimensionless distance is smaller than 10. The approximate radius of influence given by equation (147) corresponds to the point where the gray dashed line crosses the x-axis, which is clearly an underestimation of the actual radius of influence. Chapter 10 elaborates on the concept of the radius of influence and critically reviews its use in the context of assessing the environmental impact of permanent groundwater extractions.

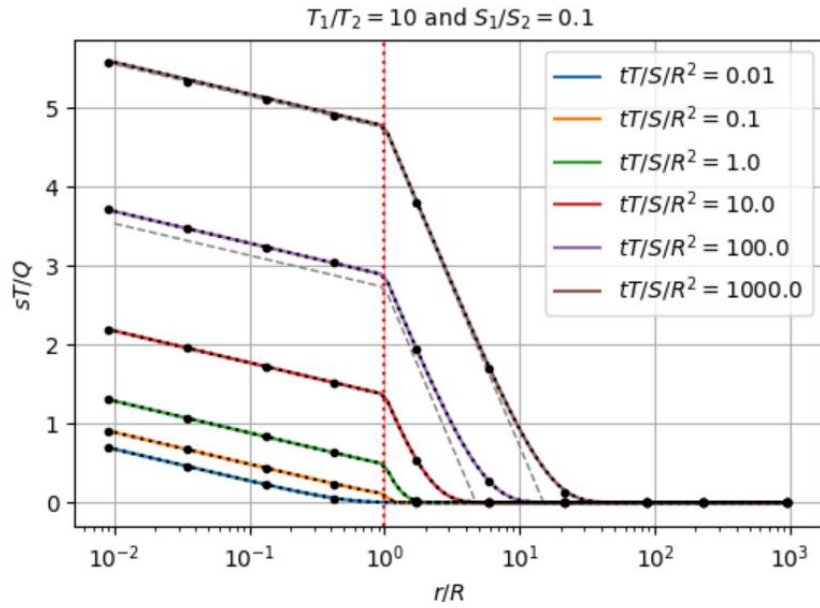


Figure 7. Dimensionless drawdown as a function of dimensionless radial distance at different dimensionless times for the model that simulates transient flow to a fully penetrating pumping well surrounded by a gravel pack with radius R , constant transmissivity T_1 , and constant storativity S_1 . Distance R is indicated by the vertical red dotted line. The well extracts water at constant rate Q from a confined aquifer with constant transmissivity T_2 and constant storativity S_2 . Parameters T and S are the total transmissivity and storativity, respectively. The solid lines are calculated using the semi-analytical solution by Butler (1988), the black dotted lines are simulated using the generalized semi-analytical solution presented in this chapter, and the black dots are the finite-difference solution. The gray dashed lines represent the approximate analytical solution for large values of time by Barker and Herbert (1982). See text for definition of parameters and derivation of solutions.

5.5.6. Slug test in confined aquifer

In the next Chapter 6, the semi-analytical solution developed in this chapter is extended to define more realistic boundary conditions at the well-face. This extension allows for taking into account the wellbore storage, which is required for the simulation of slug tests. However, using the solution method presented in this chapter, it is also possible to include the effect of the wellbore storage by applying a simple modeling trick: instead of letting the well-face coincide with the inner model boundary so that the well is a boundary condition, the well as a whole is included in the model and corresponds to the most inner zone. Since the well contains water only, a very high value is assigned to the transmissivity of the zone representing the well, and its storativity is set to one. This ‘high transmissivity’ approach is illustrated here and verified against the well-known analytical model for the simulation of a slug test conducted in a finite-diameter well fully penetrating a confined aquifer (Cooper et al., 1967).

5.5.6.1. Problem statement

Consider a confined aquifer with constant transmissivity T and constant storativity S . Axisymmetric transient flow in the aquifer is governed by the well-known diffusion equation:

$$\frac{\partial^2 s}{\partial r^2} + \frac{1}{r} \frac{\partial s}{\partial r} = \frac{S}{T} \frac{\partial s}{\partial t} \quad (150)$$

Partial differential equation (150) is the same as the one that is applied to obtain the famous Theis (1935) equation. Similarly, an aquifer of infinite lateral extent is assumed:

$$s(\infty, t) = 0 \quad (151)$$

The condition at the inner model boundary is different, however, since a well of finite radius r_w [L] is considered in which an instantaneous head change H_0 [L] occurs. This means the initial drawdown at $t = 0$ is equal to zero in the aquifer and to H_0 at the well-face:

$$s(r, 0) = \begin{cases} 0 & (r > r_w) \\ H_0 & (r = r_w) \end{cases} \quad (152)$$

As the radius of the well is not infinitesimal, wellbore storage must be taken into account by defining the wellbore balance:

$$2\pi r T \frac{\partial s}{\partial r} = \pi r_c^2 \frac{dH}{dt} \quad (r = r_w; t > 0) \quad (153)$$

with r_c the radius [L] of the well-casing where the change of water level H [L] inside the wellbore takes place. It is assumed that the water level change H equals the drawdown at the well face or $H(t) = s(r_w, t)$.

5.5.6.2. Solution

As the aquifer is of infinite extent in the radial direction according to boundary condition (151), the general solution to the Laplace transform of equation (150) is $\bar{s}(r, p) = \beta K_0(r\sqrt{d})$, with $d = \sqrt{pS/T}$, and β an arbitrary constant, which is found by introducing the general solution into the remaining boundary condition (153). The Laplace transform of boundary condition (153) requires the first derivative of \bar{s} with respect to r , which equals $-\beta\sqrt{d}K_1(r\sqrt{d})$. Recalling that $H(t) = s(r_w, t)$, and using initial condition (152), the Laplace transform of dH/dt is $p\bar{s}(r_w, p) - H_0$. Using the general solution, the Laplace transform of boundary condition (153) is thus written as:

$$-2\pi r_w T \beta \sqrt{d} K_1(r_w \sqrt{d}) = \pi r_c^2 [p\beta K_0(r_w \sqrt{d}) - H_0] \quad (154)$$

From equation (154), an expression for constant β is found, which is substituted in the general solution to finally yield the exact solution in the Laplace domain:

$$\bar{s}(r, p) = \frac{r_w S H_0 K_0(r\sqrt{d})}{T \sqrt{d} \left[r_w \sqrt{d} K_0(r_w \sqrt{d}) + 2 \frac{r_w^2}{r_c^2} S K_1(r_w \sqrt{d}) \right]} \quad (155)$$

The exact solution in the Laplace domain given by equation (155) is also found in Cooper et al. (1967). Note that the modified Bessel functions of the second kind in the nominator must have order 0 and 1 respectively. In equation (7) of the original paper of Cooper et al. (1967), the modified Bessel functions of the second kind are all of order 0, which is probably a typo.

The solution in Laplace space for the head change inside the well is found by setting r in equation (155) to r_w . Cooper et al. (1967) invert expression (155) analytically to obtain a closed-form solution. Because this solution contains an improper integral that must be approximated numerically, it is more straightforward to invert expression (155) numerically applying the Stehfest (1970) algorithm.

As already explained briefly in the introduction of this section, the stated problem of axisymmetric flow toward a well in which a slug test is conducted can also be solved applying the semi-analytical approach presented in this chapter. In this case, one layer and two zones are defined, where the first zone corresponds to the well and the second zone to the aquifer. This means distance R_1 of the boundary between the two zones is set to r_w . The inner model boundary has an infinitesimal radius; the outer model boundary is at an infinitely large distance. Because the well only contains water, a very large value is assigned to the transmissivity of the first zone, e.g. $T_1 = 10^5$, and its storativity is

defined so that wellbore balance equation (153) is fulfilled: $S_1 = r_c^2/r_w^2$. The aquifer parameters are assigned to the parameters of the second zone: $T_2 = T$ and $S_2 = S$. As the aquifer is confined, resistances c are all infinitely large. According to initial condition (152), initial head φ_2 in the second zone is zero, and initial head φ_1 in the first zone representing the well must be set to H_0 .

The stated problem can also be solved using the finite-difference approach, in which case the same trick may be applied to define an inner zone with high transmissivity that conceptualizes the well. However, a more effective approach is to assign a small width to the first grid cell representing the well, and to set its storativity to the horizontal wellbore surface area (Louwyck et al., 2012, 2014). This approach is discussed in more detail in section 6.4.1 of the next Chapter 6; in this section, the ‘high transmissivity’ approach is applied.

5.5.6.3. Example

Figure 8 shows the normalized head change H/H_0 as a function of dimensionless time tT/r_c^2 for different values of dimensionless parameter Sr_w^2/r_c^2 . Figure 8 is actually a reproduction of Fig. 3 in the original paper of Cooper et al. (1967).

The solid lines correspond to the numerically inverted Laplace solution (155) by Cooper et al. (1967), the black dotted lines are simulated using the generalized semi-analytical solution derived in section 5.3, and the black dots are the finite-difference solution. All methods virtually give the same results, even though the well is conceptualized as a ‘large transmissivity’ zone in both the generalized semi-analytical and the finite-difference model. As already mentioned, a mathematically more rigorous approach is developed to deal with finite-diameter wells open to one or more layers in the next Chapter 6.

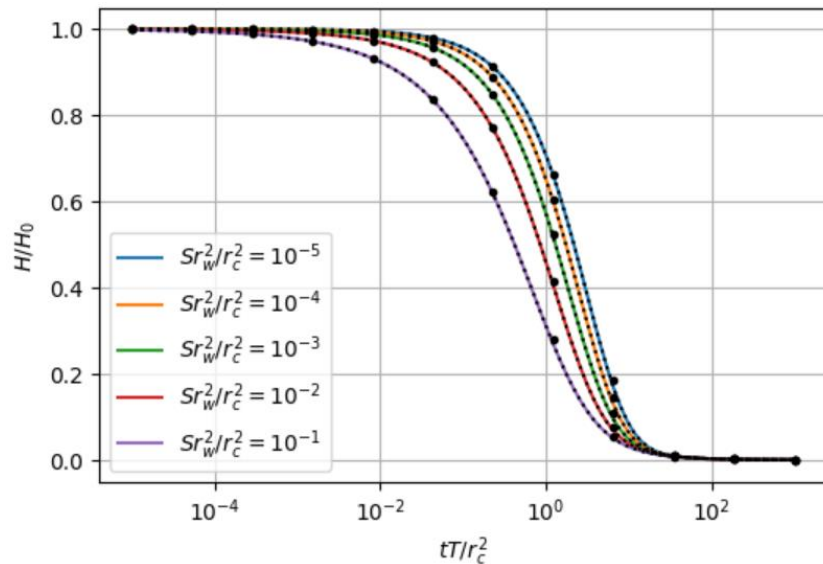


Figure 8. Plot of the normalized head change inside the well as a function of dimensionless time for the Cooper et al. (1967) model simulating axisymmetric flow toward a fully penetrating well in a confined aquifer with transmissivity T and storativity S . The well is stressed by an instantaneous head change H_0 at time $t = 0$. The well-screen radius is r_w , the radius of the casing is r_c . The solid lines are the numerically inverted Laplace solution by Cooper et al. (1967), the black dotted lines are simulated applying the generalized semi-analytical solution presented in this chapter, and the black dots are the finite-difference solution. See text for definition of parameters and derivation of solutions.

5.5.7. Embanked river infiltrating a multilayer aquifer system

The ‘high transmissivity’ trick can also be applied to simulate the effect of a water level change in a river that is interacting with the groundwater reservoir, which is illustrated in the final test case of this chapter. In this example, the effect of a permanent average water level rise of 1 m in an

embanked river is simulated. The river infiltrates an aquifer system consisting of multiple layers. Figure 9 shows the schematization of the system. It is assumed the effect of the water level rise only affects the four uppermost aquifers, which explains why only these aquifers are included in the model. The interaction with the deeper part of the groundwater reservoir is simplified by the leaky lower boundary condition, which comprises resistance c_4 of the bounding aquitard and a constant-head at the bottom of this aquitard. The three aquitards separating the four aquifers are also conceptualized as resistance layers of zero thickness. This means the model consists of four layers corresponding to the four aquifers. The parameter values are given in Figure 9.

The river has a width of 20 m; the dike embanking it also has a width of 20 m. As the water level rise in the river is permanent, steady groundwater flow in the aquifer system is simulated. Parallel flow is assumed which is perpendicular to the river axis. This means the three-dimensional problem is reduced to a two-dimensional profile model that represents a vertical cross section of the groundwater flow system. That is why only half of the river is included in the model, as is seen on Figure 9.

Adjacent to the river, there is a polder area that extends up to 500 m from the middle of the river. This low-lying area is drained by a dense system of ditches with constant drainage level and an average drainage resistance of 10 d. The interaction between this drainage system and the top aquifer is also conceptualized as a leaky boundary condition. Next to the polder area, a recharge area occurs where the excess of rainfall infiltrates the top aquifer at a constant average rate of 100 mm per year. Because of the leaky boundary conditions at the top and bottom of the model, it is justified to assume this area has an infinitely large extent.

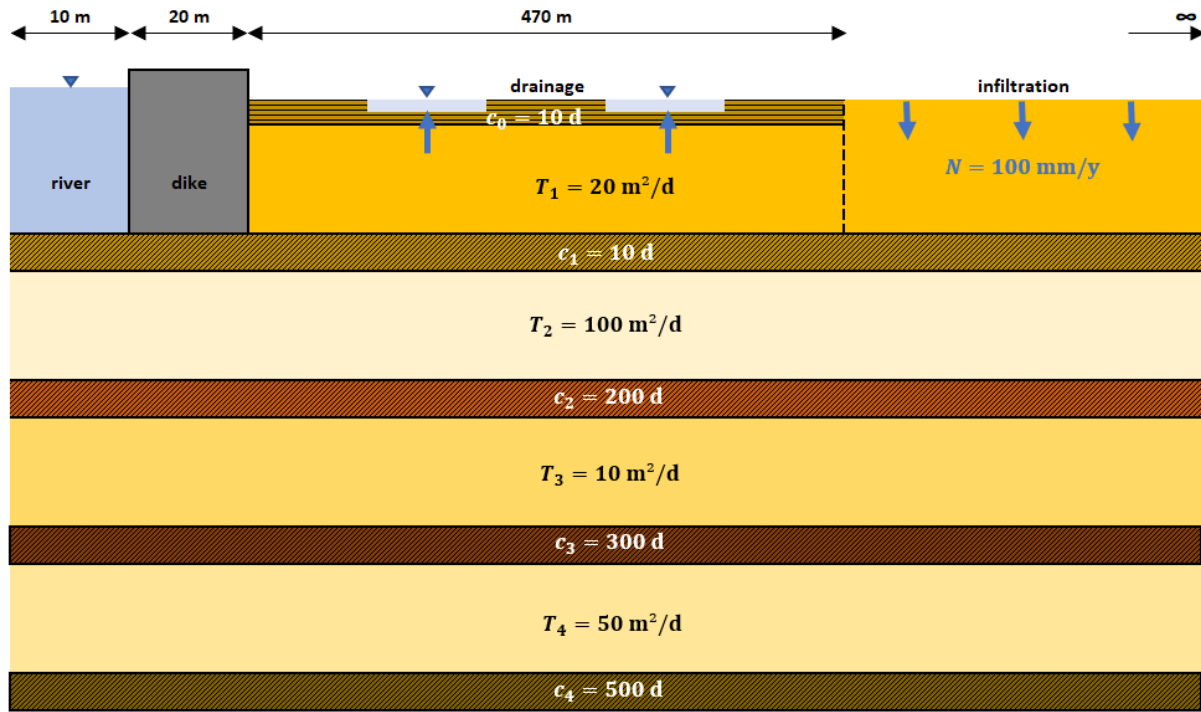


Figure 9. Schematization of the multi-aquifer system recharged by an embanked river with constant water level. The aquifers are characterized by transmissivities T_i , the aquitards by resistances c_i . The aquifer system has a leaky lower boundary. Close to the river, the top aquifer is discharged by a drainage system with constant level and resistance c_0 . Further away, the top aquifer is infiltrated at constant flux N . Horizontal and vertical distances are not to scale. See text for definition of parameters.

Three model setups are considered to solve the two-dimensional parallel flow problem. First, the semi-analytical solution method discussed in Chapter 2 is used. This method developed by Hemker

(1984) assumes the layers are homogeneous, which comes down to defining only one zone using the solution method discussed in this chapter. As a consequence, the river cannot be part of the model in this setup, so the inner model boundary at distance R_0 equal to 10 m, which implies the presence of the dike is ignored. Since the change in head close to the river is of interest here, the infiltration is also omitted, and the top layer is drained over its full horizontal extent.

Mathematically, the inner boundary condition is a mixed-type condition: in the top layer, a constant head is defined which corresponds to the head rise in the river, whereas a no-flux condition is required in the other layers. This difficulty is circumvented by defining a constant infiltration rate from river to upper layer that equals 1 and applying the superposition principle. As the system of equations and boundary conditions is linear, the head change s_i [L] in layer i is proportional to infiltration rate Q [L^3/T]:

$$s_i(r) = Q\sigma_i(r) \quad (156)$$

with σ_i the head change [L] due to unit recharge. The validity of expression (156) was discussed exhaustively in section 2.4 of Chapter 2. The unknown infiltration rate Q can be derived by setting $Q\sigma_1(R_0)$ in (156) to the known head change in the river $s_1(R_0)$, which equals 1 in this example. This gives:

$$s_i(r) = \frac{\sigma_i(r)}{\sigma_1(R_0)} \quad (157)$$

Expression (157) simply states that the head changes $\sigma_i(r)$ simulated using the model with unit recharge must be divided by the simulated head change $\sigma_1(R_0)$ in the river to obtain the head changes $s_i(r)$ due to a head rise of 1 m in the river.

In the second model setup, three zones are defined: the first zone has a width of 10 m and contains the river, the second zone corresponds to the drained polder area, and the third zone conceptualizes the recharge area. The effect of the dike is also neglected in this case. The difference with the previous setup is that the interaction between river and aquifer system is not restricted to the top aquifer, but there is also vertical flow through the first aquitard from the river to the second aquifer. In the first zone, the transmissivity of the first layer is set to $10^5 \text{ m}^2/\text{d}$ to simulate the effect of the surface water body and the upper resistance in this zone is set to an infinitely large value.

To deal with the mixed-type boundary condition in this setup, additionally, a dummy zone of width 10^3 m is defined at the inner boundary. In each layer of this zone, a constant head is defined: in the first layer, this constant head is set to the head rise in the river equal to 1 m, and in the other layers the constant head is set to 0. To nullify the effect of these constant heads in the lower layers, a very small value of $10^{-5} \text{ m}^2/\text{d}$ is assigned to the layer transmissivities of this zone, except the transmissivity of the first layer, which is set to $10^5 \text{ m}^2/\text{d}$, as this layer is part of the river.

The third and final model setup is the same as the second one, with the exception of an extra zone that is defined to include the semi-pervious dike in the first layer, to which a small value of $10^{-3} \text{ m}^2/\text{d}$ is assigned. In this way the horizontal flow from the river to the top aquifer is impeded, which is a more realistic scenario. Furthermore, there is no difference between the second and the third setup. Figure 10 summarizes the differences between the three scenarios by visualizing how the inner model boundary is defined in the three model setups.

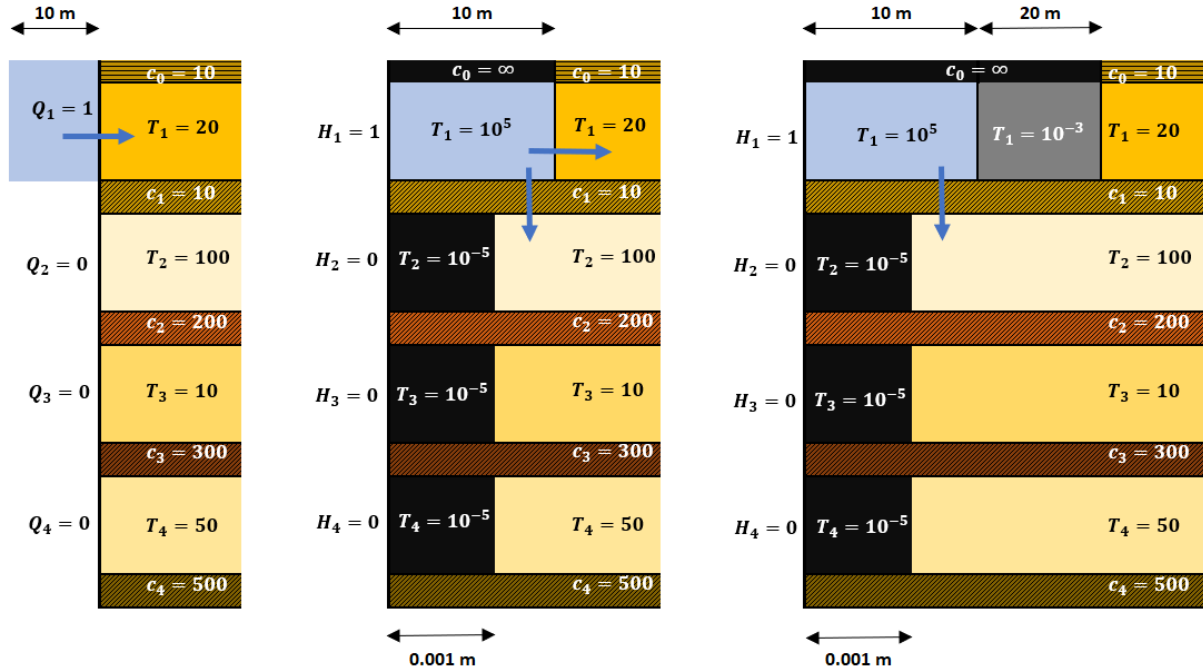


Figure 10. Visualization of the three model setups that are applied to simulate the effect of a permanent water level rise of 1 m in an embanked river infiltrating a multi-aquifer system. The first scheme visualizes the first model setup, in which the river is conceptualized as a constant-recharge boundary condition. Recharge Q_1 is set to 1 and superposition is applied to ensure the head rise in the river is 1 m. The middle scheme is the second model setup in which the river corresponds to the blue zone with high transmissivity equal to 10^5 . The water level rise in the river is simulated using a constant-head boundary $H_1 = 1$ m. In the other layers, the effect of the constant heads is nullified by introducing the black small zone with a low transmissivity of 10^{-5} . The right scheme corresponds to the third model setup, which is the same as the second setup. The only difference is the extra gray low transmissive zone in the first layer that conceptualizes the river embankment. For the sake of visibility, horizontal and vertical distances are not to scale, and parameter units are omitted. Transmissivities T are in m^2/d , resistances c are in d , recharges Q are in $m^3/d/m$, and heads H are in m . See text for definitions and a more detailed explanation of the model setups.

Figure 11 shows the head changes in the four aquifers as a function of the horizontal distance to the center of the river. The left graph is the result for the second scenario without dike, the right graph for the third scenario with dike. In both plots, the solid lines are simulated using the generalized semi-analytical solution derived in section 5.3, and the black dotted lines are the finite-difference solution. It is seen that both solution techniques yield virtually the same results. The head changes simulated using the semi-analytical model with homogeneous layers according to the first model setup are displayed on both plots as cyan colored thin solid lines. Comparing the results of this first scenario with the other simulations shows that neglecting the vertical flow between river and aquifer system clearly underestimates the effect of the head rise in the river. On the other hand, this effect only occurs close to the river, and it is mitigated by the river embankment.

Although this example solves a fictitious problem with the sole purpose of demonstrating and verifying the semi-analytical multilayer-multizone solution developed in this chapter, the situation of a wide embanked river recharging a low-lying polder area is very typical in Flanders and the Netherlands. It is also not hard to imagine the typical cross-sectional groundwater flow pattern of an infiltrating river next to a discharging area from Figure 11. Indeed, below the river, the heads decrease with depth which implies groundwater flow goes down, whereas the heads are reversed and flow goes up in the drainage area.

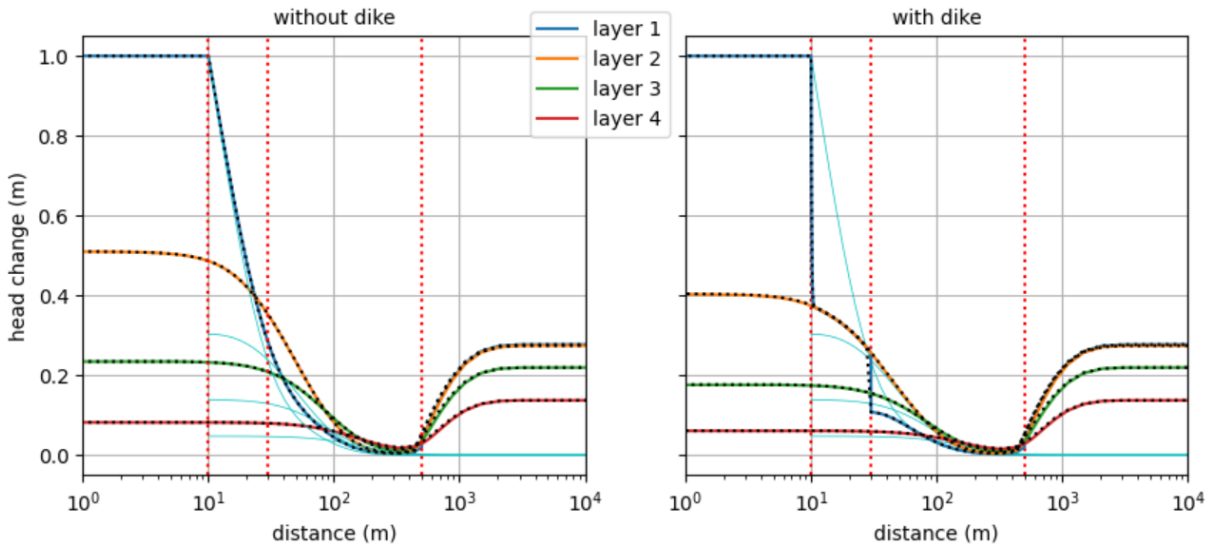


Figure 11. Plots of head change as a function of horizontal distance for different models simulating the effect of a permanent water level rise in an embanked river infiltrating a four-aquifer system that is drained close to the river and infiltrated by precipitation excess further away from the river. The first model contains homogeneous layers corresponding to the four aquifers. It has a leaky upper and lower boundary, which means the recharge area is omitted. The river is conceptualized as a boundary condition with specified recharge. The model is simulated using the generalized semi-analytical method by Hemker (1984) and the results are the cyan thin solid lines drawn on both plots. In the second and third model, the river is modeled as a separate high-transmissivity zone in which a constant head of 1 m is defined. In the second model, the effect of the river embankment is neglected (left plot), whereas the dike enclosing the river is a separate low-transmissivity zone in the third model (right plot). The vertical red dotted lines indicate the boundaries between the different zones: the first and second zone contain river and dike, respectively; the third and fourth zone have a draining and infiltrating top aquifer, respectively. Both models are simulated using the generalized semi-analytical solution presented in this chapter (solid lines), and applying the finite-difference method (black dotted lines). See Figure 9 for the problem schematization and the parameter values, and Figure 10 for a visualization of the three model setups. See text for definition of parameters and derivation of solutions.

Because it is a typical situation in the Netherlands, Hemker (1984) not only presents the generalized solution for parallel flow in a system consisting of an arbitrary number of homogeneous aquifers separated by aquitards, he also gives an example involving a more complicated river boundary condition that is similar to the example presented in this section. In his example, however, the stream partially penetrates a leaky semi-pervious top layer instead of a phreatic aquifer. Hemker (1984) solves the problem by coupling two models consisting of the same layers but with different leaky top boundary conditions: the first model represents the river and the aquifer system below it, the second model simulates the flow in the remaining part of the aquifer system. This approach is basically the same as the semi-analytical solution method developed in this chapter, and using this method, the example given by Hemker (1984) could be solved easily by defining a model that consists of two leaky zones, where each zone has a different hydraulic resistance at the top.

5.6. Skin effect

The most relevant application of a multizone model is undoubtedly the analysis of the effect of a finite-thickness skin on the simulation and interpretation of aquifer tests. To underline the importance of the skin effect, Houben et al. (2016) did a search on the Scopus database, and found more than 1000 papers containing the term “wellbore skin”, most of them related to the petroleum industry. Kruseman and de Ridder (1990) also refer to petroleum engineering where the head losses in the vicinity of the well are called the “skin effect”, as they are caused by a thin, resistant “skin” against the wall of the borehole. Similarly, Houben et al. (2016) describe the wellbore skin – also termed “skin layer” or “filter cake” – as a thin layer of low conductivity deposited close to the borehole wall, usually formed during the drilling process.

Due to its low conductivity, the wellbore skin can be one of the largest contributors to the total well-loss, despite its relatively small thickness (Houben, 2015). As it may have a significant negative effect on well-yield, well-performance tests are conducted to quantify the skin effect, such as the classical step-drawdown test and the recovery test (Kruseman & de Ridder, 1990). Traditionally, the skin effect is simulated assuming a wellbore skin of infinitesimal thickness (e.g. Cassiani et al., 1999; Cassiani & Kabala, 1998; Chang & Chen, 2002; Dougherty & Babu, 1984; Hemker, 1999b; Moench, 1997). Under this assumption, a dimensionless skin factor may be used to estimate the linear head losses due to the skin and correct the drawdown inside the well accordingly (Houben, 2015; Kruseman & de Ridder, 1990).

However, more sophisticated models can handle a finite-thickness skin by defining a cylindrical zone around the well to which hydraulic parameters are assigned that characterize the wellbore skin. These skin parameters are different from the aquifer parameters. The model presented by Butler (1988) and discussed in section 5.5.5 is one of the many semi-analytical models found in the literature that include a finite-thickness skin around the well (e.g. Barua & Bora, 2010; Chang & Chen, 2002; Chang et al., 2010; Chiu et al., 2007a, 2007b; Feng & Wen, 2016; Feng & Zhan, 2016, 2019; Huang et al., 2015; Hyder et al., 1994; Novakowski, 1993; Perina & Lee, 2006; Yang et al., 2014; Yang & Yeh, 2005, 2009; Yeh & Yang, 2006).

In this section, the analysis of the skin effect presented by Louwyck et al. (2010, 2014) is revisited. Louwyck et al. (2010) analyze step-drawdown tests and quantify the well-losses using the inverse numerical model developed by Lebbe (1999). Remarkably, the interpretation of some of the tests yield a negative well-loss coefficient, which the authors attribute to the fact the pumping well is effectively developed in these cases. Here, it is theoretically explained under which conditions a negative well-loss coefficient could be derived.

Louwyck et al. (2014) use the Butler (1988) solution to show that the dimensionless skin factor may be derived from the approximate solution for large values of time. As discussed in section 5.5.5, this approximate solution is the corresponding steady-state solution with an outer model boundary that expands with time. Using the steady-state multizone solution derived in section 5.5.3, the dimensionless skin factor assuming a zero-thickness skin can be generalized to estimate linear well-losses due to multiple cylindrical zones of different hydraulic conductivity around the pumping well. Theoretically, this solution is valid only for wells fully penetrating a confined aquifer. Therefore, it is investigated if it is still justified to apply the skin factor to estimate the linear well-losses in a pumping well extracting water from a multilayer system.

5.6.1. Linear and non-linear well losses

Kruseman and de Ridder (1990) divide the drawdown inside the pumping well up into aquifer losses and well losses. As the names suggest, the first are attributed to the laminar Darcian flow of groundwater in the aquifer, whereas the latter are caused by the flow in the disturbed zone around the well, the flow through the well-screen, and the flow inside the borehole. Concerning the well losses, Kruseman and de Ridder (1990) also distinguish between linear and nonlinear head losses. These three types of head losses – aquifer losses and linear and nonlinear well losses – can be expressed in the following formula :

$$s_w(t) = B_1 Q + B_2 Q + C Q^p \quad (158)$$

with s_w the drawdown [L] in the pumping well which is a function of time t [T], Q the constant pumping rate [L^3/T], B_1 the linear aquifer-loss coefficient [T/L^2], B_2 the linear well-loss coefficient [T/L^2], and C the nonlinear well-loss coefficient [T/L^{3p-1}].

Exponent p in equation (158) is a number that may be determined empirically, for instance, by interpreting step-drawdown test data (Lebbe, 1999), although deriving both C and p reliably along with the aquifer parameters that determine B_1 is mathematically challenging or even impossible as the inverse system is ill-posed (Louwyck et al., 2010). Therefore, the value for p is mostly estimated a priori. Jacob (1947) suggests $p = 2$, a value which is still widely accepted (Houben & Kenrick, 2022), although p may range between 1.5 and 3.5 (Kruseman & de Ridder, 1990), or even between 0.35 and 6.01 (Kurtulus et al., 2019).

If the linear head losses at the well are combined into a single term, then equation (158) reduces to:

$$s_w(t) = B(r_e, t)Q + CQ^p \quad (159)$$

where $B(r_e, t) = B_1 + B_2$. Coefficient B [T/L²] not only depends on time t , but also on radius r_e [L], the effective well-radius, which Jacob (1947) defines as the radial distance at which the theoretical drawdown, based on the logarithmic head distribution, equals the drawdown just outside the well screen.

Houben (2015) divides the total drawdown in the pumping well into five components:

$$s_w = s_{aq} + s_{sk} + s_{gp} + s_{sc} + s_{up} \quad (160)$$

with s_{aq} the aquifer loss [L], s_{sk} the skin-layer loss [L], s_{gp} the gravel-pack loss [L] which also includes convergence loss [L], s_{sc} the well-screen loss [L], and s_{up} the upflow loss [L] in the well-interior, which is the sum of losses in screen and casing. The wellbore skin refers to the filter cake, that is the fine material covering the borehole wall (Houben, 2015). The gravel pack is the artificially-graded coarser material immediately surrounding the well-screen, with a recommended thickness in the range of 8 to 15 cm (Kruseman & de Ridder, 1990). In some cases, there is an inner and an outer gravel pack, where the inner gravel is finer than the outer, or vice versa. If there is a skin, then it is located between the gravel pack and the aquifer (Houben, 2015; Houben et al., 2016). Convergence refers to the flow at the interface between gravel pack and screen, where flow paths in the gravel pack indeed converge toward the screen slots (Houben, 2015). Although gravel pack and screen are more pervious than the aquifer, they may be affected by mechanical and biogeochemical clogging processes, which constrict the hydraulically effective area, and consequently increase the head losses (Houben et al., 2018). In this case, a well-skin in the strict sense of the word is present.

Flow in the aquifer, the skin, and the gravel pack include both viscous and inertial flow components, although nonlinear laminar flow commonly becomes relevant only in the gravel pack (Houben, 2015; Houben & Kenrick, 2022). The first is generally referred to as Darcian or linear flow, as it is governed by Darcy's law, whereas the latter is referred to as non-Darcian or nonlinear flow, and may be described, for instance, by the Forchheimer (1901) equation. If this equation is applied according to Engelund (1953) with the modification suggested by Barker and Herbert (1992), then the nonlinear gravel pack loss is proportional to the square of the pumping rate. Flow in the screen slots and the well interior is turbulent under almost all circumstances, and different approaches exist to simulate their effect (Houben, 2015). If the orifice equation by Barker and Herbert (1992) is used to describe the flow in the screen, and the Darcy-Weisbach equation (Weisbach, 1845) for the flow inside the casing, then the well-screen and upflow losses are also proportional to the square of the pumping rate (Houben, 2015). In this case, equation (160) relates to equation (159) as follows (Houben & Kenrick, 2022):

$$s_w = (s_{aq} + s_{sk} + s_{gp}) + (s_{gpn} + s_{sc} + s_{up}) = BQ + CQ^2 \quad (161)$$

with $s_{gp} = s_{gpl} + s_{gpnl}$. Equation (161) shows that the linear head losses BQ are composed of the aquifer loss s_{aq} , the skin loss s_{sk} , and the linear gravel-pack loss s_{gpl} , whereas the nonlinear head losses CQ^2 comprise the nonlinear gravel-pack loss s_{gpnl} , the screen loss s_{sc} , and the upflow loss s_{up} .

5.6.2. Dimensionless skin factor

According to Kruseman and de Ridder (1990), the theoretical concept of wellbore skin relates to the concept of linear well-loss which comprises head losses due to compaction or plugging of the aquifer during drilling, and head losses in the gravel pack and in the screen. These head losses are lumped together into the linear well-loss component, i.e. term $B_2 Q$ in equation (158) which equals $s_{sk} + s_{gpl}$. The linear well-loss component may be characterized by a dimensionless skin factor F_{skin} defined as (Hemker, 1999b; Houben, 2015; Kruseman & de Ridder, 1990):

$$F_{skin} = \frac{K^h \Delta r_s}{K_s^h r_w} \quad (162)$$

with r_w the well-screen radius [L], Δr_s the thickness [L] of the skin, and K^h and K_s^h the conductivity [L/T] of aquifer and skin, respectively. In this case, the skin comprises the gravel pack and a possible filter cake. If nonlinear well-loss due to inertial flow in the gravel pack and friction losses and turbulent flow in the screen and the wellbore is neglected, total drawdown in the pumping well is calculated as (Kruseman & de Ridder, 1990):

$$s_w(t) = s(r_w, t) = s(r_s, t) + \frac{Q}{2\pi K^h L} F_{skin} \quad (163)$$

with L the screen length [L], and r_s the outer radius [L] of the skin, i.e. $r_s = r_w + \Delta r_s$. If flow and friction losses are neglected, then there is a hydrostatic equilibrium within the borehole (Bennett et al., 1982), which implies the drawdown in the well $s_w(t)$ is equal to the drawdown at the well-face $s(r_w, t)$. Drawdown $s(r_s, t)$ is the drawdown in the aquifer at the outer boundary of the skin.

According to equation (163), drawdown s_w in the pumping well is equal to the drawdown $s(r_s, t)$ at the outer radius of the skin, obtained from an analytical or numerical model considering a homogeneous aquifer, plus a supplementary drawdown, which is a linear function of the pumping rate Q . Comparing equation (163) to equation (158) with $C = 0$, it is concluded that $s(r_s, t) = B_1 Q$ and:

$$B_2 = \frac{F_{skin}}{2\pi K^h L} \quad (164)$$

The skin effect may be positive or negative, respectively if the conductivity of the skin is smaller or larger than the aquifer conductivity (Barrash & Dougherty, 1997; Chiu et al., 2007b; Kruseman & de Ridder, 1990; Lebbe, 1999). Although well development should result in a zone of improved conductivity around the wellbore, it is indeed possible that a filter cake is present at the end of the drilling operation, which causes a smaller conductivity (Houben, 2015). Obviously, clogging of screen and/or gravel pack may also result in a smaller conductivity (Houben et al., 2018).

In case of a negative skin effect, the total drawdown in the well is less than the theoretical drawdown in the well without skin effect, which may result into a negative well loss coefficient if well performance is evaluated through analysis of step-drawdown test data, as is illustrated by Louwyck et al. (2010). This needs some clarification, as it is hydraulically impossible the head in the well is higher than the head at the outer boundary of the skin, which would imply groundwater is flowing away from the well. Louwyck et al. (2010) apply the method proposed by Lebbe (1999) who defines the head in the well as follows:

$$s_w(t) = B_1 Q + C Q^p \quad (165)$$

Comparing equation (165) with equation (158) by Kruseman and de Ridder (1990), it is seen that Lebbe (1999) does not take into account the linear well-loss equal to $B_2 Q$. Reformulating equation (165) by Lebbe (1999) using equation (161) by Houben and Kenrick (2022) gives:

$$s_w = s_{aq} + (s_{gpnl} + s_{sc} + s_{up}) = B_1 Q + C Q^2 \quad (166)$$

where Lebbe (1999) sets s_{aq} to $s(r_w, t)$ instead of $s(r_s, t)$.

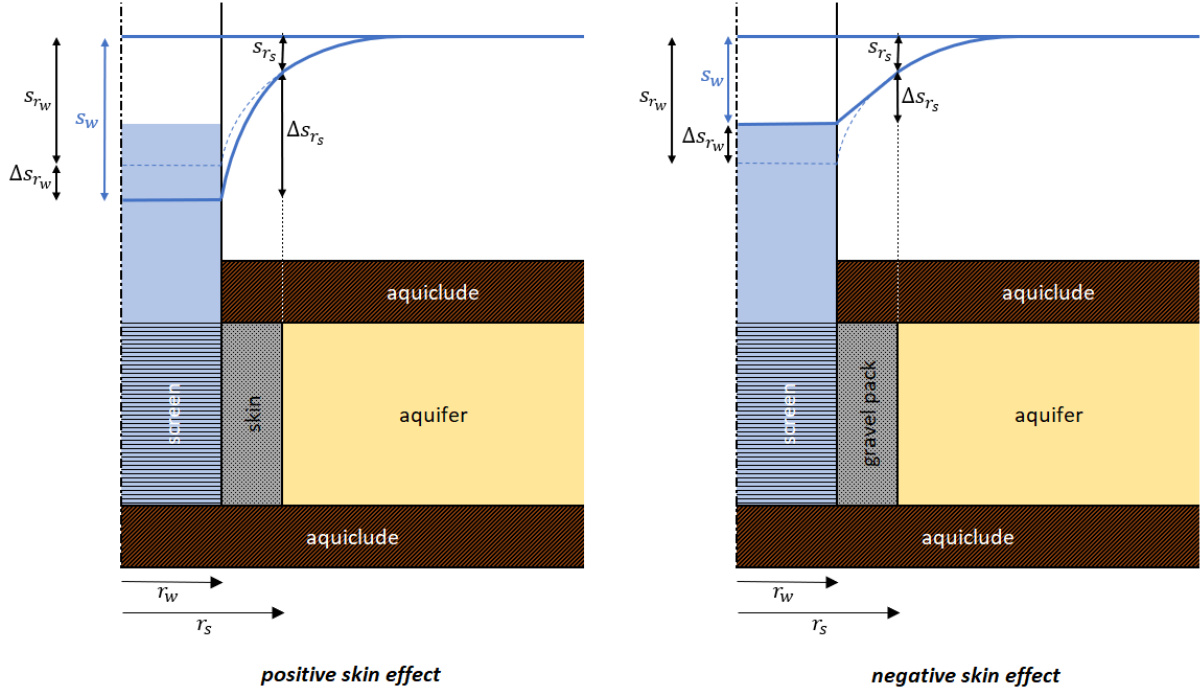


Figure 12. Illustration of the skin effect on drawdown s_w in a pumping well with radius r_w . The left drawing shows the positive skin effect of a low conductivity skin with radius r_s , which results into an additional drawdown Δs_{r_w} in the well compared with the theoretical drawdown s_{r_w} without skin. The right drawing shows the negative skin effect of a highly permeable gravel pack with radius r_s , which results into a smaller drawdown s_w in the well than the theoretical drawdown s_{r_w} without gravel pack. Traditionally, drawdown s_w in the well is estimated by simulating drawdown s_{r_s} at the interface between skin or gravel pack and aquifer, and adding the head loss Δs_{r_s} due to skin or gravel pack, which is calculated using the dimensionless skin factor (Kruseman & de Ridder, 1990). This theory is applicable if the pumping well is fully penetrating a confined aquifer, as is shown on the drawings. It is also possible to simulate the theoretical drawdown s_{r_w} at the well-face, and correct it by estimating Δs_{r_w} from step-drawdown test data (Lebbe, 1999). Drawdown difference Δs_{r_w} is positive in case of a positive skin effect and negative in case of a negative skin effect. Distances are not to scale. See text for definitions and further explanation.

Summarizing, Lebbe (1999) simulates the drawdown at the face of the well-screen and adds the non-linear well-loss term $C Q^2$ to this drawdown, while Kruseman and de Ridder (1990) suggest to calculate drawdown at the outer boundary of the skin and to correct this drawdown for linear and nonlinear well-losses. In the latter case, it is impossible to have negative well-loss coefficients B_2 and C , whereas in the first case, the well-loss coefficient C is negative indeed if there is a negative skin effect, which is demonstrated by Louwyck et al. (2010) through interpretation of synthetic and real step-drawdown test data. Figure 12 illustrates the difference between positive and negative skin effect and the way it is calculated according to Kruseman and de Ridder (1990), amongst others, and according to Lebbe (1999).

5.6.3. Multi-zone skin factor

Theoretically, skin factor F_{skin} applies to an infinitely thin skin only, i.e. $\Delta r_s \rightarrow 0$. In practice, the thickness of the skin should be negligibly small. If the thickness of the skin is not negligibly small, then the skin factor should be calculated as (Louwyck et al., 2014):

$$F_{skin} = \frac{K^h}{K_s^h} \ln\left(\frac{r_s}{r_w}\right) = \frac{K^h}{K_s^h} \ln\left(1 + \frac{\Delta r_s}{r_w}\right) \quad (167)$$

As $\ln(1 + x) \rightarrow x$ if $x \rightarrow 0$, it is seen that expression (162) approximates (167) if $\Delta r_s \rightarrow 0$. Equation (167) is also found in Houben (2015).

The skin factor applies to a single cylindrical zone around the well. In reality, however, more than one zone may be present, in which case the skin factor should incorporate the linear head losses due to each of these zones. Using solution (116) for steady flow in a confined aquifer consisting of multiple zones given in section 5.5.3, it is straightforward to extend the definition of the skin factor to multiple zones. If constant head φ at the outer model boundary is set to zero, then equation (116) expresses the head change s . If drawdown at the well-face is considered, (116) simplifies to:

$$s(R_0) = \frac{Q}{2\pi} \sum_{k=0}^{n_z-1} \frac{\ln(R_{k+1}/R_k)}{T_{k+1}} \quad (168)$$

Houben (2015) presents an approach considering both linear and nonlinear well losses in which the first head losses are calculated using equation (168) with 3 zones: gravel pack, skin, and aquifer.

Rearranging equation (168) by splitting off the last term which corresponds to the actual aquifer:

$$s(R_0) = \frac{Q}{2\pi T_{n_z}} \ln\left(\frac{R_{n_z}}{R_{n_z-1}}\right) + \frac{Q}{2\pi} \sum_{k=0}^{n_z-2} \frac{\ln(R_{k+1}/R_k)}{T_{k+1}} \quad (169)$$

Generalizing equation (163) to include n_z zones instead of 2:

$$s_w = s(R_0) = s(R_{n_z-1}) - \frac{Q}{2\pi T_{n_z}} F_{skin} \quad (170)$$

Note that radius R_0 corresponds to the well-radius r_w , radius R_{n_z-1} to radius r_s of the boundary between disturbed zone and aquifer, and transmissivity T_{n_z} equals $K^h L$. Comparing equations (169) and (170), it is seen that the multizone skin factor must be defined as:

$$F_{skin} = T_{n_z} \sum_{k=0}^{n_z-2} \frac{\ln(R_{k+1}/R_k)}{T_{k+1}} \quad (171)$$

If the skin consists of only one zone, and consequently, two zones are considered in the model, equation (171) indeed reduces to equation (167):

$$F_{skin} = \frac{T_2}{T_1} \ln\left(\frac{R_1}{R_0}\right) \quad (172)$$

with $T_2 = K^h L$, $T_1 = K_s^h L$, $R_1 = r_s$, and $R_0 = r_w$. Theoretically, equations (170) and (171) are valid only for a fully penetrating well, in which case screen length L equals the aquifer thickness.

5.6.4. Skin effect in case of transient flow

As discussed in section 5.5.5, it is also justified to use equation (169) for large values of time in case of transient axisymmetric flow toward a fully penetrating well in a confined aquifer. Recall that in the transient case, R_{n_z} is time-dependent, and given by equation (149). Substituting R_{n_z} in equation (169) gives:

$$s(R_0, t) = \frac{Q}{4\pi T_{n_z}} \ln \left(\frac{4T_{n_z}t}{\eta S_{n_z} R_{n_z-1}^2} \right) + \frac{Q}{2\pi} \sum_{k=0}^{n_z-2} \frac{\ln(R_{k+1}/R_k)}{T_{k+1}} \quad (173)$$

From equation (173), it follows that definition (171) for skin factor F_{skin} is still valid for large values of time in the transient case of a fully penetrating well extracting water from a confined aquifer.

In case of two zones, equation (173) simplifies to solution (146) presented by Barker and Herbert (1982) and by Butler (1988), with $r = R_0$ and $R = R_1$. As already mentioned, Houben (2015) also applies an expression similar to equation (173) considering 3 zones to evaluate the linear head-losses in gravel pack, skin, and aquifer, and he also proposes to use the time-dependent radius of influence formula similar to expression (149) based on the Cooper and Jacob (1946) approximation of the Theis (1935) equation.

Summarizing, equations (170) and (171) applying the multizone skin factor are not only valid for steady flow toward a fully penetrating well in a confined aquifer, but they may be used for transient flow as well. In the transient case, the skin factor is applicable for large times only when a pseudo steady state occurs in the disturbed zone around the pumping well. This implies that the radial discharge at the interface between aquifer and skin should be approximately equal to the pumping rate, or $Q^h(R_{n_z-1}, t) \approx Q$.

As an example, reconsider the test case discussed in section 5.5.5 in which transient flow is simulated toward a pumping well encircled by a gravel pack and fully penetrating a confined aquifer. The simulations are carried out again, and this time, the horizontal discharge Q^h in the aquifer is also calculated. The results are shown in Figure 13. Recall that transmissivity T_1 of the gravel pack is 10 times larger than the aquifer transmissivity T_2 , and that its storativity S_1 is 10 times smaller than the aquifer storativity S_2 . The left plot shows the dimensionless drawdown sT/Q as a function of relative distance r/R at different dimensionless times $\frac{tT}{SR^2}$, with $T = T_1 + T_2$, $S = S_1 + S_2$, and R the outer radius of the gravel pack.

For this example, dimensionless skin factor F according to (167) is 0.230, and linear well-loss coefficient B_2 according to (164) is 0.403, which also equals the dimensionless linear well-loss, as the problem is formulated in dimensionless form. Substituting F into equation (163), the approximated dimensionless drawdown at the well-face is obtained, which is indicated by crosses on the left graph of Figure 13. This approximated solution is equal to the sum of the well-loss and the drawdown at distance R calculated using the corresponding solution for a homogeneous layer (Theis, 1935), which is indicated by the dotted lines. It is seen the approximation deviates more from the exact drawdown at smaller values of time. This is because the radial discharge $Q^h(R, t)$ at the interface between aquifer and gravel pack is significantly smaller than the pumping rate Q , which is illustrated by the right graph of Figure 13.

This plot shows the relative radial discharge Q^h/Q as a function of relative distance r/R . If the relative discharge at distance R is very close to 1, then the storage change in wellbore and gravel pack is negligibly small, and the flow in this area is in a pseudo steady state. Under this condition,

applying the approximate solution based on the skin factor is justified. However, at the beginning of the extraction, the storage change cannot be neglected, which explains why the approximate drawdown is inaccurate at small values of time.

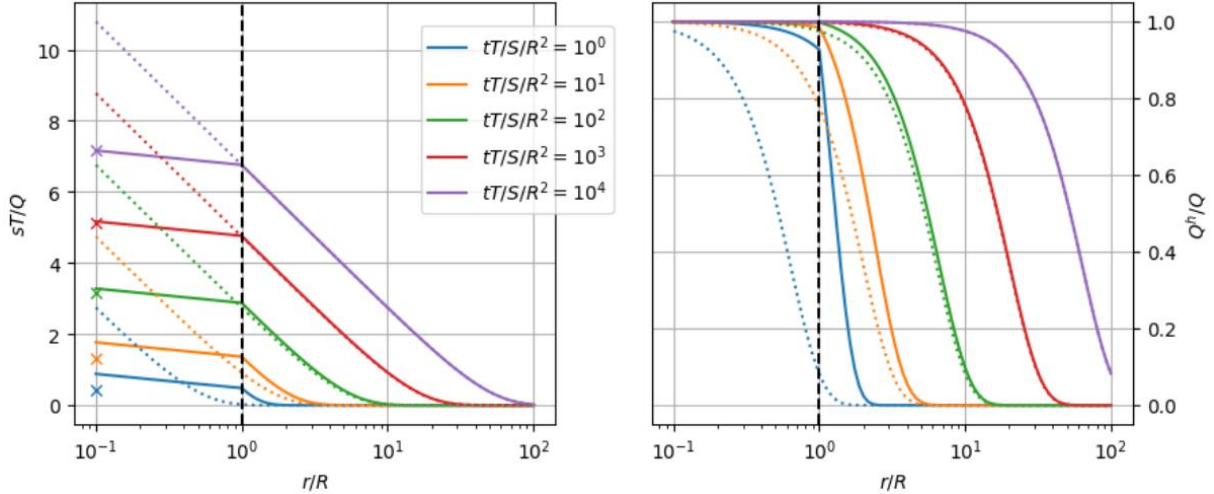


Figure 13. The left plot shows the dimensionless drawdown as a function of dimensionless radial distance at different dimensionless times for the model that simulates transient flow to a fully penetrating pumping well surrounded by a gravel pack with radius R , constant transmissivity T_1 , and constant storativity S_1 . Distance R is indicated by the vertical black dashed line. The well extracts water at constant rate Q from a confined aquifer with constant transmissivity T_2 and constant storativity S_2 . Parameters T and S are the total transmissivity and storativity, respectively. The solid lines are the exact solution, the crosses are the approximate solution calculated using the skin factor and the corresponding solution for a homogeneous layer indicated by dotted lines (Theis, 1935). The right plot shows the corresponding dimensionless radial discharge as a function of dimensionless radial distance. See text for definition of parameters and derivation of solutions.

5.6.5. Skin effect for a well in a multilayer system

If the pumped aquifer is part of a multilayer system, then leakage from the adjacent layers should be taken into account to analyze whether the dimensionless skin factor is applicable or not. Let us first introduce two new variables to make the analysis mathematically more comprehensible. The first variable is the total volume of water per unit of time Q_{ij}^s [L^3/T] that comes from storage change in zone j situated in layer i :

$$Q_{ij}^s(t) = 2\pi S_{ij} \int_{R_{j-1}}^{R_j} \frac{\partial S_{ij}}{\partial t} r dr \quad (1 \leq i \leq n_l; 1 \leq j \leq n_z) \quad (174)$$

The second variable is the total volume of water per unit of time Q_{ij}^v [L^3/T] that is exchanged between layers i and $i + 1$ in zone j :

$$Q_{ij}^v = 2\pi \int_{R_{j-1}}^{R_j} \frac{s_{ij} - s_{i+1,j}}{c_{ij}} r dr \quad (0 \leq i \leq n_l; 1 \leq j \leq n_z) \quad (175)$$

Both variables are defined as a function of drawdown s instead of head h , since the head losses in the well are analyzed, which are basically drawdowns. This also implies the superposition principle is applied and infiltration is canceled out or $N = 0$.

Definitions (174) and (175) can be applied to partial differential equation (4) formulated in terms of drawdown by multiplying both sides of the equation by $2\pi r$ and integrating both sides between distances R_{j-1} and R_j . This gives the total volumetric budget equation for zone j in layer i :

$$Q_{ij}^h(R_{j-1}, t) - Q_{ij}^h(R_j, t) = Q_{ij}^s(t) + Q_{ij}^v(t) - Q_{i-1,j}^v(t) \quad (0 \leq i \leq n_l; 1 \leq j \leq n_z) \quad (176)$$

If n_z zones are considered, then the most distal zone is the aquifer, and the other zones are part of the disturbed zone around the well. Hence, the total volumetric budget equation of this disturbed zone comprises the first $n_z - 1$ zones, and it is found by summing both sides of equation (176):

$$\sum_{j=1}^{n_z-1} [Q_{ij}^h(R_{j-1}, t) - Q_{ij}^h(R_j, t)] = \sum_{j=1}^{n_z-1} [Q_{ij}^s(t) + Q_{ij}^v(t) - Q_{i-1,j}^v(t)] \quad (0 \leq i \leq n_l) \quad (177)$$

Simplifying the left-hand side of equation (177) and applying boundary condition (11) which states that $Q_{i,1}^h(R_0, t) = Q_i$:

$$Q_i - Q_{ij}^h(R_{n_z-1}, t) = \sum_{j=1}^{n_z-1} Q_{ij}^s(t) + \sum_{j=1}^{n_z-1} Q_{ij}^v(t) - \sum_{j=1}^{n_z-1} Q_{i-1,j}^v(t) \quad (0 \leq i \leq n_l) \quad (178)$$

The right-hand side of equation (177) is also rearranged to clarify that it is equal to the sum of the total storage change and the total leakage from the adjacent layers in the first $n_z - 1$ zones.

The approach applying the dimensionless skin factor is valid only if $Q_i = Q_{ij}^h(R_{n_z-1}, t)$, which is true if the left-hand side of equation (178) is zero. This implies the storage change in the first $n_z - 1$ zones is zero, and in these zones, there is no exchange of water between the pumped layer i and its adjacent layers. Theoretically, this only occurs in case of steady flow toward a well fully penetrating a confined aquifer. In practice, however, it suffices that $Q_{ij}^h(R_{n_z-1}, t)$ is close to the pumping rate Q_i . This less strict condition is fulfilled when the transient flow in the disturbed zone is in a pseudo steady state and if this disturbed zone around the well is relatively small.

The effect of the storage change has already been illustrated in previous section 5.6.4 using the model of Butler (1988). In this case, the total leakage terms are absent from equation (178) as the aquifer is confined, and the skin factor is applicable if the storage change term is close to zero, which is the case for large values of time. The effect of the leakage can be demonstrated using the steady state solution for a leaky two-zone aquifer derived in section 5.5.4. Indeed, the leaky aquifer may be interpreted as part of a three-aquifer system with constant heads in the upper and lower aquifers. This makes the leakage from the bounding aquifers even more pronounced than in the case of bounding variable-head layers.

As an example, reconsider the first scenario discussed in section 5.5.4 in which steady flow is simulated to a pumping well with radius R_0 extracting water at constant rate Q from a leaky aquifer with constant transmissivity T_2 . The well is surrounded by a finite-thickness skin with radius R_1 and transmissivity T_1 which is 10 times smaller than the aquifer transmissivity. The resistances of upper and lower aquifer boundary are the same, i.e. $c_0 = c_1$.

The left plot of Figure 14 shows dimensionless drawdown sT/Q as a function of dimensionless distance r/\sqrt{Tc} , with $T = T_1 + T_2$ and $c = c_0 + c_1$. Dimensionless well radius R_0/\sqrt{Tc} is 0.01 and solutions are simulated for different values of dimensionless skin radius R_1/\sqrt{Tc} , which are indicated by the vertical dashed lines. The solid lines are simulated using the analytical solution (131) derived in section 5.5.4. The black dotted line is the corresponding solution of de Glee (1930) without skin. The crosses are the drawdown at the well-face estimated using equation (163) applying the dimensionless skin factor. As expected, the larger the skin, the more the estimated drawdown deviates from the exact drawdown. Because the skin effect is positive, the estimated drawdown is an

overestimation, whereas it would be an underestimation in case of a negative skin effect, as is seen in Figure 13.

The right plot of Figure 14 shows the corresponding relative radial discharge Q^h/Q as a function of relative distance r/\sqrt{Tc} . If the relative discharge at distance R_1 is very close to 1, then the leakage from the bounding layers in the zone corresponding to the skin is negligibly small, and the flow in this area may be approximated using the confined aquifer solution. Under this condition, estimating drawdown in the well using the skin factor is justified as $Q^h \approx Q$. However, if the skin is relatively thick, then the leakage may not be neglected, which explains why the approximate drawdown is inaccurate in these cases.

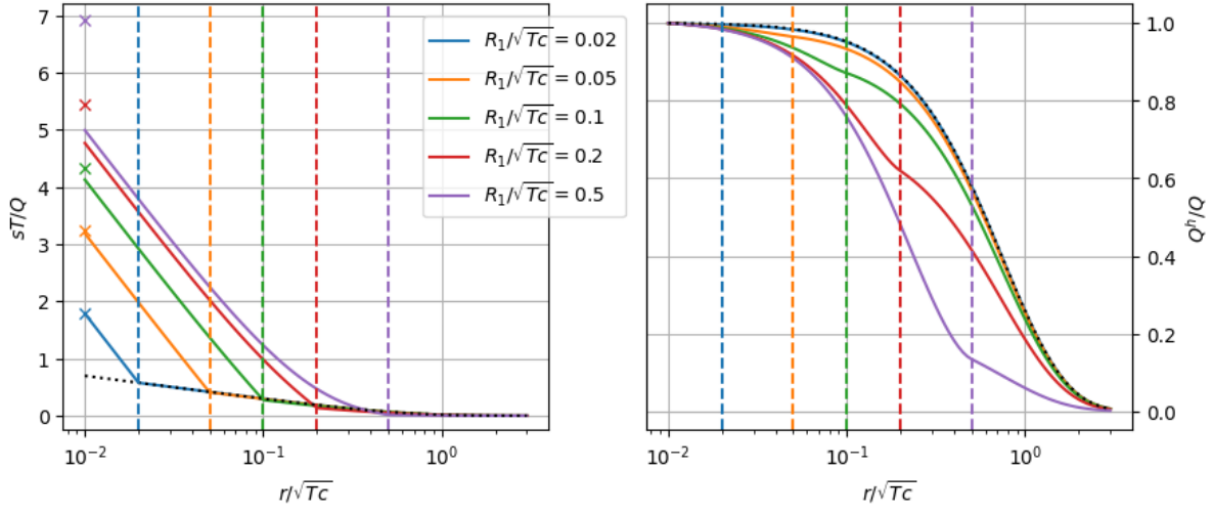


Figure 14. The left plot shows the dimensionless drawdown as a function of dimensionless radial distance for the model that simulates steady flow to a fully penetrating pumping well surrounded by a finite-thickness skin with radius R_1 and constant transmissivity T_1 . Different values for R_1 are considered, which are indicated by the vertical dashed lines. The well extracts water at constant rate Q from a leaky aquifer with constant transmissivity T_2 that is 10 times larger than T_1 . The resistances of the bounding aquitards are the same, i.e. $c_0 = c_1$. Parameters T and c are the total transmissivity and resistance, respectively. The crosses are the approximate solution calculated using the dimensionless skin factor and the corresponding solution without skin (de Glee, 1930), which is indicated by a black dotted line. The right plot shows the corresponding dimensionless radial discharge as a function of dimensionless radial distance. See text for definition of parameters and derivation of solutions.

In most real-world cases, the thickness of gravel pack and skin are indeed relatively small, so one could argue that the use of the dimensionless skin factor approach to estimate the total linear head loss inside the well at relatively large values of time is justified from a practical point of view. There is, however, another important condition that must be fulfilled, and that is the well-screen must be fully penetrating, and it may not extend over more than one layer. This condition is rarely met in practice, as fully penetrating wells are the exception and not the rule.

When flow toward a partially penetrating well is simulated, the vertical flow component cannot be neglected in most cases. Moreover, a more realistic mixed-type boundary condition must be defined at the inner model boundary, which imposes a uniform drawdown vertically along the well-face instead of a uniform discharge equal to the pumping rate. Such a mixed-type boundary condition is also required if the well-screen is open to more than one layer characterized by different hydraulic properties. Because of the importance of partially penetrating wells and multi-aquifer wells, the next Chapter 6 is devoted to analytical and numerical solutions that define more realistic boundary conditions for these types of wells. The dimensionless skin factor is not applicable in many of these cases.

5.7. Summary and conclusions

This chapter presents a generalized semi-analytical solution for the simulation of axisymmetric or parallel flow in multilayered aquifer systems consisting of multiple zones characterized by different hydraulic parameters and/or boundary conditions. Both steady and transient flow can be simulated in confined or leaky systems that may include areal recharge. The aquifer system is allowed to be laterally bounded or unbounded, and the source or sink at the inner boundary is a specified head or a constant discharge. In case of transient flow, the Laplace transform is applied and numerically inverted using the Stehfest (1970) algorithm.

The presented solution method is an extension of the semi-analytical approach for multilayer systems discussed in Chapter 2. In the latter, layers are assumed homogeneous, while in the former, the layers may contain lateral heterogeneities. The multilayer-multizone solution is found by coupling homogeneous multilayer models and preserving continuity of flow at the common boundaries of these models. As a consequence, the homogeneous multilayer solution is the same as the multilayer-multizone solution applied to a single zone. The coupling of models involves solving a linear system of equations for which a new algorithm is developed inspired by the Thomas (1949) algorithm. Alternatively, standard LU decomposition may be applied, which is more robust.

The semi-analytical solution method is carefully compared with the finite-difference method presented in Chapter 3, and verified against several analytical and semi-analytical solutions described in the literature (Bakker & Strack, 2003; Barker & Herbert, 1982; Blom, 1973; Butler, 1988; Cooper et al., 1967; Haitjema, 1995; Strack, 1989). Additionally, the analytical steady-state solutions for multizone flow in a single confined aquifer are derived and used as test cases. Both axisymmetric and parallel flow are considered, and the solutions for specified-discharge as well as specified-head conditions at the inner model boundary are developed. The analytical steady state solution for a fully penetrating pumping well with finite-thickness skin in a leaky aquifer is also presented. This solution extends the well-known de Glee (1930) formula. It is concluded that the semi-analytical solution method for multilayer-multizone flow gives accurate results that compare very well to the finite-difference simulations and the analytical solutions.

Analyzing these multizone models, three types of applications may be distinguished. First, the multilayer-multizone solution can be applied to model a circular infiltration area in a multiple aquifer system. The analytical steady-state solution is well-known in the hydrogeological literature (Bakker & Strack, 2003), and embedding the circular infiltration area into a leaky aquifer system may be used to simulate the effect of drainage. In this chapter, the boundary between the zones with infiltration and drainage, respectively, is specified by the user. It is more realistic, however, to determine this boundary by checking the head against the drainage level. As is explained in Chapter 7, this requires solving a nonlinear inverse problem. The one-layer model for steady flow subject to areal infiltration and drainage is presented by Ernst (1971). It will be discussed in Chapter 7, and additionally in Chapter 10 and Chapter 11, respectively discussing the radius of influence and the difference between linear and nonlinear models.

The second type of application is the simulation of the effect of a finite-thickness skin around the well. As the skin effect may have a significant impact on the performance of a pumping well, this topic gets a lot of attention in the literature (Houben et al., 2016). A distinction is made between linear and nonlinear well-losses (Kruseman & de Ridder, 1990), the latter being attributed to the non-Darcian flow in the disturbed zone around the well, and to the turbulent flow through the well-screen and inside the borehole (Houben, 2015). The skin effect is linear, and traditionally, it is characterized by a dimensionless skin factor (Kruseman & de Ridder, 1990). It expresses a linear

relation between well-loss and pumping rate, and strictly speaking, it holds for steady radial flow to a fully penetrating well with zero-thickness skin. It is also assumed that there is a hydrostatic equilibrium within the borehole. In case of a skin that is less permeable than the aquifer, the skin effect is positive, while a gravel pack that is usually more permeable, gives a negative skin effect.

Using the analytical one-dimensional multizone solution derived in this chapter, it is straightforward to generalize the dimensionless skin factor to include multiple zones of finite width. The solution by Butler (1988) also shows that the skin factor is applicable in case of transient flow toward a fully penetrating well with finite-thickness skin, if storage change within the cylindrical zone representing the skin is negligibly small. In most real-world cases, the thickness of gravel pack and skin are relatively small, which justifies using the dimensionless skin factor to estimate the total linear head loss inside the well at relatively large values of time. The assumption of a fully penetrating well, however, implies the absence of vertical flow inside the skin zone. This condition is rarely met in practice, as most wells are partially penetrating, in which case a mixed-type boundary condition must be defined at the inner model boundary. Next Chapter 6 extends both the semi-analytical solution discussed in this chapter and the finite-difference method presented in Chapter 3 to deal with this type of boundary condition.

Finally, the multilayer-multizone solution may also be used to include the effect of wellbore storage or to model the draining or irrigating effect of a wide stream. In this case, the well or stream is conceptualized as a separate zone of high transmissivity. This is illustrated by reproducing the type curves calculated by Cooper et al. (1967) for simulating a slug test in a confined aquifer. In a second example, the effect of a permanent water level rise in an embanked river interacting with a multilayered aquifer system is simulated. Although the emphasis of the presented two-dimensional multilayer solution method is on the simulation of axisymmetric flow toward a well, this last example shows how it can also be used to accurately solve parallel flow problems.

Without pretending that such two-dimensional cross-sectional models can replace a complex three-dimensional model, they have the advantage of not being time-consuming and data hungry. Therefore, it could be useful to conceptualize a given groundwater problem as a one- or two-dimensional problem which can be solved analytically before building a full-fledged three-dimensional numerical model. In this way, one is able to explore the problem and to get a better idea of the order of magnitude of the simulated heads and the sensitivity of the input parameters and boundary conditions that are involved. These are valuable insights that may help the modeler to substantiate some of the inevitable choices that must be made when building a complex three-dimensional numerical model (Haitjema, 2006).

The two examples in this chapter show that defining a high-transmissivity zone to model a large-diameter well or a stream of large width results in accurate simulations. However, a mathematically more rigorous way is to include the storage change inside the well or stream in the inner boundary condition representing this well or stream. Moreover, if this well or stream is open to more than one model layer, then it is also more effective to define a mixed-type boundary condition. As already mentioned, this is the subject of next Chapter 6, in which the multilayer-multizone solution presented in this chapter is extended to model multilayer wells with a finite diameter or multilayer streams with a finite width. The multilayer-multizone solution is also applied in Chapter 7 to solve the nonlinear problems of confined-unconfined flow and drainage, and in Chapter 8 to simulate nonlinear unconfined flow.

5.8. References

- Bakker, M. (2001). An analytic, approximate method for modeling steady, three-dimensional flow to partially penetrating wells. *Water Resources Research*, 37(5).
<https://doi.org/10.1029/2000WR900400>
- Bakker, M. (2013). Semi-analytic modeling of transient multi-layer flow with TTim. *Hydrogeology Journal*, 21(4), 935–943. <https://doi.org/10.1007/s10040-013-0975-2>
- Bakker, M., & Strack, O. D. L. (2003). Analytic elements for multiaquifer flow. *Journal of Hydrology*, 271(1–4). [https://doi.org/10.1016/S0022-1694\(02\)00319-0](https://doi.org/10.1016/S0022-1694(02)00319-0)
- Barker, J. A., & Herbert, R. (1982). Pumping Tests in Patchy Aquifers. *Ground Water*, 20(2), 150–155.
<https://doi.org/10.1111/j.1745-6584.1982.tb02742.x>
- Barker, J. A., & Herbert, R. (1992). A Simple Theory For Estimating Well Losses: With Application To Test Wells In Bangladesh. *Applied Hydrogeology*, 0(0), 20–31.
<https://doi.org/10.1007/PL00010959>
- Barrash, W., & Dougherty, M. E. (1997). Modeling Axially Symmetric and Nonsymmetric Flow to a Well with MODFLOW, and Application to Goddard2 Well Test, Boise, Idaho. *Ground Water*, 35(4), 602–611. <https://doi.org/10.1111/j.1745-6584.1997.tb00125.x>
- Barua, G., & Bora, S. N. (2010). Hydraulics of a partially penetrating well with skin zone in a confined aquifer. *Advances in Water Resources*, 33(12), 1575–1587.
<https://doi.org/10.1016/j.advwatres.2010.09.008>
- Bateman, H. (1954). *Tables of Integral Transforms*. (A. Erdélyi, Ed.) (Vol. 1). New York: McGraw-Hill Book Company.
- Bear, J. (1972). *Dynamics of Fluids in Porous Media*. New York: American Elsevier Publishing Company.
- Bennett, G. D., Kontis, A. L., & Larson, S. P. (1982). Representation of Multiaquifer Well Effects in Three-Dimensional Ground-Water Flow Simulation. *Ground Water*, 20(3), 334–341.
<https://doi.org/10.1111/j.1745-6584.1982.tb01354.x>
- Blom, J. (1973). *Verlagingen van het freatisch vlak bij grondwateronttrekking in een gebied met vrije afwatering (Drenthe)* (in Dutch). RID Mededeling 74-7, Rijksinstituut voor Drinkwatervoorziening (RID), The Netherlands.
- Bruggeman, G. A. (1999). *Analytical solutions of geohydrological problems. Developments in Water Science 46*. Amsterdam: Elsevier.
- Butler, J. J. (1988). Pumping tests in nonuniform aquifers — The radially symmetric case. *Journal of Hydrology*, 101(1–4), 15–30. [https://doi.org/10.1016/0022-1694\(88\)90025-X](https://doi.org/10.1016/0022-1694(88)90025-X)
- Cassiani, G., & Kabala, Z. J. (1998). Hydraulics of a partially penetrating well: solution to a mixed-type boundary value problem via dual integral equations. *Journal of Hydrology*, 211(1–4), 100–111.
[https://doi.org/10.1016/S0022-1694\(98\)00223-6](https://doi.org/10.1016/S0022-1694(98)00223-6)
- Cassiani, G., Kabala, Z. J., & Medina, M. A. (1999). Flowing partially penetrating well: solution to a mixed-type boundary value problem. *Advances in Water Resources*, 23(1), 59–68.
[https://doi.org/10.1016/S0309-1708\(99\)00002-0](https://doi.org/10.1016/S0309-1708(99)00002-0)

- Chang, C.-C., & Chen, C.-S. (2002). An integral transform approach for a mixed boundary problem involving a flowing partially penetrating well with infinitesimal well skin. *Water Resources Research*, 38(6), 7-1-7-7. <https://doi.org/10.1029/2001WR001091>
- Chang, Y. C., Yeh, H. D., & Chen, G. Y. (2010). Transient solution for radial two-zone flow in unconfined aquifers under constant-head tests. *Hydrological Processes*, 24(11), 1496–1503. <https://doi.org/10.1002/hyp.7610>
- Chiu, P.-Y., Yeh, H.-D., & Yang, S.-Y. (2007a). A new solution for a partially penetrating constant-rate pumping well with a finite-thickness skin. *International Journal for Numerical and Analytical Methods in Geomechanics*, 31(15), 1659–1674. <https://doi.org/10.1002/nag.607>
- Chiu, P.-Y., Yeh, H.-D., & Yang, S.-Y. (2007b). A new solution for a partially penetrating constant-rate pumping well with a finite-thickness skin. *International Journal for Numerical and Analytical Methods in Geomechanics*, 31(15), 1659–1674. <https://doi.org/10.1002/nag.607>
- Cooper, H. H., & Jacob, C. E. (1946). A generalized graphical method for evaluating formation constants and summarizing well-field history. *Transactions, American Geophysical Union*, 27(4), 526–534. <https://doi.org/10.1029/TR027i004p00526>
- Cooper, H. H., Bredehoeft, J. D., & Papadopoulos, I. S. (1967). Response of a finite-diameter well to an instantaneous charge of water. *Water Resources Research*, 3(1), 263–269. <https://doi.org/10.1029/WR003i001p00263>
- de Glee, G. J. (1930). *Over grondwaterstroomingen bij wateronttrekking door middel van putten (in Dutch)* (PhD thesis). Technische Hoogeschool Delft, Drukkerij J. Waltman. Jr., Delft.
- Dougherty, D. E., & Babu, D. K. (1984). Flow to a Partially Penetrating Well in a Double-Porosity Reservoir. *Water Resources Research*, 20(8), 1116–1122. <https://doi.org/10.1029/WR020i008p01116>
- Engelund, F. (1953). *On the laminar and turbulent flow of groundwater through homogeneous sands*. Copenhagen: Akademiet for de Tekniske Videnskaber.
- Ernst, L. F. (1971). Analysis of groundwater flow to deep wells in areas with a non-linear function for the subsurface drainage. *Journal of Hydrology*, 14(2). [https://doi.org/10.1016/0022-1694\(71\)90004-7](https://doi.org/10.1016/0022-1694(71)90004-7)
- Feng, Q., & Wen, Z. (2016). Non-Darcian flow to a partially penetrating well in a confined aquifer with a finite-thickness skin. *Hydrogeology Journal*, 24(5), 1287–1296. <https://doi.org/10.1007/s10040-016-1389-8>
- Feng, Q., & Zhan, H. (2016). Integrated aquitard-aquifer flow with a mixed-type well-face boundary and skin effect. *Advances in Water Resources*, 89, 42–52. <https://doi.org/10.1016/j.advwatres.2016.01.003>
- Feng, Q., & Zhan, H. (2019). Constant-head test at a partially penetrating well in an aquifer-aquitard system. *Journal of Hydrology*, 569, 495–505. <https://doi.org/10.1016/j.jhydrol.2018.12.018>
- Forchheimer, P. Z. (1901). Wasserbewegung durch Boden (in German). *Zeitschrift Des Vereins Deutscher Ingenieure*, 50, 1781–1788.
- Haitjema, H. (1995). *Analytic Element Modeling of Groundwater Flow*. San Diego: Academic Press. <https://doi.org/10.1016/B978-0-12-316550-3.X5000-4>

- Haitjema, H. (2006). The Role of Hand Calculations in Ground Water Flow Modeling. *Ground Water*, 44(6). <https://doi.org/10.1111/j.1745-6584.2006.00189.x>
- Hantush, M. S. (1949). Plain potential flow of ground water with linear leakage. (PhD Thesis). University of Utah, Salt Lake City.
- Hantush, M. S., & Jacob, C. E. (1955). Non-steady radial flow in an infinite leaky aquifer. *Transactions, American Geophysical Union*, 36(1), 95–100. <https://doi.org/10.1029/TR036i001p00095>
- Harbaugh, A. W. (2005). MODFLOW-2005, the U.S. Geological Survey modular ground-water model - the Ground-Water Flow Process. U.S. Geological Survey Techniques and Methods 6-A16. <https://doi.org/https://doi.org/10.3133/tm6A16>
- Harbaugh, A. W., Banta, E. R., Hill, M. C., & McDonald, M. G. (2000). MODFLOW-2000, The U.S. Geological Survey Modular Ground-Water Model: User Guide to Modularization Concepts and the Ground-Water Flow Process. U.S. Geological Survey Open-File Report 00-92. <https://doi.org/https://doi.org/10.3133/ofr200092>
- Hemker, C. J. (1984). Steady groundwater flow in leaky multiple-aquifer systems. *Journal of Hydrology*, 72(3–4), 355–374. [https://doi.org/10.1016/0022-1694\(84\)90089-1](https://doi.org/10.1016/0022-1694(84)90089-1)
- Hemker, C. J. (1985). Transient well flow in leaky multiple-aquifer systems. *Journal of Hydrology*, 81(1–2), 111–126. [https://doi.org/10.1016/0022-1694\(85\)90170-2](https://doi.org/10.1016/0022-1694(85)90170-2)
- Hemker, C. J. (1999a). Transient well flow in vertically heterogeneous aquifers. *Journal of Hydrology*, 225(1–2), 1–18. [https://doi.org/10.1016/S0022-1694\(99\)00137-7](https://doi.org/10.1016/S0022-1694(99)00137-7)
- Hemker, C. J. (1999b). Transient well flow in layered aquifer systems: the uniform well-face drawdown solution. *Journal of Hydrology*, 225(1–2), 19–44. [https://doi.org/10.1016/S0022-1694\(99\)00093-1](https://doi.org/10.1016/S0022-1694(99)00093-1)
- Hemker, C. J. (2000). *Groundwater flow in layered aquifer systems* (PhD thesis). VU, Amsterdam.
- Houben, G. J. (2015). Review: Hydraulics of water wells—head losses of individual components. *Hydrogeology Journal*, 23(8), 1659–1675. <https://doi.org/10.1007/s10040-015-1313-7>
- Houben, G. J., & Kenrick, M. A. P. (2022). Step-drawdown tests: linear and nonlinear head loss components. *Hydrogeology Journal*, 30(4), 1315–1326. <https://doi.org/10.1007/s10040-022-02467-8>
- Houben, G. J., Halisch, M., Kaufhold, S., Weidner, C., Sander, J., & Reich, M. (2016). Analysis of Wellbore Skin Samples-Typology, Composition, and Hydraulic Properties. *Groundwater*, 54(5), 634–645. <https://doi.org/10.1111/gwat.12403>
- Houben, G. J., Wachenhausen, J., & Guevara Morel, C. R. (2018). Effects of ageing on the hydraulics of water wells and the influence of non-Darcy flow. *Hydrogeology Journal*, 26(4), 1285–1294. <https://doi.org/10.1007/s10040-018-1775-5>
- Huang, C.-S., Yang, S.-Y., & Yeh, H.-D. (2015). Technical Note: Approximate solution of transient drawdown for constant-flux pumping at a partially penetrating well in a radial two-zone confined aquifer. *Hydrology and Earth System Sciences*, 19(6), 2639–2647. <https://doi.org/10.5194/hess-19-2639-2015>
- Hunt, B. (1986). Solutions for steady groundwater flow in multi-layer aquifer systems. *Transport in Porous Media*, 1(4), 419–429. <https://doi.org/10.1007/BF00208046>

- Hyder, Z., Butler, J. J., McElwee, C. D., & Liu, W. (1994). Slug tests in partially penetrating wells. *Water Resources Research*, 30(11), 2945–2957. <https://doi.org/10.1029/94WR01670>
- Jacob, C. E. (1946). Radial flow in a leaky artesian aquifer. *Transactions, American Geophysical Union*, 27(2). <https://doi.org/10.1029/TR027i002p00198>
- Jacob, C. E. (1947). Drawdown Test to Determine Effective Radius of Artesian Well. *Transactions of the American Society of Civil Engineers*, 112(1), 1047–1064. <https://doi.org/10.1061/TACEAT.0006033>
- Kitterød, N.-O. (2004). Dupuit-Forchheimer solutions for radial flow with linearly varying hydraulic conductivity or thickness of aquifer. *Water Resources Research*, 40(11). <https://doi.org/10.1029/2004WR003115>
- Kooper, J. (1914). Beweging van het water in den bodem bij onttrekking door bronnen (in Dutch). *Ingenieur*, 29, 697–716.
- Kruseman, G. P., & de Ridder, N. A. (1990). *Analysis and Evaluation of Pumping Test Data* (2nd ed.). ILRI Publication 47, Wageningen.
- Kurtulus, B., Yayılm, T. N., Avşar, O., Kulac, H. F., & Razack, M. (2019). The Well Efficiency Criteria Revisited—Development of a General Well Efficiency Criteria (GWEC) Based on Rorabaugh's Model. *Water*, 11(9), 1784. <https://doi.org/10.3390/w11091784>
- Langevin, C. D. (2008). Modeling Axisymmetric Flow and Transport. *Ground Water*, 46(4), 579–590. <https://doi.org/10.1111/j.1745-6584.2008.00445.x>
- Lebbe, L. C. (1999). *Hydraulic Parameter Identification. Generalized Interpretation Method for Single and Multiple Pumping Tests*. Berlin Heidelberg: Springer-Verlag.
- Louwyck, A., Vandenbohede, A., & Lebbe, L. C. (2010). Numerical analysis of step-drawdown tests: Parameter identification and uncertainty. *Journal of Hydrology*, 380(1–2), 165–179. <https://doi.org/10.1016/j.jhydrol.2009.10.034>
- Louwyck, A., Vandenbohede, A., Bakker, M., & Lebbe, L. C. (2012). Simulation of axi-symmetric flow towards wells: A finite-difference approach. *Computers & Geosciences*, 44, 136–145. <https://doi.org/10.1016/j.cageo.2011.09.004>
- Louwyck, A., Vandenbohede, A., Bakker, M., & Lebbe, L. C. (2014). MODFLOW procedure to simulate axisymmetric flow in radially heterogeneous and layered aquifer systems. *Hydrogeology Journal*, 22(5), 1217–1226. <https://doi.org/10.1007/s10040-014-1150-0>
- Louwyck, A., Vandenbohede, A., Libbrecht, D., Van Camp, M., & Walraevens, K. (2022). The Radius of Influence Myth. *Water*, 14(2), 149. <https://doi.org/10.3390/w14020149>
- Moench, A. F. (1997). Flow to a well of finite diameter in a homogeneous, anisotropic water table aquifer. *Water Resources Research*, 33(6), 1397–1407. <https://doi.org/10.1029/97WR00651>
- Neville, C. J., & Tonkin, M. J. (2004). Modeling Multiaquifer Wells with MODFLOW. *Ground Water*, 42(6), 910–919. <https://doi.org/10.1111/j.1745-6584.2004.t01-9-.x>
- Novakowski, K. S. (1993). Interpretation of the transient flow rate obtained from constant-head tests conducted in situ in clays. *Canadian Geotechnical Journal*, 30(4), 600–606. <https://doi.org/10.1139/t93-052>

- Perina, T., & Lee, T.-C. (2006). General well function for pumping from a confined, leaky, or unconfined aquifer. *Journal of Hydrology*, 317(3–4), 239–260. <https://doi.org/10.1016/j.jhydrol.2005.05.020>
- Peterson, P., Oliphant, T., & Vanderplas, J. (2022). SciPy (version 1.8.1) documentation for function linalg.solve. Retrieved July 18, 2022, from <https://docs.scipy.org/doc/scipy/reference/generated/scipy.linalg.solve.html>
- Şen, Z. (2014). Hydraulic Conductivity Variation in a Confined Aquifer. *Journal of Hydrologic Engineering*, 19(3), 654–658. [https://doi.org/10.1061/\(ASCE\)HE.1943-5584.0000832](https://doi.org/10.1061/(ASCE)HE.1943-5584.0000832)
- Stehfest, H. (1970). Algorithm 368: Numerical inversion of Laplace transforms [D5]. *Communications of the ACM*, 13(1), 47–49. <https://doi.org/10.1145/361953.361969>
- Strack, O. D. L. (1989). *Groundwater Mechanics*. Old Tappan, N. J.: Prentice-Hall.
- Theis, C. V. (1935). The relation between the lowering of the Piezometric surface and the rate and duration of discharge of a well using ground-water storage. *Transactions, American Geophysical Union*, 16(2), 519–524. <https://doi.org/10.1029/TR016i002p00519>
- Thiem, A. (1870). Die Ergiebigkeit artesischer Bohrlöcher, Schachtbrunnen und Filtergalerien (in German). *Journal Für Gasbeleuchtung Und Wasserversorgung*, 13, 450–467.
- Thiem, G. (1906). *Hydrologische Methoden (in German)*. Leipzig: Gebhardt.
- Thomas, L. H. (1949). *Elliptic Problems in Linear Difference Equations Over a Network*. Watson Science Computer Laboratory, Colombia University, New York.
- Weisbach, J. (1845). *Lehrbuch der Ingenieur- und Maschinen-Mechanik (in German)*. Braunschweig, Germany: Friedrich Vieweg.
- Yang, S.-Y., & Yeh, H.-D. (2005). Laplace-Domain Solutions for Radial Two-Zone Flow Equations under the Conditions of Constant-Head and Partially Penetrating Well. *Journal of Hydraulic Engineering*, 131(3), 209–216. [https://doi.org/10.1061/\(ASCE\)0733-9429\(2005\)131:3\(209\)](https://doi.org/10.1061/(ASCE)0733-9429(2005)131:3(209))
- Yang, S.-Y., & Yeh, H.-D. (2009). Radial groundwater flow to a finite diameter well in a leaky confined aquifer with a finite-thickness skin. *Hydrological Processes*, 23(23), 3382–3390. <https://doi.org/10.1002/hyp.7449>
- Yang, S.-Y., Huang, C.-S., Liu, C.-H., & Yeh, H.-D. (2014). Approximate Solution for a Transient Hydraulic Head Distribution Induced by a Constant-Head Test at a Partially Penetrating Well in a Two-Zone Confined Aquifer. *Journal of Hydraulic Engineering*, 140(7). [https://doi.org/10.1061/\(ASCE\)HY.1943-7900.0000884](https://doi.org/10.1061/(ASCE)HY.1943-7900.0000884)
- Yeh, H.-D., & Yang, S.-Y. (2006). A novel analytical solution for a slug test conducted in a well with a finite-thickness skin. *Advances in Water Resources*, 29(10), 1479–1489. <https://doi.org/10.1016/j.advwatres.2005.11.002>

Chapter 6. Modeling Multilayer Wells

6.1. Introduction

In this chapter, both the finite-difference approach discussed in Chapter 3 and the semi-analytical solution developed in previous Chapter 5 are extended to simulate flow to a well that is open across two or more layers in the aquifer system. In case of a multi-aquifer well, these layers represent aquifers characterized by different hydraulic properties. It is also possible that the layers have the same hydraulic parameters but different hydraulic heads, for instance, in case of a partially penetrating well. Radial flow toward a partially penetrating well has been studied intensively as fully penetrating wells are the exception rather than the rule. Because the solution presented in this chapter is applicable to both multi-aquifer wells and partially penetrating wells, the more general term multilayer well is used here. In the context of the finite-difference model MODFLOW, the term multi-node well is well-established (Halford & Hanson, 2002; Konikow et al., 2009).

To simulate flow toward a multilayer well, a mixed-type boundary value problem must be solved. Indeed, a first-type or Dirichlet boundary condition is defined at the well-face which equates the head at that boundary to the water level in the well, while a second-type or Neumann boundary condition is required for the impervious non-screened parts of the aquifer system (Cassiani et al., 1999; Cassiani & Kabala, 1998). The mixed-type well-face boundary condition is also referred to as integrated well-face flux (IWFF) (Ruud & Kabala, 1997), uniform well-face drawdown (UWD) (Hemker, 1999a), or nonuniform flux (NUF) (Feng & Zhan, 2016). A mixed-type boundary condition at the well-face is also required when simulating flow to a well in a heterogeneous aquifer where conductivity is modeled by a three-dimensional stationary random space function (Dagan & Lessoff, 2011; Indelman et al., 1996). However, this chapter only treats radial flow in vertically heterogeneous aquifers toward a well that may be surrounded by a number of cylindrical zones characterized by different hydraulic properties.

The solutions discussed and presented in this chapter simplify the actual hydrodynamics of the flow system close to and inside the well in two ways. First, it is assumed that there is hydrostatic equilibrium within the borehole (Bennett et al., 1982), which means flow and friction losses are neglected. Approaches that consider non-linear flow inside the wellbore are presented by, among others, Cooley and Cunningham (1979), Chen and Jiao (1999), and Mathias and Wen (2015). Second, flow close to the well is assumed to be linear and laminar, although this Darcian approach is not fully applicable, as nonlinear inertial flow may occur in the gravel pack (Houben, 2015). Models that simulate non-Darcian flow to a partially penetrating well are developed by Wen et al. (2014), Wen et al. (2016), and Feng and Wen (2016).

6.1.1. Multi-aquifer wells

Sokol (1963) published the analytical solution to calculate the steady water level in an abandoned non-pumping well perforating more than one confined aquifer. As it is assumed the aquifers are separated by impervious layers, the Thiem (1870, 1906) formula is applicable, and Sokol (1963) shows that the water level in the multi-aquifer well is affected by each aquifer in proportion to the aquifer transmissivities. Extending this solution to a well that is extracting water from the aquifers, is straightforward, and the resulting formula can be found in Neville and Tonkin (2004). Xiang (1994) derives the steady state solution for a constant-head well surrounded by a disturbed zone in a layered aquifer, treating both the radial and the vertical component of flow analytically, the latter by applying the finite Fourier cosine transformation.

The multi-aquifer well problem for transient flow is tackled first by Papadopoulos (1966) who considers a pumping well connected to two confined aquifers. Papadopoulos (1966) derives the exact solution in Laplace space, inverts this solution analytically, and presents some asymptotic solutions that are more easy to evaluate. Mishra et al. (1985) apply a discrete kernel approach to solve the same problem, and a computationally more simple semi-analytical approach is proposed for both the case with and without crossflow by Singh (2008) and Singh (2009), respectively. Khader and Veerankutty (1975) apply integral transforms to solve the problem of a multi-aquifer well extracting water from both a water table aquifer and the underlying confined aquifer. Wikramaratna (1984) presents the solution in the Laplace domain for a finite-diameter well open to multiple aquifers separated by aquiclude, and inverts the solution analytically for the case of two aquifers. Using this two-aquifer solution, Wikramaratna (1985) analyzes how wellbore storage and flow from the two aquifers contribute to the pumping rate of the well. Mishra and Chandra (1990, 1992) solve the same problem as Wikramaratna (1984) applying a discrete kernel approach.

With the exception of the models developed by Singh (2008) and Xiang (1994), the other models discussed so far share the assumption there is no crossflow between the aquifers, which means the multi-aquifer well is the only connection between the aquifers. Hemker (1999a) solves the problem of a multilayer well in a vertically heterogeneous aquifer system considering vertical flow by extending the semi-analytical multilayer well-flow solution he developed earlier (Hemker, 1985, 1999b). The latter solution can also be used to simulate flow to a multilayer well, assuming a uniform gradient at the well-face (UWG), whereas in the former solution, a uniform drawdown is assumed at the well-face (UWD), which is a more realistic boundary condition. The UWD solution also takes into account wellbore storage, and it is even possible to define a zero-thickness skin around the well-screen. According to Hemker (1999a), the synthesized analytical numerical (SAN) method developed by Székely (1990) and applied by Székely (1992, 1995) to simulate flow to a partially penetrating well or a well with long screen or multiple screens, is similar to the solutions developed by Hemker (1985, 1999a, 1999b), although extensions in the SAN method to include aquifer heterogeneity, aquitard storage, or turbulent flow within wellbore and surrounding skin are based on numerically obtained approximations and corrections.

6.1.2. Partially penetrating wells

As it is not required to connect all layers to the multilayer well, the UWD solution developed by Hemker (1999a) is also capable of simulating the effect of partial penetration. This may be done by dividing the aquifer containing the partially penetrating well into a number of model layers to take into account the vertical flow. The approach is illustrated by Bakker (2001) for steady state flow. Interesting is that Bakker (2001) only applies this vertical discretization locally around the well, which is justified as the partially penetrating effect is observable only close to the well (Hantush, 1964). Hemker (1999a) regards this approach as an extension of the method in which the well is replaced by a number of point sources and corresponding image sinks, where the unknown discharges are determined by solving a linear system of equations.

According to Dagan (1978), assuming a continuous distribution of point sources along the well axis can be traced back to Muskat (1937), who applies this technique to simulate steady flow to a partially penetrating well in a confined aquifer. However, de Glee (1930) also uses the method of images to model a partially penetrating well in a leaky aquifer. Tarshish (1993, 1998) applies the method to simulate steady flow to a well partially penetrating a confined aquifer, whereas Dagan (1978) considers an unconfined aquifer and uses Green's function, which can be seen as a way to mathematically structure the method of images (Pantoja & Elias, 2020). Kipp (1973) applies the method of images to simulate transient flow to a finite-diameter well in an unconfined aquifer. More

recently, the Green function method is applied by Dagan and Lessoff (2011) to analyze transient flow to a partially penetrating well in an unconfined heterogeneous aquifer, and by Wang et al. (2021) to model a multi-aquifer well with partially penetrating screen in each aquifer of a confined two-aquifer system. Previously, Javandel and Witherspoon (1980) simulated transient flow to a partially penetrating well in the top layer of a two-layer system with impervious top and unbounded lower layer. Although Javandel and Witherspoon (1980) define a continuous point source, they still assume a uniform gradient along the well-face (UWG).

Inspired by the work of Muskat (1937) and Dagan (1978), Haitjema (1985) and Haitjema and Kraemer (1988) apply line sinks along the well axis instead of point sinks, which has the advantage that axial symmetry is not required. Anjaneyulu (1991) uses an approach based on the analogy of flow of electric current to simulate steady flow toward a partially penetrating well in an unconfined aquifer, whereas Barua and Bora (2010) consider a partially penetrating well with finite radius and well-skin in a confined aquifer, and solve the differential equation governing steady state flow by means of the method of separation of variables. The same method in combination with the Laplace transform is applied by Chang et al. (2010, 2011) to simulate transient flow to a finite-diameter well partially penetrating an unconfined aquifer during a constant-head test. Feng and Zhan (2015, 2016) also combine the Laplace transform and the method of separation of variables to model a partially penetrating pumping well with finite radius and finite-thickness skin in a leaky aquifer overlain by a compressible aquitard. Both Barua and Bora (2010) and Chang et al. (2011) take into account flow below the well, which most other models for partially penetrating wells neglect. Nevertheless, one of the first models to simulate the partially penetrating effect of a well also considers the zone below the borehole (Kirkham, 1959).

Separation of variables is one method to solve the governing differential equation; integral transforms are, however, the most commonly applied technique to solve the equation analytically or semi-analytically. The Laplace transform has already been mentioned. It is used to eliminate the partial derivative of the hydraulic head with respect to the time. The infinite zero-order Hankel transform may be applied with respect to the radial distance, and the finite Fourier cosine transform with respect to the vertical distance. Transient models almost always apply the Laplace transform in combination with one of the two other transforms. The inversions are usually done by applying a numerical algorithm, such as the Stehfest (1970) algorithm, which is used to invert solutions in the Laplace domain. Because of the use of numerical algorithms, these solutions are called semi-analytical.

Table 1 and Table 2 give a non-exhaustive overview of studies in which an analytical or semi-analytical model is developed for transient radial Darcian flow to a single partially penetrating well, respectively assuming a constant flux or a constant head along the well-screen. Only the models defining a nonuniform flux are relevant for this study, although it seems that solutions assuming a uniform flux are more frequently applied to interpret aquifer test data (Ciftci, 2019; Duffield, 2007; Kruseman & de Ridder, 1990). As already mentioned, assuming a constant head or drawdown along the well-screen is more realistic, but fortunately, the mathematical simplification of a uniform well-face flux boundary condition does not lead to unacceptably inaccurate results at distances that are not extremely close to the pumping well (Yeh & Chang, 2013). In any case, solving the mixed-type boundary value problem analytically is more challenging, and in general, additional mathematical techniques are required. For instance, some researchers discretize the well-screen (Chang & Chen, 2002, 2003; Feng & Zhan, 2016; Perina & Lee, 2006), whereas Cassiani and Kabala (1998) and Cassiani et al. (1999) apply a dual integral method, Wilkinson and Hammond (1990) a perturbation

method, Chang and Yeh (2009) a dual series equations and a perturbation method, and Chang and Yeh (2010) a triple series equations method.

Table 1 and Table 2 show that models are developed to simulate pumping tests, slug tests, and constant-head tests conducted in partially penetrating wells. The well may have an infinitesimal or finite diameter, and may be surrounded by a skin of zero or finite thickness. If the well has a finite diameter, then wellbore storage may be taken into account. Most of the models are restricted to a single homogeneous anisotropic aquifer with impervious lower boundary, although some models consider an aquifer with infinite thickness which has no lower boundary (Cassiani et al., 1999; Cassiani & Kabala, 1998; Javandel & Witherspoon, 1980; Kipp, 1973). The top of the aquifer may be an impervious or leaky boundary, or a water table. The solution developed by Tartakovsky and Neuman (2007) for a water table aquifer even includes the unsaturated zone where flow is governed by Richards' equation. Dougherty and Babu (1984) model a dual-porosity reservoir, Dagan and Lessoff (2011) a heterogeneous aquifer, and some solutions consider two layers (Feng et al., 2019; Feng & Zhan, 2015, 2016, 2019; Javandel & Witherspoon, 1980, 1983; Zlotnik & Zhan, 2005) or even three layers (Feng et al., 2020, 2021; Malama et al., 2008). The vertical position of the partially penetrating well-screen can be chosen by the user in most models, except when the aquifer has an infinite thickness, in which case the well-screen must extend from the top of the aquifer. In most two-layer models, the well is located in the lower aquifer; in the three-layer models, the well is located in the top layer (Malama et al., 2008), the lower layer (Feng et al., 2020), or the middle layer (Feng et al., 2021).

Table 1. Analytical models for transient radial flow to a partially penetrating well assuming a uniform well-face gradient (UWG). The models assume a homogeneous vertically anisotropic aquifer of infinite radial extent with impervious lower boundary, unless otherwise stated. Specific details of the model assumptions and the applied solution method can be found in the referenced study.

Study	Aquifer system	Partially penetrating well				Solution method
		Finite radius	Storage	Skin	Stress	
Hantush (1961a, 1961b, 1964)	Confined or leaky aquifer	No	No	No	Constant pumping	Fourier + Laplace transforms
Neuman (1974)	Unconfined aquifer	No	No	No	Constant pumping	Hankel + Laplace transforms
Javandel and Witherspoon (1980)	System of two isotropic layers with impervious top and no lower boundary	No	No	No	Constant pumping	Laplace transform + method of images
Javandel and Witherspoon (1983)	Confined system of two isotropic layers	No	No	No	Constant pumping	Hankel + Laplace transforms
Dougherty and Babu (1984)	Confined double-porosity aquifer	Yes	Yes	Zero-thickness	Constant pumping + instantaneous head change	Fourier + Laplace transforms
Novakowski (1993)	Confined aquifer	Yes	No	Finite-thickness	Constant head	Fourier + Laplace transforms
Moench (1996)	Unconfined aquifer	No	No	No	Constant pumping	Fourier + Laplace transforms
Moench (1997)	Unconfined aquifer	Yes	Yes	Zero-thickness	Constant pumping	Fourier + Laplace transforms
Zlotnik and Zhan (2005)	Unconfined aquifer above infinitely thick aquitard	No	No	No	Constant pumping	Fourier + Laplace transforms + superposition of point sinks

Yang and Yeh (2005)	Confined aquifer	Yes	No	Finite-thickness	Constant head	Fourier + Laplace transforms
Yang et al. (2006)	Confined aquifer	Yes	No	No	Constant pumping	Fourier + Laplace transforms
Chiu et al. (2007)	Confined aquifer	Yes	No	Finite-thickness	Constant pumping	Fourier + Laplace transforms
Tartakovsky and Neuman (2007)	Unconfined aquifer + unsaturated zone	No	No	No	Constant pumping	Hankel + Laplace transforms
Malama et al. (2008)	Unconfined and confined aquifer separated by compressible aquitard	No	No	No	Constant pumping	Hankel + Laplace transforms
Chang et al. (2010)	Unconfined aquifer	Yes	No	Finite-thickness	Constant head	Laplace transform + separation of variables
Mishra et al. (2012)	Confined aquifer	Yes	Yes	No	Constant pumping(Fourier + Laplace transforms
Yang et al. (2014)	Confined aquifer	Yes	No	Finite-thickness	Constant head	Fourier transform + transient influence radius
Huang et al. (2015)	Confined aquifer	Yes	No	Finite-thickness	Constant pumping	Fourier transform + transient influence radius
Feng and Zhan (2015)	Leaky aquifer + compressible aquitard	Yes	Yes	No	Constant pumping	Laplace transform + separation of variables
Feng and Zhan (2019)	Unbounded or bounded leaky aquifer + compressible aquitard	Yes	Yes	Finite-thickness	Constant head	Fourier + Laplace transforms + separation of variables
Feng et al. (2019)	System of two anisotropic layers, confined bottom, leaky or confined top	No	No	No	Variable pumping	Hankel + Laplace transforms
Feng et al. (2020)	System of three anisotropic layers, confined bottom, leaky or confined top or water table	No	No	No	Constant pumping	Hankel + Laplace transforms
Feng et al. (2021)	System of three anisotropic layers, leaky or confined bottom, leaky or confined top or water table	No	No	No	Variable pumping	Hankel + Laplace transforms

Table 2. Analytical models for transient radial flow to a partially penetrating well assuming a uniform well-face head or drawdown (UWD). The models assume a homogeneous vertically anisotropic aquifer of infinite radial extent with impervious lower boundary, unless otherwise stated. Specific details of the model assumptions and the applied solution method can be found in the referenced study.

Study	Aquifer system	Partially penetrating well				Solution method
		Finite radius	Storage	Skin	Stress	
Kipp (1973)	Unconfined isotropic aquifer of infinite thickness	Yes	Yes	No	Variable head	Transformation to potential function + method of images

Kader and Ramadurgaiah (1978)	Bounded confined Aquifer	Yes	Yes	No	Constant pumping	Fourier + Laplace transforms
Hyder et al. (1994)	Confined or leaky aquifer	Yes	Yes	Finite-thickness	Instantaneous head change	Fourier + Laplace transforms
Cassiani and Kabala (1998)	Aquifer with impervious top and no lower boundary	Yes	Yes	Zero-thickness	Constant pumping + instantaneous head change	Fourier + Laplace transforms
Cassiani et al. (1999)	Aquifer with impervious top and no lower boundary	Yes	Yes	Zero-thickness	Constant head	Fourier + Laplace transforms
Chang and Chen (2002)	Confined aquifer	Yes	No	Zero-thickness	Constant head	Fourier + Laplace transforms
Chang and Chen (2003)	Confined aquifer	Yes	No	No	Constant head	Fourier + Laplace transforms
Perina and Lee (2006)	Confined, leaky or unconfined aquifer	Yes	Yes	Finite-thickness	Constant pumping	Fourier + Laplace transforms
Chang and Yeh (2009)	Confined aquifer	Yes	No	No	Constant head	Fourier + Laplace transforms
Chang and Yeh (2010)	Confined aquifer	Yes	No	No	Constant head	Fourier + Laplace transforms
Chang et al. (2011)	Unconfined aquifer	Yes	No	No	Constant head	Laplace transform + separation of variables
Dagan and Lessoff (2011)	Unconfined heterogeneous aquifer	Yes	No	No	Constant pumping	Green's function method
Feng and Zhan (2016)	Leaky aquifer + compressible aquitard	Yes	Yes	Finite-thickness	Constant pumping	Laplace transform + separation of variables

6.1.3. Numerical methods

Numerical models applying the finite-difference method (Bennett et al., 1982; Cooley, 1971; Ruud & Kabala, 1996, 1997; Tjahjanto & Kassim, 2004) or the finite-element method (Cooley & Cunningham, 1979; Javandel & Witherspoon, 1969; Neuman & Witherspoon, 1971; Sudicky et al., 1995; Widdowson et al., 1990) are also an option to solve the problem of flow to a multilayer well.

Numerical models may also be used to calculate discrete pulse kernels for applying the convolution method (Olsthoorn, 2008). Approaches that use an analytical solution as discrete kernel have already been mentioned (Mishra et al., 1985; Mishra & Chandra, 1990, 1992); models that use MODFLOW (McDonald & Harbaugh, 1988) to obtain the kernels for simulating flow to a well tapping from two aquifers are presented by Mani et al. (1999) and Singh (2010).

Although numerical solutions are in general more easily obtained (Hemker, 1999a), the issue of choosing between a uniform or a non-uniform well-face flux remains. As for the semi-analytical methods, defining a uniform well-face flux for a numerical solution is more straightforward as it simply comes down to adding an extra source term to the nodes which represent the well. In the frequently used finite-difference model MODFLOW, for instance, the WEL package (Harbaugh et al., 2000) is used for that purpose. However, implementing a uniform head or drawdown at the well-face is more involved, and there are a number of possible techniques in which the well screen is defined as a model boundary or in which the well is part of the model grid.

In the first case of a model boundary, the head or drawdown inside the well can be calculated applying the superposition principle (Huang, 1973; Javandel & Witherspoon, 1969; Neuman &

Witherspoon, 1969; Sudicky et al., 1995) or using an iterative procedure (Bennett et al., 1982; Chen & Jiao, 1999; Cooley, 1971; Mathias & Wen, 2015; Neuman & Witherspoon, 1971; Ruud & Kabala, 1996, 1997; Tjahjanto & Kassim, 2004; Widdowson et al., 1990). In some models applying an iterative method, the integrated well-face flux is obtained by numerical integration (Mathias & Wen, 2015; Ruud & Kabala, 1996, 1997). MODFLOW's Multi-Node Well packages MNW (Halford & Hanson, 2002) and MNW2 (Konikow et al., 2009) also apply an iterative procedure. These packages are built from the earlier Multi-Aquifer Well package MAW1 (McDonald, 1984, 1986) which is based on the ideas by Bennet et al. (1982). MODFLOW 6 provides a new Multi-Aquifer Well package MAW which replaces the MNW and MNW2 packages (Langevin et al., 2017).

If the well is part of the model domain, then the friction losses and nonuniform flow within the wellbore may be taken into account (Cooley & Cunningham, 1979), or a hydrostatic water level inside the well may be assumed, in which case a high value can be assigned to the vertical conductivity between the well nodes (Behrooz-Koohenjani et al., 2011; Louwyck et al., 2012). The value for the vertical conductivity may also be estimated from the Hagen-Poiseuille equation for laminar flow of an incompressible fluid through a long cylindrical pipe (Sudicky et al., 1995). Using the unstructured grid option of MODFLOW 6 (Langevin et al., 2017), it is also possible to connect the cells that are part of the well instead of assigning a high value to the vertical conductivity.

Neville and Tonkin (2004) compare three approaches for simulating multi-aquifer wells using MODFLOW (Harbaugh et al., 2000; Harbaugh & McDonald, 1996; McDonald & Harbaugh, 1988): (1) the conventional application of the WEL package, where transmissivity weighting is used to calculate flow crossing the screen at each well node; (2) a modified application of the WEL package, where a high value is assigned to the vertical conductivity between the well nodes; (3) the multi-node well approach, implemented in the MNW package (Halford & Hanson, 2002). Neville and Tonkin (2004) conclude that (1) the conventional approach based on transmissivity weighting is inappropriate; (2) the high-K_v approach may be used if the vertical conductivity is sufficiently high and if the dimension of the well block is similar to the actual dimension of the well; (3) the MNW approach is relatively insensitive to grid refinement and is recommended to represent wells in models with relatively coarse grid.

Verifying the WEL and MNW approaches against analytical solutions is done by Gastélum et al. (2011), while Szucs et al. (2013) evaluate the MNW2 package (Konikow et al., 2009) using different analytical and numerical solutions, including the SAN method developed by Székely (1990; 1995). Szucs et al. (2013) conclude that the MNW approach provides accurate results in general, but do not recommend it in case of short-term transient simulations. Louwyck et al. (2012) present a method similar to the method of Langevin (2008) for tricking MODFLOW into simulating axisymmetric flow, and apply the high-K_v approach to accurately model a slug test conducted in a partially penetrating well. The MODFLOW procedure has been discussed in detail in section 3.4 of Chapter 3.

Vandenbohede et al. (2014) use SEAWAT to simulate axisymmetric heat transport employing the method of Langevin (2008) to convert the Cartesian grid geometry into an axisymmetric grid geometry. Both the conventional WEL and the MNW approach are applied, and it is concluded that the latter yields more accurate results, although the difference between both approaches is more pronounced for heat transport than for solute transport.

The MNW and MNW2 packages are implemented in MODFLOW to define wells with long screens extending over more than one cell in a rectangular grid. The MNW2 package can also deal with the effects of partial penetration, linear and nonlinear head losses, and pumping rate constraints. In this way, it allows for more accurate and realistic representations of well-field conditions in local and regional groundwater flow models for minimal computational costs (Konikow et al., 2009). The MNW

and MNW2 packages may also be used to simulate the effects of long-screen multi-aquifer wells on solute transport (Konikow & Hornberger, 2006), contaminant movement (Johnson et al., 2011; Yager & Heywood, 2014), water samples chemistry (Poulsen et al., 2019), and seawater intrusion (Coulon et al., 2022). The approach presented by Vandenbohede et al. (2014) differs from these applications because it applies the MNW2 package to connect the cells from a multilayer well in the center of an axisymmetric grid. In that sense, it is similar to finite-difference models using cylindrical coordinates to simulate axisymmetric flow to a multilayer well (Mathias & Wen, 2015; Ruud & Kabala, 1996, 1997).

6.1.4. Objectives

This chapter also treats the case of axisymmetric flow to a single well that has one or more screens connected to multiple layers. First, a semi-analytical solution is derived which is based on the work of Hemker (1984, 1985, 1999a, 1999b), and in particular on the UWD solution for axisymmetric flow to a multilayer well with single screen and zero-thickness skin (Hemker, 1999a). The solution presented in this chapter may be seen as an extension of the UWD solution, as multiple screens are allowed. Additionally, an arbitrary number of cylindrical zones of finite width around the well may be defined, just like in previous Chapter 5. Infiltration can be included and the solution is formulated in terms of hydraulic heads instead of drawdowns. Both steady and transient flow are considered, and the solution for parallel flow to a multilayer stream is also presented. The solution technique is similar to the one applied by Hemker (1999a, 1999b): the Laplace transform is applied and the system of partial differential equations is uncoupled by performing the eigendecomposition of the system matrix for each cylindrical zone. The obtained solution in the Laplace domain is numerically inverted using the Stehfest (1970) algorithm.

The second objective is to extend the finite-difference method presented in Chapter 3 with the option of defining a multi-node well. A simple algorithm is developed to connect any number of cells within the finite-difference grid. In this way, the multi-layer well is part of the model grid, which makes it easy to include the effect of wellbore storage by assigning a value to the storativity of the connected cells. Taking into account wellbore storage is, however, not possible if MODFLOW is used to simulate axisymmetric flow (Langevin, 2008; Louwyck et al., 2012, 2014) in combination with the MNW2 package (Konikow et al., 2009) to connect the cells that belong to the multi-node well. As already mentioned, this approach is applied by Vandenbohede et al. (2014) to simulate axisymmetric heat transport, in which case it is justified to neglect the wellbore storage. Unfortunately, Vandenbohede et al. (2014) do not elaborate on the MODFLOW-MNW2 procedure to simulate axisymmetric flow to a multi-node well. Therefore, the third objective is to explain this procedure in detail, which could also be applied to MODFLOW 6 and its new MAW package, that replaces the MNW2 package, and is capable of taking into account the wellbore storage (Langevin et al., 2017).

Finally, the presented semi-analytical and numerical solutions are verified against existing analytical solutions described in the hydrogeological literature. The first test case uses the formula derived by Sokol (1963) to calculate the steady water level in an abandoned multi-aquifer well and the extended formula for the case the well is extracted (Neville & Tonkin, 2004). The second test case considers the transient model for a well tapping multiple confined aquifers without crossflow. The two-aquifer solution by Papadopoulos (1966) and the solution for an arbitrary number of aquifers by Wikramaratna (1984) are used. The generalized UWD solution by Hemker (1999a) for multiple layers with crossflow is used as a third case. From the plethora of analytical solutions developed for partially penetrating wells, the UWG solution developed by Mishra et al. (2012) is compared with Hemker's multilayer UWD solution, and the KGS model (Hyder et al., 1994) is used to verify whether the newly developed solutions give accurate results when applied to simulate a slug test in a partially

penetrating well with finite-thickness skin. This case is extra challenging as a slug test is highly sensitive to effects of wellbore storage and skin. Slug test models also have to deal with very small values of time.

The added value of the developed solutions is finally illustrated by simulating axisymmetric flow to a partially penetrating well in a multi-aquifer system with combined infiltration and drainage in the top layer. The well-screen extends over multiple layers with different hydraulic properties and it has a finite-thickness skin. The well is surrounded by a gravel pack with a clay seal above it. Between the developed zone and the aquifer a second skin occurs. The model is solved using both the semi-analytical and the finite-difference solutions developed in this chapter.

Before presenting and verifying these new solutions, the problem is stated mathematically in the next section. The semi-analytical solution is derived after the problem statement. The algorithm to connect cells in the finite-difference grid is given next, and it is explained how the MNW2 package may be used to define a multi-node well by applying the procedure to trick MODFLOW into simulating radial flow. Finally, the developed solutions are verified against the well-known solutions discussed above.

6.2. Problem statement

The stated problem is the same as in previous Chapter 5, with the only difference the inner boundary condition represents a multilayer well with finite diameter for which the change in wellbore storage is taken into account (Figure 1). In case of parallel flow, this inner boundary condition may conceptualize a single stream interacting with more than one layer in the aquifer system.

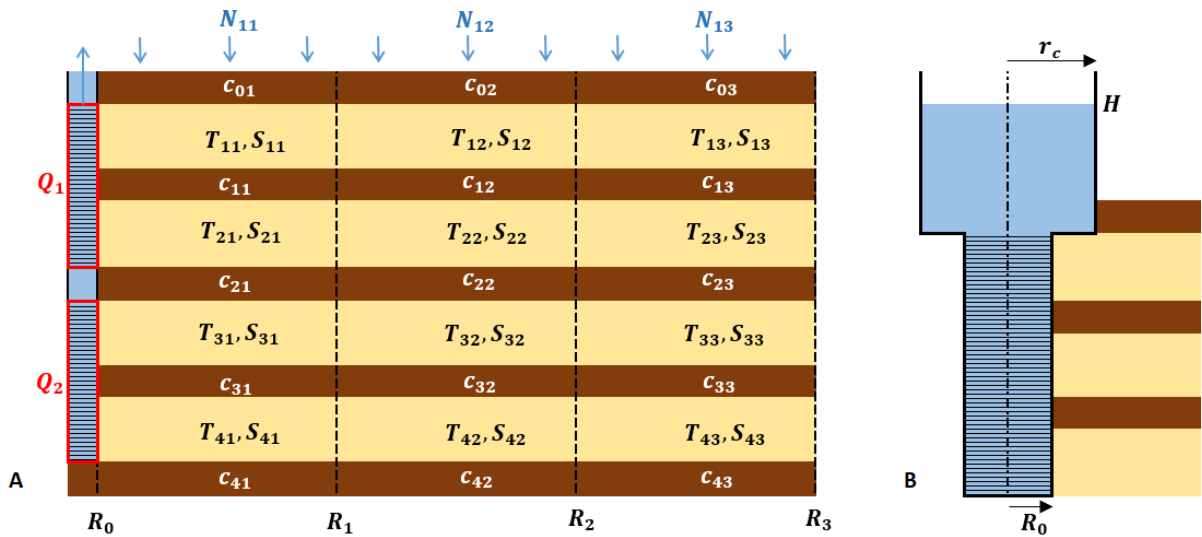


Figure 1. The left plot (A) visualizes the problem stated and solved in this chapter. The difference with the problem stated in previous chapter 5 is the possibility to connect well-screens. The right plot (B) zooms in on such a multilayer well, with R_0 the radius of the well-screen, and r_c the radius of the well-casing. Wellbore storage is considered in this chapter, which is determined by the radius of the well-casing and the change in water level H . In case of parallel flow, the inner boundary may represent a stream that is open to more than one layer. See text for the mathematical statement of the problem and definitions of parameters.

The system of partial differential equations describing flow in each zone and layer is:

$$\nabla^2 h_{ij} = \frac{S_{ij}}{T_{ij}} \frac{\partial h_{ij}}{\partial t} + \frac{-N_{ij}}{T_{ij}} + \frac{h_{ij} - h_{i-1,j}}{c_{i-1,j} T_{ij}} + \frac{h_{ij} - h_{i+1,j}}{c_{ij} T_{ij}} \quad (1 \leq i \leq n_l; 1 \leq j \leq n_z) \quad (1)$$

with $\nabla^2 h = \frac{\partial^2 h}{\partial r^2} + \frac{1}{r} \frac{\partial h}{\partial r}$ in case of axisymmetric flow, and $\nabla^2 h = \frac{\partial^2 h}{\partial r^2}$ in case of parallel flow. Hydraulic head h_{ij} [L] in layer i and zone j is a function of time t [T]. The head also depends on radial or horizontal distance r [L], depending on the type of flow. If flow is in a steady state, then $\frac{\partial h_{ij}}{\partial t} = 0$, by definition, and the head only depends on distance r .

The total number of layers is n_l ; the total number of zones is n_z . Layers are numbered from top to bottom; zones from inner boundary at distance R_0 [L] to outer boundary at distance R_{n_z} [L]. The boundary between zones j and $j + 1$ is at distance R_j [L] (Figure 1A). Layer i has constant thickness D_i [L]. Each zone j in layer i is characterized by a constant transmissivity T_{ij} [L^2/T], a constant storativity S_{ij} [-], and a constant infiltration flux N_{ij} [L/T], which is positive in case of recharge. Zones j in adjacent layers i and $i + 1$ are separated by an incompressible resistance layer with zero thickness characterized by hydraulic resistance c_{ij} [T]. See previous Chapter 5 for a more detailed explanation about these parameters.

In case of axisymmetric flow, radial discharge Q^h [L^3/T] is defined as:

$$Q_{ij}^h = -2\pi T_{ij} r \frac{\partial h_{ij}}{\partial r} \quad (1 \leq i \leq n_l; 1 \leq j \leq n_z) \quad (2)$$

In case of parallel flow, horizontal discharge Q^h [L^2/T] is defined as:

$$Q_{ij}^h = -T_{ij} \frac{\partial h_{ij}}{\partial r} \quad (1 \leq i \leq n_l; 1 \leq j \leq n_z) \quad (3)$$

The leaky upper and the lower boundary of the aquifer system are characterized by resistances $c_{0,j}$ and $c_{n_l,j}$, and constant heads $\varphi_{0,j}$ [L] and $\varphi_{n_l+1,j}$ [L], respectively:

$$h_{0,j}(r, t) = \varphi_{0,j} \quad (1 \leq j \leq n_z) \quad (4)$$

$$h_{n_l+1,j}(r, t) = \varphi_{n_l+1,j} \quad (1 \leq j \leq n_z) \quad (5)$$

At the outer model boundary, a constant head φ_{i,n_z} [L] is defined in each layer i :

$$h_{i,n_z}(R_{n_z}, t) = \varphi_{i,n_z} \quad (1 \leq i \leq n_l) \quad (6)$$

Head and flow are continuous at the boundary between zones j and $j + 1$ in layer i :

$$h_{ij}(R_j, t) = h_{i,j+1}(R_j, t) \quad (1 \leq i \leq n_l; 1 \leq j < n_z) \quad (7)$$

$$Q_{ij}^h(R_j, t) = Q_{i,j+1}^h(R_j, t) \quad (1 \leq i \leq n_l; 1 \leq j < n_z) \quad (8)$$

In this chapter, a well with radius R_0 or a stream with half width equal to R_0 is considered that is open to more than one layer in the aquifer system (Figure 1B). Although it is not very likely to have more than one stream in case of parallel flow, it is realistic to have a well with more than one screen, and therefore, the general case considering more than one multilayer well or stream is stated mathematically.

The water level H_w [L] at time t in the w -th multilayer well or stream is equal to the head h_{i_w} at the inner model boundary at distance R_0 and time t in the layers i_w that are connected to this well or stream:

$$H_w(t) = h_{i_w}(R_0, t) \quad (w = 1, 2, \dots, n_w) \quad (9)$$

where the total number of multilayer wells or streams equals n_w . The wellbore balance for well w at time t is:

$$Q_w = \pi r_{c,w}^2 \frac{dH_w}{dt} + \sum_{i_w} Q_{i_w,1}^h(R_0, t) \quad (w = 1, 2, \dots, n_w) \quad (10)$$

with Q_w the constant pumping rate of well w , which is negative if water is removed from the aquifer system; $r_{c,w}$ [L] is the radius of the casing of well w , or more precisely, the part of the well where the water level movements take place. The first term of the right-hand side of equation (10) defines the change in wellbore storage, which is zero if steady flow is considered, as H_w is independent of time in this case. If parallel flow is simulated, then the change in storage in the stream must be considered:

$$Q_w = r_{c,w} \frac{dH_w}{dt} + \sum_{i_w} Q_{i_w,1}^h(R_0, t) \quad (w = 1, 2, \dots, n_w) \quad (11)$$

where $r_{c,w}$ is half the width of the part of the w -th stream where the water level is changing.

The unscreened layers in the aquifer system have a no-flux condition at the inner model boundary:

$$Q_{i_u,1}^h(R_0, t) = 0 \quad (12)$$

where i_u refers to the indices of the unscreened layers.

Finally, initial conditions at $t = 0$ are required in case of transient flow. These conditions are defined by setting the initial head in each zone j and layer i to the initial head φ_{ij} :

$$h_{ij}(r, 0) = \varphi_{ij} \quad (1 \leq i \leq n_l; 1 \leq j \leq n_z) \quad (13)$$

Note that the initial heads φ_{i,n_z} in the outer zones equal the constant heads at the outer model boundary defined by (6). An initial water level is also required for each well or stream w :

$$H_w(0) = \varphi_{w,0} \quad (w = 1, 2, \dots, n_w) \quad (14)$$

where subscript 0 in $\varphi_{w,0}$ refers to the multilayer wells or streams, which may be regarded as zone 0.

6.3. Semi-analytical solution

As the stated problem is just an extension to the one stated in Chapter 5, it is possible to conduct the same solution method. The Laplace transform is applied as suggested by Hemker (1999a, 1999b, 2000), after which the system of ordinary differential equations for each zone is uncoupled by decomposing the system matrix into its eigenvalues and eigenvectors, as proposed by Hemker (1984, 1985). The general solution for each zone is the same as the general solution for multilayer flow without zones presented in Chapter 2, and particular solutions are obtained by solving the system of boundary conditions numerically, as discussed in Chapter 5. If there is no lateral variation in hydraulic parameters, which implies there is only one zone, then the system of boundary conditions can be solved analytically, as shown by (Hemker, 1999a). In this case, a zero-thickness skin may be taken into account. In the transient case, particular solutions in the Laplace domain are inverted numerically using the Stehfest (1970) algorithm.

6.3.1. General solution

The problem stated in section 6.2 is first Laplace transformed and written in matrix form, after which system matrix A_j is decomposed into its eigenvalues and corresponding eigenvectors:

$$\mathbf{A}_j = \mathbf{V}_j \mathbf{D}_j \mathbf{V}_j^{-1} \quad (1 \leq j \leq n_z) \quad (15)$$

with \mathbf{D}_j a diagonal matrix holding the eigenvalues d_{ij} , and \mathbf{V}_j a matrix containing the corresponding eigenvectors in its columns. System matrix \mathbf{A}_j is an $n_l \times n_l$ tridiagonal matrix, where the entry on the i -th row and the k -th column is:

$$\mathbf{A}_{jik} = \begin{cases} \frac{1}{c_{i-1,j} T_{ij}} + \frac{1}{c_{ij} T_{ij}} + \frac{S_{ij}}{T_{ij}} p & (i = k) \\ \frac{-1}{c_{i-1,j} T_{ij}} & (i = k + 1) \\ \frac{-1}{c_{ij} T_{ij}} & (i = k - 1) \end{cases} \quad (16)$$

If $i = k$, then the entry is on the main diagonal of \mathbf{A}_j ; if $i = k + 1$, then the entry is on the lower diagonal; and if $i = k - 1$, then the entry is on the upper diagonal. All other elements in \mathbf{A}_j are zero. In case of steady state, the term containing the storativity and Laplace variable p [1/T] is omitted, which may be obtained by setting S_{ij} to zero.

The general solution for the resulting system of uncoupled differential equations is:

$$\mathbf{V}_j^{-1} \mathbf{h}_j(r) = \mathbf{g}_j(r) = \mathbf{I}_j(r) \boldsymbol{\alpha}_j + \mathbf{K}_j(r) \boldsymbol{\beta}_j + \mathbf{m}_j(r) \quad (1 \leq j \leq n_z) \quad (17)$$

where the i -th entry in $n_l \times 1$ vector \mathbf{h}_j is $h_{ij}(r)$ in case of steady state, while it is the Laplace transform of head $\bar{h}_{ij}(r, p)$ in case of transient flow; \mathbf{I}_j and \mathbf{K}_j are $n_l \times n_l$ diagonal matrices, and $\boldsymbol{\alpha}_j$, $\boldsymbol{\beta}_j$, and \mathbf{m}_j are $n_l \times 1$ vectors. In case of axisymmetric flow, the nonzero entries of \mathbf{I}_j , \mathbf{K}_j , and \mathbf{m}_j are defined as, respectively:

$$\mathbf{I}_{jii}(r) = \begin{cases} \ln(r) & (d_{ij} = 0) \\ I_0\left(r \sqrt{d_{ij}}\right) & (d_{ij} \neq 0) \end{cases} \quad (18)$$

$$\mathbf{K}_{jii}(r) = \begin{cases} 1 & (d_{ij} = 0) \\ K_0\left(r \sqrt{d_{ij}}\right) & (d_{ij} \neq 0) \end{cases} \quad (19)$$

$$\mathbf{m}_{ji}(r) = \begin{cases} -\frac{\mathbf{v}_{ji} r^2}{4} & (d_{ij} = 0) \\ \frac{\mathbf{v}_{ji}}{d_{ij}} & (d_{ij} \neq 0) \end{cases} \quad (20)$$

Functions I_0 and K_0 are the zero order modified Bessel functions of the first and second kind, respectively; \mathbf{v}_{ji} is the i -th element of $n_l \times 1$ vector $\mathbf{v}_j = \mathbf{V}_j^{-1} \mathbf{b}_j$, with \mathbf{b}_j an $n_l \times 1$ vector defined as:

$$\mathbf{b}_{ji} = \begin{cases} \frac{N_{1,j}}{p T_{1,j}} + \frac{\varphi_{0,j}}{p c_{0,j} T_{1,j}} + \frac{S_{1,j}}{T_{1,j}} \varphi_{1,j} & (i = 1) \\ \frac{N_{n_l,j}}{p T_{n_l,j}} + \frac{\varphi_{n_l+1,j}}{p c_{n_l,j} T_{n_l,j}} + \frac{S_{n_l,j}}{T_{n_l,j}} \varphi_{n_l,j} & (i = n_l) \\ \frac{N_{ij}}{p T_{ij}} + \frac{S_{ij}}{T_{ij}} \varphi_{ij} & (1 < i < n_l) \end{cases} \quad (21)$$

In the steady-state case, the terms containing the storativity are omitted, as is Laplace variable p . This may be obtained by setting S_{ij} to zero for all i , and setting p to 1.

In case of parallel flow, the nonzero entries of \mathbf{I}_j , \mathbf{K}_j , and \mathbf{m}_j are:

$$\mathbf{I}_{jii}(r) = \begin{cases} r & (d_{ij} = 0) \\ e^{(r\sqrt{d_{ij}})} & (d_{ij} \neq 0) \end{cases} \quad (22)$$

$$\mathbf{K}_{jii}(r) = \begin{cases} 1 & (d_{ij} = 0) \\ e^{-(r\sqrt{d_{ij}})} & (d_{ij} \neq 0) \end{cases} \quad (23)$$

$$\mathbf{m}_{ji}(r) = \begin{cases} -\frac{\nu_{ji}r^2}{2} & (d_{ij} = 0) \\ \frac{\nu_{ji}}{d_{ij}} & (d_{ij} \neq 0) \end{cases} \quad (24)$$

The first order derivative \mathbf{g}_j with respect to r is also needed:

$$\nabla \mathbf{g}_j(r) = \mathbf{I}'_j(r)\boldsymbol{\alpha}_j + \mathbf{K}'_j(r)\boldsymbol{\beta}_j + \mathbf{m}'_j(r) \quad (25)$$

where \mathbf{I}'_j and \mathbf{K}'_j are $n_l \times n_l$ diagonal matrices, and \mathbf{m}'_j is an $n_l \times 1$ vector. In case of axisymmetric flow, $\nabla \mathbf{g}_j = r \frac{\partial \mathbf{g}_j}{\partial r}$, and the nonzero entries of \mathbf{I}'_j , \mathbf{K}'_j , and \mathbf{m}'_j are defined as, respectively:

$$\mathbf{I}'_{jii}(r) = \begin{cases} 1 & (d_{ij} = 0) \\ \left(r\sqrt{d_{ij}}\right) I_1\left(r\sqrt{d_{ij}}\right) & (d_{ij} \neq 0) \end{cases} \quad (26)$$

$$\mathbf{K}'_{jii}(r) = \begin{cases} 0 & (d_{ij} = 0) \\ -\left(r\sqrt{d_{ij}}\right) K_1\left(r\sqrt{d_{ij}}\right) & (d_{ij} \neq 0) \end{cases} \quad (27)$$

$$\mathbf{m}'_{ji}(r) = \begin{cases} -\frac{\nu_{ji}r^2}{2} & (d_{ij} = 0) \\ 0 & (d_{ij} \neq 0) \end{cases} \quad (28)$$

Functions I_1 and K_1 are the first order modified Bessel functions of the first and second kind, respectively. In case of parallel flow, $\nabla \mathbf{g}_j = \frac{\partial \mathbf{g}_j}{\partial r}$, and these nonzero entries are:

$$\mathbf{I}'_{jii}(r) = \begin{cases} 1 & (d_{ij} = 0) \\ \left(\sqrt{d_{ij}}\right) e^{(r\sqrt{d_{ij}})} & (d_{ij} \neq 0) \end{cases} \quad (29)$$

$$\mathbf{K}'_{jii}(r) = \begin{cases} 0 & (d_{ij} = 0) \\ -\left(\sqrt{d_{ij}}\right) e^{-(r\sqrt{d_{ij}})} & (d_{ij} \neq 0) \end{cases} \quad (30)$$

$$\mathbf{m}'_{ji}(r) = \begin{cases} -\nu_{ji}r & (d_{ij} = 0) \\ 0 & (d_{ij} \neq 0) \end{cases} \quad (31)$$

Chapter 5 also presents this general solution and discusses it in more detail.

6.3.2. Particular solutions

Vectors α_j and β_j contain the unknown integration constants which are determined by applying the boundary conditions. These are also Laplace transformed and written in matrix form. The constant-head conditions (6) at the outer model boundary are rewritten as:

$$\mathbf{V}_{n_z} \mathbf{g}_{n_z}(R_{n_z}) = \boldsymbol{\varphi}_{n_z} \quad (32)$$

with $\boldsymbol{\varphi}_{n_z}$ an $n_l \times 1$ vector in which the i -th entry is φ_{i,n_z} in case of steady flow, and $\varphi_{i,n_z}/p$ in case of transient flow. The conditions (7) and (8) at the boundary between zones j and $j + 1$ are reformulated as, respectively:

$$\mathbf{V}_j \mathbf{g}_j(R_j) = \mathbf{V}_{j+1} \mathbf{g}_{j+1}(R_j) \quad (1 \leq j < n_z) \quad (33)$$

$$\mathbf{T}_j \mathbf{V}_j \nabla \mathbf{g}_j(R_j) = \mathbf{T}_{j+1} \mathbf{V}_{j+1} \nabla \mathbf{g}_{j+1}(R_j) \quad (1 \leq j < n_z) \quad (34)$$

where \mathbf{T}_j is an $n_l \times n_l$ diagonal matrix, with nonzero entries equal to $2\pi T_{ij}$ in case of axisymmetric flow, and T_{ij} in case of parallel flow.

In order to write the inner boundary conditions in matrix form, matrices \mathbf{E} , \mathbf{U} , and \mathbf{C} are introduced. All three matrices contain zeros and ones only. In case of matrix \mathbf{E} , the nonzero entries indicate which layers are screened, whereas the nonzero entries in \mathbf{U} correspond to the unscreened layers, and the nonzero entries in \mathbf{C} show which of the screened layers are connected. If n_s is the number of screened layers, then matrix \mathbf{E} is an $n_l \times n_s$ matrix in which only the entries $\mathbf{E}_{i_w,j}$ are equal to 1, matrix \mathbf{U} is an $n_l \times (n_l - n_s)$ matrix in which only the entries $\mathbf{U}_{i_u,j}$ are equal to 1, and matrix \mathbf{C} is an $n_s \times n_w$ matrix in which only the entries $\mathbf{C}_{i_w,w}$ are equal to 1. Recall that i_w represents the indices of all layers open to well w . Similarly, i_u represents the indices of all unscreened layers. Index j in $\mathbf{E}_{i_w,j}$ refers to a screened layer, while it refers to an unscreened layer in $\mathbf{U}_{i_u,j}$.

Consider the following example to explain how matrices \mathbf{E} , \mathbf{U} , and \mathbf{C} are defined in a specific case. Suppose the aquifer system has 7 layers, from which the first, the fourth, the sixth, and the last layer have no screen, while the second and third layer are connected to the first well, and the fifth layer is open to the second well. In this case, $n_l = 7$, $n_s = 3$, and $n_w = 2$, and matrices \mathbf{E} , \mathbf{U} , and \mathbf{C} are defined as:

$$\mathbf{E} = \begin{bmatrix} 0 & 0 & 0 \\ 1 & 0 & 0 \\ 0 & 1 & 0 \\ 0 & 0 & 0 \\ 0 & 0 & 1 \\ 0 & 0 & 0 \\ 0 & 0 & 0 \end{bmatrix} \quad \mathbf{U} = \begin{bmatrix} 1 & 0 & 0 & 0 \\ 0 & 0 & 0 & 0 \\ 0 & 0 & 0 & 0 \\ 0 & 1 & 0 & 0 \\ 0 & 0 & 0 & 0 \\ 0 & 0 & 1 & 0 \\ 0 & 0 & 0 & 1 \end{bmatrix} \quad \mathbf{C} = \begin{bmatrix} 1 & 0 \\ 1 & 0 \\ 0 & 1 \end{bmatrix} \quad (35)$$

It is straightforward to prove that $\mathbf{E}^T \mathbf{E}$ equals the $n_s \times n_s$ identity matrix (Hemker, 1999a), and that $\mathbf{E} \mathbf{E}^T$ is an $n_l \times n_l$ diagonal matrix in which entry \mathbf{E}_{ii} on the main diagonal is one if layer i has a well screen, and zero otherwise. Similarly, $\mathbf{U}^T \mathbf{U}$ equals the identity matrix, and $\mathbf{U} \mathbf{U}^T$ is an $n_l \times n_l$ diagonal matrix in which the only entries that equal 1 correspond to layers without well screen.

Condition (9) that states the heads at the well-face of layers with connected screens are equal to the water level in the well can now be written in matrix form using matrices \mathbf{E} and \mathbf{C} :

$$\mathbf{E}^T \mathbf{h}_1(R_0) = \mathbf{C} \mathbf{H} \quad (36)$$

The corresponding wellbore balances (10) are written in matrix form as follows:

$$\mathbf{Q} = \mathbf{R}_c(p\mathbf{H} - \boldsymbol{\varphi}_0) + (\mathbf{E}\mathbf{C})^T \mathbf{T}_1 \nabla \mathbf{h}_1(R_0) \quad (37)$$

Vectors \mathbf{Q} , \mathbf{H} , and $\boldsymbol{\varphi}_0$ contain n_w values. The first term in (37) is omitted in the steady-state case. If steady flow is simulated, then the w -th entry in \mathbf{Q} is the pumping rate of well w :

$$Q_w = Q_w \quad (38)$$

In the transient-state case, the w -th entry is the Laplace transform of Q_w :

$$Q_w = \frac{Q_w}{p} \quad (39)$$

Vector \mathbf{H} contains the unknown water level in the well. In the steady-state case, the w -th entry in \mathbf{H} is:

$$H_w = H_w \quad (40)$$

In the transient-state case, the w -th entry is the Laplace transform \bar{H} of the water level in the well:

$$H_w = \bar{H}_w \quad (41)$$

Vector $\boldsymbol{\varphi}_0$ contains the initial heads in the n_w wells:

$$\boldsymbol{\varphi}_{0,w} = \varphi_{w,0} \quad (42)$$

In (37), \mathbf{R}_c is an $n_w \times n_w$ diagonal matrix. In case of axisymmetric flow, the nonzero diagonal entries are:

$$R_{c,w,w} = \pi r_{c,w}^2 \quad (43)$$

with $r_{c,w}$ the radius of the casing of the w -th well. In case of parallel flow, these entries are:

$$R_{c,w,w} = r_{c,w} \quad (44)$$

with $r_{c,w}$ the half width of the w -th stream. The no-flux conditions (12) defined for the unscreened layers are written in matrix form as follows:

$$\mathbf{U}^T \mathbf{T}_1 \nabla \mathbf{h}_1(R_0) = \mathbf{0} \quad (45)$$

Rewriting the inner boundary conditions (36), (37), and (45) as a function of \mathbf{g}_1 finally gives, respectively:

$$\mathbf{E}^T \mathbf{V}_1 \mathbf{g}_1(R_0) = \mathbf{C} \mathbf{H} \quad (46)$$

$$\mathbf{Q} = \mathbf{R}_c(p\mathbf{H} - \boldsymbol{\varphi}_0) + (\mathbf{E}\mathbf{C})^T \mathbf{T}_1 \mathbf{V}_1 \nabla \mathbf{g}_1(R_0) \quad (47)$$

$$\mathbf{U}^T \mathbf{T}_1 \mathbf{V}_1 \nabla \mathbf{g}_1(R_0) = \mathbf{0} \quad (48)$$

The resulting system of equations that considers all boundary conditions is:

$$\begin{cases} \mathbf{R}_c p \mathbf{H} + (\mathbf{E}\mathbf{C})^T \mathbf{X}'_1 \boldsymbol{\alpha}_1 + (\mathbf{E}\mathbf{C})^T \mathbf{Y}'_1 \boldsymbol{\beta}_1 = \mathbf{Q} + \mathbf{R}_c \boldsymbol{\varphi}_0 + (\mathbf{E}\mathbf{C})^T \mathbf{z}'_1 & (r = R_0) \\ \mathbf{C} \mathbf{H} - \mathbf{E}^T \mathbf{X}_1 \boldsymbol{\alpha}_1 - \mathbf{E}^T \mathbf{Y}_1 \boldsymbol{\beta}_1 = \mathbf{E}^T \mathbf{z}_1 & (r = R_0) \\ -\mathbf{U}^T \mathbf{X}'_1 \boldsymbol{\alpha}_1 - \mathbf{U}^T \mathbf{Y}'_1 \boldsymbol{\beta}_1 = \mathbf{U}^T \mathbf{z}'_1 & (r = R_0) \\ \mathbf{X}_j \boldsymbol{\alpha}_j + \mathbf{Y}_j \boldsymbol{\beta}_j - \mathbf{X}_{j+1} \boldsymbol{\alpha}_{j+1} - \mathbf{Y}_{j+1} \boldsymbol{\beta}_{j+1} = \mathbf{z}_{j+1} - \mathbf{z}_j & (r = R_j; 1 \leq j < n_z) \\ \mathbf{X}'_j \boldsymbol{\alpha}_j + \mathbf{Y}'_j \boldsymbol{\beta}_j - \mathbf{X}'_{j+1} \boldsymbol{\alpha}_{j+1} - \mathbf{Y}'_{j+1} \boldsymbol{\beta}_{j+1} = \mathbf{z}'_{j+1} - \mathbf{z}'_j & (r = R_j; 1 \leq j < n_z) \\ \mathbf{X}_{n_z} \boldsymbol{\alpha}_{n_z} + \mathbf{Y}_{n_z} \boldsymbol{\beta}_{n_z} = \boldsymbol{\varphi}_{n_z} - \mathbf{z}_{n_z} & (r = R_{n_z}) \end{cases} \quad (49)$$

with $\mathbf{X}_j = \mathbf{V}_j \mathbf{I}_j$; $\mathbf{Y}_j = \mathbf{V}_j \mathbf{K}_j$; $\mathbf{z}_j = \mathbf{V}_j \mathbf{m}_j$; $\mathbf{X}'_j = \mathbf{T}_j \mathbf{V}_j \mathbf{I}'_j$; $\mathbf{Y}'_j = \mathbf{T}_j \mathbf{V}_j \mathbf{K}'_j$; $\mathbf{z}'_j = \mathbf{T}_j \mathbf{V}_j \mathbf{m}'_j$.

In total, there are $n = 2n_l \cdot n_z + n_w$ equations in (49). Solving (49) yields the integration constants, which are the entries of vectors α_j and β_j , and the unknown heads \mathbf{H} in the n_w multilayer wells or streams:

$$\boldsymbol{\gamma} = \mathbf{M}^{-1} \boldsymbol{\omega} \quad (50)$$

where vector $\boldsymbol{\gamma}$ in (50) contains the n_w unknown water levels in the wells or streams, and the $2n_l \cdot n_z$ unknown integration constants:

$$\boldsymbol{\gamma} = \begin{bmatrix} \mathbf{H} \\ \boldsymbol{\beta}_1 \\ \boldsymbol{\alpha}_1 \\ \vdots \\ \boldsymbol{\beta}_{n_z} \\ \boldsymbol{\alpha}_{n_z} \end{bmatrix} \quad (51)$$

\mathbf{M} in (50) is the $n \times n$ matrix containing the known coefficients:

$$\mathbf{M} = \begin{bmatrix} \mathbf{W} & -\mathbf{M}_{10} & \mathbf{0} & \cdots & \cdots & \mathbf{0} \\ \mathbf{0} & \mathbf{M}_{11} & -\mathbf{M}_{21} & \mathbf{0} & & \vdots \\ \vdots & \mathbf{0} & \mathbf{M}_{22} & -\mathbf{M}_{32} & \mathbf{0} & \vdots \\ & \vdots & \mathbf{0} & & & \mathbf{0} \\ \vdots & \vdots & & \mathbf{0} & \mathbf{M}_{n_z-1,n_z-1} & -\mathbf{M}_{n_z,n_z-1} \\ \mathbf{0} & \mathbf{0} & \cdots & \cdots & \mathbf{0} & \mathbf{M}_{n_z,n_z} \end{bmatrix} \quad (52)$$

with:

$$\mathbf{W} = \begin{bmatrix} \mathbf{R}_c p \\ \mathbf{C} \\ \mathbf{0} \end{bmatrix} \quad (53)$$

$$\mathbf{M}_{10} = \begin{bmatrix} -(\mathbf{E}\mathbf{C})^T \mathbf{Y}'_1(R_0) & -(\mathbf{E}\mathbf{C})^T \mathbf{X}'_1(R_0) \\ \mathbf{E}^T \mathbf{Y}_1(R_0) & \mathbf{E}^T \mathbf{X}_1(R_0) \\ \mathbf{U}^T \mathbf{Y}'_1(R_0) & \mathbf{U}^T \mathbf{X}'_1(R_0) \end{bmatrix} \quad (54)$$

$$\mathbf{M}_{jk} = \begin{bmatrix} \mathbf{Y}_j(R_k) & \mathbf{X}_j(R_k) \\ \mathbf{Y}'_j(R_k) & \mathbf{X}'_j(R_k) \end{bmatrix} \quad (0 < k < n_z; j \in \{k, k+1\}) \quad (55)$$

$$\mathbf{M}_{n_z,n_z} = [\mathbf{Y}_{n_z}(R_{n_z}) \quad \mathbf{X}_{n_z}(R_{n_z})] \quad (56)$$

In (53), \mathbf{W} is an $(n_l + n_w) \times n_w$ matrix.

The entries of vector $\boldsymbol{\omega}$ in (50) are the $2n$ known terms in the right-hand side of the equations in (49):

$$\boldsymbol{\omega} = \begin{bmatrix} (\mathbf{E}\mathbf{C})^T \mathbf{z}'_{10} + \mathbf{Q} + \mathbf{R}_c \boldsymbol{\varphi}^w \\ \mathbf{E}^T \mathbf{z}_{10} \\ \mathbf{U}^T \mathbf{z}'_{10} \\ \mathbf{z}_{21} - \mathbf{z}_{11} \\ \mathbf{z}'_{21} - \mathbf{z}'_{11} \\ \vdots \\ \mathbf{z}_{n_z,n_z-1} - \mathbf{z}_{n_z-1,n_z-1} \\ \mathbf{z}'_{n_z,n_z-1} - \mathbf{z}'_{n_z-1,n_z-1} \\ \boldsymbol{\varphi}_{n_z} - \mathbf{z}_{n_z,n_z} \end{bmatrix} \quad (57)$$

Matrix system (50) is solved using the standard solver available with SciPy (Peterson et al., 2022). Once the integration constants α_j and β_j are determined for all j , hydraulic heads for all zones j , for all layers i , and at any given distance r , are found by evaluating:

$$\mathbf{h}_j(r) = \mathbf{V}_j \mathbf{g}_j(r) \quad (58)$$

Horizontal discharges for all zones j , for all layers i , and at any given distance r , are found by evaluating:

$$\mathbf{Q}_j^h(r) = -\mathbf{T}_j \mathbf{V}_j \nabla \mathbf{g}_j(r) \quad (59)$$

where vector \mathbf{Q}_j^h contains the n_l radial or horizontal discharges in zone j at distance r . In the transient-state case, the Laplace transformed heads \mathbf{h}_j and Laplace transformed discharges \mathbf{Q}_j^h need to be inverted to the real time domain. This is done numerically by applying the Stehfest (1970) algorithm.

The principle of superposition may be applied to simulate time-dependent discharge in the multilayer wells or streams, as explained in section 2.4 of Chapter 2. Because of the radial variations in hydraulic parameters, superposition in space is not possible, except if only one zone is considered. The solution for this one-zone problem is derived in the next section.

6.3.3. Solution for homogeneous layers

If only one zone is considered, then vectors $\boldsymbol{\alpha}$ and $\boldsymbol{\beta}$ holding the integration constants can be determined analytically. For notational convenience, subscript $j = 1$ referring to this zone is omitted. In this case, system of matrix equations (49) simplifies to:

$$\begin{cases} \mathbf{R}_c p \mathbf{H} + (\mathbf{EC})^T \mathbf{X}' \boldsymbol{\alpha} + (\mathbf{EC})^T \mathbf{Y}' \boldsymbol{\beta} = \mathbf{Q} + \mathbf{R}_c \boldsymbol{\varphi}_0 + (\mathbf{EC})^T \mathbf{z}' & (r = R_0) \\ \mathbf{CH} - \mathbf{E}^T \mathbf{X} \boldsymbol{\alpha} - \mathbf{E}^T \mathbf{Y} \boldsymbol{\beta} = \mathbf{E}^T \mathbf{z} & (r = R_0) \\ -\mathbf{U}^T \mathbf{X}' \boldsymbol{\alpha} - \mathbf{U}^T \mathbf{Y}' \boldsymbol{\beta} = \mathbf{U}^T \mathbf{z}' & (r = R_0) \\ \mathbf{X} \boldsymbol{\alpha} + \mathbf{Y} \boldsymbol{\beta} = \boldsymbol{\varphi} - \mathbf{z} & (r = R_1) \end{cases} \quad (60)$$

To solve system of equations (60), the method proposed by Hemker (1999a) is used. First, system (60) is rearranged into two separate systems of equations:

$$\begin{cases} \mathbf{R}_c p \mathbf{H} + (\mathbf{EC})^T \mathbf{Q}^h = \mathbf{Q} + \mathbf{R}_c \boldsymbol{\varphi}_0 & (r = R_0) \\ \mathbf{CH} = \mathbf{E}^T \mathbf{h} & (r = R_0) \end{cases} \quad (61)$$

$$\begin{cases} -\mathbf{I}' \boldsymbol{\alpha} - \mathbf{K}' \boldsymbol{\beta} - \mathbf{m}' = \mathbf{V}^{-1} \mathbf{T}^{-1} \mathbf{Q}^h & (r = R_0) \\ \mathbf{I} \boldsymbol{\alpha} + \mathbf{K} \boldsymbol{\beta} + \mathbf{m} = \mathbf{V}^{-1} \boldsymbol{\varphi} & (r = R_1) \end{cases} \quad (62)$$

In the upper system of equations (61), vectors \mathbf{Q}^h and \mathbf{H} are unknown, whereas vectors $\boldsymbol{\alpha}$ and $\boldsymbol{\beta}$ are unknown in the lower system of equations (62). The solution for the lower system (62) has already been derived in Chapter 2. In case of axisymmetric flow, the integration constants are:

$$\boldsymbol{\alpha}_i = \begin{cases} \frac{\mathbf{v}_i R_0^2}{2} - \mathbf{q}_i & (d_i = 0) \\ \frac{(R_0 \sqrt{d_i}) K_1(R_0 \sqrt{d_i})}{(R_0 \sqrt{d_i}) [K_0(R_1 \sqrt{d_i}) I_1(R_0 \sqrt{d_i}) + K_1(R_0 \sqrt{d_i}) I_0(R_1 \sqrt{d_i})]} \left[\mathbf{w}_i - \frac{\mathbf{v}_i}{d_i} \right] - K_0(R_1 \sqrt{d_i}) \mathbf{q}_i & (d_i \neq 0) \end{cases} \quad (63)$$

$$\boldsymbol{\beta}_i = \begin{cases} \frac{\mathbf{v}_i R_1^2}{4} + \mathbf{w}_i - \boldsymbol{\alpha}_i \ln(R_1) & (d_i = 0) \\ \frac{(R_0 \sqrt{d_i}) I_1(R_0 \sqrt{d_i})}{(R_0 \sqrt{d_i}) [K_0(R_1 \sqrt{d_i}) I_1(R_0 \sqrt{d_i}) + K_1(R_0 \sqrt{d_i}) I_0(R_1 \sqrt{d_i})]} \left[\mathbf{w}_i - \frac{\mathbf{v}_i}{d_i} \right] + I_0(R_1 \sqrt{d_i}) \mathbf{q}_i & (d_i \neq 0) \end{cases} \quad (64)$$

with $\mathbf{q} = \mathbf{V}^{-1} \mathbf{T}^{-1} \mathbf{Q}^h(R_0)$ and $\mathbf{w} = \mathbf{V}^{-1} \boldsymbol{\varphi}$. In case of parallel flow, the constants are:

$$\boldsymbol{\alpha}_i = \begin{cases} \mathbf{v}_i R_0 - \mathbf{q}_i & (d_i = 0) \\ \frac{\sqrt{d_i} e^{-(R_0 \sqrt{d_i})}}{\sqrt{d_i} [e^{(R_0 - R_1) \sqrt{d_i}} + e^{(R_1 - R_0) \sqrt{d_i}}]} \left[\mathbf{w}_i - \frac{\mathbf{v}_i}{d_i} \right] - e^{-(R_1 \sqrt{d_i})} \mathbf{q}_i & (d_i \neq 0) \end{cases} \quad (65)$$

$$\boldsymbol{\beta}_i = \begin{cases} \frac{\mathbf{v}_i R_1^2}{2} + \mathbf{w}_i - \boldsymbol{\alpha}_i R_1 & (d_i = 0) \\ \frac{e^{(R_1 \sqrt{d_i})} \mathbf{q}_i + \sqrt{d_i} e^{(R_0 \sqrt{d_i})}}{\sqrt{d_i} [e^{(R_0 - R_1) \sqrt{d_i}} + e^{(R_1 - R_0) \sqrt{d_i}}]} \left[\mathbf{w}_i - \frac{\mathbf{v}_i}{d_i} \right] & (d_i \neq 0) \end{cases} \quad (66)$$

As $\mathbf{Q}^h(R_0)$ is unknown, vector \mathbf{q} is also unknown in this case, and therefore, general solution (17) is rewritten as a function of \mathbf{q} :

$$\mathbf{g}(r) = \mathbf{I}(r) \boldsymbol{\alpha} + \mathbf{K}(r) \boldsymbol{\beta} + \mathbf{m}(r) = \boldsymbol{\zeta}(r) + \mathbf{Z}(r) \mathbf{q} \quad (67)$$

In the axisymmetric case, the i -th element in vector $\boldsymbol{\zeta}$ is defined as:

$$\boldsymbol{\zeta}_i(r) = \begin{cases} \frac{\mathbf{v}_i R_0^2}{2} \ln\left(\frac{r}{R_1}\right) + \frac{\mathbf{v}_i (R_1^2 - r^2)}{4} + \mathbf{w}_i & (d_i = 0) \\ \frac{K_1(R_0 \sqrt{d_i}) I_0(r \sqrt{d_i}) + I_1(R_0 \sqrt{d_i}) K_0(r \sqrt{d_i})}{I_1(R_0 \sqrt{d_i}) K_0(R_1 \sqrt{d_i}) + K_1(R_0 \sqrt{d_i}) I_0(R_1 \sqrt{d_i})} \left(\mathbf{w}_i - \frac{\mathbf{v}_i}{d_i} \right) + \frac{\mathbf{v}_i}{d_i} & (d_i \neq 0) \end{cases} \quad (68)$$

\mathbf{Z} is an $n_l \times n_l$ diagonal matrix with diagonal entries equal to:

$$\mathbf{Z}_{ii}(r) = \begin{cases} \ln\left(\frac{R_1}{r}\right) & (d_i = 0) \\ \frac{I_0(R_1 \sqrt{d_i}) K_0(r \sqrt{d_i}) - K_0(R_1 \sqrt{d_i}) I_0(r \sqrt{d_i})}{R_0 \sqrt{d_i} [I_1(R_0 \sqrt{d_i}) K_0(R_1 \sqrt{d_i}) + K_1(R_0 \sqrt{d_i}) I_0(R_1 \sqrt{d_i})]} & (d_i \neq 0) \end{cases} \quad (69)$$

In the multilayer well case, distance R_0 is always finite. The outer boundary R_1 may be at an infinitely large distance if $d_i \neq 0$, in which case expressions (68) and (69) reduce to, respectively:

$$\boldsymbol{\zeta}_i(r) = \frac{\mathbf{v}_i}{d_i} \quad (70)$$

$$\mathbf{Z}_{ii}(r) = \frac{K_0(r \sqrt{d_i})}{R_0 \sqrt{d_i} K_1(R_0 \sqrt{d_i})} \quad (71)$$

In case of parallel flow, the i -th entry of vector $\boldsymbol{\zeta}$ is:

$$\zeta_i(r) = \begin{cases} \mathbf{v}_i R_0 (r - R_1) + \frac{\mathbf{v}_i (R_1^2 - r^2)}{2} + \mathbf{w}_i & (d_i = 0) \\ \frac{e^{(r-R_0)\sqrt{d_i}} + e^{(R_0-r)\sqrt{d_i}}}{e^{(R_0-R_1)\sqrt{d_i}} + e^{(R_1-R_0)\sqrt{d_i}}} \left(\mathbf{w}_i - \frac{\mathbf{v}_i}{d_i} \right) + \frac{\mathbf{v}_i}{d_i} & (d_i \neq 0) \end{cases} \quad (72)$$

and the nonzero elements of diagonal matrix \mathbf{Z} are:

$$\mathbf{Z}_{ii}(r) = \begin{cases} R_1 - r & (d_i = 0) \\ \frac{e^{(R_1-r)\sqrt{d_i}} - e^{(r-R_1)\sqrt{d_i}}}{\sqrt{d_i} [e^{(R_0-R_1)\sqrt{d_i}} + e^{(R_1-R_0)\sqrt{d_i}}]} & (d_i \neq 0) \end{cases} \quad (73)$$

In the parallel case, the outer model boundary may also be at an infinitely large distance if $d_i \neq 0$. If $R_1 \rightarrow \infty$, then (72) and (73) simplify to, respectively:

$$\zeta_i(r) = \frac{\mathbf{v}_i}{d_i} \quad (74)$$

$$\mathbf{Z}_{ii}(r) = \frac{e^{-(r\sqrt{d_i})}}{\sqrt{d_i} e^{-(R_0\sqrt{d_i})}} \quad (75)$$

Introducing (67) into condition (36), using $\mathbf{h} = \mathbf{Vg}$ and $\mathbf{q} = \mathbf{V}^{-1}\mathbf{T}^{-1}\mathbf{Q}^h(R_0)$, gives:

$$\mathbf{CH} = \mathbf{E}^T \mathbf{V} \zeta(R_0) + \mathbf{E}^T \mathbf{VZ}(R_0) \mathbf{V}^{-1} \mathbf{T}^{-1} \mathbf{Q}^h(R_0) \quad (76)$$

from which it follows that:

$$\mathbf{Q}^h(R_0) = \mathbf{E} \boldsymbol{\Psi}^{-1} [\mathbf{CH} - \mathbf{E}^T \mathbf{V} \zeta(R_0)] \quad (77)$$

with $\boldsymbol{\Psi} = (\mathbf{E}^T \mathbf{VZ}(R_0) \mathbf{V}^{-1} \mathbf{T}^{-1} \mathbf{E})$, and where $\mathbf{Q}^h(R_0)$ in (76) is replaced by $\mathbf{E} \mathbf{E}^T \mathbf{Q}^h(R_0)$ so that only the nonzero discharges for the screened layers are selected in $\mathbf{Q}^h(R_0)$, as the discharges for the unscreened layers are zero. Introducing expression (77) into (37) gives:

$$\mathbf{Q} = \mathbf{R}_c(p\mathbf{H} - \boldsymbol{\varphi}_0) - \mathbf{C}^T \boldsymbol{\Psi}^{-1} [\mathbf{CH} - \mathbf{E}^T \mathbf{V} \zeta(R_0)] \quad (78)$$

Recall that $\mathbf{E}^T \mathbf{E}$ equals the identity matrix. From (78), the solution for \mathbf{H} is found:

$$\mathbf{H} = \boldsymbol{\Theta}^{-1} [\mathbf{Q} + \mathbf{R}_c \boldsymbol{\varphi}_0 - \mathbf{C}^T \boldsymbol{\Psi}^{-1} \mathbf{E}^T \mathbf{V} \zeta(R_0)] \quad (79)$$

with $\boldsymbol{\Theta} = (p\mathbf{R}_c - \mathbf{C}^T \boldsymbol{\Psi}^{-1} \mathbf{C})$. Solution (79) is introduced into (77):

$$\mathbf{Q}^h(R_0) = \mathbf{E} \boldsymbol{\Psi}^{-1} \{ \mathbf{C} \boldsymbol{\Theta}^{-1} [\mathbf{Q} + \mathbf{R}_c \boldsymbol{\varphi}_0 - \mathbf{C}^T \boldsymbol{\Psi}^{-1} \mathbf{E}^T \mathbf{V} \zeta(R_0)] - \mathbf{E}^T \mathbf{V} \zeta(R_0) \} \quad (80)$$

Equation (80) is introduced into (67) to finally obtain the solution for multilayer well-flow:

$$\mathbf{h}(r) = \mathbf{V} \zeta(r) + \mathbf{VZ}(r) \mathbf{V}^{-1} \mathbf{T}^{-1} \mathbf{E} \boldsymbol{\Psi}^{-1} \{ \mathbf{C} \boldsymbol{\Theta}^{-1} [\mathbf{Q} + \mathbf{R}_c \boldsymbol{\varphi}_0 - \mathbf{C}^T \boldsymbol{\Psi}^{-1} \mathbf{E}^T \mathbf{V} \zeta(R_0)] - \mathbf{E}^T \mathbf{V} \zeta(R_0) \} \quad (81)$$

where use is made of $\mathbf{h} = \mathbf{Vg}$ and $\mathbf{q} = \mathbf{V}^{-1}\mathbf{T}^{-1}\mathbf{Q}^h(R_0)$. Recall that $\mathbf{R}_c = \mathbf{0}$ in (81) if flow is steady, and that (81) must be inverted numerically in case of transient flow.

The horizontal discharge vector \mathbf{Q}^h is found by evaluating the following expression:

$$\mathbf{Q}^h(r) = -\mathbf{T} \nabla \mathbf{h} = \mathbf{TV} [\zeta'(r) + \mathbf{Z}'(r) \mathbf{q}] \quad (82)$$

In case of axisymmetric flow, the i -th element in vector ζ' is defined as:

$$\zeta'_i(r) = \begin{cases} \frac{\mathbf{v}_i(r^2 - R_0^2)}{2} & (d_i = 0) \\ \frac{r\sqrt{d_i}[\text{I}_1(R_0\sqrt{d_i})\text{K}_1(r\sqrt{d_i}) - \text{K}_1(R_0\sqrt{d_i})\text{I}_1(r\sqrt{d_i})]}{\text{I}_1(R_0\sqrt{d_i})\text{K}_0(R_1\sqrt{d_i}) + \text{K}_1(R_0\sqrt{d_i})\text{I}_0(R_1\sqrt{d_i})} \left(\mathbf{w}_i - \frac{\mathbf{v}_i}{d_i}\right) & (d_i \neq 0) \end{cases} \quad (83)$$

Matrix \mathbf{Z}' is an $n_l \times n_l$ diagonal matrix with diagonal entries equal to:

$$\mathbf{Z}'_{ii}(r) = \begin{cases} 1 & (d_i = 0) \\ \frac{r\sqrt{d_i}[\text{I}_0(R_1\sqrt{d_i})\text{K}_1(r\sqrt{d_i}) + \text{K}_0(R_1\sqrt{d_i})\text{I}_1(r\sqrt{d_i})]}{R_0\sqrt{d_i}[\text{I}_1(R_0\sqrt{d_i})\text{K}_0(R_1\sqrt{d_i}) + \text{K}_1(R_0\sqrt{d_i})\text{I}_0(R_1\sqrt{d_i})]} & (d_i \neq 0) \end{cases} \quad (84)$$

Recall that the outer boundary R_1 may be at an infinitely large distance if $d_i \neq 0$, in which case expressions (83) and (84) reduce to, respectively:

$$\zeta'_i(r) = 0 \quad (85)$$

$$\mathbf{Z}'_{ii}(r) = \frac{r\sqrt{d_i}\text{K}_1(r\sqrt{d_i})}{R_0\sqrt{d_i}\text{K}_1(R_0\sqrt{d_i})} \quad (86)$$

When parallel flow is simulated, the i -th entry of vector ζ' is:

$$\zeta'_i(r) = \begin{cases} \mathbf{v}_i(r - R_0) & (d_i = 0) \\ \frac{\sqrt{d_i}[e^{(R_0-r)\sqrt{d_i}} - e^{(r-R_0)\sqrt{d_i}}]}{e^{(R_0-R_1)\sqrt{d_i}} + e^{(R_1-R_0)\sqrt{d_i}}} \left(\mathbf{w}_i - \frac{\mathbf{v}_i}{d_i}\right) & (d_i \neq 0) \end{cases} \quad (87)$$

and the nonzero entries of \mathbf{Z}'_{ii} are:

$$\mathbf{Z}'_{ii}(r) = \begin{cases} 1 & (d_i = 0) \\ \frac{e^{(R_1-r)\sqrt{d_i}} + e^{(r-R_1)\sqrt{d_i}}}{e^{(R_0-R_1)\sqrt{d_i}} + e^{(R_1-R_0)\sqrt{d_i}}} & (d_i \neq 0) \end{cases} \quad (88)$$

If $d_i \neq 0$ and $R_1 \rightarrow \infty$, then expressions (87) and (88) simplify to, respectively:

$$\zeta'_i(r) = 0 \quad (89)$$

$$\mathbf{Z}'_{ii}(r) = \frac{e^{-(r\sqrt{d_i})}}{e^{-(R_0\sqrt{d_i})}} \quad (90)$$

6.3.4. Zero-thickness skin

The solution developed by Hemker (1999a) also includes the effect of an infinitesimally thin well skin, which is defined using the dimensionless skin factor F :

$$F_{i_w} = \frac{T_{i_w}}{T_{skin}} \ln \frac{R_{skin}}{R_0} \quad (91)$$

with T_{skin} the transmissivity [L^2/T] of the skin with outer radius R_{skin} [L]. Recall that i_w represents the indices of the layers in which well w has a screen. The dimensionless skin factor is discussed exhaustively in Chapter 5. In case of a zero-thickness skin, condition (9) needs to be extended:

$$H_w(t) = h_{i_w}(R_0, t) + \frac{Q_{i_w}^h(R_0, t)F_{i_w}}{2\pi T_{i_w}} \quad (w = 1, 2, \dots, n_w) \quad (92)$$

In case of steady flow, head H_w and radial discharge Q^h are not dependent of time:

$$H_w = h_{i_w}(R_0) + \frac{Q_{i_w}^h(R_0)F_{i_w}}{2\pi T_{i_w}} \quad (w = 1, 2, \dots, n_w) \quad (93)$$

In the transient case, the Laplace transform of (92) is required:

$$\bar{H}_w = \bar{h}_{i_w}(R_0) + \frac{\bar{Q}_{i_w}^h(R_0)F_{i_w}}{2\pi T_{i_w}} \quad (w = 1, 2, \dots, n_w) \quad (94)$$

Conditions (93) and (94) are expressed in matrix form as follows:

$$\mathbf{CH} = \mathbf{E}^T [\mathbf{h}(R_0) + \mathbf{FT}^{-1} \mathbf{Q}^h(R_0)] \quad (95)$$

with \mathbf{F} an $n_l \times n_l$ diagonal matrix with nonzero entry F_{ii} equal to the skin factor F_i for layer i . If there is no skin defined for layer i , then F_i is set to zero.

Substituting $[\mathbf{V}\zeta(R_0) + \mathbf{VZ}(R_0)\mathbf{V}^{-1}\mathbf{T}^{-1}\mathbf{Q}^h(R_0)]$ for $\mathbf{h}(R_0)$ according to (67) in expression (95) gives:

$$\mathbf{CH} = \mathbf{E}^T \mathbf{V}\zeta(R_0) + \mathbf{E}^T [\mathbf{VZ}(R_0)\mathbf{V}^{-1} + \mathbf{F}] \mathbf{T}^{-1} \mathbf{Q}^h(R_0) \quad (96)$$

Comparing expression (96) to the corresponding expression (76) for \mathbf{CH} without skin, it is seen that $\Psi = \mathbf{E}^T [\mathbf{VZ}(R_0)\mathbf{V}^{-1} + \mathbf{F}] \mathbf{T}^{-1} \mathbf{E}$ in the well-skin case. This means that equations (79), (80), and (81) to calculate \mathbf{H} , $\mathbf{Q}^h(R_0)$, and $\mathbf{h}(r)$, respectively, are still valid in case of zero-thickness well-skins, provided that the extended expression for Ψ is used.

Note that in the well-skin case, head $\mathbf{h}(R_0)$ at the well-face is not equal to head \mathbf{H} in the well. The reason why there are two heads at distance R_0 , is because the skin is conceptualized as an interface between well and aquifer with thickness equal to zero. Hence, inner and outer radius of the skin coincide at distance R_0 . If the inner radius is denoted by R_0^- , then head \mathbf{H} in the well equals $\mathbf{h}(R_0^-)$, whereas $\mathbf{h}(R_0)$ is the head at the outer radius R_0^+ , which equals the head in the well without head loss.

6.4. Finite-difference solution

The problem stated in section 6.2 can also be solved by applying the finite-difference approach outlined in Chapter 3. Only two modifications are required to include wellbore storage and to connect grid cells that correspond to the screen of a multilayer well.

6.4.1. Wellbore storage

As discussed in section 3.3.1, a model grid is defined consisting of layers and columns, where the latter are determined by distances $r_{b,j}$ [L]. Louwyck et al. (2012, 2014) propose to assign a small width δ [L] to the first column representing the well by setting distance $r_{b,1}$ of the inner grid boundary to $R_0 - \delta$. Distance $r_{b,2}$ is set to R_0 ; hence, the outer boundary of the first column coincides with the well-face. The wellbore storage is taken into account by setting the storativity of the inner cells corresponding to a well accordingly:

$$S_{i_w,1} = \pi r_{c,w}^2 \quad (w = 1, 2, \dots, n_w) \quad (97)$$

Recall that i_w are the indices of the layers open to well w , and that n_w is the number of wells.

If parallel flow is simulated, then the storage change in the stream is considered, and equation (97) is replaced by:

$$S_{i_w,1} = r_{c,w} \quad (w = 1, 2, \dots, n_w) \quad (98)$$

6.4.2. Connected cells

Simulating flow to multilayer wells or streams applying the finite-difference approach is realized by connecting the cells in the model grid that define the multilayer well or stream. Implementing connected grid cells is straightforward as it only requires a simple update of the finite-difference matrix system.

As discussed in Chapter 3, the finite-difference approach comes down to solving a system of $n_l \times n_r$ equations for each time step k , with n_r the number of columns that are defined in the model grid, and n_l the number of layers:

$$\mathbf{A}_k \mathbf{h}_k = \mathbf{b}_k \quad (99)$$

Each row in matrix system (99) corresponds to the water budget equation of one cell ij in the grid, where i refers to the layer index, and j to the column index:

$$Q_{i,j+1,k}^h - Q_{ijk}^h + Q_{i+1,j,k}^v - Q_{ijk}^v + Q_{i,j,k-1}^s + Q_{ijk} + Q_{ijk}^c = 0 \quad (2 \leq k \leq n_t) \quad (100)$$

Q_{ijk}^h is the horizontal or radial discharge [L^3/T] between cells $i, j - 1$ and ij at time k :

$$Q_{ijk}^h = Q_{ij}^{hc}(h_{ijk} - h_{i,j-1,k}) \quad (101)$$

with Q_{ij}^{hc} the horizontal or radial conductance [L^2/T] between cells $i, j - 1$ and ij . Q_{ijk}^v is the vertical discharge [L^3/T] between cells $i - 1, j$ and ij at time k :

$$Q_{ijk}^v = Q_{ij}^{vc}(h_{ijk} - h_{i-1,j,k}) \quad (102)$$

with Q_{ij}^{vc} the vertical conductance [L^2/T] between cells $i - 1, j$ and ij . Q_{ijk}^s is the storage change [L^3/T] in cell ij between times k and $k + 1$:

$$Q_{ijk}^s = Q_{ijk}^{sc}(h_{i,j,k+1} - h_{ijk}) \quad (103)$$

with Q_{ijk}^{sc} the constant storage change term [L^2/T] for cell ij and time step k . Q_{ijk} is the known recharge [L^3/T] in cell ij during time step k , whereas Q_{ijk}^c is the recharge [L^3/T] in cell ij during time step k induced by a head-dependent flux boundary condition with constant head φ_{ijk} [L] and conductance Q_{ij}^{cc} [L^2/T]:

$$Q_{ijk}^c = Q_{ij}^{cc}(h_{ijk} - \varphi_{ijk}) \quad (104)$$

Definitions of Q_{ij}^{hc} , Q_{ij}^{vc} , Q_{ijk}^{sc} , and Q_{ij}^{cc} depend on the type of flow and are given in sections 3.3.2 and 3.3.3 of Chapter 3.

If cell ij is connected to cell uv , the hydraulic head in both cells is the same for all time steps k :

$$h_{ijk} = h_{uvk} \quad (1 \leq k \leq n_t) \quad (105)$$

As the two cells are connected, the total inflow to both cells must equal their total outflow. This implies that the water budget equation for both cells must be taken together:

$$\begin{aligned} & Q_{i,j+1,k}^h + Q_{u,v+1,k}^h - Q_{ijk}^h - Q_{uvk}^h + Q_{i+1,j,k}^v + Q_{u+1,v,k}^v - Q_{ijk}^v - Q_{uvk}^v \\ & + Q_{i,j,k-1}^s + Q_{u,v,k-1}^s + Q_{ijk} + Q_{uvk} + Q_{ijk}^c + Q_{uvk}^c = 0 \quad (2 \leq k \leq n_t) \end{aligned} \quad (106)$$

Rearranging (106) using (105) and applying the definitions of the discharge terms (101), (102), (103), and (104), gives:

$$\begin{aligned}
& Q_{i,j+1}^{hc} h_{i,j+1,k} + Q_{u,v+1}^{hc} h_{u,v+1,k} + Q_{ij}^{hc} h_{i,j-1,k} + Q_{uv}^{hc} h_{u,v-1,k} - (Q_{i,j+1}^{hc} + Q_{u,v+1}^{hc} + Q_{ij}^{hc} + Q_{uv}^{hc}) h_{ijk} \\
& + Q_{i+1,j}^{vc} h_{i+1,j,k} + Q_{u+1,v}^{vc} h_{u+1,v,k} + Q_{ij}^c h_{i-1,j,k} + Q_{uv}^{vc} h_{u-1,v,k} \\
& - (Q_{i+1,j}^{vc} + Q_{u+1,v}^{vc} + Q_{ij}^{vc} + Q_{uv}^{vc}) h_{ijk} \\
& + (Q_{i,j,k-1}^{sc} + Q_{u,v,k-1}^{sc}) h_{ijk} + (Q_{ij}^{cc} + Q_{uv}^{cc}) h_{ijk} \\
& = (Q_{i,j,k-1}^{sc} + Q_{u,v,k-1}^{sc}) h_{i,j,k-1} + (Q_{ijk} + Q_{uvk}) + (Q_{ij}^{cc} \varphi_{ijk} + Q_{uv}^{cc} \varphi_{uvk}) \quad (2 \leq k \leq n_t)
\end{aligned} \tag{107}$$

If two neighboring cells are connected, then there is no flow between those cells. Consider two adjacent cells j and $j + 1$ in the same layer i , then horizontal or radial flow $Q_{i,j+1,k}^h$ is canceled out from equation (106) indeed, as $Q_{i,j+1,k}^h = Q_{uvk}$. In the same way, $Q_{i+1,j,k}^v$ is canceled out if cells i and $i + 1$ in column j are connected, as $Q_{i+1,j,k}^v = Q_{uvk}$ in this case. Although connected cells are mostly neighboring cells, this is not a requirement. A typical example of two cells that are connected but not adjacent to each other are cells that conceptualize a well having a screen in each of two aquifers separated by an aquitard in which there is no well-screen.

As the water budget equations are written in matrix form, equation (107) must be translated into operations performed on matrix \mathbf{A}_k and on vectors \mathbf{b}_k and \mathbf{h}_k . Suppose the linear index for cell ij is $l = (i - 1)n_r + j$, and the linear index for cell uv is $w = (u - 1)n_r + v$. To take into account equation (107), matrix system (99) needs to be updated as follows:

1. Add row w in matrix \mathbf{A}_k to row l : $\mathbf{A}_{klj} \leftarrow \mathbf{A}_{klj} + \mathbf{A}_{kwj}$ for $j = 1, 2, 3, \dots, n_l \cdot n_r$.
2. Add column w in matrix \mathbf{A}_k to column l : $\mathbf{A}_{kjl} \leftarrow \mathbf{A}_{kjl} + \mathbf{A}_{kjw}$ for $j = 1, 2, 3, \dots, n_l \cdot n_r$.
3. Add element w in vector \mathbf{b}_k to element l : $\mathbf{b}_{kl} \leftarrow \mathbf{b}_{kl} + \mathbf{b}_{kw}$.
4. Remove row w from matrix \mathbf{A}_k .
5. Remove column w from matrix \mathbf{A}_k .
6. Remove element w from vector \mathbf{b}_k
7. Remove element w from vector \mathbf{h}_k .

The step numbering is indicative. The only requirement is that the adding steps are performed before the removing steps.

Recall that matrix system (99) only applies to cells with a variable head; hence, rows in \mathbf{A}_k and elements in \mathbf{b}_k that correspond to inactive or constant-head cells are removed. As explained in Chapter 3, the terms that contain a constant head must be added to vector \mathbf{b}_k before deleting those rows, columns, and elements.

The above algorithm that is executed to modify matrix system (99) results into an updated matrix \mathbf{A}_k that is not pentadiagonal anymore. As a consequence, algorithms such as SIP or ADI are not applicable to solve the system, but standard LU-decomposition is. In this chapter, the standard solver implemented in SciPy (Peterson et al., 2022) is used.

The modified finite-difference approach presented in this section is verified in section 6.5. The discretization of distance r and time t is generally discussed in section 3.3.1 of Chapter 3. Here, the same ‘logspace’ scheme is applied as in previous Chapter 5, which is explained in section 5.4.

6.4.3. MODFLOW procedure

It is also possible to use MODFLOW-2005 (Harbaugh, 2005) to simulate flow to a multilayer well by applying the procedure presented by Louwyck et al. (2012, 2014). This procedure is similar to the one developed by Langevin (2008), but it is more effective in defining radial inhomogeneities, as it allows for defining multiple cylindrical zones around the well characterized by different hydraulic properties

and boundary conditions such as recharge. In fact, it results in the same finite-difference formulation as presented in Chapter 3 (Louwyck et al., 2012).

Louwyck et al. (2012) apply the high-K_v approach (Neville & Tonkin, 2004) to connect the cells that belong to a multilayer well. By defining a very high vertical conductivity inside the cells of a multilayer well, the heads in these cells are virtually the same indeed. In practice, however, the resulting high conductances make convergence more difficult or even impossible. On the other hand, this approach has the advantage that wellbore storage can be taken into account, as is illustrated by Louwyck et al. (2012), who simulate a slug test in a partially penetrating well using this approach.

If wellbore storage may be ignored, then using the revised Multi-Node Well package MNW2 (Konikow et al., 2009) is a more effective way to define a multilayer well. In this case, equation (10) expressing the wellbore balance reduces to:

$$Q_w = \sum_{i_w} Q_{i_w}^h(R_0, t) \quad (w = 1, 2, \dots, n_w) \quad (108)$$

with i_w the indices of the layers connected to well w , and where index 1 referring to the first zone is omitted. Equation (108) corresponds to equation 1 in the MNW2 package manual (Konikow et al., 2009). In the finite-difference formulation discussed in this section, the radial discharge $Q_{i_w}^h$ is defined as:

$$Q_{i_w,2}^h = Q_{i_w,2}^{hc}(h_{i_w,2} - h_{i_w,1}) = 2\pi T_{i_w} \frac{h_{i_w,2} - h_{i_w,1}}{\ln(r_2/r_1)} \quad (109)$$

where $h_{i_w,j}$ is the head in layer i_w at distance r_j [L]. If $j = 1$, then the head in the well is simulated:

$$Q_{i_w,2}^h = 2\pi T_{i_w} \frac{h_{i_w,2} - H_w}{\ln(r_2/r_1)} \quad (110)$$

Recall that distance r_j is at the center of column j . Substituting (110) into (108) gives:

$$Q_w = \sum_{i_w} \frac{2\pi T_{i_w}}{\ln(r_2/r_1)} h_{i_w,2} - \sum_{i_w} \frac{2\pi T_{i_w}}{\ln(r_2/r_1)} H_w \quad (w = 1, 2, \dots, n_w) \quad (111)$$

Equation (111) corresponds to equation 17 in the MNW2 package manual, with $Q_{net} = -Q_w$; $n = i_w$; $h_n = h_{i_w,2}$; $h_{WELL} = H_w$; and cell-to-well conductance CWC [L²/T]:

$$CWC_n = Q_{i_w,2}^{hc} = \frac{2\pi T_{i_w}}{\ln(r_2/r_1)} \quad (112)$$

The MNW2 package can also be used to simulate parallel flow to a stream that is connected to more than one grid layer. In this case, the cell-to-well conductance is defined as:

$$CWC_n = Q_{i_w,2}^{hc} = \frac{T_{i_w}}{r_2 - r_1} \quad (113)$$

Recall that when simulating parallel flow, a vertical profile model is constructed using a grid consisting of one row of unit width. The input parameters are not modified as the grid represents correct distances in this case.

Figure 2 shows the similarity between the finite-difference method presented in this chapter and the MODFLOW-MNW2 approach. In the first approach, the multilayer well is implemented by connecting the cells in the first column. As a consequence, these cells are part of the finite-difference grid. If

MODFLOW is used, however, then the multilayer well is a boundary condition defined for the cells in the second column. This means the first column is omitted in the MODFLOW grid and the radial conductances $Q_{i_w,2}^{hc}$ are the cell-to-well conductances CWC_n in the MNW2 input file according to equation (112).

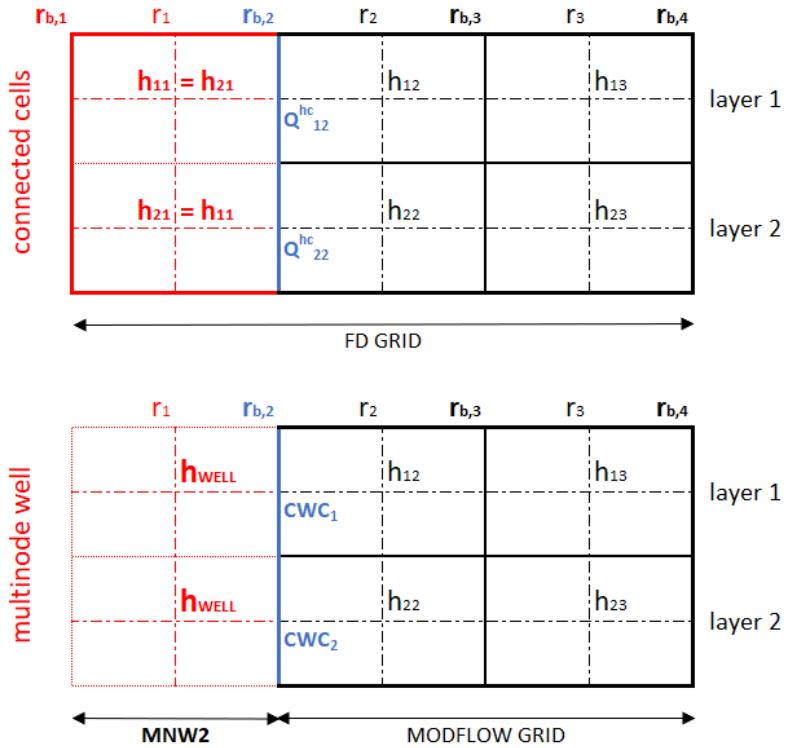


Figure 2. Defining the model grid for a multilayer well interacting with the first two model layers. The upper model grid is used in the finite-difference approach that uses connected cells for the multilayer well, the lower grid is used in the MODFLOW procedure that applies the revised Multi-Node Well (MNW2) package. The grid nodes are at radial distances r , the vertical cell boundaries are at distances r_b , and the heads at the nodes are denoted by h . The radial conductances Q^{hc} between the cells representing the multilayer well and the aquifer in the first approach are equal to the cell-to-well conductances CWC of the multi-node well in the MODFLOW-MNW2 approach. See text for a more detailed explanation.

To define multilayer wells using the MNW2 package, the procedure outlined in section 3.4.2 of Chapter 3 to use MODFLOW-2005 for the simulation of axisymmetric flow must be extended by the following steps.

1. The multilayer wells are defined in the MNW2-file:
 - a. The maximum number of multi-node wells MNWMAX is set to the number of wells n_w ; the maximum number of nodes NODTOT is not required.
 - b. For each well w , the WELLID may be set to index w . The number of nodes NNODES is equal to the number of layers connected to well w . The LOSSTYPE is set to SPECIFYCWC. Variables PUMPLOC, QLIMIT, PPFLAG, and PUMPCAP are set to zero as they are not relevant. Variable CWC is set to -1 as each layer has a different radial conductance.
 - c. For each node i_w of well w , variable LAY is set to i_w , and variables ROW and COL are set to 1 as the grid contains one row only and the multi-node well is added to the first column. The cell-to-well conductance CWC is set to radial conductance $Q_{i_w,2}^{hc}$ according to equation (112).
 - d. For each stress period, ITMP is equal to the number of wells n_w , and for each multi-node well w , its WELLID is given and its pumping rate Q_w is assigned to variable QDES.

2. The MNWI package is used to record the heads simulated for the multi-node wells:
 - a. Flags WEL1FLAG, QSUMFLAG, and BYND are set to 0, and variable MNWOBS is equal to the number of wells n_w .
 - b. For each multi-node well w , the WELLID is given, and the UNIT number of the file to which the output data are written. This DATA-file is added to the NAME-file, and it contains the calculated heads $h_{WELL} = H_w$ at each simulation time for each well w . If the radial flow $Q_{l_w,2}^h$ between multi-node well w and the layers i_w is required, then QNDFLAG must be set to 1 for this well; otherwise it is set to 0.

The MNW2 package assumes there is hydrostatic equilibrium within the pumping well, which means there are no head gradients within the borehole (Konikow et al., 2009).

It is possible that nodes in the multi-node well go dry if the water level in the borehole is lower than the bottom of the model layer to which the node belongs, even if the layer is confined and cannot go dry. As a consequence, the thickness of confined layers should be set to a sufficiently large value, and hydraulic parameters should be modified accordingly so that transmissivities, resistances, and storativities do not change. Alternatively, one may increase the initial and constant heads.

In MODFLOW 6 (Langevin et al., 2017), the MNW2 package is replaced by the Multi-Aquifer Well (MAW) package, which still allows the user to specify the cell-to-well conductance. Moreover, the wellbore storage can be taken into account, in which case the radius of the casing of the multilayer well is required. In MODFLOW 6, the multi-aquifer well flow terms are incorporated into the groundwater flow equation (Langevin et al., 2017), which means the heads in those wells are derived simultaneously with the heads at the nodes of the model grid, whereas the MNW2 package applies an iterative process in which the heads at the grid nodes and the water levels in the multi-node wells are calculated alternately (Konikow et al., 2009). Using MODFLOW6, multilayer wells can also be defined as part of an unstructured model grid in which the cells belonging to a multilayer well are connected in a similar way as the method described in section 6.4.2.

In the next section 6.5, the procedure using MODFLOW-2005 (Harbaugh, 2005) and the MNW2 package (Konikow et al., 2009) is verified against analytical solutions and compared with the semi-analytical and finite-difference methods presented in this chapter.

6.5. Verification

Several test cases are considered to verify the semi-analytical solution derived in section 6.3 and the finite-difference approach outlined in section 6.4. The two methods are compared with each other, and additionally, they are verified against analytical solutions presented in the hydrogeological literature. The MODFLOW procedure presented in section 6.4.3 is tested in the first two cases. All solutions are coded with Python. This includes the semi-analytical and the finite-difference method developed in this chapter as well as the existing analytical solutions from the literature.

The first test case is the steady state solution for a fully penetrating well in a system of multiple confined aquifers. Sokol (1963) gives the formula to calculate the steady water level in the multi-aquifer well in case the well is not extracted, Neville and Tonkin (2004) generalize to the case of a pumping well. Here, the solution for any distance from the well is presented for both steady radial and parallel flow. The transient state model is discussed in the second test case. The solution for two confined aquifers is given by Papadopoulos (1966), whereas Wikramaratna (1984) generalizes to multiple confined aquifers. The exact solution in the Laplace domain is presented; the inversion is done numerically by applying the Stehfest (1970) algorithm.

The third case verifies the semi-analytical and finite-difference solution against the UWD solution developed by Hemker (1999a), whereas the fourth case compares the UWD solution with the UWG solution for a partially penetrating pumping well in a confined aquifer developed by Mishra et al. (2012). The fifth case discusses the KGS model to simulate slug tests in partially penetrating wells (Hyder et al., 1994). The final case presents a model of a partially penetrating multilayer well with well-skin and gravel pack, which extracts groundwater from a phreatic multi-aquifer system subject to areal infiltration and drainage.

6.5.1. Steady flow to a multi-aquifer well

In the first test case, steady flow is considered to a single well or stream that penetrates multiple aquifers separated by impervious aquiclude. This reduces the system of differential equations (1) to:

$$\nabla^2 h_i = 0 \quad (1 \leq i \leq n_l) \quad (114)$$

As there is one zone only, the subscript referring to this single zone is omitted. The outer boundary condition (6) at distance R_1 reduces to:

$$h_i(R_1) = \varphi_i \quad (1 \leq i \leq n_l) \quad (115)$$

The inner boundary conditions (9) and the wellbore balance equation (10) reduce to:

$$H = h_i(R_0) \quad (1 \leq i \leq n_l) \quad (116)$$

$$Q = \sum_{i=1}^{n_l} Q_i^h(R_0) \quad (117)$$

It is straightforward to solve this system of ordinary differential equations and associated boundary conditions to obtain the steady water level in the well or stream. In case of axisymmetric flow, the solution for H is (Neville & Tonkin, 2004):

$$H = \frac{\frac{Q}{2\pi} \ln\left(\frac{R_1}{R_0}\right) + \sum_i T_i \varphi_i}{\sum_i T_i} \quad (118)$$

In case of parallel, the solution is:

$$H = \frac{Q(R_1 - R_0) + \sum_i T_i \varphi_i}{\sum_i T_i} \quad (119)$$

To go from the parallel to the radial flow solution, distances must be replaced by their logarithms, and Q must be divided by 2π . Taking a closer look at both solutions, it is seen that the first term equals the head in the comprehensive system with transmissivity equal to the sum of the transmissivities of the individual layers, and that the second term redistributes the head according to the relative transmissivities. The first term corresponds to the comprehensive potential (Bakker & Strack, 2003; Strack, 1989), and in case of radial flow, it is calculated using the well-known Thiem (1870, 1906) formula. If there is no pumping, i.e. $Q = 0$, then only the second term remains:

$$H = \frac{\sum_i T_i \varphi_i}{\sum_i T_i} \quad (120)$$

Expression (120) is valid for both radial and parallel flow, and is given by Sokol (1963).

Once the head in the well or stream is known, the head at any distance r can be calculated. In case of axisymmetric flow, the head h_i in the i -th aquifer is:

$$h_i(r) = \varphi_i + \frac{H - \varphi_i}{\ln\left(\frac{R_0}{R_1}\right)} \ln\left(\frac{r}{R_1}\right) \quad (1 \leq i \leq n_l) \quad (121)$$

In case of parallel flow:

$$h_i(r) = \varphi_i + \frac{H - \varphi_i}{R_0 - R_1} (r - R_1) \quad (1 \leq i \leq n_l) \quad (122)$$

It is seen again that the distances are replaced by their logarithms if radial flow is considered instead of parallel flow.

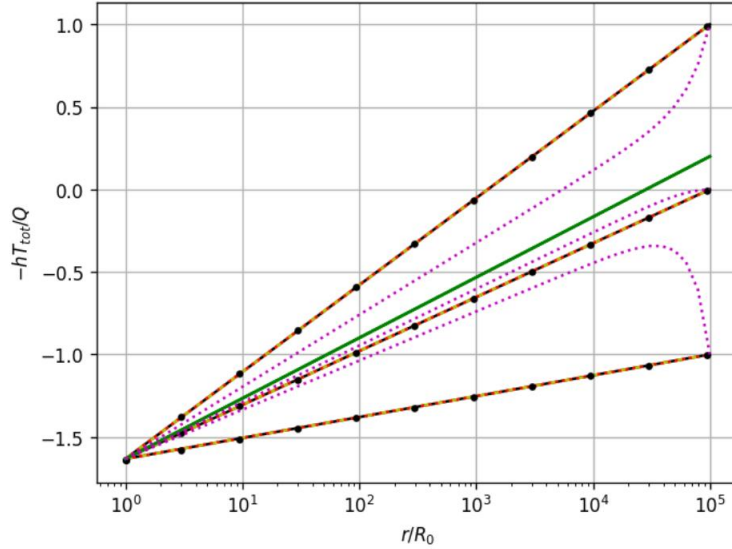


Figure 3. Dimensionless head versus dimensionless distance for the steady flow model of a multi-aquifer well with radius R_0 . The aquifer system consists of three aquifers with relative transmissivities equal to 0.1, 0.6, and 0.3, respectively. The outer boundary of the system is at a relative distance of 10^5 . At this boundary, constant heads are defined in each aquifer, with dimensionless values equal to -1, 0, and 1, respectively. The black solid lines give the analytical solution, the yellow dashed lines the generalized semi-analytical solution, the red dotted lines the finite-difference solution for the case in which the aquifers are separated by infinitely large resistance layers, and the black dots the MODFLOW-MN2 solution. The green solid line is the analytical solution for the case of infinitesimal resistances. The magenta dotted lines show the solution for dimensionless resistances equal to 10^{10} . T_{tot} equals the sum of the transmissivities of the three aquifers. See text for a more detailed explanation.

Figure 3 shows the solution for a three-aquifer system characterized by the dimensionless input parameters given in Table 3. The dimensionless constant head is defined for the outer model boundary at relative distance $R_1/R_0 = 10^5$. Dimensionless head $-h_i \sum_i T_i/Q$ is plotted as a function of dimensionless distance r/R_0 due to steady pumping (i.e. $Q < 0$) of a multi-aquifer well with radius R_0 that is fully connected to the three aquifers.

Table 3. Dimensionless parameters for three aquifers open to a multi-aquifer well. The steady-state model simulating radial flow to this well is discussed in the text.

Aquifer	Dimensionless transmissivity $T_i / \sum_i T_i$	Dimensionless constant head $-\varphi_i \sum_i T_i/Q$
$i = 1$	0.1	-1.0
$i = 2$	0.6	0.0
$i = 3$	0.3	1.0

In Figure 3, the analytical solution expressed by equation (118) is represented by the black solid lines, the semi-analytical solution discussed in section 6.3 by the yellow dashed lines, the finite-difference solution by the red dotted lines, and the MODFLOW-MNW2 solution by the black dots. The four solutions are virtually the same. The green solid line shows the analytical solution for the corresponding system with infinitesimal resistance between the aquifers. In this case, the head in all aquifers is the same and equal to:

$$h_i(r) = H + \frac{Q}{2\pi \sum_i T_i} \ln\left(\frac{R_0}{r}\right) \quad (1 \leq i \leq n_l) \quad (123)$$

where H is given by equation (118). Equation (123) is the Thiem (1870, 1906) formula for the comprehensive system with total transmissivity $\sum_i T_i$, known pumping rate Q , and known head H at distance R_0 . The magenta dotted lines in the plot of Figure 3 correspond to the semi-analytical solution for the same system with dimensionless resistance between the layers $c \sum_i T_i / R_0^2 = 10^{10}$. It is seen the resistance between the aquifers has no effect on the head H in the well.

6.5.2. Transient flow to a multi-aquifer well

If the transient-state case of previous model discussed in section 6.5.1 is considered, then the system of equations (1) reduces to:

$$\nabla^2 h_i = \frac{S_i}{T_i} \frac{\partial h_i}{\partial t} \quad (1 \leq i \leq n_l) \quad (124)$$

Recall that there is no vertical flow between the aquifers as they are separated by aquiclude. The associated boundary conditions are the same as for the steady-state case, except that heads h_i and H are time-dependent now, and that the storage change inside the wellbore is taken into account in the wellbore balance:

$$h_i(R_1, t) = \varphi_i \quad (1 \leq i \leq n_l) \quad (125)$$

$$H(t) = h_i(R_0, t) \quad (1 \leq i \leq n_l) \quad (126)$$

$$Q = \pi r_c^2 \frac{\partial H}{\partial t} + \sum_{i=1}^{n_l} Q_i^h(R_0, t) \quad (127)$$

Recall that r_c is the radius of the well-casing.

Additionally, an initial condition at $t = 0$ is required for both aquifer and well, respectively:

$$h_i(r, 0) = \varphi_i \quad (1 \leq i \leq n_l) \quad (128)$$

$$H(0) = \varphi_0 \quad (1 \leq i \leq n_l) \quad (129)$$

It is straightforward to find the exact solution in the Laplace domain for an aquifer system of infinite radial extent, i.e. $R_1 \rightarrow \infty$. First, the Laplace transform of the head \bar{H} in the multi-aquifer well is determined:

$$\bar{H}(p) = \frac{\frac{Q}{p} + \pi r_c^2 \varphi_0 + \sum_i \frac{2\pi R_0 T_i \varphi_i \sqrt{d_i} K_1(R_0 \sqrt{d_i})}{p K_0(R_0 \sqrt{d_i})}}{\pi r_c^2 p + \sum_i \frac{2\pi R_0 T_i \sqrt{d_i} K_1(R_0 \sqrt{d_i})}{K_0(R_0 \sqrt{d_i})}} \quad (130)$$

with eigenvalues $d_i = p \frac{S_i}{T_i}$.

Once the Laplace transform of the head in the well is known, the Laplace transform of the head \bar{h}_i in layer i at any distance r can be calculated using equation (130):

$$\bar{h}_i(r, p) = \frac{\varphi_i}{p} + \left(\bar{H}(p) - \frac{\varphi_i}{p} \right) \frac{K_0(r\sqrt{d_i})}{K_0(R_0\sqrt{d_i})} \quad (131)$$

Expressions (130) and (131) are inverted numerically by applying the Stehfest (1970) algorithm.

The solution in terms of drawdown is found by setting φ_i and φ_0 to zero, and it is presented by Wikramaratna (1984). Simplifying equation (130) in this way gives the solution for the Laplace transform of the change in water level in the well $\Delta\bar{H}$ [L]:

$$\Delta\bar{H}(p) = \frac{Q}{\pi r_c^2 p^2 + \sum_i \frac{2\pi R_0 p T_i \sqrt{d_i} K_1(R_0\sqrt{d_i})}{K_0(R_0\sqrt{d_i})}} \quad (132)$$

The corresponding solution for the Laplace transform of the drawdown \bar{s}_i [L] in aquifer i is found by simplifying equation (131):

$$\bar{s}_i(r, p) = \Delta\bar{H}(p) \frac{K_0(r\sqrt{d_i})}{K_0(R_0\sqrt{d_i})} \quad (133)$$

For two aquifers, this solution simplifies to (Wikramaratna, 1984):

$$\Delta\bar{H}(p) = \frac{Q}{\pi p} \left[\frac{1}{r_c^2 p} + \frac{K_0(R_0\sqrt{d_1}) K_0(R_0\sqrt{d_2})}{2R_0 G(d_1, d_2)} \right] \quad (134)$$

$$\begin{cases} \bar{s}_1(r, p) = \frac{Q K_0(r\sqrt{d_1})}{\pi p} \left[\frac{1}{r_c^2 p K_0(R_0\sqrt{d_1})} + \frac{K_0(R_0\sqrt{d_2})}{2R_0 G(d_1, d_2)} \right] \\ \bar{s}_2(r, p) = \frac{Q K_0(r\sqrt{d_2})}{\pi p} \left[\frac{1}{r_c^2 p K_0(R_0\sqrt{d_2})} + \frac{K_0(R_0\sqrt{d_1})}{2R_0 G(d_1, d_2)} \right] \end{cases} \quad (135)$$

with:

$$G(d_1, d_2) = T_1 \sqrt{d_1} K_1(R_0\sqrt{d_1}) K_0(R_0\sqrt{d_2}) + T_2 \sqrt{d_2} K_1(R_0\sqrt{d_2}) K_0(R_0\sqrt{d_1}) \quad (136)$$

The exact solution in Laplace space for two aquifers with nonzero initial heads and without wellbore storage in the well, i.e. $r_c \rightarrow 0$, is given by Papadopoulos (1966):

$$\begin{cases} \bar{h}_1(r, p) = \frac{\varphi_1}{p} + \left[(\varphi_2 - \varphi_1) T_2 \sqrt{d_2} K_1(R_0\sqrt{d_2}) + \frac{Q}{2\pi R_0} K_0(R_0\sqrt{d_2}) \right] \frac{K_0(r\sqrt{d_1})}{p G(d_1, d_2)} \\ \bar{h}_2(r, p) = \frac{\varphi_2}{p} + \left[(\varphi_1 - \varphi_2) T_1 \sqrt{d_1} K_1(R_0\sqrt{d_1}) + \frac{Q}{2\pi R_0} K_0(R_0\sqrt{d_1}) \right] \frac{K_0(r\sqrt{d_2})}{p G(d_1, d_2)} \end{cases} \quad (137)$$

with $G(d_1, d_2)$ according to (136).

The exact solution in the Laplace domain for one aquifer that includes wellbore storage is:

$$\bar{h}(r, p) = \frac{\varphi}{p} + \left(\bar{H}(p) - \frac{\varphi}{p} \right) \frac{K_0(r\sqrt{d})}{K_0(R_0\sqrt{d})} \quad (138)$$

with \bar{H} the Laplace transform of the head in the large-diameter well:

$$\bar{H}(p) = \frac{\frac{Q}{p} + \pi r_c^2 \varphi_0 + \frac{2\pi R_0 T \varphi \sqrt{d} K_1(R_0 \sqrt{d})}{p K_0(R_0 \sqrt{d})}}{\pi r_c^2 p + \frac{2\pi R_0 T \sqrt{d} K_1(R_0 \sqrt{d})}{K_0(R_0 \sqrt{d})}} \quad (139)$$

and eigenvalue $d = p \frac{S}{T}$. The Laplace space solution in terms of drawdown is found by setting φ and φ_0 in (138) and (139) to zero:

$$\bar{s}(r, p) = \frac{Q K_0(r \sqrt{d})}{\pi r_c^2 p^2 K_0(R_0 \sqrt{d}) + 2\pi R_0 p T \sqrt{d} K_1(R_0 \sqrt{d})} \quad (140)$$

Expression (140) is presented by Papadopoulos and Cooper (1967), who also give the analytically inverted solution in the real-time domain.

To find the solution for parallel flow, the modified Bessel functions $K_0(x)$ and $K_1(x)$ in equations (130) and (131) for axisymmetric flow are replaced by e^{-x} , πr_c^2 is replaced by r_c , and $2\pi R_0$ is deleted. After simplifying the expression for \bar{H} , this gives:

$$\bar{H}(p) = \frac{\frac{Q}{p} + r_c \varphi_w + \sum_i \frac{\varphi_i}{p} T_i \sqrt{d_i}}{r_c p + \sum_i T_i \sqrt{d_i}} \quad (141)$$

$$\bar{h}_i(r, p) = \frac{\varphi_i}{p} + \left(\bar{H}(p) - \frac{\varphi_i}{p} \right) \frac{e^{-(r \sqrt{d_i})}}{e^{-(R_0 \sqrt{d_i})}} \quad (142)$$

Figure 4 shows the solution for a three-aquifer system characterized by the dimensionless input parameters given in Table 4. Dimensionless head $-h_i \sum_i T_i / Q$ is plotted as a function of dimensionless time $t \sum_i T_i / (R_0^2 \sum_i S_i)$ due to pumping (i.e. $Q < 0$) of a multi-aquifer well with radius R_0 that is fully connected to the three aquifers.

Table 4. Dimensionless parameters for three aquifers open to a multi-aquifer well. The transient-state model simulating radial flow to this well is discussed in the text.

Aquifer	Dimensionless transmissivity $T_i / \sum_i T_i$	Dimensionless storativity $S_i / \sum_i S_i$	Dimensionless initial head $-\varphi_i \sum_i T_i / Q$
$i = 1$	0.1	0.25	-1.0
$i = 2$	0.6	0.50	0.0
$i = 3$	0.3	0.25	1.0

Figure 4 plots the head in the pumping well and in an observation well with separate screen in each aquifer and at relative distance r/R_0 equal to 100. The semi-analytical solution (131) is represented by the black solid lines, the generalized semi-analytical solution given in section 6.3 by the yellow dashed lines, the finite-difference solution by the red dotted lines, and the MODFLOW-MNW2 solution by the black dots. The four solutions are virtually the same. Concerning the pumping well, there is a scenario that neglects the wellbore storage and one in which the storage change is taken into account. In the latter case, the initial dimensionless water level in the well $-H \sum_i T_i / Q$ is -0.5, and the dimensionless radius of the casing $r_c / (R_0 \sqrt{\sum_i S_i})$ is 10. This scenario cannot be simulated using the MNW2 package as it does not support the option to include wellbore storage.

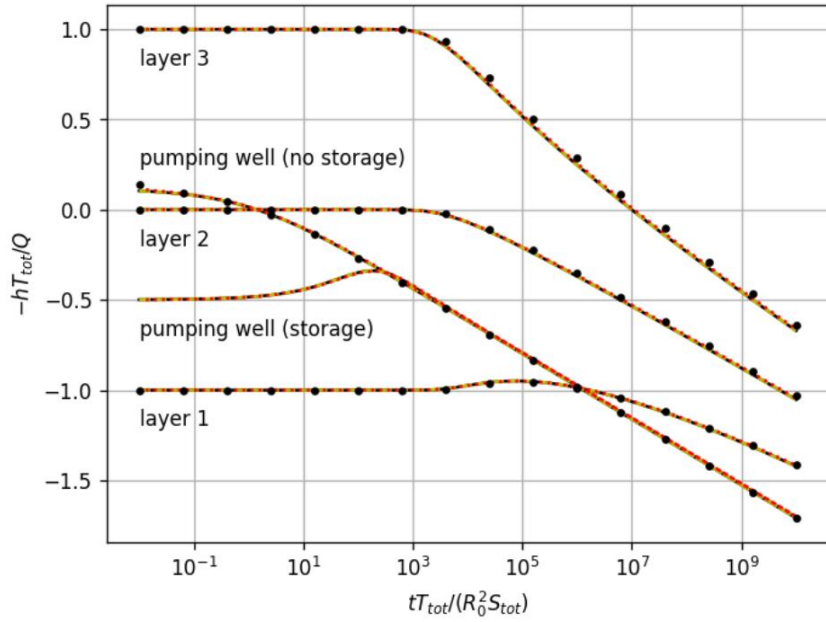


Figure 4. Dimensionless head versus dimensionless time for the transient flow model of a multi-aquifer well with radius R_0 . The aquifer system consists of three aquifers with relative transmissivities equal to 0.1, 0.6, and 0.3, and relative storativities equal to 0.25, 0.5, and 0.25, respectively. The outer boundary of the system is at an infinitely large distance. The dimensionless initial heads in the aquifers equal -1, 0, and 1, respectively. The black solid lines give the semi-analytical solution, the yellow dashed lines the generalized semi-analytical solution, the red dotted lines the finite-difference solution, and the black dots the MODFLOW-MNW2 solution. The head is simulated for the pumping well and for an observation well in each aquifer at a relative distance r/R_0 of 100. A scenario with and without wellbore storage is simulated. In the latter case, the initial dimensionless water level in the well is -0.5, and the dimensionless radius of the well-casing is 10. T_{tot} and S_{tot} are the sum of the transmissivities and the storativities of the three aquifers, respectively. See text for a more detailed explanation.

6.5.3. The UWD solution

Hemker (1999a) solves the same problem as in previous section 6.5.2, but replaces the separating aquiclude by incompressible aquitards, which means there is vertical crossflow between the aquifers. The Hemker (1999a) solution also considers the effects of wellbore storage and an infinitesimal well-skin. Transient flow is considered to a single multilayer well with constant pumping rate Q , well-screen radius R_0 , well-casing radius r_c , and dimensionless well-skin factor F . The solution is expressed in terms of drawdown instead of head, and it is called the uniform well-face drawdown (UWD) solution (Hemker, 1999a). As the superposition principle applies, no infiltration is included, and all initial and constant heads are set to zero.

The UWD solution is obtained by simplifying solution (81) for homogeneous layers derived in section 6.3.3. As there is no infiltration and all initial heads are zero, $\zeta(r) = \mathbf{0}$ and $\boldsymbol{\varphi}_0 = \mathbf{0}$, which gives:

$$\mathbf{s}(r) = \mathbf{VZ}(r)\mathbf{V}^{-1}\mathbf{T}^{-1}\mathbf{E}\boldsymbol{\Psi}^{-1}\mathbf{C} \frac{Q}{p\theta} \quad (143)$$

Recall that $\boldsymbol{\Psi} = \mathbf{E}^T [\mathbf{VZ}(R_0)\mathbf{V}^{-1} + \mathbf{F}]\mathbf{T}^{-1}\mathbf{E}$, with \mathbf{E} an $n_l \times n_s$ matrix that indicates the screened layers, and \mathbf{F} an $n_l \times n_l$ diagonal matrix with nonzero entry \mathbf{F}_{ii} equal to the skin factor F if layer i is connected to the well and zero otherwise. As there is one well only, matrix \mathbf{C} reduces to an $n_s \times 1$ vector of ones, vector \mathbf{Q} in (81) simplifies to scalar Q/p , and matrix $\boldsymbol{\Theta}$ in (81) also reduces to a scalar:

$$\theta = p\pi r_c^2 - \mathbf{C}^T \boldsymbol{\Psi}^{-1} \mathbf{C} \quad (144)$$

Vector \mathbf{s} contains the Laplace transform $\bar{s}_i(r, p)$ of the drawdown in each layer i at distance r . Solution (143) is inverted numerically using the Stehfest (1970) algorithm. The outer boundary is at

an infinitely large distance, and all eigenvalues are nonzero as transient flow is simulated. Hence, matrix \mathbf{Z} is fully determined by expression (71), or $Z_{ii}(r) = K_0(r\sqrt{d_i})/[R_0\sqrt{d_i}K_1(R_0\sqrt{d_i})]$.

Table 5. Dimensionless parameters for the three aquifers in the UWD model discussed in the text.

Aquifer	Dimensionless transmissivity $T_i/\sum_i T_i$	Dimensionless storativity $S_i/\sum_i S_i$	Dimensionless resistance $c_{i-1} \sum_i T_i/R_0^2$
$i = 1$	0.1	0.25	10^5
$i = 2$	0.6	0.50	10^{10}
$i = 3$	0.3	0.25	10^{15}

Consider the same three-aquifer system as in the previous section, but with aquitards instead of aquiclude, a leaky top, and an impervious bottom. The dimensionless parameters are given in Table 5. The aquifer system has an infinite extent; the initial and constant heads are zero. The multilayer well has a screen with radius R_0 , and its casing has a dimensionless radius $r_c/(R_0\sqrt{\sum_i S_i}) = 10$. The well is surrounded by a skin with relative width $R_{skin}/R_0 = 1.01$, and with relative transmissivity $T_{skin}/\sum_i T_i = 0.01$. This implies the skin is less pervious than the aquifer.

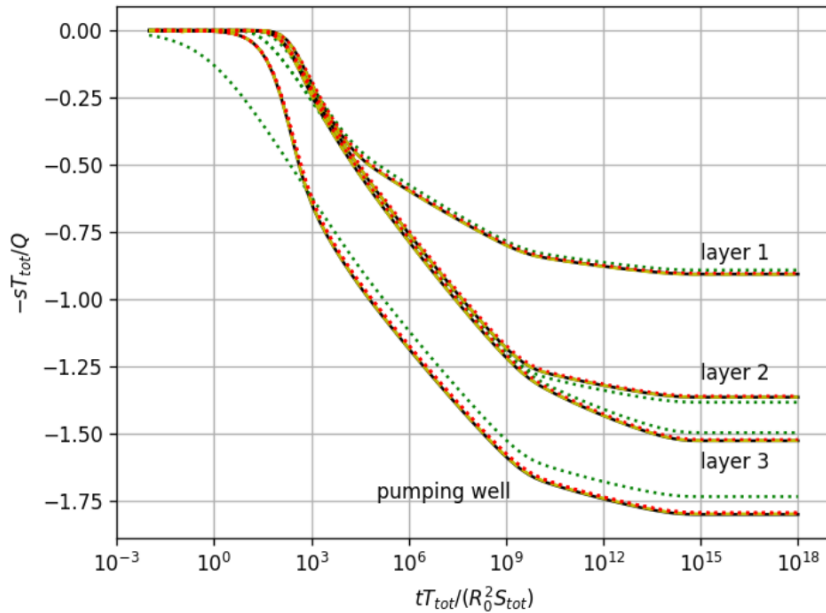


Figure 5. Dimensionless drawdown versus dimensionless time for the UWD model (Hemker, 1999a) of a multi-aquifer well with radius R_0 , wellbore storage, and less pervious well-skin. The leaky aquifer system has an impervious bottom and consists of three aquifers with relative transmissivities equal to 0.1, 0.6, and 0.3, and relative storativities equal to 0.25, 0.5, and 0.25, respectively. The dimensionless resistance of the aquitards on top of the aquifers are 10^5 , 10^{10} , and 10^{15} , respectively. The black solid lines give the UWD solution, the yellow dashed lines are the generalized semi-analytical solution, and the red dotted lines are the finite-difference solution. Drawdown is simulated for the pumping well and for an observation well in each aquifer at a relative distance r/R_0 of 10. The green dotted lines are the corresponding solution without the effect of wellbore storage and well-skin. T_{tot} and S_{tot} are the sum of the transmissivities and the storativities of the three aquifers, respectively. See text for a more detailed explanation.

Figure 5 shows the dimensionless drawdown $-s_i T_i / Q$ as a function of dimensionless time $t \sum_i T_i / (R_0^2 \sum_i S_i)$ due to pumping (i.e. $Q < 0$) of the multi-aquifer well. Drawdown is simulated for the pumping well, and for an observation well with separate screen in each aquifer and at dimensionless distance $r/R_0 = 10$. The UWD solution (143) is represented by the black solid lines, the generalized semi-analytical solution presented in section 6.3 by the yellow dashed lines, and the finite-difference solution by the red dotted lines. The UWD model applies the dimensionless skin

factor defined by (91), while the other two models implement a finite-thickness skin. It is seen that the three solutions are virtually the same.

The green dotted lines are the corresponding semi-analytical solution without wellbore storage and well-skin. The effects of wellbore storage and well-skin are observable in both the pumping and the observation well. The effect of the wellbore storage decreases and is relevant only at small values of time, whereas the skin effect remains throughout the extraction. Note that a new state of equilibrium is reached after a long time of pumping since the system is leaky.

6.5.4. Partially penetrating wells: UWD versus UWG

Previous section 6.5.3 presents the uniform well-face drawdown (UWD) solution developed by Hemker (1999a). As explained in the introductory section 6.1, this mixed-type boundary condition is not only necessary for modeling multi-aquifer wells, but it also defines a more realistic well-face condition for partially penetrating wells compared to the commonly applied and mathematically more straightforward uniform well-face gradient (UWG) condition. In this section, the semi-analytical UWG solution developed by Mishra et al. (2012) to simulate radial flow to a partially penetrating well with storage in an anisotropic confined aquifer is compared with the UWD solution.

The governing partial differential equation for radial flow in a confined aquifer of infinite lateral extent with uniform thickness B [L] is:

$$\frac{\partial^2 s}{\partial r^2} + \frac{1}{r} \frac{\partial s}{\partial r} + \frac{K^v}{K^h} \frac{\partial^2 s}{\partial z^2} = \frac{K^v}{K^h} \frac{\partial s}{\partial t} \quad (0 \leq z \leq B) \quad (145)$$

with K^h the horizontal conductivity [L/T], K^v the vertical conductivity [L/T], and S^s the specific elastic storage [1/L] of the aquifer. In this case, drawdown $s(r, z, t)$ [L] is a function of radial distance r [L], vertical distance z [L], and time t [T]. This means the solution by Mishra et al. (2012) takes the vertical direction fully into account.

The upper and lower boundaries, respectively at vertical distances $z = 0$ and $z = B$, are impervious:

$$\frac{\partial s}{\partial z} = 0 \quad (R_0 < r < \infty; z = 0 \text{ and } z = B; t > 0) \quad (146)$$

Recall that the inner model boundary is at distance R_0 [L], which coincides with the radius of the well-screen in this case. The outer model boundary is at an infinite distance from the well. Drawdown is constant and equal to zero at this boundary:

$$s(\infty, z, t) = 0 \quad (0 < z < B; t > 0) \quad (147)$$

The initial drawdown in the aquifer is also zero:

$$s(r, z, 0) = 0 \quad (R_0 < r < \infty; 0 < z < B) \quad (148)$$

The wellbore storage mass-balance expression assumes a constant flux across the well-screen:

$$Q = \pi r_c^2 \frac{\partial s}{\partial t} - 2\pi K^h b r \frac{\partial s}{\partial r} \quad (r = R_0; a \leq z \leq a + b; t > 0) \quad (149)$$

with b the length [L] of the well-screen, and a the distance between the top of the screen and the top of the aquifer. Recall that r_c is the radius [L] of the well-casing. Expression (149) is a UWG boundary condition that includes the effect of wellbore storage. There is a no-flow condition at the portion of the well-casing that is not open to the aquifer:

$$r \frac{\partial s}{\partial r} = 0 \quad (r = R_0; z < a \text{ or } z > a + b; t > 0) \quad (150)$$

Mishra et al. (2012) solve the stated problem by applying the Laplace transform with respect to time t and the finite cosine transform with respect to vertical distance z . They also introduce the following dimensionless parameters:

$$\rho = \frac{r}{B}; \eta = \frac{z}{B}; \tau = \frac{tK^h}{r^2 S^s}; \xi = \frac{R_0}{r}; \beta = \frac{a+b}{B}; \zeta = \frac{a}{B}; A = \frac{K^v}{K^h}; \alpha = \frac{r_c^2}{R_0^2 S^s B} \quad (151)$$

Note that Mishra et al. (2012) use S^s instead $S^s B$ to define α , which seems to be a mistake as α is not dimensionless if S^s is not multiplied by B .

The solution for the Laplace transform \bar{s} of drawdown is:

$$\bar{s}(\rho, \eta, \theta) = \frac{Qt}{4\pi K^h B} \left\{ F_0 + \frac{2}{\pi(\beta - \zeta)} \sum_{n=1}^{\infty} \frac{[\sin(\pi n \beta) - \sin(\pi n \zeta)] \cos(\pi n \eta)}{n} F_n \right\} \quad (152)$$

with $\theta = pt$, $\gamma_n = \sqrt{\theta/\tau + A(\pi n \rho)^2}$, and:

$$F_n = \frac{2K_0(\gamma_n)}{\theta \left[\xi \gamma_n K_1(\xi \gamma_n) + \frac{\alpha \xi^2 \gamma_n^2}{2(\beta - \zeta)} K_0(\xi \gamma_n) \right]} \quad (153)$$

K_0 and K_1 in (153) are the zeroth and first order modified Bessel functions of the second kind, respectively. Solution (152) corresponds to equation (6) in Mishra et al. (2012), which also seems to contain a typo in the denominator of the first term ($n = 0$): it should be $K_1(\xi \gamma_0)$ instead of $K_1(\xi \gamma_n)$.

Mishra et al. (2012) apply the algorithm of de Hoog et al. (1982) to invert solution (152) numerically. Here, the Stehfest (1970) algorithm is used. The infinite sum is approximated by a finite yet sufficiently large number of terms so that the truncation error is negligibly small.

Mishra et al. (2012) also derive the solution for the average drawdown between depths z_1 and z_2 :

$$\bar{s}(\rho, \Delta\eta, \theta) = \frac{Qt}{4\pi K^h B} \left\{ F_0 + \frac{2}{\pi^2(\beta - \zeta)\Delta\eta} \sum_{n=1}^{\infty} \frac{[\sin(\pi n \beta) - \sin(\pi n \zeta)][\sin(\pi n \eta_2) - \sin(\pi n \eta_1)]}{n^2} F_n \right\} \quad (154)$$

with $\Delta\eta = \eta_2 - \eta_1 = (z_2 - z_1)/B$. Equation (154) is found by integrating expression (152) from $\eta_1 = z_1/B$ to $\eta_2 = z_2/B$, and dividing the result by $\Delta\eta$. It corresponds to equation (8) in Mishra et al. (2012), which contains the same typo as their equation (6).

As shown by Mishra et al. (2012), expression (152) reduces to the Laplace domain solution of Yang et al. (2006) if wellbore storage is neglected, and to the Laplace domain solution of Hantush (1964) if the well also has an infinitesimal well-screen radius:

$$\bar{s}(\rho, \eta, \theta) = \frac{Qt}{4\pi K^h B} \left\{ \frac{2K_0(\gamma_0)}{\theta} + \frac{4}{\pi\theta(\beta - \zeta)} \sum_{n=1}^{\infty} \frac{[\sin(\pi n \beta) - \sin(\pi n \zeta)] \cos(\pi n \eta)}{n} K_0(\gamma_n) \right\} \quad (155)$$

Expression (155) corresponds to equation (11) in Mishra et al. (2012), and it can be further reduced to the Laplace domain solution of Theis (1935) if the well is fully penetrating, as in this case, the infinite sum disappears:

$$\bar{s}(\rho, \theta) = \frac{Qt}{2\pi K^h B \theta} K_0(\gamma_0) \quad (156)$$

Equation (156) corresponds to equation (12) in Mishra et al. (2012). Solution (152) simplifies to the Laplace domain solution of Papadopoulos and Cooper (1967) if the well is fully penetrating, if it has a finite well-screen radius, and if wellbore storage is taken into account:

$$\bar{s}(\rho, \theta) = \frac{Qt}{4\pi K^h B} F_0 \quad (157)$$

Equation (157) corresponds to equation (9) in Mishra et al. (2012).

As an example, consider a confined aquifer with thickness $B = 10$ m from which a partially penetrating well with radius $R_0 = r_c = 0.1$ m extracts water at a constant rate $Q = -100 \text{ m}^3/\text{d}$. The well-screen of length $b = 5$ m is located in the upper part of the aquifer. The schematization of well and aquifer is visualized in Figure 6. The horizontal conductivity of the aquifer $K^h = 10 \text{ m/d}$, the vertical conductivity $K^v = 1 \text{ m/d}$, and the specific storage $S^s = 0.001 \text{ m}^{-1}$.

The graph in Figure 6 shows drawdown s at the well-face as a function of time t simulated using the UWG solution by Mishra et al. (2012) as well as the UWD approach by Hemker (1999a). Recall that the latter does not take the vertical direction fully into account, and therefore, the aquifer in the UWD model is subdivided into ten layers of 1 m thickness. The well-screen is connected to the first five sublayers, as is shown on the schematization drawn in Figure 6. The UWD condition keeps drawdown the same for the nodes at distance R_0 in the middle of each of these sublayers. On the time-drawdown graph in Figure 6, this drawdown is represented by the black dashed line. The blue dashed line corresponds to the UWG solution (154), which is the average drawdown at the well-face over the entire length of the well-screen.

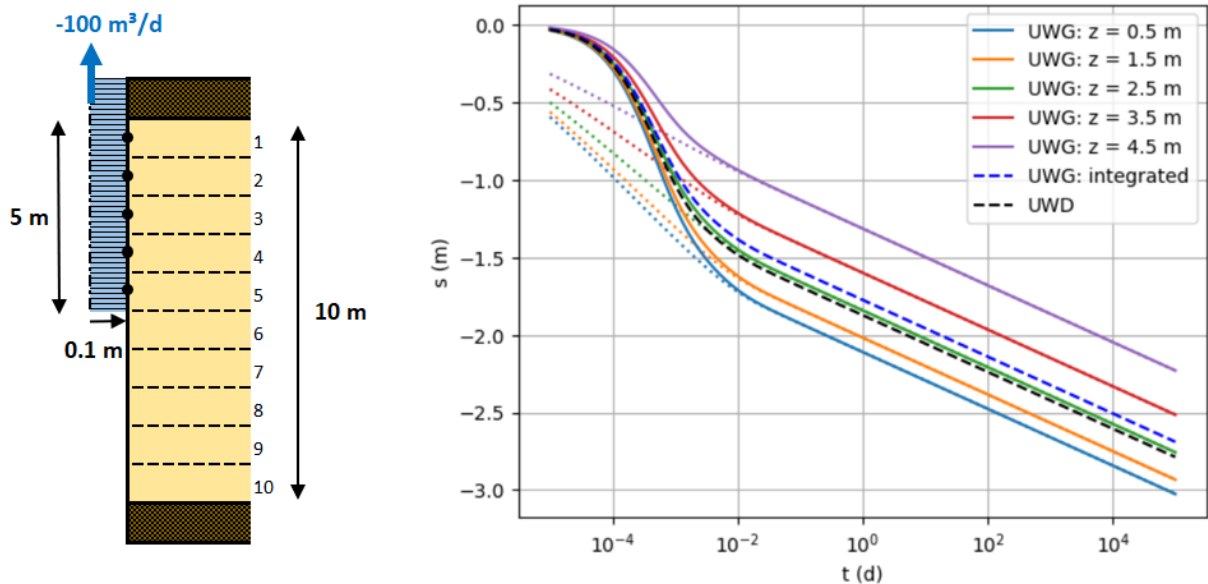


Figure 6. Left: Schematization of the example model that simulates radial flow to a pumping well partially penetrating a homogeneous confined aquifer. The aquifer has a thickness of 10 m; the length of the well-screen is 5 m. Right: Plot of drawdown s versus time t at the face of the well-screen with a radius of 0.1 m. The solid and dotted lines are simulated using the UWG solution by Mishra et al. (2012), respectively including and neglecting the wellbore storage; the blue dashed line represents the average drawdown integrated over the entire screen length. The black dashed line corresponds to the UWD solution developed by Hemker (1999a). In the UWD model, the aquifer is subdivided into 10 sublayers, and a multi-node well is defined in the upper five sublayers, as can be observed in the drawing on the left. See text for a more detailed explanation.

Finally, the drawdown at the well-face is calculated using the UWG solution (152) at the vertical distances of the nodes within the multi-node well defined in the UWD model. These correspond to the solid and dotted lines on the graph in Figure 6, representing the results that include and neglect

wellbore storage, respectively. It can be observed that the drawdown is greatest at the top and smallest at the bottom of the screen. The drawdown in the middle aligns closely with the UWD result, even more so than the average UWG drawdown integrated over the entire screen length. The effect of the wellbore storage is noticeable only at small values of time, more specifically when time t is smaller than 0.01 d.

6.5.5. The KGS model

The KGS model is developed at the Kansas Geological Survey (KGS) by Hyder et al. (1994) to simulate over-damped slug tests conducted in partially penetrating wells. The model considers a homogeneous vertically anisotropic aquifer of infinite extent with an impervious lower boundary. The upper boundary may be impervious as well, or it may be a steady water table. Wellbore storage is taken into account, and it is possible to introduce the effect of a finite-thickness well skin.

The governing partial differential equation for radial flow in both skin (zone 1) and aquifer (zone 2) is:

$$\frac{\partial^2 s_j}{\partial r^2} + \frac{1}{r} \frac{\partial s_j}{\partial r} + \frac{K_j^v}{K_j^h} \frac{\partial^2 s_j}{\partial z^2} = \frac{S_j^s}{K_j^h} \frac{\partial s_j}{\partial t} \quad (j = 1,2) \quad (158)$$

with K_j^h the horizontal conductivity [L/T], K_j^v the vertical conductivity [L/T], and S_j^s the specific elastic storage [1/L] in zone j . In this case, head change s is a function of radial distance r [L], vertical distance z [L], and time t [T]. Note that the KGS model does not discretize the aquifer into a number of sublayers and takes the vertical direction fully into account.

If the upper boundary is at distance $z = 0$, and the aquifer thickness is B [L], then the lower no-flux boundary condition is:

$$\frac{\partial s_j}{\partial z} = 0 \quad (R_0 < r < \infty; z = B; t > 0; j = 1,2) \quad (159)$$

Recall that the inner model boundary is at distance R_0 [L], which coincides with the radius of the well-screen in this case. The upper boundary condition depends on whether the aquifer is confined or phreatic:

$$\begin{cases} \frac{\partial s_j}{\partial z} = 0 & \text{(confined)} \\ s_j = 0 & \text{(unconfined)} \end{cases} \quad (R_0 < r < \infty; z = 0; t > 0; j = 1,2) \quad (160)$$

Note that in the phreatic case, the water table is conceptualized as a constant-head boundary, which is translated into a zero head change condition according to the principle of superposition. Similarly, the head change at the outer model boundary at infinity is also zero, as is the initial head change in the aquifer at $t = 0$:

$$s_2 = 0 \quad (r = \infty; 0 < z < B; t > 0) \quad (161)$$

$$s_j = 0 \quad (R_0 < r < \infty; 0 < z < B; t = 0; j = 1,2) \quad (162)$$

Inside the well, however, there is an instantaneous head change φ_0 [L] at $t = 0$:

$$H = \varphi_0 \quad (t = 0) \quad (163)$$

where $H(t)$ is the relative water level [L] within the well. As there is no vertical discretization, the drawdown at the face of the well-screen is vertically integrated:

$$\frac{1}{b} \int_a^{a+b} s_1 dz = H \quad (r = R_0; t > 0) \quad (164)$$

with b the length [L] of the well-screen, and a the distance [L] between the top of the screen and the top of the aquifer. The wellbore balance is:

$$2\pi R_0 K_1^h \frac{\partial s_1}{\partial r} = \begin{cases} \frac{\pi r_c^2}{b} \frac{dH}{dt} & (a \leq z \leq a + b) \\ 0 & (z < a \text{ or } z > a + b) \end{cases} \quad (r = R_0; t > 0) \quad (165)$$

with r_c the radius [L] of the well casing.

Finally, continuity of flow is required at the boundary between skin and aquifer at distance R_1 [L]:

$$s_1 = s_2 \quad (r = R_1; 0 < z < B; t > 0) \quad (166)$$

$$K_1^h \frac{\partial s_1}{\partial r} = K_2^h \frac{\partial s_2}{\partial r} \quad (r = R_1; 0 < z < B; t > 0) \quad (167)$$

Hyder et al. (1994) obtain the semi-analytical solution by employing a series of integral transforms: a Laplace transform in time and finite Fourier transforms in the vertical direction. Evaluation and inversion of the Fourier transforms is done numerically using discrete Fourier transforms (Brigham, 1974; Cooley & Tukey, 1965; Press et al., 1992), and the algorithm of Stehfest (1970) is applied to perform the numerical Laplace inversion.

Hyder et al. (1994) rewrite the problem in nondimensional form defining the following dimensionless parameters:

$$\rho = \frac{r}{R_0}; \eta = \frac{z}{b}; \tau = \frac{t K_2^h b}{r_c^2}; \xi = \frac{R_1}{R_0}; \beta = \frac{B}{b}; \zeta = \frac{a}{b}; A_j = \frac{K_j^v}{K_1^h}; \gamma = \frac{K_2^h}{K_1^h}; \lambda = \frac{S_2^s}{S_1^s}; \alpha = \frac{2R_0^2 S_2^s b}{r_c^2} \quad (168)$$

The exact solution in Laplace space for the normalized head H/φ_0 is (Hyder et al., 1994):

$$\mathcal{L}\left\{\frac{H(t)}{\varphi_0}\right\}(p) = \frac{(\gamma/2)\Omega}{1 + p(\gamma/2)\Omega} \quad (169)$$

with:

$$\Omega = \int_{\zeta}^{\zeta+1} \{\mathcal{F}^{-1}[\mathcal{F}(\omega)f_1]\} d\eta \quad (170)$$

$$f_1 = \frac{\Delta_2 K_0(\nu_1) - \Delta_1 I_0(\nu_1)}{\nu_1 [\Delta_2 K_1(\nu_1) - \Delta_1 I_1(\nu_1)]} \quad (171)$$

$$\Delta_1 = K_0(\nu_1 \xi) K_1(\nu_2 \xi) - \frac{\nu_1}{\nu_2 \gamma} K_0(\nu_2 \xi) K_1(\nu_1 \xi) \quad (172)$$

$$\Delta_2 = I_0(\nu_1 \xi) K_1(\nu_2 \xi) + \frac{\nu_1}{\nu_2 \gamma} K_0(\nu_2 \xi) I_1(\nu_1 \xi) \quad (173)$$

$$\nu_1 = \sqrt{\frac{A_1 b^2}{R_0^2} \omega^2 + \frac{\alpha \gamma}{2\lambda} p} \quad (174)$$

$$v_2 = \sqrt{\frac{A_2 b^2}{R_0^2} \omega^2 + \frac{\alpha}{2} p} \quad (175)$$

In (169), \mathcal{L} denotes the Laplace transform with variable p . In case of a confined aquifer, \mathcal{F} in (170) is the finite Fourier cosine transform of the boxcar function that maps z to 1 if $a \leq z \leq a + b$, and to 0 otherwise. In the unconfined case, \mathcal{F} in (170) is the modified finite Fourier sine transform of that function. In both cases, ω is the Fourier transform variable. In the confined case, $\omega = n\pi/\beta$ for $n = 1, 2, 3, \dots$, whereas $\omega = n\pi/(2\beta)$ for $n = 1, 3, 5, \dots$ in the unconfined case. Hyder et al. (1994) also present the continuous forms of Ω :

$$\Omega = \begin{cases} \frac{f_1(n=0)}{\beta} + \frac{8\beta}{\pi^2} \sum_{n=1}^{\infty} \frac{f_1(n)}{n^2} \sin^2\left(\frac{n\pi}{2\beta}\right) \cos^2\left(\frac{n\pi(1+2\zeta)}{2\beta}\right) & \text{(confined)} \\ \frac{16\beta}{\pi^2} \sum_{n=1}^{\infty} [1 + (-1)^{n+1}] \frac{f_1(n)}{n^2} \sin^2\left(\frac{n\pi}{4\beta}\right) \sin^2\left(\frac{n\pi(1+2\zeta)}{4\beta}\right) & \text{(unconfined)} \end{cases} \quad (176)$$

In this study, the continuous form of Ω given by (176) is used to evaluate expression (169), and the Stehfest (1970) algorithm is applied to perform the Laplace inversion. The original KGS model coded with FORTRAN is rewritten completely using Python.

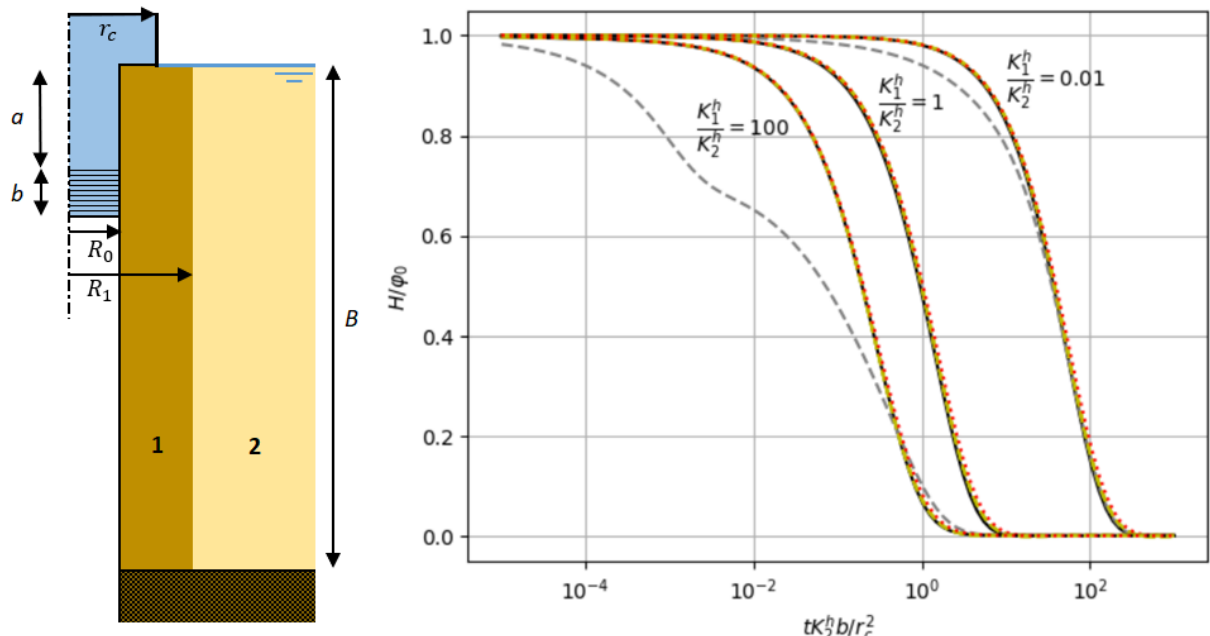


Figure 7. Left: Schematization of the example model simulating a slug test in a well with finite-thickness skin (zone 1) partially penetrating a homogeneous phreatic aquifer with steady water table (zone 2). Right: Plot of normalized head versus dimensionless time for the example model. Length b of the well-screen is 10% of the aquifer thickness B , distance a between the aquifer top and the top of the screen is 20% of the aquifer thickness. Radius r_c of the well casing is 2 times larger than radius R_0 of the well-screen, and outer radius R_1 of the skin is 3 times the screen radius. The vertical anisotropy K_2^v/K_2^h of the aquifer equals 0.5. Three scenarios are simulated: in the first, the horizontal conductivity K_1^h of the skin is 100 times larger than the horizontal conductivity K_2^h of the aquifer, in the second, the horizontal conductivity of the skin is the same, and in the third, the horizontal conductivity of the skin is 100 times smaller. The vertical anisotropy of the skin is 1, and the specific storage of skin and aquifer are the same. Dimensionless storage coefficient α is 10^{-3} . The black solid lines are simulated using the KGS model (Hyder et al., 1994), the yellow dashed lines using the generalized semi-analytical solution, and the red dotted lines using the finite-difference method. In the last two models, the aquifer is discretized into 30 sublayers of equal thickness. The gray dashed curves are simulated by assigning a 100 times larger value to the specific storage of the well-skin than to the specific storage of the aquifer. See text for a more detailed explanation.

The test case considers an unconfined aquifer with partially penetrating well and finite-thickness skin. The aquifer thickness B is 10 times length b of the screen, and the distance a between the top of the screen and the top of the aquifer is one fifth of the aquifer thickness. The outer radius R_1 of the skin is 3 times larger than radius R_0 of the well-screen, and radius r_c of the well-casing is 2 times larger than the radius of the well-screen. This is schematized in the left drawing of Figure 7. The horizontal conductivity K_2^h of the aquifer is 2 times larger than its vertical conductivity K_2^v , whereas the vertical anisotropy for the well-skin is 1, that is $K_1^h = K_1^v$. The specific storage of the skin and the aquifer are the same, that is $S_1^s = S_2^s$, and dimensionless storage α equals 10^{-3} .

The graph in Figure 7 shows the normalized head H/φ_0 as a function of dimensionless time τ for different values of the dimensionless horizontal conductivity of the skin: $K_2^h/K_1^h = 0.01$, $K_2^h/K_1^h = 1$, and $K_2^h/K_1^h = 100$. The black lines are the KGS solution that is obtained by numerically inverting expression (169), whereas the yellow dashed lines and the red dotted lines are the generalized semi-analytical solution and the finite-difference solution presented in sections 6.3 and 6.4, respectively. It is seen that the simulated heads correspond well, although the solutions presented in this chapter slightly deviate from the KGS solution, which is mainly due to the vertical discretization.

In both the semi-analytical and the finite-difference solution method, the aquifer is discretized into 30 sublayers of equal thickness, i.e. $D_i = B/n_l$ with $n_l = 30$. Recall that $T_{ij} = K_j^h D_i$ and $S_{ij} = S_j^s D_i$ for $i = 1, 2, \dots, n_l$ and $j = 1, 2$. Resistance between model layers is $c_i = D_i/K_j^v$ for $i = 1, 2, \dots, n_l - 1$ and $j = 1, 2$. The resistance of the bottom of the aquifer $c_{n_l,j}$ is infinitely large. The top of the aquifer is leaky with $c_{0,j} = D_0/(2K_j^v)$ and constant head equal to 0. The well screen is situated in model layers 7, 8, and 9.

Although the vertical anisotropy of the skin and the aquifer are not the same, the second scenario may be regarded as the reference case without well-skin. When the well-skin is less pervious than the aquifer, the recovery is significantly slower than for the other scenarios, and when the skin is more pervious than the aquifer, the recovery happens faster than when there is no skin. To check the effect of the well-skin storage, additional simulations are performed in which the specific storage of the skin is 100 times smaller and 100 times greater than the specific storage of the aquifer. Assigning a smaller specific storage to the skin has no effect (not indicated on the graph in Figure 7), while there is a significant effect when the specific storage of the skin is larger than the specific storage of the aquifer (gray dashed curves on the graph in Figure 7). Especially in case of a more permeable well-skin, the effect is very pronounced, and it is seen that the curve consists of two parts: the first part is largely determined by the hydraulic properties of the first zone, whereas it is the second zone that mainly shapes the second part. In this scenario, the more pervious zone around the well could be a gravel pack, and its effect has already been described by Bouwer (1989). Indeed, when applying the well-known interpretation method of Bouwer and Rice (1976), the gravel pack may cause a double straight-line effect when the logarithm of the head change is plotted against the time.

6.5.6. A multilayer well surrounded by multiple zones

In the final test case, axisymmetric flow is simulated toward a partially penetrating multilayer well extracting groundwater from a two-aquifer system at a constant pumping rate of $-500 \text{ m}^3/\text{d}$. The well radius is 150 mm, the well-screen has a length of 15 m and is situated in the lower part of the lower aquifer. A gravel pack of 110 mm width surrounds the screen. It has a conductivity of 50 m/d and a specific storage of 0.1 m^{-1} . The gravel pack suffers from clogging and a skin of 10 mm thickness occurs at the inner and outer boundary. The skin between well-screen and gravel pack has a conductivity of 0.1 m/d, the skin between gravel pack and aquifer has a conductivity of 1 m/d. The specific storage of

both skins is 10^{-5} m^{-1} . Above the gravel pack, a clay seal of 100 mm width is present with conductivity equal to 10^{-5} m/d and specific storage equal to 10^{-5} m^{-1} .

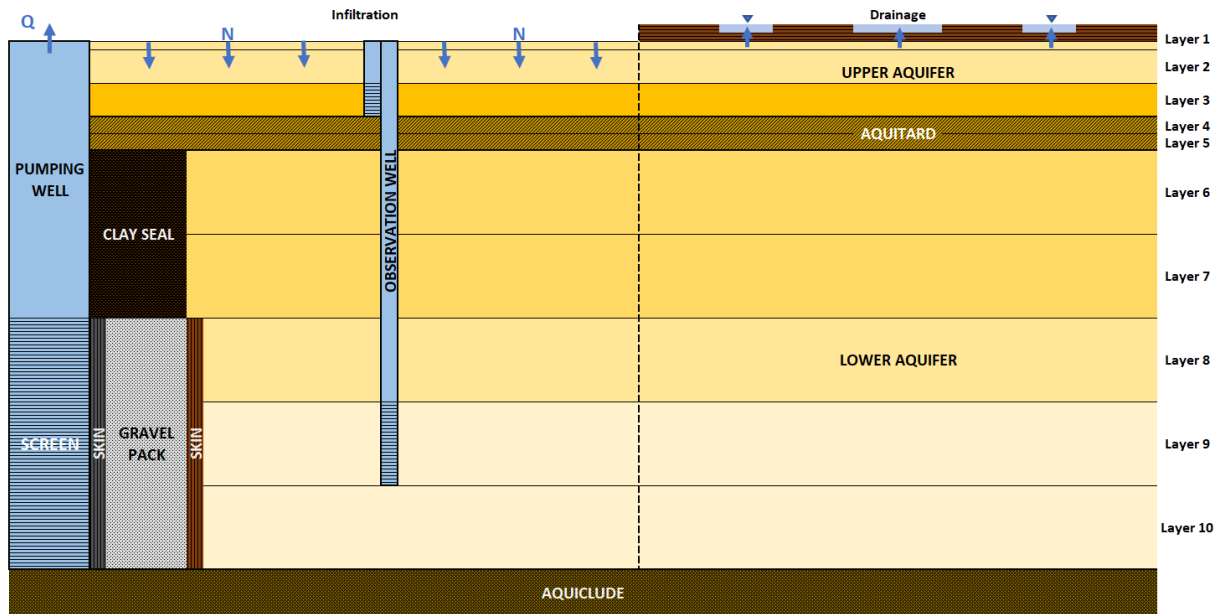


Figure 8. Schematization of the two-aquifer system from which groundwater is extracted by a partially penetrating multilayer well with skin and gravel pack. Radial and vertical distances are not to scale. See text for correct distances and Table 6 for the hydraulic parameters of the layers.

The upper aquifer is phreatic and has a total thickness of 5 m. The upper part of 2.5 m thickness is more pervious than the lower part: horizontal conductivities are 5 m/d and 1 m/d, respectively, and vertical conductivities are 1 m/d and 0.1 m/d, respectively. The specific storage of the upper aquifer is $5 \times 10^{-3} \text{ m}^{-1}$, the specific yield is 0.15. The effect of the water table is simulated by introducing a thin model layer of 0.01 m thickness on top of the model to which the specific yield is assigned. The upper aquifer is drained by a dense network of ditches with drainage resistance equal to 1000 d. In the area around the well, the ditches went dry due to the extraction. In this area with radius of 100 m, the phreatic aquifer is recharged by infiltration with a constant flux equal to 250 mm/y.

Table 6. Hydraulic parameters assigned to the layers of the model simulating a partially penetrating multilayer well with skin and gravel pack extracting water from a two-aquifer system: D is the layer thickness, K^h the horizontal conductivity, K^v the vertical conductivity, S^s the specific elastic storage, and S^y the specific yield. See Figure 7 for a visualization of the model schematization.

	Layer	D (m)	K^h (m/d)	K^v (m/d)	S^s (1/m)	S^y (-)
Upper aquifer	1	0.01	5.0	1.0	-	0.15
	2	2.5	5.0	1.0	0.005	-
	3	2.5	1.0	0.1	0.005	-
Aquitard	4	1.0	0.5	0.025	0.0001	-
	5	1.0	0.5	0.025	0.0001	-
Lower aquifer	6	5.0	2.0	0.2	0.001	-
	7	5.0	2.0	0.2	0.001	-
	8	5.0	5.0	1.0	0.0005	-
	9	5.0	10.0	3.0	0.0005	-
	10	5.0	10.0	3.0	0.0005	-

The lower aquifer is 25 m thick and lies on an impervious aquiclude. The upper part of 10 m thickness has a horizontal conductivity of 2 m/d, a vertical conductivity of 0.2 m/d, and a specific storage equal to 10^{-3} m^{-1} ; the middle part is 5 m thick and has a horizontal conductivity of 5 m/d, a vertical conductivity of 1 m/d, and a specific storage equal to $5 \times 10^{-4} \text{ m}^{-1}$; the lower part is 10 m thick, and has a horizontal conductivity of 10 m/d, a vertical conductivity of 3 m/d, and a specific storage equal to $5 \times 10^{-4} \text{ m}^{-1}$. The well screen is connected to the middle and the lower part. The upper and lower part of the aquifer are divided in two sublayers of 5 m thickness.

Finally, an aquitard of 2 m thickness separates both aquifers. Its horizontal conductivity is 0.5 m/d, its vertical conductivity is 0.025 m/d, and its specific storage is 10^{-4} m^{-1} . The aquitard consists of two model layers of 1 m thickness. The schematization of the system is visualized in Figure 8, and Table 6 summarizes the hydraulic parameters of the ten model layers.

Figure 9 shows the drawdown as a function of time from the start of the extraction, in the pumping well and in an observation well at a distance of 2 m from the well. The observation well has a screen in the lower part of the phreatic aquifer, which is the third model layer, and a screen in the lower part of the pumped aquifer, which is model layer 9. Both the pumping and the observation well are displayed on the plot of the aquifer system in Figure 8.

Two scenarios were simulated: in the first, the wellbore storage is neglected, and the pumping well has neither a skin nor a gravel pack; in the second, the effect of wellbore storage, skin, and gravel pack are taken into account. Both the semi-analytical and the finite-difference solution presented in this chapter are shown, and it is seen that both solutions are very close to each other. The observations in the phreatic layer are not affected by the wellbore storage, nor by the skin and the gravel pack, whereas the observations in the pumped aquifer clearly are. The effect of the wellbore storage is observable only at small values of time, while the effect of the skins and the gravel pack are permanent and do not vanish with time.

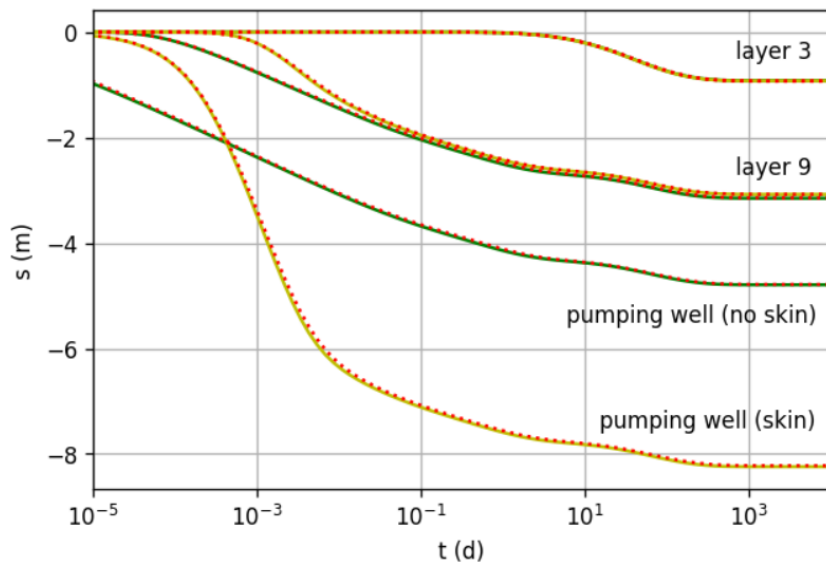


Figure 9. Drawdown versus time for the model simulating flow to a partially penetrating multilayer well in a phreatic two-aquifer system with infiltration and drainage. The solid lines are calculated using the semi-analytical approach, the red dotted lines give the finite-difference solution. The green lines correspond to the model in which wellbore storage and skin effects are neglected, whereas the yellow lines represent the solution that takes into account those effects. Figure 8 shows the model schematization, Table 6 the corresponding input parameters. The details concerning the well construction are given in the text.

6.6. Summary

In this chapter, a generalized semi-analytical solution is developed for the simulation of axisymmetric flow to a multilayer well that may be surrounded by an arbitrary number of cylindrical zones characterized by different hydraulic properties. The presented solution could be seen as an extension of the uniform well-face drawdown (UWD) solution derived by (Hemker, 1999a) that only includes a zero-thickness skin. Both steady and transient flow are considered; in the latter case, the Laplace transform is applied. The storage change in the wellbore can be taken into account if flow is transient. The well is located in a layered aquifer system with confined or leaky upper and lower boundaries. Areal recharge can be included and the aquifer system may be laterally bounded or unbounded. The corresponding semi-analytical solution for parallel flow is also given, which is straightforward given the similarity between two-dimensional axisymmetric and parallel flow.

A simple algorithm is developed to update the finite-difference matrix system in order to connect cells in the model grid. This option to connect cells is a straightforward way to define multi-node wells. In the presented method, the multi-node well is part of the model grid, and consequently, the head in the well is calculated simultaneously with the heads in the other cells of the grid. A direct solver is used to solve the resulting matrix system of finite-difference equations, which is no longer pentadiagonal due to the connected cells. This is in contrast with the iterative method applied by MODFLOW's MNW2 package (Konikow et al., 2009) that considers the multi-node well as a boundary condition. Using the method of Langevin (2008) or Louwyck et al. (2012, 2014) in combination with the MNW2 package, it is also possible to simulate axisymmetric flow to a multilayer well. In this case, the cell-to-well conductance needs to be calculated using the Thiem (1870, 1906) equation and specified in the MNW2 input file. It is not possible to include the effect of wellbore storage using the MNW2 package, but it is using the new MAW package which is available with MODFLOW 6 (Langevin et al., 2017).

Both the generalized semi-analytical and the finite-difference solution can be used to simulate axisymmetric flow to a multi-aquifer well or a partially penetrating well. This is demonstrated by discussing several test cases. In the first and second case, respectively, steady and transient flow to a multi-aquifer well open to multiple confined aquifers is simulated. The analytical solution for the steady case is derived by Sokol (1963) for an abandoned well, and by Neville and Tonkin (2004) for a pumped well. The transient-state solution for a two-aquifer system without crossflow is presented by Papadopoulos (1966), and for multiple confined aquifers by Wikramaratna (1984). The multilayer UWD solution developed by Hemker (1999a) is the third example, and the next example compares this UWD solution with the UWG solution for a partially penetrating pumping well in a confined aquifer developed by Mishra et al. (2012). The KGS model (Hyder et al., 1994) to simulate slug tests conducted in a partially penetrating well is the fifth test case. The generalized semi-analytical solution and the finite-difference solution developed in this chapter correspond very well for all of these solutions.

Finally, the added value of the developed solutions is illustrated by simulating axisymmetric flow to a partially penetrating well located in a multi-aquifer system, and having a screen extending over multiple layers in the aquifer system, characterized by different hydraulic parameters. The well has a finite-thickness skin and is surrounded by a gravel pack with a clay seal above it and a second finite-thickness skin at the boundary with the aquifer. Close to the well, the aquifer system is recharged by a constant infiltration flux, whereas drainage is still active further away from the well. This multilayer-multizone model is solved using both the semi-analytical and the finite-difference methods developed in this chapter, and it is seen that both solutions are very close to each other.

6.7. References

- Anjaneyulu, B. (1991). Partially penetrating wells in unconfined aquifers. *Agricultural Water Management*, 20(3), 185–201. [https://doi.org/10.1016/0378-3774\(91\)90016-C](https://doi.org/10.1016/0378-3774(91)90016-C)
- Bakker, M. (2001). An analytic, approximate method for modeling steady, three-dimensional flow to partially penetrating wells. *Water Resources Research*, 37(5).
<https://doi.org/10.1029/2000WR900400>
- Bakker, M., & Strack, O. D. L. (2003). Analytic elements for multiaquifer flow. *Journal of Hydrology*, 271(1–4). [https://doi.org/10.1016/S0022-1694\(02\)00319-0](https://doi.org/10.1016/S0022-1694(02)00319-0)
- Barua, G., & Bora, S. N. (2010). Hydraulics of a partially penetrating well with skin zone in a confined aquifer. *Advances in Water Resources*, 33(12), 1575–1587.
<https://doi.org/10.1016/j.advwatres.2010.09.008>
- Behrooz-Koohenjani, S., Samani, N., & Kompani-Zare, M. (2011). Steady flow rate to a partially penetrating well with seepage face in an unconfined aquifer. *Hydrogeology Journal*, 19(4), 811–821. <https://doi.org/10.1007/s10040-011-0717-2>
- Bennett, G. D., Kontis, A. L., & Larson, S. P. (1982). Representation of Multiaquifer Well Effects in Three-Dimensional Ground-Water Flow Simulation. *Ground Water*, 20(3), 334–341.
<https://doi.org/10.1111/j.1745-6584.1982.tb01354.x>
- Bouwer, H. (1989). The Bouwer and Rice Slug Test - An Update. *Ground Water*, 27(3), 304–309.
<https://doi.org/10.1111/j.1745-6584.1989.tb00453.x>
- Bouwer, H., & Rice, R. C. (1976). A slug test for determining hydraulic conductivity of unconfined aquifers with completely or partially penetrating wells. *Water Resources Research*, 12(3), 423–428. <https://doi.org/10.1029/WR012i003p00423>
- Brigham, E. O. (1974). *The Fast Fourier Transform*. Englewood Cliffs, N.J.: Prentice-Hall.
- Cassiani, G., & Kabala, Z. J. (1998). Hydraulics of a partially penetrating well: solution to a mixed-type boundary value problem via dual integral equations. *Journal of Hydrology*, 211(1–4), 100–111.
[https://doi.org/10.1016/S0022-1694\(98\)00223-6](https://doi.org/10.1016/S0022-1694(98)00223-6)
- Cassiani, G., Kabala, Z. J., & Medina, M. A. (1999). Flowing partially penetrating well: solution to a mixed-type boundary value problem. *Advances in Water Resources*, 23(1), 59–68.
[https://doi.org/10.1016/S0309-1708\(99\)00002-0](https://doi.org/10.1016/S0309-1708(99)00002-0)
- Chang, C.-C., & Chen, C.-S. (2002). An integral transform approach for a mixed boundary problem involving a flowing partially penetrating well with infinitesimal well skin. *Water Resources Research*, 38(6), 7-1-7–7. <https://doi.org/10.1029/2001WR001091>
- Chang, C.-C., & Chen, C.-S. (2003). A flowing partially penetrating well in a finite-thickness aquifer: a mixed-type initial boundary value problem. *Journal of Hydrology*, 271(1–4), 101–118.
[https://doi.org/10.1016/S0022-1694\(02\)00323-2](https://doi.org/10.1016/S0022-1694(02)00323-2)
- Chang, Y. C., & Yeh, H. D. (2009). New solutions to the constant-head test performed at a partially penetrating well. *Journal of Hydrology*, 369(1–2), 90–97.
<https://doi.org/10.1016/j.jhydrol.2009.02.016>

- Chang, Y. C., Yeh, H. D., & Chen, G. Y. (2010). Transient solution for radial two-zone flow in unconfined aquifers under constant-head tests. *Hydrological Processes*, 24(11), 1496–1503. <https://doi.org/10.1002/hyp.7610>
- Chang, Y.-C., & Yeh, H.-D. (2010). A new analytical solution solved by triple series equations method for constant-head tests in confined aquifers. *Advances in Water Resources*, 33(6), 640–651. <https://doi.org/10.1016/j.advwatres.2010.03.010>
- Chang, Y.-C., Chen, G.-Y., & Yeh, H.-D. (2011). Transient Flow into a Partially Penetrating Well during the Constant-Head Test in Unconfined Aquifers. *Journal of Hydraulic Engineering*, 137(9), 1054–1063. [https://doi.org/10.1061/\(ASCE\)HY.1943-7900.0000392](https://doi.org/10.1061/(ASCE)HY.1943-7900.0000392)
- Chen, C., & Jiao, J. J. (1999). Numerical Simulation of Pumping Tests in Multilayer Wells with Non-Darcian Flow in the Wellbore. *Ground Water*, 37(3), 465–474. <https://doi.org/10.1111/j.1745-6584.1999.tb01126.x>
- Chiu, P.-Y., Yeh, H.-D., & Yang, S.-Y. (2007). A new solution for a partially penetrating constant-rate pumping well with a finite-thickness skin. *International Journal for Numerical and Analytical Methods in Geomechanics*, 31(15), 1659–1674. <https://doi.org/10.1002/nag.607>
- Ciftci, E. (2019). A New Approach for Analyzing Drawdown Data from a Partially Penetrating Well. *Water Resources Management*, 33(8), 2727–2739. <https://doi.org/10.1007/s11269-019-02246-3>
- Cooley, J. W., & Tukey, J. W. (1965). An algorithm for the machine calculation of complex Fourier series. *Mathematics of Computation*, 19(90), 297–301. <https://doi.org/10.1090/S0025-5718-1965-0178586-1>
- Cooley, R. L. (1971). A Finite Difference Method for Unsteady Flow in Variably Saturated Porous Media: Application to a Single Pumping Well. *Water Resources Research*, 7(6), 1607–1625. <https://doi.org/10.1029/WR007i006p01607>
- Cooley, R. L., & Cunningham, A. B. (1979). Consideration of total energy loss in theory of flow to wells. *Journal of Hydrology*, 43(1–4), 161–184. [https://doi.org/10.1016/0022-1694\(79\)90171-9](https://doi.org/10.1016/0022-1694(79)90171-9)
- Coulon, C., Lemieux, J. -M., Priet, A., Bayer, P., Young, N. L., & Molson, J. (2022). Pumping Optimization Under Uncertainty in an Island Freshwater Lens Using a Sharp-Interface Seawater Intrusion Model. *Water Resources Research*, 58(8). <https://doi.org/10.1029/2021WR031793>
- Dagan, G. (1978). A note on packer, slug, and recovery tests in unconfined aquifers. *Water Resources Research*, 14(5), 929–934. <https://doi.org/10.1029/WR014i005p00929>
- Dagan, G., & Lessoff, S. C. (2011). Flow to partially penetrating wells in unconfined heterogeneous aquifers: Mean head and interpretation of pumping tests. *Water Resources Research*, 47(6). <https://doi.org/10.1029/2010WR010370>
- de Glee, G. J. (1930). *Over grondwaterstroomingen bij wateronttrekking door middel van putten (in Dutch)* (PhD thesis). Technische Hoogeschool Delft, Drukkerij J. Waltman. Jr., Delft.
- de Hoog, F. R., Knight, J. H., & Stokes, A. N. (1982). An Improved Method for Numerical Inversion of Laplace Transforms. *SIAM Journal on Scientific and Statistical Computing*, 3(3), 357–366. <https://doi.org/10.1137/0903022>

- Dougherty, D. E., & Babu, D. K. (1984). Flow to a Partially Penetrating Well in a Double-Porosity Reservoir. *Water Resources Research*, 20(8), 1116–1122.
<https://doi.org/10.1029/WR020i008p01116>
- Duffield, G. M. (2007). *AQTESOLVTM for Windows Version 4.5, User's Guide*. HydroSOLVE, Inc., Reston, VA.
- Feng, Q., & Wen, Z. (2016). Non-Darcian flow to a partially penetrating well in a confined aquifer with a finite-thickness skin. *Hydrogeology Journal*, 24(5), 1287–1296.
<https://doi.org/10.1007/s10040-016-1389-8>
- Feng, Q., & Zhan, H. (2015). On the aquitard–aquifer interface flow and the drawdown sensitivity with a partially penetrating pumping well in an anisotropic leaky confined aquifer. *Journal of Hydrology*, 521, 74–83. <https://doi.org/10.1016/j.jhydrol.2014.11.058>
- Feng, Q., & Zhan, H. (2016). Integrated aquitard-aquifer flow with a mixed-type well-face boundary and skin effect. *Advances in Water Resources*, 89, 42–52.
<https://doi.org/10.1016/j.advwatres.2016.01.003>
- Feng, Q., & Zhan, H. (2019). Constant-head test at a partially penetrating well in an aquifer-aquitard system. *Journal of Hydrology*, 569, 495–505. <https://doi.org/10.1016/j.jhydrol.2018.12.018>
- Feng, Q., Yuan, X., & Zhan, H. (2019). Flow to a partially penetrating well with variable discharge in an anisotropic two-layer aquifer system. *Journal of Hydrology*, 578, 124027.
<https://doi.org/10.1016/j.jhydrol.2019.124027>
- Feng, Q., Luo, Y., & Zhan, H. (2020). Three-dimensional response to a partially penetration well pumping in a general anisotropic three-layer aquifer system. *Journal of Hydrology*, 585, 124850.
<https://doi.org/10.1016/j.jhydrol.2020.124850>
- Feng, Q., Liu, Z., & Zhan, H. (2021). Semi-analytical solutions for transient flow to a partially penetrated well with variable discharge in a general three-layer aquifer system. *Journal of Hydrology*, 598, 126329. <https://doi.org/10.1016/j.jhydrol.2021.126329>
- Gastélum, J. R., Sheng, Z., Wang, C., & Zhao, S. (2011). Evaluation of Well Heads by Using Different Approaches: Well Package, Multi-Node Well Package, and Analytical Solution. In *World Environmental and Water Resources Congress 2011* (pp. 898–903). Reston, VA: American Society of Civil Engineers. [https://doi.org/10.1061/41173\(414\)92](https://doi.org/10.1061/41173(414)92)
- Haitjema, H. M. (1985). Modeling Three-Dimensional Flow in Confined Aquifers by Superposition of Both Two- and Three-Dimensional Analytic Functions. *Water Resources Research*, 21(10), 1557–1566. <https://doi.org/10.1029/WR021i010p01557>
- Haitjema, H. M., & Kraemer, S. R. (1988). A new analytic function for modeling partially penetrating wells. *Water Resources Research*, 24(5), 683–690. <https://doi.org/10.1029/WR024i005p00683>
- Halford, K. J., & Hanson, R. T. (2002). *User guide for the drawdown-limited, multi-node well (MNW) package for the U.S. Geological Survey's modular three-dimensional finite-difference ground-water flow model, versions MODFLOW-96 and MODFLOW-2000*. U.S. Geological Survey Open-File Report 02-293. <https://doi.org/10.3133/ofr02293>
- Hantush, M. S. (1961a). Aquifer tests on partially penetrating wells. *Journal of the Hydraulics Division, Proceedings of the American Society of Civil Engineers*, 87(HY5), 171–194.

- Hantush, M. S. (1961b). Drawdown around a partially penetrating well. *Journal of the Hydraulics Division, Proceedings of the American Society of Civil Engineers*, 87(HY4), 83–98.
- Hantush, M. S. (1964). Hydraulics of wells. In V. T. Chow (Ed.), *Advances in Hydroscience* (Vol. I, pp. 281–432). New York and London: Academic Press.
- Harbaugh, A. W. (2005). *MODFLOW-2005, the U.S. Geological Survey modular ground-water model - the Ground-Water Flow Process*. U.S. Geological Survey Techniques and Methods 6-A16. <https://doi.org/https://doi.org/10.3133/tm6A16>
- Harbaugh, A. W., & McDonald, M. G. (1996). *User's documentation for MODFLOW-96, an update to the U.S. Geological Survey modular finite-difference ground-water flow model*. U.S. Geological Survey Open-File Report 96-485. <https://doi.org/https://doi.org/10.3133/ofr96485>
- Harbaugh, A. W., Banta, E. R., Hill, M. C., & McDonald, M. G. (2000). *MODFLOW-2000, The U.S. Geological Survey Modular Ground-Water Model: User Guide to Modularization Concepts and the Ground-Water Flow Process*. U.S. Geological Survey Open-File Report 00-92. <https://doi.org/https://doi.org/10.3133/ofr200092>
- Hemker, C. J. (1984). Steady groundwater flow in leaky multiple-aquifer systems. *Journal of Hydrology*, 72(3–4), 355–374. [https://doi.org/10.1016/0022-1694\(84\)90089-1](https://doi.org/10.1016/0022-1694(84)90089-1)
- Hemker, C. J. (1985). Transient well flow in leaky multiple-aquifer systems. *Journal of Hydrology*, 81(1–2), 111–126. [https://doi.org/10.1016/0022-1694\(85\)90170-2](https://doi.org/10.1016/0022-1694(85)90170-2)
- Hemker, C. J. (1999a). Transient well flow in layered aquifer systems: the uniform well-face drawdown solution. *Journal of Hydrology*, 225(1–2), 19–44. [https://doi.org/10.1016/S0022-1694\(99\)00093-1](https://doi.org/10.1016/S0022-1694(99)00093-1)
- Hemker, C. J. (1999b). Transient well flow in vertically heterogeneous aquifers. *Journal of Hydrology*, 225(1–2), 1–18. [https://doi.org/10.1016/S0022-1694\(99\)00137-7](https://doi.org/10.1016/S0022-1694(99)00137-7)
- Hemker, C. J. (2000). *Groundwater flow in layered aquifer systems* (PhD thesis). VU, Amsterdam.
- Houben, G. J. (2015). Review: Hydraulics of water wells—flow laws and influence of geometry. *Hydrogeology Journal*, 23(8), 1633–1657. <https://doi.org/10.1007/s10040-015-1312-8>
- Huang, C.-S., Yang, S.-Y., & Yeh, H.-D. (2015). Technical Note: Approximate solution of transient drawdown for constant-flux pumping at a partially penetrating well in a radial two-zone confined aquifer. *Hydrology and Earth System Sciences*, 19(6), 2639–2647. <https://doi.org/10.5194/hess-19-2639-2015>
- Huang, Y. H. (1973). Unsteady flow toward an artesian well. *Water Resources Research*, 9(2), 426–433. <https://doi.org/10.1029/WR009i002p00426>
- Hyder, Z., Butler, J. J., McElwee, C. D., & Liu, W. (1994). Slug tests in partially penetrating wells. *Water Resources Research*, 30(11), 2945–2957. <https://doi.org/10.1029/94WR01670>
- Indelman, P., Fiori, A., & Dagan, G. (1996). Steady Flow Toward Wells in Heterogeneous Formations: Mean Head and Equivalent Conductivity. *Water Resources Research*, 32(7), 1975–1983. <https://doi.org/10.1029/96WR00990>
- Javandel, I., & Witherspoon, P. A. (1969). A Method of Analyzing Transient Fluid Flow in Multilayered Aquifers. *Water Resources Research*, 5(4), 856–869. <https://doi.org/10.1029/WR005i004p00856>

- Javandel, I., & Witherspoon, P. A. (1980). A semianalytical solution for partial penetration in two-layer aquifers. *Water Resources Research*, 16(6), 1099–1106.
<https://doi.org/10.1029/WR016i006p01099>
- Javandel, I., & Witherspoon, P. A. (1983). Analytical solution of a partially penetrating well in a two-layer aquifer. *Water Resources Research*, 19(2), 567–578.
<https://doi.org/10.1029/WR019i002p00567>
- Johnson, R. L., Clark, B. R., Landon, M. K., Kauffman, L. J., & Eberts, S. M. (2011). Modeling the Potential Impact of Seasonal and Inactive Multi-Aquifer Wells on Contaminant Movement to Public Water-Supply Wells. *Journal of the American Water Resources Association*, 47(3), 588–596. <https://doi.org/10.1111/j.1752-1688.2011.00526.x>
- Khader, M. H. A., & Ramadurgaiah, D. (1978). Flow toward a partially penetrating well in a bounded artesian aquifer. *Journal of Hydrology*, 36(1–2), 95–107. [https://doi.org/10.1016/0022-1694\(78\)90040-9](https://doi.org/10.1016/0022-1694(78)90040-9)
- Khader, M. H. A., & Veerankutty, M. K. (1975). Transient well-flow in an unconfined-confined aquifer system. *Journal of Hydrology*, 26(1–2), 123–140. [https://doi.org/10.1016/0022-1694\(75\)90129-8](https://doi.org/10.1016/0022-1694(75)90129-8)
- Kipp, K. L. (1973). Unsteady flow to a partially penetrating, finite radius well in an unconfined aquifer. *Water Resources Research*, 9(2), 448–462. <https://doi.org/10.1029/WR009i002p00448>
- Kirkham, D. (1959). Exact theory of flow into a partially penetrating well. *Journal of Geophysical Research*, 64(9), 1317–1327. <https://doi.org/10.1029/JZ064i009p01317>
- Konikow, L. F., & Hornberger, G. Z. (2006). Modeling Effects of Multinode Wells on Solute Transport. *Ground Water*, 44(5), 648–660. <https://doi.org/10.1111/j.1745-6584.2006.00231.x>
- Konikow, L. F., Hornberger, G. Z., Halford, K. J., Hanson, R. T., & Harbaugh, A. W. (2009). *Revised multi-node well (MNW2) package for MODFLOW ground-water flow model*. U.S. Geological Survey Techniques and Methods 6-A30. <https://doi.org/10.3133/tm6A30>
- Kruseman, G. P., & de Ridder, N. A. (1990). *Analysis and Evaluation of Pumping Test Data* (2nd ed.). Wageningen: ILRI Publication 47.
- Langevin, C. D. (2008). Modeling Axisymmetric Flow and Transport. *Ground Water*, 46(4), 579–590. <https://doi.org/10.1111/j.1745-6584.2008.00445.x>
- Langevin, C. D., Hughes, J. D., Banta, E. R., Niswonger, R. G., Panday, S., & Provost, A. M. (2017). *Documentation for the MODFLOW 6 Groundwater Flow Model*. U.S. Geological Survey Techniques and Methods 6-A55. <https://doi.org/10.3133/tm6A55>
- Louwyck, A., Vandenbohede, A., Bakker, M., & Lebbe, L. C. (2012). Simulation of axi-symmetric flow towards wells: A finite-difference approach. *Computers & Geosciences*, 44, 136–145. <https://doi.org/10.1016/j.cageo.2011.09.004>
- Louwyck, A., Vandenbohede, A., Bakker, M., & Lebbe, L. C. (2014). MODFLOW procedure to simulate axisymmetric flow in radially heterogeneous and layered aquifer systems. *Hydrogeology Journal*, 22(5), 1217–1226. <https://doi.org/10.1007/s10040-014-1150-0>

- Malama, B., Kuhlman, K. L., & Barrash, W. (2008). Semi-analytical solution for flow in a leaky unconfined aquifer toward a partially penetrating pumping well. *Journal of Hydrology*, 356(1–2), 234–244. <https://doi.org/10.1016/j.jhydrol.2008.03.029>
- Mani, S. K., Singh, S. K., Pandey, S. N., & Pachauri, A. K. (1999). Numerical Modelling of Flow towards a Well in a Two Layer Aquifer. *ISH Journal of Hydraulic Engineering*, 5(1), 68–76. <https://doi.org/10.1080/09715010.1999.10514644>
- Mathias, S. A., & Wen, Z. (2015). Numerical simulation of Forchheimer flow to a partially penetrating well with a mixed-type boundary condition. *Journal of Hydrology*, 524, 53–61. <https://doi.org/10.1016/j.jhydrol.2015.02.015>
- McDonald, M. G. (1984). Development of a multi-aquifer well option for a modular ground-water flow model. In *Proceedings of the National Water Well Association Conference on Practical Applications of Ground Water Models: Columbus, Ohio*, National Water Well Association (pp. 786–796). Columbus, Ohio.
- McDonald, M. G. (1986). Development of a multi-aquifer well option for a modular groundwater flow model. In R. M. Khanbilvardi & J. Fillos (Eds.), *Groundwater Hydrology, Contamination, and Remediation* (pp. 383–398). Washington, D.C.: Scientific Publications.
- McDonald, M. G., & Harbaugh, A. W. (1988). *A modular three-dimensional finite-difference ground-water flow model*. U.S. Geological Survey Techniques of Water-Resources Investigations 06-A1. <https://doi.org/10.3133/twri06A1>
- Mishra, G. C., & Chandra, S. (1990). Unsteady flow to a multi-aquifer artesian well . In *Groundwater monitoring and management: proceedings of the symposium held at Dresden, German Democratic Republic (GDR) in March 1987* (pp. 293–303). IAHS Press, Institute of Hydrology.
- Mishra, G. C., & Chandra, S. (1992). Unsteady Flow to a Multi-Aquifer Artesian Well. In *Proceedings of the Seminar on Ground Water Hydrology, 17-18 July 1992 at New Delhi, Vol-I* (pp. 131–144). New Delhi: National Institute of Hydrology.
- Mishra, G. C., Nautiyal, M. D., & Chandra, S. (1985). Unsteady flow to a well tapping two aquifers separated by an aquiclude. *Journal of Hydrology*, 82(3–4), 357–369. [https://doi.org/10.1016/0022-1694\(85\)90027-7](https://doi.org/10.1016/0022-1694(85)90027-7)
- Mishra, P. K., Vesselinov, V. v., & Neuman, S. P. (2012). Radial flow to a partially penetrating well with storage in an anisotropic confined aquifer. *Journal of Hydrology*, 448–449, 255–259. <https://doi.org/10.1016/j.jhydrol.2012.05.010>
- Moench, A. F. (1996). Flow to a Well in a Water-Table Aquifer: An Improved Laplace Transform Solution. *Ground Water*, 34(4), 593–596. <https://doi.org/10.1111/j.1745-6584.1996.tb02045.x>
- Moench, A. F. (1997). Flow to a well of finite diameter in a homogeneous, anisotropic water table aquifer. *Water Resources Research*, 33(6), 1397–1407. <https://doi.org/10.1029/97WR00651>
- Muskat, M. (1937). *The Flow of Homogeneous Fluids Through Porous Media*. New York: McGraw-Hill.
- Neuman, S. P. (1974). Effect of partial penetration on flow in unconfined aquifers considering delayed gravity response. *Water Resources Research*, 10(2), 303–312. <https://doi.org/10.1029/WR010i002p00303>

- Neuman, S. P., & Witherspoon, P. A. (1969). *Transient flow of groundwater to wells in multiple-aquifer systems*. Publication 69-1, Department of Civil Engineering, University of California, Berkeley.
- Neuman, S. P., & Witherspoon, P. A. (1971). Analysis of Nonsteady Flow with a Free Surface Using the Finite Element Method. *Water Resources Research*, 7(3), 611–623.
<https://doi.org/10.1029/WR007i003p00611>
- Neville, C. J., & Tonkin, M. J. (2004). Modeling Multiaquifer Wells with MODFLOW. *Ground Water*, 42(6), 910–919. <https://doi.org/10.1111/j.1745-6584.2004.t01-9-x>
- Novakowski, K. S. (1993). Interpretation of the transient flow rate obtained from constant-head tests conducted in situ in clays. *Canadian Geotechnical Journal*, 30(4), 600–606.
<https://doi.org/10.1139/t93-052>
- Olsthoorn, T. N. (2008). Do a Bit More with Convolution. *Groundwater*, 46(1), 13–22.
<https://doi.org/10.1111/j.1745-6584.2007.00342.x>
- Pantoja, G. C. F., & Elias, W. S. (2020). Green's functions and method of images: an interdisciplinary topic usually cast aside in physics textbooks. *ArXiv: Physics Education*.
<https://doi.org/10.48550/arXiv.2006.09999>
- Papadopoulos, I. S. (1966). Nonsteady flow to multiaquifer wells. *Journal of Geophysical Research*, 71(20), 4791–4797. <https://doi.org/10.1029/JZ071i020p04791>
- Papadopoulos, I. S., & Cooper, H. H. (1967). Drawdown in a well of large diameter. *Water Resources Research*, 3(1), 241–244. <https://doi.org/10.1029/WR003i001p00241>
- Perina, T., & Lee, T.-C. (2006). General well function for pumping from a confined, leaky, or unconfined aquifer. *Journal of Hydrology*, 317(3–4), 239–260.
<https://doi.org/10.1016/j.jhydrol.2005.05.020>
- Peterson, P., Oliphant, T., & Vanderplas, J. (2022). SciPy (version 1.8.1) documentation for function linalg.solve. Retrieved July 18, 2022, from
<https://docs.scipy.org/doc/scipy/reference/generated/scipy.linalg.solve.html>
- Poulsen, D. L., Cook, P. G., Simmons, C. T., McCallum, J. L., & Dogramaci, S. (2019). Effects of Intraborehole Flow on Purging and Sampling Long-Screened or Open Wells. *Groundwater*, 57(2), 269–278. <https://doi.org/10.1111/gwat.12797>
- Press, W. H., Teukolsky, S. A., Vetterling, W. T., & Flannery, B. P. (1992). *Numerical Recipes in FORTRAN*. New York: Cambridge University Press.
- Ruud, N. C., & Kabala, Z. J. (1996). Numerical Evaluation of Flowmeter Test Interpretation Methodologies. *Water Resources Research*, 32(4), 845–852.
<https://doi.org/10.1029/96WR00004>
- Ruud, N. C., & Kabala, Z. J. (1997). Response of a partially penetrating well in a heterogeneous aquifer: integrated well-face flux vs. uniform well-face flux boundary conditions. *Journal of Hydrology*, 194(1–4), 76–94. [https://doi.org/10.1016/S0022-1694\(96\)03217-9](https://doi.org/10.1016/S0022-1694(96)03217-9)
- Singh, S. K. (2008). Simple Model for Analyzing Transient Pumping from Two Aquifers with Cross Flow. *Journal of Irrigation and Drainage Engineering*, 134(2), 228–234.
[https://doi.org/10.1061/\(ASCE\)0733-9437\(2008\)134:2\(228\)](https://doi.org/10.1061/(ASCE)0733-9437(2008)134:2(228))

- Singh, S. K. (2009). Simple Model for Analyzing Transient Pumping from Two Aquifers without Cross Flow. *Journal of Irrigation and Drainage Engineering*, 135(1), 102–107. [https://doi.org/10.1061/\(ASCE\)0733-9437\(2009\)135:1\(102\)](https://doi.org/10.1061/(ASCE)0733-9437(2009)135:1(102))
- Singh, S. K. (2010). Modeling the Transient Pumping from Two Aquifers Using MODFLOW. *Journal of Irrigation and Drainage Engineering*, 136(4), 276–281. [https://doi.org/10.1061/\(ASCE\)IR.1943-4774.0000162](https://doi.org/10.1061/(ASCE)IR.1943-4774.0000162)
- Sokol, D. (1963). Position and fluctuations of water level in wells perforated in more than one aquifer. *Journal of Geophysical Research*, 68(4), 1079–1080. <https://doi.org/10.1029/JZ068i004p01079>
- Stehfest, H. (1970). Algorithm 368: Numerical inversion of Laplace transforms [D5]. *Communications of the ACM*, 13(1), 47–49. <https://doi.org/10.1145/361953.361969>
- Strack, O. D. L. (1989). *Groundwater Mechanics*. Old Tappan, N. J.: Prentice-Hall.
- Sudicky, E. A., Unger, A. J. A., & Lacombe, S. (1995). A Noniterative Technique for the Direct Implementation of Well Bore Boundary Conditions in Three-Dimensional Heterogeneous Formations. *Water Resources Research*, 31(2), 411–415. <https://doi.org/10.1029/94WR02854>
- Székely, F. (1990). Drawdown around a well in a heterogeneous, leaky aquifer system. *Journal of Hydrology*, 118(1–4), 247–256. [https://doi.org/10.1016/0022-1694\(90\)90261-U](https://doi.org/10.1016/0022-1694(90)90261-U)
- Székely, F. (1992). Pumping test data analysis in wells with multiple or long screens. *Journal of Hydrology*, 132(1–4), 137–156. [https://doi.org/10.1016/0022-1694\(92\)90176-V](https://doi.org/10.1016/0022-1694(92)90176-V)
- Székely, F. (1995). Estimation of Unsteady, Three-Dimensional Drawdown in Single, Vertically Heterogeneous Aquifers. *Ground Water*, 33(4), 669–674. <https://doi.org/10.1111/j.1745-6584.1995.tb00323.x>
- Szucs, P., Székely, F., & Zakanyi, B. (2013). Comparison of analytical and numerical approaches for simulating groundwater flow to multi screen wells. *Carpathian Journal of Earth and Environmental Sciences*, 8(2), 69–76.
- Tarshish, M. (1993). Combined Mathematical Model of Flow in an Aquifer-Vertical Well System. *Ground Water*, 31(4), 545–550. <https://doi.org/10.1111/j.1745-6584.1993.tb00586.x>
- Tarshish, M. (1998). Modifications of Combined Mathematical Model of Flow in an Aquifer-Vertical Well System. *Ground Water*, 36(1), 7–8. <https://doi.org/10.1111/j.1745-6584.1998.tb01060.x>
- Tartakovsky, G. D., & Neuman, S. P. (2007). Three-dimensional saturated-unsaturated flow with axial symmetry to a partially penetrating well in a compressible unconfined aquifer. *Water Resources Research*, 43(1). <https://doi.org/10.1029/2006WR005153>
- Theis, C. V. (1935). The relation between the lowering of the Piezometric surface and the rate and duration of discharge of a well using ground-water storage. *Transactions, American Geophysical Union*, 16(2), 519–524. <https://doi.org/10.1029/TR016i002p00519>
- Thiem, A. (1870). Die Ergiebigkeit artesischer Bohrlöcher, Schachtbrunnen und Filtergalerien (in German). *Journal Für Gasbeleuchtung Und Wasserversorgung*, 13, 450–467.
- Thiem, G. (1906). *Hydrologische Methoden (in German)*. Leipzig: Gebhardt.

- Tjahjanto, D., & Kassim, A. H. M. (2004). Numerical solution for transient well flow in an unconfined-confined aquifer system. *Journal of Environmental Hydrology*, 12(Paper 19).
- Vandenbohede, A., Louwyck, A., & Vlamynck, N. (2014). SEAWAT-Based Simulation of Axisymmetric Heat Transport. *Groundwater*, 52(6), 908–915. <https://doi.org/10.1111/gwat.12137>
- Wang, J., Zhou, H., Qiu, K., Dong, W., Chu, D., & Wang, L. (2021). A semi-analytical approach to simulate cross-flow effect on the flow behavior of partially penetrating well in two-layer confined aquifer by Green function method. *Journal of Hydrology*, 597, 126141. <https://doi.org/10.1016/j.jhydrol.2021.126141>
- Wen, Z., Liu, K., & Zhan, H. (2014). Non-Darcian flow toward a larger-diameter partially penetrating well in a confined aquifer. *Environmental Earth Sciences*, 72(11), 4617–4625. <https://doi.org/10.1007/s12665-014-3359-6>
- Wen, Z., Wu, F., & Feng, Q. (2016). Non-Darcian Flow to a Partially Penetrating Pumping Well in a Leaky Aquifer Considering the Aquitard–Aquifer Interface Flow. *Journal of Hydrologic Engineering*, 21(12). [https://doi.org/10.1061/\(ASCE\)HE.1943-5584.0001446](https://doi.org/10.1061/(ASCE)HE.1943-5584.0001446)
- Widdowson, M. A., Molz, F. J., & Melville, J. G. (1990). An Analysis Technique for Multilevel and Partially Penetrating Slug Test Data. *Ground Water*, 28(6), 937–945. <https://doi.org/10.1111/j.1745-6584.1990.tb01730.x>
- Wikramaratna, R. S. (1984). An Analytical Solution for the Effects of Abstraction From a Multiple-Layered Confined Aquifer With No Cross Flow. *Water Resources Research*, 20(8), 1067–1074. <https://doi.org/10.1029/WR020i008p01067>
- Wikramaratna, R. S. (1985). On the Components of Flow Resulting From Abstraction in a Two-Layered Confined Aquifer With No Cross Flow. *Water Resources Research*, 21(7), 985–989. <https://doi.org/10.1029/WR021i007p00985>
- Wilkinson, D., & Hammond, P. S. (1990). A perturbation method for mixed boundary-value problems in pressure transient testing. *Transport in Porous Media*, 5(6). <https://doi.org/10.1007/BF00203331>
- Xiang, J. (1994). Steady-state flow distributions in the disturbed zone of layered aquifers. *Advances in Water Resources*, 17(5), 275–281. [https://doi.org/10.1016/0309-1708\(94\)90031-0](https://doi.org/10.1016/0309-1708(94)90031-0)
- Yager, R. M., & Heywood, C. E. (2014). Simulation of the Effects of Seasonally Varying Pumping on Intraborehole Flow and the Vulnerability of Public-Supply Wells to Contamination. *Groundwater*, 52(S1), 40–52. <https://doi.org/10.1111/gwat.12150>
- Yang, S.-Y., & Yeh, H.-D. (2005). Laplace-Domain Solutions for Radial Two-Zone Flow Equations under the Conditions of Constant-Head and Partially Penetrating Well. *Journal of Hydraulic Engineering*, 131(3), 209–216. [https://doi.org/10.1061/\(ASCE\)0733-9429\(2005\)131:3\(209\)](https://doi.org/10.1061/(ASCE)0733-9429(2005)131:3(209))
- Yang, S.-Y., Yeh, H.-D., & Chiu, P.-Y. (2006). A closed form solution for constant flux pumping in a well under partial penetration condition. *Water Resources Research*, 42(5). <https://doi.org/10.1029/2004WR003889>
- Yang, S.-Y., Huang, C.-S., Liu, C.-H., & Yeh, H.-D. (2014). Approximate Solution for a Transient Hydraulic Head Distribution Induced by a Constant-Head Test at a Partially Penetrating Well in a Two-Zone Confined Aquifer. *Journal of Hydraulic Engineering*, 140(7). [https://doi.org/10.1061/\(ASCE\)HY.1943-7900.0000884](https://doi.org/10.1061/(ASCE)HY.1943-7900.0000884)

Yeh, H.-D., & Chang, Y.-C. (2013). Recent advances in modeling of well hydraulics. *Advances in Water Resources*, 51, 27–51. <https://doi.org/10.1016/j.advwatres.2012.03.006>

Zlotnik, V., & Zhan, H. (2005). Aquitard effect on drawdown in water table aquifers. *Water Resources Research*, 41(6). <https://doi.org/10.1029/2004WR003716>

Chapter 7. Radial Flow in Head-Dependent Two-Zone Multi-Aquifer Systems

7.1. Introduction

This chapter explores the possibility to use the multilayer-multizone approach discussed in Chapter 5 to solve nonlinear multilayer flow problems. The semi-analytical solutions developed in Chapter 2, Chapter 5, and Chapter 6 are linear, which implies linear boundary conditions and input parameters that are not a function of the hydraulic head. This requirement is not fulfilled for the problems stated in this chapter, as at least one parameter is head-dependent or one boundary condition is nonlinear.

In particular, two types of nonlinear problems are studied. The first type of problems deals with the conversion from confined to unconfined flow, which occurs when the head in a confined aquifer drops below the aquifer top. In the unconfined part close to the well, the specific yield is taken into account to calculate the storage change instead of the specific elastic storage. The second type of problems considers a pumping well in a phreatic aquifer system subject to areal infiltration and drainage. In this case, drainage in the vicinity of the well becomes inactive when the head is lower than the drainage level. In the first case, the aquifer storativity is head-dependent, whereas it is the drainage resistance in the second case.

Analytical one-layer solutions for these two problems are described in the literature and are used to test the proposed semi-analytical approach. The semi-analytical multilayer solution is also compared with the finite-difference method, which can deal with nonlinearities more easily. In particular, the use of Picard iterations is a simple and effective technique for solving nonlinear saturated groundwater flow problems (Mehl, 2006), which is illustrated in this chapter and next Chapter 8.

7.1.1. Confined-unconfined flow

Moench and Prickett (1972) are the first to present the solution for transient flow in a single confined aquifer that becomes unconfined near the well. Their solution is translated from a solution for an analogous heat conduction problem by Carslaw and Jaeger (1959). Moench and Prickett (1972) only consider the change in storativity, that is the conversion from elastic storage to specific yield in the proximal zone around the well where the head drops below the aquifer top. In reality, the transmissive property of this zone also changes, since the saturated aquifer thickness becomes smaller due to the decrease in head.

Hu and Chen (2008) take into account the head-dependent transmissivity in the unconfined part of the aquifer by applying the Girinski potential (Girinski, 1946). The analytical solution method by Hu and Chen (2008) is based on earlier work published in Chinese by Chen (1974, 1983). The method suggested by Girinski (1946) is also applied by Strack (1989) and Haitjema (1995) to derive the analytical solution for combined confined and unconfined steady flow toward a fully penetrating well in a single aquifer. The same solution is used by Chen et al. (2006) to simulate steady confined-unconfined flow induced by multiple wells in an aquifer bounded by a river with constant water level. Chen et al. (2006) apply the superposition method and the method of images, which is allowed since the Girinski (1946) potential satisfies the Laplace equation.

The Hu and Chen (2008) solution for confined-unconfined well-flow is valid for transient state conditions. However, the problem statement is simplified by assuming the aquifer diffusivity remains constant, which is theoretically doubtful, as the storage coefficient of the unconfined zone near the well is much larger than the storage coefficient of the confined part. This issue is addressed by Wang and Zhan (2009) and by Xiao et al. (2018), who both refine the Moench and Prickett (1972) solution by making the transmissivity in the unconfined zone around the well head-dependent. In this case, the unconfined flow in the proximal zone is governed by the nonlinear Boussinesq (1877, 1904) equation, which is discussed in next Chapter 8. Wang and Zhan (2009) solve this equation using a numerical Runge-Kutta method (Kutta, 1901; Runge, 1895), whereas Xiao et al. (2018) develop an analytical approach by linearizing the equation using a relation proposed by Bear (1972). In both methods, the Boltzmann transform is applied to simplify the governing partial differential equations by combining the radial distance and the time into a single variable.

Both Wang and Zhan (2009) and Xiao et al. (2018) present a solution method that considers the conversion of the storage coefficient as well as the head-dependent saturated thickness of the unconfined part of the aquifer. However, in both cases, it is assumed that the slope of the phreatic surface is relatively small so that the vertical component of the unconfined flow can be neglected. In the hydrogeological literature, neglecting the resistance to flow in the vertical direction is known as the Dupuit-Forchheimer approximation (Haitjema, 1995; Strack, 1989), which is explained in next Chapter 8. Xiao et al. (2022) develop a semi-analytical solution that does consider the vertical anisotropy in the unconfined region, and additionally, the drainage from the unsaturated zone above the water table. The latter is the well-known phenomenon of delayed yield (Boulton, 1954, 1963) or delayed gravity response (Neuman, 1972, 1974, 1979). The approach applied by Xiao et al. (2022) to consider drawdown delayed response in the context of confined-unconfined flow is based on earlier work by Moench (1995), who reconciles the Boulton (1954, 1963) and Neuman (1972, 1974) models. Next Chapter 8 also elaborates on the issues regarding delayed yield.

7.1.2. Combined areal infiltration and drainage

The analytical solution for steady radial flow toward a well in a single phreatic aquifer subject to areal uniform infiltration and drainage is given by Ernst (1971). The transient state solution based on the Laplace transform is presented by Louwyck et al. (2022), who show how the solution with draining top boundary condition is related to the Theis (1935) solution for transient radial flow in a confined aquifer, and to the steady-state and transient-state solutions for well-flow in a leaky aquifer by de Glee (1930) and Jacob (1946), and Hantush and Jacob (1955), respectively. The study by Louwyck et al. (2022) is presented in Chapter 10 discussing the validity of calculating the radius of influence to assess the environmental impact of a groundwater extraction.

The solution by Ernst (1971) is also revisited by Louwyck et al. (2023) in the context of the water budget myth (Bredehoeft, 2002; Bredehoeft et al., 1982) and its recharge controversy. Most analytical models for simulating axisymmetric flow toward a pumping well are based on the implicit assumption of linearity. In the strictest sense, this assumption only applies to homogeneous linear differential equations, as discussed in Chapter 2. The homogeneous differential equation describing axisymmetric flow does not take into account areal infiltration. In fact, it is canceled out when the initial steady head is subtracted from the head during pumping to obtain a solution in terms of drawdown. Because of that, some authors are convinced that recharge is not relevant in assessing the sustainability of a groundwater extraction (Bredehoeft, 1997, 2002, 2007; Devlin & Sophocleous, 2005, 2006), which only requires the simulation of the cone of depression.

Louwyck et al. (2023) point to the difference between linear and nonlinear models, and explain how the initial recharge determines whether the assumption of linearity is valid or not. They use the Ernst (1971) model as an example of a nonlinear problem and illustrate that recharge may be important in assessing the sustainability of the extraction. If the nonlinear drainage boundary condition is active at all distances from the pumping well, then the cone of depression is described by the de Glee formula (de Glee, 1930; Jacob, 1946). This equation expresses a linear relation between pumping rate and drawdown, and does not require knowledge of the initial conditions. However, if there is a relatively large zone around the well where the drainage is inactive due to the decrease in head, then the problem cannot be approximated by a linear equation, in which case the initial conditions are relevant. Whether or not the problem can be approximated by a linear equation, is also determined by the recharge, as a relatively large infiltration rate in combination with a relatively large leakage factor is required to keep the no-drainage zone around the well negligibly small (Louwyck et al., 2023). The study by Louwyck et al. (2023) is presented in Chapter 11.

7.1.3. Finite-difference method

Nowadays, the finite-difference method in general and the MODFLOW code in particular (Harbaugh, 2005; Harbaugh et al., 2000; Langevin et al., 2017) are considered state-of-the-art for solving complex groundwater flow problems. These problems are nonlinear in many cases. Examples relevant to this chapter are the convertible layer available with the BCF6 and LPF packages that is used to simulate confined-unconfined flow, and the DRAIN package that is used to define head-dependent boundary conditions which are only allowed to remove water from the aquifer (Harbaugh, 2005; Harbaugh et al., 2000).

Nonlinear problems can be solved by applying Picard and Newton iterations (Mehl, 2006). Earlier versions of MODFLOW apply the former (Harbaugh, 1995; Hill, 1990), while the latest MODFLOW 6 version uses the latter (Langevin et al., 2017). Nonlinearities may cause convergence difficulties, which can be overcome by applying an effective damping strategy. According to Mehl (2006), nonlinear head-dependent boundary conditions can cause more convergence difficulties than the nonlinearity that arises from unconfined flow.

To test the semi-analytical approach presented in this chapter, the Louwyck et al. (2012, 2014) procedure to trick MODFLOW (Harbaugh, 2005) into simulating axisymmetric flow is applied. This procedure is very similar to the method developed by Langevin (2008). However, the Louwyck et al. (2012, 2014) method is more flexible in taking into account radial variations of input parameters, and it can be used to simulate the two types of nonlinear problems studied in this chapter. To model the conversion from confined to unconfined flow, the BCF6 package is used which offers the option to define limited convertible layers. Like the Moench and Prickett (1972) problem, these layers only adapt the storage coefficient when flow changes from confined to unconfined while keeping the transmissivity constant.

The effect of combined areal infiltration and drainage can be simulated easily using the RECHARGE and DRAIN packages available with MODFLOW (Harbaugh, 2005; Harbaugh et al., 2000). In this study, however, the MAxSym code (Louwyck, 2011) is used, which is extended with the option to define drawdown-limited cells (Louwyck, 2015). If a node in the finite-difference grid is drawdown-limited, then a minimum or maximum value for the drawdown is specified, together with an inflow or outflow resistance. In this way, it is possible to define a nonlinear drainage boundary condition, which comprises a drainage level and a drainage resistance given by the user. This is similar to defining a head-dependent flux boundary condition using MODFLOW's DRAIN package (Harbaugh, 2005; Harbaugh et al., 2000). The nonlinearities associated with drawdown-limited cells are solved

using Picard iterations, which are integrated into the SIP solver (Louwyck, 2011). The strongly implicit procedure (Stone, 1968), abbreviated as SIP, is also one of the standard solvers implemented in MODFLOW (Harbaugh, 2005; Harbaugh et al., 2000).

7.1.4. Objective

As already mentioned, two specific well-flow problems will be solved that are described in the hydrogeological literature for a single aquifer: the Moench and Prickett (1972) problem of confined-unconfined flow and the Ernst (1971) problem of combined areal infiltration and drainage. These problems will be generalized to transient axisymmetric flow in a multi-aquifer system. This means the first problem deals with the conversion from confined to unconfined flow in the top layer of the groundwater reservoir, whereas the second problem is about a phreatic system with areal infiltration and drainage in the top layer. Figure 1 visualizes how the aquifer system is schematized in these two cases.

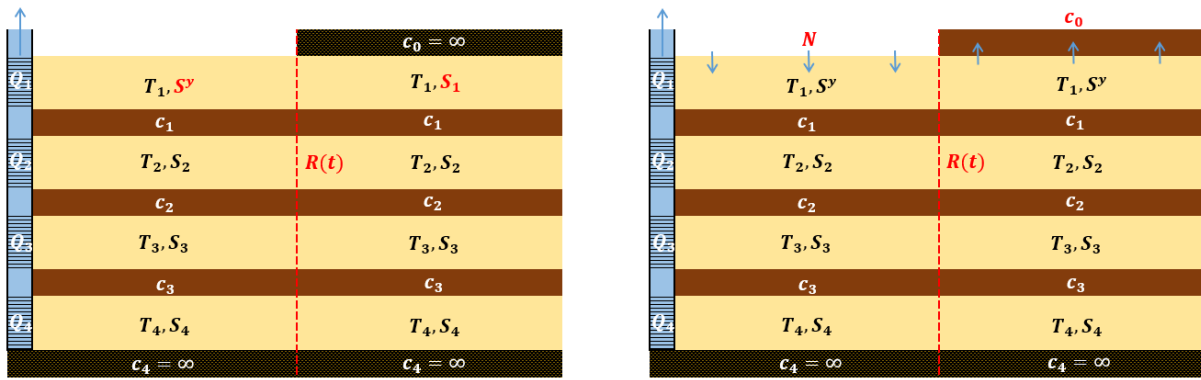


Figure 1. Schematization of the head-dependent two-zone multi-aquifer system for the two types of problems studied in this chapter. The left plot schematizes a confined system which becomes unconfined at distances where the head is lower than the top of the system. The conversion between confined and unconfined flow takes place in the top layer at distance R , which is a function of time t . In the proximal zone around the well, the storativity equals the specific yield S^y of the top aquifer, as this part of the aquifer is unconfined. In the distal zone, which is confined, the storativity S_1 is calculated using the specific storage. The right plot schematizes a phreatic system that is infiltrated at constant rate N and drained by a boundary condition characterized by resistance c_0 . In the proximal zone around the well, the drainage becomes inactive, as the head drops below the drainage level, whereas the drainage is still active in the distal zone. The conversion between drainage and no drainage also occurs in the top layer at distance R . In both cases, transmissivity T_1 is kept constant, even if the flow in the aquifer is unconfined. Discharge Q in each layer is also constant. Aquitards are conceptualized as zero-thickness layers with resistance c . The lower boundary of the aquifer system is impervious. See text for the mathematical statement of the two problems which may include as many aquifers as required.

To solve these problems analytically, they are conceptualized as two models that are coupled by means of a common boundary at which continuity of flow is preserved. More precisely, the outer boundary of the first model representing the proximal zone around the pumping well coincides with the inner boundary of the model representing the distal zone. At this shared boundary, the head and the radial discharge through the cylindrical surface must be the same in each layer of both models. Each of the two models are characterized by the same input parameters, except for the parameters that are head dependent.

In case of a confined aquifer system in which flow in the top layer becomes unconfined where the head is below the top of the system, the storativity in the proximal zone around the pumping well equals the specific yield, while it is equal to the elastic storage coefficient in the distal zone. This is shown in the left plot of Figure 1. If the top layer in the aquifer system is drained, then the resistance of the leaky top boundary condition is infinitely large in the proximal zone where the head is below the drainage level. This infinitely large resistance deactivates the drainage. In the distal zone around

the pumping well, where the drainage is still active, the resistance equals the drainage resistance, as is seen on the right plot of Figure 1.

A semi-analytical solution method is developed in Chapter 5 for simulating axisymmetric multilayer-multizone flow. This method is based on the work of Hemker (1984, 1985, 1999) who decomposes the system matrix into its eigenvalues and eigenvectors in order to uncouple the system of governing differential equations. Hemker's solutions only consider homogeneous layers. In case of multiple zones, the eigendecomposition is applied to each cylindrical zone, and these zones are coupled by preserving continuity of flow at the common boundaries. This leads to a system of linear equations that is solved numerically using LU decomposition, as is explained in Chapter 5. If transient flow is considered, then the Laplace transform is applied first, and the solution obtained in Laplace space is inverted numerically using Stehfest's (1970) algorithm. The problems discussed in this chapter only require two cylindrical zones. In this case, the system of linear equations that determines the integration constants can be solved analytically. This solution is derived first in next section 7.2.

Once the appropriate two-zone model is constructed, an inverse problem must be solved to determine the distance R of the boundary between the two zones. At this distance, the head in the top layer is specified. Because distance R is head-dependent, the inverse problem is nonlinear. It is solved iteratively, starting with an initial guess for R , and optimizing its value by minimizing an objective function that is the absolute difference between the required and the calculated drawdown at distance R in the top layer. A distinction must be made between steady and transient state problems. In case of steady flow, distance R is fixed and must be derived only once. In case of transient flow, distance R is time-dependent, which means the inverse problem must be solved for each time t .

For the two types of problems studied in this chapter, there is no proximal zone at time $t = 0$ when the extraction starts, which implies distance R initially equals zero. The maximum value for R is reached when the aquifer system is brought into a new state of equilibrium. If the system never reaches a new steady state, then the proximal zone continues to enlarge. As the boundary between the two zones is expanding with time, the question arises whether it is justified to apply the fixed two-zone solution for solving these kinds of problems. This question is answered by examining the initial conditions defined for the proximal zone. The exact solution in the Laplace domain derived in this chapter shows that the drawdown simulated for the proximal zone often is insensitive to these initial conditions. If this is true, then it is safe to determine R for each time t using the fixed two-zone solution, in the same way as is done for the steady case.

The main objective of this chapter is to demonstrate how the fixed two-zone solution can be applied to accurately solve the nonlinear problems of confined-unconfined flow and combined areal infiltration and drainage in the top layer of a multi-aquifer system that is extracted by a pumping well. After deriving the exact solution in Laplace space for axisymmetric flow in a multilayered aquifer system consisting of two cylindrical zones, the two problems of interest are stated mathematically. The general two-zone solution is reformulated and simplified taking into account the specific initial and boundary conditions defined for these two problems, and the strategy to solve the inverse problem is discussed specifically for each problem.

The proposed method is semi-analytical as it applies numerical algorithms to perform the eigendecomposition, to invert the solution in Laplace space, and to solve the minimization problem. The stated problems are also solved fully numerically using the finite-difference method. It is explained in detail how the Louwyck et al. (2012, 2014) method for modeling axisymmetric multilayer well-flow using MODFLOW can be applied to simulate confined-unconfined flow and to

take into account areal infiltration and drainage. It is also discussed how the MAXSYM code (Louwyck, 2011) is extended to include nonlinear draining and irrigating boundary conditions (Louwyck, 2015).

The finite-difference method is used to test the semi-analytical approach. For both problems, the test cases are the one-layer model and an example of a hypothetical three-layer system. The analytical one-layer solutions by Moench and Pricket (1972) and by Ernst (1971) are also used to verify the semi-analytical approach. Each example presents the corresponding linear solution, and it is seen that the drawdown may be underestimated significantly if the nonlinear solution is approximated by this linear solution. However, discussing the difference between linear and nonlinear models is not within the scope of this chapter. This important topic is investigated profoundly in Chapter 11.

7.2. Semi-analytical multilayer two-zone solution

In this section, the analytical solution is derived for axisymmetric flow in a multilayer system consisting of two cylindrical zones with fixed boundary. As explained in the introductory section 7.1.4, this solution will be applied to solve the nonlinear problems of confined-unconfined well-flow in a multilayer system and well-flow in an infiltrated and drained multi-aquifer system.

The stated problem is a specific case of the multilayer-multizone problem that was solved in Chapter 5. The difference lies in the way the integration constants are derived from the boundary conditions. Chapter 5 discusses the generalized solution method for an arbitrary number of zones. In the general case, determining the integration constants requires solving a system of $2n_z$ matrix equations, with n_z the number of zones. This is done numerically, for instance, by applying standard LU decomposition. As the number of zones n_z equals 2 in the specific case treated here, the number of matrix equations is 4, which makes it possible to solve the system of equations analytically.

First, the problem of axisymmetric flow in a multilayer system consisting of two cylindrical zones with fixed boundary is stated mathematically. Second, the solution for one zone is derived, which is the same as the solution for a multilayer system consisting of homogeneous layers. This solution is presented in Chapter 2, although it needs to be reformulated here so that the solutions for both zones can be coupled. This is done by applying the conditions at the common boundary that preserve continuity of flow. In this way, the exact solution is obtained in case of steady flow, while it is the exact solution in the Laplace domain in case of transient flow. In the latter case, the Stehfest (1970) algorithm can be applied to invert the Laplace-solution back to the real time domain.

7.2.1. Problem statement

Consider an aquifer system consisting of n_l layers and 2 zones. Transient axisymmetric flow in zone j of layer i is governed by the following partial differential equation:

$$\frac{\partial^2 h_{ij}}{\partial r^2} + \frac{1}{r} \frac{\partial h_{ij}}{\partial r} = \frac{S_{ij}}{T_{ij}} \frac{\partial h_{ij}}{\partial t} + \frac{-N_{ij}}{T_{ij}} + \frac{h_{ij} - h_{i-1,j}}{c_{i-1,j} T_{ij}} + \frac{h_{ij} - h_{i+1,j}}{c_{i,j} T_{ij}} \quad (1 \leq i \leq n_l; j \in \{1,2\}) \quad (1)$$

Hydraulic head h_{ij} [L] is a function of radial distance r [L] and time t [T]. If steady flow is considered, then $\partial h_{ij}/\partial t = 0$ in (1), by definition. In this study, only radial flow is considered, although the problem could also be stated for parallel flow, as is done in previous chapters.

In (1), transmissivity T_{ij} [L^2/T] and storativity S_{ij} [-] of zone j in layer i with constant thickness D_i [L] are defined as, respectively:

$$T_{ij} = K_{ij}^h D_i \quad (1 \leq i \leq n_l; j \in \{1,2\}) \quad (2)$$

$$S_{ij} = S_{ij}^s D_i \quad (1 \leq i \leq n_l; j \in \{1,2\}) \quad (3)$$

with K_{ij}^h the horizontal conductivity [L/T] and S_{ij}^S the specific elastic storage [L^{-1}] of zone j in layer i .

Adjacent layers i and $i + 1$ in zone j are separated by an incompressible resistance layer with zero thickness characterized by hydraulic resistance c_{ij} [T]:

$$c_{ij} = \frac{D_i}{2K_{ij}^v} + \frac{D_{i+1}}{2K_{i+1,j}^v} \quad (1 \leq i < n_l; j \in \{1,2\}) \quad (4)$$

with K_{ij}^v the vertical conductivity [L/T] of zone j in layer i . As explained in section 2.2.1 of Chapter 2, these resistance layers may also be interpreted as incompressible aquitards. The upper and lower boundary of the aquifer system is characterized by resistances $c_{0,j}$ and $c_{n_l,j}$. If a boundary is impervious, then its resistance is infinitely large. Zone j in layer i may be recharged by a constant flux N_{ij} [L/T], which is positive in case of infiltration.

The radial discharge Q_{ij}^h [L^3/T] is defined as the volume of groundwater per unit of time that is flowing through a cylindrical surface with radius r in zone j of layer i at time t :

$$Q_{ij}^h(r, t) = -2\pi T_{ij} r \frac{\partial h_{ij}}{\partial r} \quad (1 \leq i \leq n_l; j \in \{1,2\}) \quad (5)$$

At the inner model boundary, a constant discharge Q_i [L^3/T] is specified in each layer i . This boundary coincides with the face of the pumping well which has a radius equal to r_w [L]:

$$Q_{i,1}^h(r_w, t) = Q_i \quad (1 \leq i \leq n_l) \quad (6)$$

where Q_i is negative in case of pumping. It is assumed that the well-screen in each layer is fully penetrating and not connected to a well-screen in another layer, although it would be possible to state the problem for multilayer wells, as is done in previous Chapter 6.

A constant head φ [L] is defined for the upper and lower boundary conditions and for the outer model boundary condition at distance R_{out} [L]:

$$h_{ij}(r, t) = \varphi_{ij} \quad (i \in \{0, n_l + 1\}; j \in \{1,2\}) \quad (7)$$

$$h_{i,2}(R_{out}, t) = \varphi_{i,2} \quad (1 \leq i \leq n_l) \quad (8)$$

Continuity of flow requires that the head and the radial flow in each layer i is the same in zones 1 and 2 at distance R [L], which corresponds to the boundary between the two zones:

$$h_{i,1}(R, t) = h_{i,2}(R, t) \quad (1 \leq i \leq n_l) \quad (9)$$

$$Q_{i,1}^h(R, t) = Q_{i,2}^h(R, t) \quad (1 \leq i \leq n_l) \quad (10)$$

If transient state is considered, the pumping starts at $t = 0$, and the initial heads [L] are:

$$h_{ij}(r, 0) = \varphi_{ij} \quad (1 \leq i \leq n_l; j \in \{1,2\}) \quad (11)$$

Note that the initial head $\varphi_{i,2}$ in each layer i of the second zone equals the constant head at the outer model boundary according to (8).

7.2.2. Solution for one zone

The solution for one zone is the same as the solution for axisymmetric flow in a laterally bounded aquifer system consisting of homogeneous layers presented in Chapter 2, where the distance for the inner boundary of zone j is r_{in} [L], and the distance of the outer boundary is r_{out} [L]. As discussed in Chapter 2 and Chapter 5, system of equations (1) for zone j may be written in matrix form:

$$\nabla^2 \mathbf{h}_j = \mathbf{A}_j \mathbf{h}_j - \mathbf{b}_j \quad (j \in \{1,2\}) \quad (12)$$

In the steady-state case, $n_l \times 1$ vectors \mathbf{h}_j and \mathbf{b}_j , and $n_l \times n_l$ matrix \mathbf{A}_j are defined as:

$$\mathbf{h}_{ji}(r) = h_{ij}(r) \quad (1 \leq i \leq n_l; j \in \{1,2\}) \quad (13)$$

$$\mathbf{b}_{ji} = \begin{cases} \frac{N_{1,j}}{T_{1,j}} + \frac{\varphi_{0,j}}{c_{0,j} T_{1,j}} & (i = 1) \\ \frac{N_{n_l,j}}{T_{n_l,j}} + \frac{\varphi_{n_l+1,j}}{c_{n_l,j} T_{n_l,j}} & (i = n_l) \quad (j \in \{1,2\}) \\ \frac{N_{ij}}{T_{ij}} & (1 < i < n_l) \end{cases} \quad (14)$$

$$\mathbf{A}_{jik} = \begin{cases} \frac{1}{c_{i-1,j} T_{ij}} + \frac{1}{c_{ij} T_{ij}} & (i = k) \\ \frac{-1}{c_{i-1,j} T_{ij}} & (i = k + 1) \quad (j \in \{1,2\}) \\ \frac{-1}{c_{ij} T_{ij}} & (i = k - 1) \end{cases} \quad (15)$$

In case of transient flow, the Laplace transform \mathcal{L} is applied to (1), and vector \mathbf{h}_j contains the Laplace transformed heads \bar{h} :

$$\mathbf{h}_{ji}(r) = \mathcal{L}\{h_{ij}(r, t)\}(p) = \bar{h}_{ij}(r, p) \quad (1 \leq i \leq n_l; j \in \{1,2\}) \quad (16)$$

where p is the frequency variable [T^{-1}]. Vector \mathbf{b}_j and matrix \mathbf{A}_j are defined accordingly:

$$\mathbf{b}_{ji} = \begin{cases} \frac{N_{1,j}}{p T_{1,j}} + \frac{\varphi_{0,j}}{p c_{0,j} T_{1,j}} + \frac{S_{1,j}}{T_{1,j}} \varphi_{1,j} & (i = 1) \\ \frac{N_{n_l,j}}{p T_{n_l,j}} + \frac{\varphi_{n_l+1,j}}{p c_{n_l,j} T_{n_l,j}} + \frac{S_{n_l,j}}{T_{n_l,j}} \varphi_{n_l,j} & (i = n_l) \quad (j \in \{1,2\}) \\ \frac{N_{ij}}{p T_{ij}} + \frac{S_{ij}}{T_{ij}} \varphi_{ij} & (1 < i < n_l) \end{cases} \quad (17)$$

$$\mathbf{A}_{jik} = \begin{cases} \frac{1}{c_{i-1,j} T_{ij}} + \frac{1}{c_{ij} T_{ij}} + \frac{S_{ij}}{T_{ij}} p & (i = k) \\ \frac{-1}{c_{i-1,j} T_{ij}} & (i = k + 1) \quad (j \in \{1,2\}) \\ \frac{-1}{c_{ij} T_{ij}} & (i = k - 1) \end{cases} \quad (18)$$

Radial discharge Q_{ij}^h can also be written in matrix form:

$$\mathbf{Q}_j^h(r) = -r \mathbf{T}_j \frac{\partial \mathbf{h}_j(r_{in})}{\partial r} \quad (j \in \{1,2\}) \quad (19)$$

where \mathbf{T}_j is an $n_l \times n_l$ diagonal matrix with diagonal terms defined as:

$$\mathbf{T}_{jii} = 2\pi T_{ij} \quad (1 \leq i \leq n_l; j \in \{1,2\}) \quad (20)$$

In the steady-state case, the entries of vector \mathbf{Q}_j^h are:

$$\mathbf{Q}_j^h(r) = Q_{ij}^h(r) \quad (1 \leq i \leq n_l; j \in \{1,2\}) \quad (21)$$

In the transient-state case, vector \mathbf{Q}_j^h contains the Laplace transformed radial discharges:

$$\mathbf{Q}_j^h(r) = \mathcal{L}\{Q_{ij}^h(r, t)\}(p) = \bar{Q}_{ij}^h(r, p) \quad (1 \leq i \leq n_l; j \in \{1,2\}) \quad (22)$$

Using matrices to formulate the inner and outer boundary conditions at distance r_{in} and r_{out} , respectively:

$$\mathbf{Q}_j^h(r_{in}) = \mathbf{Q}_j \quad (j \in \{1,2\}) \quad (23)$$

$$\mathbf{h}_j(r_{out}) = \boldsymbol{\varphi}_j \quad (j \in \{1,2\}) \quad (24)$$

In case of steady state, $n_l \times 1$ vectors \mathbf{Q}_j and $\boldsymbol{\varphi}_j$ are defined as:

$$\mathbf{Q}_{ji} = Q_{ij} \quad (1 \leq i \leq n_l; j \in \{1,2\}) \quad (25)$$

$$\boldsymbol{\varphi}_{ji} = \varphi_{ij} \quad (1 \leq i \leq n_l; j \in \{1,2\}) \quad (26)$$

where Q_{ij} and φ_{ij} are the specified discharge at the inner model boundary and the constant head at the outer model boundary in layer i , respectively. In the transient-state case, the elements of vectors \mathbf{Q}_j and $\boldsymbol{\varphi}_j$ are the Laplace transforms of these constants:

$$\mathbf{Q}_{ji} = Q_{ij}/p \quad (1 \leq i \leq n_l; j \in \{1,2\}) \quad (27)$$

$$\boldsymbol{\varphi}_{ji} = \varphi_{ij}/p \quad (1 \leq i \leq n_l; j \in \{1,2\}) \quad (28)$$

To uncouple the system of differential equations (1), matrix \mathbf{A}_j is decomposed into its eigenvalues and eigenvectors:

$$\mathbf{A}_j = \mathbf{V}_j \mathbf{D}_j \mathbf{V}_j^{-1} \quad (j \in \{1,2\}) \quad (29)$$

with \mathbf{D}_j an $n_l \times n_l$ diagonal matrix containing the n_l strictly positive eigenvalues d_{ij} , and \mathbf{V}_j an $n_l \times n_l$ matrix holding the corresponding eigenvectors in its columns. Only if steady flow is considered and if the lower and upper model boundaries of zone j are impervious, then exactly one eigenvalue d_{ij} equals zero.

The general solution for this problem is well-known and discussed in Chapter 2 and Chapter 5:

$$\mathbf{h}_j(r) = \mathbf{V}_j [\mathbf{I}_j(r) \boldsymbol{\alpha}_j + \mathbf{K}_j(r) \boldsymbol{\beta}_j + \mathbf{m}_j(r)] \quad (j \in \{1,2\}) \quad (30)$$

where \mathbf{I}_j and \mathbf{K}_j are $n_l \times n_l$ diagonal matrices with the following diagonal terms:

$$\mathbf{I}_{jii}(r) = \begin{cases} I_0\left(r\sqrt{d_{ij}}\right) & (d_{ij} \neq 0) \\ \ln(r) & (d_{ij} = 0) \end{cases} \quad (1 \leq i \leq n_l; j \in \{1,2\}) \quad (31)$$

$$\mathbf{K}_{jii}(r) = \begin{cases} K_0\left(r\sqrt{d_{ij}}\right) & (d_{ij} \neq 0) \\ 1 & (d_{ij} = 0) \end{cases} \quad (1 \leq i \leq n_l; j \in \{1,2\}) \quad (32)$$

with I_0 and K_0 the zero order modified Bessel functions of the first and second kind, respectively. Vector \mathbf{m}_j has the following n_l entries:

$$\mathbf{m}_{ji}(r) = \begin{cases} v_{ji}/d_{ij} & (d_{ij} \neq 0) \\ -v_{ji}r^2/4 & (d_{ij} = 0) \end{cases} \quad (1 \leq i \leq n_l; j \in \{1,2\}) \quad (33)$$

with:

$$\mathbf{v}_j = \mathbf{V}_j^{-1} \mathbf{b}_j \quad (j \in \{1,2\}) \quad (34)$$

The radial discharge is also expressed using general solution (30):

$$\mathbf{Q}_j^h(r) = -\mathbf{T}_j \mathbf{V}_j [\mathbf{I}'_j(r) \boldsymbol{\alpha}_j + \mathbf{K}'_j(r) \boldsymbol{\beta}_j + \mathbf{m}'_j(r)] \quad (j \in \{1,2\}) \quad (35)$$

where \mathbf{I}'_j , \mathbf{K}'_j , and \mathbf{m}'_j contain the first derivative with respect to r of the elements in \mathbf{I}_j , \mathbf{K}_j , and \mathbf{m}_j , respectively:

$$\mathbf{I}'_{jii}(r) = \begin{cases} \left(r \sqrt{d_{ij}} \right) \text{I}_1 \left(r \sqrt{d_{ij}} \right) & (d_{ij} \neq 0) \\ 1 & (d_{ij} = 0) \end{cases} \quad (1 \leq i \leq n_l; j \in \{1,2\}) \quad (36)$$

$$\mathbf{K}'_{jii}(r) = \begin{cases} -\left(r \sqrt{d_{ij}} \right) \text{K}_1 \left(r \sqrt{d_{ij}} \right) & (d_{ij} \neq 0) \\ 0 & (d_{ij} = 0) \end{cases} \quad (1 \leq i \leq n_l; j \in \{1,2\}) \quad (37)$$

$$\mathbf{m}'_{ji}(r) = \begin{cases} 0 & (d_{ij} \neq 0) \\ -\mathbf{v}_{ji} r^2 / 2 & (d_{ij} = 0) \end{cases} \quad (1 \leq i \leq n_l; j \in \{1,2\}) \quad (38)$$

with I_1 and K_1 the first order modified Bessel functions of the first and second kind, respectively.

Vectors $\boldsymbol{\alpha}_j$ and $\boldsymbol{\beta}_j$ hold the integration constants that are derived by applying the general solution (30) to boundary conditions (23) and (24). This solution has already been presented in Chapter 2:

$$\boldsymbol{\alpha}_j = -X_j \{ \mathbf{K}_j(r_{out}) [\mathbf{V}_j^{-1} \mathbf{T}_j^{-1} \mathbf{Q}_j + \mathbf{m}'_j(r_{in})] + \mathbf{K}'_j(r_{in}) [\mathbf{V}_j^{-1} \boldsymbol{\varphi}_j - \mathbf{m}_j(r_{out})] \} \quad (j \in \{1,2\}) \quad (39)$$

$$\boldsymbol{\beta}_j = X_j \{ \mathbf{I}_j(r_{out}) [\mathbf{V}_j^{-1} \mathbf{T}_j^{-1} \mathbf{Q}_j + \mathbf{m}'_j(r_{in})] + \mathbf{I}'_j(r_{in}) [\mathbf{V}_j^{-1} \boldsymbol{\varphi}_j - \mathbf{m}_j(r_{out})] \} \quad (j \in \{1,2\}) \quad (40)$$

with:

$$X_j = \{ \mathbf{K}_j(r_{out}) \mathbf{I}'_j(r_{in}) - \mathbf{I}_j(r_{out}) \mathbf{K}'_j(r_{in}) \}^{-1} \quad (j \in \{1,2\}) \quad (41)$$

If $r_{out} \rightarrow \infty$, then $\boldsymbol{\alpha}_j \rightarrow \mathbf{0}$ and $\boldsymbol{\beta}_j \rightarrow -[\mathbf{K}'_j(r_{in})]^{-1} [\mathbf{V}_j^{-1} \mathbf{T}_j^{-1} \mathbf{Q}_j + \mathbf{m}'_j(r_{in})]$. The particular solution for heads \mathbf{h}_j and radial discharges \mathbf{Q}_j^h is found by introducing solution (39) for vector $\boldsymbol{\alpha}_j$ and solution (40) for vector $\boldsymbol{\beta}_j$ into general solution (30) and (35), respectively.

7.2.3. Coupled solution for two zones

To solve the two-zone problem stated in section 7.2.1, the particular solutions for both the proximal zone and the distal zone must be coupled. This means the heads $\boldsymbol{\varphi}_1$ at the outer boundary of the proximal zone and the discharges \mathbf{Q}_2 at the inner boundary of the distal zone must be determined by applying the two additional boundary conditions (9) and (10) that preserve the continuity of flow between the two zones. In matrix form, these internal boundary conditions are reformulated as, respectively:

$$\mathbf{h}_1(R) = \mathbf{h}_2(R) \quad (42)$$

$$\mathbf{Q}_1^h(R) = \mathbf{Q}_2^h(R) \quad (43)$$

In order to couple the solutions for both zones, the particular solution for zone j derived in previous section 7.2.2, is written first in terms of $\boldsymbol{\varphi}_j$ and \mathbf{Q}_j :

$$\mathbf{h}_j(r) = \mathbf{Y}_j(r) \mathbf{Q}_j + \mathbf{Z}_j(r) \boldsymbol{\varphi}_j + \mathbf{z}_j(r) \quad (j \in \{1,2\}) \quad (44)$$

with:

$$\mathbf{Y}_j(r) = \mathbf{V}_j \mathbf{X}_j [\mathbf{K}_j(r) \mathbf{I}_j(r_{out}) - \mathbf{I}_j(r) \mathbf{K}_j(r_{out})] \mathbf{V}_j^{-1} \mathbf{T}_j^{-1} \quad (j \in \{1,2\}) \quad (45)$$

$$\mathbf{Z}_j(r) = \mathbf{V}_j \mathbf{X}_j [\mathbf{K}_j(r) \mathbf{I}'_j(r_{in}) - \mathbf{I}_j(r) \mathbf{K}'_j(r_{in})] \mathbf{V}_j^{-1} \quad (j \in \{1,2\}) \quad (46)$$

$$\begin{aligned} \mathbf{z}_j(r) = & \mathbf{V}_j \mathbf{X}_j [\mathbf{K}_j(r) \mathbf{I}_j(r_{out}) - \mathbf{I}_j(r) \mathbf{K}_j(r_{out})] \mathbf{m}'_j(r_{in}) \\ & + \mathbf{V}_j \mathbf{X}_j [\mathbf{I}_j(r) \mathbf{K}'_j(r_{in}) - \mathbf{K}_j(r) \mathbf{I}'_j(r_{in})] \mathbf{m}_j(r_{out}) \\ & + \mathbf{V}_j \mathbf{m}_j(r) \quad (j \in \{1,2\}) \end{aligned} \quad (47)$$

If $r_{out} \rightarrow 0$, then $\mathbf{X}_j [\mathbf{K}_j(r) \mathbf{I}_j(r_{out}) - \mathbf{I}_j(r) \mathbf{K}_j(r_{out})] \rightarrow -[\mathbf{K}'_j(r_{in})]^{-1} \mathbf{K}_j(r)$.

Similarly, the solution for the radial discharge is rearranged to:

$$\mathbf{Q}_j^h(r) = \mathbf{Y}'_j(r) \mathbf{Q}_j + \mathbf{Z}'_j(r) \boldsymbol{\varphi}_j + \mathbf{z}'_j(r) \quad (j \in \{1,2\}) \quad (48)$$

with:

$$\mathbf{Y}'_j(r) = \mathbf{T}_j \mathbf{V}_j \mathbf{X}_j [\mathbf{I}'_j(r) \mathbf{K}_j(r_{out}) - \mathbf{K}'_j(r) \mathbf{I}_j(r_{out})] \mathbf{V}_j^{-1} \mathbf{T}_j^{-1} \quad (j \in \{1,2\}) \quad (49)$$

$$\mathbf{Z}'_j(r) = \mathbf{T}_j \mathbf{V}_j \mathbf{X}_j [\mathbf{I}'_j(r) \mathbf{K}'_j(r_{in}) - \mathbf{K}'_j(r) \mathbf{I}'_j(r_{in})] \mathbf{V}_j^{-1} \quad (j \in \{1,2\}) \quad (50)$$

$$\begin{aligned} \mathbf{z}'_j(r) = & \mathbf{T}_j \mathbf{V}_j \mathbf{X}_j [\mathbf{I}'_j(r) \mathbf{K}_j(r_{out}) - \mathbf{K}'_j(r) \mathbf{I}_j(r_{out})] \mathbf{m}'_j(r_{in}) \\ & + \mathbf{T}_j \mathbf{V}_j \mathbf{X}_j [\mathbf{K}'_j(r) \mathbf{I}'_j(r_{in}) - \mathbf{I}'_j(r) \mathbf{K}'_j(r_{in})] \mathbf{m}_j(r_{out}) \\ & - \mathbf{T}_j \mathbf{V}_j \mathbf{m}'_j(r) \quad (j \in \{1,2\}) \end{aligned} \quad (51)$$

For the proximal zone ($j = 1$), distances r_{in} and r_{out} must be substituted by r_w and R , respectively, whereas these distances must be substituted by R and R_{out} , respectively, for the distal zone ($j = 2$). The specified discharges at the inner boundary of the first zone are equal to the pumping rates Q_i according to boundary condition (6), while the constant heads at the outer boundary of the second zone are equal to $\varphi_{i,2}$ according to boundary condition (8). This means $\mathbf{Q}_1 = \mathbf{Q}$ and $\boldsymbol{\varphi}_2 = \boldsymbol{\varphi}$, where \mathbf{Q} and $\boldsymbol{\varphi}$ are $n_l \times 1$ vectors. In the steady-state case, the entries of these vectors are, respectively:

$$Q_i = Q_i \quad (1 \leq i \leq n_l) \quad (52)$$

$$\boldsymbol{\varphi}_i = \varphi_{i,2} \quad (1 \leq i \leq n_l) \quad (53)$$

In the transient-state case, these vectors contain the Laplace transform of the pumping rates and the constant heads, respectively:

$$Q_i = Q_i/p \quad (1 \leq i \leq n_l) \quad (54)$$

$$\boldsymbol{\varphi}_i = \varphi_{i,2}/p \quad (1 \leq i \leq n_l) \quad (55)$$

Additionally, internal boundary conditions (42) and (43) must be applied; hence, $\boldsymbol{\varphi}_1 = \mathbf{h}_2(R)$ and $\mathbf{Q}_2 = \mathbf{Q}_1^h(R)$. Performing all of these substitutions gives the exact solution for the problem stated in section 7.2.1:

$$\begin{cases} \mathbf{h}_1(r) = \mathbf{Y}_1(r) \mathbf{Q} + \mathbf{Z}_1(r) \mathbf{h}_2(R) + \mathbf{z}_1(r) & (r \leq R) \\ \mathbf{h}_2(r) = \mathbf{Y}_2(r) \mathbf{Q}_1^h(R) + \mathbf{Z}_2(r) \boldsymbol{\varphi} + \mathbf{z}_2(r) & (r \geq R) \end{cases} \quad (56)$$

with:

$$\mathbf{Q}_1^h(R) = \mathbf{Y}'_1(R) \mathbf{Q} + \mathbf{Z}'_1(R) \mathbf{h}_2(R) + \mathbf{z}'_1(R) \quad (57)$$

Expression (57) is used to substitute $\mathbf{Q}_1^h(R)$ in the second equation of (56) with $r = R$. Rearranging the obtained expression finally gives the expression to calculate $\mathbf{h}_2(R)$:

$$\mathbf{h}_2(R) = [\mathbf{I} - \mathbf{Y}_2(R)\mathbf{Z}'_1(R)]^{-1}\{\mathbf{Y}_2(R)[\mathbf{Y}'_1(R)\mathbf{Q} + \mathbf{z}'_1(R)] + \mathbf{Z}_2(R)\boldsymbol{\varphi} + \mathbf{z}_2(R)\} \quad (58)$$

with \mathbf{I} the $n_l \times n_l$ identity matrix.

Summarizing, the two-zone solution is found by calculating $\mathbf{h}_2(R)$ using equation (58). Introducing this vector into equation (57) gives $\mathbf{Q}_1^h(R)$. Both vectors are required to calculate $\mathbf{h}_1(r)$ and $\mathbf{h}_2(r)$ using (56). Similarly, the radial discharge is found by evaluating the following expression:

$$\begin{cases} \mathbf{Q}_1^h(r) = \mathbf{Y}'_1(r)\mathbf{Q} + \mathbf{Z}'_1(r)\mathbf{h}_2(R) + \mathbf{z}'_1(r) & (r \leq R) \\ \mathbf{Q}_2^h(r) = \mathbf{Y}'_2(r)\mathbf{Q}_1^h(R) + \mathbf{Z}'_2(r)\boldsymbol{\varphi} + \mathbf{z}'_2(r) & (r \geq R) \end{cases} \quad (59)$$

Recall that in case of transient flow, solutions (56) and (59) are the Laplace transform of the heads and the discharges, respectively. These solutions need to be inverted, which is done numerically by applying the Stehfest (1970) algorithm.

7.2.4. Verification

As the solution derived in previous section 7.2.3 is just a special case of the general multilayer-multizone solution presented in Chapter 5, the latter can be used to test the first. Results are not shown here, but the exact same results are obtained using both solution methods. It is also interesting to notice that in case of a single confined aquifer consisting of two zones with different transmissivities and storativities, the solution in the Laplace domain simplifies to the one presented by Butler (1988).

7.3. Multilayer head-dependent two-zone problems

In this section, the problem of axisymmetric flow toward a pumping well in a multilayer system consisting of two head-dependent cylindrical zones is discussed in general. Next sections 7.4 and 7.5 focus on two specific problems that are covered by this problem statement: confined-unconfined well-flow in a multilayer system, and well-flow in an infiltrated and drained multi-aquifer system.

First, the problem is stated mathematically, after which a semi-analytical solution method is presented. The semi-analytical approach applies the solution derived in previous section 7.2, which can be simplified here, as the problem is formulated in terms of drawdown, and because of some specific boundary conditions, such as an infinitesimal well. To find the distance of the boundary between the two zones, an inverse problem must be solved, which is done using a nonlinear solver. In the transient case, this distance is time-dependent, and therefore, it is examined whether it is justified to apply the fixed two-zone solution. This is achieved by investigating the sensitivity of the initial conditions for the proximal zone.

Finally, it is discussed how the problem can be solved numerically using the finite-difference method. Although it is generally more straightforward to solve nonlinear problems numerically, convergence difficulties may arise. It is explained how Picard iterations are used to deal with the nonlinearities. Confined-unconfined flow can be simulated using the limited convertible layer option implemented in the BCF6 package, whereas the DRAIN package can be used to define areal drainage (Harbaugh, 2005; Harbaugh et al., 2000). Both options are allowed if MODFLOW is used to simulate axisymmetric multilayer flow according to the Louwyck et al. (2012, 2014) method. Alternatively, the extended version of the MAxSym tool (Louwyck, 2011) can be used to simulate the effect of combined infiltration and drainage (Louwyck, 2015).

7.3.1. Problem statement

The solutions of the head-dependent two-zone problems solved in this chapter are expressed in terms of drawdown. This implies the principle of superposition is applicable, and if not, then it is assumed there is no flow in the aquifer system before the pumping starts, which means that the head in each layer i and at all distances r is the same and equal to φ [L]. Drawdown s [L] is defined as:

$$s_{ij}(r, t) = h_{ij}(r, t) - h_{ij}(r, 0) \quad (1 \leq i \leq n_l; j \in \{1,2\}) \quad (60)$$

Partial differential equation (1) is rewritten using definition (60):

$$\frac{\partial^2 s_{ij}}{\partial r^2} + \frac{1}{r} \frac{\partial s_{ij}}{\partial r} = \frac{S_{ij}}{T_{ij}} \frac{\partial s_{ij}}{\partial t} + \frac{-N_{ij}}{T_{ij}} + \frac{s_{ij} - s_{i-1,j}}{c_{i-1,j} T_{ij}} + \frac{s_{ij} - s_{i+1,j}}{c_{ij} T_{ij}} \quad (1 \leq i \leq n_l; j \in \{1,2\}) \quad (61)$$

Infiltration flux N_{ij} is only relevant if the aquifer system is phreatic, in which case the upper resistance $c_{0,j}$ is set to an infinitely large value, and a positive value is assigned to parameters $N_{1,j}$ of the infiltrated top layer. The infiltration flux of the other layers is set to zero. Note that the thickness of the top layer is implicitly kept constant in each zone, which implies the head change remains negligibly small with respect to the saturated thickness of the top layer.

Radial discharge Q_{ij}^h according to (5) is also redefined using drawdown s :

$$Q_{ij}^h(r, t) = -2\pi T_{ij} r \frac{\partial s_{ij}}{\partial r} \quad (1 \leq i \leq n_l; j \in \{1,2\}) \quad (62)$$

It is assumed the pumping well has an infinitesimal radius r_w :

$$\lim_{r_w \rightarrow 0} Q_{i,1}^h(r_w, t) = Q_i \quad (1 \leq i \leq n_l) \quad (63)$$

The constant drawdowns at the top of the aquifer system and at the outer boundary are all equal to zero, respectively:

$$s_{0,j}(r, t) = 0 \quad (j \in \{1,2\}) \quad (64)$$

$$s_{i,2}(\infty, t) = 0 \quad (1 \leq i \leq n_l) \quad (65)$$

Note that there is no constant head defined for the lower boundary as it is assumed impervious, or $c_{n_l,1} = c_{n_l,2} = \infty$. It is also assumed the aquifer system is unbounded which explains the outer boundary at infinity in equation (65).

The conditions (9) and (10) at the boundary between the two zones are also reformulated using drawdown s :

$$s_{i,1}(R, t) = s_{i,2}(R, t) \quad (1 \leq i \leq n_l) \quad (66)$$

$$Q_{i,1}^h(R, t) = Q_{i,2}^h(R, t) \quad (1 \leq i \leq n_l) \quad (67)$$

So far, the problem statement is just a reformulation of the problem stated in section 7.2.1 for axisymmetric flow in an aquifer system consisting of two fixed zones. Recall that the boundary between the two zones is at distance R , which is specified by the user. However, in this chapter, two problems are studied in which distance R depends on the head in the top layer that is specified at that distance. This means an additional condition is defined for the drawdown at distance R :

$$s_{1,1}(R, t) = s_{1,2}(R, t) = s_c \quad (68)$$

where drawdown s_c [L] is specified in advance. Condition (68) states that the drawdown in the top layer ($i = 1$) at the boundary between zones 1 and 2 must be equal to s_c , which is specified by the user. Drawdown s_c is assumed constant here, although it may be time-varying. It may also be defined for other than the top layer.

In case of steady flow, the drawdowns in the aquifer system are not a function of time; hence, R is a fixed distance that needs to be determined by applying condition (68). In the transient case, heads do vary with time, and consequently, so does distance R , which is a function of time t in this case. This implies that in general, distance $R(t)$ has to be derived from condition (68) for each time t .

When the pumping starts at $t = 0$, distance $R(0)$ is equal to the inner model radius, i.e. $r_w \rightarrow 0$. As a consequence, the initial conditions only apply to the drawdowns in the second zone, which are zero:

$$s_{i,2}(r, 0) = 0 \quad (1 \leq i \leq n_l) \quad (69)$$

During the extraction, $R(t)$ increases until a new state of equilibrium is reached, and the proximal zone stops expanding. In this case, $R(\infty)$ coincides with distance R of the boundary between the two zones in the corresponding steady-state model. If the system never reaches a new steady state, then the proximal zone continues to expand until it reaches the outer model boundary. In this case, $R(\infty)$ equals the distance of the outer model boundary, which is infinitely large according to (65).

7.3.2. Semi-analytical solution method

This section explains how the two-zone solution derived in section 7.2 can be used to solve the problem stated in previous section 7.3.1. The solution can be simplified as the problem is expressed in terms of drawdown and because it defines specific boundary conditions. Especially the transient-state solution is reduced drastically, revealing that the initial conditions defined for the proximal zone are not relevant in many cases. Although this is not a mathematical proof that justifies the use of the fixed two-zone solution to solve the problem of transient flow in an aquifer system with head-dependent zones, it is a plausible explanation why this solution could be very accurate, as is demonstrated by the examples in the next sections.

Finally, it is discussed how the two-zone solution is coupled to a nonlinear solver to determine the distance of the boundary between the two zones. The drawdown in the top layer at this distance is known, which means an inverse problem must be solved. The objective function is defined as the absolute value of the difference between the required and the calculated drawdown. In the steady-state case, this distance only needs to be determined once, while the minimization problem is solved for each simulation time in the transient-state case.

7.3.2.1. Steady state solution

The steady-state problem can be solved easily using the solution derived in section 7.2.3. As the problem stated in section 7.3.1 is expressed in terms of drawdown, vector \mathbf{s}_j is defined holding the drawdowns for each layer i :

$$s_{ji}(r) = s_{ij}(r) \quad (1 \leq i \leq n_l; j \in \{1,2\}) \quad (70)$$

The two-zone solution (56) can now be formulated using vector \mathbf{s}_j :

$$\begin{cases} \mathbf{s}_1(r) = \mathbf{Y}_1(r)\mathbf{Q} + \mathbf{Z}_1(r)\mathbf{s}_2(R) + \mathbf{z}_1(r) & (r \leq R) \\ \mathbf{s}_2(r) = \mathbf{Y}_2(r)\mathbf{Q}^h(R) + \mathbf{z}_2(r) & (r \geq R) \end{cases} \quad (71)$$

with:

$$\mathbf{Q}^h(R) = \mathbf{Y}'_1(R)\mathbf{Q} + \mathbf{Z}'_1(R)\mathbf{s}_2(R) + \mathbf{z}'_1(R) \quad (72)$$

$$\mathbf{s}_2(R) = [\mathbf{I} - \mathbf{Y}_2(R)\mathbf{Z}'_1(R)]^{-1}\{\mathbf{Y}_2(R)[\mathbf{Y}'_1(R)\mathbf{Q} + \mathbf{z}'_1(R)] + \mathbf{z}_2(R)\} \quad (73)$$

The radial discharge \mathbf{Q}_j^h in each zone is:

$$\begin{cases} \mathbf{Q}_1^h(r) = \mathbf{Y}'_1(r)\mathbf{Q} + \mathbf{Z}'_1(r)\mathbf{s}_2(R) + \mathbf{z}'_1(r) & (r \leq R) \\ \mathbf{Q}_2^h(r) = \mathbf{Y}'_2(r)\mathbf{Q}_1^h(R) + \mathbf{z}'_2(r) & (r \geq R) \end{cases} \quad (74)$$

Since the constant drawdowns are all equal to zero according to boundary conditions (64) and (65), $\boldsymbol{\varphi} = \mathbf{0}$, which explains why the term containing $\boldsymbol{\varphi}$ in the second equation of (71) and (74) is absent.

The inner model boundary is infinitesimal, i.e. $r_w \rightarrow 0$. This results in the following simplifications for the proximal zone ($j = 1$):

$$\lim_{r_w \rightarrow 0} \mathbf{I}'_{1,ii}(r_w) = \begin{cases} 0 & (d_{i,1} \neq 0) \\ 1 & (d_{i,1} = 0) \end{cases} \quad (1 \leq i \leq n_l) \quad (75)$$

$$\lim_{r_w \rightarrow 0} \mathbf{K}'_{1,ii}(r_w) = \begin{cases} -1 & (d_{i,1} \neq 0) \\ 0 & (d_{i,1} = 0) \end{cases} \quad (1 \leq i \leq n_l) \quad (76)$$

$$\lim_{r_w \rightarrow 0} \mathbf{m}'_{1,ii}(r_w) = 0 \quad (1 \leq i \leq n_l) \quad (77)$$

The outer boundary is infinitely large; hence, all eigenvalues must be nonzero to assure a finite solution is obtained. As $d_{i,2} > 0$ for $1 \leq i \leq n_l$, and $R_{out} \rightarrow \infty$, the following simplifications hold for the distal zone:

$$\lim_{R_{out} \rightarrow \infty} \mathbf{I}_{2,ii}(R_{out}) = \infty \quad (1 \leq i \leq n_l) \quad (78)$$

$$\lim_{R_{out} \rightarrow \infty} \mathbf{K}_{2,ii}(R_{out}) = 0 \quad (1 \leq i \leq n_l) \quad (79)$$

$$\mathbf{m}_2(r) = \mathbf{D}_2^{-1}\mathbf{V}_2^{-1}\mathbf{b}_2 \quad (80)$$

$$\mathbf{m}'_2(r) = \mathbf{0} \quad (81)$$

This simplifies \mathbf{Y}_2 , \mathbf{z}_2 , \mathbf{Y}'_2 , and \mathbf{z}'_2 to the following expressions:

$$\mathbf{Y}_2(r) = -\mathbf{V}_2[\mathbf{K}'_2(R)]^{-1}\mathbf{K}_2(r)\mathbf{V}_2^{-1}\mathbf{T}_2^{-1} \quad (82)$$

$$\mathbf{z}_2(r) = \mathbf{V}_2\mathbf{D}_2^{-1}\mathbf{V}_2^{-1}\mathbf{b}_2 \quad (83)$$

$$\mathbf{Y}'_2(r) = \mathbf{T}_2\mathbf{V}_2[\mathbf{K}'_2(R)]^{-1}\mathbf{K}'_2(r)\mathbf{V}_2^{-1}\mathbf{T}_2^{-1} \quad (84)$$

$$\mathbf{z}'_2(r) = \mathbf{0} \quad (85)$$

7.3.2.2. Transient state solution

Using the two-zone solution derived in section 7.2.3 to solve the transient-state problem stated in section 7.3.1 is not as obvious as it is for the steady-state problem. Indeed, the two-zone solution assumes a fixed boundary between the proximal and the distal zone, whereas the stated transient problem defines a boundary that expands with time. Therefore, the working hypothesis is that an approximate solution for the problem stated in section 7.3.1 can be obtained by simulating axisymmetric flow in a multilayered aquifer system with two fixed zones, where the initial drawdowns in the proximal zone are set to the required drawdown s_c at distance $R(t)$ according to condition (68):

$$s_{i,1}(r, 0) = s_c \quad (1 \leq i \leq n_l) \quad (86)$$

Under the assumption expressed by (86), the transient state problem for a given time t can be solved in the same way as the steady state problem by solving equation (68) to determine distance $R(t)$. Therefore, the general solution derived in section 7.2.3 is adopted here.

In the transient case, vector \mathbf{s}_j holds the Laplace transform of the drawdowns:

$$\mathbf{s}_{ji}(r) = \mathcal{L}\{s_{ij}(r, t)\}(p) = \bar{s}_{ij}(r, p) \quad (1 \leq i \leq n_l; j \in \{1, 2\}) \quad (87)$$

Taking into account initial condition (86) and boundary condition (64), vector \mathbf{b}_1 for the proximal zone is defined as:

$$\mathbf{b}_{1,i} = \frac{N_{i,1}}{pT_{i,1}} + \frac{S_{i,1}}{T_{i,1}} s_{i,2}(R, t) = \frac{N_{i,1}}{pT_{i,1}} + \frac{S_{i,1}}{T_{i,1}} s_c \quad (1 \leq i \leq n_l) \quad (88)$$

As the constant and initial drawdowns in the distal zone are all equal to zero according to (64), (65), and (69), the entries of vector \mathbf{b}_2 reduce to:

$$\mathbf{b}_{2,i} = \frac{N_{i,2}}{pT_{i,2}} \quad (1 \leq i \leq n_l) \quad (89)$$

Vectors \mathbf{b}_1 and \mathbf{b}_2 can be written in matrix form:

$$\mathbf{b}_1 = \mathbf{v}_1 + \Psi_1 s_c \quad (90)$$

$$\mathbf{b}_2 = \mathbf{v}_2 \quad (91)$$

The elements of $n_l \times 1$ vector \mathbf{v}_j are:

$$\mathbf{v}_{ji} = \begin{cases} \frac{N_{ij}}{pT_{ij}} & (i = 1) \\ 0 & (1 < i \leq n_l) \end{cases} \quad (92)$$

Matrix Ψ_j is an $n_l \times n_l$ diagonal matrix with nonzero entries equal to:

$$\Psi_{jii} = \frac{S_{ij}}{T_{ij}} \quad (1 \leq i \leq n_l) \quad (93)$$

Expressing the generalized two-zone solution (56) using vector \mathbf{s}_j with $\boldsymbol{\varphi} = \mathbf{0}$ gives:

$$\begin{cases} \mathbf{s}_1(r) = \mathbf{Y}_1(r)\mathbf{Q} + \mathbf{Z}_1(r)\mathbf{s}_2(R) + \mathbf{z}_1(r) & (r \leq R) \\ \mathbf{s}_2(r) = \mathbf{Y}_2(r)\mathbf{Q}_1^h(R) + \mathbf{z}_2(r) & (r \geq R) \end{cases} \quad (94)$$

with:

$$\mathbf{Q}_1^h(R) = \mathbf{Y}'_1(R)\mathbf{Q} + \mathbf{Z}'_1(R)\mathbf{s}_2(R) + \mathbf{z}'_1(R) \quad (95)$$

$$\mathbf{s}_2(R) = [\mathbf{I} - \mathbf{Y}_2(R)\mathbf{Z}'_1(R)]^{-1}[\mathbf{Y}_2(R)[\mathbf{Y}'_1(R)\mathbf{Q} + \mathbf{z}'_1(R)] + \mathbf{z}_2(R)] \quad (96)$$

The radial discharge \mathbf{Q}_j^h in each zone is:

$$\begin{cases} \mathbf{Q}_1^h(r) = \mathbf{Y}'_1(r)\mathbf{Q} + \mathbf{Z}'_1(r)\mathbf{s}_2(R) + \mathbf{z}'_1(r) & (r \leq R) \\ \mathbf{Q}_2^h(r) = \mathbf{Y}'_2(r)\mathbf{Q}_1^h(R) + \mathbf{z}'_2(r) & (r \geq R) \end{cases} \quad (97)$$

Since the radius of the inner model boundary is infinitesimal, i.e. $r_w \rightarrow 0$, and all eigenvalues are nonzero as transient flow is considered, that is $d_{i,1} > 0$ for $1 \leq i \leq n_l$, the following simplifications are valid for the proximal zone ($j = 1$):

$$\lim_{r_w \rightarrow 0} \mathbf{I}'_{1,ii}(r_w) = 0 \quad (1 \leq i \leq n_l) \quad (98)$$

$$\lim_{r_w \rightarrow 0} \mathbf{K}'_{1,ii}(r_w) = -1 \quad (1 \leq i \leq n_l) \quad (99)$$

$$\mathbf{m}_1(r) = \mathbf{D}_1^{-1} \mathbf{V}_1^{-1} [\mathbf{v}_1 + \boldsymbol{\Psi}_1 s_c] \quad (100)$$

$$\mathbf{m}'_1(r) = \mathbf{0} \quad (101)$$

This reduces \mathbf{Y}_1 , \mathbf{Z}_1 , \mathbf{z}_1 , \mathbf{Y}'_1 , \mathbf{Z}'_1 , and \mathbf{z}'_1 to the following expressions:

$$\mathbf{Y}_1(r) = \mathbf{V}_1 [\mathbf{K}_1(r) - \mathbf{U}(r) \mathbf{K}_1(R)] \mathbf{V}_1^{-1} \mathbf{T}_1^{-1} \quad (102)$$

$$\mathbf{Z}_1(r) = \mathbf{V}_1 \mathbf{U}(r) \mathbf{V}_1^{-1} \quad (103)$$

$$\mathbf{z}_1(r) = \mathbf{V}_1 [\mathbf{I} - \mathbf{U}(r)] \mathbf{D}_1^{-1} \mathbf{V}_1^{-1} [\mathbf{v}_1 + \boldsymbol{\Psi}_1 s_c] \quad (104)$$

$$\mathbf{Y}'_1(r) = \mathbf{T}_1 \mathbf{V}_1 [\mathbf{U}'(r) \mathbf{K}_1(R) - \mathbf{K}'_1(r)] \mathbf{V}_1^{-1} \mathbf{T}_1^{-1} \quad (105)$$

$$\mathbf{Z}'_1(r) = -\mathbf{T}_1 \mathbf{V}_1 \mathbf{U}'(r) \mathbf{V}_1^{-1} \quad (106)$$

$$\mathbf{z}'_1(r) = \mathbf{T}_1 \mathbf{V}_1 \mathbf{U}'(r) \mathbf{D}_1^{-1} \mathbf{V}_1^{-1} [\mathbf{v}_1 + \boldsymbol{\Psi}_1 s_c] \quad (107)$$

with:

$$\mathbf{U}(r) = [\mathbf{I}_1(R)]^{-1} \mathbf{I}_1(r) \quad (108)$$

$$\mathbf{U}'(r) = [\mathbf{I}_1(R)]^{-1} \mathbf{I}'_1(r) \quad (109)$$

As $d_{i,2} > 0$ for $1 \leq i \leq n_l$, and $R_{out} \rightarrow \infty$, the following is true for the distal zone ($j = 2$):

$$\lim_{R_{out} \rightarrow \infty} \mathbf{I}_{2,ii}(R_{out}) = \infty \quad (1 \leq i \leq n_l) \quad (110)$$

$$\lim_{R_{out} \rightarrow \infty} \mathbf{K}_{2,ii}(R_{out}) = 0 \quad (1 \leq i \leq n_l) \quad (111)$$

$$\mathbf{m}_2(r) = \mathbf{D}_2^{-1} \mathbf{V}_2^{-1} \mathbf{v}_2 \quad (112)$$

$$\mathbf{m}'_2(r) = \mathbf{0} \quad (113)$$

This simplifies \mathbf{Y}_2 , \mathbf{z}_2 , \mathbf{Y}'_2 , and \mathbf{z}'_2 to:

$$\mathbf{Y}_2(r) = -\mathbf{V}_2 \mathbf{W}(r) \mathbf{V}_2^{-1} \mathbf{T}_2^{-1} \quad (114)$$

$$\mathbf{z}_2(r) = \mathbf{V}_2 \mathbf{D}_2^{-1} \mathbf{V}_2^{-1} \mathbf{v}_2 \quad (115)$$

$$\mathbf{Y}'_2(r) = \mathbf{T}_2 \mathbf{V}_2 \mathbf{W}'(r) \mathbf{V}_2^{-1} \mathbf{T}_2^{-1} \quad (116)$$

$$\mathbf{z}'_2(r) = \mathbf{0} \quad (117)$$

with:

$$\mathbf{W}(r) = [\mathbf{K}'_2(R)]^{-1} \mathbf{K}_2(r) \quad (118)$$

$$\mathbf{W}'(r) = [\mathbf{K}'_2(R)]^{-1} \mathbf{K}'_2(r) \quad (119)$$

Recall that \mathbf{Z}_2 and \mathbf{Z}'_2 are irrelevant here as the constant drawdowns at the outer boundary are zero, that is $\boldsymbol{\phi} = \mathbf{0}$.

Introducing (102-107) and (114-117) into (94), simplifies the transient drawdown solution to:

$$\begin{cases} \mathbf{s}_1(r) = \mathbf{V}_1[\mathbf{K}_1(r) - \mathbf{U}(r)\mathbf{K}_1(R)]\mathbf{V}_1^{-1}\mathbf{T}_1^{-1}\mathbf{Q} + \mathbf{V}_1\mathbf{U}(r)\mathbf{V}_1^{-1}\mathbf{s}_2(R) \\ \quad + \mathbf{V}_1[\mathbf{I} - \mathbf{U}(r)]\mathbf{D}_1^{-1}\mathbf{V}_1^{-1}[\mathbf{v}_1 + \Psi_1 s_c] \\ \mathbf{s}_2(r) = -\mathbf{V}_2\mathbf{W}(r)\mathbf{V}_2^{-1}\mathbf{T}_2^{-1}\mathbf{Q}_1^h(R) + \mathbf{V}_2\mathbf{D}_2^{-1}\mathbf{V}_2^{-1}\mathbf{v}_2 \end{cases} \quad (120)$$

Similarly, solution (59) for the radial discharge can be simplified to:

$$\begin{cases} \mathbf{Q}_1^h(r) = \mathbf{T}_1\mathbf{V}_1[\mathbf{U}'(r)\mathbf{K}_1(R) - \mathbf{K}'_1(r)]\mathbf{V}_1^{-1}\mathbf{T}_1^{-1}\mathbf{Q} - \mathbf{T}_1\mathbf{V}_1\mathbf{U}'(r)\mathbf{V}_1^{-1}\mathbf{s}_2(R) \\ \quad + \mathbf{T}_1\mathbf{V}_1\mathbf{U}'(r)\mathbf{D}_1^{-1}\mathbf{V}_1^{-1}[\mathbf{v}_1 + \Psi_1 s_c] \\ \mathbf{Q}_2^h(r) = \mathbf{T}_2\mathbf{V}_2\mathbf{W}'(r)\mathbf{V}_2^{-1}\mathbf{T}_2^{-1}\mathbf{Q}_1^h(R) \end{cases} \quad (121)$$

Solution (120) and (121) are inverted numerically by applying the Stehfest (1970) algorithm.

Taking a closer look at diagonal matrix $\mathbf{U}(r)$, it is seen the diagonal terms all contain the function $I_0(x)/I_0(X)$ where $x \leq X$. This function is always between 0 and 1, as is seen in Figure 2. Moreover, if X is small, then the function is always very close or equal to 1, whereas it is close or equal to 0 if X is large and $x < X$. Recall that $x = r\sqrt{d_{i,1}}$ and $X = R\sqrt{d_{i,1}}$ with $d_{i,1}$ an eigenvalue of system matrix \mathbf{A}_1 . For small values of time t , distance R is very small; hence, $\mathbf{U}(r) \rightarrow \mathbf{I}$. For large values of time t , Laplace variable p approximates zero, and consequently, the eigenvalues are small, and $\mathbf{U}(r) \rightarrow \mathbf{I}$. Summarizing, diagonal matrix \mathbf{U} can be approximated by the identity matrix \mathbf{I} in many cases.

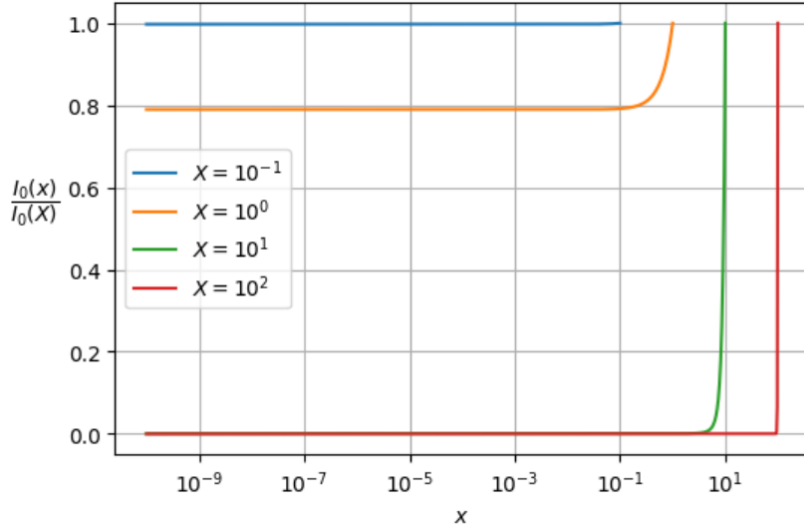


Figure 2. Plot of function $I_0(x)/I_0(X)$ where $x \leq X$ for different values of X . It is seen that the function approximates 1 for small values of X .

If it is assumed that $\mathbf{U}(r) \approx \mathbf{I}$, then solution (120) can be approximated as:

$$\begin{cases} \mathbf{s}_1(r) = \mathbf{V}_1[\mathbf{K}_1(r) - \mathbf{K}_1(R)]\mathbf{V}_1^{-1}\mathbf{T}_1^{-1}\mathbf{Q} + \mathbf{s}_2(R) + \mathbf{V}_1[\mathbf{I} - \mathbf{U}(r)]\mathbf{D}_1^{-1}\mathbf{V}_1^{-1}\mathbf{v}_1 \\ \mathbf{s}_2(r) = -\mathbf{V}_2\mathbf{W}(r)\mathbf{V}_2^{-1}\mathbf{T}_2^{-1}\mathbf{Q}_1^h(R) + \mathbf{V}_2\mathbf{D}_2^{-1}\mathbf{V}_2^{-1}\mathbf{v}_2 \end{cases} \quad (122)$$

with:

$$\mathbf{Q}_1^h(R) = -\mathbf{T}_1\mathbf{V}_1\mathbf{K}'_1(R)\mathbf{V}_1^{-1}\mathbf{T}_1^{-1}\mathbf{Q} + \mathbf{T}_1\mathbf{V}_1\mathbf{U}'(R)\mathbf{D}_1^{-1}\mathbf{V}_1^{-1}\mathbf{v}_1 \quad (123)$$

As $\mathbf{Q}_1^h(R)$ does not depend on $\mathbf{s}_2(R)$ in this approximate solution, $\mathbf{s}_2(R)$ is found simply by evaluating the second equation in (122) for $r = R$, after substituting $\mathbf{Q}_1^h(R)$ using expression (123). Note that the term containing \mathbf{v}_1 is not left out of the first equation in (122), as it turns out it may not be ignored for large values of time if there is a nonzero infiltration flux defined for the top layer. The reason is that $N_{1,1}/p$ becomes significantly large as $p \rightarrow 0$ for large values of time.

In the approximate solution given by (122), there is no term containing $\Psi_1 s_c$, which means the initial drawdowns are not relevant. In this case, it is justified to use the two-zone solution with fixed boundary to solve the transient-state problem with time-dependent distance R , as drawdown in the proximal zone at a given time t is not affected significantly by the evolution of drawdown in the period between $t = 0$ and time t .

Theoretically, the following approximation must hold for time t : $I_0(r\sqrt{d_{i,1}})/I_0(R\sqrt{d_{i,1}}) \rightarrow 1$ for all distances $r < R$ and for all layers i . In practice, this can be easily verified by checking whether the simulated drawdown is sensitive to the initial drawdown in the proximal zone or not. This verification is done for the examples discussed in this chapter, and it is seen that the initial condition defined for the proximal zone indeed has no significant impact on the calculated solutions.

7.3.2.3. Solving the inverse problem

To fulfill condition (68) that requires the drawdown in the top layer is s_c at distance R , an inverse problem must be solved. As the boundary between the two zones is head-dependent, and therefore, also the values of the parameters that differ in the two zones, the problem is generally nonlinear. Since only one head is considered, a nonlinear solver to optimize a scalar function could be used, which is standard available with Python package SciPy (Virtanen et al., 2020).

Mathematically, the inverse problem is formulated as a minimization problem by rearranging condition (68):

$$\min_{R \in \mathbb{R}^+} |s_c - s_{1,2}(R, t)| \quad (\forall t > 0) \quad (124)$$

Statement (124) defines the objective function as the absolute difference between the required drawdown s_c and the calculated drawdown $s_{1,2}$ at distance R of the boundary between the two zones. In the problems studied in this chapter, the logarithm of R is optimized to facilitate convergence:

$$\min_{\log R \in \mathbb{R}} |s_c - s_{1,2}(R, t)| \quad (\forall t > 0) \quad (125)$$

By logarithmically transforming distance R , the minimization always yields a strictly positive distance.

If steady flow is considered, then distance R is not a function of time t ; hence, the minimization problem defined in (124) or (125) has to be solved only once. If transient flow is simulated, then the minimization problem must be solved for each time t to determine $R(t)$. In this case, the logarithm of R is also optimized, and an upper boundary u is defined if possible:

$$\min_{\log R \leq u} |s_c - s_{1,2}(R, t)| \quad (\forall t > 0) \quad (126)$$

In case of an extraction, the largest time t gives the largest value for R ; hence, the upper bound u may be determined by solving the corresponding steady-state problem:

$$\min_{\log R \in \mathbb{R}} |s_c - s_{1,2}(R, t)| \quad (t \rightarrow \infty) \quad (127)$$

Once R is determined for the corresponding steady-state problem, the upper bound u is defined as:

$$u = \lim_{t \rightarrow \infty} \log R(t) \quad (128)$$

It is possible, however, the flow in the aquifer system never attains a new state of equilibrium. In this case, the upper bound u may be determined as follows:

$$u = \log R(t_{max}) \quad (\forall t < t_{max}) \quad (129)$$

where t_{max} [T] is the largest time that is required to solve the problem at hand. Time t_{max} is used to determine the maximum distance $R(t_{max})$. This distance is determined solving (125) without upper bound, and it is used as upper bound to solve (126) for all other times t that are smaller than t_{max} . In practice, the times are sorted from large to small, and distance $R(t_k)$ is used as upper bound to determine distance $R(t_{k+1})$, with $t_k > t_{k+1}$.

7.3.3. Finite-difference approach

In general, the finite-difference method discussed in Chapter 3 is well-chosen to deal with parameters that vary with the radial distance, as it is very easy to include heterogeneities into the finite-difference grid. Therefore, one may expect it is also very straightforward to apply the finite-difference method for solving the two-zone problem stated in section 7.3.1. It is true that using the finite-difference approach is less cumbersome than using the semi-analytical approach, although there is a small caveat: the two zones are not fixed as their boundary expands with time.

Mathematically, the width of the proximal zone depends on the value of one parameter that is head-dependent, which implies the problem is nonlinear. In case of confined-unconfined flow, it is the storage coefficient that changes from elastic storage to specific yield when the head drops below the top of the aquifer system, and in case of a draining boundary condition, its resistance becomes infinitely large to cut off the drainage when the head is lower than the drainage level. The head-dependent proximal zone that expands with time cannot be defined explicitly in the finite-difference grid. However, since the grid consists of a fixed number of rings as part of the radial discretization, it is straightforward to check for each of these rings if it belongs to the proximal or the distal zone. This is simply done by evaluating if the head in the ring respectively is lower or greater than the specified head that defines the conversion, after which the head-dependent parameter is changed accordingly. In this way, the distance of the boundary between proximal and distal zone is determined implicitly.

Changing one of the parameters assigned to a ring depending on the value of the head calculated for that ring may affect the heads simulated in the other nodes of the grid. As a consequence, these heads need to be updated, and hopefully, they are closer to the correct heads. The updated heads may in turn affect the value of some of the head-dependent parameters, which are also updated. If convergence happens, then further iterations will successively improve the accuracy of the heads and the head-dependent parameters. This iterative procedure is referred to as Picard iterations (Harbaugh, 1995; Hill, 1990), and it is used in earlier versions of MODFLOW (Harbaugh, 2005; Harbaugh et al., 2000; Harbaugh & McDonald, 1996; McDonald & Harbaugh, 1988), for instance, to simulate unconfined flow in a layer with head-dependent saturated thickness. It is interesting to mention that the current MODFLOW 6 version applies the Newton-Raphson method to deal with nonlinearities (Langevin et al., 2017).

In section 3.3.4 of Chapter 3, it is described in detail how the finite-difference method comes down to solving the following system of linear equations for each time step k :

$$\mathbf{A}_k \mathbf{h}_k = \mathbf{b}_k \quad (130)$$

Matrix \mathbf{A}_k is an $n \times n$ matrix, and both \mathbf{h}_k and \mathbf{b}_k are $n \times 1$ vectors, with n the number of nodes in the model grid. Matrix \mathbf{A}_k and vector \mathbf{b}_k hold the known terms that are calculated using the input parameters and boundary conditions, whereas vector \mathbf{h}_k contains the unknown heads for each node in the grid. This means the heads are found by solving matrix system (130):

$$\mathbf{h}_k = \mathbf{A}_k^{-1} \mathbf{b}_k \quad (131)$$

As explained in section 3.3.5 of Chapter 3, solving (131) can be done using an iterative solver or a direct solver. If the system is linear, which implies all input parameters are independent of head and all boundary conditions are linear, then matrix \mathbf{A}_k and vector \mathbf{b}_k are independent of head and system (130) only needs to be solved once for each time step k . However, if at least one of the input parameters are head-dependent or one of the boundary conditions is nonlinear, then matrix \mathbf{A}_k and/or vector \mathbf{b}_k are head-dependent:

$$\mathbf{A}_k(h)\mathbf{h}_k = \mathbf{b}_k(h) \quad (132)$$

As explained above, the following iterative procedure can be used to solve nonlinear matrix system (132):

$$\mathbf{h}_k^{(m)} = [\mathbf{A}_k^{(m-1)}(h^{(m-1)})]^{-1} \mathbf{b}_k^{(m-1)}(h^{(m-1)}) \quad (133)$$

where superscript m refers to the iteration. According to (133), the heads in iteration m are found by solving matrix system (132) in which matrix \mathbf{A}_k and vector \mathbf{b}_k are updated using the heads of the previous iteration ($m - 1$). In the first iteration, that is $m = 1$, the heads from previous time step ($k - 1$) are used. If it concerns the first time step, that is $k = 1$, then the initial heads are used.

As for any other iterative procedure, a criterion of convergence is required. In this case, the maximum absolute difference between the heads in successive iterations ($m - 1$) and m can be verified against a specified convergence tolerance: If the maximum absolute head difference is smaller than this given tolerance, the heads are considered sufficiently accurate and the iterative procedure is stopped. It is also recommended to define a maximum number of iterations to avoid running into an infinite loop when the algorithm does not converge.

If an iterative solver is used, then the iterative procedure expressed by (133) is sometimes referred to as the outer iterations (Hill, 1990). Consequently, the iterations executed by the iterative method to actually solve the matrix system are referred to as the inner iterations. Some iterative solvers, such as ADI (Peaceman & Rachford, 1955) and SIP (Stone, 1968), which are discussed in section 3.3.5 of Chapter 3, allow the integration of both iterative procedures. For instance, the AS2D model developed by Lebbe (1988, 1999) is capable of simulating unconfined flow in the top layer of the multilayer grid by updating its saturated thickness after each ADI iteration.

The same approach to deal with unconfined flow is implemented in the MAxSym code (Louwyck, 2011) that applies both ADI and SIP as iterative solvers. As will be discussed in section 7.5.4, this Matlab tool is extended with the option to define drawdown-limited cells (Louwyck, 2015), which can be used to add a drainage boundary condition to the model. This option is required to simulate the effect of combined infiltration and drainage on pumping, which is examined in section 7.5. Alternatively, the MODFLOW procedure developed by Louwyck et al. (2012, 2014) can be applied, in which case the DRAIN package (Harbaugh, 2005; Harbaugh et al., 2000) can be used. The MODFLOW procedure is discussed in section 3.4 of Chapter 3; the use of the DRAIN package is addressed in section 7.5.4.

Although it is possible to simulate unconfined flow using the MAxSym tool (Louwyck, 2011), it cannot handle the conversion from confined to unconfined flow, a problem that is examined in the next section 7.4. Fortunately, this option is built in MODFLOW (Harbaugh, 2005), and layers that convert from confined to unconfined are called convertible layers. Both the BCF6 and the LPF package support the use of convertible layers (Harbaugh, 2005; Harbaugh et al., 2000), and a distinction must be made between limited and fully convertible layers. A limited convertible layer only changes its

storativity from elastic storage to specific yield when the head is below the layer thickness, and keeps its thickness constant, whereas a fully convertible layer also adapts its saturated thickness.

The problem that will be stated in section 7.4 assumes that all layers in the aquifer system have a constant thickness. This is also true for the top layer, to which the specific yield is assigned once it becomes unconfined. As such, the top layer in these problems is a limited convertible layer and not a fully convertible layer, as the saturated thickness is assumed constant. Therefore, the MODFLOW procedure by Louwyck et al. (2012, 2014) defining a limited convertible top layer is used to test the semi-analytical approach developed in this chapter. As will be explained in section 7.4.3, the limited convertible option is available with the BCF6 package (Harbaugh, 2005; Harbaugh et al., 2000).

7.4. Confined-unconfined flow

The first type of nonlinear problems that is examined applying the semi-analytical approach explained in section 7.3.2 deals with the conversion from confined to unconfined flow. More specifically, the analytical one-layer solution by Moench and Prickett (1972) is generalized to multiple layers. The conversion only applies to the top layer of the aquifer system. The storativity of this layer is changed when the head drops below the top of the system, while the transmissivity remains unmodified. This is in agreement with the assumptions underlying the Moench and Prickett (1972) model.

The problem is stated mathematically and the semi-analytical approach is reformulated to solve this specific head-dependent two-zone problem. The analytical solution by Moench and Prickett (1972) is discussed in detail, and it is examined if it corresponds to the proposed Laplace transform solution reduced to one layer. It is also explained how the MODFLOW procedure by Louwyck et al. (2012, 2014) can be applied to solve the problem numerically.

The Moench and Prickett (1972) solution is compared with the results simulated using the semi-analytical approach and the finite-difference method. A final example of a three-layer system is used to compare the semi-analytical multilayer solution with the finite-difference solution.

7.4.1. Problem statement

The problem generally stated in section 7.3.1 is adopted here, which means the partial differential equations are formulated in terms of drawdown s :

$$\begin{cases} \frac{\partial^2 s_{11}}{\partial r^2} + \frac{1}{r} \frac{\partial s_{11}}{\partial r} = \frac{S^y}{T_1} \frac{\partial s_{11}}{\partial t} + \frac{s_{11} - s_{21}}{c_1 T_1} \\ \frac{\partial^2 s_{12}}{\partial r^2} + \frac{1}{r} \frac{\partial s_{12}}{\partial r} = \frac{S_1}{T_1} \frac{\partial s_{12}}{\partial t} + \frac{s_{12} - s_{22}}{c_1 T_1} \\ \frac{\partial^2 s_{ij}}{\partial r^2} + \frac{1}{r} \frac{\partial s_{ij}}{\partial r} = \frac{S_i}{T_i} \frac{\partial s_{ij}}{\partial t} + \frac{s_{ij} - s_{i-1,j}}{c_{i-1} T_i} + \frac{s_{ij} - s_{i+1,j}}{c_i T_i} \quad (2 \leq i \leq n_l; j \in \{1,2\}) \end{cases} \quad (134)$$

Parameter S^y in the first differential equation of (134) is the specific yield, which is dimensionless. It expresses the unconfined conditions in the proximal zone ($j = 1$) around the well of the top layer. In the distal zone ($j = 2$), the top layer is still confined, and storativity S_1 is calculated using the specific elastic storage of the top layer, which is expressed by the storage change term in the second equation of (134). The difference between the two zones thus only lies in the storativity of the top layer:

$$\begin{cases} S_{1,1} = S^y \\ S_{1,2} = S_1^s D_1 \end{cases} \quad (135)$$

with S_1^s the specific elastic storage of the top layer, and D_1 the thickness of the top layer.

The third equation of (134) describes the flow in the deeper layers of the aquifer system. The other head-independent parameters are the same in both zones, and therefore, subscript j referring to the zone is omitted. As the lower boundary of the aquifer system is impervious, $c_{n_l} = \infty$. Resistance c_0 is also infinitely large since there is no leakage at the top of the aquifer system. There is also no infiltration; hence, $N_i = 0$ for all layers i .

The initial conditions and the boundary conditions are also adopted from section 7.3.1:

$$s_{i,2}(r, 0) = 0 \quad (1 \leq i \leq n_l) \quad (136)$$

$$\lim_{r_w \rightarrow 0} Q_{i,1}^h(r_w, t) = Q_i \quad (1 \leq i \leq n_l) \quad (137)$$

$$s_{i,2}(\infty, t) = 0 \quad (1 \leq i \leq n_l) \quad (138)$$

$$s_{1,1}(R, t) = s_{1,2}(R, t) = s_c = D_1 - \varphi \quad (139)$$

$$Q_{i,1}^h(R, t) = Q_{i,2}^h(R, t) \quad (1 \leq i \leq n_l) \quad (140)$$

The flow converts from confined to unconfined when the head in the upper layer drops below the top of that layer. This means the head is equal to thickness D_1 of the top layer at distance R , or $h_{1,1}(R) = h_{1,2}(R) = D_1$. Therefore, the specified drawdown s_c at distance R is equal to $D_1 - \varphi$, which is expressed by condition (139). Recall that φ is the initial head in the aquifer.

7.4.2. Semi-analytical solution method

The semi-analytical solution method discussed in section 7.3.2 is adopted here to solve the specific problem of confined-unconfined flow stated in previous section 7.4.1. First, the solution for multiple layers is presented, after which solving the inverse problem to determine R is discussed. Finally, the one-layer solution is derived, and compared with the analytical Moench and Pricket (1972) solution.

7.4.2.1. Solution for multiple layers

To solve the stated problem semi-analytically, the transient-state solution presented in section 7.3.2.2 is applied. The exact solution for the drawdown in the Laplace domain is given by (120). The solution can be reduced by removing the terms containing \mathbf{v}_1 and \mathbf{v}_2 , as there is no infiltration:

$$\begin{cases} \mathbf{s}_1(r) = \mathbf{V}_1 \{ [\mathbf{K}_1(r) - \mathbf{U}(r)\mathbf{K}_1(R)]\mathbf{V}_1^{-1}\mathbf{T}^{-1}\mathbf{Q} + \mathbf{U}(r)\mathbf{V}_1^{-1}\mathbf{s}_2(R) + [\mathbf{I} - \mathbf{U}(r)]\mathbf{D}_1^{-1}\mathbf{V}_1^{-1}\mathbf{\Psi}_1 s_c \} \\ \mathbf{s}_2(r) = -\mathbf{V}_2 \mathbf{W}(r)\mathbf{V}_2^{-1}\mathbf{T}^{-1}\mathbf{Q}_1^h(R) \end{cases} \quad (141)$$

Similarly, the exact solution for the Laplace transform of the radial discharge given by (121) simplifies to:

$$\begin{cases} \mathbf{Q}_1^h(r) = \mathbf{T}\mathbf{V}_1 \{ [\mathbf{U}'(r)\mathbf{K}_1(R) - \mathbf{K}'_1(r)]\mathbf{V}_1^{-1}\mathbf{T}^{-1}\mathbf{Q} - \mathbf{U}'(r)\mathbf{V}_1^{-1}\mathbf{s}_2(R) + \mathbf{U}'(r)\mathbf{D}_1^{-1}\mathbf{V}_1^{-1}\mathbf{\Psi}_1 s_c \} \\ \mathbf{Q}_2^h(r) = \mathbf{T}\mathbf{V}_2 \mathbf{W}'(r)\mathbf{V}_2^{-1}\mathbf{T}^{-1}\mathbf{Q}_1^h(R) \end{cases} \quad (142)$$

Note that $\mathbf{T}_1 = \mathbf{T}_2 = \mathbf{T}$ as the aquifer transmissivities are the same in both zones. Vector $\mathbf{Q}_1^h(R)$ in the second equation of (141) and (142) is given by the first equation of (142) with $r = R$:

$$\mathbf{Q}_1^h(R) = \mathbf{T}\mathbf{V}_1 \{ [\mathbf{U}'(R)\mathbf{K}_1(R) - \mathbf{K}'_1(R)]\mathbf{V}_1^{-1}\mathbf{T}^{-1}\mathbf{Q} - \mathbf{U}'(R)\mathbf{V}_1^{-1}\mathbf{s}_2(R) + \mathbf{U}'(R)\mathbf{D}_1^{-1}\mathbf{V}_1^{-1}\mathbf{\Psi}_1 s_c \} \quad (143)$$

Vector $\mathbf{s}_2(R)$ is found by introducing (143) into the second equation of (141) with $r = R$:

$$\begin{aligned} \mathbf{s}_2(R) &= \{ \mathbf{I} - \mathbf{V}_2 \mathbf{W}(R)\mathbf{V}_2^{-1}\mathbf{V}_1 \mathbf{U}'(R)\mathbf{V}_1^{-1} \}^{-1} \cdot \\ &\quad \{ \mathbf{V}_2 \mathbf{W}(R)\mathbf{V}_2^{-1}\mathbf{V}_1 [\mathbf{K}'_1(R) - \mathbf{U}'(R)\mathbf{K}_1(R)]\mathbf{V}_1^{-1}\mathbf{T}^{-1}\mathbf{Q} - \mathbf{U}'(R)\mathbf{D}_1^{-1}\mathbf{V}_1^{-1}\mathbf{\Psi}_1 s_c \} \end{aligned} \quad (144)$$

As explained in section 7.3.2.2, matrix $\mathbf{U}(r)$ may be approximated by the unity matrix in many cases, which leads to the following approximation of solution (141):

$$\begin{cases} \mathbf{s}_1(r) = \mathbf{V}_1[\mathbf{K}_1(r) - \mathbf{K}_1(R)]\mathbf{V}_1^{-1}\mathbf{T}^{-1}\mathbf{Q} + \mathbf{s}_2(R) & (r \leq R) \\ \mathbf{s}_2(r) = -\mathbf{V}_2\mathbf{W}(r)\mathbf{V}_2^{-1}\mathbf{T}^{-1}\mathbf{Q}_1^h(R) & (r \geq R) \end{cases} \quad (145)$$

with:

$$\mathbf{Q}_1^h(R) = \mathbf{T}\mathbf{V}_1\mathbf{K}'_1(R)\mathbf{V}_1^{-1}\mathbf{T}^{-1}\mathbf{Q} \quad (146)$$

$$\mathbf{s}_2(R) = \mathbf{V}_2\mathbf{W}(R)\mathbf{V}_2^{-1}\mathbf{V}_1\mathbf{K}'_1(R)\mathbf{V}_1^{-1}\mathbf{T}^{-1}\mathbf{Q} \quad (147)$$

Introducing (146) and (147) into (145) gives the approximate solution for the drawdown in the Laplace domain:

$$\begin{cases} \mathbf{s}_1(r) = \{\mathbf{V}_1[\mathbf{K}_1(r) - \mathbf{K}_1(R)] + \mathbf{V}_2\mathbf{W}(R)\mathbf{V}_2^{-1}\mathbf{V}_1\mathbf{K}'_1(R)\}\mathbf{V}_1^{-1}\mathbf{T}^{-1}\mathbf{Q} & (r \leq R) \\ \mathbf{s}_2(r) = \mathbf{V}_2\mathbf{W}(r)\mathbf{V}_2^{-1}\mathbf{V}_1\mathbf{K}'_1(R)\mathbf{V}_1^{-1}\mathbf{T}^{-1}\mathbf{Q} & (r \geq R) \end{cases} \quad (148)$$

As the given solutions are expressed in the Laplace domain, they need to be inverted, which is done numerically using the Stehfest (1970) algorithm.

7.4.2.2. Solving the inverse problem

To find distance $R(t)$ of the time-dependent boundary between the two zones, an inverse problem must be solved, as is explained in section 7.3.2.3. As the value for drawdown s_c is specified by (139), the minimization problem expressed by (125) can be reformulated as:

$$\min_{\log R \in \mathbb{R}} |D_1 - \varphi - s_{1,2}(R, t)| \quad (\forall t > 0) \quad (149)$$

Initially, $R = 0$ at time $t = 0$. As there is no interaction with external sources or sinks, the aquifer system never reaches a new state of equilibrium, and consequently, $R \rightarrow \infty$ if $t \rightarrow \infty$.

Solving (149) for $\log R$ is difficult for small values of time t if no bounds are imposed. Therefore, the unbounded inverse problem is solved first for the largest value of time t_{max} [T] that is required to solve the problem at hand:

$$R_{max} = \min_{\log R \in \mathbb{R}} |D_1 - \varphi - s_{1,2}(R, t_{max})| \quad (150)$$

Once R_{max} [L] is found, the other values for $R(t)$ can be determined recursively starting with the second largest time, etc.:

$$\begin{aligned} R(t_k) &= \min_{\log R \in [l, u]} |D_1 - \varphi - s_{1,2}(R, t_k)| \quad (0 < t_k < t_{k+1}) \\ &\text{with } l = \log(R(t_{k+1})/x) \text{ and } u = \log R(t_{k+1}) \end{aligned} \quad (151)$$

Recall that $t_{max} = \max_k t_k$. Variables l and u in (151) are the lower and upper bound, respectively, which are defined using $R(t_{k+1})$, that is determined during the previous iteration. Constant x is greater than 1 and must be chosen sufficiently large.

7.4.2.3. The one-layer solution

Solution (141) may be reformulated for one layer. For notational convenience, index $i = 1$ referring to the single layer is omitted. For the same reason, the specific yield S^y of this layer is assigned to variable S_1 and its storage coefficient S is assigned to variable S_2 . This means that subscripts 1 and 2 refer to the proximal unconfined zone and the distal confined zone, respectively, which is in agreement with (135).

If solution (141) is reduced to one layer, the single eigenvalue d_j equals the single element of A_j , that is $S_j p/T$, and the corresponding eigenvector \mathbf{V}_j is 1:

$$\begin{cases} \bar{s}_1(r, p) = \frac{D - \varphi}{p} + \frac{Q}{2\pi T p} \left[K_0(x_1) - \frac{I_0(x_1)}{I_0(X_1)} K_0(X_1) \right] & (r \leq R) \\ \bar{s}_2(r, p) = \bar{Q}_1^h(R, p) \frac{K_0(x_2)}{2\pi T X_2 K_1(X_2)} & (r \geq R) \end{cases} \quad (152)$$

with $x_j = r \sqrt{\frac{S_j}{T} p}$ and $X_j = R \sqrt{\frac{S_j}{T} p}$. In the first equation of (152), the Laplace transform of (139) is used to replace $\bar{s}_2(R, p)$:

$$\bar{s}_2(R, p) = \frac{s_c}{p} = \frac{D - \varphi}{p} \quad (153)$$

In expression (153), subscript 1 is omitted from aquifer thickness D . Quantity $\bar{Q}_1^h(R, p)$ in the second equation of (152) is found by evaluating:

$$\bar{Q}_1^h(R, p) = \left[\frac{X_1 I_1(X_1)}{I_0(X_1)} K_0(X_1) + X_1 K_1(X_1) \right] \frac{Q}{p} \quad (154)$$

Distance R is found by introducing (154) in the second equation of (152), which is used to substitute $\bar{s}_2(R, p)$ in equation (153). Rearranging and inverting the obtained equation gives:

$$\mathcal{L}^{-1} \left\{ \left[\frac{X_1 I_1(X_1)}{I_0(X_1)} K_0(X_1) + X_1 K_1(X_1) \right] \frac{Q K_0(X_2)}{2\pi T p X_2 K_1(X_2)} \right\} + \varphi - D = 0 \quad (155)$$

where \mathcal{L}^{-1} denotes the inverse Laplace transform. Using equations (153) and (155), the second equation in solution (152) can be reduced:

$$\begin{cases} \bar{s}_1(r, p) = \frac{D - \varphi}{p} + \frac{Q}{2\pi T_1 p} \left[K_0(x_1) - \frac{I_0(x_1)}{I_0(X_1)} K_0(X_1) \right] & (r \leq R) \\ \bar{s}_2(r, p) = \left(\frac{D - \varphi}{p} \right) \frac{K_0(x_2)}{K_0(X_2)} & (r \geq R) \end{cases} \quad (156)$$

As explained in section 7.3.2.2, the first equation in solution (156) can be approximated by assuming $\frac{I_0(x_1)}{I_0(X_1)} \approx 1$:

$$\begin{cases} \bar{s}_1(r, p) = \frac{D - \varphi}{p} + \frac{Q}{2\pi T_1 p} [K_0(x_1) - K_0(X_1)] & (r \leq R) \\ \bar{s}_2(r, p) = \left(\frac{D - \varphi}{p} \right) \frac{K_0(x_2)}{K_0(X_2)} & (r \geq R) \end{cases} \quad (157)$$

Taking the derivative of the first equation in (157) with respect to r , and using it to simplify (154) gives:

$$\bar{Q}_1^h(R, p) = X_1 K_1(X_1) \frac{Q}{p} \quad (158)$$

Introducing (158) into the second equation of (152) gives the equation that must be solved to find R :

$$\mathcal{L}^{-1} \left\{ \frac{K_0(X_2)}{2\pi T X_2 K_1(X_2)} X_1 K_1(X_1) \frac{Q}{p} \right\} + \varphi - D = 0 \quad (159)$$

Moench and Prickett (1972) give the analytical solution in the real time domain for the one-layer problem of transient confined-unconfined flow:

$$\begin{cases} s_1(r, t) = D - \varphi + \frac{Q}{4\pi T} \left[W\left(\frac{r^2 S_1}{4tT}\right) - W\left(\frac{R^2 S_1}{4tT}\right) \right] & (r \leq R) \\ s_2(r, t) = (D - \varphi) W\left(\frac{r^2 S_2}{4tT}\right) / W\left(\frac{R^2 S_2}{4tT}\right) & (r \geq R) \end{cases} \quad (160)$$

where distance R is found by evaluating:

$$\frac{Q}{4\pi T} \exp\left(\frac{-R^2 S_1}{4tT}\right) - \frac{(D - \varphi)}{W\left(\frac{R^2 S_2}{4tT}\right)} \exp\left(\frac{-R^2 S_2}{4tT}\right) = 0 \quad (161)$$

Recall that $S_1 = S^y$ and $S_2 = S$. It is straightforward to verify that solution (160) subject to (161) simplifies to the Theis (1935) solution if $S_1 = S_2$. Equation (161) can be written in dimensionless form:

$$W(v)\exp(v[1 - \alpha]) - \sigma = 0 \quad (162)$$

with $v = \frac{R^2 S_2}{4tT}$, $\alpha = \frac{S_1}{S_2}$, and $\sigma = \frac{4\pi T(D - \varphi)}{Q}$. This means that for a given α and σ , parameter v needs to be determined only once using (162). Indeed, as v is constant and proportional to R^2/t , distance R can be derived directly from v for any time t .

Expansion $W(u) \approx -\gamma - \ln(u) = -\ln(ue^\gamma)$ is valid for small distances and large values of time according to the Cooper and Jacob (1946) approximation, which simplifies (160) to:

$$\begin{cases} s_1(r, t) = \varphi - D + \frac{Q}{2\pi T} \ln\left(\frac{R}{r}\right) & (r \leq R) \\ s_2(r, t) = \frac{Q}{2\pi T} \ln\left(\frac{1}{r} \sqrt{\frac{4tT}{S_2 e^\gamma}}\right) & (r \geq R) \end{cases} \quad (163)$$

Solution (163) corresponds to the steady state solution presented in Chapter 5 for a confined aquifer consisting of two-zones with time-dependent outer boundary. In this case, expression (161) that determines R reduces to:

$$s_2(R, t) = \frac{Q}{2\pi T} \ln\left(\frac{1}{R} \sqrt{\frac{4tT}{S_2 e^\gamma}}\right) = \varphi - D \quad (164)$$

Rearranging (164) gives:

$$R = \sqrt{\frac{4tT}{S_2 e^\gamma}} \exp\left(\frac{2\pi T[D - \varphi]}{Q}\right) \quad (165)$$

To apply the Cooper and Jacob (1946) approximation, u must be smaller than 0.02. Therefore, approximation (165) and corresponding solution (163) are justified only if $\frac{R^2 S_1}{4tT} < 0.02$.

The same approximation can be obtained from the Laplace transform solution (157) by applying $xK_1(x) \rightarrow 1$ if $x \rightarrow 0$ to the second equation, and using the well-known inversion $\mathcal{L}^{-1}[K_0(a\sqrt{p})/p] = W(a^2/4t)/2$ to both equations (see page 303 of Hantush, 1964):

$$\begin{cases} s_1(r, t) = \varphi - D + \frac{Q}{4\pi T} \left[W\left(\frac{r^2 S_1}{4tT}\right) - W\left(\frac{R^2 S_1}{4tT}\right) \right] & (r \leq R) \\ s_2(r, t) = \frac{Q}{4\pi T} W\left(\frac{r^2 S_2}{4tT}\right) & (r \geq R) \end{cases} \quad (166)$$

Solution (166) results into (163) if the Cooper and Jacob (1946) approximation is applied.

The analytical inversion of the second equation of (157) can be done using the following known inversion $\mathcal{L}^{-1}\{K_0(a\sqrt{p})/[pK_0(b\sqrt{p})]\} = A(t/b^2, a/b)$ (see page 335 of Carslaw and Jaeger, 1959; or page 303 and page 309 of Hantush, 1964), where function A is defined as:

$$A(\tau, \rho) = 1 - \frac{2}{\pi} \int_0^\infty \frac{J_0(u)Y_0(\rho u) - Y_0(u)J_0(\rho u)}{[J_0(u)]^2 + [Y_0(u)]^2} \exp(-\tau u^2) \frac{du}{u} \quad (167)$$

with J_0 and Y_0 the zero order Bessel functions of the first and second kind, respectively. According to Hantush (1964), function $A(\tau, \rho)$ may be approximated by $W(\rho^2/4\tau)/\ln(2.25\tau)$ if $\tau > 500$. This results into the following approximate solution:

$$\begin{cases} s_1(r, t) = \varphi - D + \frac{Q}{4\pi T} \left[W\left(\frac{r^2 S_1}{4tT}\right) - W\left(\frac{R^2 S_1}{4tT}\right) \right] & (r \leq R) \\ s_2(r, t) = (\varphi - D) W\left(\frac{r^2 S_2}{4tT}\right) / \ln\left(2.25 \frac{tT}{R^2 S_2}\right) & (r \geq R) \end{cases} \quad (168)$$

Note that solution (168) and solution (160) by Moench and Prickett (1972) are the same if the Cooper and Jacob (1946) approximation is applied: $W\left(\frac{R^2 S_2}{4tT}\right) \approx \ln\left(\frac{4tT}{R^2 S_2 e^r}\right) \approx \ln\left(2.25 \frac{tT}{R^2 S_2}\right)$.

Rearranging the Laplace transform of equation (159) that is applied to determine distance R :

$$\frac{Q}{2\pi T p} K_0(X_2) [X_1 K_1(X_1)] = \frac{\varphi - D}{p} [X_2 K_1(X_2)] \quad (169)$$

Applying the following known inversions to the corresponding subparts of equation (169): $\mathcal{L}^{-1}\{a/p\} = a$, $\mathcal{L}^{-1}[K_0(a\sqrt{p})/p] = W(a^2/4t)/2$, and $\mathcal{L}^{-1}\{(\sqrt{a/p})K_1(\sqrt{ap})\} = \exp(-a/4t)$ (see inversion 25 on page 146 of Bateman, 1954; or inversion 29.3.122 on page 1028 of Abramowitz and Stegun, 1965), and multiplying the inverted functions:

$$\frac{Q}{4\pi T} W\left(\frac{R^2 S_2}{4tT}\right) \exp\left(-\frac{R^2 S_1}{4tT}\right) = (\varphi - D) \exp\left(-\frac{R^2 S_2}{4tT}\right) \quad (170)$$

Rearranging (170) gives expression (161) to find R presented by Moench and Prickett (1972). This is remarkable as the convolution theorem should be applied here which implies it is generally not allowed to multiply the inverted Laplace transformed expressions. However, proving that the analytical inversion of expression (169) results into expression (170) is out of scope, and instead, it is shown through a well-chosen example that both solutions are virtually the same.

A final note on the Moench and Prickett (1972) solution that was translated from an analogous heat conduction problem solved by Carslaw and Jaeger (1959). The original equations in the paper by Moench and Prickett (1972) are:

$$\begin{cases} s_1(r, t) = \varphi - D + \frac{Q}{4\pi T} \left[W\left(\frac{r^2 S_1}{4tT}\right) - W\left(\frac{R^2 S_1}{4tT}\right) \right] & (r \leq R) \\ s_2(r, t) = \frac{Q}{4\pi T} \exp\left(\frac{R^2 [S_2 - S_1]}{4tT}\right) W\left(\frac{r^2 S_2}{4tT}\right) & (r \geq R) \end{cases} \quad (171)$$

To be precise, the first and second equation of (171) correspond to equations (14) and (15) in Moench and Prickett (1972), respectively. However, drawdown $\varphi - D$ is missing from equation (14) in Moench and Prickett (1972), which seems to be a mistake, as the initial head at $t = 0$ in the aquifer is φ at all distances r and not D . The second equation in (171) is simplified to the second equation in (160) by using equation (161), which corresponds to equation (13) in Moench and Prickett (1972).

7.4.3. Finite-difference approach

It is possible to solve the problem stated in section 7.4.1 numerically by applying the MODFLOW procedure proposed by Louwyck et al. (2012, 2014) and discussed in section 3.4.2 of Chapter 3. The numerical solution may be used to test the semi-analytical approach presented in previous section 7.4.2. The MODFLOW procedure by Louwyck et al. (2012, 2014) uses LPF as flow package (Harbaugh, 2005; Harbaugh et al., 2000). As explained in section 7.3.3, the top layer in the model grid is defined as limited convertible, since only the storativity changes from elastic storage to specific yield when the flow in the layer becomes unconfined, while the transmissivity is not modified. This option is implemented in the BCF6 package (Harbaugh, 2005; Harbaugh et al., 2000). Using the BCF6 package instead of the LPF package is not an issue to apply the MODFLOW procedure by Louwyck et al. (2012, 2014), as hydraulic parameters defined in the BCF6 input file can be converted in the same way as in the LPF input file in order to trick MODFLOW into simulating axisymmetric flow.

The MODFLOW grid is defined in the DIS file (Harbaugh, 2005; Harbaugh et al., 2000). It consists of 1 row (NROW=1) of unit width (DELC=1), n_l layers (NLAY= n_l), and n_r columns (NCOL= n_r), which are conceptualized as concentric rings, since flow is axially symmetric. Index i refers to layer i , and index j to ring j . The inner radius [L] of ring j is $r_{b,j}$; the outer radius [L] is $r_{b,j+1}$. However, cell width DELR is set to 1, since the width of each ring is included by modifying the aquifer parameters. Layer i is characterized by its thickness D_i ; variables BOTM and TOP, defining top and bottom of each layer, are set accordingly. The starting or initial heads are defined in the BA6 file by setting variable STRT (Harbaugh, 2005; Harbaugh et al., 2000). Recall that in this case, STRT is set to φ for all layers i . The head in node j is calculated at the nodal circle with radius r_j [L], which is equal to the harmonic mean of inner and outer radius. Time t is discretized into time steps. Head h_{ijk} [L] is the head in layer i , ring j , and time step k .

Defining the top layer as limited convertible using the BCF6 package is done by setting the LAYCON variable for the first layer to 2. In MODFLOW-2005 (Harbaugh, 2005), the LAYCON variable is the same as in MODFLOW-88 (McDonald & Harbaugh, 1988), although it is part of the LTYPE variable, which determines not only the layer type, but also the method of calculating the interblock transmissivity. More precisely, the LTYPE variable consists of two digits, where the left digit determines the interblock transmissivity, and the right digit indicates the layer type, which may be confined (LAYCON=0), unconfined (LAYCON=1), limited convertible (LAYCON=2), or fully convertible (LAYCON=3). Here, the harmonic mean is used to calculate the interblock transmissivity, which is option 0, and therefore, LTYPE must be set to 02. Digit zero may be omitted as the harmonic mean is the default way to calculate the interblock transmissivity; hence, it suffices to set the LTYPE variable of the first layer to 2.

Concerning the storativities, the BCF6 package has two variables: SF1 and SF2. If LAYCON is 2, then SF1 is the confined storage coefficient, whereas SF2 is the specific yield (Harbaugh, 2005; Harbaugh et al., 2000). This means that the top layer's elastic storage coefficient S_1 is assigned to SF1, and its specific yield S^y is assigned to SF2. For the other layers, which are confined, only variable SF1 needs to be defined. Both variables must be multiplied by the horizontal surface areas of the rings in order to convert the parallel flow into axisymmetric flow (Louwyck et al., 2012, 2014):

$$SF1_{ij} = \pi(r_{b,j+1}^2 - r_{b,j}^2)S_i \quad (1 < i \leq n_l; \ 1 \leq j \leq n_r) \quad (172)$$

$$SF2_{ij} = \pi(r_{b,j+1}^2 - r_{b,j}^2)S^y \quad (i = 1; \ 1 \leq j \leq n_r) \quad (173)$$

Transmissivity TRAN for cell ij is corrected as follows (Louwyck et al., 2012, 2014):

$$TRAN_{ij} = \frac{2\pi K_{ij}^h D_i}{\ln(r_{b,j+1}/r_{b,j})} \quad (1 < i \leq n_l; \ 1 \leq j \leq n_r) \quad (174)$$

Recall that LTYPE is set to 2 if $i = 1$ and to 0 otherwise as the other layers are confined. Variable HY is not relevant here as the layers are neither unconfined nor fully convertible. Variable TRPY is set to 1 as there is no horizontal anisotropy. The hydraulic resistances between the model layers are assigned to the VCONT variable of each layer:

$$VCONT_{ij} = \frac{\pi(r_{b,j+1}^2 - r_{b,j}^2)}{c_i} \quad (1 < i < n_l; \ 1 \leq j \leq n_r) \quad (175)$$

Variables related to the wetting capability are not relevant here. Simulations are performed using the SIP solver (Harbaugh, 2005; Harbaugh et al., 2000). Radial distance and time are discretized according to a 'logspace' scheme, which is explained in section 3.3.1 of Chapter 3 and section 5.4 of Chapter 5.

7.4.4. Verification

To verify the semi-analytical approach presented in section 7.4.2, it is first compared with the analytical Moench and Prickett (1972) solution. Because this model considers a single layer, a three-layer example is also worked out in which the semi-analytical solution is compared with the finite-difference solution. The latter is simulated using the MODFLOW procedure by Louwyck et al. (2012, 2014), which is explained in section 7.4.3.

7.4.4.1. One-layer solution

In the first test case, the Moench and Prickett (1972) model is used to simulate axisymmetric flow toward a fully penetrating well in a confined aquifer that is converted into an unconfined aquifer where the head drops below the aquifer top. The proximal zone around the pumping well is unconfined and characterized by storativity S_1 , which equals the specific yield of the aquifer, whereas the distal zone remains confined, and therefore, it is characterized by the elastic storage coefficient S_2 .

Figure 3 is a plot of dimensionless drawdown $-sT/Q$ versus dimensionless time $tT/(r^2 S_1)$ for different relative storativities S_1/S_2 . Drawdown $s_c = D - \varphi$, that determines the conversion between confined and unconfined flow, is equal to Q/T in this example. The colored solid lines are calculated using analytical solution (171) by Moench and Prickett (1972), the black dotted lines are simulated using the semi-analytical approach presented in section 7.4.2, and the black dots are obtained by employing the MODFLOW procedure discussed in section 7.4.3. The semi-analytical approach applies solution (156) given in section 7.4.2.3, which is numerically inverted using the Stehfest (1970) algorithm. It is seen that all methods virtually give the same results.

The vertical colored dashed lines indicate the corresponding dimensionless time $tT/(R^2S_1)$ when the conversion takes place. As explained in section 7.4.2.3, distance R at which the boundary between the unconfined and confined occurs, is found by solving equation (162) for dimensionless parameter $v = R^2S_2/(4tT)$. As this parameter is proportional to t/R^2 , equation (162) only needs to be solved once for each model, which is done using SciPy function “root” that applies a modified Powell’s method (More et al., 1980). In case of the semi-analytical approach, minimization problem (149) is solved using SciPy function “fmin” to find the dimensionless time $tT/(R^2S_1)$. This function applies the Nelder and Mead (1965) method. Although the values for the point of conversion determined using the “fmin” function deviate up to 10% from the values determined using the “root” function, they have not a significant impact on the accuracy of the calculated drawdowns. Moreover, the difference between the two function results is almost not visible on the semi-logarithmic plot of Figure 3.

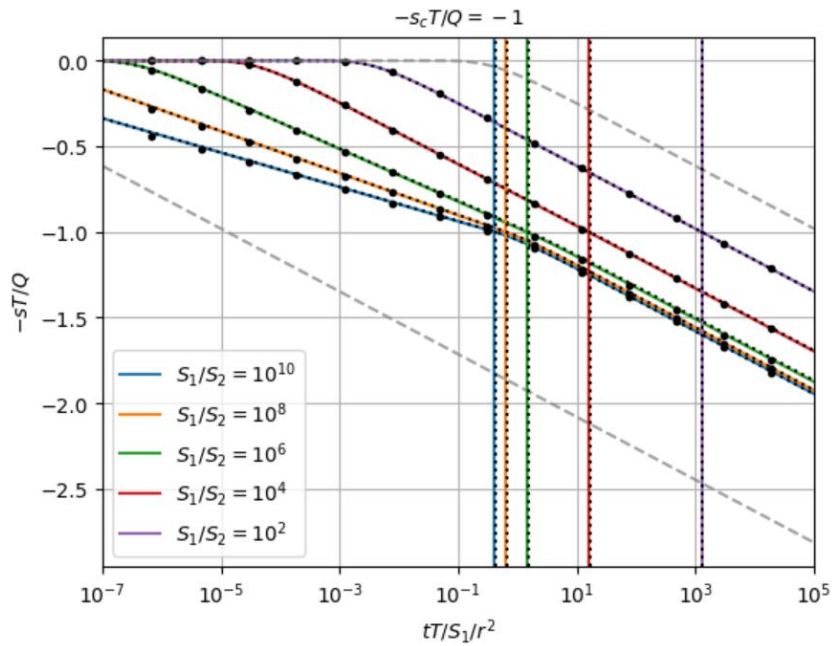


Figure 3. Dimensionless drawdown versus dimensionless time for the model simulating axisymmetric flow toward a fully penetrating well in a confined aquifer that becomes unconfined if the head drops below the top of the aquifer. The conversion takes place at the distance from the well where drawdown s_c equals the aquifer thickness minus the initial head. The proximal zone around the pumping well is the unconfined part of the aquifer characterized by storativity S_1 which equals the aquifer's specific yield. The distal zone is the confined part and is characterized by storativity S_2 which equals the aquifer's elastic storage coefficient. The solid lines are the analytical solution by Moench & Pricket (1972), the dotted black lines are the numerically inverted solution in the Laplace domain presented in this chapter, the black dots are simulated using the finite-difference method. The vertical lines indicate the dimensionless time when the conversion occurs. In this example, drawdown s_c equals Q/T , with Q the pumping rate and T the aquifer transmissivity. Variables r and t are the radial distance and the time, respectively. The gray dashed lines are the corresponding Theis (1935) solution for a homogeneous aquifer, where the upper curve is calculated using S_1 as storativity, and the lower curve using S_2 . See text for definitions of parameters and a more detailed discussion about the different solution methods.

The gray dashed curves added to the plot of Figure 3 are the corresponding Theis (1935) solution for a homogeneous aquifer with constant storativity. The curve showing the largest drawdowns in absolute value is calculated using elastic storage coefficient S_2 , whereas the other curve is calculated using the specific yield S_1 of the aquifer. The approximate solution (163) that is obtained by applying the Cooper and Jacob (1946) approximation is also calculated, but the results are not plotted on the graph in Figure 3. Recall that this approximation is valid if $R^2S_1/(4tT) < 0.02$, which is only true for the two models with the smallest ratio S_1/S_2 . This means that only the purple and red curves may be approximated using solution (163), and it is seen that for large values of dimensionless time, these

curves nearly exhibit a straight line indeed, as the storage change in the proximal zone is negligibly small. However, if ratio S_1/S_2 is large, then the curves clearly consist of two straight lines that intersect at the point of conversion.

7.4.4.2. Three-layer example

To test the semi-analytical multilayer approach outlined in sections 7.4.2.1 and 7.4.2.2, an example of a confined three-aquifer system is given in which the top layer is converted into a partially unconfined aquifer when the head drops below the top of the system due to the extraction of groundwater. Recall that the general schematization of this aquifer system is visualized in the left plot of Figure 1. This plot shows a system of four aquifers, while the example discussed here considers a system that comprises three aquifers.

The transmissivities of the aquifers counted from top to bottom are $T_1 = 20 \text{ m}^2/\text{d}$, $T_2 = 100 \text{ m}^2/\text{d}$, and $T_3 = 250 \text{ m}^2/\text{d}$; the elastic storage coefficients are $S_1 = 10^{-4}$, $S_2 = 5 \times 10^{-4}$, and $S_3 = 10^{-5}$. The two incompressible aquitards separating the aquifers have resistances $c_1 = 500 \text{ d}$ and $c_2 = 100 \text{ d}$, respectively. A pumping well with infinitesimal radius and a separate fully penetrating well-screen in the lower and upper aquifer extracts water from the system at pumping rates $Q_1 = -100 \text{ m}^3/\text{d}$ and $Q_3 = -250 \text{ m}^3/\text{d}$, respectively. As the middle aquifer is not extracted, $Q_2 = 0$.

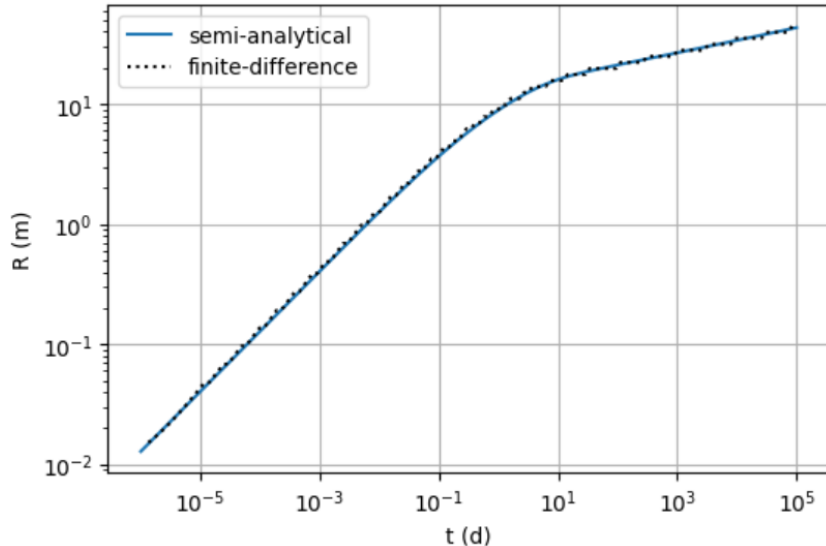


Figure 4. Distance R at which confined flow is converted into unconfined flow as a function of time t for the three-aquifer model discussed in the text. The solid blue curve is determined using the semi-analytical approach presented in this chapter, while the dotted black line is derived from the drawdowns simulated using a finite-difference model. See text for a detailed explanation.

The specific yield of the top aquifer is 0.2, and this value replaces the value for its elastic storage coefficient S_1 in the proximal zone around the pumping well where flow becomes unconfined. This conversion occurs when the drawdown in the top aquifer is smaller than -2 m. Distance R at which this conversion takes place, expands with time t , which is shown by the plot in Figure 4. The solid blue line is determined using the procedure outlined in section 7.4.2.2; the dotted black line represents the distance of the first node for which the finite-difference model simulates a drawdown that is smaller than -2 m. Because of the radial discretization, the finite-difference curve is not smooth. It is also clear that the relation between distance R and time t is nonlinear.

The largest time t_{max} is 10^5 d and it is used to find R_{max} by solving the unbounded minimization problem expressed by (150). Using R_{max} , distance R is determined for the other simulations times by solving the bounded minimization problem given by (151) with constant $x = 2$. The considered

time interval between 10^{-6} d and 10^5 d is discretized into 100 simulation times that are spaced evenly on a logarithmic scale. The unbounded minimization is performed using SciPy function “fmin” that applies the Nelder and Mead (1965) method, while SciPy function “fminbound” is used to solve the bounded minimization problem through the method of Brent (1973).

Once distance $R(t)$ is determined for each simulation time t , drawdowns are simulated in the Laplace domain using (141), and numerically inverted by applying the Stehfest (1970) algorithm. The left plot in Figure 5 shows drawdown s as a function of radial distance r after 0.1 days of pumping, while the right plot shows drawdown s as a function of time t at a distance of 0.1 m from the pumping well with infinitesimal radius. The colored solid lines are simulated using the semi-analytical approach, the black dotted lines employing the MODFLOW procedure by Louwyck et al. (2012, 2014) outlined in section 7.4.3. In the left plot, the vertical red dashed line indicates distance R at the considered time of 0.1 d. The gray dashed lines in the plots of Figure 5 are the corresponding solution for a confined aquifer system without conversion. It is seen that the fully confined solution only deviates from the confined-unconfined solution in the top layer at small values of time.

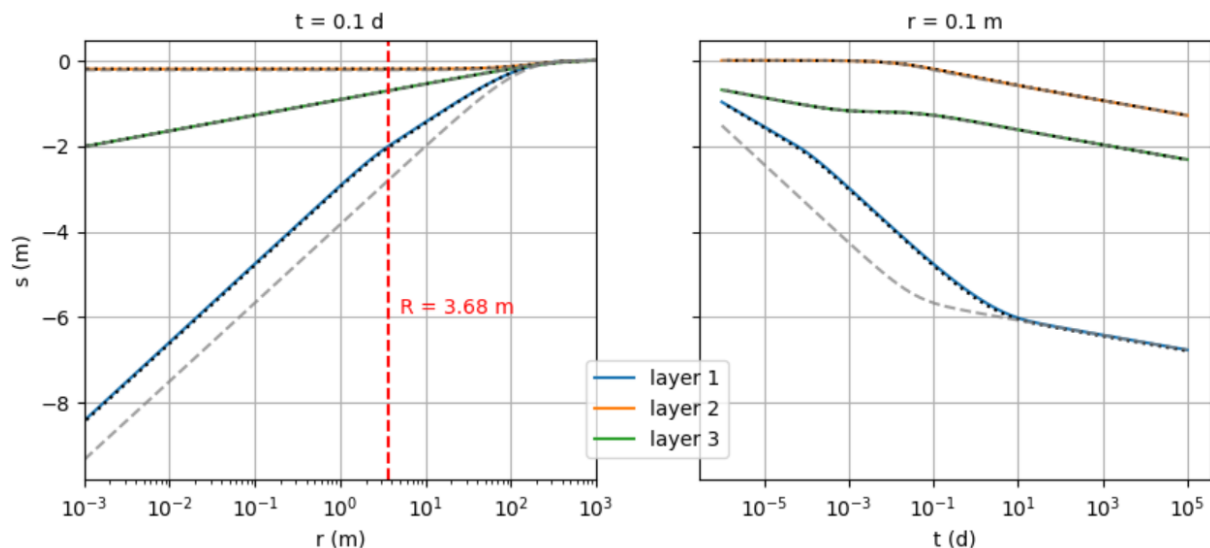


Figure 5. Drawdown s versus distance r at time $t = 0.1$ d (left plot), and drawdown s versus time t at distance $r = 0.1$ m (right plot) for the three-layer model discussed in the text. The aquifer system is confined and a pumping well extracts water from the upper and lower aquifer. Because of the extraction, the flow in the top layer converts from confined to unconfined at distance R . The colored solid lines are simulated using the semi-analytical approach presented in this chapter, the black dotted lines using the finite-difference method. The gray dashed lines are the corresponding solution without conversion. See text for a detailed explanation.

7.5. Combined areal infiltration and drainage

The second type of non-linear problems that is examined in this chapter concerns the simulation of the combined effect of areal infiltration and drainage on a groundwater extraction. It is the analytical steady-state solution developed by Ernst (1971) for a fully penetrating pumping well in a single aquifer that is generalized here to transient flow to a well in a multilayered aquifer system. Uniform infiltration and drainage are defined for the top layer, where drainage becomes inactive close to the well due to the lowering of the hydraulic head. Although this top layer is phreatic, its transmissivity is kept constant for mathematical convenience, which is in agreement with the assumptions underlying the Ernst (1971) model.

Before the problem is stated mathematically, it is shown first that there is no flow in the aquifer system before the pumping starts. More precisely, it is proven that the head in each layer of the system equals the product of infiltration rate and drainage resistance. In this way, the problem

stated in this section is a specific case of the general problem addressed in section 7.3, and consequently, the semi-analytical approach outlined in section 7.3.2 is applicable here.

The steady state solution by Ernst (1972) is discussed in detail, as is the corresponding transient-state solution by Louwyck et al. (2022). The latter also applies the Laplace transform and is very similar to the simplified one-layer solution presented here. The only difference lies in the initial conditions defined for the proximal zone: the Louwyck et al. (2022) solution sets the initial drawdown to zero, whereas the solution proposed in this study sets it to the drawdown specified for the boundary between the proximal zone without drainage and the distal zone with drainage.

The difference between both solutions is discussed in detail and compared with the finite-difference approach. It is explained how the MODFLOW procedure by Louwyck et al. (2012, 2014) can be applied to solve the stated problem numerically. In this case, however, the MAXSYM tool (Louwyck, 2011) is used to evaluate the semi-analytical results. This Matlab tool is developed specifically to simulate axisymmetric flow, and it is extended with the option to define a nonlinear drainage condition (Louwyck, 2015). Besides the transient one-layer solution, the steady-state solution by Ernst (1971) is applied to verify the results simulated using the semi-analytical approach and the finite-difference method. A final model of a three-layer system is used to compare the semi-analytical multilayer solution with the finite-difference solution when there is more than one layer.

7.5.1. Solving the initial head problem

The initial heads are found by simulating the steady flow before pumping, that is if $Q_i = 0$ for all layers i . The drainage level is set to zero, as are the constant heads at the outer model boundary:

$$h_{0,2}(r, t) = h_{i,2}(\infty, t) = 0 \quad (176)$$

The generalized solution for this problem is given in Chapter 2 and in section 7.2.2. Because of the leaky top, all eigenvalues are nonzero. As $r_{in} \rightarrow 0$, $r_{out} \rightarrow \infty$, and $Q_i = 0$, the integration constants are zero, i.e. $\alpha = \mathbf{0}$ and $\beta = \mathbf{0}$. The solution given in Chapter 2 and in section 7.2.2 thus simplifies to:

$$\mathbf{h} = \mathbf{V}\mathbf{D}^{-1}\mathbf{V}^{-1}\mathbf{b} \quad (177)$$

where vector \mathbf{h} contains the initial heads at time $t = 0$:

$$\mathbf{h}_i = h_i(r, 0) = \varphi_i \quad (1 \leq i \leq n_l) \quad (178)$$

Recall that matrices \mathbf{V} and \mathbf{D} are found by performing the following eigendecomposition:

$$\mathbf{A} = \mathbf{V}\mathbf{D}\mathbf{V}^{-1} \quad (179)$$

where system matrix \mathbf{A} is defined as:

$$\mathbf{A}_{ij} = \begin{cases} \frac{1}{c_{i-1}T_i} + \frac{1}{c_iT_i} & (i = j) \\ \frac{-1}{c_{i-1}T_i} & (i = j + 1) \\ \frac{-1}{c_iT_i} & (i = j - 1) \end{cases} \quad (180)$$

In this specific case where there is infiltration only in the top layer, vector \mathbf{b} is defined as:

$$\mathbf{b}_i = \begin{cases} N & (i = 1) \\ T_1 & (i > 1) \\ 0 & \end{cases} \quad (181)$$

From (179), it follows that:

$$\mathbf{A}^{-1} = \mathbf{V}\mathbf{D}^{-1}\mathbf{V}^{-1} \quad (182)$$

Introducing (182) into (177) gives:

$$\mathbf{h} = \mathbf{A}^{-1}\mathbf{b} \quad (183)$$

or:

$$\mathbf{A}\mathbf{h} = \mathbf{b} \quad (184)$$

Using definition (181) for \mathbf{b} :

$$\mathbf{A}\mathbf{h} = [N/T_1 \quad 0 \quad \cdots \quad 0]^T \quad (185)$$

As $c_{n_l} = \infty$, it follows from definition (180) for \mathbf{A} that:

$$\mathbf{A}\mathbf{1} = [(c_0 T_1)^{-1} \quad 0 \quad \cdots \quad 0]^T \quad (186)$$

with $\mathbf{1}$ an $n_l \times 1$ vector of ones. Expression (186) states that the sum of each row in \mathbf{A} is zero, except the sum of the first row, which equals $(c_0 T_1)^{-1}$. Multiplying both sides of equation (186) by Nc_0 gives:

$$\mathbf{A}\mathbf{1}Nc_0 = [N/T_1 \quad 0 \quad \cdots \quad 0]^T \quad (187)$$

It is seen that the right-hand side of equations (185) and (187) are the same, which implies the left-hand sides are also equal:

$$\mathbf{h} = \mathbf{1}Nc_0 \quad (188)$$

This means the initial head φ in each layer equals Nc_0 . The problem stated in section 7.3.1 assumes the initial head in each layer i and at all distances r is the same and equal to φ [L]. In this case, the initial condition can be defined as:

$$h_{i,2}(r, 0) = \varphi = Nc_0 \quad (1 \leq i \leq n_l) \quad (189)$$

Recall that initial condition (189) is required only for the distal zone, as initially, R is equal to zero. Note that this condition is only true if $c_{n_l} = \infty$. If the bottom of the aquifer system is leaky, then the initial heads are found by evaluating equation (183), in which case there is still no horizontal flow within the layers, but there is vertical flow between the layers induced by the leakage through the lower boundary.

7.5.2. Problem statement

If initial condition (189) is valid and there is no flow in the aquifer system before pumping, then the problem can be reformulated in terms of drawdown. Using definition (60):

$$s_{ij}(r, t) = h_{ij}(r, t) - \varphi = h_{ij}(r, t) - Nc_0 \quad (1 \leq i \leq n_l; j = 1, 2) \quad (190)$$

Using (190), the system of partial differential equations for the proximal zone ($j = 1$) is rewritten as:

$$\begin{cases} \frac{\partial^2 s_{11}}{\partial r^2} + \frac{1}{r} \frac{\partial s_{11}}{\partial r} = \frac{S^y}{T_1} \frac{\partial s_{11}}{\partial t} + \frac{-N}{T_1} + \frac{s_{11} - s_{21}}{c_2 T_1} \\ \frac{\partial^2 s_{i1}}{\partial r^2} + \frac{1}{r} \frac{\partial s_{i1}}{\partial r} = \frac{S_i}{T_i} \frac{\partial s_{i1}}{\partial t} + \frac{s_{i1} - s_{i-1,1}}{c_{i-1} T_i} + \frac{s_{i1} - s_{i+1,1}}{c_i T_i} \quad (2 \leq i \leq n_l) \end{cases} \quad (191)$$

Note that there is no drainage in the proximal zone; hence, $c_0 = \infty$. As the drainage level $h_{0,2}$ is zero according to (176), and consequently, $s_{0,2} = -Nc_0$, the set of partial differential equations for the distal zone ($j = 2$) simplifies to the equations of a leaky multilayer system without infiltration:

$$\begin{cases} \frac{\partial^2 s_{12}}{\partial r^2} + \frac{1}{r} \frac{\partial s_{12}}{\partial r} = \frac{S^y}{T_1} \frac{\partial s_{12}}{\partial t} + \frac{s_{12}}{c_0 T_1} + \frac{s_{12} - s_{22}}{c_2 T_1} \\ \frac{\partial^2 s_{i2}}{\partial r^2} + \frac{1}{r} \frac{\partial s_{i2}}{\partial r} = \frac{S_i}{T_i} \frac{\partial s_{i2}}{\partial t} + \frac{s_{i2} - s_{i-1,2}}{c_{i-1} T_i} + \frac{s_{i2} - s_{i+1,2}}{c_i T_i} \quad (2 \leq i \leq n_l) \end{cases} \quad (192)$$

Flux N is canceled out in the first equation of (192). Recall that $c_{n_l} = \infty$ in both zones. The boundary conditions are also rewritten as a function of drawdown and are adopted from section 7.3.1:

$$\lim_{r_w \rightarrow 0} Q_{i,1}^h(r_w, t) = Q_i \quad (1 \leq i \leq n_l) \quad (193)$$

$$s_{i,2}(\infty, t) = 0 \quad (1 \leq i \leq n_l) \quad (194)$$

$$s_{i,1}(R, t) = s_{i,2}(R, t) \quad (1 \leq i \leq n_l) \quad (195)$$

$$Q_{i,1}^h(R, t) = Q_{i,2}^h(R, t) \quad (1 \leq i \leq n_l) \quad (196)$$

Drainage becomes inactive when the head in the top layer is below the drainage level, which equals zero; hence, $h_{1,1}(R) = h_{1,2}(R) = 0$. Reformulating additional condition (68) in terms of drawdown gives:

$$s_{1,1}(R, t) = s_{1,2}(R, t) = 0 - \varphi = -Nc_0 \quad (197)$$

As transient flow is considered, initial conditions are required:

$$s_{i,2}(r, 0) = 0 \quad (1 \leq i \leq n_l) \quad (198)$$

Recall that the initial drawdowns are required only for the distal zone ($j = 2$), as initially, R is equal to zero. The aquifer system always attains a new state of equilibrium, which means the maximum value for distance R is found by solving the corresponding steady-state problem.

7.5.3. Semi-analytical solution method

The semi-analytical solution method discussed in section 7.3.2 is adopted here to simulate the effect on pumping of combined areal infiltration and drainage. First, the solution for multiple layers is presented, after which solving the inverse problem to determine R is discussed. Finally, the one-layer solutions for steady and transient flow are derived, and compared with the solutions by Ernst (1971) and by Louwyck et al. (2022), respectively.

7.5.3.1. Solution for multiple layers

To solve the stated problem semi-analytically, the transient-state solution presented in section 7.3.2.2 is applied. The exact solution for the drawdown in the Laplace domain is given by (120). The numerical inversion is done using the Stehfest (1970) algorithm. The solution in Laplace space may be approximated by (122) assuming $\mathbf{U}(r) \approx \mathbf{I}$. As explained in section 7.3.2.2, the term containing \mathbf{v}_1 in the first equation of (122) cannot be ignored for large values of time since N/p becomes significantly large if $p \rightarrow 0$. If steady flow is simulated, then solution (71) presented in section 7.3.2.1 is used.

Recall that the difference between the two zones only lies in the upper boundary conditions of the top layer. In the proximal zone ($j = 1$), there is infiltration, or $N_{1,1} = N$ with $N > 0$, yet there is no drainage, or $c_{0,1} = \infty$, while in the distal zone ($j = 2$), there is no infiltration, or $N_{1,2} = 0$, yet there is drainage, or $c_{0,2} = c_0$, where c_0 is finite. The corresponding drainage level is set to zero. As there is

no infiltration in the distal zone, $\mathbf{b}_2 = \mathbf{v}_2 = \mathbf{0}$. In the distal zone, the initial drawdowns are zero according to initial condition (198). The aquifer transmissivities are the same in both zones; hence, $\mathbf{T}_1 = \mathbf{T}_2 = \mathbf{T}$.

7.5.3.2. Solving the inverse problem

As explained in section 7.3.2.3, it is advisable to first determine distance R_{max} for the steady-state problem. Using (127) with $s_c = -Nc_0$ according to (197), the minimization problem to be solved in the steady-state case is:

$$R_{max} = \min_{\log R \in \mathbb{R}} |-Nc_0 - s_{1,2}(R, t)| \quad (t \rightarrow \infty) \quad (199)$$

Once R_{max} [L] is found, the values for $R(t_k)$ that are required to simulate transient flow at time t_k can be determined starting with the largest time $t_{max} = \max_k t_k$:

$$R(t_{max}) = \min_{\log R \leq u} |-Nc_0 - s_{1,2}(R, t_{max})| \quad \text{with } u = \log R_{max} \quad (200)$$

The other values for $R(t_k)$ can be determined recursively starting with the second largest time, etc.:

$$R(t_k) = \min_{\log R \in [l, u]} |-Nc_0 - s_{1,2}(R, t_k)| \quad (0 < t_k < t_{k+1}) \quad \text{with } l = \log(R(t_{k+1})/x) \text{ and } u = \log R(t_{k+1}) \quad (201)$$

As explained in section 7.4.2.2, variables l and u are the lower and upper bound, respectively, which are defined using $R(t_{k+1})$, that is determined during the previous iteration. Constant x is greater than 1 and must be chosen sufficiently large.

7.5.3.3. The steady-state one-layer solution

In this section, the analytical solution for the model of Ernst (1971) is derived from the steady-state multilayer solution (71) presented in section 7.3.2.1. In the one-layer case, the single eigenvalue d_j equals the single element of \mathbf{A}_j , and the corresponding eigenvector $\mathbf{V}_j = 1$. For the first zone, $d_1 = 0$ and $b_1 = N/T$, which gives:

$$s_1(r) = s_2(R) + \frac{Q}{2\pi T} \ln\left(\frac{R}{r}\right) + \frac{N}{4T} (R^2 - r^2) \quad (202)$$

For the second zone, $d_2 = \frac{1}{cT}$ and $b_2 = 0$, which gives:

$$s_2(r) = \frac{K_0(x_2)}{2\pi T X_2 K_1(X_2)} Q_1^h(R) \quad (203)$$

with $x_2 = r \sqrt{\frac{1}{cT}}$ and $X_2 = R \sqrt{\frac{1}{cT}}$. The extra condition at the point of conversion between infiltration and drainage states that:

$$s_2(R) = -Nc \quad (204)$$

Finally, the radial discharge $Q_1^h(R)$ is found by evaluating:

$$Q_1^h(R) = Q + N\pi R^2 \quad (205)$$

Summarizing, the solution for the steady state one-layer model is (Louwyck et al., 2022, 2023):

$$\begin{cases} s_1(r) = -Nc + \frac{Q}{2\pi T} \ln\left(\frac{R}{r}\right) + \frac{N}{4T}(R^2 - r^2) & (r \leq R) \\ s_2(r) = \frac{K_0(x_2)}{2\pi T X_2 K_1(X_2)} (Q + N\pi R^2) & (r \geq R) \end{cases} \quad (206)$$

Distance R is found by evaluating $s_2(R) = -Nc$ according to (204):

$$\frac{K_0(X_2)}{2\pi T X_2 K_1(X_2)} (Q + N\pi R^2) + Nc = 0 \quad (207)$$

Expression (207) may be rearranged to obtain equation (29) in Ernst (1971):

$$\frac{-Q}{\pi T N c} = X_2 \left[X_2 + 2 \frac{K_1(X_2)}{K_0(X_2)} \right] \quad (208)$$

Using (207), the second equation in (206) can be simplified:

$$\begin{cases} s_1(r) = -Nc + \frac{Q}{2\pi T} \ln\left(\frac{R}{r}\right) + \frac{N}{4T}(R^2 - r^2) & (r \leq R) \\ s_2(r) = -Nc \frac{K_0(x_2)}{K_0(X_2)} & (r \geq R) \end{cases} \quad (209)$$

The first and second equation in (209) correspond to equations (27) and (26) in Ernst (1971), respectively. In Ernst (1971), a positive value is assigned to pumping rate Q , and resistance c is defined as the sum of the effective drainage resistance and the vertical resistance of a semi-impervious layer overlaying the extracted aquifer. This is a typical situation in the western part of the Netherlands, and therefore, it is commonly referred to as the “Holland profile” (Maas, 2002).

7.5.3.4. The transient-state one-layer solution

To simulate transient flow in a single aquifer subject to uniform drainage and infiltration, the transient state multilayer solution presented in section 7.3.2.2 is applied. In this case, the eigenvalues for zone 1 and 2 are $d_1 = \frac{s}{T}p$ and $d_2 = \frac{1}{ct} + \frac{s}{T}p$, respectively, and $\nu_2 = 0$ as there is no infiltration in zone 2. Simplifying solution (120) gives:

$$\begin{cases} \bar{s}_1(r, p) = \frac{-Nc}{p} + \frac{Q}{2\pi T p} \left[K_0(x_1) - \frac{I_0(x_1)}{I_0(X_1)} K_0(X_1) \right] + \left[1 - \frac{I_0(x_1)}{I_0(X_1)} \right] \frac{N}{Sp^2} & (r \leq R) \\ \bar{s}_2(r, p) = \bar{Q}_1^h(R, p) \frac{K_0(x_2)}{2\pi T X_2 K_1(X_2)} & (r \geq R) \end{cases} \quad (210)$$

with $x_j = r\sqrt{d_j}$ and $X_j = R\sqrt{d_j}$. In the first equation of (210), the Laplace transform of condition (197) is used to replace $\bar{s}_2(R, p)$:

$$\bar{s}_2(R, p) = -\frac{Nc}{p} \quad (211)$$

The Laplace transform of the radial discharge at distance R is:

$$\bar{Q}_1^h(R, p) = 2\pi T \left\{ \left[\frac{X_1 I_1(X_1)}{I_0(X_1)} K_0(X_1) + X_1 K_1(X_1) \right] \frac{Q}{2\pi T p} + \left[\frac{X_1 I_1(X_1)}{I_0(X_1)} \right] \frac{N}{Sp^2} \right\} \quad (212)$$

Distance R is found by solving the inverse Laplace transform of (211), where the second equation of (210) is used to substitute $\bar{s}_2(R, p)$:

$$\mathcal{L}^{-1} \left\{ \bar{Q}_1^h(R, p) \frac{K_0(X_2)}{2\pi T X_2 K_1(X_2)} \right\} + Nc = 0 \quad (213)$$

Recall that \mathcal{L}^{-1} denotes the inverse Laplace transform. In equation (213), $\bar{Q}_1^h(R, p)$ must be replaced by the right-hand side of expression (212). Using equations (211) and (213), the second equation of solution (210) can be reduced:

$$\begin{cases} \bar{s}_1(r, p) = -\frac{Nc}{p} + \frac{Q}{2\pi T p} \left[K_0(x_1) - \frac{I_0(x_1)}{I_0(X_1)} K_0(X_1) \right] + \left[1 - \frac{I_0(x_1)}{I_0(X_1)} \right] \frac{N}{Sp^2} & (r \leq R) \\ \bar{s}_2(r, p) = -\frac{Nc}{p} \frac{K_0(x_2)}{K_0(X_2)} & (r \geq R) \end{cases} \quad (214)$$

The equations in (214) must be inverted back to the real time domain, which can be done numerically using the Stehfest (1970) algorithm. The same is true for the inversion in equation (213).

Louwyck et al. (2022) solve the same problem by setting the initial drawdown in the proximal zone to zero, which yields the following solution in the Laplace domain:

$$\begin{cases} \bar{s}_1 = \frac{-Nc}{p} \left[\frac{I_0(x_1)}{I_0(X_1)} \right] + \frac{Q}{2\pi T p} \left[K_0(x_1) - \frac{I_0(x_1)}{I_0(X_1)} K_0(X_1) \right] + \left[1 - \frac{I_0(x_1)}{I_0(X_1)} \right] \frac{N}{Sp^2} & (r \leq R) \\ \bar{s}_2 = \bar{Q}_1^h(R, p) \frac{K_0(x_2)}{2\pi T X_2 K_1(X_2)} & (r \geq R) \end{cases} \quad (215)$$

with:

$$\bar{Q}_1^h(R) = 2\pi T \left\{ \left[\frac{X_1 I_1(X_1)}{I_0(X_1)} K_0(X_1) + X_1 K_1(X_1) \right] \frac{Q}{2\pi T p} + \left[\frac{X_1 I_1(X_1)}{I_0(X_1)} \right] \left(\frac{1}{Sp} + c \right) \frac{N}{p} \right\} \quad (216)$$

Comparing solution (215) with solution (214), it is seen that in the first equation of (215), $-Nc/p$ is multiplied by $I_0(x_1)/I_0(X_1)$. As explained in section 7.3.2.2, it may be assumed that this function approximates 1, in which case both solutions are identical. Moreover, if this assumption is true, then both solutions may be approximated as:

$$\begin{cases} \bar{s}_1(r, p) = -\frac{Nc}{p} + \frac{Q}{2\pi T p} [K_0(x_1) - K_0(X_1)] + \left[1 - \frac{I_0(x_1)}{I_0(X_1)} \right] \frac{N}{Sp^2} & (r \leq R) \\ \bar{s}_2(r, p) = -\frac{Nc}{p} \left[\frac{K_0(x_2)}{K_0(X_2)} \right] & (r \geq R) \end{cases} \quad (217)$$

where distance R is determined by finding the root of the following equation:

$$\mathcal{L}^{-1} \left\{ \left[\frac{X_1 K_1(X_1) K_0(X_2)}{X_2 K_1(X_2)} \right] \frac{Q}{2\pi T p} + \left[\frac{X_1 I_1(X_1) K_0(X_2)}{X_2 K_1(X_2) I_0(X_1)} \right] \frac{N}{Sp^2} \right\} + Nc = 0 \quad (218)$$

Note that the first equation of (217) still takes into account the term containing N/p^2 . This term may be omitted for small values of time t , as in this case, Laplace variable $p \rightarrow \infty$. However, for large values of time, $p \rightarrow 0$, and therefore, this term cannot be ignored, even if $I_0(x_1)/I_0(X_1)$ approximates 1.

7.5.4. Finite-difference approach

To solve the problem stated in section 7.5.2 numerically, the MAxSym code (Louwyck, 2011), that implements the finite-difference approach proposed by Louwyck et al. (2012) and summarized in Chapter 3, is extended with the option to define drawdown-limited cells (Louwyck, 2015). The finite-

difference grid is two-dimensional: row i corresponds to layer i , and column j to ring j , as flow is axially symmetric. The inner radius [L] of ring j is $r_{b,j}$; the outer radius [L] is $r_{b,j+1}$. Drawdown in node j is calculated at the nodal circle with radius r_j [L], which is equal to the harmonic mean of inner and outer radius. Time t is discretized into time steps. Drawdown s_{ijk} [L] is the drawdown in layer i , for ring j , and at time step k , which is negative if the head is lowering.

If a node in the finite-difference grid is drawdown-limited, then a minimum or maximum value for the drawdown is defined. As drawdown is negative in case of a decrease in head, a maximum drawdown value s^{max} [L] must be defined to implement a draining boundary condition, and the amount of water Q^{out} [L^3/T] drained from cell ij per unit of time during time step k is calculated as:

$$Q_{ijk}^{out} = \begin{cases} \pi(r_{b,j+1}^2 - r_{b,j}^2) \frac{(s_{ijk}^{max} - s_{ijk})}{c_{ij}^{out}} & (s_{ijk} > s_{ijk}^{max}) \\ 0 & (s_{ijk} \leq s_{ijk}^{max}) \end{cases} \quad (219)$$

with c_{ij}^{out} the outflow resistance [T]. In the same way, a minimum drawdown value s^{min} [L] is defined to implement an irrigating boundary condition, and the amount of water Q^{in} [L^3/T] infiltrating into cell ij per unit of time during time step k is calculated as:

$$Q_{ijk}^{in} = \begin{cases} \pi(r_{b,j+1}^2 - r_{b,j}^2) \frac{(s_{ijk}^{min} - s_{ijk})}{c_{ij}^{in}} & (s_{ijk} < s_{ijk}^{min}) \\ 0 & (s_{ijk} \geq s_{ijk}^{min}) \end{cases} \quad (220)$$

with c_{ij}^{in} the inflow resistance [T]. Figure 6 visualizes the draining and irrigating boundary condition expressed by (219) and (220), respectively. Quantities Q_{ijk}^{out} and/or Q_{ijk}^{in} must be added to the total water budget equation for node ij . The total water budget equation is given in section 3.3.4 of Chapter 3 (equation 27).

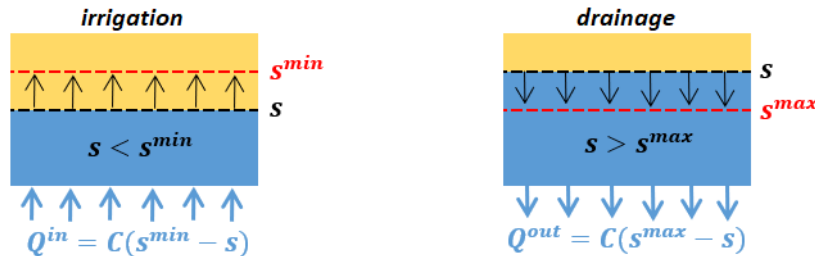


Figure 6. Visualization of the drawdown-limited boundary condition implemented in the extended version of MAxSym (Louwyck, 2011, 2015). The left case shows an irrigating boundary condition adding water to the grid cell at rate Q^{in} if the actual drawdown s is lower than the specified minimum drawdown s^{min} . The right case shows a draining boundary condition removing water from the grid cell at rate Q^{out} if the actual drawdown s is higher than the specified maximum drawdown s^{max} . Parameter C is the conductance which is equal to the horizontal surface area of the grid cell divided by the user-defined resistance. See text for exact definitions.

MAxSym (Louwyck, 2011) applies the Strongly Implicit Procedure (SIP) developed by Stone (1968) to solve the system of finite-difference equations. This procedure needs to be modified to account for imposed drawdown limits. This means that after each iteration, condition (219) and/or (220) must be checked for each cell in which a maximum or minimum drawdown is defined, respectively, and its finite-difference equation has to be updated accordingly. As boundary conditions (219) or (220) are non-linear, a larger number of iterations is required for the SIP solver to converge to a solution than usually is the case when solving a linear system of equations.

Using the MAxSym code to simulate flow towards a well in a multi-aquifer system is demonstrated by Louwyck (2011) and Louwyck et al. (2012). To simulate the problem stated in this study, recharge needs to be defined in each cell of the top layer:

$$Q_{ijk} = \pi(r_{b,j+1}^2 - r_{b,j}^2)N \quad (i = 1) \quad (221)$$

Q_{ijk} is the user defined discharge [L^3/T] in cell ij during timestep k , which is negative if water is removed from the cell. Recall that N is the constant infiltration flux defined for the top layer, which is positive since it adds water to the system. Additionally, a drainage boundary condition at the top of the multi-aquifer system is defined. Therefore, a maximum drawdown s^{max} equal to zero must be defined in each node of the top layer as the drainage level is assumed equal to zero. The outflow resistance c^{out} must be equal to the drainage resistance c_0 according to (219).

Alternatively, the MODFLOW procedure outlined by Louwyck et al. (2014) and discussed in Chapter 3 may be applied using MODFLOW 2005 (Harbaugh, 2005). To account for recharge and drainage, the RECHARGE and DRAIN packages are used (Harbaugh, 2005; Harbaugh et al., 2000). The MODFLOW grid has the same number of rows and columns as the MAxSym grid, but cells have unit width in the former. Therefore, hydraulic parameters and boundary conditions in each MODFLOW grid cell need to be corrected to account for the corresponding ring dimensions (Louwyck et al., 2014). In the RECHARGE package (Harbaugh, 2005; Harbaugh et al., 2000), the infiltration flux, denoted by RECH [L/T], is multiplied by the horizontal surface of the ring:

$$\text{RECH}(i,j) = \pi(r_{j+0.5}^2 - r_{j-0.5}^2)N \quad (i = 1) \quad (222)$$

In the DRAIN package (Harbaugh, 2005; Harbaugh et al., 2000), drainage level ELEVATION [L] is set to zero, and conductance COND [L^2/T] is defined as:

$$\text{COND}(i,j) = \frac{\pi(r_{b,j+1}^2 - r_{b,j}^2)}{c_0} \quad (i = 1) \quad (223)$$

The SIP solver is also available with MODFLOW 2005, as are many other solvers (Harbaugh, 2005; Harbaugh et al., 2000). Radial distance and time are discretized according to a ‘logspace’ scheme, which is explained in section 3.3.1 of Chapter 3 and section 5.4 of Chapter 5.

7.5.5. Verification

To verify the semi-analytical approach presented in section 7.5.3, it is compared with the steady state solution by Ernst (1971) and the transient state solution by Louwyck et al. (2022). Because these solutions consider one layer only, additionally, a three-layer example is presented in which the semi-analytical solution is compared with the finite-difference solution. The latter is simulated using the extended version of the MAxSym tool (Louwyck, 2011, 2015), as discussed in previous section 7.5.4.

7.5.5.1. Steady-state one-layer solution

The first test case involves the steady-state solution initially derived by Ernst (1971) and revisited by Louwyck et al. (2022, 2023). Figure 7 shows dimensionless drawdown $-sT/Q$ as a function of dimensionless distance r/\sqrt{Tc} for different values of dimensionless recharge $-NTc/Q$. The colored solid lines are the analytical solution by Ernst (1971), which is discussed in section 7.5.3.3. The solution is given by (209). Distance R where drainage becomes inactive, is found by solving (208) for X_2 . This is done using SciPy function “fmin” which applies the Nelder and Mead (1965) method. In this case, dimensionless distance R/\sqrt{Tc} is determined, and dimensionless drawdown at this distance equals $-NTc/Q$.

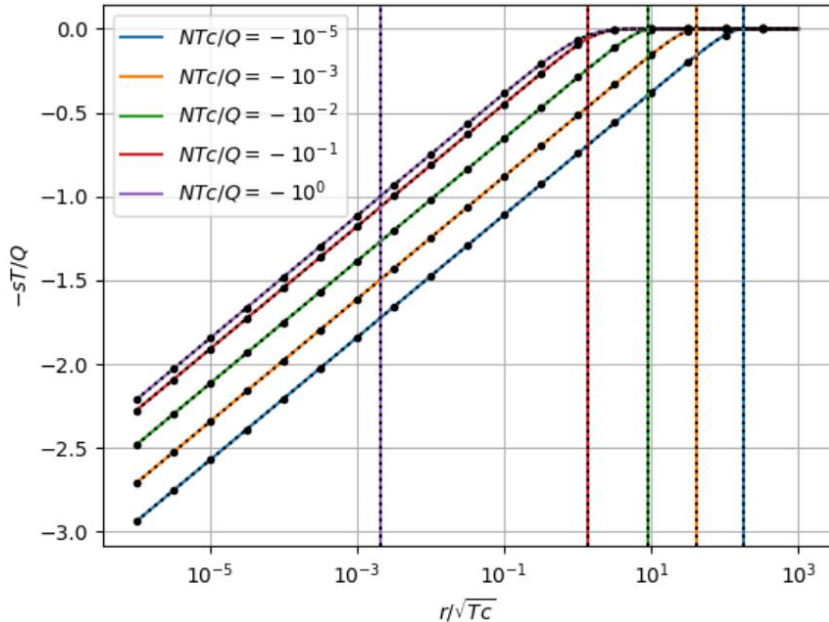


Figure 7. Dimensionless drawdown versus dimensionless distance for the model that simulates axisymmetric flow toward a fully penetrating well that extracts water at constant rate Q from a homogeneous aquifer with transmissivity T that is infiltrated at constant flux N and with areal drainage characterized by constant resistance c . The colored solid lines are the analytical solution by Ernst (1971), the black dotted lines are simulated using the semi-analytical approach presented in this chapter, and the black dots are the finite-difference solution. The vertical lines indicate the distance of the boundary between the proximal zone around the well without drainage and the distal zone with drainage. See text for the definition of the parameters and a more detailed explanation about the solution methods.

The dotted black lines are simulated using the semi-analytical approach outlined in sections 7.5.3.1 and 7.5.3.2. Although the Ernst (1971) solution is found by simplifying the steady-state multilayer solution, as is shown in section 7.5.3.3, it is still useful to test whether or not solving the multilayer problem for $n_l = 1$ in combination with the generalized minimization problem effectively gives the same results. Figure 7 confirms that both distance R and drawdown s are indeed the same. In the semi-analytical approach, distance R is determined by solving the inverse problem expressed by (199) using SciPy function “fmin”.

Finally, the finite-difference method is applied to simulate the Ernst (1971) model, and the results of these computations are indicated by black dots on the graph in Figure 7. As explained in section 7.5.4, the MODFLOW procedure developed by Louwyck et al. (2012, 2014) could be applied, but in this case, the MAxSym code (Louwyck, 2011) is used, which is extended with the option to define a drainage boundary condition in the nodes of the model grid (Louwyck, 2015). It is seen that the finite-difference results approximate the analytical solution very well.

Figure 7 shows that distance R may be interpreted as the radius of influence of the extraction if dimensionless infiltration $-NTc/Q$ is small, as in this case, drawdown $s(R)$, which equals $-Nc$, is very close to zero. If leakage factor \sqrt{Tc} is large and ratio $-N/Q$ is relatively small, then the proximal zone without drainage is negligibly small, and the Ernst (1971) solution may be approximated by the de Glee formula (de Glee, 1930; Jacob, 1946). These implications of the Ernst (1971) model are discussed exhaustively in Chapter 10 and Chapter 11 about the radius of influence and the water budget myth, respectively.

7.5.5.2. Transient-state one-layer solution

The second test case uses the transient state one-layer model presented by Louwyck et al. (2022). As explained in section 7.5.3.4, semi-analytical solution (215) by Louwyck et al. (2022) is a simplification

of the multilayer two-zone solution with fixed boundary derived in section 7.2.2. Recall that solution (215) is obtained by assigning a zero initial drawdown to the proximal zone around the well where drainage is inactive. The other solution presented in section 7.5.3.4, solution (214), is also a simplification of the multilayer two-zone solution, but in this case, the initial drawdown in the proximal zone is set to drawdown $s(R, t)$ that defines the distance where the conversion occurs. Recall that drawdown $s(R, t)$ equals $-Nc$.

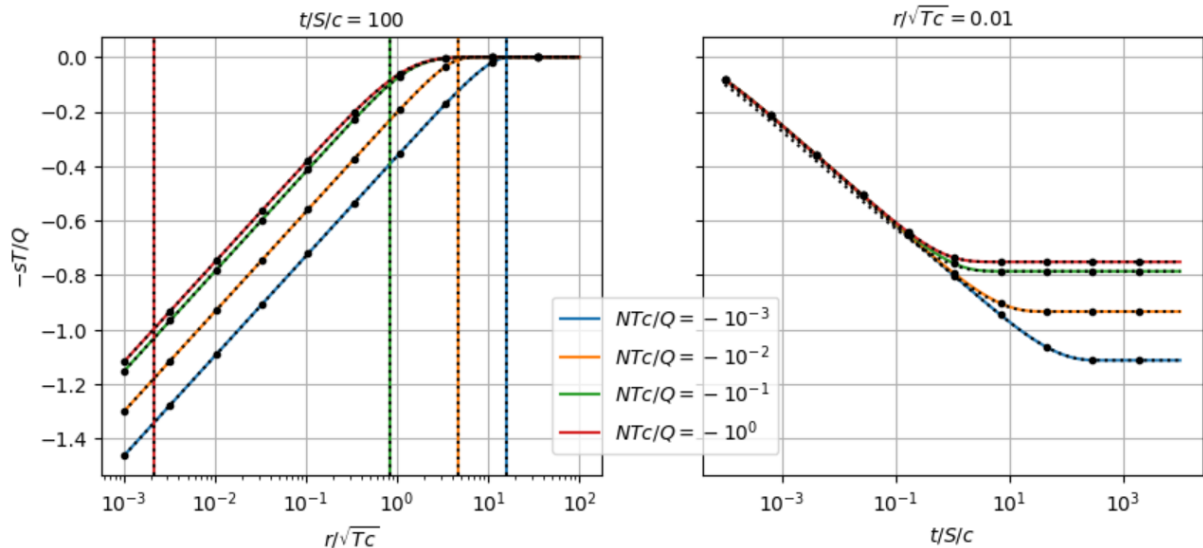


Figure 8. Dimensionless drawdown versus dimensionless distance at dimensionless time equal to 100 (left plot) and dimensionless drawdown versus dimensionless time at dimensionless distance equal to 0.01 (right plot) for the model simulating axisymmetric flow toward a fully penetrating well in a phreatic aquifer subject to areal infiltration and drainage. As indicated by the legend, the four models are simulated considering different values for the dimensionless infiltration, which is also equal to the dimensionless drawdown that determines the boundary between the proximal zone around the well where drainage is inactive and the distal zone where drainage is still active. The vertical lines in the left plot indicate the dimensionless distance at which the conversion takes place. The colored solid lines and the black dotted lines are simulated using the semi-analytical two-zone solution method presented in this chapter. The initial drawdown in the proximal zone is set to zero for the first simulations according to Louwyck et al. (2022), whereas the simulations represented by the black dotted lines set the initial drawdown equal to the drawdown at the distance where the conversion occurs. The black dots are the results obtained from the finite-difference method. See text for the definition of the parameters and a detailed discussion about the different solution methods.

The left plot in Figure 8 shows dimensionless drawdown $-sT/Q$ as a function of dimensionless distance r/\sqrt{Tc} at dimensionless time $t/(Sc)$ equal to 100, while the right plot shows dimensionless drawdown $-sT/Q$ as a function of dimensionless time $t/(Sc)$ at dimensionless distance r/\sqrt{Tc} equal to 0.01. Four different values for dimensionless recharge $-NTc/Q$ are considered. Both the colored solid lines and the black dotted lines are simulated using the semi-analytical two-zone approach discussed in this chapter. The difference between the two solutions only lies in the initial drawdown assigned to the proximal zone. The solid lines are according to Louwyck et al. (2022) approach in which the initial drawdown is set to zero, whereas the solution producing the dotted lines sets the initial drawdown to $s(R, t)$. Both solutions are virtually the same, except for small values of time.

The black dots added to the plots in Figure 8 are simulated using the finite-difference method implemented in the MAXSYM code (Louwyck, 2011, 2015). Alternatively, the MODFLOW procedure developed by Louwyck et al. (2012, 2014) may be applied, as explained in section 7.5.4. It is seen that the finite-difference results approximate the semi-analytical solutions very well, and for small values of time, they are closer to the solution that sets initial drawdowns to zero in the proximal zone. This is more clearly visible on Figure 9 that plots the dimensionless distance R/\sqrt{Tc} versus the

dimensionless time $t/(Sc)$ for the four scenarios of dimensionless recharge – NTc/Q . The semi-analytical solution with nonzero initial drawdown assigned to the proximal zone slightly deviates from the other two solutions.

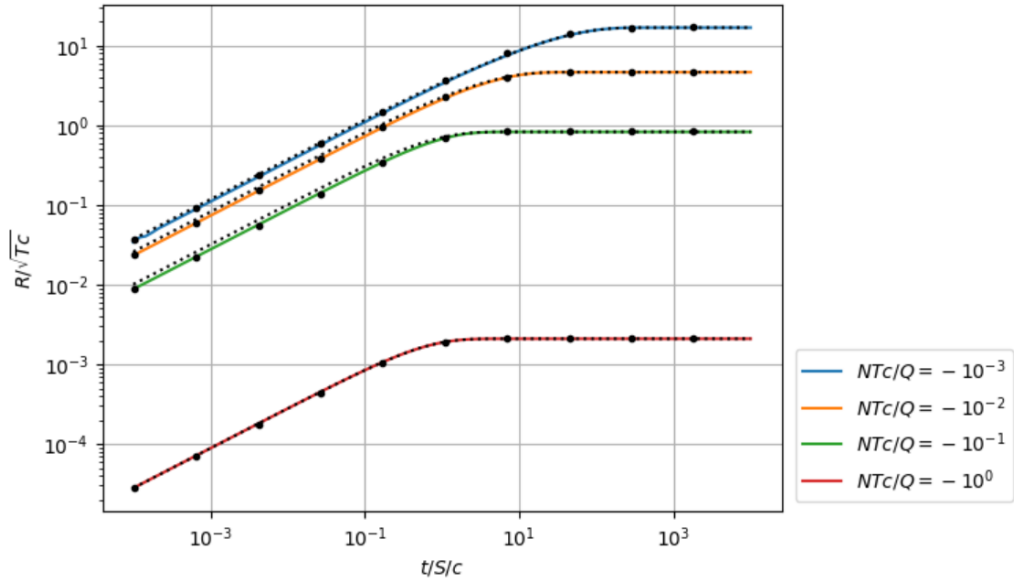


Figure 9. Dimensionless distance at which drainage becomes inactive as a function of dimensionless time for the four models simulating axisymmetric flow toward a fully penetrating pumping well in a phreatic aquifer subject to areal infiltration and drainage. The models are characterized by different values for the dimensionless infiltration, which are indicated by the legend in the plot. The corresponding drawdowns are shown in Figure 8. The colored solid lines and the black dotted lines are simulated using the semi-analytical two-zone solution method presented in this chapter. The initial drawdown in the proximal zone is set to zero for the first simulations according to Louwyck et al. (2022), whereas the initial drawdown is set to the drawdown at the distance where the conversion occurs for the simulations represented by the black dotted lines. The black dots are the results obtained from the finite-difference method. See text for the definition of the parameters and a detailed discussion about the different solution methods.

Using the semi-analytical approach, distance R is determined by solving the inverse problem as explained in section 7.5.3.2. First, the maximum possible distance R_{max} is determined by solving the minimization problem expressed by (199), which employs the corresponding steady-state model. This is done using SciPy function “fmin” that applies the Nelder and Mead (1965) method. It is seen on both the plot in Figure 9 and the time-drawdown graph in Figure 8 that the curves indeed become horizontal after a certain time of pumping, which indicates that a new steady state is reached. Once R_{max} is determined, it can be used as an upper bound to determine the values for $R(t)$. Solving the bounded minimization is done using SciPy function “fminbound” that applies Brent’s (1973) method. The considered dimensionless time interval between 10^{-4} and 10^4 is discretized into 100 evenly spaced points on a logarithmic scale. Applying the finite-difference approach to determine $R(t)$, the distance of the first node is taken for which the model simulates a drawdown that is smaller than dimensionless drawdown $s(R, t)T/Q = -NTc/Q$. Note that the vertical lines on the left plot in Figure 8 also indicate dimensionless distance R/\sqrt{Tc} at dimensionless time $t/(Sc) = 100$.

The transient-state solution may be approximated by the solution developed by Ernst (1971) when the aquifer reaches a new steady state. If leakage factor \sqrt{Tc} is large and ratio $-N/Q$ is relatively small, then the proximal zone without drainage is negligibly small, and the solution can be approximated by the Hantush and Jacob (1955) solution. In this case, the Theis (1935) formula is applicable for small values of time, and the de Glee formula (de Glee, 1930; Jacob, 1946) for large values of time when steady state is reached. The relation between the transient-state one-aquifer model subject to infiltration and drainage and other well-known one-aquifer solutions that are

frequently applied by groundwater practitioners, is clarified in Chapter 10 discussing the significance of the radius of influence.

7.5.5.3. Three-layer example

To test the semi-analytical multilayer approach presented in sections 7.5.3.1 and 7.5.3.2, an example of a three-aquifer system is discussed here, which is similar to the one given in section 7.4.4.2. Recall that the general schematization of such an aquifer system is visualized in the right plot of Figure 1, which shows a system consisting of four aquifers. The example discussed in this section considers a system that comprises three horizontal aquifers of infinite lateral extent, separated by two incompressible aquitards. The transmissivities of the aquifers counted from top to bottom are $T_1 = 200 \text{ m}^2/\text{d}$, $T_2 = 100 \text{ m}^2/\text{d}$, and $T_3 = 250 \text{ m}^2/\text{d}$; the storativities are $S_1 = 0.2$, $S_2 = 5 \times 10^{-3}$, and $S_3 = 10^{-3}$. The two incompressible aquitards separating the aquifers have resistances $c_1 = 100 \text{ d}$ and $c_2 = 500 \text{ d}$, respectively. Note that c_3 is infinitely large as the lower boundary of the multi-aquifer system is impervious.

The top of the system is infiltrated at a constant rate $N = 5 \times 10^{-4} \text{ m/d}$, and drained by a uniform head-dependent boundary condition with resistance $c_0 = 1 \text{ d}$, if the hydraulic head in the top aquifer is greater than the drainage level. When the head is below this level, resistance is set to an infinitely large value to avoid induced infiltration. Because transmissivities and storativities are assumed constant, the drainage level may be set to zero. A pumping well with infinitesimal radius and a separate fully penetrating well screen in the lower and upper aquifer extracts water from the system at pumping rates $Q_1 = -500 \text{ m}^3/\text{d}$ and $Q_3 = -250 \text{ m}^3/\text{d}$, respectively. As no water is extracted from the middle aquifer, $Q_2 = 0$.

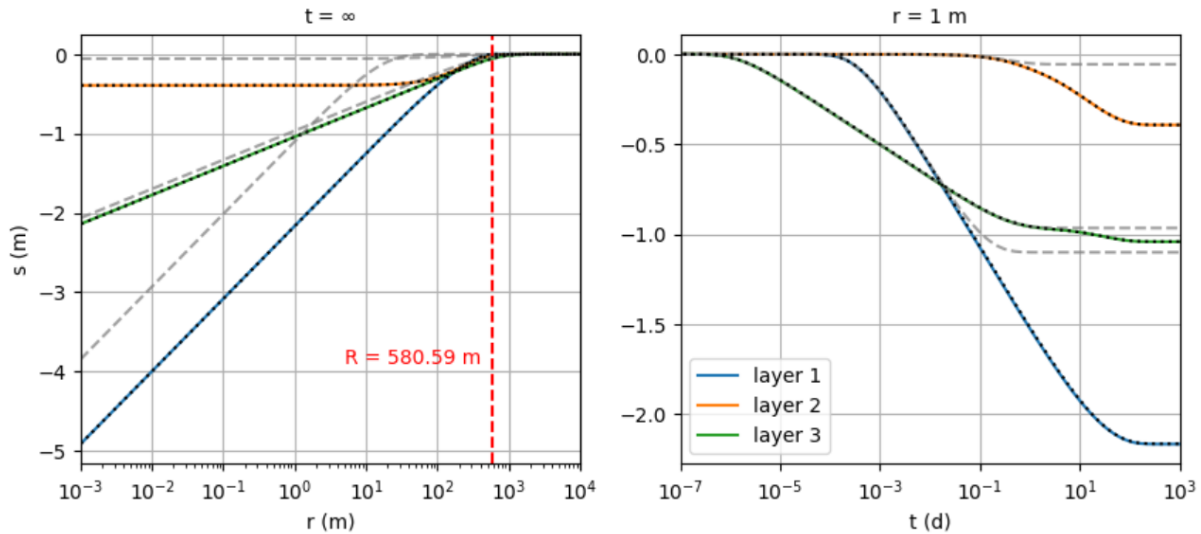


Figure 10. Steady drawdown s versus distance r (left plot) and transient drawdown s versus time t at radial distance r equal to 1 m (right plot) for the three-layer model discussed in the text. The aquifer system is phreatic and a pumping well extracts water from the upper and lower aquifer at constant pumping rate. The top aquifer is recharged at constant infiltration rate and discharged by areal drainage characterized by constant resistance. Because of the extraction, the head in the top layer drops below the drainage level, and the drainage becomes inactive in the proximal zone around the well with radius R . The colored solid lines are simulated using the semi-analytical approach presented in this chapter, the black dotted lines using the finite-difference method. The gray dashed lines are the corresponding solution for a leaky system developed by Hemker (1984, 1985, 1999). See text for a detailed explanation.

The model is simulated using the semi-analytical approach outlined in sections 7.5.3.1 and 7.5.3.2 and the finite-difference method discussed in section 7.5.4. The MODFLOW procedure by Louwyck et al. (2012, 2014) could be applied. However, the extended version of the MAXSYM code (Louwyck, 2011, 2015) is used here, which implements the finite-difference approach proposed by Louwyck et

al. (2012). Figure 10 plots the simulated drawdown versus distance and time. The left plot shows the steady-state drawdown s as a function of radial distance r , whereas the right plot shows drawdown s as a function of time t at distance $r = 1$ m. The colored solid lines correspond to the semi-analytical solution, while the black dotted lines are the result of the finite-difference simulations. It is seen that both solutions are virtually the same.

The MAxSym model consists of 3 layers and 1000 rings. The inner model radius is 0.001 m, which is small enough to approximate the infinitesimal well radius; the outer radius is 10^6 m, which is sufficiently large to approximate the analytical outer boundary at infinity. The rings are defined by discretizing radial distance in logarithmic space, and time is also discretized in logarithmic space, as suggested by Louwyck et al. (2012). The number of time steps is 200, ranging from 10^{-6} d to 984 d. Since all aquifers have constant saturated thickness, it is justified to set all model layer thicknesses to unity, and to assign aquifer transmissivities and storativities to the layer conductivities and specific storages, respectively.

The vertical resistances of the aquitards are assigned to the resistance layers of zero thickness between the model layers. Top and bottom of the model grid are no-flow boundaries. However, in each cell of the top layer, a maximum drawdown s^{max} equal to zero and an outflow resistance c^{out} equal to $c_0 = 1$ d are defined according to (219), and a constant discharge according to (221) is added to account for the constant infiltration. Finally, the pumping well is included in the model by defining constant discharges equal to the pumping rates in the first rings of the model grid.

In both the semi-analytical and the finite-difference approach, the steady initial heads are simulated first. This is required because the drainage boundary condition is nonlinear. Using MAxSym, these initial heads are easily obtained by excluding time steps, storage coefficients, and well discharges from the model. The semi-analytical solution is also straightforward and given in section 7.5.1. As there is no pumping in the initial state, the head in the top layer is greater than the drainage level at all distances. Hence, there is no proximal zone without drainage, and the semi-analytical solution is obtained by solving a leaky three-layer model with infiltration. Both solutions confirm that the calculated initials heads are the same and equal to $Nc_0 = 5 \times 10^{-4}$ m in all layers i and at all distances r from the well..

In the next step, the well is added to the MAxSym model in order to simulate the steady heads during extraction. The left plot in Figure 10 shows the corresponding drawdown, which is the difference between the steady head during pumping and the steady initial head. Note that the initial head is only needed to calculate the drawdown, since the steady state model does not require initial heads. Total volumetric budget, which should be close to zero, is smaller than 10^{-4} m³/d for both finite-difference models, which is very accurate, considering that the total recharge is greater than 10^9 m³/d.

The corresponding semi-analytical steady-state solution is obtained by applying the multilayer two-zone solution method outlined in section 7.3.2.1. Distance R at which the boundary occurs between the proximal zone without drainage and the distal zone with drainage, is determined by solving the unbounded minimization problem expressed by (199). This is done using using SciPy function “fmin” that applies the Nelder and Mead (1965) method. As explained in section 7.5.3.2, distance R obtained from the steady-state model, is the maximum possible distance R_{max} , and it is equal to 580.6 m.

The left plot in Figure 10 also shows the corresponding leaky multi-aquifer solution developed by Hemker (1984) as gray dashed lines. In this steady-state solution, the boundary condition at the top of the aquifer system is linear, which implies the drainage system can also irrigate if the head in the

top aquifer drops below the drainage level. Since the Hemker (1984) model is linear, the superposition principle holds, and drawdown may be simulated directly without knowing the initial heads. As the infiltration flux is constant, it is also canceled out from the governing differential equation formulated in terms of drawdown. In the nonlinear model, initial heads and recharge are not canceled out.

The left plot in Figure 10 shows that in this example, the leaky multilayer solution can be used to approximate drawdown in the lower aquifer, but it underestimates drawdown in the upper aquifer because of the induced infiltration. The extent of the cone of depression in the linear Hemker (1984) model is mainly determined by the largest leakage factor (Bakker & Strack, 2003), whereas it is also determined by the ratio of pumping to infiltration rate in the nonlinear model (Louwyck et al., 2022, 2023). In fact, the larger this ratio, the larger the no-drainage zone, and the more the nonlinear solution deviates from the linear multilayer solution by Hemker (1984).

Finally, the transition from the initial steady state under virgin conditions to the new steady state under pumping conditions is simulated. The right plot in Figure 10 shows the transient drawdowns simulated using the extended version of the MAxSym code (Louwyck, 2011, 2015) and according to the semi-analytical solution presented in section 7.3.2.2. Recall that the Stehfest (1970) algorithm is applied to numerically invert the Laplace space solution (120). The MAxSym model is made transient by including time steps and storativities. Total volumetric budget for each time step is examined, and the maximum value is $0.0044 \text{ m}^3/\text{d}$, which is still very accurate, although the convergence rate seems slower than in case of the steady state simulation.

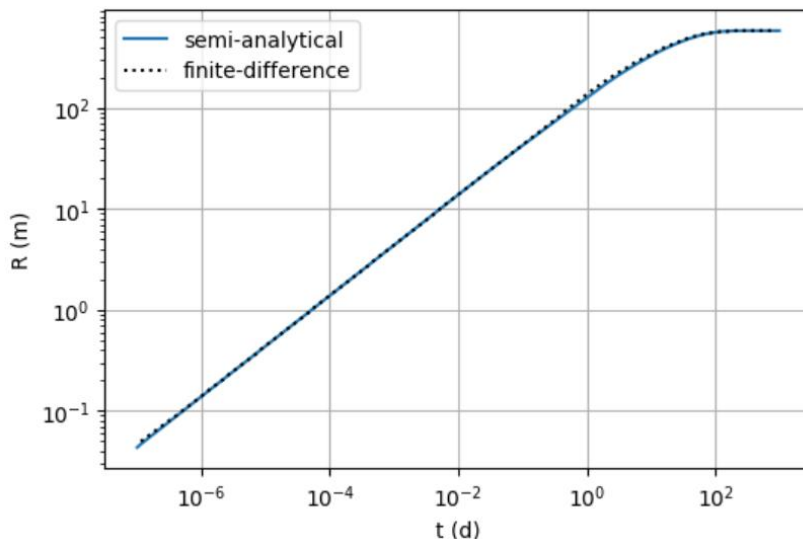


Figure 11. Distance R at which drainage becomes inactive due to pumping as a function of time t for the three-aquifer model discussed in the text. The solid blue curve is determined using the semi-analytical approach presented in this chapter, while the dotted black line is derived from the drawdowns simulated using a finite-difference model. See text for a detailed explanation.

To apply the semi-analytical approach in the transient case, distance $R(t_k)$ needs to be determined first for each simulation time t_k by solving the bounded minimization problem expressed by (201). This is done using SciPy function “fminbound” that implements Brent’s (1973) method. As explained in section 7.5.3.2, R_{max} obtained from the steady-state model is used as an upper bound for the largest simulation time, after which the other values for $R(t_k)$ are determined recursively starting with the second largest time, and so on. At every iteration, the previous value $R(t_{k+1})$ is used to define the lower and upper bound according to (201). In this example, constant x is set to 2, and the

considered time interval between 10^{-7} d and 10^3 d is discretized into 150 evenly spaced points on a logarithmic scale.

The solid blue line on the plot in Figure 11 shows the result of these optimizations. The black dotted line is distance $R(t)$ derived from the transient-state finite-difference model. There is a good match between both curves. Note that the finite-difference model does not simulate distance R explicitly; hence, R is estimated by taking the distance of the first node for which the model simulates a drawdown that is smaller than $-Nc_0$. It is seen on both the plot in Figure 11 and the time-drawdown graph in Figure 10 that the curves become horizontal after approximately 100 days of pumping, which indicates that a new steady state is reached.

The right plot in Figure 10 also indicates a good correspondence between the drawdowns simulated using the semi-analytical approach and the finite-difference method. The first are represented by colored solid lines, the latter by black dotted lines. The gray dashed lines are the corresponding transient leaky multi-aquifer solution developed by Hemker (1985, 1999). This solution is virtually the same at small values of time ($t < 0.1$ d), although the difference between both increases with time, and is maximal when steady state is reached. The difference is largest in the top layer, which is also seen on the distance-drawdown graph in Figure 10.

Notice that not only drawdown is underestimated using the linear Hemker (1985, 1999) solution, but also the time at which a new equilibrium is attained, which is approximately 1 d according to this linear model instead of 100 d. Since the superposition property holds for the leaky multilayer solution, the time to full capture is independent of discharge and recharge. However, in the nonlinear model, which replaces leakage by drainage, the ratio of pumping to infiltration rate also determines how long it takes to reach a new state of equilibrium. The larger this ratio, the larger the extent of the no-drainage zone around the well, and the further the cone of depression has to expand, since the volume of extracted water must be balanced by reducing the drainage with the same amount. Chapter 11 elaborates on this topic and explains in more detail why recharge is relevant in simulating the cone of depression if aquifers cannot be analyzed mathematically as if they are linear systems.

7.6. Summary and conclusions

In this chapter, the solution for axisymmetric flow in a multilayer system consisting of two fixed cylindrical zones is developed. It applies the eigendecomposition method developed by Hemker (1984, 1985, 1999). In the transient case, the Laplace transform is applied and the inversion is performed numerically using the Stehfest (1970) algorithm. The solution may be considered as a special case of the general multilayer-multizone solution presented in Chapter 5. Where the latter applies a numerical method to determine the integration constants, here the related system of equations is solved analytically. Although both solution methods give the same results, the analytical approach yields an expression that gives more insight in the parameter sensitivities. In particular, it reveals that the initial conditions in the proximal zone are not relevant in many cases, which suggests the solution with fixed boundary between the two zones may be applied to solve head-dependent two-zone problems with expanding boundary.

Certainly, the solution may be applied to solve steady-state problems considering two head-dependent zones. In this case, the boundary is fixed, and it can be determined easily by solving an inverse problem that minimizes the absolute difference between required and simulated drawdown in the top layer at the common boundary between the two zones. In the transient case, the same inverse problem needs to be solved for each simulation time. In both cases, a standard nonlinear solver may be applied that minimizes a scalar function. If steady flow is simulated, then an

unbounded optimization can be performed, although it is more effective to log-transform the distance of the boundary between the two zones. In case of transient flow, it is recommended to define an upper bound for the distance, especially at small values of time. This upper bound may be the distance determined for a larger value of time.

Two types of nonlinear problems are examined to evaluate the developed semi-analytical method. The first type deals with the conversion between confined and unconfined flow, and is inspired by the one-layer model presented by Moench and Prickett (1972). Here, the head-dependent parameter is the storativity, which equals the specific yield in the proximal zone where flow is unconfined, and which equals the elastic storage coefficient in the confined part of the aquifer. The second type considers a phreatic aquifer system that is infiltrated and drained at the top, a problem that was tackled first by Ernst (1971), who solved the problem for steady flow in a single aquifer. The transient-state one-layer solution is given by Louwyck et al. (2022), who apply the same solution method as described in this chapter. In this case, the head-dependent parameter is the drainage resistance, which is infinitely large in the proximal zone around the well where the drainage is inactive.

Louwyck et al. (2022) set the initial drawdown in the proximal zone to zero, whereas the solution developed in this chapter defines the initial drawdown equal to the required drawdown at the boundary between the two head-dependent zones. Because these initial drawdowns are not or less sensitive, both approaches give results that are very close to each other, although the latter seems to be in agreement with the Moench and Prickett (1972) solution. One should also keep in mind that the specified drawdown at the boundary of the two zones is kept relatively small for all examples presented in this study. In either way, all solution methods virtually give the same results for each of these one-layer cases. To test the presented semi-analytical approach for the general multilayer case, a three-layer example is given for each type of problem. In these examples, the simulated drawdown is compared with the finite-difference solution, and it is seen that both solution methods give results that approximate each other very well. It is also concluded that the finite-difference method is more straightforward to implement than the semi-analytical approach.

The MODFLOW procedure by Louwyck et al. (2012, 2014) is applied in the confined-unconfined case, where use is made of the limited convertible layer option implemented in the BCF6 package (Harbaugh, 2005; Harbaugh et al., 2000). The MAXSYM tool (Louwyck, 2011) is extended with the option to define nonlinear head-dependent boundary conditions (Louwyck, 2015) and is used to evaluate the semi-analytical approach in case of combined infiltration and drainage. It is concluded that the proposed solution method is able to simulate drawdown very accurately in both cases. It is, however, not proven mathematically that it is justified indeed to use the fixed two-zone solution in the transient case. Further research is needed to study the problem analytically, for instance, by applying the Boltzman transform instead of the Laplace transform (Wang & Zhan, 2009; Xiao et al., 2018).

Although it is not within the scope of this chapter, some examples clearly show that the corresponding linear solution may underestimate the simulated drawdown significantly. This is certainly true for the case of combined areal infiltration and drainage. Chapter 11 discusses the difference between linear and nonlinear models, and possible ramifications of applying the principle of superposition inconsiderately for assessing the sustainability of groundwater extractions. The nonlinear Ernst (1971) solution and its linear counterpart (de Glee, 1930; Jacob, 1940) are used to illustrate the importance of carefully considering whether or not the aquifer system can be analyzed as if it is a linear system. The semi-analytical solution method presented in this chapter may

contribute to a better understanding of nonlinear behavior of radial flow toward a pumping well in a multi-aquifer system.

7.7. References

- Abramowitz, M., & Stegun, I. A. (1965). *Handbook of Mathematical Functions: With Formulas, Graphs, and Mathematical Tables*. In M. Abramowitz & I. A. Stegun (Eds.), *Dover Books on Advanced Mathematics*. New York: Dover Publications.
- Bakker, M., & Strack, O. D. L. (2003). Analytic elements for multiaquifer flow. *Journal of Hydrology*, 271(1–4). [https://doi.org/10.1016/S0022-1694\(02\)00319-0](https://doi.org/10.1016/S0022-1694(02)00319-0)
- Bateman, H. (1954). *Tables of Integral Transforms*. (A. Erdélyi, Ed.) (Vol. 1). New York: McGraw-Hill Book Company.
- Bear, J. (1972). *Dynamics of Fluids in Porous Media*. New York: American Elsevier Publishing Company.
- Boulton, N. S. (1954). Unsteady radial flow to a pumped well allowing for delayed yield from storage. *General Assembly of Rome, Tome II, Groundwater, IAHS publ. 37*, 472–477.
- Boulton, N. S. (1963). Analysis of data from non-equilibrium pumping tests allowing for delayed yield from storage. *Proceedings of the Institution of Civil Engineers*, 26(3), 469–482. <https://doi.org/10.1680/icep.1963.10409>
- Boussinesq, J. (1877). *Essai sur la théorie des eaux courantes, Mémoires présentées par divers savants à l'Académie des Sciences (in French)*. Imprimerie Nationale, Paris.
- Boussinesq, J. (1904). Recherches théoriques sur l’écoulement des nappes d’eau infiltrées dans le sol et sur le débit des sources (in French). *Journal De Mathématiques Pures Et Appliquées*, 10, 5–78.
- Bredehoeft, J. D. (1997). Safe Yield and the Water Budget Myth. *Ground Water*, 35(6), 929–929. <https://doi.org/10.1111/j.1745-6584.1997.tb00162.x>
- Bredehoeft, J. D. (2002). The Water Budget Myth Revisited: Why Hydrogeologists Model. *Ground Water*, 40(4). <https://doi.org/10.1111/j.1745-6584.2002.tb02511.x>
- Bredehoeft, J. D. (2007). It Is the Discharge. *Ground Water*, 45(5), 523–523. <https://doi.org/10.1111/j.1745-6584.2007.00305.x>
- Bredehoeft, J. D., Papadopoulos, S. S., & Cooper, H. H. (1982). The water budget myth. In *Scientific Basis of Water Resources management Studies in Geophysics* (pp. 51–57). National Academy Press.
- Brent, R. P. (1973). *Algorithms for Minimization Without Derivatives*. Englewood Cliffs NJ: Prentice-Hall, Inc.
- Butler, J. J. (1988). Pumping tests in nonuniform aquifers — The radially symmetric case. *Journal of Hydrology*, 101(1–4), 15–30. [https://doi.org/10.1016/0022-1694\(88\)90025-X](https://doi.org/10.1016/0022-1694(88)90025-X)
- Carslaw, H. S., & Jaeger, J. C. (1959). *Conduction of Heat in Solids* (2nd ed.). Oxford: Oxford University Press.
- Chen, C.-X. (1974). *Analytical Solutions to Ground Water Flow Toward Wells in a Confined-Unconfined Aquifer (in Chinese)*. Beijing, China: Beijing College of Geology.

- Chen, C.-X. (1983). *Calculation Methods of Ground Water Unsteady Flow to Wells (in Chinese)*. Beijing, China: Geology Publishing House.
- Chen, C.-X., Hu, L.-T., & Wang, X.-S. (2006). Analysis of Steady Ground Water Flow Toward Wells in a Confined-Unconfined Aquifer. *Ground Water*, 44(4), 609–612. <https://doi.org/10.1111/j.1745-6584.2006.00170.x>
- Cooper, H. H., & Jacob, C. E. (1946). A generalized graphical method for evaluating formation constants and summarizing well-field history. *Transactions, American Geophysical Union*, 27(4), 526–534. <https://doi.org/10.1029/TR027i004p00526>
- de Glee, G. J. (1930). *Over grondwaterstroomingen bij wateronttrekking door middel van putten (in Dutch)* (PhD thesis). Technische Hoogeschool Delft, Drukkerij J. Waltman. Jr., Delft.
- Devlin, J. F., & Sophocleous, M. (2005). The persistence of the water budget myth and its relationship to sustainability. *Hydrogeology Journal*, 13(4). <https://doi.org/10.1007/s10040-004-0354-0>
- Devlin, J. F., & Sophocleous, M. (2006). Reply to Comment on “The persistence of the water budget myth and its relationship to sustainability” by J.F. Devlin and M. Sophocleous, *Hydrogeology Journal* (2005), 13:549–554. *Hydrogeology Journal*, 14(7), 1386–1386. <https://doi.org/10.1007/s10040-006-0033-4>
- Ernst, L. F. (1971). Analysis of groundwater flow to deep wells in areas with a non-linear function for the subsurface drainage. *Journal of Hydrology*, 14(2). [https://doi.org/10.1016/0022-1694\(71\)90004-7](https://doi.org/10.1016/0022-1694(71)90004-7)
- Girinski, N. K. (1946). Complex potential of flow with free surface in a stratum of relatively small thickness and $k = f(z)$ (in Russian). *Doklady Akademii Nauk SSSR*, 51(5), 337–338.
- Haitjema, H. (1995). *Analytic Element Modeling of Groundwater Flow*. San Diego: Academic Press. <https://doi.org/10.1016/B978-0-12-316550-3.X5000-4>
- Hantush, M. S. (1964). Hydraulics of wells. In V. T. Chow (Ed.), *Advances in Hydroscience* (Vol. I, pp. 281–432). New York and London: Academic Press.
- Hantush, M. S., & Jacob, C. E. (1955). Non-steady radial flow in an infinite leaky aquifer. *Transactions, American Geophysical Union*, 36(1), 95–100. <https://doi.org/10.1029/TR036i001p00095>
- Harbaugh, A. W. (1995). *Direct solution package based on alternating diagonal ordering for the U.S. Geological Survey modular finite-difference ground-water flow model*. U.S. Geological Survey Open-File Report 95-288. <https://doi.org/https://doi.org/10.3133/ofr95288>
- Harbaugh, A. W. (2005). *MODFLOW-2005, the U.S. Geological Survey modular ground-water model - the Ground-Water Flow Process*. U.S. Geological Survey Techniques and Methods 6-A16. <https://doi.org/https://doi.org/10.3133/tm6A16>
- Harbaugh, A. W., & McDonald, M. G. (1996). *User's documentation for MODFLOW-96, an update to the U.S. Geological Survey modular finite-difference ground-water flow model*. U.S. Geological Survey Open-File Report 96-485. <https://doi.org/https://doi.org/10.3133/ofr96485>
- Harbaugh, A. W., Banta, E. R., Hill, M. C., & McDonald, M. G. (2000). *MODFLOW-2000, The U.S. Geological Survey Modular Ground-Water Model: User Guide to Modularization Concepts and the Ground-Water Flow Process*. U.S. Geological Survey Open-File Report 00-92. <https://doi.org/https://doi.org/10.3133/ofr200092>

- Hemker, C. J. (1984). Steady groundwater flow in leaky multiple-aquifer systems. *Journal of Hydrology*, 72(3–4), 355–374. [https://doi.org/10.1016/0022-1694\(84\)90089-1](https://doi.org/10.1016/0022-1694(84)90089-1)
- Hemker, C. J. (1985). Transient well flow in leaky multiple-aquifer systems. *Journal of Hydrology*, 81(1–2), 111–126. [https://doi.org/10.1016/0022-1694\(85\)90170-2](https://doi.org/10.1016/0022-1694(85)90170-2)
- Hemker, C. J. (1999). Transient well flow in vertically heterogeneous aquifers. *Journal of Hydrology*, 225(1–2), 1–18. [https://doi.org/10.1016/S0022-1694\(99\)00137-7](https://doi.org/10.1016/S0022-1694(99)00137-7)
- Hill, M. C. (1990). *PRECONDITIONED CONJUGATE-GRADIENT 2 (PCG2), a computer program for solving ground-water flow equations*. U.S. Geological Survey Water-Resources Investigations Report 90-4048. <https://doi.org/10.3133/wri904048>
- Hu, L.-T., & Chen, C.-X. (2008). Analytical Methods for Transient Flow to a Well in a Confined-Unconfined Aquifer. *Ground Water*, 46(4), 642–646. <https://doi.org/10.1111/j.1745-6584.2008.00436.x>
- Jacob, C. E. (1940). On the flow of water in an elastic artesian aquifer. *Transactions, American Geophysical Union*, 21(2), 574. <https://doi.org/10.1029/TR021i002p00574>
- Jacob, C. E. (1946). Radial flow in a leaky artesian aquifer. *Transactions, American Geophysical Union*, 27(2). <https://doi.org/10.1029/TR027i002p00198>
- Kutta, W. (1901). Beitrag zur näherungsweisen Integration totaler Differentialgleichungen (in German). *Zeitschrift Für Mathematik Und Physik*, 46, 435–453.
- Langevin, C. D. (2008). Modeling Axisymmetric Flow and Transport. *Ground Water*, 46(4), 579–590. <https://doi.org/10.1111/j.1745-6584.2008.00445.x>
- Langevin, C. D., Hughes, J. D., Banta, E. R., Niswonger, R. G., Panday, S., & Provost, A. M. (2017). *Documentation for the MODFLOW 6 Groundwater Flow Model*. U.S. Geological Survey Techniques and Methods 6-A55. <https://doi.org/10.3133/tm6A55>
- Lebbe, L. C. (1988). *Uitvoering van pomproeven en interpretatie door middel van een invers model (in Dutch)*. Ghent University, Ghent, Belgium.
- Lebbe, L. C. (1999). *Hydraulic Parameter Identification. Generalized Interpretation Method for Single and Multiple Pumping Tests*. Berlin Heidelberg: Springer-Verlag.
- Louwyck, A. (2011). *MAxSym - A MATLAB Tool to Simulate Two-Dimensional Axi-Symmetric Groundwater Flow*. Research Unit Groundwater Modeling, Ghent University. Retrieved from <https://github.com/alouwyck/MAxSym>
- Louwyck, A. (2015). *Module Projectwerk programmeren B5 - Ontwikkeling MAxSymMer (in Dutch)* (Associate Degree Programming). CVO Lethas, Brussels.
- Louwyck, A., Vandenbohede, A., Bakker, M., & Lebbe, L. C. (2012). Simulation of axi-symmetric flow towards wells: A finite-difference approach. *Computers & Geosciences*, 44, 136–145. <https://doi.org/10.1016/j.cageo.2011.09.004>
- Louwyck, A., Vandenbohede, A., Bakker, M., & Lebbe, L. C. (2014). MODFLOW procedure to simulate axisymmetric flow in radially heterogeneous and layered aquifer systems. *Hydrogeology Journal*, 22(5), 1217–1226. <https://doi.org/10.1007/s10040-014-1150-0>

- Louwyck, A., Vandenbohede, A., Libbrecht, D., Van Camp, M., & Walraevens, K. (2022). The Radius of Influence Myth. *Water*, 14(2), 149. <https://doi.org/10.3390/w14020149>
- Louwyck, A., Vandenbohede, A., Heuvelmans, G., Van Camp, M., & Walraevens, K. (2023). The Water Budget Myth and Its Recharge Controversy: Linear vs. Nonlinear Models. *Groundwater*, 61(1), 100–110. <https://doi.org/10.1111/gwat.13245>
- Maas, C. (2002). Weerstanden in het Hollandse Profiel (in Dutch). *Stromingen*, 8(3), 5–15.
- McDonald, M. G., & Harbaugh, A. W. (1988). *A modular three-dimensional finite-difference ground-water flow model*. U.S. Geological Survey Techniques of Water-Resources Investigations 06-A1. <https://doi.org/10.3133/twri06A1>
- Mehl, S. W. (2006). Use of Picard and Newton Iteration for Solving Nonlinear Ground Water Flow Equations. *Ground Water*, 44(4), 583–594. <https://doi.org/10.1111/j.1745-6584.2006.00207.x>
- Moench, A. F. (1995). Combining the Neuman and Boulton Models for Flow to a Well in an Unconfined Aquifer. *Ground Water*, 33(3), 378–384. <https://doi.org/10.1111/j.1745-6584.1995.tb00293.x>
- Moench, A. F., & Prickett, T. A. (1972). Radial flow in an infinite aquifer undergoing conversion from artesian to water table conditions. *Water Resources Research*, 8(2), 494–499. <https://doi.org/10.1029/WR008i002p00494>
- More, J. J., Burton, S. G., & Hillstrom, K. E. (1980). User Guide for MINPACK-1.
- Nelder, J. A., & Mead, R. (1965). A Simplex Method for Function Minimization. *The Computer Journal*, 7(4), 308–313. <https://doi.org/10.1093/comjnl/7.4.308>
- Neuman, S. P. (1972). Theory of flow in unconfined aquifers considering delayed response of the water table. *Water Resources Research*, 8(4), 1031–1045. <https://doi.org/10.1029/WR008i004p01031>
- Neuman, S. P. (1974). Effect of partial penetration on flow in unconfined aquifers considering delayed gravity response. *Water Resources Research*, 10(2), 303–312. <https://doi.org/10.1029/WR010i002p00303>
- Neuman, S. P. (1979). Perspective on ‘Delayed yield.’ *Water Resources Research*, 15(4), 899–908. <https://doi.org/10.1029/WR015i004p00899>
- Peaceman, D. W., & Rachford, Jr., H. H. (1955). The Numerical Solution of Parabolic and Elliptic Differential Equations. *Journal of the Society for Industrial and Applied Mathematics*, 3(1), 28–41. <https://doi.org/10.1137/0103003>
- Runge, C. (1895). Ueber die numerische Auflösung von Differentialgleichungen (in German). *Mathematische Annalen*, 46(2), 167–178. <https://doi.org/10.1007/BF01446807>
- Stehfest, H. (1970). Algorithm 368: Numerical inversion of Laplace transforms [D5]. *Communications of the ACM*, 13(1), 47–49. <https://doi.org/10.1145/361953.361969>
- Stone, H. L. (1968). Iterative Solution of Implicit Approximations of Multidimensional Partial Differential Equations. *SIAM Journal on Numerical Analysis*, 5(3), 530–558. <https://doi.org/10.1137/0705044>
- Strack, O. D. L. (1989). *Groundwater Mechanics*. Old Tappan, N. J.: Prentice-Hall.

Theis, C. V. (1935). The relation between the lowering of the Piezometric surface and the rate and duration of discharge of a well using ground-water storage. *Transactions, American Geophysical Union*, 16(2), 519–524. <https://doi.org/10.1029/TR016i002p00519>

Virtanen, P., Gommers, R., Oliphant, T. E., Haberland, M., Reddy, T., Cournapeau, D., et al. (2020). SciPy 1.0: fundamental algorithms for scientific computing in Python. *Nature Methods*, 17(3), 261–272. <https://doi.org/10.1038/s41592-019-0686-2>

Wang, X.-S., & Zhan, H. (2009). A new solution of transient confined–unconfined flow driven by a pumping well. *Advances in Water Resources*, 32(8), 1213–1222. <https://doi.org/10.1016/j.advwatres.2009.04.004>

Xiao, L., Ye, M., & Xu, Y. (2018). A New Solution for Confined-Unconfined Flow Toward a Fully Penetrating Well in a Confined Aquifer. *Groundwater*, 56(6), 959–968. <https://doi.org/10.1111/gwat.12642>

Xiao, L., Guo, G., Chen, L., Gan, F., & Xu, Y. (2022). Theory of transient confined-unconfined flow in a confined aquifer considering delayed responses of water table. *Journal of Hydrology*, 608, 127644. <https://doi.org/10.1016/j.jhydrol.2022.127644>

Chapter 8. Modeling Unconfined Flow

8.1. Introduction

An unconfined aquifer, also referred to as phreatic, gravity, or water table aquifer (Mishra & Kuhlman, 2013), is one whose upper boundary is the water table (Strack, 1989). If a pumping well extracts water from a phreatic aquifer, then the lowering of the water table decreases its saturated thickness. If this decrease is significant, then the assumption of constant transmissivity is no longer justified, and flow is governed by a nonlinear equation (e.g. Louwyck et al., 2023). In case of a fully penetrating well, the resistance to flow in the vertical direction typically is neglected according to the Dupuit-Forchheimer approximation (Haitjema, 1995; Strack, 1989). The first to describe steady flow to a well in an aquifer with head-dependent saturated thickness was Dupuit (1857, 1863).

The lowering of the water table also causes drainage of the overlying unsaturated zone (González-Quirós & Fernández-Álvarez, 2021; Moench, 2004). Time-drawdown curves obtained from a pumping test conducted in an unconfined aquifer show a typical S-shape (Kruseman & de Ridder, 1990), which may be attributed to this drainage. Boulton (1954a, 1963) extended the theory of transient confined flow to a well by Theis (1935) to include this effect of delayed yield. However, his proposed solution is semi-empirical, and it is Neuman (1972) who presented the first physically based model by treating the water table as a moving material boundary. As the latter does not include the unsaturated zone, there is controversy and confusion in the literature about the effect of the unsaturated zone (Mao et al., 2011; Moench, 2004). Recent models, however, mostly couple the aquifer explicitly with a linearized form of Richards' unsaturated flow equation. Mishra and Kuhlman (2013) give an overview of the most important models for unconfined flow, from Dupuit (1857) until the increasingly realistic saturated-unsaturated models of present day.

Most models for unconfined flow consider one aquifer only. This chapter deals with the problem of modeling axisymmetric flow to a well extracting water from an unconfined aquifer that is part of a layered aquifer system. The effect of both the head-dependent transmissivity and the delayed yield are considered, although these are addressed separately. In the first section, the multilayer system has a top layer with head-dependent thickness. The nonlinear problem is linearized by discretizing the radial distance into cylindrical zones around the well. In this way, it is possible to use the semi-analytical multilayer-multizone solution method presented in Chapter 5 to approximate the nonlinear unconfined flow in the top layer. This technique is similar to the finite-difference approach for simulating axisymmetric multilayer well-flow (e.g. Louwyck et al., 2012).

The second section is about modeling the effect of delayed yield in the top layer of a phreatic multilayer system. In this case, the transmissivity of the top layer remains constant, which implies the mathematical problem is linear. Hemker (1999) already applied his leaky multilayer solution to simulate this kind of multilayer well-flow very accurately, which is possible as the Boulton (1954a, 1963) solution can be reproduced by modeling an aquifer-aquitard system (Cooley & Case, 1973). Hemker (1999) defines a dummy layer with near-zero transmissivity to include the effect of delayed yield. In this chapter, however, the delayed yield is defined as an upper boundary condition, which only requires minor modification of the multilayer solution presented in Chapter 2.

Each section starts with a literature overview, after which the problem is stated mathematically. It is explained in detail how both problems can be solved semi-analytically and numerically using the finite-difference approach by Louwyck et al. (2012). In both cases, these solution methods are verified against a well-known analytical one-layer solution: in case of nonlinear unconfined flow, this solution is the Dupuit (1857, 1863) equation, in case of delayed yield, it is the Boulton (1954a, 1963)

solution. A three-layer example is used as a final test case to compare the semi-analytical method with the finite-difference method.

8.2. Nonlinear unconfined flow

The problem of steady flow to a well in a phreatic aquifer with head-dependent saturated thickness has been addressed first by Dupuit (1857, 1863), who derived the well-known formulas for both confined and unconfined aquifers. In the hydrogeological literature, the equation for confined well-flow is known as the Thiem equation, since Thiem (1906) was possibly the first to apply this equation for the interpretation of pumping test data (Houben & Batelaan, 2021; Mishra & Kuhlman, 2013). Of interest here is the unconfined well-flow equation and the assumptions underlying this solution. The first assumption is that the pores of the soil below the phreatic surface are completely filled with water, whereas those above it only contain air (Strack, 1989). This implies that the saturated aquifer thickness is equal to the head in the aquifer, which results in a nonlinear problem.

The second assumption neglects the vertical flow component, and is usually referred to as the Dupuit approximation or the Dupuit-Forchheimer approximation, since Forchheimer (1886; 1901) also applied this approximation independently from Dupuit (1857, 1863) (Strack, 1989). Forchheimer (1886) was, however, the first to recognize the Laplace equation governing steady confined flow to which the Thiem equation is a solution, and Forchheimer (1901) presented the differential equation governing steady unconfined flow to which the nonlinear Dupuit equation is a solution (Mishra & Kuhlman, 2013). The partial differential equation governing transient unconfined flow was developed by Boussinesq (1877, 1904) (Bartlett & Porporato, 2018). Strack (1989) refers to the strictly horizontal flow in a phreatic aquifer as shallow unconfined flow, and instead of neglecting the vertical flow component, he assumes the resistance to flow in the vertical direction is negligible, which results into the same mathematical statement of the problem. This alternative explanation for the Dupuit-Forchheimer approximation is also given by Strack (1984) and Haitjema (1995), and was initially proposed by Kirkham (1967).

The third assumption ignores the seepage face which develops between the water level in the well and the elevation where the water table intersects the well-face (Rushton, 2006). In general, a seepage face boundary is the interface at atmospheric pressure where the water exits the porous medium, and in its vicinity, the phreatic surface is above the elevation of the external surface water level, which can be a lake or an open drain, or in this case, a pumping well (Bear, 1972). The seepage face is often ignored in simulations of flow and transport, despite its significance, especially when the thickness of the unsaturated zone is comparable to that of the unconfined aquifer (Yakirevich et al., 2010). In contrast, some other research indicates that the seepage face position mostly is independent of the properties of the unsaturated zone in case of a pumping well (Chenaf & Chapuis, 2007). Occurrence of a seepage face may affect well performance, often leading to well yields that are less than values determined by conventional analysis (Rushton, 2006). Pumping rates estimated under the Dupuit-Forchheimer assumption, for instance, may be in error by 12% to 20% (Shamsai & Narasimhan, 1991). As the actual water level in the pumping well is lower than the simulated water level ignoring the seepage face, its effect may be estimated using models that account for well loss (Ojha & Gopal, 1999). A seepage face along the soil-well interface may also play an important role in solute and chemical transport to wells in variably saturated, unconfined aquifers (Yakirevich et al., 2010).

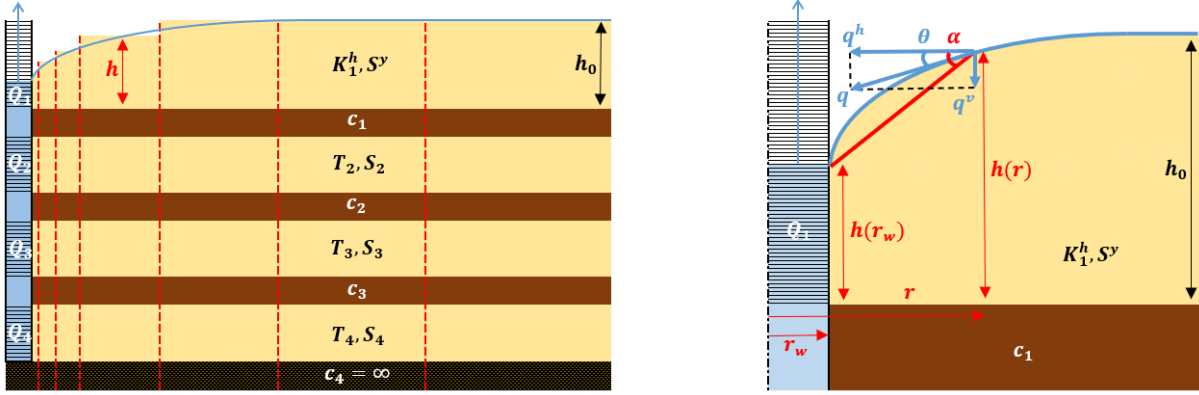


Figure 1. The left plot shows the schematization of the unconfined multi-aquifer system in which the saturated thickness of the top layer is equal to the hydraulic head h . As the governing equation for the top layer is nonlinear, it is linearized by defining cylindrical zones around the well (vertical red lines) in which the saturated thickness is constant. This discretization of the radial distance is applied to the semi-analytical approach presented in this chapter as well as to the finite-difference method. T and S are the aquifer transmissivity and storativity, respectively, K^h is the horizontal conductivity, S^y is the specific yield, and Q is the pumping rate. Aquitards are conceptualized as zero-thickness layers with resistance c . Here, a system consisting of 4 aquifers bounded below by an aquiclude is plotted. In general, any number of aquifers can be treated, and the lower boundary may be leaky instead of confined. The right plot visualizes the Dupuit-Forchheimer approximation for the top layer, where q is the velocity, h_0 is the initial head, and r_w is the radius of the pumping well. See text for definitions and a detailed explanation.

This section treats unconfined flow in a multilayered aquifer system under these three assumptions. To be more precise, the top layer of the aquifer system is unconfined. But instead of assuming an impervious lower boundary like in the Dupuit (1857, 1863) model, there is interaction with the deeper layers, which have constant thickness, as is shown in the left plot of Figure 1. This implies the three assumptions are applicable only to the top layer: (1) its saturated thickness is head-dependent, (2) the vertical flow component is ignored, and (3) there is no seepage face. This is clearly visualized in the right plot of Figure 1. According to Xiao et al. (2018), who refer to Bear (1972), the Dupuit-Forchheimer approximation is valid if the head $h(r)$ [L] at radial distance r [L] from the center of the well with radius r_w [L] meets the following condition:

$$h(r) < 0.58r + h(r_w) \quad (1)$$

with $h(r_w)$ the head at the face of the well. This is illustrated in the right plot of Figure 1. Velocity $q(r)$ [L/T] at distance r is approximated by the horizontal component $q^h(r)$ [L] while the vertical component $q^v(r)$ [L] is ignored. This means $q(r) \approx q^h(r)$ under the condition that $\theta < 30^\circ$. In practice, angle α is taken, thus $\tan \theta < \tan \alpha < \tan 30^\circ$. If $r_w \ll r$, then $\tan \alpha = [h(r) - h(r_w)]/r$. As $\tan 30^\circ = 0.58$, condition (1) is obtained by rearranging this equation. If condition (1) is not met, then r should be sufficiently large, that is $r > 1.72h_0$, with h_0 [L] the initial saturated thickness (Xiao et al., 2018).

Since the saturated thickness of the top layer is head-dependent, radial flow in that layer is described by a nonlinear differential equation. Consequently, the solution method by Hemker (1984, 1985, 1999), which has been used in previous chapters, is not readily applicable here, even not in case of steady state. In case of transient flow, solving the Boussinesq (1877, 1904) equation that considers a single layer, is mathematically even more challenging, and only a few analytical solutions are known (Bartlett & Porporato, 2018; Haitjema, 1995). Boussinesq (1904) developed an analytical solution himself, and recently, Bartlett and Porporato (2018) presented a class of exact solutions for horizontal and sloping aquifers. In most cases, approximate solutions are derived by linearizing the partial differential equation (Brutsaert, 1994; Troch et al., 2003, 2013; Verhoest & Troch, 2000).

In this section, the multilayer-multizone approach discussed in Chapter 5 is used to linearize the system of equations in a similar way as applied by the finite-difference approach. As illustrated in the left plot of Figure 1, the radial distance is discretized by defining cylindrical zones around the pumping well in which the saturated thickness is constant and equal to the head in the middle of the zone. The width of these zones increases with the distance from the well in order to obtain a more accurate approximation of the declining water table near the well.

After stating the problem mathematically, it is explained how the problem can be solved by applying Picard iterations (Mehl, 2006) to the semi-analytical multilayer-multizone approach and the finite-difference method. Both methods are verified against the analytical Dupuit (1857, 1863) solution for steady flow to a well in an unconfined aquifer. A second test case discusses transient flow in a phreatic three-aquifer system. The numerical simulations are performed using the MAxSym code (Louwyck, 2011), which implements the finite-difference approach by Louwyck et al. (2012).

8.2.1. Problem statement

Consider a phreatic aquifer system consisting of n_l layers. Axisymmetric flow in the top layer of the system is governed by the following nonlinear partial differential equation:

$$\frac{K_1^h}{r} \frac{\partial}{\partial r} \left(r h_1 \frac{\partial h_1}{\partial r} \right) = (S^y + S_1^s h_1) \frac{\partial h_1}{\partial t} - N + \frac{h_1 - h_2}{c_1} \quad (2)$$

Hydraulic head h [L] is a function of radial distance r [L] and time t [T]. Subscript 1 in equation (2) refers to the first layer, as layers are numbered from top to bottom. The following parameters are considered: horizontal conductivity K^h [L/T], specific storage S^s [1/L], specific yield S^y [-], vertical resistance c [T] of the bounding aquitard, and infiltration flux N [L/T]. In case of recharge, N is positive, although infiltration is ignored for the problems studied in this chapter, which implies $N = 0$. The term containing the specific storage S_1^s may be neglected if it is much smaller than the specific yield. In this case, and if a single layer is considered, that is $S_1^s = 0$ and $c_1 = \infty$, equation (2) is called the Boussinesq (1877, 1904) equation.

Axisymmetric flow in layer i that is not the top layer, is described by the same linear partial differential equation that is dealt with in previous chapters:

$$\frac{\partial^2 h_i}{\partial r^2} + \frac{1}{r} \frac{\partial h_i}{\partial r} = \frac{S_i}{T_i} \frac{\partial h_i}{\partial t} + \frac{h_i - h_{i-1}}{c_{i-1} T_i} + \frac{h_i - h_{i+1}}{c_i T_i} \quad (2 \leq i \leq n_l) \quad (3)$$

Transmissivity T_i [L²/T] and storativity S_i [-] of layer i are defined as, respectively:

$$T_i = K_i^h D_i \quad (2 \leq i \leq n_l) \quad (4)$$

$$S_i = S_i^s D_i \quad (2 \leq i \leq n_l) \quad (5)$$

with D_i [L] the constant layer thickness. Adjacent layers i and $i + 1$ in zone j are separated by an incompressible resistance layer with zero thickness characterized by hydraulic resistance c_i [T]. If the finite-difference approach is applied to discretize the vertical flow component, then c_i is defined as (Hemker, 1999):

$$c_i = \frac{D_i}{2K_i^v} + \frac{D_{i+1}}{2K_{i+1}^v} \quad (2 \leq i < n_l) \quad (6)$$

with K_i^v [L/T] the vertical conductivity of layer i . The lower boundary of the aquifer system is characterized by c_{n_l} [T]. If this boundary is impervious, then c_{n_l} is infinitely large. If the finite-

difference technique is applied, then resistance c_1 between the top layer and the layer underneath is defined as:

$$c_1(r, t) = \frac{h_1(r, t)}{2K_1^v} + \frac{D_2}{2K_2^v} \quad (7)$$

Note that c_1 is a function of radial distance r and time t as it is a function of head h_1 in the top layer. The same is true for the transmissivity of the top layer, and the storativity, if the specific elastic storage is not neglected:

$$T_1(r, t) = K_1^h h_1(r, t) \quad (8)$$

$$S_1(r, t) = S^y + S_1^s h_1(r, t) \quad (9)$$

If flow is in a steady state, $\partial h_i / \partial t = 0$, by definition, and equations (2) and (3) are reduced to ordinary differential equations. In this study, only radial flow is considered, although the problem could also be stated for parallel flow, as was done in previous chapters.

At the inner model boundary, a constant discharge Q_i [L^3/T] is specified in each layer i . This boundary coincides with the face of the pumping well with radius r_w [L]:

$$\begin{cases} 2\pi K_1^h h_1 r \frac{\partial h_1}{\partial r} = -Q_1 & (r = r_w) \\ 2\pi T_i r \frac{\partial h_i}{\partial r} = -Q_i & (r = r_w; 2 \leq i \leq n_l) \end{cases} \quad (10)$$

where Q_i is negative in case of pumping. It is assumed that the well-screen in each layer is fully penetrating and not connected to a well-screen in another layer. The change in wellbore storage is not taken into account. It would be possible, however, to state the problem for multilayer wells with finite diameter including wellbore storage, as is done in Chapter 6. As already mentioned in the introduction 8.1, the effect of a seepage face is ignored here.

For the sake of simplicity, it is assumed that there is no flow in the aquifer system before the pumping starts, which means that the head in each layer i and at all distances r is the same and equal to h_0 [L] at time $t = 0$:

$$h_i(r, 0) = h_0 \quad (1 \leq i \leq n_l) \quad (11)$$

At the outer model boundary at distance r_{out} [L], a constant head is defined in each layer i , which is equal to the initial head h_0 :

$$h_i(r_{out}, t) = h_0 \quad (1 \leq i \leq n_l) \quad (12)$$

The initial head h_0 is equal to the initial saturated thickness of the top layer.

8.2.2. Semi-analytical method

To solve the problem stated in the previous section, the multilayer-multizone solution discussed in Chapter 5 is applied in a similar way as the finite-difference method treats the radial dependence of the hydraulic head. This means not only the vertical distance is discretized, but also radial distance r . As the gradient is steeper close to the well, it is common practice to discretize the radial dimension into distances that are spaced evenly on a logarithmic scale (Anderson & Woessner, 1992; Barrash & Dougherty, 1997; Lebbe, 1999; Louwyck et al., 2012; Reilly & Harbaugh, 1993):

$$r_{j+1} = a_r r_j \quad (1 \leq j \leq n_z - 1) \quad (13)$$

with n_z the number of zones, and a_r an expansion factor larger than 1 and preferably smaller than 1.5 (Anderson & Woessner, 1992). Section 3.3.1 of Chapter 3 elaborates on this finite-difference discretization of radial distance r . The left drawing in Figure 1 visually illustrates that the idea of this log-spacing is to enlarge the zones with distance r from the pumping well. Distance r_j is defined as the harmonic mean of distances R_{j-1} [L] and R_j [L] of inner and outer boundary of zone j , respectively:

$$r_j = \sqrt{R_{j-1} \cdot R_j} \quad (1 \leq j \leq n_z) \quad (14)$$

Similar to the finite-difference approach (Harbaugh, 1995), Picard iterations are applied to solve the nonlinear problem of the head-dependent saturated thickness. Starting with assigning the initial head to the aquifer thickness, the head in each zone is simulated using the semi-analytical approach presented in Chapter 5, after which these simulated heads are used to modify the saturated thickness for each zone. These steps are repeated until the heads do not change significantly, which may be verified using a criterion of convergence. The algorithm is as follows:

0. Initialization: Assign initial head $h_1(r_j, 0) = h_0$ defined by (11) to thickness $D_{1,j}$ of the upper layer in each zone j , with $1 \leq j \leq n_z$, and calculate $T_{1,j}$ according to (8). If required, also calculate $S_{1,j}$ and $c_{1,j}$ according to (9) and (7), respectively.
1. Iteration: Go through the following steps starting with $m = 1$:

- a. Simulate head $h_i^{(m)}(r_j, t)$ at time t for each layer i and at each distance r_j with $1 \leq j \leq n_z$ and $1 \leq i \leq n_l$.
- b. Assign head $h_1^{(m)}(r_j, t)$ simulated for the top layer in previous step to thickness $D_{1,j}$ of the upper layer in each zone j , with $1 \leq j \leq n_z$, and modify $T_{1,j}$ according to (8). If required, also modify $S_{1,j}$ and $c_{1,j}$ according to (9) and (7), respectively.
- c. Calculate the maximum absolute difference [L] between the simulated heads from previous iteration $m - 1$ and current iteration m :

$$\Delta h = \max_j |h_1^{(m)}(r_j, t) - h_1^{(m-1)}(r_j, t)|$$

with $1 \leq j \leq n_z$, and where $m = 0$ refers to the initialization step 0, which implies the initial head h_0 is assigned to $h_1^{(0)}$.

2. Convergence criterion: Check if the maximum absolute difference Δh is smaller than a given tolerance δ [L]:

- a. If $\Delta h < \delta$, then stop.
- b. If $\Delta h \geq \delta$, then go back to step 1 and go through the next iteration $k + 1$.

It is also common practice to define a maximum number of iterations M , in which case the iterative procedure is aborted if $m + 1 > M$.

It is very straightforward to implement this algorithm, for instance, using a while-loop with Python or Matlab.

8.2.3. Finite-difference approach

As discussed in section 7.1.3 of previous Chapter 7, nonlinear problems are solved by applying Picard or Newton iterations when a finite-difference model is used (Mehl, 2006). In case of Picard iterations, the same procedure is followed as outlined in previous section 8.2.2. When an iterative solver is applied, it may be more convenient, however, to integrate these iterations into the algorithm used to solve the system of finite-difference equations.

The MODFLOW procedure by Louwyck et al. (2012, 2014) can be applied to solve the problem stated in section 8.2.1. If the BCF6 package (Harbaugh, 2005) is used, then the top layer's LTYPE variable must be set to 1 to define the layer as unconfined, which means the layer transmissivity is calculated from the head-dependent saturated thickness and the conductivity. The Louwyck et al. (2012, 2014) method is very similar to the Langevin (2008) method.

However, to test the semi-analytical approach outlined in section 8.2.2, the MAXSym code (Louwyck, 2011) is used here, which implements the finite-difference method presented by Louwyck et al. (2012). Flow simulated in the upper layer of a MAXSym model may be confined or unconfined. In the latter case, Picard iterations are applied that are integrated into the SIP (Stone, 1968) solver. This means the thickness of each cell belonging to the top layer is adapted at the end of each iteration, and the hydraulic parameters of the top layer are modified accordingly (Louwyck, 2011; Louwyck et al., 2012).

Section 3.3.1 of Chapter 3 explains how the time dimension is discretized into n_t simulation times t_k :

$$t_{k+1} = a_t t_k \quad (2 \leq k \leq n_t - 1) \quad (15)$$

with a_t a constant greater than 1, to obtain simulation times that are evenly spaced on a logarithmic scale. The first simulation time t_1 is set to zero and corresponds to the initial conditions. The discretization of radial and vertical distance is adopted from the semi-analytical approach, which means n_l layers are defined and n_z nodes according to (13).

MAXSym simulates drawdown s_{ijk} [L] for each layer i and for each node j at each simulation time t_k [T], which is negative in case of pumping (Louwyck, 2011). This means that transmissivity T_1 and storativity S_1 assigned to the top layer are modified at the end of each iteration m performed by the SIP solver:

$$T_{1,j,k}^{(m)} = K_1^h \cdot (D_1 + s_{1,j,k}^{(m)}) \quad (16)$$

$$S_{1,j,k}^{(m)} = S^y + S_1^s \cdot (D_1 + s_{1,j,k}^{(m)}) \quad (17)$$

The vertical resistance between the two uppermost layers is also adapted:

$$c_{1,j,k}^{(m)} = \frac{D_1 + s_{1,j,k}^{(m)}}{2K_1^v} + \frac{D_2}{2K_2^v} \quad (18)$$

Expressions (16), (17), and (18) are equivalent to (8), (9), and (7), respectively. The same criterion of convergence is used as for the semi-analytical approach (Louwyck, 2011; Louwyck et al., 2012).

In simulating unconfined flow, the semi-analytical approach outlined in section 8.2.2 and the finite-difference method implemented in the MAXSym tool (Louwyck, 2011) are very similar. The main difference between the two methods is that the semi-analytical approach calculates the head within each zone j exactly, whereas the finite-difference method approximates the head using the Thiem (1870; 1906) equation. The finite-difference method also discretizes the time dimension, while the semi-analytical approach applies the Laplace transform, and inverts the obtained solution numerically using the Stehfest (1970) algorithm.

8.2.4. Verification

First, the nonlinear Dupuit (1857, 1863) model is discussed in detail and used to verify the semi-analytical solution method outlined in section 8.2.2. Because this model only defines one layer, a second example of a three-layer model is considered to test the method. In both cases, the MAXSym

tool (Louwyck, 2011) is used to check the results numerically. Recall this tool implements the finite-difference approach by Louwyck et al. (2012), which is explained in Chapter 3 and summarized in previous section 8.2.3.

8.2.4.1. One-layer solution

The Dupuit (1857, 1863) model simulates axisymmetric flow toward a pumping well fully penetrating a phreatic aquifer that is not being recharged. It is assumed the flow to the well is strictly horizontal. The saturated thickness of the aquifer is equal to the hydraulic head. Steady flow is considered; hence, partial differential equation (2) simplifies to the following homogeneous ordinary differential equation:

$$\frac{d}{dr} \left(rh \frac{dh}{dr} \right) = 0 \quad (19)$$

where hydraulic head h is a function of radial distance r only. Condition (10) at the inner model boundary representing the well-face with diameter r_w reduces to:

$$2\pi K^h hr \frac{dh}{dr} = -Q \quad (r = r_w) \quad (20)$$

with K^h the aquifer conductivity and Q the pumping rate. The aquifer is laterally bounded, and the outer boundary condition (12) at distance r_{out} can be adopted without modification:

$$h(r_{out}) = h_0 \quad (21)$$

with h_0 the initial uniform head in the aquifer. Rearranging (19) and integrating both sides gives the following general solution:

$$h(r) = \sqrt{\alpha \ln r + \beta} \quad (22)$$

Introducing (22) into boundary condition (20) gives $\alpha = -Q/(\pi K^h)$, and introducing (22) into boundary condition (21) gives $\beta = h_0^2 + Q \ln r_{out}/(\pi K^h)$. Substituting these expressions for α and β in general solution (22) finally gives the well-known Dupuit (1857, 1863) equation for axisymmetric flow to a pumping well in an unconfined aquifer:

$$h(r) = \sqrt{h_0^2 - \frac{Q}{\pi K^h} \ln \frac{r}{r_{out}}} \quad (23)$$

Since $\sqrt{1-x} \rightarrow \left(1 - \frac{x}{2}\right)$ if $x \rightarrow 0$, equation (23) simplifies to the well-known Thiem (1870; 1906) equation if $h > 0.9h_0$ (Louwyck et al., 2022):

$$h(r) = h_0 - \frac{Q}{2\pi K^h h_0} \ln \frac{r}{r_{out}} \quad (24)$$

The equations of Dupuit (1857, 1863) and Thiem (1870; 1906) are discussed exhaustively in Chapter 10 about the radius of influence, and in Chapter 11 on the relevance of recharge in assessing the sustainability of groundwater extractions. Another interesting relation between equations (23) and (24) is found by applying the relation $h^2 - h_0^2 = (h + h_0)(h - h_0)$ (Dupuit, 1863):

$$h = h_0 - \frac{Q}{2\pi K^h (h + h_0)/2} \ln \frac{r}{r_{out}} \quad (25)$$

Expression (25) indicates that the Dupuit formula (23) and the Thiem formula (24) are equivalent if the saturated thickness in the latter is set to the average head $(h + h_0)/2$.

Figure 2 shows relative head h/h_0 versus relative distance r/r_{out} for different values of dimensionless discharge $Q/(\pi K^h h_0^2)$ according to the Dupuit equation (23) (colored solid lines) and the corresponding Thiem equation (24) (gray dashed lines). It is noticed that the latter is very close to the first if the relative head is greater than 0.9 indeed. The Dupuit (1857, 1863) solution is also approximated using the semi-analytical approach outlined in section 8.2.2 (black dotted lines) and the finite-difference method implemented in the MAxSym tool (Louwyck, 2011) (black dots). It is seen that all solutions are virtually the same.

In both solution methods, 100 nodes are considered at radial distances that are spaced evenly on a logarithmic scale according to (13). A constant head is defined at the outer boundary according to condition (21). Therefore, an additional constant-head cell is defined in the MAxSym model at distance r_{out} , and a very small width of 10^{-5} m is assigned to this cell. Criterion of convergence δ is set to 10^{-8} m, and the maximum number of Picard iterations required to obtain this accuracy is 13. The SIP solver also needs no more than 13 iterations to obtain the same accuracy, and the total water balance for each of the 4 simulations is smaller than 10^{-13} m³/d.

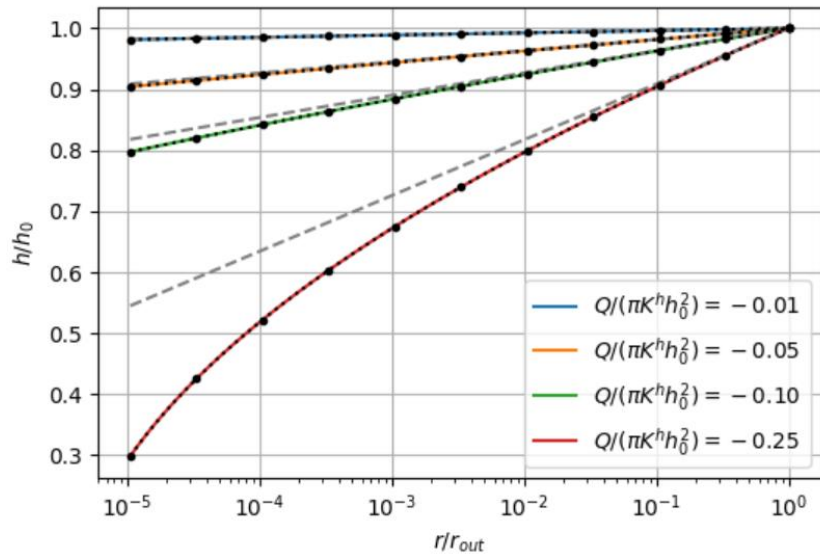


Figure 2. Relative head h/h_0 versus relative distance r/r_{out} according to the Dupuit (1857, 1863) model for axisymmetric flow to a well in an unconfined aquifer. The solid lines are the analytical solution according to Dupuit (1857, 1863), the dotted black lines are simulated using the semi-analytical multizone approach presented in this chapter, and the black dots are simulated using the finite-difference model MAxSym. The gray dashed lines are the corresponding solution of Thiem (1870; 1906) for confined flow. Variable h is the head, h_0 the initial head, r the radial distance, r_{out} the outer model boundary, Q the pumping rate, and K^h the aquifer conductivity. See text for definitions and explanation of solution methods.

8.2.4.2. Three-layer example

Consider a phreatic groundwater reservoir consisting of three aquifers separated by aquitards, and bounded below by an aquiclude. The top layer has an initial saturated thickness D_1 equal to 50 m, its horizontal conductivity K_1^h is 4 m/d, its specific yield S^y is 0.2, and its specific storage is negligibly small. The middle layer has a transmissivity T_2 equal to 100 m²/d and a storativity S_2 equal to 0.005. The bottom layer has a transmissivity T_3 equal to 250 m²/d and a storativity S_3 equal to 0.001. Vertical resistance c_1 of the upper aquitard between layers 1 and 2 is 100 d; vertical resistance c_2 of the lower aquitard between layers 2 and 3 is 500 d. A pumping well with fully penetrating screen in layer 1 and layer 3 extracts water from these layers at constant rates $Q_1 = -2500$ m³/d and $Q_3 = -1250$ m³/d, respectively. The well radius r_w is 0.1 m.

Figure 3 shows the head in the three layers simulated by applying the semi-analytical approach outlined in section 8.2.2 (colored lines) and the finite-difference method implemented in the

MAxSym tool (Louwyck, 2011) (black dotted lines). The left graph plots head h as a function of distance r after 10^4 days of pumping, whereas the right graph plots head h in the pumping well (that is at distance r equal to 0.1 m) as a function of time t . Both solutions are virtually the same. The solution for the corresponding confined system is also plotted (gray dashed lines), and it is seen that it underestimates the drawdown in the top layer at distances close to the well. This underestimation of the drawdown increases with time and decreases with the distance.

In both the semi-analytical and the finite-difference model, the outer model boundary is at a very large distance r_{out} equal to 10^7 m, in order to avoid that it affects the simulated heads. The interval between r_w and r_{out} is discretized into 150 nodes, which are at distances that are spaced evenly on a logarithmic scale according to (13). An additional constant-head cell of width 10^{-5} m is defined in the MAxSym model at distance r_{out} . Criterion of convergence δ is set to 10^{-7} m, and the maximum number of Picard iterations required to obtain this accuracy is 18. The SIP solver needs no more than 26 iterations to obtain the same accuracy, and the maximum total water balance for all time steps is smaller than 7×10^{-4} m³/d. The semi-analytical result in the right plot of Figure 3 is obtained by simulating the heads for 50 simulation times generated according to (15). In the finite-difference model, 150 time steps are defined that are also evenly spaced on a logarithmic scale, with the first time step equal to 10^{-7} d.

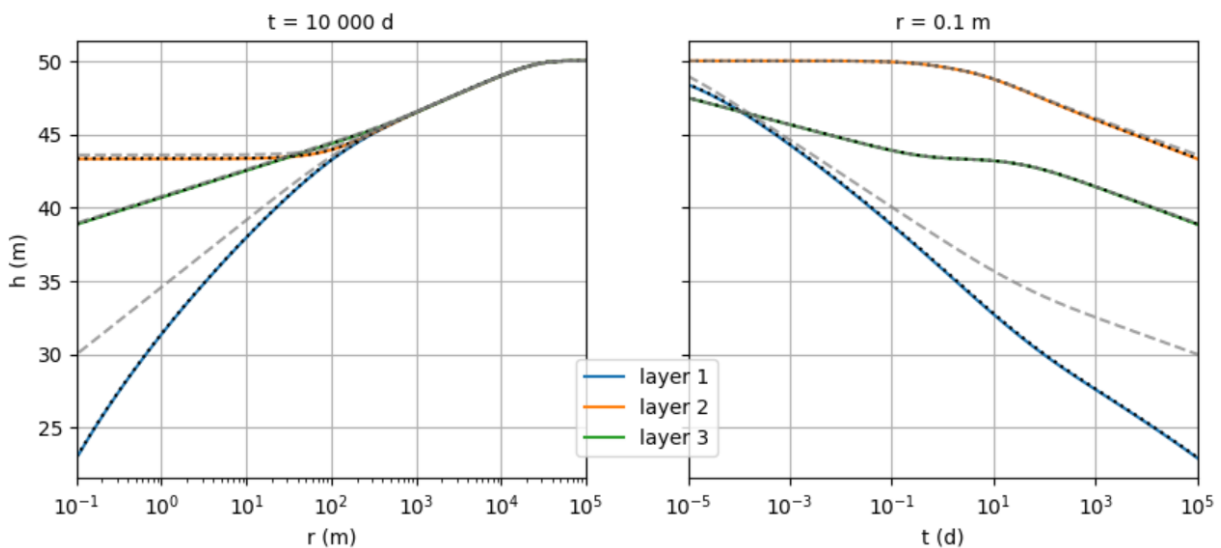


Figure 3. Head h versus distance r after 10 000 days of pumping (left plot), and head h versus time t at the face of the pumping well with a radius of 0.1 m (right plot), for the unconfined three-layer model discussed in the text. The colored lines are simulated using the semi-analytical multizone approach presented in this chapter, the black dotted lines are simulated using the finite-difference model MAxSym (2011). The gray dashed lines are the solution for the corresponding confined three-layer model.

8.3. Delayed yield

When interpreting constant-rate pumping tests conducted in phreatic aquifers, it is often seen that time-drawdown curves plotted on a logarithmic time scale exhibit a typical S-shape. In the absence of sources and sinks, the early-time segment implies that some water is released from aquifer storage instantaneously in response to the lowering of the hydraulic head (Neuman, 1979; Tartakovsky & Neuman, 2007). The shape of this steep early-time segment is similar to the Theis (1935) type curve as the unconfined aquifer initially reacts in the same way as a confined aquifer (Kruseman & de Ridder, 1990). The flat intermediate-time segment suggests the presence of an additional source of water released from storage, a phenomenon known as delayed yield or delayed response (Neuman, 1979; Tartakovsky & Neuman, 2007). It reflects the effect of the dewatering that accompanies the

falling water table, and its effect is comparable to that of leakage (Kruseman & de Ridder, 1990). The late-time segment represents the combined effect of both storage mechanisms (Tartakovsky & Neuman, 2007), and it tends to conform again to the Theis (1935) type curve (Kruseman & de Ridder, 1990).

The first formal effort to mimic the delayed yield behavior of a phreatic aquifer is made by Boulton (1954a), and a graphical procedure is developed by Boulton (1963) and by Prickett (1965) to estimate the hydraulic parameters from pumping test data (Neuman, 1979). The theory of delayed yield is extended to account for vertical anisotropy (Boulton, 1970) and partial penetration of the pumping well (Boulton & Pontin, 1971). In the Boulton (1954a, 1963) model, the rate of delay is controlled by the delay index, which is an empirical constant, as its physical meaning is unclear (Moench, 1995; Neuman, 1972, 1979). The delay index allows the specific yield to vary exponentially with time (Neuman, 1979). Boulton (1954a) attributes delayed yield to leakage either from an aquitard containing the water table and overlying the extracted aquifer or from fine-grained compressible layers interbedded with the aquifer material, whereas Boulton (1963) refers to water table conditions in the aquifer itself. Neuman (1972, 1973) developed an analytical solution capable of reproducing the three segments of the typical S-shaped drawdown curves by treating the water table as a moving material boundary, like Boulton (1954b) and Dagan (1964, 1967), and without having to rely on empirical constants. This solution is extended by Neuman (1974) to include the effect of partial penetration, and it is used by Neuman (1975) to develop methods of analysis to determine the hydraulic properties of anisotropic unconfined aquifers from pumping test data.

From the above explanation, any explicit mention of the vadose or unsaturated zone is missing, which is the zone extending from the top of the ground surface to the water table where the groundwater is – by definition – at atmospheric pressure (Lohman, 1972). For decades, there has been controversy and confusion in the literature about the effect of the unsaturated zone on the drawdowns observed during pumping tests conducted in unconfined aquifers (Mao et al., 2011; Moench, 2004). Although Boulton (1954a, 1963) originally does not refer to the unsaturated zone, his concept of delayed yield is interpreted by many researchers as the non-instantaneous release of water from the vadose zone above the falling water table (Moench, 1995, 2004; Neuman, 1979). On the other hand, the model by Neuman (1972, 1973, 1974), which may be considered the standard in groundwater industry, implies instantaneous and complete drainage, and is based on the assumption that unsaturated zone processes have no significant effect (González-Quirós & Fernández-Álvarez, 2021; Moench, 2004). In the Neuman (1972, 1973, 1974) model, the unconfined aquifer is treated as a compressible system and the water table as a moving free surface. A similar approach by Streltsova (1972a, 1972b, 1973) shows that delayed yield can be simulated indeed assuming constant values for the specific elastic storage and the specific yield, and without including the vadose zone.

Neuman (1979) defends the latter perspective by referring to, amongst others, Kroszynski and Dagan (1975), who conclude that ignoring the effect of the unsaturated zone, for mathematical simplicity, has no serious consequences. Kroszynski and Dagan (1975) draw that conclusion from the development of a two-dimensional axisymmetric analytical model that approximates the effect of the vadose zone through simple exponential relations (Moench, 2004). However, interpretation of pumping tests and comparison with results obtained from laboratory tests, volume balance methods, and numerical experiments, prove that neglecting the interaction with the unsaturated zone is not always justified, and could lead to biased parameter estimates, in particular, unrealistically low values for the specific yield (Akindunni & Gillham, 1992; Bevan et al., 2005; Endres et al., 2007; Moench, 1994, 2008; Moench et al., 2001; Narasimhan & Zhu, 1993; Nwankwor et al., 1984, 1992). Likewise, the exponential relation assumed in the Boulton (1954a, 1963) model is an

oversimplification of the actual drainage of the vadose zone (Moench, 1995, 2004; Narasimhan & Zhu, 1993). Some of these researchers attribute the S-shaped time-drawdown curves to the expansion of the capillary fringe (Narasimhan & Zhu, 1993; Nwankwor et al., 1992), which is the saturated part of the vadose zone above the water table at less than atmospheric pressure (Lohman, 1972).

A pragmatic solution is offered by Moench (1995, 1996, 1997), who replaces the boundary condition at the water table in the Neuman (1972, 1973, 1974) model by the convolution integral for delayed yield (Boulton, 1954a) combined with Darcy's law. The resulting semi-analytical solution is implemented in the WTAQ2 code (Barlow & Moench, 2011), and it seems to improve the match between theoretical type curves and field data (Moench, 1995, 1997). An alternative hypothesis by Malama (2011) attributes the anomalous values of specific yield estimated using the Neuman (1972, 1973, 1974) model to its linearization of the nonlinear kinematic condition at the water table, which is based on the work of Dagan (1964, 1967). Instead of conceptualizing the water table as a sharp interface between saturated and unsaturated zone, Malama (2011) proposes to model it as a diffuse interface. Other researchers develop more advanced semi-analytical solutions that fully incorporate the unsaturated zone (Mathias & Butler, 2006; Mishra & Neuman, 2010, 2011; Tartakovsky & Neuman, 2007). In these models, a linearized version of Richards' equation is used to describe the movement of water in the unsaturated zone. Mao et al. (2011) also include aquifer heterogeneity and advocate the use of a multidimensional variably saturated flow model, which considers the transition of water release mechanisms and vertical flow, and accounts for heterogeneity in the unconfined aquifer.

From this brief literature overview, it is clear that several models are described in the literature to take into account the interaction with the vadose zone, some of them fully implementing the unsaturated zone, others relying on simplified assumptions ranging from instantaneous to delayed drainage (González-Quirós & Fernández-Álvarez, 2021). Many of these models implicitly or explicitly assume that the unsaturated zone acts as a source of recharge, although the typically S-shaped time-drawdown curves can be reproduced in the absence of an initial unsaturated zone (Mao et al., 2011; Neuman, 1972; Tartakovsky & Neuman, 2007). Simple microgravity observations, that can be done while pumping, may help to decide whether the dynamic behavior of the vadose zone should be included in the model or not (González-Quirós & Fernández-Álvarez, 2021). One may expect, however, that most groundwater practitioners use either the model of Boulton (1954a, 1963) or the model of Neuman (1972, 1973, 1974) without even considering a full implementation of the unsaturated zone as it is mathematically too much involved. Some researchers report similar results when comparing parameters derived from pumping test data interpreted using these two models (Al-Turbak et al., 1993; Ismail & Mawlood, 2020).

The objective of this section is therefore not to take a stand on the different explanations about the nature of the S-shaped time-drawdown curves and the role of the unsaturated zone. Instead the problem of transient unconfined flow is approached from a more practical point of view by explaining how the multilayer well-flow solution by Hemker (1985, 1999), which has been presented in Chapter 2, can be used to simulate the effect of delayed yield. Hemker (1999) himself elaborates on this topic by verifying his semi-analytical solution against the model of Boulton (1954a, 1963) for unconfined flow with delayed yield toward a fully penetrating well. This is possible because of the equivalence between the Boulton (1954a, 1963) model and the solution of a well extracting from an aquifer overlain by an aquitard containing the water table. Recall that one of Boulton's (1954a) initial explanations for the phenomenon of delayed yield is leakage from a water table aquitard, which has been validated numerically by Cooley (1971, 1972). Cooley and Case (1973) theoretically derive an

expression for the delay index as a function of the specific yield and the vertical resistance of the aquitard. Boulton (1973) explicitly derives the solution for an aquifer-aquitard system and obtains the same expression as Boulton (1963), whereas Boulton and Streltsova (1975) present new equations for solving the same problem. More recently, Zlotnik and Zhan (2005) reinvestigated the aquitard effect on transient unconfined well-flow, and they conclude that it can be described indeed by a drainage-type boundary condition, although they propose a different kernel than the one applied by Boulton (1954a).

Hemker (1999) also shows how the partially penetrating effect can be accounted for using his multilayer solution by dividing the aquifer into a sufficient number of sublayers. This finite-difference technique gives results that are very close to the solution for a partially penetrating well in an unconfined aquifer by Moench (1993). The latter is a more efficient implementation of the Neuman (1974) solution, which Moench (1993) accomplishes by numerically inverting the solution in the Laplace domain using the Stehfest (1970) algorithm. Hemker (1999) also discusses the Moench (1995, 1996) solution that combines the models of Boulton (1954a, 1963) and Neuman (1972, 1973, 1974). The Hemker (1999) solution also considers the effect of wellbore storage, which has been discussed in Chapter 6. Hemker (1999) compares multilayer simulations including the effect of wellbore storage with the analytical solution developed by Boulton and Streltsova (1976) for a large-diameter well in an unconfined aquifer in which the water table is treated as a constant-head boundary. Hemker (1999) discovers systematic differences between both solutions, and using a finite-element model, he even invalidates some of the results presented by Boulton and Streltsova (1976).

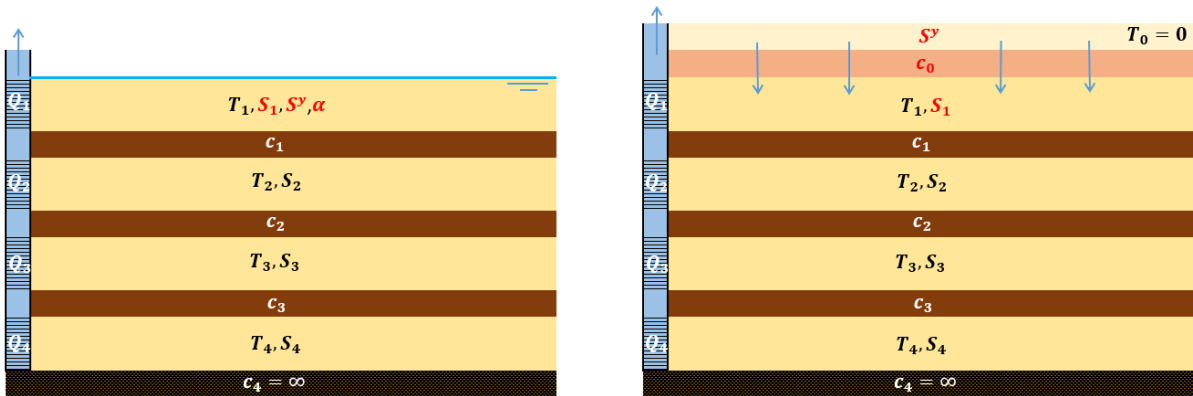


Figure 4. Schematization of the unconfined multi-aquifer system considering the process of delayed yield. The left plot depicts the actual situation where the phreatic top layer contains the water table, while the right plot visualizes the equivalent interpretation introducing a dummy layer on top of the phreatic layer that represents a reservoir producing the delayed drainage. The delayed yield in the first interpretation (left plot) is controlled by Boulton's delay index $1/\alpha$, while it is the drainage resistance c_0 that determines the rate of delay in the second interpretation (right plot). Both are equivalent if $1/\alpha$ is set to c_0S^y , with S^y the specific yield. T and S are the aquifer transmissivity and storativity, respectively, and Q is the pumping rate. Aquitards are conceptualized as zero-thickness layers with resistance c . See text for definitions. A system consisting of 4 aquifers bounded below by an aquiclude is shown here. In general, any number of aquifers can be included, and the lower boundary may be leaky instead of confined.

Hemker (1999) tricks the leaky multilayer well-flow solution into simulating the effect of delayed yield by defining a dummy layer on top of the model (Figure 4). This dummy layer acts as a reservoir that produces the delayed drainage, and therefore, its storage coefficient is set to the specific yield. The horizontal flow in the dummy layer is impeded by assigning a near-zero value to its transmissivity. The resistance between the dummy layer and the actual unconfined top layer may be interpreted as the drainage resistance (Hemker, 1999). The product of this resistance and the specific yield is equal to Boulton's delay index (Cooley & Case, 1973). The same trick is applied by Louwyck et

al. (2012, 2014) who simulate transient flow to a well in a multi-aquifer system with phreatic top, and verify the finite-difference approach presented in Chapter 3 against the semi-analytical solution by Hemker (1999) implemented in TTIm (Bakker, 2013a, 2013b). Note that the dummy layer is not required if the phreatic layer is divided into sublayers, in which case the specific yield can be assigned to the upper sublayer and the elastic storage to the other sublayers.

Instead of applying the low-transmissivity trick, the problem of transient multilayer flow to a well is restated here by defining the delayed drainage as a boundary condition that replaces the leaky upper boundary condition in the Hemker (1999) solution. Applying the Laplace transform, a similar system of modified Bessel equations is obtained as for the leaky multilayer system, which can be solved by decomposing the system matrix into its eigenvalues and corresponding eigenvectors (Hemker, 1985, 1999). This means the semi-analytical solution method presented in Chapter 2 can also be applied here and only requires minor modification. The method is verified against Boulton's (1954a, 1963) analytical solution and compared with the finite-difference approach by Louwyck et al. (2012) implemented in the MAXSym code (Louwyck, 2011). The second test case revisits the example of the three-aquifer model discussed in section 8.2.4.2, by adding delayed yield to the top layer and keeping its transmissivity constant. In both cases, the finite-difference model uses a dummy layer with near-zero transmissivity to simulate the effect of delayed yield.

8.3.1. Problem statement

Axisymmetric flow in layer i is described again by the following linear partial differential equation:

$$\frac{\partial^2 h_i}{\partial r^2} + \frac{1}{r} \frac{\partial h_i}{\partial r} = \frac{S_i}{T_i} \frac{\partial h_i}{\partial t} + \frac{-N_i}{T_i} + \frac{h_i - h_{i-1}}{c_{i-1} T_i} + \frac{h_i - h_{i+1}}{c_i T_i} \quad (1 \leq i \leq n_l) \quad (26)$$

subject to the following conditions at inner, outer, and lower boundary, respectively:

$$r \frac{\partial h_i}{\partial r} = \frac{-Q_i}{2\pi T_i} \quad (r = r_w; 1 \leq i \leq n_l) \quad (27)$$

$$h_i(r_{out}, t) = \varphi_i \quad (1 \leq i \leq n_l) \quad (28)$$

$$h_{n_l+1}(r, t) = \varphi_{n_l+1} \quad (29)$$

Note that the differential equations in (26) include infiltration N_i . In this chapter, however, infiltration is ignored, which is a common practice, although there are exceptions (Zlotnik & Ledder, 1992). The upper boundary condition differs from the leaky multilayer case discussed in previous chapters as it must implement the process of delayed yield:

$$S^y \frac{\partial h_0}{\partial t} + \frac{h_0 - h_1}{c_0} = 0 \quad (30)$$

The initial condition for each layer i at time $t = 0$ is:

$$h_i(r, 0) = \varphi_i \quad (0 \leq i \leq n_l) \quad (31)$$

Note that (31) also defines the initial condition for the upper boundary condition (30), that is $h_0(r, 0) = \varphi_0$. In previous section 8.2, h_0 denotes the initial steady head in the aquifer system, whereas it refers to the head in the dummy layer ($i = 0$) in this section.

8.3.2. Semi-analytical solution

Using initial condition (31), the Laplace transform is applied to partial differential equation (26) and its associated boundary conditions (27), (28), (29), and (30):

$$\frac{\partial^2 \bar{h}_i}{\partial r^2} + \frac{1}{r} \frac{\partial \bar{h}_i}{\partial r} = \frac{S_i}{T_i} (p \bar{h}_i - \varphi_i) + \frac{-N_i}{p T_i} + \frac{\bar{h}_i - \bar{h}_{i-1}}{c_{i-1} T_i} + \frac{\bar{h}_i - \bar{h}_{i+1}}{c_i T_i} \quad (1 \leq i \leq n_l) \quad (32)$$

$$r \frac{\partial \bar{h}_i}{\partial r} = \frac{-Q_i}{2\pi T_i p} \quad (r = r_w; 1 \leq i \leq n_l) \quad (33)$$

$$\bar{h}_i(r_{out}, p) = \frac{\varphi_i}{p} \quad (1 \leq i \leq n_l) \quad (34)$$

$$\bar{h}_{n_l+1}(r, p) = \frac{\varphi_{n_l+1}}{p} \quad (35)$$

$$S^y (p \bar{h}_0 - \varphi_0) + \frac{\bar{h}_0 - \bar{h}_1}{c_0} = 0 \quad (36)$$

From (36) it follows that:

$$\bar{h}_0 = \frac{\bar{h}_1 + c_0 S^y \varphi_0}{1 + c_0 S^y p} \quad (37)$$

Rearranging the differential equations in (32) and substituting (37) for \bar{h}_0 in the first equation ($i = 1$) and (35) for \bar{h}_{n_l+1} in the last equation ($i = n_l$) gives:

$$\begin{cases} \nabla^2 \bar{h}_1 = \frac{\bar{h}_1}{T_1} \left[p S_1 + \frac{1}{c_0} + \frac{1}{c_1} - \frac{1}{c_0(1 + c_0 S^y p)} \right] - \frac{\bar{h}_2}{c_1 T_1} - \frac{1}{T_1} \left[S_1 \varphi_1 + \frac{N_1}{p} + \frac{S^y \varphi_0}{(1 + c_0 S^y p)} \right] \\ \nabla^2 \bar{h}_i = \frac{\bar{h}_i}{T_i} \left[p S_i + \frac{1}{c_{i-1}} + \frac{1}{c_i} \right] - \frac{\bar{h}_{i-1}}{c_{i-1} T_i} - \frac{\bar{h}_{i+1}}{c_i T_i} - \frac{1}{T_i} \left[S_i \varphi_i + \frac{N_i}{p} \right] \quad (1 < i < n_l) \\ \nabla^2 \bar{h}_{n_l} = \frac{\bar{h}_{n_l}}{T_{n_l}} \left[p S_{n_l} + \frac{1}{c_{n_l-1}} + \frac{1}{c_{n_l}} \right] - \frac{\bar{h}_{n_l-1}}{c_{n_l-1} T_{n_l}} - \frac{1}{T_{n_l}} \left[S_{n_l} \varphi_{n_l} + \frac{\varphi_{n_l+1}}{c_{n_l} p} + \frac{N_{n_l}}{p} \right] \end{cases} \quad (38)$$

with $\nabla^2 \bar{h}_i = \frac{\partial^2 \bar{h}_i}{\partial r^2} + \frac{1}{r} \frac{\partial \bar{h}_i}{\partial r}$.

A similar system of ordinary modified Bessel differential equations subject to boundary conditions (33) and (34) is obtained for the leaky multilayer system discussed in Chapter 2. System of equations (38) is written in matrix form:

$$\nabla^2 \mathbf{h} = \mathbf{A} \mathbf{h} - \mathbf{b} \quad (39)$$

where \mathbf{h} and \mathbf{b} are $n_l \times 1$ vectors and \mathbf{A} is an $n_l \times n_l$ tridiagonal matrix, defined as, respectively:

$$\mathbf{h}_i = \bar{h}_i(r, p) \quad (40)$$

$$\mathbf{b}_i = \begin{cases} \frac{N_1}{p T_1} + \frac{S_1}{T_1} \varphi_1 + \frac{S^y \varphi_0}{T_1 (1 + c_0 S^y p)} & (i = 1) \\ \frac{N_i}{p T_i} + \frac{S_i}{T_i} \varphi_i & (1 < i < n_l) \\ \frac{N_{n_l}}{p T_{n_l}} + \frac{S_{n_l}}{T_{n_l}} \varphi_{n_l} + \frac{\varphi_{n_l+1}}{p c_{n_l} T_{n_l}} & (i = n_l) \end{cases} \quad (41)$$

$$A_{ij} = \begin{cases} \frac{1}{c_0 T_1} + \frac{1}{c_1 T_1} + \frac{S_1}{T_1} p - \frac{1}{c_0 T_1 (1 + c_0 S^y p)} & (i = j = 1) \\ \frac{1}{c_{i-1} T_i} + \frac{1}{c_i T_i} + \frac{S_i}{T_i} p & (i = j; 1 < i \leq n_l) \\ \frac{-1}{c_{i-1} T_i} & (i = j + 1; 1 < i \leq n_l) \\ \frac{-1}{c_i T_i} & (i = j - 1; 1 \leq i < n_l) \end{cases} \quad (42)$$

The i -th entry in \mathbf{h} and \mathbf{b} is denoted by \mathbf{h}_i and \mathbf{b}_i , respectively, and the entry on the i -th row and the j -th column of matrix \mathbf{A} is referred to as A_{ij} . If $i = j$, then the entry is on the main diagonal of \mathbf{A} , if $i = j + 1$, then the entry is on the lower diagonal, and if $i = j - 1$, then the entry is on the upper diagonal; all other elements in \mathbf{A} are zero.

Boundary conditions (33) and (34) are also written in matrix form, respectively:

$$r_w \frac{\partial \mathbf{h}(r_w)}{\partial r} = -\mathbf{T}^{-1} \mathbf{Q} \quad (43)$$

$$\mathbf{h}(r_{out}) = \boldsymbol{\varphi} \quad (44)$$

In expression (43), \mathbf{T} is an $n_l \times n_l$ diagonal matrix, and \mathbf{Q} is an $n_l \times 1$ vector. The nonzero entries in \mathbf{T} are defined as:

$$\mathbf{T}_{ii} = 2\pi T_i \quad (45)$$

The i -th entry in \mathbf{Q} is:

$$\mathbf{Q}_i = \frac{Q_i}{p} \quad (46)$$

In equation (44), $\boldsymbol{\varphi}$ is an $n_l \times 1$ vector in which the i -th entry is:

$$\boldsymbol{\varphi}_i = \frac{\varphi_i}{p} \quad (47)$$

Comparing equations (41) and (42) to expressions (37) and (38) in Chapter 2 defining \mathbf{b} and \mathbf{A} , respectively, for a leaky multilayer system, it is seen that only the elements \mathbf{b}_1 and \mathbf{A}_{11} are defined differently here. As a consequence, solving (39) subject to (43) and (44) can be done in the same way as discussed in Chapter 2.

Matrix \mathbf{A} is decomposed into its eigenvalues and corresponding eigenvectors:

$$\nabla^2 \mathbf{h} = \mathbf{V} \mathbf{D} \mathbf{V}^{-1} \mathbf{h} - \mathbf{b} \quad (48)$$

where \mathbf{D} is an $n_l \times n_l$ diagonal matrix containing the n_l eigenvalues d_i , and \mathbf{V} is an $n_l \times n_l$ matrix containing the corresponding eigenvectors in its columns. As only the transient case is considered here, there are no eigenvalues equal to zero. Multiplying both sides of (48) by \mathbf{V}^{-1} gives:

$$\nabla^2 \mathbf{V}^{-1} \mathbf{h} = \mathbf{D} \mathbf{V}^{-1} \mathbf{h} - \mathbf{V}^{-1} \mathbf{b} \quad (49)$$

The general solution of matrix system (49) is:

$$\mathbf{h}(r) = \mathbf{V} [\mathbf{I}(r) \boldsymbol{\alpha} + \mathbf{K}(r) \boldsymbol{\beta} + \mathbf{D}^{-1} \mathbf{V}^{-1} \mathbf{b}] \quad (50)$$

where $\mathbf{I}(r)$ and $\mathbf{K}(r)$ are $n_l \times n_l$ diagonal matrices with the following diagonal terms, respectively:

$$I_{ii}(r) = I_0(r\sqrt{d_i}) \quad (1 \leq i \leq n_l) \quad (51)$$

$$K_{ii}(r) = K_0(r\sqrt{d_i}) \quad (1 \leq i \leq n_l) \quad (52)$$

with I_0 and K_0 the zero order modified Bessel functions of the first and second kind, respectively.

Vectors α and β in (50) hold the integration constants that are determined by introducing general solution (50) into boundary conditions (43) and (44). This gives the particular solution, which has already been derived in Chapter 2:

$$\alpha = -X\{\mathbf{K}(r_{out})V^{-1}\mathbf{T}^{-1}\mathbf{Q} + \mathbf{K}'(r_w)[V^{-1}\boldsymbol{\varphi} - \mathbf{D}^{-1}V^{-1}\mathbf{b}]\} \quad (53)$$

$$\beta = X\{\mathbf{I}(r_{out})V^{-1}\mathbf{T}^{-1}\mathbf{Q} + \mathbf{I}'(r_w)[V^{-1}\boldsymbol{\varphi} - \mathbf{D}^{-1}V^{-1}\mathbf{b}]\} \quad (54)$$

with:

$$\mathbf{X} = \{\mathbf{K}(r_{out})\mathbf{I}'(r_w) - \mathbf{I}(r_{out})\mathbf{K}'(r_w)\}^{-1} \quad (55)$$

The nonzero entries in diagonal matrices $\mathbf{I}'(r_w)$ and $\mathbf{K}'(r_w)$ are defined as:

$$I'_{ii}(r_w) = (r_w\sqrt{d_i})I_1(r_w\sqrt{d_i}) \quad (1 \leq i \leq n_l) \quad (56)$$

$$K'_{ii}(r_w) = -(r_w\sqrt{d_i})K_1(r_w\sqrt{d_i}) \quad (1 \leq i \leq n_l) \quad (57)$$

If $r_w \rightarrow 0$, then $\alpha \rightarrow [\mathbf{I}(r_{out})]^{-1}[V^{-1}\boldsymbol{\varphi} - \mathbf{D}^{-1}V^{-1}\mathbf{b} - \mathbf{K}(r_{out})V^{-1}\mathbf{T}^{-1}\mathbf{Q}]$ and $\beta \rightarrow V^{-1}\mathbf{T}^{-1}\mathbf{Q}$.

If $r_{out} \rightarrow \infty$, then $\alpha \rightarrow \mathbf{0}$ and $\beta \rightarrow -[\mathbf{K}'(r_w)]^{-1}V^{-1}\mathbf{T}^{-1}\mathbf{Q}$.

Recall that solution (50) is expressed in the Laplace domain. The solution in the real time domain is found by numerically inverting the Laplace-transformed heads \mathbf{h} according to (50) using the Stehfest (1970) algorithm.

8.3.3. Finite-difference approach

The semi-analytical solution method outlined in previous section 8.3.2 is compared with the finite-difference approach described by Louwyck et al. (2012) and presented in Chapter 3. The MAxSym tool (Louwyck, 2011) is used here, which implements this method. Alternatively, the MODFLOW procedure by Louwyck et al. (2012, 2014) may be used, which is also summarized in Chapter 3. Recall that this procedure converts rectilinear flow into axisymmetric flow simply by modifying the input parameters of the MODFLOW (Harbaugh, 2005) model. Since these models do not provide the option of including delayed yield as a boundary condition, a low transmissive layer is defined representing the delayed drainage, in the same way Hemker (1999) applied his semi-analytical leaky multilayer well-flow solution to reproduce the Boulton (1954a, 1963) type-curves. Radial distance r and time t are discretized on a logarithmic scale according to (13) and (15), respectively.

8.3.4. Verification

The Boulton (1954a, 1963) model is discussed first and applied to verify the semi-analytical solution method outlined in section 8.3.2, after which the three-layer example discussed in section 8.2.4.2 is used as a second test case. Delayed yield is added to the top layer of this three-layer model, and its transmissivity is assumed constant here. In both cases, the MAxSym tool (Louwyck, 2011) is used to check the results numerically.

8.3.4.1. Boulton model

The partial differential equation describing unconfined transient radial flow according to the Boulton (1954a, 1963) model is the same as the diffusion equation that governs confined flow in the Theis

(1935) model. There is, however, an additional term containing a convolutional integral for the delayed yield (Boulton, 1954a, 1963):

$$T \left(\frac{\partial^2 s}{\partial r^2} + \frac{1}{r} \frac{\partial s}{\partial r} \right) = S_1^y \frac{\partial s}{\partial t} + \alpha S_2^y \int_0^t \frac{\partial s}{\partial t} e^{-\alpha(t-\tau)} d\tau \quad (58)$$

where s is the drawdown in the phreatic aquifer at distance r and at time t . The aquifer has a constant transmissivity T , and it is characterized by an early time apparent specific yield S_1^y [-], and a larger time specific yield S_2^y [-] (Lohman, 1972). The additional delayed yield term contains the empirical constant α [1/T] of which the reciprocal $1/\alpha$ is called the delay index. The convolutional integral in (58) is obtained from integration of the following empirical relation (Boulton, 1954a):

$$\partial v_d = -\partial s \cdot \alpha S_2^y e^{-\alpha(t-\tau)} \quad (59)$$

where ∂v_d [L/T] is the rate of delayed yield at time t due to an infinitesimal change in drawdown ∂s during an infinitesimal time interval $\partial\tau$ (with $\tau < t$). The minus sign in expression (59) indicates that the direction of ∂v_d is downward (Cooley & Case, 1973).

The initial condition and the boundary conditions are the same as for the Theis (1935) model: there is no drawdown in the aquifer before pumping, the fully penetrating well of infinitesimal radius extracts water from the aquifer at constant rate Q , and the aquifer is laterally unbounded. These three conditions are mathematically translated into the following equations, respectively:

$$s(r, 0) = 0 \quad (60)$$

$$\lim_{r \rightarrow 0} \left(r \frac{\partial s}{\partial r} \right) = \frac{-Q}{2\pi T} \quad (61)$$

$$s(\infty, t) = 0 \quad (62)$$

The particular solution of differential equation (58) subject to conditions (60), (61), and (62) is (Boulton, 1963):

$$s(r, t) = \frac{-Q}{4\pi T} \int_0^\infty \frac{2}{x} \left\{ 1 - e^{-\mu_1} \left[\cosh \mu_2 + \frac{\alpha t \eta (1-x^2)}{2\mu_2} \sinh \mu_2 \right] \right\} J_0 \left(\frac{rx}{\gamma B} \right) dx \quad (63)$$

with J_0 the zero order Bessel function of the first kind, and variables η , γ , B , μ_1 , and μ_2 defined as:

$$\eta = 1 + S_2^y / S_1^y \quad (64)$$

$$\gamma = \sqrt{1 - 1/\eta} \quad (65)$$

$$B = \sqrt{T / (\alpha S_2^y)} \quad (66)$$

$$\mu_1 = \alpha t \eta (1+x^2)/2 \quad (67)$$

$$\mu_2 = \left(\alpha t \sqrt{\eta^2 (1+x^2)^2 - 4\eta x^2} \right) / 2 \quad (68)$$

Of interest here is the approximate solution for $\eta \rightarrow \infty$ (Boulton, 1963):

$$s(r, t) = \frac{-Q}{2\pi T} \int_0^\infty \left\{ 1 - \frac{1}{x^2+1} \exp \left(\frac{-\alpha t x^2}{x^2+1} \right) - \frac{x^2}{x^2+1} e^{-2\mu_1} \right\} J_0 \left(\frac{rx}{B} \right) \frac{dx}{x} \quad (69)$$

In practice, solution (69) is valid if the early time specific yield S_1^y is much smaller than the larger time specific yield S_2^y . The improper integral in (69) can be solved numerically using the vectorized adaptive quadrature implemented in Matlab function ‘quadgk’ (Shampine, 2008). The term containing $e^{-2\mu_1}$ may be omitted for large values of time t .

As already mentioned, Cooley and Case (1973) show theoretically that the Boulton (1954a, 1963) model can be reproduced by a two-layer model in which the lower layer represents the extracted aquifer and the upper layer the source responsible for the delayed yield. This top layer may be conceptualized as an aquitard containing the falling water table in which flow is strictly vertical. Recall that this is also one of the possible interpretations initially proposed by Boulton (1954a). Cooley and Case (1973) additionally prove the delay index has a physical meaning following this interpretation:

$$1/\alpha = cS_2^y \quad (70)$$

with c the vertical resistance of the aquitard and S_2^y its specific yield. The early time specific yield S_1^y equals the elastic storage S_1 of the extracted aquifer with transmissivity $T_1 = T$. The elastic storage of the aquitard is neglected and its transmissivity is zero, or $S_2 = 0$ and $T_2 = 0$. Only the aquifer is extracted; hence, $Q_1 = Q$ and $Q_2 = 0$.

However, the typical S-shaped drawdown curves are also observed when extracting a phreatic aquifer that is not bounded by an overlying aquitard. In this case, the delayed yield may be attributed to the transition of water release mechanisms, from the expansion of water and compaction of the porous medium to the drainage of the unsaturated zone above the falling water table (Mao et al., 2011). Translated to the two specific yield parameters considered by Boulton (1954a, 1963), this implies that the elastic storage coefficient of the aquifer, i.e. $S = S^s D$, is assigned to the early time specific yield S_1^y , while the actual specific yield S^y of the aquifer equals the later time specific yield S_2^y ; or more precisely, the latter is the sum of both coefficients, that is $S_2^y = S + S^y$ (Gambolati, 1976; Herrera et al., 1978). Recall that D is the initial saturated thickness of the aquifer, which is assumed constant. Lebbe (1999) distinguishes this interpretation from the one that involves an aquifer-aquitard system by referring to the first as ‘immediate yield’, and to the latter as ‘delayed yield’.

Applying the interpretation of a single unconfined aquifer, relation (70) is still valid, and parameter c may be seen as the delayed drainage resistance (Hemker, 1999). A physical meaning for this parameter is not required if the model is used to fit pumping test data. One may compare this to the conductance parameter defined for the MODFLOW river and drainage boundary conditions (Harbaugh, 2005). The conductance is not a pure physical parameter either, but should be seen as a lumped model parameter which comprises actual soil characteristics and mathematical simplifications relying on Darcy’s law (Maas, 2003). On the other hand, drainage resistance c may be linked to the resistance of the extracted aquifer. For instance, Streltsova (1972a, 1972b, 1973) demonstrates that her model is equivalent to that of Boulton (1954a, 1963) if $\alpha = 3K^v/(DS^y)$, with K^v the vertical conductivity of the aquifer. This implies that the drainage resistance c is equal to $D/(3K^v)$, which is one third of the vertical resistance of the aquifer. Neuman (1975) finds a similar relation in reconciling his solution with the Boulton (1954a, 1963) solution:

$$\alpha = \frac{K^v}{DS^y} \left[3.063 - 0.567 \log \left(\frac{K^v r^2}{K^h D^2} \right) \right] \quad (71)$$

Note that relation (71) defines α as a function of radial distance r . However, if the term containing the logarithm is omitted, then expression (71) by Neuman (1975) is the same as α found by Streletsova (1972a, 1972b, 1973). Neuman (1979) also derives a relation between α and $K^y/(DS^y)$ that links the Boulton (1954a, 1963) model to the integrodifferential approach by Herrera et al. (1978).

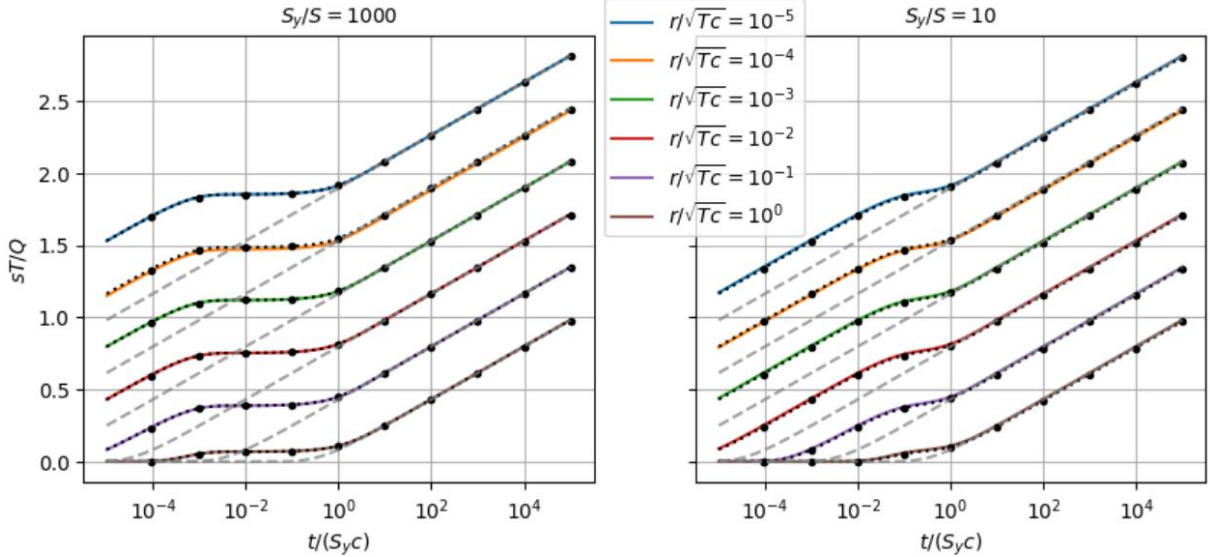


Figure 5. Dimensionless drawdown versus dimensionless time for different values of dimensionless distance according to Boulton's model describing axisymmetric flow to a fully penetrating well in an unconfined aquifer considering delayed yield. The colored solid lines are the analytical solution by Boulton (1954a, 1963), the black dotted lines are the semi-analytical solution by Hemker (1999) modified to include the effect of delayed yield, and the black dots are simulated using the finite-difference approach by Louwyck et al. (2012). The gray dashed lines are the corresponding Theis (1935) solution taking into account specific yield only. The left and right plot consider different values for the ratio between the aquifer's specific yield S_y and its elastic storage coefficient S . The transmissivity of the aquifer is T , the delayed drainage resistance is c , the pumping rate is Q . Drawdown s is a function of radial distance r and time t . See text for definitions and a detailed explanation.

Figure 5 shows dimensionless drawdown sT/Q versus dimensionless time $t\alpha$, with $1/\alpha = cS^y$ according to (70), for different dimensionless distances r/\sqrt{Tc} . Two models are simulated defining different values for S^y/S in order to illustrate the effect of the delayed yield. The left plot in Figure 5 visualizes the results for the model in which this ratio equals 1000, while the right plot is simulated considering a ratio that is equal to 10. Both graphs clearly show the typical S-shaped curves consisting of a steep early-time segment, a flat intermediate-time segment, and a steep late-time segment.

The colored solid lines are calculated using the approximate analytical solution (69) by Boulton (1963), the black dotted lines are simulated using the semi-analytical approach outlined in section 8.3.2, and the black dots are the finite-difference results simulated using MAXSYM (Louwyck, 2011). In the finite-difference model consisting of two layers, the simulation period is divided into 150 timesteps according to (15), and 1200 rings are generated according to (13). Linear interpolation is applied to obtain the drawdowns at the required distances. The maximum total water balance for all time steps is smaller than $10^{-11} \text{ m}^3/\text{d}$, indicating the matrix system is solved very accurately for each time step. All results are virtually the same, which confirms the Boulton (1954a, 1963) model can be reproduced indeed by a two-layer model using Hemker's (1999) solution.

It is seen that the larger ratio S^y/S , the more pronounced the flat intermediate segment is. The late-time segment coincides with the Theis (1935) solution assigning the specific yield S^y to the aquifer storativity. This solution is indicated by gray dashed lines on the graphs in Figure 5. Not indicated by

Figure 5 but easy to verify is that the early-time segment can also be approximated by the Theis (1935) solution if the specific storage coefficient is used, and both the early-time and the intermediate-time segment may be approximated by the Hantush and Jacob (1955) solution for a pumping well in a leaky aquifer.

8.3.4.2. Three-layer example

In the three-layer example discussed in section 8.2.4.2, the process of delayed yield has been neglected. As a result, the time-drawdown curve for the top layer does not exhibit a typical S-shape (Figure 3). The curve for the lower layer, however, does show an S-shape due to the leakage from the layer above, which illustrates the similarity between the processes of delayed yield and leakage. Here, the model is simulated again, this time including delayed yield, but keeping the top layer's transmissivity constant. The semi-analytical solution presented in section 8.3.2 is compared with the finite-difference approach applying the dummy layer trick as discussed in section 8.3.3.

Recall that the example considers a phreatic groundwater reservoir consisting of three aquifers separated by incompressible aquitards, and bounded below by an aquiclude. The initial head in the system is constant and equals 50 m. The aquifer transmissivities are, respectively, $T_1 = 200 \text{ m}^2/\text{d}$, $T_2 = 100 \text{ m}^2/\text{d}$, and $T_3 = 250 \text{ m}^2/\text{d}$; the aquifer storativities are, respectively, $S_1 = 0.005$, $S_2 = 0.005$, and $S_3 = 0.001$. The vertical resistances of the aquitards are, respectively, $c_1 = 100 \text{ d}$ and $c_2 = 500 \text{ d}$. Additionally, a drainage resistance c_0 of 1 d is defined to simulate the effect of delayed yield according to (30). In previous example, storage coefficient S_1 of the upper aquifer was ignored, and only the specific yield S^y was taken into account which equals 0.2. Obviously, both coefficients are required here. Finally, the pumping well has a radius r_w of 0.1 m, and it extracts water from the upper and the lower aquifer at rates $Q_1 = -2500 \text{ m}^3/\text{d}$ and $Q_3 = -1250 \text{ m}^3/\text{d}$, respectively.

The finite-difference grid consists of 150 nodes between r_w and r_{out} , generated using expression (13). Distance r_{out} of the outer grid boundary equals 10^7 m , and an additional constant-head cell of width 10^{-5} m is defined at this distance. Using expression (15), the simulation period is discretized into 150 time steps, starting with a time step equal to 10^{-7} d . The finite-difference grid consists of 4 layers, as a dummy layer is defined on top of the layer representing the upper aquifer to mimic the effect of delayed drainage. This dummy layer has a very small transmissivity equal to $10^{-5} \text{ m}^2/\text{d}$, and its storativity is equal to the specific yield S^y . The system of finite-difference equations is solved using the SIP solver (Stone, 1968), which yields very accurate results, as the maximum total water balance for all time steps is smaller than $2.5 \times 10^{-4} \text{ m}^3/\text{d}$.

Figure 6 shows the head in the three layers simulated using the semi-analytical approach outlined in section 8.3.2 (colored lines) and the finite-difference method implemented in the MAxSym tool (Louwyck, 2011) (black dots). The left graph plots head h as a function of distance r after 10^4 days of pumping; the right graph plots head h in the pumping well (that is at distance r equal to 0.1 m) as a function of time t . Both solutions are very close to each other. The solution for the corresponding confined system is also plotted (gray dashed lines), as is the solution for the unconfined system presented in section 8.2.4.2 simulating nonlinear flow in the upper layer (black dotted lines).

As is seen on the right plot of Figure 6, the time-drawdown curve for the top aquifer clearly exhibits an S-shape due to the effect of delayed yield. At early times, only elastic storage releases water and affects the drawdown, which explains why it is larger than the drawdown simulated using the confined model considering specific yield as the sole water release mechanism. At larger values of time, the specific yield dominates; hence, the time-drawdown curve coincides with the curve according to the confined model. This also explains why there is no difference between the results of both models after 10^4 days of pumping. In the upper aquifer, the nonlinear effect of the head-

dependent transmissivity is significant close to the well, which is clearly seen on the left plot of Figure 6. As already discussed in section 8.2.4.2, this effect increases with time.

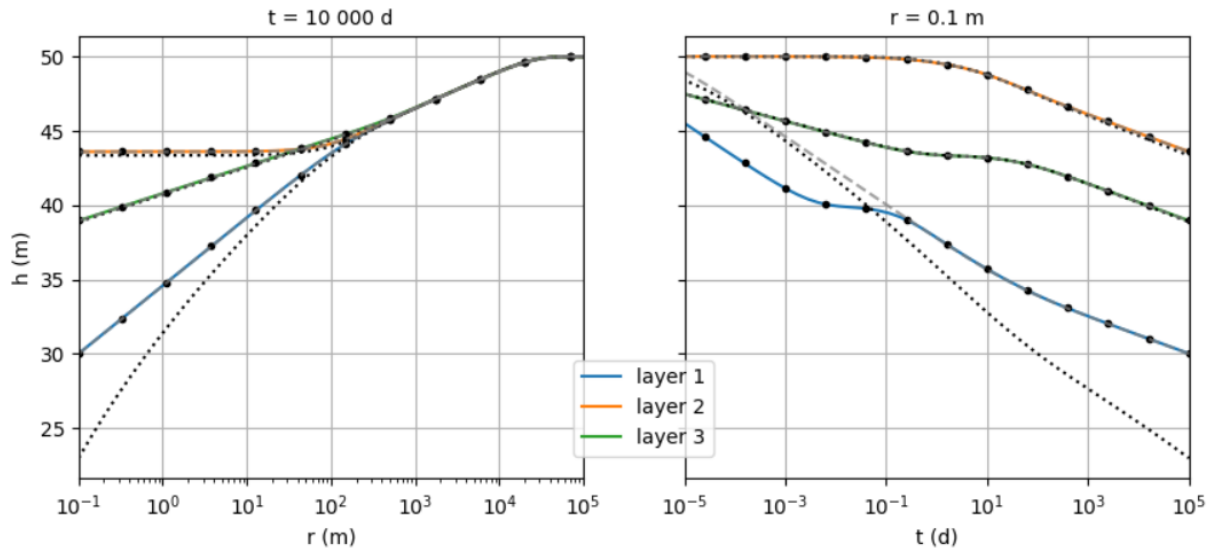


Figure 6. Head h versus distance r after 10 000 days of pumping (left plot), and head h versus time t at the face of the pumping well with a radius of 0.1 m (right plot), for the three-layer model discussed in the text that includes delayed yield in the top layer. The colored lines are according to the semi-analytical solution by Hemker (1999) modified to include the effect of delayed yield, while the black dots are simulated using the finite-difference model MAXSYM (2011). The black dotted lines are the corresponding unconfined solution considering nonlinear flow in the top layer (see Figure 3), whereas the gray dashed lines are the solution for the corresponding confined three-layer model without delayed yield.

8.4. Summary and conclusions

This chapter only scratches the surface of the study of flow to a well in an unconfined aquifer. Two important aspects of unconfined flow are treated separately: the nonlinear behavior associated with the head-dependent saturated thickness of the water table aquifer, and the phenomenon of delayed yield.

Although there is controversy and confusion in the literature about the latter, it is relatively straightforward to simulate the effect of delayed yield by simply defining a low transmissive dummy layer to which the specific yield is assigned on top of the model. This ‘modeling trick’ is based on the fact that the semi-empirical solution by Boulton (1954a, 1963) can be simulated using an aquifer-aquitard system (Cooley & Case, 1973). Hemker (1999) already showed that his semi-analytical solution method can be applied in this way to accurately reproduce results obtained from well-known unconfined well-flow models such as Boulton (1954a, 1963), Neuman (1972, 1973, 1974), and Moench (1995, 1996). Here, the Hemker (1999) solution is extended by treating the delayed yield layer as a real upper boundary condition, which is mathematically more elegant. It is reconfirmed that the Boulton (1954a, 1963) solution indeed corresponds to a model of well-flow in an aquifer bounded on top by a reservoir that produces the delayed drainage determined by the specific yield.

To simulate the effect of the head-dependent transmissivity, the governing partial differential equation is linearized by discretizing the aquifer system into cylindrical zones around the well. The saturated thickness of each zone equals the head at the center of this zone, and within each zone, it does not vary with the radial distance. The width of the zones increases with the distance from the well to obtain an accurate approximation of the declining water table near the well. Using Picard iterations (Mehl, 2006), the heads and the head-dependent transmissivities are alternately updated until convergence is reached. This technique is implemented in the MAXSYM code (Louwyck, 2011;

Louwyck et al., 2012) to simulate unconfined flow in the top layer of a multilayer aquifer system. Alternatively, the MODFLOW procedure by Louwyck et al. (2012, 2014) can be used, as it allows for radial variation of input parameters. This finite-difference technique can also be applied to the semi-analytical multilayer-multizone solution developed in Chapter 5.

Applying this linearization, it is seen that both the finite-difference approach and the semi-analytical solution method give results that are very close to the exact solution for steady unconfined flow to a fully penetrating well (Dupuit, 1857, 1863). Modeling a three-layer example, both solution methods yield virtually the same results again. The same example is also used to test the effect of delayed yield. Comparing the results with the corresponding three-layer model that does not consider nonlinear unconfined flow and neglects the effect of delayed yield, it is seen that ignoring these effects may significantly underestimate drawdown.

An attempt was made to combine both effects, which was unsuccessful. Picard iterations do not seem to be effective in the combined case, and further research is needed to develop a better algorithm, for instance, using Newton iterations (Mehl, 2006). Once an effective algorithm is found, it may also be used to solve the problem of confined-unconfined flow in a more realistic way than is done in previous Chapter 7, where only the change in storage coefficient is considered. It is worth mentioning that MODFLOW-NWT (Niswonger et al., 2011), MODFLOW-USG (Panday et al., 2013), and MODFLOW 6 (Langevin et al., 2017) are able to simulate systems with a head-dependent transmissivity and a storage coefficient that changes between elastic storage and specific yield using the Newton method. Another aspect that is not discussed here, is the presence of a seepage face, and interaction with the unsaturated zone could be taken into account by extending the multilayer models with a linearized form of Richards' unsaturated flow equation.

8.5. References

- Al-Turbak, A. S., Al-Hassoun, S. A., & Al-Othman, A. A. (1993). Determination of Unconfined Aquifer Parameters Using Boulton, Neuman and Streletsova Methods. *Journal of King Saud University - Engineering Sciences*, 5(2), 155–169. [https://doi.org/10.1016/S1018-3639\(18\)30578-6](https://doi.org/10.1016/S1018-3639(18)30578-6)
- Akindunni, F. F., & Gillham, R. W. (1992). Unsaturated and Saturated Flow in Response to Pumping of an Unconfined Aquifer: Numerical Investigation of Delayed Drainage. *Ground Water*, 30(6), 873–884. <https://doi.org/10.1111/j.1745-6584.1992.tb01570.x>
- Anderson, M. P., & Woessner, W. W. (1992). *Applied Groundwater Modeling — Simulation of Flow and Advective Transport*. San Diego, California: Academic Press.
- Bakker, M. (2013a). Analytic Modeling of Transient Multilayer Flow. In P. K. Mishra & K. Kuhlman (Eds.), *Advances in Hydrogeology* (pp. 95–114). New York, NY: Springer, Heidelberg. https://doi.org/10.1007/978-1-4614-6479-2_5
- Bakker, M. (2013b). Semi-analytic modeling of transient multi-layer flow with TTim. *Hydrogeology Journal*, 21(4), 935–943. <https://doi.org/10.1007/s10040-013-0975-2>
- Barlow, P. M., & Moench, A. F. (2011). *WTAQ version 2 - A computer program for analysis of aquifer tests in confined and water-table aquifers with alternative representations of drainage from the unsaturated zone*. U.S. Geological Survey Techniques and Methods 3-B9. <https://doi.org/10.3133/tm3B9>

- Barrash, W., & Dougherty, M. E. (1997). Modeling Axially Symmetric and Nonsymmetric Flow to a Well with MODFLOW, and Application to Goddard2 Well Test, Boise, Idaho. *Ground Water*, 35(4), 602–611. <https://doi.org/10.1111/j.1745-6584.1997.tb00125.x>
- Bartlett, M. S., & Porporato, A. (2018). A Class of Exact Solutions of the Boussinesq Equation for Horizontal and Sloping Aquifers. *Water Resources Research*, 54(2), 767–778. <https://doi.org/10.1002/2017WR022056>
- Bear, J. (1972). *Dynamics of Fluids in Porous Media*. New York: American Elsevier Publishing Company.
- Bevan, M. J., Endres, A. L., Rudolph, D. L., & Parkin, G. (2005). A field scale study of pumping-induced drainage and recovery in an unconfined aquifer. *Journal of Hydrology*, 315(1–4), 52–70. <https://doi.org/10.1016/j.jhydrol.2005.04.006>
- Boulton, N. S. (1954a). Unsteady radial flow to a pumped well allowing for delayed yield from storage. *General Assembly of Rome, Tome II, Groundwater, IAHS publ. 37*, 472–477.
- Boulton, N. S. (1954b). The drawdown of the watertable under non-steady conditions near a pumped well in an unconfined formation. *Proceedings of the Institution of Civil Engineers*, 3(4), 564–579. <https://doi.org/10.1680/ipeds.1954.12586>
- Boulton, N. S. (1963). Analysis of data from non-equilibrium pumping tests allowing for delayed yield from storage. *Proceedings of the Institution of Civil Engineers*, 26(3), 469–482. <https://doi.org/10.1680/iicep.1963.10409>
- Boulton, N. S. (1970). Analysis of data from pumping tests in unconfined anisotropic aquifers. *Journal of Hydrology*, 10(4), 369–378. [https://doi.org/10.1016/0022-1694\(70\)90223-4](https://doi.org/10.1016/0022-1694(70)90223-4)
- Boulton, N. S. (1973). The influence of delayed drainage on data from pumping tests in unconfined aquifers. *Journal of Hydrology*, 19(2), 157–169. [https://doi.org/10.1016/0022-1694\(73\)90077-2](https://doi.org/10.1016/0022-1694(73)90077-2)
- Boulton, N. S., & Pontin, J. M. A. (1971). An extended theory of delayed yield from storage applied to pumping tests in unconfined anisotropic aquifers. *Journal of Hydrology*, 14(1), 53–65. [https://doi.org/10.1016/0022-1694\(71\)90092-8](https://doi.org/10.1016/0022-1694(71)90092-8)
- Boulton, N. S., & Streltsova, T. D. (1975). New equations for determining the formation constants of an aquifer from pumping test data. *Water Resources Research*, 11(1), 148–153. <https://doi.org/10.1029/WR011i001p00148>
- Boulton, N. S., & Streltsova, T. D. (1976). The drawdown near an abstraction well of large diameter under non-steady conditions in an unconfined aquifer. *Journal of Hydrology*, 30(1–2), 29–46. [https://doi.org/10.1016/0022-1694\(76\)90087-1](https://doi.org/10.1016/0022-1694(76)90087-1)
- Boussinesq, J. (1877). *Essai sur la théorie des eaux courantes, Mémoires présentées par divers savants à l'Académie des Sciences* (in French). Imprimerie Nationale, Paris.
- Boussinesq, J. (1904). Recherches théoriques sur l’écoulement des nappes d’eau infiltrées dans le sol et sur le débit des sources (in French). *Journal De Mathématiques Pures Et Appliquées*, 10, 5–78.
- Brutsaert, W. (1994). The unit response of groundwater outflow from a hillslope. *Water Resources Research*, 30(10), 2759–2763. <https://doi.org/10.1029/94WR01396>

- Chenaf, D., & Chapuis, R. P. (2007). Seepage Face Height, Water Table Position, and Well Efficiency at Steady State. *Ground Water*, 45(2), 168–177. <https://doi.org/10.1111/j.1745-6584.2006.00277.x>
- Cooley, R. L. (1971). A Finite Difference Method for Unsteady Flow in Variably Saturated Porous Media: Application to a Single Pumping Well. *Water Resources Research*, 7(6), 1607–1625. <https://doi.org/10.1029/WR007i006p01607>
- Cooley, R. L. (1972). Numerical simulation of flow in an aquifer overlain by a water table aquitard. *Water Resources Research*, 8(4), 1046–1050. <https://doi.org/10.1029/WR008i004p01046>
- Cooley, R. L., & Case, C. M. (1973). Effect of a water table aquitard on drawdown in an underlying pumped aquifer. *Water Resources Research*, 9(2), 434–447. <https://doi.org/10.1029/WR009i002p00434>
- Dagan, G. (1964). Second order linearized theory of free surface flow in porous media. *La Houille Blanche*, 8, 901–910.
- Dagan, G. (1967). A method of determining the permeability and effective porosity of unconfined anisotropic aquifers. *Water Resources Research*, 3(4), 1059–1071. <https://doi.org/10.1029/WR003i004p01059>
- Dupuit, J. (1857). Mouvement de l'eau à travers les terrains perméables (in French). *Comptes Rendus de l'Académie Des Sciences*, 45, 92–96.
- Dupuit, J. (1863). *Etude Théoriques et Pratiques Sur le Mouvement Des Eaux Dans Les Canaux Découverts et à Travers Les Terrains Perméables* (in French). Paris: Dunot.
- Endres, A. L., Jones, J. P., & Bertrand, E. A. (2007). Pumping-induced vadose zone drainage and storage in an unconfined aquifer: A comparison of analytical model predictions and field measurements. *Journal of Hydrology*, 335(1–2), 207–218. <https://doi.org/10.1016/j.jhydrol.2006.07.018>
- Forchheimer, P. (1886). Über die Ergiebigkeit von Brunnen-Anlagen und Sickerschlitten (in German). *Zeitschrift Des Architekten- Und Ingenieur-Vereins*, 32, 539–563.
- Forchheimer, P. Z. (1901). Wasserbewegung durch Boden (in German). *Zeitschrift Des Vereins Deutscher Ingenieure*, 50, 1781–1788.
- Gambolati, G. (1976). Transient free surface flow to a well: An analysis of theoretical solutions. *Water Resources Research*, 12(1), 27–39. <https://doi.org/10.1029/WR012i001p00027>
- González-Quirós, A., & Fernández-Álvarez, J. P. (2021). Use of microgravity for identification of delayed gravity drainage and conceptual model selection in unconfined aquifers. *Journal of Hydrology*, 597, 126285. <https://doi.org/10.1016/j.jhydrol.2021.126285>
- Haitjema, H. (1995). *Analytic Element Modeling of Groundwater Flow*. San Diego: Academic Press. <https://doi.org/10.1016/B978-0-12-316550-3.X5000-4>
- Hantush, M. S., & Jacob, C. E. (1955). Non-steady radial flow in an infinite leaky aquifer. *Transactions, American Geophysical Union*, 36(1), 95–100. <https://doi.org/10.1029/TR036i001p00095>
- Harbaugh, A. W. (1995). *Direct solution package based on alternating diagonal ordering for the U.S. Geological Survey modular finite-difference ground-water flow model*. U.S. Geological Survey Open-File Report 95-288. <https://doi.org/https://doi.org/10.3133/ofr95288>

- Harbaugh, A. W. (2005). *MODFLOW-2005, the U.S. Geological Survey modular ground-water model - the Ground-Water Flow Process*. U.S. Geological Survey Techniques and Methods 6-A16. <https://doi.org/https://doi.org/10.3133/tm6A16>
- Hemker, C. J. (1984). Steady groundwater flow in leaky multiple-aquifer systems. *Journal of Hydrology*, 72(3–4), 355–374. [https://doi.org/10.1016/0022-1694\(84\)90089-1](https://doi.org/10.1016/0022-1694(84)90089-1)
- Hemker, C. J. (1985). Transient well flow in leaky multiple-aquifer systems. *Journal of Hydrology*, 81(1–2), 111–126. [https://doi.org/10.1016/0022-1694\(85\)90170-2](https://doi.org/10.1016/0022-1694(85)90170-2)
- Hemker, C. J. (1999). Transient well flow in vertically heterogeneous aquifers. *Journal of Hydrology*, 225(1–2), 1–18. [https://doi.org/10.1016/S0022-1694\(99\)00137-7](https://doi.org/10.1016/S0022-1694(99)00137-7)
- Herrera, I., Minzoni, A., & Flores, E. Z. (1978). Theory of flow in unconfined aquifers by integrodifferential equations. *Water Resources Research*, 14(2), 291–298. <https://doi.org/10.1029/WR014i002p00291>
- Houben, G. J., & Batelaan, O. (2021). The Thiem team – Adolf and Günther Thiem, two forefathers of hydrogeology. *Hydrology and Earth System Sciences Discussions*.
- Ismail, S. O., & Mawlood, D. K. (2020). Comparing pumping test between Boulton and Neuman in unconfined aquifer. *Zanco Journal of Pure and Applied Sciences*, 32(2), 7–14.
- Kirkham, D. (1967). Explanation of paradoxes in Dupuit-Forchheimer Seepage Theory. *Water Resources Research*, 3(2), 609–622. <https://doi.org/10.1029/WR003i002p00609>
- Kroszynski, U. I., & Dagan, G. (1975). Well pumping in unconfined aquifers: The influence of the unsaturated zone. *Water Resources Research*, 11(3), 479–490. <https://doi.org/10.1029/WR011i003p00479>
- Kruseman, G. P., & de Ridder, N. A. (1990). *Analysis and Evaluation of Pumping Test Data* (2nd ed.). Wageningen: ILRI Publication 47.
- Langevin, C. D. (2008). Modeling Axisymmetric Flow and Transport. *Ground Water*, 46(4), 579–590. <https://doi.org/10.1111/j.1745-6584.2008.00445.x>
- Langevin, C. D., Hughes, J. D., Banta, E. R., Niswonger, R. G., Panday, S., & Provost, A. M. (2017). *Documentation for the MODFLOW 6 Groundwater Flow Model*. U.S. Geological Survey Techniques and Methods 6-A55. <https://doi.org/10.3133/tm6A55>
- Lebbe, L. C. (1999). *Hydraulic Parameter Identification. Generalized Interpretation Method for Single and Multiple Pumping Tests*. Berlin Heidelberg: Springer-Verlag.
- Lohman, S. W. (1972). *Ground-water Hydraulics*. U.S. Geological Survey.
- Louwyck, A. (2011). *MAxSym - A MATLAB Tool to Simulate Two-Dimensional Axi-Symmetric Groundwater Flow*. Research Unit Groundwater Modeling, Ghent University. Retrieved from <https://github.com/alouwyck/MAxSym>
- Louwyck, A., Vandenbohede, A., Bakker, M., & Lebbe, L. C. (2012). Simulation of axi-symmetric flow towards wells: A finite-difference approach. *Computers & Geosciences*, 44, 136–145. <https://doi.org/10.1016/j.cageo.2011.09.004>

- Louwyck, A., Vandenbohede, A., Bakker, M., & Lebbe, L. C. (2014). MODFLOW procedure to simulate axisymmetric flow in radially heterogeneous and layered aquifer systems. *Hydrogeology Journal*, 22(5), 1217–1226. <https://doi.org/10.1007/s10040-014-1150-0>
- Louwyck, A., Vandenbohede, A., Libbrecht, D., Van Camp, M., & Walraevens, K. (2022). The Radius of Influence Myth. *Water*, 14(2), 149. <https://doi.org/10.3390/w14020149>
- Louwyck, A., Vandenbohede, A., Heuvelmans, G., Van Camp, M., & Walraevens, K. (2023). The Water Budget Myth and Its Recharge Controversy: Linear vs. Nonlinear Models. *Groundwater*, 61(1), 100–110. <https://doi.org/10.1111/gwat.13245>
- Maas, C. (2003). Ondiepe wateropen in MODFLOW (in Dutch). *Stromingen*, 9(3), 37–45.
- Malama, B. (2011). Alternative linearization of water table kinematic condition for unconfined aquifer pumping test modeling and its implications for specific yield estimates. *Journal of Hydrology*, 399(3–4), 141–147. <https://doi.org/10.1016/j.jhydrol.2010.11.007>
- Mao, D., Wan, L., Yeh, T.-C. J., Lee, C.-H., Hsu, K.-C., Wen, J.-C., & Lu, W. (2011). A revisit of drawdown behavior during pumping in unconfined aquifers. *Water Resources Research*, 47(5). <https://doi.org/10.1029/2010WR009326>
- Mathias, S. A., & Butler, A. P. (2006). Linearized Richards' equation approach to pumping test analysis in compressible aquifers. *Water Resources Research*, 42(6). <https://doi.org/10.1029/2005WR004680>
- Mehl, S. W. (2006). Use of Picard and Newton Iteration for Solving Nonlinear Ground Water Flow Equations. *Ground Water*, 44(4), 583–594. <https://doi.org/10.1111/j.1745-6584.2006.00207.x>
- Mishra, P. K., & Kuhlman, K. L. (2013). Unconfined Aquifer Flow Theory: From Dupuit to Present. In P. K. Mishra & K. L. Kuhlman (Eds.), *Advances in Hydrogeology* (pp. 185–202). New York, NY: Springer New York. https://doi.org/10.1007/978-1-4614-6479-2_9
- Mishra, P. K., & Neuman, S. P. (2010). Improved forward and inverse analyses of saturated-unsaturated flow toward a well in a compressible unconfined aquifer. *Water Resources Research*, 46(7). <https://doi.org/10.1029/2009WR008899>
- Mishra, P. K., & Neuman, S. P. (2011). Saturated-unsaturated flow to a well with storage in a compressible unconfined aquifer. *Water Resources Research*, 47(5). <https://doi.org/10.1029/2010WR010177>
- Moench, A. F. (1993). Computation of Type Curves for Flow to Partially Penetrating Wells in Water-Table Aquifers. *Ground Water*, 31(6), 966–971. <https://doi.org/10.1111/j.1745-6584.1993.tb00870.x>
- Moench, A. F. (1994). Specific Yield as Determined by Type-Curve Analysis of Aquifer-Test Data. *Ground Water*, 32(6), 949–957. <https://doi.org/10.1111/j.1745-6584.1994.tb00934.x>
- Moench, A. F. (1995). Combining the Neuman and Boulton Models for Flow to a Well in an Unconfined Aquifer. *Ground Water*, 33(3), 378–384. <https://doi.org/10.1111/j.1745-6584.1995.tb00293.x>
- Moench, A. F. (1996). Flow to a Well in a Water-Table Aquifer: An Improved Laplace Transform Solution. *Ground Water*, 34(4), 593–596. <https://doi.org/10.1111/j.1745-6584.1996.tb02045.x>

- Moench, A. F. (1997). Flow to a well of finite diameter in a homogeneous, anisotropic water table aquifer. *Water Resources Research*, 33(6), 1397–1407. <https://doi.org/10.1029/97WR00651>
- Moench, A. F. (2004). Importance of the Vadose Zone in Analyses of Unconfined Aquifer Tests. *Ground Water*, 42(2), 223–233. <https://doi.org/10.1111/j.1745-6584.2004.tb02669.x>
- Moench, A. F. (2008). Analytical and numerical analyses of an unconfined aquifer test considering unsaturated zone characteristics. *Water Resources Research*, 44(6). <https://doi.org/10.1029/2006WR005736>
- Moench, A. F., Garabedian, S. P., & LeBlanc, D. R. (2001). *Estimation of Hydraulic Parameters from an Unconfined Aquifer Test Conducted in a Glacial Outwash Deposit, Cape Cod, Massachusetts*. U.S. Geological Survey Professional Paper 1629.
- Narasimhan, T. N., & Zhu, M. (1993). Transient flow of water to a well in an unconfined aquifer: Applicability of some conceptual models. *Water Resources Research*, 29(1), 179–191. <https://doi.org/10.1029/92WR01959>
- Neuman, S. P. (1972). Theory of flow in unconfined aquifers considering delayed response of the water table. *Water Resources Research*, 8(4), 1031–1045. <https://doi.org/10.1029/WR008i004p01031>
- Neuman, S. P. (1973). Supplementary Comments on ‘Theory of flow in unconfined aquifers considering delayed response of the water table.’ *Water Resources Research*, 9(4), 1102–1103. <https://doi.org/10.1029/WR009i004p01102>
- Neuman, S. P. (1974). Effect of partial penetration on flow in unconfined aquifers considering delayed gravity response. *Water Resources Research*, 10(2), 303–312. <https://doi.org/10.1029/WR010i002p00303>
- Neuman, S. P. (1975). Analysis of pumping test data from anisotropic unconfined aquifers considering delayed gravity response. *Water Resources Research*, 11(2), 329–342. <https://doi.org/10.1029/WR011i002p00329>
- Neuman, S. P. (1979). Perspective on ‘Delayed yield.’ *Water Resources Research*, 15(4), 899–908. <https://doi.org/10.1029/WR015i004p00899>
- Niswonger, R. G., Pandy, S., & Ibaraki, M. (2011). *MODFLOW-NWT, A Newton formulation for MODFLOW-2005*. U.S. Geological Survey Techniques and Methods 6-A37. <https://doi.org/10.3133/tm6A37>
- Nwankwor, G. I., Cherry, J. A., & Gillham, R. W. (1984). A Comparative Study of Specific Yield Determinations for a Shallow Sand Aquifer. *Ground Water*, 22(6), 764–772. <https://doi.org/10.1111/j.1745-6584.1984.tb01445.x>
- Nwankwor, G. I., Gillham, R. W., Kamp, G., & Akindunni, F. F. (1992). Unsaturated and Saturated Flow in Response to Pumping of an Unconfined Aquifer: Field Evidence of Delayed Drainage. *Ground Water*, 30(5), 690–700. <https://doi.org/10.1111/j.1745-6584.1992.tb01555.x>
- Ojha, C. S. P., & Gopal, V. (1999). Seepage Face Modeling for Large-Diameter Well in Unconfined Aquifer. *Journal of Hydrologic Engineering*, 4(3), 275–279. [https://doi.org/10.1061/\(ASCE\)1084-0699\(1999\)4:3\(275\)](https://doi.org/10.1061/(ASCE)1084-0699(1999)4:3(275))

- Panday, S., Langevin, C. D., Niswonger, R. G., Ibaraki, M., & Hughes, J. D. (2013). *MODFLOW-USG version 1: An unstructured grid version of MODFLOW for simulating groundwater flow and tightly coupled processes using a control volume finite-difference formulation*. U.S. Geological Survey Techniques and Methods 6-A45. <https://doi.org/10.3133/tm6A45>
- Prickett, T. A. (1965). Type-Curve Solution to Aquifer Tests under Water-Table Conditions. *Ground Water*, 3(3), 5–14. <https://doi.org/10.1111/j.1745-6584.1965.tb01214.x>
- Reilly, T. E., & Harbaugh, A. W. (1993). Simulation of Cylindrical Flow to a Well Using the U.S. Geological Survey Modular Finite-Difference Ground-Water Flow Model. *Ground Water*, 31(3), 489–494. <https://doi.org/10.1111/j.1745-6584.1993.tb01851.x>
- Rushton, K. R. (2006). Significance of a seepage face on flows to wells in unconfined aquifers. *Quarterly Journal of Engineering Geology and Hydrogeology*, 39(4), 323–331. <https://doi.org/10.1144/1470-9236/06-004>
- Shampine, L. F. (2008). Vectorized adaptive quadrature in MATLAB. *Journal of Computational and Applied Mathematics*, 211(2). <https://doi.org/10.1016/j.cam.2006.11.021>
- Shamsai, A., & Narasimhan, T. N. (1991). A numerical investigation of free surface-Seepage face relationship under steady state flow conditions. *Water Resources Research*, 27(3), 409–421. <https://doi.org/10.1029/90WR01905>
- Stehfest, H. (1970). Algorithm 368: Numerical inversion of Laplace transforms [D5]. *Communications of the ACM*, 13(1), 47–49. <https://doi.org/10.1145/361953.361969>
- Stone, H. L. (1968). Iterative Solution of Implicit Approximations of Multidimensional Partial Differential Equations. *SIAM Journal on Numerical Analysis*, 5(3), 530–558. <https://doi.org/10.1137/0705044>
- Strack, O. D. L. (1984). Three-Dimensional Streamlines in Dupuit-Forchheimer Models. *Water Resources Research*, 20(7), 812–822. <https://doi.org/10.1029/WR020i007p00812>
- Strack, O. D. L. (1989). *Groundwater Mechanics*. Old Tappan, N. J.: Prentice-Hall.
- Streltsova, T. D. (1972a). Unconfined aquifer and slow drainage. *Journal of Hydrology*, 16(2), 117–124. [https://doi.org/10.1016/0022-1694\(72\)90117-5](https://doi.org/10.1016/0022-1694(72)90117-5)
- Streltsova, T. D. (1972b). Unsteady radial flow in an unconfined aquifer. *Water Resources Research*, 8(4), 1059–1066. <https://doi.org/10.1029/WR008i004p01059>
- Streltsova, T. D. (1973). Flow near a pumped well in an unconfined aquifer under nonsteady conditions. *Water Resources Research*, 9(1), 227–235. <https://doi.org/10.1029/WR009i001p00227>
- Tartakovsky, G. D., & Neuman, S. P. (2007). Three-dimensional saturated-unsaturated flow with axial symmetry to a partially penetrating well in a compressible unconfined aquifer. *Water Resources Research*, 43(1). <https://doi.org/10.1029/2006WR005153>
- Theis, C. V. (1935). The relation between the lowering of the Piezometric surface and the rate and duration of discharge of a well using ground-water storage. *Transactions, American Geophysical Union*, 16(2), 519–524. <https://doi.org/10.1029/TR016i002p00519>
- Thiem, A. (1870). Die Ergiebigkeit artesischer Bohrlöcher, Schachtbrunnen und Filtergalerien (in German). *Journal Für Gasbeleuchtung Und Wasserversorgung*, 13, 450–467.

- Thiem, G. (1906). *Hydrologische Methoden (in German)*. Leipzig: Gebhardt.
- Troch, P. A., Paniconi, C., & van Loon, E. (2003). Hillslope-storage Boussinesq model for subsurface flow and variable source areas along complex hillslopes: 1. Formulation and characteristic response. *Water Resources Research*, 39(11). <https://doi.org/10.1029/2002WR001728>
- Troch, P. A., Berne, A., Bogaart, P., Harman, C., Hilberts, A. G. J., Lyon, S. W., et al. (2013). The importance of hydraulic groundwater theory in catchment hydrology: The legacy of Wilfried Brutsaert and Jean-Yves Parlange. *Water Resources Research*, 49(9), 5099–5116. <https://doi.org/10.1002/wrcr.20407>
- Verhoest, N. E. C., & Troch, P. A. (2000). Some analytical solutions of the linearized Boussinesq equation with recharge for a sloping aquifer. *Water Resources Research*, 36(3), 793–800. <https://doi.org/10.1029/1999WR900317>
- Xiao, L., Ye, M., & Xu, Y. (2018). A New Solution for Confined-Unconfined Flow Toward a Fully Penetrating Well in a Confined Aquifer. *Groundwater*, 56(6), 959–968. <https://doi.org/10.1111/gwat.12642>
- Yakirevich, A., Gish, T. J., Šimunek, J., van Genuchten, M. Th., Pachepsky, Y. A., Nicholson, T. J., & Cady, R. E. (2010). Potential Impact of a Seepage Face on Solute Transport to a Pumping Well. *Vadose Zone Journal*, 9(3), 686–696. <https://doi.org/10.2136/vzj2009.0054>
- Zlotnik, V., & Ledder, G. (1992). Groundwater flow in a compressible unconfined aquifer with uniform circular recharge. *Water Resources Research*, 28(6), 1619–1630. <https://doi.org/10.1029/92WR00462>
- Zlotnik, V., & Zhan, H. (2005). Aquitard effect on drawdown in water table aquifers. *Water Resources Research*, 41(6). <https://doi.org/10.1029/2004WR003716>

Chapter 9. Understanding Axisymmetric Multilayer Well-Flow

9.1. Introduction

In this chapter, the solution for transient axisymmetric flow to a well of infinitesimal radius extracting water at constant rate from a confined multilayer system of infinite extent is studied. The semi-analytical solution method presented by Hemker (1984, 1985, 1999a) is applied, which is also discussed in Chapter 2 and Chapter 4. The exact solution in Laplace space is compared with the corresponding steady state solution, and by expanding this Laplace space solution for large values of time, an asymptotic solution is found that is equal to the steady state solution, except for the comprehensive potential term, which is described by the Theis (1935) equation instead of the Thiem (1870; 1906) formula.

Analyzing the leakage between the layers of the system shows that in the proximal zone around the well, the extracted water is redistributed according to the transmissive properties of the layers, whereas in the distal zone, flow is corrected to account for the storative properties. Once the distribution of water in the proximal zone has been completed and the hydraulic gradient does not change anymore, flow is in a pseudo-steady state, and drawdown may be approximated by the asymptotic solution. The corresponding drawdown curves plotted on semi-logarithmic axes are parallel straight lines with slope given by the Cooper and Jacob (1946) approximation for the equivalent single-layer model. Hence, the presented theory confirms the spatial averaging in drawdown data measured during pumping tests, and exposes an inherent limitation of multi-level tests.

9.1.1. Semi-analytical multi-aquifer solutions

The theory of multi-aquifer flow toward a pumping well is well-established within the hydrogeological community, and both semi-analytical and numerical methods exist to solve the problem. Hemker (1984) is the first in the English literature to publish the analytical solution for steady flow in a leaky multi-aquifer system, although earlier work on multilayer well-flow problems is published in Russian and Hungarian (Halász, 1975; Halász & Székely, 1979; Székely, 1978). Hemker (1984) applies the technique of eigendecomposition to uncouple the system of ordinary differential equations. Hunt (1985, 1986) uses the solution of a generalized eigenvalue problem, and Yu (1987) presents a method similar to Hemker (1984), while Maas (1986, 1987a) makes use of matrix differential calculus. Steady flow in systems of aquifers separated by leaky layers is also treated by Strack (1989).

Hemker (1985), Hunt (1985) and Maas (1987b) extended their steady-state solution method to obtain a solution for transient flow to a well in a confined or leaky multi-aquifer system. Hemker (1985) applies the Laplace and Hankel transforms, Maas (1987b) the Hankel and generalized Fourier transforms. Maas (1987b) also considers the compressibility of the separating aquitards. Both Hemker (1985) and Maas (1987b) apply analytical inversion techniques, whereas Hemker and Maas (1987) use the Stehfest (1970) algorithm to invert the obtained solution in Laplace space. The solution of Hemker and Maas (1987) completely accounts for the effect of elastic storage in separating and bounding aquitards. Unaware of these results, Cheng and Morohunfola (1993) published a similar but less concise solution several years later (Hemker, 2000), and Bruggeman (1999) presented an alternative expression to the solution by Hemker (1985).

Previously, axisymmetric well-flow models were restricted to one or two layers (Hemker, 2000), such as the well-known analytical solutions by Theis (1935), de Glee (1930), Jacob (1946), Hantush and Jacob (1955), Hantush (1967), and Neuman and Witherspoon (1969). In that sense, the multi-aquifer solutions were a major breakthrough in well hydraulics. On the other hand, these models still adopt some of the simplifying assumptions made by their predecessors. The infinitesimal well diameter, for instance, is tackled by Hemker (1999a, 1999b), whereas solutions for anisotropic layered aquifer systems are developed by Bakker and Hemker (2002) and Meesters et al. (2004). Relevant to this study is the assumption of strictly horizontal flow in each layer of the system according to the Dupuit-Forchheimer approximation (Bakker, 1999). This issue may be resolved by applying the finite-difference technique of dividing an aquifer layer in a number of sublayers separated by resistance layers of thickness zero (Bakker, 1999, 2001; Hemker, 1984, 1985, 1999a). The vertical direction can also be fully taken into account by applying the integral transform strategies presented by Veling and Maas (2009).

9.1.2. Objective

Since axisymmetric multi-aquifer flow has been fully described mathematically by Veling and Maas (2009), one could argue that theoretical studies on this subject have become pointless. Nevertheless, a full mathematical description does not automatically lead to a full understanding of the problem. In a recent paper by Pfannkuch et al. (2021), for instance, it is stated that “in a highly stratified aquifer with layers of high hydraulic conductivity contrasts [...] the high conductivity layers contribute early to discharge from the well and need less drawdown. [...] As the lower permeability layers contribute more of the pumped discharge, the curve steepens.” In Fig. 4f of the paper, an example is shown of such a steepening time-drawdown curve that consists of three straight lines, where the steepest line indeed corresponds to the largest values of time. However, this statement by Pfannkuch et al. (2021) cannot be confirmed by the multi-aquifer well-flow theory developed by Hemker (1984, 1985, 1999a, 1999b), which is examined in depth in this study.

The main objective of this chapter is thus to get more insight in the dynamics of transient multi-aquifer flow to a well. First, the transient-state problem for a confined multi-layer system originally solved by Hemker (1985) is re-evaluated in Laplace space, as suggested by Hemker (1999a, 2000). Second, it is shown how this solution is related to the steady-state solution. As mentioned above, Hemker (1984) was the first to present the steady-state solution for a leaky multi-aquifer system. In case the system is confined, however, the resulting matrix is singular, and therefore the method presented by Bakker (2001) and Bakker and Strack (2003) is adopted, who formulate the problem in terms of discharge potentials.

Bakker (2001) shows that in the confined case, one eigenvalue is zero and corresponds to the comprehensive potential, which is defined as the sum of the potentials in all layers and is determined by the Thiem (1870; 1906) solution. This means radial flow in the aquifer system can be described as if it is a single confined layer with transmissivity equal to the sum of the transmissivities of all layers. Close to the well, however, this flow is redistributed according to the transmissive properties of the individual layers in the system, whereas at large distances, the leakage between these layers becomes negligibly small, and the system actually behaves as a single homogeneous layer. The distance from which interaction between layers can be ignored, is determined by the largest leakage factor (Bakker & Strack, 2003).

The concept of a comprehensive potential is introduced by Strack (1981a, 1981b) to solve the problem of flow in aquifers with clay laminae, and it is applied by Strack and Haitjema (1981a, 1981b) to model double aquifer flow. The comprehensive potential is also discussed by Strack (1989) and

Haitjema (1995). In these studies and in the work of Bakker (2001) and Bakker and Strack (2003), the comprehensive potential is used to simulate steady flow. The question that is answered in this study is to what extent the comprehensive potential also applies to the transient axisymmetric case. Or more specifically, when is it allowed to use the Theis (1935) solution to calculate the comprehensive potential of a transient multilayer system extracted by a pumping well. Hemker (1985) shows that this is always the case if the diffusivities of all layers in the system are equal, and Hunt and Scott (2007) prove that it is always justified for large values of time in a two-layer system. Inspired by the work of Hunt and Scott (2007), the multi-layer Laplace space solution is expanded for large values of time, resulting in an asymptotic solution similar to the steady-state solution by Bakker (2001), but in which the comprehensive potential given by the Thiem (1870; 1906) formula is replaced indeed by the Theis (1935) solution.

By evaluating the water budget of the individual layers using this approximate solution, it is shown that after a long period of pumping at constant rate, flow close to the well is redistributed according to the transmissive properties of the individual layers, resulting in a pseudo-steady state, which is also referred to as steady shape conditions (Bohling et al., 2002). However, at distances larger than a distance determined by the largest leakage factor, leakage still occurs if layer diffusivities are not equal, since flow needs to be redistributed according to the storative properties of the layers. Recall that the system is confined, and consequently, the total volume of pumped water is always balanced by the total storage change. This explains why in the distal part of the aquifer, vertical flow may occur from a pumped layer to an unpumped layer, which is clearly demonstrated by the theoretical example given in this study to clarify the derived expressions.

The developed asymptotic solution is verified by analyzing a large number of random simulations, and the consequences of the presented theory are discussed for the interpretation of pumping tests in multi-aquifer systems. The theory supports the steady shape analysis of tomographic pumping tests proposed by Bohling et al. (2002, 2007), and it also confirms the spatial averaging in pumping induced drawdown data. It is argued that deriving the hydraulic parameters of individual layers from drawdown measurements, is limited in space and time, and a rule of thumb is proposed to guide modelers in determining the window of opportunity. A second and final theoretical example clearly illustrates the inherent limitations of the hydraulic tomography due to this spatial averaging in drawdown (Bohling, 2009; Bohling & Butler, 2010).

9.2. Problem statement

In this section, the problem of transient axisymmetric flow to a well with infinitesimal radius in a confined multilayer aquifer system of infinite extent, first stated by Hemker (1985), is reformulated in terms of discharge potentials, as proposed by Bakker (2001) and Bakker and Strack (2003). The different layers in the system may correspond to real aquifers, or they may be the result of a vertical finite-difference discretization (Hemker, 1999a).

Consider a confined multilayer aquifer system of infinite extent that is discretized vertically in n_l horizontal homogeneous layers, where layer i is characterized by transmissivity T_i [L^2/T] and storativity S_i [-]. Within each layer, resistance to vertical flow is neglected according to the Dupuit-Forchheimer approximation. Between layers i and $i + 1$, a resistance layer of zero thickness is present, characterized by vertical resistance c_i [T], where $c_1 = c_{n_l+1} = \infty$, as the system is confined. Layers are numbered from top to bottom.

A cylindrical (r, z) coordinate system is adopted with the z -axis pointing vertically upward. Transient axisymmetric flow in the system is described by the following set of partial differential equations:

$$\frac{\partial^2 \Phi_i}{\partial r^2} + \frac{1}{r} \frac{\partial \Phi_i}{\partial r} = \frac{S_i}{T_i} \frac{\partial \Phi_i}{\partial t} + \frac{\Phi_i}{T_i c_i} - \frac{\Phi_{i-1}}{T_{i-1} c_i} + \frac{\Phi_i}{T_i c_{i+1}} - \frac{\Phi_{i+1}}{T_{i+1} c_{i+1}} \quad (1 \leq i \leq n_l) \quad (1)$$

where r is the radial distance [L], and t is the time [T]. The discharge potential Φ_i [L^3/T] in layer i is defined as (e.g. Strack, 1989):

$$\Phi_i(r, t) = T_i \varphi_i(r, t) \quad (1 \leq i \leq n_l) \quad (2)$$

where φ_i is the piezometric head [L] in layer i .

In case of pumping or injection, it is common to study the change in head s [L]:

$$s_i(r, t) = \varphi_i(r, t) - \varphi_i(r, 0) \quad (1 \leq i \leq n_l) \quad (3)$$

where $\varphi_i(r, 0)$ is the initial head [L] before pumping at $t = 0$. The head change is positive when the head is rising and negative otherwise; in the latter case, head change s is called drawdown.

Since the differential equations in (1) are linear, the head change is independent of the initial head, and therefore, it is not required to assume a constant initial head. For the sake of simplicity, however, the initial head is assumed zero, resulting into the following set of initial conditions:

$$\Phi_i(r, 0) = 0 \quad (1 \leq i \leq n_l) \quad (4)$$

In case of (4), the potential $\Phi_i(r, t)$ reflects the change in potential, and head $\varphi_i(r, t)$ equals the change in head $s_i(r, t)$, which may be superimposed on initial head $\varphi_i(r, 0)$ to obtain the total head during pumping or injection.

The multilayer aquifer system is discharged or recharged by means of a vertical cylindrical well with vertical axis coinciding with the z -axis of the coordinate system. The well has a separate fully penetrating screen in each layer. If an infinitesimal well-radius is assumed, the set of inner boundary conditions is:

$$\lim_{r \rightarrow 0} 2\pi r \frac{\partial \Phi_i}{\partial r} = -Q_i \quad (1 \leq i \leq n_l) \quad (5)$$

where Q_i is the pumping ($Q_i < 0$) or injection ($Q_i > 0$) rate [L^3/T] in layer i . In this chapter, only pumping is considered, which implies head change s is always a drawdown of the initial head.

As the multilayer system has an infinite extent, the set of outer boundary conditions is defined at an infinite radial distance:

$$\lim_{r \rightarrow \infty} \Phi_i(r, t) = \Phi_i(r, 0) = 0 \quad (1 \leq i \leq n_l) \quad (6)$$

where initial potential $\Phi_i(r, 0)$ is zero according to (4).

The radial discharge $Q_i^r(r, t)$ [L^3/T] is the amount of water per unit of time that flows through the cylindrical surface with radius r in layer i at time t :

$$Q_i^r(r, t) = -2\pi r \frac{\partial \Phi_i}{\partial r} \quad (1 \leq i \leq n_l) \quad (7)$$

The vertical discharge $Q_i^v(r_1, r_2, t)$ is the amount of water per unit of time that flows through the ring-shaped vertical surface between layer i and layer $i - 1$, and determined by the radii r_1 and r_2 at time t :

$$Q_i^v(r_1, r_2, t) = 2\pi \int_{r_1}^{r_2} \left(\frac{\Phi_i}{T_i c_i} - \frac{\Phi_{i-1}}{T_{i-1} c_i} \right) r dr \quad (2 \leq i \leq n_l) \quad (8)$$

The storage change $Q_i^s(r_1, r_2, t)$ is the amount of water per unit of time released by or stored in the ring determined by radii r_1 and r_2 in layer i at time t :

$$Q_i^s(r_1, r_2, t) = 2\pi \frac{S_i}{T_i} \int_{r_1}^{r_2} \frac{\partial \Phi_i}{\partial t} r dr \quad (1 \leq i \leq n_l) \quad (9)$$

The total water budget for each layer is found by multiplying both sides of the equations (1) by $2\pi r$ and integrating them between 0 and ∞ . Using definitions (7), (8), and (9), the following relation is found:

$$-Q_i^r(\infty, t) + Q_i^r(0, t) - Q_i^s(0, \infty, t) - Q_i^v(0, \infty, t) + Q_{i+1}^v(0, \infty, t) = 0 \quad (1 \leq i \leq n_l) \quad (10)$$

9.3. Analytical solution

First, the exact solution in the Laplace domain is given for the problem stated in the previous section. Second, the corresponding steady-state solution is presented, which is theoretically valid for an infinite time. Finally, the asymptotic pseudo-steady state solution is derived for times that are both finite and large. The latter is equal to the steady-state solution in which the comprehensive potential given by the Thiem (1870; 1906) formula is replaced by the Theis (1935) equation.

9.3.1. Exact solution in Laplace space

Hemker (1985) solved the problem stated in the previous section by applying the Hankel and Laplace transform, and inverted the obtained solution in Laplace space analytically. In this study, however, it is more convenient to keep the solution in Laplace space because of its simplicity and its similarity to the steady-state solution.

Laplace transform \mathcal{L} of discharge potential Φ is denoted by $\bar{\Phi}$:

$$\mathcal{L}\{\Phi_i(r, t)\}(p) = \bar{\Phi}_i(r, p) \quad (1 \leq i \leq n_l) \quad (11)$$

with p the frequency variable [T^{-1}].

Applying the Laplace transform (11) to the set of partial differential equations (1) subject to boundary conditions (5) and (6) respectively gives:

$$\frac{\partial^2 \bar{\Phi}_i}{\partial r^2} + \frac{1}{r} \frac{\partial \bar{\Phi}_i}{\partial r} = \frac{S_i}{T_i} p \bar{\Phi}_i + \frac{\bar{\Phi}_i}{T_i c_i} - \frac{\bar{\Phi}_{i-1}}{T_{i-1} c_i} + \frac{\bar{\Phi}_i}{T_i c_{i+1}} - \frac{\bar{\Phi}_{i+1}}{T_{i+1} c_{i+1}} \quad (1 \leq i \leq n_l) \quad (12)$$

$$\lim_{r \rightarrow 0} 2\pi r \frac{\partial \bar{\Phi}_i}{\partial r} = \frac{-Q_i}{p} \quad (1 \leq i \leq n_l) \quad (13)$$

$$\lim_{r \rightarrow \infty} \bar{\Phi}_i(r, p) = 0 \quad (1 \leq i \leq n_l) \quad (14)$$

The Laplace transform of radial discharge (7), vertical discharge (8), and storage change (9) is, respectively:

$$\bar{Q}_i^r(r, p) = -2\pi r \frac{\partial \bar{\Phi}_i}{\partial r} \quad (1 \leq i \leq n_l) \quad (15)$$

$$\bar{Q}_i^v(r_1, r_2, p) = 2\pi \int_{r_1}^{r_2} \left(\frac{\bar{\Phi}_i}{T_i c_i} - \frac{\bar{\Phi}_{i-1}}{T_{i-1} c_i} \right) r dr \quad (1 \leq i \leq n_l) \quad (16)$$

$$\bar{Q}_i^s(r_1, r_2, p) = 2\pi \frac{S_i}{T_i} \int_{r_1}^{r_2} p \bar{\Phi}_i r dr \quad (1 \leq i \leq n_l) \quad (17)$$

To find the solution in Laplace space, it is convenient to rewrite the problem in matrix form. The set of equations (12) is rewritten as:

$$\nabla^2 \bar{\Phi} = \mathbf{A} \bar{\Phi} \quad (18)$$

where $\bar{\Phi}$ is an $n_l \times 1$ vector containing the discharge potentials $\bar{\Phi}_i$, and \mathbf{A} is the system matrix, a tridiagonal $n_l \times n_l$ matrix with diagonal terms:

$$A_{i,i} = \frac{1}{T_i c_i} + \frac{1}{T_i c_{i+1}} + \frac{S_i}{T_i} p \quad (1 \leq i \leq n_l) \quad (19)$$

and off-diagonal terms:

$$A_{i,i-1} = \frac{-1}{T_{i-1} c_i} \quad (2 \leq i \leq n_l) \quad (20)$$

$$A_{i,i+1} = \frac{-1}{T_{i+1} c_{i+1}} \quad (1 \leq i \leq n_l - 1) \quad (21)$$

Performing the eigendecomposition of system matrix \mathbf{A} , matrix equation (18) can be uncoupled to a set of modified Bessel differential equations for which the general solution is well-known:

$$\nabla^2 \mathbf{V}^{-1} \bar{\Phi} = \Lambda \mathbf{V}^{-1} \bar{\Phi} \quad (22)$$

with Λ an $n_l \times n_l$ diagonal matrix with the eigenvalues λ_i on the diagonal entries, and \mathbf{V} an $n_l \times n_l$ matrix with the corresponding eigenvectors.

The particular solution to (12) subject to boundary conditions (13) and (14) is:

$$\bar{\Phi}_i(r, p) = \frac{1}{2\pi p} \sum_{j=1}^{n_l} \sum_{k=1}^{n_l} V_{i,k} K_0(r\sqrt{\lambda_k}) V'_{k,j} Q_j \quad (1 \leq i \leq n_l) \quad (23)$$

with $V_{i,k}$ the i -th element of the k -th eigenvector, $V'_{k,j}$ the entry in the k -th row and j -th column of \mathbf{V}^{-1} , the inverse of matrix \mathbf{V} , and K_0 the zero order modified Bessel function of the second kind.

Using definitions (2) and (3) and applying initial condition (4) to (23), the Laplace transform of drawdown is found:

$$\bar{s}_i(r, p) = \frac{1}{2\pi T_i p} \sum_{j=1}^{n_l} \sum_{k=1}^{n_l} V_{i,k} K_0(r\sqrt{\lambda_k}) V'_{k,j} Q_j \quad (1 \leq i \leq n_l) \quad (24)$$

Solution (24) is usually inverted back into the time domain numerically, and in this work, the Stehfest (1970) algorithm is used. Alternatively, the method by de Hoog et al. (1982) may be applied.

Introducing (23) into (15), (16), and (17) gives the Laplace transform of radial discharge, vertical discharge, and storage change, respectively:

$$\bar{Q}_i^r(r, p) = \frac{1}{p} \sum_{j=1}^{n_l} \sum_{k=1}^{n_l} V_{i,k} r \sqrt{\lambda_k} K_1(r \sqrt{\lambda_k}) V'_{k,j} Q_j \quad (1 \leq i \leq n_l) \quad (25)$$

$$\bar{Q}_i^v(r_1, r_2, p) = \frac{1}{c_i p} \sum_{j=1}^{n_l} \sum_{k=1}^{n_l} \left(\frac{V_{i,k}}{T_i} - \frac{V_{i-1,k}}{T_{i-1}} \right) \frac{V'_{k,j} Q_j}{\sqrt{\lambda_k}} [r_1 K_1(r_1 \sqrt{\lambda_k}) - r_2 K_1(r_2 \sqrt{\lambda_k})] \quad (2 \leq i \leq n_l) \quad (26)$$

$$\bar{Q}_i^s(r_1, r_2, p) = \frac{S_i}{T_i} \sum_{j=1}^{n_l} \sum_{k=1}^{n_l} \frac{V_{i,k} V'_{k,j} Q_j}{\sqrt{\lambda_k}} [r_1 K_1(r_1 \sqrt{\lambda_k}) - r_2 K_1(r_2 \sqrt{\lambda_k})] \quad (1 \leq i \leq n_l) \quad (27)$$

where use is made of $\int x K_0(x) dx = -x K_1(x)$, with K_1 the first order modified Bessel function of the second kind.

As $x K_1(x) \rightarrow 1$ if $x \rightarrow 0$, and $x K_1(x) \rightarrow 0$ if $x \rightarrow \infty$, it is found that:

$$Q_i^r(0, t) = Q_i \quad (1 \leq i \leq n_l) \quad (28)$$

$$Q_i^r(\infty, t) = 0 \quad (1 \leq i \leq n_l) \quad (29)$$

$$\bar{Q}_i^v(0, \infty, p) = \frac{1}{c_i p} \sum_{j=1}^{n_l} \sum_{k=1}^{n_l} \left(\frac{V_{i,k}}{T_i} - \frac{V_{i-1,k}}{T_{i-1}} \right) \frac{V'_{k,j} Q_j}{\lambda_k} \quad (2 \leq i \leq n_l) \quad (30)$$

$$\bar{Q}_i^s(0, \infty, p) = \frac{S_i}{T_i} \sum_{j=1}^{n_l} \sum_{k=1}^{n_l} \frac{V_{i,k} V'_{k,j} Q_j}{\lambda_k} \quad (1 \leq i \leq n_l) \quad (31)$$

Expression (28) is in agreement with boundary condition (5).

Applying (28) and (29) simplifies equation (10) to:

$$Q_i - Q_i^s(0, \infty, t) - Q_i^v(0, \infty, t) + Q_{i+1}^v(0, \infty, t) = 0 \quad (1 \leq i \leq n_l) \quad (32)$$

The solution given in this section is valid for finite values of time t . The next section presents the solution for $t \rightarrow \infty$.

9.3.2. Steady state solution

Since the multilayer aquifer system is confined and its outer boundary with constant head is at an infinite radial distance, steady-state flow is reached only after an infinite time of pumping:

$$\lim_{t \rightarrow \infty} \Phi_i(r, t) = \hat{\Phi}_i(r) \quad (1 \leq i \leq n_l) \quad (33)$$

with $\hat{\Phi}_i(r)$ the steady discharge potential in layer i at distance r . The steady-state flow, which is valid for $t \rightarrow \infty$, is governed by the same set of differential equations (1), except for the storage change term which is zero by definition:

$$\frac{d^2 \hat{\Phi}_i}{dr^2} + \frac{1}{r} \frac{d \hat{\Phi}_i}{dr} = \frac{\hat{\Phi}_i}{T_i c_i} - \frac{\hat{\Phi}_{i-1}}{T_{i-1} c_i} + \frac{\hat{\Phi}_i}{T_i c_{i+1}} - \frac{\hat{\Phi}_{i+1}}{T_{i+1} c_{i+1}} \quad (1 \leq i \leq n_l) \quad (34)$$

The boundary conditions are also the same as (5) and (6):

$$\lim_{r \rightarrow 0} 2\pi r \frac{d \hat{\Phi}_i}{dr} = -Q_i \quad (1 \leq i \leq n_l) \quad (35)$$

$$\lim_{r \rightarrow \infty} \hat{\Phi}_i(r) = 0 \quad (1 \leq i \leq n_l) \quad (36)$$

Radial and vertical discharge are calculated in the same way as (7) and (8):

$$\hat{Q}_i^r(r) = -2\pi r \frac{d\hat{\Phi}_i}{dr} \quad (1 \leq i \leq n_l) \quad (37)$$

$$\hat{Q}_i^v(r_1, r_2) = 2\pi \int_{r_1}^{r_2} \left(\frac{\hat{\Phi}_i}{T_i c_i} - \frac{\hat{\Phi}_{i-1}}{T_{i-1} c_i} \right) r dr \quad (2 \leq i \leq n_l) \quad (38)$$

The total water budget for each layer (10) can also be adopted, except that $\hat{Q}_i^s = 0$, by definition:

$$-\hat{Q}_i^r(\infty) + \hat{Q}_i^r(0) - \hat{Q}_i^v(0, \infty) + \hat{Q}_{i+1}^v(0, \infty) = 0 \quad (1 \leq i \leq n_l) \quad (39)$$

Similar to (18), the steady-state problem is expressed in matrix form, where in this case, system matrix $\hat{\mathbf{A}}$ is a tridiagonal $n_l \times n_l$ matrix with diagonal terms:

$$\hat{A}_{i,i} = \frac{1}{T_i c_i} + \frac{1}{T_{i+1} c_{i+1}} \quad (1 \leq i \leq n_l) \quad (40)$$

and off-diagonal terms:

$$\hat{A}_{i,i-1} = \frac{-1}{T_{i-1} c_i} \quad (2 \leq i \leq n_l) \quad (41)$$

$$\hat{A}_{i,i+1} = \frac{-1}{T_{i+1} c_{i+1}} \quad (1 \leq i \leq n_l - 1) \quad (42)$$

The solution to (34) is again found by performing the eigendecomposition of system matrix $\hat{\mathbf{A}}$ to obtain an $n_l \times n_l$ diagonal matrix $\hat{\Lambda}$ with the eigenvalues $\hat{\lambda}_i$ and an $n_l \times n_l$ matrix $\hat{\mathbf{V}}$ with the corresponding eigenvectors. However, in case of steady state flow, system matrix $\hat{\mathbf{A}}$ is singular because the sum of the elements of each column equals zero (Bakker, 2001). This summation corresponds to the following differential equation:

$$\frac{d^2\hat{\Phi}_c}{dr^2} + \frac{1}{r} \frac{d\hat{\Phi}_c}{dr} = 0 \quad (43)$$

where the comprehensive potential $\hat{\Phi}_c$ [L^3/T] in (43) is defined as (Bakker, 2001; Bakker & Strack, 2003):

$$\hat{\Phi}_c = \sum_{i=1}^{n_l} \hat{\Phi}_i \quad (44)$$

The corresponding boundary conditions are:

$$\lim_{r \rightarrow 0} 2\pi r \frac{d\hat{\Phi}_c}{dr} = -Q \quad (45)$$

$$\lim_{r \rightarrow \infty} \hat{\Phi}_c(r) = 0 \quad (46)$$

with Q [L^3/T] the total pumping rate equal to $\sum_{i=1}^{n_l} Q_i$.

The solution to (43) subject to (45) and (46) is known as the Thiem (1870; 1906) equation:

$$\hat{\Phi}_c(r) = \lim_{R \rightarrow \infty} \frac{Q}{2\pi} \ln(R/r) \quad (47)$$

with R [L] the radial distance of the outer boundary which is infinitely large according to (46).

Because the right-hand side of equation (43) is zero, the corresponding eigenvalue of system matrix $\hat{\mathbf{A}}$ is also zero. All elements of the corresponding row in $\hat{\mathbf{V}}^{-1}$, the inverse of matrix $\hat{\mathbf{V}}$, are equal to one, which follows from (44). The sum of all elements of the corresponding eigenvector $\hat{\mathbf{v}}_0$ must be one as $\hat{\mathbf{V}}^{-1}\hat{\mathbf{V}}$ equals the identity matrix. Combining this requirement with the definition of eigenvector, that is $\hat{\mathbf{A}}\hat{\mathbf{v}}_0 = 0$, it is found that eigenvector $\hat{\mathbf{v}}_0$ is equal to:

$$\hat{\mathbf{v}}_0 = \mathbf{T}/T \quad (48)$$

where \mathbf{T} is an $n_l \times 1$ vector with T_i as elements, and total transmissivity T [L^2/T] is equal to $\sum_{i=1}^{n_l} T_i$. A slightly different proof is given by Bakker (2001).

The remaining equations corresponding to the $n_l - 1$ nonzero eigenvalues are modified Bessel differential equations, and the particular solution to (34) subject to boundary conditions (35) and (36) is:

$$\hat{\Phi}_i(r) = \lim_{R \rightarrow \infty} \frac{QT_i}{2\pi T} \ln(R/r) + \frac{1}{2\pi} \sum_{j=1}^{n_l} \sum_{k=1}^{n_l-1} \hat{V}_{i,k} K_0 \left(r \sqrt{\hat{\lambda}_k} \right) \hat{V}'_{k,j} Q_j \quad (1 \leq i \leq n_l) \quad (49)$$

with $\hat{V}_{i,k}$ the i -th element of the k -th eigenvector, and $\hat{V}'_{k,j}$ the entry in the k -th row and j -th column of $\hat{\mathbf{V}}^{-1}$. The first term in (49) corresponds to the zero eigenvalue and is equal to the comprehensive potential according to (47) multiplied by the i -th element in $\hat{\mathbf{v}}_0$ given by (48). The other terms in (49) correspond to the nonzero eigenvalues. Because radius R of the outer boundary is infinitely large, the potentials in (49) are also infinitely large. Therefore, solution (49) only has a practical meaning if the outer boundary is at a finite distance R , which still is large enough to neglect the terms containing $K_0(R\hat{\lambda}_k^{1/2})$ so that the outer boundary condition (36) is still satisfied, albeit approximately.

Steady-state drawdown \hat{s} is found using definitions (2) and (3) and applying initial condition (4) to (49):

$$\hat{s}_i(r) = \lim_{R \rightarrow \infty} \frac{Q}{2\pi T} \ln(R/r) + \frac{1}{2\pi T_i} \sum_{j=1}^{n_l} \sum_{k=1}^{n_l-1} \hat{V}_{i,k} K_0 \left(r \sqrt{\hat{\lambda}_k} \right) \hat{V}'_{k,j} Q_j \quad (1 \leq i \leq n_l) \quad (50)$$

Radial and vertical discharge are found by introducing solution (49) into definitions (37) and (38), respectively:

$$\hat{Q}_i^r(r) = \frac{T_i}{T} Q + \sum_{j=1}^{n_l} \sum_{k=1}^{n_l-1} \hat{V}_{i,k} \hat{V}'_{k,j} Q_j r \sqrt{\hat{\lambda}_k} K_1 \left(r \sqrt{\hat{\lambda}_k} \right) \quad (1 \leq i \leq n_l) \quad (51)$$

$$\hat{Q}_i^v(r_1, r_2) = \sum_{j=1}^{n_l} \sum_{k=1}^{n_l-1} \left(\frac{\hat{V}_{i,k}}{T_i} - \frac{\hat{V}_{i-1,k}}{T_{i-1}} \right) \frac{\hat{V}'_{k,j} Q_j}{c_i \sqrt{\hat{\lambda}_k}} \left[r_1 K_1 \left(r_1 \sqrt{\hat{\lambda}_k} \right) - r_2 K_1 \left(r_2 \sqrt{\hat{\lambda}_k} \right) \right] \quad (2 \leq i \leq n_l) \quad (52)$$

Radial discharge at the boundaries and total vertical discharge are found taking into account that $xK_1(x) \rightarrow 1$ if $x \rightarrow 0$ and $xK_1(x) \rightarrow 0$ if $x \rightarrow \infty$:

$$\hat{Q}_i^r(0) = Q_i \quad (1 \leq i \leq n_l) \quad (53)$$

$$\hat{Q}_i^r(\infty) = \frac{T_i}{T} Q \quad (1 \leq i \leq n_l) \quad (54)$$

$$\hat{Q}_i^v(0, \infty) = \sum_{j=1}^{n_l} \sum_{k=1}^{n_l-1} \left(\frac{\hat{V}_{i,k}}{T_i} - \frac{\hat{V}_{i-1,k}}{T_{i-1}} \right) \frac{\hat{V}'_{k,j} Q_j}{c_i \hat{\lambda}_k} \quad (2 \leq i \leq n_l) \quad (55)$$

The right-hand side of (54) shows that radial discharge in each layer at the outer boundary is proportional to the layer's transmissivity. This proportionality is consistent with the well-known solution of steady parallel flow between two constant head boundaries in a layered system, and it is, for instance, used by Hemker (1999a) to redistribute the radial discharge along a well-screen extending over more than one layer.

Introducing (53) and (54) into total water budget equation (39) gives:

$$-\frac{T_i}{T} Q + Q_i = \hat{Q}_i^v(0, \infty) - \hat{Q}_{i+1}^v(0, \infty) \quad (1 \leq i \leq n_l) \quad (56)$$

System of equations (56) can be solved recursively starting with $\hat{Q}_1^v(0, \infty) = 0$ to find a solution for $\hat{Q}_i^v(0, \infty)$:

$$\hat{Q}_i^v(0, \infty) = \sum_{j=1}^{i-1} \frac{T_j}{T} Q - Q_j \quad (2 \leq i \leq n_l) \quad (57)$$

In this context, it is common to introduce the leakage factors L_i [L] (Hemker, 1984):

$$L_i = 1/\sqrt{\hat{\lambda}_i} \quad (\hat{\lambda}_i \neq 0; 1 \leq i \leq n_l - 1) \quad (58)$$

with $\hat{\lambda}_i$ a nonzero eigenvalue.

Since $K_0(x)$ and $xK_1(x)$ are negligibly small when $x \geq 8$, there is virtually no vertical flow at distances larger than $R_m = 8L_m$, with L_m the largest leakage factor. Bakker and Strack (2003) even state $6L_m$ is sufficiently large for most practical purposes. Consequently, the following approximations are justified:

$$\hat{\Phi}_i(r \geq R_m) \sim \frac{QT_i}{2\pi T} \ln(R/r) \quad (1 \leq i \leq n_l) \quad (59)$$

$$\hat{s}_i(r \geq R_m) \sim \frac{Q}{2\pi T} \ln(R/r) \quad (1 \leq i \leq n_l) \quad (60)$$

$$\hat{Q}_i^r(r \geq R_m) \sim \frac{T_i}{T} Q \quad (1 \leq i \leq n_l) \quad (61)$$

$$\hat{Q}_i^v(0, R_m) \sim \sum_{j=1}^{i-1} \frac{T_j}{T} Q - Q_j \quad (2 \leq i \leq n_l) \quad (62)$$

At the well-face ($r = 0$), the radial discharge in layer i according to (53) equals the pumping rate, which is in agreement with boundary condition (35). At small distances $r < R_m$, radial flow is redistributed according to the transmissive properties of the system. The amount of water exchanged between two layers according to (57) reflects this redistribution of water. At large distances $r \geq R_m$, vertical flow between the layers is negligibly small, which explains (62), and drawdown in each layer is equal to drawdown in the equivalent single-layer system with total transmissivity T and total pumping rate Q governed by the Thiem (1870; 1906) equation (60). Redistribution of water is virtually complete at these large distances, which means radial discharge in each layer i is equal to fraction T_i/T of the total pumping rate Q , which explains (61).

This section discussed the steady-state solution, which is valid for $t \rightarrow \infty$. In the next section, an approximate solution is derived for large values of time t .

9.3.3. Asymptotic solution for large values of time

In previous section, it is explained that steady state flow is reached after an infinite time of pumping, which is expressed by statement (33). Using solution (23) in Laplace space, the following statement is equivalent to (33):

$$\lim_{p \rightarrow 0} \bar{\Phi}_i(r, p) = \hat{\Phi}_i(r) \quad (1 \leq i \leq n_l) \quad (63)$$

The time dependent terms in solution (23) are the eigenvalues λ_i and corresponding eigenvectors \mathbf{V} , and therefore, the following statements are an implication of (63):

$$\lim_{p \rightarrow 0} \lambda_i = \hat{\lambda}_i \quad (1 \leq i \leq n_l) \quad (64)$$

$$\lim_{p \rightarrow 0} \mathbf{V} = \hat{\mathbf{V}} \quad (65)$$

where $\hat{\lambda}_i$ and $\hat{\mathbf{V}}$ are the eigenvalues and corresponding eigenvectors, respectively, in steady-state solution (49). In fact, the nonzero eigenvalues $\hat{\lambda}_i$ and eigenvectors $\hat{\mathbf{V}}$ are asymptotic for the corresponding time-dependent eigenvalues and eigenvectors. Hence, the following expansions are justified for finitely large values of time t :

$$\lambda_i \sim \hat{\lambda}_i \quad (\hat{\lambda}_i \neq 0; p \rightarrow 0) \quad (66)$$

$$\mathbf{V} \sim \hat{\mathbf{V}} \quad (p \rightarrow 0) \quad (67)$$

The smallest time dependent eigenvalue λ_s corresponds to the zero eigenvalue in the steady state case, but cannot be approximated by zero as the corresponding infinitely large comprehensive potential is reached only after an infinite time of pumping. Thus λ_s is zero only after an infinite time, and at finitely large values of time, it is still time-dependent.

To find the expansion for λ_s if $p \rightarrow 0$, the total water budget for the multilayer system is checked:

$$\frac{Q}{p} - \sum_{i=1}^{n_l} \bar{Q}_i^s(0, \infty, p) = 0 \quad (68)$$

Applying expansions (66) and (67) to (31):

$$\bar{Q}_i^s(0, \infty, p) \sim \frac{S_i}{T_i} \left(\frac{T_i Q}{T \lambda_s} + \sum_{j=1}^{n_l} \sum_{k=1}^{n_l-1} \frac{\hat{V}_{i,k} \hat{V}'_{k,j} Q_j}{\hat{\lambda}_k} \right) \quad (p \rightarrow 0; 1 \leq i \leq n_l) \quad (69)$$

The first term in the expression between parentheses of equation (69) uses solution (48) for eigenvector $\hat{\mathbf{V}}_0$ corresponding to the zero eigenvalue; the last $n_l - 1$ terms may be omitted since they are independent of p . Introducing (69) into (68) and rearranging terms gives:

$$\lambda_s \sim \frac{S}{T} p \quad (p \rightarrow 0) \quad (70)$$

with total storativity S [-] equal to $\sum_{i=1}^{n_l} S_i$.

Applying expansions (66), (67), and (70) to solution (23) in Laplace space:

$$\bar{\Phi}_i(r, p) \sim \frac{Q T_i}{2\pi T p} K_0\left(r \sqrt{\frac{S}{T}} p\right) + \frac{1}{2\pi p} \sum_{j=1}^{n_l} \sum_{k=1}^{n_l-1} \hat{V}_{i,k} K_0\left(r \sqrt{\hat{\lambda}_k}\right) \hat{V}'_{k,j} Q_j \quad (p \rightarrow 0; 1 \leq i \leq n_l) \quad (71)$$

As the eigenvalues $\hat{\lambda}_k$ and corresponding eigenvectors are independent of p , the last $n_l - 1$ terms in (71) are inverted to the same terms of steady state solution (49). The first term in (71), replacing the comprehensive potential in steady-state solution (49), is the well-known Laplace inversion of the Theis' well function W (Hantush, 1964):

$$\mathcal{L}^{-1}\left\{\frac{1}{p} K_0\left(r \sqrt{\frac{S}{T}} p\right)\right\} = \frac{1}{2} W\left(\frac{r^2 S}{4tT}\right) \quad (72)$$

This gives the approximate solution for large values of time t :

$$\Phi_i(r, t) \sim \frac{Q T_i}{4\pi T} W\left(\frac{r^2 S}{4tT}\right) + \frac{1}{2\pi} \sum_{j=1}^{n_l} \sum_{k=1}^{n_l-1} \hat{V}_{i,k} K_0\left(r \sqrt{\hat{\lambda}_k}\right) \hat{V}'_{k,j} Q_j \quad (t \rightarrow \infty; 1 \leq i \leq n_l) \quad (73)$$

The Theis' well function or exponential integral W is defined as (Theis, 1935):

$$W(u) = \int_u^\infty \frac{e^{-x}}{x} dx = -\gamma - \ln(u) - \sum_{n=1}^{\infty} \frac{(-u)^n}{n \cdot n!} \quad (74)$$

with γ the Euler constant equal to 0.57721....

Using definitions (2) and (3) and applying initial condition (4), drawdown at large values of time t may be approximated as:

$$s_i(r, t) \sim \frac{Q}{4\pi T} W\left(\frac{r^2 S}{4tT}\right) + \frac{1}{2\pi T_i} \sum_{j=1}^{n_l} \sum_{k=1}^{n_l-1} \hat{V}_{i,k} K_0\left(r \sqrt{\hat{\lambda}_k}\right) \hat{V}'_{k,j} Q_j \quad (t \rightarrow \infty; 1 \leq i \leq n_l) \quad (75)$$

Solution (75) is the same as steady state solution (50) except for the first term, which is the Thiem (1870; 1906) equation for the equivalent single-layer system in the latter, whereas the first uses the Theis (1935) equation for the equivalent single-layer system with total transmissivity T , total storativity S , and total pumping rate Q .

Introducing solution (75) into definitions (7) and (8), respectively, the approximations for radial and vertical discharge are found:

$$Q_i^r(r, t) \sim \sum_{j=1}^{n_l} \sum_{k=1}^{n_l-1} \hat{V}_{i,k} \hat{V}'_{k,j} Q_j r \sqrt{\hat{\lambda}_k} K_1\left(r \sqrt{\hat{\lambda}_k}\right) + \frac{Q T_i}{T} e^{\frac{-r^2 S}{4tT}} \quad (t \rightarrow \infty; 1 \leq i \leq n_l) \quad (76)$$

$$Q_i^v(r_1, r_2, t) \sim \sum_{j=1}^{n_l} \sum_{k=1}^{n_l-1} \left(\frac{\hat{V}_{i,k}}{T_i} - \frac{\hat{V}_{i-1,k}}{T_{i-1}} \right) \frac{\hat{V}'_{k,j} Q_j}{c_i \sqrt{\hat{\lambda}_k}} \left[r_1 K_1\left(r_1 \sqrt{\hat{\lambda}_k}\right) - r_2 K_1\left(r_2 \sqrt{\hat{\lambda}_k}\right) \right] \quad (t \rightarrow \infty; 2 \leq i \leq n_l) \quad (77)$$

where the approximated vertical discharge (77) is equal to steady state solution (52) as the time-dependent term containing the comprehensive potential is canceled out. On the other hand, the storage change only contains the time-dependent term:

$$Q_i^s(r_1, r_2, t) \sim \frac{S_i}{S} Q \left(e^{-\frac{r_1^2 S}{4tT}} - e^{-\frac{r_2^2 S}{4tT}} \right) \quad (t \rightarrow \infty; 1 \leq i \leq n_l) \quad (78)$$

The total storage change in each layer i is:

$$Q_i^s(0, \infty, t) \sim \frac{S_i}{S} Q \quad (t \rightarrow \infty; 1 \leq i \leq n_l) \quad (79)$$

Expression (79) shows that each layer contributes to the extraction proportionally to its relative storativity S_i/S .

As $K_0(x)$ and $xK_1(x)$ are negligibly small when $x \geq 8$, the following approximations are justified:

$$\Phi_i(r \geq R_m, t) \sim \frac{QT_i}{4\pi T} W\left(\frac{r^2 S}{4tT}\right) \quad (t \rightarrow \infty; 1 \leq i \leq n_l) \quad (80)$$

$$s_i(r \geq R_m, t) \sim \frac{Q}{4\pi T} W\left(\frac{r^2 S}{4tT}\right) \quad (t \rightarrow \infty; 1 \leq i \leq n_l) \quad (81)$$

$$Q_i^r(r \geq R_m, t) \sim \frac{T_i}{T} Q e^{-\frac{r^2 S}{4tT}} \quad (t \rightarrow \infty; 1 \leq i \leq n_l) \quad (82)$$

$$Q_i^v(0, R_m, t) \sim \sum_{j=1}^{i-1} \frac{T_j}{T} Q - Q_j \quad (t \rightarrow \infty; 2 \leq i \leq n_l) \quad (83)$$

with $R_m = 8L_m$, where L_m is the largest of the leakage factors defined by (58).

Total water budget equation (32) is still valid and substituting (79) for $Q_i^s(0, \infty, t)$ gives:

$$Q_i - \frac{S_i}{S} Q - Q_i^v(0, \infty, t) + Q_{i+1}^v(0, \infty, t) \sim 0 \quad (t \rightarrow \infty; 1 \leq i \leq n_l) \quad (84)$$

Solving (84) recursively, an expression for $Q_i^v(0, \infty, t)$ is found:

$$Q_i^v(0, \infty, t) \sim \sum_{j=1}^{i-1} \frac{S_j}{S} Q - Q_j \quad (t \rightarrow \infty; 2 \leq i \leq n_l) \quad (85)$$

Expression (85) is in agreement with (79) and shows that the extracted water is redistributed between the layers to have each layer contribute proportionally to its relative storativity.

Recall that there is also a redistribution of water given by (83), which is driven by the transmissive properties of the system. This redistribution takes place in the proximal part of the well ($r < R_m$), where flow is in pseudo-steady state. The latter is confirmed by (78) as Q_i^s is negligibly small indeed at small distances. In the daily practice of analyzing pumping test data, the concept of pseudo-steady state is well known (Hemker, 1984). According to Kruseman and de Ridder (1990), it is said that steady flow is attained if the change in drawdown has become negligibly small. In reality, the water level may drop further as pumping continues and the system is not recharged by an outside source. If, however, the hydraulic gradient induced by the pumping does not change anymore, the flow towards the well has attained a pseudo-steady state (Kruseman & de Ridder, 1990).

An additional vertical flow occurs in the distal part of the well ($r \geq R_m$) in order to obtain the total redistribution as a function of the storative properties of the layers. This additional vertical flow is found by subtracting (83) from (85):

$$Q_i^v(R_m, \infty, t) \sim \sum_{j=1}^{i-1} \left(\frac{S_j}{S} - \frac{T_j}{T} \right) Q \quad (t \rightarrow \infty; 2 \leq i \leq n_l) \quad (86)$$

However, as the horizontal surface covered by the distal part is very large at large values of time, the vertical gradient between the layers is negligibly small in this part, which explains approximations (80) and (81). Only when the diffusivities S_i/T_i of all layers are the same, there actually is no vertical flow in the distal part. Note that Hemker (1985) treated the equal diffusivity case as a special case, since the solution to this particular problem is easier than for the general case where diffusivities are different. The direction of vertical flow in the distal part ($r \geq R_m$) can be counterintuitive as it is possible water flows from a pumped to an unpumped layer.

The next section presents an example of a three-layer system in which the direction of the vertical flow in the proximal part ($r < R_m$) is opposite to the direction of the vertical flow in the distal part ($r \geq R_m$). After discussing this simple example clarifying the presented theory, the asymptotic solution (75) is verified by analyzing a thousand random multilayer models. A final example demonstrates the spatial averaging in drawdown observations from multilevel pumping tests.

9.4. Example

Consider a confined aquifer system consisting of three layers ($n_l = 3$) in which groundwater flow induced by a vertical well is described by system of equations (1) subject to initial condition (4) and boundary conditions (5) and (6), and with the following known parameters:

- Layer 1: $Q_1 = -100 \text{ m}^3/\text{d}$, $T_1 = 100 \text{ m}^2/\text{d}$, $S_1 = 0.003$;
- Between layer 1 and 2: $c_2 = 1000 \text{ d}$;
- Layer 2: $Q_2 = -100 \text{ m}^3/\text{d}$, $T_2 = 200 \text{ m}^2/\text{d}$, $S_2 = 0.002$;
- Between layer 2 and 3: $c_3 = 2000 \text{ d}$;
- Layer 3: $Q_3 = -100 \text{ m}^3/\text{d}$, $T_3 = 300 \text{ m}^2/\text{d}$, $S_3 = 0.001$.

Top and bottom resistance, respectively c_1 and c_4 , are infinitely large, as the system is confined.

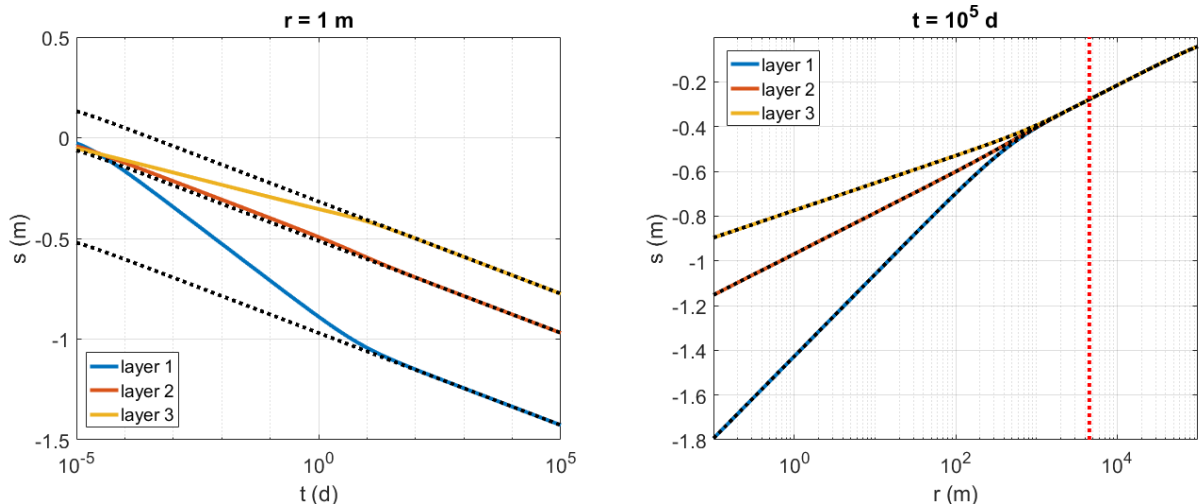


Figure 1. Exact (solid lines) and approximate (dotted lines) drawdown $s(r, t)$ as a function of time t at 1 m from the well (left plot), and as a function of distance r at 10^5 days after the start of the extraction (right plot), for the three-layer system described in the text. The red dashed line in the right graph indicates distance $R_m = 8L_m$ (with L_m the maximum leakage factor), which is equal to 4533 m in this example.

First, drawdown $s(r, t)$ according to the numerically inverted exact solution (24) is compared to the approximated solution (75). The left graph in Figure 1 shows the exact and the approximate

drawdown as a function of time t at 1 m from the well. It is seen that both solutions are virtually the same indeed at times larger than 100 d.

The right graph in Figure 1 shows both exact and approximate drawdown as a function of distance r at 10^5 d after the extraction started. As expected, both solutions are virtually the same at all distances. At distances larger than $R_m = 8L_m = 4533$ m, drawdown is the same in each layer and may be approximated by the Theis (1935) equation for a single layer with total transmissivity T , total storativity S , and total pumping rate Q .

The exact radial discharge $Q^r(r, t)$ is calculated by inverting (25) numerically using the Stehfest (1970) algorithm. At large values of time, the radial discharge may be approximated using (76). The left plot in Figure 2 shows that both solutions coincide because time $t = 10^5$ d is larger than 100 d. At small distances, radial discharge in each layer i equals the pumping rate $Q_i = -100$ m³/d. At distances larger than $8L_m = 4533$ m, radial discharge may be approximated using expression (82). Because $e^{-x} \rightarrow 1$ if $x \rightarrow 0$ and $e^{-x} \rightarrow 0$ if $x \rightarrow \infty$, radial discharge approximates QT_i/T at distance $R_m = 8L_m$ and is negligibly small at very large distances. In this example, radial discharge in layers 1, 2, and 3 is redistributed respectively from -50 m³/d, -100 m³/d, and -150 m³/d to -100 m³/d. Hence, 50 m³/d of water is flowing from layer 3 via layer 2 to layer 1 in the proximal part to the well ($r < 8L_m$).

At distances smaller than 10^4 m, groundwater flow is in pseudo-steady state, as $Q^s(0, r, t)$ is negligibly small in all layers, as indicated by the right plot of Figure 2. Here, transient radial discharge can be approximated by the steady radial discharge given by (51). This zone of pseudo-steady state expands with time t . At distances larger than 5.10^5 m, radial discharge is zero, which means the extraction has no impact yet. At distances between 10^4 and 5.10^5 m, storage change is not negligibly small, which is seen in the right plot of Figure 2.

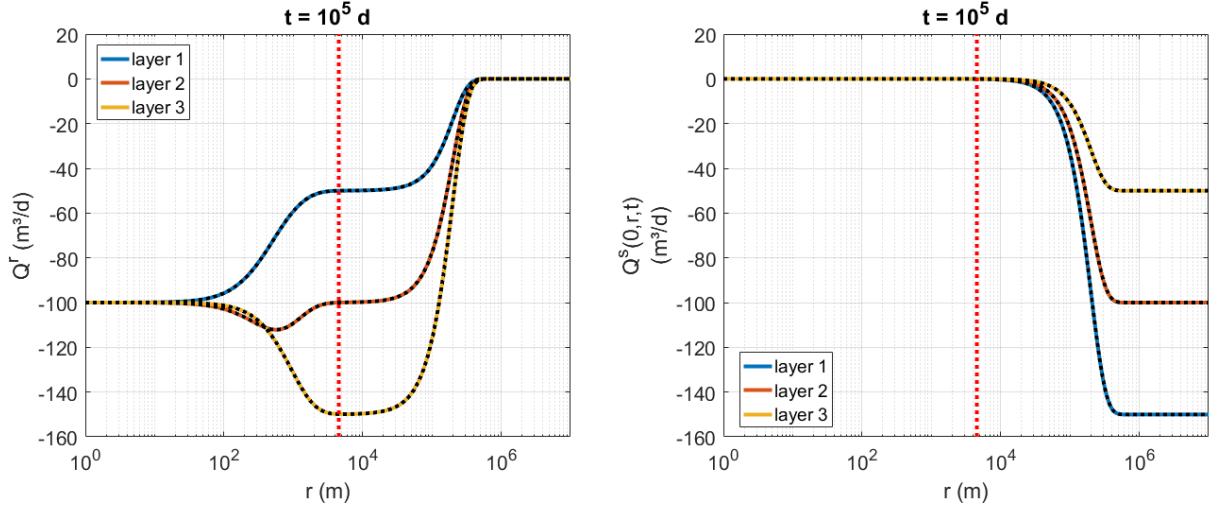


Figure 2. Exact (solid lines) and approximate (dotted black lines) radial discharge $Q^r(r, t)$ (left plot) and cumulative storage change $Q^s(0, r, t)$ (right plot) as a function of distance r at 10^5 d after the start of the extraction for the three-layer system described in the text. The red dotted line indicates distance $R_m = 8L_m$ (with L_m the maximum leakage factor) which is equal to 4533 m in this example.

This graph shows both the exact and the approximate cumulative storage change $Q^s(0, r, t)$ as a function of distance r . The first is obtained by inverting (27) numerically using the Stehfest (1970) algorithm, whereas the latter is calculated using (78). As time $t = 10^5$ d is larger than 100 d, both solutions are virtually the same. Because the system is confined without any sources or sinks, the total amount of water delivered by the storage change equals the total pumping rate of 300 m³/d, which is in agreement with the total water budget equation.

According to (79), each layer contributes proportionally to its relative storativity S_i/S , which is seen on the graph indeed, as layer 1 delivers $150 \text{ m}^3/\text{d}$, layer 2 delivers $100 \text{ m}^3/\text{d}$, and layer 3 delivers $50 \text{ m}^3/\text{d}$. Recall that radial flow is $50 \text{ m}^3/\text{d}$ in layer 1, $100 \text{ m}^3/\text{d}$ in layer 2, and $150 \text{ m}^3/\text{d}$ in layer 3, and that $50 \text{ m}^3/\text{d}$ of water is flowing from layer 3 to layer 1 via layer 2 in the proximal part around the well ($r < 8L_m$). Hence, $100 \text{ m}^3/\text{d}$ of water is flowing from layer 1 to layer 3 via layer 2 in the distal part around the well ($r > 8L_m$).

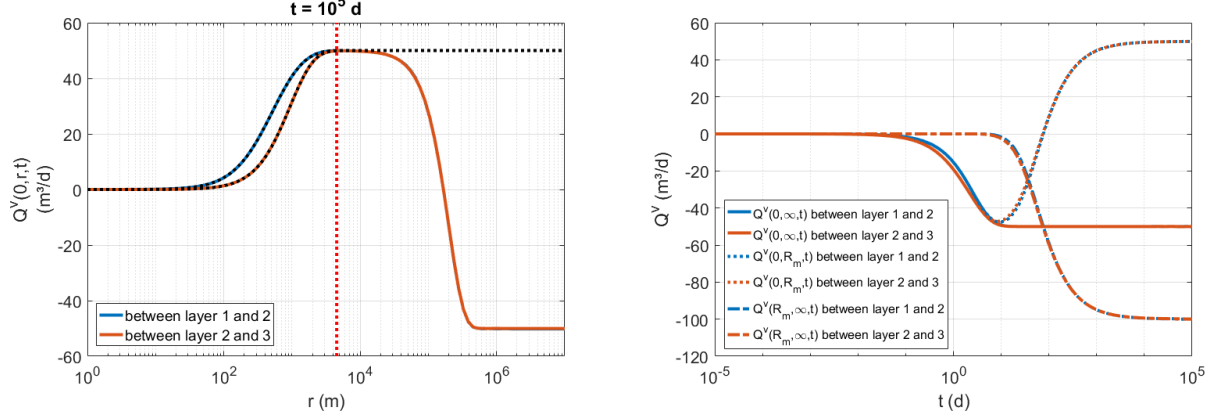


Figure 3. Left: Exact (solid lines) and approximate (dotted black lines) cumulative vertical discharge $Q^v(0,r,t)$ as a function of distance r at 10^5 d after the start of the extraction for the three-layer system described in the text. The red dotted line indicates distance $R_m = 8L_m$ (with L_m the maximum leakage factor) which is equal to 4533 m in this example. Right: Total vertical discharge Q^v between the layers as a function of time t over the full extent of the aquifer system (solid lines), in the proximal part, i.e. $r < R_m$ (dotted lines), and in the distal part, i.e. $r \geq R_m$ (dashed lines).

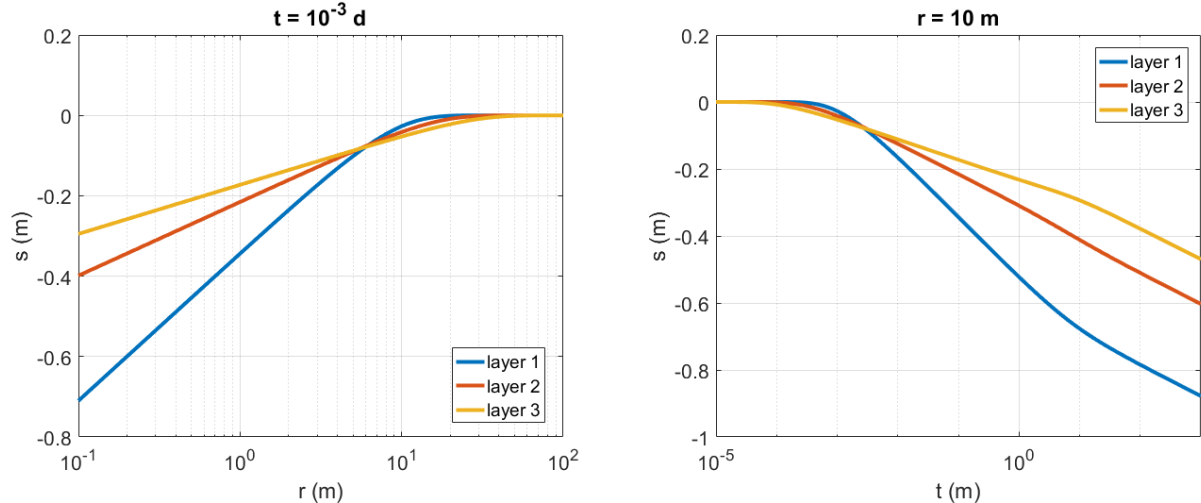


Figure 4. Left: Exact drawdown $s(r,t)$ as a function of distance r , at 10^{-3} d after the start of the extraction, for the three-layer system described in the text. In the proximal part around the well ($r < 6 \text{ m}$), water is flowing from layer 2 to 1 and from layer 3 to 2. In the distal part around the well ($r \geq 6 \text{ m}$), water is flowing from layer 1 to 2 and from layer 2 to 3. Right: Exact drawdown $s(r,t)$ as a function of time t , at a distance equal to 10 m. The inversion of flow at this distance is between 10^{-4} d and 3.10^{-3} d .

This is confirmed by the left plot of Figure 3, which shows the cumulative vertical discharge $Q^v(0,r,t)$ as a function of distance r at time $t = 10^5 \text{ d}$. The total amount of water flowing from layer 2 to layer 1 and from layer 3 to layer 2 in the proximal part ($r < 8L_m$) is $50 \text{ m}^3/\text{d}$ indeed, while $100 \text{ m}^3/\text{d}$ of water is flowing from layer 1 to layer 2 and from layer 2 to layer 3 in the distal part of the aquifer ($r > 8L_m$). Both the exact and the approximate solutions are plotted, which are obtained by numerically inverting (26) and (77), respectively. Because the approximate equation for the vertical discharge is the same as steady state equation (52), the exchange of water between the layers in the

distal part is neglected by the approximate solution. Consequently, the approximate cumulative vertical discharge $Q^v(0, r, t)$ remains $50 \text{ m}^3/\text{d}$ for large values of distance r , whereas it should be $-50 \text{ m}^3/\text{d}$, which is correctly calculated by the exact solution.

In this example, the redistribution of water driven by the transmissive properties of the layers in the proximal part is opposite to the redistribution of water driven by the storative properties of the layers. This explains the inversion of vertical flow occurring in the distal part, which is noticed even at small values of time t (Figure 4). This is because the process of redistribution of water already takes place immediately after pumping has started, in order to let the extracted water flow to the well as efficiently as possible by making use of all layers in the aquifer system.

The distal zone, in which the inversion of vertical flow occurs, moves away from the well and expands with time. After a certain period of pumping, the inversion is not visible anymore on the drawdown versus distance graphs because of the large aquifer volumes that are involved. At large values of time, the boundary between the proximal and distal part has become steady, and may be defined at a distance equal to $R_m = 8L_m$. The redistribution of water in the proximal part, driven by the transmissive properties of the layers, is completed then, and thus, the flow has attained a pseudo-steady state. On the other hand, the distal part continues to expand as the model does not include outside sources that could bring the aquifer system in a true state of steady flow.

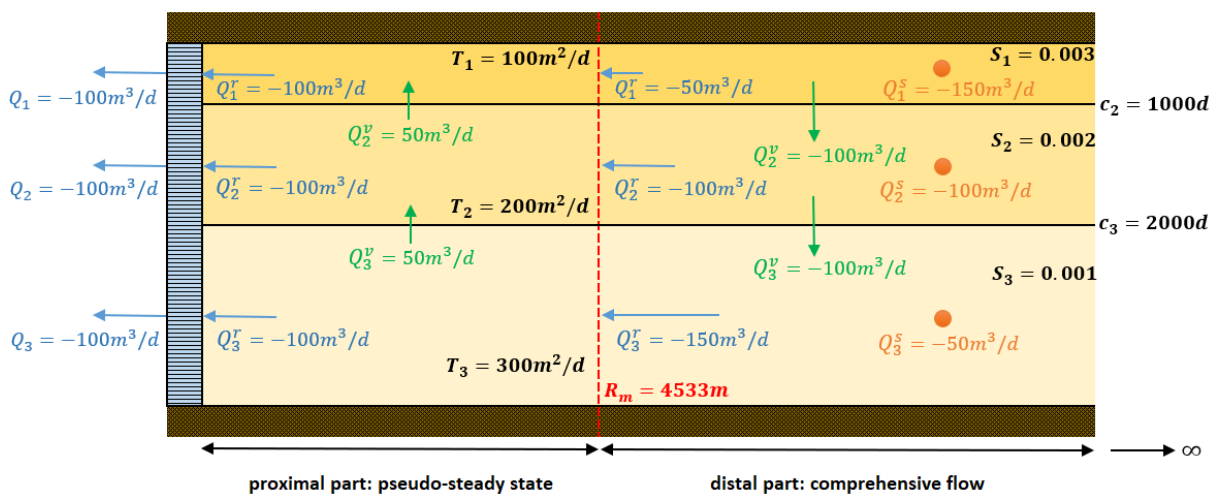


Figure 5. Schematic overview of flow at large values of time in and between layers of the three-layer system described in the text. Distance $R_m = 8L_m$ (with L_m the maximum leakage factor) equals 4533 m in this example. Q is the pumping rate (m^3/d), T is the transmissivity (m^2/d), S is the storativity (-), c is the vertical resistance (d), Q^r is the radial discharge (m^3/d), Q^v is the vertical discharge (m^3/d), Q^s is the storage change (m^3/d). See text for definitions.

This process of redistribution of water as a function of time is clearly illustrated by the right plot of Figure 3. It shows the total vertical discharge $Q^v(0, \infty, t)$ as a function of time t over the full extent of the aquifer, the vertical discharge $Q^v(0, R_m, t)$ as a function of time for the proximal part, and the vertical discharge $Q^v(R_m, \infty, t)$ as a function of time for the distal part. The total amount of water that should flow from layer 1 to layer 3 via layer 2 is $50 \text{ m}^3/\text{d}$. This exchange is given by (85) and is necessary in order to let each layer contribute proportionally to its relative storativity S_i/S . The relative transmissivity T_i/T of each layer is responsible for the exchange between layers in the proximal part, for the horizontal flow to the well to be as efficient as possible. According to (83), $50 \text{ m}^3/\text{d}$ of water should flow in the opposite direction in the proximal part, i.e. from layer 3 to layer 1 via layer 2. The exchange in the distal part given by (86) is the difference between both: $100 \text{ m}^3/\text{d}$ of water should flow from layer 1 to layer 3 via layer 2. The necessary exchange of water between the

three layers is fully attained only after a long period of pumping, in this example 10^4 days, according to the right plot of Figure 3.

Summarizing, Figure 5 gives a schematic overview of groundwater flow in the aquifer system for large values of time, i.e. $t > 10^4$ d. This figure clearly shows how each layer in the system contributes to the total amount of water being extracted, and how this water is redistributed according to the transmissive properties of the layers. In this example, that redistribution of water causes a counterintuitive inversion of the vertical flow between the layers.

9.5. Verification

In this section, the asymptotic solution (75) is verified against the numerically inverted exact solution in Laplace space (24). Thousand models are simulated with a randomly generated number of layers between 2 and 20. Transmissivities, storativities, and vertical resistances are randomly sampled from a lognormal distribution:

$$X = 10^{\sigma Z} \quad (87)$$

with σ the standard deviation equal to 0.25, and Z a standard normal variable. Simulations are performed after reformulating the problem statement using dimensionless parameters. These parameters, denoted by an asterisk superscript, are $s_i^* = s_i T / Q$, $T_i^* = T_i / T$, $S_i^* = S_i / S$, $c_i^* = c_i / c$, $Q_i^* = Q_i / Q$, $r^* = r / \sqrt{Tc}$, $t^* = t / (Sc)$, for $1 \leq i \leq n_l$, and with $c = \sum_{i=2}^{n_l} c_i$ the total vertical resistance [T]. In this way, only the relative hydraulic parameter values are important. Since the problem is linear, the superposition principle (Bruggeman, 1999; Haitjema, 1995; Strack, 1989) may be applied, and therefore, it suffices that only one layer is extracted, which is also randomly selected.

Comparing both solutions is conveniently done by applying the Cooper and Jacob (1946) method. Taking a closer look to the approximate solution (75), it is seen that the only time-dependent term is the one related to the comprehensive potential given by the Theis (1935) equation. Since this solution holds for large values of time, it is justified to apply the Cooper and Jacob (1946) approximation, which simplifies (75) to:

$$s_i(r, t) \sim \frac{Q}{4\pi T} \ln \left(\frac{4tT}{r^2 S} e^{-\gamma} \right) + \frac{1}{2\pi T_i} \sum_{j=1}^n \sum_{k=1}^{n-1} \hat{V}_{i,k} K_0 \left(r \sqrt{\hat{\lambda}_k} \right) \hat{V}'_{k,j} Q_j \quad (t \rightarrow \infty; 1 \leq i \leq n_l) \quad (88)$$

with γ the Euler–Mascheroni constant equal to 0.57721.... The derivative of (88) with respect to $\log(t)$ is:

$$\frac{\partial s_i(r, t)}{\partial \log(t)} \sim \ln(10) \frac{Q}{4\pi T} \quad (t \rightarrow \infty; 1 \leq i \leq n_l) \quad (89)$$

According to (89), drawdown s plotted versus $\log(t)$ approximates a straight line at large values of time, which is true at all distances and in each layer. In dimensionless form, both Q^* and T^* are 1, and the right-hand side of (89) reduces to $\ln(10)/(4\pi)$, which is equal to 0.1832. The derivative in the left-hand side of (89) may be approximated by the slope of the straight line:

$$\frac{\partial s_i(r, t)}{\partial \log(t)} \sim \frac{s_i(r, t.f) - s_i(r, t)}{\log(f)} \quad (t \rightarrow \infty; 1 \leq i \leq n_l) \quad (90)$$

with f a constant factor. To apply (90), it is sufficient that the drawdowns at time t and time $(t.f)$ are calculated at an arbitrary distance r . At large values of time, the right-hand side of (90) approximates the right-hand side of (89), and in dimensionless form, it is close to 0.1832. The relative difference δ between the simulated slope (90) and the expected slope (89) is calculated as:

$$\delta = \left| 1 - \frac{s_i^*(r^*, t^*f) - s_i^*(r^*, t^*)}{\log(f)} \frac{4\pi}{\ln(10)} \right| \quad (91)$$

where dimensionless drawdown s^* is the numerical inverted exact Laplace solution (24). As both (89) and (90) hold for all layers i , index i in (91) may refer to any layer in the aquifer system. At large values of time, when the exact solution may be approximated by the asymptotic solution, relative difference δ should always be close to zero.

Figure 6 shows the maximum relative difference δ for all simulations as a function of dimensionless time t^* . In each simulation, index i in (91) refers to the pumped layer, dimensionless distance r^* is 0.01, and f is equal to 2. The maximum transmissivity ratio ($\max_i T_i / \min_i T_i$) is 28.3, the maximum resistance ratio ($\max_i c_i / \min_i c_i$) is 31.4, and the maximum storativity ratio ($\max_i S_i / \min_i S_i$) is 34.2. The graph clearly confirms that in each simulation, the relative difference is close to zero when dimensionless time t^* is greater than 10. For $t^* \geq 1$, the relative difference is smaller than 70%, for $t^* \geq 10$, it is smaller than 5%, and for $t^* \geq 100$ it is smaller than 1.8%. As a rule of thumb, one could state that the asymptotic solution for large values of times is valid when $t \geq 10Sc$.

Returning to the example discussed in previous example, Figure 1 shows indeed that exact and approximate solutions are virtually the same when $t \geq 10Sc$, which is 180 d in this case. It is also seen that all drawdown versus $\log(t)$ curves are straight lines, and their slope can be approximated by (89). One could even apply the Cooper and Jacob (1946) method to derive total transmissivity T from this slope, since total pumping rate Q is known.

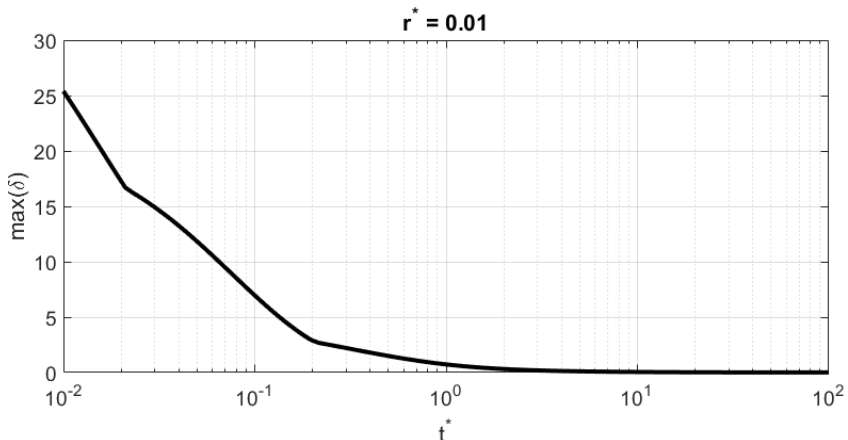


Figure 6. Maximum relative difference δ as a function of dimensionless time $t^* = t/(Sc)$ for the 1000 simulations performed to verify the validity of the asymptotic solution. See text for definitions and for more information.

9.6. Hydraulic parameter identification

For modeling purposes, rules of thumb like the $8L_m$ and the $10Sc$ rules, are very useful, since modelers need to know when vertical discretization is required and when not. An example is given by Bakker (2001), who only divides an extracted aquifer up locally in a number of sublayers to correct the steady flow to the well for its partially penetrating effect. This study proves the technique can also be applied to simulate transient flow to a partially penetrating well. The developed theory for transient multi-aquifer flow also confirms the spatial averaging in the measurements of pumping induced drawdown. According to Bohling and Butler (2010), this process causes the non-uniqueness of groundwater flow inverse problems, and in order to obtain a unique solution, they need to be regularized or biased by incorporating other sources of data.

Indeed, drawdown measured at distances $r \geq 8L_m$ and at times $t \geq 10Sc$ is sensitive only to total transmissivity T and to total storativity S . Recall that vertical flow between the individual layers is negligibly small at these distances; hence, drawdown is the same in each layer, and can be approximated by the Theis (1935) equation (81). Moreover, drawdown at these large distances is zero at the beginning of the extraction. On the other hand, close to the well, at distances smaller than $8L_m$, drawdown curves definitely are characterized by the hydraulic properties of individual layers, although this is only true at the beginning of extraction, since the individual storage coefficients S_i are not present in the asymptotic solutions (75) and (88).

In many cases, groundwater practitioners are interested in the hydraulic properties of the individual layers. This analysis shows that deriving the hydraulic parameters of individual layers from drawdown measurements is limited in space and time. The window of opportunity is different for each aquifer system and therefore needs to be examined on a case by case basis. But it is clear that it is much smaller than $r = 8L_m$ and $t = 10Sc$, since the sensitivities of the drawdown observations to the individual layer parameters need to be sufficiently large. Drawdown data observed close to the pumping well yet at larger values of time, may be included in the analysis as well, since they are still sensitive to the transmissivities of the individual layers.

As an example, consider a 5-layer system with the following dimensionless parameters, which were generated randomly:

- Layer 1: $T_1^* = 0.2235, S_1^* = 0.3161$
- Resistance layer 1: $c_1^* = 0.1269$
- Layer 2: $T_2^* = 0.2362, S_2^* = 0.1117$
- Resistance layer 2: $c_2^* = 0.2434$
- Layer 3: $T_3^* = 0.1159, S_3^* = 0.0857$
- Resistance layer 3: $c_3^* = 0.3146$
- Layer 4: $T_4^* = 0.1389, S_4^* = 0.2655$
- Resistance layer 4: $c_4^* = 0.3151$
- Layer 5: $T_5^* = 0.2854, S_5^* = 0.2210$

Water is extracted subsequently from each layer with the same steady pumping rate. In this way, 5 separated pumping tests are conducted which could be interpreted simultaneously. Drawdown data may be sampled from the pumping well and/or from different observation wells with screen in the pumped layer or in one of the unpumped layers. Figure 7 shows dimensionless drawdown s^* as a function of dimensionless time t^* (left plot) and dimensionless distance r^* (right plot) in the pumped layer during the five tests. The time-drawdown graph shows that the exact drawdown (solid lines) is very close to the asymptotic solution (dotted lines) when dimensionless time is 0.2 or larger. The dimensionless distance equal to 8 times the largest leakage factor is 3.3, but the distance-drawdown graph indicates that drawdown must be measured at much smaller distances as all curves virtually are the same if $r^* > 0.1$.

Suppose the graphs in Figure 7 show drawdown data observed during the performance of a hydraulic tomography test in an aquifer with total thickness equal to 5 m, total transmissivity T equal to 5 m^2/d , total resistance c equal to 10 d, and total storativity S equal to 0.0025. In this case, to get the real values of distance, time, and drawdown, respectively, dimensionless distance r^* must be multiplied by $\sqrt{Tc} = 7$, dimensionless time t^* by $Sc = 0.025$, and dimensionless drawdown by Q/T . Hence, dimensionless distance equal to 0.1 corresponds to 0.7 m, and dimensionless time equal to 0.2 corresponds to 0.005 d or 7.2 minutes. This implies drawdown must be observed at a distance smaller than 0.7 m, and at times smaller than 7.2 minutes, if storativities also need to be identified.

In practice, this certainly is not impossible, although this example clearly illustrates the inherent limitations of hydraulic tomography, as discussed by Bohling and Butler (2010).

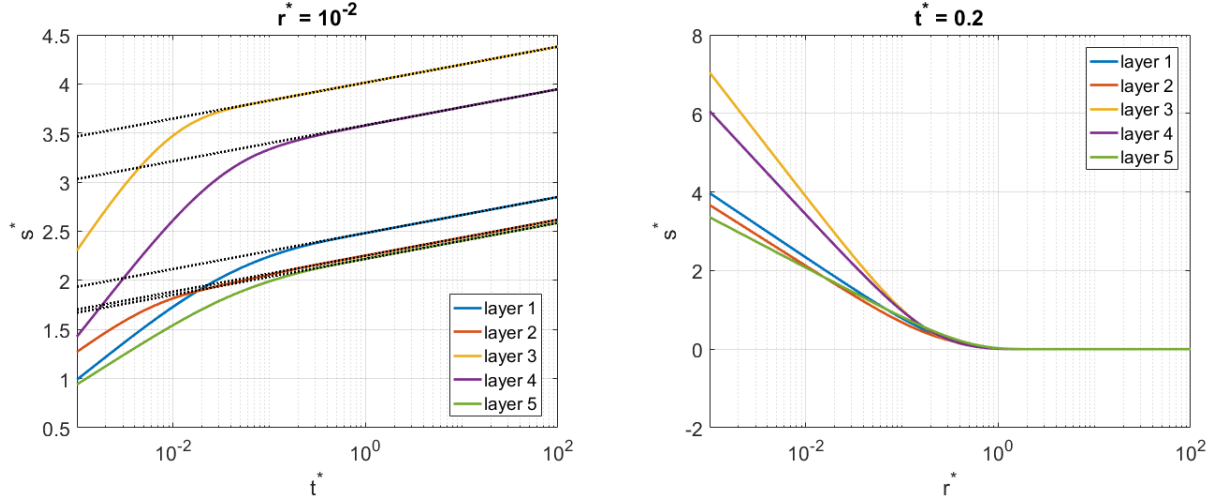


Figure 7. Dimensionless drawdown s^* as a function of dimensionless time t^* at dimensionless distance $r^* = 0.01$ (left plot) and as a function of dimensionless distance r^* at dimensionless time $t^* = 0.2$ (right plot) in the pumped layer of a 5-layer system in which water is extracted subsequently from each layer. Solid lines are exact solutions, dotted lines are the corresponding asymptotic solutions for large values of time. The dimensionless distance equal to 8 times the largest leakage factor, is 3.3. See text for the definition of the dimensionless parameters and the values of the aquifer parameters.

Bohling (1993) is among the first to propose the hydraulic tomography as a sequential aquifer test for characterizing aquifer heterogeneity, independently from other researchers (Gottlieb, 1992; Gottlieb & Dietrich, 1995; Tosaka et al., 1993). Butler et al. (1999) demonstrate, through laboratory and field experiments, the practical feasibility of obtaining accurate transient drawdown data that are required to perform and interpret such a series of short-term pumping tests. To overcome the computational burden associated with the analysis of transient data from these tests and to reduce the time required to reach steady state, Bohling et al. (2002) introduce the concept of steady shape for the inversion of hydraulic tomography data. Steady shape is a synonym for the term pseudo-steady state used in this study. According to Bohling et al. (2002), it has its origins in the early work of Theis (1940), and it enables transient drawdown data to be analyzed with a steady state model.

Bohling et al. (2002) refer to Butler (1988), who proves that hydraulic gradients under steady shape conditions are the same as those that exist under true steady state conditions. As is discussed in section 5.5.5 of Chapter 5, Butler (1988) develops a solution for transient flow to a well in a single aquifer consisting of two zones, and he shows that the late-time approximation, which is valid under steady shape conditions, indeed simplifies to the Thiem (1870; 1906) equation. Bohling et al. (2002) state that this equivalence also holds for higher dimensions, which can easily be verified numerically. This chapter substantiates this statement by actually proving its validity in the context of multilayer systems, which is highly relevant to the application of tomographic pumping tests for characterizing the vertical heterogeneity of aquifers. Furthermore, the developed approximate solution for large values of time could be used to efficiently and effectively interpret hydraulic tomography data based on the steady shape concept introduced by Bohling et al. (2002).

While this chapter provides theoretical support for the inherent limitations of multilevel pumping tests as argued by Bohling and Butler (2010), it is important to note that these limitations do not make these tests entirely useless; quite the opposite. Compared with traditional interpretation methods for pumping tests, the simultaneous interpretation of multiple pumping tests performed in different layers of the same aquifer system results in a more reliable characterization of the hydraulic

properties of these layers (Lebbe, 1999). This is illustrated in Chapter 12, which discusses the simultaneous interpretation of a double pumping test conducted in a layered aquifer situated in the western Belgian coastal plain. To obtain a unique solution in this particular case, the inverse problem is biased by carefully schematizing the aquifer using the existing geological knowledge about the aquifer (Louwyck et al., 2005).

Concerning the hydraulic tomography, Bohling et al. (2007) successfully apply the developed steady shape interpretation method to tests carried out in a coarse sand and gravel alluvial aquifer. The inverse problem is also regularized by defining layers that are determined from geophysical measurements. However, Bohling et al. (2007) do mention that they have difficulty creating a vertical gradient over significant distances, which corroborates the theory elaborated in this chapter. Bohling (2009) further analyzes sensitivity and resolution of the conducted tomographic tests and also concludes that it is possible to resolve variations in hydraulic conductivity only within a limited distance of pumping intervals and observation points.

Imposing an assumed geostatistical model for the spatial variability of the parameters is another way of regularizing the inverse problem (Bohling, 2009). Yeh and Liu (2000) are the first to introduce a geostatistical inverse method for interpretation of hydraulic tomography data, although it is worth noting that Neuman (1987) had already advocated the statistical analysis of tests that sample small volumes which are not representative for the conductivity of a larger portion of the aquifer. This is true especially for fractured rocks and karst aquifers (Dong et al., 2019; Fischer et al., 2020; Illman, 2014; Li et al., 2021; Ringel et al., 2021; Tiedeman & Barrash, 2020; Wang et al., 2023). Currently, geostatistical inversion forms the backbone of most hydraulic tomography algorithms as the estimated parameters can be treated as a stochastic process because of their spatial variability (Illman et al., 2015).

By applying a geostatistical inversion technique, one also recognizes that obtaining the exact parameter fields in a highly heterogeneous aquifer is impossible, and therefore, the statistically most likely parameter fields are derived that fit the sampled drawdowns (Hou et al., 2023). Additionally, geostatistical inverse modeling has the advantage of providing uncertainty estimates (Illman et al., 2015). The vast number of papers published on this subject, especially during the last decade, indicates that the hydraulic tomography has been accepted as a mature and viable technology for characterizing aquifer heterogeneity (Wen et al., 2020). In many cases, it may perform even better than traditional approaches (Berg & Illman, 2015; Illman et al., 2015). A thorough discussion about the effectiveness of the hydraulic tomography and the application of geostatistical inverse methods is, however, beyond the scope of this study.

9.7. Summary and conclusions

Radial flow to a well in a multilayer aquifer system has been subject of investigation for more than a century. Hemker (1985) was the first to publish a generalized transient state solution for a leaky or confined system consisting of an arbitrary number of Dupuit layers separated by resistance layers of zero thickness. In this study, the exact solution in Laplace space for a confined multilayer system is re-evaluated, and compared to the corresponding steady-state solution given by Bakker (2001). The Laplace space solution is expanded for large values of time and inverted analytically, resulting in an approximate solution that equals the steady-state solution in which the comprehensive potential given by the Thiem (1870; 1906) formula is replaced by the Theis (1935) equation.

By evaluating the water budget for the individual layers using this approximate solution for large values of time, it is shown that close to the well, at distances smaller than about 8 times the largest leakage factor, flow is redistributed according to the transmissive properties of the individual layers,

resulting in a pseudo-steady state, also called steady shape conditions. Drawdown curves plotted on semi-logarithmic axes are parallel straight lines at large values of time, and the slope of these lines is equal to the slope of the straight line given by the Cooper and Jacob (1946) approximation of the Theis (1935) solution for the equivalent single-layer model. In the latter, total transmissivity and storativity of the multilayer system is considered, and the total pumping rate of all wells in the system.

At distances larger than the distance determined by the largest leakage factor, flow continues to be redistributed according to the storative properties of the layers, as the system is confined. A theoretical example is given in which this redistribution of water in the distal part of the multilayer system causes a counterintuitive inversion of the vertical flow between the layers of the system. This vertical flow is, however, negligibly small because of the large volumes involved. Hence, drawdown in the individual layers is virtually the same at distances larger than about 8 times the largest leakage factor, a conclusion that also holds for steady multilayer flow (Bakker & Strack, 2003).

The asymptotic solution for large values of time is verified against the numerically inverted exact Laplace space solution by simulating a thousand randomly generated multilayer models. Reformulating both solutions using dimensionless parameters, it is concluded for all simulations that the exact solution approximates the asymptotic solution after a period of pumping which is larger than 10 times the product of the total storativity and the sum of all vertical resistances. Combined with the observation of uniform drawdown at distances larger than 8 times the largest leakage factor, this conclusion is a useful rule of thumb that may help modelers decide whether vertical discretization is required or not.

The developed theory also confirms the spatial averaging in the measurements of pumping induced drawdown. As a consequence, deriving the hydraulic parameters of individual layers in the multilayer aquifer system from drawdown measurements, is limited in space and time. The window of opportunity is different for each aquifer system and needs to be examined on a case by case basis. A second theoretical example shows, however, that drawdown must be sampled at distances that are much smaller than 8 times the largest leakage factor. This example clearly demonstrates the inherent limitations of hydraulic tomography, as discussed by Bohling and Butler (2010).

9.8. References

- Bakker, M. (1999). Simulating groundwater flow in multi-aquifer systems with analytical and numerical Dupuit-models. *Journal of Hydrology*, 222(1–4), 55–64.
[https://doi.org/10.1016/S0022-1694\(99\)00089-X](https://doi.org/10.1016/S0022-1694(99)00089-X)
- Bakker, M. (2001). An analytic, approximate method for modeling steady, three-dimensional flow to partially penetrating wells. *Water Resources Research*, 37(5).
<https://doi.org/10.1029/2000WR900400>
- Bakker, M., & Hemker, C. J. (2002). A Dupuit formulation for flow in layered, anisotropic aquifers. *Advances in Water Resources*, 25(7), 747–754. [https://doi.org/10.1016/S0309-1708\(02\)00074-X](https://doi.org/10.1016/S0309-1708(02)00074-X)
- Bakker, M., & Strack, O. D. L. (2003). Analytic elements for multiaquifer flow. *Journal of Hydrology*, 271(1–4). [https://doi.org/10.1016/S0022-1694\(02\)00319-0](https://doi.org/10.1016/S0022-1694(02)00319-0)
- Berg, S. J., & Illman, W. A. (2015). Comparison of Hydraulic Tomography with Traditional Methods at a Highly Heterogeneous Site. *Groundwater*, 53(1), 71–89. <https://doi.org/10.1111/gwat.12159>

- Bohling, G. C. (1993). Hydraulic tomography in two-dimensional, steady state groundwaterflow (abstract). *Eos Trans. AGU*, 74(16), Spring Meet. Suppl., 141.
- Bohling, G. C. (2009). Sensitivity and resolution of tomographic pumping tests in an alluvial aquifer. *Water Resources Research*, 45(2), 1–21. <https://doi.org/10.1029/2008WR007249>
- Bohling, G. C., & Butler, J. J. (2010). Inherent Limitations of Hydraulic Tomography. *Ground Water*, 48(6), 809–824. <https://doi.org/10.1111/j.1745-6584.2010.00757.x>
- Bohling, G. C., Butler, J. J., Zhan, X., & Knoll, M. D. (2007). A field assessment of the value of steady shape hydraulic tomography for characterization of aquifer heterogeneities. *Water Resources Research*, 43(5), 1–23. <https://doi.org/10.1029/2006WR004932>
- Bohling, G. C., Zhan, X., Butler, J. J., & Zheng, L. (2002). Steady shape analysis of tomographic pumping tests for characterization of aquifer heterogeneities. *Water Resources Research*, 38(12), 60_1-60_15. <https://doi.org/10.1029/2001WR001176>
- Bruggeman, G. A. (1999). *Analytical solutions of geohydrological problems. Developments in Water Science* 46. Amsterdam: Elsevier.
- Butler, J. J. (1988). Pumping tests in nonuniform aquifers — The radially symmetric case. *Journal of Hydrology*, 101(1–4), 15–30. [https://doi.org/10.1016/0022-1694\(88\)90025-X](https://doi.org/10.1016/0022-1694(88)90025-X)
- Butler, J. J., McElwee, C. D., & Bohling, G. C. (1999). Pumping tests in networks of multilevel sampling wells: Motivation and methodology. *Water Resources Research*, 35(11), 3553–3560. <https://doi.org/10.1029/1999WR900231>
- Cheng, A. H.-D., & Morohunfola, O. K. (1993). Multilayered leaky aquifer systems: 1. Pumping well solutions. *Water Resources Research*, 29(8), 2787–2800. <https://doi.org/10.1029/93WR00768>
- Cooper, H. H., & Jacob, C. E. (1946). A generalized graphical method for evaluating formation constants and summarizing well-field history. *Transactions, American Geophysical Union*, 27(4), 526–534. <https://doi.org/10.1029/TR027i004p00526>
- de Glee, G. J. (1930). *Over grondwaterstroomingen bij wateronttrekking door middel van putten (in Dutch)* [PhD thesis]. Technische Hoogeschool Delft, Drukkerij J. Waltman. Jr.
- de Hoog, F. R., Knight, J. H., & Stokes, A. N. (1982). An Improved Method for Numerical Inversion of Laplace Transforms. *SIAM Journal on Scientific and Statistical Computing*, 3(3), 357–366. <https://doi.org/10.1137/0903022>
- Dong, Y., Fu, Y., Yeh, T. -C. J., Wang, Y. -L., Zha, Y., Wang, L., & Hao, Y. (2019). Equivalence of Discrete Fracture Network and Porous Media Models by Hydraulic Tomography. *Water Resources Research*, 55(4), 3234–3247. <https://doi.org/10.1029/2018WR024290>
- Fischer, P., Jardani, A., & Jourde, H. (2020). Hydraulic tomography in coupled discrete-continuum concept to image hydraulic properties of a fractured and karstified aquifer (Lez aquifer, France). *Advances in Water Resources*, 137, 103523. <https://doi.org/10.1016/j.advwatres.2020.103523>
- Gottlieb, J. (1992). *Hydraulische Tomographie: Identifikation räumlich verteilter Durchlässigkeiten im Untergrund (in German)* (Patent P4236692.5 vom 30.10.1992).
- Gottlieb, J., & Dietrich, P. (1995). Identification of the permeability distribution in soil by hydraulic tomography. *Inverse Problems*, 11(2), 353–360. <https://doi.org/10.1088/0266-5611/11/2/005>

- Haitjema, H. (1995). *Analytic Element Modeling of Groundwater Flow*. San Diego: Academic Press.
<https://doi.org/10.1016/B978-0-12-316550-3.X5000-4>
- Halász, B. (1975). Eigenheiten von geschichteten hydrogeologischen Systemen (in Hungarian). *Hidrol. Közl.*, 11, 505–507.
- Halász, B., & Székely, F. (1979). Computation of drawdown in wells in stratified aquifer systems (In Russian). *I.A.H. Methods for Evaluation of Groundwater Resources. XV-1. Congr. Vilnius*, 50–53.
- Hantush, M. S. (1964). Hydraulics of wells. In V. T. Chow (Ed.), *Advances in Hydroscience: Vol. I* (pp. 281–432). New York and London: Academic Press.
- Hantush, M. S. (1967). Flow to wells in aquifers separated by a semipervious layer. *Journal of Geophysical Research*, 72(6), 1709–1720. <https://doi.org/10.1029/JZ072i006p01709>
- Hantush, M. S., & Jacob, C. E. (1955). Non-steady radial flow in an infinite leaky aquifer. *Transactions, American Geophysical Union*, 36(1), 95–100. <https://doi.org/10.1029/TR036i001p00095>
- Hemker, C. J. (1984). Steady groundwater flow in leaky multiple-aquifer systems. *Journal of Hydrology*, 72(3–4), 355–374. [https://doi.org/10.1016/0022-1694\(84\)90089-1](https://doi.org/10.1016/0022-1694(84)90089-1)
- Hemker, C. J. (1985). Transient well flow in leaky multiple-aquifer systems. *Journal of Hydrology*, 81(1–2), 111–126. [https://doi.org/10.1016/0022-1694\(85\)90170-2](https://doi.org/10.1016/0022-1694(85)90170-2)
- Hemker, C. J. (1999a). Transient well flow in vertically heterogeneous aquifers. *Journal of Hydrology*, 225(1–2), 1–18. [https://doi.org/10.1016/S0022-1694\(99\)00137-7](https://doi.org/10.1016/S0022-1694(99)00137-7)
- Hemker, C. J. (1999b). Transient well flow in layered aquifer systems: the uniform well-face drawdown solution. *Journal of Hydrology*, 225(1–2), 19–44. [https://doi.org/10.1016/S0022-1694\(99\)00093-1](https://doi.org/10.1016/S0022-1694(99)00093-1)
- Hemker, C. J. (2000). *Groundwater flow in layered aquifer systems* [PhD thesis]. VU, Amsterdam.
- Hemker, C. J., & Maas, C. (1987). Unsteady flow to wells in layered and fissured aquifer systems. *Journal of Hydrology*, 90(3–4), 231–249. [https://doi.org/10.1016/0022-1694\(87\)90069-2](https://doi.org/10.1016/0022-1694(87)90069-2)
- Hou, X., Hu, R., Yeh, T. -C. J., Li, Y., Qi, J., Song, Y., & Qiu, H. (2023). A Short-Term Pumping Strategy for Hydraulic Tomography Based on the Successive Linear Estimator. *Water Resources Research*, 59(4), 1–18. <https://doi.org/10.1029/2022WR033831>
- Hunt, B. (1985). Flow to a Well in a Multiaquifer System. *Water Resources Research*, 21(11), 1637–1641. <https://doi.org/10.1029/WR021i011p01637>
- Hunt, B. (1986). Solutions for steady groundwater flow in multi-layer aquifer systems. *Transport in Porous Media*, 1(4), 419–429. <https://doi.org/10.1007/BF00208046>
- Hunt, B., & Scott, D. (2007). Flow to a Well in a Two-Aquifer System. *Journal of Hydrologic Engineering*, 12(2), 146–155. [https://doi.org/10.1061/\(ASCE\)1084-0699\(2007\)12:2\(146\)](https://doi.org/10.1061/(ASCE)1084-0699(2007)12:2(146))
- Illman, W. A. (2014). Hydraulic Tomography Offers Improved Imaging of Heterogeneity in Fractured Rocks. *Groundwater*, 52(5), 659–684. <https://doi.org/10.1111/gwat.12119>
- Illman, W. A., Berg, S. J., & Zhao, Z. (2015). Should hydraulic tomography data be interpreted using geostatistical inverse modeling? A laboratory sandbox investigation. *Water Resources Research*, 51(5), 3219–3237. <https://doi.org/10.1002/2014WR016552>

- Jacob, C. E. (1946). Radial flow in a leaky artesian aquifer. *Transactions, American Geophysical Union*, 27(2). <https://doi.org/10.1029/TR027i002p00198>
- Kruseman, G. P., & de Ridder, N. A. (1990). *Analysis and Evaluation of Pumping Test Data* (2nd ed.). ILRI Publication 47, Wageningen.
- Lebbe, L. C. (1999). *Hydraulic Parameter Identification. Generalized Interpretation Method for Single and Multiple Pumping Tests*. Berlin Heidelberg: Springer-Verlag.
<https://doi.org/https://doi.org/10.1007/978-3-642-60117-0>
- Li, S., Wang, X., Xu, Z., Mao, D., & Pan, D. (2021). Numerical investigation of hydraulic tomography for mapping karst conduits and its connectivity. *Engineering Geology*, 281, 105967.
<https://doi.org/10.1016/j.enggeo.2020.105967>
- Louwyck, A., Vandenbohede, A., & Lebbe, L. C. (2005). The role of hydrogeological research in the realization of a combined pumping and deep infiltration system at the excavation "Duinenabdij." In J.-L. Herrier, J. Mees, A. Salman, J. Seys, H. Van Nieuwenhuyse, & I. Dobbelaere (Eds.), *Proceedings "Dunes and Estuaries 2005": International Conference on nature restoration practices in European coastal habitats, Koksijde, Belgium 19-23 September 2005*. (pp. 317–326). VLIZ Special Publication 19.
- Maas, C. (1986). The use of matrix differential calculus in problems of multiple-aquifer flow. *Journal of Hydrology*, 88(1–2). [https://doi.org/10.1016/0022-1694\(86\)90196-4](https://doi.org/10.1016/0022-1694(86)90196-4)
- Maas, C. (1987a). Groundwater flow to a well in a layered porous medium: 1. Steady flow. *Water Resources Research*, 23(8), 1675–1681. <https://doi.org/10.1029/WR023i008p01675>
- Maas, C. (1987b). Groundwater flow to a well in a layered porous medium: 2. Nonsteady multiple-aquifer flow. *Water Resources Research*, 23(8), 1683–1688.
<https://doi.org/10.1029/WR023i008p01683>
- Meesters, A. G. C. A., Hemker, C. J., & van den Berg, E. H. (2004). An approximate analytical solution for well flow in anisotropic layered aquifer systems. *Journal of Hydrology*, 296(1–4), 241–253.
<https://doi.org/10.1016/j.jhydrol.2004.03.021>
- Neuman, S. P. (1987). Stochastic continuum representation of fractured rock permeability as an alternative to the REV and fracture network concepts. *Proc. U.S. Rock Mech. Symp.*, 28, 533–561.
- Neuman, S. P., & Witherspoon, P. A. (1969). Theory of Flow in a Confined Two Aquifer System. *Water Resources Research*, 5(4), 803–816. <https://doi.org/10.1029/WR005i004p00803>
- Pfannkuch, H.-O., Mooers, H. D., Siegel, D. I., Quinn, J. J., Rosenberry, D. O., & Alexander, S. C. (2021). Review: "Jacob's Zoo"—how using Jacob's method for aquifer testing leads to more intuitive understanding of aquifer characteristics. *Hydrogeology Journal*, 29(6).
<https://doi.org/10.1007/s10040-021-02363-7>
- Ringel, L. M., Jalali, M., & Bayer, P. (2021). Stochastic Inversion of Three-Dimensional Discrete Fracture Network Structure With Hydraulic Tomography. *Water Resources Research*, 57(12), 1–16. <https://doi.org/10.1029/2021WR030401>
- Stehfest, H. (1970). Algorithm 368: Numerical inversion of Laplace transforms [D5]. *Communications of the ACM*, 13(1), 47–49. <https://doi.org/10.1145/361953.361969>

- Strack, O. D. L. (1981a). Flow in aquifers with clay laminae: 1. The comprehensive potential. *Water Resources Research*, 17(4), 985–992. <https://doi.org/10.1029/WR017i004p00985>
- Strack, O. D. L. (1981b). Flow in aquifers with clay laminae: 2. Exact solutions. *Water Resources Research*, 17(4), 993–1004. <https://doi.org/10.1029/WR017i004p00993>
- Strack, O. D. L. (1989). *Groundwater Mechanics*. Old Tappan, N. J.: Prentice-Hall.
- Strack, O. D. L., & Haitjema, H. M. (1981a). Modeling double aquifer flow using a comprehensive potential and distributed singularities: 1. Solution for homogeneous permeability. *Water Resources Research*, 17(5), 1535–1549. <https://doi.org/10.1029/WR017i005p01535>
- Strack, O. D. L., & Haitjema, H. M. (1981b). Modeling double aquifer flow using a comprehensive potential and distributed singularities: 2. Solution for inhomogeneous permeabilities. *Water Resources Research*, 17(5), 1551–1560. <https://doi.org/10.1029/WR017i005p01551>
- Székely, F. (1978). *Computing problems in well hydraulics (in Hungarian)*. Res. Cent. Water Resour. Res. Dev. (VITUKI), Budapest.
- Theis, C. V. (1935). The relation between the lowering of the Piezometric surface and the rate and duration of discharge of a well using ground-water storage. *Transactions, American Geophysical Union*, 16(2), 519–524. <https://doi.org/10.1029/TR016i002p00519>
- Theis, C. V. (1940). The source of water derived from wells: essential factors controlling the response of an aquifer to development. *Civil Engineering*, 10, 277–280.
- Thiem, A. (1870). Die Ergiebigkeit artesischer Bohrlöcher, Schachtbrunnen und Filtergalerien (in German). *Journal Für Gasbeleuchtung Und Wasserversorgung*, 13, 450–467.
- Thiem, G. (1906). *Hydrologische Methoden (in German)*. Leipzig: Gebhardt.
- Tiedeman, C. R., & Barrash, W. (2020). Hydraulic Tomography: 3D Hydraulic Conductivity, Fracture Network, and Connectivity in Mudstone. *Groundwater*, 58(2), 238–257. <https://doi.org/10.1111/gwat.12915>
- Tosaka, H., Masumoto, K., & Kojima, K. (1993). Hydropulse tomography for identifying 3-d permeability distribution, in High Level Radioactive Waste Management. *Proceedings of the Fourth Annual International Conference of the ASCE, Am. Soc. of Civ. Eng., Reston VA*, 955–959.
- Veling, E. J. M., & Maas, C. (2009). Strategy for solving semi-analytically three-dimensional transient flow in a coupled N-layer aquifer system. *Journal of Engineering Mathematics*, 64(2), 145–161. <https://doi.org/10.1007/s10665-008-9256-9>
- Wang, X., Kong, X.-Z., Hu, L., & Xu, Z. (2023). Mapping conduits in two-dimensional heterogeneous karst aquifers using hydraulic tomography. *Journal of Hydrology*, 617, 129018. <https://doi.org/10.1016/j.jhydrol.2022.129018>
- Wen, J. -C., Chen, J. -L., Yeh, T. -C. J., Wang, Y. -L., Huang, S. -Y., Tian, Z., & Yu, C. -Y. (2020). Redundant and Nonredundant Information for Model Calibration or Hydraulic Tomography. *Groundwater*, 58(1), 79–92. <https://doi.org/10.1111/gwat.12879>
- Yeh, T.-C. J., & Liu, S. (2000). Hydraulic tomography: Development of a new aquifer test method. *Water Resources Research*, 36(8), 2095–2105. <https://doi.org/10.1029/2000WR900114>

Yu, W. S. (1987). Steady ground-water flow through layered media. *Transport in Porous Media*, 2(2), 103–127. <https://doi.org/10.1007/BF00142654>

Chapter 10. The Radius of Influence Myth

10.1. Introduction

This chapter is a revision of the Louwyck et al. (2022) paper about the use of empirical formulas to estimate the radius of influence in general, and the Sichardt formula in particular. Author contributions are given in section 1.5 of the introductory Chapter 1. The sections of the paper are rearranged to be consistent with the other chapters. References are reformatted for the same reason. Additional figures are included to visualize and clarify the analytical models discussed in the paper, and the literature overview is updated. Finally, a section is added in which the analytical Ernst model is validated by means of a MODFLOW model. The one-dimensional solutions by de Glee (1930), Theis (1935), and Hantush and Jacob (1955) are also presented in Chapter 2, whereas the solution by Ernst (1971) is also discussed in Chapter 7 and Chapter 11.

Empirical formulas to estimate the radius of influence, such as the Sichardt formula (Kyrieleis & Sichardt, 1930), occasionally appear in studies assessing the environmental impact of groundwater extractions. As they are inconsistent with fundamental hydrogeological principles, the term “radius of influence myth” is used by analogy with the water budget myth. In this study, alternative formulations based on the well-known de Glee (1930) and Theis (1935) equations are presented, and the contested formula that estimates the radius of influence by balancing pumping and infiltration rate, is derived from an asymptotic solution of an analytical model developed by Ernst (1971). The Ernst (1971) model that assumes uniform recharge and drainage, is validated by means of a MODFLOW (Harbaugh, 2005) model that simulates flow to a well in a recharged aquifer with non-uniform drainage.

The transient-state solution of the Ernst (1971) model is developed by applying the Laplace transform, and it is compared with the finite-difference solution. Examining drawdown and total storage change reveals the relations between the presented one-dimensional radial flow solutions. The assumptions underlying these solutions are discussed in detail to show their limitations and to refute misunderstandings about their applicability. The discussed analytical models and the formulas derived from it to estimate the radius of influence, cannot be regarded as substitutes for advanced modeling, although they offer valuable insights on relevant parameter combinations.

10.1.1. The Sichardt formula

This study stems from the concern about the use of empirical formulas to assess the impact of groundwater extractions. Zhai et al. (2021) and Motyka and d’Obyn (2022) give an overview of different empirical relations that are in use. This work focuses on the formula of Sichardt as it is frequently applied by groundwater consultants in Flanders and the Netherlands to estimate the radius of influence in case of pumping or dewatering (Bot, 2016; Janssen, 2003; OVAM, 2018; VMM, 2019, 2020; Willems et al., 2009). Since the formula and its variants are recommended in many textbooks on geotechnical engineering (Cashman & Preene, 2013; Coduto et al., 2011; Dachroth, 2017; Desoet & Reiffsteck, 2020; Fraco and Associates Inc., 1971; Mansur & Kaufman, 1962; Merkl, 2008; Powers, 1981, 1992; Powers et al., 2007; Powrie, 2004; Puller, 2003; Punmia et al., 1995; Sanglerat et al., 1984; Smoltczyk, 2003), and applied in dewatering and groundwater studies published in peer-reviewed journals (Amartya Kumar et al., 2012; Ergun & Nalçakan, 1993; De Filippi et al., 2020; Houben, 2015; Khadka, 2021; Masoud, 2020; Niu et al., 2013; Rabie, 2013; Yihdego,

2018; Yihdego & Drury, 2016; Yihdego & Paffard, 2017), it may be concluded its use is worldwide spread, although some researchers advise against it (Bair & O'Donnell, 1983; El-Hames, 2020; Fileccia, 2015; Moh et al., 1996; Motyka & d'Obrynn, 2022; Zhai et al., 2021) or suggest applying a correction factor to enhance its reliability (Desens & Houben, 2022, 2023).

The formula was published first by Kyrieleis and Sichardt in 1930 (Kyrieleis & Sichardt, 1930), but they mention Sichardt as the discoverer, unfortunately without citation. Some authors refer to Sichardt (1928), and although the problem concerning the radius of influence is addressed in Sichardt's dissertation, the formula itself, however, is not given. Cashman and Preene (2013) state that the formula was based on earlier work by Weber, but they give no references. According to Narasimhan (1998), Weber (1928) made the first successful attempt to analyze transient flow toward a well. But it is not clear if Sichardt was inspired by this work, as the Sichardt equation holds for steady-state conditions (Kyrieleis & Sichardt, 1930). In many cases, however, the Sichardt formula is applied without citation, which may indicate it has become a standard tool in dewatering studies.

Since empirical formulas such as the Sichardt equation are widely used, yet not in agreement with some of the fundamental principles of groundwater flow (Zhai et al., 2021), we consider the term "radius of influence myth" well-placed by analogy with the groundwater budget myth introduced by Bredehoeft et al. (1982), and revisited by Bredehoeft (2002). The main objective of this study is to debunk the myth and to present alternative formulas that are consistent with fundamental laws and principles applied in hydrogeology. In fact, the work of Bredehoeft et al. (1982) and Bredehoeft (2002) is highly relevant, as it addresses sustainable groundwater development, and brings up the fundamental hydrological principles that were stated first by Theis (1940), and revisited recently by Konikow and Leake (2014). According to Theis (1940), the essential factors controlling the response of an aquifer system to pumping are (1) the distance to, and character of the recharge, (2) the distance to the locality of natural discharge, and (3) the character of the cone of depression.

When the extraction starts, groundwater is taken from storage to create gradients towards the well (Bredehoeft et al., 1982), and the resulting decline of water levels is observed only locally around the well. When pumping continues, the cone of depression expands and deepens, as more groundwater is released from storage to support the extraction. When it reaches areas of natural recharge or discharge, the lowering of the water table in these areas induces additional recharge or reduces the discharge (Theis, 1940). Examples of the first are an increase in vertical soil percolation or infiltration from streams, whereas a decrease in evapotranspiration or drainage are examples of the latter. The cone of depression ceases to expand when the amount of extracted water is balanced completely by the total change in recharge and discharge, which is called the capture (Bredehoeft, 2002; Bredehoeft et al., 1982; Bredehoeft & Durbin, 2009; Konikow & Leake, 2014; Lohman, 1972). Note that this concept of capture has a distinct meaning from the capture zone of a well (Barlow et al., 2018; Seward et al., 2015). The capture zone is defined as the three-dimensional volumetric portion of a groundwater-flow field that discharges water to a well (Barlow et al., 2018), and it may not be confused with the cone of depression (Brown, 1963).

When the pumping rate is balanced completely by the capture, a further decline of water levels is not needed anymore, hence, the aquifer system is brought into a new state of dynamic equilibrium. The time to full capture may range from seconds to centuries (Bredehoeft & Durbin, 2009; Sophocleous, 2012), and depends on the hydraulic properties of the aquifer system, the interacting sources and sinks, and the positioning of the extraction within the system (Bredehoeft et al., 1982). It is also possible, however, the capture may never be large enough to balance the pumping. In this case, the aquifer continues to be depleted, until the well goes dry (Bredehoeft & Durbin, 2009), which may also occur when sources and sinks, such as streams, dry up.

When evaluating sustainable pumping, it may be sufficient to calculate the cone of depression to see whether a new steady state is attained or not. However, sustainable pumping may not be confused with sustainability, which is a much broader concept, as it includes other factors such as water quality, ecology, and socioeconomic considerations (Devlin & Sophocleous, 2005). It is common practice to use mathematical models to simulate the cone of depression as well as to assess other impacts caused by groundwater development. The first may be performed using traditional analytical models (Bredehoeft, 2002), whereas the latter requires advanced numerical modeling (Kalf & Woolley, 2005; Zhou, 2009). Therefore, our major concern is the use of the Sichardt formula in environmental impact studies assessing sustainability as the formula oversimplifies the hydraulics of well-flow.

The Sichardt formula determines the radius of influence of an extraction by merely considering the aquifer conductivity and the lowering of the water level in the well. The radius of influence is defined as the boundary of the cone of depression, i.e. the radial distance from the center of the well to the point where there is no lowering of the water table or potentiometric surface (Hansen, 1991), or beyond which drawdown is negligible or unobservable (Bear, 1979). This definition implies the assumption of axial symmetry around the axis of the well. Axisymmetric models simulating flow to a well, are frequently applied to analyze aquifer tests (e.g. Kruseman & de Ridder, 1990), in which case this assumption is justified because of the limited impact of such tests. It is also mathematically convenient, as it reduces the flow problem by one dimension.

However, in case of permanent groundwater extractions, the assumption of axial symmetry is rarely valid, as the cone of depression is not restricted to the vicinity of the well. In reality, the part of the aquifer system impacted by a large cone of depression is not axially symmetric, and neither are the streams and other sources and sinks interacting with the system. As a consequence, the area of influence corresponding to the cone of depression cannot be described by simply drawing a circle around the well in this case (Hansen, 1991). Moreover, the pumped aquifer mostly is part of a multi-aquifer system, i.e. a succession of aquifers separated by relatively less permeable aquitards, and a complete understanding of flow in the pumped aquifer without analyzing the multi-aquifer system as a whole is impossible (Neuman & Witherspoon, 1969a). These arguments may lead to the conclusion to abandon the radius of influence concept (Zhai et al., 2021), although it is a well-known and useful concept (Bair & O'Donnell, 1983; Bresciani et al., 2020a, 2020b; Castellazzi et al., 2016; Chu, 1994; Dragoni, 1998; Gefell et al., 1994; MacDonald & Kitanidis, 1993; Méité et al., 2023; Soni et al., 2015). Moreover, approaches applying this concept to groundwater management have proven to be valuable, provided that they are theoretically justified (Ahmadi et al., 2023; Fileccia, 2015; Seward et al., 2015; Zhou, 2011).

10.1.2. Objectives

In this study, it is shown that the radius of influence is a parameter that can be derived from well-known one-dimensional axisymmetric models. These and other analytical models are still useful, not only in an educational context (Pfannkuch et al., 2021), but also because they have some advantages over numerical models (Haitjema, 2006). In practice, groundwater studies are constrained by time and budget, often impeding the setup of data hungry numerical models, in which case the use of analytical models is an acceptable and inexpensive alternative (Fileccia, 2015). Moreover, sophisticated numerical models are not required in every case, and analytical models can help to decide whether to build a complex numerical model or not, as they offer valuable insights. Therefore, it is strongly recommended to perform hand calculations and to analyze simple analytical solutions before getting started with comprehensive numerical modeling (Haitjema, 2006). The text book written by Haitjema (1995) is a good start to extend one's analytical modeling skills, or the recently

published book by Bakker and Post (2022), in which it is illustrated how Python can be used to implement analytical models in a straightforward manner. For more advanced techniques, we refer to Bakker and Strack (2003) who present analytical elements to simulate wells, infiltration areas and streams in multi-aquifer systems, to Strack (1989, 2017) who translates a plethora of complex practical questions into mathematical formulations that can be solved analytically, and to Bruggeman (1999) who developed more than thousand analytical solutions.

The point of view defended in this work is that the radius of influence is not an erroneous concept, rather its use is problematic in many cases, because groundwater practitioners often are unaware of the assumptions underlying frequently used equations to calculate the cone of depression.

Groundwater modeling courses nowadays focus on the use of numerical models, which do not offer the same intuitions and insights that analytical models offer (Haitjema, 2006). Therefore, several well-known one-dimensional axisymmetric models are carefully explained here and suggested as valid alternatives to approaches that rely on empirical formulas. After presenting the Sichardt formula (Kyrieleis & Sichardt, 1930) and exposing its inconsistency with the Thiem (1870; 1906) equation, the solutions developed by de Glee (1930) and Theis (1935) are discussed: the former is used for steady flow in a leaky aquifer, the latter for transient flow in a confined aquifer. Based on these solutions, alternative formulas for the radius of influence are presented, and equations are derived to determine the maximum radius of influence without knowledge of the aquifer transmissivity. In the subsequent section, the model of Hantush and Jacob (1955) to simulate transient flow in a leaky aquifer is discussed to clarify the relation between the de Glee (1930) and the Theis (1935) equation, and rules of thumb are derived to distinguish between both.

Finally, the steady-state solution for well-flow in a phreatic aquifer subject to areal recharge and drainage developed by Ernst (1971) is discussed. The assumptions underlying this model are the same as those underlying the steady-state solution for a well extracting a leaky aquifer (de Glee, 1930; Jacob, 1940), except for the head-dependent boundary condition at the top, which is linear in the latter, whereas it is nonlinear in the first, as it is restricted to draining water from the aquifer. The asymptotic solution for zero resistance surprisingly yields the formula to determine the radius of influence by balancing pumping and infiltration rate, which is contested by some authors (Bredehoeft, 2002; Brown, 1963). Apparently, this formula is valid in heavily drained areas with an excess of precipitation, which are common in Flanders and the Netherlands. The applicability of the Ernst (1971) model is discussed in detail and validated by comparing the analytical Ernst (1971) solution with numerical results obtained from a MODFLOW (Harbaugh, 2005) model defining more realistic boundary conditions.

To see the relation between the Theis (1935) model and the Ernst (1971) model, the transient-state solution for the latter is developed by applying the Laplace transform, and compared with the finite-difference model MAxSym (Louwyck, 2011; Louwyck et al., 2012) extended with the option to include drainage boundary conditions (Louwyck, 2015). Next section gives the detailed derivation of this semi-analytical solution, for which the same assumptions hold as for the Hantush and Jacob (1955) model, except for the nonlinear head-dependent boundary condition at the top. In fact, all one-dimensional radial flow solutions presented in this work are related, as they are all solutions to the same differential equation. This is shown by examining the total storage change, from which some useful rules of thumb are derived. In the context of assessing the environmental impact of groundwater extractions, the presented formulas to estimate the radius of influence certainly cannot replace comprehensive numerical modeling, yet they may be considered as more reliable alternatives to the Sichardt formula.

10.2. One-dimensional axisymmetric flow: analytical solutions

This section treats the mathematical problem of axisymmetric flow to a pumping well fully penetrating a homogeneous and isotropic aquifer. The problem is stated generally, which implies both steady and transient flow are considered, the well may have a finite or infinitesimal diameter, the aquifer may be laterally bounded or unbounded, and its upper and lower boundaries may be confined or leaky. It is also possible to define uniform recharge.

The problem is solved analytically and the obtained solution is simplified to well-known solutions that are discussed in the section 10.3: Thiem (1870; 1906), de Glee (1930), Theis (1935), and Hantush and Jacob (1955). In section 10.3, the de Glee (1930) and the Theis (1935) equations are used to derive formulas for estimating the radius of influence. Finally, this section presents the solution for the Ernst (1971) model, which is a nonlinear model that combines the solution of two linear one-layer models. Using the Laplace transform, the transient-state solution of the Ernst (1971) model is derived. The exact solution in the Laplace domain is given, which is inverted numerically using the Stehfest (1970) algorithm. Results of this newly developed solution are presented in section 10.3.7.

10.2.1. Problem statement

In general, one-dimensional axisymmetric flow is governed by the following partial differential equation:

$$\frac{\partial^2 h}{\partial r^2} + \frac{1}{r} \frac{\partial h}{\partial r} = \frac{S}{T} \frac{\partial h}{\partial t} - \frac{N}{T} + \frac{h - h_{top}}{c_{top} T} + \frac{h - h_{bot}}{c_{bot} T} \quad (1)$$

with $h(r, t)$ the hydraulic head [L] in the aquifer, which is a function of radial distance r [L] and time t [T]. A homogeneous aquifer is considered with constant transmissivity T [L^2/T] and constant storativity S [-]. Transmissivity T equals KD , with K the horizontal conductivity [L/T], and D the aquifer thickness [L]. Storativity S equals $S^s D$, with S^s the specific elastic storage [L^{-1}]. However, if the aquifer is unconfined, then S equals the specific yield S_y [-]. The aquifer may be recharged at the top by a constant flux N [L/T]. This flux is positive in case of infiltration. The leaky top and bottom boundary have constant heads [L] h_{top} and h_{bot} , and corresponding hydraulic resistances [L] c_{top} and c_{bot} , respectively.

The inner boundary is a well with radius r_w [L] from which water is extracted at constant pumping rate Q [L^3/T]:

$$r_w \frac{\partial h(r_w)}{\partial r} = \frac{Q}{2\pi T} \quad (2)$$

If water is extracted, then $Q > 0$. The outer boundary at distance r_{out} [L] has a constant head h_{out} [L]:

$$h(r_{out}, t) = h_{out} \quad (3)$$

The initial condition is:

$$h(r, 0) = h_0 \quad (4)$$

The steady-state problem is also treated by differential equation (1), with $\partial h / \partial t = 0$, and subject to boundary conditions (2) and (3).

10.2.2. Laplace transform

In case of transient flow, Laplace transform \mathcal{L} is applied. The Laplace transform of head h is denoted by \bar{h} :

$$\mathcal{L}\{h(r, t)\}(p) = \bar{h}(r, p) \quad (5)$$

with p the frequency variable [T^{-1}]. The Laplace transform of the constants is:

$$\bar{Q} = \frac{Q}{p}, \bar{N} = \frac{N}{p}, \bar{h}_{out} = \frac{h_{out}}{p}, \bar{h}_{top} = \frac{h_{top}}{p}, \bar{h}_{bot} = \frac{h_{bot}}{p} \quad (6)$$

Equation (1) is transformed into:

$$\frac{\partial^2 \bar{h}}{\partial r^2} + \frac{1}{r} \frac{\partial \bar{h}}{\partial r} = \frac{S}{T} p \bar{h} - \frac{S}{T} h_0 - \frac{\bar{N}}{T} + \frac{\bar{h} - \bar{h}_{top}}{c_{top} T} + \frac{\bar{h} - \bar{h}_{bot}}{c_{bot} T} \quad (7)$$

Boundary conditions (2) and (3) are transformed into, respectively:

$$r_w \frac{\partial \bar{h}(r_w)}{\partial r} = \frac{\bar{Q}}{2\pi T} \quad (8)$$

$$\bar{h}(r_{out}) = \bar{h}_{out} \quad (9)$$

10.2.3. General solution

Both the steady-state and the Laplace transformed transient-state problem are described by an ordinary differential equation of the form:

$$\frac{d^2 y}{dr^2} + \frac{1}{r} \frac{dy}{dr} = ay - b \quad (10)$$

subject to the following boundary conditions:

$$r_w \frac{dy(r_w)}{dr} = q \quad (11)$$

$$y(r_{out}) = y_{out} \quad (12)$$

If transient flow is considered, then:

$$y = \bar{h}; a = \frac{S}{T} p + \frac{1}{c_{top} T} + \frac{1}{c_{bot} T}; b = \frac{S}{T} h_0 + \frac{\bar{N}}{T} + \frac{\bar{h}_{top}}{c_{top} T} + \frac{\bar{h}_{bot}}{c_{bot} T}; q = \frac{\bar{Q}}{2\pi T}; y_{out} = \bar{h}_{out} \quad (13)$$

If steady flow is considered, then:

$$y = h; a = \frac{1}{c_{top} T} + \frac{1}{c_{bot} T}; b = \frac{N}{T} + \frac{h_{top}}{c_{top} T} + \frac{h_{bot}}{c_{bot} T}; q = \frac{Q}{2\pi T}; y_{out} = h_{out} \quad (14)$$

The general solution of (10) is:

$$y = \alpha f(r) + \beta g(r) + z(r) = \begin{cases} \alpha \ln(r) + \beta - \frac{br^2}{4} & (a = 0) \\ \alpha I_0(r\sqrt{a}) + \beta K_0(r\sqrt{a}) + \frac{b}{a} & (a \neq 0) \end{cases} \quad (15)$$

with α and β arbitrary constants. I_0 and K_0 are the zero-order modified Bessel functions of the first and second kind, respectively. Note that $a = 0$ if flow is steady and if the aquifer is confined. In this case, $b = N/T$.

10.2.4. Particular solutions

A particular solution is found by introducing (15) into boundary conditions (11) and (12), which gives the following general expressions for constants α and β , respectively:

$$\alpha = \frac{[y_{out} - z(r_{out})]r_w g'(r_w) + [r_w z'(r_w) - q]g(r_{out})}{r_w g'(r_w)f(r_{out}) - r_w f'(r_w)g(r_{out})} \quad (16)$$

$$\beta = \frac{-[y_{out} - z(r_{out})]r_w f'(r_w) - [r_w z'(r_w) - q]f(r_{out})}{r_w g'(r_w)f(r_{out}) - r_w f'(r_w)g(r_{out})} \quad (17)$$

where f' , g' , and z' are the derivatives of f , g , and z , respectively, with respect to r .

If $a = 0$, then the constants are:

$$\alpha = q + \frac{br_w^2}{2} \quad (18)$$

$$\beta = y_{out} + \frac{br_{out}^2}{4} - \alpha \ln(r_{out}) \quad (19)$$

and the solution simplifies to:

$$h(r) = h_{out} + \left[\frac{Nr_w^2}{2T} + \frac{Q}{2\pi T} \right] \ln\left(\frac{r}{r_{out}}\right) + \frac{N}{4T}(r_{out}^2 - r^2) \quad (20)$$

Solution (20) is found, for instance, in Strack (1989) and Haitjema (1995).

Recall that in this case, flow is steady and the aquifer is confined. If $N = 0$ and h according to (20) is subtracted from h_{out} , then the Thiem (1870; 1906) equation is obtained:

$$s(r) = \frac{Q}{2\pi T} \ln\left(\frac{r_{out}}{r}\right) \quad (21)$$

If $Q = 0$ and $r_w = 0$, then equation (20) simplifies to the solution for a circular infiltration area (Haitjema, 1995; Strack, 1989):

$$h(r) = h_{out} + \frac{N}{4T}(r_{out}^2 - r^2) \quad (22)$$

If $r_w = 0$, and equation (20) is subtracted from h_{out} , the well-known solution for a well in a circular infiltration pond with radius r_{out} is obtained (Haitjema, 1995; Strack, 1989):

$$s(r) = \frac{Q}{2\pi T} \ln\left(\frac{r_{out}}{r}\right) - \frac{N}{4T}(r_{out}^2 - r^2) \quad (23)$$

If $a \neq 0$, the constants are:

$$\alpha = \frac{\left[y_{out} - \frac{b}{a}\right](r_w \sqrt{a})K_1(r_w \sqrt{a}) + qK_0(r_{out} \sqrt{a})}{(r_w \sqrt{a})[I_1(r_w \sqrt{a})K_0(r_{out} \sqrt{a}) + K_1(r_w \sqrt{a})I_0(r_{out} \sqrt{a})]} \quad (24)$$

$$\beta = \frac{\left[y_{out} - \frac{b}{a}\right](r_w \sqrt{a})I_1(r_w \sqrt{a}) - qI_0(r_{out} \sqrt{a})}{(r_w \sqrt{a})[I_1(r_w \sqrt{a})K_0(r_{out} \sqrt{a}) + K_1(r_w \sqrt{a})I_0(r_{out} \sqrt{a})]} \quad (25)$$

with I_1 and K_1 the first order modified Bessel functions of the first and second kind, respectively.

If $r_w \rightarrow 0$, expressions (24) and (25) reduce to, respectively:

$$\alpha = \frac{y_{out} - \frac{b}{a} + qK_0(r_{out}\sqrt{a})}{I_0(r_{out}\sqrt{a})} \quad (26)$$

$$\beta = -q \quad (27)$$

If $r_{out} \rightarrow \infty$, expressions (24) and (25) reduce to, respectively:

$$\alpha = 0 \quad (28)$$

$$\beta = \frac{-q}{(r_w\sqrt{a})K_1(r_w\sqrt{a})} \quad (29)$$

If $r_{out} \rightarrow \infty$ and $r_w \rightarrow 0$, then $\beta = -q$.

In general, the steady-state solution is:

$$h(r) = \alpha I_0(r\sqrt{a}) + \beta K_0(r\sqrt{a}) + \frac{b}{a} \quad (30)$$

with a , b , q , and y_{out} given by (14).

If $r_{out} \rightarrow \infty$ and the lower boundary is confined, i.e. $c_{bot} \rightarrow \infty$, the steady-state solution is:

$$h(r) = h_{top} - \frac{Q}{2\pi T} \frac{K_0\left(r\sqrt{\frac{1}{c_{top}T}}\right)}{\left(r_w\sqrt{\frac{1}{c_{top}T}}\right)K_0\left(r_w\sqrt{\frac{1}{c_{top}T}}\right)} + Nc_{top} \quad (31)$$

If $h_{top} = 0$ and $Q = 0$, then equation (31) simplifies to the solution for the head in an unbounded aquifer recharged by uniform infiltration characterized by flux N , and discharged by uniform drainage characterized by level $h_{top} = 0$ and resistance c_{top} (Ernst, 1971):

$$h(r) = Nc_{top} \quad (32)$$

If there is no infiltration, i.e. $N = 0$, and equation (31) is subtracted from h_{top} , the solution for radial flow to a well with finite radius r_w in a leaky aquifer is obtained (Bruggeman, 1999):

$$s(r) = \frac{Q}{2\pi T} \frac{K_0\left(r\sqrt{\frac{1}{c_{top}T}}\right)}{\left(r_w\sqrt{\frac{1}{c_{top}T}}\right)K_0\left(r_w\sqrt{\frac{1}{c_{top}T}}\right)} \quad (33)$$

If $r_w \rightarrow 0$, then solution (33) simplifies to the de Glee equation (de Glee, 1930; Jacob, 1946):

$$s(r) = \frac{Q}{2\pi T} K_0\left(r\sqrt{\frac{1}{c_{top}T}}\right) \quad (34)$$

The generalized steady-state solution for a pumping well in an aquifer with leaky top and bottom layer is:

$$h(r) = \frac{c_{bot}h_{top} + c_{top}h_{bot}}{c_{top} + c_{bot}} - \frac{Q}{2\pi T} K_0 \left(r \sqrt{\frac{c_{top} + c_{bot}}{c_{top}c_{bot}T}} \right) \quad (35)$$

In general, the transient-state solution in the Laplace domain is:

$$\bar{h}(r, p) = \alpha I_0(r\sqrt{a}) + \beta K_0(r\sqrt{a}) + \frac{b}{a} \quad (36)$$

with a, b, q , and y_{out} given by (13). This solution may be numerically inverted by applying the Stehfest (1970) algorithm.

If $r_w \rightarrow 0$, $r_{out} \rightarrow \infty$, and $N = 0$, and if the system is confined, i.e. $c_{top} = c_{bot} = \infty$, the following solution in Laplace space is obtained:

$$\bar{h}(r, p) = \frac{h_0}{p} - \frac{Q}{2\pi T p} K_0 \left(r \sqrt{\frac{S}{T}} p \right) \quad (37)$$

Inverting (37) analytically (Hantush, 1964; Loaiciga, 2010) gives the well-known Theis (1935) equation if h is subtracted from h_0 :

$$s(r, t) = \frac{Q}{4\pi T} W \left(\frac{r^2 S}{4tT} \right) \quad (38)$$

In (38), function W is the Theis well function (Theis, 1935):

$$W(u) = \int_u^\infty \frac{e^{-x}}{x} dx \quad (39)$$

If $r_w \rightarrow 0$, $r_{out} \rightarrow \infty$, $N = 0$, and if the system is leaky with $h_0 = h_{top}$ and $c_{bot} \rightarrow \infty$, the following solution in Laplace space is obtained:

$$\bar{h}(r, p) = \frac{h_0}{p} - \frac{Q}{2\pi T p} K_0 \left(r \sqrt{\frac{S}{T}} p + \frac{1}{c_{top}T} \right) \quad (40)$$

It is possible to invert equation (40) analytically (Hantush, 1964), which gives the solution by Hantush and Jacob (1955) if h is subtracted from h_0 :

$$s(r, t) = \frac{Q}{4\pi T} W \left(\frac{r^2 S}{4tT}, \frac{r}{\sqrt{c_{top}T}} \right) \quad (41)$$

In (41), function W is the Hantush well function (Hantush & Jacob, 1955):

$$W(u, v) = \int_u^\infty \frac{e^{-x-v^2/4x}}{x} dx \quad (42)$$

10.2.5. Radial discharge and storage change

The radial discharge $Q^r(r, t)$ [L^3/T] is the amount of water per unit of time that flows horizontally through the cylindrical surface with radius r , at time t :

$$Q^r(r, t) = 2\pi Tr \frac{\partial h}{\partial r} \quad (43)$$

In case of steady flow, and if the aquifer is leaky, i.e. $a \neq 0$, general solution (30) is used to evaluate expression (43):

$$Q^r(r) = 2\pi Tr\sqrt{a}[\alpha I_1(r\sqrt{a}) - \beta K_1(r\sqrt{a})] \quad (44)$$

with α and β according to (24) and (25), respectively, and a, b, q , and y_{out} given by (14). If the aquifer is confined, then $a = 0$, and equation (44) simplifies to:

$$Q^r(r) = Q - N\pi(r^2 - r_w^2) \quad (45)$$

In case of transient flow, the Laplace transform of (43) is evaluated using general solution (36):

$$\bar{Q}^r(r, p) = 2\pi Tr \frac{\partial \bar{h}}{\partial r} = 2\pi Tr\sqrt{a}[\alpha I_1(r\sqrt{a}) - \beta K_1(r\sqrt{a})] \quad (46)$$

with α and β according to (24) and (25), respectively, and a, b, q , and y_{out} given by (13). Expression (46) may be inverted numerically using the Stehfest (1970) algorithm.

In case of transient flow, the storage change $Q^s(r_1, r_2, t)$ is defined as the amount of water per unit of time released by or stored in the ring determined by radii r_1 and r_2 at time t :

$$Q^s(r_1, r_2, t) = -2\pi S \int_{r_1}^{r_2} \frac{\partial h}{\partial t} r dr \quad (47)$$

The Laplace transform of (47) is:

$$\bar{Q}^s(r_1, r_2, p) = -2\pi S \int_{r_1}^{r_2} \frac{\partial \bar{h}}{\partial t} r dr = -2\pi S \int_{r_1}^{r_2} (p\bar{h} - h_0) r dr \quad (48)$$

Introducing (36) into (48):

$$\bar{Q}^s(r_1, r_2, p) = -2\pi S \left[\frac{rp}{\sqrt{a}} [\alpha I_1(r\sqrt{a}) - \beta K_1(r\sqrt{a})] + \left(\frac{b}{a} p - h_0 \right) \frac{r^2}{2} \right]_{r_1}^{r_2} \quad (49)$$

with α and β according to (24) and (25), respectively, and a, b, q , and y_{out} given by (13). Expression (49) may be inverted numerically using the Stehfest (1970) algorithm.

Total storage change dV/dt is equal to $Q^s(r_w, r_{out}, t)$. In case of the Theis (1935) model, this simplifies to Q/p , which is inverted to Q . To find the total storage change in case of the Hantush and Jacob (1955) model, expression (49) is evaluated for $r_1 \rightarrow 0$ and $r_2 \rightarrow \infty$. This simplifies to $Q/[p + 1/(Sc)]$, which is inverted to (Hantush, 1964):

$$\frac{dV}{dt} = Q^s(0, \infty, t) = Q e^{-t/Sc} \quad (50)$$

10.2.6. The Ernst model

Now the problem of one-dimensional axisymmetric flow has been stated in general, we are able to present the steady-state model of Ernst (1971), and to develop its transient-state version. The Ernst (1971) model simulates axisymmetric flow to a pumping well fully penetrating an aquifer with constant transmissivity, uniform areal recharge, and uniform areal drainage. Before the pumping starts, the initial head h_0 in the aquifer equals Nc according to (32), with $c_{top} = c$.

The Ernst (1971) model combines the solution of two one-dimensional axisymmetric models. The first model calculates drawdown in the proximal zone around the well without drainage ($r \leq r_d$). It simulates flow in a bounded homogeneous aquifer with constant thickness and infiltration at the top. The second model calculates drawdown in the distal zone where drainage is still active ($r \geq r_d$). It simulates flow in a homogeneous leaky aquifer with constant thickness and infiltration at the top.

The inner boundary condition in the first model defines a constant discharge equal to the pumping rate at the well, whereas the outer boundary is a constant head equal to the drainage level. The latter is set to zero; hence, the drawdown is equal to the initial head $h_0 = Nc$. This outer boundary coincides with the inner boundary of the second model. Therefore, drawdown in both models must be the same at this boundary, and continuity of flow requires the inflow to the first model must be equal to the outflow from the second model. The latter determines the constant flux at the inner boundary of the second model. The outer boundary condition in the second model is a constant head at an infinite large distance.

The solution for the drawdown in the proximal zone is found by subtracting (23) from the initial head, whereas the solution for the drawdown in the distal zone is given by (33). In equation (23), r_{out} must be replaced by r_d . In equation (33), r_w is substituted by r_d , and Q by $Q^r(r_d)$ according to (45), with $r_w = 0$. Recall that $c_{top} = c$ in both equations. This gives the following solution (Ernst, 1971):

$$\begin{cases} s_1(r) = Nc - \frac{Q}{2\pi T} \ln\left(\frac{r}{r_d}\right) - \frac{N}{4T}(r_d^2 - r^2) & (r \leq r_d) \\ s_2(r) = \frac{(Q - N\pi r_d^2)}{2\pi T} \left(\frac{\text{K}_0\left(\frac{r}{\sqrt{cT}}\right)}{\frac{r_d}{\sqrt{cT}} \text{K}_1\left(\frac{r_d}{\sqrt{cT}}\right)} \right) & (r \geq r_d) \end{cases} \quad (51)$$

At the boundary between the two zones, drawdown equals Nc , so distance r_d is found by solving the equation $s_2(r_d) = Nc$. As explained in Chapter 7, this can be done easily using a standard nonlinear solver available with Matlab or SciPy.

The transient solution is found in the same way. However, in this case, the boundary between both models is time dependent. The Laplace transform of transient head \bar{h}_1 and \bar{h}_2 in the proximal zone without drainage and the distal zone with drainage, respectively, is given by (36). In the proximal zone, $c_{top} = c_{bot} = \infty$, $r_{out} = r_d$, $h_{out} = 0$, and $h_0 = Nc$, whereas in the distal zone, $c_{bot} = \infty$, $c_{top} = c$, $r_w = r_d$, $h_{top} = h_{out} = 0$, and $h_0 = Nc$. Using (13), the exact solution in Laplace space is:

$$\begin{cases} \bar{h}_1(r, p) = \alpha_1 I_0(r\sqrt{a_1}) + \beta_1 K_0(r\sqrt{a_1}) + \frac{Nc}{p} \left(1 + \frac{1}{Scp}\right) & (r \leq r_d) \\ \bar{h}_2(r, p) = \beta_2 K_0(r\sqrt{a_2}) + \frac{Nc}{p} & (r \geq r_d) \end{cases} \quad (52)$$

with $a_1 = \frac{S}{T}p$ and $a_2 = \frac{S}{T}p + \frac{1}{cT}$. Recall that in the transient case, the boundary r_d between the proximal and the distal zone is time-dependent. However, it is not transformed, as radial distance r is not transformed either. A more substantiated explanation why it is justified to use a fixed two-zone model for each time t is given in Chapter 7.

It is assumed $r_w \rightarrow 0$ and $r_{out} \rightarrow \infty$, hence, constants α_1 and β_1 are given by (26) and (27), respectively, and constant β_2 by (29):

$$\alpha_1 = \frac{-\frac{Nc}{p} - \frac{N}{Sp^2} + \frac{Q}{2\pi T p} K_0(r_d \sqrt{a_1})}{I_0(r_d \sqrt{a_1})} \quad (53)$$

$$\beta_1 = \frac{-Q}{2\pi T p} \quad (54)$$

$$\beta_2 = \frac{-\bar{Q}_1^r(r_d, p)}{2\pi T (r_d \sqrt{a_2}) K_1(r_d \sqrt{a_2})} \quad (55)$$

Note that $\alpha_2 = 0$, according to (28). The pumping rate in (29) is replaced by the inflow $\bar{Q}_1^r(r_d, p)$ at the outer boundary of the proximal zone, which is given by (46):

$$\bar{Q}_1^r(r_d, p) = 2\pi T r_d \frac{\partial \bar{h}(r_d)}{\partial r} = 2\pi T r_d \sqrt{a_1} [\alpha_1 I_1(r_d \sqrt{a_1}) - \beta_1 K_1(r_d \sqrt{a_1})] \quad (56)$$

The unknown radius r_d is found by solving $h_2(r_d, t) = 0$, using a nonlinear solver available with Matlab or Scipy, which is discussed in more detail in Chapter 7. To find the zero head h_2 at distance r_d , the second equation of (52) is used and numerically inverted using the Stehfest (1970) algorithm. The nonlinear solver finds the value of r_d that corresponds to the root of this numerically inverted equation. Note that the logarithm of r_d is evaluated to avoid negative values.

Once r_d is found, drawdown s_1 and s_2 for the proximal and distal zone are found by numerically inverting the respective equations of (52), and by subtracting the calculated head h from the initial head $h_0 = Nc$. As r_d is time-dependent, this routine must be applied for each time t .

Total storage change dV/dt at a given time t is found by numerically inverting $\bar{Q}^s(0, \infty, p) = \bar{Q}_1^s(0, r_d, p) + \bar{Q}_2^s(r_d, \infty, p)$. Using equation (49) and simplifying the outcome gives:

$$\bar{Q}^s(0, \infty, p) = \frac{Q - \pi N r_d^2}{p} + 2\pi S p r_d \left[\frac{-\alpha_1}{\sqrt{a_1}} I_1(r_d \sqrt{a_1}) + \frac{\beta_1}{\sqrt{a_1}} K_1(r_d \sqrt{a_1}) - \frac{\beta_2}{\sqrt{a_2}} K_1(r_d \sqrt{a_2}) \right] \quad (57)$$

If $t \rightarrow 0$, then $p \rightarrow \infty$ and $r_d \rightarrow 0$, and total storage change approximates Q . If $t \rightarrow \infty$, then $p \rightarrow 0$, and total storage change is negligibly small.

10.3. Estimating the radius of influence

This section discusses several formulas for estimating the radius of influence. First, the empirical Sichardt formula (Kyrieleis & Sichardt, 1930) is discussed, which is used in combination with the equations of Dupuit (1863) and Thiem (1870; 1906). In case of a specified-discharge well, the unknown drawdown at the well-face and the unknown radius of influence are determined by solving the system of these two equations, which does not always yield a solution. In the subsequent sections, more reliable formulas to calculate the radius of influence are derived from the de Glee (1930) and the Theis (1935) solutions. Comparing these formulas with the Sichardt formula show that the latter mostly underestimates the radius of influence. Using the de Glee (1930) and the Theis (1935) solution, it is also possible to determine a maximum value for the radius of influence without

knowing the aquifer transmissivity. The Hantush and Jacob (1955) model is discussed to show the relation between the models of de Glee (1930) and Theis (1935).

The Ernst (1971) model is similar to the de Glee (1930) model except for the top boundary condition, which is not leaky but draining. If the drainage resistance is zero, then the asymptotic solution shows that the radius of influence is obtained by balancing pumping and infiltration rate. As this formula is contested in the hydrogeological literature (Bredehoeft, 2002; Brown, 1963), a MODFLOW (Harbaugh, 2005) model is constructed to validate the Ernst (1971) model, and in particular, its asymptotic solution. The transient-state solution of the Ernst (1971) model derived in previous section 10.2.6 is also discussed in detail, and it is used to synthesize the different solutions discussed in this section. Moreover, it reveals some useful rules of thumb that may help groundwater practitioners to choose between the different formulas presented here for estimating the radius of influence.

10.3.1. The Sichardt formula

As already mentioned in the introduction, the Sichardt formula first appears in a document written in German by Kyrieleis and Sichardt (1930), who present it as empirically derived by Sichardt, yet not being published, only valid for steady state, and formulated as $R = 3000sK^{1/2}$, with s the drawdown in m, K the hydraulic conductivity in m/s, and R the radius of influence in m. Kyrieleis and Sichardt (1930) do not provide further explanation. To be consistent with other solutions presented below, we reformulate the formula with K in m/d. As drawdown s is a function of radial distance r (m) to the center of the well, we explicitly indicate that drawdown at the well-face is meant in the Sichardt formula (Kyrieleis & Sichardt, 1930):

$$R = \frac{3000}{\sqrt{86400}} s(r_w) \sqrt{K} = 10.206 s(r_w) \sqrt{K} \quad (58)$$

with r_w (m) the well-radius. To simulate the cone of depression due to pumping at constant rate Q (m^3/d), formula (58) is introduced into the equation for steady well-flow in a homogeneous unconfined aquifer (Houben, 2015; VMM, 2019, 2020; Willems et al., 2009). The equation that takes into account the head-dependence of the aquifer thickness is (Dupuit, 1863):

$$s(r) = h_0 \left(1 - \sqrt{1 + \frac{Q}{\pi K h_0^2} \ln \left(\frac{r}{R} \right)} \right) \quad (59)$$

with h_0 (m) the constant initial head, which defines the saturated thickness of the aquifer before the extraction starts. Since drawdown is positive in Sichardt's formula (58), pumping rate Q in (59) is positive. Figure 1 shows a schematic of the Dupuit (1863) model in which distance R is calculated using Sichardt's formula.

If drawdown is small with respect to the saturated thickness, the following series expansion may be applied to (59): $\sqrt{1-x} \rightarrow \left(1 - \frac{x}{2}\right)$ if $x \rightarrow 0$. If $x < 0.2$ is taken, then drawdown must be smaller than 10% of the initial saturated thickness. Applying this approximation, the well-known Thiem (1870; 1906) equation for steady well-flow in a homogeneous confined aquifer is obtained:

$$s(r) = \frac{Q}{2\pi K D} \ln \left(\frac{R}{r} \right) \quad (60)$$

In (60), it is assumed the saturated thickness is constant and equal to D (m). In practice, the initial head h_0 at the well is taken. Note that distance R according to Sichardt's formula (58) sometimes is

defined as the distance to the well face, in which case r_w must be subtracted from R . At distance R , a constant-head boundary is defined in (59) and (60). Since drawdown is zero at R , this distance is the radius of influence according to the Dupuit and the Thiem formulas (59) and (60), respectively.

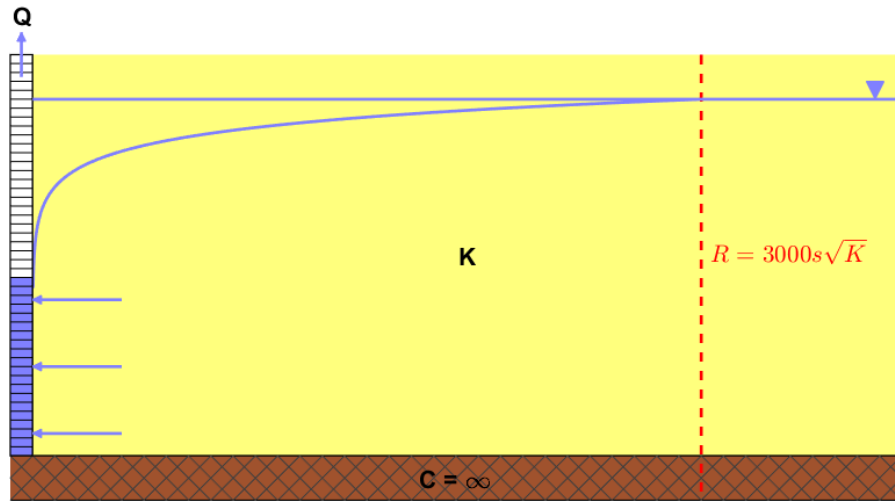


Figure 1. Schematic of the Dupuit (1863) model for steady axisymmetric flow to a well in an unconfined aquifer. The well extracts water from the aquifer at constant rate Q . The horizontal conductivity of the aquifer is K ; the lower boundary of the aquifer is impervious. The vertical flow component is neglected. A constant head is defined at the outer boundary at distance R . If the Sichardt formula (Kryieleis & Sichardt, 1930) is used to estimate the radius of influence, then distance R is set to $3000s\sqrt{K}$, with s the drawdown in the well. See text for definitions.

Figure 2 shows relative drawdown s/h_0 as a function of relative distance r/R for different values of dimensionless discharge $Q/(\pi K h_0^2)$. Both the Dupuit and the Thiem equation are plotted. It is seen that the latter approximates the former very well if $s/h_0 < 0.1$, which confirms the rule of thumb that drawdown must be smaller than 10% of the initial saturated thickness. It is also seen that the Dupuit equation (59) does not give a real solution if $s/h_0 > 1$, which indicates the pumping well goes dry. The Thiem equation (60) always gives a real solution, as a constant saturated thickness is assumed. However, the latter clearly underestimates the drawdown if $s/h_0 > 0.1$. The ramifications of using a linear solution such as the Thiem model instead of a nonlinear solution such as the Dupuit model to assess the sustainability of a groundwater extraction is discussed exhaustively by Louwyck et al. (2023) and in the next Chapter 11.

According to Houben (2015), the Sichardt formula (58) is valid only for unconfined gravelly aquifers, and drawdown according to (59) and (60) is relatively insensitive to the estimated radius of influence R as it occurs in a logarithmic term. Therefore, a roughly estimated value from the dimensionally inconsistent Sichardt equation (58) will not lead to a significant error when applied to optimize well efficiency. Desens and Houben (2022) verify the Sichardt formula (58) against the Theis (1935) solution, and conclude it is optimally applied to sandy to gravelly aquifers with porosities around 15% and thickness about 15 m. To broaden its range of application, Desens and Houben (2022) suggest to use a correction factor based on the Cooper and Jacob (1946) approximation of the Theis (1935) equation. Basically, this correction factor transforms the Sichardt formula (58) into the well-known equation to estimate the radius of influence using the aquifer diffusivity (Bear, 1972). This equation is presented in section 10.3.3 about the Theis (1935) model.

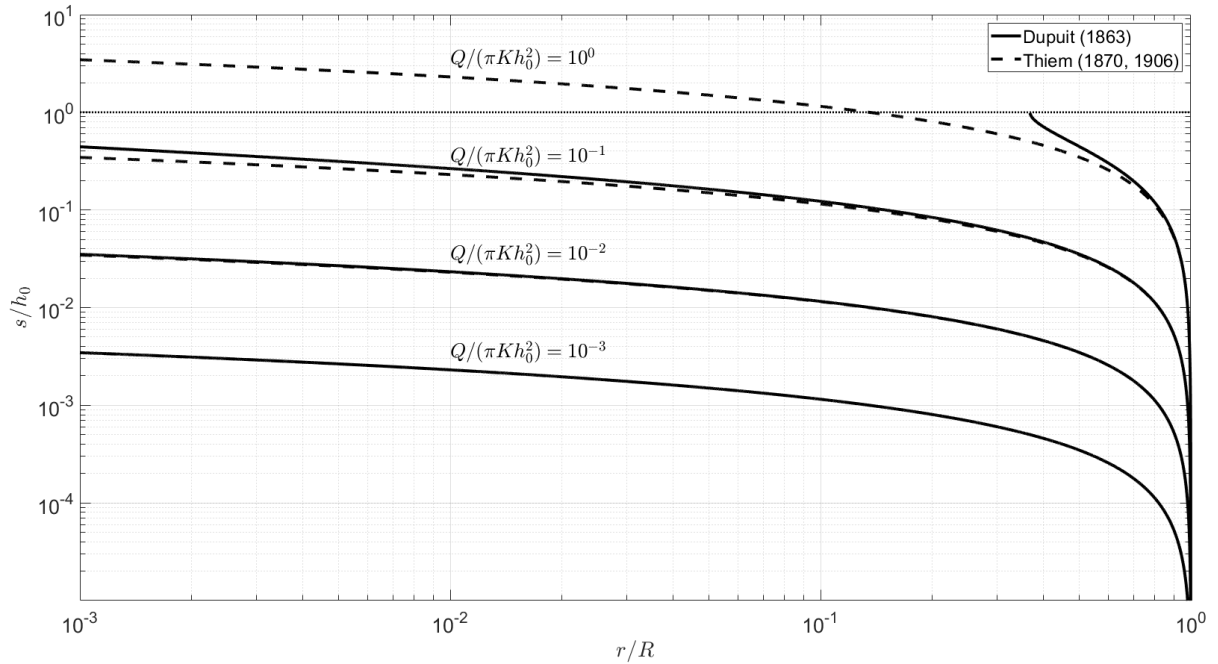


Figure 2. Relative drawdown s/h_0 versus relative distance r/R for different values of dimensionless pumping rate according to the Dupuit (1863) and the Thiem (1870; 1906) equation, with s the drawdown, h_0 the initial head, r the radial distance, R the distance of the outer model boundary at which drawdown is zero, K the aquifer conductivity, and Q the constant pumping rate of the well. See text for definitions. If relative drawdown is larger than 1, the pumping well goes dry, which is indicated by the horizontal dotted line. The Dupuit equation does not give a real solution when this is the case, while the Thiem equation does, as it is linear. Both solutions are virtually the same if relative drawdown is smaller than 0.1.

In discussing the use of the Sichardt formula (58) with geotechnical engineers, it was concluded the formula mainly serves as a rule of thumb to estimate the initial pumping rate of a dewatering well. In this case, the dewatering requires a lowering of the water table; hence, drawdown at the well face is known, and the radius of influence is calculated using Sichardt's formula (58). Introducing the obtained radius of influence into Dupuit's equation (59) gives an estimate of the unknown discharge. Some authors recommend the use of the formula only during the first 5 days of the dewatering (Janssen, 2003; VMM, 2019). This is in contrast with the assumption of steady state mentioned in the original work of Kyrieleis and Sichardt (1930), as initially, water is exclusively removed from aquifer storage (Bredehoeft et al., 1982). As already mentioned, the transient version of the radius of influence derived from the Theis (1935) solution is discussed in section 10.3.3, and it is compared to the Sichardt formula (58).

Although there exist models that are more reliable to quantify the size of a dewatering construction (El-Hames, 2020; Lyu et al., 2021; Wang et al., 2019; Wu et al., 2020; Zeng et al., 2019, 2021; Zhang et al., 2021; Zheng et al., 2021), discussing this matter is out of scope. Our concern lies with the use of the Sichardt formula (58) in assessing the environmental impact of permanent extractions. In this case, the discharge is known, and the cone of depression must be estimated. Mathematically, this comes down to solving the system of two equations, consisting of the Sichardt formula (58) and the Dupuit equation (59) for $r = r_w$, to find the two unknown variables: drawdown at the well-face and the radius of influence. For the sake of simplicity, we replace the Dupuit equation (59) by the Thiem equation (60). Multiplying each side of (60) by $(10.206 \sqrt{K}/r_w)$, and dividing both sides of the Sichardt formula (58) by r_w , gives:

$$\begin{cases} s^* = R^* \\ s^* = Q^* \ln(R^*) \end{cases} \quad (61)$$

with dimensionless drawdown $s^* = 10.206 s(r_w) \sqrt{K} / r_w$, dimensionless discharge $Q^* = 10.206 Q / (2\pi \sqrt{K} D r_w)$, and dimensionless radius of influence $R^* = R / r_w$. If R in Sichardt's formula (58) is interpreted as the distance to the well-face, then the following system of equations must be solved:

$$\begin{cases} s^* = R^* - 1 \\ s^* = Q^* \ln(R^*) \end{cases} \quad (62)$$

Both (61) and (62) are solved by writing R^* as a function of s^* using the first equation, and introducing the result into the second equation, which gives $s^* = Q^* \ln(s^*)$ and $s^* = Q^* \ln(s^* + 1)$, respectively.

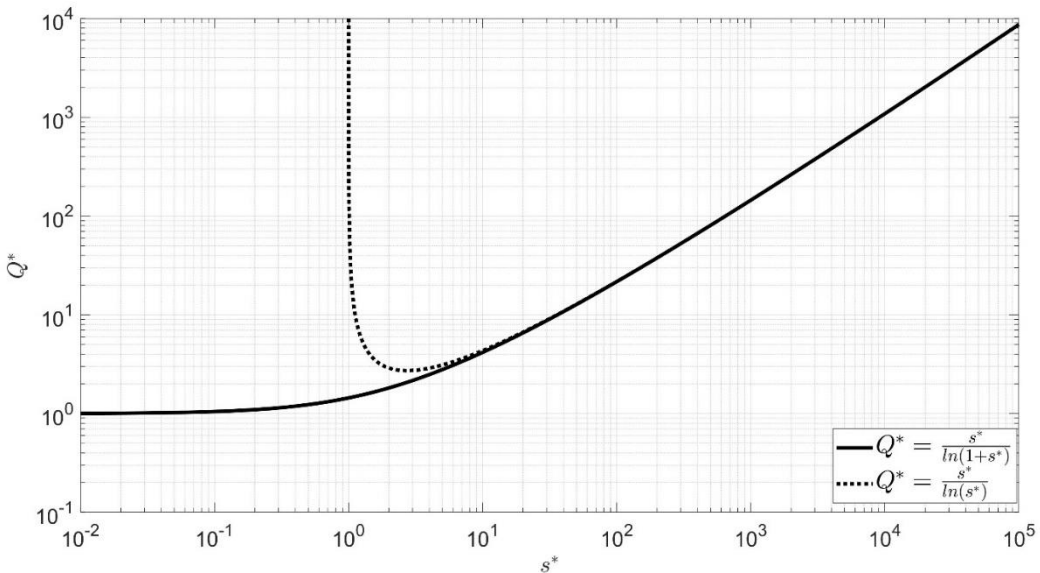


Figure 3. Dimensionless discharge Q^* as a function of dimensionless drawdown s^* resulting from combining the Sichardt formula (Kyrieleis & Sichardt, 1930) and the Thiem (1870; 1906) equation. The dimensionless parameters are defined in the text. Solid and dotted lines give the solution in which the radius of influence according to the Sichardt formula equals the distance to the well-face and to the center of the well, respectively.

Figure 3 shows both solutions. In case of (61), radius of influence R cannot be smaller than the well radius r_w , hence, dimensionless drawdown (dotted line) cannot be smaller than 1, as it equals the dimensionless radius of influence. The minimum of the curve is found by solving $dQ^*/ds^* = 0$, which gives $Q^* = 1/e$. Hence, there is no solution if dimensionless discharge is smaller than $1/e$, exactly one solution if $Q^* = 1/e$, and two solutions otherwise. In case of (62), dimensionless discharge virtually equals 1 when dimensionless drawdown (solid line) is smaller than 0.1, as $\ln(x + 1) \rightarrow x$ if $x \rightarrow 0$. There is no solution if dimensionless discharge is smaller than 1.

The Thiem equation (60) is a particular solution to differential equation (1) governing one-dimensional radial flow, which combines Darcy's law and the law of mass conservation (Bruggeman, 1999), two fundamental laws in physics. It is also required to formulate the finite-difference approximation of the two-dimensional radial flow equation (Louwyck et al., 2012). Since it expresses the fundamental laws of groundwater flow, the Sichardt formula must be consistent with the Thiem equation. However, Figure 3 shows that small yet realistic pumping rates do not yield a solution. Therefore, we strongly discourage its use. The next two sections present two valid alternatives, based on the solutions of de Glee (1930) and Theis (1935). The former solves the differential equation for steady flow, the latter for transient flow.

10.3.2. The de Glee Equation

Although examining the historical context in which the Sichardt formula was developed and applied is out of scope, it is not unthinkable German engineers at that time were struggling with the constant-head boundary condition that is required to apply the equations of Dupuit (59) and Thiem (60). According to Zhai et al. (2021), this constant-head boundary condition has been misinterpreted indeed by several authors. Nowadays, we understand the cone of depression is mathematically determined by the change of aquifer storage and the boundary conditions, but these principles were not known until they were stated first by Theis (1940).

In the Netherlands, Kooper (1914) solved the problem by assuming a constant-head resistance layer on top of the aquifer (Hemker, 2000). This leaky aquifer solution is known as the de Glee formula, as de Glee applied Kooper's formula in 1930 in his dissertation (de Glee, 1930) to evaluate field data, and he also extended it to a partially penetrating well (Hemker, 2000). In the English literature, the same solution was published by Jacob (1946):

$$s(r) = \frac{Q}{2\pi K D} K_0 \left(r \sqrt{\frac{1}{c K D}} \right) \quad (63)$$

with c (d) the resistance of the constant-head layer. Function K_0 is the zero order modified Bessel function of the second kind. This function is available with SciPy, R, Matlab, and Excel. The underlying steady state model assumes the leaky aquifer has an impermeable base and is homogeneous with constant saturated thickness D . The well is fully penetrating, an assumption which is justified when evaluating the extent of the cone of depression, as the effect of a partially penetrating well is observed only in a small zone around the well (Bakker, 2001). The system is linear, hence, drawdown according to (63) may be superimposed on the initial heads, which are assumed steady. Initial flow in the aquifer is allowed. In section 10.2, it is explained how equation (63) is derived, which is the same as equation (34) with $T = K D$ and $c_{top} = c$.

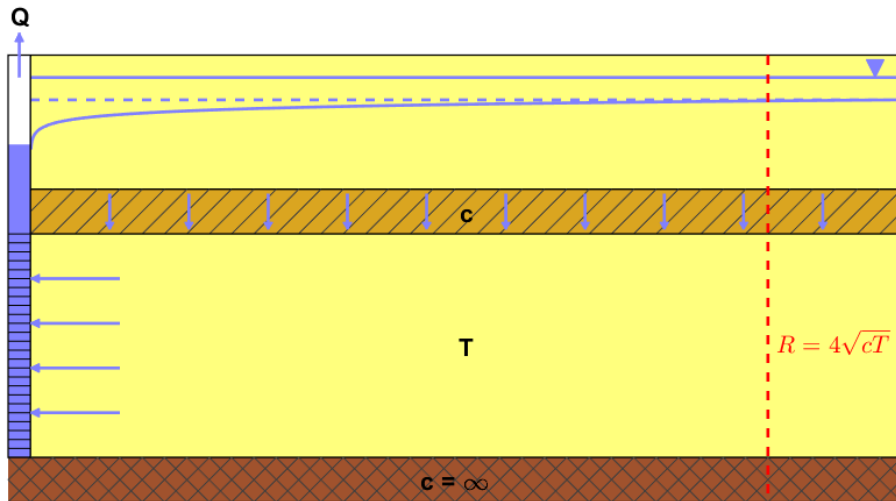


Figure 4. Schematic of the de Glee (1930) model for steady axisymmetric flow to a fully penetrating well in a leaky aquifer. The well extracts water from the aquifer at constant rate Q . The vertical flow component is neglected. The constant transmissivity of the aquifer is T ; the lower boundary of the aquifer is impervious, while the upper boundary is leaky. The latter is mostly interpreted as an aquitard with constant resistance c , and an overlying aquifer with constant head. Radius of influence R at which drawdown is negligibly small, may be estimated as 4 times the leakage factor. See text for definitions.

The upper boundary condition may be interpreted as an overlying homogeneous aquitard characterized by resistance c , in which a uniform head occurs that supplies the leakage (de Glee,

1930; Jacob, 1946). This is the case when the aquitard is continuously being replenished by rainfall, a condition that is found in polder areas of the Netherlands and Flanders. In a more common interpretation, the aquitard is in turn overlain by an aquifer with constant head (Jacob, 1946; Neuman & Witherspoon, 1969a) as shown in Figure 4. Flow in the pumped aquifer is strictly horizontal, whereas flow in the aquitard is strictly vertical.

In both interpretations, the extracted groundwater is balanced by the leakage through the overlying aquitard. Hence, the cone of depression covers an area in which the total leakage equals the pumping rate. Mathematically, this area is infinitely large; in practice, the following rule of thumb is applicable (Zhou, 2011):

$$R = 4\sqrt{cKD} \quad (64)$$

where \sqrt{cKD} is called the leakage factor (m). Formula (64) defines a cylindrical zone around the well with radius R in which the leakage is significant. Outside this zone, the vertical flow in the overlying aquitard is negligibly small, hence, drawdown in the pumped layer is also negligibly small. Therefore, R according to (64) may be interpreted as the radius of influence. Mathematically, the outer constant-head boundary is at infinity, which avoids the use of empirical formulas. Moreover, the radius of influence according to (64) has a physical interpretation, which is consistent with the fundamental hydrological principles stated by Theis (1940).

The de Glee equation (63) is related to Thiem's equation (60). As $K_0(x) \rightarrow [-\gamma - \ln(\frac{x}{2})]$ if $x \rightarrow 0$ (Abramowitz & Stegun, 1965), we may approximate (63) as:

$$s(r) = \frac{Q}{2\pi K D} \ln\left(\frac{2e^{-\gamma}\sqrt{cKD}}{r}\right) \quad (65)$$

with γ the Euler constant equal to 0.57721.... Comparing (65) with the Thiem equation (60), it is seen that the radius of influence according to (65) is (De Smedt, 2006):

$$R = 2e^{-\gamma}\sqrt{cKD} = 1.123\sqrt{cKD} \quad (66)$$

However, equation (66) is valid only for small distances and/or large leakage factor; hence, it is safer to use (64). Figure 5 plots dimensionless drawdown $2\pi K D s / Q$ versus dimensionless distance r/\sqrt{cKD} according to exact solution (63) and approximate solution (65). It also displays the radius of influence according to (64) and (66). It is seen that the approximate solution is very close to the exact solution if $r/\sqrt{cKD} < 0.02$.

A less common interpretation of the de Glee solution (63) is well-flow in a phreatic aquifer overlain by a dense network of ditches and canals interacting with the aquifer (Ernst, 1971; Hemker, 1984; Louwyck et al., 2023). This interpretation is valid in humid areas, where these ditches drain the excess of water from rainfall. The extraction of groundwater in the aquifer causes a reduced drainage, or even induces infiltration from the surface water. This interpretation is equivalent to defining a river boundary condition in each cell of the top layer of a MODFLOW model. It is also possible to define a boundary condition that only drains water, equivalent to MODFLOW drains. Definition of MODFLOW river and drain boundary conditions is given in Harbaugh (2005). The analytical solution that considers a drain-only boundary condition was developed by Ernst (1971) and is discussed in section 10.3.5. First, the well-known equation derived by Theis (1935) is discussed, who solved the problem of transient flow to a well in a confined aquifer.

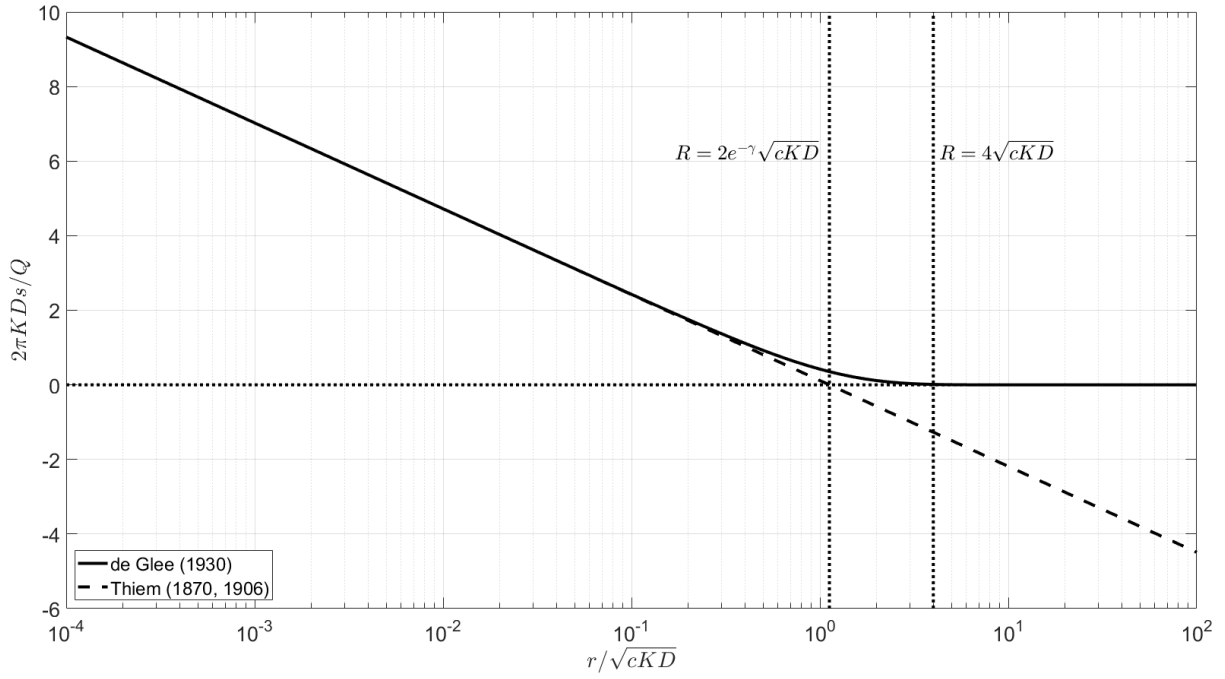


Figure 5. Dimensionless drawdown versus dimensionless distance according to the de Glee (1930) equation (solid line) and the Thiem (1870; 1906) formula (dashed line) with outer boundary at distance R equal to 1.123 times the leakage factor. This distance is indicated by the left vertical dotted line. The right vertical dotted line indicates the radius of influence R equal to 4 times the leakage factor. Variable s is the drawdown, r is the radial distance, KD is the aquifer transmissivity, c is the resistance, Q is the pumping rate, and γ is the Euler constant. The leakage factor is defined as $(cKD)^{1/2}$. See text for definitions.

10.3.3. The Theis equation

We have already mentioned Narasimhan (1998) who states that Weber (1928) made the first successful attempt to analyze non-steady flow towards a well. However, without any notion of aquifer storativity, and hence, without knowing how to mathematically describe the elastic aquifer response, this statement probably should be nuanced. Indeed, the concept of aquifer storativity was not fully understood until 1935, when Theis (1935) developed his well-known equation with the aid of the mathematician Lubin (Bredehoeft, 2008). The Theis (1935) equation is:

$$s(r, t) = \frac{Q}{4\pi K D} W\left(\frac{r^2 S}{4t K D}\right) \quad (67)$$

with t the time in days, and S the storage coefficient, which is dimensionless. Several approaches may be followed to derive (67) (Loàiciga, 2010; Masoodi & Ghanbari, 2012; Perina, 2010). Section 10.2 shows how (67) is derived using the Laplace transform. Equation (67) is the same as equation (38) with $T = KD$.

In the hydrogeological literature, function W is called the Theis' well function; in mathematics, it's called the exponential integral (Abramowitz & Stegun, 1965):

$$W(u) = \int_u^\infty \frac{e^{-x}}{x} dx = -\gamma - \ln(u) - \sum_{n=1}^{\infty} \frac{(-u)^n}{n \cdot n!} \quad (68)$$

Evaluating function W is straightforward using SciPy, R, or Matlab, as they provide a built-in function. We may also apply the well-known Cooper and Jacob (1946) approximation: for small values of u , the infinite summation in the right-hand side of (68) may be omitted, resulting into the following approximation of the Theis equation (67):

$$s(r, t) = \frac{-Q}{2\pi K D} \ln \left(r \sqrt{\frac{e^r S}{4t K D}} \right) \quad (69)$$

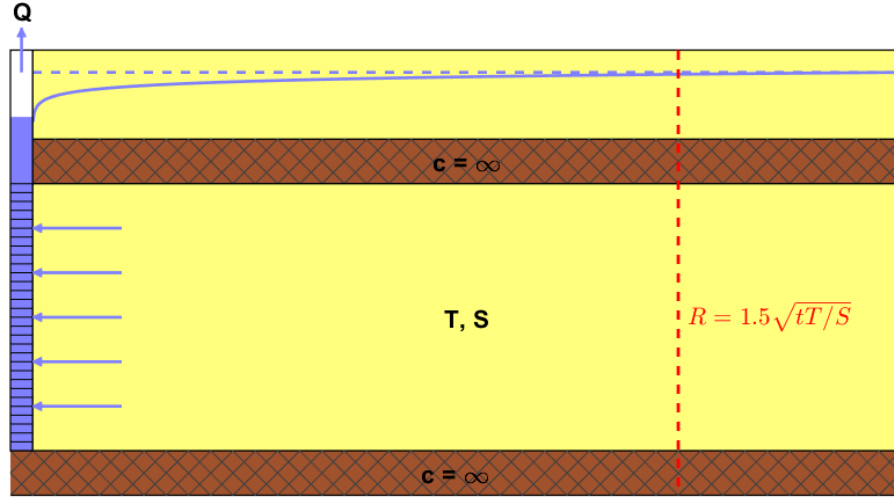


Figure 6. Schematic of the Theis (1935) model for transient axisymmetric flow to a fully penetrating well in a confined aquifer. The well extracts water from the aquifer at constant rate Q . The vertical flow component is neglected. The constant transmissivity of the aquifer is T , the constant storativity is S . Both the lower and the upper boundary of the aquifer are impervious. Radius of influence R at which drawdown is negligibly small, is time-dependent and may be estimated as 1.5 times the square root of diffusivity T/S multiplied by time t . See text for definitions.

Cooper and Jacob (1946) suggest $u < 0.02$, whereas Jacob (1950) proposes $u < 0.05$. Comparing (69) with the Thiem equation (60), the transient radius of influence according to the Theis (1935) is model obtained (Bear, 1972):

$$R(t) = \sqrt{\frac{4t K D}{e^r S}} = 1.499 \sqrt{\frac{t K D}{S}} \quad (70)$$

The Theis (1935) model assumes a fully penetrating well with infinitesimal well radius in a homogeneous confined aquifer, as is shown in Figure 6. As the well is fully penetrating, flow in the aquifer is strictly horizontal. Figure 7 plots dimensionless drawdown $4\pi K D s / Q$ versus dimensionless variable $r^2 S / (4t K D)$ according to exact solution (67) and approximate solution (69), and visually confirms both solutions are virtually the same if $r^2 S / (4t K D) < 0.02$, as suggested by Cooper and Jacob (1946). The radius of influence according to (70) is also displayed. However, Figure 7 shows it may be safer to estimate the radius of influence consistently with equation (64) that is derived for the de Glee (1930) model (Hurst, 1968):

$$R = \sqrt{2 \cdot \frac{4t K D}{S}} = 2.828 \sqrt{\frac{t K D}{S}} \quad (71)$$

Like the Thiem equation (60), the Theis equation (67) may be applied to simulate flow to a well in a phreatic aquifer, if drawdown is relatively small with respect to the aquifer's saturated thickness. In this case, storage coefficient S is replaced by the specific yield S_y , which is also dimensionless. Like the de Glee equation (63), the Theis solution (67) allows superposition, if initial heads are steady.

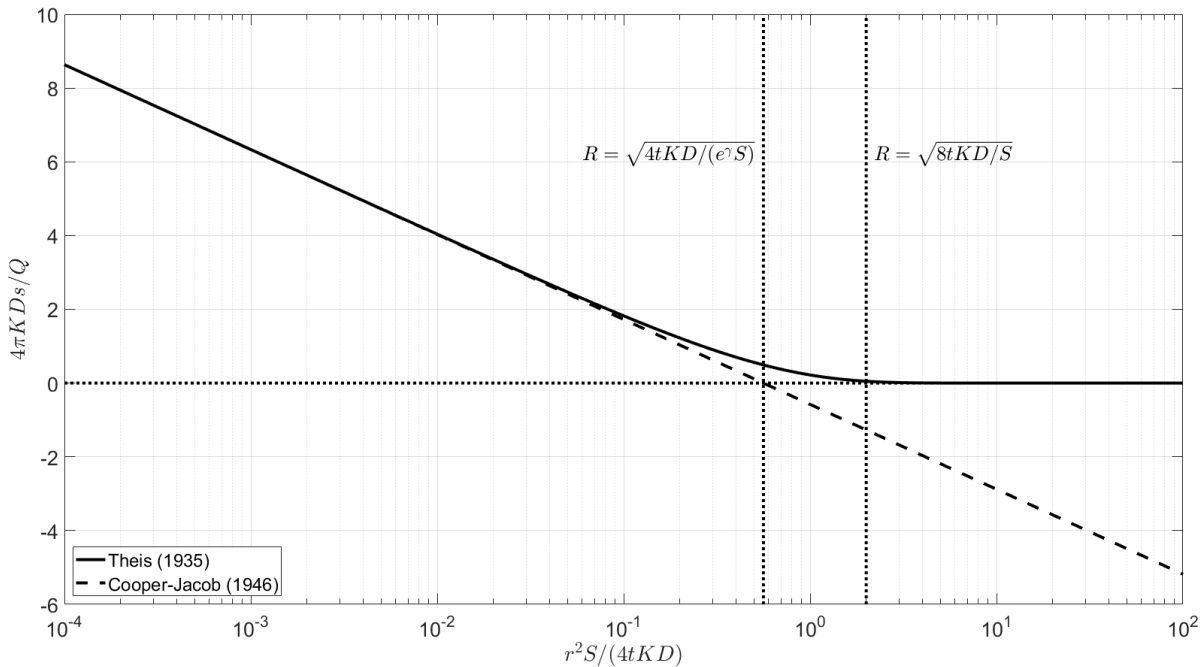


Figure 7. Dimensionless drawdown versus dimensionless distance according to the Theis (1935) equation (solid line) and the Cooper and Jacob (1946) approximation (dashed line) based on the Thiem (1870; 1906) formula with outer boundary at distance R equal to 1.5 times the square root of diffusivity KD/S multiplied by time t . This distance is indicated by the left vertical dotted line. The right vertical dotted line indicates the radius of influence R equal to 2.8 times the square root of diffusivity KD/S multiplied by time t . Variable s is the drawdown, r is the radial distance, t is the time, KD is the aquifer transmissivity, S is the aquifer storativity, Q is the pumping rate, and γ is the Euler constant. See text for definitions.

There is no interaction with sources and sinks; hence, the aquifer storage entirely yields the extracted groundwater. Mathematically, this is accomplished by defining the outer constant-head boundary at an infinitely large distance from the well. Therefore, the Theis (1935) model is best suited to simulate the initial flow to the well, when the capture is negligibly small. Equations (70) and (71) show that the cone of depression expands with time at a pace determined by the aquifer properties: it expands more rapidly if the aquifer is transmissive (high K) and stores less groundwater (small S). In case of small K and high S , the cone of depression is deeper. Because the model is linear and the outer boundary is at infinity, the aquifer can be depleted indefinitely. In reality, the well goes dry after a finite time of pumping, if the cone of depression doesn't reach sources and/or sinks from which water can be captured to sustain the pumping.

In the case of the de Glee (1930) model, this water comes from the upper boundary condition, which represents leakage through an overlying aquitard, or uniformly distributed surface water interaction. Consequently, the models of de Glee (1930) and Theis (1935) may be combined, where the latter is used at the beginning of the extraction, when capture is negligibly small, until its radius of influence according to (70) equals the radius of influence according to (64) derived from the de Glee equation (63). The corresponding time is the time to full capture, at which a new state of equilibrium is attained, and for which the de Glee solution (63) is valid. This transition to steady state may be simulated accurately by applying the model of Hantush and Jacob (1955).

10.3.4. The Hantush-Jacob model

The solution developed by Hantush and Jacob (1955) may be seen as the transient version of the de Glee equation (63) or the leaky version of the Theis equation (67). Figure 8 shows a schematic of the Hantush and Jacob (1955) model.

If a fully penetrating well of infinitesimal radius extracts water at constant rate Q from a homogeneous leaky aquifer of infinite extent, then drawdown s as a function of radial distance r and time t is calculated as (Hantush & Jacob, 1955):

$$s(r, t) = \frac{Q}{4\pi K D} W\left(\frac{r^2 S}{4t K D}, \frac{r}{\sqrt{c K D}}\right) \quad (72)$$

Section 10.2 shows how equation (72) is derived by applying the Laplace transform. Equation (72) is the same as equation (41) with $T = K D$ and $c_{top} = c$.

Like the de Glee equation (63) and the Theis equation (67), solution (72) allows superposition, if initial heads are steady. Hantush and Jacob (1955) assume that the overlying aquitard is incompressible, which means its storage is neglected. Solutions that consider storage effects in the aquitard also exist (Hantush, 1960; De Smedt, 2020), and the well-known solution of Neuman and Witherspoon (1969b) even accounts for drawdown in the unpumped aquifer overlying the bounding aquitard.

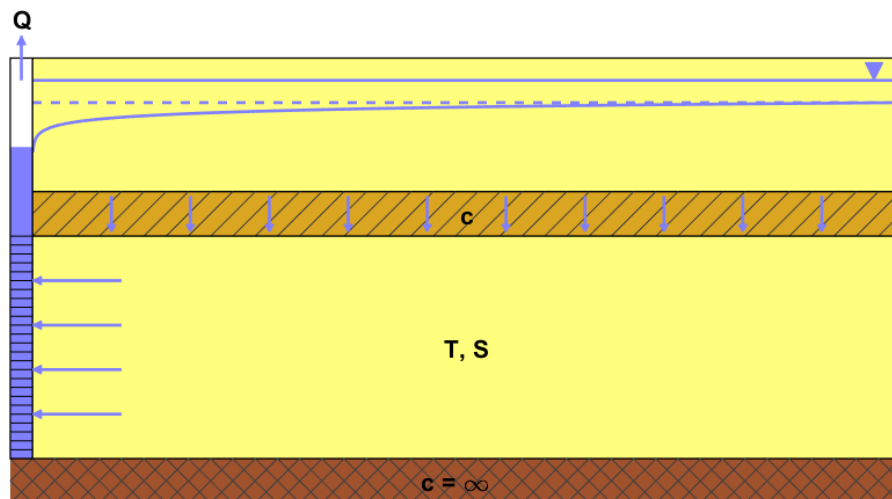


Figure 8. Schematic of the Hantush and Jacob (1955) model for transient axisymmetric flow to a fully penetrating well in a leaky aquifer. The well extracts water from the aquifer at constant rate Q . The vertical flow component is neglected. The constant transmissivity of the aquifer is T , the constant storativity is S . The lower boundary of the aquifer is impervious, the upper boundary is leaky. The latter is mostly interpreted as an aquitard with constant resistance c , and an overlying aquifer with constant head. See text for definitions.

Function W in solution (72) is the Hantush well function (Hantush & Jacob, 1955):

$$W(u, v) = \int_u^\infty \frac{e^{-x-v^2/4x}}{x} dx \quad (73)$$

The Hantush well function (73) may be evaluated by performing a numerical inversion of the Laplace transform of W , e.g. by using the Stehfest (1970) algorithm, or by applying Gaussian quadrature, e.g. using Matlab function quadgk (Shampine, 2008). Veling and Maas (2010) give an overview of existing analytical and numerical methods to calculate or approximate the Hantush well function, and derive a fast approximation of W , which is given in section 2.5.10. Comparing (73) with definition (68) of the Theis well function shows that both are identical if $v = 0$. Indeed, if c is infinitely large, then the aquifer is confined, and solution (72) must be equal to the Theis equation (67). The following relation between functions W and K_0 holds (Veling & Maas, 2010):

$$\lim_{u \rightarrow 0} W(u, v) = 2K_0(v) \quad (74)$$

From (74) it follows that the Hantush and Jacob solution (72) equals the de Glee equation (63) if steady state is attained. Thus, the Theis solution (67) and the de Glee equation (63) are asymptotic solutions for the Hantush and Jacob (1955) model. This is clearly illustrated by Figure 9 which plots dimensionless drawdown as a function of dimensionless time for different values of dimensionless distances according to solution (72) and according to those corresponding asymptotic solutions (63) and (67).

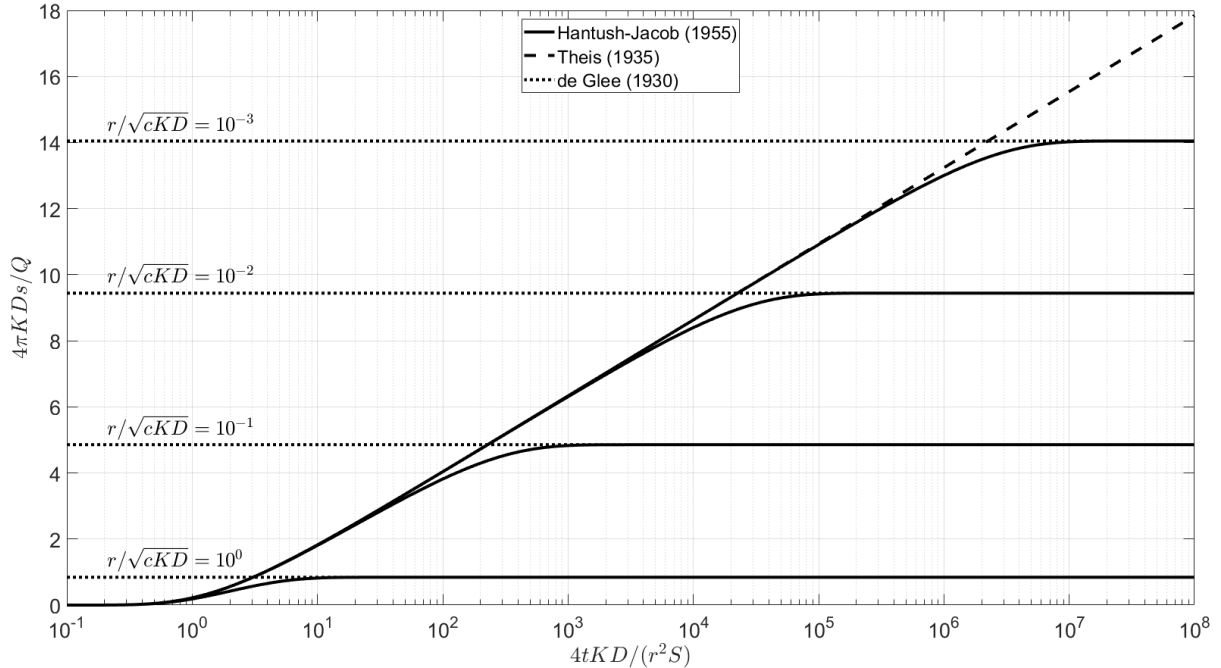


Figure 9. Dimensionless drawdown versus dimensionless time for different values of dimensionless distance according to the Hantush and Jacob (1955) model (solid lines). The asymptotic solution for small values of time corresponds to the Theis (1935) equation (dashed line), while the asymptotic solution for large values of time when steady state is reached corresponds to the de Glee (1930) formula (horizontal dotted lines). Variable s is the drawdown, r is the radial distance, t is the time, KD is the aquifer transmissivity, S is the aquifer storativity, c is the resistance of the overlying aquitard, and Q is the pumping rate. See text for definitions.

Examining the total storage change dV/dt (m^3/d) gives a better idea when leakage becomes relevant and when it is maximal:

$$\frac{dV}{dt} = Q e^{-t/Sc} \quad (75)$$

Equation (75) is the same as equation (50) in section 10.2, which is derived by applying the Laplace transform. If time t is zero, storage change equals pumping rate Q ; if t is infinitely large, then storage change is zero. As e^{-x} approximates 1 if $x < 0.01$ and 0 if $x > 10$, the Theis equation (67) may be used if $t < 0.01Sc$, and the de Glee equation (63) if $t > 10Sc$. These are also useful rules of thumb to verify if estimating the radius of influence using (70) or (64), respectively, is justified. Figure 10 compares these approximations of the radius of influence with the radius of influence according to the Sichardt formula (58). It is seen that the latter tends to underestimate the extent of the cone of depression after a period of pumping, and therefore, its use in assessing the environmental impact of permanent extractions should be avoided at all costs.

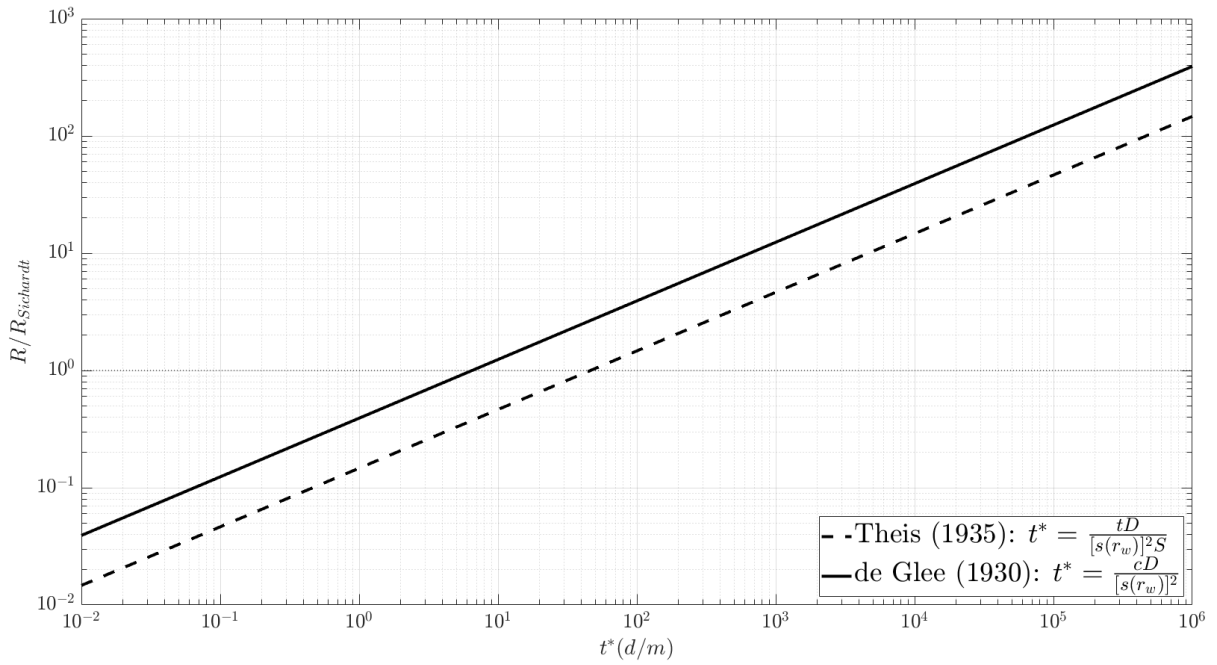


Figure 10. Plot showing the ratio of the radius of influence R approximated using the Theis (1935) or the de Glee (1930) equations, and the radius of influence $R_{Sichardt}$ according to the empirical Sichardt formula (Kyrieleis & Sichardt, 1930). Parameter t is the time, D is the saturated thickness, S is the storage coefficient, c is the resistance, $s(r_w)$ is the drawdown at the face of the well with radius r_w . See text for definitions. The Sichardt radius of influence underestimates the hydraulic impact of the extraction if the ratio is larger than 1, that is above the horizontal dotted line. See text for a more detailed explanation.

10.3.5. The Ernst model

In the model of de Glee (de Glee, 1930; Jacob, 1946) and the model of Hantush and Jacob (1955), the upper boundary condition is linear, which implies it is an infinite source of water. In reality, the hydraulic head in a layer overlying a pumped aquifer, or water levels in surface water bodies draining this aquifer, also decrease after a period of pumping, at risk of going dry.

This is accounted for in the model of Ernst (1971) by excluding this upper boundary condition at distances where the head drops below a given level. The same assumptions underlying the model of de Glee (de Glee, 1930; Jacob, 1946) also hold for the model of Ernst (1971), except that the constant-head layer is only allowed to drain water from the pumped aquifer. Hence, a proximal zone around the pumping well is considered without drainage, whereas the distal part of the aquifer is still being drained, as is shown in Figure 11. As already mentioned, this draining condition is equivalent to defining a drain boundary condition in each cell of the top layer of a MODFLOW model (Harbaugh, 2005).

Since the drainage boundary condition depends on the hydraulic head in the aquifer, the model is nonlinear. As a consequence, the superposition principle is not valid, and infiltration at the top of the aquifer cannot be ignored. Ernst (1971) assumes a constant infiltration rate N (m/d), and shows that the initial head h_0 before pumping is:

$$h_0 = Nc \quad (76)$$

where c is the drainage resistance. Equation (76) is the same as equation (32) with $c = c_{top}$. Infiltration flux N is positive if water is added to the aquifer.

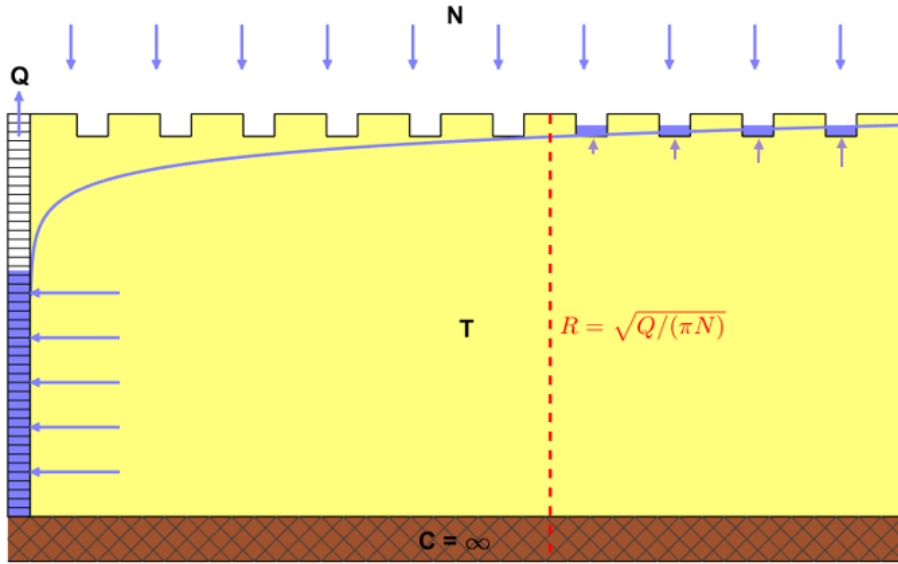


Figure 11. Schematic of the Ernst (1971) model for steady axisymmetric flow to a well in a phreatic aquifer subject to uniform areal infiltration and drainage. The well extracts water from the aquifer at constant rate Q . The vertical flow component is neglected. The constant transmissivity of the aquifer is T ; the lower boundary of the aquifer is impervious. The aquifer infiltration is determined by constant flux N . Close to the well, the upper drainage boundary condition is inactive due to the lowering of the hydraulic head. If the drainage resistance is negligibly small, then the radius of influence R may be derived from the ratio of pumping rate Q and infiltration flux N . See text for definitions.

The initial heads according to (76) are relative to the steady drainage levels. For convenience, the latter are set to zero, which is allowed as the aquifer's saturated thickness D is assumed constant. Next section 10.3.6 elaborates on this assumption. Recall that the aquifer has an infinite extent. If water at constant rate $Q > 0$ is extracted from a well of negligibly small radius, then drawdown s is:

$$\begin{cases} s_1(r) = Nc - \frac{Q}{2\pi KD} \ln\left(\frac{r}{r_d}\right) - \frac{N}{4KD}(r_d^2 - r^2) & (r \leq r_d) \\ s_2(r) = \frac{(Q - N\pi r_d^2)}{2\pi KD} \left(\frac{K_0\left(\frac{r}{\sqrt{cKD}}\right)}{\frac{r_d}{\sqrt{cKD}} K_1\left(\frac{r_d}{\sqrt{cKD}}\right)} \right) & (r \geq r_d) \end{cases} \quad (77)$$

Section 10.2 explains how solution (77) is derived, which is the same as solution (51) with $T = KD$. Function K_1 is the first order modified Bessel function of the second kind, also available with SciPy, R, Matlab, and Excel.

Distance r_d is the boundary between the proximal zone without drainage and the distal zone with drainage. This means s_1 according to the first equation of (77) is the drawdown in the proximal zone, whereas s_2 according to the second equation of (77) is the drawdown in the distal zone. Boundary r_d is found by solving equation $s_2(r_d) = Nc$, which is straightforward applying a standard nonlinear solver available with Matlab or SciPy. The left plot (a) in Figure 12 is a graphical representation of the solution of this equation, and the right plot (b) shows drawdown according to (77) expressed in dimensionless form.

If drainage is perfect, then resistance c is zero, in which case s_2 is zero, and s_1 is reduced to the well-known solution for a well in a circular infiltration pond with radius r_d (Haitjema, 1995):

$$s_1(r) = -\frac{Q}{2\pi KD} \ln\left(\frac{r}{r_d}\right) - \frac{N}{4KD}(r_d^2 - r^2) \quad (r \leq r_d) \quad (78)$$

As drawdown s_2 in the distal zone is zero, the radius of influence R equals r_d . The dotted straight line on the left plot (a) in Figure 12 shows that in this case:

$$R = \sqrt{\frac{Q}{\pi N}} \quad (79)$$

Formula (79) is used to estimate the extent of the capture zone (Haitjema, 1995), as it balances recharge and pumping rate. In most cases, however, capture zone and cone of depression do not coincide (Brown, 1963), but they do in this case. Returning to the underlying assumptions, we may conclude (79) is valid in flat areas with an excess of precipitation which is discharged by a dense system of drainage canals and ditches. In Flanders and the Netherlands, such areas are common. The left plot (a) in Figure 12 shows that using (79) to estimate the radius of influence is justified if $Q/(\pi NKDc) > 100$.

In case of gentle pumping, drainage remains active all over the aquifer, and r_d is negligibly small. In this case, solution (77) simplifies to the de Glee solution (63), which is clearly illustrated in the right plot (b) of Figure 12. From this plot, we may derive the rule of thumb that using the de Glee equation (63) is justified if $Q/(\pi NKDc) < 1$.

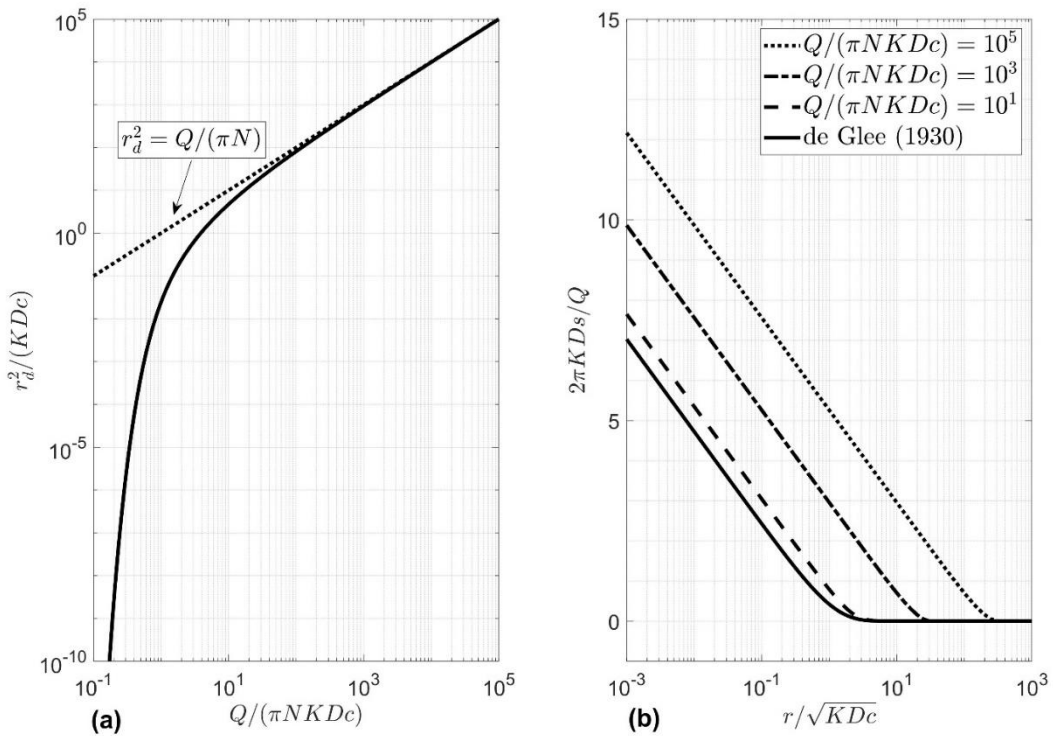


Figure 12. Solution of the Ernst (1971) model. (a) Dimensionless extent of the no-drainage zone $r_d/(KDc)^{1/2}$ versus dimensionless pumping rate $Q/(\pi NKDc)$. The dotted line is the asymptotic solution for zero resistance. (b) Dimensionless drawdown $(2\pi K D s)/Q$ versus dimensionless distance $r/(KDc)^{1/2}$ for different values of dimensionless pumping rate $Q/(\pi NKDc)$. The solid line is the de Glee (1930) solution. K is the aquifer conductivity, D the saturated thickness, c the drainage resistance, N the infiltration flux, Q the pumping rate, s the drawdown, r the radial distance, and r_d the boundary between the zones without and with drainage. See text for definitions and a more detailed explanation.

10.3.6. Validating the Ernst model

The assumption of areal drainage made by the Ernst (1971) model may seem unrealistic, since it is rare to have constant drainage levels everywhere in the field. Moreover, it is very unlikely to

encounter a real situation where a drain occurs at each distance from the well. The network of ditches is not axially symmetric either, an assumption made implicitly when the Ernst (1971) model is applied. The question thus arises whether the Ernst (1971) solution has any practical meaning at all.

Ernst (1971) elaborates on the applicability of his solution, and presents a thorough analysis of annual hydraulic head fluctuations observed in different parts of the Netherlands. Despite the simplifying assumption of combined areal drainage and infiltration, the solution is applicable in humid areas where the ground surface has only small differences in elevation and where the excess precipitation is mainly carried off by groundwater flow to a system of closely spaced surface drains. Although these drains have different size and level, it is possible to simulate their draining effect by defining a single boundary condition with average resistance. For instance, in the rather low areas of the Netherlands characterized by a dense network of ditches, this average drainage resistance is found to range between 30 and 300 days, whereas it is much larger in the higher areas, where only few and widely spaced watercourses give discharge (Ernst, 1971).

To validate the Ernst (1971) model, it is compared with a simple MODFLOW model (Harbaugh, 2005). The MODFLOW model defines more realistic nonuniform drainage boundary conditions, as opposed to the Ernst (1971) model, that considers a uniform drainage of the aquifer. This uniform drainage implies that the drainage level h_{drn} [L] is constant, as is resistance c . The initial head h_0 before pumping is also constant and equal to:

$$h_0 = h_{drn} + Nc \quad (80)$$

For mathematical convenience, drainage level h_{drn} is set to zero, which results into equation (76). This is justified as the aquifer transmissivity T is constant. However, the no-flow assumption is too strict, and it suffices the difference between the initial head h_0 and the drainage level h_{drn} is Nc . This means that it is allowed to consider an initial steady flow in the aquifer caused by spatially varying drainage levels. In this case, drawdown s may be calculated using the Ernst solution (77), and superimposed on the initial heads h_0 to obtain the heads h during pumping.

The analysis by Ernst (1971) indicates that the assumption of a constant resistance c is also too strict. The draining boundary condition is very similar to the frequently used MODFLOW drain (Harbaugh, 2005), which is also a single boundary condition defined to conceptualize the complex interaction between groundwater and surface water in the particular area covered by the grid cell to which the drain is assigned. In practice, resistance c in solution (77) may be estimated as follows:

$$c = \frac{A}{A_{drn}} c_{drn} \quad (81)$$

where A [L^2] is the horizontal surface area of the aquifer, A_{drn} [L^2] is the horizontal surface area of the drained part of the aquifer, and c_{drn} [T] is the effective drainage resistance. Note that Ernst (1971) also includes in c the vertical resistance of a semi-pervious aquitard overlying the aquifer. To illustrate how equation (81) should be interpreted, a MODFLOW model (Harbaugh, 2005) is constructed that simulates flow to a well in a homogeneous aquifer recharged by infiltration and discharged by a system of parallel ditches.

The rectangular MODFLOW grid consists of 1 layer, 101 rows, and 101 columns. The layer thickness D is 10 m; row height and column width are constant and equal to 20 m. The lower boundary of the layer is impervious, as are the lateral grid boundaries. The layer conductivity K is 5 m/d, which means transmissivity KD is 50 m²/d. The layer type is set to confined to keep the transmissivity constant. The recharge package is used to define a constant infiltration flux N equal to 0.0005 m/d or 182.5

mm/yr. A pumping well is defined in the center of the grid by assigning discharge Q of $250 \text{ m}^3/\text{d}$ to the cell in row 51 and column 51 using the well package.

Finally, the drain package is applied to add the draining streams to the model. The parallel ditches are north-south oriented, and the distance between two adjacent ditches is 40 m. This means a drain boundary condition is defined in each cell belonging to an odd column, while the cells in the even columns are not drained. The drainage level is 10 m in the cells of the first column, while it is 5 m in the cells of the last column. The drainage level in the cells of the intermediate columns is determined by linearly interpolating the drainage levels at the boundaries. To each drained cell, a conductance of $100 \text{ m}^2/\text{d}$ is assigned. The corresponding drainage resistance c_{drn} is 4 d, as it is equal to the surface area of the cell, which is $20 \text{ m} \times 20 \text{ m}$, divided by this conductance value.

First, the steady initial head is simulated without the well, after which the well is added to the model to obtain the steady head during the extraction. The SIP (Stone, 1968) solver is used in both cases. The left plot in Figure 13 shows the results of these simulations, which are considered accurate as the error on the total volumetric budget is negligibly small. The plot shows the head calculated for the cells in row 51, which must be interpreted as a cross-section from west to east through the aquifer containing the pumping well. Both the initial head h_0 and the head h during pumping are plotted, and the difference between both is drawdown s , which is also drawn. It is clearly seen that there is an initial uniform flow from west to east due to the decreasing drainage levels. The pumping well causes a cone of depression which is axially symmetric.

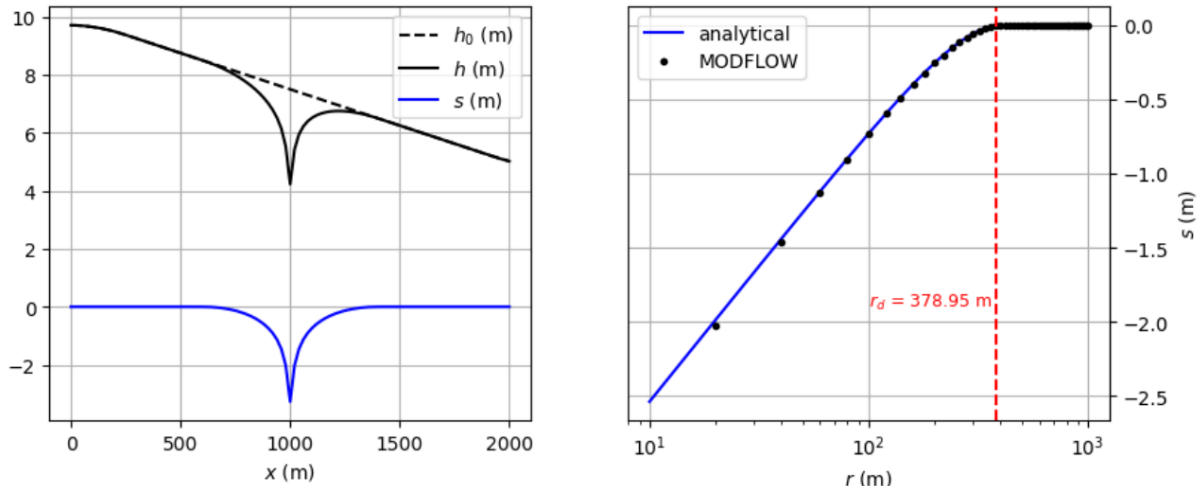


Figure 13. Results of the MODFLOW model used to validate the analytical solution by Ernst (1971) for simulating flow to a pumping well extracting water at constant rate from a homogeneous aquifer subject to uniform areal recharge and uniform areal drainage. The left plot shows the steady head h_0 and h before and during pumping, respectively, as a function of distance x . The difference between h_0 and h is drawdown s caused by the pumping. These results are simulated using the MODFLOW model defining nonuniform drainage by north-south parallel streams. The right plot compares the drawdown simulated by the MODFLOW model with the drawdown calculated using the analytical solution by Ernst (1971). Radial distance r expresses the distance from the pumping well. The outer boundary of the proximal zone around the well where drainage has become inactive due to the lowering of the head is at distance r_d . As drawdown beyond this distance is close to zero, it may be interpreted as the radius of influence, which can be estimated here by balancing pumping and infiltration rate. See text for a detailed description of the MODFLOW model setup.

The drawdown describing this cone of depression is also calculated using the analytical solution (77) by Ernst (1971). Transmissivity KD , infiltration rate N , and pumping rate Q are adopted from the MODFLOW model. To determine resistance c , effective drainage resistance c_{drn} is needed, which equals 4 d, and the ratio A/A_{drn} , which equals 2 as only half of the cells is drained. Introducing these values into expression (81), it is found that the equivalent resistance c equals 8 d. The right plot of

Figure 13 shows drawdown s according to analytical solution (77) as a function of the radial distance r to the well. The MODFLOW result is also added to the plot, and it is seen it approximates the analytical solution very well. Only close to the well there is a small deviation between both solutions, which is due to the discretization of the rectangular MODFLOW grid. Drawdown simulated in the grid cell containing the well is not accurate at all, and that is why the plot starts from $r = 10$ m, which is half the width of this cell.

The analytical solution requires distance r_d that determines the boundary between the proximal zone where the drainage is not active anymore, and the distal zone where drainage is still active. Here, distance r_d is 379 m, and drawdown $s(r_d)$ at this distance is $Nc = 0.004$ m. Distance r_d could be interpreted as the radius of influence, as $s(r_d)$ is very close to zero. The rule of thumb derived in previous section states that it is justified to estimate the radius of influence by balancing pumping and infiltration rate if $Q/(\pi NKDc) > 100$. This condition is met as $Q/(\pi NKDc)$ equals 398 in this case, and the radius of influence R according to (79) is 399 m. The right plot of Figure 13 shows that there is no drawdown indeed beyond this distance.

This example demonstrates that the assumptions underlying the Ernst (1971) model should not be interpreted too strictly. Just like the infiltration is spatially averaged, the uniform drainage condition also summarizes the hydraulic properties of surface drains of different size and level. The example also proves that the formula to estimate the radius of influence by balancing pumping and infiltration rate is not fundamentally wrong. Nevertheless, this formula is contested by Bredehoeft (2002) in the context of the water budget myth. Bredehoeft (2002) refers to Brown (1963) who shows that the cone of depression does not coincide with the capture zone, which he calls the area of diversion. Brown (1963) illustrates this by developing the analytical solution for a pumping well in a homogeneous aquifer subject to uniform recharge and bounded by two parallel streams.

This is a similar example as the one discussed here, except that there is no areal drainage. As a consequence, the cone of depression has to expand until it reaches the discharging streams at the boundaries of the aquifer, whereas the capture zone is determined by recharge only. In the Ernst (1971) model, however, recharge and discharge coincide, and so do capture zone and cone of depression, if the drainage resistance is negligibly small. Louwyck et al. (2023) discuss the relevance of recharge for estimating the cone of depression, and explain why it is important to distinguish between linear models, such as the Brown (1963) model, and nonlinear models, such as the Ernst (1971) model, as recharge is canceled out from the drawdown equation only if the model is linear. The study by Louwyck et al. (2023) is presented in the next Chapter 11.

10.3.7. Transient state solution of the Ernst model

Ernst (1971) only treats the steady-state solution. In section 10.2.6, the transient-state solution is developed by applying the Laplace transform. In Figure 14, a schematic of this model is shown.

Figure 15 shows dimensionless drawdown as a function of dimensionless distance (left plot) and dimensionless time (right plot) for different values of dimensionless discharge. The semi-analytical solution is compared with the finite-difference solution (circles) simulated using the MAXSYM code (Louwyck, 2011), that was extended with the option to include head-dependent boundary conditions (Louwyck, 2015), similar to MODFLOW rivers and drains (Harbaugh, 2005), as is explained in section 7.5.4. The finite-difference solution may also be obtained using MODFLOW (Harbaugh, 2005) by tricking it into simulating axisymmetric flow using the procedure outlined by Louwyck et al. (2012, 2014). The model grid consists of one layer, and a recharge and drain boundary condition is defined in each grid cell i . Applying this procedure, the drain conductance equals A_i/c , and the recharge flux is multiplied by A_i , where A_i (m^2) is the horizontal surface area of the ring represented by cell i .

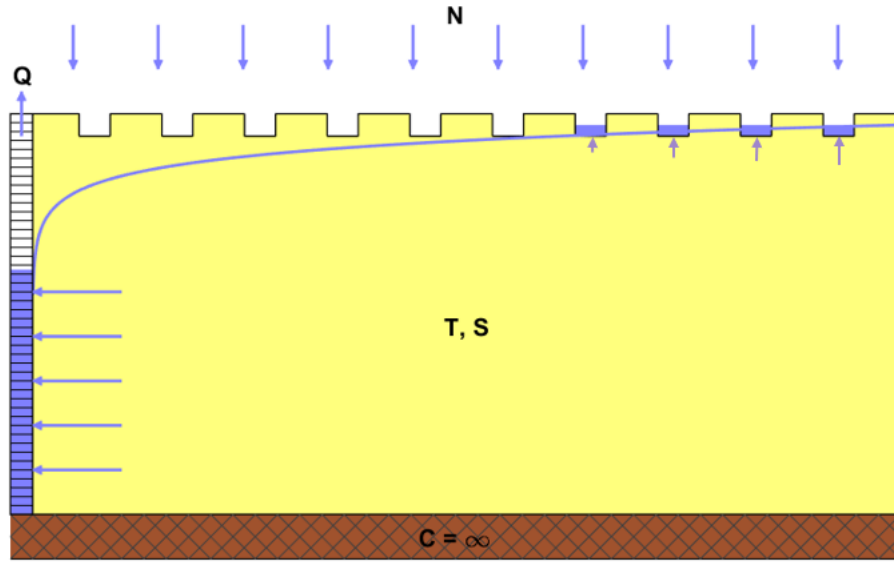


Figure 14. Schematic of the transient version of the Ernst (1971) model for simulating axisymmetric flow to a well in a phreatic aquifer subject to uniform areal infiltration and drainage. The well extracts water from the aquifer at constant rate Q . The vertical flow component is neglected. The constant transmissivity of the aquifer is T , the constant storativity is S . The lower boundary of the aquifer is impervious. The aquifer infiltration is determined by constant flux N . Close to the well, the upper drainage boundary condition is inactive due to the lowering of the hydraulic head. See text for definitions.

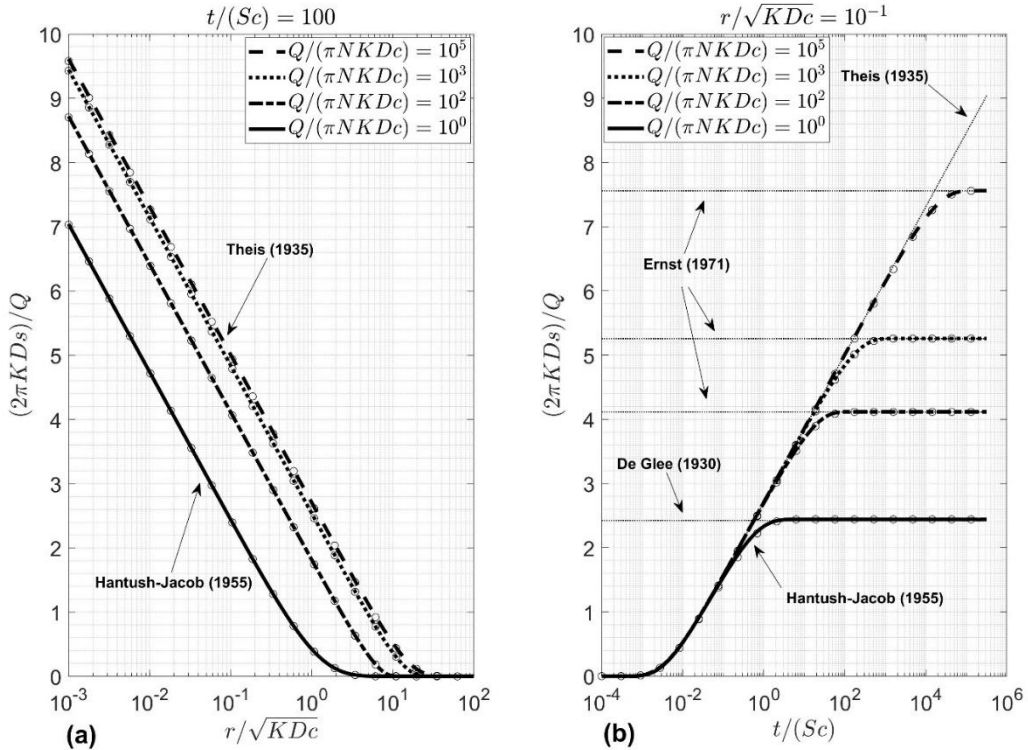


Figure 15. Transient state solution of the Ernst (1971) model developed in this study. (a) Dimensionless drawdown $(2\pi K D_s)/Q$ as a function of dimensionless distance $r/(K D_c)^{1/2}$ for dimensionless time $t/(Sc)$ equal to 100 and for different dimensionless pumping rates $Q/(\pi N K D_c)$. (b) Dimensionless drawdown $(2\pi K D_s)/Q$ as a function of dimensionless time $t/(Sc)$ for dimensionless distance $r/(K D_c)^{1/2}$ equal to 0.1 and for different dimensionless pumping rates $Q/(\pi N K D_c)$. K is the aquifer conductivity, S the storativity, D the saturated thickness, c the drainage resistance, N the infiltration flux, Q the pumping rate, s the drawdown, r the radial distance, and t the time. See text for definitions. The solution is compared with the finite-difference approach (circles), and against the asymptotic solutions developed by de Glee (1930), Theis (1935), Hantush and Jacob (1955), and Ernst (1971).

The transient-state solution of well-flow in an aquifer subject to infiltration and drainage has asymptotic solutions that correspond to the models already discussed in this study. After a period of pumping, steady state is reached, in which case drawdown may be approximated by the Ernst solution (77). If dimensionless discharge $Q/(\pi NK D c) < 1$, then the de Glee equation (63) may be used. This rule of thumb may be generalized, as it also holds for the transient-state model, in which case the solution of Hantush and Jacob (72) must be used. Finally, at small values of time, drawdown may be approximated using the Theis equation (67). The relation between the transient-state solution of the Ernst (1971) model and these asymptotic solutions is shown in Figure 15.

Figure 16 also reveals the relation between the different solutions discussed in this study. It shows the relative storage change $dV/dt/Q$ as a function of dimensionless time $t/(Sc)$ and dimensionless pumping rate $Q/(\pi NK D c)$. Figure 16 was plotted using MAXSYM (Louwyck, 2011, 2015), since the finite-difference approach is more convenient to calculate volumetric budgets. The exact Laplace space formulation of storage change is given in section 10.2.6. The left side of the contour plot is the transient part, in the right side, steady-state solutions are valid. In the upper part of the plot, drainage resistance is negligibly small and infiltration is relevant, in the lower part, infiltration may be ignored. Solution (78) may be used if both storage change and resistance are negligibly small, which is in the upper right part of the plot. The dotted lines are not strict boundaries; they only indicate the rules of thumb derived in this study that may be used to switch from one solution to another. Under the assumption of a homogeneous phreatic aquifer, infiltrated at constant rate, and discharged by area covering drainage, radius of influence (70) derived from the Theis equation (67) is applicable in the left part, radius of influence (64) derived from the de Glee equation (63) in the lower right part, and radius of influence (79) determined by balancing pumping and infiltration rate in the upper right part.

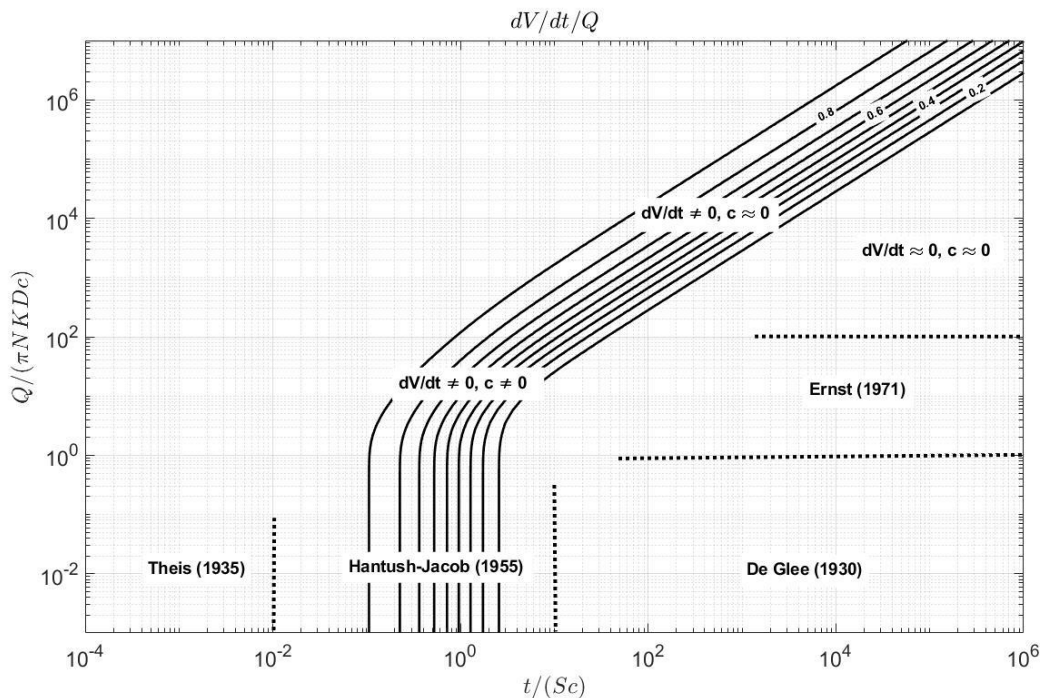


Figure 16. Contour plot of dimensionless storage change $dV/dt/Q$ as a function of dimensionless time $t/(Sc)$ and dimensionless pumping rate $Q/(\pi NK D c)$ for the transient state solution of the Ernst (1971) model developed in this study, with dV/dt the storage change, Q the pumping rate, t the time, S the storage coefficient, c the drainage resistance, N the infiltration flux, K the aquifer conductivity, and D the saturated thickness. See text for definitions. The plot reveals the relation with the solutions developed by de Glee (1930), Theis (1935), Hantush and Jacob (1955), and Ernst (1971). The dotted lines indicate the rules of thumb derived in this study.

10.3.8. Finding the maximum radius of influence

To obtain an accurate estimate of the radius of influence, reliable values for the model parameters are required. In practice, however, these parameter values often are unknown. Moreover, it is not always possible to carry out a profound hydrogeological study in which field data are collected, for instance, drawdown observations from pumping tests, that can be analyzed to identify the aquifer transmissivity and other parameter values (e.g. Kruseman & de Ridder, 1990). If relevant parameters are not available, then one should use values for these missing parameters in a conservative way. In the context of sustainable pumping, it is safer to overestimate the radius of influence. This section derives a formula from both the equations of de Glee (1930) and Theis (1935) for estimating the maximum radius of influence which is independent of the aquifer transmissivity.

The de Glee solution (63) and the Theis solution (67) are expressed by an equation of the following form:

$$s = \frac{Q}{T} f\left(\frac{r^2}{T} \prod_i P_i\right) \quad (82)$$

with s the drawdown [L], Q the pumping rate [L^3/T], $T = KD$ the transmissivity [L^2/T], r the radial distance [L], and P_i an independent variable or hydraulic parameter. In case of the de Glee equation (63), function f is defined as $f(x) = K_0(\sqrt{x})/(2\pi)$ with K_0 the zero order modified Bessel function of the second kind, whereas $f(x) = W(x)/\pi$ with W the Theis Well function in case of the Theis equation (67).

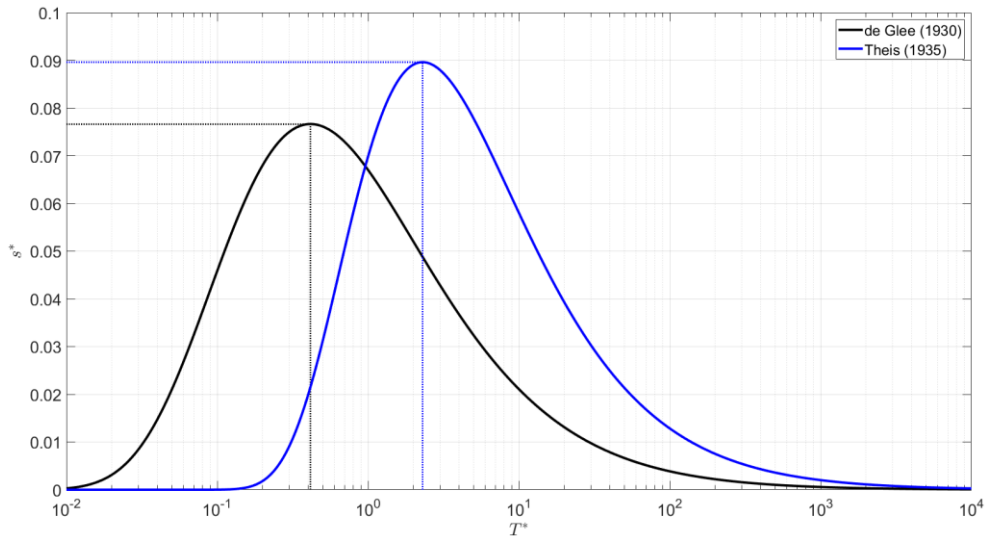


Figure 17. Plot of dimensionless drawdown versus dimensionless transmissivity for the de Glee (1930) formula and the Theis (1935) equation. The maximum value for each function is indicated by dotted lines, and it may be used to find the maximum radius of influence. See text for definitions and a detailed explanation.

Defining dimensionless drawdown $s^* = \frac{sr^2}{Q} \prod_i P_i$ and dimensionless transmissivity $T^* = \frac{T}{r^2} \prod_i P_i^{-1}$, equation (82) is written in dimensionless form:

$$s^* = f(1/T^*)/T^* = g(T^*) \quad (83)$$

As shown in Figure 17, function g reaches its maximum in point (T_{max}^*, s_{max}^*) . This point is found by numerically solving $\frac{dg}{dT^*} = 0$, after which maximum distance r_{max} is found for a given maximum drawdown s_{max} using the definition of dimensionless drawdown s^* :

$$r_{max} = \sqrt{\frac{Q s_{max}^*}{s_{max}} \prod_i P_i^{-1}} \quad (84)$$

The corresponding transmissivity T_{max} is found by applying the definition of dimensionless transmissivity T^* and replacing r_{max} by (84):

$$T_{max} = \frac{Q s_{max}^*}{s_{max}} T_{max}^* \quad (85)$$

In case of the de Glee equation (63), $s_{max}^* = 0.0766$ and $T_{max}^* = 0.4148$. The maximum radius of influence R_{max} given a maximum allowable drawdown s_{max} is:

$$R_{max} = \sqrt{\frac{0.0766 Q c}{s_{max}}} \quad (86)$$

with c the hydraulic resistance [T]. The corresponding maximum transmissivity is:

$$T_{max} = \frac{0.0318 Q}{s_{max}} \quad (87)$$

In case of the Theis equation (67), $s_{max}^* = 0.0896$ and $T_{max}^* = 2.2998$. The maximum radius of influence R_{max} given a maximum allowable drawdown s_{max} at time t [L] is:

$$R_{max} = \sqrt{\frac{0.0896 Q t}{s_{max} S}} \quad (88)$$

with S the storage coefficient [-]. The corresponding maximum transmissivity is:

$$T_{max} = \frac{0.0515 Q}{s_{max}} \quad (89)$$

10.4. Discussion

This chapter is completed by discussing the use and reliability of the formulas that were derived to calculate the cone of depression and the corresponding radius of influence. Table 1 summarizes the assumptions underlying the one-dimensional analytical models studied in this work. Each of these models simulates drawdown in the extracted aquifer only, and assumes there is no drawdown in the adjacent layers. The aquifer base is assumed impervious, the aquifer top may be impervious, leaky, or draining. The models of Thiem (1870; 1906) and Theis (1935) have an impervious upper boundary, the models of de Glee (1930) and Hantush and Jacob (1955) have a leaky top, and the upper boundary in the Ernst (1971) model is draining. In the latter, there is also a constant infiltration flux.

In the Dupuit (1863) solution, the saturated thickness of the aquifer equals the hydraulic head, hence, the upper boundary is interpreted as the water table. In all other models, the saturated thickness is constant. Therefore, the single layer is mostly interpreted as a confined aquifer in the Thiem (1870; 1906) and Theis (1935) models, and as a semi-confined aquifer in the de Glee (1930) and Hantush and Jacob (1955) models. The bounding aquitard in the latter models is assumed incompressible, and has a uniform head because it is continuously being replenished by rainfall, or it is overlain by an aquifer with constant head.

Alternatively, a phreatic aquifer may be assumed using the models of Thiem (1906), Theis (1935), de Glee (1930), and Hantush and Jacob (1955), if drawdown is small compared to the initial saturated

thickness. Implicitly, the phreatic aquifer may be recharged by a constant infiltration flux, which is canceled out in the drawdown solutions, since the governing differential equation is linear. If the aquifer is phreatic, the leaky top in the de Glee (1930) and Hantush and Jacob (1955) models is interpreted as surface water interaction similar to MODFLOW rivers (Harbaugh, 2005). This interpretation also holds for the Ernst (1971) model, although in this model, the upper boundary condition is restricted to draining water from the phreatic aquifer. Since this is a nonlinear condition similar to MODFLOW drains (Harbaugh, 2005), recharge is not canceled out in the governing equation, and therefore, the constant infiltration flux is defined explicitly.

The aquifer in these models is assumed horizontal, homogeneous and isotropic. As a consequence, the flow to the pumping well is axially symmetric. Moreover, the well is fully penetrating; hence, flow is assumed strictly horizontal. In each of these models, the well extracts water at a constant pumping rate. The well also has an infinitesimal radius, which means wellbore storage is neglected. The outer boundary in each of these models is a constant head. In the models of Dupuit (1863) and Thiem (1870; 1906), this boundary is at a finite distance from the well. Because drawdown is zero at the outer boundary, it corresponds to the radius of influence. In the other models, this outer boundary is defined at an infinitely large distance. Therefore, the derived formulas for calculating the radius of influence correspond to a distance from the well at which drawdown is negligibly small. These equations are given in the last column of Table 1.

Table 1. Summary of the analytical models discussed in this work which are used to simulate axisymmetric flow toward a fully penetrating well with infinitesimal radius and constant pumping rate in a homogeneous aquifer with impervious base. From the solutions of these models, equations and rules of thumb are derived to estimate the radius of influence R , with KD the transmissivity, c the resistance, S the storage coefficient, N the infiltration flux, Q the pumping rate, and t the time. See text for explanation and definitions.

Model	Flow regime	Outer boundary	Upper Boundary	Initial Flow	Super-position	Radius of Influence R
Dupuit (1863)	Steady	Finite	Water table	None	No ⁴	Outer boundary (= input parameter)
Thiem (1870; 1906)	Steady	Finite	Impervious ¹	Steady	Yes	Outer boundary (= input parameter)
de Glee (1930)	Steady	Infinite	Leaky ²	Steady	Yes	$R = 4\sqrt{cKD}$
Theis (1935)	Transient	Infinite	Impervious ¹	Steady	Yes	$R = 1.5 \sqrt{\frac{tKD}{S}}$
Hantush-Jacob (1955)	Transient	Infinite	Leaky ²	Steady	Yes	$R = 1.5 \sqrt{\frac{tKD}{S}}$ if $t < 0.01Sc$ $R = 4\sqrt{cKD}$ if $t > 10Sc$
Ernst (1971)	Steady	Infinite	Drainage + Recharge	None ³	No ⁴	$R = \sqrt{\frac{Q}{\pi N}}$ if $\frac{Q}{\pi NKc} > 100$ $R = 4\sqrt{cKD}$ if $\frac{Q}{\pi NKc} < 1$
Transient Ernst (this study)	Transient	Infinite	Drainage + Recharge	None ³	No ⁴	See Figure 16

¹ Or water table if drawdown is less than 10% of initial saturated thickness.

² Leakage through incompressible aquitard or linear surface water interaction (cfr. MODFLOW river).

³ Initial heads equal to Nc are relative to the steady drainage levels, which are set to zero for convenience.

⁴ Unless the solution may be approximated by its corresponding linear equation.

The models of Dupuit (1863) and Ernst (1971) are nonlinear: in the first, the saturated aquifer thickness depends on the hydraulic head, whereas the draining boundary condition is nonlinear in the latter. Because of this nonlinearity, superposition is not applicable, and the initial heads must be constant. This implies there is no initial flow in the aquifer, although the constant initials heads in the Ernst (1971) model are relative to the drainage levels that are steady but not necessarily constant. This means the Ernst (1971) solution may be superimposed on the initial heads that are the result of this steady but nonuniform drainage in the aquifer. The other models are linear and therefore allow initial steady flow in the aquifer, since the superposition principle is valid. Recall that under certain conditions the Dupuit (1863) and Ernst (1971) solutions may be approximated by the linear equations of Thiem (1870; 1906) and de Glee (1930), respectively. Superposition is explained in many hydrogeology textbooks (e.g. Bakker & Post, 2022; Bear, 1979; Bruggeman, 1999; Haitjema, 1995; Kruseman & de Ridder, 1990; Strack, 1989, 2017). It states that the drawdowns induced by individual constant-discharge wells can be summed to obtain the total drawdown caused by these extractions. Superposition may also be applied to simulate variable-discharge pumping.

The assumptions underlying the discussed models also hold for the derived formulas to estimate the radius of influence summarized in the last column of Table 1. These assumptions oversimplify the process of groundwater flow to a pumping well in many aspects. Therefore, assessing the environmental impact of a groundwater extraction by merely calculating the radius of influence must be avoided at all costs. These kinds of studies mostly require advanced numerical modeling, as estimating the extent of the cone of depression is not sufficient to evaluate the effects on groundwater flow and on sources and sinks. The impact on water quality and ecology, and other considerations must also be taken into account, which may even require additional models besides a calibrated groundwater flow model.

To check whether the pumping is sustainable or not, it may suffice to estimate the area of influence. As already discussed in the introduction, this area rarely is a circle, and in most cases, the pumped aquifer is part of a multi-aquifer system. Still, a first approach that applies one-dimensional axisymmetric solutions assuming a single aquifer could be useful, as they give an idea of the extent of the cone of depression and offer insight in the sensitivity of the hydraulic parameters. If drawdowns in the unpumped layers of a multi-aquifer system are not negligibly small, axisymmetric multi-aquifer solutions can be applied (e.g. Hemker, 1984, 1985; Hemker & Maas, 1987; Hunt, 1985, 1986; Maas, 1986), which are implemented in user-friendly Matlab and Python codes (e.g. Bakker, 2013; Louwyck et al., 2012).

In many real-world cases, reliable parameter values are not available, and examining a range of realistic values is a pragmatic way to get an idea of the worst-case impact. Because of the low computational cost, axisymmetric single- and multi-layer models are well-suited to perform these kinds of calculations. Using the de Glee equation (63) and the Theis equation (67), it is even possible to determine the maximum radius of influence R_{max} , which is independent of the aquifer transmissivity KD . The following formulas, respectively for the de Glee (1930) model and the Theis (1935) model, were derived in previous section 10.3.8:

$$R_{max} = \sqrt{\frac{0.0766 Qc}{s_{max}}} \quad (90)$$

$$R_{max} = \sqrt{\frac{0.0896 Qt}{s_{max} S}} \quad (91)$$

Formulas (90) and (91) only depend on pumping rate Q and the maximum allowable drawdown s_{max} at distance R_{max} . Additionally, formula (90) derived from the de Glee equation (63), requires resistance c , whereas formula (91) derived from the Theis equation (67), requires storage coefficient S . The latter is also time-dependent.

The maximum allowable drawdown s_{max} is necessary in (90) and (91), because the model of de Glee (1930) and the model of Theis (1935) have a boundary condition at infinity. Only at this boundary condition, drawdown is exactly zero, by definition, whereas drawdown is nonzero at all other distances from the well. Mathematically, the radius of influence is thus infinitely large. Recall that formulas (64) and (70) estimating the radius of influence, are approximations that ensure drawdown is zero at distance R . The error induced by these approximations is proportional to $Q/(KD)$ (Dragoni, 1998).

This maximum allowable drawdown is the subject of many discussions between groundwater practitioners in Flanders, who range its optimal value from 1 mm to 10 cm. Although these discussions are necessary from an ecological point of view, they are pointless if a radius of influence approach is used as a substitute for a sophisticated mathematical model. Hence, Louwyck et al. (2023) believe it is more meaningful to discuss model assumptions and reliability of input data. The formulas presented in this study may be helpful in these discussions, as they show which parameter combinations are relevant. Results calculated using these formulas, however, may never be interpreted as ground truth data.

10.5. Summary and conclusions

The radius of influence myth refers to the use of empirical formulas to assess the environmental impact of groundwater extractions. As an example, the frequently used Sichardt formula (Kyrieleis & Sichardt, 1930) was examined, which estimates the radius of influence merely considering the aquifer conductivity and the drawdown in the pumping well. It is shown that the Sichardt formula is not consistent with the fundamental Thiem (1870; 1906) equation. It also tends to underestimate the extent of the cone of depression, and therefore, its use must be discouraged.

A distinction must be made between sustainable pumping and sustainability (Devlin & Sophocleous, 2005), the latter being a much broader concept that in many cases requires advanced numerical modeling. Concerning sustainable pumping, the fundamental hydrological principles that were stated first by Theis (1940) must be kept in mind. The extraction causes a cone of depression, which is determined by the change of aquifer storage and the sources and sinks from which water is captured. As a consequence, the assumption of axial symmetry only holds close to the well, and therefore, the radius of influence rarely is an accurate measure of the extent of the cone of depression.

On the other hand, Haitjema (2006) advocates the use of simple formulas derived from one-dimensional models to get insight into the problem at hand. These formulas have minimum data requirements and may help setting up the right numerical model. Therefore, alternatives to the Sichardt formula are derived from existing one-dimensional analytical solutions developed by de Glee (1930), by Theis (1935), and by Ernst (1971). An asymptotic solution to the latter yields the contested formula to determine the radius of influence by balancing pumping and infiltration rate. Considering the assumptions underlying the Ernst (1971) model, it is concluded that this formula is valid in humid areas that are heavily drained. The applicability of the Ernst (1971) model assuming areal uniform drainage is discussed in detail, and validated by means of a MODFLOW (Harbaugh, 2005) model that simulates flow to a pumping well in an aquifer subject to nonuniform drainage.

The model of Hantush and Jacob (1955) is also discussed to see the relation between the solutions of de Glee (1930) and Theis (1935). The transient-state solution of the Ernst (1971) model is developed by applying the Laplace transform. This solution includes drainage instead of leakage at the top of the aquifer. Examining drawdown curves and total storage change as a function of dimensionless parameters reveals the relation between the presented one-dimensional radial flow solutions, from which some useful rules of thumb are derived.

Although the derived formulas are better alternatives to frequently used empirical formulas, they may not be considered as methods to accurately estimate the cone of depression of an extraction, as they rely on oversimplifying assumptions. They are not intended as a substitute for comprehensive numerical models, although they may be useful in setting up these models, as they offer valuable insights on relevant parameter combinations.

10.6. References

- Abramowitz, M., & Stegun, I. A. (1965). *Handbook of Mathematical Functions: With Formulas, Graphs, and Mathematical Tables*. In M. Abramowitz & I. A. Stegun (Eds.), *Dover Books on Advanced Mathematics*. New York: Dover Publications.
- Ahmadi, A., Chitsazan, M., Mirzaee, S. Y., & Nadri, A. (2023). The effects of influence radius and drawdown cone on the areas related to the protection of water wells. *Journal of Hydrology*, 617, 129001. <https://doi.org/10.1016/j.jhydrol.2022.129001>
- Amartya Kumar, B., Sudip, B., & Prabir, M. (2012). An Innovative Methodology for Groundwater Management with Reference to Saline Water Intrusion. *IOSR Journal of Engineering*, 2(6), 1473–1486. <https://doi.org/10.9790/3021-026114731486>
- Bair, E. S., & O'Donnell, T. P. (1983). Uses of Numerical Modeling in the Design and Licensing of Dewatering and Depressurizing Systems. *Ground Water*, 21(4). <https://doi.org/10.1111/j.1745-6584.1983.tb00742.x>
- Bakker, M. (2001). An analytic, approximate method for modeling steady, three-dimensional flow to partially penetrating wells. *Water Resources Research*, 37(5). <https://doi.org/10.1029/2000WR900400>
- Bakker, M. (2013). Semi-analytic modeling of transient multi-layer flow with TTIm. *Hydrogeology Journal*, 21(4). <https://doi.org/10.1007/s10040-013-0975-2>
- Bakker, M., & Post, V. E. A. (2022). *Analytical Groundwater Modeling: Theory and Applications using Python* (1st ed.). London: CRC Press.
- Bakker, M., & Strack, O. D. L. (2003). Analytic elements for multiaquifer flow. *Journal of Hydrology*, 271(1–4). [https://doi.org/10.1016/S0022-1694\(02\)00319-0](https://doi.org/10.1016/S0022-1694(02)00319-0)
- Barlow, P. M., Leake, S. A., & Fienen, M. N. (2018). Capture Versus Capture Zones: Clarifying Terminology Related to Sources of Water to Wells. *Groundwater*, 56(5). <https://doi.org/10.1111/gwat.12661>
- Bear, J. (1972). *Dynamics of Fluids in Porous Media*. New York: American Elsevier Publishing Company.
- Bear, J. (1979). *Hydraulics of Groundwater. McGraw-Hill series in water resources and environmental engineering*. New York: McGraw-Hill.

- Bot, B. (2016). *Grondwaterzakboekje (in Dutch)* (2nd ed.). Rotterdam, the Netherlands: Bot Raadgevend Ingenieur.
- Bredehoeft, J. D. (2002). The Water Budget Myth Revisited: Why Hydrogeologists Model. *Ground Water*, 40(4). <https://doi.org/10.1111/j.1745-6584.2002.tb02511.x>
- Bredehoeft, J. D. (2008). An interview with C.V. Theis. *Hydrogeology Journal*, 16(1). <https://doi.org/10.1007/s10040-007-0248-z>
- Bredehoeft, J. D., & Durbin, T. (2009). Ground Water Development - The Time to Full Capture Problem. *Ground Water*, 47(4). <https://doi.org/10.1111/j.1745-6584.2008.00538.x>
- Bredehoeft, J. D., Papadopoulos, S. S., & Cooper, H. H. (1982). The water budget myth. In *Scientific Basis of Water Resources management Studies in Geophysics* (pp. 51–57). National Academy Press.
- Bresciani, E., Shandilya, R. N., Kang, P. K., & Lee, S. (2020a). Evolution of the radius of investigation during recovery tests. *Journal of Hydrology*, 590, 125346. <https://doi.org/10.1016/j.jhydrol.2020.125346>
- Bresciani, E., Shandilya, R. N., Kang, P. K., & Lee, S. (2020b). Well radius of influence and radius of investigation: What exactly are they and how to estimate them? *Journal of Hydrology*, 583. <https://doi.org/10.1016/j.jhydrol.2020.124646>
- Brown, R. H. (1963). *The cone of depression and the area of diversion around a discharging well in an infinite strip aquifer subject to uniform recharge*. U.S. Geological Survey Water-Supply Paper 1545C; U.S. Government Printing Office, Washington, D.C.
- Bruggeman, G. A. (1999). *Analytical solutions of geohydrological problems. Developments in Water Science* 46. Amsterdam: Elsevier.
- Cashman, P. M., & Preene, M. (2013). *Groundwater Lowering in Construction – A Practical Guide to Dewatering. Volume 6 of Applied Geotechnics* (2nd ed.). Boca Raton, Florida: CRC Press.
- Castellazzi, P., Martel, R., Galloway, D. L., Longuevergne, L., & Rivera, A. (2016). Assessing Groundwater Depletion and Dynamics Using GRACE and InSAR: Potential and Limitations. *Groundwater*, 54(6). <https://doi.org/10.1111/gwat.12453>
- Chu, S. T. (1994). Transient Radius of Influence Model. *Journal of Irrigation and Drainage Engineering*, 120(5). [https://doi.org/10.1061/\(ASCE\)0733-9437\(1994\)120:5\(964\)](https://doi.org/10.1061/(ASCE)0733-9437(1994)120:5(964))
- Coduto, D. P., Yeung, M. R., & Kitch, W. A. (2011). *Geotechnical Engineering: Principles & Practices* (2nd ed.). New York: Pearson Prentice Hall.
- Cooper, H. H., & Jacob, C. E. (1946). A generalized graphical method for evaluating formation constants and summarizing well-field history. *Transactions, American Geophysical Union*, 27(4), 526–534. <https://doi.org/10.1029/TR027i004p00526>
- Dachroth, W. (2017). *Handbuch der Baugеologie und Geotechnik (in German)*. Berlin, Heidelberg: Springer. <https://doi.org/10.1007/978-3-662-46886-9>
- De Filippi, F. M., Iacurto, S., Ferranti, F., & Sappa, G. (2020). Hydraulic Conductivity Estimation Using Low-Flow Purging Data Elaboration in Contaminated Sites. *Water*, 12(3). <https://doi.org/10.3390/w12030898>

de Glee, G. J. (1930). *Over grondwaterstroomingen bij wateronttrekking door middel van putten (in Dutch)* (PhD thesis). Technische Hoogeschool Delft, Drukkerij J. Waltman. Jr., Delft.

Desens, A., & Houben, G. J. (2022). Jenseits von Sichardt – empirische Formeln zur Bestimmung der Absenkreichweite eines Brunnens und ein Verbesserungsvorschlag (in German). *Grundwasser*, 27(2), 131–141. <https://doi.org/10.1007/s00767-021-00500-3>

Desens, A., & Houben, G. J. (2023). Replik zu den Anmerkungen von Frieder Haakh zum Beitrag „Jenseits von Sichardt – empirische Formeln zur Bestimmung der Absenkreichweite eines Brunnens und ein Verbesserungsvorschlag“ von Anika Desens und Georg J. Houben, *Grundwasser* 27 (2), 131–141 (2022) (in German). *Grundwasser*. <https://doi.org/10.1007/s00767-022-00536-z>

De Smedt, F. (2006). *Groundwater Hydrology*. Department of Hydrology and Hydraulic Engineering, Faculty of Applied Sciences, Free University Brussels.

De Smedt, F. (2020). Constant-Rate Pumping Test in a Leaky Aquifer with Water Release from Storage in the Aquitard. *Groundwater*, 58(4). <https://doi.org/10.1111/gwat.12997>

Desoert, C., & Reiffsteck, Ph. (2020). *Géotechnique - Exercices et problèmes corrigés de mécanique des sols, avec rappels de cours (in French)* (2nd ed.). Malakoff: Dunod.

Devlin, J. F., & Sophocleous, M. (2005). The persistence of the water budget myth and its relationship to sustainability. *Hydrogeology Journal*, 13(4). <https://doi.org/10.1007/s10040-004-0354-0>

Dragoni, W. (1998). Some considerations regarding the radius or influence or a pumping well. *Hydrogéologie*, 3, 21–25.

Dupuit, J. (1863). *Etude Théoriques et Pratiques Sur le Mouvement Des Eaux Dans Les Canaux Découverts et à Travers Les Terrains Perméables (in French)*. Paris: Dunot.

El-Hames, A. S. (2020). Development of a simple method for determining the influence radius of a pumping well in steady-state condition. *Journal of Groundwater Science and Engineering*, 8(2), 97–107.

Ergun, M. U., & Nalçakan, M. S. (1993). Dewatering of a large excavation pit by wellpoints. In *Proceedings of the Third International Conference on Case Histories in Geotechnical Engineering* (pp. 707–711). St. Louis, Missouri.

Ernst, L. F. (1971). Analysis of groundwater flow to deep wells in areas with a non-linear function for the subsurface drainage. *Journal of Hydrology*, 14(2). [https://doi.org/10.1016/0022-1694\(71\)90004-7](https://doi.org/10.1016/0022-1694(71)90004-7)

Fileccia, A. (2015). Some simple procedures for the calculation of the influence radius and well head protection areas (theoretical approach and a field case for a water table aquifer in an alluvial plain). *Acque Sotterranee - Italian Journal of Groundwater*, 4(3). <https://doi.org/10.7343/as-117-15-0144>

Fruco and Associates Inc. (1971). *Dewatering and Groundwater Control for Deep Excavations. NAVFAC Manual*. Washington D.C.: Department of the Navy.

Gefell, M. J., Thomas, G. M., & Rossello, S. J. (1994). Maximum Water-Table Drawdown at a Fully Penetrating Pumping Well. *Ground Water*, 32(3). <https://doi.org/10.1111/j.1745-6584.1994.tb00658.x>

- Haitjema, H. (1995). *Analytic Element Modeling of Groundwater Flow*. San Diego: Academic Press.
<https://doi.org/10.1016/B978-0-12-316550-3.X5000-4>
- Haitjema, H. (2006). The Role of Hand Calculations in Ground Water Flow Modeling. *Ground Water*, 44(6). <https://doi.org/10.1111/j.1745-6584.2006.00189.x>
- Hansen, C. V. (1991). *Description and evaluation of selected methods used to delineate wellhead-protection areas around public-supply wells near Mt. Hope, Kansas*. U.S. Geological Survey Water-Resources Investigations Report 90-4102.
- Hantush, M. S. (1960). Modification of the theory of leaky aquifers. *Journal of Geophysical Research*, 65(11), 3713–3725. <https://doi.org/10.1029/JZ065i011p03713>
- Hantush, M. S. (1964). Hydraulics of wells. In V. T. Chow (Ed.), *Advances in Hydroscience* (Vol. I, pp. 281–432). New York and London: Academic Press.
- Hantush, M. S., & Jacob, C. E. (1955). Non-steady radial flow in an infinite leaky aquifer. *Transactions, American Geophysical Union*, 36(1), 95–100. <https://doi.org/10.1029/TR036i001p00095>
- Harbaugh, A. W. (2005). *MODFLOW-2005, the U.S. Geological Survey modular ground-water model - the Ground-Water Flow Process*. U.S. Geological Survey Techniques and Methods 6-A16. <https://doi.org/https://doi.org/10.3133/tm6A16>
- Hemker, C. J. (1984). Steady groundwater flow in leaky multiple-aquifer systems. *Journal of Hydrology*, 72(3–4), 355–374. [https://doi.org/10.1016/0022-1694\(84\)90089-1](https://doi.org/10.1016/0022-1694(84)90089-1)
- Hemker, C. J. (1985). Transient well flow in leaky multiple-aquifer systems. *Journal of Hydrology*, 81(1–2), 111–126. [https://doi.org/10.1016/0022-1694\(85\)90170-2](https://doi.org/10.1016/0022-1694(85)90170-2)
- Hemker, C. J. (2000). *Groundwater flow in layered aquifer systems* (PhD thesis). VU, Amsterdam.
- Hemker, C. J., & Maas, C. (1987). Unsteady flow to wells in layered and fissured aquifer systems. *Journal of Hydrology*, 90(3–4), 231–249. [https://doi.org/10.1016/0022-1694\(87\)90069-2](https://doi.org/10.1016/0022-1694(87)90069-2)
- Houben, G. J. (2015). Review: Hydraulics of water wells—head losses of individual components. *Hydrogeology Journal*, 23(8), 1659–1675. <https://doi.org/10.1007/s10040-015-1313-7>
- Hunt, B. (1985). Flow to a Well in a Multiaquifer System. *Water Resources Research*, 21(11), 1637–1641. <https://doi.org/10.1029/WR021i011p01637>
- Hunt, B. (1986). Solutions for steady groundwater flow in multi-layer aquifer systems. *Transport in Porous Media*, 1(4), 419–429. <https://doi.org/10.1007/BF00208046>
- Hurst, W. (1968). Radius of drainage formula: a technical note. *Society of Petroleum Engineers*.
- Jacob, C. E. (1940). On the flow of water in an elastic artesian aquifer. *Transactions, American Geophysical Union*, 21(2), 574. <https://doi.org/10.1029/TR021i002p00574>
- Jacob, C. E. (1946). Radial flow in a leaky artesian aquifer. *Transactions, American Geophysical Union*, 27(2). <https://doi.org/10.1029/TR027i002p00198>
- Jacob, C. E. (1950). Flow of groundwater. In H. Rouse (Ed.), *Engineering hydraulics* (pp. 321–386). New York: Wiley.
- Janssen, G. J. M. (2003). *Bemaling van bouwputten (in Dutch)*. Delft: Van Marken Delft Drukkers.

- Kalf, F. R. P., & Woolley, D. R. (2005). Applicability and methodology of determining sustainable yield in groundwater systems. *Hydrogeology Journal*, 13(1). <https://doi.org/10.1007/s10040-004-0401-x>
- Khadka, D. B. (2021). Experimental Design of Physical Unconfined Aquifer for Evaluation of Well Abstraction Effects: Laboratory Approach. *Journal of Engineering Research and Reports*. <https://doi.org/10.9734/jerr/2021/v20i717346>
- Konikow, L. F., & Leake, S. A. (2014). Depletion and Capture: Revisiting “The Source of Water Derived from Wells.” *Groundwater*, 52(S1). <https://doi.org/10.1111/gwat.12204>
- Kooper, J. (1914). Beweging van het water in den bodem bij onttrekking door bronnen (in Dutch). *De Ingenieur*, 29, 697–716.
- Kruseman, G. P., & de Ridder, N. A. (1990). *Analysis and Evaluation of Pumping Test Data* (2nd ed.). Wageningen: ILRI Publication 47.
- Kyrieleis, W., & Sichardt, W. (1930). *Grundwasserabsenkung bei Fundierungsarbeiten (in German)*. Berlin: Springer.
- Loaiciga, H. A. (2010). Derivation Approaches for the Theis (1935) Equation. *Ground Water*, 48(1). <https://doi.org/10.1111/j.1745-6584.2009.00568.x>
- Lohman, S. W. (1972). *Definitions of selected ground water terms – revisions and conceptual refinements*. Professional Paper 708, U.S. Geological Survey Water Supply Paper 1988, U.S. Government Printing Office, Washington, D.C.
- Louwyck, A. (2011). *MAxSym - A MATLAB Tool to Simulate Two-Dimensional Axi-Symmetric Groundwater Flow*. Research Unit Groundwater Modeling, Ghent University. Retrieved from <https://github.com/alouwyck/MAxSym>
- Louwyck, A. (2015). *Module Projectwerk programmeren B5 - Ontwikkeling MAxSymMer (in Dutch)* (Associate Degree Programming). CVO Lethas, Brussels.
- Louwyck, A., Vandenbohede, A., Bakker, M., & Lebbe, L. C. (2012). Simulation of axi-symmetric flow towards wells: A finite-difference approach. *Computers & Geosciences*, 44, 136–145. <https://doi.org/10.1016/j.cageo.2011.09.004>
- Louwyck, A., Vandenbohede, A., Bakker, M., & Lebbe, L. C. (2014). MODFLOW procedure to simulate axisymmetric flow in radially heterogeneous and layered aquifer systems. *Hydrogeology Journal*, 22(5), 1217–1226. <https://doi.org/10.1007/s10040-014-1150-0>
- Louwyck, A., Vandenbohede, A., Libbrecht, D., Van Camp, M., & Walraevens, K. (2022). The Radius of Influence Myth. *Water*, 14(2), 149. <https://doi.org/10.3390/w14020149>
- Louwyck, A., Vandenbohede, A., Heuvelmans, G., Van Camp, M., & Walraevens, K. (2023). The Water Budget Myth and Its Recharge Controversy: Linear vs. Nonlinear Models. *Groundwater*, 61(1), 100–110. <https://doi.org/10.1111/gwat.13245>
- Lyu, H.-M., Shen, S.-L., Wu, Y.-X., & Zhou, A.-N. (2021). Calculation of groundwater head distribution with a close barrier during excavation dewatering in confined aquifer. *Geoscience Frontiers*, 12(2). <https://doi.org/10.1016/j.gsf.2020.08.002>
- Maas, C. (1986). The use of matrix differential calculus in problems of multiple-aquifer flow. *Journal of Hydrology*, 88(1–2). [https://doi.org/10.1016/0022-1694\(86\)90196-4](https://doi.org/10.1016/0022-1694(86)90196-4)

- MacDonald, T. R., & Kitanidis, P. K. (1993). Modeling the Free Surface of an Unconfined Aquifer Near a Recirculation Well. *Ground Water*, 31(5). <https://doi.org/10.1111/j.1745-6584.1993.tb00850.x>
- Mansur, C. I., & Kaufman, R. I. (1962). Chapter 3 – Dewatering. In G. A. Leonards (Ed.), *Foundation Engineering* (pp. 241–350). New York: McGraw-Hill.
- Masoodi, R., & Ghanbari, R. N. (2012). Derivation of the Theis (1935) Equation by Substitution. *Ground Water*, 50(1). <https://doi.org/10.1111/j.1745-6584.2011.00886.x>
- Masoud, M. (2020). Groundwater Resources Management of the Shallow Groundwater Aquifer in the Desert Fringes of El Beheira Governorate, Egypt. *Earth Systems and Environment*, 4(1). <https://doi.org/10.1007/s41748-020-00148-8>
- Méité, D., Chesnaux, R., Rafini, S., & Ferroud, A. (2023). Characterizing the radius of influence during pumping tests using the absolute critical drawdown criterion: Cases of integer flow dimensions. *Journal of Hydrology*, 618, 129096. <https://doi.org/10.1016/j.jhydrol.2023.129096>
- Merkl, G. (2008). *Technik der Wasserversorgung: Praxisgrundlagen für Führungskräfte (in German)*. Oldenbourg: Deutscher Industrieverlag.
- Moh, Z.-C., Chuay, H.-Y., & Hwang, R. N. (1996). Large scale pumping test and hydraulic characteristics of Chingmei gravels. In *Proceedings of Twelfth Southeast Asian Geotechnical Conference and the Fourt International Conference on Tropical Soils* (Vol. 1). (pp. 119–124). Kuala Lumpur, Malaysia.
- Motyka, J., & d'Obryn, K. (2022). The radius of influence of mine drainage – Definitions, methods of determination, and practical issues. *Journal of Hydrology*, 613, 128422. <https://doi.org/10.1016/j.jhydrol.2022.128422>
- Narasimhan, T. N. (1998). Hydraulic characterization of aquifers, reservoir rocks, and soils: A history of ideas. *Water Resources Research*, 34(1). <https://doi.org/10.1029/97WR02714>
- Neuman, S. P., & Witherspoon, P. A. (1969a). Applicability of Current Theories of Flow in Leaky Aquifers. *Water Resources Research*, 5(4). <https://doi.org/10.1029/WR005i004p00817>
- Neuman, S. P., & Witherspoon, P. A. (1969b). Theory of Flow in a Confined Two Aquifer System. *Water Resources Research*, 5(4), 803–816. <https://doi.org/10.1029/WR005i004p00803>
- Niu, W.-J., Wang, Z., Chen, F., & Li, H. (2013). Settlement Analysis of a Confined Sand Aquifer Overlain by a Clay Layer due to Single Well Pumping. *Mathematical Problems in Engineering*, 2013. <https://doi.org/10.1155/2013/789853>
- OVAM. (2018). *Standaardprocedure Bodemsaneringsproject (in Dutch)*. Openbare Vlaamse Afvalstoffenmaatschappij, Mechelen, Belgium.
- Perina, T. (2010). Derivation of the Theis (1935) Equation by Substitution. *Ground Water*, 48(1). <https://doi.org/10.1111/j.1745-6584.2009.00610.x>
- Pfannkuch, H.-O., Mooers, H. D., Siegel, D. I., Quinn, J. J., Rosenberry, D. O., & Alexander, S. C. (2021). Review: “Jacob’s Zoo” - how using Jacob’s method for aquifer testing leads to more intuitive understanding of aquifer characteristics. *Hydrogeology Journal*, 29(6). <https://doi.org/10.1007/s10040-021-02363-7>
- Powers, J. P. (1981). *Construction Dewatering – A Guide to Theory and Practice*. New York: John Wiley & Sons.

- Powers, J. P. (1992). *Construction Dewatering: new methods and applications* (2nd ed.). New York: John Wiley & Sons.
- Powers, J. P., Corwin, A. B., Schmall, P. C., & Kaeck, W. E. (2007). *Construction Dewatering and Groundwater Control: New Methods and Applications*. New York: John Wiley & Sons.
- Powrie, W. (2004). *Soil mechanics: concepts and applications* (2nd ed.). New York: Taylor & Francis.
- Puller, M. (2003). *Deep Excavations: a practical manual*. London: Thomas Telford.
- Punmia, B. C., Ashok, K. J., & Arun, K. J. (1995). *Water Supply Engineering* (2nd ed.). New Delhi: Laxmi Publications (P) LTD.
- Rabie, M. H. (2013). Comparative Study between Predicted and Observed Records of Implementation Dewatering Systems at Abu Qir Intake Power Plant, Alexandria. *Journal of American Science*, 9(5), 106–114.
- Sanglerat, G., Olivari, G., & Cambou, B. (1984). *Practical Problems in Soil Mechanics and Foundation Engineering, 1 – Developments in Geotechnical Engineering* (Vol. 34A). Amsterdam: Elsevier Science Publishers B.V.
- Seward, P., Xu, Y., & Turton, A. (2015). Investigating a spatial approach to groundwater quantity management using radius of influence with a case study of South Africa. *Water SA*, 41(1). <https://doi.org/10.4314/wsa.v41i1.10>
- Shampine, L. F. (2008). Vectorized adaptive quadrature in MATLAB. *Journal of Computational and Applied Mathematics*, 211(2). <https://doi.org/10.1016/j.cam.2006.11.021>
- Sichardt, W. (1928). *Das Fassungsvermögen von Rohrbrunnen und seine Bedeutung für die Grundwasserabsenkung, insbesondere für größere Absenkungstiefen (in German)*. Berlin: Verlag Von Julius Springer.
- Smoltczyk, U. (2003). Ground Dewatering. In U. Smoltczyk (Ed.), *Geotechnical Engineering handbook* (Vol. 2, pp. 365–398). John Wiley & Sons.
- Soni, A. K., Sahoo, L. K., Ghosh, U. K., & Khond, M. V. (2015). Importance of Radius of Influence and its Estimation in a Limestone Quarry. *Journal of The Institution of Engineers (India): Series D*, 96(1). <https://doi.org/10.1007/s40033-014-0059-z>
- Sophocleous, M. (2012). Retracted: On Understanding and Predicting Groundwater Response Time. *Groundwater*, 50(4). <https://doi.org/10.1111/j.1745-6584.2011.00876.x>
- Stehfest, H. (1970). Algorithm 368: Numerical inversion of Laplace transforms [D5]. *Communications of the ACM*, 13(1). <https://doi.org/10.1145/361953.361969>
- Stone, H. L. (1968). Iterative Solution of Implicit Approximations of Multidimensional Partial Differential Equations. *SIAM Journal on Numerical Analysis*, 5(3), 530–558. <https://doi.org/10.1137/0705044>
- Strack, O. D. L. (1989). *Groundwater Mechanics*. Old Tappan, N. J.: Prentice-Hall.
- Strack, O. D. L. (2017). *Analytical Groundwater Mechanics*. Cambridge University Press.
- Theis, C. V. (1935). The relation between the lowering of the Piezometric surface and the rate and duration of discharge of a well using ground-water storage. *Transactions, American Geophysical Union*, 16(2), 519–524. <https://doi.org/10.1029/TR016i002p00519>

- Theis, C. V. (1940). The source of water derived from wells: essential factors controlling the response of an aquifer to development. *Civil Engineering*, 10, 277–280.
- Thiem, A. (1870). Die Ergiebigkeit artesischer Bohrlöcher, Schachtbrunnen und Filtergalerien (in German). *Journal Für Gasbeleuchtung Und Wasserversorgung*, 13, 450–467.
- Thiem, G. (1906). *Hydrologische Methoden (in German)*. Leipzig: Gebhardt.
- Veling, E. J. M., & Maas, C. (2010). Hantush Well Function revisited. *Journal of Hydrology*, 393(3–4). <https://doi.org/10.1016/j.jhydrol.2010.08.033>
- VMM. (2019). *Richtlijnen bemalingen ter bescherming van het milieu (in Dutch)*. Vlaamse Milieumaatschappij, Aalst, Belgium.
- VMM. (2020). *Handleiding berekeningsinstrument bemalingen (in Dutch)*. Vlaamse Milieumaatschappij, Aalst, Belgium.
- Wang, X.-W., Yang, T.-L., Xu, Y.-S., & Shen, S.-L. (2019). Evaluation of optimized depth of waterproof curtain to mitigate negative impacts during dewatering. *Journal of Hydrology*, 577. <https://doi.org/10.1016/j.jhydrol.2019.123969>
- Weber, H. (1928). *Die Reichweite von Grundwasserabsenkungen mittels Rohrbrunnen (in German)*. Berlin: Springer-Verlag.
- Willems, E., Monseré, T., & Dierckx, J. (2009). *Geactualiseerd richtlijnenboek milieueffectrapportage - Basisrichtlijnen per activiteitengroep – Landbouwdieren (in Dutch)*. Dienst MER, Afdeling Milieu-, Natuur- en Energiebeleid, Departement Leefmilieu, Natuur en Energie, Brussels.
- Wu, Y.-X., Shen, S.-L., Lyu, H.-M., & Zhou, A.-N. (2020). Analyses of leakage effect of waterproof curtain during excavation dewatering. *Journal of Hydrology*, 583. <https://doi.org/10.1016/j.jhydrol.2020.124582>
- Yihdego, Y. (2018). Engineering and enviro-management value of radius of influence estimate from mining excavation. *Journal of Applied Water Engineering and Research*, 6(4). <https://doi.org/10.1080/23249676.2017.1287022>
- Yihdego, Y., & Drury, L. (2016). Mine dewatering and impact assessment in an arid area: Case of Gulf region. *Environmental Monitoring and Assessment*, 188(11). <https://doi.org/10.1007/s10661-016-5542-6>
- Yihdego, Y., & Paffard, A. (2017). Predicting Open Pit Mine Inflow and Recovery Depth in the Durvuljin soum, Zavkhan Province, Mongolia. *Mine Water and the Environment*, 36(1). <https://doi.org/10.1007/s10230-016-0419-z>
- Zeng, C.-F., Zheng, G., & Xue, X.-L. (2019). Responses of deep soil layers to combined recharge in a leaky aquifer. *Engineering Geology*, 260. <https://doi.org/10.1016/j.enggeo.2019.105263>
- Zeng, C.-F., Wang, S., Xue, X.-L., Zheng, G., & Mei, G.-X. (2021). Evolution of deep ground settlement subject to groundwater drawdown during dewatering in a multi-layered aquifer-aquitard system: Insights from numerical modelling. *Journal of Hydrology*, 603. <https://doi.org/10.1016/j.jhydrol.2021.127078>
- Zhai, Y., Cao, X., Jiang, Y., Sun, K., Hu, L., Teng, Y., et al. (2021). Further Discussion on the Influence Radius of a Pumping Well: A Parameter with Little Scientific and Practical Significance That Can Easily Be Misleading. *Water*, 13(15). <https://doi.org/10.3390/w13152050>

Zhang, X., Wang, X., & Xu, Y. (2021). Influence of Filter Tube of Pumping Well on Groundwater Drawdown during Deep Foundation Pit Dewatering. *Water*, 13(22).
<https://doi.org/10.3390/w13223297>

Zheng, Y., Lei, J., Wang, F., Xiang, L., Yang, J., & Xue, Q. (2021). Investigation on Dewatering of a Deep Shaft in Strong Permeable Sandy Pebble Strata on the Bank of the Yellow River. *Geofluids*, 2021.
<https://doi.org/10.1155/2021/9994477>

Zhou, Y. (2009). A critical review of groundwater budget myth, safe yield and sustainability. *Journal of Hydrology*, 370(1–4). <https://doi.org/10.1016/j.jhydrol.2009.03.009>

Zhou, Y. (2011). Sources of water, travel times and protection areas for wells in semi-confined aquifers. *Hydrogeology Journal*, 19(7). <https://doi.org/10.1007/s10040-011-0762-x>

Chapter 11. The Water Budget Myth and Its Recharge Controversy: Linear versus Nonlinear Systems

11.1. Introduction

This chapter stems from a discussion about the validity of estimating an extraction's radius of influence by assuming the pumping rate is balanced by the infiltration rate, an idea which Brown (1963) and Bredehoeft (2002) call fallacious. In Flanders and in the Netherlands, it is not an unusual practice, however, to include infiltration in models simulating pumping induced drawdown (e.g. Blom, 1973; Ernst, 1971; De Smedt, 2006; Verruijt, 1970), although it is true that most axisymmetric models applied to calculate the cone of depression do not consider recharge (e.g. de Glee, 1930; Hantush & Jacob, 1955; Hemker, 1984, 1985, 1999; Jacob, 1946; Theis, 1935). As explained in Chapter 2, omitting the recharge is allowed if the superposition principle is valid, in which case it is assumed the groundwater reservoir can be analyzed mathematically as if it is a linear system (Bredehoeft, 2007).

The discussion is part of a more general controversy in the hydrogeological literature about the role of recharge in assessing whether a groundwater extraction is sustainable or not. This controversy originates in the water budget myth (Bredehoeft, 2002; Bredehoeft et al., 1982), which is the idea that safe pumping must not exceed the initial recharge. To refute the concept of safe yield, a simplified water budget equation is used, which equates the total pumping rate to the sum of capture and storage change (Bredehoeft, 2002; Bredehoeft et al., 1982). Since initial recharge and discharge are canceled out from this equation, it is concluded that sustainable pumping has nothing to do with recharge (Bredehoeft, 1997, 2002, 2007). After summarizing the literature about the recharge controversy, the assumptions underlying this equation are investigated, and it is seen that it indeed expresses the superposition principle.

However, one should always be aware of the underlying model assumptions, and keep in mind they are meant to simplify the problem at hand, and therefore cannot be generalized. Two analytical solutions for one-dimensional radial flow to a well are used to demonstrate the assumption of linearity, supporting the idea that sustainable pumping has nothing to do with initial recharge, may not be generalized either. First, the island example presented by Bredehoeft et al. (1982) and Bredehoeft (2002) is discussed, and the solution for unconfined flow is given to show that the recharge is one of the key parameters determining whether the system can be analyzed as if it is a linear system or not. In the subsequent section, a dense network of draining ditches and canals is added to the island, and a solution presented by Ernst (1971) is given that implements these draining elements as a nonlinear function. This solution is also presented in Chapter 7 and Chapter 10.

In the second island example, the recharge is again one of the key parameters that determine whether the drains are active or not. The asymptotic solution for zero resistance even shows that the cone of depression stops expanding when the pumping rate is balanced by the recharge rate. Although it is true the cone of depression almost never coincides with the capture zone, which Brown (1963) calls the area of diversion, it is not fundamentally wrong to estimate the radius of influence from the area in which the same volume of water is infiltrated as the extracted volume. In

fact, the Ernst (1971) model is in complete agreement with the water budget equations presented by Bredehoeft et al. (1982) and Bredehoeft (2002).

Linear models implicitly assume the groundwater reservoir can be depleted indefinitely and boundary conditions are an infinite source of water. If an aquifer is modeled assuming its saturated thickness is constant, then a pumping well extracting from this aquifer can never go dry. Similarly, a linear boundary condition that defines a source or sink interacting with an aquifer, never goes dry either. To evaluate sustainability, however, the limits of the aquifer system must be examined accurately. Theoretically, this can only be accomplished by applying nonlinear models, in which case setting up the simplified water budget equation is impossible without knowing the initial conditions. Hence, excluding recharge when assessing sustainable pumping may not be done inconsiderately.

A shortened version of this chapter is published in *Ground Water* (Louwyck et al., 2023). Author contributions are given in section 1.5 of the introductory Chapter 1. The literature overview is updated, and references are reformatted to be consistent with the other chapters. The section presenting the finite-difference approximation of the simplified water budget equation (Bredehoeft, 2002; Bredehoeft et al., 1982) is not discussed in Louwyck et al. (2023). As numerical models, and especially MODFLOW (Harbaugh, 2005; Harbaugh et al., 2000; Langevin et al., 2017), are considered state-of-the-art for evaluating the impacts of a groundwater development (Zhou, 2009), this section is added to prove the recharge controversy is not about the difference between traditional analytical modeling and the present-day approach that advocates numerical modeling. More specifically, it is illustrated that the superposition principle not only applies to analytical models by revisiting the numerical example presented by Zhou (2009).

11.1.1. The recharge controversy

This section addresses the controversy in the hydrogeological literature about the role of recharge in assessing whether or not a groundwater extraction is sustainable. The controversy started with an editorial written by Sophocleous (1997) explaining why the concept of safe yield, which limits groundwater pumping to the natural recharge, leads to continued groundwater depletion, stream dewatering, and loss of wetland and riparian ecosystems. Sophocleous (1997) refers to Theis (1940), who concisely stated the underlying hydrologic principles, which are revisited by Konikow and Leake (2014). Under natural conditions, aquifer systems are in a dynamic state of equilibrium; hence, recharge is balanced by discharge. If water is pumped from an aquifer system, the extracted volume is balanced by storage change, an increase in recharge, and/or a decrease in discharge. When pumping starts, the water almost exclusively comes from storage, whereas it is the capture, i.e. the increase in recharge plus the decrease in discharge (Lohman, 1972a), which balances the extracted amount of water when the system is brought into a new state of equilibrium. According to Sophocleous (1997), the timing of this transition is a key factor in developing sustainable water-use policies, but as it is exceedingly difficult to distinguish between natural and induced recharge, further research is needed in this area, for instance by calibrating stream-aquifer models which are capable of generating these transition curves. These ideas are further developed and translated into practice by Sophocleous (2000, 2002, 2005).

In a subsequent editorial, Bredehoeft (1997) called the editorial written by Sophocleous (1997) an especially important one, as it explains why the idea of safe yield is fallacious. Bredehoeft (1997) also refers to Theis (1940), and to Bredehoeft et al. (1982), who term this idea the groundwater budget myth. Bredehoeft (1997) elaborates on the dynamic nature of the capture that depends on both the geometry of the aquifer system and the hydraulic properties such as permeability and specific storage. In his experience, the change in recharge due to pumping is difficult or even impossible to

quantify. Recharge usually is fixed by rainfall and does not increase by development; hence, only reduced discharge may bring the groundwater system into a new state of equilibrium. Bredehoeft (1997) concludes sustainable groundwater development has almost nothing to do with recharge, and therefore, the focus of research should not be on induced recharge, as suggested by Sophocleous (1997).

Bredehoeft (2002) revisits the water budget myth, because the Bredehoeft et al. (1982) paper appeared in an obscure publication. Again, Bredehoeft (2002) refers to Theis (1940), and additionally, to Brown (1963), who also debunks the water budget myth. He also mentions more recent studies (Alley et al., 1999; Sophocleous, 2000), but remarks that the fundamental principles stated by Theis (1940) are not well understood by many groundwater professionals. Bredehoeft (2002) explains how traditional analytical models apply the principle of superposition to assess the impact of wells on the groundwater system. These models calculate the cone of depression which is superimposed on the initial head. The infiltration flux is required only to solve the initial boundary value problem. To simulate the cone of depression, only the aquifer diffusivity, the boundary conditions, and the pumping rates are needed; initial recharge and discharge are not required. Bredehoeft (2002) thus concludes that the initial rate of recharge is not important at all in determining the size of a sustainable extraction. This is in line with Maddock and Vionnet (1998) who show that even seasonal variations of recharge and discharge do not determine capture.

Sophocleous and Devlin (2004) agree with the arguments given by Bredehoeft (2002), but they believe he condemns the association between recharge and sustainability so forcefully, groundwater practitioners may get the impression that recharge is not worth considering at all. According to Sophocleous and Devlin (2004), recharge is important because sustainability encompasses more than sustainable pumping; other factors such as water quality, ecology and socioeconomic considerations also play an important role. Another argument given by Sophocleous and Devlin (2004) is that a large initial discharge, originating from initial recharge of the same volume, can support a large reduced discharge to balance the pumping rate. Devlin and Sophocleous (2005) elaborate on the arguments discussed by Sophocleous and Devlin (2004), and suggest to separate the concepts of sustainable pumping and sustainability, since recharge rates are deemed irrelevant to the first, whereas they are not to the latter, as sustainability is a much broader concept and cannot be considered from solely a groundwater perspective.

This is in agreement with Alley et al. (1999) who define groundwater sustainability as the development and use of groundwater in a manner that can be maintained for an indefinite time without causing unacceptable environmental, economic, or social consequences. Alley and Leake (2004) even argue that sustainability is not a purely scientific concept, but an evolving perspective that challenges hydrologists to translate complex and vague socioeconomic questions into quantifiable problems. This requires “integrated groundwater management”, which is an approach of “thinking beyond the aquifer” to get to a more encompassing view of steps needed to have sustainable groundwater resources (Jakeman et al., 2016). Maimone (2004) also points to the confusion between the simple concept of aquifer yield and sustainable yield which cannot be summarized in a single and correct number. Similarly, Seward et al. (2006) distinguishes between borehole yield, which is dependent on what capture of groundwater is possible, and basin yield that adds to this how much capture is permissible. Wood (2020) emphasizes that the societal value of groundwater includes both quantity and quality aspects, and even suggests replacing the term sustainability with a word that incorporates both aspects, such as groundwater durability.

Loáiciga (2006) comments on the paper written by Devlin and Sophocleous (2005), and finds the distinction between sustainable pumping and sustainability superfluous. Mathematically, Loáiciga’s

(2006) interpretation comes down to a maximization problem, and the solution to this problem shows that the sustainable pumping rate cannot exceed the initial recharge. Loáiciga (2006) concludes that the water budget myth is an innocuous, if not laudable concept, as it is a meaningful and correctly derived pumping rate under the definition of sustainable pumping proposed by Loáiciga (2002). Loáiciga (2006) also solves the transient groundwater budget equation, which yields a sustainable pumping rate as a function of time. This adaptive sustainable pumping requires knowledge of the recharge, which is also a function of time, as precipitation varies with time (Loáiciga, 2006). Devlin and Sophocleous (2006) argue that Loáiciga's (2006) comment illustrates there is confusion in the hydrogeological community about sustainable pumping and sustainability, which is partially semantic. According to Devlin and Sophocleous (2006), Loáiciga's (2006) definition of sustainable pumping is consistent with use of the term sustainability by Devlin and Sophocleous (2005), and introducing the transient case redefines the scope of the discussion. Consequently, Devlin and Sophocleous (2006) maintain that recharge estimates are not necessary for the calculation of sustainable pumping rates, whereas they are required for the assessment of sustainability.

Kalf and Woolley (2005) agree with Bredehoeft (2002) to the extent that a determination of natural recharge alone is an oversimplification for determining sustainability, but conclude that the water budget myth is not necessarily a myth, from a basin groundwater sustainability perspective, and that natural recharge is not irrelevant. It is required to determine the pre-development conditions, and the interception of natural discharge must always be equal or less than an equal rate of natural recharge, given the basin initially was in equilibrium. Kalf and Woolley (2005) also discuss the hypothetical Basin and Range example given by Bredehoeft et al. (1982), Bredehoeft (2002), and Bredehoeft and Durbin (2009), and consider the same basin in a more humid environment with a large permanent river meandering across it. In this case, the well-field performance would be controlled largely by induced recharge provided that this river flow is comprised of runoff. By contrast, Bredehoeft et al. (1982) assume recharge is independent of the pumping in the basin, which is a typical condition in the arid west of the United States.

As already mentioned above, Bredehoeft (1997, 2002) generalizes this assumption to most groundwater situations, arguing recharge is a function of external conditions such as rainfall and vegetation. This implies there is no change in recharge and the extracted water is balanced by a decrease in initial discharge. In an editorial titled "It is the discharge", Bredehoeft (2007) repeats his point of view, and advocates to examine the discharge of a groundwater system, as it is more fruitful than focusing on the recharge; the latter is difficult to quantify, and human activities that impact a groundwater system ultimately impact the former. Bredehoeft (2007) also states that many aquifers can be analyzed mathematically as if they are linear systems, even water table aquifers where the change in head does not change the saturated thickness greatly. Leake (2011) emphasizes that rates and directions of groundwater flow do not matter when determining capture in a reasonably linear system. If the system is linear, it is justified to apply the principle of superposition, which is discussed in more detail by Bredehoeft (2002). The nonlinear case is discussed by Leake et al. (2010), who conclude that in general, the capture is overestimated when nonlinearities are linearized.

Zhou (2009) agrees that the traditional idea of safe yield is a misconception, but states that both the natural recharge and the dynamic development of the capture determine the sustainability of a groundwater development. Zhou (2009) concludes that the aquifer storage will be depleted if the pumping rate is larger than the total recharge, i.e. initial plus induced recharge. Zhou (2009) also believes that it is difficult to determine the capture, whereas it is more convenient to determine total recharge and total discharge under development conditions, an argument that is also given by van

der Gun and Lippinen (2010). Both Zhou (2009) and van der Gun and Lippinen (2010) mention that the natural recharge and the sustainable pumping rate, which is balanced by the maximum capture, are correlated. Van der Gun and Lippinen (2010) indicate this correlation is strong when capture mainly consists of reduced discharge, and they argue that in case of a closed arid groundwater basin, such as the Basin and Range example discussed by Bredehoeft (2002), a model is not required to see the maximum capture is virtually equal to the initial recharge. The situation is different when the groundwater system interacts with a permanent surface water body, in which case the induced recharge from the latter plays an important role. In many other cases, however, the maximum rate of sustainable pumping may be expressed as a fraction of the initial recharge (Van der Gun & Lippinen, 2010).

Seward et al. (2015) question Zhou's (2009) statement that aquifer sustainability depends on both natural recharge and capture, as the first is missing in Bredehoeft's (2002) capture equation. Seward et al. (2015) also believe a large part of the hydrogeological community see no harm in 'pumping the recharge' approaches to sustainability, referring to Balleau (2013), although the latter suggests to abandon the traditional concept of safe yield from the administrative functions, as the concept was dismissed by groundwater experts long time ago. Balleau (2013) even disapproves the use of a ratio of natural recharge to well-field withdrawals as indicator of sustainability by Wada et al. (2010). Ferguson (2021) also criticizes Wada (2016) and Bierkens and Wada (2019) for applying recharge based approaches, and substantiates his comment referring to Bredehoeft (2002).

11.1.2. Objective

The cited literature proves that there is still controversy about the role of recharge in studying groundwater sustainability. Devlin and Sophocleous' (2005) suggestion to distinguish between basin sustainability and sustainable pumping is very useful, as the recharge controversy indeed is not about sustainability. Even Bredehoeft (2007) admits that recharge is of interest to fully understand the groundwater system, as it determines, for instance, how contaminants are transported through the system. Moreover, if recharge had nothing to do with sustainability, managed aquifer recharge, which is considered an effective technique to secure groundwater resources (Zhang et al., 2020), would be a false promise.

Therefore, discussing sustainability is not within the scope of this study, which aims to show that, within the context of sustainable pumping, making the distinction between linear and nonlinear models is of utmost importance. This means recharge is irrelevant for the estimation of sustainable pumping rates if and only if the aquifer system can be analyzed mathematically as if it is a linear system, as pointed out by Bredehoeft (2007). If this assumption is not met, then recharge must be taken into account, even when the problem at hand only requires the simulation of the cone of depression caused by the pumping. Additionally, it is argued that the mathematical assumption of a linear system comes down to the assumption that the extraction is sustainable. This underlying circular reasoning makes the use of linear models theoretically questionable if applied to evaluate sustainable pumping and sustainability in general, even if these models are preferred over nonlinear models, from a practical point of view, as the latter cause more convergence difficulties (Mehl, 2006).

These ideas are illustrated by discussing two simple well-flow problems that can be solved by applying analytical models. First, the Bredehoeft et al. (1982) and Bredehoeft (2002) example of a circular island is used to demonstrate that the nonlinear solution with head-dependent aquifer transmissivity requires knowledge of the initial conditions. In this case, the initial recharge also determines whether the pumping is sustainable or not, and superposition is applicable only if specific

conditions are met. Second, Ernst's (1971) analytical solution is discussed in detail by adopting the circular island example and reframing it to humid climatic conditions. As the Ernst (1971) model includes a nonlinear drainage boundary condition, it is examined again under what conditions superposition is applicable. And again, the recharge appears to be one of the key parameters in determining whether the system can be analyzed as a linear system or not.

Using the Ernst (1971) model, it is also shown that balancing pumping and infiltration rate to determine the extent of the cone of depression corresponds to the asymptotic solution with zero drainage resistance, which is a misconception according to Brown (1963) and Bredehoeft (2002). In Flanders and in the Netherlands, it is not an unusual practice, however, to take into account the recharge when simulating pumping induced drawdown (Blom, 1973; De Smedt, 2006), and the solution presented by Ernst (1971) proves that balancing pumping and infiltration rate is in complete agreement with the water budget equations presented by Bredehoeft et al. (1982) and Bredehoeft (2002).

The island examples may be considered atypical, however, and since numerical models nowadays predominate, the finite-difference formulation of the water budget equation is also examined, and applied to the numerical modeling example given by Zhou (2009). Although numerical models are capable of incorporating more realistic boundary conditions, by definition, a groundwater model is a simplified mathematical description of reality, whether it is numerical or analytical. Therefore, it may not be confused with the real aquifer system, as it is based on a series of assumptions. In the next section, the assumptions underlying the simplified water budget equation presented by Bredehoeft et al. (1982) and Bredehoeft (2002) are unraveled, and it is explained why applying the superposition method implicitly assumes the extraction is sustainable.

11.2. The water budget equation revisited

The basic idea that the amount of extracted groundwater is balanced by a change in storage, a change in recharge, and a change in discharge, is stated first by Theis (1940), and expressed using water balance equations by Lohman (1972b), who mentions Cooper formulating these equations back in 1967. The same equations are presented by Bredehoeft et al. (1982) and Bredehoeft (2002) to debunk the water budget myth, and therefore, they are an integral part of almost every article discussing the myth.

In general, the groundwater balance at time t [T] is:

$$R_t - D_t - \frac{dV_t}{dt} = 0 \quad (1)$$

with R_t the total recharge [L^3/T], D_t the total discharge [L^3/T], and V_t the groundwater storage [L^3]. Note that R and D in equation (1) are always positive, whereas storage change dV/dt is positive when water is removed from the aquifer. If $dV/dt = 0$, then the aquifer system is in a steady state. In natural circumstances, recharge may result from rainfall percolating through the soil or from surface water infiltrating into the aquifer system (Theis, 1940). If equation (1) expresses the total water balance of a multi-aquifer system, it includes all layers in the system, in which case the vertical flow between layers is not considered as recharge.

To study the hydrological impact of a groundwater extraction with pumping rate Q_t [L^3/T], the water budget equation (1) is reformulated as:

$$(R_0 + \Delta R_t) - (D_0 + \Delta D_t) - Q_t - \frac{dV_t}{dt} = 0 \quad (2)$$

with R_0 and D_0 the initial recharge and discharge, respectively, at time $t = 0$, when the extraction starts; $\Delta R_t = R_t - R_0$ is the change in initial recharge at time t , and $\Delta D_t = D_t - D_0$ is the change in initial discharge at time t . Note that in equation (2), total pumping rate Q_t is separated from the other sinks that discharge water from the aquifer system. When discussing the water budget myth, a constant pumping rate is assumed, hence $Q_t = Q$, which is positive if water is extracted. Moreover, Q should be interpreted as the net pumping rate. The distinction between total and net pumping rates is relevant, especially in cases such as pumping for irrigation (Devlin & Sophocleous, 2005; Kendy, 2003).

From (1), it follows that $R_0 = D_0$ if it is assumed the groundwater system is in a state of dynamic equilibrium at $t = 0$, as storage change is zero by definition under this assumption. This reduces equation (2) to:

$$Q = \Delta R_t - \Delta D_t - \frac{dV_t}{dt} \quad (3)$$

with $\Delta R_t - \Delta D_t$ the capture at time t , also termed “depletion” according to Leake (2011). Equation (3) expresses the basic principle that the extracted water is balanced by the capture and the storage change. The initial recharge R_0 is absent from equation (3); hence, the concept of safe yield is a myth, as it states that pumping is safe if $Q \leq R_0$ (Bredehoeft, 2002; Bredehoeft et al., 1982). Another water budget myth is the idea that the volume V of groundwater in storage is by itself meaningful in the analyses of water availability (Alley, 2007). Besides the fact that not all groundwater in storage is recoverable with pumping wells (Alley, 2007), equation (3) shows indeed that aquifer storage is not the only quantity that must be taken into account.

If the system is brought into a new state of equilibrium, then the pumping rate is only balanced by the capture:

$$Q = \lim_{t \rightarrow \infty} (\Delta R_t - \Delta D_t) \quad (4)$$

Mathematically, (4) is obtained after an infinitely large period of pumping. In reality, the time to full capture is finite, ranging from a few seconds to centuries or possibly millions of years (Bredehoeft & Durbin, 2009; Sophocleous, 2012). It is also possible a new steady state may never be reached if the pumping rate is too large to be balanced by the capture. In this case, the groundwater reservoir continues to be depleted until the extraction runs dry. Therefore, sustainable pumping means that the aquifer system can be brought into a new state of dynamic equilibrium, which implies equation (4) has a real solution. As already mentioned in the introduction, sustainable pumping may not be confused with sustainability, which is a much broader concept (Devlin & Sophocleous, 2005).

Recall that equation (3) is only valid under certain assumptions: the first assumption is the constant pumping rate Q , the second is the initial steady state, from which it follows that $R_0 = D_0$. In many real-world cases, however, pumping rates are time-dependent, and new extractions may be planned in exploited aquifer systems that are not in a state of dynamic equilibrium. The transient case is discussed by Loáiciga (2006), who shows that in this case, recharge as a function of time may be considered. If the second assumption is not met, then the initial recharge does not equal the initial discharge, which means that both are required to simulate the initial conditions before pumping. Otherwise, equation (3) is true, from which it is concluded that sustainable pumping is independent of initial recharge and discharge (Bredehoeft, 1997, 2002, 2007; Devlin & Sophocleous, 2005; Sophocleous & Devlin, 2004).

However, a third assumption mentioned by Bredehoeft (2002, 2007) must also be taken into account: the superposition property, which is explained in section 2.4 of Chapter 2 and in many hydrogeology textbooks (e.g. Bruggeman, 1999; Haitjema, 1995; Kruseman & de Ridder, 1990;

Verruijt, 1970). Applied to pumping wells, the principle of superposition or linearity principle states that drawdowns due to individual constant-discharge wells can be summed to obtain the total drawdown caused by these extractions. However, this principle is only valid if the governing differential equation is homogeneous and linear, and if all individual solutions satisfy the boundary and initial conditions (Bruggeman, 1999). The differential equation describing horizontal flow in an unconfined aquifer is the canonical example of a nonlinear problem for which the superposition principle does not hold, because the saturated aquifer thickness is a function of the hydraulic head. Superposition is also not allowed if the aquifer is recharged by a constant infiltration flux, as in this case, the governing differential equation is nonhomogeneous, and a typical example of a nonlinear boundary condition is the MODFLOW drain (Harbaugh, 2005; Harbaugh et al., 2000), because its conductance is head-dependent.

The total amount of water V_t available in the groundwater reservoir at time t is found by solving differential equation (1) subject to given initial and boundary conditions. As already mentioned, this volume is less than the product of the horizontal area of the aquifer, the saturated thickness, and the specific yield, as it is impossible to remove all water from storage with pumping wells (Alley, 2007). In most cases, equation (1) can only be solved by applying a groundwater model, since total recharge, total discharge, and storage change are dependent on the hydraulic head h [L], which is a function of space and time. Indeed, the response of the aquifer system is not immediate, nor is it equally distributed, but it depends on the position of the pumping wells and their distance to the sources and sinks, and on the hydraulic properties of the aquifer system (Bredehoeft et al., 1982).

Equation (1) only expresses the law of conservation of matter (Devlin & Sophocleous, 2005), whereas flow within the system is determined by the hydraulic heads according to Darcy's law. Hence, R , D , and V are functions of hydraulic head h [L], and therefore, the change in recharge ΔR_t and the change in discharge ΔD_t should be written as:

$$\Delta R_t = R(h_t) - R(h_0) \quad (5)$$

$$\Delta D_t = D(h_t) - D(h_0) \quad (6)$$

In essence, the discussion about the relevance of the initial recharge (and discharge) comes down to the question if ΔR_t (and ΔD_t) can be calculated directly without knowing R_0 (and D_0). Since this question is not answered yet, equation (3) needs to be rewritten using (5) and (6):

$$Q = [R(h_t) - R(h_0)] - [D(h_t) - D(h_0)] - \frac{\partial V(h_t)}{\partial t} \quad (7)$$

Drawdown s [L] expresses the effect of pumping on the hydraulic head, as it is defined as the change in head due to pumping:

$$s_t = h_t(h_0) - h_0 \quad (8)$$

Note that in general, hydraulic head h_t at time t is a function of initial head h_0 at $t = 0$. However, if h_0 is constant, then there is no flow in the pre-developed aquifer system, hence, initial recharge and discharge are zero, and hydraulic head h_t is independent of initial head h_0 . Under this assumption, equation (7) simplifies to:

$$Q = R(s_t) - D(s_t) - \frac{\partial V(s_t)}{\partial t} \quad (9)$$

Since equation (9) is equivalent to equation (3), quantity $R(s_t) - D(s_t)$ is the capture.

Assuming a horizontal piezometric surface before pumping is common in aquifer test interpretation (Kruseman & de Ridder, 1990), although equation (9) is also valid under a less strict assumption.

Indeed, if the differential equation and the boundary conditions describing the groundwater flow problem are linear, then the superposition principle holds:

$$L(ah_t + bh_0) = aL(h_t) + bL(h_0) \quad (10)$$

with a and b arbitrary constants, and L a response function, in this case R , D , and V . If (10) holds and $dV_0/dt = 0$ implying h_0 is independent of time, equation (7) can be written as:

$$Q = R(h_t - h_0) - D(h_t - h_0) - \frac{\partial V(h_t - h_0)}{\partial t} \quad (11)$$

Applying equation (8) to equation (11) indeed results in equation (9), which is the water budget equation for models simulating drawdown s_t directly by applying the principle of superposition. In these models, hydraulic head h_t is independent of initial head h_0 , which follows from (10). Recall that the initial head must be steady, although uniformity is not required, which means constant groundwater flow is allowed in the initial aquifer system.

Models that simulate drawdown directly, under the assumption of linearity, only consider changes in recharge and discharge, and they do not distinguish between both. That is why “rates and directions of groundwater flow don’t matter”, to quote Leake (2011). If it is assumed recharge through percolation is not affected by the pumping, then it is not included in these models. And that is exactly the point made by Bredehoeft (1997, 2002, 2007). To evaluate the change in flow in the aquifer system or the alterations in the interactions with sources and sinks, the drawdowns are superimposed on the initial heads afterwards.

If some of the equations involved in the mathematical problem statement are not linear, however, then superposition is not possible, and equation (11) cannot be applied. This means that hydraulic head h_t during pumping depends on initial head h_0 , and the capture on initial recharge R_0 and initial discharge D_0 . In other words, equation (7) cannot be reduced to equation (11) if the problem is not linear. Therefore, the question whether initial recharge is relevant or not in evaluating sustainable pumping comes down to the question if the assumption of linearity is justified when assessing the sustainability of an extraction.

As already mentioned, it is common practice to apply superposition models when interpreting aquifer tests. Since these tests are temporary and mostly have limited impact on the hydraulic head, the assumption of linearity is justified in most cases. Using superposition to evaluate the impact of permanent groundwater extractions, however, is questionable or at least subject to caution, since linear systems implicitly assume unlimited resources of water. In a linear model, the saturated thickness of aquifers and aquitards are constant, as are the boundary conditions implementing the interaction with surface water bodies. As a consequence, a new state of equilibrium is always reached, and if not, the system continues to be depleted, because wells cannot go dry and sources cannot dry up.

Obviously, simulation results can always be verified against drawdown and flux constraints. This may be done manually or through application of optimization techniques such as linear programming (Ahlfeld et al., 2005, 2009). But linear models also tend to underestimate drawdown, and therefore, the impact of the extraction. For instance, if a well in an unconfined aquifer extracts water, then the water table is lowering, which in reality reduces the transmissivity of the aquifer. This can only be simulated accurately using a nonlinear model that calculates transmissivity as a function of the saturated thickness. A linear model keeping transmissivity constant, simulates a shallower cone of depression, and therefore, underestimates the aquifer depletion.

Another example is a stream that is only capable of draining groundwater and dries up when the water table drops below a certain level. The interaction between aquifer and stream may be modeled using a head-dependent flux defined by a constant drainage level and drainage resistance. The latter should be head-dependent, as it must become infinitely large if the head drops below the drainage level. MODFLOW's drain package (Harbaugh, 2005; Harbaugh et al., 2000), for instance, provides such a nonlinear boundary condition. However, in a linear model that keeps the resistance constant, the stream may become an extra source, as it starts to irrigate when the head is lower than the drainage level, which may result in an underestimation of the cone of depression.

Sheets et al. (2015) investigated the approximation error produced by the simulation of water-table aquifers using a constant saturated thickness, and they report a maximum error of about 20 % when maximum drawdowns are about 35 % of the initial saturated thickness. Therefore, they recommend the use of the specified-thickness approximation in early phases of model development and in applications that require many model runs to save execution time and improve solution stability. Leake et al. (2010) argue that nonlinear responses are more likely to occur when pumping rates are large, but weaken the importance of nonlinearities by stating that their general effect is to overestimate the capture when they are removed from the model. However, water budget equation (3) clearly indicates that overestimating the capture leads to an underestimation of the storage change, and hence, the cone of depression. This confirms that applying superposition should be done carefully, not only to assess sustainability in the broadest sense of the word, but also to evaluate whether an extraction is sustainable or not.

11.3. Bredehoeft's island

Consider the circular island situated in a freshwater lake shown in Figure 1 and discussed by Bredehoeft et al. (1982) and Bredehoeft (2002). The phreatic aquifer on the island is recharged by rainfall and discharges into the lake. It is bounded below by an impermeable aquiclude, and a well at the center of the island extracts water from it at constant pumping rate.

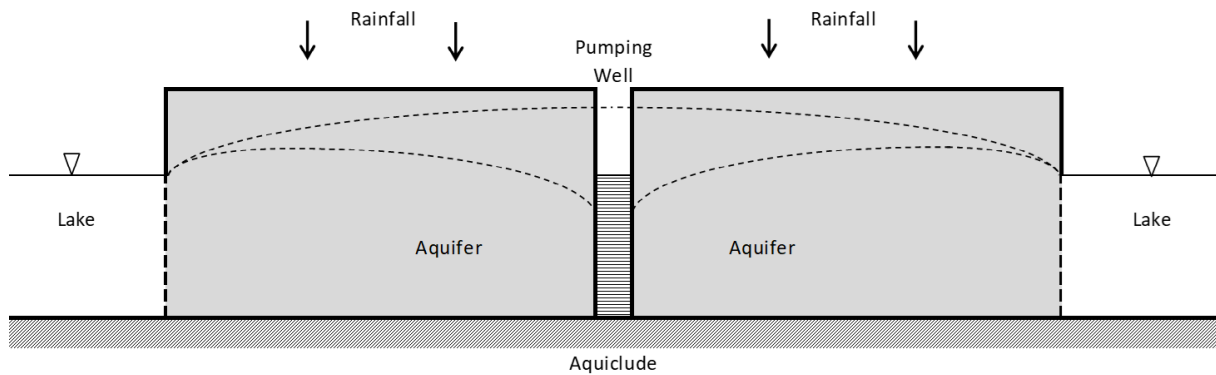


Figure 1. Sketch of the circular island aquifer system discussed by Bredehoeft et al. (1982) and Bredehoeft (2002).

After a period of pumping, the system is brought into a new equilibrium, and the steady head in the unconfined aquifer is calculated using the following nonlinear equation (Verruijt, 1970):

$$h(r) = \sqrt{h_c^2 + \frac{N}{2K}(r_c^2 - r^2) + \frac{Q}{\pi K} \ln \frac{r}{r_c}} \quad (12)$$

where h is the hydraulic head [L]; r is the radial distance [L] to the well; h_c is the water level in the lake, which defines the constant head [L] at the outer boundary of the island at distance r_c , the radius [L] of the island; K is the hydraulic conductivity [L/T] of the aquifer; N is the infiltration flux

[L/T]; and Q is the pumping rate [L³/T] of the well. In case of recharge, N is positive. Recall that Q is positive in case of extraction. The initial steady head h_0 , before the extraction starts, is also given by (12) for $Q = 0$. If there is no infiltration, i.e. $N = 0$, then $h_0 = h_c$, which means the aquifer's initial saturated thickness is equal to the water level in the lake. If $N = 0$, then equation (12) simplifies to the well-known Dupuit (1863) equation for radial flow in an unconfined aquifer.

Drawdown s [L] according to (8) is found by taking the difference between the head h during pumping and the initial head h_0 :

$$s(r) = h(r) - h_0(r) = \sqrt{h_c^2 + \frac{N}{2K}(r_c^2 - r^2) + \frac{Q}{\pi K} \ln \frac{r}{r_c}} - \sqrt{h_c^2 + \frac{N}{2K}(r_c^2 - r^2)} \quad (13)$$

Because equation (13) is not linear, it cannot be simplified to obtain an expression independent of initial head h_0 and recharge N . Rearranging and rewriting (13) as a function of initial head h_0 gives:

$$s(r) = h_0 \left[\sqrt{1 + \frac{Q}{\pi K h_0^2} \ln \frac{r}{r_c}} - 1 \right] \quad (14)$$

Equation (14) is valid only if the argument of the square root is positive. If this is not the case at distance r_w , the radius [L] of the well, then the latter goes dry, and the extraction is not sustainable. Therefore, the condition to have a sustainable development is:

$$\frac{Q}{\pi K h_0^2} \ln \frac{r_c}{r_w} \leq 1 \quad (15)$$

Usually $r_w^2 \ll r_c^2$, in which case $h_0^2 \approx h_c^2 + \frac{Nr_c^2}{2K}$; hence, condition (15) may be rearranged into:

$$N\pi r_c^2 \geq Q \ln \frac{r_c^2}{r_w^2} - 2\pi K h_c^2 \quad (16)$$

Before the extraction begins, the system is in a steady state, and both initial recharge R_0 and initial discharge D_0 equal $N\pi r_c^2$, which is the left-hand side of equation (16). The groundwater budget myth erroneously states that the pumping rate should not exceed the initial recharge for the extraction to be safe. That would imply the right-hand side of equation (16) should be equal to Q , which is clearly not the case. Sustainable pumping in this example also depends on the relative distance r_w/r_c between well and lake, on the constant water level h_c in the lake, and on the aquifer's conductivity K : if the lake is too far away from the well, and/or the aquifer transmissivity is too low, the well goes dry before the cone of depression reaches the lake. This confirms Bredehoeft's (1997, 2002, 2007) point of view. On the other hand, condition (16) clearly shows that whether the well goes dry or not, also depends on the initial recharge R_0 .

Applying series expansion $\sqrt{1-x} \rightarrow \left(1 - \frac{x}{2}\right)$ if $x \rightarrow 0$, equation (14) may be approximated as:

$$s(r) \approx \frac{Q}{2\pi K h_0} \ln \frac{r}{r_c} \quad (17)$$

To approximate equation (14) by equation (17), $\frac{Q}{\pi K h_0^2} \ln \frac{r_c}{r}$ must be much smaller than 1. Rearranging this condition after substituting h_0^2 by $h_c^2 + \frac{Nr_c^2}{2K}$ gives:

$$\cdot \frac{Q}{2\pi K h_c} \ln \frac{r_c}{r} \ll \frac{h_c}{2} + \frac{N(r_c^2 - r^2)}{4K h_c} \quad (18)$$

Recall that if there is no infiltration, then $h_0 = h_c$, and equation (17) is the well-known Thiem (1870; 1906) equation with constant transmissivity $K h_c$ [L^2/T]. This means the left-hand side of (18) is the absolute value of the drawdown according to the Thiem (1870; 1906) equation. The latter may be used if drawdown is smaller than 10% of the initial saturated aquifer thickness (Louwyck et al., 2022), and if the infiltration flux is negligibly small. Only if these conditions are met, the aquifer transmissivity may be assumed constant, in which case applying superposition is justified. However, if superposition is applied inaccurately in this case, then the approximated drawdown will underestimate the exact drawdown, unless it is corrected (Jacob, 1944).

Devlin and Sophocleous (2005) also discuss the island example, and they show that the aquifer continues to discharge into the lake in case of gentle pumping, i.e. $Q < R_0$. In this case, the capture only consists of reduced discharge ΔD , and there is no induced recharge ΔR as infiltration flux N is constant. If $Q > R_0$, then water flows from the lake into the aquifer, and there is also induced recharge. Note that the constant-head boundary conceptualizes the lake as an infinite source of water which never dries up, and therefore, the amount of water in the lake is not a limiting factor to the extraction in this model.

11.4. Polder island

The previous example illustrates that the superposition principle may be applied if recharge is negligibly small, and if the aquifer's saturated thickness is relatively large, a typical condition in the arid west of the USA, according to Bredehoeft et al. (1982). Suppose now the circular island is reclaimed from the lake in an area where the climate is humid and infiltration cannot be ignored (Figure 2). This is a typical condition in deltaic or low lying polder areas (Ernst, 1971). On the island, a dense network of canals and ditches is present which drains the excess of water from rainfall.

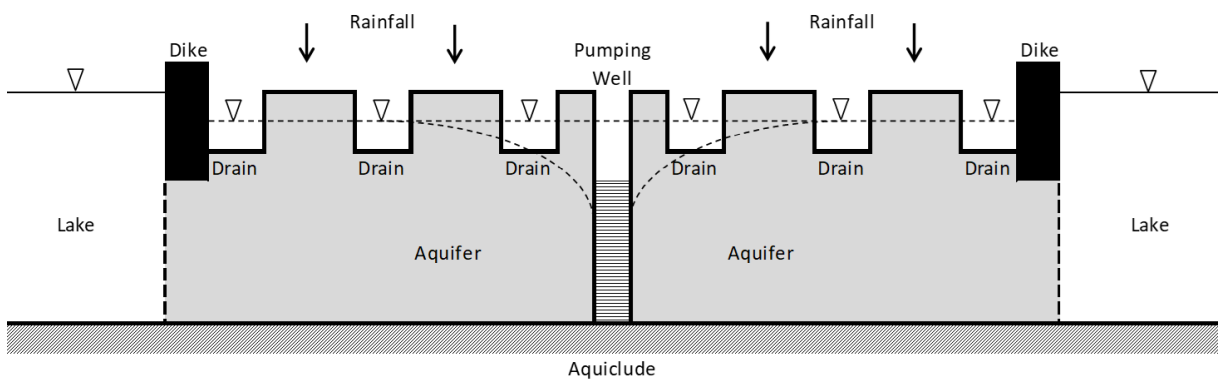


Figure 2. Sketch of the polder island aquifer system.

11.4.1. The linear case

The interaction between the aquifer and the draining elements may be conceptualized in a similar way a river boundary condition is defined in MODFLOW (Harbaugh, 2005; Harbaugh et al., 2000):

$$Q_d = 2\pi \int_0^{r_c} \frac{h_d(r) - h(r)}{c} r dr \quad (19)$$

with Q_d [L^3/T] the total amount of water per unit of time drained by the network of ditches, h_d [L] the drainage level, and c [T] the drainage resistance. Note that Q_d is negative if water is removed from the aquifer.

If it is assumed drainage resistance c and aquifer transmissivity T [L^2/T] are constant, the problem is linear. In this case, superposition may be applied by simulating hydraulic head h relatively to drainage level h_d . Hence, it is allowed to set h_d to zero in (19), and superimpose the calculated head on drainage level h_d afterwards. If the island's radius r_c is large enough so that the outer boundary condition has no impact on the pumping induced drawdown, it is also justified to assume the aquifer is unbounded, i.e. $r_c \rightarrow \infty$. Under these assumptions, the problem of flow to a well in the middle of the polder island is equivalent to the problem of well-flow in a leaky aquifer of infinite extent (Ernst, 1971; Hemker, 1984). If the aquifer's outer boundary is at large distance, the initial steady state head h_0 is uniform (Ernst, 1971):

$$h_0 = Nc \quad (20)$$

In contrast to Bredehoeft's island case, the infiltrated water is not discharged by outflow into the lake, but by drainage. Substituting (20) into (19), and taking into account $h_d = 0$, the drained amount of water per unit of time at $t = 0$ is:

$$D_0 = N\pi r_c^2 = R_0 \quad (21)$$

When the system is brought into a new dynamic equilibrium after a period of pumping, the head is given by the following equation (Bruggeman, 1999):

$$h(r) = h_0 - \frac{Q}{2\pi T} \left(\frac{K_0\left(\frac{r}{\lambda}\right)}{\frac{r_w}{\lambda} K_1\left(\frac{r_w}{\lambda}\right)} \right) \quad (22)$$

with $\lambda = \sqrt{Tc}$, the leakage factor [L]; K_0 and K_1 are the modified Bessel functions of the second kind with order zero and one, respectively. If $r_w \rightarrow 0$, then $\frac{r_w}{\lambda} K_1\left(\frac{r_w}{\lambda}\right) \rightarrow 1$, and equation (22) simplifies to:

$$h(r) = h_0 - \frac{Q}{2\pi T} K_0\left(\frac{r}{\lambda}\right) \quad (23)$$

Introducing (23) into (19), and making use of $\int_0^\infty r K_0(r) dr = 1$, the amount of water per unit of time Q_d exchanged between the aquifer and the network of ditches during pumping is obtained:

$$Q_d = Q - N\pi r_c^2 \quad (24)$$

Using (4) and (21), it follows from (24) that:

$$Q_d = -D_0 - \Delta D + \Delta R \quad (25)$$

Recharge through infiltration N is unchanged, and therefore, the extracted water is balanced by reduced drainage, and possibly induced infiltration from the ditches. Indeed, if head h drops below the drainage level h_d , the ditches will start to irrigate. As a consequence, two zones around the well can be distinguished: a proximal zone where $h < h_d$ in which irrigation takes place, and a distal zone where $h > h_d$ in which groundwater is still being drained. Taking into account $h_d = 0$, it follows from (20) and (23) that the boundary r_d [L] between those two zones is found by solving the following equation:

$$\frac{2\pi N \lambda^2}{Q} = K_0\left(\frac{r_d}{\lambda}\right) \quad (26)$$

If well-radius r_w is greater than r_d , there will be no induced recharge. It can be proven mathematically that this is the case when the pumping rate is smaller than the initial recharge given by (21). Otherwise, there is always induced recharge.

Since the system is linear, it is possible to calculate drawdown s directly according to the principle of superposition, and equation (23) becomes the well-known formula to calculate drawdown due to pumping in a leaky aquifer (de Glee, 1930; Jacob, 1946):

$$h(r) - h_0(r) = s(r) = \frac{-Q}{2\pi T} K_0 \left(\frac{r}{\lambda} \right) \quad (27)$$

In case of a leaky aquifer, the leakage is usually interpreted as an increase of vertical flow through the overlying aquitard (Jacob, 1946). If it is assumed there is no flow before the extraction, this interpretation of induced recharge is correct. However, the polder island example clearly demonstrates the no-flow assumption is too strict, and the leakage may be reduced discharge.

No prior knowledge about the infiltration is required in order to assess the impact of the extraction on the water table applying (27). The leakage, which is equal to the capture $\Delta R - \Delta D$, can also be calculated directly using (27) without knowing the initial recharge or discharge:

$$\Delta Q_d = 2\pi \int_0^\infty \frac{-s(r)}{c} r dr = Q \quad (28)$$

Note that (28) gives a change in flow ΔQ_d [L^3/T], as it uses the change in head s . In fact, equation (28) is equivalent to equation (9), with $\partial V(s_t)/\partial t = 0$. As a consequence, no distinction can be made between induced recharge and reduced discharge. To distinguish between those two components, the initial head $h_0 = Nc$ is needed. Therefore, knowing the infiltration flux N is required to evaluate the impact of the extraction on the ditches and canals as they may switch from draining to irrigating.

11.4.2. The nonlinear case

This is even more pronounced if the ditches are restricted to draining. The steady-state solution for this system is developed by Ernst (1971), whereas the transient-state solution is presented by Louwyck et al. (2022). In this case, boundary condition (19) expressing the interaction between groundwater and surface water needs to be redefined as:

$$Q_d = 2\pi \int_0^{r_c} \frac{h_d(r) - h(r)}{f(h)} r dr \quad (29)$$

with:

$$f(h) = \begin{cases} c & \text{if } h > h_d \\ \infty & \text{if } h \leq h_d \end{cases} \quad (30)$$

Equation (29) states that there is drainage in the distal zone ($r > r_d$), and no interaction in the proximal zone ($r \leq r_d$). If boundary condition (29) is applied instead of (19), the system is nonlinear, as drainage resistance c depends on head h in the aquifer, which is expressed by function f defined in (30). In the proximal zone, $Q_d = 0$, because of the infinitely large resistance c , whereas $Q_d < 0$ in the distal zone. Note that boundary condition (29) can be seen as a MODFLOW drain (Harbaugh, 2005; Harbaugh et al., 2000) defined over the whole area of the island.

As resistance c is infinitely large in the proximal zone around the well where drainage is inactive, the steady-state head h_1 in this zone must be calculated as (Haitjema, 1995):

$$h_1(r) = \left[\frac{Nr_w^2}{2T} + \frac{Q}{2\pi T} \right] \ln \left(\frac{r}{r_d} \right) + \frac{N}{4T} (r_d^2 - r^2) \quad (r \leq r_d) \quad (31)$$

The constant head at boundary r_d equals the drainage level h_d which is set to zero. The head h_2 in the distal zone, where the drainage is still active, is given by equation (22). To ensure continuity of flow at boundary r_d , pumping rate Q in (22) must be replaced by:

$$-2\pi Tr_d \frac{dh_1(r_d)}{dr} = N\pi r_d^2 - Q \quad (32)$$

Inserting the right-hand side of equation (32) into equation (22) and replacing r_w by r_d gives:

$$h_2(r) = h_0 + \frac{(N\pi r_d^2 - Q)}{2\pi T} \left(\frac{K_0 \left(\frac{r}{\lambda} \right)}{\frac{r_d}{\lambda} K_1 \left(\frac{r_d}{\lambda} \right)} \right) \quad (r > r_d) \quad (33)$$

Recall that initial head $h_0 = Nc$ according to (20). As the system is nonlinear, this initial head cannot be removed from equation (33). Drawdown in the proximal and distal zone is found by subtracting h_0 from equations (31) and (33), respectively.

Using (33), distance r_d is found by solving $h_2(r_d) = h_d = 0$. Rearranging this equation gives:

$$\left[2 \frac{K_1 \left(\frac{r_d}{\lambda} \right)}{K_0 \left(\frac{r_d}{\lambda} \right)} + \frac{r_d}{\lambda} \right] \frac{r_d}{\lambda} - \frac{Q}{N\pi\lambda^2} = 0 \quad (34)$$

As explained in Chapter 7, finding the root of the left-hand side of (34) can be done numerically using a nonlinear solver. Equation (34) clearly indicates that for a given leakage factor λ , ratio Q/N determines the distance r_d up to where the draining elements are depleted. Louwyck et al. (2022) show that the largest possible value for r_d^2 is $Q/(\pi N)$, and that this maximum radius is attained if $Q > 100\pi N \lambda^2$. Mathematically, the no-drainage zone is maximal if the drainage is perfect or $c \rightarrow 0$. In this case, there is no flow in the distal zone, and head $h_2 = 0$, as $xK_1(x) \rightarrow 0$ if $x \rightarrow \infty$. This implies the left-hand side of equation (32) is zero, from which the following well-known formula can be derived:

$$Q = N\pi r_d^2 \quad (35)$$

Equation (35) is used to calculate the radius of the capture zone (Haitjema, 1995), also called the area contributing recharge to the well (Reilly & Pollock, 1996). Note that this “capture” may not be confused with the water budget capture (Barlow et al., 2018; Seward et al., 2015). Since h_2 is zero in this case, by definition, r_d is also the radius of influence. As a consequence, the radius of the cone of depression and the radius of the capture zone coincide in this special case, an idea Brown (1963) called fallacious. This example shows, however, it is justified to estimate the radius of influence using equation (35) for wells in densely drained areas with a flat water table.

Taking a closer look at the total groundwater budget, it is clear that equations (21) and (24) still hold if the ditches can only drain water, but in this case, it is certain that the capture only contains reduced discharge as there is no induced recharge, given the outer boundary is at a sufficiently large distance from the well. Therefore, equation (25) is reduced to:

$$Q^d = -D_0 - \Delta D \quad (36)$$

From equations (24) and (35), it follows that $\Delta D = -Q$, which confirms the extracted amount of water is balanced by reduced drainage only. According to Ernst (1971), deep well pumping of groundwater in this case primarily involves a smaller discharge of water by the drains, whereas changes in evaporation by plants are of less importance, which justifies the assumption of a constant infiltration flux N . This is in complete agreement with the statements made by Bredehoeft (1997, 2002, 2007).

If the proximal zone without drainage is negligibly small, then this zone may be neglected. Indeed, if $r_d \rightarrow 0$, then $\frac{r_d}{\lambda} K_1\left(\frac{r_d}{\lambda}\right) \rightarrow 1$, and equation (33) reduces to equation (23), the solution for the linear system. Louwyck et al. (2022) show that this approximation is justified if $Q < \pi N \lambda^2$. If this constraint is satisfied, no ditches are depleted, and the interaction between the groundwater system and the draining surface water is given by boundary condition (19), which is a linear function of the hydraulic head. Recall that in this case, the superposition principle is valid and drawdown may be calculated directly using the de Glee (1930) equation (27). However, if this equation is used to approximate drawdown when superposition is not allowed, the resulting cone of depression will be underestimated.

In this example, whether superposition is allowed or not, thus depends on ratio Q/N and leakage factor λ : if there is relatively much infiltration, and/or if the aquifer transmissivity and/or the resistance to drainage are large, then the problem is linear, which implies drawdown can be calculated without knowledge of the initial steady state conditions. Under the assumption of linearity, prior knowledge about the infiltration rate is not required, although infiltration flux N is one of the parameters that implicitly determine whether this assumption is valid or not. Recall that a similar conclusion was drawn from the previous island example without drainage.

11.5. Finite-difference approach

Since numerical models are considered the best available tools to evaluate the impacts of a groundwater development (Zhou, 2009), this section examines the finite-difference approximation of the water budget equations presented above. The hypothetical case presented by Zhou (2009) is also revisited to show the superposition principle not only applies to analytical models. As explained in previous chapters 2 to 8, analytical and numerical models apply different mathematical methods to solve the same differential equation. This means the analysis on the water budget equation discussed in section 11.2 is also valid for complex numerical models, which is proven in this section.

Numerical models are more flexible than analytical models, and therefore, they are capable of solving more realistic problems. Moreover, many groundwater flow problems cannot be solved analytically, in which case applying a numerical method is the sole alternative. Unfortunately, numerical models do not offer the same insight as studying one-dimensional analytical solutions does (Haitjema, 2006). The one-dimensional models discussed in previous sections clearly reveal which parameters are relevant, and in particular, when infiltration should be taken into account and when not. Although it is possible to analyze parameter sensitivities numerically, which also gives an idea on whether or not a parameter is relevant, it is not easy to get an understanding of the problem as profound as the insight offered by the corresponding analytical solution, if it exists.

Kalf and Woolley (2005) recommend the use of numerical models over classical analytical models, as the latter are not able to produce volumetric balances. It is true that calculating volumetric balances is very straightforward using a numerical model. However, it was shown in previous sections 11.3 and 11.4 discussing the island examples that volumetric balances can also be calculated analytically.

According to Haitjema (2006), such basic water balance calculations are very useful, for instance, to check on numerically simulated capture zones.

11.5.1. Finite-difference equations

The common approach to assess the effect of groundwater extractions on the groundwater system, is to first build a model to simulate the pre-development conditions without the pumping, after which the extractions are included in the model to simulate the development conditions. The difference between both simulations gives an idea of the combined effect of the extractions. Like analytical models, numerical models also solve a differential equation subject to a set of boundary conditions. The finite-difference method is a frequently applied numerical method that converts these equations into a system of algebraic equations (Harbaugh, 2005). In matrix form, the first model without pumping is written as:

$$\mathbf{A}_0 \mathbf{h}_0 - \mathbf{b}_0 = \mathbf{0} \quad (37)$$

Matrix \mathbf{A} contains the known conductance terms, \mathbf{h} is the vector with unknown heads, and \mathbf{b} contains the known terms of the boundary conditions. In general, the boundary conditions define the sources and sinks interacting with the modeled groundwater system. If the finite-difference grid contains n nodes, then \mathbf{A} is an $n \times n$ matrix, whereas \mathbf{h} and \mathbf{b} are $n \times 1$ vectors. Subscript 0 refers to time $t = 0$, when the extraction starts. The unknown heads \mathbf{h} are found by inverting matrix \mathbf{A} :

$$\mathbf{h}_0 = \mathbf{A}_0^{-1} \mathbf{b}_0 \quad (38)$$

The calculated heads according to (38) are adopted as initial heads by the second model simulating the extraction. Similar to equation (37), this model can be written in matrix form:

$$\mathbf{A}_k \mathbf{h}_k - \mathbf{b}_k = \mathbf{0} \quad (39)$$

where index k refers to time t_k after the start of the extraction. System of equations (39) is solved in the same way as (38):

$$\mathbf{h}_k = \mathbf{A}_k^{-1} \mathbf{b}_k \quad (40)$$

Primarily, the hydraulic effect of the extraction is evaluated by calculating the difference between (38) and (40):

$$\mathbf{s}_k = \mathbf{h}_k - \mathbf{h}_0 = \mathbf{A}_k^{-1} \mathbf{b}_k - \mathbf{A}_0^{-1} \mathbf{b}_0 \quad (41)$$

with \mathbf{s}_k the vector with drawdowns according to (8). If $\mathbf{A}_k = \mathbf{A}_0 = \mathbf{A}$, then expression (41) simplifies to:

$$\mathbf{s}_k = \mathbf{A}^{-1} (\mathbf{b}_k - \mathbf{b}_0) \quad (42)$$

Solving (42) is mathematically more convenient, since drawdown is calculated directly without having to simulate the pre-development state of the groundwater system. The question rises, however, under which assumptions solution (42) is valid.

Matrix \mathbf{A} contains the conductance terms C [L^2/T] to calculate flow F [L^3/T] according to Darcy's law between adjacent cells or between cells and head-dependent boundary conditions:

$$F_{ijk} = C_{ijk} (h_{ik} - h_{jk}) \quad (43)$$

Recall that index k refers to simulation time t_k . Index i refers to cell i , whereas index j may refer to cell j adjacent to cell i , or to a head-dependent boundary condition that interacts with cell i , such as a MODFLOW river or drain boundary condition (Harbaugh, 2005; Harbaugh et al., 2000). This implies h_j

may be an unknown head or a known constant head. Matrix \mathbf{A} also contains the terms V [L²/T] to calculate the storage change $\Delta V/\Delta t$ [L³/T] in each cell i during time step k :

$$\frac{\Delta V_i}{\Delta t_k} = V_{ik}(h_{ik} - h_{i,k-1}) \quad (44)$$

Vector \mathbf{b} contains the known constant heads multiplied by their respective conductances C , the known terms $V_{ik}h_{i,k-1}$ from equation (44), and the known discharges Q_i [L³/T] from the flux boundary conditions, such as MODFLOW recharge and well boundary conditions (Harbaugh, 2005; Harbaugh et al., 2000).

Considering these different terms, system of equation (37) and (39) can be rewritten as, respectively:

$$(\mathbf{F}_0 + \mathbf{C}_0 - \mathbf{V}_0)\mathbf{h}_0 + \mathbf{V}_0\mathbf{h}_{-1} - \mathbf{c}_0 + \mathbf{q}_0 = \mathbf{0} \quad (45)$$

$$(\mathbf{F}_k + \mathbf{C}_k - \mathbf{V}_k)\mathbf{h}_k + \mathbf{V}_k\mathbf{h}_{k-1} - \mathbf{c}_k + \mathbf{q}_k = \mathbf{0} \quad (46)$$

In (45) and (46), matrix \mathbf{F} holds the conductances C to calculate flow between cells with unknown heads, matrix \mathbf{C} holds the conductances C that determine the interaction with head-dependent boundary conditions, matrix \mathbf{V} contains the storage change terms, the elements of vector \mathbf{c} are the known constant heads multiplied by their respective conductances C , and the entries in vector \mathbf{q} are the known discharges Q .

To obtain drawdown according to (42), it is required that all conductances C are constant, and that the initial heads are steady so that there is initially no storage change, and matrix \mathbf{V}_0 in (45) only contains zeros. Under these assumptions, subtracting (45) from (46) gives:

$$(\mathbf{F} + \mathbf{C})\mathbf{s}_k - \mathbf{V}_k(\mathbf{s}_k - \mathbf{s}_{k-1}) - (\mathbf{c}_k - \mathbf{c}_0) + (\mathbf{q}_k - \mathbf{q}_0) = \mathbf{0} \quad (47)$$

The assumptions underlying (46) are the same that are made to derive water budget equation (11). Equation (47), which is the same as equation (42), indeed expresses the principle of superposition. It may be applied if the conductances are constant, which makes the system of equations linear. This implies all hydraulic conductivities and resistances are constant, as are all distances required to calculate the conductances such as layer thicknesses. This also holds for the boundary conditions; hence, vectors $(\mathbf{c}_k - \mathbf{c}_0)$ and $(\mathbf{q}_k - \mathbf{q}_0)$ only contain changes in constant head and changes in discharge, respectively. If all constant heads and all discharges are time-independent, except the pumping rates defined for the new extractions, then these changes are zero, and expression (47) further simplifies to:

$$(\mathbf{F} + \mathbf{C})\mathbf{s}_k - \mathbf{V}_k(\mathbf{s}_k - \mathbf{s}_{k-1}) + \mathbf{q}_k^{new} = \mathbf{0} \quad (48)$$

where vector \mathbf{q}_k^{new} contains the pumping rates of the added wells.

System of equations (48) is the finite-difference formulation for many well-known axisymmetric models to simulate flow to a well (e.g. de Glee, 1930; Hantush & Jacob, 1955; Hemker, 1984, 1985; Jacob, 1946; Theis, 1935). These are examples of the traditional analytical models Bredehoeft (2002, 2007) refers to when he states that pumping has nothing to do with recharge. Indeed, (48) clearly shows that flux boundary conditions, such as infiltration in the top layer, are canceled out. However, when the system is not linear, equations (47) and (48) are not valid, and consequently, this statement cannot be generalized.

The finite-difference formulation for total water budget equation (1) at time t_k is:

$$R_k - D_k - \frac{\Delta V}{\Delta t_k} = 0 \quad (49)$$

Recall that R is the total recharge, which is the sum of all sources, and D is the total discharge, which is the sum of all sinks, whereas $\Delta V/\Delta t$ is the total change in storage.

Using the system of finite-difference equations (39), total volumetric budget is obtained by taking the sum of all these equations:

$$[\mathbf{A}_k \mathbf{h}_k - \mathbf{b}_k]^T \mathbf{1} = 0 \quad (50)$$

with $\mathbf{1}$ an $n \times 1$ vector in which each entry equals one.

To see the link between (49) and (50), a distinction must be made in equation (46) between sources and sinks. Denoting the first by superscript *in*, and the latter by superscript *out*, equation (50) is reformulated as:

$$[(\mathbf{C}_k^{in} \mathbf{h}_k - \mathbf{c}_k^{in} + \mathbf{q}_k^{in}) + (\mathbf{C}_k^{out} \mathbf{h}_k - \mathbf{c}_k^{out} + \mathbf{q}_k^{out}) - \mathbf{V}_k(\mathbf{h}_k - \mathbf{h}_{k-1})]^T \mathbf{1} = 0 \quad (51)$$

Note that the $\mathbf{F}_k \mathbf{h}_k$ terms in (46) are canceled out since the sum of all rows in \mathbf{F} is zero. This implies matrix \mathbf{F} is singular, which explains why at least one constant-head or head-dependent flux boundary condition is required in case of steady flow to ensure matrix \mathbf{A} can be inverted. Comparing (49) with (51), it is clearly seen now that:

$$R_k = [\mathbf{C}_k^{in} \mathbf{h}_k - \mathbf{c}_k^{in} + \mathbf{q}_k^{in}]^T \mathbf{1} \quad (52)$$

$$D_k = -[\mathbf{C}_k^{out} \mathbf{h}_k - \mathbf{c}_k^{out} + \mathbf{q}_k^{out}]^T \mathbf{1} \quad (53)$$

$$\frac{\Delta V}{\Delta t_k} = [\mathbf{V}_k(\mathbf{h}_k - \mathbf{h}_{k-1})]^T \mathbf{1} \quad (54)$$

The finite-difference formulation for total budget equation (2) in terms of change in recharge and discharge for the developed system is:

$$(R_0 + \Delta R_k) - (D_0 + \Delta D_k) - Q_k - \frac{\Delta V}{\Delta t_k} = 0 \quad (55)$$

where subscript 0 refers to time $t = 0$, the start of the extraction, and subscript k to time t_k after the start of the extraction. Q_k is the total pumping rate [L^3/T] of the new extractions at time t_k .

Using (52) and (53), respectively, the change in recharge and discharge is calculated as:

$$\Delta R_k = R_k - R_0 = [\mathbf{C}_k^{in} \mathbf{h}_k - \mathbf{c}_k^{in} + \mathbf{q}_k^{in} - \mathbf{C}_0^{in} \mathbf{h}_0 + \mathbf{c}_0^{in} - \mathbf{q}_0^{in}]^T \mathbf{1} \quad (56)$$

$$\Delta D_k = D_k - D_0 = -[\mathbf{C}_k^{out} \mathbf{h}_k - \mathbf{c}_k^{out} + \mathbf{q}_k^{out} - \mathbf{C}_0^{out} \mathbf{h}_0 + \mathbf{c}_0^{out} - \mathbf{q}_0^{out}]^T \mathbf{1} \quad (57)$$

Note that (57) does not include the discharges of the newly added wells; hence, $Q_k = [\mathbf{q}_k^{new}]^T \mathbf{1}$.

If the system is linear and all conductances are constant, (56) and (57) may be written as a function of drawdown:

$$\Delta R_k = [\mathbf{C}^{in} \mathbf{s}_k - (\mathbf{c}_k^{in} + \mathbf{c}_0^{in}) + (\mathbf{q}_k^{in} - \mathbf{q}_0^{in})]^T \mathbf{1} \quad (58)$$

$$\Delta D_k = -[\mathbf{C}^{out} \mathbf{s}_k - (\mathbf{c}_k^{out} + \mathbf{c}_0^{out}) + (\mathbf{q}_k^{out} - \mathbf{q}_0^{out})]^T \mathbf{1} \quad (59)$$

If all boundary conditions do not change with time, then (58) and (59) are further reduced to, respectively:

$$\Delta R_k = [\mathbf{C}^{in} \mathbf{s}_k]^T \mathbf{1} \quad (60)$$

$$\Delta D_k = -[\mathbf{C}^{out} \mathbf{s}_k]^T \mathbf{1} \quad (61)$$

Using (42) or (47), it is possible to calculate drawdown without having to simulate the initial heads first, if the pre-development system is in a state of steady flow, and if the mathematical problem is linear, which implies the hydraulic properties of the groundwater system and its sources and sinks are constant. Under these assumptions, the capture can also be calculated directly using (58) and (59), or using (60) and (61). In these cases, knowing the initial recharge and discharge is not required. In all other cases, it is necessary to simulate the pre-development conditions to assess the hydrological effect of new extractions in the groundwater system. The same conclusion was drawn in the section discussing the water budget equations, which is no surprise, as these equations are approximated in this section applying the finite-difference method.

11.5.2. Numerical example

To refute the idea numerical models always require to set up the pre-development steady-state conditions, as stated by Kalf and Woolley (2005), the hypothetical case presented by Zhou (2009) is simulated using (48).

In this example, a homogeneous aquifer is considered bounded by a river in the west, a drainage canal in the east, and no-flow boundaries in the north and the south. The extent of the aquifer is 5500 m by 5500 m, the saturated thickness is 60 m, the hydraulic conductivity is 20 m/d, the specific yield is 0.25. Infiltration recharges the aquifer at a constant rate of 1 mm/d. In the center, water is pumped from the aquifer at a constant rate of 24000 m³/d, which corresponds to Zhou's (2009) first pumping case. The model grid consists of 1 layer, 55 rows of equal height, and 55 columns of equal width. The river stage is 100 m, the drainage level is 95 m; resistances or conductances are not mentioned by Zhou (2009), neither is the layer type. By trial and error, the same result was obtained keeping the saturated thickness constant, and setting river and drainage conductance to 26 m²/d and 24 m²/d, respectively. This result is shown in the left plot of Figure 3, which is virtually the same as Figure 1 in Zhou (2009).

Zhou (2009) first simulates the initial heads, after which he adds the wells to the model to obtain drawdown, calculated as the difference between the head during pumping and the initial head. Drawdown in the left plot of Figure 3, however, is calculated directly by solving (48). Zhou (2009) performs transient simulations, but since the steady drawdown is shown, attained after a period of pumping, storage change may be set to zero, in which case expression (48) simplifies to:

$$(\mathbf{F} + \mathbf{C})\mathbf{s} + \mathbf{q}^{new} = \mathbf{0} \quad (62)$$

Because all cells have the same size, only the transmissivity of the aquifer is needed to construct matrix \mathbf{F} , whereas matrix \mathbf{C} requires the river and drainage conductances. Since the river and drainage elevations are constant, they are excluded. Vector \mathbf{q}^{new} contains the pumping rate; the infiltration flux is also excluded as it is constant. Zhou (2009) defines 12 wells, but doesn't mention their exact location. Therefore, a single well is defined in the middle cell of the grid. Once matrices \mathbf{F} and \mathbf{C} and vector \mathbf{q}^{new} are constructed, drawdowns are found by solving (62):

$$\mathbf{s} = -(\mathbf{F} + \mathbf{C})^{-1} \mathbf{q}^{new} \quad (63)$$

Evaluating (63) is straightforward applying a standard linear algebra solver. Using equations (60) and (61), the capture is calculated, which equals the pumping rate, as it should. If river and drain cells are kept separate in the calculation, then it is seen that 51.28 % and 48.72 % of the extracted volume is balanced by loss of water in river and drain, respectively.

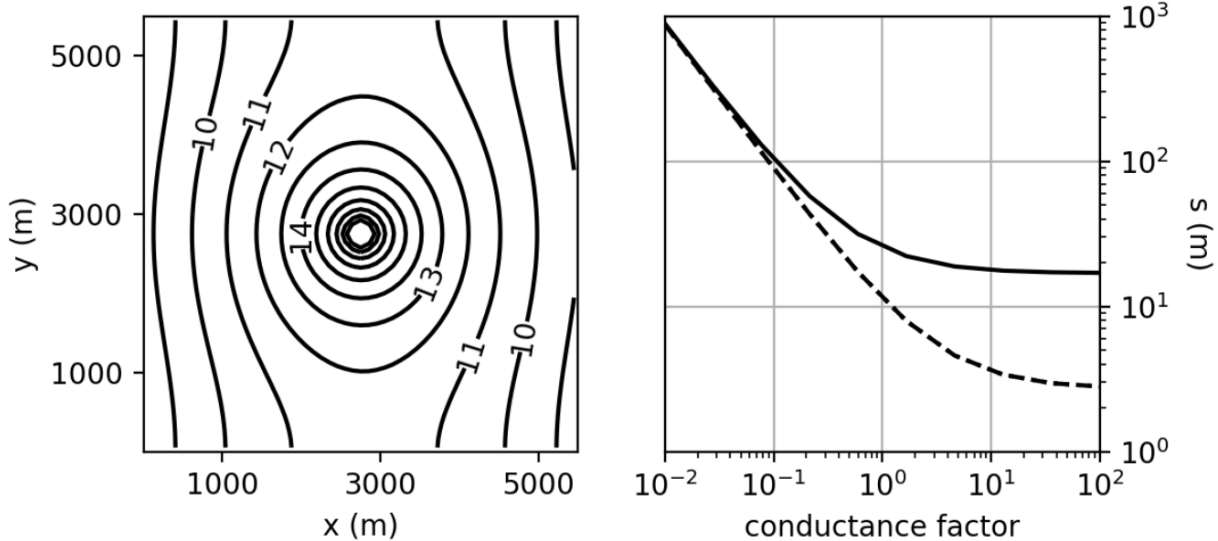


Figure 3. Left: contour plot of drawdown for the hypothetical case discussed by Zhou (2009). See text for a detailed description of the case. Right: drawdown s as a function of the conductance factor, by which the original river and drain conductances are multiplied. Solid and dashed lines respectively show drawdown for the cell containing the well and for the river cell in the middle row. Note that the drawdown defined in the text is negative in case of extraction, so the negative drawdown is displayed here.

Since a linear model is used to calculate drawdown and capture, knowing the infiltration flux is not required, which confirms the statements made by Bredehoeft (1997, 2002, 2007). However, without knowing the initial heads, it is not possible to distinguish between reduced exfiltration and induced infiltration. These initial heads depend on the initial recharge, which determines whether there is induced recharge or not. Because the pumping rate is smaller than the initial recharge, which is $30250 \text{ m}^3/\text{d}$, the extracted water can be balanced completely by reduced drainage. Zhou (2009) simulates a second scenario in which the total pumping rate is $36000 \text{ m}^3/\text{d}$, and in this case, the extraction causes a complete depletion of the drainage canal, and it induces infiltration from the river. As explained in section 11.4.2, the nonlinear response of the drainage canal cannot be simulated without knowledge of the initial conditions.

Whether the second scenario is feasible or not, also depends on the cone of depression. As the aquifer is phreatic, its saturated thickness equals the hydraulic head, and if the cone of depression becomes too deep, the wells will go dry. This can only be simulated using a nonlinear model that updates the saturated thickness according to the water table height. As explained in section 11.3 discussing the example of Bredehoeft's island, the parameters determining the sustainability of the extraction are the pumping rate, the infiltration rate, the distance between wells and streams, and the aquifer conductivity. The polder island example showed the drain resistance also plays a role. The right plot in Figure 3 indeed confirms that river and drain conductances are important: if the conductances are small, resistance to stream outflow is large, and drawdown increases.

This example clearly demonstrates that the initial conditions are irrelevant indeed if a groundwater development can be simulated as if it is a linear system. This is in agreement with the point of view defended by Bredehoeft (1997, 2002, 2007). However, it also illustrates that the assumption of

linearity depends on these initial conditions. In fact, a more accurate evaluation of the sustainability of the extraction requires a model that simulates the nonlinear response of the aquifer and the drains. Since the initial heads are needed in such a nonlinear model, modeling the pre-development conditions is inevitable, which requires knowledge of the initial recharge and discharge. Therefore, the statement by Bredehoeft (1997) that sustainable groundwater development has nothing to do with recharge, and the conclusion by Devlin and Sophocleous (2005, 2006) that recharge rates are irrelevant to sustainable pumping, should be nuanced.

11.6. Summary and conclusions

The groundwater budget myth, contested by Bredehoeft et al. (1982) and Bredehoeft (2002), gave rise to a controversy about the role of recharge in assessing the sustainability of groundwater development. Devlin and Sophocleous (2005) pointed to a confusion in terminology, and argued a distinction must be made between sustainable pumping, which only requires examining the drawdown induced by the extraction, and sustainability, which is a broader and more encompassing concept.

Bredehoeft (2002) explains how traditional analytical models apply the principle of superposition to assess the impact of wells on groundwater systems. These models calculate the cone of depression which is superimposed on the initial head. The recharge flux is required only to solve the initial boundary value problem. To simulate the cone of depression, only the aquifer diffusivity, the boundary conditions, and the pumping rate are needed; initial recharge and discharge are not required.

The irrelevance of the initial conditions is based on a simplified water budget equation, which equates the total pumping rate to the sum of capture and storage change (Bredehoeft, 2002; Bredehoeft et al., 1982). After examining the assumptions underlying this equation, it is proven that it indeed expresses the superposition principle, which assumes a linear system. Under this assumption, drawdown is independent of initial conditions, including initial recharge.

However, like any other model assumption, this is a simplification of reality, as it implicitly assumes the groundwater reservoir can be depleted indefinitely and boundary conditions are an infinite source of water. In reality, capture and storage are limited, and this requires modeling nonlinear responses, in which case the superposition principle is not applicable, and simulating the initial conditions is inevitable. In fact, the initial conditions determine the limits of the system, and as a consequence, they paradoxically determine whether the assumption of linearity is valid or not. Therefore, it is concluded that applying linear models to assess sustainability should be subject to caution, as they tend to underestimate the cone of depression.

Two analytical examples are given to demonstrate nonlinear models are dependent on the initial conditions indeed. Bredehoeft's island case (Bredehoeft, 2002; Bredehoeft et al., 1982) is discussed first. In this model, recharge implicitly determines the aquifer's saturated thickness, and hence, the sustainability of the extraction. It is also shown that in this case the superposition principle is valid only under specific conditions: recharge must be negligibly small and drawdown must be much smaller than the saturated aquifer thickness. Otherwise a nonlinear model is required in which the initial conditions, including recharge, are of importance.

The second example discusses the analytical model developed by Ernst (1971) to simulate flow to a well in a polder area with a nonlinear function for drainage. The ratio of the recharge to the pumping rate together with the leakage factor determine whether superposition can be applied or not. If drainage resistance is negligibly small, the cone of depression even coincides with the capture zone.

Although this asymptotic solution is an exceptional case, it proves that the idea of balancing pumping and infiltration rate is not fallacious, but in agreement with the fundamental principles stated by Theis (1940), as in this case, the pumping rate is balanced by reduced drainage.

Although both one-dimensional models are oversimplifications of reality, they clearly demonstrate that the initial recharge cannot always be ignored if the model is not linear. The same is concluded after examining the finite-difference approximation of the water budget equation. Although it is common practice to simulate the initial steady state of the aquifer system when using a numerical model such as MODFLOW (Harbaugh, 2005), it is allowed to skip this step if input parameters are constant and boundary conditions are linear. In this case, the initial recharge is irrelevant, which is illustrated using a numerical example adopted from Zhou (2009). However, if some of the hydraulic parameters are head-dependent, then it is necessary to simulate the initial flow in the groundwater reservoir, which requires knowledge of the recharge.

In conclusion, the question if recharge is important in assessing the sustainability of groundwater development comes down to the question if superposition can be applied in the analysis of the groundwater system. In many cases, applying this traditional method of analysis is still justified indeed, but in many other real-word cases, defining nonlinear and time-dependent stresses on the groundwater system is inevitable, making recharge a relevant parameter. And this, to quote Bredehoeft (2002), is “why hydrogeologists model”.

11.7. References

- Ahlfeld, D. P., Barlow, P. M., & Mulligan, A. E. (2005). *GWM-a ground-water management process for the U.S. Geological Survey modular ground-water model (MODFLOW-2000)*. U.S. Geological Survey Open-File Report 2005-1072.
- Ahlfeld, D. P., Baker, K. M., & Barlow, P. M. (2009). *GWM-2005 - A Groundwater-Management Process for MODFLOW-2005 with Local Grid Refinement (LGR) Capability*. U.S. Geological Survey Techniques and Methods 6-A33.
- Alley, W. M. (2007). Another Water Budget Myth: The Significance of Recoverable Ground Water in Storage. *Ground Water*, 45(3), 251–251. <https://doi.org/10.1111/j.1745-6584.2006.00274.x>
- Alley, W. M., & Leake, S. A. (2004). The Journey from Safe Yield to Sustainability. *Ground Water*, 42(1), 12–16. <https://doi.org/10.1111/j.1745-6584.2004.tb02446.x>
- Alley, W. M., Reilly, T. E., & Franke, O. L. (1999). *Sustainability of ground-water resources*. U.S. Geological Survey Circular 1186.
- Balleau, W. P. (2013). The Policy of “Pumping the Recharge” Is Out of Control. *Eos, Transactions American Geophysical Union*, 94(1), 4–4. <https://doi.org/10.1002/2013EO010007>
- Barlow, P. M., Leake, S. A., & Fienen, M. N. (2018). Capture Versus Capture Zones: Clarifying Terminology Related to Sources of Water to Wells. *Groundwater*, 56(5). <https://doi.org/10.1111/gwat.12661>
- Bierkens, M. F. P., & Wada, Y. (2019). Non-renewable groundwater use and groundwater depletion: a review. *Environmental Research Letters*, 14(6), 063002. <https://doi.org/10.1088/1748-9326/ab1a5f>

- Blom, J. (1973). *Verlagingen van het freatisch vlak bij grondwateronttrekking in een gebied met vrije afwatering (Drenthe) (in Dutch)*. RID Mededeling 74-7, Rijksinstituut voor Drinkwatervoorziening (RID), The Netherlands.
- Bredehoeft, J. D. (1997). Safe Yield and the Water Budget Myth. *Ground Water*, 35(6), 929–929. <https://doi.org/10.1111/j.1745-6584.1997.tb00162.x>
- Bredehoeft, J. D. (2002). The Water Budget Myth Revisited: Why Hydrogeologists Model. *Ground Water*, 40(4). <https://doi.org/10.1111/j.1745-6584.2002.tb02511.x>
- Bredehoeft, J. D. (2007). It Is the Discharge. *Ground Water*, 45(5), 523–523. <https://doi.org/10.1111/j.1745-6584.2007.00305.x>
- Bredehoeft, J. D., & Durbin, T. (2009). Ground Water Development - The Time to Full Capture Problem. *Ground Water*, 47(4). <https://doi.org/10.1111/j.1745-6584.2008.00538.x>
- Bredehoeft, J. D., Papadopoulos, S. S., & Cooper, H. H. (1982). The water budget myth. In *Scientific Basis of Water Resources management Studies in Geophysics* (pp. 51–57). National Academy Press.
- Brown, R. H. (1963). *The cone of depression and the area of diversion around a discharging well in an infinite strip aquifer subject to uniform recharge*. U.S. Geological Survey Water-Supply Paper 1545C; U.S. Government Printing Office, Washington, D.C.
- Bruggeman, G. A. (1999). *Analytical solutions of geohydrological problems. Developments in Water Science* 46. Amsterdam: Elsevier.
- de Glee, G. J. (1930). *Over grondwaterstroomingen bij wateronttrekking door middel van putten (in Dutch)* (PhD thesis). Technische Hoogeschool Delft, Drukkerij J. Waltman. Jr., Delft.
- De Smedt, F. (2006). *Groundwater Hydrology*. Department of Hydrology and Hydraulic Engineering, Faculty of Applied Sciences, Free University Brussels.
- Devlin, J. F., & Sophocleous, M. (2005). The persistence of the water budget myth and its relationship to sustainability. *Hydrogeology Journal*, 13(4). <https://doi.org/10.1007/s10040-004-0354-0>
- Devlin, J. F., & Sophocleous, M. (2006). Reply to Comment on “The persistence of the water budget myth and its relationship to sustainability” by J.F. Devlin and M. Sophocleous, *Hydrogeology Journal* (2005), 13:549–554. *Hydrogeology Journal*, 14(7), 1386–1386. <https://doi.org/10.1007/s10040-006-0033-4>
- Dupuit, J. (1863). *Etude Théoriques et Pratiques Sur le Mouvement Des Eaux Dans Les Canaux Découverts et à Travers Les Terrains Perméables (in French)*. Paris: Dunot.
- Ernst, L. F. (1971). Analysis of groundwater flow to deep wells in areas with a non-linear function for the subsurface drainage. *Journal of Hydrology*, 14(2). [https://doi.org/10.1016/0022-1694\(71\)90004-7](https://doi.org/10.1016/0022-1694(71)90004-7)
- Ferguson, G. (2021). Interactive comment on “Large-scale sensitivities of groundwater and surface water to groundwater withdrawal” by Marc F. P. Bierkens et al. *Hydrology and Earth System Sciences Discussions*. <https://doi.org/10.5194/hess-2020-632-RC2>
- Haitjema, H. (1995). *Analytic Element Modeling of Groundwater Flow*. San Diego: Academic Press. <https://doi.org/10.1016/B978-0-12-316550-3.X5000-4>

- Haitjema, H. (2006). The Role of Hand Calculations in Ground Water Flow Modeling. *Ground Water*, 44(6). <https://doi.org/10.1111/j.1745-6584.2006.00189.x>
- Hantush, M. S., & Jacob, C. E. (1955). Non-steady radial flow in an infinite leaky aquifer. *Transactions, American Geophysical Union*, 36(1), 95–100. <https://doi.org/10.1029/TR036i001p00095>
- Harbaugh, A. W. (2005). *MODFLOW-2005, the U.S. Geological Survey modular ground-water model - the Ground-Water Flow Process*. U.S. Geological Survey Techniques and Methods 6-A16. <https://doi.org/https://doi.org/10.3133/tm6A16>
- Harbaugh, A. W., Banta, E. R., Hill, M. C., & McDonald, M. G. (2000). *MODFLOW-2000, The U.S. Geological Survey Modular Ground-Water Model: User Guide to Modularization Concepts and the Ground-Water Flow Process*. U.S. Geological Survey Open-File Report 00-92. <https://doi.org/https://doi.org/10.3133/ofr200092>
- Hemker, C. J. (1984). Steady groundwater flow in leaky multiple-aquifer systems. *Journal of Hydrology*, 72(3–4), 355–374. [https://doi.org/10.1016/0022-1694\(84\)90089-1](https://doi.org/10.1016/0022-1694(84)90089-1)
- Hemker, C. J. (1985). Transient well flow in leaky multiple-aquifer systems. *Journal of Hydrology*, 81(1–2), 111–126. [https://doi.org/10.1016/0022-1694\(85\)90170-2](https://doi.org/10.1016/0022-1694(85)90170-2)
- Hemker, C. J. (1999). Transient well flow in vertically heterogeneous aquifers. *Journal of Hydrology*, 225(1–2), 1–18. [https://doi.org/10.1016/S0022-1694\(99\)00137-7](https://doi.org/10.1016/S0022-1694(99)00137-7)
- Jacob, C. E. (1944). *Notes on determining permeability by pumping tests under water-table conditions*. U.S. Geological Survey Open File Report.
- Jacob, C. E. (1946). Radial flow in a leaky artesian aquifer. *Transactions, American Geophysical Union*, 27(2). <https://doi.org/10.1029/TR027i002p00198>
- Jakeman, A. J., Barreteau, O., Hunt, R. J., Rinaudo, J.-D., & Ross, A. (2016). *Integrated Groundwater Management: Concepts, Approaches, Challenges*. Switzerland: Springer International Publishing. https://doi.org/10.1007/978-3-319-23576-9_1
- Kalf, F. R. P., & Woolley, D. R. (2005). Applicability and methodology of determining sustainable yield in groundwater systems. *Hydrogeology Journal*, 13(1). <https://doi.org/10.1007/s10040-004-0401-x>
- Kendy, E. (2003). The False Promise of Sustainable Pumping Rates. *Ground Water*, 41(1), 2–4. <https://doi.org/10.1111/j.1745-6584.2003.tb02559.x>
- Konikow, L. F., & Leake, S. A. (2014). Depletion and Capture: Revisiting “The Source of Water Derived from Wells.” *Groundwater*, 52(S1). <https://doi.org/10.1111/gwat.12204>
- Kruseman, G. P., & de Ridder, N. A. (1990). *Analysis and Evaluation of Pumping Test Data* (2nd ed.). Wageningen: ILRI Publication 47.
- Langevin, C. D., Hughes, J. D., Banta, E. R., Niswonger, R. G., Panday, S., & Provost, A. M. (2017). *Documentation for the MODFLOW 6 Groundwater Flow Model*. U.S. Geological Survey Techniques and Methods 6-A55. <https://doi.org/10.3133/tm6A55>
- Leake, S. A. (2011). Capture-Rates and Directions of Groundwater Flow Don’t Matter! *Ground Water*, 49(4), 456–458. <https://doi.org/10.1111/j.1745-6584.2010.00797.x>

- Leake, S. A., Reeves, H. W., & Dickinson, J. E. (2010). A New Capture Fraction Method to Map How Pumpage Affects Surface Water Flow. *Ground Water*, 48(5), 690–700. <https://doi.org/10.1111/j.1745-6584.2010.00701.x>
- Loáiciga, H. A. (2002). Sustainable Ground-Water Exploitation. *International Geology Review*, 44(12), 1115–1121. <https://doi.org/10.2747/0020-6814.44.12.1115>
- Loáiciga, H. A. (2006). Comment on “The persistence of the water budget myth and its relationship to sustainability” by J.F. Devlin and M. Sophocleous, *Hydrogeology Journal* (2005) 13:549–554. *Hydrogeology Journal*, 14(7), 1383–1385. <https://doi.org/10.1007/s10040-006-0032-5>
- Lohman, S. W. (1972a). *Definitions of selected ground water terms – revisions and conceptual refinements*. Professional Paper 708, U.S. Geological Survey Water Supply Paper 1988, U.S. Government Printing Office, Washington, D.C.
- Lohman, S. W. (1972b). *Ground-water Hydraulics*. U.S. Geological Survey.
- Louwyck, A., Vandenbohede, A., Libbrecht, D., Van Camp, M., & Walraevens, K. (2022). The Radius of Influence Myth. *Water*, 14(2), 149. <https://doi.org/10.3390/w14020149>
- Louwyck, A., Vandenbohede, A., Heuvelmans, G., Van Camp, M., & Walraevens, K. (2023). The Water Budget Myth and Its Recharge Controversy: Linear vs. Nonlinear Models. *Groundwater*, 61(1), 100–110. <https://doi.org/10.1111/gwat.13245>
- Maddock III, T., & Vionnet, L. B. (1998). Groundwater capture processes under a seasonal variation in natural recharge and discharge. *Hydrogeology Journal*, 6(1), 24–32. <https://doi.org/10.1007/s100400050131>
- Maimone, M. (2004). Defining and Managing Sustainable Yield. *Ground Water*, 42(6), 809–814. <https://doi.org/10.1111/j.1745-6584.2004.tb02739.x>
- Mehl, S. W. (2006). Use of Picard and Newton Iteration for Solving Nonlinear Ground Water Flow Equations. *Ground Water*, 44(4), 583–594. <https://doi.org/10.1111/j.1745-6584.2006.00207.x>
- Reilly, T. E., & Pollock, D. W. (1996). Sources of Water to Wells for Transient Cyclic Systems. *Ground Water*, 34(6), 979–988. <https://doi.org/10.1111/j.1745-6584.1996.tb02163.x>
- Seward, P., Xu, Y., & Brendonck, L. (2006). Sustainable groundwater use, the capture principle, and adaptive management. *Water SA*, 32(4), 473–482. <https://doi.org/10.4314/wsa.v32i4.5287>
- Seward, P., Xu, Y., & Turton, A. (2015). Investigating a spatial approach to groundwater quantity management using radius of influence with a case study of South Africa. *Water SA*, 41(1). <https://doi.org/10.4314/wsa.v41i1.10>
- Sheets, R. A., Hill, M. C., Haitjema, H. M., Provost, A. M., & Masterson, J. P. (2015). Simulation of Water-Table Aquifers Using Specified Saturated Thickness. *Groundwater*, 53(1), 151–157. <https://doi.org/10.1111/gwat.12164>
- Sophocleous, M. (1997). Managing water resources systems: why “safe yield” is not sustainable. *Ground Water*, 35(4), 561–561. <https://doi.org/10.1111/j.1745-6584.1997.tb00116.x>
- Sophocleous, M. (2000). From safe yield to sustainable development of water resources—the Kansas experience. *Journal of Hydrology*, 235(1–2), 27–43. [https://doi.org/10.1016/S0022-1694\(00\)00263-8](https://doi.org/10.1016/S0022-1694(00)00263-8)

- Sophocleous, M. (2002). Interactions between groundwater and surface water: the state of the science. *Hydrogeology Journal*, 10(1), 52–67. <https://doi.org/10.1007/s10040-001-0170-8>
- Sophocleous, M. (2005). Groundwater recharge and sustainability in the High Plains aquifer in Kansas, USA. *Hydrogeology Journal*, 13(2), 351–365. <https://doi.org/10.1007/s10040-004-0385-6>
- Sophocleous, M. (2012). *Retracted: On Understanding and Predicting Groundwater Response Time. Groundwater*, 50(4). <https://doi.org/10.1111/j.1745-6584.2011.00876.x>
- Sophocleous, M., & Devlin, J. F. (2004). Discussion on the paper “The Water Budget Myth Revisited: Why Hydrogeologists Model,” by John D. Bredehoeft, July-August 2002 issue, v. 40, no. 4: 340–345. *Ground Water*, 42(4), 618–618. <https://doi.org/10.1111/j.1745-6584.2004.tb02630.x>
- Theis, C. V. (1935). The relation between the lowering of the Piezometric surface and the rate and duration of discharge of a well using ground-water storage. *Transactions, American Geophysical Union*, 16(2), 519–524. <https://doi.org/10.1029/TR016i002p00519>
- Theis, C. V. (1940). The source of water derived from wells: essential factors controlling the response of an aquifer to development. *Civil Engineering*, 10, 277–280.
- Thiem, A. (1870). Die Ergiebigkeit artesischer Bohrlöcher, Schachtbrunnen und Filtergalerien (in German). *Journal Für Gasbeleuchtung Und Wasserversorgung*, 13, 450–467.
- Thiem, G. (1906). *Hydrologische Methoden (in German)*. Leipzig: Gebhardt.
- Van der Gun, J., & Lipponen, A. (2010). Reconciling Groundwater Storage Depletion Due to Pumping with Sustainability. *Sustainability*, 2(11), 3418–3435. <https://doi.org/10.3390/su2113418>
- Verruijt, A. (1970). *Theory of Groundwater Flow*. London: Macmillan Press.
- Wada, Y. (2016). Modeling Groundwater Depletion at Regional and Global Scales: Present State and Future Prospects. *Surveys in Geophysics*, 37(2), 419–451. <https://doi.org/10.1007/s10712-015-9347-x>
- Wada, Y., van Beek, L. P. H., van Kempen, C. M., Reckman, J. W. T. M., Vasak, S., & Bierkens, M. F. P. (2010). Global depletion of groundwater resources. *Geophysical Research Letters*, 37(20), n/a-n/a. <https://doi.org/10.1029/2010GL044571>
- Wood, W. W. (2020). Groundwater “Durability” Not “Sustainability”? *Groundwater*, 58(6), 858–859. <https://doi.org/10.1111/gwat.13032>
- Zhang, H., Xu, Y., & Kanyerere, T. (2020). A review of the managed aquifer recharge: Historical development, current situation and perspectives. *Physics and Chemistry of the Earth, Parts A/B/C*, 118–119, 102887. <https://doi.org/10.1016/j.pce.2020.102887>
- Zhou, Y. (2009). A critical review of groundwater budget myth, safe yield and sustainability. *Journal of Hydrology*, 370(1–4). <https://doi.org/10.1016/j.jhydrol.2009.03.009>

Chapter 12. Using Linear Programming to Revisit the Optimization of a Combined Pumping and Deep Infiltration System

12.1. Introduction

This chapter revisits the study by Louwyck et al. (2005) to illustrate how the axisymmetric multilayer solutions discussed throughout this dissertation can be used in practice. Author contributions are given in section 1.5 of the introductory Chapter 1. The paper by Louwyck et al. (2005) summarizes the hydrogeological studies that were carried out to realize a more effective drainage system at the excavation site 'Duinenabdij', which may be translated as 'Abbey of the Dunes' (Lebbe et al., 2002; Louwyck, 2001; Lust, 2002). As the name suggests, the archeological site is located in the dunes of the town of Koksijde on the western North Sea coast of Belgium. One of the step-drawdown tests analyzed by Louwyck et al. (2010) - the one called the Dune test - was also conducted on this site. As the involved aquifer system consists of three permeable layers separated by two semi-pervious layers, it is necessary to apply a multilayer model to simulate groundwater flow in this system accurately, making this study an excellent case to discuss in this dissertation on multilayer flow.

The relatively shallow upper semi-pervious layer caused problems of high groundwater levels at the excavation site. To prevent flooding, a new drainage system was realized consisting of 26 pumping wells enclosing the site and extracting groundwater from the middle permeable layer. To protect the surrounding dunes, the extracted water is deep infiltrated back into the aquifer system by means of 24 injection wells with screen in the middle and lower permeable layer. Louwyck et al. (2005) emphasize the role of hydrogeological research preceding the on-site realization of this new drainage system. Relevant literature was studied and field data were gathered on the site, such as borings and geophysical borehole measurements, all of them giving a profound insight into the constitution of the aquifer system (Louwyck, 2001; Lust, 2002). A double pumping test was conducted to estimate the hydraulic parameters of the different layers in the aquifer system (Lebbe et al., 2002; Lust, 2002), and the effectiveness of the drainage system was investigated through mathematical modeling (Louwyck, 2001; Lust, 2002).

12.1.1. Inverse problems

Up to this chapter, the dissertation discussed the simulation of axisymmetric flow in multilayer aquifer systems applying analytical or numerical solution methods. Simulating heads or drawdowns using a mathematical model with known hydraulic parameters and boundary conditions is called a forward problem (Sun, 1999). In practice, however, axisymmetric models are frequently used to solve inverse problems. In Chapter 7 discussing nonlinear two-zone problems, an inverse problem has to be solved to find the boundary between the two zones. According to Sun (1999), this is a type 3 inverse problem, as it involves inferring boundary conditions.

In this chapter, the more frequently applied type 1 and type 2 inverse problems are addressed. Both the interpretation of the step-drawdown test, the aforementioned Dune test (Louwyck et al., 2010), and the interpretation of the double pumping test (Lebbe et al., 2002; Lust, 2002) are examples of

type 1 inverse problems, which are solved to find optimal hydraulic parameters (Sun, 1999). In both analyses, the inverse model combines the forward AS2D model discussed in Chapter 4 with the nonlinear Gauss-Newton regression algorithm to fit the simulated drawdown to the drawdowns observed during the aquifer test (Lebbe, 1988, 1999). Least-squares minimization has been applied extensively to interpret aquifer tests (Yeh, 2015). An example is the frequently used MLU program (Hemker & Post, 2019), which couples the semi-analytical solution by Hemker (1999a) to the Levenberg-Marquardt regression algorithm (Hemker, 1985a). Both the Gauss-Newton algorithm and the Levenbergh-Marquardt algorithm are discussed by Yeh (2015).

Estimating the pumping and injection rates to achieve the desired lowering of the water table at the excavation site is an example of a type 2 inverse problem (Sun, 1999). In the original studies (Louwyck, 2001; Louwyck et al., 2005; Lust, 2002), finding these pumping and injection rates was done via a trial-and-error procedure. The numerical AS2D model simulates flow to one well, and superposition is applied to obtain the total change in head due to all pumping and injection wells (Lebbe, 1988, 1999). Pumping and injection rates were modified manually until the drawdown of the water table was sufficiently large. As it is very likely that this educated guess is suboptimal, the exact optimal rates are derived here using linear programming. Instead of AS2D, the analytical solution by Hemker (1984) is applied to simulate the flow to one well. As discussed in Chapter 4, the latter is more accurate.

12.1.2. Linear programming

Linear programming, also called linear optimization, is an optimization method to achieve the optimal outcome in a mathematical model whose requirements are represented by linear relationships (Dantzig & Mukund, 1997). This optimal outcome may be the maximum profit or the lowest cost, or in the context of groundwater management, the optimal pumping rates of a groundwater development (Naseer & Honma, 2014; Psilovikos, 1999). The method is usually attributed to Dantzig (1947), who developed the simplex method, an efficient algorithm to tackle linear optimization problems, although the problem of solving a system of linear inequalities dates back at least as far as Fourier in the 19th century (Dantzig, 1982).

Linear programming is a technique that is well-known in the hydrogeological literature. The USGS, for instance, developed the GWM code, which is the groundwater management process for MODFLOW using optimization, and one of the optimization techniques is linear programming (Ahlfeld et al., 2005, 2009; Banta & Ahlfeld, 2013). Another example is the MODMAN code (Greenwald, 1994, 1998) that also couples a linear optimization model to MODFLOW (McDonald & Harbaugh, 1988). It seems linear programming is mostly applied in the context of quantitative groundwater management (Danapour et al., 2021; Jha et al., 2020; Naseer & Honma, 2014; Psilovikos, 1999; Stoecker et al., 1985), although it may also be used to optimize problems involving groundwater quality and contamination (Bretas & Haith, 1990). Linear programming is straightforward to use, but it is restricted to relatively small linear problems. More robust optimization methods exist that can handle nonlinear problems, e.g. quadratic and nonlinear programming, or can deal with non-differentiable and discontinuous functions, e.g. simulated annealing and genetic algorithms (Yeh, 2015).

12.1.3. Objective

The main objective of this chapter is to revisit the optimization of pumping and injection rates by Louwyck et al. (2005) using linear programming. As it concerns a multilayer aquifer system, the case is also a nice illustration of applying the analytical multilayer solution discussed in Chapter 2 to efficiently solve real-world problems without having to build a complicated, data-hungry, and

computationally expensive groundwater flow model. It is, however, not the purpose to validate the original simulations by Louwyck et al. (2005) or to evaluate the effectiveness of the realized drainage system. Therefore, the configuration of the wells suggested by Louwyck et al. (2005) is not modified, and only the pumping and injection rates are optimized.

In the next section 12.2, the original study by Louwyck et al. (2005) is presented. In fact, the text of this paper is adopted completely with only a few minor modifications to make it consistent with the other chapters in this dissertation. It discusses the interpretation of the double pumping test that was conducted to identify the hydraulic parameters for the different layers in the aquifer system (Lebbe et al., 2002; Lust, 2002). It also presents the simulation of the drainage system using the manually optimized pumping and injection rates. The subsequent section 12.3 revisits the optimization part of the study. It explains in detail how linear programming is applied to find the minimal pumping and injection rates that are needed to achieve a lowering of the water table of 1 m at the excavation site. In contrast to the previous chapters, this chapter also discusses in great detail the Python code that is written to perform the combined simulation and optimization.

Python scripting is becoming increasingly popular among groundwater practitioners (Bakker, 2014). A nice example is the FloPy package which consists of a set of scripts to run most MODFLOW related programs (Bakker et al., 2016). Another example is TTim, a multilayer analytical element model developed in Python (Bakker, 2013). Because TTim implements the semi-analytical transient state solution by Hemker (1999a, 1999b), it could be used as a forward model in the optimization of the drainage system. However, it is opted to implement the steady-state solution by Hemker (1984) from scratch, which is justified as it is the steady drawdown that has to be evaluated. It also demonstrates how easily this analytical solution is coded using scientific Python packages such as SciPy and NumPy, which provide all the necessary functions to perform the required matrix manipulations. PuLP is used for the optimization, which is a linear programming modeler written in Python that wraps several frequently applied solvers. Using PuLP, only a few lines of code are needed to define and solve the minimization problem, which is far more efficient than the original trial-and-error procedure by Louwyck et al. (2005).

12.2. The original study

Hydrogeological interventions in ecological valuable areas must be well studied beforehand. Modeling these interventions based on field observations and field studies is herein a valuable step. This is illustrated with an example in the western Belgian coastal plain. A new drainage system had to be designed for the preservation of the archeological excavation site ‘OLV Ten Duinen’. This site is situated in a valuable and protected dune area. A system of pumping and injection of water was studied to optimize the draining of the site and to minimize the effects in the nearby dunes. A double pumping test was conducted to derive the relevant parameters. These parameters were used to simulate and find the optimal configuration of the extraction and deep-infiltration wells.

12.2.1. Introduction

The archeological site of the medieval abbey ‘OLV Ten Duinen’ is situated in the dunes of Koksijde, Belgium (Figure 1). Because of its low topographic level and the occurrence of a shallow semi-permeable layer, the excavation suffered from high water levels during the winter periods. Since the former draining was ineffective, a new drainage system was needed to preserve the archeological relics. Furthermore, the conservation of the ecologically valuable dunes surrounding the site was a

second objective in the realization of the system. A profound knowledge about the hydrogeological characteristics of the concerning aquifer was indispensable to plan this system.



Figure 1. Situation of the study area and preserved dune areas.

A study of relevant literature (Baeteman, 1985; Lebbe, 1973, 1978; Lebbe et al., 1984, 1996; Van Houtte, 1998; Van Houtte et al., 1992) provided a first insight in the hydrogeological constitution of the groundwater reservoir. The aquifer system is composed of Quaternary sediments existing of three sandy, permeable layers, which are separated by two silty, semi-permeable layers (Figure 2). Underneath, the aquifer is bounded by a Palaeogene clay layer that could be considered impermeable in the scope of this study. The occurrence of the two semi-permeable layers was confirmed by the interpretation of borings and geophysical borehole measurements, viz. high electrical conductivity measurements, in wells at different locations on the site (Louwyck, 2001; Lust, 2002). Because the entire groundwater reservoir contains fresh water (De Breuck et al., 1974), the fluctuations of these conductivity measurements give a qualitative insight in the lithological constitution of the aquifer.

The former drainage system extracted only water above the shallow semi-permeable layer which caused a worse infiltration through this layer, and this explained largely its ineffectiveness to drain most of the recharge water away. A solution is to pump below the shallow semi-permeable layer so that a large part of the recharge water would flow through this layer deeper in the groundwater reservoir. However, this pumping would not only cause a descent of the water table at the excavation site, but it would also affect the surrounding dunes. Therefore, it is necessary to deep-infiltrate the pumped water in the two undermost permeable layers at the borders of the site.

Modeling this system of combined pumping and deep-infiltration, given the specific hydrogeological constitution, revealed the importance of an accurate knowledge of the hydraulic parameters of the concerning hydrogeological layers, particularly the hydraulic resistance of the two semi-permeable layers (Louwyck, 2001). Estimations of the parameters based on the interpretation of pumping tests executed in the vicinity of the study area were not reliable, because of the heterogeneous nature of Quaternary deposits in the Belgian coastal plain (Baeteman, 1999). The performance of a pumping test at the excavation site was therefore inevitable. Moreover, in order to achieve a reliable

deduction of the hydraulic resistance of both semi-permeable layers, it was necessary to execute a double pumping test affecting the two undermost permeable layers.

The drawdowns recorded during these two tests were simultaneously interpreted by means of an inverse numerical model, and this interpretation resulted in reliable parameter values. The model simulating the system of combined pumping and deep infiltration based on the deduced parameter values gave a profound insight in the system's effectiveness: not only the excavation would be drained properly, also the surrounding valuable dunes would be protected (Lebbe et al., 2002; Lust, 2002).

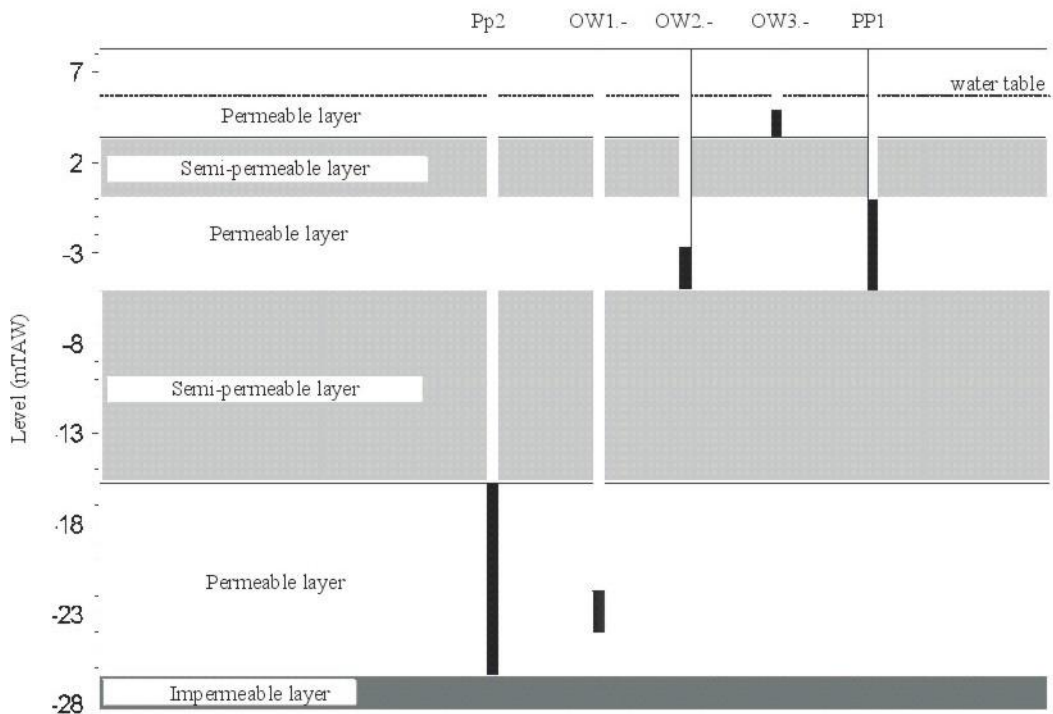


Figure 2. Schematic constitution of groundwater reservoir and position of screens (black) of pumping (PP-) and observation (OW-) wells. The mTAW is the Belgian ordnance datum, referring to mean low low seawater level, about 2.3 m below mean sea level.

12.2.2. Methodology

Figure 3 shows schematically the groundwater flow during a pumping test in an aquifer with permeable (B , D_1 , D_2) and semi-permeable (A , C) layers (Vandenbohede & Lebbe, 2003). An amount of water is extracted from the permeable layer B , which causes a horizontal movement of water in this layer towards the pumping well. This groundwater flow is mainly characterized by layer B 's horizontal conductivity K^h (m/d) and specific elastic storage S^s (1/m). The effect of pumping can be observed by the lowering of hydraulic head or drawdown s (m) in observation wells with screen in this layer. The pumping also causes a vertical movement of water from the adjacent semi-permeable layers to the permeable layer. This is called hydraulic leakage and it is mainly determined by the vertical conductivity K^v (m/d) and specific elastic storage S^s of layers A and C . The drawdown in observation wells with screen in D_1 or D_2 is caused by this leakage.

The resulting axisymmetric flow towards the pumping well is treated by the following partial differential equation (Lebbe, 1999):

$$K^h \left(\frac{\partial^2 s}{\partial r^2} + \frac{1}{r} \frac{\partial s}{\partial r} \right) + K^v \frac{\partial^2 s}{\partial z^2} = S^s \frac{\partial s}{\partial t} \quad (1)$$

with r (m) the distance from the pumping well, z (m) the depth, and t (d) the time after starting the test. Groundwater flow toward a pumping well may be conceptualized here as axisymmetric flow in a layered groundwater reservoir, where constant parameter values are assigned to each layer. This implies the vertical distance z is discretized into n_l layers, which converts partial differential equation (1) into a system of n_l partial differential equations (Hemker, 1985b, 1999b):

$$K_i^h D_i \left(\frac{\partial^2 s_i}{\partial r^2} + \frac{1}{r} \frac{\partial s_i}{\partial r} \right) = S_i^s D_i \frac{\partial s_i}{\partial t} + \frac{s_i - s_{i-1}}{c_{i-1}} + \frac{s_i - s_{i+1}}{c_i} \quad (1 \leq i \leq n_l) \quad (2)$$

where index i refers to layer i with thickness D_i (m), horizontal conductivity K_i^h , and specific elastic storage S_i^s . Drawdown s_i (m) in layer i is a function of radial distance r and time t . As part of the vertical discretization, resistance layers of zero thickness are defined between the layers. Resistance layer i is situated between layer i and layer $i + 1$, and its resistance c_i (d) is defined as:

$$c_i = \frac{D_i}{2K_i^v} + \frac{D_{i+1}}{2K_{i+1}^v} \quad (1 \leq i < n_l) \quad (3)$$

with K_i^v the vertical conductivity of layer i . The upper and lower boundary of the aquifer system are impervious, which means $c_0 = c_{n_l} = \infty$. The layers are strictly horizontal and laterally unbounded:

$$s_i(\infty, t) = 0 \quad (1 \leq i \leq n_l) \quad (4)$$

The superposition principle is applied; hence, the constant drawdown equal to zero in (4), which also explains the initial condition:

$$s_i(r, 0) = 0 \quad (1 \leq i \leq n_l) \quad (5)$$

At the inner model boundary, a constant discharge Q_i (m^3/d) is defined for each layer i , which defines the pumping rate of the well:

$$\lim_{r \rightarrow 0} \left(r \frac{\partial s_i}{\partial r} \right) = \frac{-Q_i}{2\pi K_i^h D_i} \quad (1 \leq i \leq n_l) \quad (6)$$

Pumping rate Q_i is positive if water is extracted. As the effect of wellbore storage is neglected, an infinitesimal radius is assumed in (6).

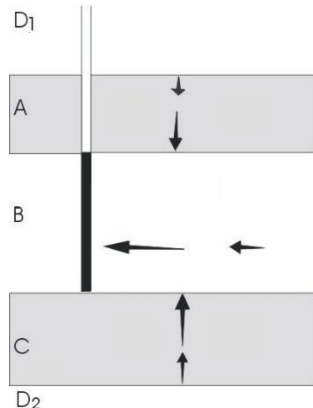


Figure 3. Schematized flow towards pumping well in layered aquifer (Vandenbohede & Lebbe, 2003).

HYPARIDEN (HYdraulic PARameter IDENTification) is a set of computer codes developed as a generalized interpretation method for single and multiple pumping tests in layered heterogeneous aquifers (Lebbe, 1999). It is based on an axially symmetric, numerical model AS2D, specifically designed for the simulation of pumping tests (Lebbe, 1988, 1999). AS2D solves system of equations (2) subject to conditions (4), (5), and (6) using the hybrid finite-difference finite-element method, which is discussed exhaustively in Chapter 4. Because of the assumption of axial symmetry, the model has several advantages over frequently used numerical groundwater flow models in the analysis of pumping tests. HYPARIDEN also includes an inverse numerical model allowing for the derivation of optimal values of hydraulic parameters or groups of hydraulic parameters from the observed drawdowns.

All observations from different wells at different times are involved together in the parameter identification process, and in the case of a multiple pumping test, all observations from all tests are simultaneously interpreted. The algorithm of the inverse model is obtained by the combination of the forward numerical model and the Gauss-Newton algorithm for nonlinear regression. In the first step, the forward model calculates the drawdowns at the concerning observation places and times. The second step involves a number of sensitivity analyses. Based on these sensitivities and the differences between calculated and observed data, the calculation of adjustment factors for the derivable hydraulic parameters is finally performed. By successive execution of these three steps, the optimal values for the hydraulic parameters are derived iteratively along with their joint confidence region (Lebbe, 1988, 1999).

In this study, a double pumping test was executed in the north eastern corner of the site. The relative position of pumping and observation wells is pictured in Figure 4. The location of the well screens is shown in Figure 2. During the first pumping test, a discharge of $178 \text{ m}^3/\text{d}$ was pumped on pumping well PP1 with screen situated over the entire depth interval of the middle permeable layer.

Drawdown measurements were performed in this pumping well and in the observation wells at different times during the duration of the test, which is two days. In the second test, PP2 with screen in the deepest permeable layer was used as pumping well. The discharge was $599 \text{ m}^3/\text{d}$ and the duration of the test was three days. Again, drawdown was measured in the pumping and observation wells at different times. Between the two tests, a recovery period of two days was needed to ensure the observations of the second test were not influenced by the first test.

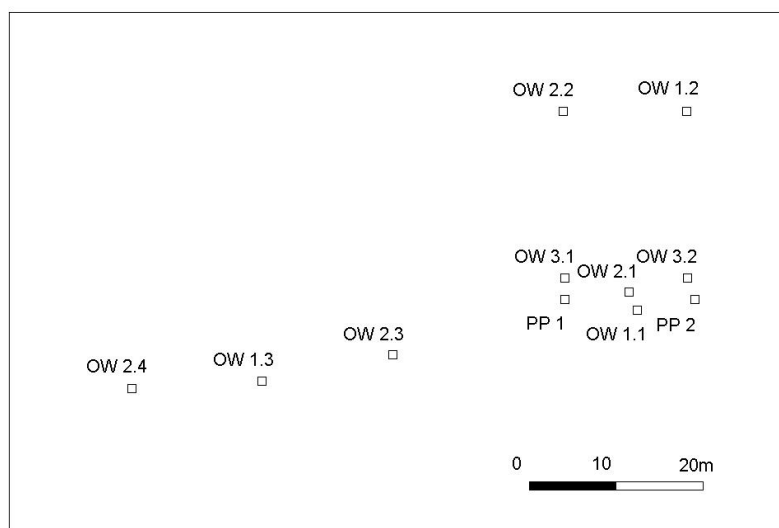


Figure 4. Position of pumping and observation wells.

The interpretation of the observed drawdowns by means of HYPARIDEN resulted in reliable parameter values, after which it was possible to simulate the system of combined pumping and deep-infiltration. To be more precise, an estimate of the drawdown due to simultaneously pumping and deep-infiltrating in the different wells of the system was simulated. Knowing the hydraulic parameters of the groundwater reservoir and the discharges for the individual wells, this drawdown can be calculated by application of the rule of superposition (Lebbe, 1999), which is also discussed in Chapter 2:

$$s_i(x, y, t) = \sum_{p=1}^{n_w} \frac{Q_p}{Q_{ref}} s_i(r_p, t) \text{ with } r_p = \sqrt{(x_p - x)^2 + (y_p - y)^2} \quad (7)$$

where $s_i(x, y, t)$ is the drawdown in layer i at node (x, y) of a mesh-centered grid and at time t after starting the drainage system; (x_p, y_p) is the coordinate of the point representing the p -th pumping well extracting at pumping rate Q_p ; n_w is the number of pumping wells; $s_i(r_p, t)$ is the drawdown calculated using AS2D at time t in layer i and at distance r_p from the p -th pumping well extracting at a specified pumping rate Q_{ref} used as reference. Here, Q_{ref} is set to the maximum pumping rate, i.e. $\max_p Q_p$. Note that discharge Q_p is less than zero when the p -th well is a deep-infiltration well. The superposition rule expressed by (7) thus states that the drawdown due to a multiple well field is equal to the sum of drawdowns due to each individual well.

The MULTPU-code in HYPARIDEN is designed to simulate drawdown due to a multiple well field by application of (7). Remark that the superposition method according to (7) is only valid if the groundwater flow is linear, meaning that in case of considerable drawdown in the top layer, this model is not appropriate. In this study, the assumption of linearity is justified; hence, drawdown calculated using MULTPU is as accurate as drawdown that would be simulated using MODFLOW (Harbaugh et al., 2000). In this particular case, one could even state the requirement of a laterally bounded aquifer system makes the MODFLOW model less realistic and the estimated drawdown less accurate (Lust, 2002).



Figure 5. Location of pumping (closed bold line) and deep infiltration (northern bold line) zone.

To simulate the combined pumping and deep-infiltration system by application of (7), knowledge about its technical design is required, viz. the exact location of the different wells, the position of

their screen, and their individual discharge rate. Figure 5 shows the exact location of the pumping and deep-infiltration zone. The 26 pumping wells with screen in the middle permeable layer are located around the relics of the excavation site; the 24 deep-infiltration wells with screen in the middle permeable layer are located at the northern boundary of the site. In between the latter wells, 12 deep-infiltration wells with screen in the deepest permeable layer were constructed. The simulation of the system was performed with a pumping rate equal to $60 \text{ m}^3/\text{d}$ for each pumping well, an injection rate equal to $-49,33 \text{ m}^3/\text{d}$ for each deep-infiltration well with screen in the middle permeable layer, and an injection rate equal to $-40 \text{ m}^3/\text{d}$ for each deep-infiltration well with screen in the deepest permeable layer. Pumping wells are surrounded by a gravel pack over the full depth, and in the absence of a clay seal, it is estimated that each well extracts $4 \text{ m}^3/\text{d}$ from the upper permeable layer (Lust, 2002).

12.2.3. Results

The sensitivity analyses indicate that the optimal value of seven relevant hydraulic parameters or parameter groups could be deduced from the observations of the double pumping test (Lebbe et al., 2002; Lust, 2002). Table 1 gives an overview of these parameters and their optimal value calculated by means of the inverse numerical model. The subscripts of the parameters refers to the layer numbering which is according to Figure 2, taking into account the layers are counted starting with the upper permeable layer, the upper semi-permeable layer, etc. Parameter c is the hydraulic resistance of a semi-permeable layer, which is the thickness of the layer divided by its vertical conductivity. The optimal values in Table 1 are sorted by reliability, which means the inferred value for the horizontal conductivity K_5^h of the lowest permeable layer is the most reliable one.

Table 1. Optimal values for relevant parameters.

Parameter	Optimal value
K_5^h	42.00 m/d
K_3^h	13.80 m/d
c_4	49.70 d
S_5^s	$7.12 \times 10^{-5} \text{ m}^{-1}$
$S_2^s = S_3^s$	$7.80 \times 10^{-5} \text{ m}^{-1}$
S_4^s	$2.09 \times 10^{-5} \text{ m}^{-1}$
c_2	735.00 d

Figure 6 and Figure 7 show the time-drawdown and distance-drawdown graphs for the first and second pumping test, respectively. The crosses indicate the observed drawdowns, the solid lines are calculated with the forward numerical model AS2D by using the optimal values of the hydraulic parameters. At first sight, one can observe a good agreement between the observed and calculated drawdowns. Analyzing the 424 residuals, their distribution is inferred as normal with zero mean and total sum of squares equal to 1.919. Remark the absence of observations in the uppermost permeable layer because of their insignificance: the high hydraulic resistance of the uppermost semi-permeable layer causes a drawdown with the same magnitude of observed natural head fluctuations. This high resistance is also the reason why the hydraulic parameters of the uppermost permeable layer, that is layer 1, are not identifiable, which means these parameters have little influence on the drawdown in the other layers. A rough estimate of their values is thus sufficient in the interpretation of the double pumping test and the simulation of the combined pumping and deep-infiltration system.

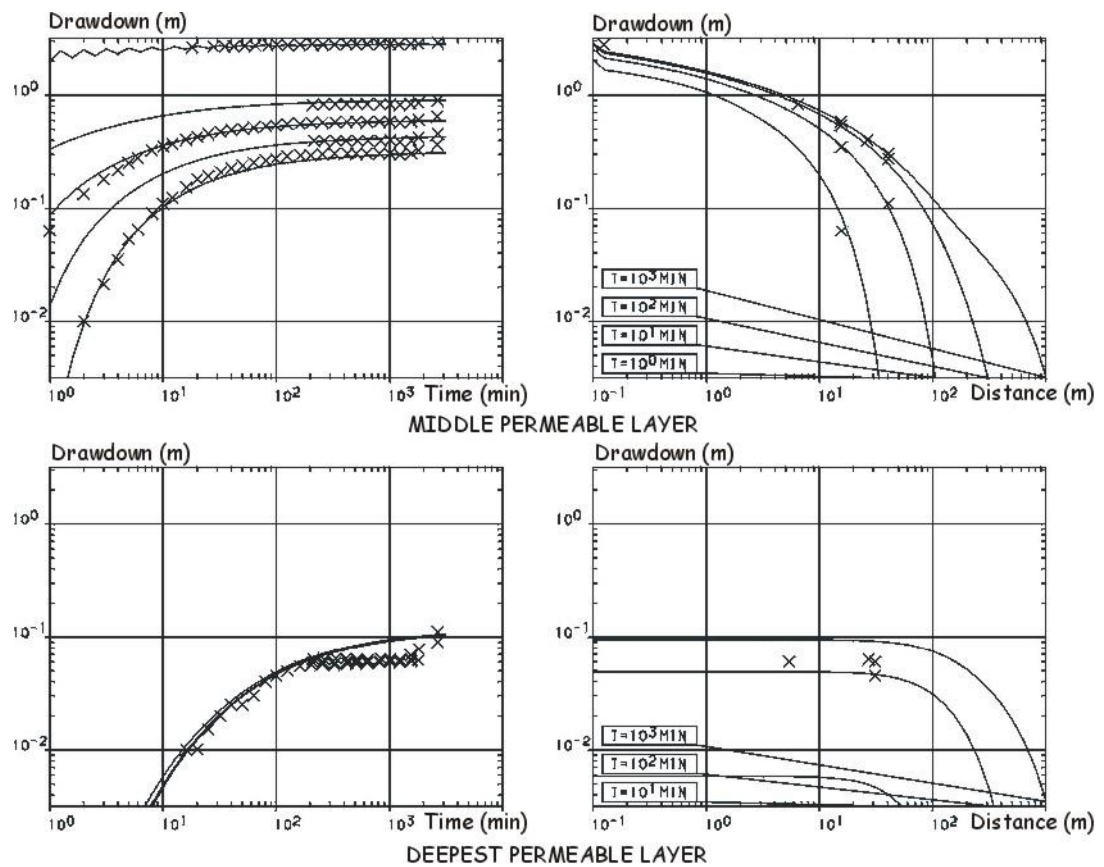


Figure 6. Observed (crosses) and calculated (solid lines) drawdowns for the first pumping test.

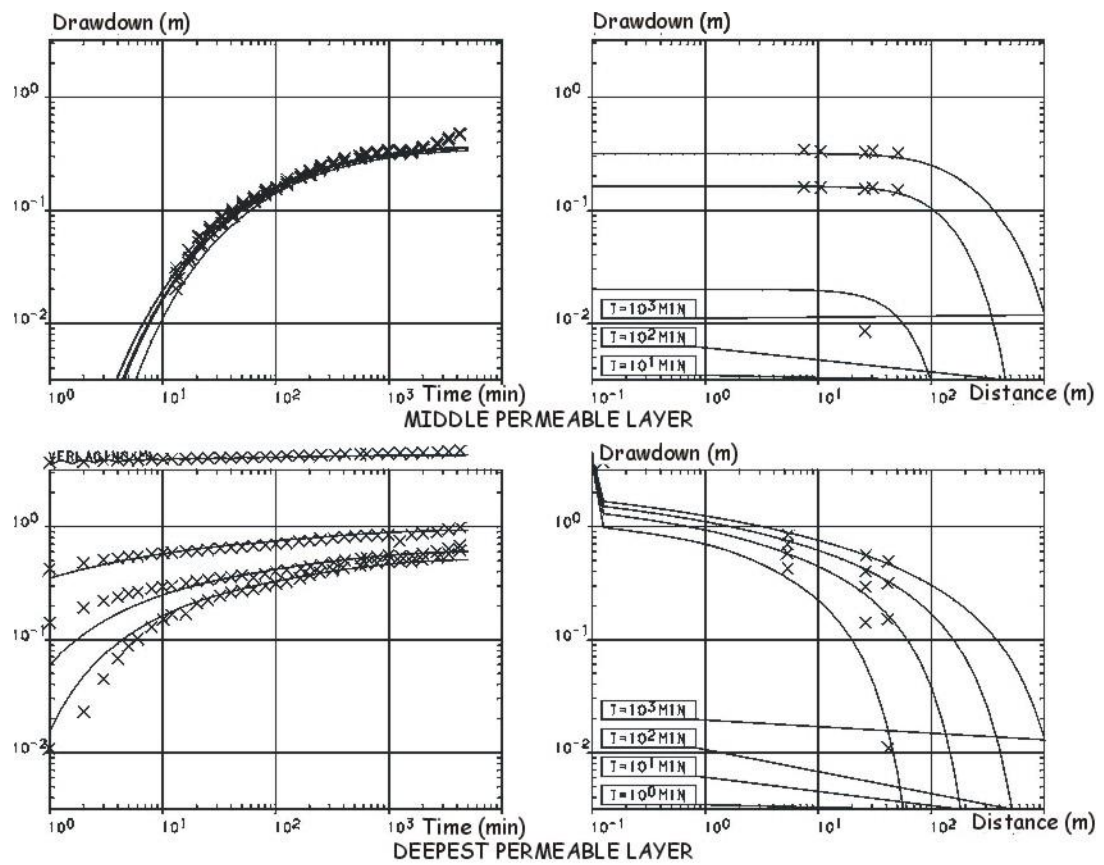


Figure 7. Observed (crosses) and calculated (solid lines) drawdowns for the second pumping test.

It has already been mentioned HYPARIDEN allows for deducing the optimal values along with their joint confidence region. The analysis of this confidence region gives an idea about the accuracy of the deduced values and their mutual dependency (Lebbe, 1999). For the double pumping test in this study, all parameter values show a moderate mutual dependency (Lebbe et al., 2002; Lust, 2002). Moreover, the first five parameter groups in Table 1 are inferred accurately. The optimal value for S_4^S , the specific elastic storage for the deepest semi-permeable layer, is less reliable. Finally, the deduction of the hydraulic resistance c_2 of the shallow semi-permeable layer is not accurate due to the lack of significant drawdown measurements in the uppermost permeable layer.

However, by calculating the difference between the hydraulic head in the two uppermost permeable layers and estimating the infiltration rate of groundwater through the shallow semi-permeable layer, a more reliable value can be assigned to this parameter by application of Darcy's law (Louwyck, 2001; Lust, 2002). When assuming the infiltration rate is twice the annual average infiltration rate and thus equal to 1.53 mm/d (Lebbe, 1978), the estimated hydraulic resistance c_2 of the uppermost semi-permeable layer equals to 1300 d (Lebbe et al., 2002).

Figure 8, Figure 9, and Figure 10 show the horizontal contour lines of the drawdown simulated by means of MULTPU in the three permeable layers due to the combined pumping and deep-infiltration of the drainage system. The dimension of the simulated area is 600 m x 600 m and the y-axis is parallel to the north-south direction. Negative drawdown values are indicating a rising of the hydraulic head. In the middle permeable layer, which is directly influenced by the system, the appearance of a large 'depression funnel' and 'infiltration cone' at respectively the pumping and deep infiltration zone is seen. A funnel and cone are also appearing in the deepest permeable layer, although less accentuated and not following the exact shape of the well configuration because of the absence of pumping wells in this layer and the occurrence of the deepest semi-permeable layer.

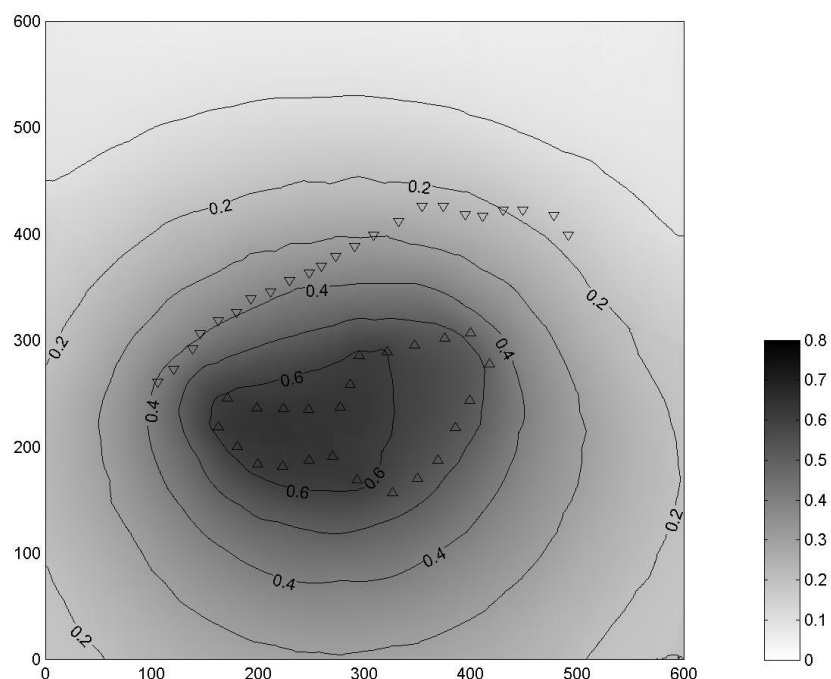


Figure 8. Calculated drawdown due to drainage system in upper permeable layer. Triangles indicate the position of pumping (triangle up) and deep infiltration (triangle down) wells.

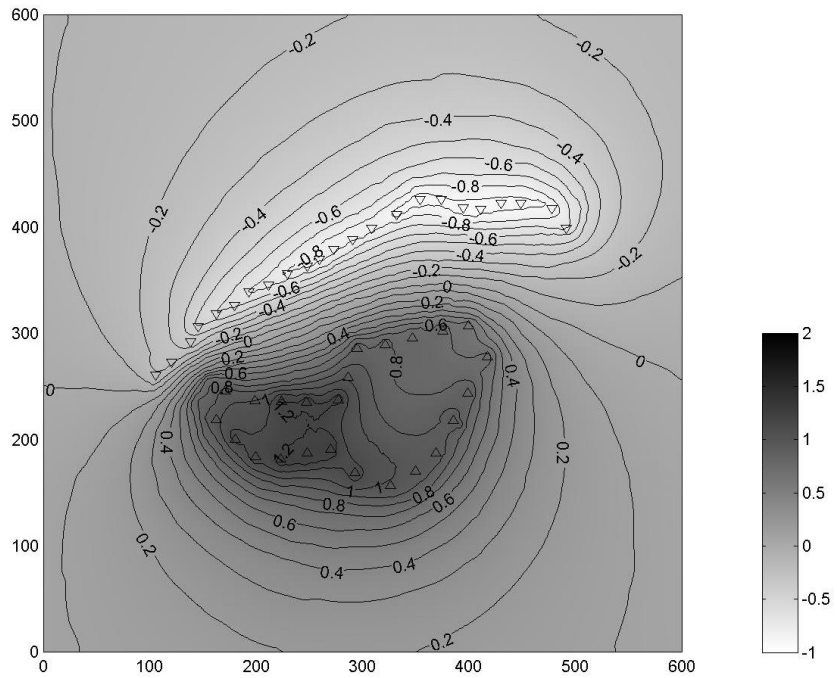


Figure 9. Calculated drawdown due to drainage system in middle permeable layer. Triangles indicate the position of pumping (triangle up) and deep infiltration (triangle down) wells.

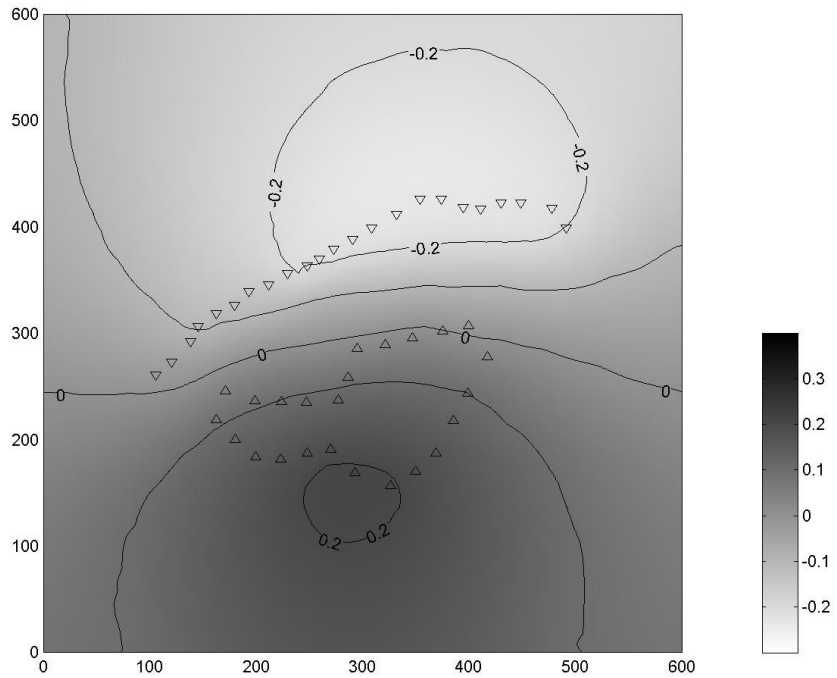


Figure 10. Calculated drawdown due to drainage system in lower permeable layer. Triangles indicate the position of pumping (triangle up) and deep infiltration (triangle down) wells.

The high hydraulic resistance of the shallow semi-permeable layer and the dispersal of deep-infiltrated water over the two undermost permeable layers are the reason why an infiltration cone is absent in the uppermost permeable layer. Looking more closely at this graph, the simulated lowering of the water table at the excavation site is significant. Note that the lowering at the western part is higher than the lowering at the eastern part. It is also seen that the drawdown in the surroundings is minimal, and especially, the northern part of the area is protected because of the location of the deep-infiltration zone. In this particular case, a configuration with a deep-infiltration zone

surrounding the entire area could be considered as ideal (Louwyck, 2001). However, not only hydrogeological requirements were playing a role in determining the most suitable configuration.

12.2.4. Conclusions

Simulating the system of combined pumping and deep-infiltration has proven its effectiveness in draining the excavation site without endangering the surrounding valuable dune area. In general, the system of combined pumping and deep-infiltration is an outstanding method to create a local lowering of the water table. Moreover, the location of the deep-infiltration zone can be chosen in a way the vulnerable area is optimally protected.

Furthermore, this study has illustrated the important role of field tests and mathematical modeling in the planning of hydrogeological interventions in ecologically valuable areas. In fact, the different steps in handling a hydrogeological problem in an efficient and scientific justified way are discussed. Relevant literature was consulted to gain initial insight into the hydrogeological constitution of the studied groundwater reservoir. Then supplementary information was gathered by means of borings, geophysical borehole measurements (conductivity measurements) and the performance of a double pumping test. The interpretation of these field data makes it possible to fill the gaps in the hydrogeological knowledge required to accurately model the designed drainage system. Finally, analyzing the simulation of the system has shown its effectiveness in taking care of the problem.

12.3. Revisiting the optimization

To protect the archeological relics at the excavation site ‘Duinenabdij’, about 1 m lowering of the water table was required (Louwyck, 2001; Lust, 2002). Taking a closer look at the simulated drawdown in the top layer (Figure 8), it is seen this objective is not achieved. In reality, vertical sand drains perforating the upper semi-pervious layer were installed to decrease its resistance and to increase the drawdown in the top layer (Lust, 2002).

In this section, the combined simulation and optimization problem is revisited to find the minimum pumping rate that is required to achieve a lowering of the water table of at least 1 m at the excavation site. The configuration of pumping and injection wells is adopted from the original study. In this original study, finding the optimal pumping and injection rates was done manually via trial-and-error (Louwyck et al., 2005; Lust, 2002). Here, linear programming is used to minimize the pumping rate subject to the hard constraint of 1 m drawdown in the top layer at the site.

Drawdown in the three permeable layers due to the drainage system is simulated again by applying the superposition method expressed by (7). However, instead of solving system of differential equations (2) numerically, the analytical solution by Hemker (1984) is used. This solution is exact and easy to implement, which is illustrated by discussing the Python code developed to perform the simulations. For the optimization, Python package PuLP is applied which implements different solvers for linear programming.

Applying superposition and linear programming is only allowed if the groundwater flow problem is linear. Although the stated problem is linear indeed, it should be noted the upper layer contains the water table, which means its saturated thickness is head-dependent. Therefore, a more accurate simulation of the drainage system would require a more advanced numerical model that can handle the nonlinear flow in the upper layer, such as MODFLOW 6 (Langevin et al., 2017). In case of unconfined flow, successive linear programming (Ahlfeld & Baro-Montes, 2008) can be applied to minimize the pumping rates, which is implemented in GWM (Banta & Ahlfeld, 2013). On the other hand, one may argue that the error due to the assumption of linearity is much smaller than the inevitable parameter uncertainty associated with the interpretation of the pumping tests.

Linear programming is an exact solution method that finds the global optimum. Therefore, it can only be used in practice to solve relatively small problems, such as the case discussed here. In many other practical situations, however, finding the exact global optimum would take too much time, in which case an optimization method should be used that approximates the global optimum. Metaheuristics like simulated annealing, tabu search, and genetic algorithms are examples of such methods. An excellent overview of the different optimization methods applied to solve groundwater management problems is given by Yeh (2015).

12.3.1. Methodology

The original study applies the numerical AS2D model (Lebbe, 1988, 1999) to simulate the double pumping tests as well as the drainage system consisting of pumping and deep-infiltration wells. In this model, the Quaternary aquifer system is discretized into 13 model layers (Lebbe et al., 2002; Louwyck et al., 2005; Lust, 2002). More precisely, the upper permeable layer containing the water table and the semi-pervious layers (Figure 2) are divided into sublayers, in order to simulate the vertical flow in these layers more accurately. As flow in the semi-pervious layers is predominantly vertical indeed, a discretization beyond the lithostratigraphic units is required for a reliable interpretation of the double pumping tests (Lebbe et al., 2002; Lust, 2002). Furthermore, the AS2D model is transient, which is also necessary to simulate the double pumping tests accurately. The effect of the drainage system is modelled after 100.000 minutes of pumping and deep infiltrating (Lust, 2002). As the total pumping rate equals the total injection rate, it is expected the aquifer system is in a steady state again after this period of almost 70 days.

Here, the simulation of the combined pumping and deep-infiltration system is revisited and optimized by applying linear programming. A new steady-state multilayer model is built for that purpose. As explained in Chapter 2, such a model can be simulated easily by applying the superposition method to the analytical solution by Hemker (1984). The new steady-state model is also reduced to 3 layers which correspond to the three aquifers, while the separating aquitards are conceptualized as zero-thickness resistance layers. This is justified as the focus is on the drawdown in the top layer, which does not require a very accurate simulation of the vertical flow within these semi-pervious layers.

The thickness of the upper layer is 2.9 m and its conductivity is estimated as 12 m/d, the thickness of the middle layer is 5.2 m, and the thickness of the lower layer is 10.7 m (Lust, 2002). As the upper layer is phreatic, its saturated thickness was estimated from the mean water table height. Using Table 1, the transmissivity for each layer is found by multiplying its thickness by its horizontal conductivity: $T_1 = 34.80 \text{ m}^2/\text{d}$, $T_2 = 71.76 \text{ m}^2/\text{d}$, and $T_3 = 449.40 \text{ m}^2/\text{d}$. Note that only the permeable layers are numbered here, and the aquitards get the index of the overlying aquifer. Therefore, resistance of the lower aquitard is 49.70 d, which is c_4 in Table 1 and c_2 in the new steady-state model, whereas resistance of the upper aquitard, which is c_1 in the new model, is estimated 1300 d, as explained in section 12.2.3.

As already mentioned, the flow induced by the system of combined pumping and deep-infiltration will eventually reach a new steady state if the total discharge equals the total recharge, which is translated into the following condition:

$$\sum_{j=1}^4 n_j P_j = 0 \quad (8)$$

where n_j is a number of wells, and P_j is the corresponding pumping or injection rate (m^3/d) for each of these wells. P_1 is the amount of water per unit of time that each pumping well extracts from the

top layer through its gravel pack, P_2 is the pumping rate for each well extracting water from the middle layer, P_3 is the injection rate for each well injecting water in the middle layer, and P_4 is the injection rate for each well deep-infiltrating water in the lower layer. This means $n_1 = n_2$ is the number of pumping wells, which is 26, n_3 is the number of injections wells, which is 24, and n_4 is 12 as only half of the injection wells also recharge the lower layer. In the scenario proposed by Louwyck et al. (2005) and discussed in section 12.2.2, P_1 is 4 m³/d, P_2 is 60 m³/d, and P_4 is -40 m³/d. By solving (8), it is found that injection rate P_3 equals -49.33 m³/d indeed.

By definition, drawdown s is independent of time in case of steady state, or $\partial s / \partial t = 0$, which simplifies (2) to a system of ordinary differential equations. As explained in Chapter 2, this system of equations can be written in matrix form:

$$\frac{d^2\mathbf{s}}{dr^2} + \frac{1}{r} \frac{ds}{dr} = \mathbf{As} \quad (9)$$

where \mathbf{s} is an $n_l \times 1$ vector holding drawdown $s_i(r)$ at distance r for each layer i :

$$s_i = s_i(r) \quad (1 \leq i \leq n_l) \quad (10)$$

and \mathbf{A} is an $n_l \times n_l$ tridiagonal matrix with nonzero entries defined as:

$$A_{ij} = \begin{cases} \frac{1}{c_{i-1}T_i} + \frac{1}{c_i T_i} & (1 \leq i \leq n_l; j = i) \\ \frac{-1}{c_{i-1}T_i} & (1 < i \leq n_l; j = i - 1) \\ \frac{-1}{c_i T_i} & (1 \leq i < n_l; j = i + 1) \end{cases} \quad (11)$$

Boundary conditions (4) and (6) are also written in matrix form, respectively:

$$\mathbf{s}(R) = \mathbf{0} \quad (12)$$

$$\lim_{r \rightarrow 0} \left(r \frac{ds}{dr} \right) = -\mathbf{T}^{-1} \mathbf{Q} \quad (13)$$

with \mathbf{T} an $n_l \times n_l$ diagonal matrix with nonzero entries equal to:

$$T_{ii} = 2\pi T_i \quad (1 \leq i \leq n_l) \quad (14)$$

and \mathbf{Q} an $n_l \times 1$ vector holding the pumping rates Q_i for each layer i :

$$Q_i = Q_i \quad (1 \leq i \leq n_l) \quad (15)$$

Note that boundary condition (12) defines the outer model boundary at a finite distance R [L], which is required for an aquifer system in steady state, extracted by a single well, and without other sources and sinks.

As explained in Chapter 2, matrix system (9) is solved by decomposing matrix \mathbf{A} into its eigenvalues and corresponding eigenvectors (Hemker, 1984):

$$\mathbf{A} = \mathbf{V} \mathbf{D} \mathbf{V}^{-1} \quad (16)$$

where \mathbf{D} is an $n_l \times n_l$ diagonal matrix containing the n_l eigenvalues d_i , and \mathbf{V} is an $n_l \times n_l$ matrix containing the corresponding eigenvectors in its columns. As steady state is considered and the upper and lower boundary are impervious, i.e. $c_0 = c_{n_l} = \infty$, matrix \mathbf{A} has $n_l - 1$ strictly positive

eigenvalues and 1 zero eigenvalue corresponding to the solution of the comprehensive system (Bakker & Strack, 2003).

The solution for (9) subject to conditions (12) and (13) is given in Chapter 2:

$$\mathbf{s}(r) = \mathbf{V}\mathbf{K}(r, R)\mathbf{V}^{-1}\mathbf{T}^{-1}\mathbf{Q} \quad (17)$$

with $\mathbf{K}(r, R)$ an $n_l \times n_l$ diagonal matrix containing the following nonzero entries:

$$\mathbf{K}_{ii}(r, R) = \begin{cases} \ln(R/r) & (d_i = 0) \\ K_0(r\sqrt{d_i}) - \frac{K_0(R\sqrt{d_i})}{I_0(R\sqrt{d_i})} I_0(r\sqrt{d_i}) & (d_i \neq 0) \end{cases} \quad (18)$$

As explained in Chapter 9, the zero eigenvalue corresponds to the Thiem (1870; 1906) solution for the comprehensive system (Bakker & Strack, 2003).

Using (17), equation (7) expressing the principle of superposition can be reformulated as:

$$\mathbf{s}(x, y) = \sum_{p=1}^{n_w} \mathbf{V}\mathbf{K}(r_p, R_p)\mathbf{V}^{-1}\mathbf{T}^{-1}\mathbf{Q}_p \text{ with } r_p = \sqrt{(x_p - x)^2 + (y_p - y)^2} \quad (19)$$

An additional constant head must be defined in a single point (x_0, y_0) :

$$\mathbf{s}(x_0, y_0) = \mathbf{0} \quad (20)$$

Preferably, this point is specified at a far distance from the wells so it has no impact on the calculated drawdown (Bakker & Strack, 2003). For each well p in (19), R_p can now be determined using point (x_0, y_0) :

$$R_p = \sqrt{(x_p - x_0)^2 + (y_p - y_0)^2} \quad (21)$$

Equation (21) is required to fulfill boundary condition (12) for each well p . As drawdown is proportional to the pumping rate according to the superposition property, expression (19) may be written as:

$$\mathbf{s}(x, y) = \sum_{j=1}^4 P_j \sum_{p=1}^{n_j} \mathbf{V}\mathbf{K}(r_p, R_p)\mathbf{V}^{-1}\mathbf{T}^{-1}\mathbf{U}_j \text{ with } r_p = \sqrt{(x_p - x)^2 + (y_p - y)^2} \quad (22)$$

and with:

$$\mathbf{U}_1 = \begin{bmatrix} 1 \\ 0 \\ 0 \end{bmatrix}, \mathbf{U}_2 = \begin{bmatrix} 0 \\ 1 \\ 0 \end{bmatrix}, \mathbf{U}_3 = \begin{bmatrix} 0 \\ 0 \\ 1 \end{bmatrix}, \mathbf{U}_4 = \begin{bmatrix} 0 \\ 0 \\ 0 \end{bmatrix} \quad (23)$$

Vector \mathbf{U}_j has 3 elements as there are 3 layers in the aquifer system. The entry in \mathbf{U}_j equal to 1 indicates the extracted layer, which implies $P_j \mathbf{U}_j = \mathbf{Q}_p$. For each of the 4 types of pumping or injection wells defined by (8), equation (22) first simulates drawdown \mathbf{u}_j using a unit discharge vector \mathbf{U}_j , and then multiplies the output by the required pumping or injection rate P_j :

$$\mathbf{s}(x, y) = \sum_{j=1}^4 P_j \mathbf{u}_j \quad (24)$$

Expression (19) is rearranged to expression (22) since the latter can be used to optimize the pumping rates applying linear programming. Here, pumping rate P_2 must be minimized, which means P_2 is the objective function. Pumping rate P_1 is a constant equal to $4 \text{ m}^3/\text{d}$. Two optimization problems will be solved: the first considers P_4 as a constant equal to $-40 \text{ m}^3/\text{d}$, whereas P_4 is a variable in the second problem. Injection rate P_3 is always determined by (8).

In order to be able to minimize the objective function, the following constraints are required:

$$P_2 \geq 0 \quad (25)$$

$$\forall (x, y) \in C: \sum_{j=1}^4 P_j u_j \geq 1 \quad (26)$$

Constraint (26) defines a set C of control points at which the drawdown according to (22) must be larger than 1 m. These points are located at the excavation site, where the objective is to lower the water table by 1 m indeed (Louwyck, 2001; Lust, 2002). Four points are defined with coordinates (300, 200), (300, 250), (350, 200), and (350, 250), respectively. In the second scenario defining P_4 as variable, the additional constraint $P_4 \leq 0$ is required.

12.3.2. Implementation

Solving the minimization problem as outlined in previous section 12.3.1 can be done easily in Python using packages specifically developed for scientific computing. This section discusses the Python implementation in detail. A basic knowledge of Python syntax and object-oriented programming is required to understand the code presented in this section. Readers who are new to these topics are recommended to read the “Python Crash Course” by Matthes (2023), and readers interested in solving groundwater problems analytically using Python certainly will appreciate the textbook by Bakker and Post (2022). The Jupyter notebook with the Python code for this problem can be downloaded from GitHub⁹, and running this notebook is straightforward in the Google Colaboratory environment, which is free of charge and doesn’t require any installation of packages.

The hardest part is to implement solution (17), although manipulating matrices is very straightforward using the NumPy library, while the SciPy package offers functions to perform the eigendecomposition, matrix inversion, and the evaluation of special functions like the modified Bessel functions. Visualizing the model output is also easy using the Matplotlib library. To be able to use the required functions provided with these packages, the following import statements must be evaluated:

```
import numpy as np
import matplotlib.pyplot as plt
from numpy.linalg import multi_dot as mdot
import warnings
from scipy.linalg import eig, inv, solve, LinAlgWarning
from scipy.special import i0, k0
```

The object-oriented programming paradigm is applied to structure the code (e.g. Bakker & Kelson, 2009). As indicated by the class diagram in Figure 11, three classes are defined: the `AquiferSystem` class which represents the multilayer aquifer system, the `Well` class which conceptualizes a pumping or injection well, and the `MultiLayerSteadyWellFlow` class which is used to simulate the drawdown due to one well using the Hemker (1984) solution. As is seen on the diagram in Figure 11, an `AquiferSystem` object may contain several `Well` objects, whereas a `Well` object uses exactly one `MultiLayerSteadyWellFlow` object to simulate the drawdown the well causes. Each class has

⁹ <https://github.com/alouwyck/PhD>

an `__init__` method, which may be seen as the class constructor, as it is used to instantiate a particular object belonging to that class. An object consists of attributes holding its specific data, and it also has methods which are functions that operate on the object. For instance, a `Well` object has attribute `Q` to which the pumping rate of the well is assigned, and it has a method `s` that calculates the drawdown caused by the well at points passed to the method as coordinates (x, y) . In the following subsections, the code for each class is discussed in detail.

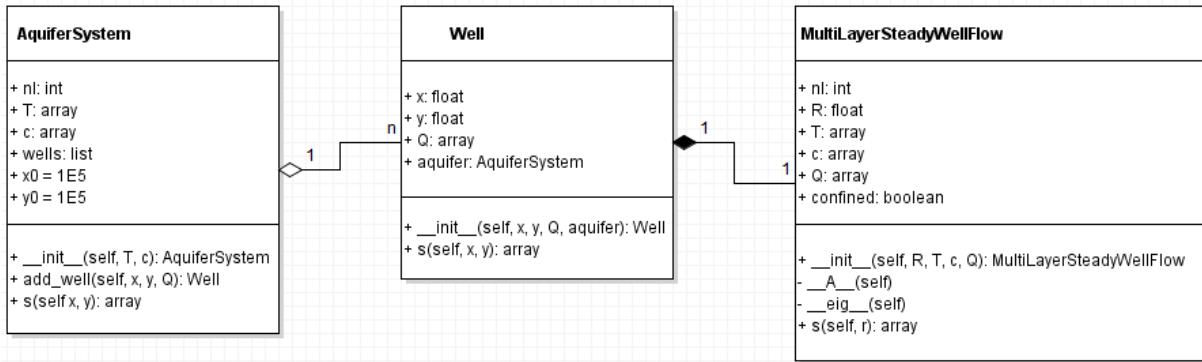


Figure 11. Class diagram summarizing attributes and methods for the three Python classes defined to simulate the steady-state effect of multiple wells extracting from a multilayer aquifer system. Drawdown is calculated using the superposition method and the analytical solution by Hemker (1984). Relations between the classes are also indicated: an `AquiferSystem` object aggregates many `Well` objects, and each `Well` object is composed of exactly one `MultiLayerSteadyWellFlow` object. The latter is used to calculate the drawdown in the aquifer system induced by the well it represents. See text for the Python code and a more detailed explanation.

12.3.2.1. Class AquiferSystem

The `AquiferSystem` class represents the multilayer aquifer system and must contain the hydraulic parameters of the layers of which the system consists. As the model is steady-state, only transmissivities `T` and resistances `c` are required, which are passed to the constructor as array-like objects and stored as NumPy arrays. Attribute `nl` is the total number of layers n_l , and attributes `x0` and `y0` are the coordinates of point (x_0, y_0) at which a constant head is defined according to (20). By default, a value of 10^5 is assigned to both. Attribute `wells` is a list of `Well` objects representing the wells interacting with the aquifer system. These wells are added by invoking method `add_well`. The input parameters of this method are the coordinate (x, y) of the well and the pumping rate `Q`. The latter is an array-like object as it must indicate the pumping rate Q_i for each layer i . Finally, there is method `s` which calculates the total drawdown due to all wells in the aquifer system by applying superposition. This method uses a `for`-loop to calculate the drawdown caused by each individual well, after which this drawdown is added to the total drawdown `s` returned by the method.

```

class AquiferSystem:
    """
    class to define a multilayer aquifer system that is extracted by pumping wells
    """

    def __init__(self, T, c):
        """
        T is vector with layer transmissivities [L2/T] (array-like)
        c is vector with resistances [T] (array-like)
        """
        self.T = np.array(T, dtype=float) # shape (nl,)
        self.c = np.array(c, dtype=float) # shape (nl+1,)
        self.nl = len(self.T) # number of layers nl
        self.x0, self.y0 = 1e5, 1e5 # constant-head point (x0, y0)
        self.wells = [] # list of wells extracting from the aquifer system

```

```

def add_well(self, x, y, Q):
    """
    adds a pumping well to the aquifer system
    x and y are the coordinates [L] of the well
    Q are the pumping rates [L³/T] for each layer (Q > 0: extracting water)
    returns Well object
    """
    well = Well(x=x, y=y, Q=Q, aquifer=self) # create Well object
    self.wells.append(well) # append Well object to list of wells
    return well

def s(self, x, y):
    """
    calculates drawdown s [L] due to all wells in the aquifer system
    at nodes (x, y) applying the superposition method
    x and y are the coordinates [L] of the nodes (array-like)
    x and y both have shape (nrow, ncol)
    returns drawdown array s of shape (nl, nrow, ncol)
    """
    x, y = np.array(x), np.array(y)
    s = np.zeros((self.nl, ) + x.shape) # initialize drawdown array s
    for well in self.wells: # run through all wells
        s += well.s(x, y) # add well drawdown to s
    return s

```

12.3.2.2. Class Well

The `Well` class represents a pumping or injection well. The attributes passed to the constructor are the position of the well expressed by coordinates `x` and `y`, and the pumping rate `Q`, which is positive in case of pumping. There is also an attribute `aquifer` which stores the `AquiferSystem` object to which the `Well` object belongs. Method `s` calculates the drawdown caused by the well at the points defined by coordinates `x` and `y`. Using the hydraulic parameters assigned to the attributes of the `AquiferSystem` object, a `MultiLayerSteadyWellFlow` object is created, which implements the model that performs the actual simulations. As this model is axisymmetric, (`x`, `y`) coordinates need to be converted to radial distances `r`. The outer boundary `R` is determined in the same way using constant-head point (`x0`, `y0`).

```

class Well:
    """
    class to define a well in a multilayer aquifer
    """

    def __init__(self, x, y, Q, aquifer):
        """
        x and y are the coordinates [L] of the well
        Q are the pumping rates [L³/T] for each layer (Q > 0: extracting water)
        aquifer is an AquiferSystem object
        """
        self.x = float(x)
        self.y = float(y)
        self.Q = np.array(Q, dtype=float) # shape (nl,)
        self.aquifer = aquifer

    def s(self, x, y):
        """
        calculates drawdown s [L] caused by the well at nodes (x, y)
        x and y are the coordinates [L] of the nodes (array-like)
        x and y both have shape (nrow, ncol)
        returns drawdown array s of shape (nl, nrow, ncol)
        """
        x, y = np.array(x), np.array(y)
        x0, y0 = self.aquifer.x0, self.aquifer.y0
        T, c = self.aquifer.T, self.aquifer.c
        shape = (self.aquifer.nl, ) + x.shape # shape of s is (nl, nrow, ncol)
        R = np.sqrt((self.x - x0)**2 + (self.y - self.aquifer.y0)**2) # determine R
        m = MultiLayerSteadyWellFlow(R=R, T=T, c=c, Q=self.Q) # create model
        r = np.sqrt((self.x - x)**2 + (self.y - y)**2) # determine distances r
        return np.reshape(m.s(r=r.reshape(-1, 1)), shape) # return drawdown array s

```

12.3.2.3. Class MultiLayerSteadyWellFlow

The `MultiLayerSteadyWellFlow` implements the steady-state multilayer model to simulate axisymmetric flow to a pumping well. It calculates drawdown analytically according to the Hemker (1984) solution. Like any other class, it has a constructor, which accepts the parameters that define the model: outer model boundary R , layer transmissivities T , resistances c , and pumping rates Q . It sets attribute `nl` which is the number of layers, and attribute `confined` which is a boolean indicating whether the system is confined or not. Recall that the system is confined if both upper and lower resistances are infinitely large. It also assigns `True` to `no_warnings` to suppress runtime warnings. Method `s` is invoked to calculate drawdown at distances r . It uses two private methods, which are methods that cannot be called by other objects. The first private method is `__A__` which constructs system matrix A , the second private method is `__eig__` which performs the eigendecomposition of system matrix A .

```

class MultiLayerSteadyWellFlow:
    """
    class to build models for axisymmetric multilayer well-flow
    """

    def __init__(self, R, T, c, Q):
        """
        R is distance [L] of outer model boundary (float)
        T is vector with layer transmissivities [L2/T] (array-like)
        c is vector with resistances [T] (array-like)
        Q is vector with pumping rates [L3/T] (array-like)
        if there are nl layers, then len(T) == len(Q) == nl and len(c) == nl + 1
        """
        self.R = float(R)
        self.T = np.array(T, dtype=float) # shape (nl,)
        self.c = np.array(c, dtype=float) # shape (nl+1,)
        self.Q = np.array(Q, dtype=float) # shape (nl,)
        self.nl = len(self.T) # number of layers nl
        self.confined = np.all(np.isinf([self.c[0], self.c[-1]])) # confined?
        self.no_warnings = True # suppress warnings?

    def __A__(self):
        """constructs system matrix A"""
        Tc0 = 1 / (self.T * self.c[:-1])
        Tc1 = 1 / (self.T * self.c[1:])
        irow, icol = np.diag_indices(self.nl)
        self._A = np.zeros((self.nl, self.nl))
        self._A[irow, icol] = Tc0 + Tc1
        self._A[irow[:-1], icol[:-1] + 1] = -Tc1[:-1]
        self._A[irow[-1], icol[-1]] = -Tc0[-1]

    def __eig__(self):
        """performs eigenvalue decomposition of system matrix A"""
        self._d, self._V = eig(self._A) # eigenvalue decomposition of A
        self._d = np.real(self._d) # keep real part of eigenvalues d
        self._inz = np.arange(self.nl) # indices of nonzero eigenvalues
        if self.confined: # if confined, then there's one zero eigenvalue!
            self._iz = np.argmin(np.abs(self._d)) # index of zero eigenvalue
            self._inz = np.setdiff1d(self._inz, self._iz)
        if len(self._inz) > 0: # if there are nonzero eigenvalues
            self._sd = np.sqrt(self._d[self._inz]) # sqrt of nonzero eigenvalues
            X = self.R * self._sd
            self._KI = k0(X) / i0(X)
            self._KI[np.isnan(self._KI)] = 0.0 # if X -> inf, then i0(X) -> inf
            self._iV = inv(self._V) # inverse of matrix V
            self._q = np.dot(self._iV, self.Q / 2 / np.pi / self.T)

```

```

def s(self, r):
    """
    calculates drawdown s [L] at radial distance r [L]
    r is vector with distances (array-like)
    returns array s of shape (nl, nr) with len(r) == nr
    """
    r = np.array(r, dtype=float) # convert r into numpy array
    if r.ndim == 0: r = r[np.newaxis] # if scalar
    nr = len(r)
    with warnings.catch_warnings():
        if self.no_warnings: # suppress scipy.linalg and runtime warnings
            warnings.filterwarnings('ignore', category=LinAlgWarning)
            warnings.filterwarnings('ignore', category=RuntimeWarning)
        self.__A__() # construct system matrix A
        self.__eig__() # eigenvalue decomposition of A
        K = np.zeros((self.nl, self.nl)) # initialize K
        s = np.zeros((self.nl, nr)) # initialize s
        for i in range(nr): # loop over vector r
            if self.confined: # there's one zero eigenvalue
                K[self._iz, self._iz] = np.log(self.R / r[i])
            if len(self._inz) > 0: # if there are nonzero eigenvalues
                x = r[i] * self._sd
                y = k0(x) - self._KI * i0(x)
                y[np.isnan(y)] = 0.0 # if x -> inf, then KI * i0(x) -> 0
                K[self._inz, self._inz] = y
            s[:, i] = mdot((self._V, K, self._q)) # calculate s
    return s

```

12.3.2.4. Using superposition to simulate total drawdown

In order to simulate total drawdown in the layered aquifer, the location of the pumping and injection wells is needed. These are estimated from the figures in Louwyck et al. (2005).

The (x,y) coordinates of the 26 pumping wells are (first column is the x-coordinate, second column the y-coordinate):

```

pwalls = np.array([
    [170.61611374, 246.2633452],
    [197.63033175, 237.01067616],
    [223.93364929, 236.29893238],
    [248.81516588, 234.87544484],
    [278.67298578, 237.72241993],
    [287.91469194, 259.0747331],
    [296.44549763, 286.12099644],
    [320.61611374, 289.6797153],
    [345.49763033, 294.66192171],
    [375.35545024, 302.4911032],
    [400.9478673, 307.47330961],
    [418.00947867, 276.8683274],
    [398.81516588, 243.41637011],
    [386.72985782, 217.08185053],
    [370.37914692, 186.47686833],
    [351.18483412, 170.81850534],
    [326.30331754, 155.87188612],
    [293.60189573, 168.68327402],
    [270.85308057, 191.45907473],
    [248.81516588, 187.90035587],
    [222.51184834, 181.49466192],
    [199.0521327, 183.62989324],
    [181.99052133, 200.],
    [162.79620853, 217.79359431],
    [409.47867299, 292.17081851],
    [408.41232227, 260.14234875]
])

```

The (x,y) coordinates of the 24 injection wells are:

```
iwells = np.array([
    [106.63507109, 261.20996441],
    [120.14218009, 272.59786477],
    [138.62559242, 292.52669039],
    [145.73459716, 306.76156584],
    [161.37440758, 318.86120996],
    [179.85781991, 326.69039146],
    [193.36492891, 338.79003559],
    [212.55924171, 346.61921708],
    [231.04265403, 355.87188612],
    [248.1042654, 362.27758007],
    [260.18957346, 368.68327402],
    [272.98578199, 381.49466192],
    [290.04739336, 388.61209964],
    [310.66350711, 397.86476868],
    [330.56872038, 412.8113879],
    [352.60663507, 427.75800712],
    [375.35545024, 425.6227758],
    [393.12796209, 417.08185053],
    [411.61137441, 417.08185053],
    [429.38388626, 423.48754448],
    [450., 423.48754448],
    [477.72511848, 417.08185053],
    [491.23222749, 397.86476868],
    [463.86255924, 420.28469751]
])
```

The pumping and injection rates according to Louwyck et al. (2005) are also assigned to variables:

```
npw, niw = len(pwells), len(iwells) # number of pumping and injection wells
Q_grav = 4.0 # P1: gravel pack discharge (upper layer)
Q_pump = 60.0 # P2: pumping rate (middle layer)
Q_deep = -40.0 # P4: deep injection rate (lower layer)
# determining P3: injection rate (middle layer)
Q_inj = -(npw * (Q_pump + Q_grav) + niw / 2 * Q_deep) / niw
```

The gravel pack discharge P_1 is assigned to variable Q_{grav} , pumping rate P_2 to Q_{pump} , and injection rate P_4 to Q_{deep} . Finally, injection rate P_3 for the wells injecting the middle layer is determined by solving equation (8). The result is $-49.33 \text{ m}^3/\text{d}$, which is assigned to Q_{inj} .

In the next step, four superposition models are created using class `AquiferSystem`, one for each type of well: (1) `gravel` for the gravel packs extracting water from the top layer, (2) `pump` for the wells pumping the middle layer, (3) `inject` for the wells injecting the pumped water back into the middle layer, and (4) `deep` for the wells doing the same into the lower layer. To each `AquiferSystem` object, all wells of the type it represents are added, and the pumping or injection rate is set to unity using vectors \mathbf{U}_j according to (23). Recall that only half of the wells are injecting water into the lower layer, which explains the last if statement.

```
# transmissivities T (m2/d) and resistances c (d)
T = [2.9 * 12, 5.2 * 13.8, 10.7 * 42.0] # T = D * Kh
c = [np.inf, 1300.0, 49.70, np.inf] # confined system

# instantiating an AquiferSystem object for each type of pumping or injection
gravel = AquiferSystem(T=T, c=c) # gravel pack discharge upper layer
pump = AquiferSystem(T=T, c=c) # pumping middle layer
inject = AquiferSystem(T=T, c=c) # injection middle layer
deep = AquiferSystem(T=T, c=c) # deep infiltration lower layer

# adding pumping wells with unit discharge
for well in pwells:
    x, y = tuple(well)
    gravel.add_well(x=x, y=y, Q=[1.0, 0.0, 0.0]) # U1
    pump.add_well(x=x, y=y, Q=[0.0, 1.0, 0.0]) # U2

# adding injection wells with unit discharge
for i, well in enumerate(iwells):
    x, y = tuple(well)
    inject.add_well(x=x, y=y, Q=[0.0, 1.0, 0.0]) # U2
    if i % 2: # only half of the injection wells recharge the lower layer
        deep.add_well(x=x, y=y, Q=[0.0, 0.0, 1.0]) # U3
```

The models are used to simulate drawdown due to unit discharge for a 600 m x 600 m grid similar to the grid defined by Louwyck et al. (2005). Both the x and y dimensions are discretized into 100 nodes.

```
# creating the grid
coord = np.linspace(0, 600, 100)
xgrid, ygrid = np.meshgrid(coord, coord)

# simulating drawdown using unit discharge
s_grav = gravel.s(xgrid, ygrid)
s_pump = pump.s(xgrid, ygrid)
s_inj = inject.s(xgrid, ygrid)
s_deep = deep.s(xgrid, ygrid)
```

Finally, total drawdown is calculated according to expression (22). Additionally, a plot is created showing the exact position of the wells and the calculated drawdown in the three permeable layers.

```
# simulating drawdown according to Louwyck et al. (2005)
s = Q_grav * s_grav + Q_pump * s_pump + Q_inj * s_inj + Q_deep * s_deep

# plotting
fig, ax = plt.subplots(2, 2, figsize=(7, 7), sharex=True, sharey=True)
lim, d, fontsize = (0, 600), 100, 8
labels = ['pumping middle layer',
          'injection middle layer',
          'injection middle + lower layer']

ax[0][0].plot(pwells[:, 0], pwells[:, 1], 'r.', label=labels[0]);
ax[0][0].plot(iwells[:, 0], iwells[:, 1], 'g.', label=labels[1]);
ax[0][0].plot(iwells[:, 0], iwells[:, 1], 'b.', label=labels[2]);
ax[0][0].set_xlim(lim);
ax[0][0].set_ylim(lim);
ax[0][0].set_aspect('equal', 'box');
ax[0][0].grid();

for i, a in enumerate([ax[0][1], ax[1][0], ax[1][1]]):
    step = 0.25 if i == 1 else 0.1
    cs = a.contour(xgrid, ygrid, s[i, :, :], levels=np.arange(-2, 2, step))
    a.clabel(cs, cs.levels, inline=True);
    a.set_title('layer ' + str(i+1), fontsize=fontsize);
    a.set_xlim(lim);
    a.set_ylim(lim);
    a.set_aspect('equal', 'box');
    a.grid()

ax[0][0].set_yticks(np.arange(lim[0], lim[1] + d, d));
ax[0][0].set_yticklabels(np.arange(lim[0], lim[1] + d, d), fontsize=fontsize);
ax[1][0].set_yticks(np.arange(lim[0], lim[1] + d, d), fontsize=fontsize);
ax[1][0].set_xticks(np.arange(lim[0], lim[1] + d, d));
ax[1][0].set_xticklabels(np.arange(lim[0], lim[1] + d, d), fontsize=fontsize);
ax[1][1].set_xticks(np.arange(lim[0], lim[1] + d, d));
ax[1][1].set_xticklabels(np.arange(lim[0], lim[1] + d, d), fontsize=fontsize);
ax[0][0].set_ylabel('y (m)', fontsize=fontsize);
ax[1][0].set_ylabel('y (m)', fontsize=fontsize);
ax[1][0].set_xlabel('x (m)', fontsize=fontsize);
ax[1][1].set_xlabel('x (m)', fontsize=fontsize);
ax[0][0].legend(fontsize=fontsize);
```

The results obtained after running this code is shown in Figure 12. As expected, a similar drawdown pattern is observed as for the simulations performed using AS2D in the original study (Figure 8, Figure 9, and Figure 10). However, the new simulations show larger values for the drawdown, especially in the upper layer. As discussed in Chapter 4, the AS2D model may produce less accurate results. Its model grid also contains more sublayers, which may affect the results, although the most likely explanation is the 10^5 minutes simulation period is not long enough to attain a new steady state. Despite these larger values, the required 1 m lowering of the water table is still not achieved in the top layer at the excavation site, which is the zone enclosed by the pumping wells (red dots in the left upper plot of Figure 12). Next section shows how to apply linear programming to derive the minimum pumping rate that does satisfy this constraint of 1 m drawdown.

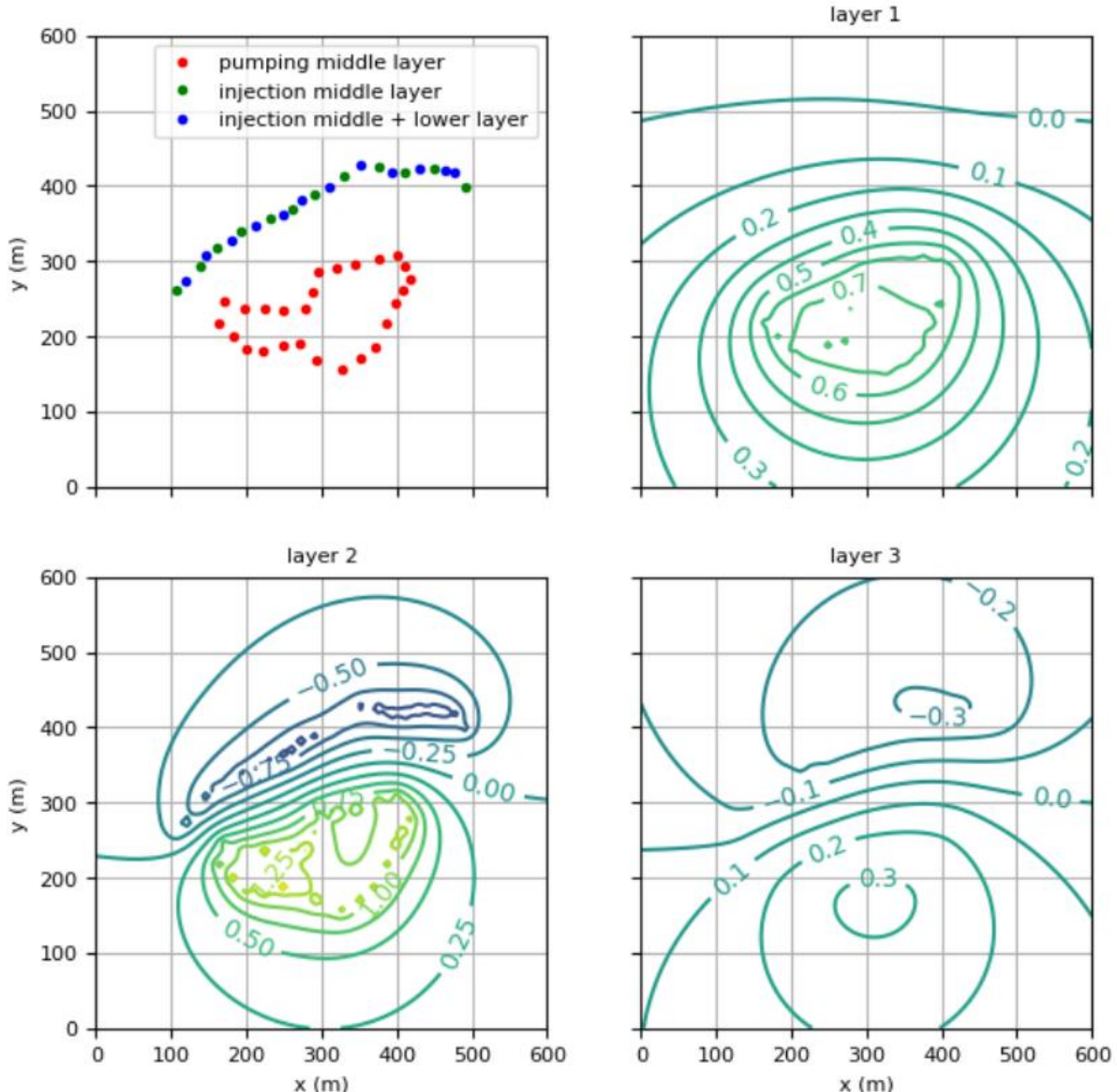


Figure 12. Results obtained from the steady-state model simulating the combined pumping and deep-infiltration system to drain the excavation site ‘Duinenabdij’. The upper left plot indicates the location of the pumping and infiltration wells. The excavation site is enclosed by pumping wells (red dots). The other plots show the horizontal contour lines of drawdown (in meters) for the three permeable layers in the aquifer system. Drawdown is calculated by applying the superposition method to the analytical solution by Hemker (1984). Pumping and injection rates are adopted from the original study by Louwyck et al (2005). See text for more information.

12.3.2.5. Minimizing the pumping rate

As explained in the methodology section 12.3.1, linear programming can be applied to minimize the total pumping rate subject to certain constraints. Python package PuLP will be used to perform the optimization:

```
from pulp import *
```

Recall that 4 control points at the excavation site are defined where the drawdown should be at least 1 m. Using the superposition models, drawdown due to unit discharge is calculated for these points:

```
# control points (xc, yc)
xc = [300, 300, 350, 350]
yc = [200, 250, 200, 250]
```

```

# drawdown in these points (top layer only)
s1 = gravel.s(xc, yc)[0, :]
s2 = pump.s(xc, yc)[0, :]
s3 = inject.s(xc, yc)[0, :]
s4 = deep.s(xc, yc)[0, :]

```

As explained in section 12.3.1, the objective is to minimize pumping rate P_2 , which is the pumping rate assigned to each well extracting water from the middle layer. This means the objective function to minimize simply equals P_2 , which is variable `Q_pump` in the code. This minimization is subject to the constraints that drawdown must be at least 1 m in the control points (xc, yc) . Another constraint states that the total volume of water extracted from the aquifer system per unit of time must equal the total amount of water that is reinjected per unit of time. This constraint determines the rates P_3 and P_4 for the injection wells in the middle and lower layer, respectively. In the first scenario, P_4 is constant and equal to $-40 \text{ m}^3/\text{d}$, whereas it is variable in the second scenario. Gravel pack discharge P_1 is constant and equal to $4 \text{ m}^3/\text{d}$ in both scenarios.

The code for the first scenario is:

```

# instantiating LpProblem object (linear programming problem)
prob = LpProblem("Scenario_1", LpMinimize) # it's a minimization problem

# defining the variables
Q_pump1 = LpVariable("Q_pump", lowBound=0) # pumping rate middle layer (Q>0)
Q_inj1 = LpVariable("Q_inj", upBound=0) # injection rate middle layer (Q<0)

# defining the objective function
prob += Q_pump1, "minimize total pumping rate"

# adding constraint Q_out == Q_in
prob += npw * (Q_grav + Q_pump1) + niw * Q_inj1 + niw / 2 * Q_deep == 0

# add constraint at the 4 control points
for i in range(len(xc)):
    # drawdown in top layer must be at least 1 m: P1*s1 + P2*s2 + P3*s3 + P4*s4 >= 1
    prob += Q_grav * s1[i] + Q_pump1 * s2[i] + Q_inj1 * s3[i] + Q_deep * s4[i] >= 1.0

# solving the problem
prob.solve()
print(LpStatus[prob.status]) # checking the status of the solution
print(Q_pump1.value(), Q_inj1.value(), Q_deep) # checking the optimized variables

```

First, an `LpProblem` object is created to define the linear programming problem, which is a minimization problem in this case, as is indicated by `LpMinimize`. Next, the variables are defined as `LpVariable`. In this first scenario, only rates P_2 and P_3 are variable. The first variable is a pumping rate, and therefore, must be positive, which is accomplished by setting the lower bound to zero. The second variable is an injection rate, which must be negative; hence, the upper bound equals zero. In the next step, the objective function is added to the `LpProblem` object, which is variable `Q_pump1` to which the optimal value for P_2 will be assigned according to scenario 1. Finally, the constraints are added to the `LpProblem` object.

Calling method `solve` on the `LpProblem` object solves the problem. The problem status indicates that an optimal solution is found, which assigns $182.73 \text{ m}^3/\text{d}$ to P_2 and $-182.29 \text{ m}^3/\text{d}$ to P_3 . Checking the constraints, it is seen the drawdown in the top layer at the control points is equal to or greater than 1 m indeed. The error on the total budget constraint is $2 \times 10^{-5} \text{ m}^3/\text{d}$, which is negligibly small. In conclusion, the pumping rate has to be 3 times larger than the pumping rate estimated in the original study to obtain a drawdown of 1 m at least at the excavation site.

Using these optimized values for the pumping and the injection rates, drawdown in each layer is simulated and plotted again for the $600 \text{ m} \times 600 \text{ m}$ grid:

```

# simulating drawdown: P1*s1 + P2*s2 + P3*s3 + P4*s4
s = Q_grav * s_grav + Q_pump1.value() * s_pump + \
    Q_inj1.value() * s_inj + Q_deep * s_deep

# plotting
fig, ax = plt.subplots(2, 2, figsize=(7, 7), sharex=True, sharey=True);
lim, d, fontsize = (0, 600), 100, 8
labels = ['pumping middle layer', 'injection middle layer',
          'injection middle + lower layer', 'control points']

ax[0][0].plot(pwells[:, 0], pwells[:, 1], 'r.', label=labels[0]);
ax[0][0].plot(iwells[:, 0], iwells[:, 1], 'g.', label=labels[1]);
ax[0][0].plot(iwells[1::2, 0], iwells[1::2, 1], 'b.', label=labels[2]);
ax[0][0].plot(xc, yc, 'k.', label=labels[3]);
ax[0][0].set_xlim(lim);
ax[0][0].set_ylim(lim);
ax[0][0].set_aspect('equal', 'box');
ax[0][0].grid();

for i, a in enumerate([ax[0][1], ax[1][0], ax[1][1]]):
    step = 0.5 if i == 1 else 0.2
    cs = a.contour(xgrid, ygrid, s[i, :, :], levels=np.arange(-2, 2, step))
    a.clabel(cs, cs.levels, inline=True);
    a.set_title('layer ' + str(i+1), fontsize=fontsize);
    a.set_xlim(lim);
    a.set_ylim(lim);
    a.set_aspect('equal', 'box');
    a.grid()

ax[0][0].set_yticks(np.arange(lim[0], lim[1] + d, d));
ax[0][0].set_yticklabels(np.arange(lim[0], lim[1] + d, d), fontsize=fontsize);
ax[1][0].set_yticks(np.arange(lim[0], lim[1] + d, d));
ax[1][0].set_yticklabels(np.arange(lim[0], lim[1] + d, d), fontsize=fontsize);
ax[1][0].set_xticks(np.arange(lim[0], lim[1] + d, d));
ax[1][0].set_xticklabels(np.arange(lim[0], lim[1] + d, d), fontsize=fontsize);
ax[1][1].set_xticks(np.arange(lim[0], lim[1] + d, d));
ax[1][1].set_xticklabels(np.arange(lim[0], lim[1] + d, d), fontsize=fontsize);
ax[0][0].set_ylabel('y (m)', fontsize=fontsize);
ax[1][0].set_ylabel('y (m)', fontsize=fontsize);
ax[1][0].set_xlabel('x (m)', fontsize=fontsize);
ax[1][1].set_xlabel('x (m)', fontsize=fontsize);
ax[0][0].legend(fontsize=fontsize, loc=(0.075, 0.8));

```

The result of running this code is shown in Figure 13. The contour lines of drawdown for the top layer (layer 1) clearly show that a lowering of the water table of at least 1 m is obtained at the excavation site, which is the zone surrounded by the pumping wells (red dots in the left upper plot of Figure 13). Compared with the original scenario, the ‘depression funnel’ simulated for this new scenario is significantly deeper as the optimized pumping rates are three times larger. Accordingly, the ‘infiltration cone’ is also more pronounced than in the original scenario as the corresponding injection rates are also larger. As a consequence, there is a larger decrease of the water table in the dune area to the south of the site, whereas the water table in the dune area in the north increases more than in the original scenario.

In the second scenario, injection rate P_4 is also variable, and the optimization code only needs one additional statement that defines $Q_{\text{deep}2}$ representing P_4 as LpVariable with upper bound equal to zero as it is an injection rate:

```

# instantiating LpProblem object (linear programming problem)
prob = LpProblem("Scenario_2", LpMinimize) # it's a minimization problem

# defining the variables
Q_pump2 = LpVariable("Q_pump", lowBound=0) # pumping rate middle layer (Q > 0)
Q_inj2 = LpVariable("Q_inj", upBound=0) # injection rate middle layer (Q < 0)
Q_deep2 = LpVariable("Q_deep", upBound=0) # injection rate lower layer (Q < 0)

# defining the objective function
prob += Q_pump2, "minimize total pumping rate"

# adding constraint Q_out == Q_in
prob += npw * (Q_grav + Q_pump2) + niw * Q_inj2 + niw / 2 * Q_deep2 == 0

```

```

# add constraint at the 4 control points
for i in range(len(xc)):
    # drawdown in top layer must be at least 1 m: P1*s1 + P2*s2 + P3*s3 + P4*s4 >= 1
    prob += Q_grav * s1[i] + Q_pump2 * s2[i] + Q_inj2 * s3[i] + Q_deep2 * s4[i] >= 1.0

# solving the problem
prob.solve()
print(LpStatus[prob.status]) # checking the status of the solution
print(Q_pump2.value(), Q_inj2.value(), Q_deep2.value()) # the optimized variables

```

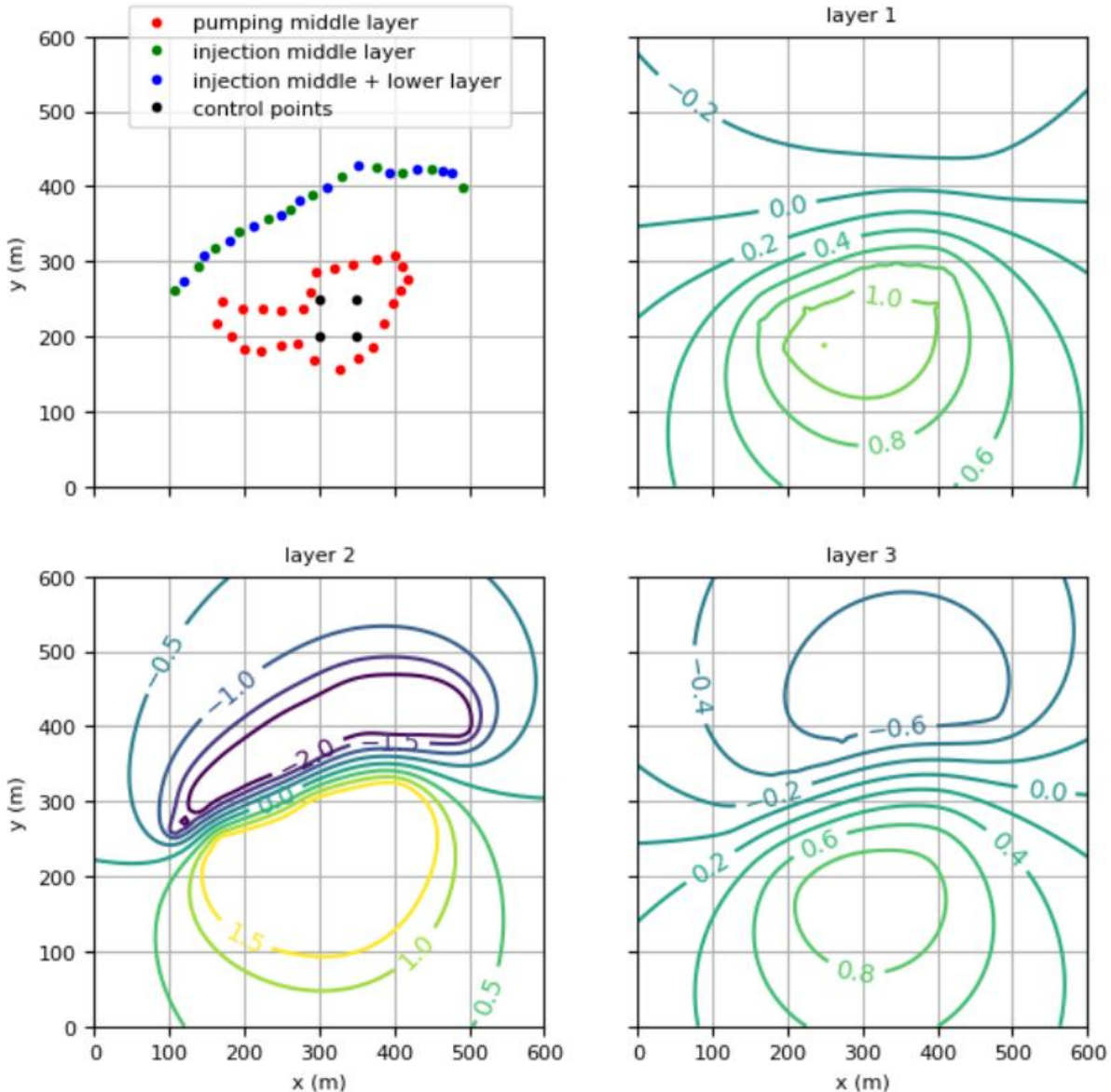


Figure 13. Results obtained from the steady-state model simulating the combined pumping and deep-infiltration system to drain the excavation site 'Duinenabdij'. The upper left plot indicates the location of the pumping and infiltration wells. The excavation site is enclosed by pumping wells (red dots). The other plots show the horizontal contour lines of drawdown (in meters) for the three permeable layers in the aquifer system. Drawdown is calculated by applying the superposition method to the analytical solution by Hemker (1984). Linear programming is used to optimize the pumping and injection rates assigned to the wells discharging and recharging the middle layer according to the first scenario with fixed injection rate for wells recharging the lower layer. See text for more information.

Again an optimal solution is found, and as expected, there is no injection in the middle layer, or P_3 is zero. The optimal pumping rate P_2 equals $107.96 \text{ m}^3/\text{d}$, which is significantly smaller than the optimal value determined in the first scenario, but it is still much larger than the $60 \text{ m}^3/\text{d}$ estimated in the

original study. Injection rate P_4 is $-242.59 \text{ m}^3/\text{d}$. All constraints are satisfied and the error on the total budget constraint is smaller than $10^{-12} \text{ m}^3/\text{d}$. Using these optimized values for pumping and injection rates, drawdown in each layer is simulated again for the $600 \text{ m} \times 600 \text{ m}$ grid:

```
# simulating drawdown: P1*s1 + P2*s2 + P3*s3 + P4*s4
s = Q_grav * s_grav + Q_pump2.value() * s_pump + \
    Q_inj2.value() * s_inj + Q_deep2.value() * s_deep
```

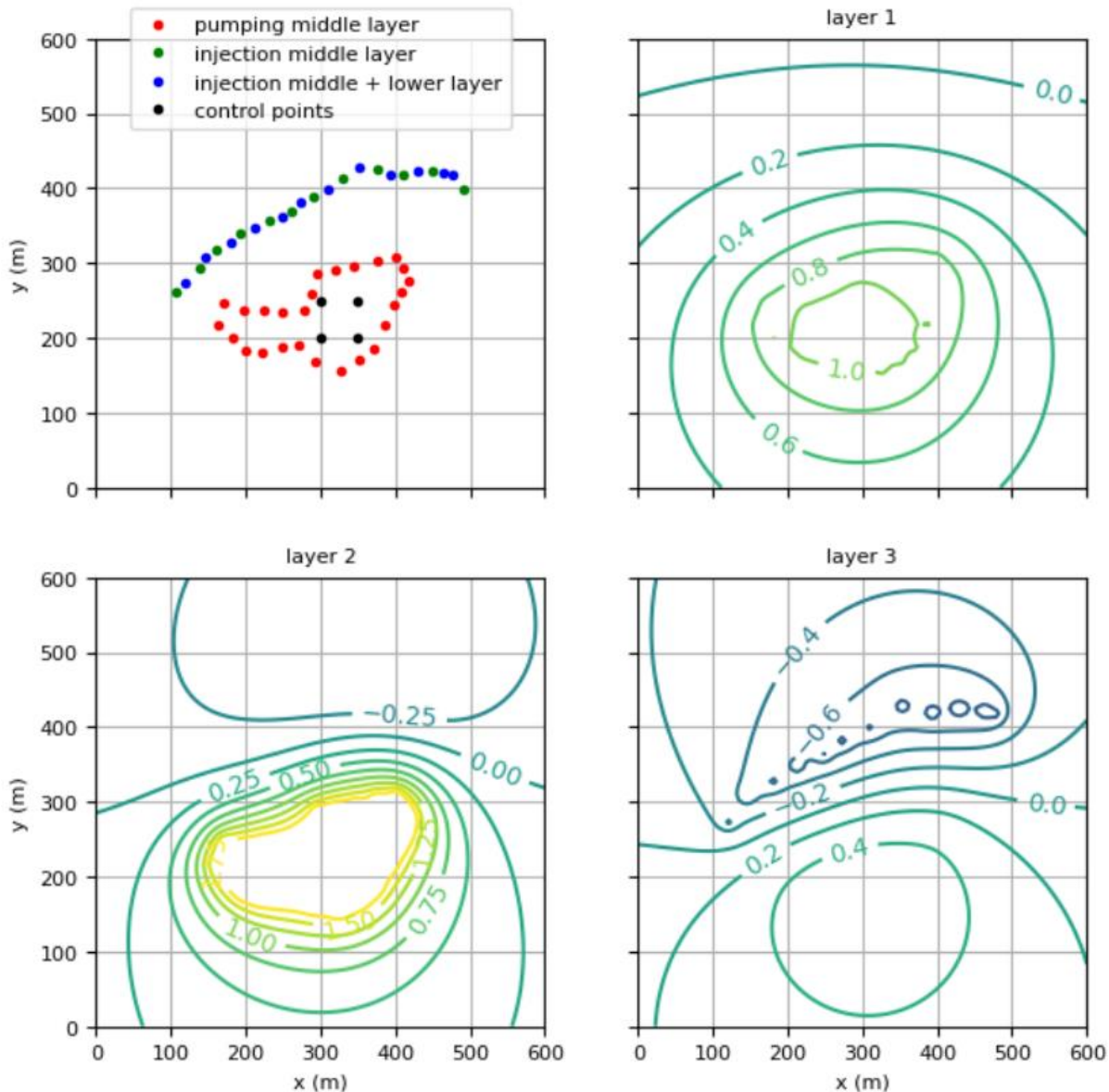


Figure 14. Results obtained from the steady-state model simulating the combined pumping and deep-infiltration system to drain the excavation site 'Duinenabdij'. The upper left plot indicates the location of the pumping and infiltration wells. The excavation site is enclosed by pumping wells (red dots). The other plots show the horizontal contour lines of drawdown (in meters) for the three permeable layers in the aquifer system. Drawdown is calculated by applying the superposition method to the analytical solution by Hemker (1984). Linear programming is used to optimize pumping and injection rates according to the second scenario described in the text. The optimal solution suggests to inject the water extracted from the middle layer into the lower layer only.

The code to plot this result as seen in Figure 14 is the same as the code given above to plot the results of the first scenario. Compared with the first scenario, the differences are most noticeable for the drawdown in the middle and lower layer. In this second scenario, the 'depression funnel' in the

middle layer is deeper, whereas the ‘infiltration cone’ is higher in the lower layer as there is no injection in the middle layer. The objective of lowering the water table at least 1 m in the top layer at the excavation site is also achieved here, although there is a larger decrease of the water table in the dunes to the south of the site. On the other hand, the water table in the dunes in the north is less affected by the drainage system.

12.3.3. Conclusions

Using linear programming, two scenarios are found for the existing configuration of pumping and injection wells that satisfy the requirement of decreasing the water table by at least 1 m at the excavation site, while drawdown in the valuable dune areas surrounding the site remains limited. However, deciding which of these two optimization scenarios is the best solution is not the aim of revisiting the optimization of the drainage system. As already mentioned, finding the optimal configuration is not only constrained by purely hydrogeological requirements.

The objective is to show that linear programming is a very effective and useful technique to solve these kinds of optimization problems in which several possibly conflicting interests must be balanced. In this case, the lowering of the water table at the excavation site is needed to preserve the archeological relics. On the other hand, a lowering of the water table in the protected dune areas is undesirable. A hard drawdown constraint has not been imposed on these areas, although this would be possible, and by applying linear programming, one could easily determine whether the problem is feasible or not. If it is infeasible, then there is no solution for the optimization problem, in which case the hard drawdown constraints could be turned into soft constraints by adding them to the objective function. This implies it is allowed to violate the constraints at the cost of being penalized. However, by minimizing the objective function, these penalties are also minimized, and additionally, the conflicting soft constraints are weighted up. In this way, it is possible to prioritize the different constraints.

It is also demonstrated that the Python packages, specifically designed for scientific computing and data science, are easy to use in solving the optimization problem. These packages are open source and may be used free of charge, which is also a big advantage. To simulate the drainage system, the steady-state multilayer solution by Hemker (1984) is implemented using NumPy and SciPy. These Python libraries provide all the necessary functions to deal with matrices, perform the eigendecomposition, and evaluate the modified Bessel functions. Once the analytical solution for simulating radial flow to one well is coded, it is straightforward to apply the superposition method to simulate the drawdown caused by the drainage system comprising several pumping and injection wells. Matplotlib, another popular Python library, is used to plot the results in a very customized way. Finally, the PuLP package is applied to perform the linear programming, which is also very straightforward, and only requires a few lines of code.

12.4. Summary

The study by Louwyck et al. (2005) summarizes the hydrogeological studies conducted to realize a more effective drainage system at the excavation site ‘Duinenabdij’ (Lebbe et al., 2002; Louwyck, 2001; Lust, 2002). The aquifer system consists of three permeable layers separated by two semi-pervious layers. The shallow semi-pervious layer caused problems of flooding at the site. The new drainage system consisting of multiple pumping and injection wells, extracts water from the middle permeable layer, and injects the pumped water into the middle and lower permeable layers in order to protect the dunes surrounding the site. The relevant hydraulic parameters of the aquifer system were identified through interpretation of a double pumping test conducted at the site (Lebbe et al., 2002; Lust, 2002). Before realizing the drainage system, its effectiveness was evaluated through

mathematical modeling (Louwyck, 2001; Lust, 2002). HYPARIDEN (Lebbe, 1988, 1999) was used for the interpretation of the pumping test as well as for the modeling of the drainage system.

In the original studies, finding the optimal pumping and injection rates was done manually via trial-and-error (Louwyck et al., 2005; Lust, 2002). In this chapter, the combined simulation and optimization problem is revisited to find the minimum pumping rate that is required to achieve the desired lowering of the water table at the excavation site. Drawdown in the three permeable layers due to the drainage system is simulated by applying the superposition method to the solution by Hemker (1984) for axisymmetric steady-state multilayer well-flow. This analytical solution is coded with Python, which is straightforward using Python's packages for scientific computing. For the optimization, linear programming is applied, which is implemented in Python package PuLP. It is shown that only a few lines of code are needed to define and solve the problem of finding the minimum pumping and injection rates. In summary, this case study illustrates how the analytical multilayer solution discussed in Chapter 2 can be applied to solve a real-world problem very efficiently without having to build a complicated, data-hungry, and computationally expensive groundwater flow model.

12.5. References

- Ahlfeld, D. P., Baker, K. M., & Barlow, P. M. (2009). *GWM-2005 - A Groundwater-Management Process for MODFLOW-2005 with Local Grid Refinement (LGR) Capability*. U.S. Geological Survey Techniques and Methods 6-A33.
- Ahlfeld, D. P., Barlow, P. M., & Mulligan, A. E. (2005). *GWM-a ground-water management process for the U.S. Geological Survey modular ground-water model (MODFLOW-2000)*. U.S. Geological Survey Open-File Report 2005-1072.
- Ahlfeld, D. P., & Baro-Montes, G. (2008). Solving Unconfined Groundwater Flow Management Problems with Successive Linear Programming. *Journal of Water Resources Planning and Management*, 134(5), 404–412. [https://doi.org/10.1061/\(ASCE\)0733-9496\(2008\)134:5\(404\)](https://doi.org/10.1061/(ASCE)0733-9496(2008)134:5(404))
- Baeteman, C. (1985). *Beschrijving van Boring 35E/150 (in Dutch)*. Geological Survey of Belgium, Brussels.
- Baeteman, C. (1999). The Holocene depositional history of the IJzer paleovalley (western Belgian coastal plain) with reference to the factors controlling the formation of intercalated peat beds. *Geologica Belgica*, 2(3–4), 39–72.
- Bakker, M. (2013). Semi-analytic modeling of transient multi-layer flow with TTIm. *Hydrogeology Journal*, 21(4), 935–943. <https://doi.org/10.1007/s10040-013-0975-2>
- Bakker, M. (2014). Python Scripting: The Return to Programming. *Groundwater*, 52(6), 821–822. <https://doi.org/10.1111/gwat.12269>
- Bakker, M., & Kelson, V. A. (2009). Writing Analytic Element Programs in Python. *Ground Water*, 47(6), 828–834. <https://doi.org/10.1111/j.1745-6584.2009.00583.x>
- Bakker, M., & Post, V. (2022). *Analytical Groundwater Modeling - Theory and Applications using Python*. CRC Press.
- Bakker, M., Post, V., Langevin, C. D., Hughes, J. D., White, J. T., Starn, J. J., & Fienen, M. N. (2016). Scripting MODFLOW Model Development Using Python and FloPy. *Groundwater*, 54(5), 733–739. <https://doi.org/10.1111/gwat.12413>

- Bakker, M., & Strack, O. D. L. (2003). Analytic elements for multiaquifer flow. *Journal of Hydrology*, 271(1–4). [https://doi.org/10.1016/S0022-1694\(02\)00319-0](https://doi.org/10.1016/S0022-1694(02)00319-0)
- Banta, E. R., & Ahlfeld, D. P. (2013). *GWM-VI -- Groundwater Management with Parallel Processing for Multiple MODFLOW versions*. U.S. Geological Survey Techniques and Methods 6-A48.
- Bretas, F. S., & Haith, D. A. (1990). Linear Programming Analysis of Pesticide Pollution of Groundwater. *Transactions of the ASAE*, 33(1), 0167–0172. <https://doi.org/10.13031/2013.31312>
- Danapour, M., Fienen, M. N., Højberg, A. L., Jensen, K. H., & Stisen, S. (2021). Multi-Constrained Catchment Scale Optimization of Groundwater Abstraction Using Linear Programming. *Groundwater*, 59(4), 503–516. <https://doi.org/10.1111/gwat.13083>
- Dantzig, G. B. (1947). Maximization of a linear function of variables subject to linear inequalities. In T. C. Koopmans (Ed.), *Activity Analysis of Production and Allocation* (pp. 339–347). New York – London: Wiley & Chapman-Hall.
- Dantzig, G. B. (1982). Reminiscences about the origins of linear programming. *Operations Research Letters*, 1(2), 43–48.
- Dantzig, G. B., & Mukund, N. (1997). *Linear programming 1: Introduction*. New York: Springer-Verlag.
- De Breuck, W. G., De Moor, R., Maréchal, R., & Tavernier, R. (1974). *Diepte van het grensvlak tussen zoet en zout water in de freatisch watervoerende laag van het Belgische Kustgebied (1963-1973) (in Dutch)*. Map, Militair Geografisch Instituut, Brussels.
- Greenwald, R. M. (1994). *MODflow MANagement: An Optimization Module for MODFLOW, version 3.02, IGWMC*.
- Greenwald, R. M. (1998). *Documentation and user's guide - MODMAN, an optimization module for MODFLOW, version 4.0*. HSI GeoTrans, Freehold, NJ.
- Harbaugh, A. W., Banta, E. R., Hill, M. C., & McDonald, M. G. (2000). *MODFLOW-2000, The U.S. Geological Survey Modular Ground-Water Model: User Guide to Modularization Concepts and the Ground-Water Flow Process*. U.S. Geological Survey Open-File Report 00-92. <https://doi.org/https://doi.org/10.3133/ofr200092>
- Hemker, C. J. (1984). Steady groundwater flow in leaky multiple-aquifer systems. *Journal of Hydrology*, 72(3–4), 355–374. [https://doi.org/10.1016/0022-1694\(84\)90089-1](https://doi.org/10.1016/0022-1694(84)90089-1)
- Hemker, C. J. (1985a). A General Purpose Microcomputer Aquifer Test Evaluation Technique. *Ground Water*, 23(2), 247–253. <https://doi.org/10.1111/j.1745-6584.1985.tb02799.x>
- Hemker, C. J. (1985b). Transient well flow in leaky multiple-aquifer systems. *Journal of Hydrology*, 81(1–2), 111–126. [https://doi.org/10.1016/0022-1694\(85\)90170-2](https://doi.org/10.1016/0022-1694(85)90170-2)
- Hemker, C. J. (1999a). Transient well flow in layered aquifer systems: the uniform well-face drawdown solution. *Journal of Hydrology*, 225(1–2), 19–44. [https://doi.org/10.1016/S0022-1694\(99\)00093-1](https://doi.org/10.1016/S0022-1694(99)00093-1)
- Hemker, C. J. (1999b). Transient well flow in vertically heterogeneous aquifers. *Journal of Hydrology*, 225(1–2), 1–18. [https://doi.org/10.1016/S0022-1694\(99\)00137-7](https://doi.org/10.1016/S0022-1694(99)00137-7)

- Hemker, C. J., & Post, V. E. A. (2019). *MLU for Windows*. Retrieved from <https://www.microfem.com/products/mlu.html>
- Jha, M. K., Peralta, R. C., & Sahoo, S. (2020). Simulation-Optimization for Conjunctive Water Resources Management and Optimal Crop Planning in Kushabhadra-Bhargavi River Delta of Eastern India. *International Journal of Environmental Research and Public Health*, 17(10), 3521. <https://doi.org/10.3390/ijerph17103521>
- Langevin, C. D., Hughes, J. D., Banta, E. R., Niswonger, R. G., Panday, S., & Provost, A. M. (2017). *Documentation for the MODFLOW 6 Groundwater Flow Model*. U.S. Geological Survey Techniques and Methods 6-A55. <https://doi.org/10.3133/tm6A55>
- Lebbe, L. C. (1973). *Hydrogeologisch onderzoek van het duingebied te Oostduinkerke (in Dutch)* [MSc Thesis]. Ghent University.
- Lebbe, L. C. (1978). *Hydrogeologie van het duingebied ten westen van De Panne (in Dutch)* [PhD Thesis]. Ghent University.
- Lebbe, L. C. (1988). *Uitvoering van pompproeven en interpretatie door middel van een invers model (in Dutch)*. Ghent University.
- Lebbe, L. C. (1999). *Hydraulic Parameter Identification. Generalized Interpretation Method for Single and Multiple Pumping Tests*. Berlin Heidelberg: Springer-Verlag.
- Lebbe, L. C., Pede, K., & Van Houtte, E. (1984). Analyse van pompproeven in een veellagig grondwaterreservoir met behulp van een matematisch model (in Dutch). *Tijdschrift Becewa*, 78, 132–146.
- Lebbe, L. C., Vandenbohede, A., & Louwyck, A. (2002). *Uitvoering en interpretatie van dubbele pompproef nabij de abdijsite te Koksijde (in Dutch)*. Report GROMO2002/01, Ghent University.
- Lebbe, L. C., Vermoortel, Y., & De Breuck, W. (1996). *Mathematisch model van de grondwaterstromingen van het militair vliegveld te Koksijde en de omringende gebieden*. Report TGO96/10, Ghent University.
- Louwyck, A. (2001). *Hydrogeologische studie van de archeologische site ‘Duinenabdij’, Koksijde (in Dutch)* [MSc. Thesis]. Ghent University.
- Louwyck, A., Vandenbohede, A., & Lebbe, L. C. (2005). The role of hydrogeological research in the realization of a combined pumping and deep infiltration system at the excavation “Duinenabdij.” In J.-L. Herrier, J. Mees, A. Salman, J. Seys, H. Van Nieuwenhuyse, & I. Dobbelaere (Eds.), *Proceedings “Dunes and Estuaries 2005”: International Conference on nature restoration practices in European coastal habitats, Koksijde, Belgium 19-23 September 2005*. (pp. 317–326). VLIZ Special Publication 19.
- Louwyck, A., Vandenbohede, A., & Lebbe, L. C. (2010). Numerical analysis of step-drawdown tests: Parameter identification and uncertainty. *Journal of Hydrology*, 380(1–2), 165–179. <https://doi.org/10.1016/j.jhydrol.2009.10.034>
- Lust, H. (2002). *Bijdrage tot de optimalisatie van de diepe drainage op de Duinenabdijsite te Koksijde (in Dutch)* [MSc. Thesis]. Ghent University.
- Matthes, E. (2023). *Python Crash Course, 3rd Edition: A Hands-On, Project-Based Introduction to Programming*. No Starch Press.

- McDonald, M. G., & Harbaugh, A. W. (1988). *A modular three-dimensional finite-difference ground-water flow model*. U.S. Geological Survey Techniques of Water-Resources Investigations 06-A1. <https://doi.org/10.3133/twri06A1>
- Naseer, A., & Honma, S. (2014). A Method for Optimizing Groundwater Management. *Proceedings of the School of Engineering, Tokai University, Series E*, 39, 19–26.
- Psilovikos, A. A. (1999). Optimization models in groundwater management, based on linear and mixed integer programming. An application to a greek hydrogeological basin. *Physics and Chemistry of the Earth, Part B: Hydrology, Oceans and Atmosphere*, 24(1–2), 139–144. [https://doi.org/10.1016/S1464-1909\(98\)00025-2](https://doi.org/10.1016/S1464-1909(98)00025-2)
- Stoecker, A. L., Seidmann, A., & Lloyd, G. S. (1985). A Linear Dynamic Programming Approach to Irrigation System Management with Depleting Groundwater. *Management Science*, 31(4), 422–434. <https://doi.org/10.1287/mnsc.31.4.422>
- Sun, N.-Z. (1999). *Inverse Problems in Groundwater Modeling* (Vol. 6). Dordrecht: Springer Netherlands. <https://doi.org/10.1007/978-94-017-1970-4>
- Thiem, A. (1870). Die Ergiebigkeit artesischer Bohrlöcher, Schachtbrunnen und Filtergalerien (in German). *Journal Für Gasbeleuchtung Und Wasserversorgung*, 13, 450–467.
- Thiem, G. (1906). *Hydrologische Methoden (in German)*. Leipzig: Gebhardt.
- Vandenbohede, A., & Lebbe, L. C. (2003). Combined interpretation of pumping and tracer tests: theoretical considerations and illustration with a field test. *Journal of Hydrology*, 277(1–2), 134–149. [https://doi.org/10.1016/S0022-1694\(03\)00090-8](https://doi.org/10.1016/S0022-1694(03)00090-8)
- Van Houtte, E. (1998). *Beschrijving van ondiepe boring in opdracht van de gemeente Koksijde (in Dutch)*. Report, Intercommunale Waterleidings-maatschappij van Veurne-Ambacht (IWVA), Veurne, Belgium.
- Van Houtte, E., Lebbe, L. C., & De Breuck, W. (1992). *Studie van de huidige en toekomstige waterwinningsmogelijkheden in de Westhoek (in Dutch)*. Report TGO91/07, Ghent University.
- Yeh, W. W.-G. (2015). Review: Optimization methods for groundwater modeling and management. *Hydrogeology Journal*, 23(6), 1051–1065. <https://doi.org/10.1007/s10040-015-1260-3>

Chapter 13. Summary and Conclusions

13.1. Main objective

As discussed in section 1.2 of Chapter 1, the main objective of this PhD research is to get a better understanding of axisymmetric flow to a well in a multilayered aquifer system. This goal is achieved by studying and comparing existing multilayer solutions, by developing and implementing new solutions, and by solving real-world problems involving radial flow. As such, the dissertation can be divided into four major parts: chapter 2 to 4 synthesize and compare existing solution methods for axisymmetric multilayer flow, chapters 5 to 8 extend these solution methods to solve more advanced problems, chapters 9 to 11 discuss some theoretical insights obtained from the axisymmetric multilayer solutions examined and developed in previous chapters, and chapter 12 presents a practical case involving multilayer well-flow. This final chapter follows this subdivision in summarizing the different chapters and formulating some major conclusions and recommendations.

13.2. Existing solutions

In Chapter 2, the existing semi-analytical theory is presented, which goes back to the publications of Hemker (1984, 1985, 1999a). A generalized solution is developed that can handle both steady and transient flow in confined and leaky systems possibly including areal recharge. The aquifer system may be laterally bounded or unbounded, and the inner model boundary condition can be a specified head or a constant discharge. In case of transient flow, the Laplace transform is applied and the inversion is performed numerically using the Stehfest (1970) algorithm. The superposition method is explained, which makes it possible to define time-varying boundary conditions or to simulate flow due to multiple wells. One- and two-layer solutions described in the hydrogeological literature are presented as special cases obtained by simplifying the generalized semi-analytical solution. The similarity between axisymmetric and parallel flow makes extending the solution to include the latter very straightforward.

Chapter 3 presents the finite-difference approach by Louwyck et al. (2012) to solve the problem of axisymmetric multilayer flow as stated in Chapter 2. The method is an extension of and an improvement to the axisymmetric model AS2D developed by Lebbe (1988, 1999), and it is implemented in the Matlab tool M^AxSym (Louwyck, 2011). The tool contains new features such as initial drawdowns, inactive and constant-head cells, recharge, and stress periods, and most importantly, it also allows for radial variation of input parameters, which makes it possible, for instance, to simulate the effects of the change in wellbore storage and a finite-thickness skin.

To test the new semi-analytical solutions developed in this study, the finite-difference method is also coded with Python, in which case standard LU decomposition is used to solve the system of equations, instead of an iterative solver. Similarity between axisymmetric and parallel flow led to the development of a new procedure to trick the unmodified version of MODFLOW (Harbaugh, 2005) into simulating radial multilayer flow (Louwyck et al., 2012, 2014). This procedure is inspired by the approach by Langevin (2008), yet more flexible in including radially varying input parameters.

Chapter 4 reviews the hybrid finite-difference finite-element method developed by Lebbe (1988, 1999) to simulate axisymmetric flow to a well in an aquifer system consisting of homogeneous layers. Basically, the method is an alternative finite-difference formulation that interpolates calculated drawdowns in both space and time. The temporal interpolation is very similar to the Crank and Nicolson (1947, 1996) method, and therefore, it may suffer from spurious oscillations during the first time steps. However, this issue is solved easily by defining a very small initial time step. The vertical

interpolation is more problematic as it may lead to head rises, which Lebbe (1988) calls a “numerical Noordbergum effect”, and which he attenuates by means of empirical correction factors. It is argued, however, that it is safer to abolish the vertical interpolation according to the Dupuit-Forchheimer approximation. Finally, it is shown that the radial interpolation has no added value, and since it is computationally more demanding, it is also recommended to omit this interpolation.

The hybrid method by Lebbe (1988, 1999) has been used extensively during the past thirty-five years at the Department of Geology of Ghent University to identify hydraulic parameters from pumping test data for a wide range of lithological layers in Flanders. It is concluded, however, that the computational errors had no significant impact on the reliability of these parameters, as in general, observed data are also impacted by measurement errors, and models are prone to conceptual errors. On the other hand, it is preferable to use the semi-analytical solution method (e.g. Hemker, 1999a) or the backward Euler finite-difference method (e.g. Louwyck et al., 2012) which is also implemented in MODFLOW (Harbaugh, 2005).

13.3. New solutions

In Chapter 5, the generalized semi-analytical solution for radial flow in a multilayer system is extended to include lateral variation, similar to the finite-difference approach discussed in Chapter 3. This is achieved by defining multiple cylindrical zones around the well. Each zone can be seen as a separate multilayer model that is solved using the method presented in Chapter 2. The different models are coupled to each other by preserving continuity of flow at their common boundaries. This results in a system of linear equations that is solved to obtain the integration constants associated with each zone. A new algorithm similar to the Thomas (1949) algorithm is developed to solve this system of equations. Alternatively, standard LU decomposition may be used which is more robust. The solution method is also applicable to simulate parallel flow in multilayer systems characterized by laterally varying parameters.

The multilayer-multizone solution can be used to solve more advanced and more realistic problems. For instance, it allows for defining mixed boundary conditions at the top of the aquifer system, such as a combination of infiltration by precipitation and drainage from a dense system of ditches. Another important application is the simulation of the effect of a finite-thickness skin. In Chapter 5, the theory of the dimensionless skin factor is reviewed, which describes the effect of linear well-loss (Kruseman & de Ridder, 1990). In a strict sense, it is applicable to steady flow toward a fully penetrating well with zero-thickness skin, although the dimensionless skin factor can be generalized to include multiple finite-thickness zones. The solution by Butler (1988) proves that it is also justified to use the skin factor in case of transient flow toward a fully penetrating well at large values of time. However, the dimensionless skin factor is generally not applicable to partially penetrating wells and multilayer wells.

To simulate the effect of wellbore storage, a well of large diameter can be represented by a separate highly transmissive zone in the model. It is, however, mathematically more convenient to include this effect in the boundary condition conceptualizing the well. If the well extends over more than one model layer, then the uniform well-face drawdown solution (UWD) can be applied to define the required mixed-type boundary condition (Hemker, 1999b). This offers a more realistic way to implement partially penetrating wells and multi-aquifer wells than the traditional uniform well-face gradient (UWG) approach which assigns transmissivity weighted discharges to the inner model boundary. In Chapter 6, the solution technique developed in Chapter 5 is applied to generalize the UWD solution by Hemker (1999b) to make it possible to define multiple zones of finite width.

The UWD solution can also be obtained numerically by defining multi-node wells. For that purpose, the finite-difference approach presented in Chapter 3 is extended with the option to connect grid cells. A simple algorithm is developed to update the finite-difference matrix system, which is solved easily using standard LU decomposition. As the multi-node well is part of the model grid, the head in the well is calculated simultaneously with the heads in the other cells of the grid. Alternatively, the MODFLOW procedure by Louwyck et al. (2012, 2014) discussed in Chapter 3 can be used in combination with the MNW2 package (Konikow et al., 2009). The latter defines the multi-node well as a boundary condition and applies an iterative solution method. Unlike the extended finite-difference method, the MNW2 package cannot account for the effect of the change in wellbore storage.

Chapter 7 generalizes the one-dimensional radial flow solutions by Moench and Prickett (1972) and Ernst (1971). The first simulates the conversion from confined to unconfined flow, only considering the change in storage coefficient, whereas the latter simulates steady flow to a well in an aquifer subject to areal uniform infiltration and drainage. Both models consist of two cylindrical zones, and the boundary between the two is specified by a head condition. In case of confined-unconfined flow, this condition expresses the fact that flow becomes unconfined when the head drops below the aquifer top, while the drainage becomes inactive when the head is lower than the drainage level.

Solving both of these two problems requires a two-zone model; hence, the semi-analytical multilayer-multizone solution developed in Chapter 5 can be used to include confined-unconfined flow or drainage in the top layer of a multilayer aquifer system. As the distance of the boundary between the two zones representing the two different conditions is determined by a specified head, a nonlinear inverse problem must be solved to find this distance. In case of steady flow, only one distance is required, which can be derived using a standard nonlinear solver available with Python. In case of transient flow, the boundary between the two zones expands with time, and its distance must be determined for each time. For small values of time, it is recommended to use a later-time distance as upper bound to constrain the optimization problem.

In the transient case, the Laplace transform is applied, which raises the question about the validity of the initial conditions. The boundary for each simulation time is determined assuming this boundary was already there at the initial time when the pumping started. This is not how the problem is stated mathematically. However, it is found that the initial conditions defined for the proximal zone are irrelevant in most cases, which seems to be confirmed by the analytical one-layer solution for confined-unconfined flow developed by Moench and Prickett (1972). The presented semi-analytical approach for the general multilayer case is also compared with the finite-difference solution for both confined-unconfined flow and transient flow subject to drainage, and it is seen that both solution methods give results that are very close to each other. It is, however, not proven mathematically that it is justified to apply the fixed two-zone solution in the transient case, and further research is needed to study the problem analytically.

The multilayer-multizone solution developed in Chapter 5 is also used in Chapter 8 to simulate unconfined flow in the upper layer considering head-dependent transmissivity. The governing differential equation is linearized by discretizing the aquifer system into cylindrical zones around the well, similar to the finite-difference discretization of the radial distance (Louwyck et al., 2012). Using Picard iterations, the heads and the head-dependent transmissivities are alternately updated until convergence is reached. This technique is also implemented in the MAxSym code (Louwyck, 2011; Louwyck et al., 2012) to simulate unconfined flow in the top layer of a multilayer aquifer system. Alternatively, the MODFLOW procedure by Louwyck et al. (2012, 2014) can be used, as it allows for

radial variation of input parameters. The semi-analytical and finite-difference methods give results that are virtually the same.

Chapter 8 also discusses the effect of delayed yield, which is straightforward to simulate using the equivalence between the semi-empirical solution by Boulton (1954, 1963) and an aquifer-aquitard model adopting the corresponding hydraulic parameters (Cooley & Case, 1973). Based on this equivalence, Hemker (1999a) simply defines a highly transmissive dummy layer to which the specific yield is assigned on top of the model. In Chapter 8, the Hemker (1999a) solution is extended by treating the delayed yield layer as an upper boundary condition, which is mathematically more convenient. It is reconfirmed that the Boulton (1954, 1963) solution corresponds to a model of well-flow in an aquifer bounded on top by a reservoir that produces the delayed drainage determined by the specific yield (Cooley & Case, 1973). An attempt to combine the nonlinear effect of unconfined flow and the linear effect of delayed yield was unsuccessful. Further research is needed to find a more effective algorithm than Picard iterations that can deal with nonlinear unconfined flow that accounts for delayed yield.

The newly developed solution methods are tested very carefully. They are verified against several analytical solutions presented in the hydrogeological literature, and in each test case, the semi-analytical multilayer solution is compared with the finite-difference result. It is concluded that both solution methods perform equally well in terms of accuracy. In case of the finite-difference method, the accuracy mainly depends on the discretization of time and space, whereas the accuracy of the semi-analytical solution depends on the precision of the Stehfest (1970) algorithm, which is determined by the Stehfest number. Theoretically, the bigger the Stehfest number, the more accurate the inversion. In practice, however, the inversion tends to be unstable due to numerical approximation errors if the Stehfest number becomes too large. In our experience, a Stehfest number equal to 8 gives good results, and a number greater than 18 is not recommended if standard double precision floating points are used. Other existing numerical inversion algorithms, such as the method by de Hoog et al. (1982), are not applied in this work.

Defining a higher resolution for the finite-difference discretization and using a bigger Stehfest number both are computationally more expensive. This tradeoff between precision and computational speed makes it difficult to state which of the two solution methods is fastest. As it depends on many factors, it is actually problem-specific, although it seems that semi-analytically solving the nonlinear problems discussed in Chapter 7 and Chapter 8 is significantly slower. Certainly, implementing nonlinearities is more straightforward applying the finite-difference approach, which is also true for including heterogeneity. On the other hand, the user input for the semi-analytical approach is simpler because it does not require radial and temporal discretization, and the most pronounced benefit of using analytical methods is the insight they offer (Haitjema, 2006).

Several test cases presented in chapters 5 to 8 also include the solution for the simplified model that neglects the studied effect: well-skin, wellbore storage, drainage, nonlinear unconfined flow, or delayed yield. Comparing the solutions with and without this effect, it is seen that the latter may significantly over- or underestimate the drawdown. This underlines the importance of developing more advanced axisymmetric solutions that allow for defining more realistic boundary conditions. Under the assumption of axial symmetry, the governing differential equation is reduced by one dimension, making these models relatively easy to set up and fast to run. Therefore, it is highly recommended to perform one- and two-dimensional simulations to get a better understanding of the problem to solve before building advanced three-dimensional numerical models. As a matter of fact, these kinds of simulations led to the theoretical insights discussed in chapters 9 to 11 and summarized in the next section.

13.4. Theoretical considerations

Chapter 9 studies the solution by Hemker (1985) for transient flow to a pumping well of infinitesimal diameter extracting from a confined multi-aquifer system of infinite extent. The exact solution in Laplace space is derived and compared to the corresponding steady-state solution given by Bakker (2001). The Laplace-space solution is expanded for large values of time and inverted analytically, resulting in an approximate solution that is equal to the steady-state solution in which the comprehensive potential is expressed by the Theis (1935) equation instead of the Thiem (1870; 1906) formula. The comprehensive potential is obtained from the solution for the equivalent single-layer model adopting the total transmissivity, the total storativity, and the total pumping rate.

By evaluating the water balances for the individual layers using this approximate solution for large values of time, it is shown that close to the well, at distances smaller than about 8 times the largest leakage factor, flow is redistributed according to the transmissive properties of the individual layers, resulting in a pseudo-steady state, also referred to as steady shape conditions (Bohling et al., 2002). At distances larger than the distance determined by the largest leakage factor, flow continues to be redistributed according to the storative properties of the layers, which may result in a counterintuitive inversion of the vertical flow between the layers. Drawdown curves plotted on semi-logarithmic axes are parallel straight lines at large values of time, and the slope of these lines equals the slope of the straight line given by the Cooper and Jacob (1946) approximation of the Theis (1935) solution for the equivalent single-layer model.

By simulating randomly generated multi-layer models, it is seen that the exact solution approximates the asymptotic solution after a period of pumping which is larger than about 10 times the product of the total storativity and the sum of all vertical resistances. It is concluded that deriving the hydraulic parameters for individual layers in the multilayer system from drawdown measurements is limited in space and time, and the window of opportunity is different for each aquifer system. The developed theory substantiates the steady shape interpretation method of hydraulic tomography data by Bohling et al. (2002). It also confirms the spatial averaging in the measurements of pumping induced drawdown and clearly demonstrates the inherent limitations of hydraulic tomography (Bohling & Butler, 2010).

Since a confined multi-aquifer system extracted at constant rate behaves as a homogeneous aquifer beyond a certain distance and at large values of time, the Theis (1935) solution can be used to estimate the radius of influence. At least if the cone of depression is not affected by sources and sinks that are not axially symmetric, such as streams. In reality, this is not often the case, and therefore, assessing the environmental impact of an extraction by solely estimating its radius of influence is questionable. Unfortunately, this is a common practice, and in Flanders, groundwater practitioners even apply empirical formulas such as the Sichardt formula (Kyrieleis & Sichardt, 1930). Louwyck et al. (2022) call this practice “the radius of influence myth” as these formulas are not consistent with the fundamental hydrological principles stated by Theis (1940).

Chapter 10 examines the Sichardt formula, which estimates the radius of influence by merely considering the aquifer conductivity and the drawdown in the pumping well. It is shown that the Sichardt formula is not consistent with the fundamental Thiem equation (1870; 1906). It also tends to underestimate the extent of the cone of depression; hence, its use must be discouraged in the context of environmental impact assessments (Louwyck et al., 2022). It is also imperative to distinguish between sustainable pumping and sustainability (Devlin & Sophocleous, 2005), the latter being a much broader concept that encompasses aspects such as water quality, ecology, and

socioeconomic considerations, and therefore, requiring advanced numerical modeling in many, if not all cases.

On the other hand, the use of axisymmetric models in the initial stage of a groundwater study is recommended to get insight into the problem to solve. As already argued, these models have minimum data requirements and may help setting up the right three-dimensional model. Therefore, alternatives to the Sichardt formula are presented in Chapter 10, which are derived from existing one-dimensional analytical solutions developed by de Glee (1930), by Theis (1935), and by Ernst (1971). An asymptotic solution to the latter yields the contested formula to determine the radius of influence by balancing pumping and infiltration rate (Louwyck et al., 2022, 2023). Considering the assumptions underlying the Ernst (1971) model, it is concluded that this formula is valid in humid areas that are heavily drained, which has been validated by means of a MODFLOW model.

The superposition principle is another argument in favor of the use of axisymmetric models in the context of evaluating sustainable pumping. This principle is discussed in Chapter 2 and it states that the total drawdown due to multiple extractions is the sum of the drawdown caused by the individual pumping wells. As a consequence, the effect of each well can be isolated by calculating its cone of depression independently from the effect of the other wells. However, there is a caveat, as this principle is valid only if the boundary value problem is expressed by linear equations. Since linear models tend to underestimate the cone of depression, it is concluded that applying linear models to assess sustainability should be subject to caution (Louwyck et al., 2023).

Distinguishing between linear and nonlinear models is the essence of the debate on the role of recharge in evaluating the sustainability of groundwater development (Louwyck et al., 2023). The controversy originates in the groundwater budget myth, which is the idea that safe pumping must not exceed the initial recharge. To refute this idea of safe yield, a simplified water budget equation is used, which equates the total pumping rate to the sum of capture and storage change (Bredehoeft, 2002; Bredehoeft et al., 1982). Since initial recharge and discharge are canceled out from this equation, Bredehoeft (1997, 2002, 2007) concludes that sustainable pumping has nothing to do with recharge.

In Chapter 11, it is proven that this water budget equation expresses the superposition principle. Under this assumption, drawdown is independent of initial conditions, including initial recharge. However, like any other model assumption, this is a simplification of reality, as it implicitly assumes the groundwater reservoir can be depleted indefinitely and boundary conditions are an infinite source of water. In reality, capture and storage are limited, and this requires modeling nonlinear responses, in which case the superposition principle is not applicable, and simulating the initial conditions is inevitable. Moreover, the initial conditions determine the limits of the system, and as a consequence, they paradoxically determine whether the assumption of linearity is valid or not (Louwyck et al., 2023).

Using the solution for nonlinear unconfined flow to a well pumping a circular island subject to areal recharge (Verruijt, 1970) and the solution by Ernst (1971) that defines a nonlinear function for the drainage, it is demonstrated that the question if recharge is important in assessing the sustainability of groundwater development comes down to the question if superposition can be applied in the analysis of the groundwater system. The finite-difference approximation of the simplified water budget equation shows that this question is generally applicable and does not only concern analytical models. In many cases, using superposition models is still justified indeed, but in many other cases, defining nonlinear and time-dependent stresses on the groundwater system is inevitable, making

recharge a relevant parameter. And this, to quote Bredehoeft (2002), is “why hydrogeologists model”.

13.5. A practical case study

The last Chapter 12 demonstrates how the axisymmetric multilayer solution is used to solve a real-word groundwater problem. For that purpose, Chapter 12 summarizes the hydrogeological studies conducted to realize a drainage system at the excavation site ‘Duinenabdij’ (Louwyck et al., 2005).

The aquifer system at the site consists of three permeable layers separated by two semi-pervious layers, where the shallow semi-pervious layer has caused problems of flooding in the past. The new drainage system extracts water from the middle permeable layer to lower the water table at the site, and it re-injects the pumped water to protect the dunes surrounding the site. Using the numerical model by Lebbe (1988, 1999), the relevant hydraulic parameters of the aquifer system were estimated from data observed during a double pumping test, and the feasibility of the drainage system was evaluated through mathematical modeling. Finding the optimal pumping and injection rates was done manually via trial-and-error (Louwyck et al., 2005).

In Chapter 12, linear programming is applied to minimize the pumping and injection rates of the drainage system. Drawdown in the three permeable layers is simulated by applying the superposition method to the solution by Hemker (1984) for axisymmetric steady-state multilayer well-flow. The combined simulation and optimization is coded with Python, which is very straightforward using Python’s packages for scientific computing. This confirms it is possible indeed to solve practical groundwater problems efficiently using the solutions discussed in this dissertation without having to build a complicated, data-hungry, and computationally expensive groundwater flow model.

13.6. Final conclusions and recommendations

This PhD research aimed at getting a better understanding of axisymmetric flow to a well in a multilayered aquifer system. The most important finding is that leakage from adjacent layers to the extracted layer is limited in both space and time. It is proven that the drawdown curves conform to the Theis (1935) solution again after a certain time of pumping when the aquifer system has reached a pseudo-steady state. This confirms the spatial averaging in the measurements of pumping induced drawdown, and therefore, it is concluded that multilevel tests, such as the hydraulic tomography, have inherent limitations.

Axisymmetric models are well-known to groundwater practitioners as they are frequently used to analyze aquifer tests. There are many solutions described in the hydrogeological literature which require a thorough knowledge of the underlying assumptions. The multilayer-multizone solution developed in this work generalizes these solutions, and it is capable of including different effects, such as the presence of a finite-thickness skin, the change in wellbore storage, unconfined flow in the upper layer, and a combination of areal infiltration and drainage. It is shown that neglecting these effects may severely under- or overestimate the actual drawdown.

Axisymmetric models are also used to assess the environmental impact of permanent groundwater extractions. In its simplest form, only the radius of influence is calculated, a common practice that is questionable, as the assumption of axial symmetry is rarely valid in these cases, which implies the cone of depression cannot be described by simply drawing a circle around the well. Empirical formulas to estimate the radius of influence are also widely-used, a common practice which should be discouraged, as these formulas are not consistent with fundamental hydrogeological principles. On the other hand, when properly applied, axisymmetric models may offer valuable insights, and therefore, their usage preliminary to advanced numerical modeling is recommended.

In combination with the superposition method, axisymmetric models are powerful tools which may eliminate the need to build complex and expensive groundwater flow models in some cases. This is illustrated by solving a practical problem in which a drainage system consisting of multiple pumping and injection wells is optimized using linear programming. One should keep in mind, however, that the superposition principle is valid only if the governing equations are linear, which implicitly assumes the groundwater reservoir can be depleted indefinitely and boundary conditions are an infinite source of water. Therefore, it is concluded that applying superposition models to assess sustainability is subject to caution.

The stated multilayer problems are solved using the semi-analytical approach based on the Laplace transform and the finite-difference method. It is concluded they are both very accurate. Implementing the finite-difference approach is more straightforward if the model includes heterogeneities or nonlinearities, although it is also relatively easy to code most of the analytical solutions presented in this work. The Python programming language has become very popular among groundwater practitioners and is highly recommended, as it offers all the required libraries for scientific computing free of charge. Python scripting using interactive notebooks certainly fills the gap between simple spreadsheet calculations and expensive software for advanced groundwater modeling.

13.7. References

- Bakker, M. (2001). An analytic, approximate method for modeling steady, three-dimensional flow to partially penetrating wells. *Water Resources Research*, 37(5).
<https://doi.org/10.1029/2000WR900400>
- Bohling, G. C., & Butler, J. J. (2010). Inherent Limitations of Hydraulic Tomography. *Ground Water*, 48(6), 809–824. <https://doi.org/10.1111/j.1745-6584.2010.00757.x>
- Bohling, G. C., Zhan, X., Butler, J. J., & Zheng, L. (2002). Steady shape analysis of tomographic pumping tests for characterization of aquifer heterogeneities. *Water Resources Research*, 38(12), 60_1-60_15. <https://doi.org/10.1029/2001WR001176>
- Boulton, N. S. (1954). Unsteady radial flow to a pumped well allowing for delayed yield from storage. *General Assembly of Rome, Tome II, Groundwater, IAHS publ. 37*, 472–477.
- Boulton, N. S. (1963). Analysis of data from non-equilibrium pumping tests allowing for delayed yield from storage. *Proceedings of the Institution of Civil Engineers*, 26(3), 469–482.
<https://doi.org/10.1680/iicep.1963.10409>
- Bredehoeft, J. D. (1997). Safe Yield and the Water Budget Myth. *Ground Water*, 35(6), 929–929.
<https://doi.org/10.1111/j.1745-6584.1997.tb00162.x>
- Bredehoeft, J. D. (2002). The Water Budget Myth Revisited: Why Hydrogeologists Model. *Ground Water*, 40(4). <https://doi.org/10.1111/j.1745-6584.2002.tb02511.x>
- Bredehoeft, J. D. (2007). It Is the Discharge. *Ground Water*, 45(5), 523–523.
<https://doi.org/10.1111/j.1745-6584.2007.00305.x>
- Bredehoeft, J. D., Papadopoulos, S. S., & Cooper, H. H. (1982). The water budget myth. In *Scientific Basis of Water Resources management Studies in Geophysics* (pp. 51–57). National Academy Press.

- Butler, J. J. (1988). Pumping tests in nonuniform aquifers — The radially symmetric case. *Journal of Hydrology*, 101(1–4), 15–30. [https://doi.org/10.1016/0022-1694\(88\)90025-X](https://doi.org/10.1016/0022-1694(88)90025-X)
- Cooley, R. L., & Case, C. M. (1973). Effect of a water table aquitard on drawdown in an underlying pumped aquifer. *Water Resources Research*, 9(2), 434–447. <https://doi.org/10.1029/WR009i002p00434>
- Cooper, H. H., & Jacob, C. E. (1946). A generalized graphical method for evaluating formation constants and summarizing well-field history. *Transactions, American Geophysical Union*, 27(4), 526–534. <https://doi.org/10.1029/TR027i004p00526>
- Crank, J., & Nicolson, P. (1947). A practical method for numerical evaluation of solutions of partial differential equations of the heat-conduction type. *Mathematical Proceedings of the Cambridge Philosophical Society*, 43(1), 50–67. <https://doi.org/10.1017/S0305004100023197>
- Crank, J., & Nicolson, P. (1996). A practical method for numerical evaluation of solutions of partial differential equations of the heat-conduction type. *Advances in Computational Mathematics*, 6(1), 207–226. <https://doi.org/10.1007/BF02127704>
- de Glee, G. J. (1930). *Over grondwaterstroomingen bij wateronttrekking door middel van putten (in Dutch)* [PhD thesis]. Technische Hoogeschool Delft, Drukkerij J. Waltman. Jr., Delft.
- de Hoog, F. R., Knight, J. H., & Stokes, A. N. (1982). An Improved Method for Numerical Inversion of Laplace Transforms. *SIAM Journal on Scientific and Statistical Computing*, 3(3), 357–366. <https://doi.org/10.1137/0903022>
- Devlin, J. F., & Sophocleous, M. (2005). The persistence of the water budget myth and its relationship to sustainability. *Hydrogeology Journal*, 13(4). <https://doi.org/10.1007/s10040-004-0354-0>
- Ernst, L. F. (1971). Analysis of groundwater flow to deep wells in areas with a non-linear function for the subsurface drainage. *Journal of Hydrology*, 14(2). [https://doi.org/10.1016/0022-1694\(71\)90004-7](https://doi.org/10.1016/0022-1694(71)90004-7)
- Haitjema, H. (2006). The Role of Hand Calculations in Ground Water Flow Modeling. *Ground Water*, 44(6). <https://doi.org/10.1111/j.1745-6584.2006.00189.x>
- Harbaugh, A. W. (2005). *MODFLOW-2005, the U.S. Geological Survey modular ground-water model - the Ground-Water Flow Process*. U.S. Geological Survey Techniques and Methods 6-A16. <https://doi.org/https://doi.org/10.3133/tm6A16>
- Hemker, C. J. (1984). Steady groundwater flow in leaky multiple-aquifer systems. *Journal of Hydrology*, 72(3–4), 355–374. [https://doi.org/10.1016/0022-1694\(84\)90089-1](https://doi.org/10.1016/0022-1694(84)90089-1)
- Hemker, C. J. (1985). Transient well flow in leaky multiple-aquifer systems. *Journal of Hydrology*, 81(1–2), 111–126. [https://doi.org/10.1016/0022-1694\(85\)90170-2](https://doi.org/10.1016/0022-1694(85)90170-2)
- Hemker, C. J. (1999a). Transient well flow in vertically heterogeneous aquifers. *Journal of Hydrology*, 225(1–2), 1–18. [https://doi.org/10.1016/S0022-1694\(99\)00137-7](https://doi.org/10.1016/S0022-1694(99)00137-7)
- Hemker, C. J. (1999b). Transient well flow in layered aquifer systems: the uniform well-face drawdown solution. *Journal of Hydrology*, 225(1–2), 19–44. [https://doi.org/10.1016/S0022-1694\(99\)00093-1](https://doi.org/10.1016/S0022-1694(99)00093-1)

- Konikow, L. F., Hornberger, G. Z., Halford, K. J., Hanson, R. T., & Harbaugh, A. W. (2009). *Revised multi-node well (MNW2) package for MODFLOW ground-water flow model*. U.S. Geological Survey Techniques and Methods 6-A30. <https://doi.org/10.3133/tm6A30>
- Kruseman, G. P., & de Ridder, N. A. (1990). *Analysis and Evaluation of Pumping Test Data* (2nd ed.). ILRI Publication 47, Wageningen.
- Kyrieleis, W., & Sichardt, W. (1930). *Grundwasserabsenkung bei Fundierungsarbeiten (in German)*. Berlin: Springer.
- Langevin, C. D. (2008). Modeling Axisymmetric Flow and Transport. *Ground Water*, 46(4), 579–590. <https://doi.org/10.1111/j.1745-6584.2008.00445.x>
- Lebbe, L. C. (1988). *Uitvoering van pomproeven en interpretatie door middel van een invers model (in Dutch)*. Ghent University.
- Lebbe, L. C. (1999). *Hydraulic Parameter Identification. Generalized Interpretation Method for Single and Multiple Pumping Tests*. Berlin Heidelberg: Springer-Verlag.
- Louwyck, A. (2011). *MAxSym - A MATLAB Tool to Simulate Two-Dimensional Axi-Symmetric Groundwater Flow*. Research Unit Groundwater Modeling, Ghent University. Retrieved from <https://github.com/alouwyck/MAxSym>
- Louwyck, A., Vandenbohede, A., Bakker, M., & Lebbe, L. C. (2012). Simulation of axi-symmetric flow towards wells: A finite-difference approach. *Computers & Geosciences*, 44, 136–145. <https://doi.org/10.1016/j.cageo.2011.09.004>
- Louwyck, A., Vandenbohede, A., Bakker, M., & Lebbe, L. C. (2014). MODFLOW procedure to simulate axisymmetric flow in radially heterogeneous and layered aquifer systems. *Hydrogeology Journal*, 22(5), 1217–1226. <https://doi.org/10.1007/s10040-014-1150-0>
- Louwyck, A., Vandenbohede, A., Heuvelmans, G., Van Camp, M., & Walraevens, K. (2023). The Water Budget Myth and Its Recharge Controversy: Linear vs. Nonlinear Models. *Groundwater*, 61(1), 100–110. <https://doi.org/10.1111/gwat.13245>
- Louwyck, A., Vandenbohede, A., & Lebbe, L. C. (2005). The role of hydrogeological research in the realization of a combined pumping and deep infiltration system at the excavation “Duinenabdij.” In J.-L. Herrier, J. Mees, A. Salman, J. Seys, H. Van Nieuwenhuyse, & I. Dobbelaere (Eds.), *Proceedings “Dunes and Estuaries 2005”: International Conference on nature restoration practices in European coastal habitats, Koksijde, Belgium 19-23 September 2005*. (pp. 317–326). VLIZ Special Publication 19.
- Louwyck, A., Vandenbohede, A., Libbrecht, D., Van Camp, M., & Walraevens, K. (2022). The Radius of Influence Myth. *Water*, 14(2), 149. <https://doi.org/10.3390/w14020149>
- Moench, A. F., & Prickett, T. A. (1972). Radial flow in an infinite aquifer undergoing conversion from artesian to water table conditions. *Water Resources Research*, 8(2), 494–499. <https://doi.org/10.1029/WR008i002p00494>
- Stehfest, H. (1970). Algorithm 368: Numerical inversion of Laplace transforms [D5]. *Communications of the ACM*, 13(1), 47–49. <https://doi.org/10.1145/361953.361969>

- Theis, C. V. (1935). The relation between the lowering of the Piezometric surface and the rate and duration of discharge of a well using ground-water storage. *Transactions, American Geophysical Union*, 16(2), 519–524. <https://doi.org/10.1029/TR016i002p00519>
- Theis, C. V. (1940). The source of water derived from wells: essential factors controlling the response of an aquifer to development. *Civil Engineering*, 10, 277–280.
- Thiem, A. (1870). Die Ergiebigkeit artesischer Bohrlöcher, Schachtbrunnen und Filtergalerien (in German). *Journal Für Gasbeleuchtung Und Wasserversorgung*, 13, 450–467.
- Thiem, G. (1906). *Hydrologische Methoden (in German)*. Leipzig: Gebhardt.
- Thomas, L. H. (1949). *Elliptic Problems in Linear Difference Equations Over a Network*. Watson Science Computer Laboratory, Colombia University, New York.
- Verruijt, A. (1970). *Theory of Groundwater Flow*. London: Macmillan Press.

Appendix: Analytical Solutions

An overview is given of the analytical and semi-analytical solutions discussed in this study. The solutions are classified according to the following features:

- **flow:** the type of flow
 - **R:** radial or axisymmetric flow
 - **P:** parallel flow
- **state:** the state of the aquifer system
 - **S:** steady state
 - **U:** unsteady or transient state
- **layers:** the number of layers in the aquifer system
 - **1:** one layer
 - **2:** two layers
 - **M:** multiple layers
 - **N:** there is no cross-flow between the layers
- **zones:** the number of zones
 - **1:** one zone
 - **2:** two zones
 - **M:** multiple zones
- **lower:** the lower boundary of the aquifer system
 - **C:** confined or impervious lower boundary
 - **L:** leaky lower boundary condition defining a constant head and resistance
- **upper:** the upper boundary of the aquifer system
 - **C:** confined or impervious upper boundary (i.e. upper layer has constant thickness)
 - **L:** leaky upper boundary condition defining a constant head and resistance
 - **W:** water table (i.e. upper layer thickness is head-dependent)
 - **N:** uniform recharge
 - **D:** uniform recharge and drainage (cfr. Ernst, 1971)
 - **Y:** delayed yield from water table (cfr. Boulton, 1954, 1963)
 - **M:** conversion from confined to unconfined (cfr. Moench & Prickett, 1972)
- **outer:** the distance of the outer model boundary
 - **B:** finite distance or laterally bounded aquifer system
 - **U:** infinite distance or laterally unbounded aquifer system
- **inner:** the distance of the inner model boundary
 - **Z:** zero or infinitesimal distance
 - **F:** finite distance
- **well or stream:** the boundary condition defining the well or stream
 - **N:** no-flux boundary condition or impervious inner boundary
 - **Q:** constant nonzero flux
 - **H:** constant head
 - **C:** instantaneous head change (e.g. slug test)
 - **P:** partially penetrating with vertical distance fully taken into account
 - **M:** mixed-type boundary condition (e.g. multi-aquifer or partially penetrating well)
 - **W:** wellbore storage included
 - **S:** zero-thickness skin included (i.e. defining a dimensionless skin factor)

The following table indicates in which **section** of the dissertation the model with given features has been presented.

If values are separated by a slash, then one of the values can be chosen for that feature. For instance, value "F/Z" for feature "inner" means the inner radius may be finite or infinitesimal. If values are separated by a plus sign, then both values are considered for that feature. For instance, value "C+N" for feature "upper" indicates that the upper boundary is impervious and that a constant infiltration flux is defined. Value "C/L+N" means that the upper boundary is impervious or leaky, and that the aquifer system is recharged.

The table also mentions the **equation** of the analytical solution. In case of transient models, this equation may be the exact solution in the Laplace domain. If the model has been presented in the hydrogeological literature, then its **reference** is given.

Although not strictly applied, the rows in the table are sorted as follows:

1. models for parallel flow come before axisymmetric models;
2. the number of layers are sorted in ascending order;
3. steady-state models come before transient-state models;
4. the number of zones are sorted in ascending order;
5. specified-discharge wells come before constant-head wells;
6. boundary conditions in general are ranked according to complexity.

flow	state	layers	zones	lower	upper	outer	inner	well or stream	Section	equation	reference
P	S	1	1	C	C	B	F/Z	Q	2.5.1	115	Darcy (1856)
P	S	1	1	C	C	B	F/Z	H	2.5.1	117	Darcy (1856)
P	S	1	M	C	C	B	F/Z	Q	5.5.3.2	115	
P	S	1	M	C	C	B	F/Z	H	5.5.3.2	117	
P	S	1	1	C	C+N	B	F	H	2.5.4	122	
P	S	1	1	C	C+N	B	Z	H	2.5.4	123	Haitjema (1995)
P	S	M+N	1	C	C	B	F	Q+M	6.5.1	119+122	
P	U	1	1	C	C	U	Z	Q	2.5.9	147	Edelman (1947)
P	U	1	1	C	C	U	Z	H	2.5.9	145	Edelman (1947)
P	U	M+N	1	C	C	U	F	Q+M+W	6.5.2	141+142	
R	S	1	1	C	C	B	F/Z	Q	2.5.2 8.2.4.1 10.2.4 10.3.1 11.3	118 24 21 60 17	Thiem (1870, 1906)
R	S	1	1	C	C	B	F	H	2.5.2	119	
R	S	1	1	C	C	B	F	Q+S	5.6.2	162+163	Kruseman & de Ridder (1990)
R	S	1	2	C	C	B	F/Z	Q	5.5.3.2	119	
R	S	1	M	C	C	B	F/Z	Q	5.5.3.2	116	
R	S	1	M	C	C	B	F	H	5.5.3.2	118	
R	S	1	1	C	W	B	F/Z	Q	8.2.4.1 10.3.1	23 59	Dupuit (1857, 1863)
R	S	1	1	C	C+N	B	Z	N	2.5.3 10.2.4	120 22	Haitjema (1995)
R	S	1	1	C	C+N	B	Z	Q	10.2.4	23	Haitjema (1995)

flow	state	layers	zones	lower	upper	outer	inner	well or stream	Section	equation	reference
R	S	1	1	C	C+N	B	F	Q	2.5.3 10.2.4	121 20	Haitjema (1995)
R	S	1	1	C	W+N	B	F/Z	Q	11.3	12	Verruijt (1970)
R	S	1	1	C	C+N	B	F	H	2.5.5	125	
R	S	1	1	C	L	U	Z	Q	2.5.6 10.2.4 10.3.2 11.4.1	126 34 63 27	Kooper (1914); de Glee (1930); Jacob (1946); Hantush (1949)
R	S	1	1	C	L	U	F	Q	2.5.6 5.5.4.2 10.2.4 11.4.1	128 132 33 22	Kooper (1914); de Glee (1930); Bruggeman (1999)
R	S	1	1	L	L	U	Z	Q	10.2.4	35	
R	S	1	1	L	L	U	F	Q	2.5.6	129	
R	S	1	2	C	L	U	Z	Q	5.5.4.2	131	
R	S	1	1	C	L+N	U	F	Q	10.2.4	31	
R	S	1	2	C	C+N	B	Z	Q	5.5.1.2	96	Haitjema (1995)
R	S	1	2	C	C+N+L	U	Z	Q	5.5.2.2	104+105	Blom (1973)
R	S	1	1	C	L+N	U	Z	N	10.2.4 10.3.5 11.4.1	32 76 20	Ernst (1971)
R	S	1	2	C	D	U	Z	Q	7.5.3.3 10.2.6 10.3.5	208+209 51 77	Ernst (1971)
R	S	1	2	C	D	U	F	Q	11.4.2	31-34	Ernst (1971)
R	U	1	1	C	C	U	Z	Q	2.5.7 4.4.2 6.5.4 10.2.4 10.3.3	132 70 156 38 67	Theis (1935)
R	U	1	1	C	C	U	Z	P+Q	6.5.4	155	Hantush (1964)
R	U	1	1	C	C	U	F	Q+W	6.5.2 6.5.4	138+139 157	Papadopoulos & Cooper (1967)
R	U	1	1	C	C	U	F	P+Q+W	6.5.4	152-154	Mishra et al. (2012)
R	U	1	1	C	C	U	F	C+W	5.5.6.2	155	Cooper et al. (1967)
R	U	1	2	C	C/L	U	F	P+C+M+W	6.5.5	176	Hyder et al. (1994)
R	U	1	2	C	C	U	Z	Q	5.5.5.2	144	Butler (1988)
R	U	1	1	C	C+Y	U	Z	Q	8.3.4.1	69	Boulton (1954, 1963)
R	U	1	2	C	M	U	Z	Q	7.4.2.3	160+161	Moench & Prickett (1972)
R	U	1	1	C	L	U	Z	Q	2.5.10 10.2.4 10.3.4	149 41 72	Hantush & Jacob (1955)
R	U	1	2	C	D	U	Z	Q	7.5.3.4 10.2.6	217+218 52-56	Louwyck et al. (2022)
R	S/U	1	1	C/L	C/L+N	U/B	F/Z	Q	10.2		
R	S	2	1	C	C	B	Z	Q	2.5.13	156	Bakker & Strack (2003)
R	S	2	1	C	C+N	B	Z	N	2.5.13	157	Bakker & Strack (2003)
R	S	2	2	C	C+N	B	Z	Q	5.5.1.2	97+98	Bakker & Strack (2003)
R/P	S	2	1	L	L	U	Z	Q	2.5.11	152	Hemker (1984)
R	U	2+N	1	C	C	U	F	Q+M+W	6.5.2	134+135	Wikramaratna (1984)

flow	state	layers	zones	lower	upper	outer	inner	well or stream	Section	equation	reference
R	U	2+N	1	C	C	U	F	Q+M	6.5.2	137	Papadopoulos (1966)
R/P	U	2	1	C/L	C/L	U	Z	Q	2.5.12	154	Hemker (1985, 1999a)
R	S	M+N	1	C	C	B	F	N+M	6.5.1	120+121	Sokol (1963)
R	S	M+N	1	C	C	B	F	Q+M	6.5.1	118+121	Neville & Tonkin (2004)
R	S	M	1	C	L+N	U	Z	N	7.5.1	189	
R/P	S	M	1	L	L	U	Z	Q	2.5.11	151	Hemker (1984)
R	S	M	1	C	C	B	Z	Q	9.3.2 12.3.1	50 17+18	Hemker (1984); Bakker & Strack (2003)
R	U	M+N	1	C	C	U	F	Q+M+W	6.5.2	130+131	Wikramaratna (1984)
R	U	M	1	C	C	U	Z	Q	4.3.1 9.3.1	21 24	Hemker (1985, 1999a)
R/P	U	M	1	C/L	C/L	U	Z	Q	2.5.12	153	Hemker (1985, 1999a)
R	S/U	M	1	C/L	C/L+N	U/B	F/Z	Q	7.2.2		Hemker (1984, 1985, 1999a); Bakker & Strack (2003)
R/P	S/U	M	1	C/L	C/L+N	U/B	F/Z	Q/H	2.3		Hemker (1984, 1985, 1999a); Bakker & Strack (2003)
R	U	M	1	C/L	C+Y	U/B	F/Z	Q	8.3.2		
R	U	M	1	C/L	C/L	U	F	Q+M+ W+S	6.5.3	143	Hemker (1999b)
R/P	S/U	M	1	C/L	C/L+N	U/B	F	Q/H/C+ M+W	6.3.3		
R/P	S/U	M	1	C/L	C/L+N	U/B	F	Q/H/C+ M+W+S	6.3.4		
R	S	M	2	C	C+N	B	Z	N	5.5.1.2	93	Bakker & Strack (2003)
R	S	M	2	C	C	B	Z	Q	5.5.1.2	91	Bakker & Strack (2003)
R	S	M	2	C	C+N	B	Z	Q	5.5.1.2	95	Bakker & Strack (2003)
R	S	M	2	C	C/L+N	U	Z	Q	7.3.2.1		
R	U	M	2	C	C/L+N	U	Z	Q	7.3.2.2		
R	S/U	M	2	C/L	C/L+N	U/B	F/Z	Q	7.2.3		
R	U	M	2	C	M	U	Z	Q	7.4.2		
R	S/U	M	2	C	D	U	Z	Q	7.5.3		
R/P	S/U	M	M	C/L	C/L+N	U/B	F/Z	Q/H	5.3		
R/P	S/U	M	M	C/L	C/L+N	U/B	F	Q/H/C+ M+W	6.3.2		
R	S/U	M	M	C/L	W	U/B	F/Z	Q	8.2.2		

References:

- Bakker, M., & Strack, O. D. L. (2003). Analytic elements for multiaquifer flow. *Journal of Hydrology*, 271(1–4). [https://doi.org/10.1016/S0022-1694\(02\)00319-0](https://doi.org/10.1016/S0022-1694(02)00319-0)
- Blom, J. (1973). *Verlagingen van het freatisch vlak bij grondwateronttrekking in een gebied met vrije afwatering (Drenthe) (in Dutch)*. RID Mededeling 74-7, Rijksinstituut voor Drinkwatervoorziening (RID), The Netherlands.
- Boulton, N. S. (1954). Unsteady radial flow to a pumped well allowing for delayed yield from storage. *General Assembly of Rome, Tome II, Groundwater*, IAHS publ. 37, 472–477.

- Boulton, N. S. (1963). Analysis of data from non-equilibrium pumping tests allowing for delayed yield from storage. *Proceedings of the Institution of Civil Engineers*, 26(3), 469–482. <https://doi.org/10.1680/iicep.1963.10409>
- Bruggeman, G. A. (1999). *Analytical solutions of geohydrological problems. Developments in Water Science* 46. Amsterdam: Elsevier.
- Butler, J. J. (1988). Pumping tests in nonuniform aquifers — The radially symmetric case. *Journal of Hydrology*, 101(1–4), 15–30. [https://doi.org/10.1016/0022-1694\(88\)90025-X](https://doi.org/10.1016/0022-1694(88)90025-X)
- Cooper, H. H., Bredehoeft, J. D., & Papadopoulos, I. S. (1967). Response of a finite-diameter well to an instantaneous charge of water. *Water Resources Research*, 3(1), 263–269. <https://doi.org/10.1029/WR003i001p00263>
- Darcy, H. (1856). *Les fontaines publiques de la ville de Dijon (In French)*. Paris: Dalmont.
- de Glee, G. J. (1930). *Over grondwaterstroomingen bij wateronttrekking door middel van putten (in Dutch)* (PhD thesis). Technische Hoogeschool Delft, Drukkerij J. Waltman. Jr., Delft.
- Dupuit, J. (1857). Mouvement de l'eau à travers les terrains perméables (in French). *Comptes Rendus de l'Académie Des Sciences*, 45, 92–96.
- Dupuit, J. (1863). *Etude Théoriques et Pratiques Sur le Mouvement Des Eaux Dans Les Canaux Découverts et à Travers Les Terrains Perméables (in French)*. Paris: Dunot.
- Edelman, J. H. (1947). *Over de berekening van grondwaterstroomingen (in Dutch)*. TU Delft, Delft.
- Ernst, L. F. (1971). Analysis of groundwater flow to deep wells in areas with a non-linear function for the subsurface drainage. *Journal of Hydrology*, 14(2). [https://doi.org/10.1016/0022-1694\(71\)90004-7](https://doi.org/10.1016/0022-1694(71)90004-7)
- Haitjema, H. (1995). *Analytic Element Modeling of Groundwater Flow*. San Diego: Academic Press. <https://doi.org/10.1016/B978-0-12-316550-3.X5000-4>
- Hantush, M. S. (1949). *Plain potential flow of ground water with linear leakage*. (PhD Thesis). University of Utah, Salt Lake City.
- Hantush, M. S. (1964). Hydraulics of wells. In V. T. Chow (Ed.), *Advances in Hydroscience* (Vol. I, pp. 281–432). New York and London: Academic Press.
- Hantush, M. S., & Jacob, C. E. (1955). Non-steady radial flow in an infinite leaky aquifer. *Transactions, American Geophysical Union*, 36(1), 95–100. <https://doi.org/10.1029/TR036i001p00095>
- Hemker, C. J. (1984). Steady groundwater flow in leaky multiple-aquifer systems. *Journal of Hydrology*, 72(3–4), 355–374. [https://doi.org/10.1016/0022-1694\(84\)90089-1](https://doi.org/10.1016/0022-1694(84)90089-1)
- Hemker, C. J. (1985). Transient well flow in leaky multiple-aquifer systems. *Journal of Hydrology*, 81(1–2), 111–126. [https://doi.org/10.1016/0022-1694\(85\)90170-2](https://doi.org/10.1016/0022-1694(85)90170-2)
- Hemker, C. J. (1999a). Transient well flow in vertically heterogeneous aquifers. *Journal of Hydrology*, 225(1–2), 1–18. [https://doi.org/10.1016/S0022-1694\(99\)00137-7](https://doi.org/10.1016/S0022-1694(99)00137-7)
- Hemker, C. J. (1999b). Transient well flow in layered aquifer systems: the uniform well-face drawdown solution. *Journal of Hydrology*, 225(1–2), 19–44. [https://doi.org/10.1016/S0022-1694\(99\)00093-1](https://doi.org/10.1016/S0022-1694(99)00093-1)

- Hyder, Z., Butler, J. J., McElwee, C. D., & Liu, W. (1994). Slug tests in partially penetrating wells. *Water Resources Research*, 30(11), 2945–2957. <https://doi.org/10.1029/94WR01670>
- Jacob, C. E. (1946). Radial flow in a leaky artesian aquifer. *Transactions, American Geophysical Union*, 27(2). <https://doi.org/10.1029/TR027i002p00198>
- Kooper, J. (1914). Beweging van het water in den bodem bij onttrekking door bronnen (in Dutch). *Ingenieur*, 29, 697–716.
- Kruseman, G. P., & de Ridder, N. A. (1990). *Analysis and Evaluation of Pumping Test Data* (2nd ed.). Wageningen: ILRI Publication 47.
- Louwyck, A., Vandenbohede, A., Libbrecht, D., Van Camp, M., & Walraevens, K. (2022). The Radius of Influence Myth. *Water*, 14(2), 149. <https://doi.org/10.3390/w14020149>
- Mishra, P. K., Vesselinov, V. V., & Neuman, S. P. (2012). Radial flow to a partially penetrating well with storage in an anisotropic confined aquifer. *Journal of Hydrology*, 448–449, 255–259. <https://doi.org/10.1016/j.jhydrol.2012.05.010>
- Moench, A. F., & Prickett, T. A. (1972). Radial flow in an infinite aquifer undergoing conversion from artesian to water table conditions. *Water Resources Research*, 8(2), 494–499. <https://doi.org/10.1029/WR008i002p00494>
- Neville, C. J., & Tonkin, M. J. (2004). Modeling Multiaquifer Wells with MODFLOW. *Ground Water*, 42(6), 910–919. <https://doi.org/10.1111/j.1745-6584.2004.t01-9-.x>
- Papadopoulos, I. S. (1966). Nonsteady flow to multiaquifer wells. *Journal of Geophysical Research*, 71(20), 4791–4797. <https://doi.org/10.1029/JZ071i020p04791>
- Papadopoulos, I. S., & Cooper, H. H. (1967). Drawdown in a well of large diameter. *Water Resources Research*, 3(1), 241–244. <https://doi.org/10.1029/WR003i001p00241>
- Sokol, D. (1963). Position and fluctuations of water level in wells perforated in more than one aquifer. *Journal of Geophysical Research*, 68(4), 1079–1080. <https://doi.org/10.1029/JZ068i004p01079>
- Theis, C. V. (1935). The relation between the lowering of the Piezometric surface and the rate and duration of discharge of a well using ground-water storage. *Transactions, American Geophysical Union*, 16(2), 519–524. <https://doi.org/10.1029/TR016i002p00519>
- Thiem, A. (1870). Die Ergiebigkeit artesischer Bohrlöcher, Schachtbrunnen und Filtergalerien (in German). *Journal Für Gasbeleuchtung Und Wasserversorgung*, 13, 450–467.
- Thiem, G. (1906). *Hydrologische Methoden (in German)*. Leipzig: Gebhardt.
- Verruijt, A. (1970). *Theory of Groundwater Flow*. London: Macmillan Press.
- Wikramaratna, R. S. (1984). An Analytical Solution for the Effects of Abstraction From a Multiple-Layered Confined Aquifer With No Cross Flow. *Water Resources Research*, 20(8), 1067–1074. <https://doi.org/10.1029/WR020i008p01067>